Astrophysical parameters of M dwarfs with exoplanets

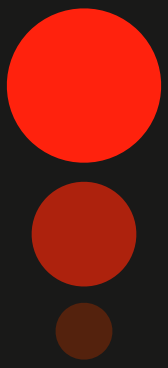

Carlos Cifuentes San Román

DOCTORAL THESIS
2023

Universidad Complutense de Madrid

Facultad de Ciencias Físicas

Tesis doctoral

Parámetros astrofísicos de enanas M con exoplanetas

Astrophysical parameters of M dwarfs with exoplanets

Memoria para optar al grado de doctor
presentada por:

Carlos Cifuentes San Román

Supervisado por:

Dr. José Antonio Caballero
Dr. Jorge Sanz Forcada

Astrophysical parameters *of* M dwarfs *with* exoplanets

Carlos Cifuentes San Román

with external refereeing by

Prof. Adam J. Burgasser
and
Prof. Andrei A. Tokovinin

Madrid, March 2023

A mi madre

"Platero es pequeño, peludo, suave;
tan blando por fuera,
que se diría todo de algodón,
que no lleva huesos."

— Juan Ramón Jiménez, *Platero y yo*

Agradecimientos

Nuestras madres son nuestro primer firmamento, nuestra primera luz, nuestro universo entero. Este libro trata sobre estrellas: sus colores, sus brillos, su lugar. Hay estrellas que aunque nacieron juntas ahora no están cerca, pero mantienen un vínculo que permanece en el espacio y en el tiempo. Yo tengo la fortuna de tener una estrella que me mira y me acompaña: este libro es para mi madre.

Mis padres me dieron la vida y lucharon por aquel futuro que *ahora* es — no puedo imaginar un regalo más valioso. Me mostraron siempre el camino del esfuerzo y la empatía. De mi hermana Judith y mi cuñado Iván he aprendido que lo que importa es la sensibilidad y el amor sencillo y sin adornos. A ellos la vida les sigue: Óliver y Mateo, os deseo lo mejor en vuestro propio camino, que es un libro que se acaba de abrir. Mis tías, Eloína y Loli, cada día han sido cariño puro, amor sincero, un hogar para el alma. Sois mi familia y os debo mucho más de lo que podría expresar en palabras.

José Caballero y Jorge Sanz me han ofrecido todo lo que se puede pedir: experiencia, paciencia y cercanía. Ellos me brindaron la libertad de poder descubrir por mi mismo. José ha sido infinitamente generoso con su tiempo, y ha tenido para mi siempre sus puertas abiertas. Una vez él y yo fuimos *The Astrophysical Brothers*, y hubo tantas otras ocasiones en las que la música nos vio unidos. Yo guardo respeto y admiración por él, le estoy profundamente agradecido. Valoro el entusiasmo y la cercanía que María Rosa Zapatero Osorio ha significado. En nuestras reuniones de los viernes yo me noto madurar como científico. En el MPIA Trifon Trifonov me enseñó muchas cosas útiles e importantes. No olvidaré el color de Königstuhl en el otoño de Heidelberg. A Félix un día le regalé miel y manzanas y él me devolvió mucho más. Con Michel Mayor conversé sobre vida en Marte, sobre Suiza, sobre chocolate. Cuando veo su nombre siempre evoco su inspiradora humildad. Me siento afortunado de haber compartido esta etapa con vosotros y vosotras, deseo poder volver a hacerlo.

Dice la RAE que la amistad es "afecto personal, puro y desinteresado, compartido con otra persona, que nace y se fortalece con el trato". Adrián, Bea, Diego, Héctor, Pepe, Sara — comparto con vosotros el placer de la amistad: somos amigos a cambio de nada. Me conocen desde esa edad en la que yo ignoraba hasta cuál era la edad del Universo. A mis colegas en el Centro de Astrobiología: ojalá que la ciencia nos una de nuevo, he sido tan feliz de haber podido compartir este tiempo juntos. Mientras escribo estas líneas, a mi lado está Olga. Ella es mi compañera en el viaje, una luz en el camino, reposo para el corazón.

Esta página no puede ser una lista exhaustiva de quienes traigo a mi memoria al querer agradecer por tanto. Aunque no leas tu nombre, yo habré pensado en ti. Puede incluso que no sepa tu nombre y algo te deba agradecer.

Es vuestro este trabajo, sois todo lo bueno que hay en mi.
Sin vuestra luz no se ven las estrellas.

Carlos, en marzo de 2023.

Contents

Abstract

M dwarfs are the most abundant stars in the Universe. They are hosts of a rich diversity of planetary companions, which are much more noticeable in these smaller stars. Advancements in technology continue to push the boundaries of what is possible to be detected on them, even when they exist as faint signals. In many cases, planets orbiting M dwarfs can also be described in remarkable detail. What makes the difference is how deeply we can characterise the host star. This includes to properly model their atmospheres, their abundance of metals, and their activity processes. If they are well described individually, these numerous stars have the potential for providing statistically robust conclusions when combined into larger samples. Carmencita is the input catalogue of nearby M dwarfs for the CARMENES project, which aims to search for potentially habitable Earth-sized planets orbiting them. It contains more than two thousand M dwarfs that are scrutinized by the consortium members from multiple angles and with a high degree of attention to detail.

This thesis contributes to the description of each one of these M dwarfs, including astrometry, photometry, activity, kinematics, and multiplicity, but also to the study of the sample as a whole. We carry out a comprehensive process that involves multi-band photometric and astrometric data analyses. With a minucious examination of every single star and their potential physical companions, we put special effort on the individualised inspection rather than on bulk searches, and in hand-picked data rather than in fully automatised crossmatches. We homogeneously derive stellar luminosities that are eminently empirical, temperatures, masses, and radii, as well as many intermediate products such as bolometric corrections, absolute magnitudes, and colours. From these, we obtain averaged values and empirical relations between fundamental parameters and observables.

Additionally, we address the topic of multiplicity of M dwarfs, describing in detail the existing multiple systems and their components, also proposing the existence of many pairs discovered for the first time. We put the focus on the unresolved binary systems that go unnoticed without spectroscopic studies, but that lead to an incomplete picture of stellar genesis, and to miscalculations of stellar parameters, which negatively impacts the planetary descriptions. The empirical observations presented in this study provide an important benchmark for testing and improving theoretical predictions, because any model of stellar formation and evolution should be able to explain the observed characteristics of these stars.

By taking a careful, individualized approach to the study of M dwarfs, we not only contribute to the study of the Universe's physical processes, but we also pave the way for future discoveries of the potential for life beyond our own planet. Overall, the findings of this study underscore the importance of continued research into the most numerous stars and their planetary systems. We expect that the wealth of data gathered in this thesis will serve as a valuable resource for astronomers and researchers in related fields, and that it will inspire further investigations and new insights into the processes that shape the Universe.

Keywords: astronomical data bases – virtual observatory tools – stars: low-mass – stars: late-type – stars: binaries – planetary systems

Resumen

Las enanas M son las estrellas más abundantes en el Universo. Albergan una rica diversidad de compañeros planetarios, que son mucho más evidentes en estas estrellas más pequeñas. Los avances tecnológicos continúan ampliando los límites de lo que es posible detectar en ellas, incluso cuando se manifiestan como señales débiles. En muchos casos, los planetas que orbitan enanas M también pueden describirse con notable detalle. Lo que marca la diferencia es la completitud con el que podemos caracterizar la estrella anfitriona. Esto incluye modelar adecuadamente sus atmósferas, su abundancia en metales y sus procesos de actividad. Si se describen adecuadamente de manera individualizada, estas numerosas estrellas tienen el potencial de proporcionar conclusiones estadísticamente robustas cuando se combinan en muestras más grandes. Carmencita es el catálogo de entrada de enanas M cercanas para el proyecto CARMENES, que tiene como objetivo buscar planetas del tamaño de la Tierra potencialmente habitables orbitando alrededor de ellas. Contiene más de dos mil enanas M que son examinadas por los miembros del consorcio desde múltiples ángulos y con un alto grado de atención al detalle.

Esta tesis contribuye a la descripción de cada una de estas enanas M, incluyendo la astrometría, fotometría, actividad, cinemática y multiplicidad, pero también al estudio de la muestra en su conjunto. Llevamos a cabo un proceso exhaustivo que implica el análisis de datos fotométricos en múltiples bandas, y astrométricos. Con un examen minucioso de cada estrella y sus posibles compañeros físicos, hemos puesto especial énfasis en la inspección individualizada en lugar de en las búsquedas masivas, y en la selección manual de datos en lugar de cruces completamente automatizados con bases de datos. Derivamos homogéneamente luminosidades estelares que son eminentemente empíricas, temperaturas, masas y radios, así como muchos productos intermedios como correcciones bolométricas, magnitudes absolutas y colores. A partir de estos, obtenemos valores promediados y relaciones empíricas entre los parámetros fundamentales y las observables.

Además, abordamos el tema de la multiplicidad de las enanas M, describiendo detalladamente los sistemas múltiples existentes y sus componentes, proponiendo también la existencia de muchas parejas descubiertas por primera vez. Ponemos el foco en los sistemas binarios no resueltos que pasan desapercibidos sin estudios espectroscópicos, pero que conducen a una imagen incompleta de la génesis estelar y a cálculos erróneos de los parámetros estelares, lo que afecta negativamente a las descripciones planetarias. Las observaciones empíricas presentadas en este estudio proporcionan un importante punto de referencia para poner a prueba y mejorar las predicciones teóricas, porque cualquier modelo de formación y evolución estelar debería ser capaz de explicar las características observadas de estas estrellas.

Al tomar un enfoque cuidadoso e individualizado para el estudio de las enanas M, no solo contribuimos al estudio de los procesos físicos del Universo, sino que también abrimos el camino para futuros descubrimientos del potencial de vida más allá de nuestro propio planeta. En general, los hallazgos de este estudio destacan la importancia de continuar la investigación en las estrellas más numerosas y sus sistemas planetarios. Esperamos que la gran cantidad de datos recopilados en esta tesis sirva como un recurso valioso para astrónomos e investigadores en campos relacionados, y que inspire nuevas investigaciones y nuevas perspectivas sobre los procesos que dan forma al Universo.

Palabras clave: Bases de datos astronómicas – herramientas del observatorio virtual – estrellas: baja masa – estrellas: tipos tardíos – estrellas: binarias – sistemas planetarios

Chapter 1

Introduction

M dwarfs are made of many lives. Their evolution is so slow that from their birth to their final light, many generations of stars like our Sun can go by. This is because M dwarfs make of hydrogen fusion an extremely efficient process. They do not have much mass to convert into energy, but their interiors do a good job at mixing the very few available. They are the first hydrogen-fusing objects that enjoy fully convective interiors, which means that hydrogen is constantly delivered from the surface to the core, making its burning steady and slow. Taking the most of the matter available in this way, however faintly, M dwarfs can glow from dozens to hundreds of billions of years. Meanwhile, the Sun will die one hundred times before the last of their least massive neighbours disappears. In other words, the Universe still needs to be older to see the first red dwarf shut down and die.

M dwarfs are the most abundant stars in the Galaxy, by far exceeding in number stars like our Sun. Planets orbiting M dwarfs are extremely ubiquitous, certainly exceeding the number of stars. With an uncountable amount of possibilities, the number of planets that are suitable for life as we know it could be exceedingly vast. These realisations can safely be extrapolated to other galaxies in the observable Universe. We could say, then, that M dwarfs might be made of many *lifes*. Today we can learn about the diversity and peculiarities of planets orbiting M dwarfs with an unprecedented detail. The problem of how hospitable they can be for life is far from being closed. The future envisions further investigation of the emergence and survival of atmospheres, made possible by the development of extraordinarily well-tailored instrumentation. Disentangling the effects resulting from a plethora of involved factors demands a highly multidisciplinary approach. Among these factors is the behaviour of the host star, which is determined by its fundamental physical parameters, such as its mass. To understand how planets form, evolve, and survive to host life, characterising the host star is the first safe step. The ways are many, and are open — it promises to be a fruitful endeavour.

1.1 Know thy star, know thy planet

Over the past two decades, there has been a surge of interest in M dwarfs, as novel horizons previously restricted by technological, instrumental, and computational limitations have been revealed. The current outlook on these stars is fresh and optimistic, particularly in the search for life-hosting exoplanet candidates. Visually discriminating an exoplanet is almost always not a possibility, let alone actually using robots to probe their atmospheres or surfaces directly and bring a sample back to Earth, and so indirect methods to discover planets must be the way. Every discovery of a planet around an M dwarf contributes to our statistical understanding of the existence and occurrence of planets, and the greater the diversity of detected planets, the more comprehensive our knowledge becomes. Bulk studies such as all-sky exoplanet surveys provide many samples to withdraw from, but there are not shortcuts to the meticulous studies of light or radial-velocity curves for individual stars. Therefore, nothing is more important than describing the stars, by empirical observation or by modelling otherwise, as perfectly as possible.

Exoplanet exploration is just one topic of research that will be indisputably benefited by a better characterisation of these cool stars, but many others exist. If we improve our understanding of the individual stars from the most common type in the Universe, we will necessarily gain knowledge about pretty much any global process in the Galaxy. Our understanding of how stars form and evolve to host planets has been achieved by studying individual stars in great detail. With M dwarfs now more accessible than ever before, the possibilities are limitless. Our understanding of the Universe and its processes fundamentally relies on the study of starlight. In order to describe any planet, one must first describe the object that it orbits. Although orphaned, free-floating planets exist and may outnumber those that orbit objects of any type, their description is inherently incomplete and subject to significant uncertainties In any case, it is highly unlikely that life could emerge or survive on these objects.

Planets are composed from the same material as their mother stars (Gonzalez, 1997; Santos et al., 2001; Fischer & Valenti, 2005). As in a family portrait, we should aim at picturing the mother in order to understand the child. Being able to describe the composition, origin, and vital status of a star is the way to go in order to properly describe her planets. In this sense, planets can be known only as good as their stars are, and the planetary diversity found is a reflection of the miscellany of stars. The mass of a planet can be considered its most fundamental property because, when combined with a radius measured from transits, it determines the bulk density. Some planets are prone to an extraordinary characterisation, for instance, if they transit the star that they orbit (e.g. Caballero et al., 2022). More precise determinations of mass and radius translates into better defined constraints on ice mass fraction and size of rocky interior of the orbiting planets, but has little effect on the composition of the gas layer (Dorn et al., 2017). Many efforts have been undertaken in the determination of stellar parameters, including empirical determination of masses, radii, and their relation to luminosity (Veeder, 1974; Henry & McCarthy, 1993; Chabrier & Baraffe, 1997; Delfosse et al., 2000; Bonfils et al., 2005a; Mann et al., 2015, 2019; Terrien et al., 2015; Benedict et al., 2016; Schweitzer et al., 2019), effective temperature, surface gravity, and metallicity (Casagrande et al., 2008; Rojas-Ayala et al., 2013; Montes et al., 2018; Passegger et al., 2018, 2019; Rajpurohit et al., 2018a), or activity and rotation periods (Stauffer & Hartmann, 1986; Reid et al., 1995; Hawley et al., 1996; Morales et al., 2008; Hawley et al., 2014; Newton et al., 2015; Jeffers et al., 2018; Díez Alonso et al., 2019; Schöfer et al., 2019; Lafarga et al., 2023).

Luckily, the parameters of star and planet are fundamentally tied during their detection. For instance, the semi-amplitude of the radial-velocity (RV) wobble that the planet with mass $\mathcal{M}_p$ imprints in the star with mass $\mathcal{M}_\star$ when orbiting with a period P is:

$$K_\star = \frac{1}{\sqrt{1-e^2}} \frac{\mathcal{M}_p \sin i}{(\mathcal{M}_p + \mathcal{M}_\star)^{2/3}} \left(\frac{2\pi \mathrm{G}}{P}\right)^{1/3}, \tag{1.1}$$

where e is the eccentricity of the orbit and i is the inclination of the orbital plane. Therefore, the mass of the planet is necessarily a fraction of that of the host star. This is even more evident in the case of the planetary radius. The surface flux F (or amount of light per unit area) that is blocked when the star of radius $\mathcal{R}_\star$ is eclipsed by the planet of radius $\mathcal{R}_p$ is directly proportional to the area that it blocks. A simplified form ignoring the limb darkening can be put as:

$$\frac{\Delta F}{F} = \frac{\mathcal{R}_p^2}{\mathcal{R}_\star^2}. \tag{1.2}$$

Large planets around relatively small stars maximise the observed semiamplitude, $K_\star$, of the reflex velocities, and the surface flux dip, $\Delta F/F$, of the partial occultation of the star, because the effects are much more notable. In the first case is the gravitational tug, in the second case is the proportion of the star that the planet eclipses. The domain of small, potentially habitable rocky planets is most easily approachable in the case of the least massive stars (Anglada-Escudé et al., 2016; Gillon et al., 2017; Zechmeister et al., 2019; Dreizler et al., 2020; Trifonov et al., 2021), and still poses a challenge in the case of Sun-like mass stars. It is important to mention that the very detectability of a planet is reigned by the nature of the star, because the amount of stellar activity or jittery fundamentally limits the precision to derive planetary characteristics.

Another essential parameter that is integral to the definition of a planet is the bolometric luminosity, $\mathcal{L}$. It corresponds to the output stellar energy per unit of time, and it is an intrinsic property directly related to its mass. The Stefann-Boltzmann's law relates the luminosity to the temperature and radius of the star, given that the energy profile as a function of the wavelength can be approximated by that of a black body: $F = \frac{\mathcal{L}}{4\pi\mathcal{R}^2} = \sigma T_{\mathrm{eff}}^4$. The luminosity determines the equilibrium temperature of the planets that orbit her, depending on the orbital separation. The equilibrium temperature of the planet, T_{eq}, is decisive for the habitability, as it dictates, for example, the fate of an atmosphere on it. If the planet orbits a star of luminosity $\mathcal{L}$ at a separation a, the general expression for the equilibrium temperature is:

$$T_{\mathrm{eq}} = \left(\frac{\mathcal{L}(1-A_B)}{16\sigma\pi a^2}\right)^{1/4}, \tag{1.3}$$

where σ is the Stefan-Boltzmann constant. This formula approximates both star and planet to a black body, and considers a planetary surface that partially reflects a fraction of the incident stellar flux, measured by the Bond albedo, A_B. Because of the interdependence of all of these properties, quantifying stellar parameters turns out to be extremely of uttermost importance when characterising the planet (e.g. von Braun et al., 2014a). This is also true for the astrometry of the star: even modest uncertainties in the distance can result in substantial uncertainties in its mass or the equilibrium temperature of the planet, which are dependent on the semi-major axis. Luckily, the *Gaia* mission[1] measured trigonometric parallaxes with unprecedented precision, providing remarkably small relative uncertainties (less than 1 % for sources with $G \lesssim 15$ mag, and 1–10 % for sources with $G \simeq$15–18 mag).

[1] *Gaia* is a space observatory of the European Space Agency (ESA), launched in 2013, which is expected to be operative at least until 2025. This is the first reference to this mission, but it will be recurrent throughout this work given the fundamental role of its data. The name was originally meant an acronym ("Global Astrometric Interferometer for Astrophysics"), but now it remains as a proper noun.

The equilibrium temperature determines the circumstellar habitable zone (CHZ), which is classically defined as the range of orbital separations from a star for which a planetary surface can support liquid water, which translates into $T_{\rm eq} \simeq 273$–373 K (Dole, 1964; Hart, 1978; Kasting et al., 1993; Kopparapu et al., 2017, and see Tarter et al. 2007 for the particular M-dwarf case). This approach provides a solid starting point since it allows for more accurate predictions of the expected observational signatures. However, this concept is constantly evolving as new findings emerge from one of the most active areas of astrobiological research, which deals with the origins of life (Ramirez, 2018). Among these findings are: the existence of extraterrestrial liquid water is possible under a range of conditions outside the habitable zone limits (e.g. Murray et al., 2012; Kopparapu et al., 2014; Glein et al., 2015; Choblet et al., 2017; Vance et al., 2018; Kite & Ford, 2018), the possibility of other energy sources besides the parent star to influence positively on biotic processes (Lindegren et al., 2018, and see again Tarter et al. 2007), the fact that life can prosper in extreme environments that do not qualify as habitable in the strict sense (Edwards et al., 2012), the hypothesis of alternative biogenic chemistry (Kan et al., 2016), or the presence and survival of an atmosphere (Lingam & Loeb, 2017). To define what habitable means, and what makes a planet capable of developing and sustaining life, one should questions what is *essential* for giving way to any form of life (see the review by Shahar et al., 2019).

To summarise, our understanding of how planets form and evolve rests fundamentally on the characterisation of their host stars. This includes a clear, updated picture of their nature of the star (Chapter 2), a precise determination of stellar parameters and how their uncertainties propagate (Chapter 3), and a detailed knowledge of the physically bound companions (Chapter 4). In the quest for exoplanets, in particular with expectations for life to prosper, knowing the host star is not only an option, but a necessity. As if it was written in stone on the Temple of Apollo: *Know thy star, know thy planet*.

1.2 Brave new worlds

Since the early discoverers of spectrum analysis in astronomy, such as Robert Bunsen and Gustav Kirchhoff, our capability to read between the lines has shifted our perspective about what can be learnt from light alone. William Huggins carried out the first spectroscopic observations in the mid-nineteenth century (Huggins & Miller, 1864), to discover that the chemistry found in the Earth and the Sun was also present in distant stars, comets, and nebulae. His major innovation occurred in 1868, when he was the first to measure the radial velocity of a star in the Doppler shift of its spectral lines (see Huggins & Huggins, 1890). In the spectrum of a white dwarf, van Maanen (1917) discovered elements heavier than helium, which might be indicative of accreted planetary debris (Zuckerman et al., 2007; Farihi, 2016), and so van Maanen's spectrum might be recognised the first early evidence of an exoplanet. Campbell et al. (1988) offered tentative detection of a planet around a star similar to our Sun. The authors considered that the role of the stellar magnetic fields in the observed periodicities was not of trivial interpretation, and therefore a solid confirmation was not possible — the existence of a planet of jovian mass would be later confirmed by Hatzes et al. (2003). Latham et al. (1989) published the first detection of a substellar object candidate outside the Solar System, which presented as 'a probable brown dwarf' in a 84-day orbit around a solar-like star.

It was epoch for many innovative works regarding exoplanetary discovery: Wolszczan & Frail (1992) and Wolszczan (1994) detected and confirmed the first planet outside the Solar System that orbits a pulsar, Hatzes & Cochran (1993) studied radial velocity variations of giant stars, and the notorious discovery of the first solid evidence of an exoplanet orbiting a main sequence, solar-like star by Mayor & Queloz (1995), which was validated later that year (Marcy & Butler, 1995). A similar discovery by Marcy & Butler

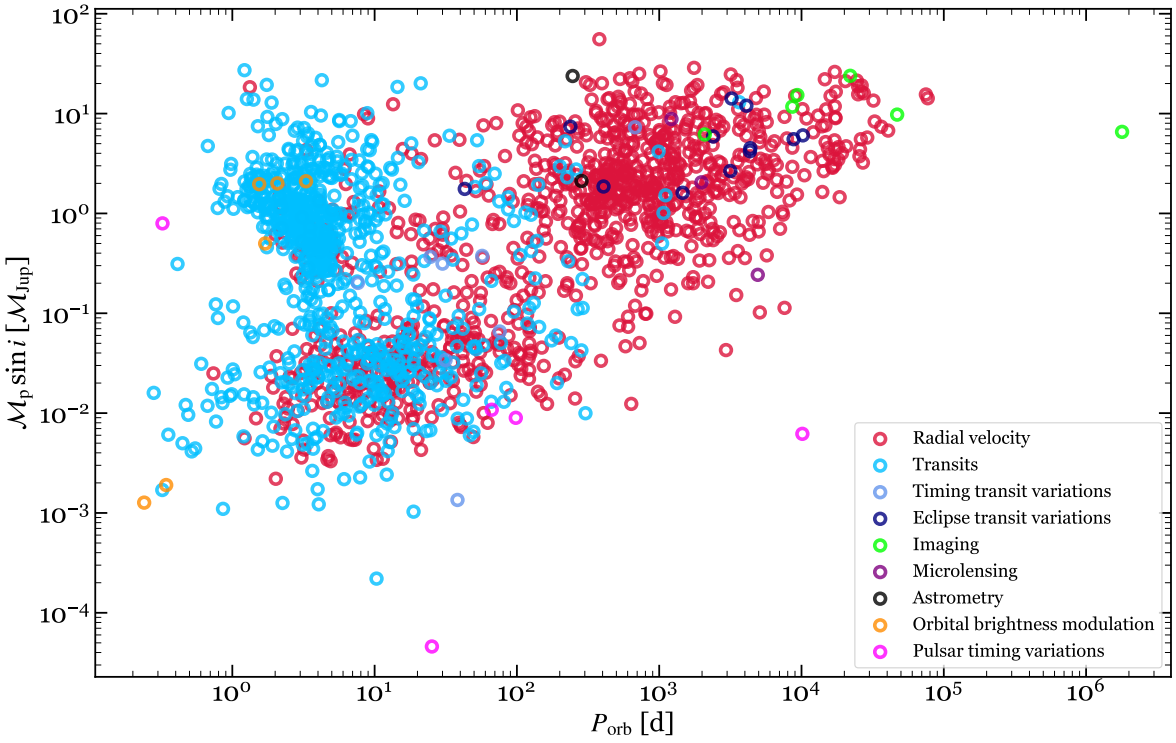

Figure 1.1: Orbital period as a function of planetary mass in jovian units for all exoplanets confirmed to date in the NASA Exoplanet Archive, coloured to differentiate by the discovery method.

(1996) and Butler & Marcy (1996) would soon follow. To the date of writing this work, 5250 detections are confirmed exoplanets[2] (Fig. 1.1). Given that three decades have gone by since the first pioneering investigations, this implies that a new planet has been discovered approximately every two days.

Except for the few dozen cases for which there is a direct imaging of the actual planet (e.g. Fig. 1.2), almost all confirmed exoplanets are detected by indirect means. Two techniques account for 95% of the discoveries (Fig. 1.3). The radial-velocity (RV) method has produced 1027 confirmed detections, but it is *eclipsed* by the transit method, with 3945 exoplanets found. In the RV method, because both star and planet revolve around the centre of mass of the system, the orbit of the planet is inferred from the star's orbit, which is measured as a back-and-forth movement in the component of the motion as seen from Earth. In the other case, a planet is said to transit when its orbital path crosses the host star as seen from our perspective. With sufficient accuracy, it is possible to measure a periodic dimming of the light from the star. The effect is equivalent to a solar eclipse, but in another star. As in the case of our Sun, these can be predicted accurately years into the future. The time between transits also tells important information regarding additional planets or other causes that disturb the regularity. Even when the transits method is only sensitive to planets with orbits that are coplanar (or near to) to our line of sight, their discoveries are much more fruitful in number because they can be carried out in all-sky surveys. The majority of the planet detections using transits are attributed to only two of these missions: *Kepler* (Borucki et al., 2010; Howell et al., 2014) and *TESS* (Ricker et al., 2015) have contributed with more than 90% of the transiting planets, with potential candidates already detected in enough number to double the size of the current pool[3]. Other methods can be potentially used during the transits: transit timing variations, eclipse tim-

[2]In this section, all the statistics and figures are made with data from the NASA Exoplanet Archive `https://exoplanets.nasa.gov`, updated as of February 20, 2023.

[3]There are 6153 *TESS*, 2054 *Kepler* and 978 K2 (*Kepler*'s extended mission) candidates to be confirmed. These are transit-like events that appear to be astrophysical in origin.

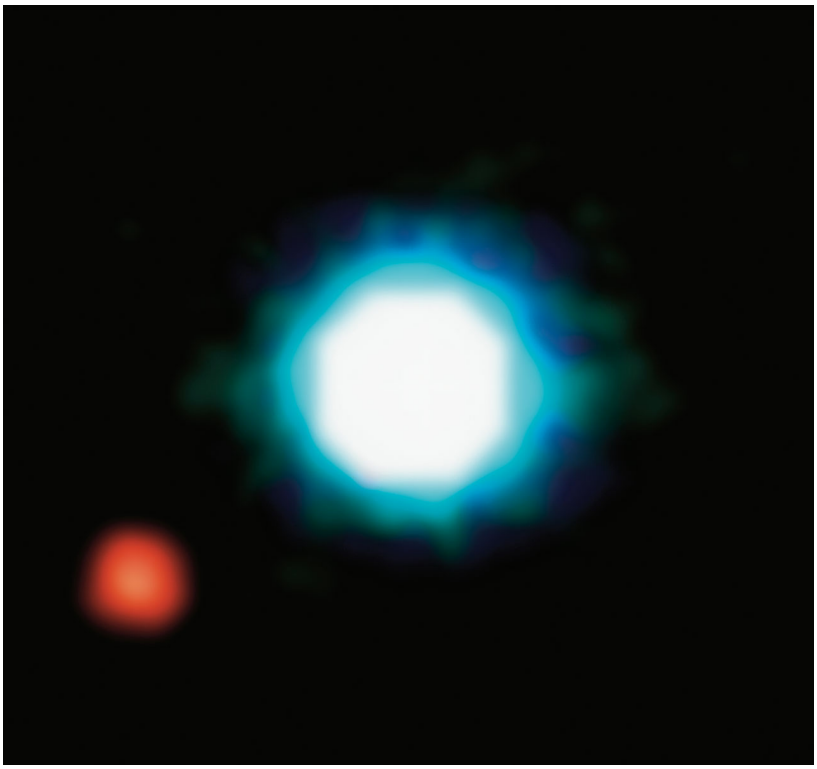

Figure 1.2: 2M1207 b (Chauvin et al., 2004; Mamajek, 2005) is a giant planet ($\sim 5\ M_{\rm Jup}$, shown in red) around a brown dwarf (2M1207, shown in blue) that constitutes a beautiful example of a directly imaged exoplanet. It is the first planetary-mass companion of a brown dwarf discovered, and the first to be directly imaged beyond the Solar System. The image is composed by three near-infrared exposures (H, K and L passbands) with the NACO adaptive-optics facility at the 8.2-m VLT Yepun telescope at the ESO Paranal Observatory (Credit: ESO).

ing variations, or orbital brightness modulation. Other are more sophisticated and demanding from the observational perspective: polarimetry, or microlensing. The latter exploits a fascinating phenomenon: the gravitational lensing effect predicted by Albert Einstein's theory of general relativity. A massive body such a star can bend the light coming from a more distant star. If a planet happens to pass in front of the distant star, it can cause a brief increase in brightness that can be measured.

The technological effort put into the discovery of exoplanets has also produced many other ground- and space-based instruments. Some of the ground based spectrographs with the greatest resolving power are summarised in Table 1.1. In this context, the future depends to a great extent on the precision that can be achieved with Doppler measurements, with a prospect of extraordinary 10-centimetre per second values (Fischer et al., 2016, and compare with the 3 metre-per-second precision of Butler et al. 1996).

One of the most exciting possibilities, for which many observational efforts have already being carried out, is the study of atmospheres of distant worlds (e.g. Ehrenreich et al., 2020). Small, Earth-sized planets are more interesting than large, gaseous worlds, because they could potentially be better hosts for life. The prospect of being able to isolate the spectral features of the atmospheres of these planets is a promising perspective for the future (Tal-Or et al., 2019). Upcoming generations of extremely large telescopes might be able to detect molecules such as O_2 in the atmosphere rocky planets in the CHZ of M dwarfs. They could combine high-contrast imaging and high-dispersion spectroscopy techniques to peer into the nearest neighbour planets (Snellen et al., 2015).

Indeed, the proximity of some confirmed exoplanets that also transit, many of them orbiting M dwarfs,

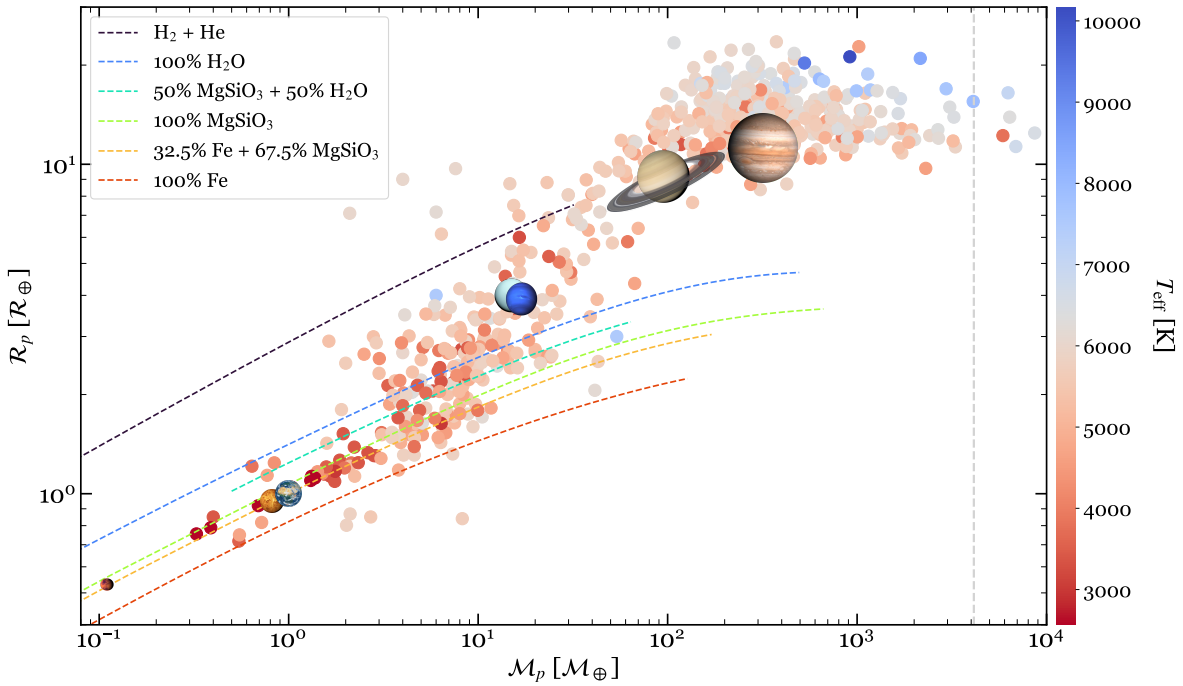

Figure 1.3: Mass-radius diagram for all the confirmed transiting exoplanets with mass determination (from RV or transit time variations), colour-coded by effective temperature of the host star, along with the planets of the Solar System. The dashed coloured curved are theoretical composition models by Zeng et al. (2019) described in the legend, and the dashed grey line represents the limiting mass for the deuterium burning (13 $\mathcal{M}_{\rm Jup}$). Figure adapted from Caballero et al. (2022).

offers a favourable opportunity to probe their atmospheres (Seager & Deming, 2010; Wunderlich et al., 2019). There is already a sizeable body of the literature devoted to these explorations. Some atomic and molecular species investigated include Hα, He I, Li I, Na I doublet, Mg I, K I, and Ca II infrared tripled (IRT) (Nortmann et al., 2018; Salz et al., 2018; Alonso-Floriano et al., 2019b; Casasayas-Barris et al., 2020; Khalafinejad et al., 2021; Casasayas-Barris et al., 2021; Czesla et al., 2022; Tabernero et al., 2022b), Si (Cont et al., 2022b), Ti and V (Cont et al., 2022a), Fe (Yan et al., 2022), TiO (Cont et al., 2021), and also H_2O (Alonso-Floriano et al., 2019a; Sánchez-López et al., 2019).

Transmission spectroscopy is the method to access to this information observationally, when the light from the star pierces the planet gaseous envelope, if this exists. It is, in some way, as seeing a sunrise (of another 'Sun') in another planet. Nowadays, to observe the atmosphere of an Earth-like planet *from* Earth falls on the edge of the technological capabilities. But the prospects are good: we have the technology, the knowledge, and the targets. Small, rocky planets in the habitable zone of red dwarfs are reachable with today's technology.

1.3 M dwarfs

Low-mass, cool stars are remarkably numerous and long-lived objects in the Galaxy. Among them, M dwarfs are by far the most common type of star in the solar neighbourhood, vastly outnumbering their more massive counterparts (Henry et al., 1994, 2006; Reid et al., 2004; Bochanski et al., 2010; Winn & Fabrycky, 2015; Reylé et al., 2021). In their mainly convective interiors, the fusion process is slow and, therefore, the lifespan is long, as they remain on the main sequence for tens of billions of years (Adams & Laughlin, 1997; Baraffe et al., 1998).

Table 1.1: Some of the highest-resolution ground-based spectrographs for exoplanet surveys.

Instrument[a]	First light	Telescope/ Observatory[b]	Resolution	λ coverage [nm]
HIRES	1993	10-m WMKO	85 000	300–1000
CORALIE[c]	1998	1.2-m LSO	60 000	390–680
HARPS	2003	3.6-m LSO	120 000	380–690
CRIRES	2006	8.2-m VLT	100 000	950–5200
HARPS-N	2012	3.6-m TNG	120 000	378–691
CARMENES	2015	3.6-m CAHA	94 600 (VIS)	520–960
			86 400 (nIR)	960–1710
ESPRESSO	2016	8.2-m VLT	200 000	380–686
EXPRES	2018	4.3-m DCT	150 000	380–780
SPIRou	2018	3.6-m CFHT	75 000	950–2350
IRD	2018	8.2-m ST	70 000	950–2450
HPF	2018	9.2-m HET	50 000	800–1300
MAROON-X	2019	8.1-m GNT	85 000	500–920
CRIRES+	2021	8.2-m VLT	100 000	1000–5000
NIRPS	2022	3.6-m LSO	100 000	950–1800
KPF	2022	10-m WMKO	98 000	440–850
ANDES[d]	[2026]	39-m ELT[e]	100 000	400–1800

[a] HIRES: HIgh Resolution Echelle Spectrometer (Vogt et al., 1994); HARPS / HARPS-N: High-Accuracy Radial velocity Planetary Searcher (Mayor et al., 2003); CRIRES / CRIRES+: CRyogenic InfraRed Echelle Spectrograph / ~ Upgrade (Kaeufl et al., 2004); CARMENES: Calar Alto high-Resolution search for M dwarfs with Exoearths with Near-infrared and optical Echelle Spectrographs (see Sect. 2.1); ESPRESSO: Echelle SPectrograph for Rocky Exoplanets and Stable Spectroscopic Observations (Pepe et al., 2010); EXPRES: EXtreme PREcision Spectrograph (Jurgenson et al., 2016); SPIRou: SpectroPolarimètre InfraRouge (Artigau et al., 2014); IRD: InfraRed Doppler (Tsujimoto et al., 2018); HPF: Habitable Zone Planet Finder (Mahadevan et al., 2012); MAROON-X: M-dwarf Advanced Radial velocity Observer Of Neighboring eXoplanets (Seifahrt et al., 2018); NIRPS: Near-InfraRed Planet Searcher (Bouchy et al., 2017); KPF: Keck Planet Finder (Gibson et al., 2016); ANDES: ArmazoNes high Dispersion Echelle Spectrograph (Marconi et al., 2022).

[b] CAHA: Centro Astronómico Hispano en Andalucía; CFHT: Canada France Hawaii Telescope; DCT: Discovery Channel Telescope; ELT: Extremely Large Telescope; GNT: Gemini North Telescope; HET: Hobby-Eberly Telescope; LSO: La Silla Observatory; ST: Subaru Telescope; TNG: Telescopio Nazionale Galileo; VLT: Very Large Telescope; WMKO: W. M. Keck Observatory.

[c] CORALIE is not an actual acronym, but the name of the baby daughter of an engineer from the Observatoire de Haute-Provence in France.

[d] Formerly known as HIRES, but was renamed due to the coincidence with Keck's HIRES, which is in operations since the 1990s.

[e] Currently under construction (first light expected in 2028).

Such abundance and prevalence make low-mass stars very attractive targets for multiple areas of astrophysical research. Collectively, M dwarfs are excellent probes for the examination of the Galactic structure (Bahcall & Soneira, 1980; Scalo, 1986; Reid et al., 1997; Chabrier, 2003a; Pirzkal et al., 2005; Caballero et al., 2008; Ferguson et al., 2017), and are also very convenient tracers of Galactic kinematics and evolution (Reid et al., 1995; Gizis et al., 2002; West et al., 2006; Bochanski et al., 2007). Individually, M dwarfs have proven to be interesting targets for the discovery of low-mass exoplanets, and a consid-

Figure 1.4: Direct image of Proxima Centauri taken using Hubble's Wide Field and Planetary Camera 2 (WFPC2). Credits: ESA/Hubble & NASA.

erable amount of the current literature pays special attention to them (e.g. Boss, 2006; Tarter et al., 2007; Zechmeister et al., 2009; Bonfils et al., 2013a; Mann et al., 2013b; Clanton & Gaudi, 2014; Dressing & Charbonneau, 2015; Fischer et al., 2016; Kopparapu et al., 2017; Reiners et al., 2018b). In particular, low-mass, small-sized stars are specially suited to the search for close-in terrestrial planets because their detection becomes easier with decreasing stellar size and planetary orbital period (Anglada-Escudé et al., 2016; Gillon et al., 2017; Zechmeister et al., 2019).

But to say that M dwarfs are simply *common* would be an understatement. In order to appreciate their ubiquity, we propose an interstellar travel[4]. Departure: our Sun — a G2 V star burning hydrogen in a reasonable peace in its main sequence existence. The nearest stellar neighbour to our Sun is a triple system that contains an M dwarf (Proxima Centauri, M5.5 V — see Fig. 1.4). More than a hundred years passed since the discovery of the star (Innes, 1915; Voûte, 1917)[5] for an Earth-like planet to be detected (Anglada-Escudé et al., 2016)[6]. The second nearest neighbour, which carries the name of its discoverer (E. E. Barnard), is an M dwarf as well (Barnard, 1916), with a controversial planet around (Ribas et al., 2018, but see Lubin et al. 2021). If we ignore the ultracool, little-or-no-glowing objects in Luhman 16 (an L8+T1 binary) and the planetary-mass object WISE 0855-0714 (Y4), the next two stars are M dwarfs, too: Wolf 359 or CN Leo (M6.0 V), and Lalande 21185 (M2.0 V). At 10 pc away from home, we will have spotted 422 stellar and substellar objects, including a few white dwarfs, from which 249 (or 59 out of 100) are spectroscopically classified as M dwarfs (Reylé et al., 2021).

[4] A super-luminous speed is assumed, so distances can be ignored.

[5] Gill (1899) noted the importance of a fair assignation of the prime discoverer.

[6] Two additional, smaller planets, in even closer orbits were found thereafter (Faria et al., 2022), one of them confirmed, and a third, 5.2-year period candidate (Damasso et al., 2020) that awaits confirmation.

None of the stars that are being studied in this research can be seen with the naked eye from Earth. This is because M dwarfs shine primarily in the infrared (the typical peak of emission for M dwarfs lies between ~0.7 and 1.5 μm), where the human eye is not sensitive. On top of this, they also shine much dimly (less than 10 %) than our Sun. They lie in the lower tail of the main sequence (see Fig. 1.5). Because of their intrinsic faintness, low-mass stars and substellar objects have been widely under-represented until relatively recent times.

With such an abundance, it is not surprising that red dwarfs contribute notably to the luminosity function and constitute an important weight in the mass function baryonic, ordinary matter of the Milky Way (Scalo, 1986; Hawkins & Bessell, 1988; Kroupa et al., 1993; Kirkpatrick et al., 1994; Gould et al., 1996, 1997; Kroupa, 2001; Zheng et al., 2001; Chabrier, 2003b; Covey et al., 2008; Bochanski et al., 2010; Kalirai et al., 2013). Both in the initial mass function (IMF) and the stellar luminosity function (SLF) the existence of unresolved binaries must have an impact that must not be neglected (Kroupa et al., 1991; Piskunov & Mal'Kov, 1991; Chabrier, 2003a; Kroupa & Jerabkova, 2018).

In dwarfs with masses of less than 0.35 $\mathcal{M}_\odot$ (i.e. M3.5-M4.0 type and onwards), convection takes over as the principal mechanism for energy transportation, and fully convective interiors dominate (Delfosse et al., 1998b; Mullan & MacDonald, 2001; Reiners & Basri, 2009). This translates into the fact that a large fraction of mid-M dwarfs to early-L objects are magnetically active (Hawley et al., 1996; Gizis et al., 2000b; West et al., 2004, 2008). In particular, young, low mass stars show very strong chromospheric activity, which intensifies the ultraviolet emission with respect to older populations (Rodriguez et al., 2011). This makes radial-velocity detections more difficult, because some signatures imprinted by active stars can adopt the appearance of the gravitational interaction with one or more planets (France et al., 2013).

If an M dwarf was selected at random, there is a good chance that it would host at least one planet about the size of Earth (Cassan et al., 2012; Bonfils et al., 2013a; Gaidos et al., 2016; Hardegree-Ullman et al., 2019; Mulders et al., 2021; Sabotta et al., 2021). Clanton & Gaudi (2014) estimated the number of planets of *any* kind per M dwarf to be of 1.9 ± 0.5. Using the full four-year of *Kepler* data, Dressing & Charbonneau (2015) estimated the cumulative occurrence rate of planets with 1–4 $\mathcal{R}_\oplus$ and orbital periods less than 200 days to be 2.5 ± 0.2 planets per M dwarf, with 16^{+17}_{-7} % and 12^{+10}_{-5} % of Earth-size and super-Earth planets per M dwarf habitable zone, respectively. For minimum masses between 1 and 10 $M_\oplus$, Sabotta et al. (2021) estimated in $1.32^{+0.33}_{-0.31}$ planets per M dwarf. More recently, Ribas et al. (2023) reported 1.44 ± 0.20 planets with $\mathcal{M} \sin i < 1000\ \mathcal{M}_\odot$ with periods of less than 1000 days. The common results that emerges from these studies is that each M dwarfs could harbour, *at least*, one planet. These statistics come to reality in the solar neighbourhood, beyond Barnard's star: Lalande 21285 (2 planets, Díaz et al., 2019; Rosenthal et al., 2021), Lacaille 9352 (2 planets, Jeffers et al., 2020), Ross 128 (1 planet, Bonfils et al., 2018b), and so on[7]. Some of them also have additional candidates, but unconfirmed. The evidence collected in the first two decades of the 21st century leaves no trace of doubt: M dwarfs are fertile ground for planetary systems.

We have learned that these planets exist in a rich diversity, which includes Jovian planets (Bayliss et al., 2018; Morales et al., 2019), Saturnian and sub-Saturnian (Hartman et al., 2009; Quirrenbach et al., 2022; Sedaghati et al., 2022), Neptunian and sub-Neptunian (Bonfils et al., 2005b; Reiners et al., 2018a; Luque et al., 2019a, 2022b; Espinoza et al., 2022), super-Earths (Udry & Santos, 2007; Charbonneau et al., 2009; Dittmann et al., 2017; Suárez Mascareño et al., 2017b; Díez Alonso et al., 2018b; Günther et al., 2019; Bluhm et al., 2021; Soto et al., 2021; Toledo-Padrón et al., 2021; Luque et al., 2022a; Damasso et al., 2022; Chaturvedi et al., 2022), and Earth-like planets (Berta-Thompson et al., 2015; Anglada-Escudé et al.,

[7] For CN Leo Tuomi et al. (2019) reported two planets, although this was a very controversial result.

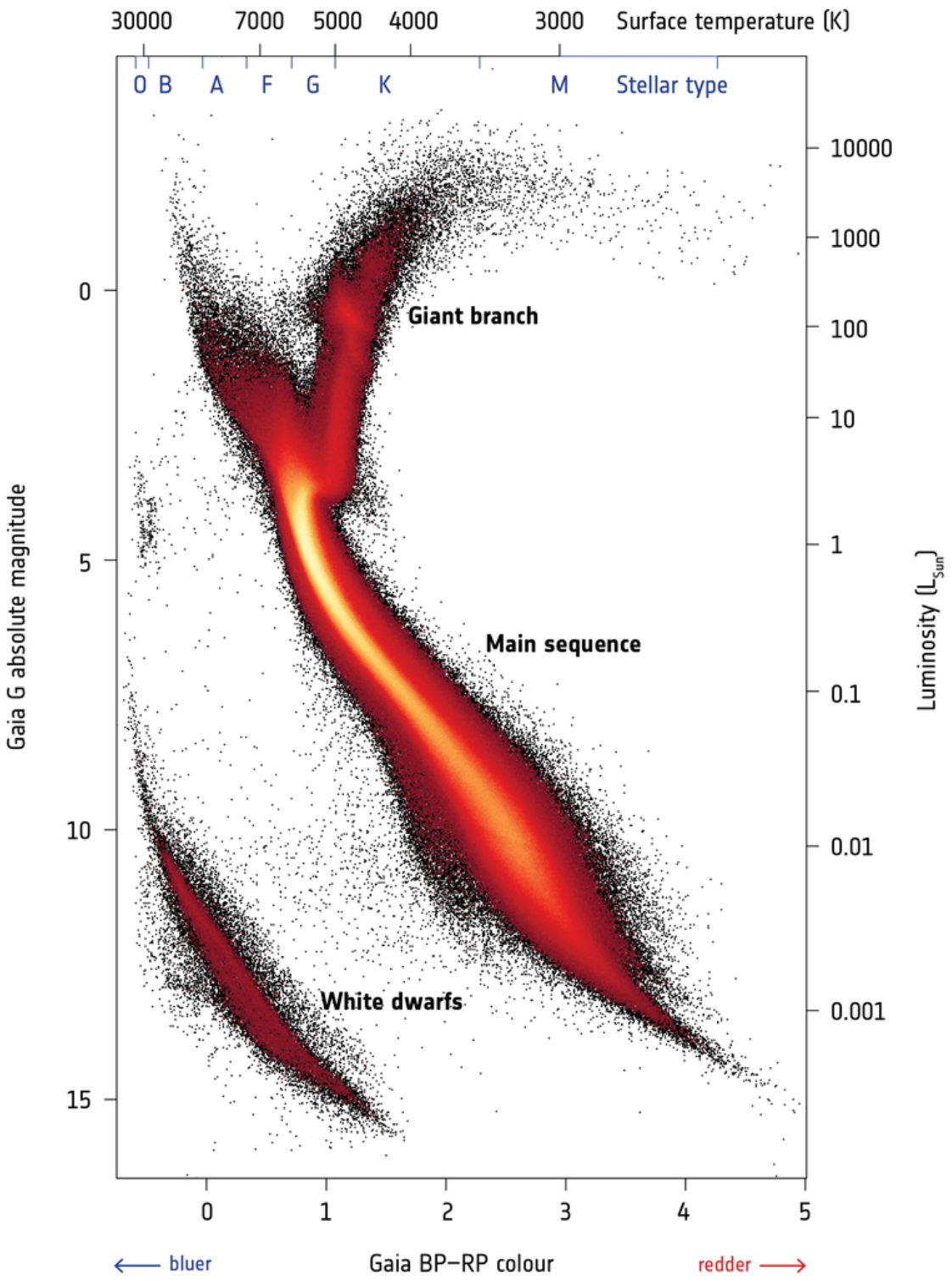

Figure 1.5: Hertzsprung-Russell diagram containing more than four million stars within 1500 parsec from the Sun with *Gaia* DR2 data. Credit: ESA/Gaia/DPAC.

2016; Gillon et al., 2017; Dittmann et al., 2017; Luque et al., 2019b; Kemmer et al., 2020; Amado et al., 2021; Trifonov et al., 2021; Kemmer et al., 2022; Luque et al., 2022a; Caballero et al., 2022).

In the case of solar-like stars, a well-studied population, it exists a strong correlation between metallicity and planet occurrence (e.g. Santos et al., 2001). It has been very well studied in the case of gas giants (Gonzalez, 1997; Santos et al., 2000; Laws et al., 2003; Santos et al., 2004; Fischer & Valenti, 2005; Johnson et al., 2010a; Mortier et al., 2012), but remains unclear for super-Earths and Neptune-mass planets (Sousa et al., 2008, 2011; Mayor et al., 2011). Observations suggest that terrestrial planets emerge without any preference on the metal content of the star (Buchhave et al., 2012).

It seems that M dwarfs are less likely to harbour giant, gaseous planets (Endl et al., 2006; Johnson et al., 2007; Mann et al., 2013a; Gan et al., 2022). However, there are counterexamples, such as GJ 3512 ('A giant exoplanet orbiting a very-low-mass star challenges planet formation models', Morales et al., 2019), or the four-planet system in the M4 dwarf IL Aqr, which contains the first jovian planet detected in such a star (Marcy et al., 1998, 2001; Rivera et al., 2005, 2010). Nevertheless, metallicity is a complicated subject in the case of cool stars (see Passegger et al., 2022). Until recent years the systematic study of correlation between fundamental properties and planet occurrence in M dwarfs have been limited due to the small size of confirmed M dwarfs with planets, specially the small-sized. Contrary to FGK stars, there was initially evidence that the planet-hosting M dwarfs had sub-solar metallicities (Bonfils et al., 2005a; Bean et al., 2006), but recent studies point towards the opposite direction (Johnson & Apps, 2009; Rojas-Ayala et al., 2010; Terrien et al., 2012; Hobson et al., 2018). On top of this, the number of low-metallicity red dwarfs does not seem to match the model predictions (Woolf & West, 2012). It has been suggested that the weakened frequency of giant planets found in the red dwarfs can be explained by the lower masses of the host stars, rather than by the effect of metallicity (Johnson & Apps, 2009). Still, the correlation between metallicity and planet occurrence is seen as strong supporting evidence of the core-accretion model of planet formation (Mizuno, 1980; Pollack et al., 1996; Lambrechts & Johansen, 2012). Under this mechanism, planet formation modelling results in a higher occurrence of lower-mass planets (Laughlin et al., 2004; Alibert & Benz, 2017).

The present thesis is all about these common, small, faint, planet-host main sequence stars called M dwarfs. We investigate in detail about 2200 nearby stars of this kind. The sample is the input catalogue of stars for the CARMENES project. The homonymous instrument looks for exo-Earths on a subsample of 350 stars. By meticulously characterising each one of them, we set the foundation for deriving solid and robust global properties for these fascinating objects.

Chapter 2

Carmencita

A catalogue should feel like a home for the stars. At home, the stars should be able to find who they are, where is their place on the sky, and how big and luminous they are. And the fingerprint of their spectra, how much *metal* is in their cores. Also, how fast they rotate, how magnetically active they are, how much they apparently shine. Chances are that some of them have a companion that moves along, very close or very wide, or both — they should know that, too. This is what *Carmencita* is about: home for many hundreds of cool stars, each one with so much to tell if one listens carefully. From its very foundation, dozens of parameters have been compiled or measured for every one of them. This has been the effort of many before me, which now embody a respectable amount of the bibliographic content of this work. In this chapter I will describe my own contribution to this catalogue, which includes a meticulous compilation and continuous update, so *Carmencita* feels like home. If I were a red dwarf, I would prefer to be in Carmencita.

Figure 2.1: Long-exposure moon-washed photography of the dome of the 3.5-m telescope at the Calar Alto Observatory (taken May, 2017).

2.1 CARMENES

Calar Alto high-Resolution search for M dwarfs with Exoearths with Near-infrared and optical Echelle Spectrographs (CARMENES) ['kar-men-es] (Caballero et al., 2013b; Quirrenbach et al., 2014) represents an instrument, a science project, and a consortium. Since prospective exercises on exoplanet search identified near-infrared as an area of potential development, CARMENES was designed with enough sensitivity to reach the scientific goal of the project: to detect and characterise terrestrial planets in the habitable zones of late-type main-sequence stars. In particular, the instrument aimed at detecting 2 $\mathcal{M}_\oplus$ planets in the habitable zone of M5 V stars. This translates into a metre-per-second precision in the measurement of radial-velocity variations in extremely faint objects and with long-term stability, which constitutes a technological challenge. CARMENES was designed in such a way that its efficiency is maximum around 1 μm, which is the emission peak of mid- to late-M dwarfs. The project was conceived as a single large survey targeted at about 300 M-type stars in the solar neighbourhood during guaranteed time observations (GTO) nights at the 3.5-m telescope at the Calar Alto Observatory[1] (Centro Astronómico Hispano en Andalucía (CAHA, Almería, Spain) — see Fig. 2.1 and Fig. 2.2, upper image.

There, the instrument CARMENES is mounted. It consists of a double channel covering two consecutive ranges in the optical (from 520 to 960 nm — VIS) and the near-infrared (from 960 to 1710 nm — NIR) with a very high spatial resolution of R = 80 400 and R = 94 600 in those respective ranges. The spectrum is distributed in 55 and 28 orders for the VIS and NIR channels, respectively (Fig. 2.3). Each channel is an échelle spectrograph, housed in a thermally stabilised vacuum vessel (at a pressure of about

[1] CAHA, https://www.caha.es/es/.

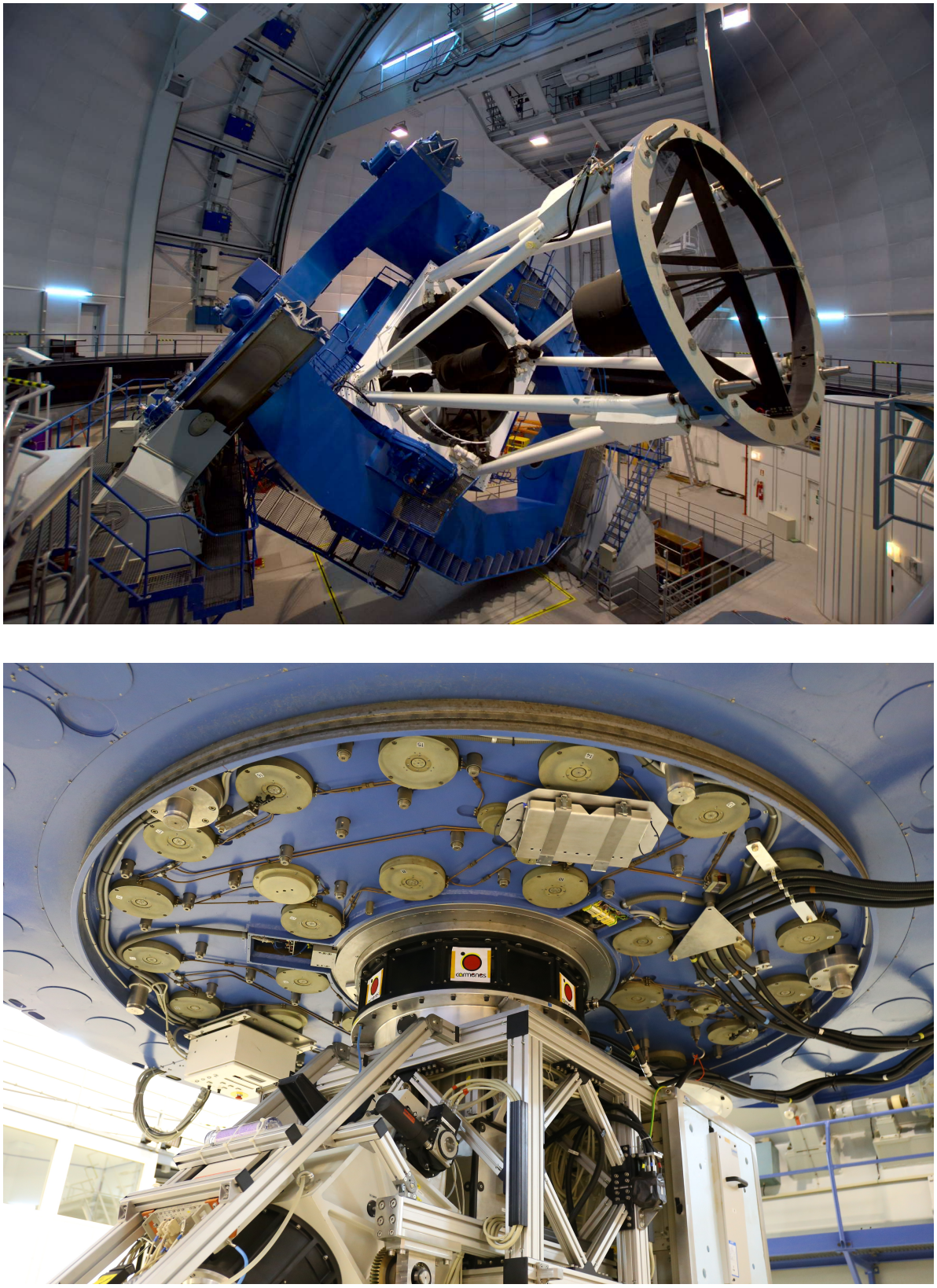

Figure 2.2: Slightly upper view of the 3.5-m telescope at the Calar Alto Observatory with open petals that expose the main mirror (*top*), and a closer view of the Cassegrain focus, which has the attachment of the instrument front-end at the telescope (*bottom*).

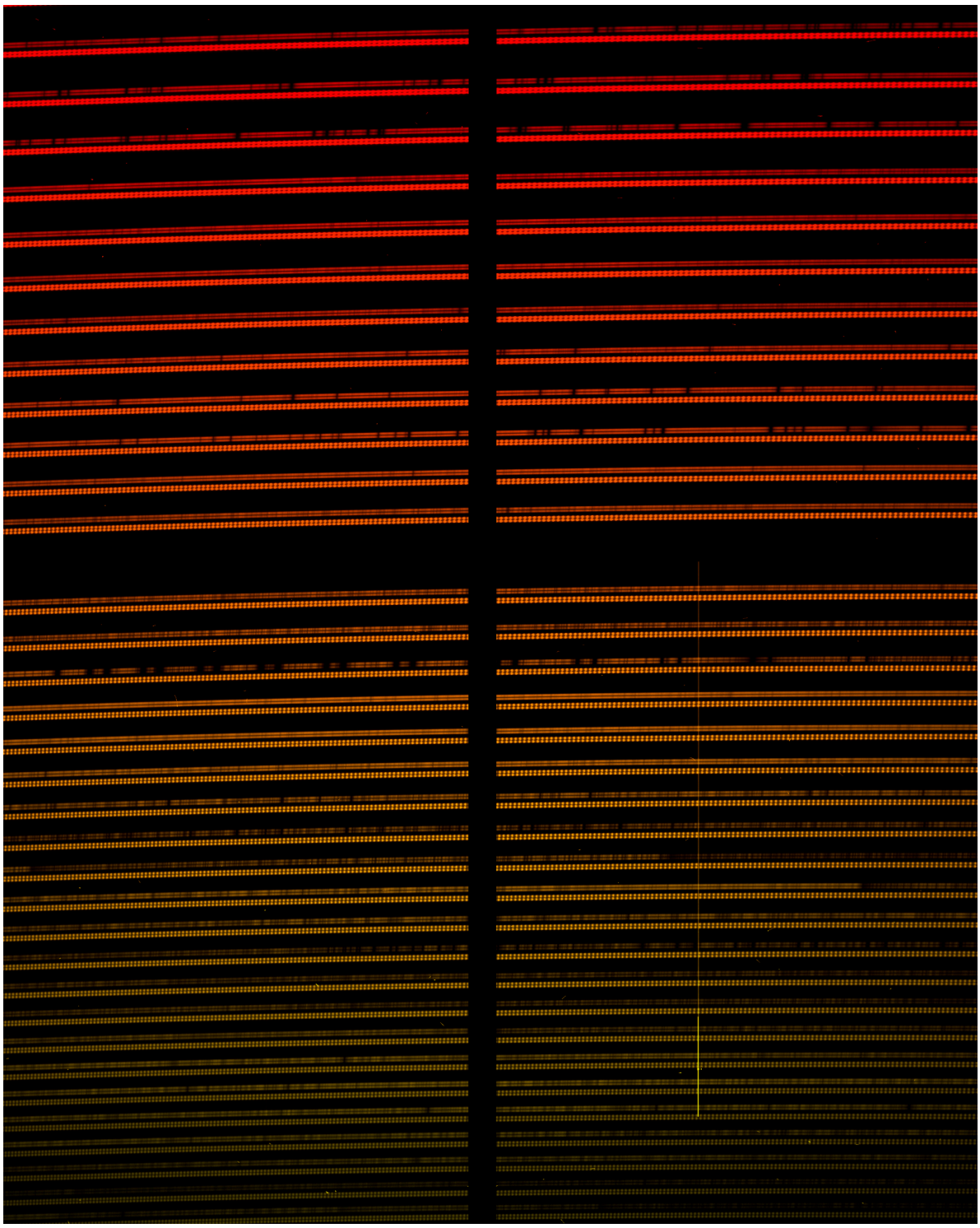

Figure 2.3: Fragment of one of the first CARMENES VIS spectra taken, corresponding to Luyten's Star, along with the Fabry-Pérot for simultaneous calibration. Absorption lines are easily visible.

10^{-5} mbar) placed in the coudé room of the dome, where exceptional levels of mechanical and thermal stabilisation are ensured. This diminishes the effects that compromise the instrumental stability, mainly pressure variations and possible convection effects. They are mounted on benches and equipped with a temperature stabilisation system that can maintain a temperature constant within 10^{-3} K. The VIS spectrograph operates at around room temperature (285 K) with a night stability of about 1 mK, while the NIR spectrograph is cooled down to about 140 K with a night stability of about 3 mK. Each one is simultaneously fed by two octagonal cross-section fibres: one is for calibration, and the other carries the light of the target from the Cassegrain focus of the telescope. Choosing non-circular fibres allows for a higher overall throughput. Using a 100 μm fibre, their projected size on the sky is 1.5 arcsec[2]. A dichroic beam splitter placed at 960 nm leads the light into these fibres. The calibration is performed with an emission-line lamp and with a Fabry-Pérot etalon, individually for each channel (Th-Ne for VIS, and U-Ne for NIR). The coating of the reflective optics is silver and gold for the VIS and NIR channels, respectively. The detectors are different for each channel: a 4k × 4k pixel CCD for the VIS, and two 2k × 2k pixel CMOS for the NIR. The optical design of the instrument is based on the FEROS design[3] (Kaufer et al., 1997). The interface of the instrument to the telescope or front-end is attached to the Cassegrain focus of the telescope (Fig. 2.2, lower image). With this, CARMENES delivers an exceptional performance in the radial-velocity measurements with an internal precision (or distribution of the formal uncertainties of the RV measurements) of 1.2 m s^{-1} for early and intermediate M-dwarf types, and 5.4 m s^{-1} for the late ones, with the maximum of the distribution (mode) at 0.91 m s^{-1} (Ribas et al., 2023). For more details on the technical side and the performance of the instrument, we also refer to Seifert et al. (2012), Quirrenbach et al. (2014), and Quirrenbach et al. (2016).

The consortium was established by more than 200 scientists and engineers from Spanish and German institutions that have contributed to the design, construction and science exploitation of the instrument. The founding members[4] of the CARMENES consortium were chosen on the basis of parity: five in Spain, five in Germany and the formerly Spanish-German Centro Astronómico Hispano en Andalucía (CAHA)[5], in cooperation by the MPG and the CSIC until 2018. The science coordination team includes representatives of these 11 institutions. Even the CARMENES logo was designed to consciously represent a cultural mixture of both Germany and Spain (Fig. 2.4). CARMENES was funded by the MPG, CSIC, Ministerio de Economía y Competitividad (MINECO), and European Regional Development Fund (ERDF), among others. The call for letters of intent for the construction of the next generation instrument for CAHA 3.5-m telescope dates back to March 2008. The first light of the whole instrument was obtained on November 11, 2015, which was prior to the instrument's formal commissioning, on December 14, 2015. The instrument began GTO operations on January 1, 2016, and operated until December 31, 2020. Since January 2021, an upgraded version of the instrument (CARMENES+), which included an enhancement of the cooling system of the NIR channel, carries out 250 additional nights as

[2]This fact motivates the definition of a boundary between 'close' and 'wide' companions (Chapters 3 and 4), which aims to avoid contamination in the spectra from nearby sources.

[3]This design is a grism cross-dispersed, white-pupil, échelle spectrograph working in quasi-Littrow mode using a two-beam, two-slice, image slicer (Seifert et al., 2012).

[4]Centro de Astrobiología (CAB, CSIC-INTA; Madrid, Spain), Consejo Superior de Investigaciones Científicas (CSIC), Hamburger Sternwarte (HS; Hamburg, Germany), Instituto de Astrofísica de Andalucía (IAA; Granada, Spain), Instituto de Astrofísica de Canarias (IAC; Tenerife, Spain), Institut für Astrophysik Göttingen (IAG; Göttingen, Germany), Institut de Ciències de l'Espai (ICE; Barcelona, Spain), Landessternwarte Königstuhl (LSW; Heidelberg, Germany), Max-Planck-Gesellschaft (MPG), Max-Planck-Institut für Astronomie (MPIA; Heidelberg, Germany), REsearch Consortium On Nearby Stars (RECONS), Thüringer Landessternwarte Tautenburg (TLS; Tautenburg, Germany), and Universidad Complutense de Madrid (UCM; Madrid, Spain).

[5]In 2005, an agreement was signed by the MPIA and IAA to operate jointly the observatory, in a 50-50 proportion, under the denomination Centro Astronómico Hispano-Alemán de Calar Alto. From 2019 to date, the Junta de Andalucía took over the German institution, and joined CSIC to conduct the observatory, making a 100 % Spanish operation, thus acquiring the new denomination.

a legacy project. Subsequent improvements of the instrumentation will incorporate a new wavelength calibration system. While CARMENES has performed radial-velocity *TESS* and K2 (*Kepler*'s extended mission) follow-up (e.g. Palle et al., 2019; Luque et al., 2019a; Nowak et al., 2020; Bluhm et al., 2021; Chaturvedi et al., 2022; Caballero et al., 2022; Radica et al., 2022; Luque et al., 2022a; Trifonov et al., 2023), CARMENES+ will do so for ESA missions *Gaia* and specially, after 2026, PLAnetary Transits and Oscillations of stars (PLATO).

Figure 2.4: The CARMENES logo is a 'Sol de Miró' (Spain) à la Bauhaus (Germany).

The first data release (DR1) of CARMENES includes all the spectra collected in four years of GTO operations, is soon to be publicly accessible (Ribas et al., 2023). While the main objective of CARMENES is the detection of exoplanets, there is potentially much more to be drawn from high quality spectra. For example, exploiting the diagnostic capabilities of many spectral features: He I infrared triplet (Fuhrmeister et al., 2019b,a; Marfil et al., 2021), K I (Fuhrmeister et al., 2022), Ti and V (Shan et al., 2021), Rb (Abia et al., 2020), or Na, Mg, Si, K, Ca, Ti, V, Cr, Mn, Fe, and Sr (Ishikawa et al., 2022a). These are proven very useful to determine stellar fundamental and atmospheric properties (e.g. Passegger et al., 2018, 2019, 2020, 2022; Schweitzer et al., 2019; Marfil et al., 2021), and also to characterise the stellar activity (e.g. Tal-Or et al., 2018; Fuhrmeister et al., 2018, 2019b; Schöfer et al., 2019; Hintz et al., 2019, 2020; Lafarga et al., 2021), and magnetic fields (Shulyak et al., 2019; Reiners et al., 2022).

2.2 Carmencita

When CARMENES saw the first light, the catalogue of M dwarfs to be observed in the guaranteed time was ready. It was baptised 'Carmencita', or the CARMENES Cool dwarf Information and daTa Archive (Caballero et al., 2013a, 2016). To the M dwarfs in Carmencita only two simple criteria were required: to be observable from Calar Alto, Almería (i.e., declination northern of $\delta > -23$ deg), and to be the brightest stars in each spectral subtype, based on the Two Micron All-Sky Survey (2MASS) J magnitude (see Table 1 in Alonso-Floriano et al., 2015b). A variety of sources in the literature provided the known M dwarfs with these characteristics. More than 90 % of the stars in Carmencita come from six works: "The Palomar/MSU nearby star spectroscopic survey" (PMSU, Reid et al., 1995, 2002), "A spectroscopic catalogue of the brightest ($J < 9$) M dwarfs in the northern sky" (Lépine et al., 2013), "G. P. Kuipers spectral classifications of proper-motion stars" (Bidelman, 1985), "An all-sky catalogue of bright M dwarfs" (Lépine & Gaidos, 2011), "Spectral types of M dwarf stars" (Joy & Abt, 1974), and "Spectral classification

of high-proper-motion stars" (Lee, 1984).

2MASS is an all-sky coverage survey that provides a photometric solution for 1.6 million sources. The first equatorial coordinates (in the epoch 2000.0 and equinox J2000) and apparent magnitudes (in the JHK_S passbands – centred in 1.24, 1.66, and 2.15 μm, respectively) were incorporated. The current version of Carmencita (v105) contains 2215 M dwarfs with spectral types from M0.0 V to M9.5 V, and three late-K dwarfs in the boundary K7/M0 V. Among these are the 378 stars intensely monitored by the consortium during GTO (Quirrenbach et al., 2018; Reiners et al., 2018b). The data products derived from the 4-year monitorisation comprise 19 633 spectra for a sample of 362 targets (see Fig. 2.5), and were publicly released on February 2023 as the first data release or DR1 (Ribas et al., 2023).

CARMENES is an extremely sensitive instrument. When looking for planets with the RV method, nearby stellar or substellar companions, physically bound or not, must be extremely well acknowledged, because they may induce real or artificial radial-velocity variations that compromise the measurements. A first classification for suitability was done, avoiding the stars with close (ρ <5 arcsec) companions, either physical or visual, that could also affect the photometric data (Alonso-Floriano et al., 2015b).

GTO dwarfs comprise 362 K7 V to M9 V single stars, which show no evidence of youth or multiplicity. This subsample will be of use throughout this work, especially in the empirical models derived in Chapter 3, because their astrometry and photometry are well-behaved, reliably outlining the main sequence. Alonso-Floriano et al. (2015b) performed a preliminary low-resolution spectral analysis using the Calar Alto Faint Object Spectrograph (CAFOS) at the 2.2-m telescope in Calar Alto, for 753 of the best suited targets.

Carmencita contains equatorial and galactic coordinates, spectral indices, astrophysical parameters, parallactic distances, proper motions, rotational and radial velocities, Hα equivalent widths, X-ray count rates and hardness ratios, broadband multi-wavelength photometry from the ultraviolet to the mid-infrared, close and wide multiplicity information, Galactocentric space velocities, and identification in three catalogues (2MASS, *Gaia* DR3, AllWISE). All these parameters are properly referenced and uncertainties are always included, if available. The technical details behind these parameters are omitted here for simplicity, but are included in the descriptions of the tables produced in this work.

Over the years, CARMENES has built Carmencita. Many of the values for different parameters have been measured or calculated by the consortium members. In Table 2.1 we acknowledge this effort by enumerating these contributions. It is important to note that older references, are superseded by newer references, if these achieve more precise determinations based on solid approaches. This is the main potential of a dynamical catalogue like Carmencita: to be able to provide up-to-date, homogeneous, and accessible information for all the members of the consortium. The mentioned table also includes in **boldface** the contributions derived during the process of this thesis[6]. If Carmencita was a house, then (with 2218 rows and 177 columns) it is certainly made of 392 586 individual bricks. A major value of this catalogue is the individual handling that every of these bricks receives, avoiding automatic-only procedures when possible and aiming for a quality-over-quantity approach. When looked as a unity, Carmencita is a statistically robust sample of well-characterised M dwarfs in the neighbourhood of our Sun, and so global properties can be safely withdrawn from its study as a whole.

[6]Additionally, since late 2020 (version 98), I (C. Cifuentes) am in charge of the update and maintenance of Carmencita, the CARMENES input catalogue.

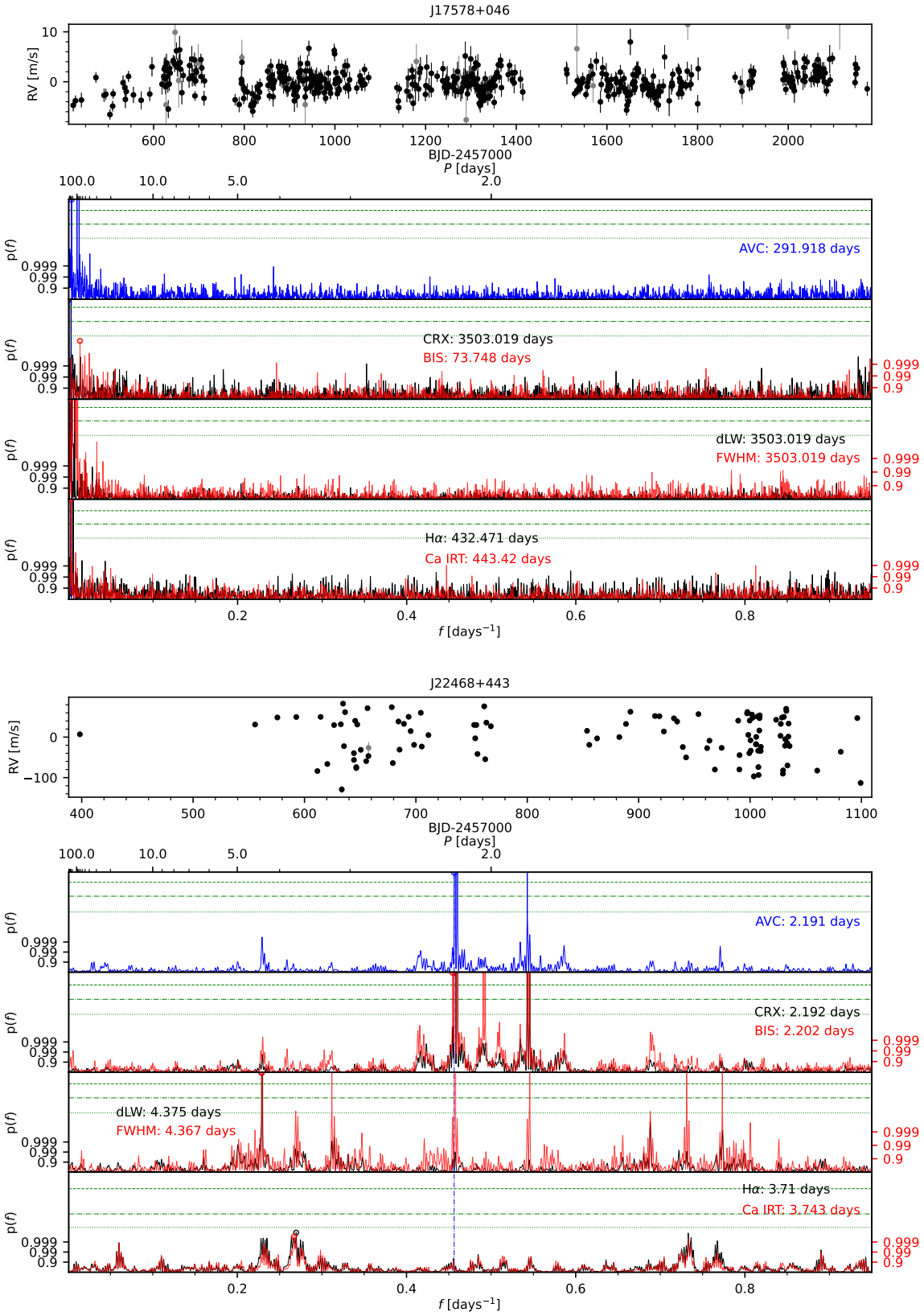

Figure 2.5: Periodograms of the quiet Barnard's Star (J17578+046, *top*) and the highly active EV Lac (J22468+443, *bottom*) obtained from the first data release (DR1) of CARMENES.

Table 2.1: Contribution to the astrophysical parameters of the stars in Carmencita from published (or close to be published) referenced works of the consortium members.

Parameter[a]	Description	Source(s)[b]
`SpT`	Spectral type	Alo15a
`Teff_K, logg, [Fe/H]`	Effective temperature, surface gravity, iron abundance	Marf21, Pas18,19,20, Cif20, Schw19
`L_Lsol, M_Msol, R_Rsol`	Bolometric luminosity, stellar mass and radius	Cif20*, Schw19, This work (**Chapter 3**)
`d_pc`	Heliocentric distance (photometric)	Cor17b, Cif20*, This work (**Chapter 3**)
`Vr_kms-1`	Radial velocity	Jef18, Laf20, Bar18,21
`U_kms-1, V_kms-1, W_kms-1,`	Galactocentric velocities	Cor23 (see Section 2.4)
`SKG`	Stellar kinematic group	Alo15b, Sha23, this work (see Section 2.4)
`P_d`	Rotational period	Die19
`pEWHalpha_A`	Hα pseudo-equivalent width	Alo15a, Fuh23, Scho19
`Activity`	Flaring/chromospheric activity indicators	Tal18
`Photometry`	Apparent magnitudes in up to 20 passbands	This work (**Chapter 3**)
`Multiplicity`	Multiplicity characteristics	Bar18,21, Jeff18, Cor17a, This work (**Chapter 4**)

[a] The uncertainties are included in all cases.

[b] Alo15a: Alonso-Floriano et al. (2015b); Alo15b: Alonso-Floriano et al. (2015a); Bar18: Baroch et al. (2018); Bar21: Baroch et al. (2021); Cif20: Cifuentes et al. (2020); Cor17a: Cortés-Contreras et al. (2017a); Cor17b: Cortés-Contreras (2017); Die19: Díez Alonso et al. (2019); Fuh20: Fuhrmeister et al. (2020); Jef18: Jeffers et al. (2018); Laf20: Lafarga et al. (2020); Marf21: Marfil et al. (2021); Pas18: Passegger et al. (2018); Pas19: Passegger et al. (2019); Pas20: Passegger et al. (2020); Scho19: Schöfer et al. (2019); Schw19: Schweitzer et al. (2019); Sha23: Shan et al., in prep. Tal18: Tal-Or et al. (2018). (*): from this reference or computed using the results in it.

2.3 Astrometry

Gaia has been a game changer, and this is specially true when it comes to astrometric characterisation. For instance, the trigonometric distances to the stars in Carmencita were originally adopted from the General Catalogue of Trigonometric Stellar Parallaxes (van Altena et al., 1995), the new Hipparcos astrometric catalogue (van Leeuwen, 2007), and the MEarth survey (Dittmann et al., 2014). These sources provided data for around 60 % of the stars, while for the remaining 40 %, the use of photometric distances was a must, even though they suffered from a much lower precision than the geometrical measurements from parallaxes. In the case of proper motions, 96 % of the original values in Carmencita came from three catalogues: Lépine and Shara Northern Stars Proper Motion (LSPM-North Lépine & Shara, 2005), the USNO-B1.0 and 2MASS combination (PPMXL; Roeser et al., 2010), and *Hipparcos* (van Leeuwen, 2007). In the present version of Carmencita, *Gaia* DR3 (or DR2) provide proper motions and parallaxes for ∼93 % of the stars. For a few stars, parallactic distances are not published, and may be necessary to adopt photometric estimations. It is important to determine potential unresolved binarity, because in those cases the photometric distance would be underestimated.

By representing a colour as a function of the absolute magnitude in one of the two passbands, it is possible to determine a photometric distance. In this work (see Chapter 3, Sect. 3.2.3) we determine a M_J vs. $r-J$ model, using only well-behaved, single stars from GTO, that can serve to approximate the distances photometrically. Using the definition of absolute magnitude in the r passband, $M_r = r - 5\log d_{\rm phot} + 5$, a photometric distance is derived as $d_{\rm phot} = 10^{\frac{5+r-M_r}{5}}$, where $M_r = M_r(r, J)$ is our model derived from polynomial fitting using stars with actual parallactic distances. This is a convenient choice of magnitudes, since they are almost always available for many relatively bright systems.

Table 2.2: Characteristic velocity dispersions in the thin disk, thick disk, and stellar halo, and asymmetric drift (extracted from Bensby et al. 2003).

	χ_{ns}	σ_u [km s^{-1}]	σ_v [km s^{-1}]	σ_w [km s^{-1}]	$V_{\rm asym}$ [km s^{-1}]
Thin Disk (D)	0.94	35	20	16	–15
Thick Disk (TD)	0.06	67	38	35	–46
Halo (H)	0.0015	160	90	90	–220

2.4 Kinematics

Some Carmencita stars belong to moving groups and associations, and some of them considered young. In broad terms, and for an easier first classification, we broadly classified as 'young' those system with an age of less than 1 Ga. These are hereafter denominated stellar kinematic group (SKG), and the column `SKG` in Carmencita contains information about them. In this work we perform a search in a number catalogues in order to update and complete this column, assigning a confirmed or probable membership to any or some kinematic groups. The relation of these SKGs found and the sources for their assignation can be found in Chapter 3 (Sect. 3.2.2). On top of this search, we performed a complementary assignation to SKGs and stellar populations using the `SteParKin` code (see Appendix E). It evaluates the membership of stars to young (< 1 Ga) kinematic moving groups and associations and assigns their stellar populations as proposed by Bensby et al. (2003, 2005), based on their positions and their Galactocentric velocities (U, V, W). These can be derived from the equatorial coordinates (α, δ), parallaxes (ϖ), proper motions $(\mu_\alpha \cos\delta, \mu_\alpha \cos\delta)$, and radial velocities (V_r), with their corresponding uncertainties:

$$\begin{bmatrix} U \\ V \\ W \end{bmatrix} = \tilde{B} \begin{bmatrix} V_r \\ \frac{k\mu_\alpha \cos\delta}{\varpi} \\ \frac{k\mu_\delta}{\varpi} \end{bmatrix}, \tag{2.1}$$

where $k = 4.74057$ km s^{-1} and $\tilde{B}$ is a 3×3 matrix, result of the converting the equatorial coordinates to the Galactic system, following the approach by Soderblom & Clements (1987). With this, the assignation of a star to a given moving group or association requires that their Galactocentric velocities are within the 3D ellipsoid that defines it.

The stellar population, thin disk (D), thick disk (TD), thin-thick transition disk (TD-D), or halo (H), is also assigned in this step. As Bensby et al. (2003) noted, there is no obvious predetermined way to define a sample of purely thick disk stars in the solar neighbourhood. From the two main methods of finding local thick or thin disk stars, there is the pure kinematical approach, or the combination of kinematics, metallicities, and stellar ages (e.g. Fuhrmann, 1998). The authors adopt the first approach: a population is roughly defined by the observed fraction in the solar neighbourhood (χ_{ns}), the characteristic velocity dispersions $(\sigma_u, \sigma_v, \sigma_w)$, and the asymmetric drift $(v_{\rm asym})$, assuming that the Galactic space velocities (U, V, W) of the stars in these populations have Gaussian distribution:

$$f(U,V,W) = k\ \exp\left(-\frac{U_{\rm LSR}^2}{2\sigma_U^2} - \frac{(V_{\rm LSR} - V_{\rm asym})^2}{2\sigma_V^2} - \frac{W_{\rm LSR}^2}{2\sigma_W^2}\right), \tag{2.2}$$

where LSR stands for the local standard of rest, and k is a normalisation parameter, defined as:

$$k = \frac{1}{(2\pi)^{3/2}\sigma_U\sigma_V\sigma_W}. \tag{2.3}$$

The values that the authors adopt for the three populations are given in Table 2.2. One caveat worth mentioning in the `SteParKin` approach is the rather optimistic definition of the UVW space of the stellar associations and moving groups as compared to other codes available in the literature. It also does not resolve by itself the overlapping between assignations, but it is labeled as member for both. The controversies found in the overlapping cases were resolved in all cases by analysing individually the consensus in the literature. For those stars with groups already assigned in any of the catalogues, there is coincidence or equivalence in the assignation. For this reason, `SteParKin` has been used as a *complement* to the literature agreement.

Two additional codes of recognition in this topic, extensively used for the probabilistic assignation to kinematic groups are `LACEwING`[7] (Riedel et al., 2017) and `BANYAN` Σ[8] (Gagné et al., 2018b). The assignations given by these tools are incorporated implicitly in the compilation of the catalogues provided by the respective authors (see Table 4.9 in Chapter 4, Sect. 4.4.5) .

The results are showcased in two figures produced by `SteParkin`: a Θ-M (or Toomre) and a Böttlinger diagrams (Figs. 2.6 and 2.7, repectively), using the derived galactocentric velocities. Only one star, namely LP 651-007 (Karmn J02462-049) is found to belong to the Galactic halo.

2.5 Fundamental astrophysical parameters

Chapter 3 is devoted to the derivation of stellar parameters and the details. Stellar parameters include bolometric luminosities ($\mathcal{L}$), masses ($\mathcal{M}$), and radii ($\mathcal{R}$). Luminosities are essentially empirically derived, because the intervention of models in the final values is greatly minimised, in favour of multi-wavelength, broadband photometry, and trigonometric distances. Radii are directly derived from the luminosities, given that the effective temperature is known, assuming a black-body approximation for the emitting behaviour of the star. The Stefan-Boltzmann law relates the power radiated from a blackbody with its (effective) temperature, $T_{\rm eff}$. In words, the total energy radiated by a blackbody per unit surface area across all wavelengths per unit time is directly proportional to the fourth power of the blackbody's thermodynamic temperature. In terms of the area of the blackbody of radius $\mathcal{R}$, it becomes: $\mathcal{L} = 4\pi\mathcal{R}^2\sigma T_{\rm eff}^4$, where σ is the Stefan-Boltzmann constant. A full derivation process can be found in, e.g., Rybicki & Lightman (1979).

Masses are a parameter of great significance, because they convey information about the past formation, and the future evolution of the star. Luckily, many roads lead to stellar masses, as we explain in Schweitzer et al. (2019) (see Sect. 3.4.1). The effective temperature ($T_{\rm eff}$), surface gravity (g), and metallicity (referred as the iron abundance, [Fe/H]), are stellar characteristics that are imprint in the spectra of the stars. The cooler the star, the more complex it becomes to reproduce its spectrum.

The luminosity of a star varies very little for the most part of its lifetime, except for the very beginning and the end. Once in the main sequence, one equation dominates, implying that the more massive a star, the more luminous it is. For instance, in Schweitzer et al. (2019) we found that the relation $\mathcal{L} \propto \mathcal{M}^{2.22\pm0.02}$ holds true for $0.1\,\mathcal{M}_\odot < \mathcal{M} < 0.5\,\mathcal{M}_\odot$ stars, or M1–M8 V. In other words, the main sequence is a sequence of masses. Before settling in this sequence, stars appear more luminous when contracting. This effect is

[7] https://github.com/ariedel/lacewing.
[8] https://github.com/jgagneastro/banyan_sigma.

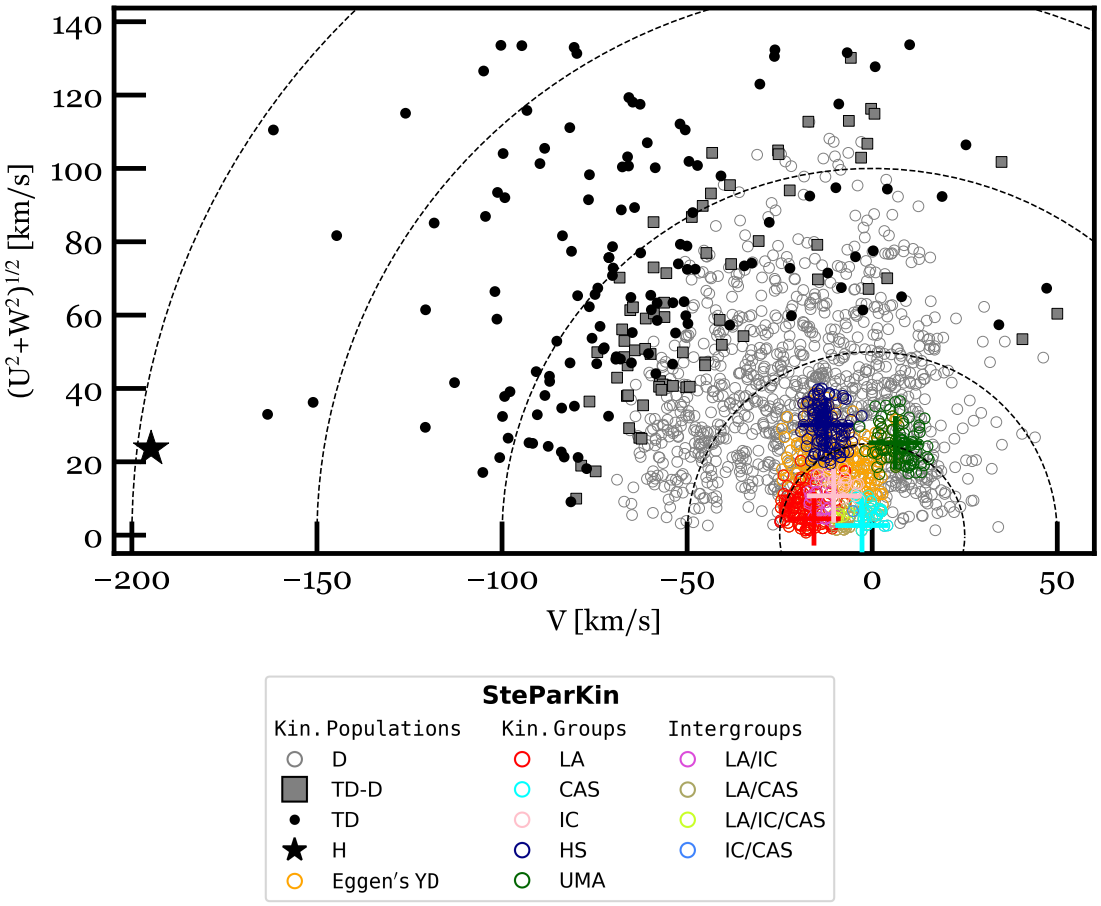

Figure 2.6: Θ-M or Toomre diagram for the Galactocentric velocities of the Carmencita stars.

not exclusive of pre-main sequence stars: unresolved binaries are disguised as single, but the measured flux (or apparent magnitude) is actually the contribution of two (in some cases even more) stars, as we investigate in Chapter 4. This makes luminosities, and the derived masses, to be artificially larger than they should be. It must be noted that not only the overluminous stars may be problematic during the mass determination. For instance, it is possible that young stars with spectral types later than ~M4-M5 do not present overluminosity, but the mass determinations derived from main sequence stars may not be not valid. Fortunately, these are very few and can be handled individually[9]. For this reason we did not make any preliminary assumption on the youth of the stars for the calculation of luminosities (see Chapter 3), but addressed each case separately. In this way, the existence of stars that were off the main sequence track in our Hertzsprung-Russell (HR) diagrams came by surprise and hinted towards possible multiplicity that had not been resolved yet.

For the most extreme cases of overluminous stars almost all of them were reported to belong to a young moving groups (YMG). For those, we first compared the membership in the literature with ours, and assigned an age interval and a median value to each of those SKGs. From the several possibilities for modelling the masses of these substellar objects based on their assigned age[10], we preferred the results

[9] One notable example is LP 944-20, a field (6.43 pc) ultracool dwarf at the brown dwarf-stellar boundary M9.5 V, which is member of the Castor moving group (see Ribas, 2003b). In Cifuentes et al. (2020) we derived luminosity, radius (from VOSA's effective temperature) and mass that is in very good agreement with its spectral classification ($T_{\rm eff}$ = 2400 K; $\mathcal{L}$ = 2.264 ± 0.022 $10^{-4}\,\mathcal{L}_\odot$; $\mathcal{M}$ = 0.0760 ± 0.0089 $\mathcal{M}_\odot$).

[10] BHAC15 (Baraffe et al., 2015), Mesa Isochrones and Stellar Tracks (MIST; Paxton et al., 2011; Choi et al., 2016), Stellar Parameters of Tracks with Starspots (SPOTS; Somers et al., 2020), PISA (Dell'Omodarme et al., 2012), FRANEC (from the Pisa and

Table 2.3: Overluminous stars identified in HR diagram for which fundamental parameters have been derived using PARSEC isochrone models.

Karmn	Name	SKG[a]	$\mathcal{L}$ $[10^{-3}\mathcal{L}_\odot]$	$\mathcal{M}$ $[\mathcal{M}_\odot]$	$\mathcal{R}$ $[\mathcal{R}_\odot]$
J01352–072†	Barta 161 12	β Pic	47.75 ± 0.37	$0.376^{+0.017}_{-0.021}$	$0.718^{+0.018}_{-0.013}$
J02088+494	G 173-039	AB Dor	17.82 ± 0.08	$0.370^{+0.078}_{-0.022}$	$0.417^{+0.045}_{-0.018}$
J02519+224	RBS 365	β Pic	26.89 ± 0.17	$0.254^{+0.014}_{-0.011}$	$0.611^{+0.016}_{-0.012}$
J03473-019	G 80-021	AB Dor	31.22 ± 0.22	$0.469^{+0.052}_{-0.005}$	$0.494^{+0.055}_{-0.021}$
J04472+206	RX J0447.2+2038	IC 2391	12.51 ± 0.08	$0.208^{+0.036}_{-0.031}$	$0.430^{+0.038}_{-0.024}$
J05019+011	1RXJ050156.7+010845	β Pic	33.83 ± 0.20	$0.297^{+0.017}_{-0.013}$	$0.652^{+0.017}_{-0.012}$
J05062+046	RX J0506.2+0439	β Pic	28.24 ± 0.19	$0.262^{+0.014}_{-0.011}$	$0.619^{+0.017}_{-0.012}$
J05084–210	2MJ05082729-2101444	β Pic	38.99 ± 0.40	$0.327^{+0.019}_{-0.015}$	$0.678^{+0.019}_{-0.014}$
J06318+414	LP 205-044	Hya	13.38 ± 0.06	$0.347^{+0.205}_{-0.017}$	$0.364^{+0.165}_{-0.010}$
J06574+740	2MJ06572616+7405265	Cas	7.03 ± 0.63	$0.269^{+0.009}_{-0.005}$	$0.284^{+0.017}_{-0.015}$
J07319+362N	BL Lyn	Cas	18.64 ± 0.08	$0.413^{+0.007}_{-0.004}$	$0.397^{+0.004}_{-0.001}$
J07446+035	YZ CMi[b]	IC 2391	11.16 ± 0.09	$0.192^{+0.033}_{-0.028}$	$0.342^{+0.161}_{-0.010}$
J09133+688	G 234-057	AB Dor	71.91 ± 1.32	$0.576^{+0.025}_{-0.023}$	$0.587^{+0.097}_{-0.024}$
J09449–123	G 161-071[b]	Arg	8.97 ± 0.05	$0.167^{+0.029}_{-0.024}$	$0.318^{+0.153}_{-0.010}$
J10196+198	AD Leo	Cas	23.59 ± 0.11	$0.446^{+0.006}_{-0.004}$	$0.429^{+0.002}_{-0.000}$
J11201–104	LP 733-099	Cas	41.65 ± 0.32	$0.527^{+0.006}_{-0.001}$	$0.507^{+0.001}_{-0.001}$
J11474+667	1RXJ114728.8+664405	Cas	8.06 ± 0.08	$0.289^{+0.011}_{-0.004}$	$0.297^{+0.006}_{-0.002}$
J12156+526	StKM 2-809	UMa	33.02 ± 0.43	$0.494^{+0.007}_{-0.002}$	$0.476^{+0.001}_{-0.001}$
J15218+209	OT Ser	LA	45.75 ± 0.22	$0.525^{+0.200}_{-0.016}$	$0.519^{+0.223}_{-0.001}$
J16102–193	K2-33	USco	102.62 ± 1.09	$0.514^{+0.066}_{-0.052}$	$0.942^{+0.052}_{-0.039}$
J17338+169	1RXJ173353.5+165515	LA	9.54 ± 0.20	$0.292^{+0.179}_{-0.022}$	$0.325^{+0.159}_{-0.013}$
J18174+483	TYC 3529-1437-1	LA	44.88 ± 0.25	$0.522^{+0.201}_{-0.016}$	$0.518^{+0.221}_{-0.002}$
J20451–313	AU Mic	β Pic	98.75 ± 0.86	$0.606^{+0.025}_{-0.016}$	$0.862^{+0.022}_{-0.018}$
J22518+317	GT Peg	IC 2391	26.39 ± 0.13	$0.346^{+0.063}_{-0.044}$	$0.537^{+0.043}_{-0.026}$

[a] AB Dor: AB Doradus, 100 ± 50 Ma (Luhman et al., 2005; Bell et al., 2015; Rodríguez et al., 2018); β Pic: β Pictoris, $18.5^{+2.0}_{-2.4}$ Ma (Miret-Roig et al., 2020a); Cas: Castor, 300 ± 100 Ma (Ribas, 2003b); IC 2391 SC: Omicron Velorum Supercluster, 40 ± 15 Ma (Barrado y Navascués et al., 1999, 2004); LA: Local Association, 150^{+150}_{-136} Ma (López-Santiago et al., 2006); UMa: Ursa Majoris, 300 ± 100 Ma (King et al., 2003); USco: Upper Scorpius, 11 ± 3 Ma (Pecaut et al., 2012).

[b] YZ Cmi and G 161-071 ages were further reviewed, as they appeared as mass outliers in a first estimation. For YZ CMi (Alonso-Floriano et al., 2015a), flagged as a β Pictoris possible member that need confirmation, posterior investigations do not mention again this membership (e.g. Loyd et al., 2018). G 161-071 is assigned to Argus/IC 2391 SC based on findings in the literature (e.g. Bell et al., 2015).
(†) Barta 161 12 was identified as a double-lined spectroscopic binary (SB2) by Malo et al. (2014a), but the detection was a false positive.

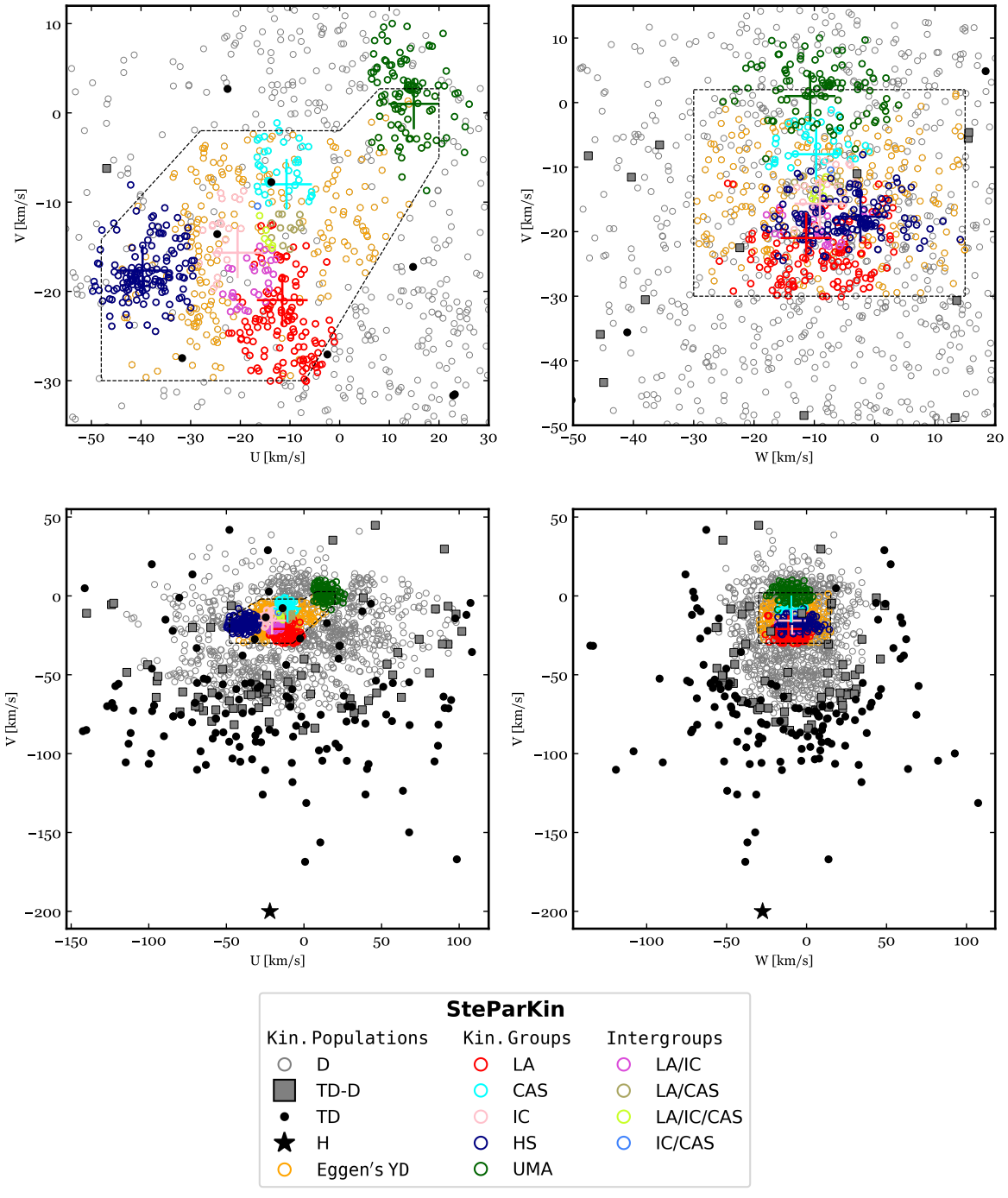

Figure 2.7: Böttlinger diagram for the Galactocentric velocities of the Carmencita stars, representing the (U, V) and (V, W) Galactocentric planes.

obtained with the PAdova and TRieste Stellar Evolution Code (PARSEC; Bressan et al., 2012, and see Nguyen et al. 2022 for the V2.0)[11]. Among the possible routes to obtain stellar masses (colour-absolute magnitude diagrams, eclipsing binaries in young open clusters, or luminosity-mass relations), we chose the relation with luminosities, as we found it to be the most consistent one, and also because it benefited from our very precise determination of them (see Chapter 3). In this line, Cardona Guillén et al. (2021)

Naples groups, Degl'Innocenti et al., 2008), or the Bag of Stellar Tracks and Isochrones (BaSTI; Pietrinferni et al., 2004; Hidalgo et al., 2018), to name a few.

[11] http://stev.oapd.inaf.it/cgi-bin/cmd.

Table 2.4: Late-type stars for which fundamental parameters have been derived using DUSTY00 isochrone models.

Karmn	Name	Spectral type	SpT ref[a]	$\mathcal{L}$ [$10^{-4}\mathcal{L}_\odot$]	$T_{\rm eff}$[b] [K]	$\mathcal{M}$ [$\mathcal{M}_\odot$]	$\mathcal{R}$ [$\mathcal{R}_\odot$]
J02465+164	LP 411-006	M6.0 V	PMSU	9.42 ± 0.05	2900 ± 50$^{(1)}$	0.103 ± 0.010	0.127 ± 0.013
J02530+168	Teegarden's Star	M7.0 V	Alo15a	7.22 ± 0.05	3034 ± 45$^{(2)}$	0.097 ± 0.010	0.120 ± 0.012
J03142+286	LP 299-036	M6.0 V	PMSU	10.68 ± 0.06	2900 ± 50$^{(1)}$	0.113 ± 0.009	0.129 ± 0.004
J04198+425	LSR J0419+4233	M8.5 V	Lep03	4.90 ± 0.03	2400 ± 38$^{(1)}$	0.089 ± 0.009	0.112 ± 0.011
J05394+406	LSR J0539+4038	M8.0 V	Lep03	5.68 ± 0.03	2600 ± 50$^{(1)}$	0.092 ± 0.009	0.115 ± 0.011
J07403-174	LP 783-002	M6.0 V	PMSU	8.39 ± 0.04	3031 ± 26$^{(2)}$	0.100 ± 0.010	0.124 ± 0.012
J08298+267	DX Cnc	M6.5 V	Alo15a	8.36 ± 0.03	2997 ± 49$^{(2)}$	0.100 ± 0.010	0.124 ± 0.012
J08536-034	LP 666-009	M9.0 V	Jen09	2.81 ± 0.02	2400 ± 38$^{(1)}$	0.081 ± 0.008	0.102 ± 0.010
J09003+218	LP 368-128	M6.5 V	Alo15a	7.94 ± 0.04	3061 ± 43$^{(2)}$	0.099 ± 0.010	0.123 ± 0.012
J09033+056	NLTT 20861	M7.0 V	New14	18.08 ± 11.03	3027 ± 19$^{(2)}$	0.139 ± 0.051	0.155 ± 0.047
J10482-113	LP 731-058	M6.5 V	Alo15a	6.75 ± 0.04	3029 ± 25$^{(2)}$	0.095 ± 0.010	0.119 ± 0.012
J10564+070	CN Leo	M6.0 V	Alo15a	10.12 ± 0.07	3071 ± 24$^{(2)}$	0.095 ± 0.008	0.112 ± 0.002
J14321+081	LP 560-035	M6.0 V	New14	18.07 ± 0.10	3161 ± 86$^{(2)}$	0.126 ± 0.011	0.142 ± 0.008
J16555-083	vB 8	M7.0 V	Alo15a	5.86 ± 0.03	3005 ± 21$^{(2)}$	0.092 ± 0.009	0.115 ± 0.012
J18356+329	LSR J1835+3259	M8.5 V	Schm07	2.62 ± 0.01	2500 ± 50$^{(1)}$	0.081 ± 0.008	0.101 ± 0.010
J19169+051S	V1298 Aql	M8.0 V	Alo15a	4.33 ± 0.03	2600 ± 50$^{(1)}$	0.087 ± 0.009	0.109 ± 0.011
J19255+096	LSPM J1925+0938	M8.0 V	New14	10.77 ± 0.12	2500 ± 50$^{(1)}$	0.161 ± 0.011	0.175 ± 0.007
J23064-050	2MUCD 12171	M8.0 V	Schm07	4.95 ± 0.03	2600 ± 50$^{(1)}$	0.089 ± 0.009	0.112 ± 0.011

[a] Alo15a: Alonso-Floriano et al. (2015b); Jen09: Jenkins et al. (2009); Lep03: Lépine et al. (2003); New14: Newton et al. (2014); PMSU: Reid et al. (1995); Schm07: Schmidt et al. (2007).
[b] (1): Obtained from DUSTY00 model fitting; (2) Obtained from spectral synthesis by Marfil et al. (2021).

also suggest PARSEC as the most appropriate grid of synthetic isochrones for mass estimation from luminosities. Therefore, we used our homogeneously derived bolometric luminosities using *Gaia*'s third data release (DR3) latest astrometry and photometry. First, we assigned a kinematic membership to a young moving group for each star (see again Sect. 2.4) and obtain minimum and maximum ages from the literature (see footnote of Table). This translates, however indirectly, into lower and upper limit of the mass. For each corresponding age, in a $\mathcal{L}$-$\mathcal{M}$ relationship from the PARSEC synthetic models, we interpolated the values of our luminosities to obtain the corresponding masses using a quadratic polynomial least-squares fit. It must be noted that, the determination of masses from these models is only as good as the models are (this 'theoretical gap' applies to all areas of astrophysics). The masses should not be interpreted as the real masses, but the ones *expected* for a given age. The uncertainty would not be limited by our knowledge (or ignorance) about the age of the SKG, but also should incorporate the uncertainty on the assignation to the kinematic group in question, based on their kinematics. Of course, luminosities do contribute with their own uncertainties. Nevertheless, *smaller* uncertainties (magnitudes, parallaxes, effective temperature, etc.) are massively eclipsed by the uncertainty in age.

In Table 2.5 we show the overluminous stars found, for which we have estimated masses from the evolutionary models, while radii are computed using these and the Stefan-Boltzmann relation, with effective temperatures coming from DUSTY model fitting or, preferentially if available, from spectral synthesis by Marfil et al. (2021)[12]. We tabulate their luminosities, the derived masses using PARSEC or DUSTY00 isochrones, the adopted SKG, along with the age range and the reference. While there still are bona fide stars in young SKGs in Carmencita that are *not* overluminous, we do not considered the necessity to redetermine masses for them, as the $\mathcal{M}$-$\mathcal{R}$ relation from Schweitzer et al. (2019) applies nevertheless.

With an analogous procedure, we derived masses for the late-type GTO stars ($\mathcal{L} < 0.1\,\mathcal{L}_\odot$, spectral type

[12]The authors employed SteParSyn, a Bayesian spectral synthesis implementation specially suited for late-type stars, following a Markov chain Monte Carlo (MCMC) approach (Tabernero et al., 2022a).

later or equal than M6.0 V), using isochrone models (Table 2.4). For these, we found incongruences in all representations that involved masses computed using the mass-radius relation by Schweitzer et al. (2019), because it does not hold true for the least massive stars. We used the Lyon group's `DUSTY00` (Chabrier et al., 2000)[13] public code, assuming constant ages of 1, 5, 10 Ga to determine new masses and radii for them. Out of the 18 stars susceptible of having their masses/radii recalculated, two of them (J14321+081 and J09033+056) cannot be characterised with `DUSTY00` models, as their luminosity is out of their validity range, and extrapolation beyond the model limits would be needed. These updated values are included in the first data release CARMENES DR1.

[13] http://perso.ens-lyon.fr/isabelle.baraffe/.

Chapter 3

Luminosities

The content of this chapter has been adapted from the article *CARMENES input catalogue of M dwarfs. V. Luminosities, colours, and spectral energy distributions*, published in *Astronomy & Astrophysics* (Cifuentes et al. 2020, A&A, 642, A115).

M dwarfs have gained much relevance in the search for potentially habitable Earth-sized planets in the last years. In our on-going effort to comprehensively and accurately characterise confirmed and potential planet-hosting M dwarfs, in particular for the CARMENES survey, we have carried out an exhaustive multi-band photometric analysis involving spectral energy distributions, luminosities, absolute magnitudes, colours, and spectral types, from which we have derived basic astrophysical parameters. We have carefully compiled photometry in 20 passbands from the ultraviolet to the mid-infrared for a sample of 2479 K5 V to L8 stars and ultracool dwarfs, including 2210 nearby, bright M dwarfs. We combined this information with the latest parallactic distances and close-multiplicity information available, mostly from *Gaia* DR2. For this task we made extensive use of Virtual Observatory tools. We have homogeneously computed accurate bolometric luminosities and effective temperatures of 1843 single stars, derived their radii and masses, studied the impact of metallicity, and compared our findings with the literature. As a result, over 40 000 individually inspected magnitudes, together with the basic data and derived parameters of the stars, individual and averaged by spectral type, have been made public to the astronomical community. In addition, we have reported 40 new close multiple systems and candidates ($\rho < 3.3$ arcsec) and 36 overluminous stars that are assigned to young Galactic populations. In the new era of exoplanet searches around M dwarfs via transit (e.g. *TESS*, *PLATO*) and radial velocity (e.g. CARMENES, NIRPS+HARPS), this work is of fundamental importance for stellar and therefore planetary parameter determination.

3.1 Introduction

This work is part of a series of papers devoted to describing the CARMENES input catalogue of M dwarfs. Here we continue the work started by Alonso-Floriano et al. (2015b) on spectral typing from low-resolution spectroscopy of M dwarfs (I), and followed up by Cortés-Contreras et al. (2017b) on multiplicity from high-resolution lucky imaging (II), Jeffers et al. (2018) on activity from high-resolution spectroscopy (III), Díez Alonso et al. (2019) on rotation periods from photometric time series (IV).

In this fifth item of the series, we focus on the analysis of multi-wavelength photometry, from the far ultraviolet to the mid infrared, of a large sample of nearby, bright M dwarfs, including those monitored by CARMENES, as well as some late K dwarfs and early and mid L dwarfs. We derive accurate bolometric luminosities, identify new close binaries, members in young stellar kinematic groups, and other outliers in colour-colour, colour-magnitude, and colour-spectral type diagrams. We also explore different relationships between colours, absolute magnitudes, spectral types, luminosities, masses, and radii. For that, we make extensive use of the second data release of *Gaia* astrometry and photometry (*Gaia* DR2; Gaia Collaboration et al., 2018b), numerous public all-sky surveys from the ground and space, and Virtual Observatory tools such as the `Aladin` interactive sky atlas (Bonnarel et al., 2000), the Tool for OPerations on Catalogues And Tables (`TOPCAT`; Taylor, 2005), and the Virtual Observatory Spectral energy distribution Analyser (`VOSA`; Bayo et al., 2008).

Our work is also connected to that of Schweitzer et al. (2019), who derived masses and radii from effective temperatures (determined from spectral synthesis) and luminosities (measured exactly as in the present work) for 293 M dwarfs monitored by CARMENES. As a result, here we complement the description of the calculation of stellar masses and radii of all planet hosts detected by CARMENES (e.g. Reiners et al., 2018a; Ribas et al., 2018; Trifonov et al., 2018; Zechmeister et al., 2019; Luque et al., 2019b; Morales et al., 2019, to cite a few).

3.1.1 Sample

In this Section we describe the building process of our sample, as well as the compilation of their photometric and astrometric data from public catalogues. Our sample is based mainly on Carmencita, the CARMENES input catalogue (Sect. 2.2). In the version used in this Chapter, Carmencita contains 2191 M dwarfs and 3 K dwarfs[1], namely J04167–120 (LP 714–47), J11110+304E (HD 97101 A), and J18198–019 (HD 168442), which satisfied simple selection criteria based on J-band magnitude and spectral type regardless of multiplicity, age, or metallicity (cf. Alonso-Floriano et al., 2015b). Except for the three K dwarfs, Carmencita includes M dwarfs visible from the Calar Alto Observatory in Southern Spain ($\delta \gtrsim -23$ deg) with spectral types from M0.0 V to M9.0 V and near-infrared brightnesses between $J = 4.2$ mag and 11.5 mag. The spectral classifications of 2028 M dwarfs (92.5 %) were taken from only three references: Hawley et al. (2002), Lépine et al. (2013), and Alonso-Floriano et al. (2015b), which are equivalent among them according to the latter authors. Of the remaining 163 M dwarfs, most spectral types also came from reliable, equivalent sources (e.g. Gray et al., 2003; Scholz et al., 2005; Riaz et al., 2006), which assures a relative homogeneity in our sample.

As described in the references above, Carmencita is unbiased except for the fact that it may include overluminous and lack underluminous stars in the J band at a fixed spectral type. This fact probably

[1] Carmencita is a catalogue in constant development and refinement. For instance, the version used in Chapter 4 includes around 20 more M dwarfs, which are part of the CARMENES follow-up of some targets from the Transiting Exoplanet Survey Satellite (*TESS*) (Ricker et al., 2015) program.

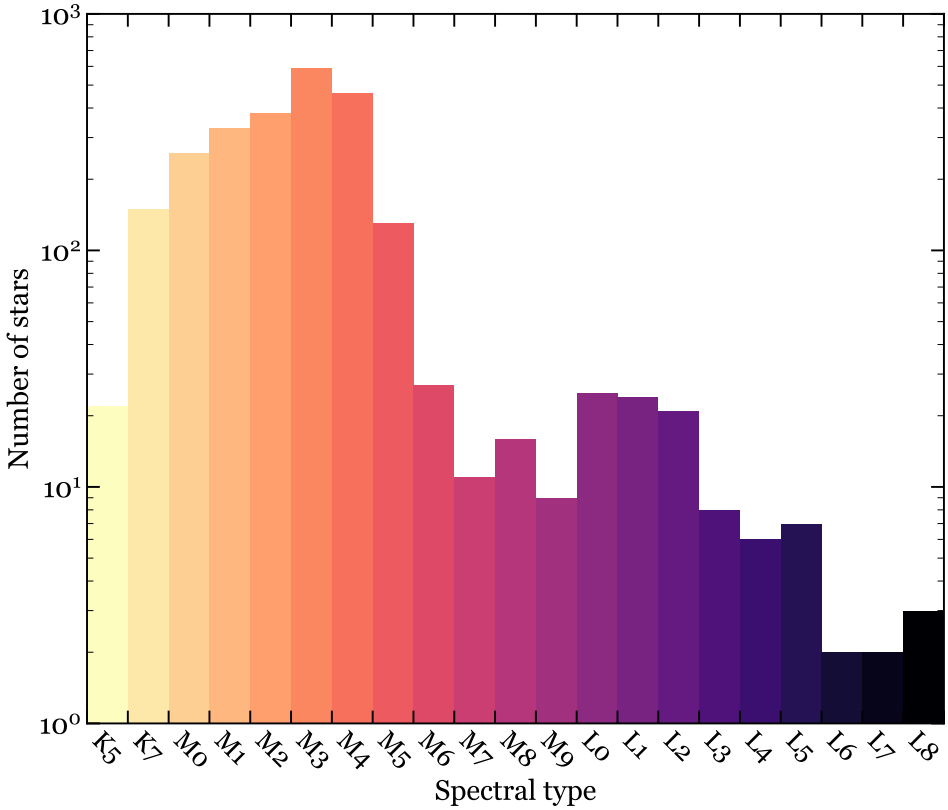

Figure 3.1: Distribution of spectral types in our sample.

translates into a larger fraction of (overluminous) close multiples and young active stars, and a lower fraction of (underluminous) very low metallicity M-type dwarfs (subdwarfs and extreme subdwarfs; Gizis, 1997; Lépine et al., 2007). From the distribution of the ζ index, a metallicity proxy measured in low-resolution spectra of a large number of Carmencita stars (cf. Alonso-Floriano et al., 2015b), we extrapolated that most of our M dwarfs have solar-like metallicities, but that there could be a significant number of them with [Fe/H] < –1.0. Nevertheless, volume-completeness samples can be safely drawn from Carmencita, as explained in Chapter 4.

In order to extend the photometric sample to a wider spectral range and to avoid any boundary value problem, we complemented Carmencita with additional stars earlier than M0.0 V, and with stars and brown dwarfs later than M6.5 V. The eventual distribution of spectral types is displayed in Fig. 3.1. On the warm side, we included 168 bright stars with spectral types between K5 V and K7 V from Kirkpatrick et al. (1991), Lépine et al. (2013), and Alonso-Floriano et al. (2015b), and the RECONS list of the 100 nearest stars[2] (Henry et al., 2006). We did not include the very bright K stars η Cas B, 36 Oph C, BD+01 3942 A, ξ Cap B, 61 Cyg A, and 61 Cyg B, whose photometry is strongly affected by saturation or blending due to close multiplicity.

On the cool side, we first included seven M5.0–9.0 V stars from RECONS with $\delta < -23$ deg. Next, we added 110 ultracool dwarfs from Smart et al. (2017) with a Two Micron All-Sky Survey (2MASS) near-infrared counterpart (Skrutskie et al., 2006) and relative error in *Gaia* DR2 parallaxes ($\delta\varpi/\varpi$) less than 1 %. That addition made 12 M8.0–9.5 V and 98 L0.0–8.0 ultracool dwarfs. We did not include four T-type brown dwarfs (SIMP J013656.57+093347.3, ULAS J141623.94+134836.30, 2MASS 15031961+2525196, and WISE J203042.79+074934.7) and one L dwarf, HD 16270 B, because of their poor 2MASS photo-

[2] http://www.recons.org/TOP100.posted.html.

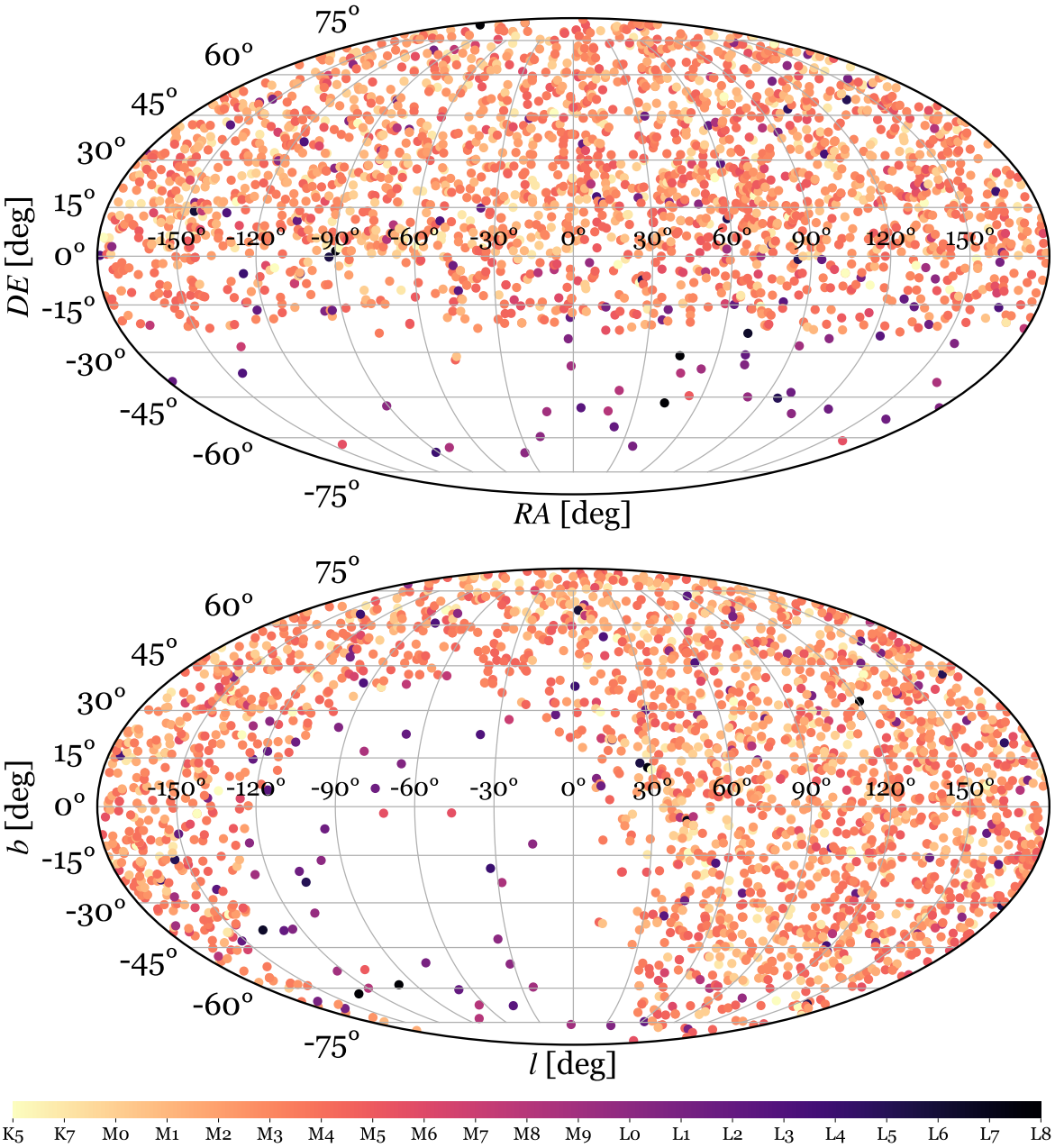

Figure 3.2: Location in the Mollweide-projection sky of the 2479 targets in our sample, which contains Carmencita stars plus the late-K and early-L stars added, colour-coded by spectral type, in equatorial (*top*) and Galactic coordinates (*bottom*). We note the absence of Carmencita M dwarfs with declinations lower than δ = –23 deg.

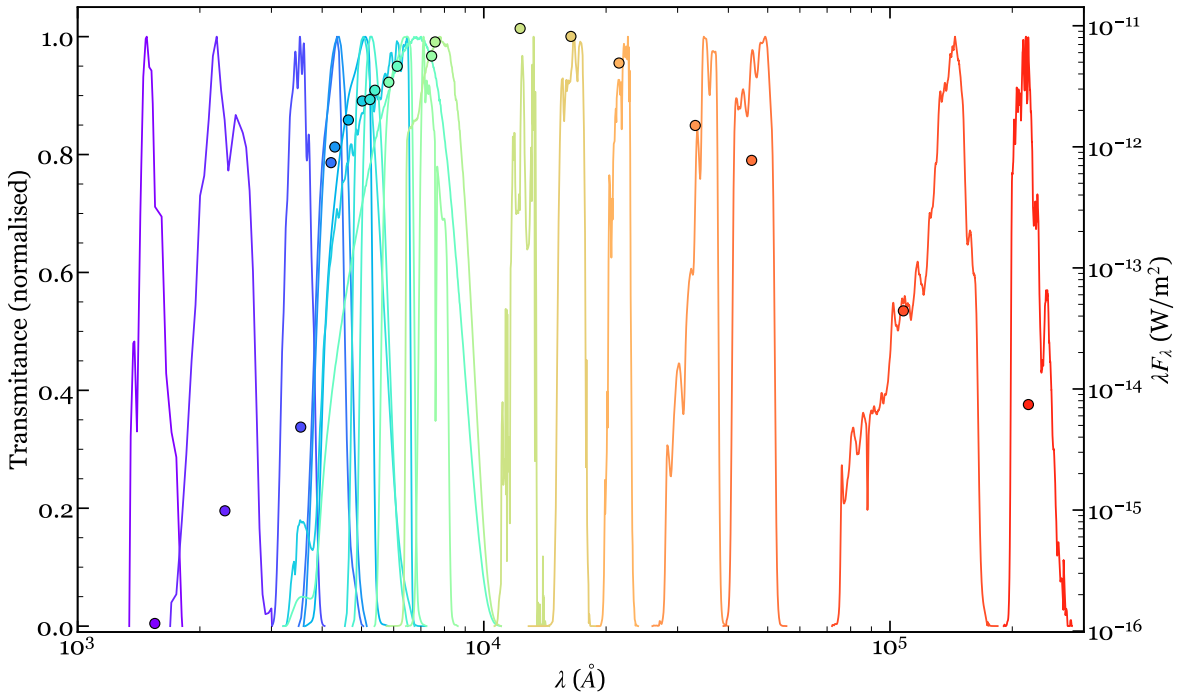

Figure 3.3: Normalised transmission curves of the 20 passbands employed for the compilation of photometry, taken from the SVO Filter Profile Service. For comparison, coloured filled circles depict the spectral energy distribution of DS Leo (Karmn J11026+219, M1.0 V).

metric quality (see Sect. 3.1.2).

As a result, the joint K-M-L spectro-photometric sample contained 2479 targets consisting on 171 late-K dwarfs, 2210 M dwarfs, and 98 L dwarfs. For all targets in the sample we employed and tabulated equatorial coordinates from *Gaia* DR2 except for the 58 stars (five K, 53 M) that were not catalogued by the ESA space mission. For all 58 stars, we used the positions at the epoch of 2MASS projected to the epoch 2015.5 with proper motions from van Leeuwen (2007) and Zacharias et al. (2012), as compiled by Caballero et al. (2016).

The spatial distribution of the 2479 targets is illustrated in Fig. 3.2. For the sake of simplicity, we will use hereafter the term "stars" for the 2479 objects in our sample, including the stellar and substellar objects later than M7 V, also known as ultracool dwarfs (Kirkpatrick et al., 1997).

3.1.2 Photometry

For every star in the sample, we compiled multiwavelength broadband photometry covering a wide spectral range from the ultraviolet to the mid-infrared, as illustrated in Fig. 3.3. First of all, with `Aladin` we manually retrieved the 2MASS equatorial coordinates, JHK_s magnitudes and uncertainties, and photometric quality flags of all 2479 stars (we had done this previously for the Carmencita stars; Caballero et al. 2016). Next, we added photometric data from different public catalogues. We started by adding *Gaia* DR2 G, G_{BP}, and G_{RP} magnitudes, obtained with the query form available in the *Gaia* Archive[3]. We followed by adding magnitudes and uncertainties of the Galaxy Evolution Explorer (*GALEX*) FUV and NUV, the Ninth Sloan Digital Sky Survey Data Release (SDSS9) $u'g'r'i'$, Tycho-2 B_T and V_T, the AAVSO Photometric All-Sky Survey Data Release 9 (APASS9) B and V, the Fourth US Naval Obser-

[3] http://gea.esac.esa.int/archive/.

Table 3.1: Passbands employed for the compilation of photometry.

Band	$\lambda_{\rm eff}$ [Å]	$W_{\rm eff}$ [Å]	F^0_λ [W m^{-2} Å^{-1}]	Survey[a]	Description
FUV	1549.0	265.6	6.491×10^{-12}	*GALEX*	GALEX *FUV*
NUV	2304.7	768.3	4.450×10^{-12}	*GALEX*	GALEX *NUV*
u'	3594.9	558.4	3.639×10^{-12}	SDSS9	SDSS u' full transmission
B_T	4206.4	708.4	6.598×10^{-12}	Tycho-2	Tycho B
B	4297.2	843.1	6.491×10^{-12}	UCAC4[b]	UCAC4 B filter
	4297.2	843.1	6.491×10^{-12}	APASS9[b]	APASS B filter
g'	4640.4	1158.4	5.521×10^{-12}	UCAC4	UCAC4 g' filter
	4640.4	1158.4	5.521×10^{-12}	SDSS9	SDSS g' full transmission
	4640.4	1158.4	5.521×10^{-12}	APASS9	APASS g' filter
	4810.8	1053.1	5.043×10^{-12}	PS1 DR1	PS1 g' filter
G_{B_P}	5020.9	2279.5	4.035×10^{-12}	*Gaia* DR2	Gaia G_{BP} filter, DR2
	5035.8	2157.5	4.079×10^{-12}	*Gaia* DR3	Gaia G_{BP} filter, DR3
V_T	5243.9	1005.7	3.984×10^{-12}	Tycho-2	Tycho V
V	5394.3	870.6	3.734×10^{-12}	UCAC4	UCAC4 V filter
	5394.3	870.6	3.734×10^{-12}	APASS9	APASS V filter
r'	6122.3	1111.2	2.529×10^{-12}	UCAC4	UCAC4 r' filter
	6122.3	1111.2	2.529×10^{-12}	SDSS9	SDSS r' full transmission
	6122.3	1111.2	2.529×10^{-12}	APASS9	APASS r' filter
	6122.3	1318.1	2.529×10^{-12}	CMC15	SDSS r' full transmission
	6156.4	1252.4	2.480×10^{-12}	PS1 DR1	PS1 r' filter
G	5836.3	4358.4	2.495×10^{-12}	*Gaia* DR2	Gaia G filter, DR2
	5822.4	4052.9	2.816×10^{-12}	*Gaia* DR3	Gaia G filter, DR3
i'	7439.5	1044.6	1.409×10^{-12}	UCAC4	UCAC4 i' filter
	7439.5	1044.6	1.409×10^{-12}	SDSS9	SDSS i' full transmission
	7439.5	1044.6	1.409×10^{-12}	APASS9	APASS i' filter
	7503.7	1206.6	1.372×10^{-12}	PS1 DR1	PS1 i' filter
G_{R_P}	7588.8	2943.7	1.294×10^{-12}	Gaia DR2	*Gaia* G_{RP} filter, DR2
	7619.9	2924.4	1.269×10^{-12}	Gaia DR3	*Gaia* G_{RP} filter, DR3
J	12285.4	1624.2	3.143×10^{-13}	2MASS	2MASS J
H	16386.1	2509.4	1.144×10^{-13}	2MASS	2MASS H
K_s	21521.6	2618.9	4.306×10^{-14}	2MASS	2MASS K_s
$W1$	33156.6	6626.4	8.238×10^{-15}	(All)WISE	WISE $W1$ filter
$W2$	45644.9	10422.7	2.431×10^{-15}	(All)WISE	WISE $W2$ filter
$W3$	107868.4	55055.7	6.570×10^{-17}	(All)WISE	WISE $W3$ filter
$W4$	219149.6	41016.8	4.995×10^{-18}	(All)WISE	WISE $W4$ filter

[a] *GALEX* DR5: Galaxy Evolution Explorer, Bianchi et al. (2011); SDSS DR9: Sloan Digital Sky Survey, Ahn et al. (2012); UCAC4: The fourth U.S. Naval Observatory CCD Astrograph Catalog, Zacharias et al. (2012); Pan-STARRS1: Panoramic Survey Telescope and Rapid Response System, Kaiser et al. (2010), Tonry et al. (2012), and Chambers et al. (2016); CMC15: Carlsberg Meridian Catalogue, Niels Bohr Institute et al. (2014); APASS9: The AAVSO Photometric All-Sky Survey, Henden et al. (2016); Tycho-2: Høg et al. (2000); 2MASS: Two Micron All-Sky Survey, Skrutskie et al. (2006); *Gaia* DR2: Gaia Collaboration et al. (2016) with the revised response curves of Maíz Apellániz & Weiler (2018); *Gaia* DR3: Gaia Collaboration et al. (2022b); WISE: Wide-field Infrared Survey Explorer, Cutri & et al. (2012); AllWISE: Cutri & et al. (2014).

[b] UCAC4 and APASS9 *BVgri* are defined as identical to `GCPD/Johnson.B_Landolt`, `GCPD/Johnson.V_Landolt`, `MISC/APASS.sdss_g` / `SLOAN/SDSS.g`, `MISC/APASS.sdss_r` / `SLOAN/SDSS.r`, and `MISC/APASS.sdss_i` / `SLOAN/SDSS.i`, respectively.

vatory CCD Astrograph Catalog (UCAC4) $BVg'r'i'$, the Carlsberg Meridian Catalogue 15 (CMC15) r', and of the Wide-field Infrared Survey Explorer (AllWISE and WISE) $W1W2W3W4$ (and their quality flags when available). For that, we used the `TOPCAT` automatic positional cross-match tool `CDS X-match` with a search radius of 5 arcsec and the "All" find option. For a few high proper-motion stars, we enlarged the search radius to 10 arcsec. Next we used `Aladin` to: (*i*) visually inspect the automatic cross-matches of all sources (and correct them, especially in mismatched cases of high proper motion and close binary sources), and (*ii*) compile, by hand, the most reliable photometry of Pan-STARRS1 DR1 only for the stars for which g', r', or i' magnitudes were not available in other catalogues (PS1 DR1 delivered up to 60 multi-epoch observations for every star over three years in the five PS1 passbands). Although the inspection must be done individually, the process of loading catalogs and images in `Aladin` can be sped up by using the macro tool option (see Appendix E).

The passband name, effective wavelength $\lambda_{\rm eff}$, effective width $W_{\rm eff}$, zero point flux F^0_λ, survey acronym, and corresponding references of the 20 compiled passbands are listed in Table 3.1. The passband parameters were calculated by `VOSA` with the latest filter transmission curves available at the Filter Profile Service[4] of the Spanish Virtual Observatory. When there were several surveys providing photometric data in the same passband (e.g. r' in UCAC4, SDSS9, APASS9, and PS1 DR1), we prioritised the surveys with the highest spatial resolution, sensitivity, and accuracy. PanSTARRS1 DR1 has slightly different passband parameters from those of the other $g'r'i'$ surveys. Virtually all our K and M dwarfs saturated or were in the non-linear regime in SDSS9 z' and PS1 DR1 $z'y'$, so we did not compile data in these passbands.

Gaia G, G_{Bp}, and G_{Rp} magnitude uncertainties were derived from the uncertainties in the fluxes, while UCAC4 *BVg'r'i'* magnitude uncertainties were collected from an additional `TOPCAT` table access protocol query. However, we chose APASS9 BV over UCAC4 BV when the UCAC4 uncertainties were 0.00 mag, 0.99 mag, or missing. In the case of poor photometric quality in AllWISE $W1$ to $W4$ (`Qflag` $\neq$ A,B), we chose the data available in WISE when it improved the quality of AllWISE data. We also identified possible flux excesses in the *Gaia* DR2 G_{BP} and G_{RP} photometric data with the keyword `phot_bp_rp_excess_factor`, following the guidelines of Evans et al. (2018) and Arenou et al. (2018) to separate well-behaved single sources from spurious ones.

J band magnitudes are available for all the stars in the sample, and the completeness in passbands g', G_{BP}, G, r', i', G_{RP}, H, K_s, $W1$, $W2$, $W3$, and $W4$ is greater than 97 %. For Johnson B and V the completeness is around 86 %, whereas for Tycho-2 B_T and V_T it is only 25 %. At the blue end, u' is complete for 50 % of the sample, and the ultraviolet passbands FUV and NUV are available for 39 % and 14 %, respectively. This is graphically summarised in Fig. 3.4.

In total, we collected 40 094 individual magnitudes. Of them, 39 896 have magnitude uncertainties and 33 594 have good quality photometry, defined as: 2MASS `Qflag` = A (with signal-to-noise ratio ≥10), WISE `Qflag` = A,B, $G_{BP} < 19.5$ mag (see Sect. 3.2.3), and no flux excess in *Gaia* G_{BP} and G_{RP}. Figure 3.5 shows the distribution of magnitudes for each band, ordered by increasing $\lambda_{\rm mean}$. The distributions of the bluest bands are broader than the reddest ones, while those of the most complete bands (e.g. g', r', G, J, $W1$) exhibit small secondary peaks at fainter magnitudes, which correspond to late M and early L dwarfs.

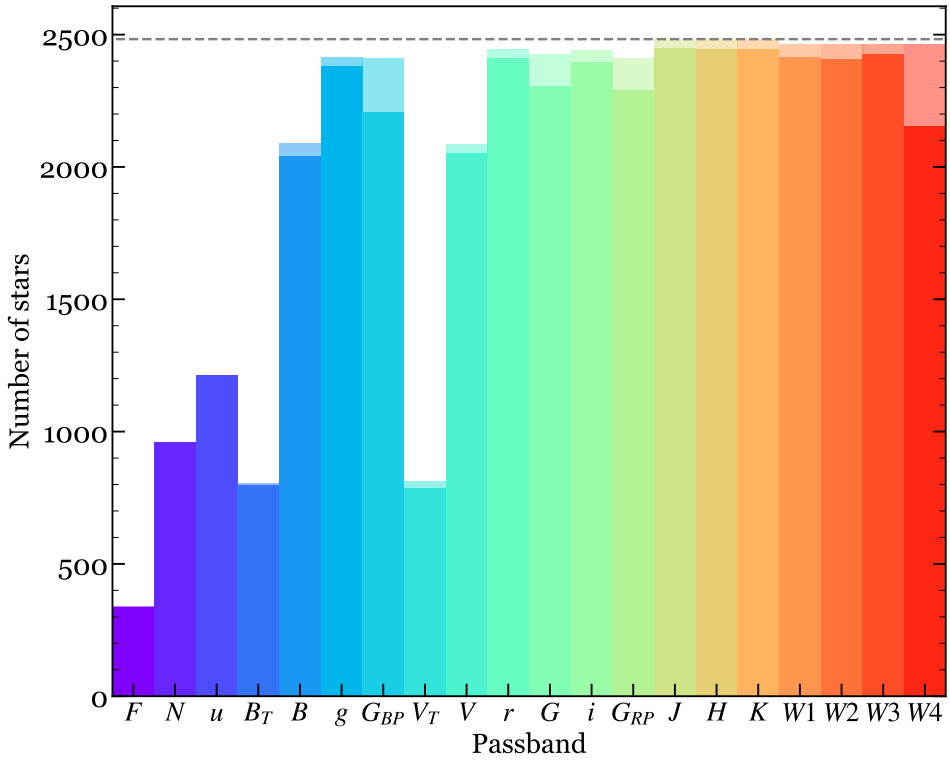

Figure 3.4: Completeness in every passband. Light shaded regions account for measurements with poor quality flags. The dashed horizontal line indicates the total number of stars in the sample.

Table 3.2: Reference of the 2425 parallactic distances in the sample.

Acronym[a]	Number of stars	Reference
Gaia2	2306	Gaia Collaboration et al. 2018b
HIP2	41	van Leeuwen 2007
Dit14	34	Dittmann et al. 2014
vAl95	16	van Altena et al. 1995
FZ16	14	Finch & Zacharias 2016
Galli18	2	Galli et al. 2018
Hen06	2	Henry et al. 2006
Jao05	2	Jao et al. 2005
Wein16	2	Weinberger et al. 2016
Dahn17	1	Dahn et al. 2017
GC09	1	Gatewood & Coban 2009
Jen52	1	Jenkins 1952
Lep09	1	Lépine et al. 2009
Ried10	1	Riedel et al. 2010
TGAS	1	Gaia Collaboration et al. 2016

[a] Achronyms used in the on-line table.

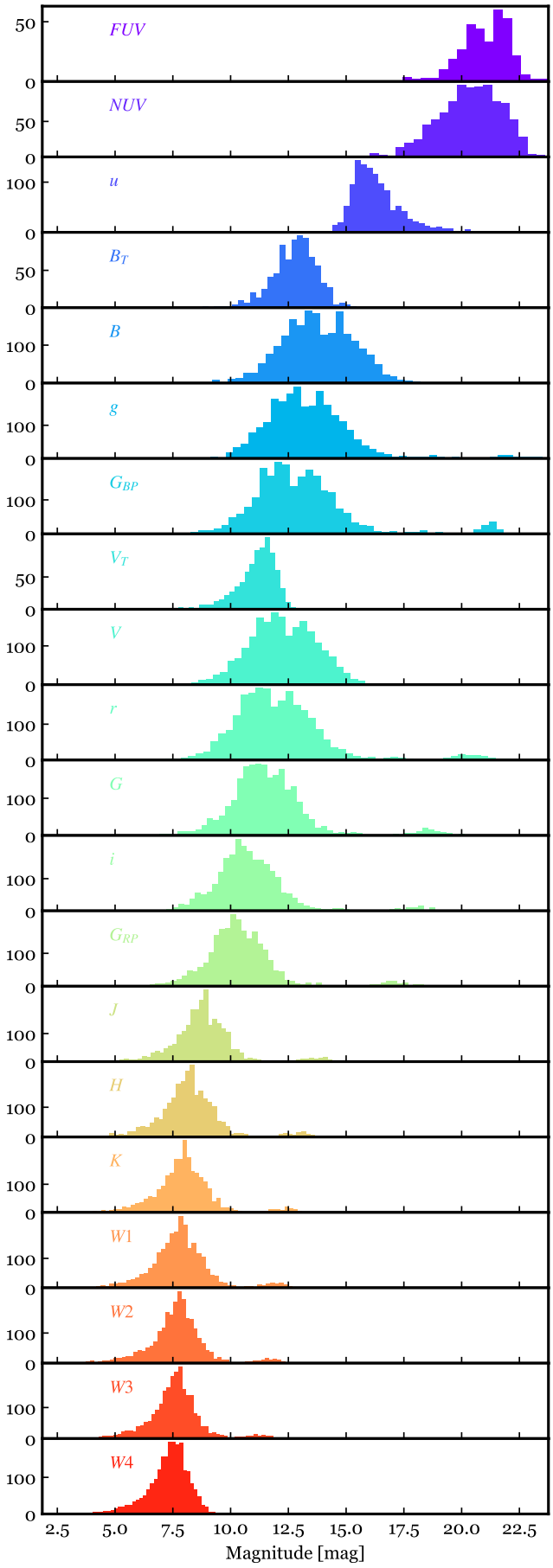

Figure 3.5: Distribution of compiled magnitudes in every passband. The width of the bins follows the Freedman-Diaconis rule.

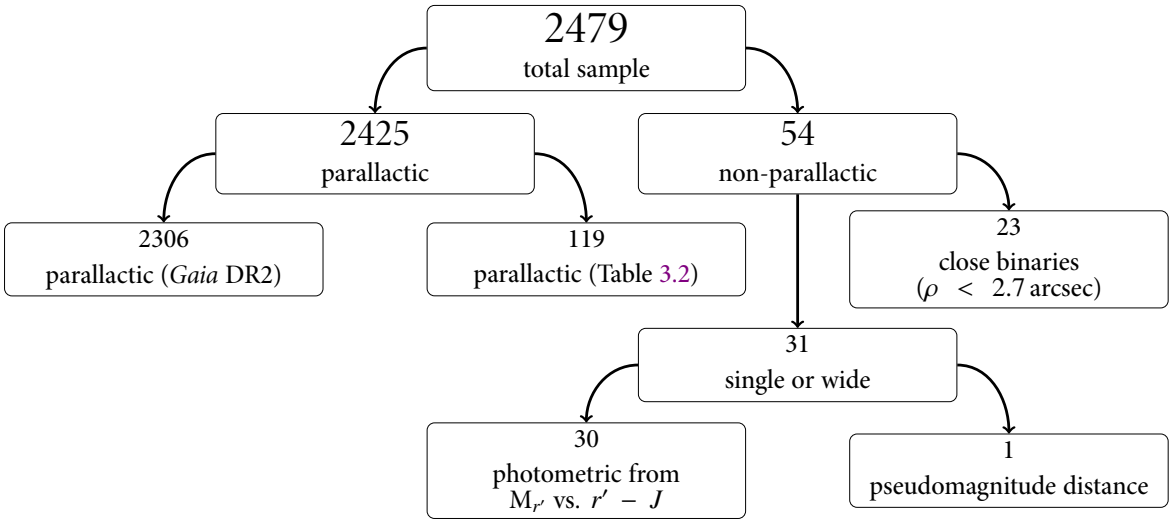

Figure 3.6: Schematic diagram of sources of heliocentric distances.

3.1.3 Distances

We compiled equatorial coordinates, proper motions, parallaxes, and astrometric quality indicators from *Gaia* DR2. Of the 2479 stars in our sample, 2425 (97.8 %) had parallactic distances. Of them, 2306 parallaxes came from *Gaia* DR2 (93.0 %) and 119 from a number of references, as detailed in Table 3.2. For 16 stars with unavailable parallactic distances, we used the trigonometric distances of their confirmed proper motion companions from *Gaia* DR2 (ten cases) and van Leeuwen (2007, six cases). As a result, there were 54 stars without parallactic distance, of which 23 are close binaries: four spectroscopic binaries from Reipurth & Mikkola (2012a) and Jeffers et al. (2018), and 19 resolved binaries (16 with $\rho \lesssim$ 0.8 arcsec, and three at ρ = 1.1–2.7 arcsec; see Sect. 3.1.4). The remaining 31 stars are single or have wide companions at angular separations of $\rho > 16$ arcsec. For 30 of them, we derived photometric distances from $r' - J$ colours following the prescription in Sect. 3.2.3. For the remaining star, a Pleiades member with an $r' - J$ colour outside the validity range, we adopted the "pseudomagnitude" distance to the open cluster of Chelli et al. (2016). As a result, we compiled or derived distances for 2456 stars (i.e. all but the 23 close binaries without parallax). Figure 3.6 shows a schematic summary of the origin of all compiled distances.

Our sample spans a distance range from 1.30 pc (Proxima Centauri) to 171 pc (Haro 6–36). However, ignoring late K dwarfs, overluminous young M dwarfs (in Taurus, Upper Scorpius, and the β Pictoris moving group; Sects. 3.2.2 and 4.4.5), and one star with a large parallax uncertainty ($\delta\varpi/\varpi \sim 8$ %), the most distant "regular" M dwarf is LP 415–17, at 73.0 pc (Díez Alonso et al., 2018b; Hirano et al., 2018). Actually, 92 % of the stars are at less than 40 pc, with only half a dozen objects further than 100 pc. The left panel in Fig. 3.7 shows the distance distribution of our K, M, and L sub-samples.

Gaia DR2 provides statistical parameters to assess the quality of the astrometric data for each source. The a posteriori mean error of unit weight (`uwe`) is a goodness-of-fit indicator that is implicit in the *Gaia* DR2 solution. Because of its strong dependence on colour and magnitude, a re-normalised `uwe`, or `ruwe`, is a more convenient indicator of well-behaved astrometric solutions (Arenou et al., 2018; Lindegren et al., 2018). The latter authors set a threshold on `ruwe` at 1.4, based on the empirical distribution of a large sample of stars, under which they retained 70 % of their sources. We derived the `ruwe` values for all stars with *Gaia* DR2 measurements in our sample (2421; there are 125 *Gaia* DR2 stars without parallax), and

[4] http://svo2.cab.inta-csic.es/theory/fps/.

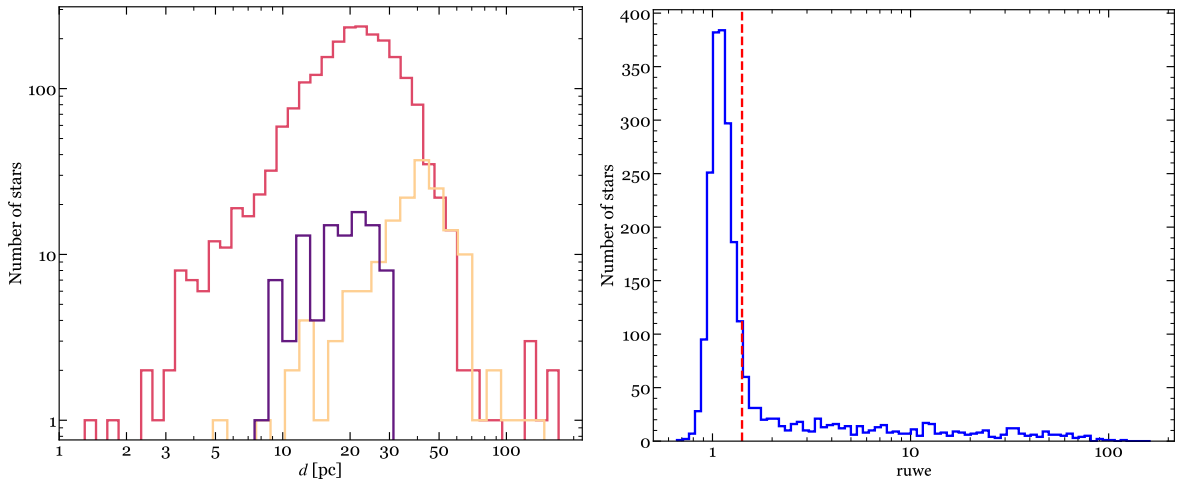

Figure 3.7: Histogram of distances for all stars in the sample, for K (yellow), M (red), and L (violet) dwarfs (*left*), and `ruwe` values for the stars identified in the *Gaia* DR2 catalogue (*right*). The vertical red dashed line in the bottom panel sets the threshold for well-behaved astrometric solutions at `ruwe` = 1.41.

display the corresponding `ruwe` histogram in the right panel of Fig. 3.7. In our case, by retaining 70 % of our sources we re-defined a cut in `ruwe` = 1.41, which is equivalent to the 1.4 value.

Our sample is not volume limited. First, its basis, the Carmencita catalogue, is not complete. Carmencita contains all known M dwarfs in the solar neighbourhood that are further north than $\delta = -23$ deg with published "spectroscopic" (i.e. non-photometric) spectral types that are brighter than the completeness magnitudes shown in Alonso-Floriano et al. (2015b), meaning they are magnitude limited by spectral subtype: M0.0–0.5 V with $J < 7.3$ mag, M1.0–1.5 V with $J < 7.8$ mag, M2.0–2.5 V with $J < 8.3$ mag, and so on. We refer the reader to the consequences of these selection criteria on the metallicity properties of the sample described in Sect. 3.1.1. Next, the K dwarf and ultracool dwarf additions are not complete either, because, for example, we discarded known K and L dwarf binaries. However, from the distribution of distances, our sample in the Calar Alto sky is complete for M0.0 V, M4.0 V, and M6.0 V stars at approximate distances of 25 pc, 15 pc, and 5 pc, respectively.

3.1.4 Close multiplicity

In order to avoid photometric disturbances caused by close sources, we searched for additional *Gaia* DR2 sources within 5 arcsec of our target stars at epoch 2015.5 using the ADQL[5] query form in the *Gaia* Archive. According to Gaia Collaboration et al. (2018b) and, especially, Arenou et al. (2018), *Gaia* can resolve equal-brightness sources separated by down to 0.4 arcsec, which were not resolved in most previous all-sky surveys, such as 2MASS or AllWISE (see Caballero et al. 2019 for a practical example of close binaries resolved for the first time by *Gaia*). For the 2421 stars in our sample that were catalogued by *Gaia*, the search provided 388 additional sources around 353 stars at $\rho < 5$ arcsec. Of them, 324 stars had only one additional source, 24 stars had two sources, 4 stars had three sources, and 1 star had four sources. Besides, for the 58 stars in our sample not tabulated in the *Gaia* catalogue, we used the projected positions as explained in Sect. 3.1.1, which resulted in 11 additional sources around 6 stars. The cases of three or more additional sources corresponded to stars in crowded regions at low Galactic latitudes.

Of the 359 stars with close *Gaia* companion candidates, 166 were already tabulated as members in known physical pairs in the Washington Double Star catalogue (Mason et al., 2001), 4 in Ansdell et al. (2015),

[5] `http://www.ivoa.net/documents/ADQL/`.

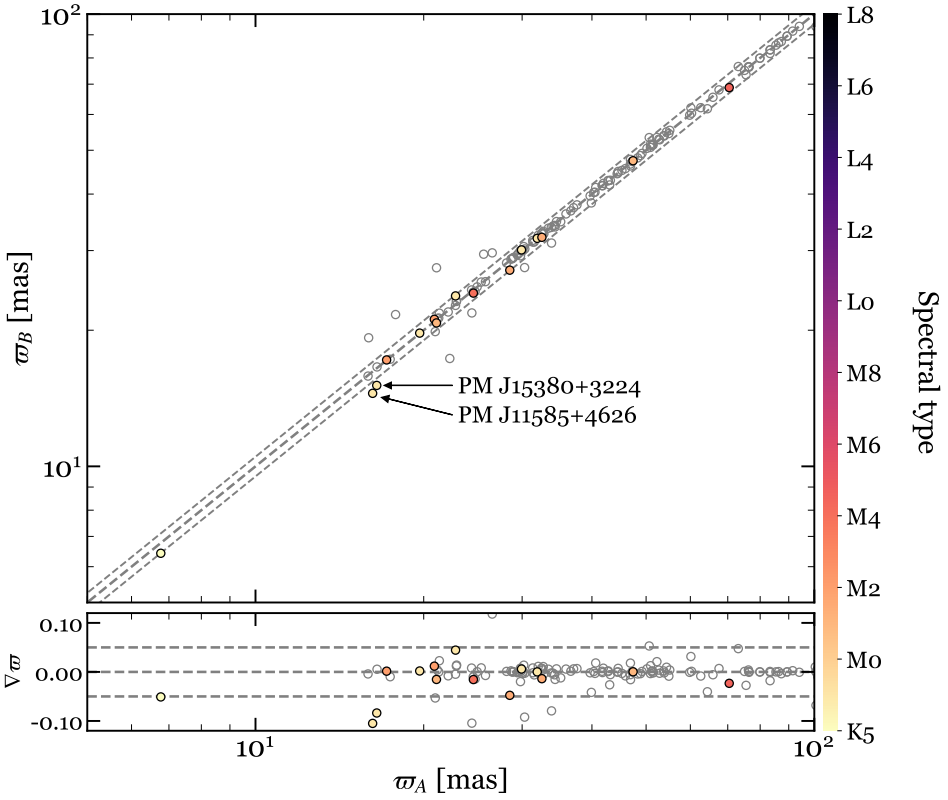

Figure 3.8: Parallax diagram of the primary (A) and secondary (B) components of the 15 new binary systems in Table C.1 with parallactic information in both components, colour-coded by spectral type. The bottom panel shows the normalised difference between both parallaxes, i.e. $\nabla\varpi = (\varpi_B - \varpi_A)/\varpi_A$. Grey empty circles are the 134 previously known pairs in our sample with parallactic information for both components and angular separation of $\rho < 5$ arcsec. The thick and thin dashed lines mark the 1:1 and 1:1 ± 0.05 (i.e. 5 % difference), respectively. Two slight outliers from our list of binary candidates are labelled with their common names.

and 1 in Heintz (1987). Next, we analysed in detail the remaining 188 systems. Of these, we classified 148 faint sources as background stars and point-like galaxies based on astrometric and photometric criteria: 96 sources have parallaxes $\varpi < 2$ mas and so are located at more than 0.5 kpc; four sources have parallaxes 2 mas $< \varpi < 7$ mas and turned to be unrelated sources at 47–225 pc (Bayesian distances computed by Bailer-Jones et al. 2018); one source with a parallax of 21.3 mas is located twice as far as the main source; and 47 sources do not have measured parallaxes, proper motions, or 2MASS near-infrared counterparts. In spite of being more than 5 mag fainter than the primary in G band, all 47 sources are visible in digitisations of blue photographic plates of the 1950s (Digitised Sky Survey I), implying that they are background sources much bluer than the stellar primaries[6].

We investigated the remaining 40 sources not included in the two previous groups. Of them, 15 are in physically bound systems with *Gaia* parallaxes for both components that agree within 1σ errors except for two cases, marked in Fig. 3.8. The two systems are bona fide high proper motion pairs, for which we see that the tangential component of the orbital motion and the *Gaia* astrometric solution has not yet taken the close binarity into account. All remaining 25 candidate companions are not visible in the Digitised Sky Survey I and satisfy $\Delta G \lesssim 5$ mag ($\Delta G \sim 0.3$ mag in three cases with G_{BP}, G, and G_{RP} photometry; see below). In Table C.1 we list the *Gaia* DR2 equatorial coordinates, proper motions,

[6]However, there are certain systems that deserve a high-resolution imaging follow-up, such as J02033–212 (G 272–145), J04429+189 (HD 285968), J05466+441 (Wolf 237), and J11311–149 (LP 732–035).

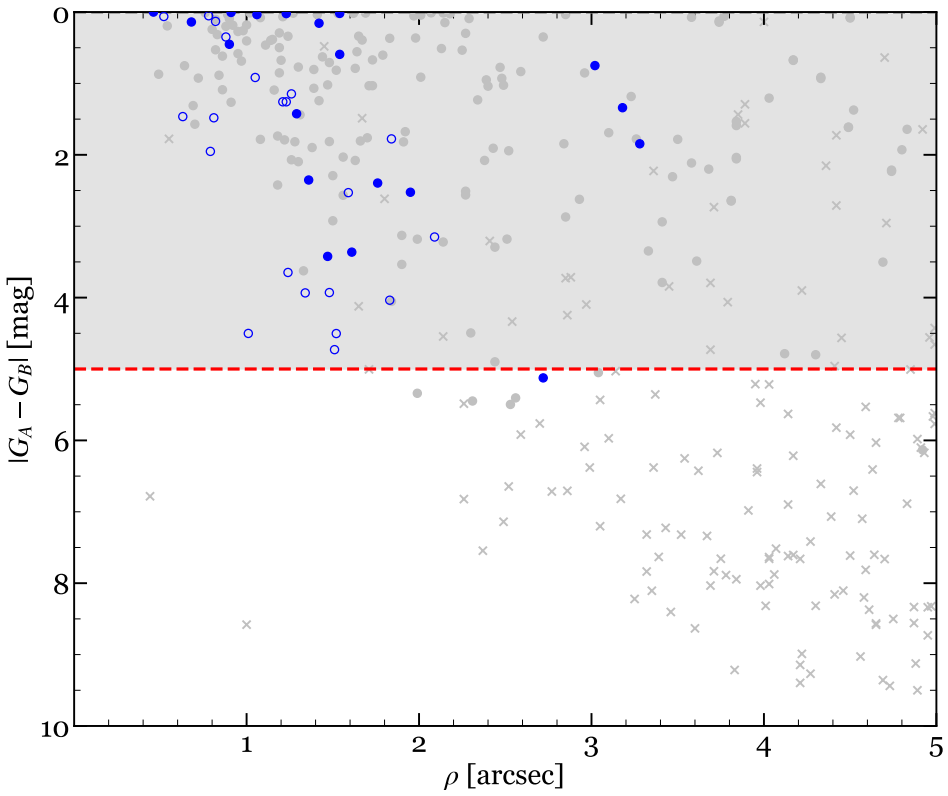

Figure 3.9: Difference in the *Gaia G* magnitude values for the 359 stars with their closest companion within 5 arcsec as a function of angular separation at epoch 2015.5. Known binaries and background stars are depicted with grey filled circles and grey crosses, respectively. New binaries are represented with blue circles, filled if they are confirmed by common parallactic distance, and open if only one component has a measured parallax. The red dashed line marks the boundary at $\Delta G = 5$ mag for contaminated sources.

parallaxes, G magnitudes, angular separations ρ, and position angles θ of the 40 new binary systems and candidates. Among them, there are three triple systems consisting of a spectroscopic binary and a fainter companion (see Table C.1 notes). All systems are separated by 3.3 arcsec at most, which explains why other surveys, such as 2MASS, were not able to resolve them.

We consider the photometry of a star as contaminated if the G flux of *any* companion at $\rho < 5$ arcsec, regardless of physical binding, is more than 1 % of its flux, that is if $\Delta G < -2.5 \log(F_{G,\mathrm{B}}/F_{G,\mathrm{A}}) = 5$ mag, where $F_{G,\mathrm{A}}$ and $F_{G,\mathrm{B}}$ represent the fluxes of the primary and secondary components in the G band, respectively. In Fig. 3.9 we plot ΔG versus ρ of the 359 pairs in our sample with $\rho < 5$ arcsec. Of them, 238 meet the criteria above, and their photometry is therefore flagged as potentially contaminated. To those 238 stars we added other 372 stars from Caballero et al. (2016) that are known to be very close physical systems unresolved by *Gaia* (but resolved with micrometers, speckle, lucky imaging, or adaptive optics systems) and spectroscopic binaries. The 610 "close binaries" are plotted as a reference in most figures afterwards with grey dots, but will not be considered in the following analysis.

The main objective of this section is to investigate the close companions, whether they are physically associated or not, with the purpose of preventing potential sources of photometric contamination. The presence of a nearby companion can adversely affect photometric measurements of a star, particularly when their brightness is similar. Such contamination can have a negative impact on the derived or observed parameters such as luminosity, distance, or colours. It is worth noting that a more comprehensive investigation of multiplicity, encompassing all separations, is the subject of Chapter 4.

Table 3.3: Set of constraints for the spectral energy distribution modelling in VOSA.

Spectral types	$T_{\rm eff}$ [K]	$\log g$ [dex]
K5 V to M2.0 V	3300–4600	4.5–5.0
M2.5 V to M5.0 V	2800–3700	4.5–5.5
M5.5 V to L8.0	1200–3200	5.0–5.5

Note: Iron abundance set to zero ([Fe/H] = 0.0).

3.2 Analysis and results

In this section we present the main products of the exploitation of the astrometric and photometric data in the sample, including luminosities, masses, radii, colours, and bolometric corrections.

3.2.1 Luminosities

After discarding the 610 close binaries ($\rho < 5$ arcsec), we kept 1843 stars with parallax and whose photometry was not affected by close multiciplicity (however, many of the latter are members of wide multiple systems, as explored in Chapter 4. We used VOSA to compute their basic stellar parameters: bolometric luminosity, $\mathcal{L}$, effective temperature, $T_{\rm eff}$, and surface gravity, $\log g$. Among the theoretical model grids available in VOSA for reproducing the observed spectral energy distribution (SED) of each target star, we used the latest BT-Settl CIFIST grid from the Lyon group (Husser et al., 2013; Baraffe et al., 2015). We conservatively constrained the possible values of $T_{\rm eff}$ and $\log g$ as a function of spectral type as discussed by Pecaut & Mamajek (2013) and Passegger et al. (2018), respectively, and summarised in Table 3.3. We fixed the metallicity to solar (BT-Settl CIFIST models are provided for [Fe/H] = 0.0 only) and visual extinction to zero ($A_V = 0$ mag, in view of the closeness of the overall sample; see Sect. 3.1.3). For each star, the VOSA input was the compiled photometry in the passbands in Table 3.1, parallactic distance, and their uncertainties.

In the fitting process, we included the observed fluxes of up to 17 passbands, from optical Tycho-2 B_T to mid-infrarred AllWISE $W4$. Since we were only interested in the photospheric emission, we excluded from the fit the other three passbands (i.e. *GALEX* FUV and NUV and SDSS9 u') because the chromospheric emission dominates in the bluest spectral range, especially in late-M dwarfs (Reipurth & Mikkola, 2012a; Stelzer et al., 2013). At wavelengths bluewards of B_T ($\lambda < 4280$ Å) and redwards of $W4$ ($\lambda > 220883$ Å) we followed the VOSA best-fit model (see example in Fig. 3.10). The uncertainty in this assumption was very small, as the estimated fraction of photospheric energy in BT-Settl CIFIST spectra bluewards of B_T (in the Wien domain) ranges from 0.46 % to 0.0002 % for M0 V and M8 V, respectively, and redwards of $W4$ (in the Rayleigh-Jeans domain) ranges from 0.0036 % to 0.0087 % for M0 V and M8 V, respectively.

For the best fit, VOSA uses a χ^2 metric, where each photometric point is weighted with its uncertainty. If this uncertainty is blank or artificially set to zero, VOSA assumes a large value instead, which depends on the largest relative error on the SED, and assigns to the point a low weight[7]. The theoretical uncertainties of $T_{\rm eff}$ and $\log g$ are determined by the BT-Settl CIFIST model grid, which provides synthetic models in steps of 100 K (50 K for spectra cooler than 2400 K) and 0.5 dex, respectively. VOSA estimates the error in the output parameters as half the grid step around the best-fit value.

[7] See http://svo2.cab.inta-csic.es/theory/vosa/.

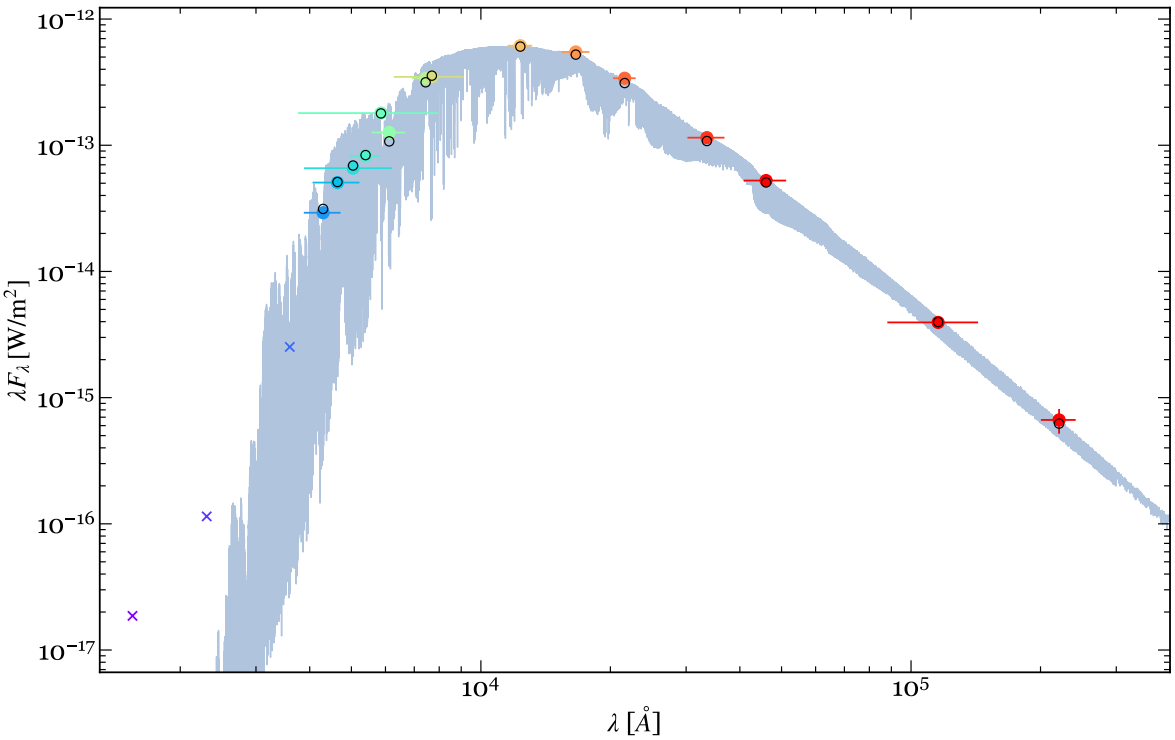

Figure 3.10: Spectral energy distribution of LP 167–071 (J10384+485, M3.0 V). The empirical fluxes (coloured empty circles, following the same colour scheme as in Fig. 3.5) are overimposed on the best-fitting `BT-Settl CIFIST` spectrum (grey; $T_{\rm eff}$ = 3300 K and log g = 5.5). The modelled fluxes are depicted as grey empty circles. Photometric data in the ultraviolet are shown as crosses, and are not considered in the modelling. Horizontal bars represent the effective widths of the bandpasses, while vertical bars (visible only for relatively large values) represent the flux uncertainty derived from the magnitude and parallax errors.

Complementing the `VOSA` automatic identification of photometric outliers in the SED, we inspected all the 1843 individual SEDs and marked 7.1 % of all data points as '`Bad`', as they had bad quality flags (Sect. 3.1.2) or clearly deviated from the SED trend in the optical and, therefore, were not included in the model fitting. After a careful inspection, we also ignored the possible infrared excesses automatically detected by `VOSA`, even for the two single, very young stars in the Taurus-Auriga association (see Sect. 3.2.2).

In Fig. 3.11 we show the distributions of luminosities, effective temperatures, and surface gravities stacked by spectral type. We derived luminosity values ranging from 1.54 10^{-5} $\mathcal{L}_\odot$ for the nearby L8 dwarf DENIS-P J0255-4700, to 0.3276 $\mathcal{L}_\odot$ for the K7 V dwarf HD 196795, except for a very young early M member of the β Pictoris moving group, namely StKM 1–1155, which has an exceptional luminosity of 1.8817 $\mathcal{L}_\odot$. Although very similar, our luminosities supersede those tabulated by Schweitzer et al. (2019) for the M dwarfs in the CARMENES GTO survey, as we updated some parallactic distances and APASS9 and PS1 DR1 optical magnitudes.

3.2.2 Young star candidates

In the two panels of Fig. 3.12 we display two related plots: a Hertzsprung-Russell (HR)[8] diagram with luminosities and effective temperatures from our `VOSA` analysis, and a colour-absolute magnitude diagram

[8]This important relation of profound impact on the understanding of stars traces back to the investigations of Hertzsprung (1923), Russell et al. (1923), and Russell (1928).

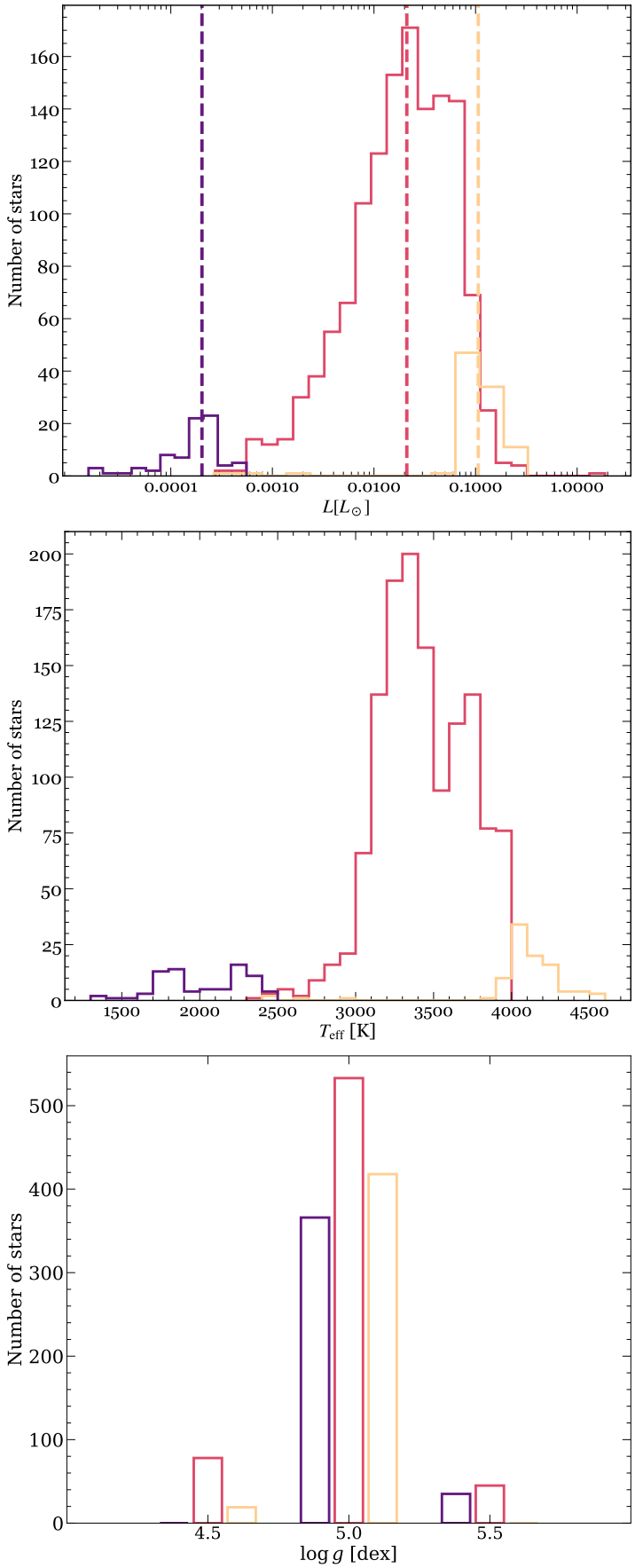

Figure 3.11: Distribution of bolometric luminosities (*top*), effective temperatures (*middle*), and surface gravities (*bottom*) for K (yellow), M (red), and L (violet) dwarfs. Dashed vertical lines mark the median values of bolometric luminosities.

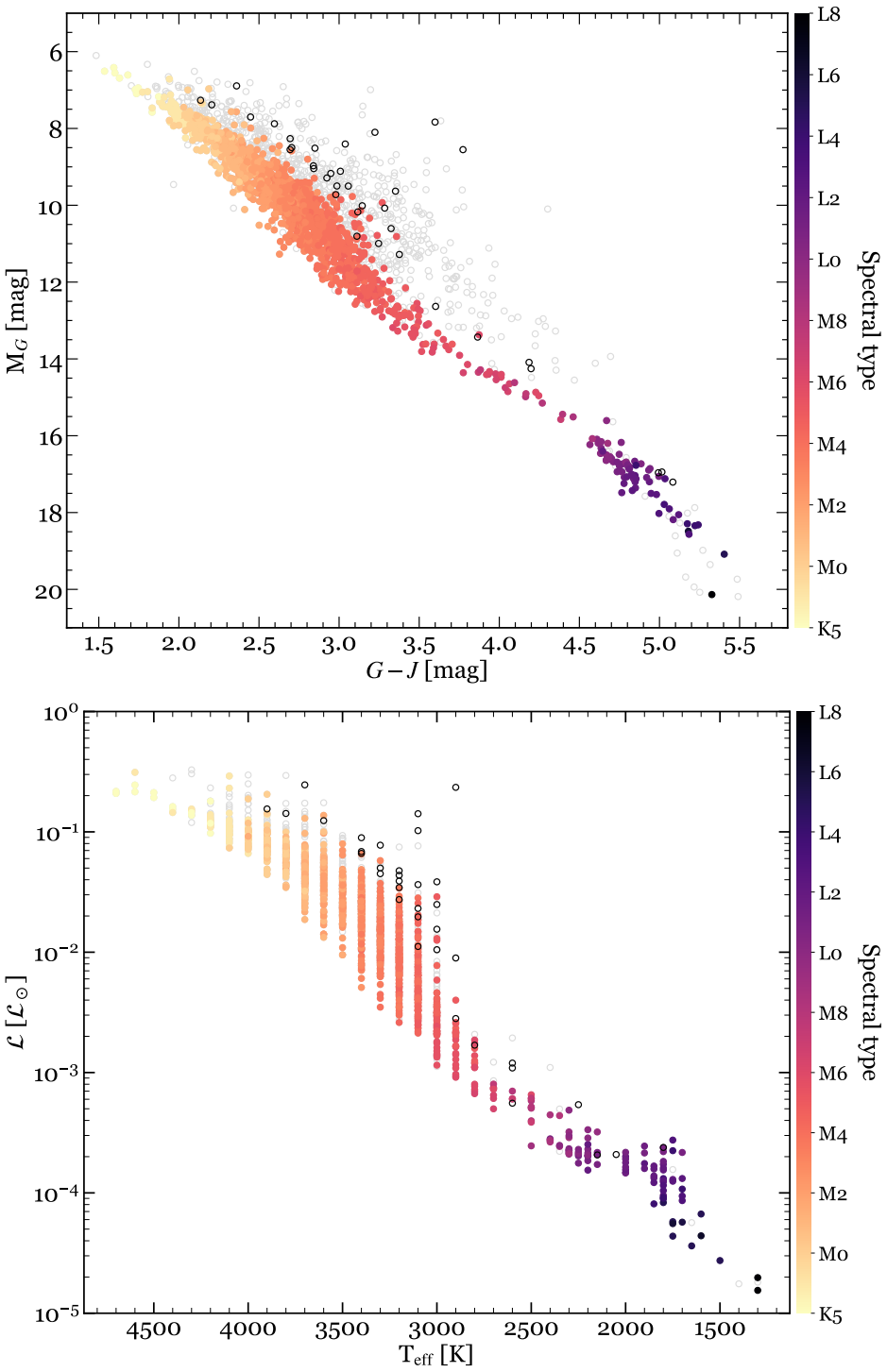

Figure 3.12: Absolute magnitude M_G against $G - J$ colour (*top*), and bolometric luminosity against effective temperature from `VOSA` (*bottom*). In the top panel, empty grey circles represent stars with poor photometric quality data in G, J, or both passbands (Sect. 3.1.2), poor astrometric quality data (`ruwe` >1.41) or non-parallactic distances (Sect. 3.1.3), and close binary stars (Sect. 3.1.4). In the bottom panel, empty grey circles represent stars with poor astrometric quality data or non-parallactic distances, and close binary stars. In both panels, black empty circles are the 36 known young overluminous stars identified in our sample. The remaining "regular" stars are colour-coded by spectral type.

Table 3.4: Overluminous young stars identified in our sample.

Karmn	Name	Stellar kinematic group	Reference
J0045+1634[a]	2MUCD 20037	Argus	Gagné et al. 2014
J01352-072	Barta 161 12	β Pictoris	Alonso-Floriano et al. 2015a
J02443+109W	MCC 401	β Pictoris	Janson et al. 2017
J03510+142	2MASS J03510078+1413398	β Pictoris	Gagné et al. 2015
J03548+163	LP 413–108	Hyades	Crain et al. 1986
J03565+319	HAT 214–02089	Hyades?	Röser et al. 2011
J04206+272	XEST 16–045	Taurus	Scelsi et al. 2007
J04238+092	LP 535–073	Hyades	Weis et al. 1979
J04238+149	IN Tau	Hyades	van Rhijn & Raimond 1934
J04252+172	V805 Tau	Hyades	van Altena 1966
J04369-162	2MASS J04365738–1613065	Tuc-Hor	Malo et al. 2014d
J04414+132	TYC 694–1183–1	Hyades	Johnson et al. 1962
J0443+0002[a]	2MUCD 10320	β Pictoris	Alonso-Floriano et al. 2015a
J04433+296	Haro 6-36	Taurus	Haro et al. 1953
J04595+017	V1005 Ori	β Pictoris	Alonso-Floriano et al. 2015a
J05019+011	1RXS J050156.7+010845	β Pictoris	Alonso-Floriano et al. 2015a
J05084-210	2MASS J05082729–2101444	β Pictoris	Alonso-Floriano et al. 2015a
J0608-2753[a]	2MASS 06085283-2753583	β Pictoris	Alonso-Floriano et al. 2015a
J07310+460	1RXS J073101.9+460030	Columba	Malo et al. 2013
J07446+035	YZ CMi	β Pictoris	Alonso-Floriano et al. 2015a
J09449-123	G 161-071	Argus	Bartlett et al. 2017
J11519+075	RX J1151.9+0731	β Pictoris	Alonso-Floriano et al. 2015a
J12508-213	DENIS J125052.6–212113	Pleiades?	Clarke et al. 2010
J14200+390	IZ Boo	Young?	Mochnacki et al. 2002
J14259+142	StKM 1–1155	β Pictoris	Alonso-Floriano et al. 2015a
J15079+762	HD 135363 B	IC 2391	Montes et al. 2001; Lépine & Bongiorno 2007
J15166+391	LP 222–065	Young disc	Jeffers et al. 2018
J1552+2948[a]	2MASS J15525906+2948485	~100 Ma	Cruz et al. 2009
J15597+440	RX J1559.7+4403	AB Dor	Binks & Jeffries 2016
J16102-193	K2–33	USco	Preibisch et al. 2001
J17572+707	LP 044–162	Argus?	Gagné et al. 2015
J21100-193	BPS CS 22898-0065	β Pictoris	Alonso-Floriano et al. 2015a
J22088+117	2MASS J22085034+1144131	β Pictoris	Shkolnik et al. 2017
J23228+787	NLTT 56725	Columba	Makarov et al. 2007; Montes et al. 2018
J23301-026	2MASS J23301129–0237227	β Pictoris	Alonso-Floriano et al. 2015a
J23317-027	AF Psc	β Pictoris	Alonso-Floriano et al. 2015a

[a] Ultra-cool dwarfs from Smart et al. (2017) not in the CARMENES catalogue of M dwarfs.

with *Gaia* and 2MASS data. After discarding stars with poor astro-photometric data or very close companions, we identified overluminous stars that departed from the main sequence defined by "regular" single stars in the M_G versus $G - J$ diagram, as in the case of StKM 1–1155. We searched the literature for information on their membership in known young kinematic groups (i.e. younger than or of the age of the Hyades, $\tau \lesssim 0.6$ Ga – Perryman et al., 1998; Montes et al., 2001; Zuckerman & Song, 2004). The 36 identified overluminous stars include members of very young associations and moving groups (Taurus-Auriga, Upper Scorpius, β Pictoris), moderately young groups (Argus, Tucana-Horologium, Columba, IC 2391 supercluster), middle-aged open clusters and groups (Pleiades, AB Doradus, Hyades), and a miscellanea classification including one star of about 100 Ma (Cruz et al., 2009), an active one that kinematically belongs to the young Galactic disc (Jeffers et al., 2018), and an ultra-fast-rotating, Hα-variable, X-ray-emitting, young star candidate (IZ Boo – Stephenson, 1986; Fleming, 1998; Mochnacki et al., 2002; Jeffers et al., 2018). The 36 stars and their respective references are listed in Table 3.4. As expected, these sources are also overluminous in the Hertzsprung-Russell diagram. Besides, there are a dozen stars neither tabulated by us nor classified as young star candidates in the literature that are also overluminous,

which will deserve attention in forthcoming works. Many of these stars will be actually proven to be two or even more stars disguised as one. In Sect. 4.3.2, and specially in Sect. 4.4.2, we explore in more detail these cases.

3.2.3 Diagrams

We present and discuss several diagrams involving colours, absolute magnitudes, and bolometric corrections.

Colour-spectral type

We computed 20 average colour indices for adjacent filters and their standard deviation for late-K to late-L dwarfs, using only the good quality photometric data. We list them in Table C.2. The size of the sample for each colour index and spectral type is shown in parentheses. Colour indices computed from samples with less than four elements are included for completeness, albeit with a word of caution. As expected, the amount of data available in the ultraviolet and optical blue passbands decreases for later spectral types (see again Fig. 3.5). In particular, for spectral types M4 V and earlier we have all possible colour combinations, and for spectral types later than M4 V and up to L5 we have all possible colour combinations only between G and $W3$. This colour compilation complements, and most of the time supersedes, previous determinations (Bessell et al., 1998; Dahn et al., 2002; Hawley et al., 2002; Knapp et al., 2004; West et al., 2005; Covey et al., 2007; Zhang et al., 2009; Bochanski et al., 2010; Lépine et al., 2013; Pecaut & Mamajek, 2013; Rajpurohit et al., 2013; Davenport et al., 2014; Filippazzo et al., 2015; Mann et al., 2015; Best et al., 2017).

From all the possible combinations, the *Gaia* DR2-2MASS colour $G - J$ provides one of the most solid estimators of spectral type from late-K to mid-L dwarfs. This is illustrated in Fig. 3.13. Firstly, $G - J$ covers a wide range in colour of about 3.6 mag between K5 V and L8, with a slight flattening restricted to the late L objects. Secondly, it exhibits one of the smallest dispersions in late-M and L dwarfs among all analysed colours, with a median deviation of 0.08 mag. Thirdly, the G and J passbands offer a high availability in this spectral type range, with 97.7 % and 100 % completeness in G and J, respectively. Also, faint objects benefit from the reliability of 2MASS and *Gaia* DR2 photometry. This colour index is superior to previous colour indices used to discriminate late spectral types, such as $i' - J$ (Reid et al., 2001; Hawley et al., 2002; West et al., 2005; Covey et al., 2008), and finds a compromise between completeness, photometric data quality (*Gaia* and 2MASS), scatter of the data, and colour interval spanned by the sequence. On the contrary, the use of *Gaia*-only and 2MASS-only colours for spectral typing presents some serious caveats, from the degeneracy of $G_{B_P} - G_{R_P}$ for spectral types M8 V and later, to the narrow interval of 1 mag of $G - G_{R_P}$ from late-K to late-M dwarfs and its pronounced flattening from late-M to mid-L dwarfs, to the blueing of $J - H$ in the M-dwarf domain. In words, it is not possible to differentiate a mid-M dwarf from an L object using the $G_{BP} - G_{RP}$ colour alone, given its degeneracy.

In Fig. 3.14, we plot six additional colour-spectral type diagrams that show the behaviour of other passbands from the near-ultraviolet to mid-infrared, and their adequacy for spectral type estimation. In all cases, data with poor photometric quality are included as empty grey circles, but not considered for any calculation. Firstly, the optical-mid-infrared $G - W3$ colour serves as a useful complement for the $G - J$ colour, especially in the late-M and early-L regime. The $G - W3$ colour also exhibits a monotonic, low-scatter, steady increase from K5 V to L8, although the median of the dispersion is 0.17 mag, twice the value obtained with the $G - J$ index. Additionally, it benefits from the widest interval in colour of all the diagrams, with approximately 7 mag separating K5 V and L8.

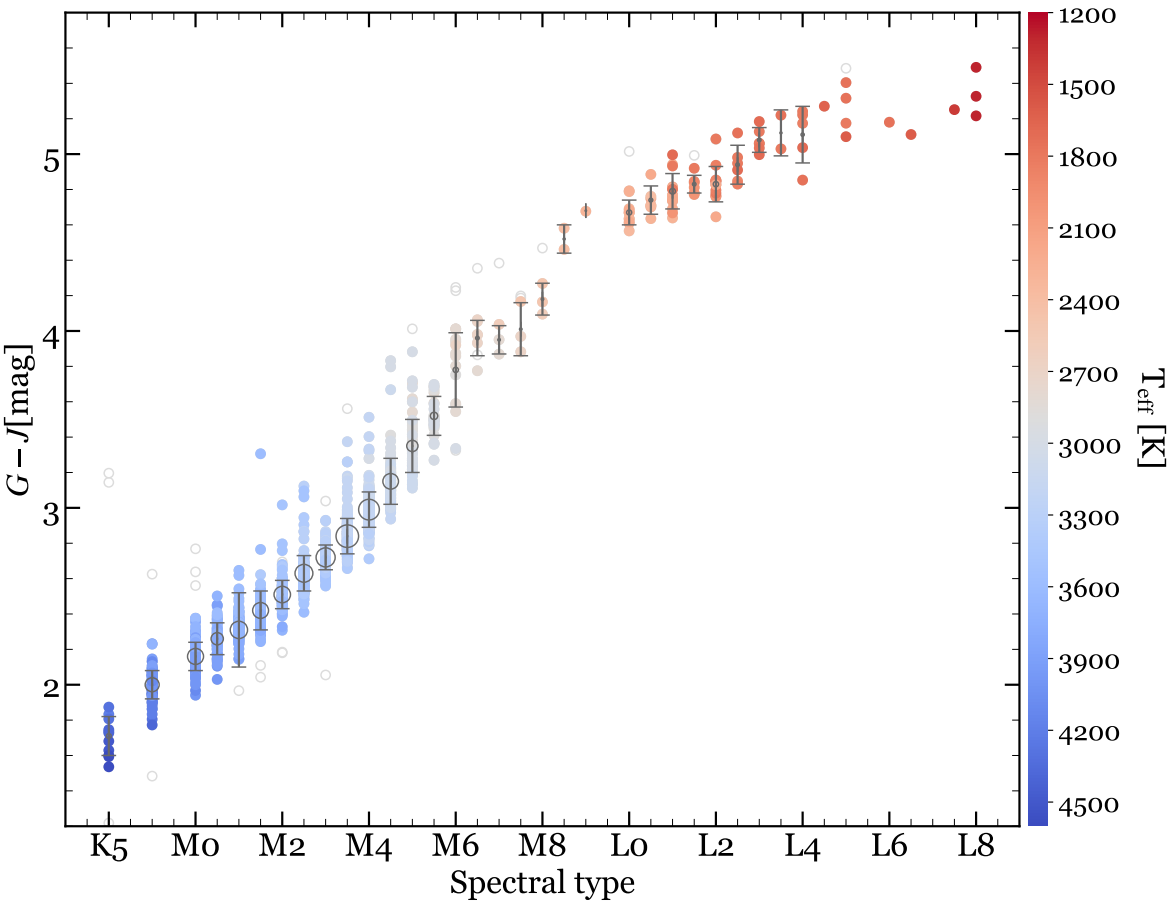

Figure 3.13: $G - J$ colour against spectral type. Grey empty circles mark the average colour for each spectral type with a size proportional to the number of stars and vertical bars accounting for their standard deviation in spectral types with more than one valid colour value. Empty light grey circles on the background depict bad photometric data, as explained in Sect. 3.1.2, and their values are not considered in the calculations of the average colours.

The purely optical colour $r' - i'$, extensively used in the literature, can help to determine spectral types of late-K to late-M dwarfs, but it fails to discriminate the types for cooler objects. It peaks at about 2.8 mag (around M7–8 V), and becomes bluer beyond this point, as shown by, e.g. Hawley et al. (2002) and Liebert & Gizis (2006).

The purely infrared colour $J - W2$ exhibits a remarkably low dispersion from M0 V to M8 V (less than 0.06 mag), but it covers a colour interval of only 0.5 mag. The colour $G_{R_P} - W1$ offers an adequate alternative, with a dispersion slightly larger in the same range (0.09 mag), but spanning five times the colour interval. Furthermore, colours including the $W4$ passband suffer from poor quality data for spectral types M8 V and later.

The $NUV - G_{RP}$ colour is sensitive to both spectral type and ultraviolet flux excesses, which may be caused by chromospheric activity and/or interaction between close binaries. The first case includes "regular" stars later than M3–4 V at the boundary of stellar full convection. The second case comprises, according to Ansdell et al. (2015), young stars (including all our overluminous young stars except one Hyades member) and unidentified binaries, which include unresolved background ultraviolet sources, unresolved old binaries with white dwarf companions, and short-period ($P < 10$ d) tidally interacting binaries that induce ongoing activity on each other. These phenomena give rise to a distinguishable

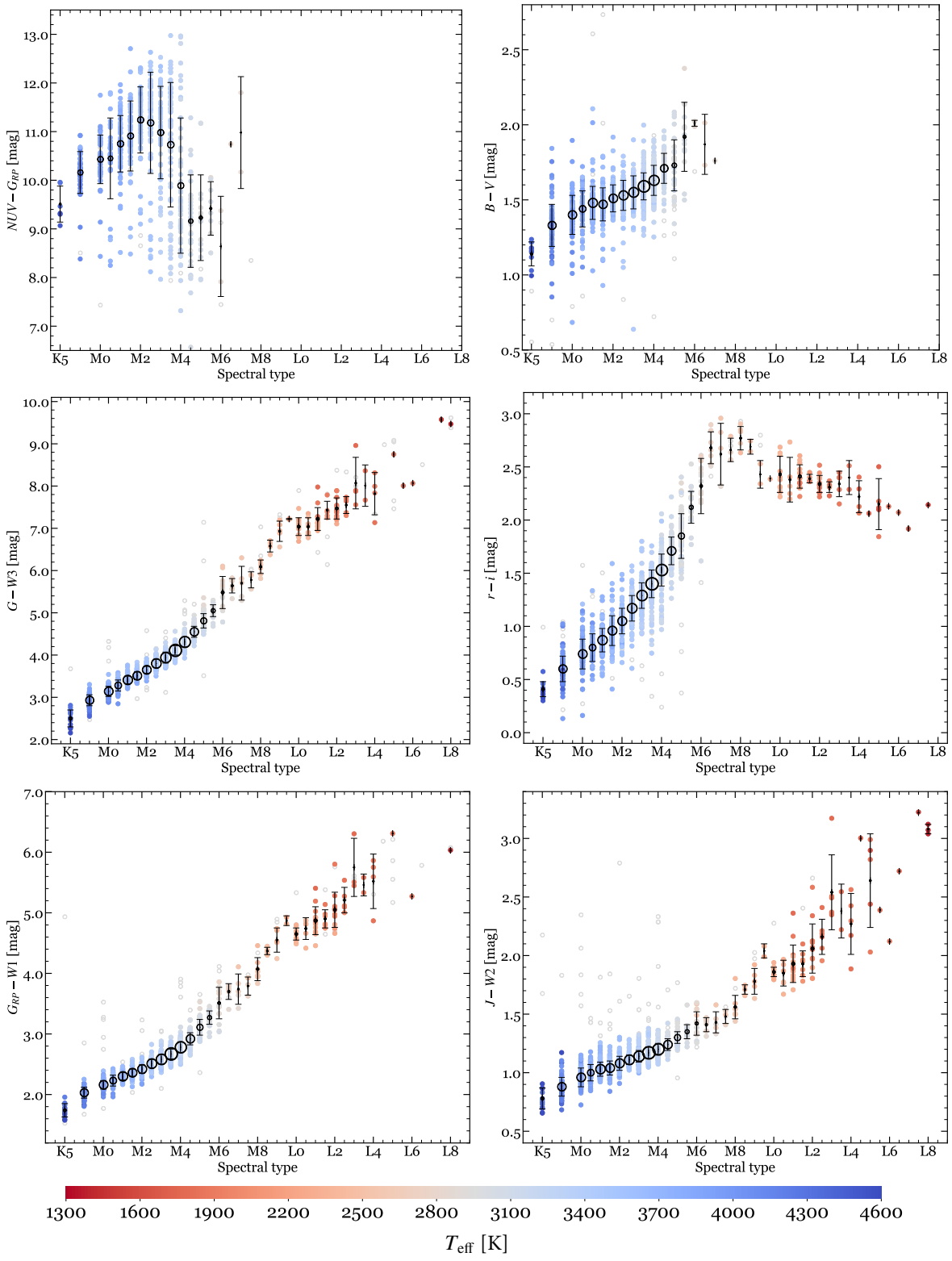

Figure 3.14: Six representative colour-spectral type diagrams, colour-coded by effective temperature.

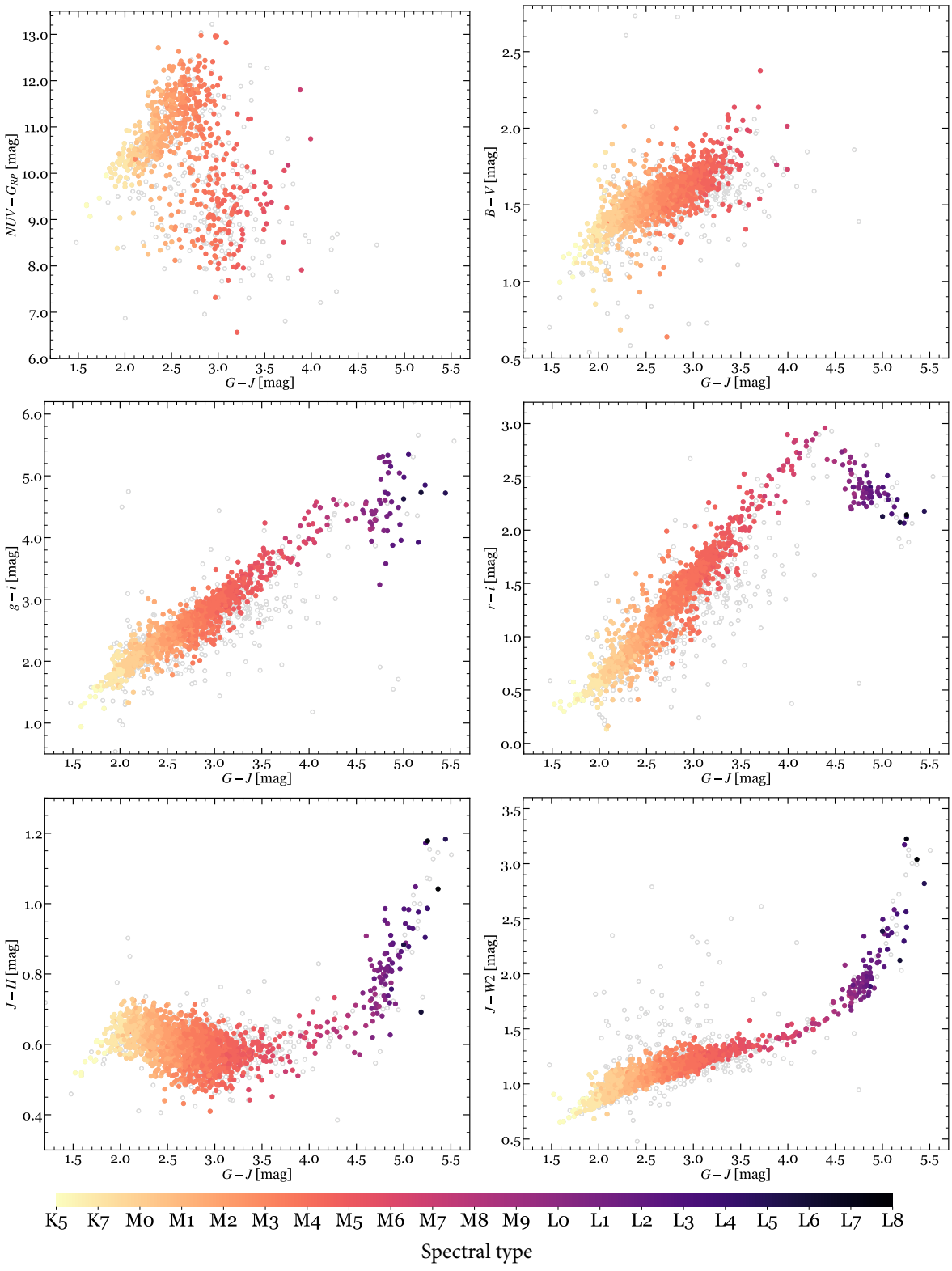

Figure 3.15: Six representative colour-colour diagrams, colour-coded by spectral type.

population appended to the main sequence.

Finally, the optical $B-V$ colour became a commonly used index in the literature, including Bessell et al. (1998), Ramírez & Meléndez (2005), Casagrande et al. (2008), Smith (2018), Sun et al. (2018), del Burgo & Allende Prieto (2018), or Cochrane & Smith (2019), just to name a few. However, the $B-V$ colour has some disadvantages in the M-dwarf domain:

- Both B and V lack the completeness in the optical range that other passbands, such as G_{BP}, r', i', or G_{RP}, deliver.
- $B-V$ fails to produce a photometric sample statistically that is consistent beyond M5 V, while the *Gaia* DR2, 2MASS, or AllWISE passbands succeed.
- $B-V$ does not correlate with spectral type beyond M5 V.
- The width of the colour interval from late K to mid M is 1 mag, only a few times the scatter of the main sequence (0.12 mag), with a striking flattening between M0 V and M3 V.
- The mean uncertainties of B and V in our sample are 0.056 mag and 0.048 mag, respectively. For comparison, the same parameters for G and J are 0.0012 mag and 0.029 mag, respectively.

Therefore, we discourage the use of $B-V$ as an estimator of spectral type for stars cooler than K5 V. This is especially applicable when the *Gaia* DR2 (and 2MASS or AllWISE) magnitudes are available. The same reasoning above also applies to the B_T and V_T Tycho-2 passbands, which are even less complete.

Colour-colour

Contrary to apparent magnitudes, observed stellar colours do not depend on distances and is possible to learn relevant information about stars from their colour indices alone. If coming from accurate photometric data, colours can serve as reliable estimators of spectral types. For instance, Strauss et al. (1999) found an extremely red object using Sloan Digital Sky Survey (SDSS) $i'-z'$ colour, which came to be the first T-type object (i.e. methane dwarf) discovered. In the same month, and even in the same journal volume but a few pages later, Burgasser et al. (1999) reported four field-methane dwarf, discovered using 2MASS $J-H$ and $H-K_s$ colours[9]. Tsvetanov et al. (2000) added a second object to the list of field Methane dwarfs, also using colours derived from 2MASS and SDSS. Soon after, Leggett et al. (2000) discovered three more similar objects using colour indices.

Diagrams that compare colours turn out to be also an useful diagnostic of the presence of binary stars, young stellar objects, white dwarfs, giant stars, or even quasars (Hawley et al., 2002; Covey et al., 2007; Casagrande et al., 2008; Davenport et al., 2014; Mann et al., 2015). These sources appear as outliers from a well-defined stellar locus, and they can be isolated and studied individually. Stars significantly brighter in a given colour exhibit an excess that may suggest the existence of relevant physical features, such as circumstellar disks associated to the early stages of evolution, which are the cause of a reddening effect (see for example White & Ghez, 2001).

As in the colour-spectral type diagrams, main sequence stars occupy a well-defined locus in colour-colour diagrams. In spite of the degeneracy beyond M8 V, the narrowest main sequence is observed in the 2MASS-*Gaia* $G_{BP}-G_{RP}$ versus $G-J$ colour-colour diagram shown in the top panel of Fig. 3.16.

[9]The authors identified extremely red objects with $J-H$ <0.2 mag and $H-K_s$<0.2 mag. Figure 3.16 (Chapter 3), can help to contextualise a Methane object as compared with an M dwarf.

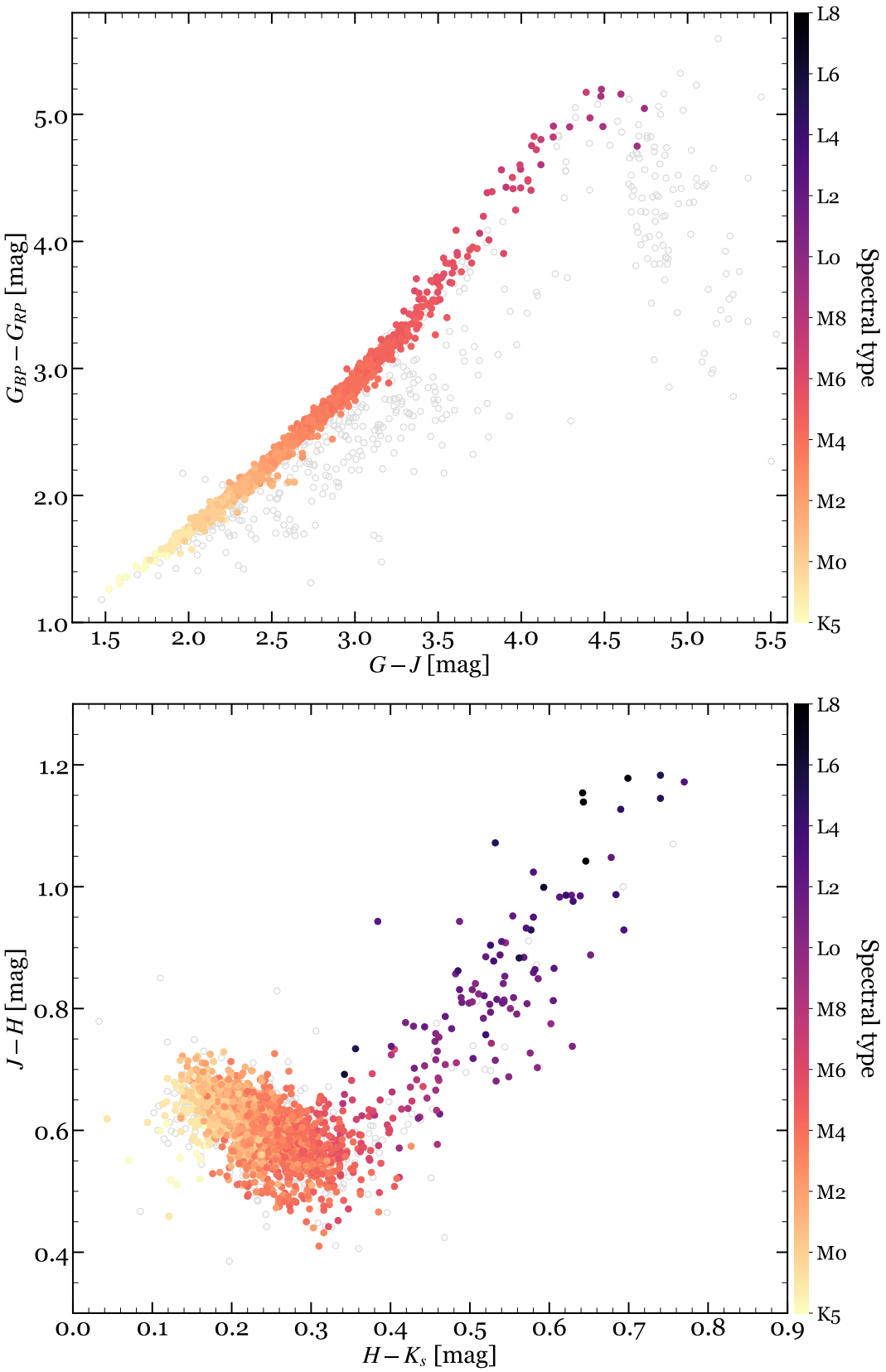

Figure 3.16: Colour-colour diagrams representing $G_{BP} - G_{RP}$ vs. $G - J$ (*top*) and $J - H$ vs. $H - K_s$ (*bottom*). In both panels, empty grey circles represent stars with poor photometric quality data in any of the involved passbands, close binaries, or young stars. The remaining "regular" stars are colour-coded by spectral type.

Outliers in the diagram are mostly unresolved binaries and young stars for colours bluer than $G - J \sim 4.5$ mag (spectral types earlier than M8 V), albeit other possibilities also exist. For example, G 78–3 (J02455+449), at 57.8 pc (Gaia Collaboration et al., 2018b), is an M5 V star (Hawley et al., 1996), which exhibits a $G - J$ colour typical of an early-M dwarf. For colours redder than $G - J \sim 4.5$ mag, we confirm the findings of Smart et al. (2019), who reported an unreliability in *Gaia* blue-band photometry of very late objects with $G_{BP} > 19.5$ mag due to background underestimation by the *Gaia* automatic pipeline (Gaia Collaboration et al., 2018a; Evans et al., 2018; Smart et al., 2019). As a comparison, in Fig. 3.16 we also show a widely used, 2MASS-only, colour-colour diagram (Kirkpatrick et al., 1999; Knapp et al., 2004; Lépine & Shara, 2005; Hewett et al., 2006; Covey et al., 2007). There, late-K to late-M dwarfs occupy a compact region that ranges from $H - K_s \sim 0.15$ mag, $J - H \sim 0.65$ mag to $H - K_s \sim 0.30$ mag, $J - H \sim 0.55$ mag, while later stars and brown dwarfs become redder (Kirkpatrick et al., 1999, and references above). We did not notice any near-infrared flux excess, as found in young T Tauri M-type stars and brown dwarfs with warm circumstellar discs (Carpenter, 2001; Caballero et al., 2004; Hernández et al., 2008).

In Fig. 3.15 we display a selection of six additional colour-colour diagrams. In all cases we plot far-ultraviolet to mid infrared-colours against $G - J$. Apart from the stars with poor photometric quality, we also discarded the 2MASS magnitudes of the extraordinarily red 2MUCD 20171 (J03552+113; Faherty et al., 2013) and blue SDSS J141624.08+134826.7 (J1416+1348A; Burgasser et al., 2010) ultracool dwarfs, which were clear outliers in many colour-colour diagrams involving 2MASS magnitudes. As in the colour-spectral type diagrams, the two colour-colour diagrams involving the bluest colours illustrate the two populations of ultraviolet active and inactive sources ($NUV - G_{RP}$) and the poor spectral sequence based on $B - V$ colour. The two diagrams involving UCAC4/SDSS9/APASS9/CMC15/PS1 DR1 $g'r'i'$ passbands, which will also be used at the Vera C. Rubin Observatory for the Legacy Survey of Space and Time (LSST), show a slightly larger spread than *Gaia* data and the double slope of the $r' - i'$ colour also found by Hawley et al. (2002) and Liebert & Gizis (2006). Interestingly, $g' - i'$ has a smaller dispersion in the late K and M dwarf domain than $r' - i'$, but a much larger dispersion at $G - J \gtrsim 4.5$ mag. This extra scatter at the reddest colours is more likely due to the intrinsic spectral variations at the M/L boundary (à la Hawley et al. 2002; e.g. metallicity) than due to data analysis systematics or Poissonian error at the survey magnitude limits (à la Smart et al. 2019; e.g. background). Finally, the colour-colour diagrams with near-infrared 2MASS and AllWISE data (specially $W3$ and $W4$) are very sensitive to $T_{\rm eff}$ variations at the L spectral types, but quite insensitive in the late-K and M dwarf domain. However, their sensitivity to metallicity must be investigated in detail with, for example, resolved photometry of M-dwarf wide common proper motion companions to FGK-type stars with well-determined stellar astrophysical parameters (Montes et al., 2018).

Absolute magnitude-colour

In Fig. 3.12 we show the M_G versus $G - J$ diagram. In Fig. 3.17 we show a similar diagram (see more examples in e.g. Dupuy & Liu, 2012), but for r' instead of G, and we overplot a quadratic polynomial fit to 278 CARMENES GTO target stars with spectral types ranging from K7 V to M9 V (Reiners et al., 2018b). All of them have well-behaved *Gaia* astrometric solutions (i.e. `ruwe` < 1.41; Fig. 3.7) and do not have close companions (Cortés-Contreras et al., 2017b; Baroch et al., 2018), extreme values of metallicity (Alonso-Floriano et al., 2015b; Passegger et al., 2018, 2019, 2020), young ages (Tal-Or et al., 2018), or large-amplitude photometric variability (Díez Alonso et al., 2019). We also fitted another quadratic polynomial to the M_G versus $G - J$ data of the GTO stars. Thus, with the parameter fits in Table 3.5 and only r' or G and J magnitudes, one can estimate a stellar distance with a median accuracy of 36 %

Table 3.5: Fit parameters for several empirical relations.

Y[a] [mag]	X [mag]	a [mag]	b [mag^{-1}]	c [mag^{-2}]	d [mag^{-3}]	e [mag^{-4}]	R^2	ΔX [mag]
$M_{r'}$	$r'-J$	+8.38 ± 2.68	−2.74 ± 2.36	+1.47 ± 0.68	−0.132 ± 0.063	0	0.9398	[2.0, 5.1]
M_G	$G-J$	+16.24 ± 4.57	−13.04 ± 4.80	+5.64 ± 1.66	−0.622 ± 0.188	0	0.9308	[2.0, 4.0]
$\log \mathcal{L}/\mathcal{L}_\odot$	M_J	+2.051 ± 0.075	−0.662 ± 0.030	+0.0267 ± 0.0039	−0.00102 ± 0.00016	0	0.9923	[4.4, 11.2)
		−3.906 ± 0.998	+0.334 ± 0.156	−0.0263 ± 0.0061	0	0	0.9477	[11.2, 14.8]
$\log \mathcal{L}/\mathcal{L}_\odot$	M_G	+0.145 ± 0.201	+0.074 ± 0.060	−0.0382 ± 0.0060	+0.00119 ± 0.00019	0	0.9901	[6.4, 14.0)
		−2.329 ± 0.687	+0.092 ± 0.084	−0.0103 ± 0.0025	0	0	0.9782	[14.0, 20.2]
BC_G	$G-J$	+0.404 ± 0.187	+0.161 ± 0.239	−0.465 ± 0.112	+0.1159 ± 0.0225	−0.0115 ± 0.0017	0.9960	(1.5, 5.4]
$BC_{r'}$	$r'-J$	+0.557 ± 0.085	−0.036 ± 0.091	−0.318 ± 0.035	+0.0552 ± 0.0056	−0.0037 ± 0.0003	0.9983	(1.5, 7.5]
BC_J	$G-J$	+0.576 ± 0.094	+0.735 ± 0.104	−0.132 ± 0.038	+0.0115 ± 0.0045	0	0.9547	(1.5, 4.0]
BC_{W3}	$G-J$	−2.592 ± 0.667	+5.845 ± 1.005	−2.611 ± 0.559	+0.586 ± 0.136	−0.0496 ± 0.0122	0.9727	(1.5, 4.0]

[a] In all cases, the polynomial fits follow the form $Y = a + bX + cX^2 + dX^3 + eX^4$ and are applicable in the range ΔX. In all cases, R^2 is the correlation coefficient from the Pearson product-moment matrix. These relations should be applied to solar-metallicity stars only (Sect. 3.3).

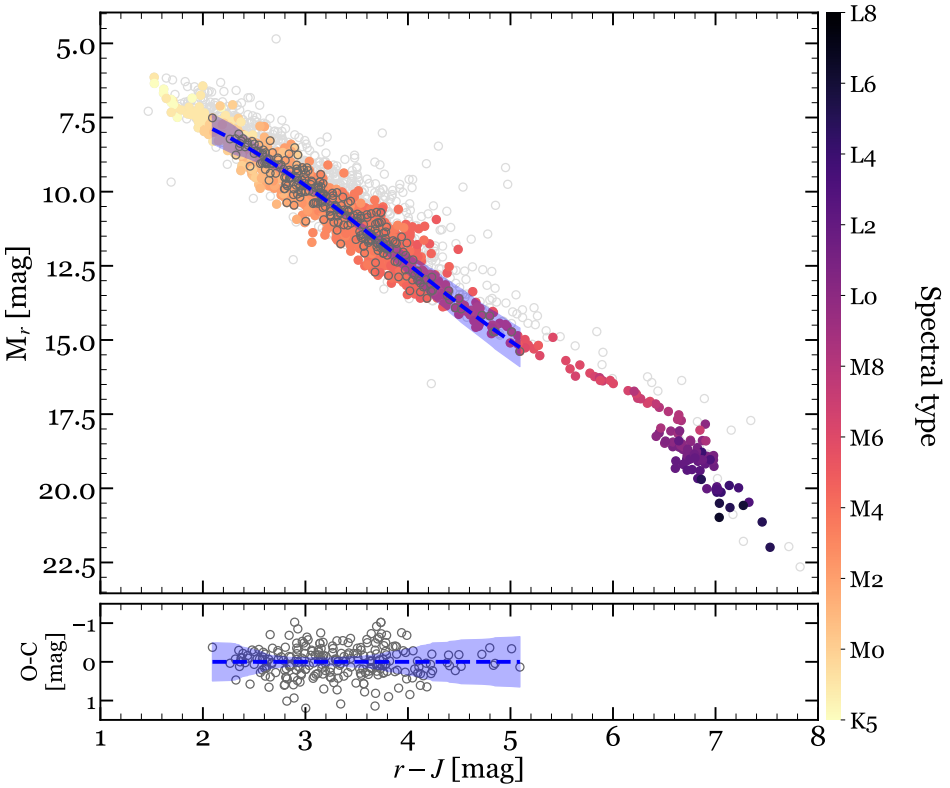

Figure 3.17: Same as Fig. 3.12 but for $M_{r'}$ vs. $r'-J$. The GTO stars in the sample are shown in dark grey. The blue dashed line represents the polynomial fit given in Table 3.5, with a blue shaded region for the 1-σ uncertainty region. The fit residuals are shown in the small bottom panel.

for stars in the colour ranges listed in the column ΔX. From our knowledge of the CARMENES GTO stars, the most important contributor to the fit uncertainty is not the parallax or magnitude error, stellar variability, or unresolved multiplicity, but the intrinsic scatter of the M-dwarf colour sequence due to different metallicity.

The M_G versus $G-J$ relation is particularly helpful because, although there are about 420 million sources with known *Gaia* DR2 and 2MASS magnitudes (Marrese et al., 2019), there are several million near-infrared sources that lack a parallax determination. However, for the 31 single stars in our sample without published trigonometric parallaxes, we estimated photometric distances homogeneously from the

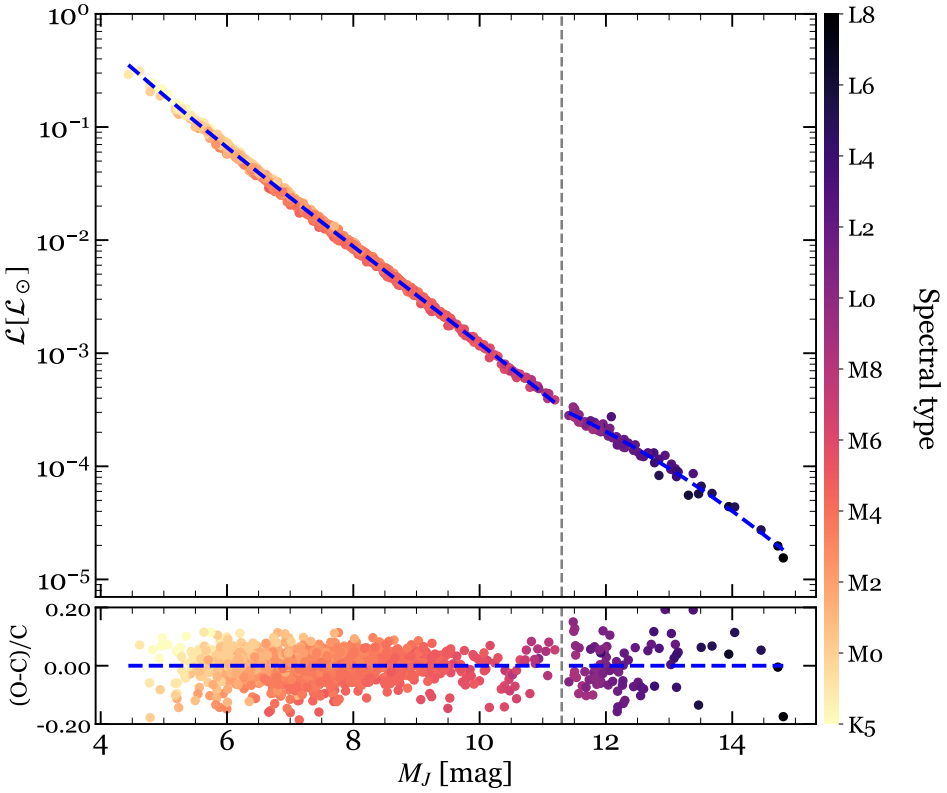

Figure 3.18: Same as Fig. 3.12, but for $\mathcal{L}_{\rm VOSA}$ vs. M_J and normalised fit residuals in the small bottom panel. The vertical dashed line separates the three-degree (late-K and M dwarfs) and two-degree (L dwarfs) fit ranges.

$M_{r'}$ versus $r' - J$ relation assuming null extinction. Because of the relatively large uncertainty in the estimates, we did not use these photometric distances throughout our work, but only tabulated them in the on-line summary table described below. In general, we only recommend the use of these relations for estimating photometric distances for stars with solar-like metallicity, as well as good photometric quality (e.g. Bochanski et al., 2007, and see Sect. 3.3).

3.2.4 Absolute magnitudes and bolometric corrections

The absolute magnitude of a star is directly related to its bolometric luminosity. In our sample, we found that the J-band absolute magnitude, M_J, provides the correlation with VOSA luminosity that is most complete and that has the smallest scatter. Figure 3.18 shows $\mathcal{L}_{\rm VOSA}$ (in solar units) versus M_J fitted in the late-K- to late-M- and L-dwarf domains, with three-degree and two-degree polynomials, respectively. Although in Table C.2 we list the fit parameters for both luminosities from 2MASS J and *Gaia* G, we preferred J over G because the larger effective width of the broad *Gaia* passband introduces more dispersion in the data, quantified by R^2. With these relationships in the M-dwarf domain, it is possible to estimate bolometric luminosities from absolute magnitudes M_J and M_G with a relative precision of 4.2 % and 4.5 %, respectively.

We calculated bolometric corrections, $BC_\lambda = M_{\rm bol} - M_\lambda$, for each investigated passband and plot them in Fig. 3.19. For the calculation, we followed the sign criterion of Böhm-Vitense (1989) and the definition of the absolute bolometric magnitude $M_{\rm bol}$ by IAU Resolution B2 (Mamajek et al., 2015), which is

independent of the solar luminosity,

$$M_{\rm bol} = -2.5 \log_{10} \frac{\mathcal{L}_\star}{\mathcal{L}_0} = -2.5 \log_{10} \mathcal{L}_\star + M_{\rm bol,0}, \tag{3.1}$$

where $\mathcal{L}_\star$ and $\mathcal{L}_0$ are the luminosity of the star and the zero point of the absolute bolometric magnitude scale, respectively, and $M_{\rm bol,0} \equiv 71.197425$ mag.

From the sample of 2479 stars, for the following analysis we discarded: (*i*) stars with poor photometric or astrometric behaviour based on quality indicators (Sects. 3.1.2 and 3.1.3), (*ii*) close binaries and stars with photometry contaminated by bright nearby companions ($\rho < 5$ arcsec; Sect. 3.1.4), (*iii*) overluminous objects known to belong to young associations and moving groups (Sect. 3.2.2), and (*iv*) stars with extraordinarily anomalous colours or absolute magnitudes.

Of the different BC_λ versus $G - J$ combinations in Fig. 3.19, the narrowest sequence is that of BC_G. However, as illustrated by Fig. 3.20, the $BC_{r'}$ versus $r' - J$ sequence is even less scattered and spans wider ranges in X ((1.5, 7.5] mag in $r' - J$ versus (1.5, 5.4] mag in $G - J$) and Y ([−5.8, 0.0] mag in $BC_{r'}$ versus [−3.8, −0.1] mag in BC_G), probably due again to the broad G effective width. We fitted polynomials to the relations BC_G versus $G-J$, $BC_{r'}$ versus $r'-J$, BC_J versus $G-J$, and BC_{W2} versus $G-J$, and provide the corresponding parameters and correlation coefficients in Table 3.5. All in all, these relationships are complementary and can help to estimate relatively precise luminosities of M dwarfs with only a handful of widely available data (G and ϖ from *Gaia*, J from 2MASS, r' from a number of surveys including the forthcoming LSST).

3.2.5 Masses and radii

Finally, we derived radii $\mathcal{R}$ and masses $\mathcal{M}$ of the well-behaved stars. For $\mathcal{R}$, we used the Stefan-Boltzmann law $L = 4\pi\mathcal{R}^2\sigma T_{\rm eff}^4$ and $\mathcal{L}$ and $T_{\rm eff}$ from `VOSA`. For $\mathcal{M}$ we used the $\mathcal{M}$-$\mathcal{R}$ relation in Eq. 6 of Schweitzer et al. (2019), which came from a compilation of detached, double-lined, double-eclipsing, main-sequence, M-dwarf binaries from the literature[10]. This relation is applicable in a wide range of metallicities for M dwarfs older than a few hundred million years. `VOSA` also computes two stellar radii, one from a model dependent dilution factor and d, the other using the Stefan-Boltzmann law, but we did not use them.

3.3 Discussion

Here we compare our $\mathcal{L}$, $T_{\rm eff}$, $\mathcal{R}$, $\mathcal{M}$, and photometric data with those in the literature. Tables 3.6 and 3.7 and Figs. 3.21 to 3.28 illustrate the discussion. In particular, in Table 3.6 we show average values of BC_G, BC_J, $\mathcal{L}$, $T_{\rm eff}$, $\mathcal{M}$, and $\mathcal{R}$ for single, main-sequence stars with spectral types from K5 V to L2.0. The last column, N, indicates the number per spectral type bin of well-behaved stars (i.e. with no companions at $\rho < 5$ arcsec, no overluminosity due to extreme youth, and of good *Gaia* DR2 astrometric and photometric quality). After applying a $3-\sigma$ clipping, we calculated three-point rolling means and standard deviations between M0.0 V and L2.0 (e.g. tabulated values for M4.0 V stars are the mean and standard deviation of all individual BC_G values of stars with spectral types M3.5, M4.0, and M4.5 V), and simple means and standard deviations for K5 V and K7 V stars. With these rolling means, we conservatively smoothed potential inter-type variability due to the small number of stars per bin at the latest spectral types and the typical uncertainty in M-dwarf spectral type determination, of 0.5 dex (Hawley et al., 2002;

[10] $\mathcal{M} = \alpha + \beta\mathcal{R}$, with $\alpha = -0.0240 \pm 0.0076\ \mathcal{M}_\odot$, $\beta = 1.055 \pm 0.017\ \mathcal{M}_\odot/\mathcal{R}_\odot$, and $\mathcal{M}$ and $\mathcal{R}$ in solar units.

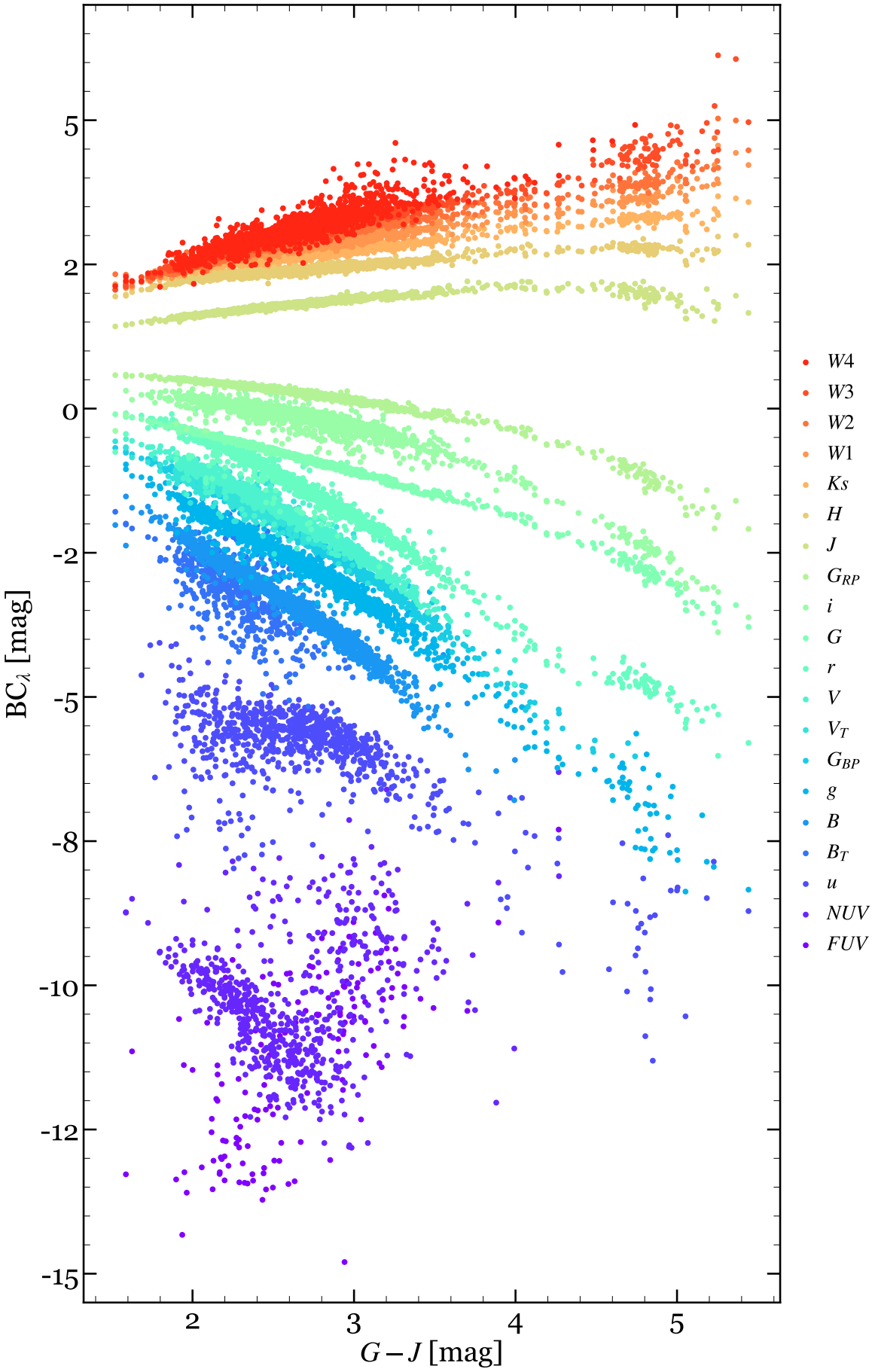

Figure 3.19: Bolometric corrections for every star and passband vs. $G - J$ colour. The coloured sets contain all stars with available photometry in G, J, and the respective passband.

Table 3.6: Average astrophysical parameters for K5 V to L5 objects.

Spectral type	BC_G [mag]	BC_J [mag]	$\mathcal{L}$ [$10^{-4} L_\odot$]	$T_{\rm eff}$ [K]	$\mathcal{R}$ [$\mathcal{R}_\odot$]	$\mathcal{M}$ [$\mathcal{M}_\odot$]	N
K5 V	–0.202 ± 0.065	1.492 ± 0.047	1760 ± 424	4430 ± 177	0.703 ± 0.054	0.718 ± 0.057	13
K7 V	–0.385 ± 0.047	1.613 ± 0.029	1000 ± 217	4057 ± 100	0.634 ± 0.047	0.645 ± 0.049	74
M0.0 V	–0.477 ± 0.082	1.654 ± 0.044	786 ± 256	3900 ± 146	0.600 ± 0.068	0.609 ± 0.072	104
M0.5 V	–0.551 ± 0.070	1.689 ± 0.039	606 ± 209	3778 ± 112	0.564 ± 0.080	0.571 ± 0.084	60
M1.0 V	–0.615 ± 0.060	1.717 ± 0.036	505 ± 171	3693 ± 85	0.541 ± 0.079	0.547 ± 0.084	112
M1.5 V	–0.664 ± 0.067	1.738 ± 0.039	424 ± 161	3633 ± 93	0.509 ± 0.089	0.513 ± 0.094	95
M2.0 V	–0.740 ± 0.077	1.768 ± 0.038	335 ± 145	3528 ± 111	0.477 ± 0.091	0.479 ± 0.096	98
M2.5 V	–0.824 ± 0.083	1.798 ± 0.035	242 ± 104	3429 ± 101	0.432 ± 0.087	0.431 ± 0.092	118
M3.0 V	–0.910 ± 0.085	1.830 ± 0.041	183 ± 87	3334 ± 88	0.393 ± 0.087	0.390 ± 0.092	142
M3.5 V	–0.992 ± 0.096	1.864 ± 0.045	133 ± 70	3260 ± 92	0.350 ± 0.086	0.345 ± 0.091	192
M4.0 V	–1.063 ± 0.103	1.892 ± 0.045	99 ± 54	3199 ± 88	0.315 ± 0.084	0.309 ± 0.088	169
M4.5 V	–1.163 ± 0.123	1.924 ± 0.042	67 ± 40	3123 ± 88	0.269 ± 0.075	0.260 ± 0.079	85
M5.0 V	–1.296 ± 0.140	1.963 ± 0.048	35 ± 18	3034 ± 91	0.211 ± 0.052	0.198 ± 0.055	47
M5.5 V	–1.445 ± 0.143	2.001 ± 0.057	20.4 ± 9.3	2941 ± 94	0.169 ± 0.032	0.155 ± 0.034	22
M6.0 V	–1.623 ± 0.217	2.067 ± 0.066	12.4 ± 5.2	2850 ± 131	0.140 ± 0.022	0.124 ± 0.023	14
M6.5 V	–1.829 ± 0.223	2.101 ± 0.065	8.5 ± 3.6	2733 ± 124	0.127 ± 0.019	0.110 ± 0.020	6
M7.0 V	–2.018 ± 0.208	2.094 ± 0.036	5.7 ± 1.1	2625 ± 108	0.115 ± 0.007	0.097 ± 0.007	6
M8.0 V	–2.189 ± 0.097	2.077 ± 0.048	5.22 ± 0.92	2492 ± 67	0.122 ± 0.007	0.105 ± 0.008	11
M9.0 V	–2.495 ± 0.223	2.067 ± 0.066	3.4 ± 1.4	2352 ± 113	0.107 ± 0.015	0.089 ± 0.016	7
L0	–2.729 ± 0.170	2.014 ± 0.087	2.22 ± 0.29	2195 ± 172	0.107 ± 0.021	0.089 ± 0.023	18
L1	–2.812 ± 0.154	1.964 ± 0.093	2.00 ± 0.46	2076 ± 203	0.112 ± 0.020	0.094 ± 0.021	22
L2	–2.924 ± 0.187	1.900 ± 0.130	1.71 ± 0.45	1961 ± 193	0.114 ± 0.020	0.096 ± 0.021	20
L3	–3.109 ± 0.285	1.845 ± 0.137	1.34 ± 0.42	1852 ± 130	0.111 ± 0.013	0.093 ± 0.014	7
L4	–3.497 ± 0.184	1.740 ± 0.136	0.78 ± 0.26	1733 ± 90	0.096 ± 0.014	0.077 ± 0.015	4
L5	–3.460 ± 0.219	1.801 ± 0.165	0.67 ± 0.24	1722 ± 98	0.090 ± 0.014	0.071 ± 0.015	7

Table 3.7: Average absolute magnitudes for K5 V to L5 objects.

Spectral type	M_B [mag]	$M_{g'}$ [mag]	$M_{G_{BP}}$ [mag]	M_V [mag]	$M_{r'}$ [mag]	M_G [mag]	$M_{i'}$ [mag]
K5 V	8.32 ± 0.37	7.81 ± 0.35	7.48 ± 0.39	7.23 ± 0.28	6.90 ± 0.31	6.85 ± 0.35	6.51 ± 0.31
K7 V	9.57 ± 0.44	9.00 ± 0.34	8.48 ± 0.34	8.27 ± 0.35	7.70 ± 0.34	7.65 ± 0.28	7.13 ± 0.26
M0.0 V	10.11 ± 0.59	9.49 ± 0.53	8.95 ± 0.52	8.73 ± 0.52	8.18 ± 0.53	8.01 ± 0.43	7.46 ± 0.43
M0.5 V	10.60 ± 0.54	9.92 ± 0.52	9.39 ± 0.52	9.16 ± 0.53	8.59 ± 0.52	8.38 ± 0.45	7.77 ± 0.42
M1.0 V	10.92 ± 0.48	10.24 ± 0.48	9.72 ± 0.45	9.47 ± 0.47	8.90 ± 0.47	8.63 ± 0.41	7.99 ± 0.41
M1.5 V	11.26 ± 0.57	10.54 ± 0.55	10.04 ± 0.54	9.78 ± 0.53	9.21 ± 0.54	8.91 ± 0.48	8.23 ± 0.49
M2.0 V	11.73 ± 0.65	10.98 ± 0.62	10.49 ± 0.60	10.21 ± 0.60	9.66 ± 0.61	9.27 ± 0.54	8.58 ± 0.55
M2.5 V	12.26 ± 0.70	11.50 ± 0.66	11.02 ± 0.64	10.73 ± 0.65	10.18 ± 0.64	9.70 ± 0.57	8.99 ± 0.58
M3.0 V	12.81 ± 0.72	12.00 ± 0.69	11.53 ± 0.69	11.26 ± 0.70	10.69 ± 0.68	10.11 ± 0.61	9.38 ± 0.59
M3.5 V	13.36 ± 0.83	12.55 ± 0.80	12.09 ± 0.79	11.79 ± 0.78	11.24 ± 0.77	10.57 ± 0.68	9.82 ± 0.69
M4.0 V	13.86 ± 0.89	13.03 ± 0.86	12.58 ± 0.84	12.25 ± 0.83	11.70 ± 0.81	10.96 ± 0.72	10.20 ± 0.72
M4.5 V	14.53 ± 0.95	13.70 ± 0.92	13.25 ± 0.91	12.88 ± 0.87	12.35 ± 0.88	11.51 ± 0.78	10.74 ± 0.79
M5.0 V	15.41 ± 1.05	14.62 ± 1.00	14.16 ± 0.99	13.68 ± 0.94	13.23 ± 0.96	12.20 ± 0.80	11.43 ± 0.81
M5.5 V	16.44 ± 0.92	15.73 ± 1.05	15.25 ± 1.01	14.61 ± 0.78	14.31 ± 0.99	13.01 ± 0.73	12.27 ± 0.68
M6.0 V	17.58 ± 0.85	16.82 ± 0.99	16.29 ± 0.96	15.63 ± 0.79	15.33 ± 0.93	13.72 ± 0.64	12.98 ± 0.64
M6.5 V	18.57 ± 0.78	17.72 ± 0.91	17.26 ± 0.89	16.67 ± 0.81	16.22 ± 0.83	14.34 ± 0.58	13.66 ± 0.58
M7.0 V	…	18.58 ± 0.71	18.17 ± 0.61	…	17.09 ± 0.60	14.89 ± 0.44	14.39 ± 0.41
M8.0 V	…	18.90 ± 0.28	18.21 ± 0.35	…	17.23 ± 0.31	15.15 ± 0.26	14.41 ± 0.24
M9.0 V	…	19.88 ± 0.66	18.78 ± 0.77	…	18.07 ± 0.54	16.01 ± 0.61	15.54 ± 0.69
L0	…	20.62 ± 0.68	19.64 ± 0.25	…	18.59 ± 0.29	16.57 ± 0.31	16.15 ± 0.34
L1	…	20.83 ± 0.71	…	…	18.74 ± 0.32	16.81 ± 0.34	16.38 ± 0.32
L2	…	21.45 ± 0.95	…	…	19.09 ± 0.48	17.07 ± 0.42	16.71 ± 0.51
L3	…	22.15 ± 0.89	…	…	19.45 ± 0.56	17.56 ± 0.59	17.14 ± 0.61
L4	…	23.40 ± 0.76	…	…	20.49 ± 0.77	18.39 ± 0.36	18.27 ± 0.75
L5	…	23.55 ± 0.79	…	…	20.69 ± 0.80	18.53 ± 0.30	18.54 ± 0.72

Spectral type	$M_{G_{RP}}$ [mag]	M_J [mag]	M_H [mag]	M_{K_s} [mag]	M_{W1} [mag]	M_{W2} [mag]	M_{W3} [mag]
K5 V	6.10 ± 0.31	5.16 ± 0.26	4.60 ± 0.24	4.46 ± 0.22	4.38 ± 0.22	4.32 ± 0.32	4.29 ± 0.35
K7 V	6.77 ± 0.25	5.65 ± 0.23	5.02 ± 0.22	4.85 ± 0.20	4.75 ± 0.20	4.78 ± 0.19	4.73 ± 0.17
M0.0 V	7.08 ± 0.38	5.89 ± 0.33	5.25 ± 0.34	5.07 ± 0.33	4.95 ± 0.30	4.93 ± 0.25	4.90 ± 0.26
M0.5 V	7.41 ± 0.41	6.14 ± 0.37	5.51 ± 0.39	5.31 ± 0.37	5.18 ± 0.36	5.13 ± 0.31	5.10 ± 0.32
M1.0 V	7.63 ± 0.39	6.30 ± 0.36	5.68 ± 0.39	5.47 ± 0.37	5.33 ± 0.36	5.26 ± 0.31	5.22 ± 0.32
M1.5 V	7.87 ± 0.46	6.50 ± 0.42	5.88 ± 0.46	5.66 ± 0.44	5.52 ± 0.44	5.44 ± 0.39	5.39 ± 0.40
M2.0 V	8.20 ± 0.52	6.75 ± 0.47	6.15 ± 0.50	5.91 ± 0.49	5.76 ± 0.48	5.67 ± 0.44	5.60 ± 0.44
M2.5 V	8.58 ± 0.55	7.06 ± 0.50	6.47 ± 0.53	6.22 ± 0.52	6.07 ± 0.51	5.95 ± 0.48	5.87 ± 0.47
M3.0 V	8.95 ± 0.56	7.36 ± 0.53	6.78 ± 0.55	6.52 ± 0.54	6.35 ± 0.53	6.22 ± 0.50	6.12 ± 0.49
M3.5 V	9.38 ± 0.65	7.70 ± 0.60	7.13 ± 0.62	6.86 ± 0.61	6.68 ± 0.59	6.53 ± 0.56	6.42 ± 0.55
M4.0 V	9.74 ± 0.69	7.99 ± 0.63	7.42 ± 0.65	7.15 ± 0.63	6.96 ± 0.62	6.79 ± 0.60	6.67 ± 0.59
M4.5 V	10.25 ± 0.74	8.41 ± 0.66	7.84 ± 0.67	7.56 ± 0.66	7.36 ± 0.64	7.19 ± 0.63	7.05 ± 0.61
M5.0 V	10.89 ± 0.76	8.94 ± 0.66	8.37 ± 0.67	8.06 ± 0.65	7.86 ± 0.64	7.67 ± 0.63	7.51 ± 0.62
M5.5 V	11.62 ± 0.58	9.56 ± 0.50	8.98 ± 0.49	8.65 ± 0.47	8.43 ± 0.46	8.23 ± 0.45	8.05 ± 0.44
M6.0 V	12.24 ± 0.54	10.03 ± 0.42	9.45 ± 0.41	9.10 ± 0.40	8.86 ± 0.39	8.65 ± 0.40	8.47 ± 0.37
M6.5 V	12.80 ± 0.52	10.40 ± 0.37	9.80 ± 0.35	9.43 ± 0.35	9.18 ± 0.34	8.98 ± 0.34	8.76 ± 0.31
M7.0 V	13.35 ± 0.39	10.78 ± 0.26	10.18 ± 0.22	9.81 ± 0.18	9.53 ± 0.22	9.32 ± 0.20	9.09 ± 0.12
M8.0 V	13.58 ± 0.24	10.88 ± 0.18	10.23 ± 0.17	9.83 ± 0.15	9.59 ± 0.15	9.36 ± 0.14	9.08 ± 0.13
M9.0 V	14.38 ± 0.59	11.45 ± 0.43	10.74 ± 0.39	10.27 ± 0.35	9.97 ± 0.32	9.70 ± 0.31	9.27 ± 0.24
L0	14.94 ± 0.31	11.86 ± 0.19	11.08 ± 0.16	10.58 ± 0.16	10.23 ± 0.15	9.98 ± 0.17	9.49 ± 0.20
L1	15.15 ± 0.38	12.03 ± 0.27	11.22 ± 0.23	10.72 ± 0.24	10.36 ± 0.21	10.10 ± 0.21	9.60 ± 0.25
L2	15.35 ± 0.32	12.30 ± 0.42	11.44 ± 0.34	10.90 ± 0.30	10.49 ± 0.23	10.22 ± 0.22	9.73 ± 0.29
L3	15.92 ± 0.60	12.62 ± 0.43	11.72 ± 0.35	11.15 ± 0.29	10.68 ± 0.21	10.40 ± 0.21	9.93 ± 0.34
L4	16.79 ± 0.35	13.29 ± 0.47	12.30 ± 0.40	11.69 ± 0.40	11.05 ± 0.33	10.71 ± 0.34	10.28 ± 0.40
L5	16.86 ± 0.29	13.39 ± 0.51	12.44 ± 0.43	11.88 ± 0.43	11.18 ± 0.35	10.85 ± 0.36	10.38 ± 0.41

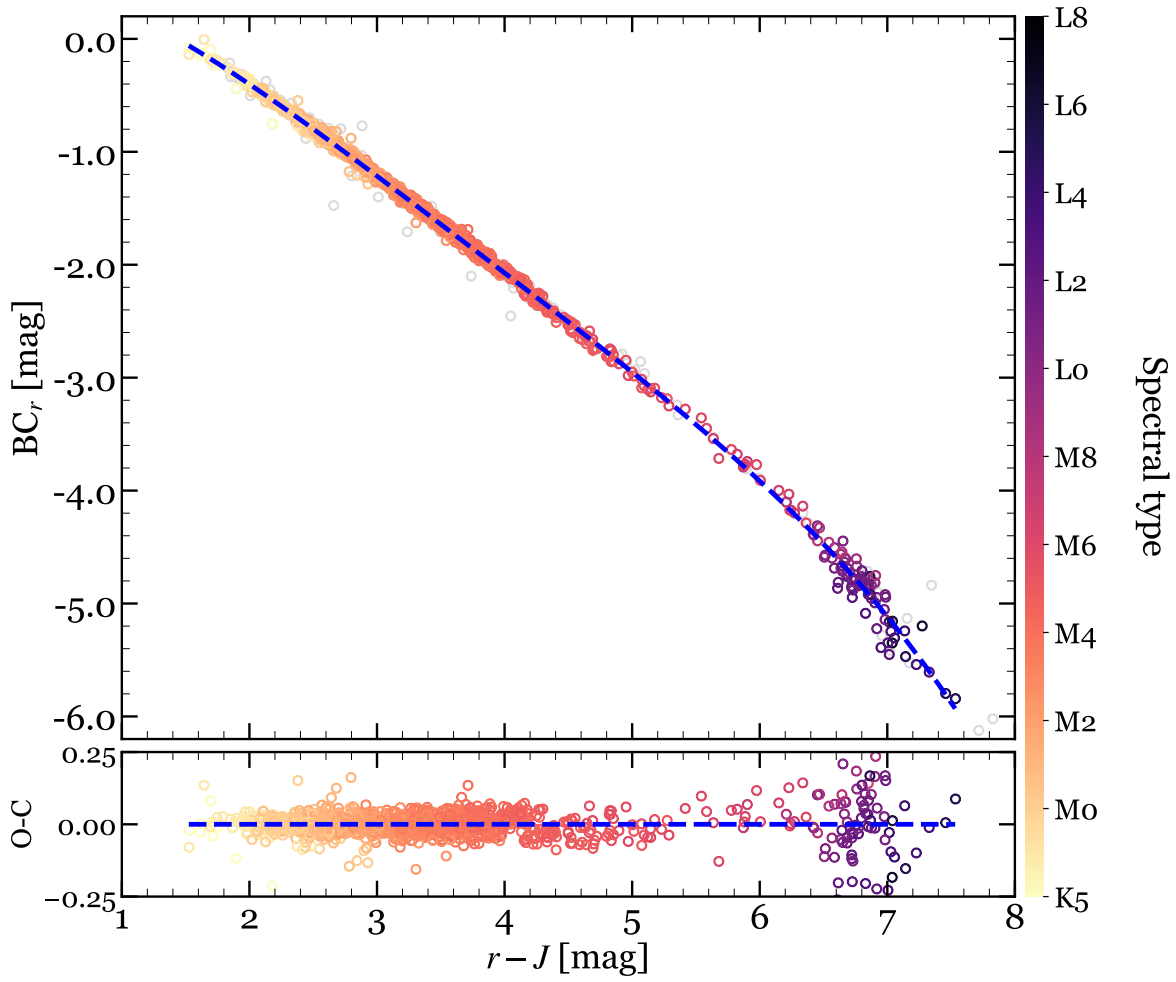

Figure 3.20: Same as Fig. 3.12 but for BC$_{r'}$ vs. $r' - J$. A polynomial fit is shown as a blue dashed line.

Lépine et al., 2013; Alonso-Floriano et al., 2015b). The correspondingly large standard deviations denote the large natural scatter of the main sequence at the earliest spectral types and the difficulty in determining precise parameters at the latest ones. The boundary values for K5 V type were not smoothed and, therefore, must be handled with care. Besides, it is not trivial to distinguish between very late K dwarfs and very early M dwarfs from low-resolution spectroscopy (see again Kirkpatrick et al., 1991; Lépine et al., 2013; Alonso-Floriano et al., 2015b), while the $T_{\rm eff}$ determination does not always help because of different temperature scales in the literature. However, the tabulated value of $\mathcal{L} \approx 0.1\,\mathcal{L}_{\odot}$ is a more accessible and reliable observational boundary in the K7 V–M0.0 V frontier. This is extensible into the M dominion, even the coolest tail. In this sense, bolometric luminosities could effectively constrain the spectral class of a main sequence star with more reliance that, for instance, the surface temperature. On the other hand, Table 3.7 complements Table C.2 and lists the average absolute magnitudes of K5 V to L2.0 objects in the 14 most representative bands (i.e. all except for *GALEX FUV* and *NUV*, SDSS9 u', Tycho-2 B_T and V_T, and *WISE W4*). We applied the same rolling mean and $3-\sigma$ clipping as in Table 3.6. For each spectral type K5–M7.0 V, a total of 6.227 10^9 different colours can be determined from the tabulated absolute magnitudes (e.g. $G - J = M_G - M_J$). For spectral types L0.0–2.0, the number of possible colours is 3 628 800.

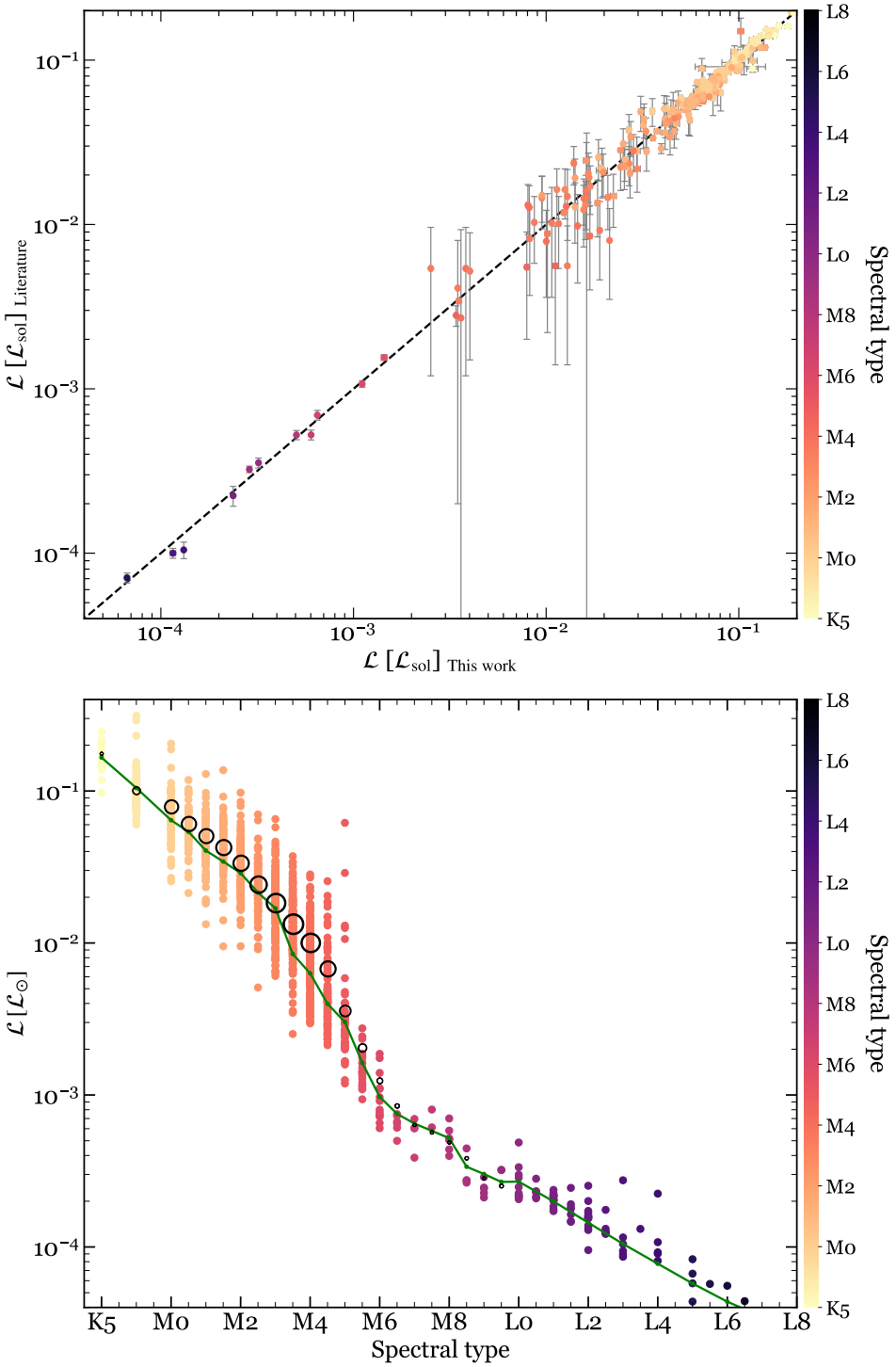

Figure 3.21: Comparison of $\mathcal{L}$ from VOSA and from the literature (*top*) and individual (coloured points) and mean $\mathcal{L}$ (black circles) as a function of spectral type as in Table 3.6 (*bottom*). In the bottom panel, the green line outlines the empirical $\mathcal{L}$-spectral type sequence of Pecaut & Mamajek (2013, with updated values for M0.0 V to M9.5 V; E. E. Mamajek, priv. comm.) and the size of the black points is proportional to the number of stars per spectral type.

Luminosities (Fig. 3.21). First, we compared our $\mathcal{L}$ computed with VOSA with those from a number of works in the literature (top panel – Golimowski et al., 2004; Vrba et al., 2004; Howard et al., 2010; Kundurthy et al., 2011; Bonfils et al., 2012; Mann et al., 2013b; Gaidos & Mann, 2014; Affer et al., 2016, 2019; Tuomi et al., 2014; Newton et al., 2015; Anglada-Escudé et al., 2016; Astudillo-Defru et al., 2017b; Dittmann et al., 2017; Gillon et al., 2017; Maldonado et al., 2017; Suárez Mascareño et al., 2017a,b; Gaia Collaboration et al., 2018b; Hirano et al., 2018; Hobson et al., 2018). In spite of (or due to) the relatively large published $\mathcal{L}$ uncertainties of a few ultracool dwarfs, the agreement is in general excellent, especially in the case of Gaia Collaboration et al. (2018b). Our median $\mathcal{L}$ values per spectral type also match those of Pecaut & Mamajek (2013, right panel). When integrated from a well-calibrated, multi-band spectral energy distribution in a wide wavelength coverage and calculated with the latest *Gaia* parallaxes as in this work, $\mathcal{L}$ can become the most reliable "observable" of low-mass stars, instead of the widely used temperature, which is inferred through colours, spectral classification, or expensive, model-dependent, spectral synthesis.

Effective temperatures (Fig. 3.22). Next, we compared our $T_{\rm eff}$ from VOSA with the values from the works referred to in the previous paragraph, except from Gaia Collaboration et al. (2018b), plus from Passegger et al. (2019), who in turn compared their $T_{\rm eff}$ with those from Rojas-Ayala et al. (2012), Gaidos & Mann (2014), Maldonado et al. (2015), Mann et al. (2015), Rajpurohit et al. (2018a), and Schweitzer et al. (2019). From the top left panel in Fig. 3.22, our $T_{\rm eff}$ are cooler than those of the literature by -86 ± 82 K. This systematic difference is within the grid step size of the theoretical models used by VOSA, of 100 K or 50 K, but appreciable in the whole $T_{\rm eff}$ = 3000–4000 K range. That VOSA does not interpolate between grid points may partly explain this systematic difference. In the empirical $T_{\rm eff}$-spectral type relation shown in the top right panel, $T_{\rm eff}$ from Rajpurohit et al. (2018a) and Passegger et al. (2019) are, again, slightly warmer than ours in the late- and early-M domains, respectively. However, the agreement with the relation of Pecaut & Mamajek (2013) is exquisite. The K/M and M/L boundaries occur at about 3900 K and 2300 K, respectively, in line with the standard values (e.g. Habets & Heintze, 1981; Kirkpatrick, 2005, see also Table 3.6). In the Hertzsprung-Russell diagram in the bottom left panel, as expected, our targets are significantly less luminous than the very young stars and brown dwarfs of the same $T_{\rm eff}$ tabulated by Pecaut & Mamajek (2013) and Farihi (2016), but our main sequence (excluding young targets) matches that of Newton et al. (2015). The most convincing plot is perhaps the M_J versus $T_{\rm eff}$ diagram in the bottom right panel, where our M-dwarf main sequence perfectly overlaps with those defined by Lépine et al. (2013) and Gaidos & Mann (2014) and extrapolates reasonably well into the ultracool dwarf sequence of Dahn et al. (2002). The absolute magnitude in the vertical axis does not depend on models, Virtual Observatory tools, spectral synthesis, or multi-band photometry, but only on reliable 2MASS J-band magnitude and *Gaia* parallaxes.

Metallicity (Figs. 3.23 to 3.25). The role of metallicity in the empirical relations between physical parameters of M dwarfs has been the subject of investigation by many teams (e.g. Bonfils et al., 2005a; Woolf & Wallerstein, 2005; Casagrande et al., 2008; Rojas-Ayala et al., 2012; Boyajian et al., 2012; von Boetticher et al., 2019, see Sect. 4.3 in Alonso-Floriano et al. 2015a for a short review). Of them, Mann et al. (2015) showed that empirical relations such as absolute magnitude-radius, radius-temperature, or colour-temperature could benefit from incorporating an additional term that accounts for metallicity. However, mainly because of the limitations of the BT-Settl CIFIST grid of theoretical models stored in the VOSA database, in our work we computed $\mathcal{L}$ and $T_{\rm eff}$ assuming a solar metallicity ([Fe/H] = 0)[11].

[11] Actually, BT-Settl CIFIST models are defined for solar metal abundance, [M/H], but here we used solar iron abundance, [Fe/H], for simplicity.

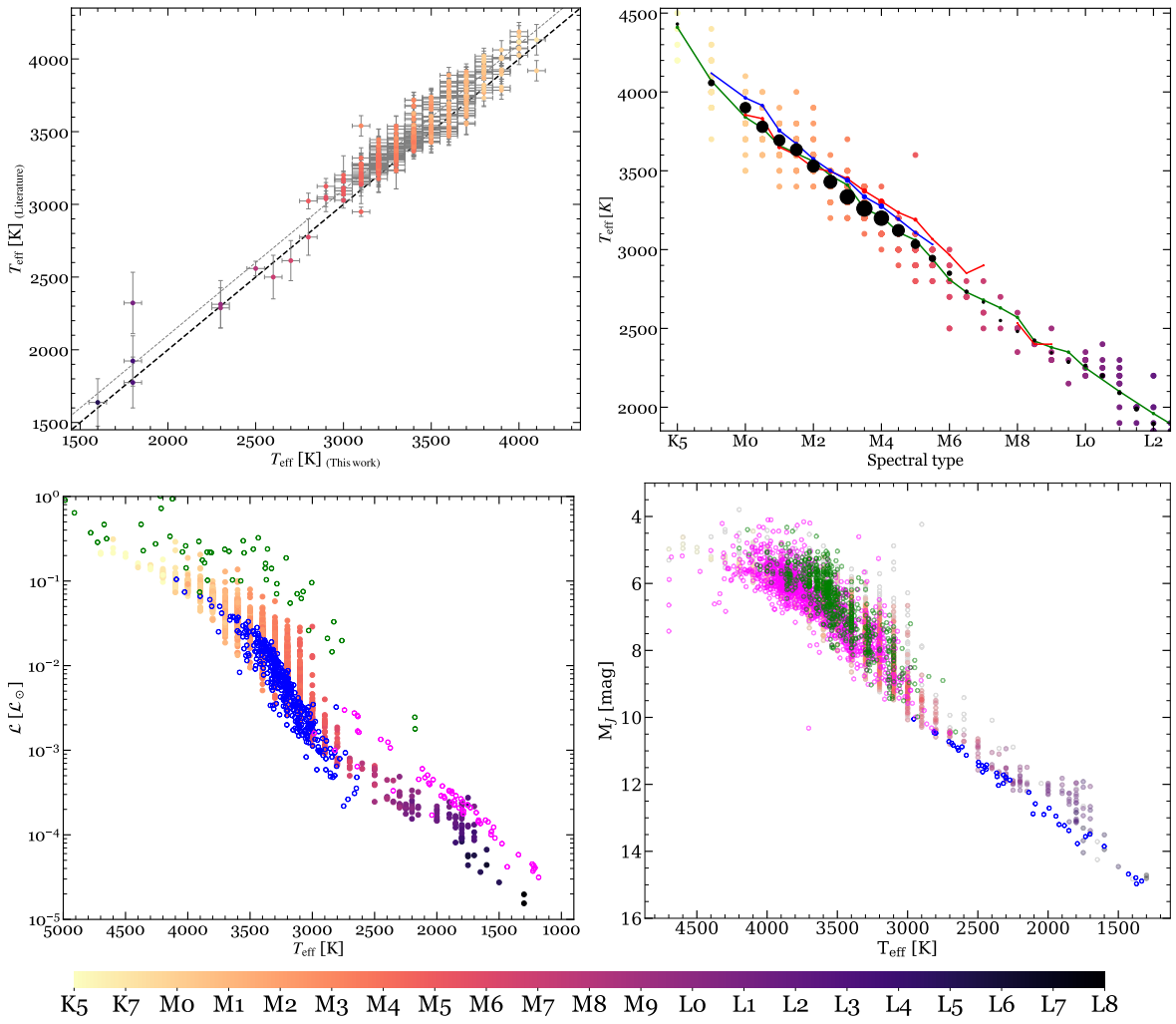

Figure 3.22: Four representative diagrams involving $T_{\rm eff}$. In the four panels our investigated stars are represented with filled circles colour-coded by spectral type. *Top left:* Comparison of $T_{\rm eff}$ from this work and from the literature. *Top right:* Individual (coloured points) and median (black circles) values of $T_{\rm eff}$ as a function of the spectral sequence shown in Table 3.6. The size of the black circles is proportional to the number of stars per spectral type. The green, red, and blue lines mark the mean values tabulated by Pecaut & Mamajek (2013), Rajpurohit et al. (2018a), and Passegger et al. (2019), respectively. *Bottom left:* $\mathcal{L}$ vs. $T_{\rm eff}$. As a comparison we also plot pre-main sequence stars with `BT-Settl` model fitting from Pecaut & Mamajek (2013, green empty circles), M dwarfs in the MEarth sample with stellar parameters from Newton et al. (2015, blue empty circles, inferred from the pseudo-equivalent width of Mg I near-infrared lines), and high-confidence moving group members from Farihi (2016, magenta empty circles) with parameters computed as in Filippazzo et al. (2015). *Bottom right:* J-band absolute magnitude vs. $T_{\rm eff}$. As a comparison we also plot the samples of Dahn et al. (2002, blue open circles), Lépine et al. (2013, green open circles), and Gaidos & Mann (2014, magenta empty circles).

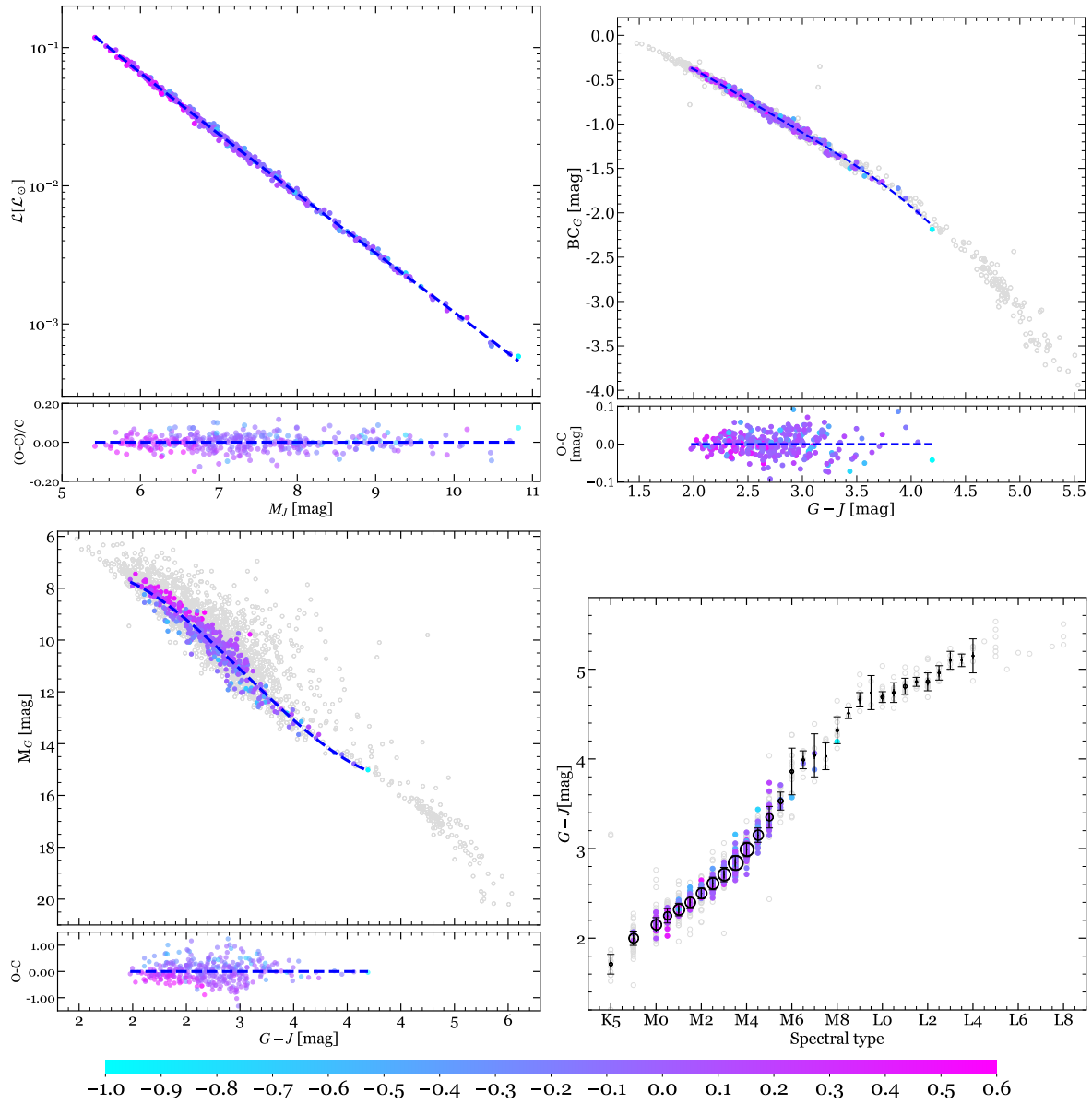

Figure 3.23: Revisiting empirical relations in Table 3.5 for stars with [Fe/H] values published in the literature, colour-coded by this parameter. *Top left:* $\mathcal{L}_{\text{VOSA,BT–Settl CIFIST}}$ vs. M_J. *Top right:* BC_G vs. $G-J$. *Bottom left:* M_G vs. $G-J$. The blue dashed lines in the three panels represent new 3-, 4-, and 3-degree polynomial fits, respectively. *Bottom right:* $G-J$ vs. spectral type. The grey circles represent the mean values with a symbol size proportional to the sample size in each type.

In order to quantify the impact of metallicity within our empirical relations in Table 3.5, first we compiled values of spectroscopically derived iron abundances of 510 single stars in our sample from Mann et al. (2015, 2019), Majewski et al. (2017), and Passegger et al. (2019). The compiled [Fe/H] values ranged from −1.63 dex for the mid-M dwarf HD 285190 to +0.59 dex for the early-M dwarf LP 397–041, with a mean and dispersion of -0.04 ± 0.26 dex.

Figure 3.23 displays the relations parametrised in Table 3.5, as well as the colour-spectral type diagram discussed in Sect. 3.2.3, colour-coded by the metallicity values from the literature. In either of the top plots ($\mathcal{L}$ vs. M_J and BC_G vs. $G-J$), the distribution of residuals did not show any correlation with the metal content of the stars. Both representations benefit from the fact that deriving $\mathcal{L}$ does not rely on precise [Fe/H] measurements. In the bottom panels, the distribution of metallicity values in the $G-J$ versus spectral type diagram shows no significant dependence on metallicity. This lack of correlation is also apparent in the additional colour diagrams displayed in this chapter. However, the M_G versus $G-J$ relation exhibits a notable correlation between metallicity and the residuals of the fit: more metallic stars appear brighter than less metallic stars of the same $G-J$ colour or, alternatively or simultaneously, more metallic stars appear redder than less metallic stars of the same M_G absolute magnitude. This dependence is most likely the main source of uncertainty for photometric distances, as we noted in Sect. 3.2.3. By using standard broad passbands in the red optical or the near infrared, such as r' or J, the effect of metallicity can be reduced compared to using wider, bluer passbands, such as G, which are more affected by the features that metallicity imprints on the spectra.

In the diagrams involving $T_{\rm eff}$, Mann et al. (2015) pointed out that the effect of metallicity can be severely masked due to the steeper dependence on the temperature. This is an important point to underline because the uncertainties in $T_{\rm eff}$ of models are a major source of uncertainties in the final products of the SED fitting. In other words, the approximation of near-solar metallicity implies an error that is always within the errors due to temperature uncertainties. We argue that, with the exception of absolute magnitude against colours and extreme cases (i.e. very metal-poor stars), the models described in this work can be treated as independent of the metal content of the star.

As an additional test, we used `VOSA` to perform a new SED fit of the CARMENES GTO stars in the sample using the `BT-Settl` grid of spectra ("no CIFIST"; Allard et al., 2012), which allowed us to explore iron abundances different from [Fe/H] = 0. In particular, we let [Fe/H] vary between −1.5 dex and +0.5 dex, with a step size of 0.5 dex, and constrained $T_{\rm eff}$ and $\log g$ as in Table 3.3. The [Fe/H] values derived from this new fit are compared to the spectroscopic values from the literature in Fig. 3.24. While the median of `VOSA` `BT-Settl` and published values are in fair agreement (−0.097 dex and +0.033 dex, respectively), the scatter of the `VOSA` [Fe/H] values is much greater than that of the literature ($\sigma_{\rm [Fe/H],VOSA} = 0.596$ dex and $\sigma_{\rm [Fe/H],literature} = 0.216$ dex). From the diagram, `VOSA` assigned artificially low [Fe/H] to stars with spectroscopically derived solar values, which reinforced our initial approach of setting [Fe/H] = 0. This is in line with the quality tests carried out by the `VOSA` team in 2017, in which they compared `VOSA` metallicities with those derived by Yee et al. (2017), Lindgren & Heiter (2017), and Rajpurohit et al. (2018b). In particular, they concluded that "metallicities [...] provided by `VOSA` are not reliable due to the minor contribution of [this parameter] to the SED shape"[12].

In Fig. 3.25 we compare the $\mathcal{L}$ and $T_{\rm eff}$ obtained for the GTO stars using `BT-Settl CIFIST` with [Fe/H] = 0 (used throughout this work) and `BT-Settl` with a free range in metallicity. While the derivation of bolometric luminosities in K dwarfs, with a normalised difference of $\Delta\mathcal{L}/\mathcal{L} = -0.0065 \pm 0.0046$, is marginally dependent on metallicity, the derivation in M dwarfs is independent: the normalised differences between $\mathcal{L}$ computed with the two methods is $\Delta\mathcal{L}/\mathcal{L} = 0.012 \pm 0.035$, consistent with zero. The

[12] http://svo2.cab.inta-csic.es/theory/vosa/.

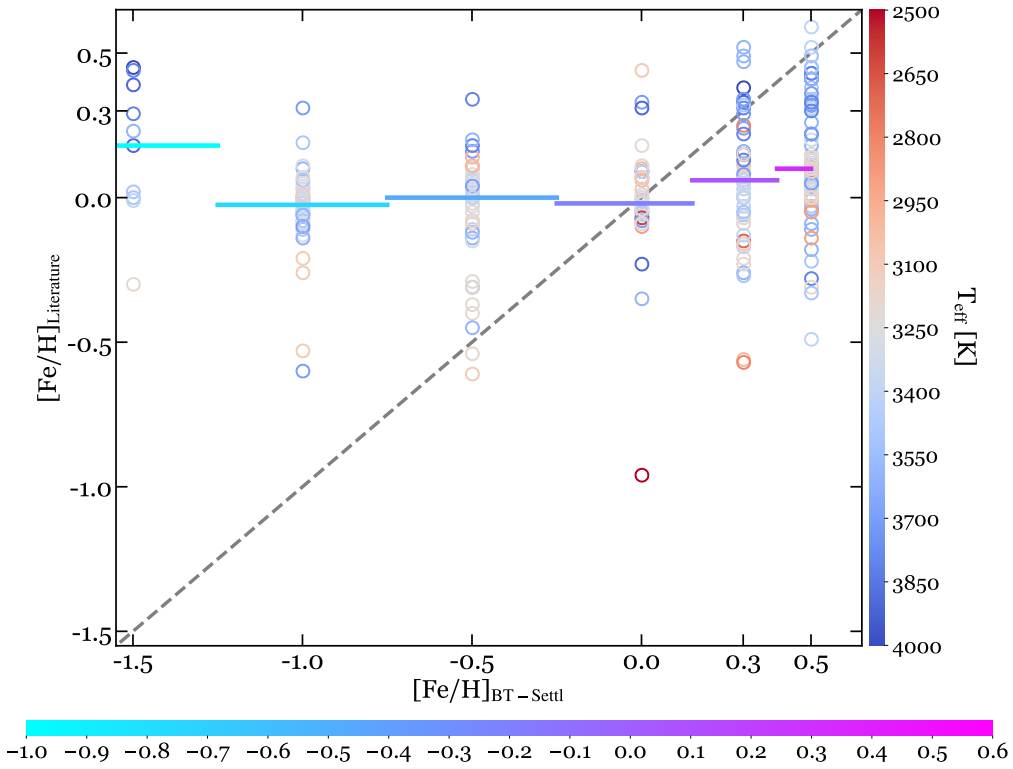

Figure 3.24: Comparison of metallicites from `VOSA` `BT-Settl` fit and from literature for CARMENES GTO M dwarfs, colour-coded by `BT-Settl CIFIST` $T_{\rm eff}$, and by [Fe/H], represented by the horizontal colourbar. Horizontal lines represent the median values in each `BT-Settl` [Fe/H] bin.

$T_{\rm eff}$ difference is also consistent with zero, and its standard deviation is 101 K, identical to the $T_{\rm eff}$ step size in the M-dwarf domain.

Radii (Fig. 3.26). We compared our $\mathcal{R}$, derived from `VOSA`'s $\mathcal{L}$ (`BT-Settl CIFIST`, [Fe/H] = 0) and $T_{\rm eff}$ using the Stefan-Boltzmann law, with the same works as in Fig. 3.21 (top left panel). Some of these works in turn compared their results with independent direct radius determinations (e.g. near-infrared interferometry – Boyajian et al., 2012; von Braun et al., 2014b). On average, our $\mathcal{R}$ are larger by $0.022 \pm 0.037\,\mathcal{R}_{\odot}$, meaning they are identical within the dispersion of the data. However, the standard deviation includes both random errors (in magnitudes, parallax, SED integration) and systematic errors (in passband $\lambda_{\rm eff}$ and $W_{\rm eff}$, `VOSA` minimisation procedure, CIFIST models), and the $\mathcal{R}$ difference appears systematically across the whole sample, so it is likely to be significant. Furthermore, because of the $T_{\rm eff}$ shift with respect to Passegger et al. (2018) and other spectral synthesis works, our $\mathcal{R}$ are also larger by about 5 % than those of Schweitzer et al. (2019), who used almost identical $\mathcal{L}$ to ours. For that reason, when $T_{\rm eff}$ from spectral synthesis on high-resolution spectra is available, we recommend using it together with our $\mathcal{L}$ for determining $\mathcal{R}$ (and $\mathcal{M}$), and use $T_{\rm eff}$ from `VOSA` when there is no spectral synthesis.

The offset in these diagrams, specially apparent in the bottom left panel, can include several causes. For one, non-resolved binarity is certainly a reason for a star to be overluminous (or oversized, in terms of the radius). As investigated in Chapter 4, this is the case for a sizeable amount of stars in the sample, but for the vast majority of cases there are only hints or clues of disguised multiplicity (specifically, via *Gaia* statistical indicators), but no actual confirmation. Because luminosities are empirical to a very large degree, we can be confident that they reflect the actual emitting power (i.e. luminosity) of the object. Also,

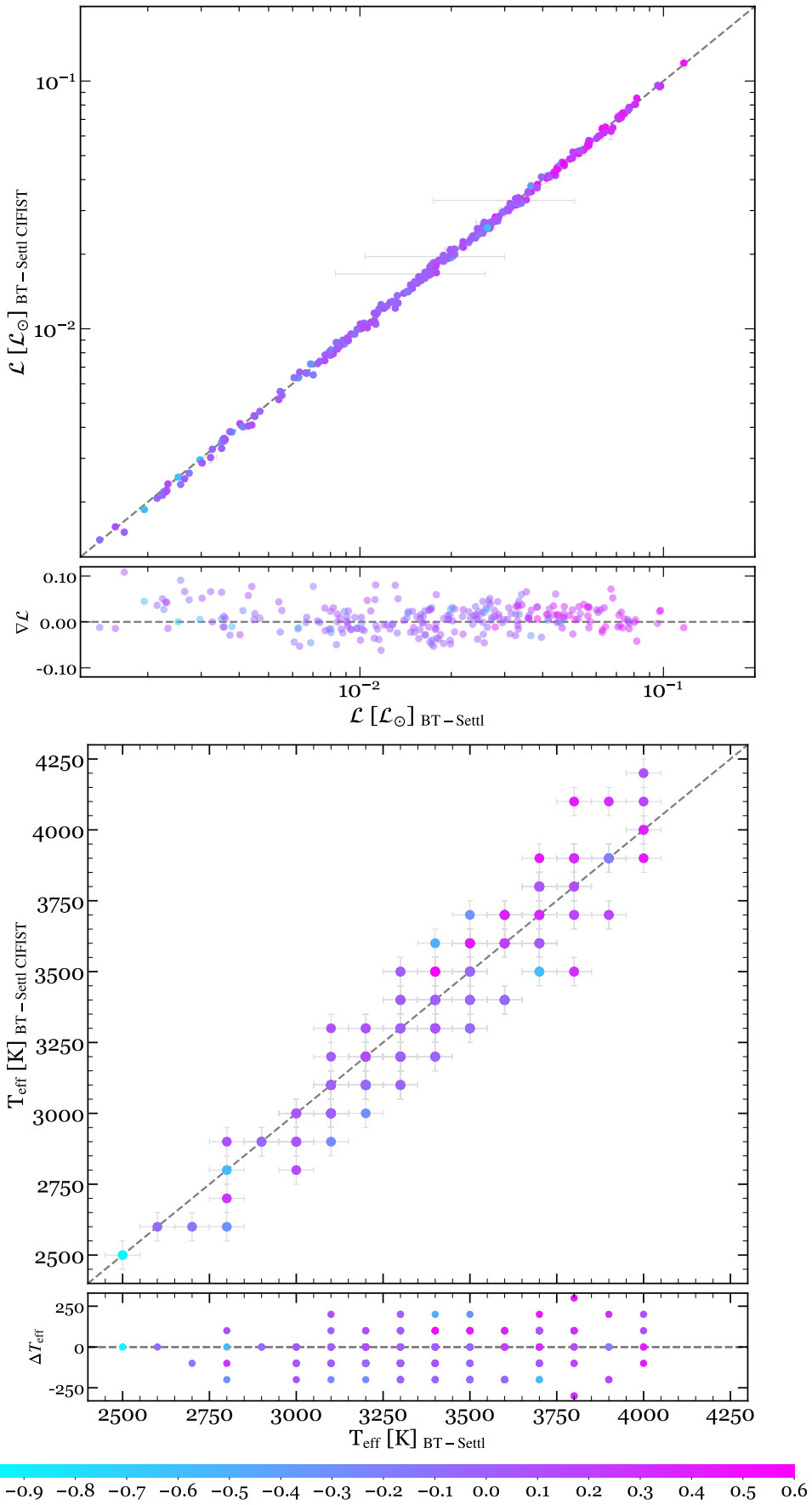

Figure 3.25: Comparison of previous and recomputed $\mathcal{L}$ (*top*) and $T_{\rm eff}$ (*bottom*) using `BT-Settl` with [Fe/H] = −1.5 to +0.5 for CARMENES GTO M dwarfs, colour-coded by metallicities published in the literature. The small bottom panels depict $\nabla L = \log \mathcal{L}_{\rm BT-Settl\,CIFIST} - \log \mathcal{L}_{\rm BT-Settl}$ and $\Delta T_{\rm eff} = T_{\rm eff,BT-Settl\,CIFIST} - T_{\rm eff,BT-Settl}$, respectively.

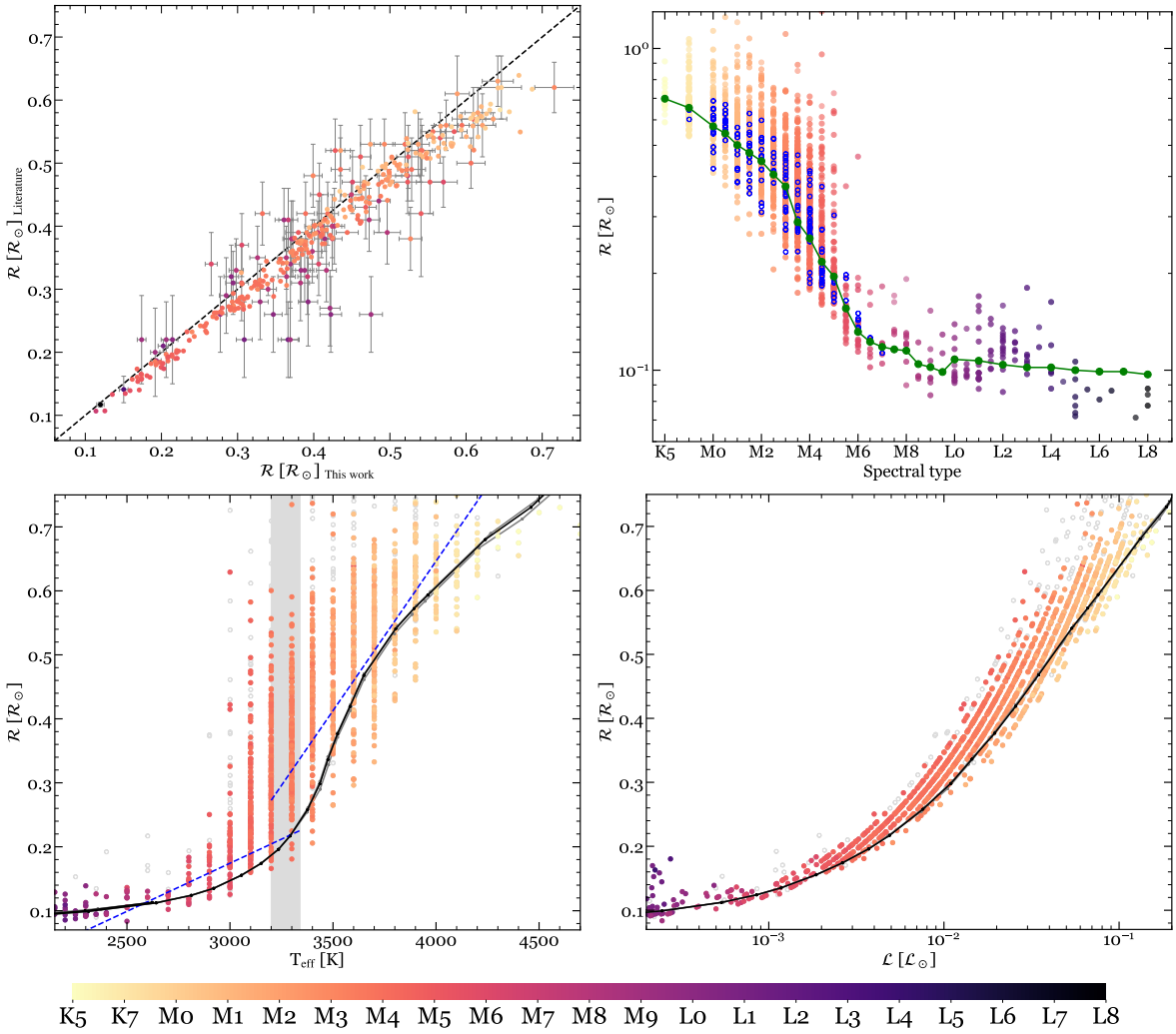

Figure 3.26: Four representative diagrams involving $\mathcal{R}$. In the four panels our investigated stars are represented with filled circles colour-coded by spectral type. *Top left:* Comparison of $\mathcal{R}$ from this work and from the literature, including Schweitzer et al. 2019 (with symbol-size error bars). *Top right:* Individual (coloured points) and median (black circles) values of $\mathcal{R}$ as a function of the spectral sequence shown in Table 3.6. The green line marks the median values from Pecaut & Mamajek (2013) and the blue circles are stars from Mann et al. (2015). *Bottom left:* $\mathcal{R}$ vs. $T_{\rm eff}$. The black and grey solid lines are the `NextGen` isochrones of the Lyon group for 1.0, 4.0, and 8.0 Ga (overlapping), the blue dashed lines are the linear fittings from Rabus et al. (2019), and the grey shaded area is the region where they reported a possible discontinuity. *Bottom right:* $\mathcal{R}$ vs. $\mathcal{L}$. The black solid lines are the same isochrones as in the bottom left panel.

their values are fundamentally unaffected by the uncertainty in synthetic models, because they almost do not rely on them. But probably a more decisive cause traces back to the models from which effective temperatures are inferred. Unfortunately, many stars lack detailed spectroscopic information, which would certainly help providing with more reliable effective temperatures (again, always preferred to those from fitted synthetic models), identifying potential compact binarity (i.e. spectroscopic binarity), and telling if a star does have signs to be young – all to better diagnose the causes for overluminosity.

In spite of the large spread at spectral types earlier than M4.5 V and some poorly sampled SEDs later than M7.0 V, the matches with the $\mathcal{R}$-spectral type relation of Pecaut & Mamajek (2013) and the values reported by Mann et al. (2015) are also good (top right panel). Our $\mathcal{R}$-$T_{\rm eff}$ diagram (bottom left panel) naturally reproduces the sigmoid shape predicted by the widely used theoretical models of Baraffe et al. (1998), but shifted by ∼100 K towards cooler $T_{\rm eff}$ (see previous paragraph). More than two decades after that cornerstone work by the Lyon group, Rabus et al. (2019) fitted an $\mathcal{R}$-$T_{\rm eff}$ relation using two linear polynomials and identified a discontinuous behaviour that the authors attributed to the transition between partially and fully convective stars at 3200–3340 K or ∼0.23 $\mathcal{M}_{\odot}$. Soon after, Cassisi & Salaris (2019) confirmed this discontinuity, but considered instead the contribution of the electron degeneracy to the gas equation of state as the physical phenomenon behind this behaviour (see also Chabrier & Baraffe, 1997). While the boundary between partially and fully convective stars is better exposed in for example the $NUV - G_{RP}$ versus spectral type diagram (see Fig. 3.15), in our data we did not find evidence for any discontinuity in the vicinity of 3250 K in the $\mathcal{R}$-$T_{\rm eff}$ diagram, but just a change of slope, as proven by Schweitzer et al. (2019, see their Fig. 11). The statistics in Rabus et al. (2019) were poorer than ours: they added around one hundred objects from Mann et al. (2015) to their sample of 22 low-mass dwarfs, while we have 1031 homogeneously investigated stars with $T_{\rm eff}$ in the 3000–3500 K interval. Furthermore, the continuity of $\mathcal{R}$ as a function of $\mathcal{L}$ is obvious in the bottom right panel of Fig. 3.26.

Masses (Fig. 3.27). We compared our $\mathcal{M}$, derived from our $\mathcal{R}$ and the $\mathcal{M}$-$\mathcal{R}$ relation of Schweitzer et al. (2019), with those from the literature (same works as in Fig. 3.21, top panel). This comparison is shown in the top panel of Fig. 3.27. Among our parameters, $\mathcal{M}$ is the one that shows more dissimilarities with respect to published values, although $\mathcal{M}_{\rm This\ work} - \mathcal{M}_{\rm lit} = 0.025 \pm 0.081\ \mathcal{M}_{\odot}$, consistent with a null difference (but probably significant as in $\mathcal{M}$ when random and systematic errors are taken into account). For example, the two stars for which our $\mathcal{M}$ deviate more than 80 % from published values are LP 229–17 (M3.5 V, $\mathcal{M}_{\rm This\ work} = 0.476 \pm 0.017\ \mathcal{M}_{\odot}$, $\mathcal{M}_{\rm lit} = 0.23 \pm 0.08\ \mathcal{M}_{\odot}$) and YZ CMi (M4.5 V, $\mathcal{M}_{\rm This\ work} = 0.368 \pm 0.008\ \mathcal{M}_{\odot}$, $\mathcal{M}_{\rm lit} = 0.19 \pm 0.08\ \mathcal{M}_{\odot}$), both from Gaidos & Mann (2014). The former star was tabulated as a spectroscopic binary by Houdebine et al. (2019), although we do not see any CARMENES radial-velocity variation attributable to binarity (Reiners et al., 2018b, see also Cortés-Contreras et al. 2017b for a lucky imaging analysis), while the latter star is a candidate member of the young β Pictoris moving group (not in Table 3.4 – Montes et al., 2001; Alonso-Floriano et al., 2015a) with strong chromospheric activity (Kahler et al., 1982; Kowalski et al., 2010; Tal-Or et al., 2018), which may partly explain the differences. In planet-host stars, such changes can translate into significant differences in the published (minimum) masses of M-dwarf planets.

We also compared our values of $\mathcal{M}$ with those calculated from the $\mathcal{M}$-M_K relations of Delfosse et al. (2000), valid for 4.5 mag ≤ M_K ≤ 9.5 mag, and Benedict et al. (2016), valid for M_K ≤ 10 mag, and the $\mathcal{M}$-M_{K_s} relation of Mann et al. (2019), valid for 4 mag ≤ M_{K_s} ≤ 11 mag, and "safe" for 4.5 mag ≤ M_{K_s} ≤ 10.5 mag. For the relations of Delfosse et al. (2000), we converted our 2MASS K_s magnitudes to CIT K values (Elias et al., 1982) using the colour transformation provided by Carpenter (2001). The means of the mass differences were: $\mathcal{M}_{\rm This\ work} - \mathcal{M}_{\rm Del00} = -0.0080 \pm 0.0320\ \mathcal{M}_{\odot}$, $\mathcal{M}_{\rm This\ work} - \mathcal{M}_{\rm Ben06} = 0.0242 \pm 0.0474\ \mathcal{M}_{\odot}$, and $\mathcal{M}_{\rm This\ work} - \mathcal{M}_{\rm Man19} = 0.0042 \pm 0.0223\ \mathcal{M}_{\odot}$ Taking into account the standard

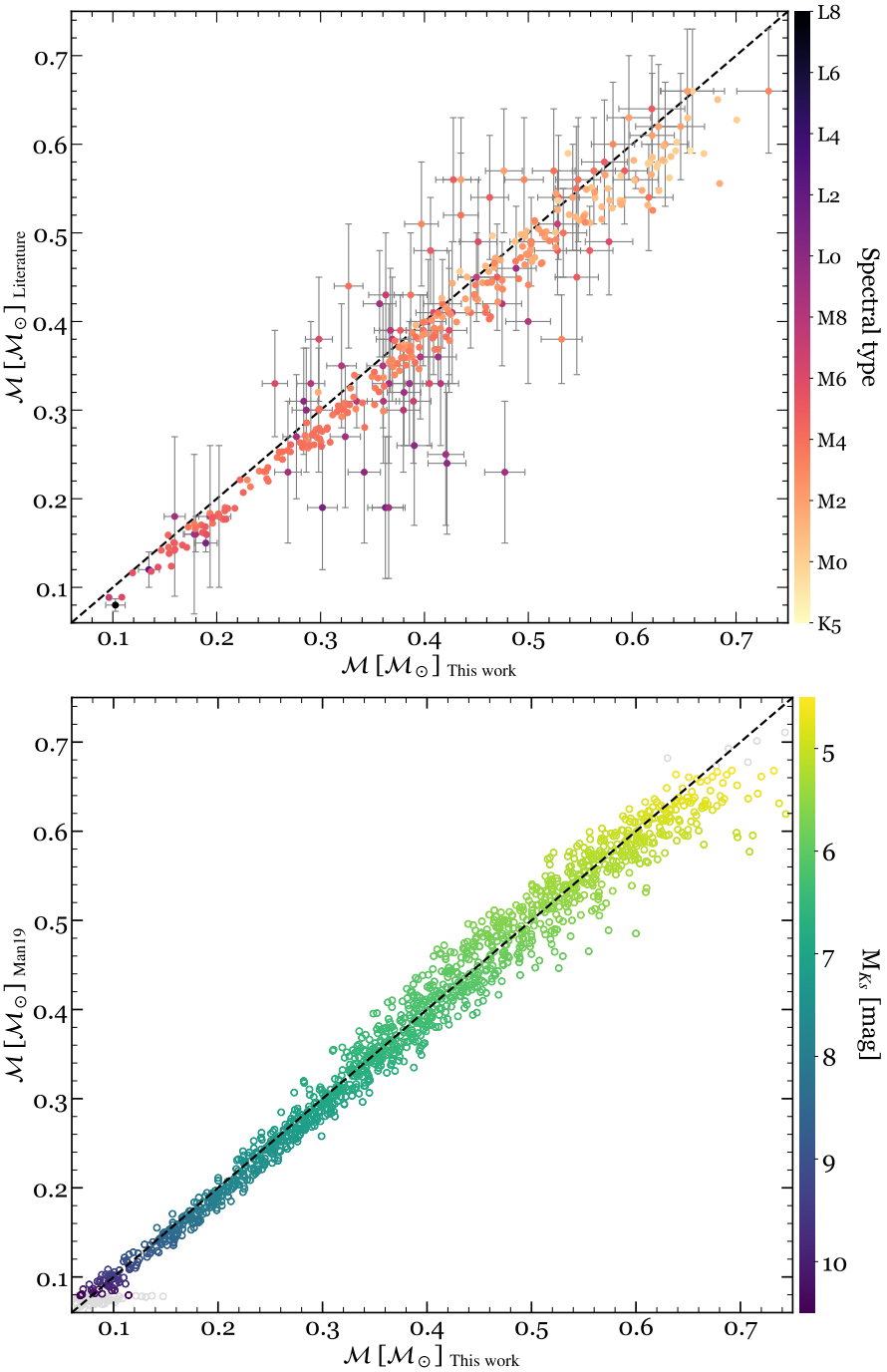

Figure 3.27: *Top:* Comparison of our masses with those from the literature. *Bottom:* Comparison with those derived from absolute magnitude M_{K_s} using the metallicity-independent relation from Mann et al. (2019) only in its validity range (4.5 mag < M_{K_s} < 10.5 mag).

deviations, Mann et al. (2019) provided the relation that best matched our $\mathcal{M}$. In the bottom panel of Fig. 3.27 we show this relation, valid in a wide mass range from 0.075 $\mathcal{M}_\odot$ to 0.70 $\mathcal{M}_\odot$. Since we fixed [Fe/H] = 0, we used the Mann et al. (2019) relation independent of metallicity ($f = 0$). Besides, the authors stated that the impact of [Fe/H] is sufficiently weak for the $f = 0$ relation to be safely used for most stars in the solar neighbourhood.

Colours (Fig. 3.28). Although with the advent of *Gaia* the $V-J$ colour should be replaced by $G-J$, the former had been used extensively in the past. The match of our mean $V-J$ colours as a function of $T_{\rm eff}$ with those of Pecaut & Mamajek (2013) is once again excellent, but the relation significantly deviates from the values tabulated by Casagrande et al. (2008). However, as noted by them, the range of applicability of their colour-temperature-metallicity relations involving $V-J$ is narrow, between 0.61 mag and 2.44 mag. As a result, from the top left panel, extrapolating the $T_{\rm eff}$ versus $V-J$ relation of Casagrande et al. (2008) beyond 2.44 mag may result in $T_{\rm eff}$ systematically cooler by more than 300 K. In the top right panel, we revisit the $r'-i'$-spectral type diagram, which is an evolution of that with $R-I$ colour in the Johnson-Cousins passbands (Veeder, 1974; Bessell, 1979; Leggett, 1992; Boyajian et al., 2012; Mann et al., 2015; Houdebine et al., 2019). We reproduce the reversal at M7.0–8.0 V ($r'-i' \sim 2.8$ mag) observed by Hawley et al. (2002), Bochanski et al. (2007), and West et al. (2008), among many others. Therefore, we confirm that the $r'-i'$ colour alone cannot be used for spectral classification beyond M5.0 V. In the optical colour-colour diagram of the bottom left panel, our $g'-r'$ colours are slightly bluer than those of Davenport et al. (2014) for a fixed $r'-i'$, and significantly bluer, by about 0.5 mag, than those of Bochanski et al. (2007). Finally, in the bottom right panel, there is a good agreement with the location of the M-dwarf main sequence of Knapp et al. (2004) in the near-infrared M_J versus $J-K_s$ diagram, but our data show instead the turnovers towards bluer and redder $J-K_s$ colours of late-K dwarfs and early-L dwarfs, respectively.

Online table We provide a summary table[13] with the compiled astro-photometric data and derived stellar parameters of all our targets. The description of the columns is given in Table D.1. The assembled catalogue in comma separated value (csv) format is available in its entirety in the electronic edition of this article. For each star or ultracool dwarf we tabulate its identifiers, equatorial coordinates, spectral type (and reference), parallax and distance (and reference), all magnitudes and their uncertainties, origin, quality flags (when available), $\mathcal{L}$, $T_{\rm eff}$, and $\log g$ from `VOSA`, $\mathcal{R}$ and $\mathcal{M}$ from the Stefan-Boltzmann law and the $\mathcal{M}$-$\mathcal{R}$ relation, *Gaia* DR2 identifier for primary and secondary sources (in the case of binary sources), four Boolean indices for close multiplicity ($\rho < 5$ arcsec), astrometric and photometric quality of the *Gaia* solution, and youth. Finally, most of the `Python` code developed by us for determining the parameters or preparing the plots shown in this work is available at GitHub[14].

3.4 Stellar characterisation

3.4.1 Different roads to radii and masses of the target stars

In Schweitzer et al. (2019) we homogeneously determined radii and masses for a sample of 293 nearby M dwarfs in Carmencita, presenting four routes to achieve it, represented by $\mathcal{M}_{\mathcal{M}-\mathcal{R}}$, $\mathcal{M}_{\log g}$, $\mathcal{M}_{K_s}$, $\mathcal{M}_{\rm P}$. Two groups of ingredients can provide these fundamental parameters, used both together and inde-

[13] https://cdsarc.cds.unistra.fr/viz-bin/cat/J/A+A/642/A115.
[14] https://github.com/ccifuentesr/CARMENES-V.

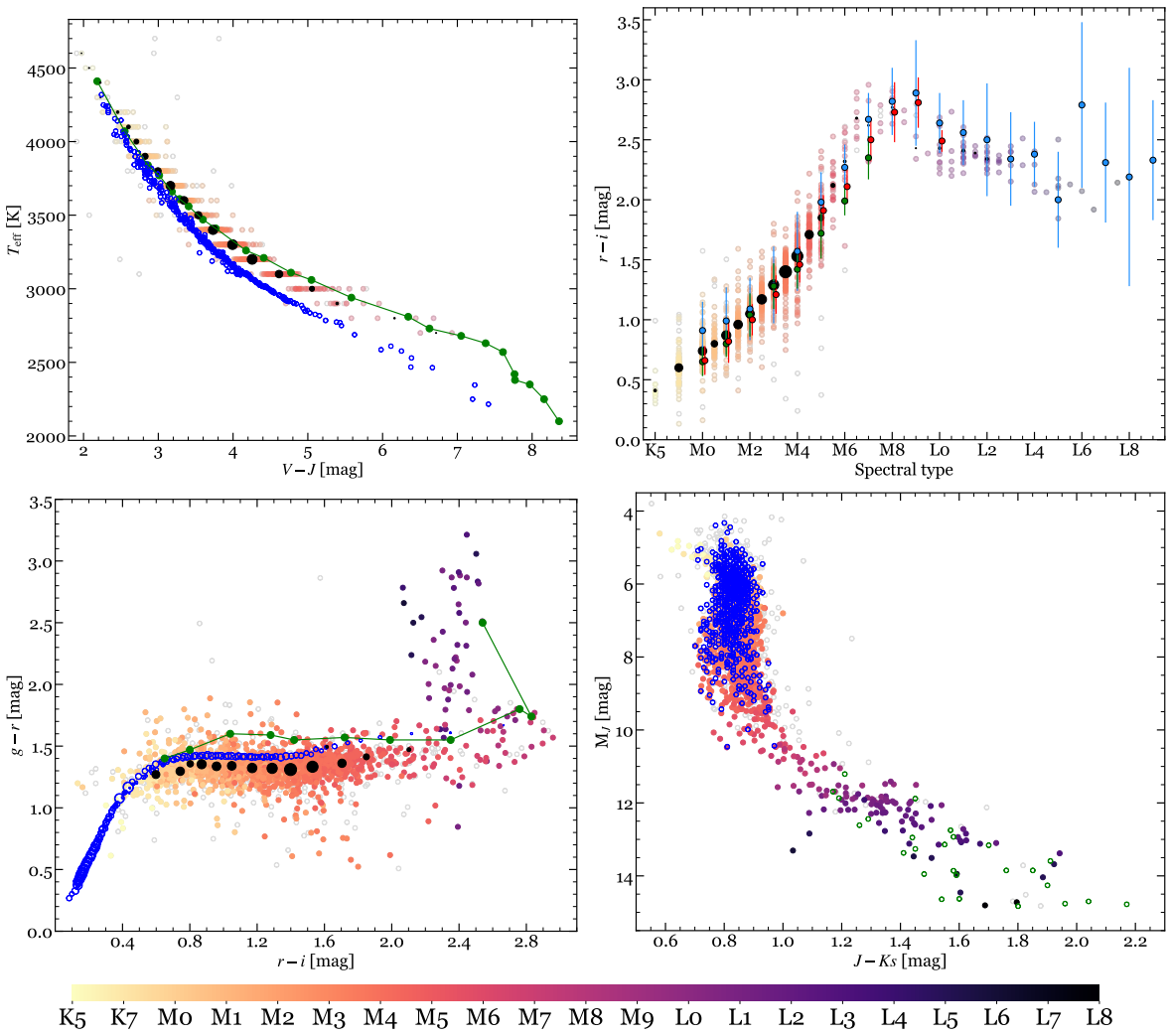

Figure 3.28: *Top left:* $T_{\rm eff}$ vs. $V-J$. The blue empty circles and green line are data from Casagrande et al. (2008) and Pecaut & Mamajek (2013), respectively. Black filled circles are the mean colours from 2700 K to 4600 K in our sample, with a size proportional to the number of stars. *Top right:* $r'-i'$ vs. spectral type. Open circles are the mean colours of Hawley et al. (2002, blue), Bochanski et al. (2007, "inactive" colours, green), and West et al. (2008, red). Black filled circles are the mean colours from K5 V to L2 in our sample, taken from Table C.2, with a size proportional to the number of stars. The error bars are the standard deviation (Hawley et al., 2002; Bochanski et al., 2007) and the intrinsic scatter of the stellar locus (West et al., 2008). *Bottom left:* $g'-r'$ vs. $r'-i'$. Black filled circles are the mean colours from K5 V to L2 in our sample, taken from Table C.2, with a size proportional to the number of stars. Blue empty circles are the mean colours by Davenport et al. (2014), with a size proportional to the numbers of stars, and the green line links the mean "inactive" colours by Bochanski et al. (2007) for spectral types M0 V to L0. *Bottom right:* M_J vs. $J-K_s$. Green and blue empty circles are data from Knapp et al. (2004) and Lépine et al. (2013), respectively. In the four panels, the stars in our sample are colour-coded by spectral type, and the discarded stars are plotted with grey empty circles.

Table 3.8: Description of the online table.

Parameter	Units	Column(s)	Description
Karmn	…	1	Carmencita star identifier (JHHMMm+DDd)[a]
Name	…	2	Discovery name or most common name[b]
RA, DE	hms	3–4	Right ascension and declination (equinox J2000, epoch 2015.5)
SpType, SpTnum	…	5–6	Spectral type and its numerical format[c]
Ref_SpT	…	7	Reference for the spectral type
Plx, ePlx	mas	8–9	Parallax and its uncertainty
Ref_Plx	…	10	Reference for the parallax
d_pc, ed_pc	pc	11–12	Distance and its uncertainty
Ref_d	…	13	Reference for the distance
Lbol, eLbol	$L_\odot$	14–15	Luminosity and its uncertainty from VOSA
Teff	K	16	Effective temperature from VOSA[d]
logg	dex	17	Surface gravity from VOSA[d]
Radius, eRadius	$\mathcal{R}_\odot$	18–19	Radius and its uncertainty
Mass, eMass	$\mathcal{M}_\odot$	20–21	Mass and its uncertainty
NN_mag, eNN_mag	mag	22–97	Magnitude and its uncertainty for the NN passband[e]
Qf_NN, Ref_NN	mag	22–97	Quality flag (if available) and reference for the NN passband[e]
Gaia_id_1	…	98	*Gaia* DR2 identifier of single or primary star
Gaia_id_2	…	99	*Gaia* DR2 identifier of secondary star in close binary system
Multiple	…	100	Boolean index for close multiple stars
Young	…	101	Boolean index for overluminous young stars
ruwe	…	102	Boolean index for stars with *Gaia* ruwe > 1.41
Excess	…	103	Boolean index for stars with photometric flux excess in *Gaia* G_{B_P} and G_{R_P} passbands

[a] For the K dwarfs, we tabulate the SUPERBLINK catalogue identifier (Lépine & Shara, 2005; Lépine et al., 2013).
[b] For the ultracool dwarfs, we tabulate the *Gaia* UltraCool Dwarf Catalogue identifier (Smart et al., 2017, 2019).
[c] SpTnum = –2 for K5 V, –1 for K7 V, 0.0 for M0.0 V, 0.5 for M0.5 V... 10.0 for L0.0, etc.
[d] VOSA uncertainties are 50 K for $T_{\rm eff}$ (25 K for $T_{\rm eff} \lesssim 2400$ K) and 0.5 dex for log g.
[e] FUV, NUV: GALEX DR5 FUV and NUV; BP, GG, RP: G_{B_P}, G, and G_{R_P} from *Gaia* DR2; BT, VT: B_T and V_T from Tycho-2; B, V: B and V from UCAC4 or APASS9; u, g, r, i: u', g', r', and i' from SDSS9, UCAC4, APASS9, PanSTARRS-1 and/or CMC15; J, H, Ks: J, H, and Ks from 2MASS; W1, W2, W3, W4: $W1$, $W2$, $W3$, and $W4$ from AllWISE or WISE.

pendently. These are broadband photometry from the ultraviolet to the mid-infrared (see Table 3.1), and photospheric parameters (effective temperature, $T_{\rm eff}$, surface gravity, $\log g$, and iron abundance, [Fe/H]), obtained by fitting PHOENIX-ACES synthetic spectra (Husser et al., 2013) to the CARMENES spectra of the visual channel as described in Passegger et al. (2016, 2018), and later extended to include the near-infrared channel, using SteParSyn (Passegger et al., 2019; Marfil et al., 2021). Figure 3.29 shows a schema of the possibilities.

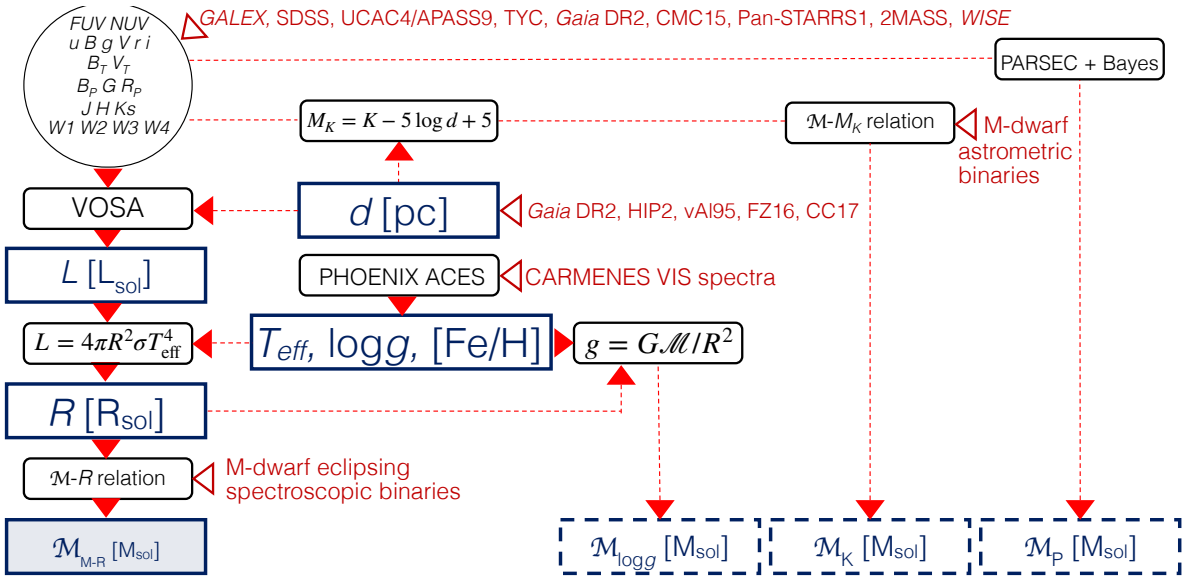

Figure 3.29: Flowchart of the different roads to masses (extracted from Schweitzer et al. 2019).

From integrated broadband photometry, together with the *Gaia* DR2 parallaxes, we obtained the bolometric luminosities $\mathcal{L}$ using VOSA, and Stefan-Boltzmann's law provides the radius, given that the effective temperature is known. The radius offers two routes for deriving masses. First, using an empirical relation between masses and radii from eclipsing binaries ($\mathcal{M}_{\mathcal{M}-\mathcal{R}}$). Second, from the definition of surface gravity, $\log g$ ($\mathcal{M}_{\log g}$), by fitting PHOENIX-ACES synthetic spectra (Husser et al., 2013) to the CARMENES spectra of the VIS channel, as in Passegger et al. (2016, 2018). From photometry alone (r and J), another method consist of a Bayesian approach that uses PARSEC library of stellar evolution models. The absolute magnitudes of our stars, M_J, were compared to synthetic models, using the colour $r - J$ and assuming solar metallicity, and the mass ($\mathcal{M}_{\rm P}$) was derived from this comparison. Finally, among the mass-magnitude relations available in the literature using infrared filters (Delfosse et al., 2000; Benedict et al., 2016, e.g.), we used the M_{K_s}-$\mathcal{M}$ relation from Mann et al. (2019). This way we obtain the mass from absolute magnitude ($\mathcal{M}_{K_s}$). The comparison between the masses obtained using the four routes is shown in Fig. 3.30). Because the metallicity was also a product of the spectral analysis, the plots account for this parameter.

The four methods used in this work delivered masses for 293 M dwarfs from the CARMENES GTO sample that we found in good agreement for the majority of our targets. These are typical field stars that are not too young, but show discrepancies in the case of very young objects. particularly when using the masses $\mathcal{M}_{\mathcal{M}-\mathcal{R}}$ and $\mathcal{M}_{\rm M-K_s}$. In the case of $\mathcal{M}_{\rm P}$, though, the relation is not restricted to a single age, and with $\mathcal{M}_{\log g}$ it is possible to use isochrones given that the age of the star is known. Between spectral types M0 V and M7 V our radii covered the range $0.1\,\mathcal{R}_\odot < \mathcal{R} < 0.6\,\mathcal{R}_\odot$ with an error of 2–3% and our masses cover $0.09\,\mathcal{M}_\odot < \mathcal{M} < 0.6\,\mathcal{M}_\odot$ with an error of 3–5%. The methods work best for a field star of at least a few hundred million years when it is possible to spectroscopically determine an effective temperature and when $\mathcal{L}$ is well determined with multiwavelength, broadband photometry, and an accurate parallax.

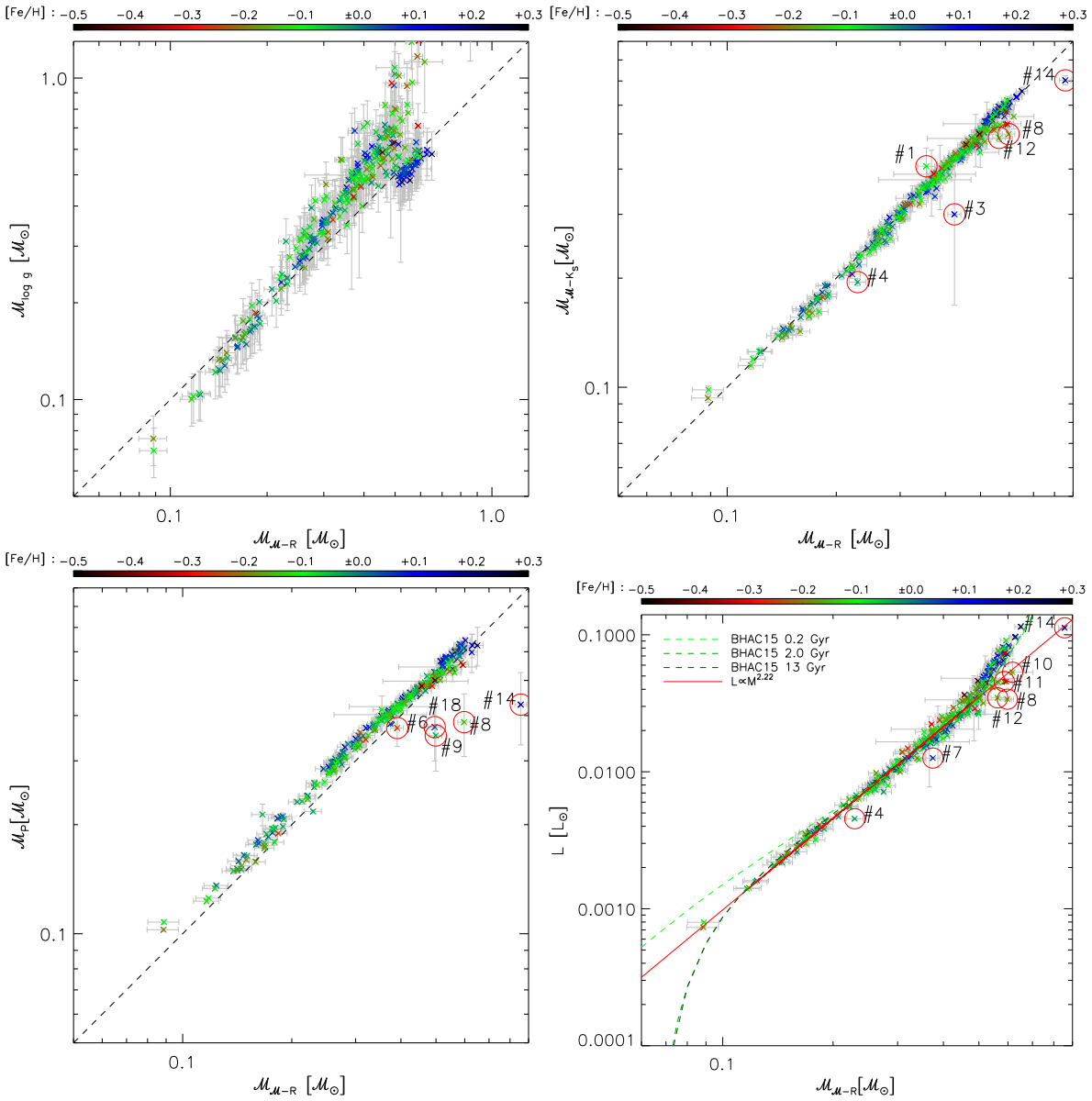

Figure 3.30: Comparison of masses for the stars studied in Schweitzer et al. (2019), obtained from detached, double-lined, double-eclipsing, main-sequence M dwarf binaries, $\mathcal{M}_{\mathcal{M}-\mathcal{R}}$, colour-coded by metallicity, against: Spectroscopic masses, using surface gravity, $\log g$, from fitting synthetic spectra $\mathcal{M}_{\log g}$ (*top left*), photometric masses from absolute magnitude M_{K_s}, as in Mann et al. (2019), $\mathcal{M}_{\mathcal{M}-\mathrm{K_s}}$ (*top right*), PARSEC-based masses with a Bayesian approach, $\mathcal{M}_\mathrm{P}$ (*bottom left*), and bolometric luminosities, with isochrones for 0.2, 2.0, and 13 Ga as dashed lines in increasingly darker green, from BHAC15 (*bottom right*). The black dashed lines marks the 1:1 relation, and the red solid line indicates the fit $\mathcal{L} \propto \mathcal{M}^{2.22\pm0.02}$. Obvious outliers are tagged in the fours plot, and discussed in detail in the original article.

3.4.2 Exomoons in the habitable zones of M dwarfs

Similarly to exoplanets, exomoons can also be targets for biosignature surveys. In Martínez-Rodríguez et al. (2019) we investigated the habitability, stability, and detectability of potential exomoons of exoplanets that orbit M dwarfs. While exoplanets in the CHZ of M dwarfs can be hostile environments to life, the existence of stable exomoons may alleviate this issue.

For 205 exoplanets orbiting 109 M dwarfs discovered with the radial velocity or transit methods, we compiled orbital, astrometric, photometric, and basic astrophysical parameters. For 192 of them, we estimated the most probable masses and radii using the models of Chen & Kipping (2017), assuming literature values for the remaining 13 planets. For the stars we derived luminosities, masses, and radii proceeding as in Cifuentes et al. (2020), and determined the inner and outer habitable zone boundaries for every star using a one-dimensional climate model. We found that 33 of the known planets orbit within the zone of habitability (Fig. 3.31). In Table C.3 we provide a complete characterisation of these systems, including whether they fall in the habitable zone[15].

For these we modelled non-eccentric, non-obliquous moons, and computed moon migration timescales for two different scenarios: strip-away from the planet, and fall-back onto the planet. Additionally, we took into consideration the planetary spin with two conditions: a maximum value equal to the orbital period (i.e. tidally locked to the star), and a minimum value of 3 h.

In the $P_0 = P_{\rm orb}$ scenario, all hypothetical moons fall back onto their planets after short time scales, except for four planets that survive because the migration time scales are longer than the Hubble time and, more interestingly, longer than protoplanetary disk dissipation times . These are Ross 1003 b, IL Aqr b and c, and CD-23 1056 b), and they may potentially harbour life and be targets for biosignature surveys. We further explored whether if their mantles would partially melt under the effects of tidal heating. Io is an example of this effect in the Solar System. Similarly to the Moon that is the main cause for the tides in the Earth oceans, Jupiter is responsible for bending the surface of Io back and forth, building up heat that makes the interior melt and boil. This may be the reason why Io is the most volcanically active object in the Solar System (see Tyler et al., 2015). Only a potential exomoon in IL Aqr c could suffer from melting. Even when most of these four planets are tidally locked to their host stars, it may still be possible for the hypothetical exomoons to retain the conditions for habitability. And even if their planets might not host liquid water because they are icy neptunians, some of their hypothetical exomoons could instead. Is in this sense that exomoons could alleviate the problem of habitability in many cases.

The two of observable effects that moons produce around exoplanets require that the planet transits. In one, the transit of the moon is superimposed of photometric transits, on the other the timing and length of the transits of the planet is perturbed (Kipping, 2009a,b). Hypothetical moons in suitable (stable) planets like the four exoplanets selected in this work would exhibit large orbital periods, which minimises the opportunities for transiting episodes. An opportunity may come first for the most massive moons, by the depth of its transit. In this eclipsing event, the massive moon might retain an atmosphere that could potentially be detected. Some of the missions that might be able to perform these detections are *CHEOPS* (Fortier et al., 2014), the upcoming *PLATO*[16] (Rauer et al., 2014), *Kepler*-class photometry (Kipping et al., 2009), or ESPRESSO (Pepe et al., 2010), via the Rossiter-McLaughlin effect as in Zhuang et al. (2012).

To end up with, it is worth mentioning the work by Tokadjian & Piro (2020), which is an extension of

[15] The list of derived parameters, as well as the code produced in this work can be found in the GitHub public repository (https://github.com/hector-mr/Exomoons_HZ_Mdwarfs).

[16] PLAnetary Transits and Oscillation of stars (*PLATO*) is an European Space Agency (ESA) mission to be launched in the last quarter of 2026.

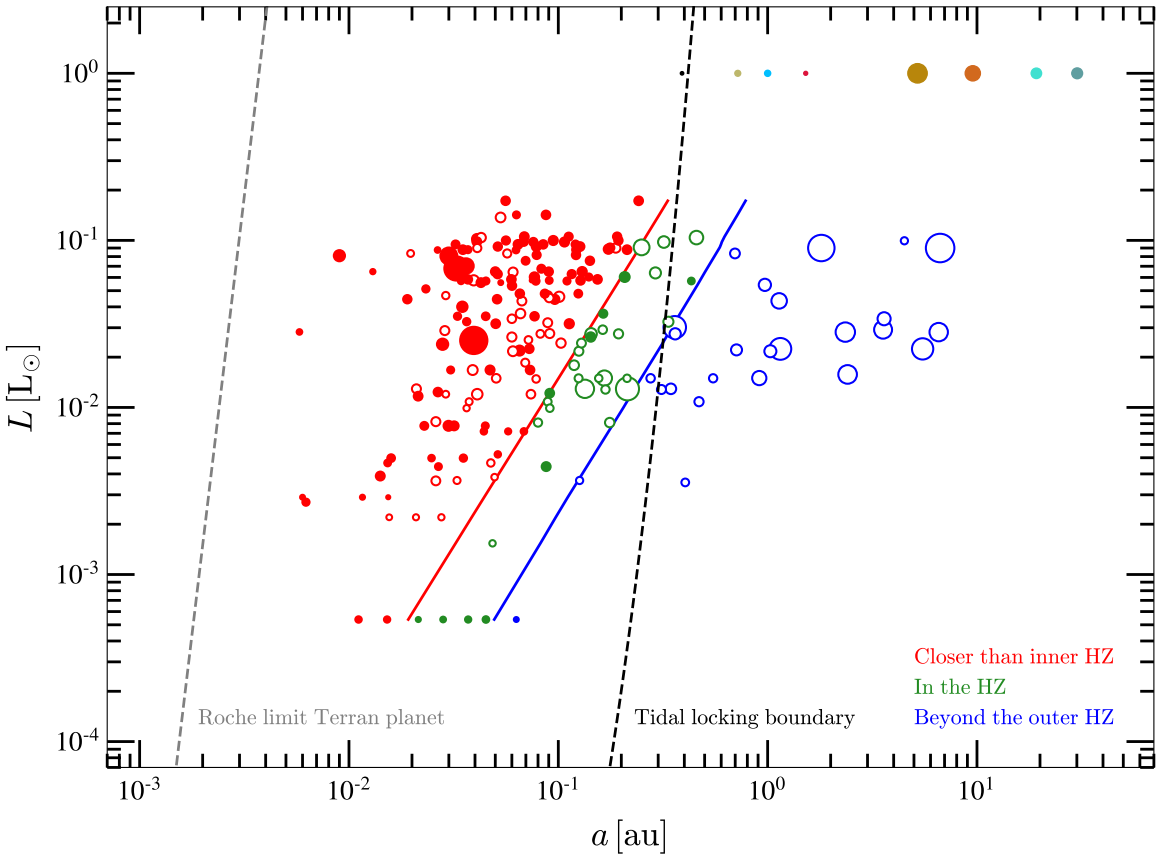

Figure 3.31: Conservative HZ for all the M dwarfs in the sample. Their hosted exoplanets are depicted with sizes proportional to their masses, with filled circles if they have been detected by transit and with open circles if they have been detected by RV measurements. Exoplanets closer than the inner HZ, in the HZ, and beyond the outer HZ are shown in red ("recent Venus"), green, and blue ("maximum greenhouse"), respectively. The dashed lines are the Roche limit for an Earth-like planet (Aggarwal & Oberbeck, 1974) in grey, and a "constant-time-lag" tidal locking model for a 10 $\mathcal{M}_\odot$-planet with rapid initial rotation after 1 Ga (Barnes, 2017), in black. The eight Solar System planets are depicted in the upper area (extracted from Martínez-Rodríguez et al. 2019).

that by Martínez-Rodríguez et al. (2019). The work explores the potential for exoplanets to host exomoons using differential equations to model the orbital and rotational evolution of planet-star-moon systems. The authors identified 36 exoplanets that may be good candidates for hosting exomoons, including Kepler-22b, Kepler-1638 b, Kepler-991 b, Kepler-1635 b, and Kepler-1625 b. The authors suggest that the detection of exomoons may be an important constraint on exoplanet structure, and call for more detailed models of tidal dissipation in future research.

3.4.3 GTO and Legacy

Many works in the last two years have benefited from astrophysical parameters derived in Schweitzer et al. (2019), Cifuentes et al. (2020), or have proceeded in the same manner as theirs with the latest astrometric, photometric and spectroscopic parameters available. In Table 3.9 we list a sample of a selection of published works, whose stellar description benefited from our characterisation, most of them corresponding to planet detections.

Table 3.9: Published planet-detection works with parameters derived by us.

Work	System	$\mathcal{L}_\star$ $[10^{-4}\,\mathcal{L}_\odot]$	$\mathcal{M}_\star$ $[\mathcal{M}_\odot]$	$\mathcal{R}_\star$ $[\mathcal{R}_\odot]$
Suárez-Mascareño et al. [2023]	GJ 1002	14.06 ± 0.19	0.120 ± 0.010	0.137 ± 0.005
Kossakowski et al. (2023)	GJ 806	29.44 ± 0.28	0.167 ± 0.011	0.1813 ± 0.0063
Palle et al. (2023)	GJ 806	259.9 ± 0.9	0.413 ± 0.011	0.4144 ± 0.0038
Blanco-Pozo et al. (2023)	GJ 1151	33.15 ± 0.18	0.1639 ± 0.0093	0.1781 ± 0.0042
Chaturvedi et al. (2022)	TOI 1468	159.5 ± 0.9	0.339 ± 0.011	0.344 ± 0.005
Kossakowski et al. (2022)	AD Leo	235.9 ± 1.1	0.423 ± 0.012	0.423 ± 0.006
Luque et al. (2022b)	G 9-40	109.6 ± 1.9	0.295 ± 0.014	0.303 ± 0.009
Caballero et al. (2022)	Gl 486	121.20 ± 0.82	0.333 ± 0.019	0.339 ± 0.015
Kemmer et al. (2022)	GJ 3929	115.5 ± 1.1	0.309 ± 0.014	0.315 ± 0.010
Espinoza et al. (2022)	TOI 1759	876.7 ± 6.3	0.606 ± 0.020	0.597 ± 0.015
Kossakowski et al. (2021)	TOI 1201	340.0 ± 5.7	0.512 ± 0.020	0.508 ± 0.016
	TOI 393	268.3 ± 2.5	0.463 ± 0.018	0.462 ± 0.014
Amado et al. (2021)	Gl 393	268.7 ± 5.4	0.426 ± 0.017	0.426 ± 0.013
	G 264-012	106.6 ± 1.1	0.297 ± 0.024	0.305 ± 0.011
Trifonov et al. (2021)	Gl 486	121.0 ± 2.3	0.333 ± 0.019	0.339 ± 0.015
Bluhm et al. (2021)	TOI-1685	303.5 ± 5.4	0.495 ± 0.019	0.492 ± 0.015
Soto et al. (2021)	LHS 1478	71.5 ± 1.2	0.236 ± 0.012	0.246 ± 0.008
Luque et al. (2021)	TOI-776	490 ± 20	0.544 ± 0.028	0.538 ± 0.024
Kemmer et al. (2020)	GJ 3473	150.0 ± 1.9	0.360 ± 0.016	0.364 ± 0.012
Baroch et al. (2020)	YZ CMi	113 ± 17	…	0.369 ± 0.055

Chapter 4

Multiplicity

Among the many possibilities of observational astronomy, stellar multiplicity may well be regarded as one of the most appealing. The existence of double stars has been recognised historically, but their true nature remained elusive even long after the invention of the telescope. Michell (1784) proposed that the odds of so many systems to appear so close by pure chance was of 500 000 to 1, at the supposition that they had been scattered by mere chance[1]. It was later admitted that the apparently fixed stars had a proper motion, hence the idea that stars that lied close in the sky were mutually affected gained interest. Observing the proper motions of several pairs, Mayer (1778) published the first catalogue of double stars, which contained 72 systems. William Herschel catalogued 898 visual doubles, which the majority were later confirmed physical pairs (Herschel & Banks, 1782; Herschel, 1785, 1822). The terrain was thereafter meticulously traveled by many others (e.g. Struve, 1837; Herschel et al., 1874; Burnham, 1906; Aitken & Doolittle, 1932, and more recently Tokovinin 1997, 2018; Mason et al. 2009; Raghavan et al. 2010). Worley (1962) carried out one of the first systematic studies of M dwarfs, which became a progenitor of the main database of astrometric double and multiple systems of use today, the Washington Double Star catalogue (WDS; Worley & Douglass, 1997; Mason et al., 2001), whose lineage traces back over 100 years. WDS collects to date 155 438 systems, with precise astrometric history and orbital description for many of the pairs.

4.1 Introduction

Mizar and Alcor (ξ Ursae Majoris) constitute an epitome of the advance of astronomical technique in this matter. Easily visible by the naked eye, at least as a single star, it is the fourth brightest star in the

[1] "The very great number of stars that have been discovered to be double, triple, &c. particularly by Mr. Herschel, if we apply the doctrine of chances, as I have heretofore done in my *Enquiry into the probable Parallax, &c. of the Fixed Stars* (Michell, 1767), cannot leave a doubt with any one [...] that by far the greatest part, if not all of them, are systems of stars so near to each other, as probably to be liable to be affected sensibly by their mutual gravitation; and it is therefore not unlikely, that the periods of the revolutions of some of these about their principals [...] may some time or other be discovered."

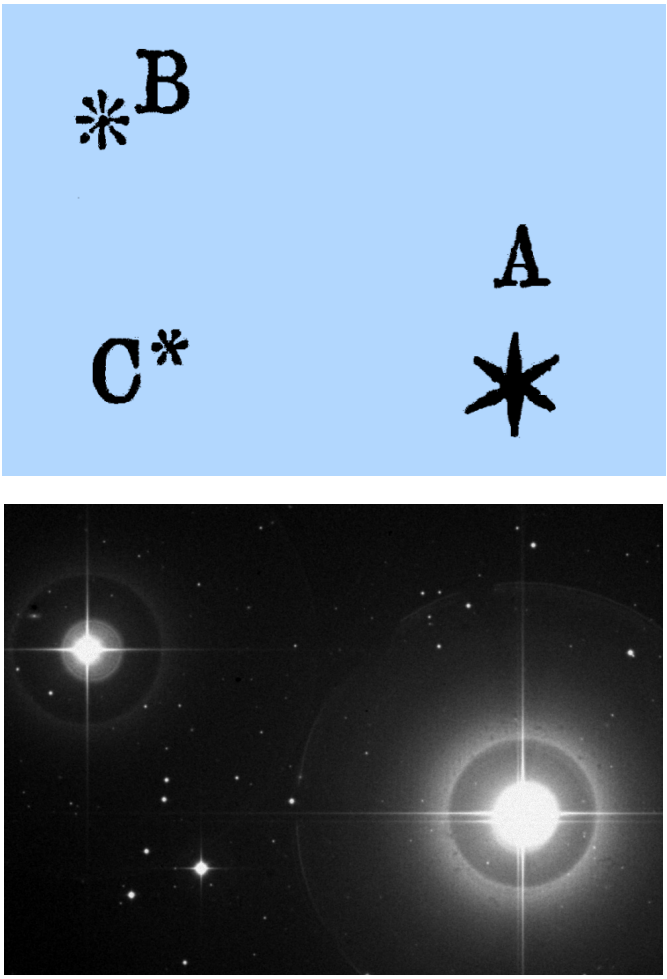

Figure 4.1: Castelli's asterism including Mizar (A), Alcor (B), and "Sidus Ludoviciana" (C). From Galileo's *Opere*, circa 1617 (*top*), and the same view from the Digitized Sky Survey (DSS) photographic plates, in red filter from the POSS-II F survey, 1991 (*bottom*).

Big Dipper. Although known to serve as a visual acuity test more than a thousand years ago (al-Sufi, 964 CE, and see Bohigian, 2008), it was the Benedictine monk Benedetto Castelli who first proposed to Galileo a systematic observation of the pair (Fig. 4.1)[2]. Through the recently invented telescope, Galileo separated the pair in 1617 (Siebert, 2005). Mizar and Alcor evolved from a visual binary, seemingly unconnected in ancient times, into a well-defined, physically bound sextuple system (Maury & Pickering, 1897; Ludendorff, 1908; Mamajek et al., 2010). Because of its relevance, stellar multiplicity has undergone intense scrutiny over the years to the point that some evidence suggest that all stars form as binaries. A successful theory of star formation should be able to explain why do we observe some stars that belong to multiple systems while many others do not, and how the multiple systems come to be as they are – for instance, how many pairs are found depending on the physical separation.

Stellar multiplicity is a common outcome of the stellar formation process (Heintz, 1969; Larson, 1972; Batten, 1973; Poveda et al., 1982; Abt, 1983; Pringle, 1989; Duquennoy & Mayor, 1991; Fischer & Marcy, 1992; Chapman et al., 1992; Mathieu et al., 2000; Tokovinin, 2008, and see Duchêne & Kraus 2013 for a review; cf. Lada 2006). The frequency of multiple systems increases with the primary stellar mass (Lada, 2006; Parker & Meyer, 2014). The observational evidence is that the percentage of OBA main

[2] Sidus Ludoviciana or Ludwig's star (HD 116798) is a bright ($G = 7.5$ mag), distant ($d \simeq 91.2$ pc), giant star (A8/F0 III), in Galileo's times mistaken for a planet by Johann Georg Liebknecht.

sequence stars that belong to a multiple system is larger than 70–80 %, and perhaps 100 % for the O type (Shatsky & Tokovinin, 2002; Mason et al., 2009), for solar type stars is around 44–67 % (Duquennoy & Mayor, 1991; Raghavan et al., 2010; Duchêne & Kraus, 2013), and in the case of low-mass stars is 10–30 % (Burgasser et al., 2003, 2006; Joergens, 2008; Guszejnov et al., 2017). Nevertheless, in the latter the efficiency in terms of the fraction of the available mass that goes into stars can be considered high (Matzner & McKee, 2000). In the particular case of M dwarfs, early studies estimated in 33–42 % the fraction of them that are part of a multiple system (Fischer & Marcy, 1992; Reid et al., 1997). More specifically, the multiplicity rate of M dwarfs has been estimated to approximate to 30 and 20 for a stellar (M dwarf) and substellar (brown dwarf) companion, respectively (Chabrier, 2003b). Recent estimates suggest that the multiplicity of M dwarfs is 26–27 %, or even lower (Delgado-Donate et al., 2004; Ward-Duong et al., 2015; Cortés-Contreras et al., 2017a; Winters et al., 2019a).

Larson (1972) first suggested that a rotating cloud would not collapse into a single star, but instead it would fragment into two or more condensations, resulting in the formation of a multiple system of stars. Now it is widely accepted that multiple systems result from the collapse and fragmentation of cloud cores (Boss & Bodenheimer, 1979; Larson, 1985; Boss, 1988; Pringle, 1989; Bate, 2000; White & Ghez, 2001; Padoan & Nordlund, 2004; Ward-Thompson et al., 2007; Reipurth et al., 2014; Tokovinin & Moe, 2020). Although it may not be the only mechanism, it is successful in explaining the mass-ratio distribution observed among the pre-main-sequence systems (Bonnell et al., 2001; Goodwin et al., 2007; Reggiani & Meyer, 2011). There is a possibility that all stars were born in multiple systems, but a majority could not remain together as they evolved (Kroupa, 2008; King et al., 2012b; Elliott et al., 2014; Sadavoy & Stahler, 2017, c.f. King et al. 2012a). This is supported by the fact that young stars are almost always found to be part of multiple systems. If the primordial population of stars was essentially of multiple systems, their diversity observed today, including the lack of multiplicity in many stars, implies that dynamical interaction must have a role in the early stages of their evolution (Goodwin, 2010; Reipurth et al., 2014). It is clear that multiple systems offer valuable insights into the ways in which stars interact and influence one another.

The dynamical interplay between the components turns into a competition for attaining stable orbits. The loss of angular momentum during the shrinkage of the closest pair is transferred to the widest, which can result in one or more of them being ejected from the original compact arrangement (Delgado-Donate et al., 2003, 2004; Tokovinin et al., 2006; Basri & Reiners, 2006; Caballero, 2007; Moeckel & Bate, 2010; Reipurth & Mikkola, 2012b, and see again Reipurth et al. 2014). This process normally unfolds during the very youth of the system with durations of less than 10^5 years (Goodwin & Kroupa, 2005). These authors also noted that ejections would produce a significant population of close binaries that are not observed. This is an important point to remember, as the topic of unresolved binaries will be proven of great relevance in this work. Ejections are not the only mechanism to account for the large separations of some binary systems, for which the theory of collapse and fragmentation does not serve satisfactorily. Other channels proposed are turbulent fragmentation (Goodwin et al., 2004; Bate, 2009; Offner et al., 2010; Tobin et al., 2016), the dissolution of clusters (Kouwenhoven et al., 2010; Moeckel & Clarke, 2011), and random bindings from slow-moving near pre-stellar cores (Leigh & Geller, 2013; Tokovinin, 2017), this latter accounting for the large fraction of young wide pairs.

Systems that contain more than two components are, in principle, unstable (Harrington, 1972, and see again Goodwin & Kroupa 2005). However, the dynamical evolution might produce a hierarchical arrangement of binaries within binaries, or nested orbits, that conduces to stability (Evans, 1968; Bonnell et al., 2003; Tokovinin, 2014). In this sense, some works such as those of Basri & Reiners (2006), Caballero (2007), and Kouwenhoven et al. (2010) predicted or pointed out to a major prevalence of wide triples over wide binaries (and see Czavalinga et al., 2023). Indeed, in many instances typically one of the

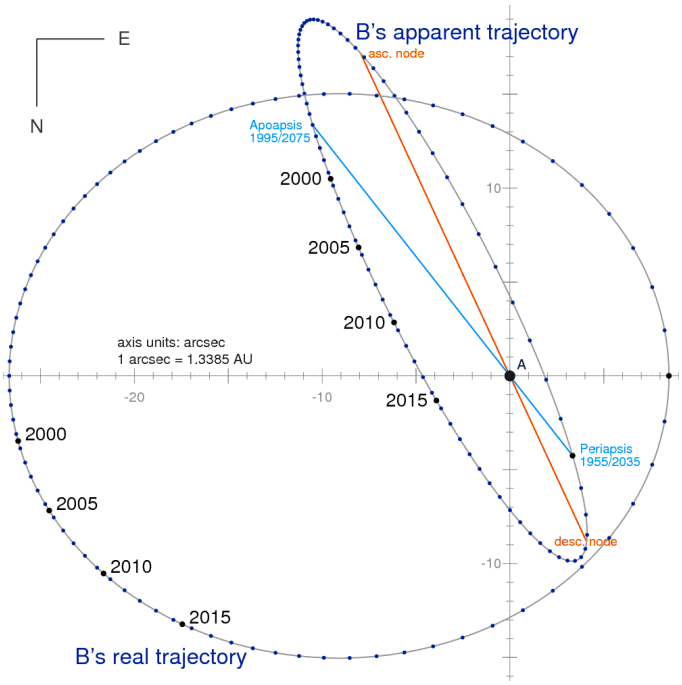

Figure 4.2: Apparent trajectory of α Centauri B orbiting α Centauri A, represented as the elongated ellipse, with the axes show the separation in arcseconds. The actual orbit of B is the less elongated ellipse with A at one of the two foci, as seen face-on (source: Wikimedia).

components of a wide binary is further resolved as a binary itself, therefore producing a triple system (see e.g. Cifuentes et al., 2021). Luckily, these can be treated individually as two-body problems (e.g. Evans, 1968). Our nearest stellar neighbour is a triple system of this kind: α Centauri consists of two Sun-like main stars (A and B) in mutual orbit. The third component (C) is Proxima Centauri, a red dwarf orbiting the pair at a separation that is 400 to 1100 times that of the pair AB[3]. Proxima orbits a double star system, but for all practical purposes, the star appears to be single. For young systems, without enough lifetime to have settled down into stable configurations, it is often unclear whether a given system can be treated as a young trapezia-like architecture, or as a mature cluster (see for instance the system of V1311 Ori in Tokovinin, 2022).

Physically bound binary systems can be found at a broad range of orbital separations. Only for the nearest stars it is feasible to physically discriminate the components in some cases, and produce detailed orbits in some others (Fig. 4.2). Still, some binaries are so closely packed that they are disguised as single objects by direct imaging, even with telescopes of the most powerful resolving capabilities. At one end, the so called contact binaries physically interact with one another (see the extreme case of the 5-minute-period white dwarf binary HM Cnc, Israel et al., 2002, and see Munday et al. 2022 for a two-decade worth of data review). The mutual pull is so strong that their gaseous envelopes fill their Roche lobes (their region of gravitational influence) and mass is transferred in the process (Lucy, 1968, and see Yakut & Eggleton 2005 for the case of low mass stars). The ultracool dwarf binary LP 413-53AB is another extreme and interesting example. Hsu et al. (2023) reported it as "the shortest-period ultracool binary discovered to date, and one of the smallest separation main sequence binaries known", with an orbital period of around 20.5 days. The authors noted that, at the current separation (around one hundredth of an astronomical unit), their larger radii at young ages would have put them in contact. While very close binaries are undetectable by direct means such as imaging, they can be recognised in the Doppler shift

[3] Harrington (1972) concluded that for a triple system in a direct orbit like α Centauri to be stable, the ratio of the periastron distance in the outer orbit to the semi-major axis of the inner orbit must be at least 3.5.

of the spectral lines (spectroscopic binaries), in the periodic eclipsing of their light (eclipsing binaries), or in the measurable change in their motion (astrometric binaries). Stars in binary systems offer the opportunity to directly measure fundamental parameters, such as masses and/or radii (Mathieu et al., 2000; Zapatero Osorio et al., 2004; Torres et al., 2010; Schweitzer et al., 2019). They are also convenient laboratories to investigate other areas, such as the nature of clusters (e.g. Kouwenhoven & de Grijs, 2008), and even a measure of gravity (e.g. Banik & Zhao, 2018).

The frontier that defines a close and a wide binary is blurry (e.g. Caballero, 2009, 2010; González-Payo et al., 2021, 2023). In the following sections we use the terms 'close' and 'wide' in a qualitative way, unless specified otherwise. As a general rule, we set a boundary between close and wide binaries at $\rho = 5$ arcsec, which results from avoiding contamination in the spectra from nearby sources in the aperture of the optical fibre of CARMENES projected on the sky (Sect. 2.1). From the CARMENES perspective, there is a quantitative difference, motivated in Sect. 3.1.4.

Wide systems have orbital periods of centuria or millennia, and thus the prospect of following them during one single orbit is unrealistic in practice, and in the best cases, full-orbit description must rely on photographic materials (see Gatewood et al., 2003). Because of this, it is not possible to discriminate between actual bound multiple systems and disintegrating clusters. Nevertheless, the components of wide pairs can be exposed individually. At these large separations, most of the binaries are fated to dissolve in timescales of a few million years (see Sect. 4.4.4). The observed separations between components of a wide system are usually smaller than 0.1 parsec (but see for instance Shaya & Olling, 2011). The youth of the system is a very common characteristic of very wide pairs, as components still undergo a process of stabilisation (Poveda & Allen, 2004). Notable examples are the system of AU Mic and AT Mic (Kalas et al., 2004; Caballero, 2009), or 'the Family of V1311 Ori', as presented by Tokovinin (2022). However, these configurations are so fragile that they are susceptible to be unbound by the dynamical encounters with different sources of perturbation, such as stars, molecular clouds, clusters, and even Stellar-mass black holes (Hills, 1975; Retterer & King, 1982; Weinberg et al., 1987; Kroupa, 1995; Kroupa et al., 1999; Caballero, 2009; Jiang & Tremaine, 2010; Parker et al., 2011; Deacon & Kraus, 2020; Cournoyer-Cloutier et al., 2021; Ryu et al., 2022). Indeed, simulations find that no binary with a separation $\geq 10^4$ au (larger than the typical size of a pre-collapse core) must be produced by isolated star formation (see Goodwin, 2010) because it cannot survive in any cluster (Parker et al., 2009). The authors argue that in binaries with semi-major axis $50 \lesssim a \lesssim 10^4$ au the effect of dynamical influence can be severe, while for $a \lesssim 50$ au they evolve almost unaffected. At these very small separations, they also note that the field population reflects the sum of all star formation. It has been suggested that very close binary systems ($r < 10$ au) are not formed by fragmentation in situ, but are a product of wider multiple systems (Bate et al., 2003).

Stars that have a common origin in space must have the same chemical imprint. Wide binaries are demonstrated to be coeval (Makarov et al., 2008) and co-chemical (Gizis, 1997; Gratton et al., 2001; Desidera et al., 2004, 2006; Makarov et al., 2008; Kraus & Hillenbrand, 2009; Hawkins et al., 2020). Sufficiently resolved pairs can serve to prove this assumption and serve as pieces in the puzzle of the Galactic formation. Fitting these pieces and reassembling the original configuration is the goal of Galactic archaeology studies, which benefits from systems of wide pairs (Andrews et al., 2019; Hawkins et al., 2020). Important applications of these are the calibration of metallicities of M dwarfs (Bonfils et al., 2005a; Bean et al., 2006; Lépine et al., 2007; Rojas-Ayala et al., 2010; Montes et al., 2018), the age-metallicity (Rebassa-Mansergas et al., 2016), age-magnetic activity relation (Garcés et al., 2011; Chanamé & Ramírez, 2012), and also studies of dark matter in the Milky Way (Yoo et al., 2004; Chanamé & Gould, 2004).

Although intrinsically small and faint ($\mathcal{M} \lesssim 0.62\,\mathcal{M}_\odot$, $\mathcal{L} \lesssim 0.076\,\mathcal{L}_\odot$, Cifuentes et al., 2020), M dwarfs make up the majority of the stars in the Universe (Henry et al., 1994, 2006; Reid et al., 2004; Bochanski

et al., 2010; Winn & Fabrycky, 2015; Reylé et al., 2021). The advances in instrumentation and image detection have opened the door to finer visions of M dwarfs. Among some of the top high-resolution ground-based spectrographs that look at the coolest stars is CARMENES (Quirrenbach et al., 2014) (see Table 1.1). The lack of detailed observations regarding individual stars carries an important observational selection effect, since very close multiple system remain undetected. In this sense, the nearest stars represent a valuable sample of study because it permits accurate photometric and astrometric measurements, which is specially true for the case of M dwarfs.

Even if the current population of M dwarfs had not evolved from a primordial one of mostly multiple systems, the frequency of binaries and higher order multiples makes their study a very important test for the theories of star formation. Also, the distributions of parameters of binary systems such as orbital periods and separations, binding energies, or masses, contain important insights into the formation process (Sterzik et al., 2003; Burgasser et al., 2007; Goodwin et al., 2007). The statistics on their frequency, their primary-companion mass ratio, and their physical separations can set meaningful constraints to the models of stellar formation and evolution, and whether the observed distribution is compatible with a primordial multiple-only population (Hartigan et al., 1994; White & Ghez, 2001; Parker et al., 2009; Reggiani & Meyer, 2011; Clark et al., 2012; Leigh & Geller, 2013; Reipurth et al., 2014; Parker & Meyer, 2014). The use of high contrast imaging techniques, like the Spectro-Polarimetric High-Contrast Exoplanet Research (SPHERE), provides a close and realistic observation of binary systems, even during the formation phase. This suggests that the interplay between different mechanisms would produce the variety of observed systems, with a possible continuum between the formation of substellar objects (massive planets and brown dwarfs) and of stellar companions (Gratton et al., 2022).

In this work we present a systematic study of the multiplicity of M dwarfs, in a volume-limited sample of more than two thousand M dwarfs with spectral subtypes form M0.0 V to M9.5 V, and separations from 0.3 au to about 206 000 au. Since the study fundamentally relies on the resolution of the systems by the *Gaia* mission, we distinguish between systems with resolved components (Sect. 4.3.1), and systems with unresolved components (Sect. 4.3.2) in *Gaia* DR3. The conclusions and prospects for a future work motivated by these investigations are summarised in Chapter 5.

4.2 Sample of study

The sample of our study is Carmencita, the CARMENES input catalogue. Carmencita contains 2216 late-K and M dwarfs, which were intentionally chosen to be independent of multiplicity, age, or metallicity. As explained in Sect. 2.2, these stars satisfy simple selection criteria based on their spectral determination, on their visibility from Calar Alto Observatory in Southern Spain ($\delta \gtrsim -23$ deg), and on their apparent brightness in the J-band magnitude, between 4.2 mag and 11.5 mag (cf. Alonso-Floriano et al., 2015b). The continuous update of the catalogue has included additional M dwarfs that are part of the Transiting Exoplanet Survey Satellite (TESS; Ricker et al., 2015) program.

We removed four late-K single stars from the original Carmencita catalogue for a more rigorous sample only populated by M dwarf objects. These are LP 415-17 (J04219+213), HD 168442 (J18198-019), TYC 4450-1440-1 (J20109+708), and Ross 176 (J20227+473), all of them classified as K7 V stars. Figure 4.3 shows the classification by spectral subtype of the 2212 M dwarfs in the sample.

A magnitude limited sample may be unintentionally overpopulated of brighter, unresolved systems (see Duquennoy & Mayor, 1991, and references therein). For this reason, we study the completeness in distance (or volume) in our sample. To address this calculation we assume a uniform distribution of the

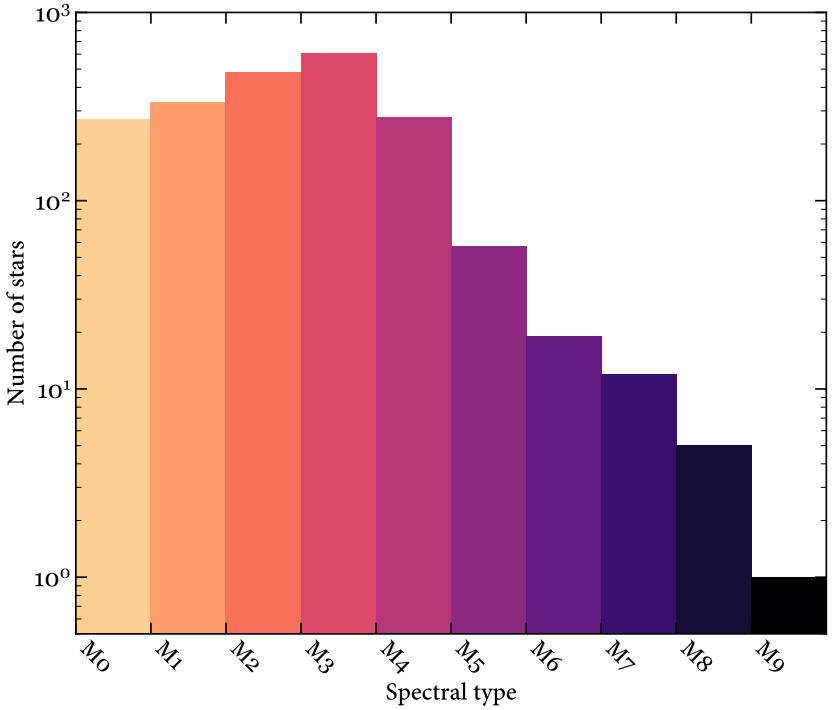

Figure 4.3: Distribution of spectral types of the stars in the sample. The M9.5 V object is Scholz's Star.

Table 4.1: Completeness distance of Carmencita as a function of spectral type.

Spectral type	$d_{\rm com}$ (pc)	Number of stars
M0.0–0.5 V	33.4	235
M1.0–1.5 V	35.3	331
M2.0–2.5 V	35.9	381
M3.0–3.5 V	33.9	560
M4.0–4.5 V	32.1	469
M5.0–5.5 V	24.2	159
M6.0–6.5 V	19.6	32
M7.0–7.5 V	15.3	16
M8.0–8.5 V	13.1	10
M9.0–9.5 V	9.9	2

stars over the area of the celestial sphere. First, we define a 'completeness distance' that depends on the spectral type, $d_{\rm com}$, using the definition of absolute magnitude in the J band, $M_J - J = -5 \log d_{\rm com} + 5$, where $J = J(\mathrm{SpT})$ (Alonso-Floriano et al., 2015b), and $M_J = M_J(\mathrm{SpT})$ using the results by Cifuentes et al. (2020). Therefore, the meaning of $d_{\rm com}$ is, for a given spectral type, the maximum distance for which we can be confident of containing all known M dwarfs identified in the literature[4]. The results are summarised in Table 4.1. Up to 30 parsec, our sample contains all M dwarfs with spectral types M4.5 V or earlier, and it is complete for all the domain of M dwarfs within 10 pc, This important fact has been checked with Reylé et al. (2021).

[4]As a reminder, Carmencita does not include stars that are not visible from Calar Alto, where CARMENES is located. As a reminder, see again the distribution of Carmencita stars in Fig. 3.2.

4.3 Analysis

For the multiplicity analysis in our sample we made extensive use of the third data release of *Gaia* astrometry and photometry (DR3, Gaia Collaboration et al., 2022b), numerous public all-sky surveys from the ground and space, the Washington Double Star catalogue (WDS; Mason et al., 2001)[5], and Virtual Observatory tools such as the `Aladin` interactive sky atlas (Bonnarel et al., 2000), the Tool for OPerations on Catalogues And Tables (`TOPCAT`; Taylor, 2005), and the Virtual Observatory Spectral energy distribution Analyzer (`VOSA`; Bayo et al., 2008).

The WDS is the principal database for astrometric double and multiple star information, and is updated nightly. Using `TOPCAT` along with `Aladin`, we looked for entries in this catalogue for all the stars in our sample and found that WDS tabulates 558 individual pairs in it. For these, we obtained the data that includes the last measured epoch, and the corresponding positional angle and separation in the 'precise' format (i.e. non-rounded values), the number of observations, and the visual magnitudes for both components.

Every star in our sample has equatorial coordinates in the 2016.0 epoch and G magnitude in the *Gaia* catalog. 95.1 % of them have the full, five-parameter astrometric solution: positions, parallaxes, and proper motions (α, δ, $\mu_\alpha \cos\delta$, μ_δ, ϖ). Among these, 61.2 % also have barycentric radial velocity, V_r, in the second or the third data releases (preferring the former in the case of availability in both). For the sources without astrometry or radial velocities provided by *Gaia*, we searched in the literature for published data, making sure that we maximise the completeness of the astrometric information in our sample.

For every star we looked for physical companions covering all ranges of separation: from compact configurations (typically binaries), only resolved employing dedicated techniques (lucky imaging, adaptive optics, speckle interferometry, etc.), to wider pairs that can be resolved using the *Gaia* astrometric solution, and in some cases other all-sky surveys, such as 2MASS or AllWISE. In this search we found a total of 800 systems in our sample. To ensure the correct interpretation of the data, sometimes within only a few arcseconds of apparent separation, we inspected individually each one of them, primarily using `Aladin` and Simbad, and we took great care to consider the existing literature and past characterisations.

Before delving into the analysis of the sample, it is crucial to note that the sample was subject to observational selection limitations. In the case of very close-in binary systems, only spectroscopic analysis can reveal the presence of pairs, as discussed in Sect. 4.3.1. Because observations of individual stars with sufficiently large telescopes and powerful instruments are not, in general, available, the very close pairs go unnoticed and do not contribute to the distributions of parameters. The consequence is that the period and mass ratio coverage lacks of uniform data at short periods. Of course, this is a fundamental concern of many investigations based on a large sample of stars.

4.3.1 Resolved systems in *Gaia*

Gaia DR3 contains data for 1 811 709 771 objects, with a complete astrometric description (positions, parallaxes, and proper motions) for 585.4 million of them. Figure 4.4 shows a relatively small sample of the stellar content identified in the catalogue within an area of 3×3 deg^2. The nominal mission of *Gaia* ended on July 2019, but the extension of their operations has been approved until 2025, when the propellant for the micropropulsion system is expected to be exhausted. In this condition, the astrometric precision for that relies on the attitude and spin rate cannot be guaranteed. By then, *Gaia* will have gained

[5] http://www.astro.gsu.edu/wds/.

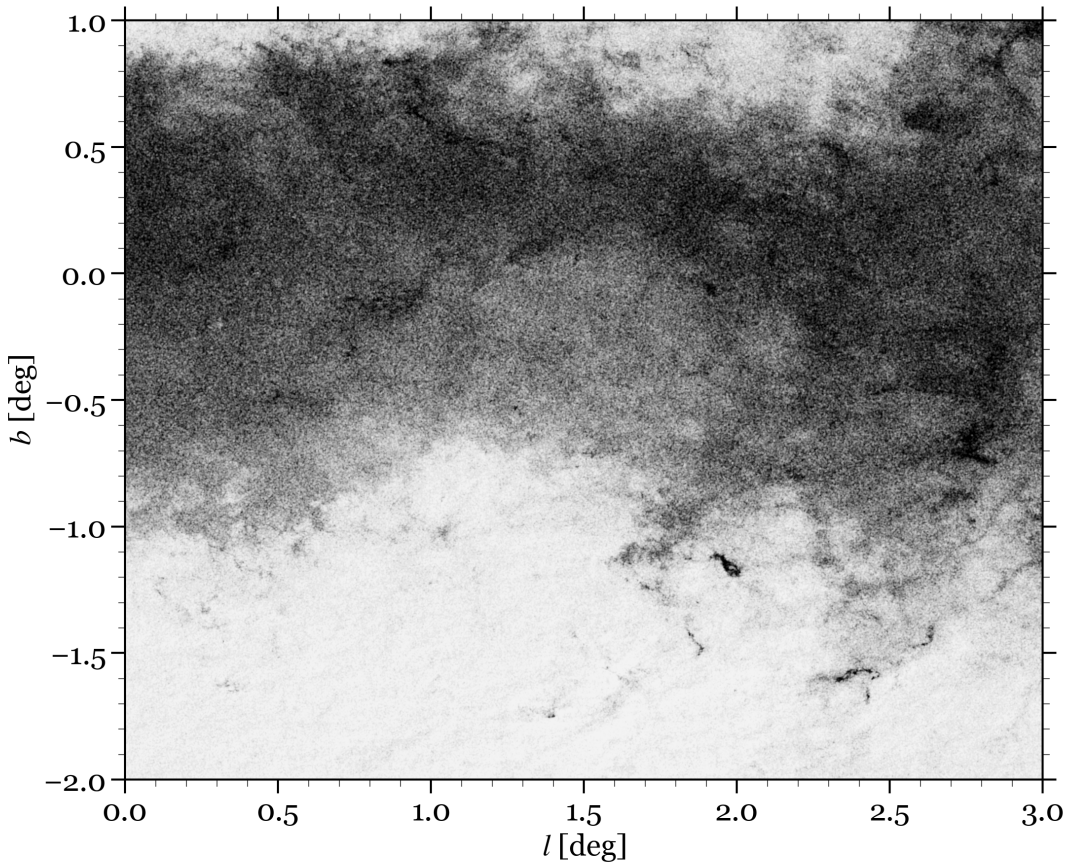

Figure 4.4: *Gaia* sources (approx. 3 million) in a $3 \times 3\,\mathrm{deg}^2$ area near the Galactic centre. Each white dot represents a source resolved by *Gaia*, in most cases with accurate astrometry, photometry, and low-resolution spectroscopy. Light-blocking dusty regions can be easily spotted in the crowded areas as darker patches.

a decade worth of precise measurements, and at least two more data releases are expected to include the results from the extended mission: DR4 (not before the end of 2025) and DR5 (not before the end of 2030). For the moment, *Gaia* has already published (in DR1, DR2, EDR3, and DR3) the most precise astrometric catalogues ever known, with accuracies ranging from 10 to 1000 μarcsec for more than one billion stars.

For the search of systems that are resolved by *Gaia*, we divided the search in two steps. Firstly, we looked for any close source in the *Gaia* DR3 catalogue using the `TOPCAT` automatic positional cross-match tool, `CDS X-match`, with a search radius of 5 arcsec. By setting the 'find' option to "All", we made sure to keep every object found in the vicinity, regardless of their kind, parallactic distance, or proper motions, even when this information was not available.

Secondly, we performed a much wider, volume-limited, blind search in the same catalog, using the AQDL form available in the *Gaia* Archive[6]. In this case, we looked for resolved sources with the full 5-parameter astrometric solution that is compatible with physical binding, based on proper motions and parallactic distances (see Sect. 4.3.1). We retrieved all elements within 10^5 au, which implies a projected separation

[6] https://gea.esac.esa.int/archive/.

of 10^4 arcsec to $\sim$ 10^3 arcsec (2.8 and ~0.3 degrees, respectively) for stars located in a range between 10 and 30 parsec, whose similarity in parallax was 10% or less, ignoring those stars without measured parallax (i.e. photometric distances). We did not impose any restriction on the proper motion because, given the small probability of finding a similar-distance source within the search radius, the benefit of finding a companion that may have perturbed motion caused by a very close companion (see Sect. 4.3.2) outweights the effort of checking individually all the potential pairs. This was done by accessing to images and catalogues via `Aladin`.

The distance on the celestial sphere from a given source was measured along a great circle or geodesic, as opposed to straight lines in the Euclidean space. Given δ_1 and δ_2 the declination of two objects, and $\Delta\alpha$ the absolute difference between their right ascensions, the central angle is given by:

$$\Delta\sigma = \arccos\left(\sin\delta_1 \sin\delta_2 + \cos\delta_1 \cos\delta_2 \cos\Delta\alpha\right), \tag{4.1}$$

and the arc length is given by $s = d\Delta\sigma = d\rho$. For all these components in the systems resolved by *Gaia*, we calculate the projected separation, ρ, and the positional angle, θ. With these variables we compute two parameters introduced by Montes et al. (2018), which are defined by pairs that are generically referred as components 1 and 2 in the formulae. These are the μ ratio, defined as:

$$(\mu\,\text{ratio})^2 = \frac{(\mu_\alpha \cos\delta_1 - \mu_\alpha \cos\delta_2)^2 + (\mu_{\delta 1} - \mu_{\delta 2})^2}{(\mu_\alpha \cos\delta_1)^2 + (\mu_{\delta 1})^2}, \tag{4.2}$$

and the proper motion position angle difference:

$$\Delta PA = |PA_1 - PA_2|, \tag{4.3}$$

to which we add a third parameter as in Cifuentes et al. (2021) and González-Payo et al. (2023), the distance ratio defined as:

$$\Delta d = \left|\frac{d_1 - d_2}{d_1}\right|. \tag{4.4}$$

We apply a preliminary criteria for multiplicity, to distinguish between physical (bound) and optical (unbound) pairs.

$$\begin{cases} \mu\,\text{ratio} < 0.15, \\ \Delta PA < 15\,\text{deg}, \\ \Delta d < 0.10. \end{cases} \tag{4.5}$$

The first two criteria account for the similarity in their movement, in particular in the modulus and orientation of their proper motions. The third criterion ensures that the components of the pair are approximately equidistant, up to a conservative difference of 10 per cent. Jointly, they serve to test if a pair is a chance alignment.

While the criteria above are sufficiently valid for resolved, relatively wide pairs with well-defined astrometry, it is indeed troublesome in the case of pairs that are too close in the sky. For these, the astrometric solution may not be accounting for the relative orbital motion, but rather for the instantaneous, tangential movement of the components. The nominal operations of *Gaia* span 1028 days, from August

5, 2014 to May 28, 2017. DR3 benefits from a good time coverage, which is an advantage with respect to DR2 during the study of proper motion anomalies (see Kervella et al., 2019). Nevertheless, this astrometric coverage is insufficient in many cases and can translate into ill-defined proper motions that cannot account for the real motion of the components in compact systems. Because of this, very close-in, physically bound systems do not comply with the criteria above.

Figure 4.5 shows these extreme cases. We show the compliance of the pairs with the criteria of Eqn. 4.5 (top panel), and the comparison of distances (bottom panel). The error bars are comparatively very small for almost all cases due to the high precision of *Gaia*'s astrometry, and had been omitted without compromising the rigour.

The distances and total proper motions of the vast majority resolved pairs compare favorably against those of their resolved companions. The criteria for physical parity also hold true for them. Nevertheless, 31 components (shown as red circles in some or all of the panels in Fig. 4.5) present anomalies in their relative positional angles proper motions, and/or distances. We have investigated their particular characteristics in further detail, and the results are presented in Table D.3, including a probable main cause for this behaviour. We encourage paying special attention to some of these pairs, because their potential closeness could make their orbital motion to be defined easier, and further characteristics of the components, such as their dynamical masses, might be obtained sooner. The vast majority of relatively wide multiple systems that are resolved in *Gaia* are known to date and collected in the WDS catalog. In Fig. 4.6 we compare the values of separations tabulated in the WDS with those computed by us using *Gaia* DR3 astrometry. The 10 stars outside the limits represented by the dashed lines have a difference in their values larger than 25 %, a characteristic typically observed in very close pairs of stars that are more strongly influenced by their mutual gravitational attraction, therefore exhibiting more noticeable common movements.

In this work we discover several pairs with an astrometry that we find to be compatible with physical parity with our stars, but that are not found either in the WDS catalogue or in the literature. Some of them are isolated pairs (i.e. binaries), whereas some are components of known systems, thus producing systems of higher order. We tabulate these 117 new systems proposed in Table D.4, including 31 binaries, 15 triples, and 4 quadruples. Apart from *Gaia* DR3 astrometric solutions (α, δ, $\mu_{\rm total}$) and G magnitudes, for each pair we tabulate the position angles (θ) and the angular separations (ρ). In a few cases, their entries in Simbad includes the denomination 'Double or multiple star', but without published references. Additionally to describing the new pairs found, we also note the impact of these findings on the general scheme of its system, and in particular on the redefinition of the class (i.e. from single to binary, binary to triple, etc.).

4.3.2 Unresolved systems in *Gaia*

Gaia is the all-sky survey with the highest angular resolution available to date. The spatial resolution of *Gaia* was limited to 0.4–0.5 arcsec in the second data release (DR2, Gaia Collaboration et al., 2018b), and slightly improved in the early third data release (EDR3, Gaia Collaboration et al., 2021). While EDR3 represented a significant advance over DR2, the third data release (DR3, Gaia Collaboration et al., 2022b) exploited in this work maintains the same astrometric data as the previous release, EDR3. Nevertheless, it incorporates a wealth of new data products, that we exploit in this work. Fabricius et al. (2021) showed that EDR3 is complete for separations above 1.5–2.0 arcsec, with severe incompleteness below 0.7 arcsec. The authors addressed the improvement of the spatial resolution of the EDR3 as compared with DR2, testing the capacity of resolving visual double stars from the WDS catalogue in both releases. Below

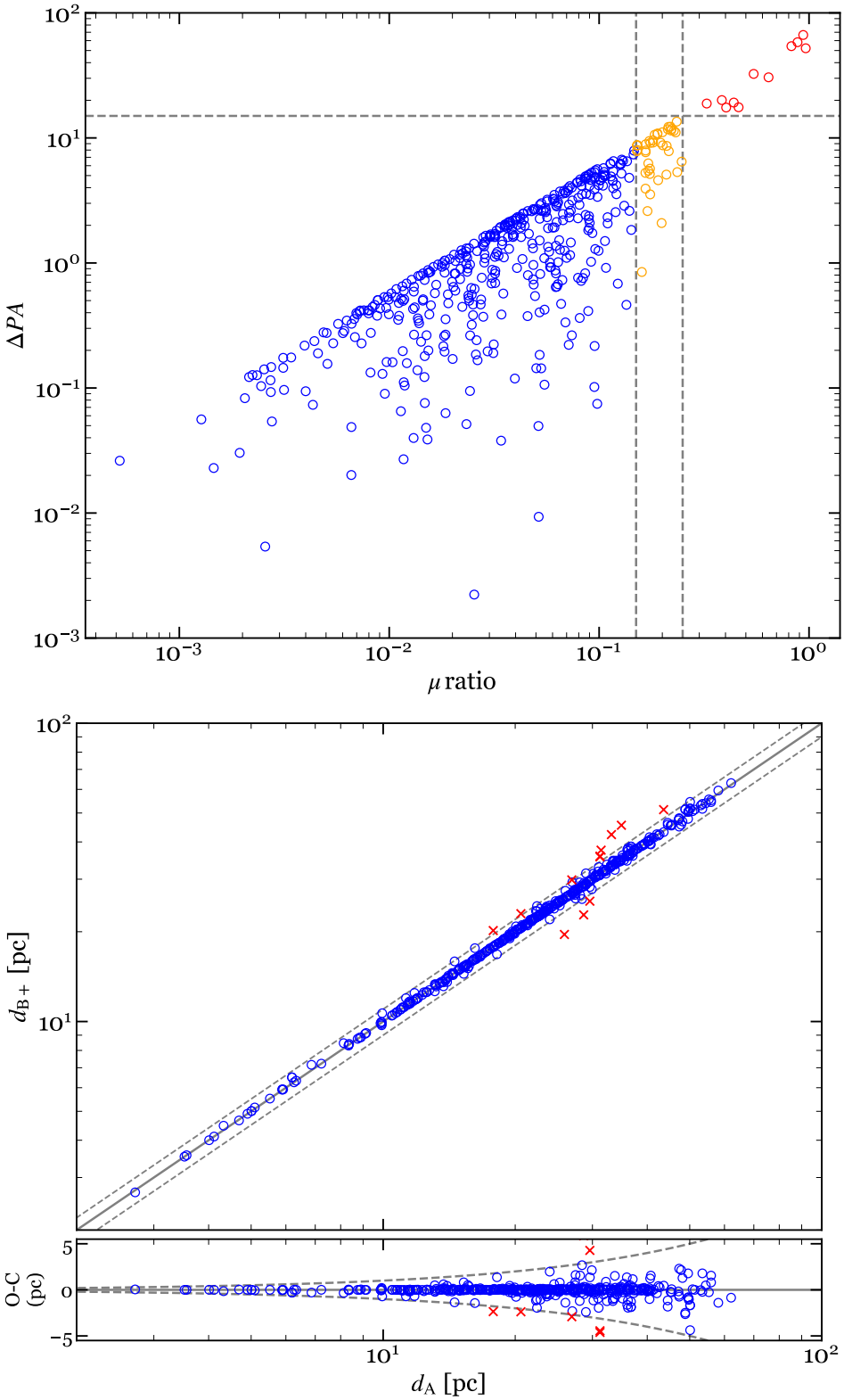

Figure 4.5: *Top*: ΔPA vs. μ ratio diagram, where the dashed grey lines set the upper limits of the criteria for physical parity (Eqn. 4.5). The red and orange empty circles are pairs that respectively do not comply, or do so partially, with that criteria. *Bottom*: Comparison of parallactic distances between the primaries and their resolved components. The dashed and dotted grey lines represent the 1:1 relation, and the differences in 10 %, respectively. The red crosses are stars out of this latter limit.

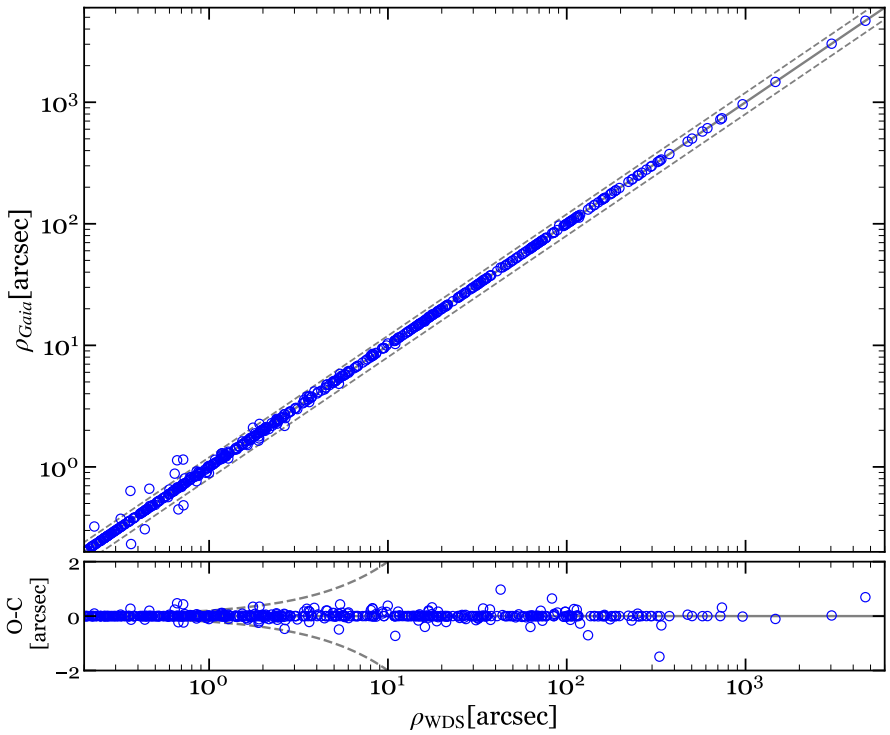

Figure 4.6: Comparison of projected separations tabulated by the WDS and measured by us using *Gaia* astrometry. The continuous and dashed grey lines represent the 1:1 relation, and the differences in 10 %, respectively.

0.7 arcsec objects can be discriminated, depending on the magnitude difference and the orientation along the dominating scan directions. Indeed, EDR3 improved the treatment of sources separated between 0.18 and 0.4 arcsec, which were erroneously considered duplicated sources in DR2.

This means that *Gaia* is unable to resolve the closest ($\rho \lesssim 0.2$ arcsec) pairs in our sample. For these, different techniques and technologies can successfully disentangle the components, such as adaptative optics, lucky imaging or, for instance, the ultra-violet vision of the Hubble Space Telescope. Therefore, we investigate in the literature for the identification of known spectroscopic binaries and triples, and the WDS for astrometric pairs. We note that this search is performed not only in the stars in our sample, but is also in their known companions.

In the case of spectroscopic systems, by definition, their components cannot be resolved by any earth- or space-based telescope, and the existence of two or more stars can only be deduced from meticulous observations in moderate or high resolution shots of their spectra (see Sect. 4.4.2). We find 132 spectroscopic multiples among the stars in our sample and their companions. We took special care with those cases for which spectroscopic binarity was reported in previous investigations (typically dated decades back), and there exist recent astrometric observations that resolve the components. Indeed, in 37 cases, the components of a binary detected by spectroscopic means are later on exposed individually, as a result of the advances in instrumentation. For these, we pay attention to the reported orbital periods and the magnitude differences reported, in order to consider the possibility that both measures, the oldest spectroscopic and the newest astrometric binaries, refer in fact to the same pair. These are not classified as 'SB', except in the case of doubt, in which case we prefer to stay conservative, and avoid losing a potential triple system (thought to be double) in a compact configuration. We list all the spectroscopic systems found in our sample in Table D.5, including their derived periods, the masses for the primary and secondary, the q ratios, and the physical separations, a, when available. The mass ratio of a star

in a multiple system indicates its mass as a fraction of the mass of the primary, $q = M_B/M_A$, where B represents a component other than the primary. For a system of equal-mass components, q is 1.

Although *Gaia* is unable to resolve very close-in systems, they are not *invisible* to its eyes. Even when the precision is not enough to discriminate the components of a very close binary, from the vast amount of data that it collects it is possible to extract information that can be much revealing, and can boast from statistical robustness.

Gaia has three different channels: astrometric, photometric and spectroscopic. The astrometric measures the movement in the sky and heliocentric distance, the photometric measures fluxes in three passbands, and the spectroscopic derives information from the spectrum, such as radial velocities by cross-correlation with theoretical spectra. *Gaia* DR3 is the first release providing analysis of the RV time-series looking for orbital motion. All together provide a coherent view of the nature of the objects.

In *Gaia* DR3 every source has been observed an average of ~70 times, and varying from ~30 to ~240, depending on the sky coordinates. Among the different types of variable stars, the Gaia data reduction identified ~2.2 million eclipsing binaries and ellipsoidal systems, with various levels of characterisation (and see Rimoldini et al., 2022). The parameters were derived by fitting the light curves (LCs) to Gaussian or cosine functions, and also to synthetic LCs of binary systems, modelling stellar surfaces as equipotentials of the Roche potential. In some cases including radial velocity data were incorporated in the study. The parameters derived include the photometric period, the times of mid-eclipse, as well as eclipse durations and depths.

Astrometrically, the full description of a system can be achieved when the orbital period is smaller than the astrometric mission time interval. As mentioned earlier, the nominal operations of *Gaia* span 1028 days (2 years, 9 months and 24 days). If the orbital period surpasses this length of time, still it is feasible to determine the orbital parameters by fitting the so called orbital models and finding the optimal goodness of fit and significance values. A binary system can be described by seven parameters (the so called Campbell's elements): the orbital period ($P_{\rm orb}$), the epoch of periastron passage (T_0), the eccentricity (e), the semi-major axis (a), the inclination of the orbital plane with respect to the sky (i), the position angle of the ascending node (Ω), and the periastron longitude measured from the ascending node (ω). However, in the present data release of *Gaia* the handling of resolved binaries was not yet possible. Nevertheless, *Gaia* comes with numerous statistical parameters, built-in indicators, and data products that are useful in the identification of unresolved systems. In Table 4.2 we summarise the different approaches that we take to make the most of the available opportunities that the third data release of *Gaia* offers. These indicators are sensitive to deviations from the single star model that is assumed in the pre-processing stage. Among the stars without known close companions (less than a few hundred astronomical units or less) we find 344 stars that comply with any of these criteria for unresolved multiplicity. Among them, 272 are single and 72 are members of multiple systems, but sufficiently separated to discard the effect of the companion as the cause. These are preliminary candidates to binaries. There are also pairs in very close proximity, but resolved by *Gaia*, which lack in some instances of parallaxes and proper motions in the DR2/DR3 catalogues. Despite of this, we deem them as candidates, as the odds for a chance alignment are much lower than that of a physical connection (El-Badry et al., 2021; Chulkov & Malkov, 2022). In a similar fashion, Vrijmoet et al. (2020) provided an analysis of unresolved astrometric multiples using two decades of astrometric data from the RECONS program along with *Gaia* DR2 observations, and recognised perturbation in its astrometric residual in a few instances.

The Non-single star tables include unresolved astrometric, spectroscopic, and eclipsing binaries (see Gaia Collaboration et al., 2022a). These solutions are distributed in four tables: `nss_two_body_orbit` when the full orbital motion is known, `nss_acceleration_astro` and `nss_non_linear_spectro` when a trend

Table 4.2: Criteria for the detection of unresolved sources based on *Gaia* DR3 statistical indicators.

Criterion	Selection	Description	Reference
1	`ruwe` > 2[a]	Measure of a poor behaviour of the centre of light.	*Gaia* Documentation
2	`ipd_gof_harmonic_amplitude` > 0.1 `ruwe` > 1.4	Useful for identifying spurious solutions of resolved doubles, not correctly handled in the *Gaia* EDR3 astrometric processing.	Fabricius et al. (2021)
3	`rv_chisq_pvalue` < 0.01 `rv_renormalised_gof` > 4 `rv_nb_transits` ≥ 10	Identification of variability in the radial velocity among all the *Gaia* measurement epochs.	Katz et al. (2022)
4	`radial_velocity_error`[b] ≥ 10 km s^{-1}	Idem.	See Katz et al. (2022)
5	`ipd_frac_multi_peak` > 30[c]	Fraction (0–100) of windows for which the IPD[d] has identified a double peak.	*Gaia* Documentation
6	`duplicated_source` = 1	Existence of a duplicated source during data processing[e]	*Gaia* Documentation
7	`non_single_star`[f]	Non-constant behaviour using binary orbit models.	Pourbaix et al. (2022)

[a] This amplitude of the centroid perturbation correlates with the physical separation between companions and scales with the binary period and the mass ratio (Belokurov et al., 2020). Instead of the generally adopted value of 1.4 (e.g. Arenou et al., 2018; Lindegren et al., 2018; Cifuentes et al., 2020), we set a conservative minimum of 2.0 (see Fig. 4.9).

[b] For the bright stars ($G \lesssim 13$ mag) it is the uncertainty on the median of the epoch radial velocities, to which a constant shift of 0.11 km s^{-1} was added to take into account a calibration floor contribution. For stars fainter than $G = 12$ mag, a method involving a cross-correlation function is used instead. This criterion applies exclusively to radial velocity values coming from *Gaia* DR2/DR3. A practical application of this metric for the discovery of unresolved pairs is developed in Sect. 4.4.2, where a selected subsample of stars with large values in this metric are spectroscopically inspected in detail, finding evidence of spectroscopic binarity in many of them using mid-resolution spectroscopy with FIES.

[c] The selected value of 30 (per cent) is based on the distribution of values and a conservative threshold. This fraction means that the detection might be a visually resolved double star (either visual or physical binary). In some cases for which this fraction is large, two or three individual detections are given by *Gaia* for the same star (i.e. separated measurements). In other, the data do not provide the full astrometric determination (i.e. lacks proper motions and parallax). Both cases are worth a further investigation for possible binarity.

[d] IPD stands for the Image Parameters Determination, which is the stage of *Gaia* data processing where the standard stellar model is fit to the image locations. The ultimate purpose of the pre-processing is to measure the key properties of the source within each window, specifically its location and flux (further details on pre-processing are given in the *Gaia* Documentation.

[e] This may indicate observational, cross-matching or processing problems, or stellar multiplicity, and probable astrometric or photometric problems in all cases. The duplicity criterion used for *Gaia* E/DR3 is an angular distance of 0.18 arcsec, while a limit of 0.4 arcsec was used for *Gaia* DR2.

[f] Flag indicating the availability of additional information in the various Non-Single Star tables. Three bits (*nnn*) indicate (*n*=1) whether it has been identified as astrometric, spectroscopic, or eclipsing binary, respectively.

is known only, and `nss_vim_fl` for variable fixed binaries. More details on the processing scheme, its validation, and the various types of solutions reached can be found in Chapter 7 of the *Gaia* documentation[7]. Additionally, we incorporate the table `vari_eclipsing_binary` (Mowlavi et al., 2022; Eyer et al., 2022) from the study of variability. The latter is the first *Gaia* catalogue of eclipsing binaries.

We look for matches of our sample with these tables, finding 49, 6, 1, 0, and 2 coincidences, respectively. This translates into 55 individual stars proposed as unresolved pairs by *Gaia*. Of them, 24 are known pairs with very close-in orbits, and 31 are bona fide single stars, or in a few cases component in very wide pairs, in principle unaffected by their companion. Of the 2 eclipsing binary candidates, one turns out to be the known eclipsing binaries Castor C (Joy & Sanford, 1926; Gizis et al., 2002) and GJ 3547 (Shkolnik et al., 2010; Reiners et al., 2012). The `non_single_star` flag fails to identify a large portion of the confirmed very close binary pairs in our sample. Additionally to this automatic categorisation, we perform a further analysis employing a combination of statistical parameters offered by DR3, which we use to flag sources that do behave as non-single objects and might have been overlooked in the automatic categorisation.

[7] https://gea.esac.esa.int/archive/documentation/GDR3.

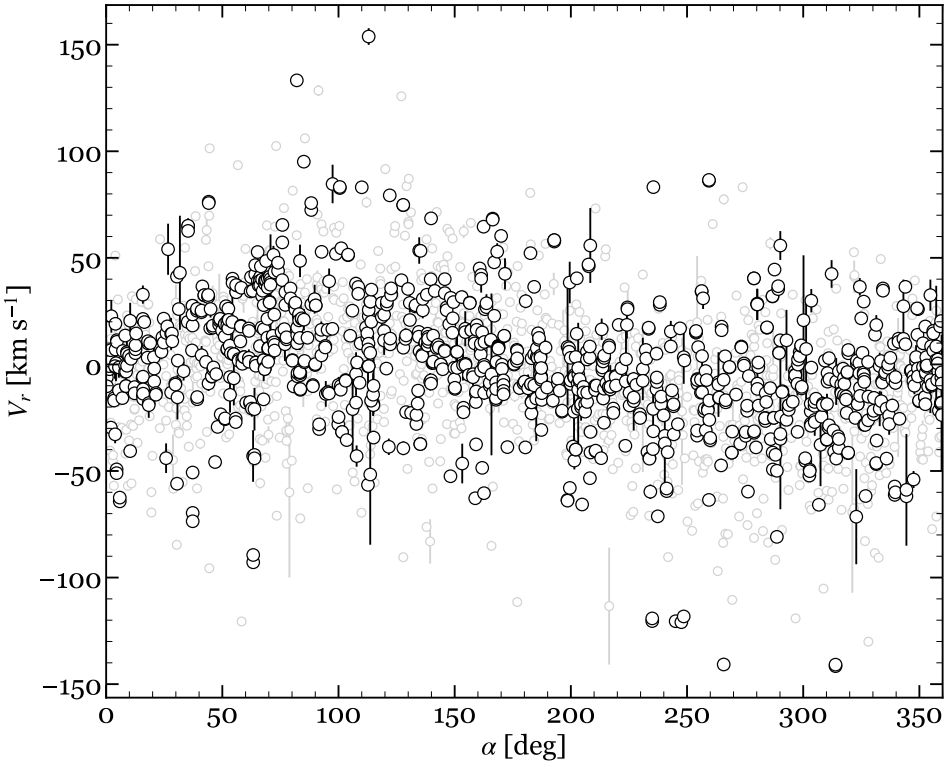

Figure 4.7: Barycentric radial velocity as a function of right ascension for the single (grey) and components of multiple systems (black), respectively.

With them we can identify potential candidates to multiple systems based on the variations of radial velocities among all the DR3 epochs. It is interesting to note the existence of stars in our sample with remarkably high values of radial velocity (Fig. 4.7), and also the existence of a wobble that is visible to a first sight in the same plot. Given that it is dependent on the right ascension of the sources, it is likely due to a positional calibration effect. The metrics that are used in this work are presented in Table 4.2, with a brief description and a general criterion recommended for each of them. More details on the specific origin of these metrics can be found in the *Gaia* DR3 documentation.

Spurious astrometric solutions can be also indicative of close binarity. The close binaries not resolved in DR2 were handled as single objects, with blended photometry and occasional spurious astrometric solutions. The approach in *Gaia* to address the consistency of these anomalous detections is to compare data from multiple transits (see Ziegler et al., 2018). In this sense, the third data release (DR3) greatly benefits from a larger number of observation epochs, which translates into the potential capability of detecting astrometric, spectroscopic or photometric (eclipsing) binaries. *Gaia* DR3 does not handle resolved binaries, but only the unresolved ones. Firstly, selects the candidates by adopting `ruwe` > 1.4. In these they added other criteria to filter out resolved system, to keep only the unresolved candidates. The spurious solutions were minimised by selecting those with a reasonable number of observations.

We apply the criteria 1–6 in Table 4.2 to all the stars in our sample without confirmed close companions. To those, we include the stars found to behave as non-single in criterion 7. By 'close' we mean here those with physical separations $s \leq 220$ au. This corresponds to a projected separation of 10.0 arcsec for a star at a distance of 22 pc, which is the median distance of the objects in our sample. Overall, we find that 344 stars in our sample comply with one or some of these criteria, but many binaries already known in the literature. But among these, 272 are single stars, without any known (close or wide) companion, and 72 are stars with known wide companions ($\rho > 5$ arcsec).

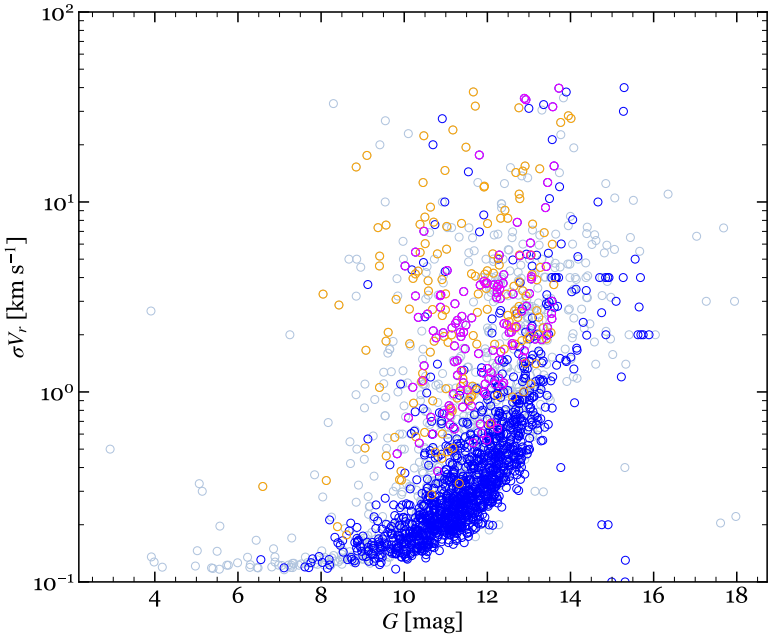

Figure 4.8: Uncertainty on the radial velocities as a function of G magnitude, shown as light and medium blue for the single and multiple stars, respectively. Stars with *evidence* for variability in the radial velocities (as hinted by criterion 3 in Table 4.2) are shown as magenta and orange empty circles, if they are single and if they are already components of a multiple system, respectively.

Gaia DR3 contains radial velocities for 33.8 million stars, with a temperature interval expanded with respect to DR2 (see Katz et al., 2022). In Sect. 4.4.2 we show the spectral analysis of a selected subsample of bona fide single stars with notable deviations from the median value of the radial velocity in *Gaia* (as high as ~ 8 km s^{-1}), as measured by the `radial_velocity_error` parameter. We estimated their periods to be of the order of months, assuming a binary in a circular orbit with equal-mass components. We also considered the parameters `ruwe` and `astrometric_excess_noise` (and its significance) as a potential signature of orbital wobble of individual components in binary star systems (Lindegren et al., 2012, and see Gan et al. 2022 for a practical example). Measuring the periodic variations in radial velocities (RV) in several epochs is a powerful method of detecting and describing binary systems. Furthermore, it allows us to discriminate true orbital acceleration due to multiplicity from the acceleration due to an effect of perspective. Figure 4.8 shows the median of the epoch radial velocities as a function of G magnitude for the stars in our sample with these available data in *Gaia*. The circles coloured in orange and magenta correspond to single and multiple stars, respectively, with evidence for variability in the radial velocities according to criterion 3 in Table 4.2. Therefore, the orange empty circles correspond to *candidates* to unresolved pairs.

4.4 Results and discussion

4.4.1 Multiplicity fraction

Approximately one-third of the M dwarfs in our sample belong to a multiple system, with binary and triple arrangements embody the majority of architectures. In this section we discuss their characteristics and provide an analysis of these statistics, including the common definitions of multiplicity and companion frequency rates.

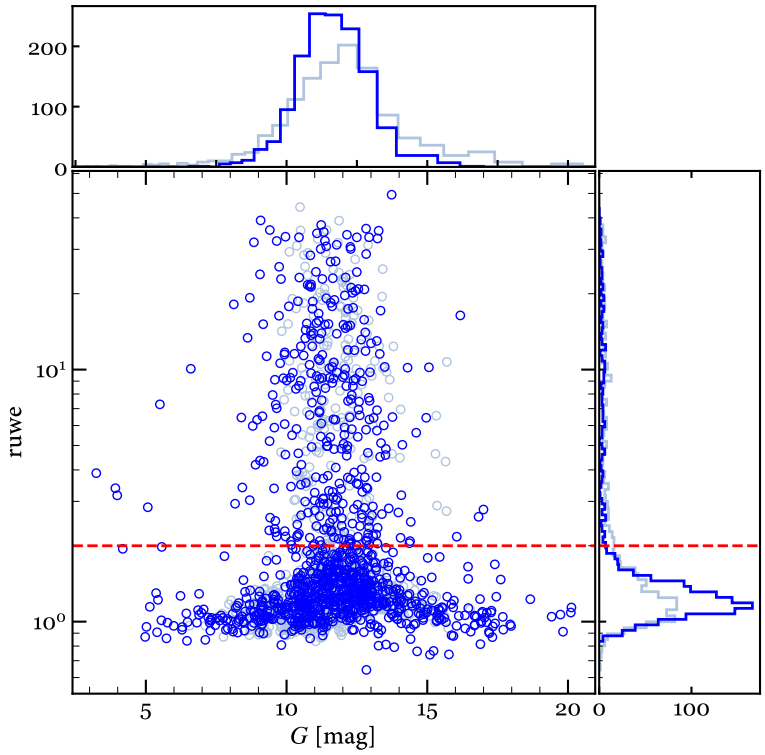

Figure 4.9: `ruwe` as a function of G magnitude for the single stars (grey circles) and the stars belonging to multiple systems (blue circles). The histograms follows the same colour codes. The dashed red line marks a conservative value of `ruwe` = 2.0.

There are 834 M dwarfs in our sample that belong to a multiple system, from which binaries and triples embody the majority of architectures, representing 81.8 % and 15.8 %, respectively. The remaining 1378 are single stars, or 62.3 % of the sample. Figure 4.10 shows the distribution of the stars, showing in red the single stars that are candidates to unresolved binaries.

Among the 834 M dwarfs in multiple systems, 641 are primary components of their systems (i.e. the most massive). For all statistical purposes, we adopt this latter definition of stellar multiplicity. In this sense, the M dwarfs in our sample that belong to systems with AFGK-type primaries *are not* computed in these statistics, but they are analysed in Sect. 4.4.5. To quantitatively asses the multiplicity of M dwarfs, we follow the notation of Batten (1973), who denoted as f_n the fraction of primaries that have n companions. Therefore, the multiplicity frequency or multiplicity fraction (MF):

$$MF = \frac{\sum\limits_{n=1} f_n}{\sum\limits_{n=0} f_n} = \frac{B + T + Q + \ldots}{S + B + T + Q + \ldots} \tag{4.6}$$

is the number of non-single systems (i.e. binaries of higher order), where S, B, T, Q denote the number of single, binary, triple, and quadruple systems, respectively. The companion star fraction (CSF), is a measure of the average number of companions per system:

$$CSF = \frac{\sum\limits_{i=1} (n-1) f_n}{\sum\limits_{i=0} f_n} = \frac{B + 2T + 3Q + \ldots}{S + B + T + Q + \ldots}, \tag{4.7}$$

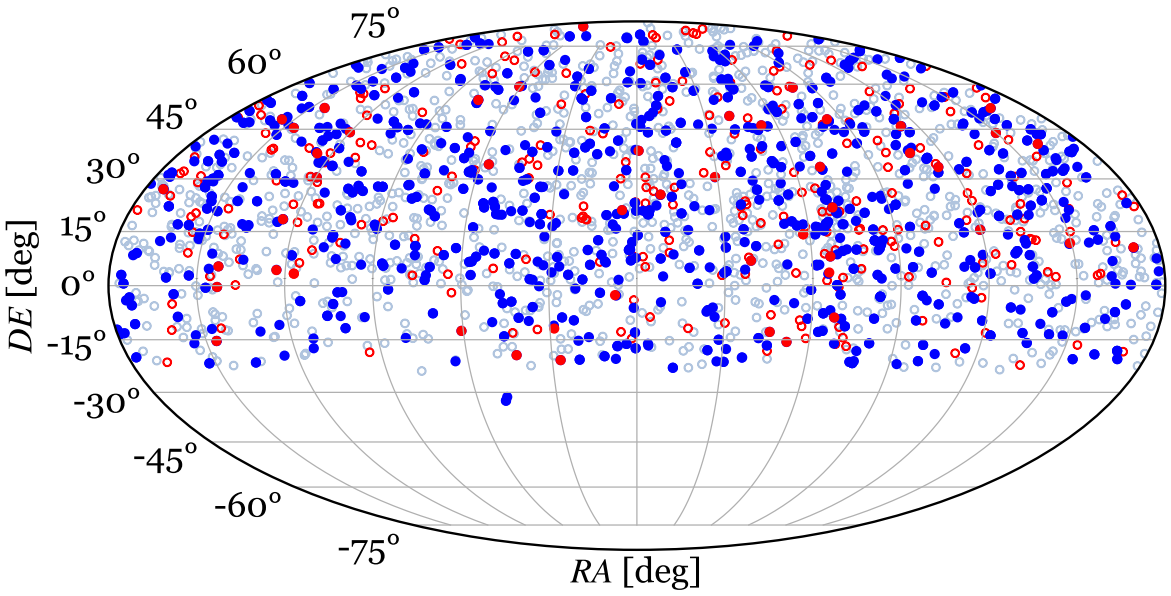

Figure 4.10: Location in the Mollweide-projection sky of all the stars in the sample of M dwarfs, including their companions, in equatorial coordinates. The coloured circles show single stars (empty grey), stars that belong to a multiple system (filled darker blue), and candidates to unresolved binarity for bona fide singles (empty red) and widely separated components of multiple systems (filled red).

which can be larger than 1. We compute these statistics globally, from M0.0–M9.5 V, and, in order to study the dependence with the mass, also for each individual spectral type, from M0.0 V to M9.5 V. We always impose that the M dwarf is the primary of each system, and we also account for observational biases by restricting the statistics to volume-limited subsamples, according to the constrains in Table 4.1. For the estimation of the uncertainties, we compute the 95 % confidence interval using the Wilson (Wilson, 1927) expression:

$$CI_{\rm Wilson} = \frac{k+\kappa^2/2}{n+\kappa^2} \pm \frac{\kappa n^{1/2}}{n+\kappa^2}\sqrt{[\hat{\epsilon}(1-\hat{\epsilon})+\kappa^2]/4n}, \tag{4.8}$$

where n is the number of trials, k is number of observed successes, $\hat{\epsilon} = k/n$, and κ is the number of standard deviations corresponding to the desired confidence interval for a normal distribution. For a confidence interval of $100(1-\alpha)$ %,

$$\kappa = \Phi^{-1}(1-\alpha/s) = \sqrt{2}\mathrm{erf}^{-1}(1-\alpha). \tag{4.9}$$

In our sample we find that the multiplicity fraction for all the range of M dwarfs, once observational biases have been taken into account, is MF = 28.9%, and the companion star fraction is CSF = 50.1%. The candidates to multiple systems found as described in Sect. 4.3.2 represent an additional 12.3% to the MF value. With this, we find that the multiplicity of M dwarfs could be *as high as* 41%.

In Table 4.4 we tabulate these statistics together with the multiplicity fraction for M dwarfs reported in the literature during the last three decades, sorted by decreasing order of publication. To compare properly, we choose works for which similar spectral ranges in the M-dwarf domain were studied, although they are rarely identical. We indicate, when possible, the relevant constrains of the studies: spectral range, sample size, completeness volume, search separations, and methodology. We help the comparison by also providing the MF in two consecutive spectral ranges: from M0.0 to M5.0 V, and from M5.5–M9.0 V.

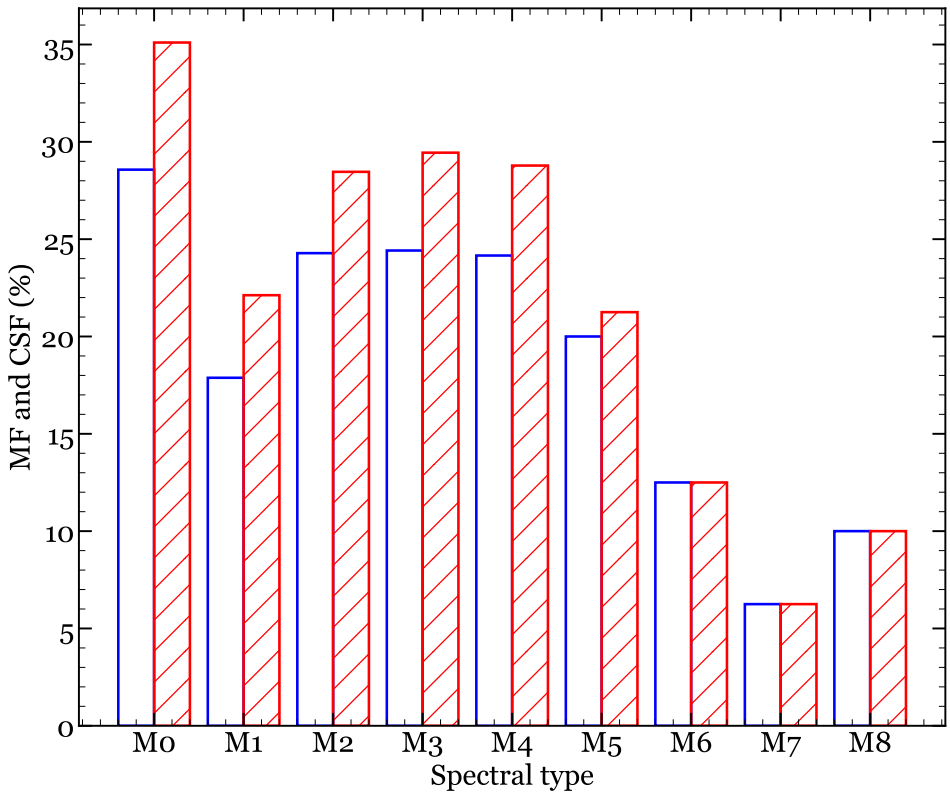

Figure 4.11: Multiplicity fraction (*MF*) and companion star fraction (*CSF*) as a function of spectral type, shown as empty blue and dashed red bar plots, respectively.

Our results are in agreement with the values reported in the literature, especially in those cases where a sizeable sample was studied. In this sense, our work doubles in size the largest sample among the compared studies.

Next, we study the dependence of multiplicity fraction on spectral type (Table 4.3). In Fig. 4.11 we show the *MF* and *CSF* percentages as a function of the spectral type, and in Table 4.4 we tabulate these fractions. The results for spectral type M7.0 V and later are omitted because of the absence of a substantial sample. The dependence of *MF* with primary mass shown is consistent with the expected values in the literature, as we introduced in Sect. 4.1. The *CSF* also reflects this dependence, meaning that the smaller the stars, the fewer the companions. With an asterisk (MF^*) we refer to the multiplicity fraction that takes into account the non-resolved candidates. We also include the mean values of the mass ratio, q, which behaviour is not monotonic (i.e. it does not indicate that the masses of the companions are comparatively smaller for smaller stars). This parameter q has calculated carefully considering what *primary* means in each system. For instance, the primary component for Proxima Centauri is the double star α Centauri, as introduced in Sect. 4.1.

Table 4.3: *MF*, *CSF*, and mean mass ratio, q, as a function of spectral type for the 2215 stars in the sample.

Spectral type	Sample size	*MF* [%]	*MF** [%]	*CSF* [%]	q
M0.0–1.0 V	245	$28.6^{+6.0}_{-5.3}$	$40.0^{+6.2}_{-5.9}$	$35.5^{+6.2}_{-5.7}$	0.75
M1.0–1.5 V	330	$17.9^{+4.5}_{-3.8}$	$30.9^{+5.2}_{-4.7}$	$22.1^{+4.8}_{-4.1}$	0.49
M2.0–2.5 V	383	$24.5^{+4.5}_{-4.0}$	$35.5^{+4.9}_{-4.6}$	$27.9^{+4.7}_{-4.3}$	0.69
M3.0–3.5 V	557	$24.4^{+3.7}_{-3.4}$	$35.9^{+4.1}_{-3.9}$	$29.6^{+3.9}_{-3.6}$	0.69
M4.0–4.5 V	476	$23.9^{+4.0}_{-3.6}$	$36.1^{+4.4}_{-4.2}$	$27.9^{+4.2}_{-3.8}$	0.72
M5.0–5.5 V	160	$20.0^{+6.9}_{-5.5}$	$34.4^{+7.6}_{-6.9}$	$21.2^{+7.0}_{-5.6}$	0.73
M6.0–6.5 V	32	$12.5^{+15.6}_{-7.5}$	$28.1^{+17.2}_{-12.6}$	$12.5^{+15.6}_{-7.5}$	…
M7.0–9.5 V	28	…	…	…	…

Table 4.4: Multiplicity fraction (*MF*) for M dwarfs calculated in this work and published in the literature.

Reference	Spectral range[a]	Sample size	$d_{\rm lim}$[b] [pc]	s [au]	Multiplicity fraction[c] [%]	Methodology[d]
This work	M0.0–M5.0	2118	~24–33	$\lesssim 10^5$	$29.2^{+2.0}_{-1.9}$ ($41.2^{+2.1}_{-2.1}$)	See Sect. 4.3
	M5.5–M9.0	94	~10–24	$\lesssim 10^5$	$23.4^{+9.5}_{-7.4}$ ($42.6^{+10.1}_{-9.5}$)	
	M0–M9	2212	~10–33	$\lesssim 10^5$	$28.9^{+1.9}_{-1.9}$ ($41.2^{+2.1}_{-2.0}$)	
Susemiehl & Meyer (2022)†	M	1550	15	$\lesssim 10^4$	22.9 ± 2.8	†
Clark et al. (2022)	M	1070	15	$\lesssim 60$	29.2–31.3	SI
Winters et al. (2019a)	M	1120	25	$\lesssim 10^4$	26.8 ± 1.4	WI
Cortés-Contreras et al. (2017b)	M0–M5	425	14 (86 %)[c]	~1.4–65.6	19.5 ± 2.3	LI
Ward-Duong et al. (2015)	K7–M6	245	15	~3–10 000	23.5 ± 3.2	AO, WI
Jódar et al. (2013)	K5–M4	451	25	$\lesssim 80$	$20.3^{+6.9}_{-5.2}$	LI
Janson et al. (2012)	M0–M5	761	52	~3–227	27 ± 3	LI
Bergfors et al. (2010)	M0–M6	108	52	~3–180	32 ± 6	LI
Law et al. (2008)	M4.5–M6.0	108	$\lesssim 20$	$\lesssim 80$	$13.6^{+6.5}_{-4.0}$	LI
Reid et al. (1997)	K2–M6	106	8	$\lesssim 1800$	32	SI, WI, RV
Leinert et al. (1997)	M0–M6	34	5	~1–100	26 ± 9	SI
Fischer & Marcy (1992)	M	62	20	$\lesssim 10^4$	42 ± 9	SI, WI
Henry (1991)	M	74	8	…	30–40 %	SI

[a] "M" must be read as "all the M dwarfs within the volume limited by $d_{\rm lim}$", when no specific limitation on the spectral classification of the sample is given.
[b] The volume-complete samples are taken for each spectral type, based on the values of Table 4.1.
[c] The percentage in parentheses takes into account the candidates to unresolved binaries detected by *Gaia*.
[d] SI: Speckle interferometry; LI: Lucky imaging; WI: Wide-field imaging; AO: Adaptive optics; RV: Radial-velocity. These methods are referred to data acquisition.
[e] The authors indicate that the percentage may increase to at least 36 % by including the pairs at $\rho < 0.2$ arcsec and $\rho > 5$ arcsec.
† Data compiled from four different works. The sample size is the sum of the individual sample sizes, and the limiting distance is the smallest one. The methodology consisted on fitting a log-normal function to the orbital separation distribution.

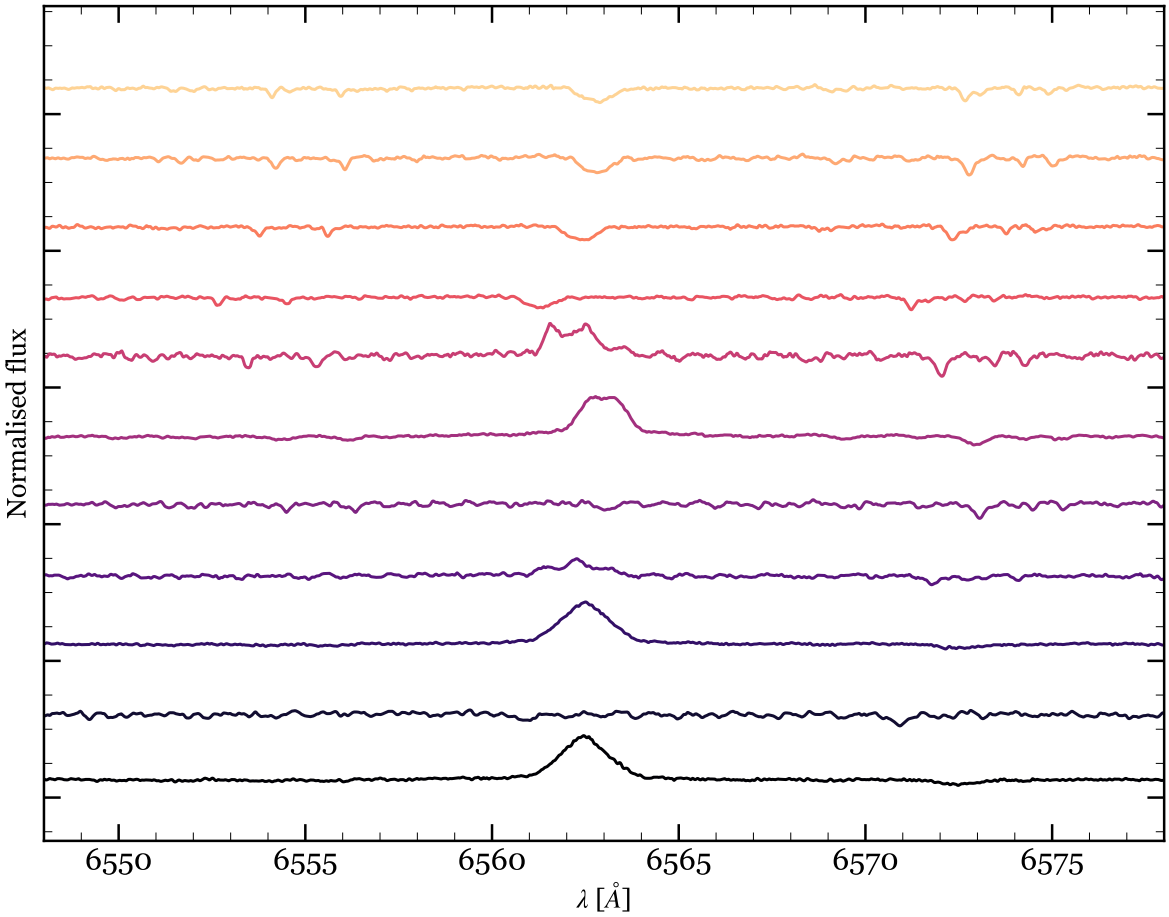

Figure 4.12: FIES spectra of early M dwarfs in our spectroscopic study, from hottest (*top*) to coolest (*bottom*). They are vertically offset for visualisation purposes.

4.4.2 Unresolved binaries resolved with FIES

Among the stars for which *Gaia* DR3 measures the largest deviations in radial velocity and the largest values of `ruwe`, we selected the brightest to study their close multiplicity using medium resolution spectra. We carried out the observations with the high-resolution FIbre-fed Echelle Spectrograph (FIES) mounted on the 2.56m Nordic Optical Telescope (NOT, Djupvik & Andersen, 2010), in the mid-resolution mode (R = 46 000). The observations took place in service mode during four nights over seven months, from April to October, 2022, and are in process in a separate proposal during four nights granted in a campaign of semester 2022B. Additionally, several spectra were obtained in mid-February with High-Efficiency and high-Resolution Mercator Échelle Spectrograph (HERMES) at the 1.2-m Mercator telescope. Finally, a follow-up proposal for this programme has been approved, also with FIES, for the semester 2023A. We have obtained so far 30 spectra of 17 targets, which were processed with automatic reduction software `FIEStool` (Stempels & Telting, 2017). Figures 4.12 and 4.13 display some representative spectra taking with FIES.

From the study of cross-correlation functions (CCFs) and radial velocities, we discovered 7 SB1 (5 of them with more observations needed to confirm), 5 SB2, 2 ST3 (one of them also to be confirmed), and 2 high-rotation stars (whose multiplicity cannot be determined with the available data). Several CCF fitting plots can be found in Fig. 4.17. We summarise the findings in Table 4.5, including the observation epochs, the heliocentric radial and rotational velocities (for both components if possible), and the

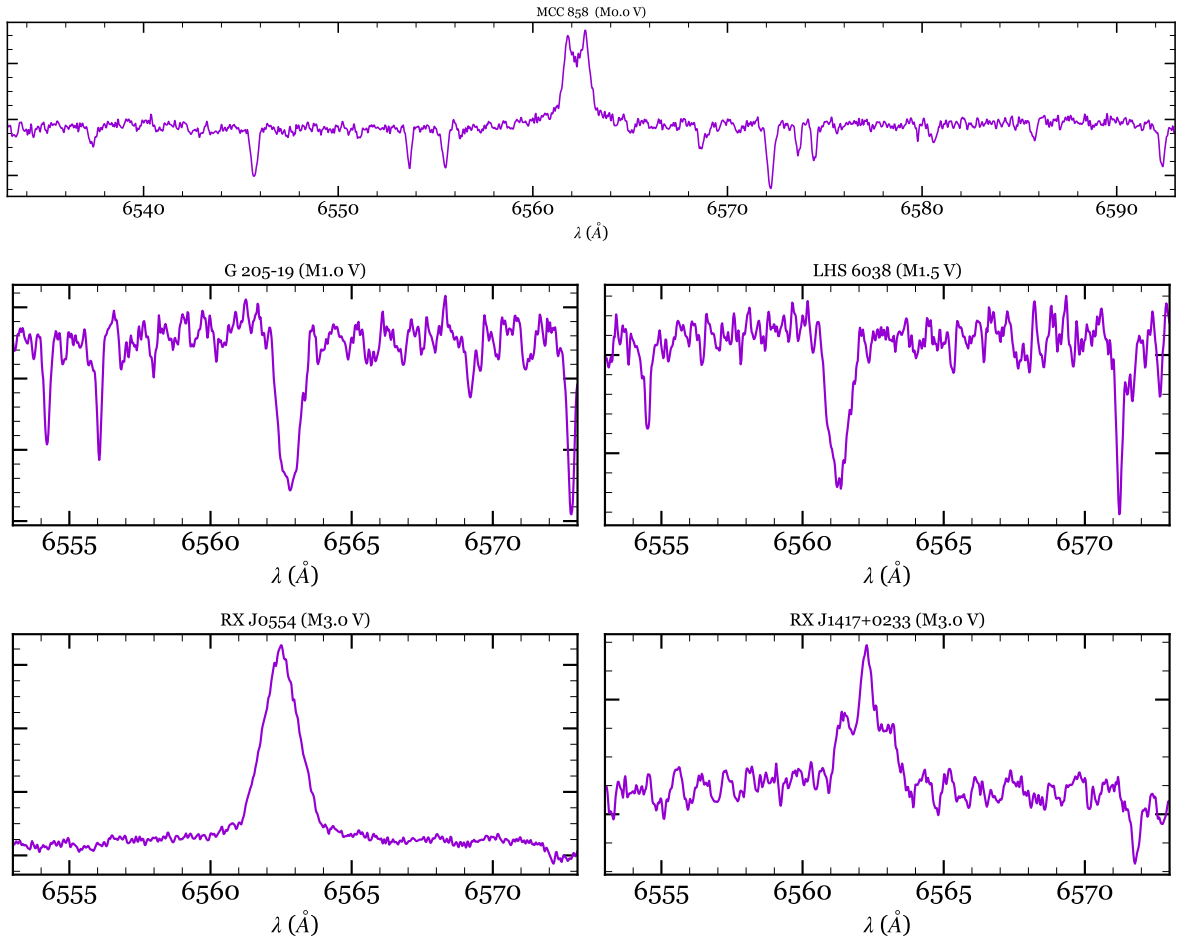

Figure 4.13: FIES mid-resolution spectra of different cases of early M dwarfs in our spectroscopic study, centred in Hα (λ = 6563 Å).

unresolved binarity criteria (1–7 in Table 4.2) that they meet. The errors associated to the heliocentric radial velocities were obtained as weighted means of the individual values deduced for each of the slices of the spectra.

Heliocentric radial velocities were obtained using the CCF technique (see e.g. Gálvez et al., 2002). The spectra of the target were cross-correlated in 6 slices in the range 4500–7500 Å, using the routine `fxcor` in the software Image Reduction and Analysis Facility (IRAF), against spectrum of a radial velocity standard. We selected Barnard's Star, because is a well-studied single, non-active, low-rotator mid-M dwarf with known radial velocity (–110 km s^{-1} Fouqué et al., 2018). We derived the radial velocity for each slice from the position of the peak of the CCF and calculated the uncertainties based on the fitted peak height and the antisymmetric noise as described by Tonry & Davis (1979). For SB2 cases, when we could discriminate the peaks in the CCF associated with both components, we fitted each peak separately.

In order to determine rotational velocities, $v \sin i$ we applied the cross-correlation technique, again using `fxcor`. The method is described in detail in Gálvez et al. (2002). In short, it is based on the fact that when a stellar spectrum with rotationally broadened lines is cross-correlated against a narrow-line spectrum, the width of the CCF will depend on the amount of rotational broadening of the former spectrum. We therefore used Barnard's Star to calibrate the relation between $v \sin i$ and the full-width half-maximum (FWHM) of the CCF. For this, we used the range 6500–7000 Å and a series of rotations between 1 and 50 km s^{-1}, fitting the relation with a 4-degree polynomial (Fig. 4.14). The rotational velocities measured

Table 4.5: Spectroscopic binaries and candidates detected from radial velocity variability and `ruwe` in *Gaia*.

Karmn	Name	SB[a]	HJD (240000–JD)	V_A [km s^{-1}]	$v \sin i_A$ [km s^{-1}]	V_B [km s^{-1}]	$v \sin i_B$ [km s^{-1}]	Note[b]
J00374+515	G 172-14	Single or SB1	59864.57	−55.68 ± 0.48	< 2	…	…	•
J01556+028	LHS 6038	SB2	59864.51	−67.32 ± 0.32	< 2	−44.66 ± 0.73	3–4	
J02069+451	V374 And	SB2	59864.44	59.13 ± 0.80	~4	64–65	…	•
			59864.74	58.82 ± 1.00	…	…	…	
			59945.46	55.27 ± 0.58	< 3	68.75 ± 1.02	< 3	
J03026-181	GJ 121.1	Single or SB1	59864.54	19.84 ± 0.13	< 2	…	…	
J03147+485	Ross 346	SB2/ST3	59864.60	30.30 ± 0.45	2–3	8.72 ± 0.95	7–8	•
			59944.56	10.92 ± 0.45	< 3	36.78 ± 0.96	~3	
			59945.55	8.62 ± 0.36	…	40.05 ± 0.72	…	
J05091+154	Ross 388	Single or SB1	59944.59	−21.60 ± 0.24	~3	…	…	
J05547+109	RX J0554.7+1055	rot	59864.62	10.51 ± 2.12	25–26	…	…	•
			59864.65	10.52 ± 1.52	…	…	…	
			59864.65	11.16 ± 2.21	~30	…	…	
J06035+155	TYC 1313-1482-1	ST3?	59864.75	49.58 ± 0.93	3–4	…	…	•
			59945.61	50.20 ± 1.00	~3	…	…	
J06105+024	TYC 135-239-1	Single or SB1	59864.72	35.76 ± 0.57	2–3	…	…	•
J08158+346	LP 311-008	SB2	59864.68	23.92 ± 0.46	2–3	43.54 ± 0.66	2–3	•
			59945.68	23.03 ± 0.47	< 3	42.22 ± 0.07	< 3	
J14175+025	RX J1417.5+0233	SB2	59697.48	−47.56 ± 0.20	2–3	−8.66 ± 0.51	4–5	•
			59723.47	−22.76 ± 0.13	…	−45.61 ± 0.38	…	
			59775.38	−18.23 ± 0.16	…	−51.4 ± 0.45	…	
J14200+390	IZ Boo	SB1?/rot	59775.38	−22.10 ± 2.87	34–36	…	…	•
J18227+379	G 205-19	Single or SB1	59864.37	−14.53 ± 0.40	< 2	…	…	•
J18394+690	RX J1839.4+6903	SB1	59723.52	−33.54 ± 0.30	1–3	…	…	•
			59775.43	−32.67 ± 0.28	…	…	…	
			59864.40	−2.19 ± 0.30	…	…	…	
			59883.31	0.54 ± 0.28	…	…	…	
J18519+130	2MJ18515965+1300034	Single or SB1	59864.30	−17.19 ± 0.68	13–14	…	…	
J22176+565	2MJ22173704+5633100	SB2	59864.45	−22.12 ± 0.53	< 2	−9.26 ± 0.9	< 2	
J23060+639	MCC 858	Single or SB1	59864.49	−22.95 ± 0.72	3–4	…	…	

[a] SB1: single-lined binary; SB2: duble-lined binary; ST3: triple-lined triple; rot: high rotation star.

[b] J00374+515: Included in Non-single table `nss_two_body_orbit` as 'SB1'.
J02069+451: Clear asymmetry found, most probably from a secondary component, but difficult to determine. Classified as eclipsing binary candidate (Malkov et al., 2006) in the Combined General Catalogue of Variable Stars (GCVS; Samus et al., 2004).
J03147+485: Probable SB3, with $V_B \simeq 17$ km s^{-1}. Unclear with a single spectrum.
J05547+109: 12.40 ± 1.88 and 12.05 ± 1.20 are the values obtained with reference star (Barnard's) rotated to the object's $v \sin i$.
J06035+155: Probable triple. 10, 50, and 70 km s^{-1} measured for the components.
J06105+024: Included in Non-single table `nss_two_body_orbit` as 'AstroSpectroSB1'.
J08158+346: Included in Non-single table `nss_two_body_orbit` as 'AstroSpectroSB1'.
J14175+025: Orbital solution attempted (Fig. 4.16).
J14200+390: −23.90 ± 4.38 is the value obtained with reference star (Barnard's) rotated to the object's $v \sin i$.
J18227+379: Probable higher order multiple.
J18394+690: Orbital solution attempted (Fig. 4.16).

this way are included in Table 4.5.

Most of our targets are not fast rotators (i.e. the rotation velocity is similar to that of Barnard's standard). Nevertheless, two objects are found to be moderate rotators: IZ Boo ($v \sin i \simeq 25$ km s^{-1}) and RX J0554.7+1055 ($v \sin i \simeq 35$ km s^{-1}). In these the lines widen and flatten, which impedes a correct fitting of the CCF to a gaussian profile (Fig. 4.15, *left*). In their spectra the lines appear as lumpy, which may look as the effect of two components, but that is not evident in the CCFs. For instance, measuring the FWHM of IZ Boo yields a rather broad range 35–45 km s^{-1} for $v \sin i$. For these two stars, we performed the CCF with the spectrum of Barnard's Star, but rotated to the corresponding $v \sin i$ esti-

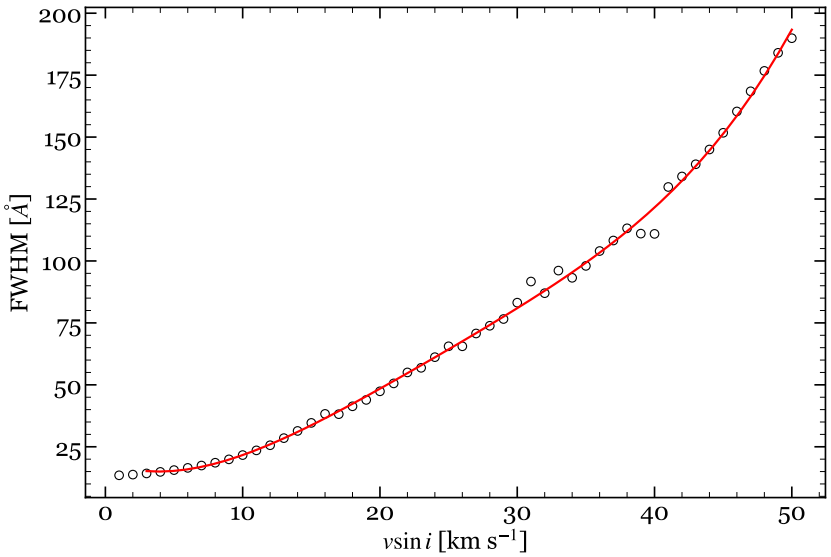

Figure 4.14: Rotational velocity, $V_{\rm rot}$, as a function of the full width half maximum (FWHM), calculated for Barnard's Star, serving as a yardstick for high-rotation objects.

Table 4.6: Prior distributions to perform the MCMC fit.

Parameter	RX J1417.5+0233	RX J1839.4+6903	Units
V_r	$\mathcal{U}(-40,-20)$	$\mathcal{U}(-40,-20)$	km s^{-1}
K	$\mathcal{G}\left(0,10^4\right)$	$\mathcal{G}\left(0,10^4\right)$	km s^{-1}
$P_{\rm orb}$	$\mathcal{G}(148,20)$	$\mathcal{G}(\mathrm{X},\mathrm{Y})$	d
T_0	$\mathcal{U}(t_1,t_1+P_{\rm orb})$	$\mathcal{U}(t_1,t_1+P_{\rm orb})$	d
$\sqrt{e}\cos\omega$	$\mathcal{G}_t(0,0.2)$	$\mathcal{G}_t(0,0.2)$	…
$\sqrt{e}\sin\omega$	$\mathcal{G}_t(0,0.2)$	$\mathcal{G}_t(0,0.2)$	…
jitter	$\mathcal{U}(0,10)$	$\mathcal{U}(0,10)$	km s^{-1}

mated for each high rotating star, as explained previously. This way we could directly measure their radial velocity and calculate the rotation velocity. With this procedure we also smoothed the profile, preventing from seeing possible close and blended companions, but a previous inspection suggest that, although very close companion or active regions may be the cause or the irregularities in the CCF, it is not possible to discriminate clearly any additional component.

For two candidates, RX J1417.5+0233 and RXJ1839.4+6903, we have made an attempt of obtaining orbital solutions, using the three and four datapoints available to date for each resolved components, respectively (Fig. 4.16). We used the sum of n Keplerian models, where n is the number of detected components in the system. We explored the parameter space by sampling the posterior distribution with the Markov chain Monte Carlo (MCMC) code `emcee` (Foreman-Mackey et al., 2013), setting the number of walkers to be four times the number of parameters (i.e. 28). Next, we iterated $3{\times}10^3$ times per walker, which sums a total of 28 000 iterations. Given the scarcity of observations per target, we can only aim at providing a preliminary orbital solution. Thus, we restrict some of the orbital parameters by employing narrow gaussian distributions ($\mathcal{G}$, or $\mathcal{G}_t$ if it is truncated) as informative priors. This is the case for the radial velocity semi-amplitude (K), the orbital period ($P_{\rm orb}$), the eccentricity (e), and the argument of periastron (ω). For the remaining parameters (epoch of periastron passage, T_0, longitude of periastron, ω, eccentricity, e, and jitter) we selected uniform prior distributions ($\mathcal{U}$).

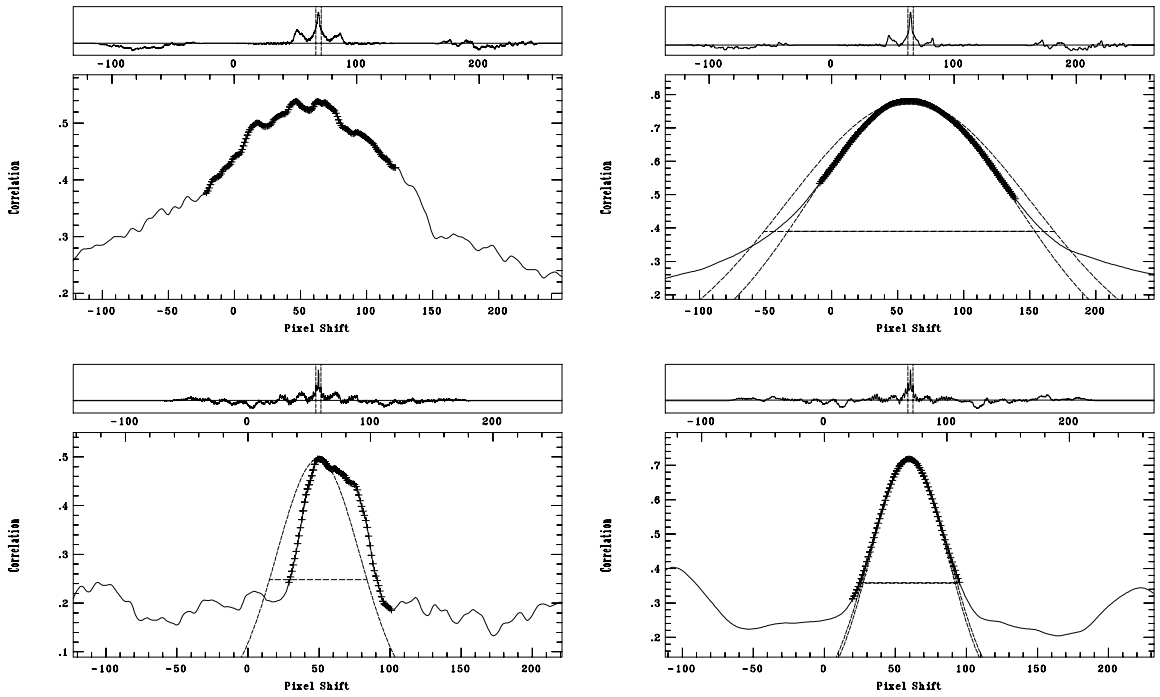

Figure 4.15: CCF of IZ Boo (*top*) and RX J0554.7+1055 (*bottom*). On the left are shown the CCFs with non-rotated Barnard's Star, while on the right are shown the CCFs with rotated Barnard's Star as standard, better suited for measuring radial velocities.

The values employed for these priors (see Table 4.6) are obtained using simple assumptions and basic physical laws. The orbital period is estimated using Kepler's Third Law (Eqn. 4.11). In it, the *maximum* separation, a, was estimated given the fact that *Gaia* DR3 is not resolving the pair, but is providing instead an altered (high) `ruwe` statistic (see Sect. 4.3.2), and therefore the physical separation must be $\rho \lesssim 0.15$ arcsec[8]. The definition $a = \rho d$ can be used inserting the parallactic distance, d, which is known. For the total mass, $\mathcal{M}_T$, we used the peak height ratio from the CCFs (Fig. 4.17) to approximate the mass of the secondary, given that the mass of the primary is known, or is approximated by the observed spectral type. Finally, the radial velocity deviation from the median measured by *Gaia*, ΔV_r, can be related to the semi-amplitude, K (Eqn. 1.1, with $\mathcal{M}_p = \mathcal{M}_\star$), as $K \simeq \frac{3}{2}\Delta V_r$. This expression comes from the fact that a full orbital revolution (equivalent to *two* semi-amplitudes, $2K$) can be related with the *Gaia* radial velocity variance since its 3-σ (that is, $3\Delta V_r$), by definition corresponds with the 99.7% of the measured radial velocities. Finally, we computed the 1-σ and 2-σ uncertainty intervals of the model from the posterior marginal distribution of each parameter.

At this point it is worth mentioning that the current release of *Gaia* (DR3) contains mean BP/RP spectra for 219 million sources (most of them with $G < 17.6$ mag), and mean radial velocity spectrometer (RVS) spectra for 1 million well-behaved objects. *Gaia* DR4 will incorporate the epoch to these spectra, and will also provide all available variable-star and non-single-star solutions, include source classifications (probabilities) plus multiple astrophysical parameters (derived from BP/RP, RVS, and astrometry) for stars, unresolved binaries, galaxies, and quasars. Therefore, DR4 (projected to no earlier than late 2025) will be of additional help in the systematic investigations such as these.

[8] The minimum angular separation for a pair resolved by *Gaia* DR3 in our sample is $\simeq 0.4$ arcsec.

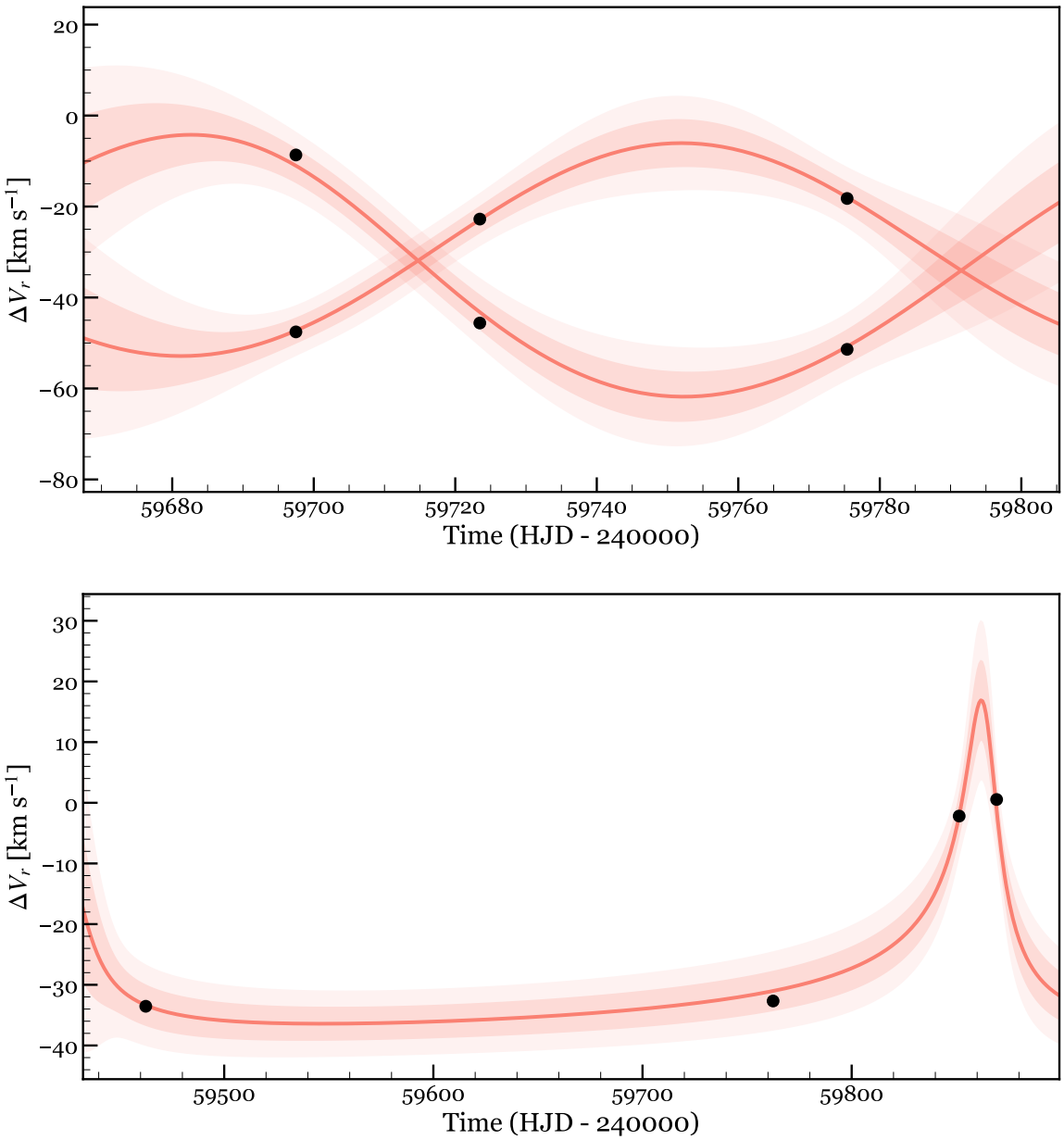

Figure 4.16: Preliminary orbital solutions for the SB2 RX J1417.5+0233 (*top*) and the SB1 RX J1839.4+6903 (*bottom*). The grey shaded regions are MCMC-derived 1- and 2-σ uncertainty intervals.

4.4.3 Astrophysical parameters

When broadband multi-wavelength photometry is available for a star, it can be arranged to produce its spectral energy distribution (SED), which contains important information about the overall emitting power of the star, or bolometric luminosity (see Chapter 3). These empirical SEDs can be approximated by synthetic models and yield the best estimation for their luminosities and effective temperatures, among other parameters. Because these models normally reproduce the stellar photosphere of the stars, we do not include magnitudes from passbands with $\lambda_{\rm eff}$ ~420 nm (i.e. ultraviolet), because these are of chromospheric origin. When combined, photometric data from different passbands serves to narrow down fundamental properties, such as masses or radii. Colours of the stars are made from the

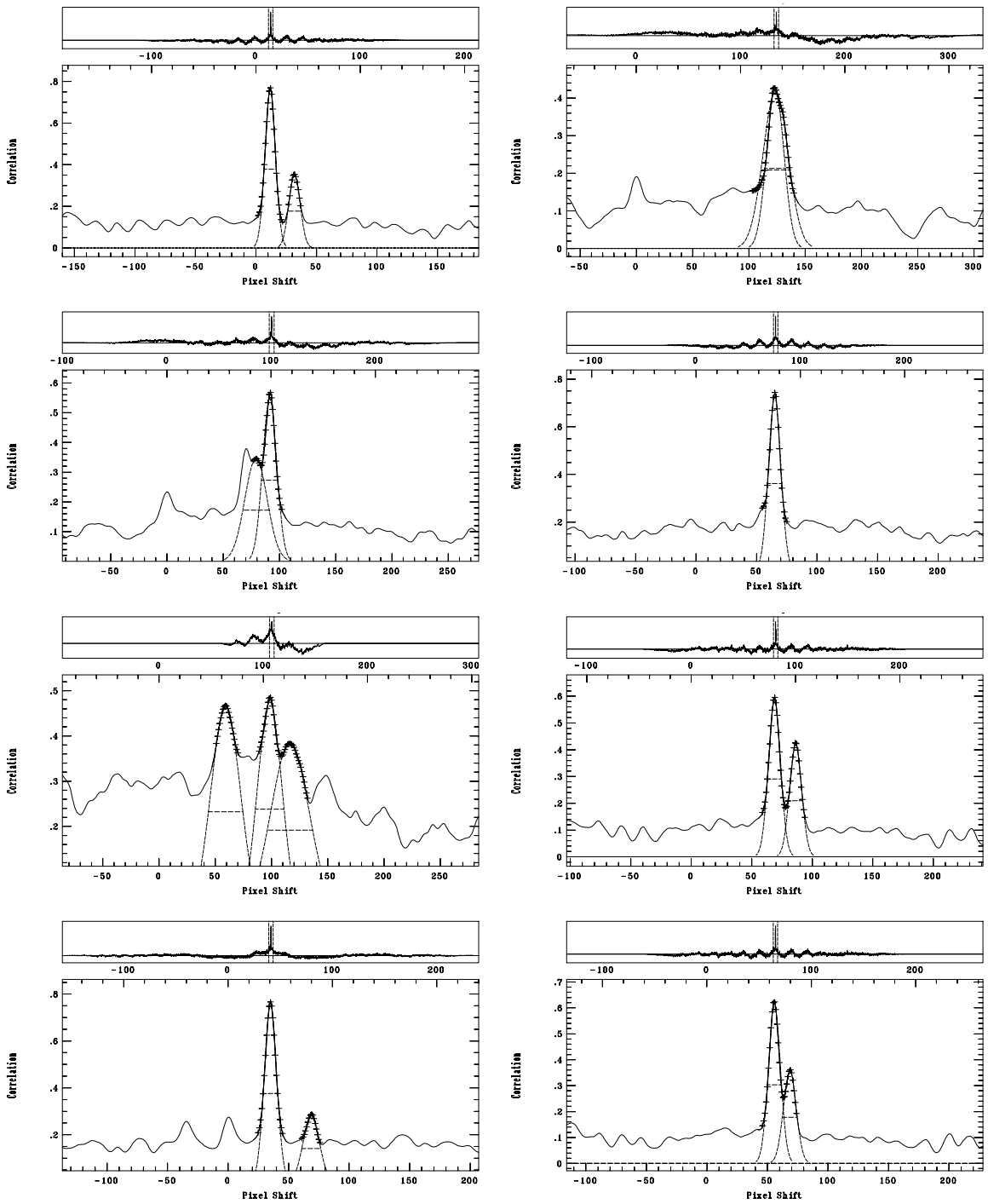

Figure 4.17: *From top to bottom, and left to right*: Cross-correlation functions of LHS 6038 (SB2), V374 And (SB2), Ross 346 (SB2/ST3), Ross 388 (single or SB1), TYC 1313-1482-1 (ST3?), LP 311-008 (SB2), RX J1417.5+0233 (SB2), and 2MASS J22173704+5633100 (SB2).

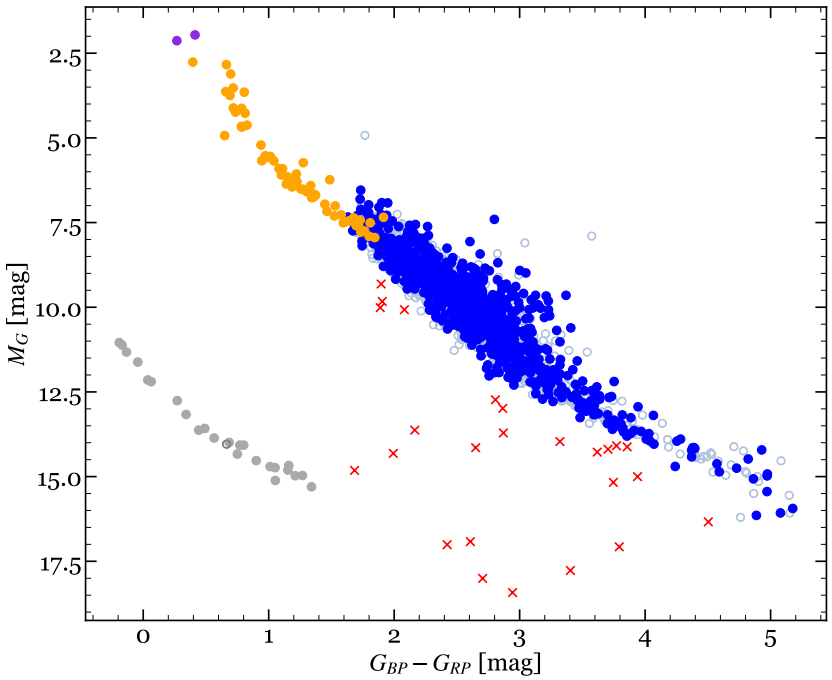

Figure 4.18: Absolute magnitude M_G against $G_{BP} - G_{RP}$ colour for all the stars with full photometry available in *Gaia* DR3. It represents M dwarfs that are single (empty light blue) or part of a multiple system (filled blue), FGK primaries (filled orange), OBA primaries (filled violet), and known and candidates to white dwarfs (filled and empty grey, respectively). Red crosses correspond to components of multiple systems that are very close, very faint, or both, resulting in compromised photometry.

difference of magnitudes in different passbands. An advantage of colours is that they do not depend on the distance to the star, which sometimes is unknown. Nevertheless, if the distance to the star is known with precision (by parallactic means), absolute magnitudes are powerful proxies for other fundamental properties, such as the bolometric luminosity (Cifuentes et al., 2020). For stars in the main sequence (MS), the close relation between the spectral classification and the absolute magnitudes, bolometric corrections, and colours, makes it possible to indirectly estimate parameters that are only accessible with direct inspection of the spectra.

We compiled up to 10 magnitudes for each star, when available: three from *Gaia* (G_{BP}, G, G_{RP}), three from the Two Micron All Sky Survey (2MASS, Skrutskie et al., 2006) (J, H, K_s), and four form the Wide-field Infrared Survey Explorer All-Sky Data Release (AllWISE, Cutri & et al., 2014) ($W1$, $W2$, $W3$, $W4$). Our attempt to include these catalogues automatically by using the 'best_neighbour' automatic crossmatch from the *Gaia* Archive was proven unsuccessful. Indeed, given the singular characteristics of these systems (only partially resolved by 2MASS and AllWISE), the use of automatic crossmatch catalogues provided by *Gaia* (`gaiaedr3.allwise_best_neighbour` and `gaiaedr3.tmass_best_neighbour` in this case) was not found appropriate. Instead, we performed this search manually to ensure a correct discrimination of the components of the systems. This is of paramount importance at this point, because the very description of each system fundamentally relies on the fact of whether 2MASS (along with *Gaia*) is able to resolve the system or not.

Unresolved binaries By definition, an unresolved binary only appears as one source in the photometric surveys, with the flux corresponding to the aggregated fluxes of all the components. As seen in Sect. 4.3.2, the latest photometric surveys like *Gaia* are able to see with better detail and discriminate very close ob-

jects previously considered as single. Still, a notable percentage of stars seen as single are most probably binaries and, to a lesser extent, triples or even multiples of higher order. Some works suggest that certain types of unresolved binarity can be discovered in apparently single stars using only photometric observations. Indeed, photometry has been employed for the identification of unresolved binaries, especially applied to clusters (e.g. Li et al., 2020; Malofeeva et al., 2023). In Fig. 4.18 we show the colour-magnitude diagram (CMD) for all the stars in our sample and their resolved companions, when the photometry in *Gaia* is available. This excludes the very close systems, and the very bright (Capella, Castor) and the very faint (e.g. GJ 570 D) stars and brown dwarfs. Several groups are highlighted: solar-like primaries (orange), OBA primaries (violet), and white dwarfs companions (light grey). All the candidates to white dwarfs based on their location in the CMD have been identified by Jiménez-Esteban et al. (2018). The authors investigated candidates to white dwarfs from the *Gaia* HR diagram using population synthesis simulator. They cut in the `phot_bp_rp_excess` factor in order to prevent against photometric errors in the G_{BP} and G_{RP} bands, especially relevant for the faintest sources. Very compact systems and resolved young stars are outliers above the main sequence. The outliers below the main sequence correspond to faint components of both very close and wide pairs. The former has its photometry affected by the brighter nearby source; for the latter, *Gaia* simply cannot provide a good measure of the flux using the blue filter, G_{BP}.

Using up to 10 magnitudes from the optical blue to the mid-infrared, and the latest parallactic distances available in *Gaia*, we derive effective temperatures and model-independent bolometric luminosities using `VOSA` to fit `BT-Settl CIFIST` models (Baraffe et al., 1998) to the observed spectral energy distribution, as in Cifuentes et al. (2020) (see Chapter 3). We only perform these calculations for the objects whose photometric data have not been compromised by the presence of a companion that is very close, or very bright, or both. These are the single stars (excluding the candidates to close binaries, as explained in Sect. 4.3.2) and, resolved components of multiple systems. For these, we assume the same condition for photometric contamination as Cifuentes et al. (2020) did. Briefly, for a star not to be affected by the presence of a nearby ($\rho \lesssim 5$ arcsec) object, the authors imposed that the flux of the latter, as measured in the G passband, should not exceed more than 1% the flux of the former. This simply translates into a minimum difference in G magnitudes, ΔG, of 5 mag. Moreover, we also restrict this condition further, by choosing only those that are resolved in at least two of the three surveys (*Gaia*, 2MASS, AllWISE), so that the SED is as complete as possible, which minimises the uncertainty in the determination of the best fitting model. This way, we make sure that the presence of a close companion with a comparable or greater luminosity does not have a negative impact on the photometry and any property derived from it. We do not compute luminosities for known spectroscopic binaries in any case.

From the luminosities we homogeneously derived radii $\mathcal{R}$ and masses $\mathcal{M}$,. In particular, we derived the masses using the $\mathcal{M}$-$\mathcal{R}$ relation in (Schweitzer et al., 2019, Eq. 6), coming from the study of detached, double-lined, double-eclipsing, main-sequence, M-dwarf binaries from the literature. This relation is valid a wide range of metallicities for M dwarfs older than a few hundred million years (Dhital et al., 2010). For the companions to the objects in our sample that are outside the M dwarf range, we use the mean values by Pecaut et al. (2012) and Pecaut & Mamajek (2013). For the stars without spectral classification provided in the literature, we estimate the spectral types photometrically, using the average values of the absolute magnitudes, M_G and M_J, which are included in Table 7 of Cifuentes et al. (2020).

For the stars for which it is not possible do derive masses directly from the bolometric luminosities, we use instead their absolute magnitudes in G. For the M dwarfs, first we fitted a 2-degree polynomial to the relation M_G versus stellar mass, $\mathcal{M}$ (Fig. 4.19), in the range $M_G \in [7.5, 15.0]$. We use the Bayesian information criterion (BIC) or Schwarz criterion to determine the preferred degree. We proceeded similarly for the M_G versus stellar radius, $\mathcal{R}$, although it is not plotted due to its similarity. The coefficients for

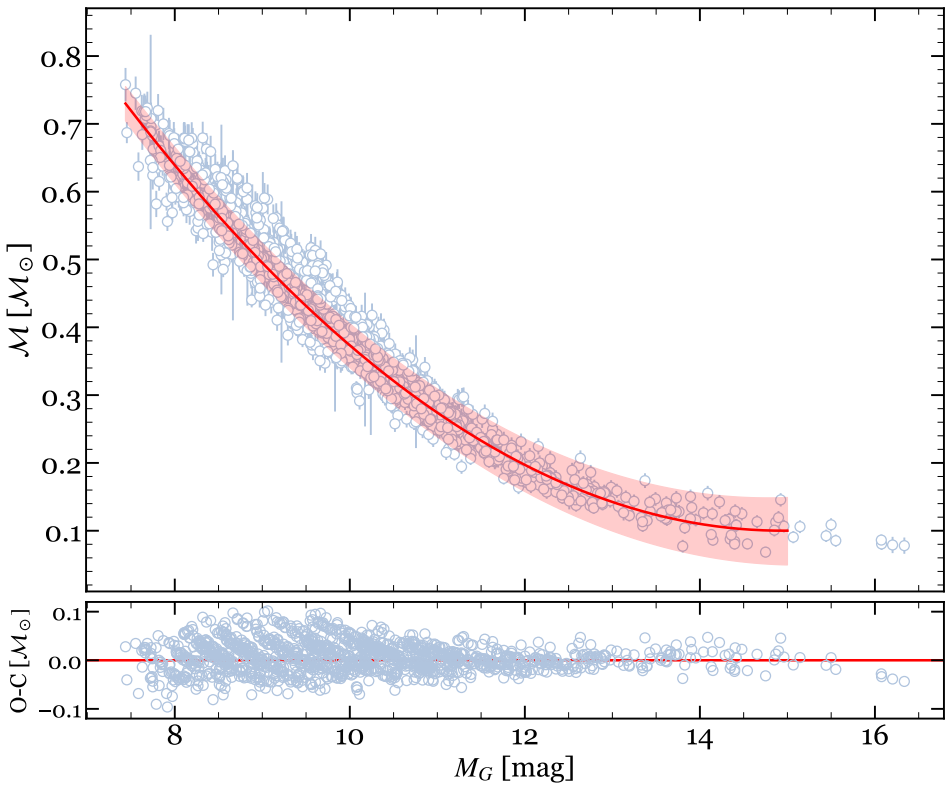

Figure 4.19: Stellar mass $\mathcal{M}$ as a function of the absolute magnitude M_G for the M dwarfs domain. The red line represents the polynomial fit described in the main text, and the red shaded area accounts the 1-σ level of uncertainty.

Table 4.7: Coefficients of the polynomial fits for $\mathcal{M}$ and $\mathcal{R}$ as a function of M_G.

Y[a] [$\mathcal{M}_\odot$]	X [$\mathcal{M}_\odot$]	a [$\mathcal{M}_\odot^{-1}$]	b [$\mathcal{M}_\odot^{-2}$]	c	r / ρ[b]	ΔX [mag]
$\mathcal{M}$	M_G	2.595 ± 0.014	−0.3338 ± 0.0026	0.01117 ± 0.00012	0.981 / 0.982	[7.5, 15.0]
$\mathcal{R}$	M_G	2.308 ± 0.007	−0.2871 ± 0.0012	0.00933 ± 0.00005	0.981 / 0.982	[7.5, 15.0]

[a] The polynomial fits follow the form $Y = a + bX + cX^2$.
[b] Pearson's r and Spearman's ρ coefficients.

both fits are given in Table 4.7, along with the correlation parameters. Both relations are valid for main sequence M dwarfs with solar metallicities, and for $M_G \in [7.5, 15.0]$ (K7/M0.0 V to M7.5 V Cifuentes et al., 2020). This upper limit was chosen with the purpose of the robustness of the fitting in mind, because least-square fitting polynomials of a higher order are prone to degeneracy. Its usage up to M_G = 16 mag still can be done in the case of necessity, but with extreme caution, considering that the masses of ultracool dwarfs are strongly dependent with age (Burgasser & Blake, 2009; Soderblom, 2010, and see Fig. 13 in Sahlmann et al. 2020). We purposefully did not include dwarfs cooler than M_G = 15 mag, because precise masses for these ultracool objects are obtained via dynamical analysis in compact astrometric binary systems (e.g. Sahlmann et al., 2011; Dupuy & Liu, 2017; Brandt et al., 2019; Sahlmann et al., 2020), and therefore *Gaia* cannot provide individual measurements for their apparent magnitudes in G.

For this fit we only selected M dwarfs with parallactic distances from *Gaia*, and excluding spectroscopic and astrometric binaries known but not resolved by it, candidates to unresolved binaries (see Sect. 4.3.2),

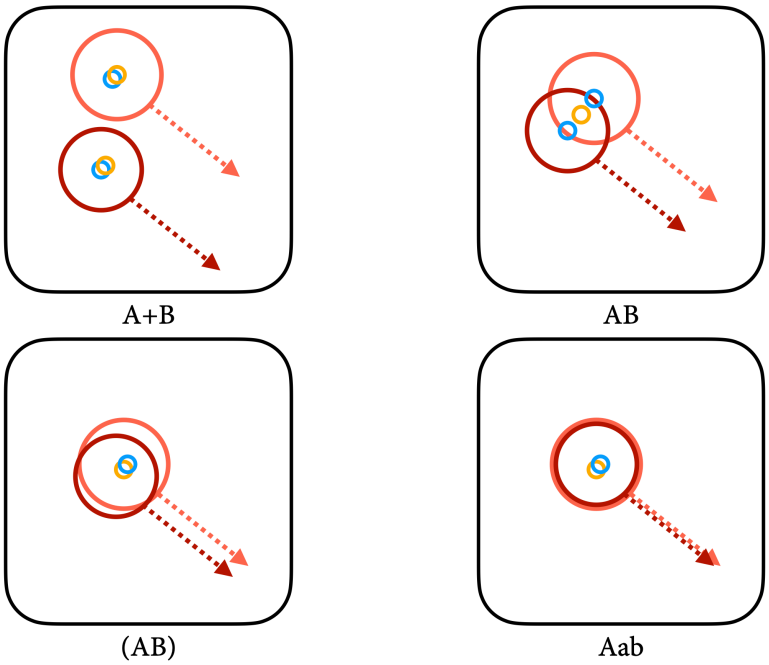

Figure 4.20: Nomenclature of multiple systems based on the resolution in *Gaia* DR3 and 2MASS, represented as blue and orange circles, respectively. *From left to right and top to bottom*: A+B (resolved in both surveys), AB (only resolved in *Gaia*), (AB) (not resolved either in *Gaia* or 2MASS, but resolved by adaptive optics, lucky imaging, or space imaging), and Aab (spectroscopic binaries, only resolved in spectral analysis). Systems may be a combination of the cases above.

and overluminous young objects, for which the masses are underestimated. For the stars outside the range of validity of the relation above, we use the M_G-$\mathcal{M}$ relation by Pecaut & Mamajek (2013). We assume a minimum of 15% of uncertainty from these tabulated values. For objects cooler than L2, we do not provide masses. For white dwarfs, we assign half a solar mass.

4.4.4 Description of the systems

About the main table of this Chapter The structure of the table that contains all the sample plus the discovered components of multiple systems found (Table D.2, and see Table D.1 for the column-by-column description) aims to be both human- and machine-readable. For the former, the systems are displayed with each component of the system resolved by *Gaia* using a single row. The stars are sorted by right ascension, but making sure that stars that belong to the same system are consecutive, in order of decreasing brightness. The nomenclature of the system is described as in Figure 4.20. The most recent version of the complete table can be found in the GitHub repository: `https://github.com/ccifuentesr/`.

Projected physical separations

The cumulative number of binaries as a function of their orbital separation can be parametrised by power laws. Öpik (1924) observed that the distribution of the semimajor axis in binary systems, $f(a)$, follows the form $f(a) \propto a^{-1}$, which in terms of the cumulative distribution is $N(a) \propto \log a$. It can be generalised as $f(a) \propto a^{-\lambda}$, or $N(a) \propto a^{-\lambda+1}$, where $\lambda = 1$ recovers the original Öpik's law. This parametrisation states the intuitive idea that as we go to wider separations, the probability of finding a bound companion strongly diminishes. These wider components are more scarce because their fragile bindings are easily

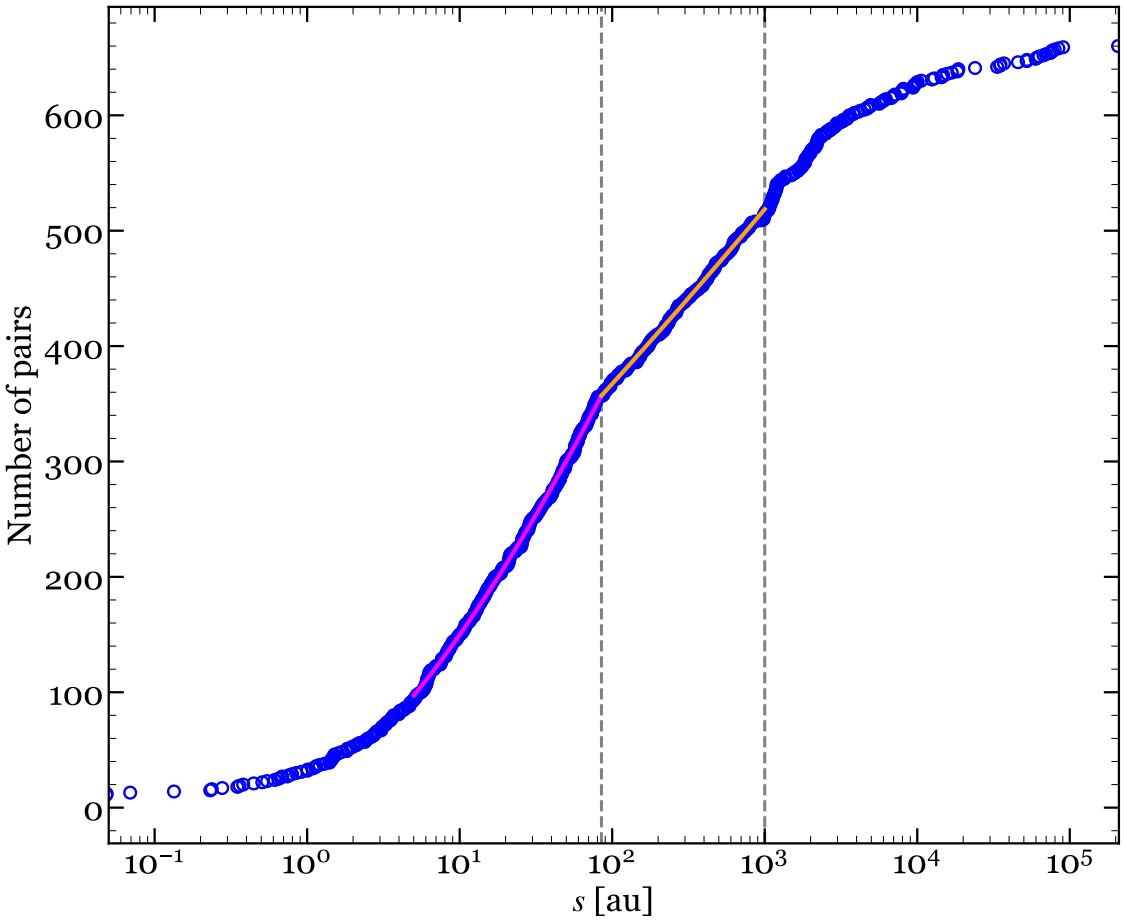

Figure 4.21: Cumulative number of pairs as a function of the physical separation, s. The grey dashed lines mark the values for s = 85 and 10^3 au. The magenta and orange lines are power-law fits for for the ranges (5, 85) and (85, 1000) au, respectively.

affected by the Galactic gravitational potential. Early investigations, such as that of van Albada (1968), suggested that binaries observed at separations greater than about 1000 au must be either "escaping" double stars (or run-away stars — see also Poveda et al. 1967), or one of the components is actually a double star, and therefore a triple system. We analyse several individual instances of this latter case using the precise astrometry of *Gaia* in Sect. 4.4.6.

Because of the small difference that exists between semi-major axis, a, and projected physical separation, s (E(log a) − E(log s) = 1.46, Couteau, 1960) it is more practical to write this expression in terms of this observed separation, $F(\log s) \propto \log s$, which can be derived from the projected angular separation, ρ, by using the small angle approximation ($\tan\rho \sim \rho$), as $s = \rho d$, given in au. Öpik's law can be satisfactorily applied to limited ranges of separation, both in pre-main sequence and main sequence stars (Poveda et al., 1982; Poveda, 1988; Poveda et al., 1994; Poveda & Allen, 2004). However, it has been indeed argued (e.g. Allen et al., 1997) that it might be preferable to describe the distribution function depending on the separation, in accordance with the two main mechanisms of binary formation: disk fragmentation and first-collapse fragmentation (see again Sect. 4.1), for which the authors propose limits of $s < 25$ au and $s > 25$ au, respectively. There also exists an interesting age-dependence of this empirical law in wide binaries, in the sense that the upper limit decreases with increasing age (see again Poveda & Allen, 2004).

In Fig. 4.21 we present the cumulative number of pairs as a function of the physical separation, s. This distribution flattens at very close ($s \lesssim 1$ au) and very wide ($s \gtrsim 10^5$ au) orbital separations. The former is

Table 4.8: Coefficients of the power-law fit for the cumulative distribution of separations, $N(\log s)$.

Range [au]	a	b	λ	R^2
[5, 85]	23.11 ± 2.11	46.428 ± 1.214	−0.3782 ± 0.0142	0.9992
(85, 10^4]	126.9 ± 16.4	44.58 ± 6.54	−0.1786 ± 0.0569	0.9982

Note: The polynomial fits follow the form $N(\log s) = a + b \log s^{\lambda-1}$.

caused by an observational bias regarding physical limitations of the data acquisition of the main high-resolution techniques (speckle, lucky imaging, adaptive optics, and also imaging). In Sect. 4.1 we already noted how investigations suggest that in binaries with semi-major axis $a \lesssim 50$ au the effect of dynamical influence is negligible towards their disruption, and they evolve essentially unaffected. In the era of *Gaia*, the flattens at large values of s occurs mainly due to the difficulty of their formation and eventual survival, rather than observational limitations.

Next, we fit the cumulative distribution between these flat regions to two power laws. This is motivated by the necessity of discriminating between at least two scenarios corresponding to different formation mechanisms, and also motivated by the changes of slope at $s \sim 85$ au and $s \sim 10^3$ au that are visually noticeable. This observational evidence also alleviates the problems that a single theory faces when explaining the existence of binaries with very wide separations. Modelling the binary formation with simple prescriptions (Tokovinin & Moe, 2020) and performing a Bayesian approach on *Gaia* data (Hwang et al., 2022), the authors found that the distribution of eccentricities is approximately uniform at $\sim 10^2$ au, becomes thermal at values larger than $10^{2.5}$–10^3 au, and superthermal[9] at $>10^3$ au. Small mass ratios ($q << 1$) might indicate that stars are formed as binary systems either by the dynamical interaction in unstable molecular clouds or by the turbulent fragmentation of molecular cloud cores. We fit the number of pairs as a function of the separation, $N(\log s)$, in the ranges $s \in [10, 85]$ au, and $s \in [85, 1000]$ au, to a more general form of Öpik's law:

$$N(\log s) = a + b \log s^{-\lambda+1}, \tag{4.10}$$

where a, b, and λ are free parameters. We tabulate the coefficients obtained for these two fits in Table 4.8, including the coefficient of determination, R^2.

In Fig. 4.22 we provide an additional view of the cumulative distributions, discriminating between three consecutive mass ranges: $\mathcal{M}/\mathcal{M}_\odot \leq 0.25$, $0.25 < \mathcal{M}/\mathcal{M}_\odot < 0.65$, and $\mathcal{M}/\mathcal{M}_\odot \geq 0.65$, which approximately correspond to M dwarfs later than M4.5, between M0.0 and M4.5, and earlier than M0.0, respectively. For visualisation purposes, we add grey dashed vertical lines as an early attempt to translate to the three ranges of mass the change in slope that is visible for the complete range of masses. These delimitations are qualitative in nature, but it can serve as a foundation for future investigations. The reason for this is the significance of the observed log-normal shape in the separation distribution and the continuing discussion about its possibility of characterising distinct populations. For instance, measuring the separation distributions of seven young star-forming regions, King et al. (2012a) noted that the separation distributions (and the multiplicity fractions) in them are very different to the field, specifically there is an excess of close binaries (the authors refer to less than 100 au) compared to the field population. They also

[9] Thermal and superthermal are terminologies that refer to the energy level of particles within a system, usually in the field of plasma physics. The energy of thermal particles follows the Maxwell-Boltzmann distribution and has an average energy that depends on the temperature of the system. Conversely, superthermal particles are characterised by energy levels that are significantly greater than the average energy of thermal particles.

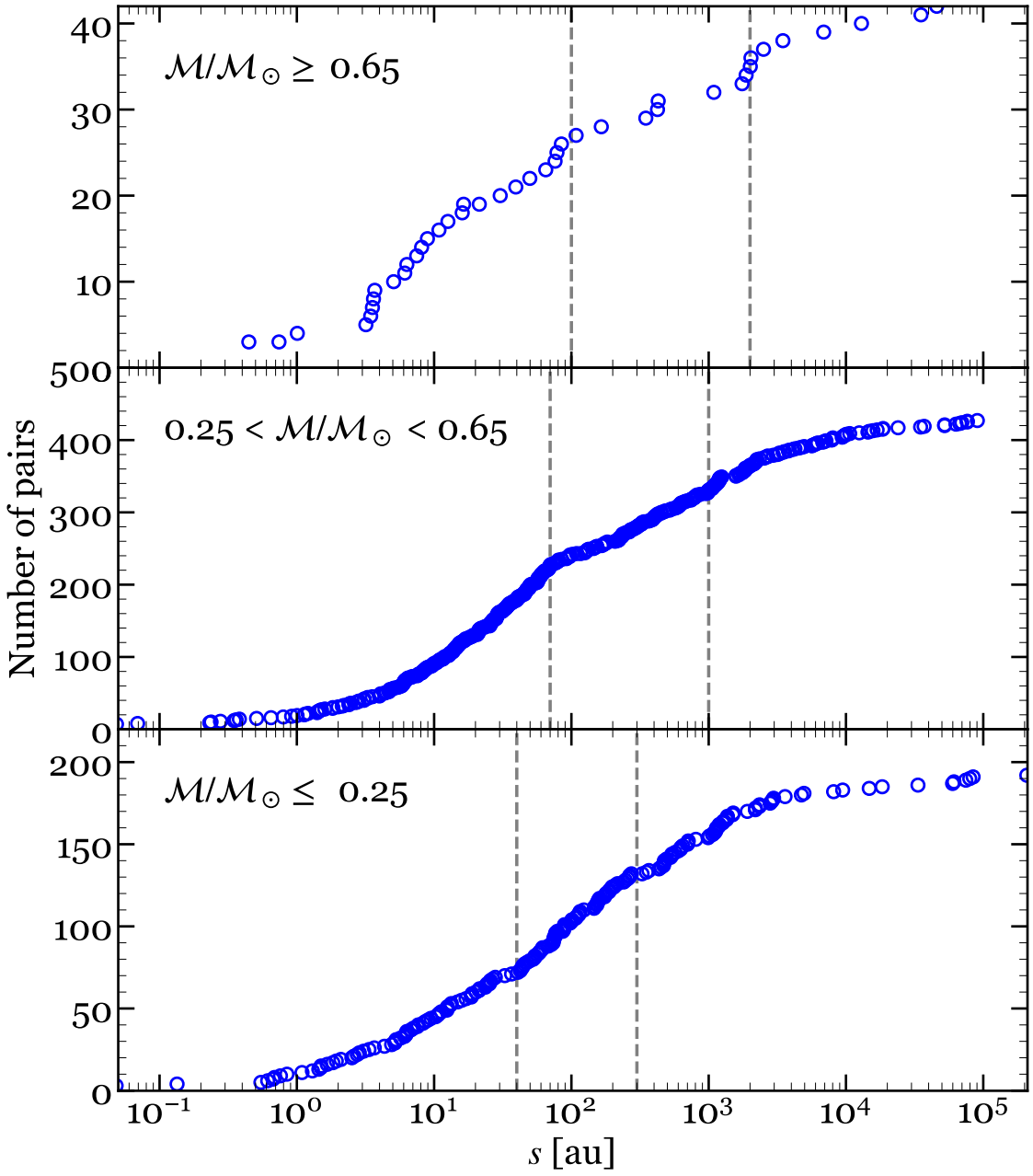

Figure 4.22: Cumulative number of pairs as a function of the physical separation, s. We show three equal-size non-overlapping ranges of primary mass: $\mathcal{M} \geq 0.65\,\mathcal{M}_\odot$ (*top*), $\mathcal{M} \in (0.25, 0.65)\,\mathcal{M}_\odot$ (*middle*), and $\mathcal{M} \leq 0.25\,\mathcal{M}_\odot$ (*bottom*). The grey dashed lines mark the values for $s \in [100, 2000]$ au (*top*), $s \in [70, 1000]$ au (*middle*), and $s \in [40, 300]$ au (*bottom*).

suggested that the separation distribution is not statistically different between the different regions, except in the 19-100 au separation range. All in all, the multifactorial nature of the separation distribution makes it a relevant characteristic that any theory of star formation should be able to account for.

Orbital periods

The orbital period of a system constrains, to a certain extent, how much detail can be poured on its description. There are binary stars for which completing a single orbit around the common centre of

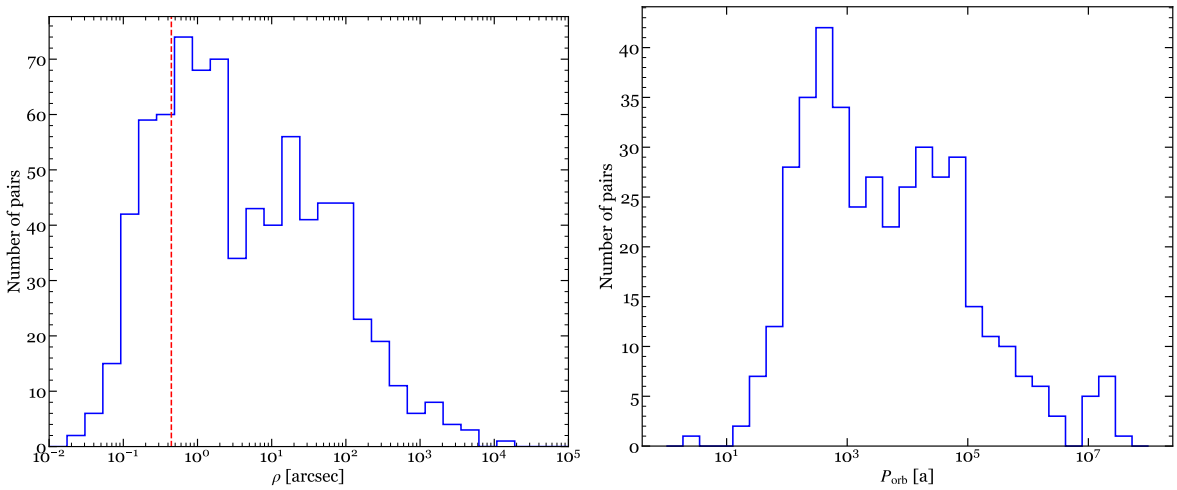

Figure 4.23: Distribution of projected separations in arcseconds (*left*) and orbital periods in years (*right*) for all the multiple systems in our sample. The red dashed vertical line represents the smallest separation that *Gaia* reports in a binary star in our sample.

mass takes millennia or even longer periods. In Fig. 4.23 (right panel) we show a distribution of the orbital periods calculated for all the pairs in our sample with available masses and orbital separations, for which we take special caution when defining the *total* mass of each system. In this sense, the definition of pair must be understood as introduced in Sect. 4.1: triple, quadruple, or even higher order systems can be treated as a binary or group of binaries in the majority of cases. This is, a close compact system can be adequately treated as a single star (with the aggregated masses) if considered from a distance much larger than the separation between its components. Masses of close binary systems need to be managed with caution, as dedicated estimation of the individual components is mandatory. The orbital periods, $P_{\rm orb}$, are calculated using the Kepler's Third Law:

$$P_{\rm orb} = 2\pi \sqrt{\frac{a^3}{G\mathcal{M}_T}}, \tag{4.11}$$

where $a \sim s = \rho d$ is the physical separation in au, and $\mathcal{M}_T$ is the total mass of the system. The majority of the orbital periods lie between 10 and 10^5 years. Without the information about their orbital orientation, these periods could be over- as well as under-estimated. As mentioned earlier in this chapter, for these systems with orbital periods of hundreds or thousands of years, the prospect of following them during one single orbit is unfeasible, only wishing for *discrete* data available from decades to attempt a draft of their orbits (as an example, in Sect. 4.4.6 we showcase two attempts of orbital characterisations with a rather scarce amount of available data, in the most favourable case of spectroscopic binary, with periods of only a few months).

Binding energies

The gravitational potential binding energy of a binary system can be interpreted as the minimum energy required to separate the components to infinity, therefore it is a measure of the strength of their attachment. In a rather intuitive denomination, Heggie (1975) introduced the categories 'soft' and 'hard' binaries as a broad classification for the class of bound that the pairs experience. The former are fragile and easy to break, the latter are highly resilient to encounters. The general expression for the binding

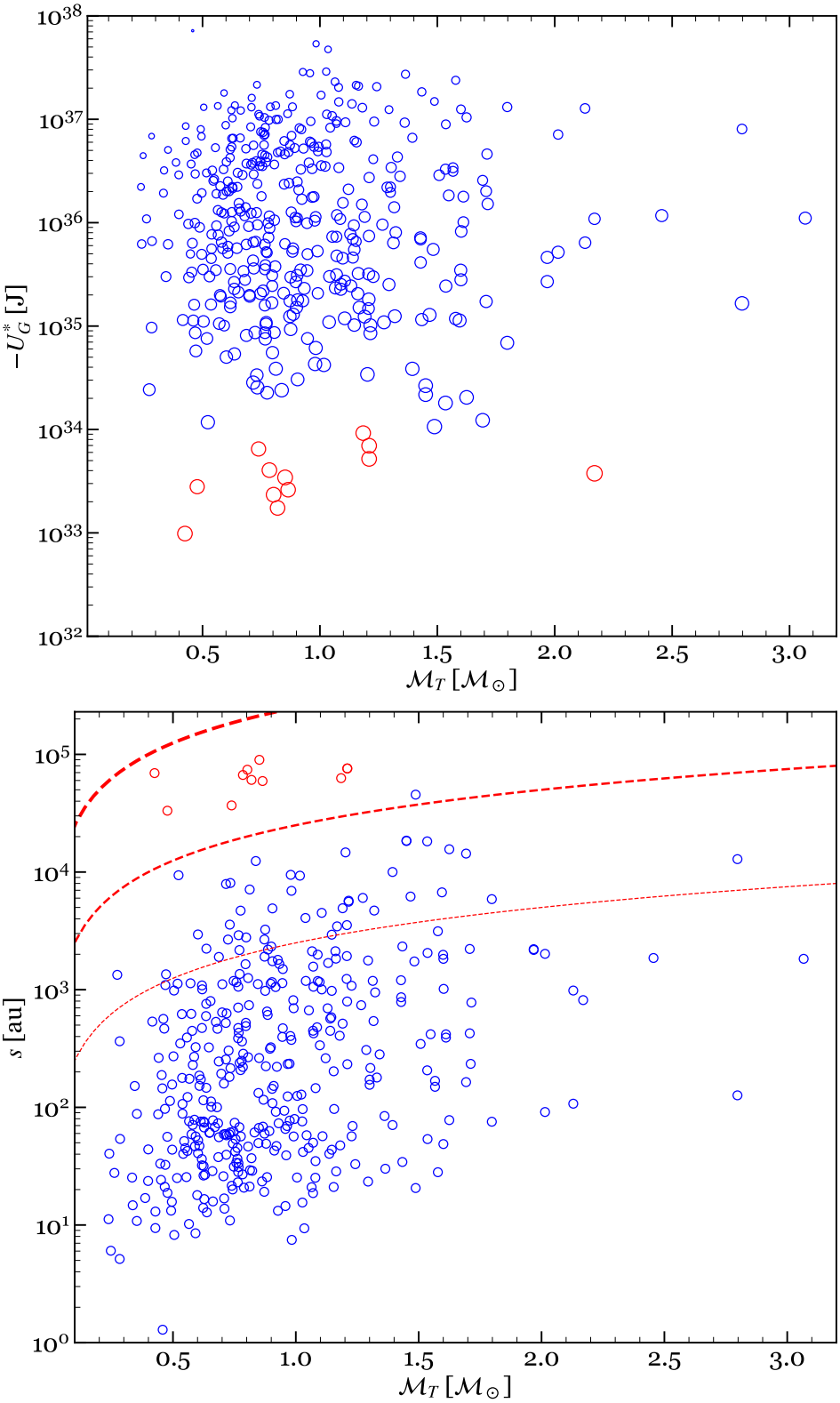

Figure 4.24: Binding energy (*top*) and physical separation (*bottom*) as a function of the total mass of the systems. In the top panel, sizes are proportional to the physical separation from the primary. Red empty circles highlight the most fragile pairs ($|U_g^*| \lesssim 10^{34}$ J). The red dashed lines represent the maximum separation, s, for expected survival in the case of 1, 10, and 100 Ga (in order of decreasing thickness).

energy of a binary system of masses $\mathcal{M}_1$ and $\mathcal{M}_2$, physically separated s (in au), can be put as:

$$-U_g^* = G\frac{\mathcal{M}_1\mathcal{M}_2}{s}. \tag{4.12}$$

Figure 4.24 (*top*) shows the binding energy with the approximation $r \sim s$ (U_g^*) as a function of the total mass $\mathcal{M}_{\rm total}$ of the system, with sizes proportional to the size of the orbit (i.e. the physical separation between the components). Although U_g^* is defined by pairs, we compute the binding energy of triple or higher order of multiplicity systems as long as they dynamically behave like a binary, as in the case of the orbital periods. Figure 4.24 (*bottom*) shows the physical separation between components as a function of the total stellar mass. The most fragile systems (see Sect. 4.4.5) are highlighted in red in both panels.

The dynamical evolution of the stars over time sets an expiring date for the binding of multiple systems, especially in the case of wide pairs. While catastrophic encounters such as collisions are not common, there are a myriad of more subtle chances to disrupt their stability. The gravitational interaction with nearby clouds or stars can be of small intensity, but it is disruptive in the long term. Weinberg et al. (1987) were interested in the fate of wide binaries in the solar neighbourhood caused by these phenomena. Based on the Fokker-Planck coefficients[10], they estimate the average lifetime of a binary (Eqn. 28 of their work) as:

$$t_*(a_0) = 1.8\times10^4\,{\rm Ma}\left(\frac{n_*}{0.05\,{\rm pc}^{-3}}\right)^{-1}\left(\frac{\mathcal{M}_{\rm tot}}{\mathcal{M}_\odot}\right)\left(\frac{\mathcal{M}_*}{\mathcal{M}_\odot}\right)^{-2}\times\left(\frac{\langle 1/V_{\rm rel}\rangle^{-1}}{20\,{\rm km\,s}^{-1}}\right)\left(\frac{a_0}{0.1\,{\rm pc}}\right)^{-1}\ln^{-1}\Lambda, \tag{4.13}$$

where n_* and $\mathcal{M}_*$ account for number density and mass of the perturbers, $V_{\rm rel}$ is the relative velocity between the binary and the perturber, $\mathcal{M}$ and a refer to the total mass and semi-major axis of the binary, and Λ is the Coulomb logarithm. The expression accounts for the stochastic gravitational perturbations and the encounters with passing stars, and can be greatly simplified (Close et al., 2007; Dhital et al., 2010) to the form:

$$s \simeq 1.212\frac{\mathcal{M}_{\rm tot}}{t_\star}. \tag{4.14}$$

Here, s represents the maximum separation in astronomical units, for a total mass $\mathcal{M}_{\rm tot}$ in solar units, to survive for a given age $t_\star$ in Gigayears. These separations are represented for the ages of 1, 10, and 100 Ga as red dashed lines in Fig. 4.24. There are 10 pairs with expected survival periods less than 10 Gigayears, while the vast majority may well be stable for hundreds or thousands of Gigayears[11], assuming a negligible occurrence of catastrophic encounters.

4.4.5 Companions to M dwarfs

FGK primaries

Modeling the atmospheres of a star is a challenging task, and the coolest the star, the harder it becomes (see e.g. Valenti et al., 1998; Woolf & Wallerstein, 2006; Önehag et al., 2012). Early attempts such as `ATLAS` (Kurucz, 1970, 1979) or `MARCS` (Gustafsson et al., 1975, and Gustafsson et al. 2008), are examples of the laudable efforts on this matter despite of the technological limitations, and from which many more

[10] In a few words: The Fokker-Planck coefficients describe the rate of diffusion and drift of particles in a stochastic process.
[11] As a reminder, the age of the Universe is around 13.77 Ga (Planck Collaboration et al., 2020).

spectral libraries would derive. PHOENIX (Hauschildt et al., 1997, and the more recent Husser et al. 2013), NEXTGEN (Hauschildt et al., 1999a,b), or BT-Settl, are just a few notable examples. In order to reproduce the spectral features successfully, models need to take into account a wider range of atomic and molecular interactions and opacities, and introducing this complexity also comes with a greater computational cost. Improvements in high-resolution spectroscopy, high-angular-resolution interferometry, and processing power have made a major difference in this important topic of research. Gaining precision in the determination of stellar abundances translates into better constrain mantle composition and relative core size of the orbiting planets (Dorn et al., 2017).

In this effort of calibrating the metallicity of the coolest stars, a Solar-type physical companion can pave a smoother passage, because their abundances are much easier to determine. Numerous works have estimated M dwarf metallicities using wide binary pairs (e.g. Rojas-Ayala et al., 2012; Montes et al., 2018; Birky et al., 2020; Ishikawa et al., 2022b). Among them, Montes et al. (2018) presented an relatively large sample of 192 wide visual binaries covering a reasonably large range in metallicity and spectral type, with atmospheric parameters of the primaries homogeneously derived using the STEPAR (Tabernero et al., 2019), and chemical abundances for 13 atomic species.

Among the M dwarfs in our sample that belong to multiple systems, we find that 54 have a Solar-type star as a primary. These are late-F to mid-K main sequence stars, including objects from F7 V to K5 V, and excluding the frontier K6/K7-M0 V. We tabulate the systems and their main astrometric properties in Table D.6. M dwarfs accompanied by a hotter, Sun-like star, are precious targets for chemical abundance studies, a promising field of investigation in the era of exoplanet discovery (see Sect. 1.3).

White dwarfs

White dwarfs (WDs) are the final stage for almost all the stars in the Milky Way (Fontaine et al., 2001). The can be considered the fossils of the stellar evolution, and similarly to the preserved remains in paleontology, white dwarfs can be used as clocks that trace back into the past history of the Universe. Several works have made use of white dwarf companions as effective chronometers for M dwarfs (Monteiro et al., 2006; Fouesneau et al., 2019; Qiu et al., 2021; Kiman et al., 2021). When physically paired with M dwarfs, WDs are a valuable source of information about their low mass companions, because, contrary to these, their modelling turns out much easier (Bergeron et al., 1995; Renedo et al., 2010). For instance, these systems represent opportunities for age estimation (Fouesneau et al., 2019), because the age estimation for WDs is based on their cooling, which is well-understood physics (see Soderblom, 2010). Other important applications include the study of mass-loss rate and the characterisation of main sequence companions in multiple systems (Pyrzas et al., 2009, 2012; Parsons et al., 2012). Regarding the observed deficit of white dwarfs compared with predictions, Williams (2004) suggested that a large portion of the missing white dwarfs might be explained if these are part of unresolved systems (e.g. Morales-Rueda et al., 2005; Toonen et al., 2017).

We list in Table D.7 the 26 systems in our sample that have at least one white dwarf. Among them, 20 are binaries, and 6 are triples [12] One of the binaries contains a known eclipsing binary (CM Dra, M4.5 V). Based on their position on the CMD, we propose the object *Gaia* DR3 2005884249925303168 (physical companion of the LF 4 +54 152, M0.0 V) as a candidate to white dwarfs, in agreement with Jiménez-Esteban et al. (2018, 2023) and Gentile Fusillo et al. (2019).

[12] Clark et al. (2022) showcases an example of the estimation for the age for one of these systems, Wolf 672 A.

Young systems

Stellar associations or moving groups are loose star clusters, containing from dozens to hundreds of stars with a common origin in space (comoving) and time (coeval), and unbound by gravity. Although sparsely located, they maintain the imprint of the mother cloud: similar motion in space, and also similar chemistry (e.g. Tabernero et al., 2017, but see Tabernero et al. (2012) about the chemical tagging of the Hyades supercluster members). Generally, 'core' stars are less dispersed members, more tied to their origin and indisputably part of a given moving group; 'stream' stars are more spatially spread members, in some cases ambiguously assigned to the group. For instance, the closest association is the Ursa Major Moving Group, which includes many of the visible stars in the constellation. Sirius was once thought to be a part of it because it moves like its members, but it turned out out be much younger (King et al., 2003). Ursa Major and the Hyades were the only moving groups known by the end of the 20th century. Dozens of co-moving associations of stars are catalogued in the solar neighbourhood. Among these associations, the YMG are of particular interest.

In regard to tracing the past, stellar associations are one of the best tale-tellers. Stars in associations convey, arguably more than any other arrangement, insights into the genesis of vast populations of stars, which ultimately reveal the tale of the Galactic population. When investigating their probable origin, younger associations are preferred because they retain a less distorted imprint of their origin, contrary to the older ones, which have necessarily endured many more perturbing effects of gravity with the environment and within the group itself. The result is that fraction of higher-order multiples decreases rapidly with age.

In Sect. 3.2.2 we identified several members of YMG motivated by the overluminosity observed in them. In this case we look for stars in our sample that belong to known stellar kinematic groups, with particular interest in the close binaries, because they provide model-independent information like no other members can. An important clarification to include here is that stars in young moving groups are *not* classified as multiple systems per se.

We compile and collate those with either solid evidence or with incontrovertible assignation, for which two or more independent authors declare the same membership, and no further studies have debated the results. We look in the literature but also use `SteParKin` code to assign a population based on the Galactocentric velocities, U, V, W, the radial velocities, V_r, and the parallaxes, ϖ. In Fig. 4.25 we show the location in the sky of the main stellar kinematic groups found in the sample. We list in Table 4.9 the associations with members among the Carmencita stars, the abbreviations used, and the reference for these assignations. Among the stars found in the sample, a few cases are pairs discovered for the first time, which means that are proposed as candidate members of the corresponding associations.

Stars with planets

Circumstellar environments of close binary stars seem to difficult or suppress the genesis of planets, both orbiting either separately, or altogether as circumbinary planets (Wang et al., 2014b,a; Kraus et al., 2016; Zagaria et al., 2022, and see Standing et al. 2023 for the first transiting circumbinary planet also measured with radial velocities). Nevertheless, planet formation does take place in binary environments (Holman & Wiegert, 1999; Mathieu et al., 2000; Naoz et al., 2012, and see Winn & Fabrycky 2015), conveniently triggering planet migration dynamics in many instances (Fabrycky & Tremaine, 2007; Petrovich, 2015, and see particular cases in Cochran et al. 1997; Wu & Murray 2003; O'Connor et al. 2021), via the Lidov-Kozai mechanism (Lidov, 1962; Kozai, 1962) .

Table 4.9: Stellar kinematic groups and associations with members found in our sample

Name	Abbreviation	In sample[a]	Reference(s)[b]
AB Doradus	AB Dor	25	9:12,20,22,23
Argus	Arg	2	11,16,20
β Pictoris	β Pic	40	6,9:16,20,22,23
Carina	Car	9	10,13,22,23
Castor[c]	Cas	30	1,6,10,12,13,27
Columba	Col	5	10,23
Hercules-Lyrae	Her-Lyr	2	4,10
Hyades/Hyades SC	Hya/HS	58/77	8,18,22:27
IC 2391	IC 2391	16	1,10,22,23
Local association	LA	98	10,23
Pleiades	Ple	2	10
Taurus	Tau	7	3,7,17,19,21
Tucana-Horologium	Tuc-Hor	5	10
TW Hydrae	TWA	2	16
Ursa Major	UMa	69	10,27
Upper Scorpius	USco	1	2
Young disk	YD	4	1,27

[a] In cases of multiple assignations for a given object, we choose a compromise between homogeneity and recent assignation.

[b] 1: Montes et al. (2001); 2: Preibisch et al. (2001); 3: Bertout & Genova (2006); 4: López-Santiago et al. (2006); 5: Caballero (2009); 6: Caballero (2010); 7: Rebull et al. (2010); 8: Röser et al. (2011); 9: Schlieder et al. (2012a); 10: Shkolnik et al. (2012); 11: Malo et al. (2013); 12: Malo et al. (2014d); 13: Elliott et al. (2014); 14: Kraus et al. (2014); 15: Alonso-Floriano et al. (2015a); 16: Gagné et al. (2015); 17: Gómez de Castro et al. (2015); 18: Kopytova et al. (2016); 19: Duchêne et al. (2017); 20: Janson et al. (2017); 21: Kraus et al. (2017); 22: Gagné et al. (2018b); 23: Gagné & Faherty (2018); 24: Gagné et al. (2018a); 25: Lodieu et al. (2019); 26: Freund et al. (2020); 27: This work.

[c] Castor is often referred as a 'dynamical stream' of non coeval stars that share kinematics (e.g. Famaey et al., 2005). Nevertheless, given the young ages of their potential members, it is considered as the other groups.

All-sky surveys such as *Kepler* or *TESS* gather data from stars in bulk portions on the sky, assuming that all the stars are single, regardless of a binarity not resolved (see Lillo-Box et al., 2012). Statistical conclusions may ignore these observational selection effects (e.g. Mulders et al., 2021). Failing to account for the possibility of stellar binarity essentially biases the planet characterisation of these searches to smaller radii (Ciardi et al., 2015). The mass of a planet derived from the mass of a star that is assumed single will be subject to a large error (see Bouma et al., 2018).

In our sample, including the individual components of the multiple systems, we find that 81 stars have confirmed exoplanets, 26 of which are detected in a multiple system (Table D.8). Of these, 12 are multiplanetary systems (2 or more planets), including the 5-planet system of 55 Cnc[13], a K0 subgiant in a binary system with components separated by ~1000 au. Although these are usually detected orbiting the primary component of wide systems, they can be also detected orbiting spectroscopic binaries (e.g. EQ Peg A, and the candidate GJ 373).

[13] Butler et al. (1997), Marcy et al. (2002), McArthur et al. (2004), and Fischer et al. (2008).

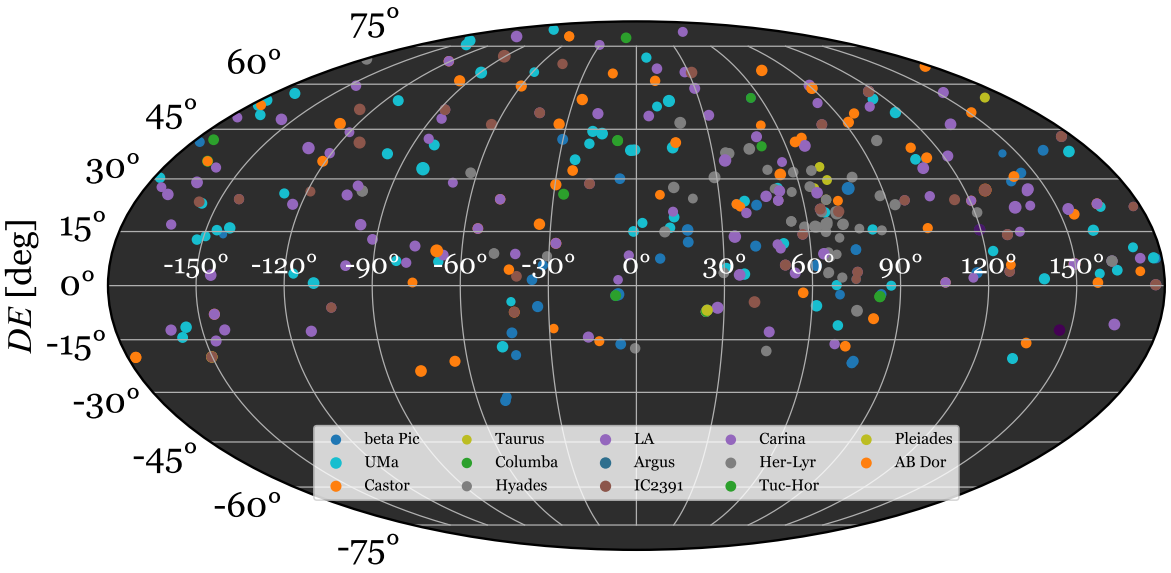

Figure 4.25: Location in the Mollweide-projection sky of the main stellar kinematic groups identified in the sample, in equatorial coordinates.

Eclipsing binaries

The cases where the orbital plane of a binary system contains our line of sight are not common. These are referred as eclipsing binaries (EB) and are a particular case of variable stars, because the components periodically eclipse each other from our point of view. This causes a periodic decrease in the brightness that depends on the relative size of the components and their physical separation. Algol (β Per) is the epitome of these systems, also being the first eclipsing binary discovered.

Eclipsing binaries are of particular interest because they are the source of empirical masses and radii[14] (Huang & Struve, 1956; Popper, 1980; Andersen, 1991). The mass of a star is perhaps its most fundamental characteristic, as the majority of its properties exhibit a strong dependence on its mass. Indeed, from binaries it is possible to accurately measure dynamical masses (in particular, in detached double-lined systems) and radii measurements (from eclipsing light curves), with accuracies of ~1–2% (Ribas, 2003a; Torres et al., 2010). Because these do not rely on models, these can be safely tested against each other, to evaluate the accuracy of model predictions. Many fields benefit from model-independent parameters, such as the non-trivial matter of determining ages (David et al., 2019). An important point to consider, specially with short-period, close-orbiting eclipsing binaries, is that the level of stellar activity can cause bias. It has been observed that inflated radii occur for young, magnetically active, or fast rotating stars (Caballero, 2010; Jackson et al., 2018; Kesseli et al., 2018; Parsons et al., 2018)[15].

When radial velocities can be measured for the components of an eclipsing binary, the size of the orbit can be calculated. The derivation of the mass and radius of Castor C serves as a good example (Torres et al., 2022). Interestingly, one of the components of the Castor system might be a flare star, which can be classified among peculiar variables. It is important to note that the properties derived for the components of these systems might not be of application to isolated stars, because of the effect that stars so close might

[14] Stellar radii have been measured for a few hundreds of stars, via optical interferometry, lunar occultation, or eclipsing binaries, whereas masses are known empirically for an even smaller number.

[15] It is worth mentioning at this point that this issue has been adknowledged by Schweitzer et al. (2019) when deriving masses from the $\mathcal{M}$-$\mathcal{R}$ relation from eclipsing binaries (see Sect. 3.4.1), as the sample mostly contained old, inactive, and slowly rotating stars.

have on one another. In our sample we identify a total of 8 eclipsing binaries, which are listed along with masses and radii in Table D.9.

The widest systems

In our search for physical companions to our stars with separations up to 10^5 au we find a number of components with $\rho > 10^4$ au. There are 32 stars of this kind in our sample. From these, 13 are known members of stellar kinematic groups and open clusters already discussed in Sect. 2.4. The remaining 19 are not recognised as members of kinematic groups or open clusters, and some of them are identified as pairs in this work for the first time. The binding energies for these systems range from $\sim$ 2 to 40 10^{33} J. In Fig. 4.24, we highlighted in red these components, showing that the survival expectancy for these fragile configurations ranges from 1 to 10 Gigayears. They are collected in Table 4.10, along with the most relevant parameters.

4.4.6 One is the loneliest number

The content of this subsection has been adapted from the article *One Is the Loneliest Number: Multiplicity in Cool Dwarfs*, published in the *Research Notes of the AAS* (RNAAS) (Cifuentes et al. 2021, *RNAAS*, 5, 129).

As multiple systems settle down into stable configurations, they result in a variety of hierarchies and a wide range of separations between the components. We examine 11 known and 11 newly discovered multiple systems including at least one M dwarf with the latest astrometric data from *Gaia* third Data Release (DR3). We find several examples that the individual components of systems at very wide separations are often multiple systems themselves.

As introduced in Chapter 1, evidence suggests that most (if not all) stars form in multiple systems, and in systems of higher order, at least one component (usually the least massive) is ejected into a distant orbit during the pre-main sequence phase (Duchêne & Kraus, 2013). Low-mass objects are preferentially ejected in three-body dynamics, and Reipurth & Mikkola (2012a) noted that these expelled companions can also be binaries. Using N-body simulations, Reipurth & Mikkola (2012a) found that extreme hierarchical architectures can be reached on timescales of millions of years with the appropriate exchange of energy and momentum. In this regard, we also call the attention to early simulations such as those of Poveda et al. (1967). In their work, one component in a triple system is dynamically scattered into a very wide orbit at the expense of shrinking the orbit of the remaining binary. In many physical star systems, seemingly single distant components are resolved as multiple systems themselves, typically binaries, which implies that known double or triple systems in wide orbits would actually be hierarchical triples or quadruples in wide configurations (see Basri & Reiners, 2006; Caballero, 2007; González-Payo et al., 2021). These findings challenge the fundamentals of star formation because the separations of wide systems cannot be the direct product of a collapsing cloud core. In this section we examine the characteristics of known and new physically bound multiple systems containing at least one M dwarf by using the astrometry from *Gaia* DR3.

We study 53 stars in 22 multiple systems, 11 of which are known systems tabulated in the Washington Double Star catalogue (Mason et al., 2001, e.g. Caballero 2007; Caballero et al. 2012; Dhital et al. 2010; Janson et al. 2014b), 4 are known systems with new candidate members, and 11 are newly discovered systems. All of them contain at least one M dwarf in different hierarchical configurations, including 12 double, 5 triple and 4 quadruple systems, plus one quintuple system. They are located between 14.1 pc and 276.1 pc. *Gaia* information is complete for all stars except two, for which we retrieved proper motions

Table 4.10: Components of multiple systems at separations larger than 10^4 au from the primary.

Karmn	Name	Spectral type	Component[a]	WDS id.	WDS disc.	s [au]	π [mas]	$\mu_\alpha \cos\delta$ [mas a^{-1}]	μ_δ [mas a^{-1}]	Note[b]
J00169+200	GJ 3022	M3.5 V	A				29.31	238.89	17.67	
	G 131-47B	M3.5 V	B	00169+2004	CRC 43	37.0	29.14	231.63	28.37	
	LP 404-54	M5.0 V	C*	*New*		60680	28.87	232.74	22.23	
J00341+253	V493 And A	M0.0 V	A				20.10	82.97	−97.36	•
	V493 And B	K7 V	B	00341+2524	SKF 220	77.9	19.72	85.93	−96.83	
	UCAC4 578-001365	M4.0 V	C*	*New*		15618	19.67	84.60	−94.78	•
J03454+729	G 221-21	M1.5 V	A				39.09	203.31	−442.85	•
	LP 31-210		B	03454+7259	LDS1581		…	…	…	
	LP 31-200	M3.5 V	C	03454+7259	WIS 99	14667	39.15	206.71	−442.36	
J04011+513	Ross 25	M3.8 V	A				39.82	365.81	−804.17	
	LSPM J0401+5131	DC8	B*	*New*		12402	39.84	367.43	−803.19	
	PM J05334+4809	M0.0 V	A				30.27	−54.57	38.76	
J05341+475	PM J05341+4732A	M2.5 V	B*	*New*		75945	30.05	−58.35	36.85	
	PM J05341+4732B	M3.0 V	C*	*New*		75899	30.04	−47.45	39.68	•
	UPM J0533+4809	M3.5 V	D*	*New*		4219	30.23	−52.55	38.28	
	1RXS J073138.4+455718	M3.0 V	Aab				17.88	−13.69	−92.77	•
J07310+460	1RXS J073101.9+460030	M4.0 V	B*	*New*		23780	18.14	−13.52	−100.85	
	G3 975312928903090560	M4.5 V	C*	*New*		16739	18.39	−12.17	−100.00	
J09579+118	GJ 3576	M4.0 V	A				39.57	−422.75	−158.52	
	LP 489-1	M5.0 V	B*	*New*		33201	40.84	−456.75	−13.67	
	PM J13255+2738	M1.0 V	A				22.00	−0.56	71.21	
J13260+275	PM J13260+2735A	M3.0 V	B*	*New*		18494	21.87	−2.47	72.85	
	PM J13260+2735B	M2.5 V	C	13260+2735	KPP3896	18344	22.03	9.15	62.91	
	HD 140232	A8 V	A				18.72	−61.65	54.32	
	G3 1197801408884577408	M3.5 V	B	15419+1828	DRS 17	127	18.64	−61.76	54.37	
J15416+184	StKM 1-1264	M1.5 V	C	15419+1828	TOK 302	12870	19.37	−65.05	64.89	
	σ CrB A	F6 V	Aab				44.06	−268.22	−87.28	•
	σ CrB B	G1 V	B	16147+3352	STF2032	164	44.13	−290.86	−78.52	
J16139+337	σ CrB C	M2.5 V	CD	16147+3352	STF2032	14346	44.27	−286.97	−89.82	•
	HD 160269A	G0 IV/V	AB	17350+6153	BU 962	9.02	69.28	236.25	−466.11	•
J17355+616	GJ 685	M0.5 V	C	17350+6153	LDS2736	10561	69.89	261.92	−514.50	
	HD 230017A	M0.0 V	A				53.42	29.43	129.98	
J18548+109	HD 230017B	M3.5 V	B	18550+1058	VYS 8	70.7	53.64	29.42	84.30	•
	PM J18542+1058	M4.0 V	C*	*New*		10010	53.84	20.21	112.82	•
J22018+164	Ross 265	M2.5 V	AB	22018+1628	YSC 165	5.75	61.79	391.82	156.08	•
	Ross 268	M3.5 V	C*	*New*		89858	56.76	361.91	84.11	
J22058−119	Wolf 1548	M0.0 V	A				38.62	−276.64	−159.37	•
	LP 759-25	M6.0 V	B	22059-1155	WNO 57	59343	51.07	−270.62	−175.40	
J23175+063	GJ 4329	M3.0 V	A				48.92	170.44	−249.49	
	GJ 4319	M3.5 V	B*	*New*		36823	48.98	173.64	−250.62	
	V368 Cep	G9 V	A				52.78	203.45	72.31	
J23194+790	HD 220140B	M3.5 V	B	23194+7900	LDS2035	206	52.84	209.25	61.43	•
J23228+787	LP 12-90	M5.0 V	C	23194+7900	MKR 1	18222	52.83	207.45	65.17	
J23317−027	AF Psc	M4.5 V	A				28.63	93.96	−72.12	•
J23301−026	2M J23301129-0237227	M6.0 V	B	23317-0245	CAB24	66834	21.98	101.33	−67.96	
J23308+157	LP 462-51	M1.0 V	AB	23309+1547	LDS5096	45.5	44.00	−164.96	−109.58	
	HD 221503	K6 V	A				68.74	341.15	−219.11	
J23302−203	GJ 1284	M2.0 V	Bab	22577-2937	SHY110	206051	62.87	314.43	−204.78	•
J23327−167	GJ 897	M3.0 V	C	23328-1651	LDS 816	21895	64.8	352.0	−216.1	•
	G3 2395220664463236992		D	23328-1645	VOU 28		…	…	…	

[a] An asterisk (∗) indicates that the component is assigned for the first time in this work.

[b] J00341+253: Member of AB Doradus (Janson et al., 2017). C is a member candidate of AB Doradus (this work).
J03454+729: Component B (G 221-21) appears an 'Inexistent' in Simbad (Not an Object – Error, Artefact, ...).
J05341+475: Absent in WDS but see the detection at 2.33 arcsec by Ansdell et al. (2015).
J07310+460: A is SB2? (Fouqué et al., 2018). B is member of the Hyades supercluster (this work).
J16139+337: A is SB2 (Strassmeier & Rice, 2003; Raghavan et al., 2009). YSC 152 Ea Eb refers to the close pair CD (0.507 arcsec).
J17355+616: SB1 according to Duquennoy & Mayor (1991) but resolved in WDS (0.625 arcsec in 2013, BU 962 AB).
J18548+109: Member of Carina (Gagné & Faherty, 2018). C is a member candidate of Carina (this work).
J22018+164: Proper motions from van Leeuwen (2007).
J22058-119: Member of Castor (Caballero, 2010).
J23194+790: Member of Columba (Gagné & Faherty, 2018).
J23317-027: Member of β Pic (Gagné et al., 2018b).
J23302-203: SB2 (Gizis et al., 2002; Jeffers et al., 2018; Cardona Guillén et al., 2021) and member of the Local Association (Cardona Guillén et al., 2021).
J23327-167: Parallax and proper motions from Tokovinin (2018).

and parallactic distances from the literature (Lépine & Shara, 2005; Dittmann et al., 2014). The spectral classifications of the primary components range from F7 V to M5.5 V, and of their physical companions from F9 V to L1. We computed the astrophysical properties as described in Chapter 3, and estimated spectral types for 22 stars from luminosities and absolute magnitudes.

We tested the physical binding of each system member candidate by applying the same criteria as in Sect. 4.3.1. Of the 22 investigated systems, 7 do not meet the conditions for actual parity. Of them, 3 are close pairs with *Gaia* proper motions perturbed by their relative orbital motion. The remaining 4 pairs are wide: one does not have parallax measured by *Gaia* for the secondary (WDS 06104+2234), one exhibits a high `ruwe` in *Gaia* (i.e. larger than 1.4, which is indicative of a problematic astrometric solution; KO 4), and only for the other two (KO 6 and SLW 1299) we disprove their physical connection based on the astrometric analysis.

We summarise the conclusions as follows:

- In 6 multiple systems the astrometric data from *Gaia* suggest additional multiplicity in at least one member.
- These are KO 1, KO 2, KO 4, 1RXS J073138.4+455718, HD 61606 A, 1RXS J074948.5–031712.
- With current data, the pairs LSPM J0651+1845/LSPM J0651+1843 and HD 77825/1RXSJ090406.8-155512 are the only wide binaries (112 and 220 arcsec, respectively) with no evidence of close binarity of the individual components in the *Gaia* solution.
- The young candidate member in β Pictoris, PYC J07311+4556, is a wide member in a quadruple, perhaps quintuple, physical system. This current configuration is expected if the system is actually young ($18.5^{+2.0}_{+2.4}$ Ma, Miret-Roig et al., 2020b) and still undergoes a process of dynamical stabilisation.
- The least-bound system in this analysis is FMR 83 with $U_g^* \sim -7.1\ 10^{33}$ J (Rica & Caballero, 2012), while the pair with largest projected separation (54 800 au) and orbital period ($10.9\ 10^6$ a) is WDS 07400-0336 (Montes et al., 2018).

In Table 4.11 we list the names of the 53 stars, spectral types, angular separations (ρ), position angles (θ), projected physical separations (s), and remarks[16]. Finally, dedicated charts with a detailed description of each system can be found in Appendix D.

[16]The full version of this table with all astro-photometric parameters and derived masses, binding energies, orbital periods, and reference codes can be downloaded in csv format from the GitHub repository (`https://github.com/ccifuentesr/cif21-multiplicity`). It has also been published in its entirety in the electronic edition of *Research Notes* (`https://iopscience.iop.org/article/10.3847/2515-5172/ac05ce`).

Table 4.11: Relative astrometry of the multiple systems investigated by Cifuentes et al. (2021).

Star name	Comp.	Spectral type[a]	ρ [arcsec]	θ [deg]	s [au]	Remarks
LEHPM 494	A	m5.5 V				Confirmed known binary (KO 1)
2M J00210589-4244433	B	L0.6: V	77.78	317.0	2083.4	B might be double
NLTT 6496	A	M4.5 V				Confirmed known binary (KO 4)
NLTT 6491	B	m4.5 V	299.13	190.6	9391.9	B might be double
LP 655-23	A	M4.0 V				Confirmed known binary (KO 2)
DENIS J043051.5-084900	B	M8 V	19.81	339.8	597.3	A and B might be double
2M J06101775+2234199	A	M4.0 V+				*New* triple. JNN 269 is visual
LP 362-121	BaBb	M6 V+m7 V	65.16	89.2	1866.9	
BD+37 1541	A	f0: V				*New* F+M binary
Karmn J06353865+3751139 B	B	m2.5 V	3.88	201.5	848.7	
LSPM J0651+1845	A	m4.5 V				Confirmed known binary (FMR 83)
LSPM J0651+1843	B	m4.5 V	111.72	150.6	7133.4	
1RXS J073138.4+455718	AaAb	M3 V+m4.5 V				*New* quadruple
1RXS J073101.9+460030	B	M4.0 V	431.39	296.0	24127.1	B might be double, probably young (β Pictoris)
[SLS2012] PYC J07311+4556	C	m4 V	307.80	266.3	17214.6	
HD 61606 A	A	K3 V				Confirmed known triple
HD 61606 B	B	K7 V	57.90	112.7	815.2	No WDS entry but reported by Poveda et al. (2009)
BD-02 2198	C	M1.0 V	3894.18	296.7	54822.6	C might be double
1RXS J074948.5-031712	A	M3.5 V				*New* triple
2M J07495087-0317194	B	m3.5 V	1.93	266.3	32.8	
2M J07494215-0320338	C	M3.5 V	234.86	214.0	4002.1	C might be double
LP 209-28	"A"	m3: V				Disproved binary (KO 6)
LP 209-27	"B"	m4 V	666.68	208.5	69836.7	
HD 77825	A	K2 V				*New* K+M binary
1RXS J090406.8-155512	B	M2.5 V	220.02	262.9	6026.0	
2M J13181352+7322073	A	m3 V				*New* M+M binary
G2 1688578285187648128	B	M3.5 V	7.39	335.7	186.8	
HD 130666	A	G5 V				*New* G+M binary
2M J14474531+4934020	B	m4.5 V	29.54	336.6	3072.3	
TYC 2565-684-1	A	g1 V				*New* G+M binary
2M J15080798+3310222	B	m3 V	43.64	306.2	8644.3	
HD 134494	A	K0 IV				Reclassified as sub-giant
BD+33 2548B	B	f9 V	23.38	285.0	6455.7	*New* m3-type companion to pair of evolved
G2 1288848427727490048	C	m3 V	5.85	180.3	1615.4	solar-mass stars
HD 149162	AaAbAc	K0 Ve+k6 V+m5 V				Confirmed quintuple (LEP 79)
G 17-23	B	M3.0 V	252.03	138.4	11405.7	
LSPM J1633+0311S	C	D:	258.42	138.4	11694.8	
G 125-15	Aab	M4.5 V+M5 V				Confirmed triple (GIC 158)
G 125-14	B	M4.5 V	45.78	347.4	1835.1	
LP 395-8 A	Aab	M3.0 V+m0 V				
LP 395-8 B	B	m3.5 V	1.92	355.5	56.6	*New* m9-type companion to trio of M dwarfs
G2 1829571684884360832	C	m9: V	11.02	307.4	325.1	
HD 212168	A	G0 V				Confirmed known quadruple (DUN 38, KO 5)
CPD-75 1748B	BaBb	k3 V+	20.90	79.3	489.2	
DENIS J222644.3-750342	C	M8 V	264.82	128.9	6198.7	
SLW J2305+0613 A	"A"	M1.7 V				Disproved triple (SLW 1300)
SLW J2305+0613 B	"B"	M3.2 V	242.37	260.9		SLW 1300 is a visual pair
SLW J2305+0613 C	"C"	M3.7 V	86.00	283.1	18656.7	
HD 221356	A	F7 V				Confirmed known quadruple (KO 3, GZA 1)
2MASSW J2331016-040618	BC	M8.0 V+L3.0 V	451.70	261.7	11668.3	
2M J23313095-0405234	D	L1 V	12.46	221.6	321.9	
StKM 2-1787[b]	A	K4 V				Confirmed known binary (VYS 11)
TYC 1174-955-2	B	M2.5 V	5.78	165.1	215.5	

[a] Lower case denotes photometrically derived spectral types.
[b] Not strictly a binary according to Montes et al. (2018), but we confirm physical parity.

Chapter 5

Conclusions and future work

We present in this thesis the most comprehensive photometric and astrometric homogeneous analysis to date of an M-dwarf sample in the close solar neighbourhood. Carmencita, the input catalogue of the CARMENES project, is a thoroughly revised and detailed catalogue with more than two thousand stars, with almost four hundred of them followed-up individually by radial-velocity and transit exoplanet surveys by the consortium. This work adds the value of a thorough, meticulous, individualised inspection of every object in Carmencita. It includes, for each star (and the physical companions, if any), a one-by-one visual examination, photometric and astrometric compilation, literature revision, catalogue data incorporation, and contextualisation in the M-dwarf big picture.

5.1 Summary

5.1.1 Astrophysical parameters

In the past, the most reliable observable of a star was the temperature, which could be obtained either through spectral analysis or through colors. This was much easier than to get a reliable luminosity, which frequently also came from spectroscopic analyses of line widths. Multi-band photometry and precise parallaxes are generally available for the vast majority of nearby stars, making it possible to integrate the spectral energy distribution, with a reduced intervention of model assumptions. With this, luminosity can be now regarded as a very reliable *observable*. We should re-consider using bolometric luminosities as a more convenient proxy for other fundamental parameters such as masses and radii, instead of using effective temperatures o spectral types. $\mathcal{M}$ vs. $\mathcal{L}$ diagrams instead of $\mathcal{M}$ vs. $T_{\rm eff}$ or $\mathcal{M}$ vs. Spectral type could be proven much more useful. Saying, for example, that $\mathcal{L} = 0.1\ \mathcal{L}_{\odot}$ may be a better boundary for separating K7 V from M0.0 V, or talking about $\mathcal{L} = 0.01\ \mathcal{L}_{\odot}$ rather than M3.5 V stars. This is of special application in the case of ultracool dwarfs. The following is a summary of the main results regarding the determination of astrophysical parameters:

- We started with the latest version of Carmencita, the CARMENES input catalogue, to which we added **168** and **117** single, nearby, bright K and ultracool dwarfs, respectively. Although our main objective was investigating luminosities, colours, and spectral energy distributions of M dwarfs, our sample contained stars and ultracool dwarfs as early as K5 V and as late as L8, in order to avoid boundary issues.

- From public all-sky surveys, we collected **40 094** photometric magnitudes for the **2479** stars and ultracool dwarfs in **20** different passbands from the far ultraviolet, through the blue and red optical and near infrared, to the mid infrared. Except for the bluest passbands, the completeness of high-quality data is of the order of **97 %**. Thanks especially to *Gaia*, we could collect parallactic distances for **98 %** of the sample and identified close multiple systems unresolved by ground all-sky surveys and *WISE*.

- We estimated spectrophotometric distances for **31** single stars without parallactic distance, using our absolute magnitude-colour relations obtained from the GTO subsample.

- We computed bolometric luminosities, effective temperatures, and surface gravities for **1843** stars and ultracool dwarfs with parallactic distance and no physical companions at less than 5 arcsec or less than 5 mag fainter in *Gaia G* than our target. For that, we used `VOSA` and all high-quality photometric data redder than SDSS u'. Because of the limitations of the `BT-Settl CIFIST` models implemented in `VOSA`, we set the metallicity to solar. However, except for a few stars with poorly sampled spectral energy distributions, the luminosities are independent of models at least at the **99.5 %** level, which supersede any pre-*Gaia* determination.

- From their loci in the Hertzsprung-Russell diagram, we identified **36** overluminous stars that had been previously assigned to young stellar kinematic groups and associations. We estimated masses and radii using isochronal models.

- We examined colour-spectral type, colour-colour, colour-magnitude, luminosity-magnitude, and bolometric correction-colour diagrams. After discarding stars with young ages, close companions, and bad photometric or astrometric quality flags (i.e. *Gaia* `phot_bp_rp_excess_factor` and `ruwe`), we fitted empirical relations of absolute magnitude-colour, bolometric correction-colour, and luminosity-absolute magnitudes including widely available G, r', and J magnitudes and *Gaia* DR2 parallaxes. In addition, we also used the Stefan-Boltzman law and the $\mathcal{M}$-$\mathcal{R}$ relation of Schweitzer et al. (2019) to derive radii and masses of all well-behaved stars in our sample.

- We tabulated median G- and J-band bolometric corrections, $\mathcal{L}$, $T_{\rm eff}$, $\mathcal{R}$, and $\mathcal{M}$, as well as absolute magnitudes in **14** passbands, for stars and ultracool dwarfs with spectral types from K5 V to L2.0.

- From the HR diagram we paid special attention to the overluminous outliers, and to the low-mass tail of the main sequence ($\mathcal{L} < 0.1\ \mathcal{L}_\odot$, M6.0–M9.5 V). The overluminous were in most cases identified as bona fide or candidate members to young kinematic groups, and so we used `PARSEC` isochrones to derive probable ranges of masses and radii, based on the ages of their stellar associations. For the least massive stars in the sample, we proceeded analogously using `DUSTY00` isochrones, not assuming a given age but an array of them. With this, we updated the masses and radii of overluminous, young stars, and of the low-mass end of Carmencita, superseding the old values in Carmencita.

- In Schweitzer et al. (2019) we used these bolometric luminosities and photometric data, together with high resolution (R >80 000) spectroscopic parameters, to determine radii and masses for **293**

nearby, bright M dwarfs in Carmencita. It was the first time that such a large and homogeneous derivation of fundamental stellar parameters was carried out.

- In Martínez-Rodríguez et al. (2019) we took advantage of this work and the same precise determination of stellar luminosities to help investigating the potential habitability, stability, and detectability of exomoons around exoplanets orbiting M dwarfs.

- The averaged astrophysical parameters ($\mathcal{L}$, $T_{\rm eff}$, $\mathcal{R}$, $\mathcal{M}$), bolometric corrections (BC_G, BC_J), absolute magnitudes in **14** passbands (from B to $W3$), and **19** adjacent colours (from FUV to $W4$) derived for K5 V to L2 objects, have served as a quick guide and reference in many published works.

5.1.2 Multiplicity

- Some multiple systems, usually young, walk on the edge of stability. There is a myriad of occasions for a bound system to be perturbed and disappear, and even bound systems are bound to fail. Some of them, though, will endure the external factors by their own gravity.

- We carried out a blind search of equidistant and comoving companions to all the stars in Carmencita, up to physical separations of 10^5 au, and for the first time, also considering the potential unresolved binaries at very close separations, by using several statistical indicators and data products in *Gaia* DR3.

- To the known physically bound systems reported in the literature, we add **48** newly discovered pairs, and propose **344** candidates to very compact binaries, to date unresolved. We incorporate these potential candidates to the discussion of multiplicity fractions and distribution of separations.

- When possible, we determined descriptive parameters of the multiplicity (angular and physical separation, positional angle, binding energies, orbital periods), fundamental parameters of the components (luminosities, masses, radii, effective temperatures, surface gravities), compile astrometry (positions, proper motions, parallaxes, radial velocities), photometry (in up to 10 passbands in *Gaia* DR2, 2MASS, AllWISE), and *Gaia* statistical indicators. Additionally, we give an individual description of the components, including their candidacy for unresolved binarity.

- We prove the adequacy of statistical data products in *Gaia* to pinpoint probable very compact binaries, or higher order systems, most of them only able to be resolved by spectroscopic scrutiny. We discovered compact multiplicity in **14** of these *Gaia* candidates, performing a systematic study with medium resolution spectra using FIES. These spectroscopic binaries included clear double- and triple-lined doubles and triples, several single-lined probable binaries, and two high rotators for which the multiplicity could not be properly confirmed. For one SB1 and one SB2 we were able to derive a potential orbital solution. Although in these studies the more amount of spectra collected, the more defined the results, it is possible to identify multiplicity in many cases from the very first spectrum.

- Approximately **38%** of the M dwarfs in Carmencita belong to an identified multiple system with a companion of *any* mass. In this broad definition of multiplicity, the number of single, binaries, triples, quadruples, and quintuples systems for every 100 M dwarfs in all the range of subtypes (from M0.0 V to M9.5 V) represented as S:B:T:Q:Q, is **62.3**:**40.1**:**13.3**:**2.8**:**0.8**.

- Defining the multiplicity of M dwarfs in this broad term (i.e. addressing the fact that a star *belongs* to a multiple system or not, regardless of the mass) is a sensible approach. For instance, all-sky surveys such as *TESS* or *Kepler* may draw conclusions, for example about planet occurrence, based on the systematic observation of brightness-limited samples of M dwarfs, without taking into consideration (at least in a first approximation) the effect of many unresolved binaries disguised as single objects.

- We computed the classically defined multiplicity fraction (*MF*) and the stellar companion fraction (*SCF*) in different un-biased samples:

  - For every individual spectral type (defined as, e.g., M0.0 V and M0.5 V).
  - For two consecutive spectral ranges: M0.0–M5.0 V, and M5.5–M9.5 V.
  - For all the range of M dwarfs (from M0.0 V to M9.5 V) in the volume-limited sample for which Carmencita is complete ($d < 10.0$ pc).

  In these definitions, the M dwarf must be the primary component in the system, that is, the most massive. This calculation has been performed with two general conditions: i) Confirmed multiplicity: including the *known* multiple systems (resolved in *Gaia* DR3 or reported in the literature with higher precision techniques) or newly discovered multiple systems (empirically compliant with astrometric criteria), at all ranges of separations, and ii) Confirmed and to be confirmed multiplicity: to the previous sample, also including the strong candidates to unresolved multiples. Regarding the *MF* and the *SCF*, once the completeness has been taking into account, we conclude that:

  - For M dwarfs in which multiplicity is confirmed, the *MF* and *SCF* are **28.9%** and **35.1%**, respectively. The MF becomes **41.2%** if the unresolved binary candidates are confirmed.
  - Binaries outnumber by far the higher order systems: For every 100 M dwarfs with a companion, the ratio S:B:T:Q:Q is **70.9**:**23.4**:**4.6**:**0.6**:**0.1**.
  - The MF and SCF *decreases* as a function of spectral type, as expected.
  - For M dwarfs later than M6 we do not provide conclusions for individual spectral types because the small sample size is not of statistical significance.

- These results are in agreement with similar studies published in the last three decades. This work, however, estimates that the actual multiplicity fraction of M dwarfs could be as high as ∼**40%**.

- The mass fraction, q, does not behave monotonically, which means that the masses of the companions are not comparatively smaller for smaller stars.

- In the cumulative distribution of physical separations, changes of slope are apparent and measurable, following Öpik's law. Based on the numerous candidacy of many single stars to binary systems, we deem the scarcity of multiple systems at very close separations to an observational effect, rather than a real configuration. In a non-cumulative distribution of projected separations, the observed peaks can be traced back to the resolving precision of surveys like *Gaia*. On the opposite side, the flattening of the distribution at wider separations is a foreseeable effect of the easier gravitational disruption of wide systems, corresponding to smaller values in their measured binding energies.

- We provide homogeneous observational data for different formation mechanisms of close and wide binaries in stars of small mass. Particularly, we provide an extensive analysis of the published data in the literature for the close binaries.

- Many are statistical indicators in *Gaia* DR3 have been regarded as useful hints of non-resolved binarity. We have demonstrated the suitability of some of these as a criteria to gauge the existence of compact multiple systems, typically of two stars, in objects previously considered to be single. If all new candidates to unresolved multiples are confirmed, the multiplicity fraction of M dwarfs can increase by **12.3%**.

5.2 Future work

5.2.1 Carmencita

- The characterisation of the stars necessarily gains precision over time. We have been keen on incorporating every new value that supersedes previous (because of its methodology and its superior handling of the uncertainties), and propagate this improvement to the parameters derived by it. As in any catalogue, a tabulated value is not (or should not be) *the* value for the parameter, but the one that, hopefully, *is very close to* the real one, given the uncertainties. In this sense, all-sky photometric and astrometric surveys, specially *Gaia*, always represent a notable improvement with regards to astrometric and photometric data, and the fundamental parameters that rely on them. Future work in Carmencita means to keep providing an up-to-date, homogeneous, and accessible information resource for the consortium members and all the scientific community, always aiming for a quality-over-quantity approach.

- Carmencita can gain in statistical robustness by incorporating late type, ultracool dwarfs, specially of spectral types M6.0 V and cooler. The same can be said about the late K dwarfs, specially in the frontier of K7/M0.0 V. We enhanced Carmencita this way in Cifuentes et al. (2020) for statistical robustness purposes, but the added objects did not remain in Carmencita. For instance, multiplicity studies would benefit from populating the least massive tail of the sequence. In the same line, Carmencita could aim for a strictly volume-complete sample, rather by a brightness-limited sample, although the former can be inferred from the latter. In this sense, volume completed censuses, such as the 10 pc scrutiny performed by Reylé et al. (2021), can be a valuable reference. One step further in this direction would be to volume-limit the sample to both hemispheres (not only limited to the Calar Alto sky), including all M dwarfs known in the solar vicinity.

5.2.2 Astrophysical parameters

There are many ways of improving our $\mathcal{L}$, $\mathcal{R}$, and $\mathcal{M}$ determinations:

- CatWISE (Eisenhardt et al., 2020), a recent NeoWISE enhanced and contributed product (Mainzer et al., 2011), represents a step forward with respect to the AllWISE mid-infrared photometry used here.

- The Legacy Survey of Space and Time (LSST), to be carried out in the Vera C. Rubin Observatory, with its spectacularly large etendue and multi-band photometry in $u'g'r'i'z'y'$ passbands, will start full survey operations in October 2024, with data scheduled to become fully public after two years.

The first data release will supersede all previous UCAC, SDSS, and Pan-STARRS optical datasets (but see also J-PAS, Benítez et al., 2014).

- The ESA *Euclid* mission (launch scheduled to Q3 2023) will complement LSST in the near infrared at Galactic latitudes far from the ecliptic, especially for the latest M dwarfs.
- Thanks to the Transiting Exoplanet Survey Satellite (*TESS*) and the discovery of new detached M-dwarf eclipsing binaries, the $\mathcal{M}$-$\mathcal{R}$ relation will be more refined and probably determined for different intervals of age and metal abundances.
- The *Gaia* DR4, will improve G, G_{BP}, and G_{RP} photometry and, especially, astrometry, with which we will have more accurate parallax and close multiplicity identifications.
- With new spectral-synthesis determinations of $T_{\rm eff}$, $\log g$, and [Fe/H] in late-type stars for calibration (e.g. with the equivalent width method or with deep learning – Marfil et al. 2018; Passegger et al. 2018, 2020; Marfil et al. 2021).
- From new studies that link kinematics, activity, and youth (and, therefore, radius and surface gravity).
- New grids of theoretical atmospheric models considering a much wider range of metallicities, which are a fundamental cornerstone of these determinations, will be available for `VOSA`.
- Among all the parameters in Carmencita, age is probably the one subject to a larger uncertainty, and with it, the values of masses and radii of the younger stars. It is accepted that age has an impact, but the actual process through which this happens remains unclear. We derived masses from isochrone models, fixing for a certain age boundaries given by the SKG assumed age. Masses could be compared by using this approach and others in which, for example, the age is a *free* parameter. Luckily, the spread of young stars in the HR diagram does represent an advantage from the point of view of discriminating the best-fitting model.

5.2.3 Multiplicity

- There are many unresolved binaries that are still overlooked. *Gaia* data have an enormous potential, and there is so much to look forward to with the following years of approved extension of the mission. Many data products of DR4 will address (as they already do in DR3) the topic of multiplicity, in particular the kind that keeps unresolved in *Gaia*. In successive data releases, *Gaia* provides more data products derived by the automatic pipelines from the original data, and the study of very close multiplicity can extensively gain in depth with *Gaia* DR4 new data, in particular with the help of radial-velocity measurements.
- The spectroscopic investigation of these suspects is the main way to prove that they are not single. These require time, constancy, and patience, because providing orbital descriptions of most of them is worth months or years of dutiful data collection.
- How multiple systems are distributed in the space of separations or mass ratios encodes fundamental clues about their very origin and interplay. Particularly, how very wide systems come to be, and how very wide pairs with *single* components may have reached that puzzling configuration.
- In more general terms, given the amount of evidence that suggests that stars are almost always born together, how *single* stars became single, is also a topic worth investigating. These discoveries

have the potential of bringing forth a new picture of the formation and dynamical evolution of stellar systems.

- The formation of planetary systems does also benefit from understanding the prevalence of multiple systems. Planetary detection and statistics, mainly based on the transit technique, are biased towards single stars.

- Despite being neither a novelty, nor groundbreaking science, the abundance studies of M dwarfs in wide physical systems with FGK primaries continues to be a topic of profound impact for the theoretical study of M dwarfs atmospheres. Because binaries are assumed to be both coeval and to have the same chemical composition, the one of the higher mass star can be extrapolated to the M-dwarf companion. We are already involved in ongoing detailed spectroscopic study using the CARMENES spectrograph, for a selected sample of these systems, which were partially selected from the study developed in this work. The proposal includes observing a sample of wide visual binaries composed of an F-, G- or K- dwarf primary and an M-dwarf secondary. These data will allow us to test the metallicity (described as the iron abundance, [Fe/H]) and chemical abundances (C, O, Na, Mg, Al, Si, Ca, Sc, Ti, V, Cr, Mn, Co, Ni, Rb, Y, Ba, and Nd), derived for the primaries with the EW method with `STEPAR` (Tabernero et al., 2019) or, equivalently, via spectral synthesis with `STEPARSYN` (Tabernero et al., 2022a). The goal of this proposal is to derive a precise spectroscopic calibration of the M-dwarf stellar parameters and chemical abundances.

- The observed cumulative distributions of separations in multiple systems under different constrains can help test the hypothesis of whether all stars form in systems, which eventually are disrupted to produce the single stars that we observe in the field. In this regard, we can use N-body analyses to study the long-term stability of these systems, with the observed distributions of orbital periods, separations, binding energies, and masses serving as valuable observational constraints.

In this thesis we contribute to our understanding of the astrometry, photometry, and multiplicity of M dwarfs. The homogeneously derived fundamental parameters and observables provide an important benchmark for testing and improving theoretical predictions, and the findings underscore the importance of continued research into M dwarfs, specially in the field of exoplanetary exploration. The study takes an individualised approach, examining each star and their potential physical companions, resulting in the discovery of many previously unknown pairs. It is hoped that the data gathered in this study will serve as a valuable resource for astronomers and researchers in related fields, providing a foundation for future discoveries.

Bibliography

Abia, C., Tabernero, H. M., Korotin, S. A., et al. 2020, A&A, 642, A227

Abt, H. A. 1983, ARA&A, 21, 343

Adams, F. C. & Laughlin, G. 1997, Reviews of Modern Physics, 69, 337

Affer, L., Damasso, M., Micela, G., et al. 2019, A&A, 622, A193

Affer, L., Micela, G., Damasso, M., et al. 2016, A&A, 593, A117

Aggarwal, H. R. & Oberbeck, V. R. 1974, ApJ, 191, 577

Ahn, C. P., Alexandroff, R., Allende Prieto, C., et al. 2012, ApJS, 203, 21

Aitken, R. G. & Doolittle, E. 1932, New General Catalogue of Double Stars within 120 degrees of the North Pole

Alibert, Y. & Benz, W. 2017, A&A, 598, L5

Allard, F., Homeier, D., & Freytag, B. 2012, Philosophical Transactions of the Royal Society of London Series A, 370, 2765

Allen, C., Poveda, A., & Herrera, M. A. 1997, in Astrophysics and Space Science Library, Vol. 223, , 133

Almenara, J. M., Astudillo-Defru, N., Bonfils, X., et al. 2015, A&A, 581, L7

Alonso-Floriano, F. J., Caballero, J. A., Cortés-Contreras, M., Solano, E., & Montes, D. 2015a, A&A, 583, A85

Alonso-Floriano, F. J., Morales, J. C., Caballero, J. A., et al. 2015b, A&A, 577, A128

Alonso-Floriano, F. J., Sánchez-López, A., Snellen, I. A. G., et al. 2019a, A&A, 621, A74

Alonso-Floriano, F. J., Snellen, I. A. G., Czesla, S., et al. 2019b, A&A, 629, A110

Amado, P. J., Bauer, F. F., Rodríguez López, C., et al. 2021, A&A, 650, A188

Andersen, J. 1991, A&A Rev., 3, 91

Andrade, M. 2007, Rev. Mexicana Astron. Astrofis., 43, 237

Andrews, J. J., Anguiano, B., Chanamé, J., et al. 2019, ApJ, 871, 42

Angelo, I., Rowe, J. F., Howell, S. B., et al. 2017, AJ, 153, 162

Anglada-Escudé, G., Amado, P. J., Barnes, J., et al. 2016, Nature, 536, 437

Anglada-Escudé, G., Arriagada, P., Tuomi, M., et al. 2014, MNRAS, 443, L89

Anglada-Escudé, G., Boss, A. P., Weinberger, A. J., et al. 2012, ApJ, 746, 37

Anglada-Escudé, G., Tuomi, M., Gerlach, E., et al. 2013, A&A, 556, A126

Ansdell, M., Gaidos, E., Mann, A. W., et al. 2015, ApJ, 798, 41

Apps, K., Clubb, K. I., Fischer, D. A., et al. 2010, PASP, 122, 156

Arenou, F., Luri, X., Babusiaux, C., et al. 2018, A&A, 616, A17

Artigau, É., Kouach, D., Donati, J.-F., et al. 2014, in Proc. SPIE, Vol. 9147, 914715

Astropy Collaboration, Price-Whelan, A. M., Lim, P. L., et al. 2022, ApJ, 935, 167

Astropy Collaboration, Robitaille, T. P., Tollerud, E. J., et al. 2013, A&A, 558, A33

Astudillo-Defru, N., Bonfils, X., Delfosse, X., et al. 2015, A&A, 575, A119

Astudillo-Defru, N., Díaz, R. F., Bonfils, X., et al. 2017a, A&A, 605, L11

Astudillo-Defru, N., Forveille, T., Bonfils, X., et al. 2017b, A&A, 602, A88

Bahcall, J. N. & Soneira, R. M. 1980, ApJS, 44, 73

Bailer-Jones, C. A. L., Rybizki, J., Fouesneau, M., Mantelet, G., & Andrae, R. 2018, AJ, 156, 58

Bakos, G. Á., Bayliss, D., Bento, J., et al. 2018, arXiv e-prints [arXiv e-prints[arXiv]1812.09406]
Banik, I. & Zhao, H. 2018, MNRAS, 480, 2660
Baraffe, I., Chabrier, G., Allard, F., & Hauschildt, P. H. 1998, A&A, 337, 403
Baraffe, I., Homeier, D., Allard, F., & Chabrier, G. 2015, A&A, 577, A42
Barnard, E. E. 1916, AJ, 29, 181
Barnes, R. 2017, Celestial Mechanics and Dynamical Astronomy, 129, 509
Baroch, D., Morales, J. C., Ribas, I., et al. 2021, A&A, 653, A49
Baroch, D., Morales, J. C., Ribas, I., et al. 2020, A&A, 641, A69
Baroch, D., Morales, J. C., Ribas, I., et al. 2018, A&A, 619, A32
Barrado y Navascués, D., Stauffer, J. R., & Jayawardhana, R. 2004, ApJ, 614, 386
Barrado y Navascués, D., Stauffer, J. R., Song, I., & Caillault, J. P. 1999, ApJ, 520, L123
Bartlett, J. L., Lurie, J. C., Riedel, A., et al. 2017, AJ, 154, 151
Basri, G. & Reiners, A. 2006, AJ, 132, 663
Bate, M. R. 2000, MNRAS, 314, 33
Bate, M. R. 2009, MNRAS, 392, 590
Bate, M. R., Bonnell, I. A., & Bromm, V. 2003, MNRAS, 339, 577
Batten, A. H. 1973, Binary and multiple systems of stars
Bauer, F. F., Zechmeister, M., Kaminski, A., et al. 2020, A&A, 640, A50
Bayliss, D., Gillen, E., Eigmüller, P., et al. 2018, MNRAS, 475, 4467
Bayo, A., Rodrigo, C., Barrado Y Navascués, D., et al. 2008, A&A, 492, 277
Bean, J. L., Benedict, G. F., & Endl, M. 2006, ApJ, 653, L65
Beard, C., Robertson, P., Kanodia, S., et al. 2022, ApJ, 936, 55
Bell, C. P. M., Mamajek, E. E., & Naylor, T. 2015, MNRAS, 454, 593
Belokurov, V., Penoyre, Z., Oh, S., et al. 2020, MNRAS, 496, 1922
Bender, C. F. & Simon, M. 2008, ApJ, 689, 416
Benedict, G. F., Henry, T. J., Franz, O. G., et al. 2016, AJ, 152, 141
Benedict, G. F., McArthur, B. E., Franz, O. G., Wasserman, L. H., & Henry, T. J. 2000, AJ, 120, 1106
Benítez, N., Dupke, R., Moles, M., et al. 2014, arXiv e-prints, arXiv:1403.5237
Bensby, T., Feltzing, S., & Lundström, I. 2003, A&A, 410, 527
Bensby, T., Feltzing, S., Lundström, I., & Ilyin, I. 2005, A&A, 433, 185
Bergeron, P., Wesemael, F., & Beauchamp, A. 1995, PASP, 107, 1047
Bergfors, C., Brandner, W., Janson, M., et al. 2010, A&A, 520, A54
Berta-Thompson, Z. K., Irwin, J., Charbonneau, D., et al. 2015, Nature, 527, 204
Bertout, C. & Genova, F. 2006, A&A, 460, 499
Bessell, M. S. 1979, PASP, 91, 589
Bessell, M. S., Castelli, F., & Plez, B. 1998, A&A, 333, 231
Best, W. M. J., Magnier, E. A., Liu, M. C., Aller, K. M., & Zhang, Z. 2017, in , Vol. 229, 240.01
Bianchi, L., Herald, J., Efremova, B., et al. 2011, Ap&SS, 335, 161
Biddle, L. I., Pearson, K. A., Crossfield, I. J. M., et al. 2014, MNRAS, 443, 1810
Bidelman, W. P. 1985, ApJS, 59, 197
Binks, A. S. & Jeffries, R. D. 2016, MNRAS, 455, 3345
Birkby, J., Nefs, B., Hodgkin, S., et al. 2012, MNRAS, 426, 1507
Birky, J., Hogg, D. W., Mann, A. W., & Burgasser, A. 2020, ApJ, 892, 31
Blanco-Pozo, J., Perger, M., Damasso, M., et al. 2023, A&A, 671, A50
Bluhm, P., Pallé, E., Molaverdikhani, K., et al. 2021, A&A, 650, A78
Bochanski, J. J., Hawley, S. L., Covey, K. R., et al. 2010, AJ, 139, 2679

Bochanski, J. J., Munn, J. A., Hawley, S. L., et al. 2007, AJ, 134, 2418

Bohigian, G. M. 2008, Survey Of Ophthalmology, 53, 536

Böhm-Vitense, E. 1989, Introduction to Stellar Astrophysics (Cambridge University Press)

Bonfils, X., Almenara, J.-M., Cloutier, R., et al. 2018a, A&A, 618, A142

Bonfils, X., Astudillo-Defru, N., Díaz, R., et al. 2018b, A&A, 613, A25

Bonfils, X., Astudillo-Defru, N., Díaz, R., et al. 2018c, A&A, 613, A25

Bonfils, X., Delfosse, X., Udry, S., et al. 2013a, A&A, 549, A109

Bonfils, X., Delfosse, X., Udry, S., et al. 2005a, A&A, 442, 635

Bonfils, X., Forveille, T., Delfosse, X., et al. 2005b, A&A, 443, L15

Bonfils, X., Gillon, M., Forveille, T., et al. 2011, A&A, 528, A111

Bonfils, X., Gillon, M., Udry, S., et al. 2012, A&A, 546, A27

Bonfils, X., Lo Curto, G., Correia, A. C. M., et al. 2013b, A&A, 556, A110

Bonfils, X., Mayor, M., Delfosse, X., et al. 2007, A&A, 474, 293

Bonnarel, F., Fernique, P., Bienaymé, O., et al. 2000, A&AS, 143, 33

Bonnell, I. A., Bate, M. R., Clarke, C. J., & Pringle, J. E. 2001, MNRAS, 323, 785

Bonnell, I. A., Bate, M. R., & Vine, S. G. 2003, MNRAS, 343, 413

Bopp, B. W. 1974, ApJ, 193, 389

Borucki, W. J., Koch, D., Basri, G., et al. 2010, Science, 327, 977

Boss, A. P. 1988, Comments on Astrophysics, 12, 169

Boss, A. P. 2006, ApJ, 643, 501

Boss, A. P. & Bodenheimer, P. 1979, ApJ, 234, 289

Bouchy, F., Doyon, R., Artigau, É., et al. 2017, The Messenger, 169, 21

Bouma, L. G., Masuda, K., & Winn, J. N. 2018, AJ, 155, 244

Bowler, B. P., Liu, M. C., Shkolnik, E. L., & Tamura, M. 2015, ApJS, 216, 7

Boyajian, T. S., von Braun, K., van Belle, G., et al. 2012, ApJ, 757, 112

Brandt, T. D., Dupuy, T. J., & Bowler, B. P. 2019, AJ, 158, 140

Bressan, A., Marigo, P., Girardi, L., et al. 2012, MNRAS, 427, 127

Buchhave, L. A., Latham, D. W., Johansen, A., et al. 2012, Nature, 486, 375

Burgasser, A. J. & Blake, C. H. 2009, AJ, 137, 4621

Burgasser, A. J., Kirkpatrick, J. D., Brown, M. E., et al. 1999, ApJ, 522, L65

Burgasser, A. J., Kirkpatrick, J. D., Cruz, K. L., et al. 2006, ApJS, 166, 585

Burgasser, A. J., Kirkpatrick, J. D., Reid, I. N., et al. 2003, ApJ, 586, 512

Burgasser, A. J., Looper, D., & Rayner, J. T. 2010, AJ, 139, 2448

Burgasser, A. J., Reid, I. N., Siegler, N., et al. 2007, in , 427

Burnham, S. W. 1906, A General Catalogue of Double Stars within 121 degrees of the North Pole

Butler, R. P., Johnson, J. A., Marcy, G. W., et al. 2006, PASP, 118, 1685

Butler, R. P. & Marcy, G. W. 1996, ApJ, 464, L153

Butler, R. P., Marcy, G. W., Williams, E., Hauser, H., & Shirts, P. 1997, ApJ, 474, L115

Butler, R. P., Marcy, G. W., Williams, E., et al. 1996, PASP, 108, 500

Butler, R. P., Vogt, S. S., Laughlin, G., et al. 2017, AJ, 153, 208

Butler, R. P., Vogt, S. S., Marcy, G. W., et al. 2004, ApJ, 617, 580

Caballero, J. A. 2007, A&A, 462, L61

Caballero, J. A. 2009, A&A, 507, 251

Caballero, J. A. 2010, A&A, 514, A98

Caballero, J. A., Béjar, V. J. S., Rebolo, R., & Zapatero Osorio, M. R. 2004, A&A, 424, 857

Caballero, J. A., Burgasser, A. J., & Klement, R. 2008, A&A, 488, 181

Caballero, J. A., Cortés-Contreras, M., Alonso-Floriano, F. J., et al. 2013a, in Protostars and Planets VI Posters

Caballero, J. A., Cortés-Contreras, M., Alonso-Floriano, F. J., et al. 2016, in , 148

Caballero, J. A., Cortés-Contreras, M., López-Santiago, J., et al. 2013b, in Highlights of Spanish Astrophysics VII, 645–645

Caballero, J. A., de Burgos, A., Alonso-Floriano, F. J., et al. 2019, A&A, 629, A114

Caballero, J. A., Genebriera, J., Miret, F. X., Tobal, T., & Cairol, J. 2012, The Observatory, 132, 252

Caballero, J. A., González-Álvarez, E., Brady, M., et al. 2022, A&A, 665, A120

Cadieux, C., Doyon, R., Plotnykov, M., et al. 2022, AJ, 164, 96

Campbell, B., Walker, G. A. H., & Yang, S. 1988, ApJ, 331, 902

Cardona Guillén, C., Lodieu, N., Béjar, V. J. S., et al. 2021, A&A, 654, A134

Carpenter, J. M. 2001, AJ, 121, 2851

Casagrande, L., Flynn, C., & Bessell, M. 2008, MNRAS, 389, 585

Casasayas-Barris, N., Orell-Miquel, J., Stangret, M., et al. 2021, A&A, 654, A163

Casasayas-Barris, N., Pallé, E., Yan, F., et al. 2020, A&A, 635, A206

Cassan, A., Kubas, D., Beaulieu, J. P., et al. 2012, Nature, 481, 167

Cassisi, S. & Salaris, M. 2019, A&A, 626, A32

Catala, C., Forveille, T., & Lai, O. 2006, AJ, 132, 2318

Chabrier, G. 2003a, PASP, 115, 763

Chabrier, G. 2003b, ApJ, 586, L133

Chabrier, G. & Baraffe, I. 1997, A&A, 327, 1039

Chabrier, G., Baraffe, I., Allard, F., & Hauschildt, P. 2000, ApJ, 542, 464

Chambers, K. C., Magnier, E. A., Metcalfe, N., et al. 2016, ArXiv e-prints [arXiv e-prints[arXiv]1612.05560]

Chanamé, J. & Gould, A. 2004, ApJ, 601, 289

Chanamé, J. & Ramírez, I. 2012, ApJ, 746, 102

Chapman, S., Pongracic, H., Disney, M., et al. 1992, Nature, 359, 207

Charbonneau, D., Berta, Z. K., Irwin, J., et al. 2009, Nature, 462, 891

Chaturvedi, P., Bluhm, P., Nagel, E., et al. 2022, A&A, 666, A155

Chauvin, G., Lagrange, A. M., Dumas, C., et al. 2004, A&A, 425, L29

Chelli, A., Duvert, G., Bourgès, L., et al. 2016, A&A, 589, A112

Chen, J. & Kipping, D. 2017, ApJ, 834, 17

Choblet, G., Tobie, G., Sotin, C., Kalousová, K., & Grasset, O. 2017, Icarus, 285, 252

Choi, J., Dotter, A., Conroy, C., et al. 2016, ApJ, 823, 102

Chulkov, D. & Malkov, O. 2022, MNRAS, 517, 2925

Ciardi, D. R., Beichman, C. A., Horch, E. P., & Howell, S. B. 2015, ApJ, 805, 16

Cifuentes, C., Caballero, J. A., & Agustí, S. 2021, Research Notes of the American Astronomical Society, 5, 129

Cifuentes, C., Caballero, J. A., Cortés-Contreras, M., et al. 2020, A&A, 642, A115

Clanton, C. & Gaudi, B. S. 2014, ApJ, 791, 91

Clark, B. M., Blake, C. H., & Knapp, G. R. 2012, ApJ, 744, 119

Clark, C. A., van Belle, G. T., Horch, E. P., et al. 2022, AJ, 164, 33

Clarke, J. R. A., Pinfield, D. J., Gálvez-Ortiz, M. C., et al. 2010, MNRAS, 402, 575

Close, L. M., Zuckerman, B., Song, I., et al. 2007, ApJ, 660, 1492

Cloutier, R., Astudillo-Defru, N., Doyon, R., et al. 2017, A&A, 608, A35

Cochran, W. D., Hatzes, A. P., Butler, R. P., & Marcy, G. W. 1997, ApJ, 483, 457

Cochrane, K. M. & Smith, G. H. 2019, PASP, 131, 114201

Cont, D., Yan, F., Reiners, A., et al. 2021, A&A, 651, A33

Cont, D., Yan, F., Reiners, A., et al. 2022a, A&A, 668, A53

Cont, D., Yan, F., Reiners, A., et al. 2022b, A&A, 657, L2

Cortés-Contreras, M. 2017, PhD thesis, Universidad Complutense de Madrid, Spain
Cortés-Contreras, M., Béjar, V. J. S., Caballero, J. A., et al. 2017a, A&A, 597, A47
Cortés-Contreras, M., Béjar, V. J. S., Caballero, J. A., et al. 2017b, A&A, 597, A47
Cortes-Contreras, M., Caballero, J. A., & Montes, D. 2014, The Observatory, 134, 348
Cournoyer-Cloutier, C., Tran, A., Lewis, S., et al. 2021, MNRAS, 501, 4464
Couteau, P. 1960, Journal des Observateurs, 43, 41
Covey, K. R., Hawley, S. L., Bochanski, J. J., et al. 2008, AJ, 136, 1778
Covey, K. R., Ivezić, Ž., Schlegel, D., et al. 2007, AJ, 134, 2398
Crain, J. N., Sanders, W. L., Fomalont, E. B., & Sramek, R. A. 1986, PASP, 98, 325
Cruz, K. L., Kirkpatrick, J. D., & Burgasser, A. J. 2009, AJ, 137, 3345
Curiel, S., Ortiz-León, G. N., Mioduszewski, A. J., & Sanchez-Bermudez, J. 2022, AJ, 164, 93
CURTIS, H. D. 1906, ApJ, 23, 351
Cutri, R. M. & et al. 2012, VizieR Online Data Catalog, 2311
Cutri, R. M. & et al. 2014, VizieR Online Data Catalog, 2328
Czavalinga, D. R., Mitnyan, T., Rappaport, S. A., et al. 2023, A&A, 670, A75
Czesla, S., Lampón, M., Sanz-Forcada, J., et al. 2022, A&A, 657, A6
Dahn, C. C., Harris, H. C., Subasavage, J. P., et al. 2017, AJ, 154, 147
Dahn, C. C., Harris, H. C., Vrba, F. J., et al. 2002, AJ, 124, 1170
Damasso, M., Del Sordo, F., Anglada-Escudé, G., et al. 2020, Science Advances, 6, eaax7467
Damasso, M., Perger, M., Almenara, J. M., et al. 2022, A&A, 666, A187
Davenport, J. R. A., Ivezić, Ž., Becker, A. C., et al. 2014, MNRAS, 440, 3430
David, T. J., Hillenbrand, L. A., Gillen, E., et al. 2019, ApJ, 872, 161
David, T. J., Hillenbrand, L. A., Petigura, E. A., et al. 2016, Nature, 534, 658
Dawson, P. C. & De Robertis, M. M. 2005, PASP, 117, 1
Deacon, N. R. & Kraus, A. L. 2020, MNRAS, 496, 5176
Dedrick, C. M., Fulton, B. J., Knutson, H. A., et al. 2021, AJ, 161, 86
Degl'Innocenti, S., Prada Moroni, P. G., Marconi, M., & Ruoppo, A. 2008, Ap&SS, 316, 25
del Burgo, C. & Allende Prieto, C. 2018, MNRAS, 479, 1953
Delfosse, X., Bonfils, X., Forveille, T., et al. 2013, A&A, 553, A8
Delfosse, X., Forveille, T., Beuzit, J. L., et al. 1999a, A&A, 344, 897
Delfosse, X., Forveille, T., Mayor, M., Burnet, M., & Perrier, C. 1999b, A&A, 341, L63
Delfosse, X., Forveille, T., Mayor, M., et al. 1998a, A&A, 338, L67
Delfosse, X., Forveille, T., Perrier, C., & Mayor, M. 1998b, A&A, 331, 581
Delfosse, X., Forveille, T., Ségransan, D., et al. 2000, A&A, 364, 217
Delgado-Donate, E. J., Clarke, C. J., & Bate, M. R. 2003, MNRAS, 342, 926
Delgado-Donate, E. J., Clarke, C. J., Bate, M. R., & Hodgkin, S. T. 2004, MNRAS, 351, 617
Dell'Omodarme, M., Valle, G., Degl'Innocenti, S., & Prada Moroni, P. G. 2012, A&A, 540, A26
Demory, B. O., Pozuelos, F. J., Gómez Maqueo Chew, Y., et al. 2020, A&A, 642, A49
Desidera, S., Chauvin, G., Bonavita, M., et al. 2021, A&A, 651, A70
Desidera, S., Gratton, R. G., Lucatello, S., & Claudi, R. U. 2006, A&A, 454, 581
Desidera, S., Gratton, R. G., Scuderi, S., et al. 2004, A&A, 420, 683
Dhital, S., West, A. A., Stassun, K. G., & Bochanski, J. J. 2010, AJ, 139, 2566
Díaz, M. R., Jenkins, J. S., Tuomi, M., et al. 2018, AJ, 155, 126
Díaz, R. F., Delfosse, X., Hobson, M. J., et al. 2019, A&A, 625, A17
Díez Alonso, E., Caballero, J. A., Montes, D., et al. 2019, A&A, 621, A126
Díez Alonso, E., González Hernández, J. I., Suárez Gómez, S. L., et al. 2018a, MNRAS, 480, L1

Díez Alonso, E., Suárez Gómez, S. L., González Hernández, J. I., et al. 2018b, MNRAS, 476, L50
Dittmann, J. A., Irwin, J. M., Charbonneau, D., & Berta-Thompson, Z. K. 2014, ApJ, 784, 156
Dittmann, J. A., Irwin, J. M., Charbonneau, D., et al. 2017, Nature, 544, 333
Djupvik, A. A. & Andersen, J. 2010, in Highlights of Spanish Astrophysics V, Vol. 14, 211
Dole, S. H. 1964, Habitable planets for man
Dorn, C., Venturini, J., Khan, A., et al. 2017, A&A, 597, A37
Dreizler, S., Crossfield, I. J. M., Kossakowski, D., et al. 2020, A&A, 644, A127
Dressing, C. D. & Charbonneau, D. 2015, ApJ, 807, 45
Dressing, C. D., Vanderburg, A., Schlieder, J. E., et al. 2017, AJ, 154, 207
Duchêne, G., Becker, A., Yang, Y., et al. 2017, MNRAS, 469, 1783
Duchêne, G. & Kraus, A. 2013, ARA&A, 51, 269
Dupuy, T. J. & Liu, M. C. 2012, ApJS, 201, 19
Dupuy, T. J. & Liu, M. C. 2017, ApJS, 231, 15
Duquennoy, A. & Mayor, M. 1991, A&A, 248, 485
Edwards, K. J., Becker, K., & Colwell, F. 2012, Annual Review of Earth and Planetary Sciences, 40, 551
Ehrenreich, D., Lovis, C., Allart, R., et al. 2020, Nature, 580, 597
Eisenhardt, P. R. M., Marocco, F., Fowler, J. W., et al. 2020, ApJS, 247, 69
El-Badry, K., Rix, H.-W., & Heintz, T. M. 2021, MNRAS, 506, 2269
Elias, J. H., Frogel, J. A., Matthews, K., & Neugebauer, G. 1982, AJ, 87, 1029
Elliott, P., Bayo, A., Melo, C. H. F., et al. 2014, A&A, 568, A26
Elliott, P., Huélamo, N., Bouy, H., et al. 2015, A&A, 580, A88
Endl, M., Cochran, W. D., Kürster, M., et al. 2006, ApJ, 649, 436
Espinoza, N., Pallé, E., Kemmer, J., et al. 2022, AJ, 163, 133
Evans, D. S. 1968, QJRAS, 9, 388
Evans, D. W., Riello, M., De Angeli, F., et al. 2018, A&A, 616, A4
Eyer, L., Audard, M., Holl, B., et al. 2022, arXiv e-prints, arXiv:2206.06416
Fabricius, C., Luri, X., Arenou, F., et al. 2021, A&A, 649, A5
Fabrycky, D. & Tremaine, S. 2007, ApJ, 669, 1298
Fabrycky, D. C., Ford, E. B., Steffen, J. H., et al. 2012, ApJ, 750, 114
Faherty, J. K., Burgasser, A. J., Walter, F. M., et al. 2012, ApJ, 752, 56
Faherty, J. K., Rice, E. L., Cruz, K. L., Mamajek, E. E., & Núñez, A. 2013, AJ, 145, 2
Famaey, B., Jorissen, A., Luri, X., et al. 2005, A&A, 430, 165
Faria, J. P., Suárez Mascareño, A., Figueira, P., et al. 2022, A&A, 658, A115
Farihi, J. 2016, New A Rev., 71, 9
Feinstein, A. D., Schlieder, J. E., Livingston, J. H., et al. 2019, AJ, 157, 40
Feng, F., Butler, R. P., Vogt, S. S., et al. 2022, ApJS, 262, 21
Feng, F., Shectman, S. A., Clement, M. S., et al. 2020, ApJS, 250, 29
Ferguson, D., Gardner, S., & Yanny, B. 2017, ApJ, 843, 141
Filippazzo, J. C., Rice, E. L., Faherty, J., et al. 2015, ApJ, 810, 158
Finch, C. T. & Zacharias, N. 2016, AJ, 151, 160
Fischer, D. A., Anglada-Escude, G., Arriagada, P., et al. 2016, PASP, 128, 066001
Fischer, D. A. & Marcy, G. W. 1992, ApJ, 396, 178
Fischer, D. A., Marcy, G. W., Butler, R. P., et al. 2008, ApJ, 675, 790
Fischer, D. A. & Valenti, J. 2005, ApJ, 622, 1102
Fleming, T. A. 1998, ApJ, 504, 461
Fontaine, G., Brassard, P., & Bergeron, P. 2001, PASP, 113, 409

Foreman-Mackey, D., Hogg, D. W., Lang, D., & Goodman, J. 2013, PASP, 125, 306

Fortier, A., Beck, T., Benz, W., et al. 2014, in Proc. SPIE, Vol. 9143,

Forveille, T., Bonfils, X., Delfosse, X., et al. 2009, A&A, 493, 645

Fouesneau, M., Rix, H.-W., von Hippel, T., Hogg, D. W., & Tian, H. 2019, ApJ, 870, 9

Fouqué, P., Moutou, C., Malo, L., et al. 2018, MNRAS, 475, 1960

France, K., Froning, C. S., Linsky, J. L., et al. 2013, ApJ, 763, 149

Freund, S., Robrade, J., Schneider, P. C., & Schmitt, J. H. M. M. 2020, A&A, 640, A66

Fuhrmann, K. 1998, A&A, 338, 161

Fuhrmeister, B., Czesla, S., Hildebrandt, L., et al. 2019a, A&A, 632, A24

Fuhrmeister, B., Czesla, S., Hildebrandt, L., et al. 2020, A&A, 640, A52

Fuhrmeister, B., Czesla, S., Nagel, E., et al. 2022, A&A, 657, A125

Fuhrmeister, B., Czesla, S., Schmitt, J. H. M. M., et al. 2018, A&A, 615, A14

Fuhrmeister, B., Czesla, S., Schmitt, J. H. M. M., et al. 2019b, A&A, 623, A24

Fukui, A., Kimura, T., Hirano, T., et al. 2022, PASJ, 74, L1

Gagné, J. & Faherty, J. K. 2018, ApJ, 862, 138

Gagné, J., Faherty, J. K., Cruz, K. L., et al. 2015, ApJS, 219, 33

Gagné, J., Faherty, J. K., & Mamajek, E. E. 2018a, ApJ, 865, 136

Gagné, J., Lafrenière, D., Doyon, R., Malo, L., & Artigau, É. 2014, ApJ, 783, 121

Gagné, J., Mamajek, E. E., Malo, L., et al. 2018b, ApJ, 856, 23

Gaia Collaboration, Arenou, F., Babusiaux, C., et al. 2022a, arXiv e-prints, arXiv:2206.05595

Gaia Collaboration, Babusiaux, C., van Leeuwen, F., et al. 2018a, A&A, 616, A10

Gaia Collaboration, Brown, A. G. A., Vallenari, A., et al. 2018b, A&A, 616, A1

Gaia Collaboration, Brown, A. G. A., Vallenari, A., et al. 2021, A&A, 649, A1

Gaia Collaboration, Brown, A. G. A., Vallenari, A., et al. 2016, A&A, 595, A2

Gaia Collaboration, Vallenari, A., Brown, A. G. A., et al. 2022b, arXiv e-prints, arXiv:2208.00211

Gaidos, E. & Mann, A. W. 2014, ApJ, 791, 54

Gaidos, E., Mann, A. W., Kraus, A. L., & Ireland, M. 2016, MNRAS, 457, 2877

Galli, P. A. B., Loinard, L., Ortiz-Léon, G. N., et al. 2018, ApJ, 859, 33

Gálvez, M. C., Montes, D., Fernández-Figueroa, M. J., et al. 2002, A&A, 389, 524

Gan, T., Wang, S. X., Wang, S., et al. 2022, arXiv e-prints, arXiv:2210.08313

Garcés, A., Catalán, S., & Ribas, I. 2011, A&A, 531, A7

Gatewood, G. & Coban, L. 2009, AJ, 137, 402

Gatewood, G., Coban, L., & Han, I. 2003, AJ, 125, 1530

Gentile Fusillo, N. P., Tremblay, P.-E., Gänsicke, B. T., et al. 2019, MNRAS, 482, 4570

Gibson, S. R., Howard, A. W., Marcy, G. W., et al. 2016, in , Vol. 9908

Gill, D. 1899, The Observatory, 22, 99

Gillon, M., Jehin, E., Lederer, S. M., et al. 2016, Nature, 533, 221

Gillon, M., Triaud, A. H. M. J., Demory, B.-O., et al. 2017, Nature, 542, 456

Gizis, J. E. 1997, AJ, 113, 806

Gizis, J. E., Monet, D. G., Reid, I. N., Kirkpatrick, J. D., & Burgasser, A. J. 2000a, MNRAS, 311, 385

Gizis, J. E., Monet, D. G., Reid, I. N., et al. 2000b, AJ, 120, 1085

Gizis, J. E., Monet, D. G., Reid, I. N., et al. 2000c, AJ, 120, 1085

Gizis, J. E., Reid, I. N., & Hawley, S. L. 2002, AJ, 123, 3356

Gizis, J. E. & Reid, N. I. 1996, AJ, 111, 365

Glein, C. R., Baross, J. A., & Waite, J. H. 2015, Geochim. Cosmochim. Acta, 162, 202

Gliese, W. & Jahreiß, H. 1991, Preliminary Version of the Third Catalogue of Nearby Stars, Vol. I; NASA/Astronomical Data Center, Goddard Space Flight Center, Greenbelt, MD

Golimowski, D. A., Leggett, S. K., Marley, M. S., et al. 2004, AJ, 127, 3516
Gómez de Castro, A. I., Lopez-Santiago, J., López-Martínez, F., et al. 2015, ApJS, 216, 26
Gonzalez, G. 1997, MNRAS, 285, 403
González-Álvarez, E., Petralia, A., Micela, G., et al. 2021, A&A, 649, A157
González-Álvarez, E., Zapatero Osorio, M. R., Caballero, J. A., et al. 2020, A&A, 637, A93
González-Álvarez, E., Zapatero Osorio, M. R., Sanz-Forcada, J., et al. 2022, A&A, 658, A138
González-Payo, J., Caballero, J. A., & Cortés-Contreras, M. 2023, A&A, 670, A102
González-Payo, J., Cortés-Contreras, M., Lodieu, N., et al. 2021, A&A, 650, A190
Goodwin, S. P. 2010, Philosophical Transactions of the Royal Society of London Series A, 368, 851
Goodwin, S. P. & Kroupa, P. 2005, A&A, 439, 565
Goodwin, S. P., Kroupa, P., Goodman, A., & Burkert, A. 2007, in Protostars and Planets V, 133
Goodwin, S. P., Whitworth, A. P., & Ward-Thompson, D. 2004, A&A, 414, 633
Gould, A., Bahcall, J. N., & Flynn, C. 1996, ApJ, 465, 759
Gould, A., Bahcall, J. N., & Flynn, C. 1997, ApJ, 482, 913
Gratton, R., Desidera, S., Marzari, F., & Bonavita, M. 2022, European Physical Journal Plus, 137, 1207
Gratton, R. G., Bonanno, G., Claudi, R. U., et al. 2001, A&A, 377, 123
Gray, R. O., Corbally, C. J., Garrison, R. F., McFadden, M. T., & Robinson, P. E. 2003, AJ, 126, 2048
Günther, M. N., Pozuelos, F. J., Dittmann, J. A., et al. 2019, Nature Astronomy, 3, 1157
Gustafsson, B., Bell, R. A., Eriksson, K., & Nordlund, A. 1975, A&A, 42, 407
Gustafsson, B., Edvardsson, B., Eriksson, K., et al. 2008, A&A, 486, 951
Guszejnov, D., Hopkins, P. F., & Krumholz, M. R. 2017, MNRAS, 468, 4093
Habets, G. M. H. J. & Heintze, J. R. W. 1981, A&AS, 46, 193
Haghighipour, N., Vogt, S. S., Butler, R. P., et al. 2010, ApJ, 715, 271
Harakawa, H., Takarada, T., Kasagi, Y., et al. 2022, PASJ, 74, 904
Hardegree-Ullman, K. K., Cushing, M. C., Muirhead, P. S., & Christiansen, J. L. 2019, AJ, 158, 75
Haro, G., Iriarte, B., & Chavira, E. 1953, Boletin de los Observatorios Tonantzintla y Tacubaya, 1, 3
Harpsøe, K. B. W., Hardis, S., Hinse, T. C., et al. 2013, A&A, 549, A10
Harrington, R. S. 1972, Celestial Mechanics, 6, 322
Harrington, R. S., Christy, J. W., & Strand, K. A. 1981a, AJ, 86, 909
Harrington, R. S., Christy, J. W., & Strand, K. A. 1981b, AJ, 86, 909
Harris, C. R., Millman, K. J., van der Walt, S. J., et al. 2020, Nature, 585, 357
Hart, M. H. 1978, Icarus, 33, 23
Hartigan, P., Strom, K. M., & Strom, S. E. 1994, ApJ, 427, 961
Hartman, J. D., Bakos, G. Á., Noyes, R. W., et al. 2011, AJ, 141, 166
Hartman, J. D., Bakos, G. Á., Torres, G., et al. 2009, ApJ, 706, 785
Hartman, J. D., Bayliss, D., Brahm, R., et al. 2015, AJ, 149, 166
Hatzes, A. P. & Cochran, W. D. 1993, ApJ, 413, 339
Hatzes, A. P., Cochran, W. D., Endl, M., et al. 2003, ApJ, 599, 1383
Hauschildt, P. H., Allard, F., & Baron, E. 1999a, ApJ, 512, 377
Hauschildt, P. H., Allard, F., & Baron, E. 1999b, ApJ, 512, 377
Hauschildt, P. H., Baron, E., & Allard, F. 1997, ApJ, 483, 390
Hawkins, K., Lucey, M., Ting, Y.-S., et al. 2020, MNRAS, 492, 1164
Hawkins, M. R. S. & Bessell, M. S. 1988, MNRAS, 234, 177
Hawley, S. L., Covey, K. R., Knapp, G. R., et al. 2002, AJ, 123, 3409
Hawley, S. L., Davenport, J. R. A., Kowalski, A. F., et al. 2014, ApJ, 797, 121
Hawley, S. L., Gizis, J. E., & Reid, I. N. 1996, AJ, 112, 2799

Heggie, D. C. 1975, MNRAS, 173, 729
Heintz, W. D. 1969, JRASC, 63, 275
Heintz, W. D. 1987, ApJS, 65, 161
Henden, A. A., Templeton, M., Terrell, D., et al. 2016, VizieR Online Data Catalog, 2336
Henry, T. J. 1991, PhD thesis, University of Arizona
Henry, T. J., Jao, W.-C., Subasavage, J. P., et al. 2006, AJ, 132, 2360
Henry, T. J., Kirkpatrick, J. D., & Simons, D. A. 1994, AJ, 108, 1437
Henry, T. J. & McCarthy, Donald W., J. 1993, AJ, 106, 773
Herbig, G. H. & Moorhead, J. M. 1965, ApJ, 141, 649
Hernández, J., Hartmann, L., Calvet, N., et al. 2008, ApJ, 686, 1195
Herschel, J. F. W., Main, R., & Pritchard, C. 1874, MmRAS, 40, 1
Herschel, M. & Banks, J. 1782, Philosophical Transactions of the Royal Society of London Series I, 72, 82
Herschel, W. 1785, Philosophical Transactions of the Royal Society of London Series I, 75, 40
Herschel, W. 1822, MmRAS, 1, 166
Hertzsprung, E. 1923, Bull. Astron. Inst. Netherlands, 2, 15
Hewett, P. C., Warren, S. J., Leggett, S. K., & Hodgkin, S. T. 2006, MNRAS, 367, 454
Hidalgo, S. L., Pietrinferni, A., Cassisi, S., et al. 2018, ApJ, 856, 125
Hills, J. G. 1975, AJ, 80, 809
Hintz, D., Fuhrmeister, B., Czesla, S., et al. 2019, A&A, 623, A136
Hintz, D., Fuhrmeister, B., Czesla, S., et al. 2020, A&A, 638, A115
Hirano, T., Dai, F., Livingston, J. H., et al. 2018, AJ, 155, 124
Hirano, T., Fukui, A., Mann, A. W., et al. 2016, ApJ, 820, 41
Hobson, M. J., Delfosse, X., Astudillo-Defru, N., et al. 2019, A&A, 625, A18
Hobson, M. J., Díaz, R. F., Delfosse, X., et al. 2018, A&A, 618, A103
Høg, E., Fabricius, C., Makarov, V. V., et al. 2000, A&A, 355, L27
Holman, M. J. & Wiegert, P. A. 1999, AJ, 117, 621
Houdebine, É. R., Mullan, D. J., Doyle, J. G., et al. 2019, AJ, 158, 56
Howard, A. W., Johnson, J. A., Marcy, G. W., et al. 2010, ApJ, 721, 1467
Howell, S. B., Sobeck, C., Haas, M., et al. 2014, PASP, 126, 398
Hsu, C.-C., Burgasser, A. J., & Theissen, C. A. 2023, arXiv e-prints, arXiv:2301.07039
Huang, S. S. & Struve, O. 1956, AJ, 61, 300
Huggins, W. & Huggins, M. 1890, Proceedings of the Royal Society of London Series I, 48, 216
Huggins, W. & Miller, W. A. 1864, Philosophical Transactions of the Royal Society of London Series I, 154, 413
Hunter, J. D. 2007, Computing in Science and Engineering, 9, 90
Husser, T. O., Wende-von Berg, S., Dreizler, S., et al. 2013, A&A, 553, A6
Hwang, H.-C., Ting, Y.-S., & Zakamska, N. L. 2022, MNRAS, 512, 3383
Innes, R. T. A. 1915, Circular of the Union Observatory Johannesburg, 30, 235
Ireland, M. J., Kraus, A., Martinache, F., Lloyd, J. P., & Tuthill, P. G. 2008, ApJ, 678, 463
Irwin, J., Charbonneau, D., Berta, Z. K., et al. 2009, ApJ, 701, 1436
Ishikawa, H. T., Aoki, W., Hirano, T., et al. 2022a, AJ, 163, 72
Ishikawa, H. T., Aoki, W., Hirano, T., et al. 2022b, AJ, 163, 72
Israel, G. L., Hummel, W., Covino, S., et al. 2002, A&A, 386, L13
Jackson, R. J., Deliyannis, C. P., & Jeffries, R. D. 2018, MNRAS, 476, 3245
Janson, M., Bergfors, C., Brandner, W., et al. 2014a, ApJS, 214, 17
Janson, M., Bergfors, C., Brandner, W., et al. 2014b, ApJ, 789, 102
Janson, M., Bergfors, C., Brandner, W., et al. 2014c, ApJ, 789, 102

Janson, M., Durkan, S., Hippler, S., et al. 2017, A&A, 599, A70
Janson, M., Hormuth, F., Bergfors, C., et al. 2012, ApJ, 754, 44
Jao, W.-C., Henry, T. J., Subasavage, J. P., et al. 2005, AJ, 129, 1954
Jeffers, S. V., Dreizler, S., Barnes, J. R., et al. 2020, Science, 368, 1477
Jeffers, S. V., Schöfer, P., Lamert, A., et al. 2018, A&A, 614, A76
Jenkins, J. S., Ramsey, L. W., Jones, H. R. A., et al. 2009, ApJ, 704, 975
Jenkins, L. F. 1952, General catalogue of trigonometric stellar parallaxes.
Jiang, Y.-F. & Tremaine, S. 2010, MNRAS, 401, 977
Jiménez-Esteban, F. M., Torres, S., Rebassa-Mansergas, A., et al. 2023, MNRAS, 518, 5106
Jiménez-Esteban, F. M., Torres, S., Rebassa-Mansergas, A., et al. 2018, MNRAS, 480, 4505
Jódar, E., Pérez-Garrido, A., Díaz-Sánchez, A., et al. 2013, MNRAS, 429, 859
Joergens, V. 2008, A&A, 492, 545
Johnson, H. L., Mitchell, R. I., & Iriarte, B. 1962, ApJ, 136, 75
Johnson, J. A., Aller, K. M., Howard, A. W., & Crepp, J. R. 2010a, PASP, 122, 905
Johnson, J. A. & Apps, K. 2009, ApJ, 699, 933
Johnson, J. A., Butler, R. P., Marcy, G. W., et al. 2007, ApJ, 670, 833
Johnson, J. A., Gazak, J. Z., Apps, K., et al. 2012, AJ, 143, 111
Johnson, J. A., Howard, A. W., Marcy, G. W., et al. 2010b, PASP, 122, 149
Johnson, J. A., Howard, A. W., Marcy, G. W., et al. 2010c, PASP, 122, 149
Jontof-Hutter, D., Rowe, J. F., Lissauer, J. J., Fabrycky, D. C., & Ford, E. B. 2015, Nature, 522, 321
Joy, A. H. 1947, ApJ, 105, 96
Joy, A. H. & Abt, H. A. 1974, ApJS, 28, 1
Joy, A. H. & Sanford, R. F. 1926, ApJ, 64, 250
Jurgenson, C., Fischer, D., McCracken, T., et al. 2016, in , Vol. 9908
Kaeufl, H.-U., Ballester, P., Biereichel, P., et al. 2004, in , Vol. 5492, 1218–1227
Kahler, S., Golub, L., Harnden, F. R., et al. 1982, ApJ, 252, 239
Kaiser, N., Burgett, W., Chambers, K., et al. 2010, in Proc. SPIE, Vol. 7733
Kalas, P., Liu, M. C., & Matthews, B. C. 2004, Science, 303, 1990
Kalirai, J. S., Anderson, J., Dotter, A., et al. 2013, ApJ, 763, 110
Kaminski, A., Trifonov, T., Caballero, J. A., et al. 2018, A&A, 618, A115
Kan, S. B. J., Lewis, R. D., Chen, K., & Arnold, F. H. 2016, Science, 354, 1048
Karataş, Y., Bilir, S., Eker, Z., & Demircan, O. 2004, MNRAS, 349, 1069
Kasting, J. F., Whitmire, D. P., & Reynolds, R. T. 1993, Icarus, 101, 108
Katoh, N., Itoh, Y., Toyota, E., & Sato, B. 2013, AJ, 145, 41
Katz, D., Sartoretti, P., Guerrier, A., et al. 2022, arXiv e-prints, arXiv:2206.05902
Kaufer, A., Wolf, B., Andersen, J., & Pasquini, L. 1997, The Messenger, 89, 1
Kemmer, J., Dreizler, S., Kossakowski, D., et al. 2022, A&A, 659, A17
Kemmer, J., Stock, S., Kossakowski, D., et al. 2020, A&A, 642, A236
Kervella, P., Arenou, F., Mignard, F., & Thévenin, F. 2019, A&A, 623, A72
Kesseli, A. Y., Muirhead, P. S., Mann, A. W., & Mace, G. 2018, AJ, 155, 225
Khalafinejad, S., Molaverdikhani, K., Blecic, J., et al. 2021, A&A, 656, A142
Khrutskaya, E. V., Izmailov, I. S., & Khovrichev, M. Y. 2010, Astronomy Letters, 36, 576
Kiman, R., Faherty, J. K., Cruz, K. L., et al. 2021, AJ, 161, 277
King, J. R., Villarreal, A. R., Soderblom, D. R., Gulliver, A. F., & Adelman, S. J. 2003, AJ, 125, 1980
King, R. R., Goodwin, S. P., Parker, R. J., & Patience, J. 2012a, MNRAS, 427, 2636
King, R. R., Parker, R. J., Patience, J., & Goodwin, S. P. 2012b, MNRAS, 421, 2025

Kipping, D. M. 2009a, MNRAS, 392, 181
Kipping, D. M. 2009b, MNRAS, 396, 1797
Kipping, D. M., Fossey, S. J., & Campanella, G. 2009, MNRAS, 400, 398
Kirkpatrick, J. D. 2005, ARA&A, 43, 195
Kirkpatrick, J. D., Henry, T. J., & Irwin, M. J. 1997, AJ, 113, 1421
Kirkpatrick, J. D., Henry, T. J., & McCarthy, Jr., D. W. 1991, ApJS, 77, 417
Kirkpatrick, J. D., McGraw, J. T., Hess, T. R., Liebert, J., & McCarthy, Donald W., J. 1994, ApJS, 94, 749
Kirkpatrick, J. D., Reid, I. N., Liebert, J., et al. 1999, ApJ, 519, 802
Kite, E. S. & Ford, E. B. 2018, ApJ, 864, 75
Knapp, G. R., Leggett, S. K., Fan, X., et al. 2004, AJ, 127, 3553
Konopacky, Q. M., Ghez, A. M., Barman, T. S., et al. 2010, ApJ, 711, 1087
Kopparapu, R. K., Ramirez, R. M., Schottelkotte, J., et al. 2014, ApJ, 787, L29
Kopparapu, R. k., Wolf, E. T., Arney, G., et al. 2017, ApJ, 845, 5
Kopytova, T. G., Brandner, W., Tognelli, E., et al. 2016, A&A, 585, A7
Kossakowski, D., Kemmer, J., Bluhm, P., et al. 2021, A&A, 656, A124
Kossakowski, D., Kürster, M., Henning, T., et al. 2022, A&A, 666, A143
Kossakowski, D., Kürster, M., Trifonov, T., et al. 2023, A&A, 670, A84
Kouwenhoven, M. B. N. & de Grijs, R. 2008, A&A, 480, 103
Kouwenhoven, M. B. N., Goodwin, S. P., Parker, R. J., et al. 2010, MNRAS, 404, 1835
Kowalski, A. F., Hawley, S. L., Holtzman, J. A., Wisniewski, J. P., & Hilton, E. J. 2010, ApJ, 714, L98
Kozai, Y. 1962, AJ, 67, 591
Kraus, A. L., Herczeg, G. J., Rizzuto, A. C., et al. 2017, ApJ, 838, 150
Kraus, A. L. & Hillenbrand, L. A. 2009, ApJ, 704, 531
Kraus, A. L., Ireland, M. J., Huber, D., Mann, A. W., & Dupuy, T. J. 2016, AJ, 152, 8
Kraus, A. L., Shkolnik, E. L., Allers, K. N., & Liu, M. C. 2014, AJ, 147, 146
Kroupa, P. 1995, MNRAS, 277, 1522
Kroupa, P. 2001, MNRAS, 322, 231
Kroupa, P. 2008, Initial Conditions for Star Clusters, Vol. 760, 181
Kroupa, P. & Jerabkova, T. 2018, arXiv e-prints, arXiv:1806.10605
Kroupa, P., Petr, M. G., & McCaughrean, M. J. 1999, New A, 4, 495
Kroupa, P., Tout, C. A., & Gilmore, G. 1991, MNRAS, 251, 293
Kroupa, P., Tout, C. A., & Gilmore, G. 1993, MNRAS, 262, 545
Kundurthy, P., Agol, E., Becker, A. C., et al. 2011, ApJ, 731, 123
Kurucz, R. L. 1970, SAO Special Report, 309
Kurucz, R. L. 1979, ApJS, 40, 1
Lada, C. J. 2006, ApJ, 640, L63
Lafarga, M., Ribas, I., Lovis, C., et al. 2020, A&A, 636, A36
Lafarga, M., Ribas, I., Reiners, A., et al. 2021, A&A, 652, A28
Lafarga, M., Ribas, I., Zechmeister, M., et al. 2023, arXiv e-prints, arXiv:2302.07916
Lalitha, S., Baroch, D., Morales, J. C., et al. 2019, A&A, 627, A116
Lambrechts, M. & Johansen, A. 2012, A&A, 544, A32
Lane, B. F., Zapatero Osorio, M. R., Britton, M. C., Martín, E. L., & Kulkarni, S. R. 2001, ApJ, 560, 390
Larson, R. B. 1972, MNRAS, 157, 121
Larson, R. B. 1985, MNRAS, 214, 379
Latham, D. W., Mazeh, T., Stefanik, R. P., Mayor, M., & Burki, G. 1989, Nature, 339, 38
Laughlin, G., Bodenheimer, P., & Adams, F. C. 2004, ApJ, 612, L73

Law, N. M., Hodgkin, S. T., & Mackay, C. D. 2006, MNRAS, 368, 1917
Law, N. M., Hodgkin, S. T., & Mackay, C. D. 2008, MNRAS, 384, 150
Laws, C., Gonzalez, G., Walker, K. M., et al. 2003, AJ, 125, 2664
Lee, S. G. 1984, AJ, 89, 702
Leggett, S. K. 1992, ApJS, 82, 351
Leggett, S. K., Geballe, T. R., Fan, X., et al. 2000, ApJ, 536, L35
Leigh, N. W. C. & Geller, A. M. 2013, MNRAS, 432, 2474
Leinert, C., Henry, T., Glindemann, A., & McCarthy, D. W., J. 1997, A&A, 325, 159
Lépine, S. & Bongiorno, B. 2007, AJ, 133, 889
Lépine, S. & Gaidos, E. 2011, AJ, 142, 138
Lépine, S., Hilton, E. J., Mann, A. W., et al. 2013, AJ, 145, 102
Lépine, S., Rich, R. M., & Shara, M. M. 2003, AJ, 125, 1598
Lépine, S., Rich, R. M., & Shara, M. M. 2007, ApJ, 669, 1235
Lépine, S. & Shara, M. M. 2005, AJ, 129, 1483
Lépine, S., Thorstensen, J. R., Shara, M. M., & Rich, R. M. 2009, AJ, 137, 4109
Li, L., Shao, Z., Li, Z.-Z., et al. 2020, ApJ, 901, 49
Lidov, M. L. 1962, Planet. Space Sci., 9, 719
Liebert, J. & Gizis, J. E. 2006, PASP, 118, 659
Lillo-Box, J., Barrado, D., & Bouy, H. 2012, A&A, 546, A10
Lindegren, L., Hernández, J., Bombrun, A., et al. 2018, A&A, 616, A2
Lindegren, L., Lammers, U., Hobbs, D., et al. 2012, A&A, 538, A78
Lindgren, S. & Heiter, U. 2017, A&A, 604, A97
Lingam, M. & Loeb, A. 2017, ApJ, 848, 41
Livingston, J. H., Dai, F., Hirano, T., et al. 2019, MNRAS, 484, 8
Lo Curto, G., Mayor, M., Benz, W., et al. 2013, A&A, 551, A59
Lodieu, N., Smart, R. L., Pérez-Garrido, A., & Silvotti, R. 2019, A&A, 623, A35
López-Santiago, J., Montes, D., Crespo-Chacón, I., & Fernández-Figueroa, M. J. 2006, ApJ, 643, 1160
Loyd, R. O. P., Shkolnik, E. L., Schneider, A. C., et al. 2018, ApJ, 867, 70
Lubin, J., Robertson, P., Stefansson, G., et al. 2021, AJ, 162, 61
Lucy, L. B. 1968, ApJ, 151, 1123
Ludendorff, H. 1908, Astronomische Nachrichten, 177, 7
Luger, R., Sestovic, M., Kruse, E., et al. 2017, Nature Astronomy, 1, 0129
Luhman, K. L., Stauffer, J. R., & Mamajek, E. E. 2005, ApJ, 628, L69
Luque, R., Fulton, B. J., Kunimoto, M., et al. 2022a, A&A, 664, A199
Luque, R., Nowak, G., Hirano, T., et al. 2022b, A&A, 666, A154
Luque, R., Nowak, G., Pallé, E., et al. 2019a, A&A, 623, A114
Luque, R., Nowak, G., Pallé, E., et al. 2018, A&A, 620, A171
Luque, R., Pallé, E., Kossakowski, D., et al. 2019b, A&A, 628, A39
Luque, R., Serrano, L. M., Molaverdikhani, K., et al. 2021, A&A, 645, A41
Maciejewski, G., Niedzielski, A., Nowak, G., et al. 2014, Acta Astron., 64, 323
Macintosh, B., Graham, J. R., Barman, T., et al. 2015, Science, 350, 64
Mahadevan, S., Ramsey, L., Bender, C., et al. 2012, in Proc. SPIE, Vol. 8446
Mahadevan, S., Stefánsson, G., Robertson, P., et al. 2021, ApJ, 919, L9
Mainzer, A., Bauer, J., Grav, T., et al. 2011, ApJ, 731, 53
Maíz Apellániz, J. & Weiler, M. 2018, A&A, 619, A180
Majewski, S. R., Schiavon, R. P., Frinchaboy, P. M., et al. 2017, AJ, 154, 94

Makarov, V. V., Zacharias, N., & Hennessy, G. S. 2008, ApJ, 687, 566

Makarov, V. V., Zacharias, N., Hennessy, G. S., Harris, H. C., & Monet, A. K. B. 2007, ApJ, 668, L155

Maldonado, J., Affer, L., Micela, G., et al. 2015, A&A, 577, A132

Maldonado, J., Petralia, A., Damasso, M., et al. 2021, VizieR Online Data Catalog, J/A+A/651/A93

Maldonado, J., Scandariato, G., Stelzer, B., et al. 2017, A&A, 598, A27

Malkov, O. Y., Oblak, E., Snegireva, E. A., & Torra, J. 2006, A&A, 446, 785

Malo, L., Artigau, É., Doyon, R., et al. 2014a, ApJ, 788, 81

Malo, L., Artigau, É., Doyon, R., et al. 2014b, ApJ, 788, 81

Malo, L., Doyon, R., Feiden, G. A., et al. 2014c, ApJ, 792, 37

Malo, L., Doyon, R., Lafrenière, D., et al. 2013, ApJ, 762, 88

Malo, L., Doyon, R., Lafreniere, D., et al. 2014d, VizieR Online Data Catalog, J/ApJ/762/88

Malofeeva, A. A., Mikhnevich, V. O., Carraro, G., & Seleznev, A. F. 2023, AJ, 165, 45

Mamajek, E. E. 2005, ApJ, 634, 1385

Mamajek, E. E., Kenworthy, M. A., Hinz, P. M., & Meyer, M. R. 2010, AJ, 139, 919

Mamajek, E. E., Torres, G., Prsa, A., et al. 2015, arXiv e-prints, arXiv:1510.06262

Mann, A. W., Brewer, J. M., Gaidos, E., Lépine, S., & Hilton, E. J. 2013a, AJ, 145, 52

Mann, A. W., Dupuy, T., Kraus, A. L., et al. 2019, ApJ, 871, 63

Mann, A. W., Feiden, G. A., Gaidos, E., Boyajian, T., & von Braun, K. 2015, ApJ, 804, 64

Mann, A. W., Gaidos, E., & Ansdell, M. 2013b, ApJ, 779, 188

Mann, A. W., Gaidos, E., Mace, G. N., et al. 2016a, ApJ, 818, 46

Mann, A. W., Newton, E. R., Rizzuto, A. C., et al. 2016b, AJ, 152, 61

Marconi, A., Abreu, M., Adibekyan, V., et al. 2022, in , Vol. 12184

Marcy, G. W. & Butler, R. P. 1995, in American Astronomical Society Meeting Abstracts, Vol. 187, 70.04

Marcy, G. W. & Butler, R. P. 1996, ApJ, 464, L147

Marcy, G. W., Butler, R. P., Fischer, D., et al. 2001, ApJ, 556, 296

Marcy, G. W., Butler, R. P., Fischer, D. A., et al. 2002, ApJ, 581, 1375

Marcy, G. W., Butler, R. P., Vogt, S. S., Fischer, D., & Lissauer, J. J. 1998, ApJ, 505, L147

Marcy, G. W., Lindsay, V., & Wilson, K. 1987, PASP, 99, 490

Marfil, E., Montes, D., Tabernero, H. M., et al. 2018, in , 32

Marfil, E., Tabernero, H. M., Montes, D., et al. 2021, A&A, 656, A162

Marrese, P. M., Marinoni, S., Fabrizio, M., & Altavilla, G. 2019, A&A, 621, A144

Martín, E. L., Koresko, C. D., Kulkarni, S. R., Lane, B. F., & Wizinowich, P. L. 2000, ApJ, 529, L37

Martínez-Rodríguez, H., Caballero, J. A., Cifuentes, C., Piro, A. L., & Barnes, R. 2019, ApJ, 887, 261

Martioli, E., Hébrard, G., Correia, A. C. M., Laskar, J., & Lecavelier des Etangs, A. 2021, A&A, 649, A177

Mason, B. D., Hartkopf, W. I., Gies, D. R., Henry, T. J., & Helsel, J. W. 2009, AJ, 137, 3358

Mason, B. D., Wycoff, G. L., Hartkopf, W. I., Douglass, G. G., & Worley, C. E. 2001, AJ, 122, 3466

Mathieu, R. D., Ghez, A. M., Jensen, E. L. N., & Simon, M. 2000, in Protostars and Planets IV, 703

Matzner, C. D. & McKee, C. F. 2000, ApJ, 545, 364

Maury, A. C. & Pickering, E. C. 1897, Annals of Harvard College Observatory, 28, 1

Mayer, C. 1778, Gründliche Vertheidigung neuer Beobachtungen von Sternwarte entdecket...

Mayor, M., Bonfils, X., Forveille, T., et al. 2009, A&A, 507, 487

Mayor, M., Marmier, M., Lovis, C., et al. 2011, arXiv e-prints, arXiv:1109.2497

Mayor, M., Pepe, F., Queloz, D., et al. 2003, The Messenger, 114, 20

Mayor, M. & Queloz, D. 1995, Nature, 378, 355

Mazeh, T., Latham, D. W., Goldberg, E., et al. 2001, MNRAS, 325, 343

McArthur, B. E., Endl, M., Cochran, W. D., et al. 2004, ApJ, 614, L81

Ment, K., Dittmann, J. A., Astudillo-Defru, N., et al. 2019, AJ, 157, 32

Mermilliod, J. C., Mayor, M., & Udry, S. 2009, A&A, 498, 949

Michell, J. 1767, Philosophical Transactions of the Royal Society of London Series I, 57, 234

Michell, J. 1784, Philosophical Transactions of the Royal Society of London Series I, 74, 35

Miret-Roig, N., Galli, P. A. B., Brandner, W., et al. 2020a, A&A, 642, A179

Miret-Roig, N., Galli, P. A. B., Brandner, W., et al. 2020b, A&A, 642, A179

Mizuno, H. 1980, Progress of Theoretical Physics, 64, 544

Mochnacki, S. W., Gladders, M. D., Thomson, J. R., et al. 2002, AJ, 124, 2868

Moeckel, N. & Bate, M. R. 2010, MNRAS, 404, 721

Moeckel, N. & Clarke, C. J. 2011, MNRAS, 415, 1179

Mohanty, S. & Basri, G. 2003, ApJ, 583, 451

Monet, D. G., Levine, S. E., Canzian, B., et al. 2003, AJ, 125, 984

Monteiro, H., Jao, W.-C., Henry, T., Subasavage, J., & Beaulieu, T. 2006, ApJ, 638, 446

Montes, D., González-Peinado, R., Tabernero, H. M., et al. 2018, MNRAS, 479, 1332

Montes, D., López-Santiago, J., Gálvez, M. C., et al. 2001, MNRAS, 328, 45

Montet, B. T., Crepp, J. R., Johnson, J. A., Howard, A. W., & Marcy, G. W. 2014, ApJ, 781, 28

Montet, B. T., Morton, T. D., Foreman-Mackey, D., et al. 2015, ApJ, 809, 25

Morales, J. C., Mustill, A. J., Ribas, I., et al. 2019, Science, 365, 1441

Morales, J. C., Ribas, I., & Jordi, C. 2008, A&A, 478, 507

Morales, J. C., Ribas, I., Jordi, C., et al. 2009, ApJ, 691, 1400

Morales-Rueda, L., Marsh, T. R., Maxted, P. F. L., et al. 2005, MNRAS, 359, 648

Mortier, A., Santos, N. C., Sozzetti, A., et al. 2012, A&A, 543, A45

Morton, T. D., Bryson, S. T., Coughlin, J. L., et al. 2016, ApJ, 822, 86

Mowlavi, N., Holl, B., Lecœur-Taïbi, I., et al. 2022, arXiv e-prints, arXiv:2211.00929

Muirhead, P. S., Johnson, J. A., Apps, K., et al. 2012, ApJ, 747, 144

Muirhead, P. S., Mann, A. W., Vanderburg, A., et al. 2015, ApJ, 801, 18

Mulders, G. D., Drążkowska, J., van der Marel, N., Ciesla, F. J., & Pascucci, I. 2021, ApJ, 920, L1

Mullan, D. J. & MacDonald, J. 2001, ApJ, 559, 353

Munday, J., Marsh, T. R., Hollands, M., et al. 2022, arXiv e-prints, arXiv:2211.09834

Murray, A. E., Kenig, F., Fritsen, C. H., et al. 2012, Proceedings of the National Academy of Science, 109, 20626

Naef, D., Mayor, M., Korzennik, S. G., et al. 2003, A&A, 410, 1051

Nagel, E., Czesla, S., Schmitt, J. H. M. M., et al. 2019, A&A, 622, A153

Naoz, S., Farr, W. M., & Rasio, F. A. 2012, ApJ, 754, L36

Newton, E. R., Charbonneau, D., Irwin, J., et al. 2014, AJ, 147, 20

Newton, E. R., Charbonneau, D., Irwin, J., & Mann, A. W. 2015, ApJ, 800, 85

Nguyen, C. T., Costa, G., Girardi, L., et al. 2022, A&A, 665, A126

Nidever, D. L., Marcy, G. W., Butler, R. P., Fischer, D. A., & Vogt, S. S. 2002, ApJS, 141, 503

Niels Bohr Institute, Institute of Astronomy, C., & Real Instituto y Observatorio de La Armada. 2014, VizieR Online Data Catalog, 1327

Nortmann, L., Pallé, E., Salz, M., et al. 2018, Science, 362, 1388

Nowak, G., Luque, R., Parviainen, H., et al. 2020, A&A, 642, A173

Obermeier, C., Henning, T., Schlieder, J. E., et al. 2016, AJ, 152, 223

O'Connor, C. E., Liu, B., & Lai, D. 2021, MNRAS, 501, 507

Offner, S. S. R., Kratter, K. M., Matzner, C. D., Krumholz, M. R., & Klein, R. I. 2010, ApJ, 725, 1485

Önehag, A., Heiter, U., Gustafsson, B., et al. 2012, A&A, 542, A33

Öpik, E. 1924, Publications of the Tartu Astrofizica Observatory, 25, 1

Padoan, P. & Nordlund, Å. 2004, ApJ, 617, 559

Palle, E., Nowak, G., Luque, R., et al. 2019, A&A, 623, A41

Palle, E., Orell-Miquel, J., Brady, M., et al. 2023, arXiv e-prints, arXiv:2301.06873

Parker, R. J., Goodwin, S. P., & Allison, R. J. 2011, MNRAS, 418, 2565

Parker, R. J., Goodwin, S. P., Kroupa, P., & Kouwenhoven, M. B. N. 2009, MNRAS, 397, 1577

Parker, R. J. & Meyer, M. R. 2014, MNRAS, 442, 3722

Parsons, S. G., Gänsicke, B. T., Marsh, T. R., et al. 2018, MNRAS, 481, 1083

Parsons, S. G., Marsh, T. R., Gänsicke, B. T., et al. 2012, MNRAS, 420, 3281

Passegger, V. M., Bello-García, A., Ordieres-Meré, J., et al. 2022, A&A, 658, A194

Passegger, V. M., Reiners, A., Jeffers, S. V., et al. 2018, A&A, 615, A6

Passegger, V. M., Schweitzer, A., Shulyak, D., et al. 2019, A&A, 627, A161

Passegger, V. M., Schweitzer, A., Shulyak, D., et al. 2020, A&A, 634, C2

Passegger, V. M., Wende-von Berg, S., & Reiners, A. 2016, A&A, 587, A19

Paxton, B., Bildsten, L., Dotter, A., et al. 2011, ApJS, 192, 3

Pecaut, M. J. & Mamajek, E. E. 2013, ApJS, 208, 9

Pecaut, M. J., Mamajek, E. E., & Bubar, E. J. 2012, ApJ, 746, 154

Pepe, F. A., Cristiani, S., Rebolo Lopez, R., et al. 2010, in Proc. SPIE, Vol. 7735,

Perez, F. & Granger, B. E. 2007, Computing in Science and Engineering, 9, 21

Perger, M., Ribas, I., Damasso, M., et al. 2017, A&A, 608, A63

Perger, M., Scandariato, G., Ribas, I., et al. 2019, A&A, 624, A123

Perryman, M. A. C., Brown, A. G. A., Lebreton, Y., et al. 1998, A&A, 331, 81

Petrovich, C. 2015, ApJ, 799, 27

Pettersen, B. R., Evans, D. S., & Coleman, L. A. 1984, ApJ, 282, 214

Pietrinferni, A., Cassisi, S., Salaris, M., & Castelli, F. 2004, ApJ, 612, 168

Pinamonti, M., Damasso, M., Marzari, F., et al. 2018, A&A, 617, A104

Pinamonti, M., Sozzetti, A., Giacobbe, P., et al. 2019, A&A, 625, A126

Pirzkal, N., Sahu, K. C., Burgasser, A., et al. 2005, ApJ, 622, 319

Piskunov, A. E. & Mal'Kov, O. I. 1991, A&A, 247, 87

Planck Collaboration, Aghanim, N., Akrami, Y., et al. 2020, A&A, 641, A6

Plavchan, P., Barclay, T., Gagné, J., et al. 2020, Nature, 582, 497

Pollack, J. B., Hubickyj, O., Bodenheimer, P., et al. 1996, Icarus, 124, 62

Popper, D. M. 1980, ARA&A, 18, 115

Pourbaix, D., Arenou, F., Gavras, P., et al. 2022, Gaia DR3 documentation Chapter 7: Non-single stars

Pourbaix, D., Tokovinin, A. A., Batten, A. H., et al. 2004, A&A, 424, 727

Poveda, A. 1988, Ap&SS, 142, 67

Poveda, A. & Allen, C. 2004, in Revista Mexicana de Astronomia y Astrofisica Conference Series, Vol. 21, 49–57

Poveda, A., Allen, C., Costero, R., Echevarría, J., & Hernández-Alcántara, A. 2009, ApJ, 706, 343

Poveda, A., Allen, C., & Parrao, L. 1982, ApJ, 258, 589

Poveda, A., Herrera, M. A., Allen, C., Cordero, G., & Lavalley, C. 1994, Rev. Mexicana Astron. Astrofis., 28, 43

Poveda, A., Ruiz, J., & Allen, C. 1967, Boletin de los Observatorios Tonantzintla y Tacubaya, 4, 86

Preibisch, T., Guenther, E., & Zinnecker, H. 2001, AJ, 121, 1040

Pringle, J. E. 1989, MNRAS, 239, 361

Pyrzas, S., Gänsicke, B. T., Brady, S., et al. 2012, MNRAS, 419, 817

Pyrzas, S., Gänsicke, B. T., Marsh, T. R., et al. 2009, MNRAS, 394, 978

Qiu, D., Tian, H.-J., Wang, X.-D., et al. 2021, ApJS, 253, 58

Quirrenbach, A., Amado, P. J., Caballero, J. A., et al. 2014, CARMENES instrument overview, Vol. 9147

Quirrenbach, A., Amado, P. J., Caballero, J. A., et al. 2016, in , Vol. 9908

Quirrenbach, A., Amado, P. J., Ribas, I., et al. 2018, in , Vol. 10702, 107020W
Quirrenbach, A., Passegger, V. M., Trifonov, T., et al. 2022, A&A, 663, A48
Rabus, M., Lachaume, R., Jordán, A., et al. 2019, MNRAS, 484, 2674
Radica, M., Artigau, É., Lafreniére, D., et al. 2022, MNRAS, 517, 5050
Raghavan, D., McAlister, H. A., Henry, T. J., et al. 2010, ApJS, 190, 1
Raghavan, D., McAlister, H. A., Torres, G., et al. 2009, ApJ, 690, 394
Rajpurohit, A. S., Allard, F., Rajpurohit, S., et al. 2018a, A&A, 620, A180
Rajpurohit, A. S., Allard, F., Teixeira, G. D. C., et al. 2018b, A&A, 610, A19
Rajpurohit, A. S., Reylé, C., Allard, F., et al. 2013, A&A, 556, A15
Ramírez, I. & Meléndez, J. 2005, ApJ, 626, 465
Ramirez, R. M. 2018, Geosciences, 8, 280
Rauer, H., Catala, C., Aerts, C., et al. 2014, Experimental Astronomy, 38, 249
Rebassa-Mansergas, A., Anguiano, B., García-Berro, E., et al. 2016, MNRAS, 463, 1137
Rebull, L. M., Padgett, D. L., McCabe, C. E., et al. 2010, ApJS, 186, 259
Reefe, M. A., Luque, R., Gaidos, E., et al. 2022, AJ, 163, 269
Reggiani, M. M. & Meyer, M. R. 2011, ApJ, 738, 60
Reid, I. N., Burgasser, A. J., Cruz, K. L., Kirkpatrick, J. D., & Gizis, J. E. 2001, AJ, 121, 1710
Reid, I. N., Cruz, K. L., Allen, P., et al. 2004, AJ, 128, 463
Reid, I. N. & Gizis, J. E. 1997, AJ, 113, 2246
Reid, I. N., Gizis, J. E., Cohen, J. G., et al. 1997, PASP, 109, 559
Reid, I. N., Gizis, J. E., & Hawley, S. L. 2002, AJ, 124, 2721
Reid, I. N., Hawley, S. L., & Gizis, J. E. 1995, AJ, 110, 1838
Reiners, A. & Basri, G. 2009, ApJ, 705, 1416
Reiners, A., Joshi, N., & Goldman, B. 2012, AJ, 143, 93
Reiners, A., Ribas, I., Zechmeister, M., et al. 2018a, A&A, 609, L5
Reiners, A., Shulyak, D., Käpylä, P. J., et al. 2022, A&A, 662, A41
Reiners, A., Zechmeister, M., Caballero, J. A., et al. 2018b, A&A, 612, A49
Reipurth, B., Clarke, C. J., Boss, A. P., et al. 2014, in Protostars and Planets VI, 267
Reipurth, B. & Mikkola, S. 2012a, Nature, 492, 221
Reipurth, B. & Mikkola, S. 2012b, Nature, 492, 221
Renedo, I., Althaus, L. G., Miller Bertolami, M. M., et al. 2010, ApJ, 717, 183
Retterer, J. M. & King, I. R. 1982, ApJ, 254, 214
Reylé, C., Jardine, K., Fouqué, P., et al. 2021, A&A, 650, A201
Riaz, B., Gizis, J. E., & Harvin, J. 2006, AJ, 132, 866
Ribas, I. 2003a, A&A, 398, 239
Ribas, I. 2003b, A&A, 400, 297
Ribas, I., Reiners, A., Zechmeister, M., et al. 2023, A&A, 670, A139
Ribas, I., Tuomi, M., Reiners, A., et al. 2018, Nature, 563, 365
Rica, F. M. & Caballero, J. A. 2012, The Observatory, 132, 305
Ricker, G. R., Winn, J. N., Vanderspek, R., et al. 2015, Journal of Astronomical Telescopes, Instruments, and Systems, 1, 014003
Riedel, A. R., Alam, M. K., Rice, E. L., Cruz, K. L., & Henry, T. J. 2017, ApJ, 840, 87
Riedel, A. R., Subasavage, J. P., Finch, C. T., et al. 2010, AJ, 140, 897
Rimoldini, L., Holl, B., Gavras, P., et al. 2022, arXiv e-prints, arXiv:2211.17238
Rivera, E. J., Laughlin, G., Butler, R. P., et al. 2010, ApJ, 719, 890
Rivera, E. J., Lissauer, J. J., Butler, R. P., et al. 2005, ApJ, 634, 625
Rodriguez, D. R., Bessell, M. S., Zuckerman, B., & Kastner, J. H. 2011, ApJ, 727, 62

Rodríguez, R., Schmidt, S. J., Jayasinghe, T., et al. 2018, Research Notes of the American Astronomical Society, 2, 8
Roeser, S., Demleitner, M., & Schilbach, E. 2010, AJ, 139, 2440
Rojas-Ayala, B., Covey, K. R., Muirhead, P. S., & Lloyd, J. P. 2010, ApJ, 720, L113
Rojas-Ayala, B., Covey, K. R., Muirhead, P. S., & Lloyd, J. P. 2012, ApJ, 748, 93
Rojas-Ayala, B., Hilton, E. J., Mann, A. W., et al. 2013, Astronomische Nachrichten, 334, 155
Rosenthal, L. J., Fulton, B. J., Hirsch, L. A., et al. 2021, ApJS, 255, 8
Röser, S., Schilbach, E., Piskunov, A. E., Kharchenko, N. V., & Scholz, R. D. 2011, A&A, 531, A92
Rowe, J. F., Bryson, S. T., Marcy, G. W., et al. 2014, ApJ, 784, 45
Russell, H. N. 1928, The Astrophysical Journal, 67, 83
Russell, H. N., Adams, W. S., & Joy, A. H. 1923, PASP, 35, 189
Rybicki, G. B. & Lightman, A. P. 1979, Radiative processes in astrophysics
Ryu, T., Perna, R., Pakmor, R., et al. 2022, arXiv e-prints, arXiv:2211.02734
Sabotta, S., Schlecker, M., Chaturvedi, P., et al. 2021, A&A, 653, A114
Sadavoy, S. I. & Stahler, S. W. 2017, MNRAS, 469, 3881
Sahlmann, J., Burgasser, A. J., Bardalez Gagliuffi, D. C., et al. 2020, MNRAS, 495, 1136
Sahlmann, J., Lazorenko, P. F., Ségransan, D., et al. 2016, A&A, 595, A77
Sahlmann, J., Ségransan, D., Queloz, D., et al. 2011, A&A, 525, A95
Salz, M., Czesla, S., Schneider, P. C., et al. 2018, A&A, 620, A97
Samus, N. N., Durlevich, O. V., & et al. 2004, VizieR Online Data Catalog, II/250
Samus', N. N., Kazarovets, E. V., Durlevich, O. V., Kireeva, N. N., & Pastukhova, E. N. 2017, Astronomy Reports, 61, 80
Sánchez-López, A., Alonso-Floriano, F. J., López-Puertas, M., et al. 2019, A&A, 630, A53
Sanchís-Ojeda, R., Rappaport, S., Pallè, E., et al. 2015, ApJ, 812, 112
Santos, N. C., Israelian, G., & Mayor, M. 2000, A&A, 363, 228
Santos, N. C., Israelian, G., & Mayor, M. 2001, A&A, 373, 1019
Santos, N. C., Israelian, G., & Mayor, M. 2004, A&A, 415, 1153
Sarkis, P., Henning, T., Kürster, M., et al. 2018, AJ, 155, 257
Scalo, J. M. 1986, Fund. Cosmic Phys., 11, 1
Scelsi, L., Maggio, A., Micela, G., et al. 2007, A&A, 468, 405
Schanche, N., Collier Cameron, A., Almenara, J. M., et al. 2019, MNRAS, 488, 4905
Schlieder, J. E., Crossfield, I. J. M., Petigura, E. A., et al. 2016, ApJ, 818, 87
Schlieder, J. E., Lépine, S., & Simon, M. 2012a, AJ, 143, 80
Schlieder, J. E., Lépine, S., & Simon, M. 2012b, AJ, 144, 109
Schmidt, S. J., Cruz, K. L., Bongiorno, B. J., Liebert, J., & Reid, I. N. 2007, AJ, 133, 2258
Schöfer, P., Jeffers, S. V., Reiners, A., et al. 2019, A&A, 623, A44
Scholz, R. D., Meusinger, H., & Jahreiß, H. 2005, A&A, 442, 211
Schweitzer, A., Passegger, V. M., Cifuentes, C., et al. 2019, A&A, 625, A68
Seager, S. & Deming, D. 2010, ARA&A, 48, 631
Sedaghati, E., Sánchez-López, A., Czesla, S., et al. 2022, A&A, 659, A44
Seifahrt, A., Stürmer, J., Bean, J. L., & Schwab, C. 2018, in , Vol. 10702
Seifert, W., Sánchez Carrasco, M. A., Xu, W., et al. 2012, in , Vol. 8446
Shahar, A., Driscoll, P., Weinberger, A., & Cody, G. 2019, Science, 364, 434
Shan, Y., Reiners, A., Fabbian, D., et al. 2021, A&A, 654, A118
Shan, Y., Yee, J. C., Bowler, B. P., et al. 2017, ApJ, 846, 93
Shara, M. M., Howell, S. B., Furlan, E., et al. 2021, MNRAS, 507, 560
Shatsky, N. & Tokovinin, A. 2002, A&A, 382, 92
Shaya, E. J. & Olling, R. P. 2011, ApJS, 192, 2

Shkolnik, E. L., Allers, K. N., Kraus, A. L., Liu, M. C., & Flagg, L. 2017, AJ, 154, 69
Shkolnik, E. L., Anglada-Escudé, G., Liu, M. C., et al. 2012, ApJ, 758, 56
Shkolnik, E. L., Hebb, L., Liu, M. C., Reid, I. N., & Collier Cameron, A. 2010, ApJ, 716, 1522
Shulyak, D., Reiners, A., Nagel, E., et al. 2019, A&A, 626, A86
Siebert, H. 2005, Journal for the History of Astronomy, 36, 251
Sinukoff, E., Howard, A. W., Petigura, E. A., et al. 2016, ApJ, 827, 78
Skinner, J., Covey, K. R., Bender, C. F., et al. 2018, AJ, 156, 45
Skrutskie, M. F., Cutri, R. M., Stiening, R., et al. 2006, AJ, 131, 1163
Skrzypinski, S. L. 2021, MSc thesis, Universidad Complutense de Madrid, Spain
Smart, R. L., Marocco, F., Caballero, J. A., et al. 2017, MNRAS, 469, 401
Smart, R. L., Marocco, F., Sarro, L. M., et al. 2019, MNRAS, 485, 4423
Smith, G. H. 2018, Ap&SS, 363, 235
Snellen, I., de Kok, R., Birkby, J. L., et al. 2015, A&A, 576, A59
Soderblom, D. R. 2010, ARA&A, 48, 581
Soderblom, D. R. & Clements, S. D. 1987, AJ, 93, 920
Somers, G., Cao, L., & Pinsonneault, M. H. 2020, ApJ, 891, 29
Soto, M. G., Anglada-Escudé, G., Dreizler, S., et al. 2021, A&A, 649, A144
Sousa, S. G., Santos, N. C., Israelian, G., Mayor, M., & Udry, S. 2011, A&A, 533, A141
Sousa, S. G., Santos, N. C., Mayor, M., et al. 2008, A&A, 487, 373
Southworth, J., Mancini, L., Madhusudhan, N., et al. 2017, AJ, 153, 191
Sperauskas, J., Deveikis, V., & Tokovinin, A. 2019, A&A, 626, A31
Standing, M. R., Sairam, L., Martin, D. V., et al. 2023, arXiv e-prints, arXiv:2301.10794
Stassun, K. G., Collins, K. A., & Gaudi, B. S. 2017, AJ, 153, 136
Stauffer, J. R., Balachandran, S. C., Krishnamurthi, A., et al. 1997, ApJ, 475, 604
Stauffer, J. R. & Hartmann, L. W. 1986, ApJS, 61, 531
Stebbins, J. 1914, ApJ, 39, 459
Stefansson, G., Cañas, C., Wisniewski, J., et al. 2020, AJ, 159, 100
Stelzer, B., Marino, A., Micela, G., López-Santiago, J., & Liefke, C. 2013, MNRAS, 431, 2063
Stempels, E. & Telting, J. 2017, FIEStool: Automated data reduction for FIber-fed Echelle Spectrograph (FIES)
Stephenson, C. B. 1986, AJ, 91, 144
Sterzik, M. F., Durisen, R. H., & Zinnecker, H. 2003, A&A, 411, 91
Stock, S., Nagel, E., Kemmer, J., et al. 2020, A&A, 643, A112
Strand, K. A. 1977, AJ, 82, 745
Strassmeier, K. G., Hall, D. S., Fekel, F. C., & Scheck, M. 1993, A catalog of chromospherically active binary stars (2nd ed.).
Strassmeier, K. G. & Rice, J. B. 2003, A&A, 399, 315
Strauss, M. A., Fan, X., Gunn, J. E., et al. 1999, ApJ, 522, L61
Struve, F. G. W. 1837, Stellarum duplicium et multiplicium mensurae micrometricae per magnum Fraunhoferi...
Suárez Mascareño, A., González-Álvarez, E., Zapatero Osorio, M. R., et al. 2023, A&A, 670, A5
Suárez Mascareño, A., González Hernández, J. I., Rebolo, R., et al. 2017a, A&A, 597, A108
Suárez Mascareño, A., González Hernández, J. I., Rebolo, R., et al. 2017b, A&A, 605, A92
Suárez Mascareño, A., González Hernández, J. I., Rebolo, R., et al. 2017c, A&A, 605, A92
Sun, M., Jiang, B. W., Zhao, H., et al. 2018, ApJ, 861, 153
Susemiehl, N. & Meyer, M. R. 2022, A&A, 657, A48
Tabernero, H. M., Marfil, E., Montes, D., & González Hernández, J. I. 2019, A&A, 628, A131
Tabernero, H. M., Marfil, E., Montes, D., & González Hernández, J. I. 2022a, A&A, 657, A66
Tabernero, H. M., Montes, D., & González Hernández, J. I. 2012, A&A, 547, A13

Tabernero, H. M., Montes, D., González Hernández, J. I., & Ammler-von Eiff, M. 2017, A&A, 597, A33
Tabernero, H. M., Zapatero Osorio, M. R., Allende Prieto, C., et al. 2022b, MNRAS, 515, 1247
Tal-Or, L., Zechmeister, M., Reiners, A., et al. 2018, A&A, 614, A122
Tal-Or, L., Zucker, S., Ribas, I., Anglada-Escudé, G., & Reiners, A. 2019, A&A, 623, A10
Tarter, J. C., Backus, P. R., Mancinelli, R. L., et al. 2007, Astrobiology, 7, 30
Taylor, M. B. 2005, in Astronomical Data Analysis Software and Systems XIV, Vol. 347, 29
Terrien, R. C., Mahadevan, S., Bender, C. F., et al. 2012, ApJ, 747, L38
Terrien, R. C., Mahadevan, S., Bender, C. F., Deshpande, R., & Robertson, P. 2015, ApJ, 802, L10
Tobin, J. J., Kratter, K. M., Persson, M. V., et al. 2016, Nature, 538, 483
Tokadjian, A. & Piro, A. L. 2020, AJ, 160, 194
Tokovinin, A. 2008, MNRAS, 389, 925
Tokovinin, A. 2014, AJ, 147, 87
Tokovinin, A. 2017, MNRAS, 468, 3461
Tokovinin, A. 2018, ApJS, 235, 6
Tokovinin, A. 2022, AJ, 163, 127
Tokovinin, A., Mason, B. D., & Hartkopf, W. I. 2010, AJ, 139, 743
Tokovinin, A. & Moe, M. 2020, MNRAS, 491, 5158
Tokovinin, A., Thomas, S., Sterzik, M., & Udry, S. 2006, A&A, 450, 681
Tokovinin, A. A. 1997, A&AS, 121, 71
Toledo-Padrón, B., Suárez Mascareño, A., González Hernández, J. I., et al. 2021, A&A, 648, A20
Tomkin, J. & Pettersen, B. R. 1986, AJ, 92, 1424
Tonry, J. & Davis, M. 1979, AJ, 84, 1511
Tonry, J. L., Stubbs, C. W., Lykke, K. R., et al. 2012, ApJ, 750, 99
Toonen, S., Hollands, M., Gänsicke, B. T., & Boekholt, T. 2017, A&A, 602, A16
Torres, G., Andersen, J., & Giménez, A. 2010, A&A Rev., 18, 67
Torres, G., Claret, A., Pavlovski, K., & Dotter, A. 2015, ApJ, 807, 26
Torres, G., Schaefer, G. H., Monnier, J. D., et al. 2022, ApJ, 941, 8
Trifonov, T., Brahm, R., Jordan, A., et al. 2023, arXiv e-prints, arXiv:2302.05694
Trifonov, T., Caballero, J. A., Morales, J. C., et al. 2021, Science, 371, 1038
Trifonov, T., Kürster, M., Zechmeister, M., et al. 2018, A&A, 609, A117
Tsujimoto, M., Morihana, K., Hayashi, T., & Kitaguchi, T. 2018, Publications of the Astronomical Society of Japan, 70, 109
Tsvetanov, Z. I., Golimowski, D. A., Zheng, W., et al. 2000, ApJ, 531, L61
Tuomi, M., Jones, H. R. A., Barnes, J. R., Anglada-Escudé, G., & Jenkins, J. S. 2014, MNRAS, 441, 1545
Tuomi, M., Jones, H. R. A., Butler, R. P., et al. 2019, arXiv e-prints, arXiv:1906.04644
Tyler, R. H., Henning, W. G., & Hamilton, C. W. 2015, ApJS, 218, 22
Udry, S. & Santos, N. C. 2007, ARA&A, 45, 397
Valenti, J. A., Piskunov, N., & Johns-Krull, C. M. 1998, ApJ, 498, 851
van Albada, T. S. 1968, Bull. Astron. Inst. Netherlands, 20, 57
van Altena, W. F. 1966, AJ, 71, 482
van Altena, W. F., Lee, J. T., & Hoffleit, E. D. 1995, The general catalogue of trigonometric [stellar] parallaxes
van Leeuwen, F. 2007, A&A, 474, 653
van Maanen, A. 1917, PASP, 29, 258
van Rhijn, P. J. & Raimond, J. J. 1934, MNRAS, 94, 508
Vance, S. D., Panning, M. P., Stähler, S., et al. 2018, Journal of Geophysical Research (Planets), 123, 180
Vanderburg, A., Rappaport, S. A., Xu, S., et al. 2020, Nature, 585, 363
Vanderspek, R., Huang, C. X., Vanderburg, A., et al. 2019, ApJ, 871, L24

Veeder, G. J. 1974, AJ, 79, 1056
Vinter Hansen, J. M., Neubauer, F. J., & Roosen-Raad, D. 1940, Lick Observatory Bulletin, 502, 89
Virtanen, P., Gommers, R., Oliphant, T. E., et al. 2020, Nature Methods, 17, 261
Vogt, S. S., Allen, S. L., Bigelow, B. C., et al. 1994, in , Vol. 2198, 362
Vogt, S. S., Butler, R. P., Marcy, G. W., et al. 2005, ApJ, 632, 638
von Boetticher, A., Triaud, A. H. M. J., Queloz, D., et al. 2019, A&A, 625, A150
von Braun, K., Boyajian, T. S., van Belle, G. T., et al. 2014a, MNRAS, 438, 2413
von Braun, K., Boyajian, T. S., van Belle, G. T., et al. 2014b, MNRAS, 438, 2413
Voûte, J. 1917, MNRAS, 77, 650
Vrba, F. J., Henden, A. A., Luginbuhl, C. B., et al. 2004, AJ, 127, 2948
Vrijmoet, E. H., Henry, T. J., Jao, W.-C., & Dieterich, S. B. 2020, AJ, 160, 215
Wang, J., Fischer, D. A., Xie, J.-W., & Ciardi, D. R. 2014a, ApJ, 791, 111
Wang, J., Xie, J.-W., Barclay, T., & Fischer, D. A. 2014b, ApJ, 783, 4
Ward-Duong, K., Patience, J., De Rosa, R. J., et al. 2015, MNRAS, 449, 2618
Ward-Thompson, D., André, P., Crutcher, R., et al. 2007, in Protostars and Planets V, ed. B. Reipurth, D. Jewitt, & K. Keil, 33
Weinberg, M. D., Shapiro, S. L., & Wasserman, I. 1987, ApJ, 312, 367
Weinberger, A. J., Boss, A. P., Keiser, S. A., et al. 2016, AJ, 152, 24
Weis, E. W., Deluca, E. E., & Upgren, A. R. 1979, PASP, 91, 766
Wells, R., Poppenhaeger, K., & Watson, C. A. 2018, MNRAS, 473, L131
Wes McKinney. 2010, in Proceedings of the 9th Python in Science Conference, 56 – 61
West, A. A., Bochanski, J. J., Hawley, S. L., et al. 2006, AJ, 132, 2507
West, A. A., Hawley, S. L., Bochanski, J. J., et al. 2008, AJ, 135, 785
West, A. A., Hawley, S. L., Walkowicz, L. M., et al. 2004, AJ, 128, 426
West, A. A., Walkowicz, L. M., & Hawley, S. L. 2005, PASP, 117, 706
White, R. J. & Ghez, A. M. 2001, ApJ, 556, 265
Williams, K. A. 2004, ApJ, 601, 1067
Wilson, E. B. 1927, Journal of the American Statistical Association, 22, 209
Winn, J. N. & Fabrycky, D. C. 2015, ARA&A, 53, 409
Winters, J. G., Cloutier, R., Medina, A. A., et al. 2022, AJ, 163, 168
Winters, J. G., Henry, T. J., Jao, W.-C., et al. 2019a, AJ, 157, 216
Winters, J. G., Medina, A. A., Irwin, J. M., et al. 2019b, AJ, 158, 152
Wittenmyer, R. A., Tuomi, M., Butler, R. P., et al. 2014, ApJ, 791, 114
Wolszczan, A. 1994, Science, 264, 538
Wolszczan, A. & Frail, D. A. 1992, Nature, 355, 145
Woolf, V. M. & Wallerstein, G. 2005, MNRAS, 356, 963
Woolf, V. M. & Wallerstein, G. 2006, PASP, 118, 218
Woolf, V. M. & West, A. A. 2012, MNRAS, 422, 1489
Worley, C. E. 1962, AJ, 67, 396
Worley, C. E. & Douglass, G. G. 1997, A&AS, 125, 523
Wright, D. J., Wittenmyer, R. A., Tinney, C. G., Bentley, J. S., & Zhao, J. 2016, ApJ, 817, L20
Wu, Y. & Murray, N. 2003, ApJ, 589, 605
Wunderlich, F., Godolt, M., Grenfell, J. L., et al. 2019, A&A, 624, A49
Yakut, K. & Eggleton, P. P. 2005, ApJ, 629, 1055
Yan, F., Reiners, A., Pallé, E., et al. 2022, A&A, 659, A7
Yee, S. W., Petigura, E. A., & von Braun, K. 2017, ApJ, 836, 77
Yoo, J., Chanamé, J., & Gould, A. 2004, ApJ, 601, 311

Zacharias, N., Finch, C. T., Girard, T. M., et al. 2012, VizieR Online Data Catalog, 1322

Zagaria, F., Clarke, C. J., Rosotti, G. P., & Manara, C. F. 2022, MNRAS, 512, 3538

Zakhozhaj, V. A. 1979, Vestnik Khar'kovskogo Universiteta, 190, 52

Zapatero Osorio, M. R., Lane, B. F., Pavlenko, Y., et al. 2004, ApJ, 615, 958

Zechmeister, M., Dreizler, S., Ribas, I., et al. 2019, A&A, 627, A49

Zechmeister, M., Kürster, M., & Endl, M. 2009, A&A, 505, 859

Zeng, L., Jacobsen, S. B., Sasselov, D. D., et al. 2019, Proceedings of the National Academy of Science, 116, 9723

Zhang, Z. H., Pokorny, R. S., Jones, H. R. A., et al. 2009, A&A, 497, 619

Zheng, Z., Flynn, C., Gould, A., Bahcall, J. N., & Salim, S. 2001, ApJ, 555, 393

Zhuang, Q., Gao, X., & Yu, Q. 2012, ApJ, 758, 111

Ziegler, C., Law, N. M., Baranec, C., et al. 2018, AJ, 156, 259

Zuckerman, B., Koester, D., Melis, C., Hansen, B. M., & Jura, M. 2007, ApJ, 671, 872

Zuckerman, B. & Song, I. 2004, ARA&A, 42, 685

Acknowledgements

I sincerely thank Prof. Adam J. Burgasser and Prof. Andrei A. Tokovinin for generously reading this work and for taking the time to provide an extremely valuable refereeing. I am grateful to Prof. E. E. Mamajek, Prof. E. Gaidos, and Dr. C. Reylé for their useful insights and suggestions at some point during the course of this thesis. F. J. Abellán de Paco, M. Cortés-Contreras, R. Dorda, G. Holgado, and I, among many others, have compiled data for Carmencita during MSc and PhD theses at the Universidad Complutense de Madrid.

This document was typeset using Leslie Lamport's LaTeX, based on Donald E. Knuth's TeX. Javier González Payo kindly provided me with the basis of this template. Robert Slimbach's Minion Pro serves as both the text and display typeface. Erik Spiekermann and Ralph du Carrois' `Fira Sans` is the monospaced font of choice.

This publication made use of `VOSA` and the Filter Profile Service, developed and maintained by the Spanish Virtual Observatory through grant AYA2017-84089, the SIMBAD database, the `Aladin` sky atlas, the VizieR catalogue access tool developed at Centre de Données astronomiques de Strasbourg (CDS) in Strasbourg Observatory, France, the Tool for OPerations on Catalogues And Tables (`TOPCAT`), and the NASA Exoplanet Archive, which is operated by the California Institute of Technology, under contract with the National Aeronautics and Space Administration under the Exoplanet Exploration Program.

Some of the material and figures included in this document have been already published in Astronomy and Astrophysics (A&A), Monthly Notices of the Royal Astronomical Society (MNRAS), and Research Notes of the American Astronomical Society (RNAAS). For scientific graphics not produced specifically for this work, due credit is given. Additional images are used under the Creative Commons[1] conditions in each particular case. No credit is mentioned for creations of my own.

All the code produced in this thesis has been written in Guido van Rossum's `Python` language. It is publicly available in my personal GitHub[2].

This thesis was mostly financed by the Spanish Ministry of Science and Innovation through grants AYA2016-79425-C3-1/2/3-P and BES-2017-080769.

CARMENES is an instrument for the Centro Astronómico Hispano-Alemán de Calar Alto (CAHA, Almería, Spain). CARMENES is funded by the German Max-Planck-Gesellschaft (MPG), the Spanish Consejo Superior de Investigaciones Científicas (CSIC), the European Union through FEDER/ERF

[1] https://creativecommons.org.
[2] https://github.com/ccifuentesr.

FICTS-2011-02 funds, and the members of the CARMENES Consortium (Max-Planck-Institut für Astronomie, Instituto de Astrofísica de Andalucía, Landessternwarte Königstuhl, Institut de Ciències de l'Espai, Insitut für Astrophysik Göttingen, Universidad Complutense de Madrid, Thüringer Landessternwarte Tautenburg, Instituto de Astrofísica de Canarias, Hamburger Sternwarte, Centro de Astrobiología and Centro Astronómico Hispano-Alemán), with additional contributions by the Spanish Ministry of Economy, the German Science Foundation through the Major Research Instrumentation Programme and DFG Research Unit FOR2544 "Blue Planets around Red Stars", the Klaus Tschira Stiftung, the states of Baden-Württemberg and Niedersachsen, and by the Junta de Andalucía.

Conventions

- The terms 'M dwarf' and 'red dwarf' are used interchangeably.
- The calligraphic $\mathcal{M}$ is used for mass, in order to be easily differentiated from other instances, such as 'M dwarf', or 'M_G'. For homogeneity, radius and luminosity are denoted as $\mathcal{R}$ and $\mathcal{L}$, respectively.
- The abbreviation 'a' is used for *year*, instead of 'yr'[3].
- Software names and parameters from electronic catalogues are shown in `monospaced` font.
- Sloan's passbands $u'g'r'i'z'$ may be simplified as *ugriz*[4].
- For simplicity purposes and to design table layouts with a better readability, some star catalog names are abbreviated (only in the tabular content): 2M for 2MASS J, G2- and G3- for *Gaia* DR2 and E/DR3, 1R for 1RXS J.
- In tabulated form, names of variable stars (e.g. 'EZ Psc', 'AD Leo') usually appear as single words (i.e. 'EZPsc', 'ADLeo').
- I predominantly use the plural pronoun 'we' instead of the singular 'I', except on a few occasions. I do this to acknowledge the collective effort of many who have worked before, and alongside me.

[3] The recognised symbol for a year is the letter 'a', rather than 'yr', which is often used in papers in English. The term 'year' should be referred to the Julian year of 365.25 days (31.5576 Ms) unless otherwise specified. See the IAU Style Manual (IAU Commission 5, IAU Transactions XXB, 1989, https://www.iau.org/publications/proceedings_rules/units/), or the NIST SP811 Special Publication 811 (https://www.nist.gov/pml/special-publication-811), and also see http://exoterrae.eu/annus.html.

[4] The *griz* photometric system (aka 'Gunn', 'Thuan-Gunn', or 'Oke-Gunn' photometric system) was developed in the decades of 1970 and 1980 to be used with electronic sensors. The *ugriz* photometric system used by SDSS is a follow-on but the passbands are not identical. The apostrophes are used to distinguish both, but are often skipped.

Appendix A

List of publications

A.1 Peer-reviewed publications

Articles in this thesis are marked with a red star (★).

2023

35. **"GJ 806 (TOI-4481): A bright nearby multi-planetary system with a transiting hot, low-density super-Earth"**
E. Pallé E., J. Orell-Miquel, M. Brady, J. Bean, A. P. Hatzes, et al. (incl. **C. Cifuentes**)
Astronomy & Astrophysics, accepted. arXiv: 2301.06873.

34. **"Searching for the nature of stars with debris disks and planets"**
R. de la Reza, C. Chavero, S. Roca-Fábrega, F. Llorente de Andrés, P. Cruz, and **C. Cifuentes**
Astronomy & Astrophysics, 671, A136. March 2023.

33. **"The CARMENES search for exoplanets around M dwarfs. A long-period planet around GJ 1151 measured with CARMENES and HARPS-N data"**
J. Blanco-Pozo, M. Perger, M. Damasso, G. Anglada Escudé, I. Ribas, D. Baroch, J. A. Caballero, **C.Cifuentes**, et al.
Astronomy & Astrophysics, 671, A50. March 2023.

32. **"The CARMENES search for exoplanets around M dwarfs. Guaranteed Time Observations Data Release 1 (2016-2020)"**
I. Ribas, A. Reiners, M. Zechmeister, J. A. Caballero, et al. (incl. **C. Cifuentes**)
Astronomy & Astrophysics, 670, A139. February 2023.

31. **"The CARMENES search for exoplanets around M dwarfs, Wolf 1069 b: Earth-mass planet in the habitable zone of a nearby, very low-mass star"**
D. Kossakowski, M. Kürster, T. Trifonov, T. Henning, J. Kemmer, et al. (incl. **C. Cifuentes**)
Astronomy & Astrophysics, 670, A84. February 2023.

2022

30. **"A quarter century of spectroscopic monitoring of the nearby M dwarf Gl 514. A super-Earth on an eccentric orbit moving in and out of the habitable zone"**
M. Damasso, M. Perger, J. M. Almenara, D. Nardiello, et al. (incl. **C. Cifuentes**)
Astronomy & Astrophysics, 666, A187. October 2022.

29. **"TOI-1468: A system of two transiting planets, a super-Earth and a mini-Neptune, on opposite sides of the radius valley"**
P. Chaturvedi, P. bluhm, E. Nagel, A. P. Hatzes, et al. (incl. **C. Cifuentes**)
Astronomy & Astrophysics, 666, A155. October 2022.

28. **"Precise mass determination for the keystone sub-Neptune planet transiting the mid-type M dwarf G 9-40"**
R. Luque, G. Nowak, T. Hirano, D. Kossakowski, et al. (incl. **C. Cifuentes**)
Astronomy & Astrophysics, 666, A154, October 2022.

27. **"The CARMENES search for exoplanets around M dwarfs. Stable radial-velocity variations at the rotation period of AD Leonis: A test case study of current limitations to treating stellar activity"**
D. Kossakowski, M. Küster, Th. Henning, T. Trifonov, et al. (incl. **C. Cifuentes**)
Astronomy & Astrophysics, 666, A143, October 2022.

26. **"A detailed analysis of the Gl 486 planetary system"**
J. A. Caballero, E. González-Alvarez, M. Brady, T. Trifonov, T. G. Ellis, C. Dorn, **C. Cifuentes**, et al.
Astronomy & Astrophysics, 665, A120, September 2022.

25. **"The CARMENES search for exoplanets around M dwarfs: Benchmarking the impact of activity in high-precision radial velocity measurements"**
S. V. Jeffers, J. R. Barnes, P. Schöfer, A. Quirrenbach, et al. (incl. **C. Cifuentes**)
Astronomy & Astrophysics, 663, A27, July 2022.

24. **"Discovery and mass measurement of the hot, transiting, Earth-sized planet, GJ 3929 b"**
J. Kemmer, S. Dreizler, D. Kossakowski, S. Stock, et al. (incl. **C. Cifuentes**)
Astronomy & Astrophysics, 659, A17, March 2022.

23. **"A Transiting, Temperate Mini-Neptune Orbiting the M Dwarf TOI-1759 Unveiled by TESS"**
N. Espinoza, E. Pallé, J. Kemmer, R. Luque, J. A. Caballero, **C. Cifuentes**, et al.
The Astronomical Journal, 163, 133, March 2022.

2021

22. **"The CARMENES search for exoplanets around M dwarfs. Stellar atmospheric parameters of target stars with SteParSyn"**
E. Marfil, H. M. Tabernero, D. Montes, J. A. Caballero, et al. (incl. **C. Cifuentes**)
Astronomy & Astrophysics, 656, A162. December 2021.

21. **"TOI-1201 b: A mini-Neptune transiting a bright and moderately young M dwarf"**
D. Kossakowski, J. Kemmer, P. Bluhm, S. Stock, J. A. Caballero, et al. (incl. **C. Cifuentes**)
Astronomy & Astrophysics, 656, A124. December 2021.

20. **"The bi-modal ^{7}Li distribution of the Milky Way's thin-disk dwarf stars. The role of Galactic-scale events and stellar evolution"**
S. Roca-Fábrega, F. Llorente de Andrés, C. Chavero, **C. Cifuentes**, and R. de la Reza
Astronomy & Astrophysics, 656, A24. December 2021.

19. **"The evolution of lithium in FGK dwarf stars: The Li rotation connection and the Li desert"**
F. Llorente de Andrés, C. Chavero, R. de la Reza, S. Roca-Fábrega, **C. Cifuentes**
Astronomy & Astrophysics, 654, A137. October 2021.

18. **"CARMENES input catalog of M dwarfs VI. A time-resolved Ca II H&K catalog from archival data"**
V. Perdelwitz, M. Mittag, L. Tal-Or, J. H. M. M. Schmitt, et al. (incl. **C. Cifuentes**)
Astronomy & Astrophysics, 652, A116. August 2021.

17. **"The CARMENES search for exoplanets around M dwarfs. Two terrestrial planets orbiting G 264-012 and one terrestrial planet orbiting Gl 393"**
P. J. Amado, F. F. Bauer, C. Rodríguez López, E. Rodríguez, et al. (incl. **C. Cifuentes**)
Astronomy & Astrophysics, 650, A188. June 2021.

16. **"A nearby transiting rocky exoplanet that is suitable for atmospheric investigation"**
T. Trifonov, J. A. Caballero, J. C. Morales, A. Seifahrt, I. Ribas, et al. (incl. **C. Cifuentes**)
Science, 371, 6533, 1038-1041. March 2021.

2020

15. **"The CARMENES search for exoplanets around M dwarfs – LP 714-47b (TOI 442.01): Populating the Neptune desert"**
S. Dreizler, M. Crossfield, D. Kossakowski, P. Plavchan, S. Jeffers, et al. (incl. **C. Cifuentes**)
Astronomy & Astrophysics, 644, A127. December 2020.

14. **"Discovery of a hot, transiting, Earth-sized planet and a second temperate, non-transiting planet around the M4 dwarf GJ 3473 (TOI-488)"**
J. Kemmer, S. Stock, D. Kossakowski, A. Kaminski, et al. (incl. **C. Cifuentes**)
Astronomy & Astrophysics, 642, A236. October 2020.

13. **"The CARMENES search for exoplanets around M dwarfs. Two planets on opposite sides of the radius gap transiting the nearby M dwarf LTT 3780"**
G. Nowak, R. Luque, H. Parviainen, E. Pallé, K. Molaverdikhani, et al. (incl. **C. Cifuentes**)
Astronomy & Astrophysics, 642, A173. October 2020.

12. (★) **"The CARMENES input catalogue of M dwarfs. V. Luminosities, colours, and spectral energy distributions"**
C. Cifuentes, J. A. Caballero, M. Cortés-Contreras, D. Montes, et al.
Astronomy & Astrophysics, 642, A115. October 2020.

11. **"The CARMENES search for exoplanets around M dwarfs. Convective shift and starspot constraints from chromatic radial velocities"**
D. Baroch, J. C. Morales, I. Ribas, E. Herrero, A. Rosich, et al. (incl. **C. Cifuentes**)
Astronomy & Astrophysics 641, A69. September 2020.

10. **"Precise mass and radius of a transiting super-Earth planet orbiting the M dwarf TOI-1235: a planet in the radius gap?"**

P. Bluhm, R. Luque, N. Espinoza, E. Pallé, J. A. Caballero, et al (incl. **C. Cifuentes**).
Astronomy & Astrophysics 639, A132. July 2020.

9. **"A He I upper atmosphere around the warm Neptune in GJ 3470 b"**
E. Pallé, S. Nortmann, N. Casasayas-Barris, M. Lampón, et al. (incl. **C. Cifuentes**)
Astronomy & Astrophysics 638, A61. June 2020.

2019

8. **"Exomoons in the habitable zones of M dwarfs"**
H. Martínez-Rodríguez, J. A. Caballero, **C. Cifuentes**, A. L. Piro, and R. Barnes.
The Astrophysical Journal, 887, 2, 261. December 2019.

7. **"A giant exoplanet around a very low mass star challenging formation models"**
J. C. Morales, A. J. Mustill, I. Ribas, M. B. Davies, A. Reiners, et al. (incl. **C. Cifuentes**)
Science, 365, 6460, 1441-1445. September 2019.

6. **"The CARMENES search for exoplanets around M dwarfs. Two temperate Earth-mass planet candidates around Teegarden's star"**
M. Zechmeister, S. Dreizler, I. Ribas, A. Reiners, J. A. Caballero, et al. (incl. **C. Cifuentes**)
Astronomy & Astrophysics. 627, A49. July 2019.

5. **"The CARMENES search for exoplanets around M dwarfs. Radii and masses of the target stars"**
A. Schweitzer, V. M. Passeger, **C. Cifuentes**, V. J. S. Béjar, M. Cortés-Contreras, et al.
Astronomy & Astrophysics 625, A68. May 2019.

2018

4. **"The CARMENES search for exoplanets around M dwarfs. A Neptune-mass planet traversing the habitable zone around HD 180617"**
A. Kaminski, T. Trifonov, J. A. Caballero, A. Quirrenbach, I. Ribas, et al. (incl. **C. Cifuentes**)
Astronomy & Astrophysics, 618, A115. October 2018.

3. **"The CARMENES search for exoplanets around M dwarfs. High-resolution optical and near-infrared spectroscopy of 324 survey stars"**
A. Reiners, M. Zechmeister, J. A. Caballero, I. Ribas, J. C. Morales, et al. (incl. **C. Cifuentes**)
Astronomy & Astrophysics, 612, A49. April 2018.

2. **"The CARMENES search for exoplanets around M dwarfs. First visual-channel radial-velocity measurements and orbital parameter updates of seven M-dwarf planetary systems"**
T. Trifonov, M. Kürster, M. Zechmeister, L. Tal-Or, J. A. Caballero, et al. (incl. **C. Cifuentes**)
Astronomy & Astrophysics, 609, A117. February 2018.

1. **"The CARMENES search for exoplanets around M dwarfs. HD 147379 b: A nearby Neptune in an early-M dwarf's temperate zone"**
A. Reiners, I. Ribas, M. Zechmeister, J. A. Caballero, et al. (incl. **C. Cifuentes**)
Astronomy & Astrophysics, 609, A49. January 2018.
Selected as an A&A Highlighted paper of the week.

A.2 Non-refereed publications

2021

2. (⋆) "One Is the Loneliest Number: Multiplicity in Cool Dwarfs"
C. Cifuentes, J. A. Caballero, and S. Agustí .
Research Notes of the AAS, Vol. 5, Number 5. June 2021.

2018

1. "Cool dwarfs in wide multiple systems: A curious quintuple system of a compact sun-like triple and a close M dwarf-white dwarf pair at a wide separation"
R. González-Peinado, J. A. Caballero, D. Montes, and **C. Cifuentes**.
The Observatory, Vol. 138, p. 292-298. December 2018.

A.3 Conference proceedings

2021

9. "Luminosities of cool stars"
C. Cifuentes, J. A. Caballero, M. Cortés-Contreras, D. Montes, and the Carmenes Consortium.
The Star-Planet Connection, On-line Workshop, October 25 – 28, 2021.

8. "CARMENES and the Frontiers of High-Resolution Spectroscopy for M dwarfs"
Y. Shan, A. Reiners, P. J. Amado, V. J. S. Béjar, J. A. Caballero, **C. Cifuentes**, and the Carmenes Consortium. *Plato Online Mission Conference 2021*, October, 2021.

7. "Stellar atmospheric parameters of CARMENES GTO M dwarfs with spectral synthesis and SteParSyn"
E. Marfil, H. M. Tabernero, D. Montes, J. A. Caballero, F. J. Lázaro-Barrasa, et al. (incl. **C. Cifuentes**)
The 20.5th Cambridge Workshop on Cool Stars, Stellar Systems, and the Sun (CS20.5). Virtually anywhere. March 2 – 4, 2021.

2020

6. "The CARMENES M-dwarf planet survey"
A. Quirrenbach, and the CARMENES Consortium (incl. **C. Cifuentes**).
Proceedings of the SPIE, Vol. 11447, id. 114473C. Ground-based and Airborne Instrumentation for Astronomy. SPIE Astronomical Telescopes + Instrumentation 2020 Digital Forum. Online. December 14 – 18, 2020.

5. "Colours and luminosities of M dwarfs in the CARMENES input catalogue"
C. Cifuentes, J. A. Caballero, M. Cortés-Contreras, D. Montes, F. J. Abellán, et al.
Contributions to the XIV.0 Scientific Meeting (virtual) of the Spanish Astronomical Society. Online. July 13 – 15 2020.

4. "Kinematics of M dwarfs in the CARMENES input catalogue"
M. Cortés-Contreras, A. J. Domínguez-Fernández, J. A. Caballero, D. Montes, C. Cardona, V. J. S. Béjar, **C. Cifuentes**, et al.

Contributions to the XIV.0 Scientific Meeting (virtual) of the Spanish Astronomical Society. Online. July 13 – 15 2020.

3. **"The bimodal A(Li) distribution of Milky Way's thin disk stars and the Galactic scale events"**
S. Roca-Fábrega, F. Llorente de Andrés, **C. Cifuentes**, C. Chavero, R. de la Reza and B. Montesinos.
Contributions to the XIV.0 Scientific Meeting (virtual) of the Spanish Astronomical Society. Online. July 13 – 15 2020.

2018

2. **"Spectral energy distributions and luminosities of M dwarfs in the CARMENES search for exoplanets"**
C. Cifuentes, J. A. Caballero, M. Cortés-Contreras, D. Montes, A. Schweitzer, I. Ribas, P. J. Amado, and the CARMENES Consortium.
Proceedings of the XIII Scientific Meeting of the Spanish Astronomical Society. Highlights on Spanish Astrophysics X Salamanca, Spain. 16 – 20 July, 2018.

1. **"CARMENES: high-resolution spectra and precise radial velocities in the red and infrared"**
A. Quirrenbach, P. J. Amado, I. Ribas, A. Reiners, J. A. Caballero, et al. (incl. **C. Cifuentes**)
Proceedings of the SPIE, Vol. 10702, id. 107020W. SPIE Astronomical Telescopes + Instrumentation. Austin, Texas, USA. 10 – 15 June, 2018.

A.4 Circulars

1. **"MPEC 2020-A99: 2020 AV2"**
P. Bacci, M. Maestripieri, M. Facchini, M. D. Grazia, L. Tesi, et al. (incl. **C. Cifuentes**).
Minor Planet Electronic Circulars, No. 2020-A99. January 2020.

A.5 VizieR online data catalogues

24. **CARMENES search for exoplanets around M dwarfs** (Ribas+, 2023)
23. **GJ 1151 CARMENES and HARPS-N data** (Blanco-Pozo+, 2023)
22. **Wolf 1069 RV and stellar activity indices** (Kossakowski+, 2023)
21. **Gl514 RVs and Activity diagnostics** (Damasso+, 2022)
20. **TOI-1468 photometry and radial velocities** (Chaturvedi+, 2022)
19. **AD Leo RV and stellar activity indices** (Kossakowski+, 2022)
18. **GJ 3929 b RVs and activity indicators** (Kemmer+, 2022)
17. **VRI photometry and radial velocity of TOI-1759** (Espinoza+, 2022)
16. **CARMENES stellar atmospheric parameters** (Marfil+, 2021)
15. **TOI-1201 RV and activity index** (Kossakowski+, 2021)
14. **Evolution of Li in FGK dwarf stars** (Llorente de Andrés+, 2021)

13. **CARMENES time-resolved CaII H&K catalog** (Perdelwitz+, 2021)
12. **G 264-012 and Gl 393 radial velocity curves** (Amado+, 2021)
11. **LP714-47 (TOI 442) radial velocity curve** (Dreizler+, 2020)
10. **GJ 3473 (TOI-488) radial velocity curve** (Kemmer+, 2020)
9. **CARMENES input catalogue of M dwarfs. V** (**Cifuentes**+, 2020)
8. **Compilation of planets around M dwarfs** (Martínez-Rodríguez+, 2019)
7. **GJ 3512 radial velocity and light curves** (Morales+, 2019)
6. **Teegarden's Star RV and Hα curves** (Zechmeister+, 2019)
5. **Radii and masses of the CARMENES targets** (Schweitzer+, 2019)
4. **A Neptune-mass planet traversing the habitable zone around HD 180617** (Kaminski+, 2018)
3. **324 CARMENES M dwarfs velocities** (Reiners+, 2018)
2. **CARMENES radial velocity curves of 7 M-dwarf** (Trifonov+, 2018)
1. **HD147379 b velocity curve** (Reiners+, 2018)

Appendix B

Long tables of Chapter 2

B.1 Carmencita, the CARMENES input catalogue[1]

[1] This table displays eight columns of carmencita, which actually includes 177 columns, as described in Chapter 2.

Table B.1: Carmencita, the CARMENES input catalogue.

Karmn	Name	α (2016.0)	δ (2016.0)	Spectral type	J [mag]	Multiplicity[a]	DR1[b]
J00012+139N	BD+13 5195A	00:01:13.21	+13:58:32.7	M0.5 V	7.798	Triple	
J00012+139S	BD+13 5195B	00:01:12.89	+13:58:22.0	M0.0 V	8.359	Triple	
J00026+383	PM J00026+3821A	00:02:40.00	+38:21:44.1	M4.0 V	9.707	Binary*	
J00033+046	StKM 1-2199	00:03:18.97	+04:41:11.6	M1.5 V	8.833		
J00056+458	HD 38B	00:05:42.30	+45:48:35.0	M0.0 V	6.142	Quadruple	•
J00051+457	GJ 2	00:05:12.22	+45:47:09.2	M1.0 V	6.704	Quadruple	
J00067-075	GJ 1002	00:06:42.32	-07:32:47.3	M5.5 V	8.323		•
J00077+603	G 217-32A	00:07:43.28	+60:22:54.0	M4.0 V	8.911	Binary	
J00078+676	PM J00078+6736	00:07:50.65	+67:36:23.9	M2.0 V	8.355		
J00079+080	GJ 3007	00:07:58.74	+08:00:12.8	M4.0 V	9.392		
J00081+479	1R000806.3+475659	00:08:06.23	+47:57:02.4	M4.0 V	8.523	Binary (SB2)	
J00084+174	GJ 3008	00:08:27.18	+17:25:26.4	M0.0 V	7.807		
J00088+208	GJ 3010	00:08:53.86	+20:50:21.4	M5.0 V	8.870	Binary	
J00110+052	G 31-29	00:11:04.89	+05:12:33.4	M1.0 V	8.530		
J00115+591	LSPM J0011+5908	00:11:29.94	+59:08:21.2	M6.0 V	9.945		•
J00118+229	LP 348-40	00:11:53.17	+22:59:01.2	M3.5 V	8.862		
J00119+330	G 130-53	00:11:55.73	+33:03:10.7	M3.5 V	9.066		
J00122+304	1R001213.6+302906	00:12:13.49	+30:28:43.8	M4.5 V	10.242		
J00131+703	TYC 4298-613-1	00:13:11.68	+70:23:54.9	M1.0 V	8.259		
J00132+693	GJ 11 A	00:13:18.00	+69:19:32.4	M3.5 V	8.556	Binary	
J00133+275	UPM J0013+2733	00:13:19.55	+27:33:29.1	M4.5 V	10.431		
J00136+806	GJ 3014	00:13:40.36	+80:39:59.8	M1.5 V	7.756	Binary	
J00137+806	GJ 3015	00:13:44.59	+80:39:52.3	M5.0 V	10.936	Binary	
J00154-161	GJ 1005	00:15:28.77	-16:08:11.7	M4.0 V	7.215	Binary	
J00156+722	LP 49-338	00:15:37.59	+72:17:03.5	M2.0 V	8.837		
J00158+135	GJ 12	00:15:49.92	+13:33:27.6	M4.0 V	8.619		
J00159-166	1R001557.5-163659	00:15:57.94	-16:36:57.5	M4.1 V	8.736	Binary	
J00162+198W	EZPsc	00:16:15.44	+19:51:25.3	M4.0 V	7.875	Triple (SB2)	•
J00162+198E	GJ 1006 B	00:16:16.96	+19:51:38.5	M4.0 V	8.893	Triple	•
J00169+051	GJ 1007	00:16:56.20	+05:07:16.4	M4.0 V	9.398		
J00169+200	GJ 3022	00:16:57.03	+20:03:55.7	M3.5 V	9.681	Triple*	
J00173+291	Ross 680	00:17:21.17	+29:11:05.7	M2.0 V	8.152		
J00176-086	GJ 3025	00:17:41.23	-08:40:55.8	M0.0 V	8.095		
J00179+209	LP 404-81	00:17:58.87	+20:57:18.6	M1.0 V	8.250	Binary	
J00182+102	GJ 16	00:18:16.59	+10:12:09.6	M1.5 V	7.564		
J00183+440	HD 1326	00:18:27.17	+44:01:29.2	M1.0 V	5.252	Binary	•
J00184+440	HD 1326B	00:18:30.07	+44:01:43.5	M3.5 V	6.789	Binary	•
J00188+278	GJ 3027	00:18:54.07	+27:48:48.1	M4.0 V	9.535		
J00190-099	GJ 1008	00:19:05.52	-09:57:58.3	M0.0 V	7.376		
J00201-170	GJ 2003	00:20:08.54	-17:03:41.2	M1+ Vk:	8.545		
J00204+330	GJ 3028	00:20:30.78	+33:04:52.6	M5.5 V	10.284		•
J00207+596	[I81] M 134	00:20:47.70	+59:36:15.6	M2.5 V	8.936		
J00209+176	StKM 1-25	00:20:57.24	+17:38:14.7	M0.0 V	8.367		
J00210+557	G 217-43	00:21:05.02	+55:43:55.6	M2.0 V	9.194		
J00218+382	G 171-51	00:21:54.79	+38:16:24.2	M3.0 V	8.953		
J00219+492	GJ 3030	00:21:58.20	+49:12:37.3	M2.5 V	9.139	Binary	
J00234+243	GJ 1011	00:23:27.73	+24:18:26.5	M4.0 V	9.753		
J00234+771	GJ 1010 A	00:23:24.80	+77:11:22.2	M2.5 V	8.042	Binary	
J00235+771	GJ 1010 B	00:23:27.78	+77:11:27.5	M4.5 V	9.934	Binary	
J00240+264	LSPM J0024+2626	00:24:03.96	+26:26:28.9	M4.0 V	10.222		
J00244+360	G 130-67	00:24:26.30	+36:03:54.0	M1.0 V	8.886		
J00245+300	GJ 3033	00:24:35.60	+30:02:29.7	M5.0 V	9.776		
J00253+228	GJ 3034	00:25:20.33	+22:53:03.7	M4.71	9.716		
J00268+701	GJ 21	00:26:52.27	+70:08:30.4	M1.0 V	7.411		
J00271+496	GJ 3035	00:27:07.39	+49:41:49.3	M4.0 V	9.733		
J00279+223	LP 349-25	00:27:56.46	+22:19:29.7	M8.0 V	10.614	Binary	
J00286-066	GJ 1012	00:28:39.11	-06:40:02.0	dM4.0	8.038		•
J00288+503	GJ 3036	00:28:54.66	+50:22:35.3	M3.7 V	8.847	Binary	

Table B.1: Carmencita, the CARMENES input catalogue (continued).

Karmn	Name	α (2016.0)	δ (2016.0)	Spectral type	J [mag]	Multiplicity[a]	DR1[b]
J00315-058	GJ 1013	00:31:35.79	-05:52:30.0	M3.7 V	8.762		
J00322+544	G 217-56	00:32:15.34	+54:28:55.3	M4.5 V	9.387		
J00324+672N	V547Cas	00:32:34.33	+67:14:03.6	M2.0 V	6.844	Triple	
J00324+672S	GJ 22 B	00:32:34.28	+67:13:59.8	M3.0 V	7.172	Triple	
J00325+074	GJ 3039	00:32:34.91	+07:29:25.7	M4.0 V	8.397	Binary	
J00328-045	GR* 50	00:32:53.21	-04:34:09.4	M4.5 V	9.276	Binary	
J00333+368	G 132-4	00:33:21.17	+36:50:28.6	M3.0 V	8.768		
J00341+253	V493AndA	00:34:08.48	+25:23:48.5	M0.0 V	8.481	Triple*	
J00346+711	GJ 3040	00:34:39.40	+71:11:36.6	M3.5 V	9.465		
J00357+025	LP 585-55	00:35:43.30	+02:33:10.9	M5.0 V	10.517	Binary	
J00358+526	G 172-11	00:35:54.70	+52:41:09.3	M2.5 V	8.932	Triple	
J00359+104	GJ 1014	00:35:56.70	+10:28:29.4	M5.0 V	10.222		•
J00361+455	GJ 3042	00:36:08.05	+45:30:55.3	M2.0 V	8.167	Binary	
J00374+515	G 172-14	00:37:25.07	+51:33:06.8	M0.5 V	8.429		
J00380+169	PM J00380+1656	00:38:03.75	+16:56:01.3	M3.0 V	9.380		
J00382+523	GJ 3044	00:38:15.16	+52:19:53.3	M0.0 V	7.714		
J00385+514	GJ 3045	00:38:33.48	+51:27:58.4	M3.0 V	8.892		
J00389+306	Wolf 1056	00:39:00.98	+30:36:58.8	M2.5 V	7.453		•
J00395+149S	LP 465-061	00:39:33.91	+14:54:19.6	M4.0 V	9.964	Triple	
J00395+149N	LP 465-62	00:39:34.16	+14:54:35.4	M4.5 V	9.826	Triple	
J00395+605	Wolf 10	00:39:33.51	+60:33:10.9	M2.42 V	9.205		
J00403+612	2M00402129+6112490	00:40:21.40	+61:12:48.2	M2.0 V	10.154		•
J00409+313	GJ 3047	00:40:56.19	+31:22:51.2	M3.3 V	9.491		
J00413+558	GJ 1015 A	00:41:21.44	+55:50:03.2	M4.2 V	9.839	Binary	
J00427+438	PM J00427+4349	00:42:47.79	+43:49:24.0	M2.5 V	8.487		
J00428+355	FFAnd	00:42:48.59	+35:32:56.9	M1.0 V	7.164	Binary (SB2)	
J00435+284	GJ 1019	00:43:35.44	+28:26:24.4	M4.0 V	10.392		
J00443+091	GJ 3052	00:44:21.54	+09:07:34.5	M4.5 V	9.501		
J00443+126	GJ 3051	00:44:19.64	+12:36:59.8	M3.5 V	8.868		
J00449-152	GJ 3053	00:44:59.68	-15:16:27.1	M4.5 V	9.612		
J00459+337	G 132-25	00:45:57.01	+33:47:11.3	M4.5 V	10.183	Binary	
J00463+353	PM J00463+3522	00:46:21.76	+35:22:10.6	M1.5 V	8.933		
J00464+506	G 172-22	00:46:30.66	+50:38:35.3	M4.0 V	9.964		
J00468+160	PM J00468+1603	00:46:53.16	+16:03:01.8	M2.0 V	8.363		
J00484+753	LSPM J0048+7518	00:48:30.66	+75:18:47.2	M3.0 V	9.469		
J00487+270	GJ 3057	00:48:45.34	+27:01:04.4	M2.5 V	8.774		
J00489+445	GJ 3058	00:48:58.46	+44:35:06.9	M3.0 V	9.125	Binary	
J00490+657	PM J00490+6544	00:49:05.09	+65:44:36.8	M2.5 V	9.304		
J00502+086	RX J0050.2+0837	00:50:17.59	+08:37:33.6	M4.5 V	9.745	Binary (SB2)	
J00505+248	FTPscA	00:50:33.49	+24:48:59.7	M3.0 Vkee	7.951	Binary	
J00511+225	BPM 84579	00:51:10.71	+22:34:43.8	M1.5 V	8.262		
J00514+583	Wolf 33	00:51:33.02	+58:18:13.8	M0.0 V	7.831		
J00515-229	HD 4967B	00:51:35.91	-22:54:35.4	M5.5 V	10.904	Binary	•
J00520+205	G 69-27	00:52:00.27	+20:34:56.6	M1.0 V	8.490		
J00532+190	LSPM J0053+1903	00:53:12.84	+19:03:25.0	M2.5 V	8.792		
J00538+459	G 172-28	00:53:53.72	+45:56:41.6	M0.0 V	8.311		
J00540+691	Ross 317	00:54:00.72	+69:10:56.9	M2.0 V	9.462		
J00548+275	G 69-32	00:54:48.49	+27:31:03.9	M4.5 V	10.340		
J00566+174	GJ 1024	00:56:39.14	+17:27:30.3	M3.8 V	9.285		
J00570+450	G 172-30	00:57:03.64	+45:05:08.7	M3.0 V	8.101		•
J00577+058	BD+05 127	00:57:44.49	+05:51:20.6	M0.0 V	7.478		
J00580+393	1R005802.4+391912	00:58:01.01	+39:19:11.5	M4.5 V	9.561		
J01008+669	GJ 3068	01:00:48.83	+66:56:53.8	M3.5 V	9.408		
J01009-044	GJ 1025	01:00:57.71	-04:26:49.5	M4.0 V	9.042		
J01013+613	Wolf 44	01:01:20.86	+61:21:43.7	M2.0 V	7.272		•
J01019+541	GJ 3069	01:01:58.94	+54:10:55.8	M5.0 V	9.778		•
J01023-104	GJ 3072	01:02:21.16	-10:25:28.7	M0.0 V	7.417		
J01025+716	Ross 318	01:02:38.16	+71:40:41.2	M3.0 V	6.301		•
J01026+623	Wolf 46	01:02:40.55	+62:20:43.6	M1.5 V	6.230	Binary	•

Table B.1: Carmencita, the CARMENES input catalogue (continued).

Karmn	Name	α (2016.0)	δ (2016.0)	Spectral type	J [mag]	Multiplicity[a]	DR1[b]
J01033+623	V388Cas	01:03:21.51	+62:21:57.2	M5.0 V	8.611	Binary	
J01032+200	GJ 1026 A	01:03:14.92	+20:05:53.1	M2.0 V	7.670	Binary	
J01032+316	GJ 3073	01:03:14.23	+31:40:59.7	M3.2 V	9.561	Binary	
J01032+712	LP 29-70	01:03:16.13	+71:13:11.8	M4.0 V	9.689	Binary	•
J01036+408	G 132-50	01:03:40.31	+40:51:26.6	M0.0 V	8.134	Quadruple	
J01037+408	G 132-51A	01:03:42.24	+40:51:13.5	M2.6 V	9.372	Quadruple	
J01041+108	StKM 1-112	01:04:11.07	+10:51:35.4	M1.0 V	8.918		
J01048-181	GJ 1028	01:04:55.25	-18:07:20.8	dM5.0	9.387		•
J01056+284	GJ 1029	01:05:39.97	+28:29:30.6	M5.5 V	9.486	Binary (SB2)	•
J01066+152	GJ 1030	01:06:41.39	+15:16:18.1	M2.0 V	8.005		
J01066+192	LSPM J0106+1913	01:06:36.93	+19:13:29.6	M3.0 V	9.343		•
J01069+804	LP 12-502	01:06:56.00	+80:27:34.0	M4.5 V	9.350		
J01078+128	G 2-21	01:07:52.53	+12:52:51.4	M1.5 V	8.787		
J01102-118	LP 707-16	01:10:17.75	-11:51:19.3	M3.0 V	8.625		
J01114+154	GJ 3076	01:11:25.63	+15:26:19.9	M5.93	9.082	Binary	
J01116+120	LP 467-15	01:11:36.66	+12:05:02.3	M2.0 V	8.914		
J01119+049N	GJ 3077	01:11:56.01	+04:54:56.6	M3.5 V	8.804	Triple	
J01119+049S	GJ 3078	01:11:58.39	+04:54:04.0	M4.0 V	9.641	Triple	
J01125-169	YZCet	01:12:31.98	-16:59:46.2	M4.0 V	7.258		•
J01133+589	Wolf 58	01:13:20.12	+58:55:20.3	M1.5 V	8.409	Binary*	
J01134-229	GJ 1033	01:13:24.20	-22:54:07.3	M4.0 V	9.896		
J01141+790	PM J01141+7904	01:14:06.69	+79:04:01.9	M3.0 V	9.667		
J01147+253	LP 351-6	01:14:49.86	+25:18:57.6	M1.5 V	8.828		
J01158+470	1R011549.5+470159	01:15:50.51	+47:02:02.1	M4.5 V	10.210	Quadruple	
J01161+601	Wolf 59	01:16:10.94	+60:09:09.6	M0.5 V	8.333		
J01178+054	GJ 3084	01:17:53.34	+05:28:16.0	M0.5 V	7.839		
J01178+286	Ross 324	01:17:50.21	+28:40:09.6	M0.5 V	8.323		
J01182-128	GJ 56.1	01:18:16.20	-12:54:10.2	M2.0 V	8.356		
J01198+841	GJ 1035	01:19:41.88	+84:09:40.4	M5.0 V	9.855		•
J01214+243	Ross 788	01:21:29.78	+24:19:50.2	M0.0 V	7.894		
J01221+221	LP 351-34	01:22:10.58	+22:09:00.6	M4.0 V	8.412	Binary	
J01227+005	GJ 3093	01:22:44.77	+00:31:55.7	M5.0 V	9.201	Binary	
J01256+097	Wolf 66 A	01:25:36.89	+09:45:18.5	M4.0 V	8.952	Binary	
J01317+209	Wolf 1523	01:32:44.80	+20:59:13.5	M2.0 V	8.825		
J01324-219	GJ 3098	01:32:25.53	-21:54:32.7	M1.5 Vk:	7.977		
J01339-176	LP 768-113	01:33:58.05	-17:38:26.8	dM4.0	8.842		•
J01352-072	1R013514.2-071254	01:35:14.03	-07:12:52.2	M4.0 V	8.964	Single	•
J01369-067	LP 648-20	01:36:55.36	-06:47:39.6	M3.5 V	9.707	Binary	
J01373+610	TYC 4031-2527-1	01:37:21.44	+61:05:27.6	M1.5 V	8.662		
J01383+572	Ross 10	01:38:21.23	+57:13:51.4	M2.5 V	8.233		
J01384+006	GJ 3103	01:38:30.49	+00:39:08.4	M2.5 V	8.189		
J01390-179	BLCet	01:39:05.17	-17:56:53.9	M5.0 V	6.283	Binary	
J01395+050	GJ 3104	01:39:31.32	+05:03:20.3	M3.0 V	9.141	Binary	
J01402+317	GJ 3105	01:40:17.16	+31:47:30.4	M4.21	9.437		
J01431+210	RX J0143.1+2101	01:43:11.75	+21:01:10.4	M4.0 V	9.249	Binary	
J01432+278	GJ 3108	01:43:16.64	+27:50:31.1	M1.0 V	7.483		
J01433+043	GJ 70	01:43:19.73	+04:19:05.7	M2.0 V	7.370		•
J01437-060	PM J01437-0602	01:43:45.20	-06:02:40.6	M3.5 V	8.770	Binary (SB2)	
J01449+163	Wolf 1530	01:44:57.63	+16:20:32.5	M4.0 V	9.584		
J01466-086	GJ 3113	01:46:37.29	-08:39:00.5	M4.0 V	8.832	Binary	
J01453+465	G 173-18	01:45:18.81	+46:32:11.3	M2.0 V	8.058	Binary (SB2)	
J01480+212	Wolf 87	01:48:04.37	+21:12:20.8	M2.5 V	8.514		
J01510-061	GJ 3119	01:51:04.69	-06:07:09.3	M4.5 V	9.413		
J01514+213	Wolf 90	01:51:24.17	+21:23:33.9	M4.0 V	9.489		
J01518+644	GJ 3117	01:51:51.72	+64:26:02.8	M2.5 V	7.838	Binary	
J01518-108	Ross 555	01:51:49.30	-10:48:21.1	M2.0 V	8.375		•
J01531-210	BD-21 332	01:53:11.67	-21:05:42.2	M2.0 V	8.066	Binary (SB2)	
J01538-149	PM J01538-1459A	01:53:50.97	-14:59:51.5	M3.0 V	7.938	Binary	
J01544+576	1R015426.6+574136	01:54:28.04	+57:41:27.7	M3.5 V	8.525	Binary	

Table B.1: Carmencita, the CARMENES input catalogue (continued).

Karmn	Name	α (2016.0)	δ (2016.0)	Spectral type	J [mag]	Multiplicity[a]	DR1[b]
J01550+379	LSPM J0155+3758	01:55:02.64	+37:57:54.6	M5.0 V	10.469		•
J01556+028	G 73-5	01:55:36.98	+02:52:53.8	M1.5 V	8.965		
J01567+305	LP 296-57	01:56:45.99	+30:33:28.6	M4.5 V	10.323	Binary	
J01592+035E	GJ 1041 A	01:59:12.66	+03:31:09.6	M1.0 V	7.906	Triple	
J01592+035W	GJ 1041 B	01:59:12.89	+03:31:12.1	M3.0 V	7.998	Triple (SB2)	
J01593+585	V596Cas	01:59:24.17	+58:31:13.0	M4.0 V	7.790		
J02000+437	GJ 3123	02:00:03.00	+43:45:23.9	M3.0 V	9.258		
J02001+366	GJ 3124	02:00:07.50	+36:39:43.8	M3.8 V	9.805		
J02002+130	TZAri	02:00:14.16	+13:02:38.7	M3.5: V	7.514		•
J02007-103	GJ 3127	02:00:46.86	-10:21:26.6	M3.5 V	9.890		
J02015+637	GJ 3126	02:01:34.72	+63:46:10.5	M2.5 V	7.265		•
J02019+735	GJ 3125	02:01:55.13	+73:32:30.2	M4.5 V	9.252	Binary	
J02020+039	Wolf 109 B	02:02:03.11	+03:56:37.4	M2.0 V	9.395	Triple	
J02022+103	GJ 3128	02:02:15.51	+10:20:09.4	M5.5 V	9.842		•
J02026+105	PM J02024+1034B	02:02:28.15	+10:34:51.9	M4.5 V	8.396	Binary	
J02027+135	GJ 3129	02:02:44.86	+13:34:31.9	M5.0 V	9.652	Binary (SB2)	
J02028+047	RX J0202.8+0446	02:02:52.00	+04:47:00.4	M3.5 V	8.975		
J02033-212	GJ 3131	02:03:20.52	-21:13:50.2	M2.5 V	7.609	Triple* (SB2)	
J02044-018	GJ 3132	02:04:26.87	-01:53:06.0	M4.5 V	9.585		
J02050-176	GJ 84	02:05:06.31	-17:36:55.5	M2.5 V	6.542	Binary	
J02055+056	Wolf 116	02:05:30.35	+05:41:43.0	M1.0 V	8.936		
J02069+451	V374And	02:06:57.61	+45:10:56.9	M0.0 V	7.397	Binary (SB2)	
J02070+496	G 173-37	02:07:04.24	+49:38:36.6	M3.5 V	8.366		•
J02071+642	GJ 3134	02:07:10.89	+64:17:08.7	M4.5 V	9.875		
J02082+802	G 242-81	02:08:18.76	+80:13:11.1	M0.0 V	8.453		
J02088+494	GJ 3136	02:08:54.01	+49:26:51.8	M4.0 V	8.423		•
J02096-143	GJ 3139	02:09:36.70	-14:21:38.2	M2.5 V	8.122		
J02116+185	G 35-32	02:11:41.19	+18:33:42.3	M3.0 V	8.672		
J02123+035	Wolf 124	02:12:19.10	+03:34:02.6	M1.5 V	6.830		•
J02133+368	1R021320.6+364837	02:13:20.68	+36:48:51.6	M4.5 V	9.367	Binary	
J02129+000	GJ 3142	02:12:55.22	+00:00:17.3	M4.0 V	9.055		
J02142-039	LP 649-72	02:14:13.11	-03:57:46.1	M5.5 V	10.481		
J02149+174	GJ 1045	02:15:00.20	+17:25:00.8	M4.0 V	9.966		
J02153+074	Wolf 127	02:15:22.39	+07:29:32.5	M1.5 V	8.632		
J02155+339	GJ 3143	02:15:34.63	+33:57:35.0	M4.2 V	9.320		
J02158-126	GJ 3145	02:15:49.43	-12:40:24.2	M3.5 V	9.051		
J02164+135	GJ 3146	02:16:30.40	+13:35:05.9	M5.0 V	9.871		•
J02171+354	GJ 3147	02:17:10.74	+35:26:28.4	M7.0 V	9.983		
J02185+207	G 35-39	02:18:35.93	+20:47:44.8	M2.5 V	8.844		
J02186+123	RX J0218.6+1219	02:18:36.75	+12:18:56.0	M2.5 V	8.797		
J02190+238	GJ 3150	02:19:02.67	+23:52:53.7	M3.6 V	9.777		
J02190+353	Ross 19	02:19:03.89	+35:21:11.8	M3.5 V	8.662		
J02204+377	GJ 3151	02:20:25.74	+37:47:29.6	M2.5 V	8.952	Binary	
J02207+029	GJ 3153	02:20:46.42	+02:58:32.9	M6.0 V	10.064		
J02210+368	GJ 1047 A	02:21:05.05	+36:52:55.2	M3.0 V	9.368	Triple	
J02222+478	GJ 96	02:22:14.99	+47:52:48.8	M0.5 V	6.377		•
J02230+181	StKM 1-261	02:23:06.15	+18:10:31.6	M0.5 V	8.493		
J02234+227	LP 353-51	02:23:26.76	+22:44:05.0	M0.5 V	8.182		
J02247+259	GJ 3156	02:24:46.00	+25:58:31.5	M0.5 V	8.456		
J02254+246	StKM 1-265	02:25:28.00	+24:40:36.9	M2.0 V	8.876		
J02256+375	GJ 3157	02:25:38.83	+37:32:32.8	M5e	9.712		
J02272+545	1R022716.4+543258	02:27:17.31	+54:32:46.1	M4.5 V	10.212	Binary	
J02274+031	PM J02274+0310	02:27:27.43	+03:10:54.7	M4.0 V	9.978		
J02277+044	HD 15285	02:27:46.05	+04:25:58.8	M1.0 V	5.990	Binary	
J02282+014	GJ 3159	02:28:17.41	+01:26:29.0	M3.0 V	9.281		
J02283+219	TYC 1221-1171-1	02:28:22.17	+21:59:45.3	M0.5 V	8.456		
J02285-200	GJ 100 C	02:28:32.62	-20:02:22.5	M2.5 V	9.181	Triple	
J02287+156	LSPM J0228+1538	02:28:47.15	+15:38:53.6	M2.0 V	8.792	Binary	
J02289+120	GJ 3160	02:28:54.68	+12:05:22.3	M2.5 V	8.373	Binary (SB2)	

Table B.1: Carmencita, the CARMENES input catalogue (continued).

Karmn	Name	α (2016.0)	δ (2016.0)	Spectral type	J [mag]	Multiplicity[a]	DR1[b]
J02289+226	StKM 2-213A	02:28:58.41	+22:36:24.5	M2.0 V	8.749	Binary	
J02292+195	LP 410-33	02:29:14.32	+19:32:31.9	M2.5 V	8.959		
J02293+884	GJ 3137	02:29:14.09	+88:24:20.3	M3.5 V	9.065		
J02314+573	Ross 21	02:31:29.87	+57:22:43.3	M3.5 V	9.218		
J02330+078	LP 530-26	02:33:04.78	+07:49:41.0	M2.0 V	8.648		
J02336+249	GJ 102	02:33:37.23	+24:55:26.9	M3.5 V	8.472		•
J02337+150	GJ 3165	02:33:47.96	+15:00:17.8	M3.0 V	9.692		
J02340+417	GJ 3164	02:34:00.46	+41:46:50.4	M3.0 V	9.638		
J02345+566	G 174-4	02:34:34.87	+56:36:42.1	M2.0 V	8.893		
J02353+235	GJ 3166	02:35:22.50	+23:34:29.5	M4.0 V	9.536		
J02358+202	GJ 104	02:35:53.59	+20:13:09.3	M2.0 V	7.208		•
J02362+068	BXCet	02:36:17.20	+06:52:41.1	M4.0 V	7.333	Triple	
J02364+554	GJ 3168	02:36:26.63	+55:28:30.2	M3.0 V	9.339		
J02367+226	G 36-26	02:36:44.08	+22:40:20.2	M5.0 V	10.081		
J02367+320	GJ 3169	02:36:47.30	+32:04:18.9	M3.5 V	8.965	Binary	
J02392+074	GJ 3174	02:39:17.85	+07:28:14.9	M3.7 V	9.881		
J02412-045	G 75-35	02:41:15.51	-04:32:18.8	M4.5 V	9.199		
J02419+435	StKM 1-291	02:41:58.94	+43:34:19.0	M1.0 V	8.244		
J02424+182	LP 410-81	02:42:25.80	+18:14:44.0	M1.5 V	8.873		
J02438-088	Wolf 1132	02:43:53.88	-08:49:57.8	M1.5 V	8.693		
J02441+492	GJ 107 B	02:44:10.79	+49:13:53.0	M1.5 V	6.688	Binary	
J02442+255	VXAri	02:44:16.53	+25:31:18.3	dM3	6.752		•
J02443+109W	MCC 401	02:44:21.45	+10:57:40.2	M1.0 V	7.973	Triple	
J02443+109E	2M02442272+1057349	02:44:22.81	+10:57:34.2	M5.0 V	10.301	Triple	
J02456+449	GJ 3178	02:45:40.30	+44:56:53.5	M0.5 V	7.818	Binary	
J02462-049	GJ 3180	02:46:16.73	-04:59:50.7	M6.0 V	10.970		
J02465+164	GJ 3181	02:46:33.79	+16:25:01.1	M6.0 V	10.971		•
J02486+621	2M02483695+6211228	02:48:37.25	+62:11:21.3	M5.5 V	12.505		•
J02489-145W	PM J02489-1432W	02:48:59.45	-14:32:14.2	M2.0 V	9.528	Binary	•
J02489-145E	PM J02489-1432E	02:49:00.02	-14:32:15.5	M2.5 V	9.733	Binary	•
J02502+628	G 246-12	02:50:16.95	+62:51:16.4	M2.5 V	9.368		
J02518+062	GJ 3184	02:51:51.15	+06:13:39.6	M3.0 V	9.415		
J02518+294	GJ 3183	02:51:49.63	+29:29:10.4	M4.0 V	9.518	Binary	
J02519+224	RBS 365	02:51:54.22	+22:27:28.2	dM4.0	8.919		•
J02524+269	GJ 3186	02:52:25.03	+26:58:26.2	M2.0 V	7.937		
J02530+168	Teegarden's Star	02:53:04.71	+16:51:51.7	M7.0 V	8.394		•
J02534+174	LP 411-18	02:53:26.14	+17:24:28.4	M3.5 V	8.716		
J02555+268	HD 18143C	02:55:36.11	+26:52:17.6	M4.0 V	9.561	Triple	
J02560-006	LP 591-156	02:56:04.17	-00:36:32.0	M5.0 V	10.421		•
J02562+239	LSPM J0256+2359	02:56:14.06	+23:59:07.4	M5.0 V	9.977	Binary	
J02565+554W	Ross 364	02:56:35.79	+55:26:06.8	M1.0 V	7.425	Binary	
J02565+554E	Ross 365	02:56:36.49	+55:26:22.3	M2.5 V	8.006	Binary	•
J02573+765	LP 14-53	02:57:21.43	+76:33:04.9	M4.0 V	9.615		•
J02575+107	Ross 791	02:57:32.96	+10:47:17.9	M4.0 V	9.162		
J02581-128	GJ 3189	02:58:10.53	-12:52:57.4	sdM3.0	8.952		
J02591+366	Ross 331	02:59:11.44	+36:36:35.7	M3.7 V	9.064	Binary	
J02592+317	GJ 3191	02:59:16.77	+31:46:27.8	M3.3 V	9.523		
J02597+389	G 134-63	02:59:46.67	+38:55:34.6	M4.5 V	10.411	Binary	
J03018-165S	GJ 3193	03:01:50.98	-16:35:40.3	M3.0 V	7.294	Binary	
J03018-165N	GJ 3192	03:01:50.63	-16:35:35.2	M2.5 V	7.110	Binary	
J03026-181	GJ 9108	03:02:38.51	-18:09:56.1	M2.5 V	8.208		
J03033-080	StM 20	03:03:21.47	-08:05:16.0	M3.0 V	9.122		
J03037-128	GJ 3197	03:03:48.10	-12:51:21.0	M3.5 V	9.283	Binary	
J03036-128	GJ 3196	03:03:40.99	-12:50:33.7	M3.5 V	9.411	Binary	
J03040-203	GJ 3198	03:04:05.05	-20:22:50.7	M4.0 V	8.634		
J03047+617	GJ 3195	03:04:45.06	+61:43:57.7	M3.0 V	8.877	Binary	
J03075-039	GJ 3202	03:07:33.51	-03:58:23.2	M0.0 V	7.950	Binary	
J03077+249	LP 355-27	03:07:47.13	+24:57:53.3	M4.5 V	10.132		
J03090+100	GJ 1055	03:09:00.48	+10:01:16.3	M5.0 V	9.926		•

Table B.1: Carmencita, the CARMENES input catalogue (continued).

Karmn	Name	α (2016.0)	δ (2016.0)	Spectral type	J [mag]	Multiplicity[a]	DR1[b]
J03095+457	GJ 125	03:09:30.17	+45:43:52.7	M2.0 V	6.730	Binary	
J03102+059	EKCet	03:10:15.34	+05:54:22.5	M2.5 V	8.363		
J03104+584	GJ 3204	03:10:26.72	+58:26:05.5	M2.0 V	8.332		
J03109+737	GJ 1053	03:11:05.27	+73:46:02.5	M6.0 V	9.850		•
J03110-046	LP 652-62	03:11:04.90	-04:36:41.1	M3.0 V	9.406		
J03112+011	1R031114.2+010655	03:11:15.60	+01:06:30.6	M5.5 V	10.682		
J03118+196	Wolf 132	03:11:48.26	+19:40:11.3	M0.5 V	8.044		
J03119+615	GJ 3206	03:11:56.89	+61:31:14.6	M0.0 V	7.374	Binary	
J03133+047	CDCet	03:13:24.78	+04:46:30.7	M4.5 V	8.775		•
J03136+653	LP 53-55	03:13:37.88	+65:21:19.5	M1.5 V	8.728		
J03142+286	GJ 3208	03:14:12.85	+28:40:27.6	M6.0 V	10.993		•
J03145+594	Ross 369A	03:14:33.17	+59:26:13.8	M2.5 V	8.448	Binary*	
J03147+114	RX J0314.7+1127	03:14:47.26	+11:27:26.7	M2.0 V	9.352		
J03147+485	Ross 346	03:14:45.11	+48:31:05.5	M1.5 V	8.174		
J03162+581S	Ross 370A	03:16:14.73	+58:09:57.3	M2.0 V	7.344	Binary	
J03162+581N	Ross 370B	03:16:14.75	+58:10:02.4	M2.0 V	7.501	Binary	
J03167+389	PM J03167+3855	03:16:46.02	+38:55:27.7	M3.5 V	9.157		
J03172+453	GJ 3213	03:17:11.82	+45:22:20.9	M3.0 V	8.422	Binary	
J03177+252	GJ 3215	03:17:46.17	+25:15:00.6	M2.5 V	8.492		
J03181+382	HD 275122	03:18:08.09	+38:14:58.3	M1.5 V	7.023		•
J03181+426	Wolf 140	03:18:07.31	+42:40:06.8	M3.5 V	9.254		
J03185+103	StKM 1-354	03:18:35.36	+10:18:43.2	M1.5 V	8.995		
J03186+326	GJ 3216	03:18:38.59	+32:39:55.3	M1.0 V	8.227		
J03187+606	Ross 371	03:18:43.66	+60:36:21.1	M3.5 V	9.450		
J03194+619	G 246-33	03:19:29.28	+61:56:01.5	M4.0 V	9.511	Binary	
J03207+397	LP 198-637 A	03:20:45.42	+39:42:59.3	M1.5 V	8.085	Binary	
J03213+799	GJ 133	03:21:24.29	+79:58:06.8	M2.0 V	7.704		•
J03217-066	GJ 3218	03:21:47.27	-06:40:25.0	M2.0 V	7.857		•
J03220+029	GJ 1058	03:22:04.46	+02:56:22.7	M4.5 V	10.314		
J03224+271	GJ 3219	03:22:28.40	+27:09:20.8	M0.0 V	8.249		
J03230+420	GJ 1059	03:23:02.16	+42:00:15.8	M5.0 V	10.389		•
J03233+116	GJ 3221	03:23:22.15	+11:41:11.0	M3.5 V	8.386		
J03236+056	1R032338.7+054117	03:23:39.25	+05:41:14.1	M4.5 V	9.867		
J03241+237	GJ 140 A	03:24:06.73	+23:47:04.2	M1.5 V	7.128	Triple	
J03242+237	GJ 140 C	03:24:13.10	+23:46:17.3	M2.5 V	8.276	Triple	
J03247+447	PM J03247+4447A	03:24:42.31	+44:47:41.4	M1.5 V	8.566	Binary	
J03257+058	GJ 3224	03:25:42.04	+05:51:48.2	M4.5 V	9.946	Binary	
J03263+171	PM J03263+1709	03:26:23.74	+17:09:30.1	M4.0 V	9.774	Binary	
J03267+192	GJ 3225	03:26:44.97	+19:14:37.7	M4.5 V	10.123		
J03272+273	CKAri	03:27:14.22	+27:23:07.8	M1.0 V	8.637		
J03275+222	ATO J051.8788+22.2102	03:27:30.94	+22:12:36.9	M4.5 V	10.044		
J03284+352	LSPM J0328+3515A	03:28:29.35	+35:15:18.6	M2.0 V	8.970	Binary	
J03286-156	GJ 3228	03:28:39.18	-15:37:16.4	M3.5 V	9.855	Binary	
J03303+346	1R033021.4+344044	03:30:23.37	+34:40:31.7	M4.0 V	9.995	Triple*	
J03288+264	GJ 3227	03:28:49.84	+26:29:10.2	M4.0 V	9.288		
J03308+542	LSPM J0330+5413	03:30:48.61	+54:13:55.1	M5.0 V	10.173		
J03309+706	LP 31-368	03:30:56.01	+70:41:06.4	M3.5 V	9.487	Binary	
J03317+143	GJ 143.3	03:31:47.18	+14:19:07.0	M2.5 V	8.695		
J03325+287	RX J0332.6+2843	03:32:35.85	+28:43:54.1	M4.5 V	9.357	Triple	
J03332+462	HD 21845B	03:33:14.16	+46:15:16.2	M0.0 V	8.382	Binary	
J03340+585	Ross 563	03:34:01.11	+58:35:52.3	M0.5 V	8.288		
J03346-048	GJ 3235	03:34:40.07	-04:50:38.5	M3.8 V	8.829	Triple (ST3)	
J03361+313	1R033609.2+311853	03:36:08.85	+31:18:37.4	M4.5 V	9.187		
J03366+034	GJ 3237	03:36:40.97	+03:29:17.6	M5.0 V	9.295		
J03372+691	GJ 3236	03:37:14.55	+69:10:47.9	M3.8 V	9.806	Binary (EB/SB2)	
J03375+178N	GJ 3239	03:37:33.54	+17:51:14.1	M2.5 V	9.100	Quadruple (SB2)	
J03375+178S	GJ 3240	03:37:34.09	+17:51:00.0	M3.5 V	9.186	Quadruple (EB?/SB2)	
J03394+249	KPTau	03:39:29.85	+24:58:05.7	M3.5 V	8.813		
J03396+254E	Wolf 204	03:39:36.47	+25:28:11.6	M3.0 V	8.747	Binary	

Table B.1: Carmencita, the CARMENES input catalogue (continued).

Karmn	Name	α (2016.0)	δ (2016.0)	Spectral type	J [mag]	Multiplicity[a]	DR1[b]
J03396+254W	Wolf 205	03:39:40.77	+25:28:39.1	M3.5 V	9.079	Binary	
J03397+334	HD 278874B	03:39:47.79	+33:28:30.7	M3.0 V	8.967	Triple	
J03416+552	TYC 3720-426-1	03:41:37.46	+55:13:05.0	M0.0 V	8.347		
J03430+459	LSPM J0343+4554A	03:43:01.79	+45:54:17.4	M4.0 V	9.668	Binary	
J03433-095	GJ 3247	03:43:22.53	-09:33:46.1	M4.5 V	9.799		
J03438+166	GJ 150.1 A	03:43:52.74	+16:40:14.2	M0.0 V	7.046	Binary	
J03437+166	GJ 150.1 B	03:43:45.42	+16:39:57.2	M1.0 V	7.533	Binary	
J03445+349	HD 278968	03:44:31.21	+34:58:20.8	M0.0 V	7.905		
J03454+729	G 221-21	03:45:28.68	+72:59:25.2	M1.5 V	8.296	Triple	
J03455+703	PM J03455+7018	03:45:32.34	+70:18:00.4	M1.0 V	8.932		
J03459+147	G 6-33	03:45:54.96	+14:42:47.2	M1.5 V	8.772		
J03463+262	HD 23453	03:46:20.60	+26:12:52.7	M1.0 V	6.689		•
J03467+821	TYC 4521-1342-1	03:46:42.67	+82:07:50.1	M1.0 V	8.987		
J03467-112	GJ 3249	03:46:46.04	-11:17:40.5	M2.5 V	9.002		
J03473+086	GJ 3250	03:47:21.40	+08:41:36.7	M5.0 V	9.849		•
J03473-019	G 80-21	03:47:23.53	-01:58:24.3	M3.0 V	7.804		•
J03479+027	Ross 588	03:47:57.68	+02:47:09.3	M0.5 V	7.964		
J03480+686	GJ 153 C	03:48:02.08	+68:40:42.9	M2 V	7.379	Triple	
J03486+735	GJ 3248	03:48:39.73	+73:32:30.9	M1.0 V	7.994		
J03505+634	GJ 3251	03:50:33.69	+63:27:14.9	M1.5 V	8.192		
J03507-060	GJ 1065	03:50:43.81	-06:06:03.6	M3.0 V	8.570		
J03510+142	PM J03510+1413	03:51:00.87	+14:13:38.7	M4.5 V	9.436	Binary	
J03510-008	GJ 3252	03:51:00.04	-00:52:52.4	M8.0 V	11.302		
J03519+397	TYC 2868-639-1	03:51:58.19	+39:46:55.8	M0.0 V	8.277	Binary	
J03526+170	Wolf 227	03:52:42.24	+17:00:53.8	M5.0 V	8.933	Binary (SB2)	
J03531+625	Ross 567	03:53:10.51	+62:34:03.8	M3.0 V	7.782		•
J03543-146	2M03542008-1437388	03:54:20.02	-14:37:37.2	M6.5 V	11.339		
J03544-091	GJ 3256	03:54:25.52	-09:09:29.2	M1.0 V	7.817	Binary*	
J03548+163	LP 413-108	03:54:53.37	+16:18:55.9	M4.0 V	9.960		
J03565+319	1R035632.5+315746	03:56:33.26	+31:57:23.8	M3.5 V	9.795		
J03567+039	Ross 23	03:56:47.95	+53:33:30.5	M1.5 V	7.809		
J03574-011	HD 24916B	03:57:28.68	-01:09:25.7	M2.5 V	7.773	Triple (SB)	
J03586+520	Ross 24	03:58:36.92	+52:01:21.7	M1.0 V	8.922		
J03588+125	G 7-14	03:58:49.38	+12:30:18.3	M4.0 V	9.757		
J03598+260	Wolf 1322	03:59:54.53	+26:05:19.5	M3.0 V	8.714		
J04011+513	Ross 25	04:01:08.18	+51:23:06.4	M3.8 V	9.665	Binary*	
J04056+057	GJ 3261	04:05:38.94	+05:44:40.4	M4 V	8.813	Triple*	
J04059+712E	LP 31-301	04:05:58.09	+71:16:34.7	M4.0 V	9.527	Triple	
J04059+712W	LP 31-302 A	04:05:57.21	+71:16:32.4	M5.0 V	10.099	Triple	
J04061-055	PM J04061-0534	04:06:06.90	-05:34:46.9	M3.5 V	9.128		
J04077+142	LP 474-123	04:07:44.14	+14:13:22.1	M0.0 V	8.041	Binary	
J04079+142	LP 474-124	04:07:54.99	+14:12:58.2	M2.5 V	9.215	Binary	
J04081+743	LP 32-16	04:08:13.87	+74:22:51.6	M3.5 V	9.247		
J04083+691	LP 31-433	04:08:24.60	+69:10:57.9	M4.5 V	10.263		
J04086+336	HD 281621	04:08:38.07	+33:38:15.3	M0.5 V	7.016	Binary	
J04093+057	LP 534-29	04:09:22.50	+05:46:25.2	M4.5 V	10.708	Binary	
J04108-128	LP 714-37	04:10:47.88	-12:51:48.4	M5.5 V	11.008	Binary	
J04112+495	Ross 27	04:11:13.29	+49:31:45.0	M3.5 V	9.486		
J04122+647	GJ 3266	04:12:18.25	+64:43:48.7	M4.0 V	9.156		
J04123+162	LP 414-117	04:12:21.90	+16:15:02.9	M4.0 V	9.736	SKG (SB2)	
J04129+526	Ross 28	04:12:58.22	+52:36:28.9	M4.0 V	8.773	Binary	
J04131+505	Ross 29A	04:13:09.43	+50:31:38.0	M4.0 V	9.260	Binary	
J04137+476	LSPM J0413+4737E	04:13:47.70	+47:37:42.5	M2.5 V	8.951		
J04139+829	GJ 3262	04:13:56.69	+82:55:03.0	M0.0 V	7.955		
J04148+277	G 39-3	04:14:53.80	+27:45:26.0	M3.5 V	8.763		
J04153-076	DYEri	04:15:19.12	-07:40:15.3	M4.5 V	6.747	Triple	•
J04166-125	GJ 2033 A	04:16:41.59	-12:33:19.3	M1.0 V	7.572	Binary	
J04167-120	LP 714-47	04:16:45.65	-12:05:05.6	M0.0 V	9.493		•
J04173+088	GJ 3270	04:17:18.68	+08:49:16.0	M5.0 V	9.030		

Table B.1: Carmencita, the CARMENES input catalogue (continued).

Karmn	Name	α (2016.0)	δ (2016.0)	Spectral type	J [mag]	Multiplicity[a]	DR1[b]
J04177+410	LSPM J0417+4103A	04:17:44.44	+41:03:10.1	M3.5 V	9.238	Binary	
J04188+013	HIP 20122	04:18:51.45	+01:23:35.0	M2.0 V	8.877		
J04191+097	UPM J0419+0944	04:19:08.15	+09:44:50.2	M3.0 V	9.990		
J04191-074	LP 654-39	04:19:06.41	-07:27:43.6	M3.5 V	9.968		
J04198+425	LSPM J0419+4233	04:19:52.90	+42:33:07.4	M8/9V	11.094		•
J04199+364	Ross 592	04:19:59.96	+36:29:04.1	M1.5 V	8.225		
J04205+815	PM J04205+8131	04:20:34.24	+81:31:54.4	M3.0 V	9.482		
J04206+272	XEST 16-045	04:20:39.20	+27:17:31.4	M4.5 V	10.497		
J04207+152	LP 415-363	04:20:48.16	+15:14:08.2	M4.0 V	9.490	Binary	
J04218+213	GJ 3274	04:21:50.22	+21:19:39.2	M3.5 V	9.080		
J04219+751	GJ 3271	04:21:59.86	+75:08:20.5	M3.0 V	8.545		•
J04221+192	GJ 3275	04:22:08.13	+19:15:21.4	M3.0 V	9.209		
J04224+036	RX J0422.4+0337	04:22:25.19	+03:37:08.5	M3.5 V	9.857	Binary*	
J04224+740	LP 31-339	04:22:28.52	+74:01:21.5	M1.5 V	8.854		
J04225+105	LSPM J0422+1031	04:22:32.25	+10:31:19.3	M3.5 V	8.471		
J04225+390	GJ 1070	04:22:34.31	+39:00:34.0	M5.0 V	10.473		•
J04227+205	LP 415-30	04:22:42.99	+20:34:11.9	M4.0 V	10.458		
J04229+259	G 8-31	04:22:59.30	+25:59:10.4	M4.5 V	9.645		
J04234+495	TYC 3337-1716-1	04:23:26.84	+49:34:15.6	M2.5 V	8.329		
J04234+809	1R042323.2+805511	04:23:29.60	+80:55:08.8	M4.0 V	9.412		
J04238+092	LP 535-73	04:23:50.83	+09:12:19.4	M3.0 V	9.117		
J04238+149	INTau	04:23:50.50	+14:55:17.0	M3.5 V	9.293		
J04247-067	1R042441.9-064725	04:24:42.78	-06:47:31.2	M4.0 V	9.566	Triple (ST3)	
J04248+324	GJ 3280	04:24:49.49	+32:26:56.0	M2.5 V	8.818		
J04251+515	PM J04251+5131	04:25:09.86	+51:31:56.2	M2.0 V	8.803		
J04252+080S	GJ 3282	04:25:15.25	+08:02:55.8	M2.5 V	8.908	SKG (SB2)	
J04252+080N	GJ 3283	04:25:17.09	+08:04:03.9	M4.0 V	10.422	SKG	
J04252+172	V805Tau	04:25:13.67	+17:16:05.1	M3.5 V	9.149	SKG	
J04274+203	TYC 1273-9-1	04:27:24.97	+20:22:44.5	M1.5 V	8.769		
J04276+595	GJ 3287	04:27:41.56	+59:35:13.5	M3.8 V	9.975	Binary	
J04278+117	GJ 3291	04:27:53.89	+11:46:46.8	M4.2 V	9.699		
J04284+176	V1102Tau	04:28:28.89	+17:41:44.9	M2.0 V	8.592	Binary	
J04290+219	HD 28343	04:29:00.05	+21:55:24.5	M0.5 V	5.674		
J04293+142	GJ 3292	04:29:18.76	+14:14:02.0	M3.8 V	9.350		•
J04294+262	FW Tau	04:29:29.71	+26:16:52.8	M5.5 V	10.340	Triple	
J04302+708	PM J04302+7049	04:30:11.72	+70:49:14.3	M1.5 V	8.753		
J04304+398	V546Per	04:30:25.67	+39:50:50.4	M5.0 V	9.113		
J04308-088	LP 655-23	04:30:52.04	-08:49:22.0	M4.0 V	9.853	Binary	
J04310+367	PM J04310+3647A	04:30:59.95	+36:47:54.7	M3.0 V	9.445	Binary	
J04311+589	GJ 169.1 A	04:31:14.21	+58:58:04.7	M4.0 V	6.622	Binary	
J04312+422	PM J04312+4217	04:31:14.99	+42:17:08.9	M2.5 V	8.349		•
J04313+241	V927Tau	04:31:23.83	+24:10:52.6	M4.5: V	9.729	Binary	
J04326+098	LP 475-1095	04:32:37.96	+09:51:06.5	M1.5 V	8.386		
J04329+001E	LP 595-23	04:32:56.07	+00:06:14.7	M0.5 V	8.421	Triple	
J04329+001S	G 82-28	04:32:55.38	+00:06:28.3	M4.0 V	9.861	Triple	
J04329+001N	LP 595-21	04:32:55.32	+00:06:33.2	M4.0 V	10.300	Triple	
J04333+239	V697TauA	04:33:23.91	+23:59:26.0	M3.0 V	8.914	Binary	
J04335+207	GJ 3296	04:33:34.48	+20:44:40.7	M5.0 V	9.769		
J04343+430	PM J04343+4302	04:34:22.55	+43:02:13.3	M2.65 V	9.616		
J04347-004	LP 595-11	04:34:45.24	-00:26:50.2	M4.0 V	9.307		•
J04350+086	StKM 1-495	04:35:02.65	+08:39:30.5	M1.0 V	8.828	Binary	
J04352-161	LP 775-31	04:35:16.33	-16:06:52.2	M8.0 V	10.406	Binary (SB2)	
J04366+112	GJ 3302	04:36:39.94	+11:13:22.8	M4.0 V	10.089		
J04369+593	LP 84-34	04:36:58.75	+59:21:57.7	M2.0 V	8.986		
J04369-162	1R043657.1-161258	04:36:57.49	-16:13:07.0	M3.5 V	9.117		
J04373+193	LP 415-1644	04:37:22.00	+19:21:16.9	M4.0 V	10.182		
J04376+528	HD 232979	04:37:41.47	+52:53:29.4	M0.0 V	5.866		
J04376-024	GJ 3305	04:37:37.51	-02:29:29.7	M1.1 V	7.299	Triple	
J04376-110	GJ 173	04:37:41.62	-11:02:23.1	M1.5 V	6.943		•

Table B.1: Carmencita, the CARMENES input catalogue (continued).

Karmn	Name	α (2016.0)	δ (2016.0)	Spectral type	J [mag]	Multiplicity[a]	DR1[b]
J04382+282	GJ 3304 A	04:38:13.13	+28:12:58.4	M4.0 V	8.173	Binary	•
J04386-115	LP 715-39	04:38:36.86	-11:30:18.6	M3.5 V	8.672		
J04388+217	G 8-48A	04:38:53.72	+21:47:51.7	M3.5 V	9.552	Triple	
J04393+335	PM J04393+3331	04:39:23.22	+33:31:48.7	M4.0 V	9.919	Triple	
J04395+162	LP 415-302	04:39:31.54	+16:15:30.2	M5.5 V	10.139		
J04398+251	PM J04398+2509	04:39:48.86	+25:09:25.4	M3.5 V	9.642		
J04403-055	LP 655-48	04:40:23.63	-05:30:06.1	M6.0 V	10.658		
J04404-091	GJ 9163 A	04:40:29.13	-09:11:48.5	M0.0 V	7.133	Binary	
J04406-128	TOI-2457	04:40:40.16	-12:53:26.6	M0.0 V	9.741		
J04407+022	GJ 3307	04:40:42.67	+02:13:52.7	M2.0 V	7.894		
J04413+327	G 39-30A	04:41:24.22	+32:42:19.9	M4.0 V	9.463	Binary	
J04414+132	TYC 694-1183-1	04:41:29.78	+13:13:16.0	M0.5 V	8.356	Binary (SB)	
J04422+577	LP 84-59	04:42:15.86	+57:42:18.2	M0.0 V	8.456		
J04423+207	LP 415-1896	04:42:23.76	+20:46:34.9	M2.0 V	8.560		
J04425+204	LP 415-345	04:42:30.40	+20:27:10.8	M3.0 V	9.396	SKG (SB2)	
J04429+095	PM J04429+0935	04:42:55.14	+09:35:53.7	M1.0 V	8.882	Binary*	
J04429+189	HD 285968	04:42:56.52	+18:57:11.5	M2.5 V	6.462		
J04429+214	PM J04429+2128	04:42:55.90	+21:28:24.8	M3.5 V	7.958		•
J04433+296	Haro 6-36	04:43:20.23	+29:40:05.7	M5.5 V	10.402		•
J04444+278	HD 283779	04:44:26.17	+27:51:37.2	M1.5 V	7.908		
J04458-144	PM J04458-1426	04:45:52.69	-14:26:23.6	M4.0 V	9.088		
J04468-112	PM J04468-1116A	04:46:51.63	-11:16:48.6	M3.0 V	8.144	Binary	
J04471+021	GJ 3313	04:47:11.55	+02:09:39.6	M0.0 V	8.308		
J04472+206	RX J0447.2+2038	04:47:12.35	+20:38:09.2	M5.0 V	9.380		
J04480+170	LP 416-43	04:48:00.98	+17:03:21.1	M0.5 V	8.214	SKG (SB)	•
J04488+100	1R044847.6+100302	04:48:47.32	+10:03:01.4	M3.0 V	8.127	Binary (SB2)	
J04494+484	G 81-34	04:49:29.77	+48:28:42.9	M4.0 V	9.059	Binary	
J04499+236	EM* LkCa 18A	04:49:56.34	+23:41:00.1	M1.0 V	8.242	Binary	
J04499+711	LP 32-204	04:49:56.29	+71:09:46.5	M3.5 V	9.633		
J04502+459	GJ 3315	04:50:15.59	+45:58:46.2	M1.0 V	8.533		
J04504+199	BPM 85800	04:50:25.49	+19:59:09.1	M1.5 V	8.731		
J04508+221	GJ 1072	04:50:51.65	+22:07:14.7	M5.0 V	9.896		
J04508+261	GJ 3316	04:50:51.21	+26:07:22.3	M2.5 V	9.152		
J04520+064	Wolf 1539	04:52:05.90	+06:28:30.7	M3.5 V	7.814		
J04524-168	LP 776-25	04:52:24.55	-16:49:25.3	M3.3 V	7.740		•
J04525+407	GJ 1073	04:52:36.26	+40:42:06.6	M5.0 V	9.071		
J04536+623	LP 84-48	04:53:40.79	+62:18:59.9	M3.5 V	9.226		
J04538+158	LSPM J0453+1549	04:53:50.10	+15:49:12.6	M2.5 V	9.432		
J04538-177	GJ 180	04:53:50.44	-17:46:34.6	M2.0 V	7.413		•
J04544+650	1R045430.9+650451	04:54:29.98	+65:04:39.5	M4.0 V	9.668		
J04559+046	HD 31412B	04:55:54.60	+04:40:13.5	M2.0 V	8.501	Triple	
J04560+432	LP 202-2	04:56:04.12	+43:13:53.0	M4.0 V	9.304		
J04587+509	GJ 1074	04:58:46.84	+50:56:32.4	M1.0 V	7.896		
J04588+498	GJ 181	04:58:50.76	+49:50:55.6	M0.0 V	6.925		
J04595+017	GJ 182	04:59:34.88	+01:46:59.2	M0.0 V	7.117		•
J05012+248	Ross 794	05:01:15.79	+24:52:18.2	M2.0 V	8.084		
J05013+226	LSPM J0501+2237	05:01:17.95	+22:36:55.3	M4.5 V	10.161		
J05018+037	GJ 3321	05:01:50.71	+03:45:53.1	M1.5 V	8.079		
J05019+011	1R050156.7+010845	05:01:56.70	+01:08:41.4	M4.0 V	8.526		
J05019+099	GJ 3322 A	05:01:58.83	+09:58:57.1	M4.0 V	7.212	Binary (SB2)	•
J05019-069	GJ 3323	05:01:56.83	-06:56:54.9	M4.0 V	7.617		•
J05024-212	HD 32450A	05:02:28.28	-21:15:28.4	M2.0 V	5.450	Binary	
J05032+213	HD 285190	05:03:16.21	+21:23:54.0	M1.5 V	7.451	Quadruple (SB2)	
J05033-173	GJ 3325	05:03:19.83	-17:22:31.8	M3.0 V	7.819		
J05034+531	GJ 184	05:03:26.22	+53:07:17.9	M0.5 V	7.001	Binary	
J05042+110	GJ 3326	05:04:14.69	+11:03:27.0	M5.0 V	9.144		•
J05050+442	UPM J0505+4414	05:05:06.06	+44:14:03.3	M5.0 V	9.829		
J05051-120	GJ 3327	05:05:11.55	-12:00:30.9	M3.0 V	9.103		
J05060+043	GJ 3328	05:06:04.44	+04:20:16.1	M1.0 V	8.303		

Table B.1: Carmencita, the CARMENES input catalogue (continued).

Karmn	Name	α (2016.0)	δ (2016.0)	Spectral type	J [mag]	Multiplicity[a]	DR1[b]
J05062+046	RX J0506.2+0439	05:06:12.96	+04:39:25.7	M4.0 V	8.909		
J05068-215E	GJ 3331	05:06:49.97	-21:35:09.4	M1.5 V	7.046	Triple	
J05068-215W	GJ 3332	05:06:49.48	-21:35:04.3	M3.5 V	7.003	Triple	•
J05072+375	RX J0507.2+3731A	05:07:14.33	+37:30:42.1	M5.0 V	10.284	Binary*	
J05076+275	TYC 1853-1649-1	05:07:36.74	+27:30:03.8	M0.5 V	8.321		
J05078+179	Wolf 230	05:07:49.34	+17:58:53.5	M3.0 V	8.023	Triple (ST2)	
J05083+756	LP 15-315	05:08:19.36	+75:38:13.3	M4.5 V	9.391	Binary	
J05084-210	2M05082729-2101444	05:08:27.34	-21:01:44.6	M5.0 V	9.716	Binary	
J05085-181	GJ 190	05:08:35.61	-18:10:41.8	M3.5 V	6.175	Binary	
J05091+154	Ross 388	05:09:10.11	+15:27:22.8	M3.5 V	8.770		•
J05103+095	G 97-23	05:10:18.12	+09:30:01.8	M2.0 V	8.864		
J05103+272	LSPM J0510+2714	05:10:19.83	+27:13:51.8	M7.0 V	10.698		
J05103+488	GJ 3336 A	05:10:22.30	+48:50:26.3	M2.5 V	7.827	Binary	
J05106+297	G 86-28	05:10:39.22	+29:46:48.9	M3.0 V	8.600		
J05109+186	GJ 3337	05:10:57.16	+18:37:24.1	M4.0 V	9.935		
J05111+158	StKM 1-549	05:11:09.78	+15:48:57.0	M1.0 V	8.974		
J05114+101	LP 477-36	05:11:29.68	+10:07:12.2	M1.0 V	8.846		
J05127+196	GJ 192	05:12:42.54	+19:40:00.2	M2.0 V	7.299		
J05151-073	GJ 3340	05:15:08.33	-07:20:55.4	M1.0 V	8.355		
J05152+236	UPM J0515+2336	05:15:17.58	+23:36:25.2	M5.0 V	10.186		•
J05155+591	LSPM J0515+5911	05:15:31.19	+59:11:01.3	M7.5 V	11.320		
J05173+321	G 86-37	05:17:20.09	+32:07:29.7	M3.5 V	9.236	Binary	
J05173+458	Capella H	05:17:24.00	+45:50:16.1	M1.0 V	6.777	Quadruple	
J05173+721	TYC 4351-466-1	05:17:21.23	+72:10:49.8	M1.0 V	8.689		
J05187+464	PM J05187+4629	05:18:44.62	+46:29:57.9	M4.5 V	9.957		
J05195+649	1R051929.3+645435	05:19:31.21	+64:54:36.2	M3.5 V	8.950		
J05206+587N	GJ 3342	05:20:41.70	+58:47:25.2	M3.5 V	9.295	Binary	
J05206+587S	GJ 3343	05:20:41.05	+58:47:12.0	M3.5 V	9.926	Binary	
J05211+557	GJ 3345	05:21:10.47	+55:45:46.5	M3.5 V	9.229		
J05223+305	PM J05223+3031	05:22:20.65	+30:31:08.3	M3.0 V	9.406		
J05226+795	TYC 4532-731-1	05:22:39.87	+79:34:30.3	M0.5 V	8.200		
J05228+202	PM J05228+2016	05:22:50.18	+20:16:36.5	M2.5 V	8.635	Binary	
J05243-160	PM J05243-1601A	05:24:19.14	-16:01:15.8	M4.5 V	8.668	Binary	
J05256-091	LP 717-36	05:25:41.70	-09:09:15.8	M3.5 V	8.454	Binary	
J05280+096	Ross 41	05:27:59.94	+09:38:26.0	M3.5 V	8.311		
J05282+029	GJ 1080	05:28:14.24	+02:57:56.6	M3.5 V	8.979	Triple (SB)	
J05289+125	GJ 3348A	05:28:56.61	+12:31:50.4	M4.0 V	9.649	Quintuple	•
J05294+155E	GJ 2043	05:29:26.92	+15:34:36.2	M0.0: V	7.557	Binary	
J05294+155W	GJ 2043 B	05:29:26.02	+15:34:43.4	M4.0 V	10.252	Binary	
J05298+320	Ross 406	05:29:52.40	+32:04:40.4	M2.5 V	8.649		
J05298-034	Wolf 1450	05:29:51.70	-03:26:37.6	M3.0 V	8.276		
J05306+152	LSPM J0530+1514	05:30:37.09	+15:14:26.3	M3.0 V	8.985		
J05314-036	HD 36395	05:31:28.21	-03:41:11.5	M1.5 V	4.999		
J05320-030	V1311Ori	05:32:04.51	-03:05:30.0	M2.0 V	7.879	Quintuple	
J05322+098	Ross 42	05:32:14.46	+09:49:11.5	M3.5 V	7.423	Binary (SB2)	•
J05328+338	G 98-7	05:32:51.57	+33:49:39.8	M3.5 V	9.391		
J05333+448	GJ 1081	05:33:19.20	+44:48:52.9	M3.5 V	8.197	Binary	
J05337+019	V371Ori	05:33:44.55	+01:56:41.0	M3.0 V	7.764	Binary (SB1)	
J05339-023	RX J0534.0-0221	05:33:59.83	-02:21:33.3	M3.0 V	8.564		
J05341+475	PM J05341+4732A	05:34:10.56	+47:32:02.8	M2.5 V	8.752	Quadruple*	•
J05341+512	GJ 3352	05:34:08.57	+51:12:52.8	M1.0 V	8.001		
J05342+103N	Ross 45	05:34:15.05	+10:19:08.0	M3.0 V	8.561	Triple	
J05342+103S	Ross 45B	05:34:15.00	+10:19:03.0	M4.5 V	9.186	Triple (SB)	
J05348+138	Ross 46	05:34:51.99	+13:52:40.4	M3.0 V	7.781		
J05360-076	Wolf 1457	05:36:00.20	-07:38:51.0	dM4.0	8.464		
J05365+113	V2689Ori	05:36:30.99	+11:19:39.4	M0.0 V	6.126	Binary	•
J05366+112	PM J05366+1117	05:36:38.46	+11:17:47.8	M4.0 V	8.266	Binary	•
J05394+406	LSPM J0539+4038	05:39:25.71	+40:38:29.5	M8.0 V	11.109		•
J05394+747	LP 33-191	05:39:25.44	+74:46:02.6	M3.5 V	9.330		•

Table B.1: Carmencita, the CARMENES input catalogue (continued).

Karmn	Name	α (2016.0)	δ (2016.0)	Spectral type	J [mag]	Multiplicity[a]	DR1[b]
J05402+126	V1402Ori	05:40:16.07	+12:38:56.4	M1.5 V	8.072	Binary (SB2)	•
J05415+534	HD 233153	05:41:30.74	+53:29:15.0	M1.0 V	6.586	Binary	
J05404+248	V780Tau	05:40:25.82	+24:48:02.0	M5.5 V	8.978	Binary	
J05419+153	GJ 9188	05:41:58.95	+15:20:13.3	M0.0 V	7.690		
J05421+124	V1352Ori	05:42:11.45	+12:28:56.5	M4.0 V	7.124		•
J05422-054	GJ 2045	05:42:12.53	-05:27:40.3	M5.0 V	10.206		
J05425+154	1R054232.1+152459	05:42:31.70	+15:25:00.2	M3.5 V	9.443		•
J05455-119	PM J05455-1158	05:45:32.04	-11:58:02.3	M4.5 V	9.590		
J05456+729	PM J05456+7255	05:45:39.09	+72:55:14.6	M3.0 V	9.395		
J05458+729	PM J05458+7254	05:45:50.02	+72:54:09.0	M2.5 V	9.338		
J05466+441	Wolf 237	05:46:37.60	+44:07:14.0	M4.0 V	8.459	Triple (SB2)	
J05468+665	TYC 4106-420-1	05:46:48.92	+66:30:13.1	M0.5 V	8.421		
J05471-052	GJ 3366	05:47:09.69	-05:12:20.3	M4.5 V	10.039		
J05472-000	GJ 3367	05:47:17.89	-00:00:49.9	M0	7.987		
J05484+077	GJ 3368	05:48:24.15	+07:45:34.3	M4.0 V	9.784		
J05511+122	PM J05511+1216	05:51:10.51	+12:16:09.4	M4.0 V	9.453		
J05530+047	G 106-7	05:53:04.75	+04:43:02.6	M1.5 V	8.950	Binary*	
J05530+251	LSPM J0553+2507	05:53:01.92	+25:07:40.9	M3.0 V	8.552	Binary	
J05532+242	Ross 59	05:53:14.24	+24:15:22.1	M1.5 V	7.485	Binary (SB2)	
J05547+109	RX J0554.7+1055	05:54:45.58	+10:55:55.9	M3.0 V	8.832		
J05558+406	PM J05558+4036	05:55:48.31	+40:36:48.0	M1.0 V	8.776	Binary*	•
J05566-103	1R055641.0-101837	05:56:40.63	-10:18:35.8	M3.5 V	9.067		
J05587+259	PM J05587+2557	05:58:47.68	+25:57:40.1	M1.0 V	8.776		
J05588+213	G 104-9	05:58:53.53	+21:20:54.5	M5.0 V	9.968	Binary	
J05596+585	EGCam	05:59:37.77	+58:35:30.8	M0.5 V	7.068	Binary	
J05599+585	GJ 3372	05:59:55.68	+58:34:11.2	M4.2 V	9.028	Binary	
J06000+027	GJ 3379	06:00:03.83	+02:42:22.9	M3.5 V	6.905		
J06008+681	GJ 3373	06:00:50.71	+68:09:05.3	M3.5 V	8.922	Binary	
J06007+681	GJ 3374	06:00:47.81	+68:08:11.6	M4.0 V	9.178	Binary	•
J06011+595	GJ 3378	06:01:10.82	+59:35:35.0	M4.0 V	7.465		
J06017+130	LSPM J0601+1305	06:01:45.54	+13:05:00.7	M2.5 V	8.444		
J06023-203	GJ 3382	06:02:22.56	-20:19:35.3	M3.5 V	9.215		•
J06024+498	GJ 3380	06:02:29.31	+49:51:42.6	M5.0 V	9.350		
J06024+663	LP 57-46	06:02:26.51	+66:20:32.3	M4.5 V	9.855		
J06025+371	PM J06025+3707	06:02:35.46	+37:07:36.2	M1.0 V	8.433		•
J06034+478	Wolf 261	06:03:29.48	+47:48:06.0	M4.2 V	9.691		
J06035+155	1R060335.0+153132	06:03:34.74	+15:31:30.4	M0.0 V	8.203		
J06035+168	1R060334.8+165128	06:03:34.49	+16:51:45.4	M4.0 V	9.387		
J06039+261	Ross 60	06:03:54.54	+26:08:46.0	M3.0 V	9.839		
J06054+608	LP 86-173	06:05:30.04	+60:49:09.8	M4.5 V	9.096		
J06066+465	PM J06066+4633A	06:06:37.78	+46:33:47.0	M3.0 V	9.231	Binary	
J06071+335	Ross 70	06:07:11.91	+33:32:30.9	M2.0 V	8.992		
J06075+472	1R060732.5+471154	06:07:31.91	+47:12:23.3	M4.5 V	9.723		
J06097+001	HD 291290	06:09:46.30	+00:09:30.8	M0.0 V	8.124		
J06102+225	PM J06102+2234	06:10:17.81	+22:34:17.2	M4.0 V	9.876	Triple	
J06103+225	LP 362-121	06:10:22.52	+22:34:18.1	M5.0 V	10.644	Triple	
J06103+722	LSPM J0610+7212	06:10:18.09	+72:11:58.0	M2.5 V	9.272		
J06103+821	GJ 226	06:10:20.24	+82:06:02.9	M2.0 V	6.869		
J06105+024	TYC 135-239-1	06:10:31.41	+02:25:30.3	M0.0 V	8.342		
J06105-218	HD 42581	06:10:34.46	-21:52:04.2	M0.5 V	5.104	Binary	•
J06107+259	Wolf 1058	06:10:46.51	+25:55:53.3	M1.5 V	8.245		•
J06109+103	Ross 79	06:10:54.88	+10:18:50.6	M2.5 V	6.795	Binary	
J06140+516	GJ 3388	06:14:01.72	+51:40:06.5	M3.5 V	8.860		
J06145+025	G 106-35	06:14:34.76	+02:30:19.7	M3.0 V	9.296		
J06171+051	GJ 231.1 B	06:17:10.42	+05:07:05.3	M3.5 V	9.088	Quadruple	
J06151-164	LP 779-34	06:15:11.90	-16:26:21.4	M4.0 V	9.283		
J06171+751	TYC 4525-194-1	06:18:07.08	+75:06:04.3	M2.0 V	8.041	Triple (ST3?)	
J06171+838	LSPM J0617+8353	06:17:04.81	+83:53:32.5	M3.5 V	8.961		
J06185+250	G 103-29	06:18:34.83	+25:03:00.6	M4.0 V	9.954		

Table B.1: Carmencita, the CARMENES input catalogue (continued).

Karmn	Name	α (2016.0)	δ (2016.0)	Spectral type	J [mag]	Multiplicity[a]	DR1[b]
J06193-066	Ross 417	06:19:20.74	-06:39:32.1	M3.0 V	9.122		
J06194+139	TYC 743-1836-1	06:19:29.61	+13:57:02.3	M0.5 V	7.841		
J06212+442	GJ 3391	06:21:13.26	+44:14:26.7	M2.0 V	8.724	Binary	
J06216+163	LP 420-5	06:21:36.85	+16:18:33.8	M1.0 V	8.482	Binary	
J06217+163	LP 420-6	06:21:44.17	+16:19:19.9	M2.5 V	9.064	Binary	
J06218-227	GJ 2049	06:21:53.08	-22:43:19.7	M1 Vk	7.832		
J06223+334	TYC 2425-1286-1	06:22:20.65	+33:26:54.6	M1.0 V	8.753		
J06236-096	LP 720-10	06:23:38.41	-09:38:51.5	M3.5 V	9.819	Binary	
J06237+020	TYC 141-24-1	06:23:46.49	+05:02:40.1	M1.5 V	8.032		
J06238+456	LP 160-22	06:23:51.20	+45:40:00.0	M5.0 V	10.348	Binary	
J06246+234	Ross 64	06:24:41.93	+23:25:50.8	M4.0 V	8.662		
J06258+561	GJ 3393	06:25:53.21	+56:10:16.9	M4.0 V	10.257		
J06262+238	1R062614.2+234942	06:26:14.52	+23:49:36.4	M1.5 V	8.636		•
J06277+093	Ross 603A	06:27:43.80	+09:23:51.3	M2.0 V	8.269	Binary	
J06293-028	V577Mon	06:29:24.18	-02:49:01.9	M4.5 V	6.376	Binary	
J06298-027	G 108-4	06:29:50.47	-02:47:49.0	M4.0 V	9.468	Binary (SB2)	
J06306+456	PM J06306+4539	06:30:37.39	+45:39:23.0	M1.0 V	8.893		
J06307+397	PM J06307+3947	06:30:47.39	+39:47:38.5	M2.0 V	9.405		
J06310+500	GJ 3395	06:31:00.97	+50:02:45.5	M0.8 V	7.873		
J06318+414	GJ 3396	06:31:50.73	+41:29:42.2	M5.84	9.680		
J06322+378	TYC 2928-1568-1	06:32:14.91	+37:48:10.6	M1.5 V	8.220		
J06323-097	PM J06323-0943	06:32:20.28	-09:43:29.9	M4.5 V	9.848		•
J06325+641	LP 57-192	06:32:31.27	+64:06:12.2	M4.0 V	9.811		
J06345+315	G 103-41	06:34:33.48	+31:30:05.1	M3.5 V	8.705		
J06354-040	1R063531.2-040314	06:35:29.75	-04:03:17.2	M5.5 V	9.272	Binary	
J06361+116	GJ 3398	06:36:06.16	+11:36:49.5	M5.0 V	9.794		
J06361+201	LP 420-4	06:36:12.05	+20:08:10.3	M2.5 V	9.434		
J06371+175	HD 260655	06:37:09.94	+17:33:58.7	M0.0 V	6.674		
J06396-210	LP 780-32	06:39:37.20	-21:01:32.4	dM4.0	8.507	Binary*	
J06400+285	GJ 3399	06:40:05.54	+28:35:10.5	M2.5 V	8.270	Binary	•
J06401-164	LP 780-23	06:40:08.72	-16:27:21.5	M2.5 V	9.121	Binary*	•
J06414+157	Wolf 289	06:41:28.23	+15:45:42.6	M4.0 V	9.570		
J06421+035	GJ 3404	06:42:11.24	+03:34:48.5	M3.0 V	8.166	Binary	
J06422+035	GJ 3405	06:42:13.39	+03:35:26.8	M4.0 V	9.112	Binary	
J06435+166	G 110-14	06:43:34.53	+16:41:35.5	M4.5 V	9.776		•
J06438+511	GJ 3406A	06:43:49.95	+51:08:06.0	M2.5 V	8.361	Binary	
J06447+718	GJ 2050	06:44:45.25	+71:53:06.7	M0.5 V	7.846	Binary	
J06461+325	HD 263175B	06:46:06.88	+32:33:16.6	M1.0 V	8.992	Binary	
J06467+159	1R064645.7+155739	06:46:45.62	+15:57:41.8	M1.0 V	7.923		
J06474+054	G 108-27	06:47:27.57	+05:24:23.3	M4.0 V	9.453		
J06486+532	LP 121-58	06:48:38.72	+53:17:24.3	M1.5 V	8.952		
J06489+211	1R064855.9+210754	06:48:55.18	+21:08:02.8	M2.5 V	9.367		
J06490+371	GJ 1092	06:49:05.73	+37:06:25.0	M4.0 V	9.561		
J06509-091	LP 661-2	06:50:59.37	-09:10:59.3	M3.5 V	9.400		
J06523-051	HD 50281B	06:52:17.42	-05:11:24.3	M2.0 V	6.579	Binary	
J06524+182	GJ 3413	06:52:24.45	+18:17:06.9	M3.5 V	9.052		
J06540+608	GJ 3412	06:54:05.43	+60:52:02.4	M3.0 V	7.128	Binary	
J06548+332	HD 265866	06:54:48.03	+33:15:59.1	M3.0 V	6.104		
J06564+121	TYC 756-1685-1	06:56:25.84	+12:07:31.4	M1.0 V	7.995		
J06564+400	GJ 3416	06:56:28.64	+40:04:58.3	M1.0 V	8.009	Binary	•
J06564+759	LP 34-110	06:53:24.30	+72:55:09.3	M1.0 V	8.918		
J06565+440	G 107-36	06:56:31.24	+44:01:45.0	M4.5 V	9.923		
J06574+740	1R065728.1+740529	06:57:25.77	+74:05:26.1	M4.0 V	8.926		
J06579+623	GJ 3417 A	06:57:57.83	+62:19:11.0	M6.0 V	8.585	Binary	
J06582+511	G 192-59	06:58:12.70	+51:08:32.4	M2.0 V	8.976		•
J06594+193	GJ 1093	06:59:29.84	+19:20:41.5	M5.0 V	9.160		
J06594+195	G 88-2	06:59:28.65	+19:30:30.4	M3.0 V	8.939		
J06596+057	PM J06596+0545	06:59:41.55	+05:45:38.9	M2.5 V	8.947		•
J07001-190	1R070005.1-190115	07:00:07.00	-19:01:25.1	M5.0 V	9.029	Binary (SB2)	

Table B.1: Carmencita, the CARMENES input catalogue (continued).

Karmn	Name	α (2016.0)	δ (2016.0)	Spectral type	J [mag]	Multiplicity[a]	DR1[b]
J07009-023	PM J07009-0221	07:00:59.74	-02:21:32.2	M3.0 V	9.301		
J07012+008	PM J07012+0052	07:01:15.54	+00:52:40.4	M2.5 V	8.794		•
J07033+346	GJ 3423	07:03:23.09	+34:41:53.6	M4.0 V	8.773		
J07034+767	LP 16-379	07:03:29.98	+76:46:21.9	M3.5 V	8.836		
J07039+527	GJ 3421	07:03:56.92	+52:41:51.8	M5.0 V	8.537	Binary	•
J07042-105	Ross 54	07:04:17.55	-10:30:44.6	M3.5 V	7.313	Binary	
J07044+682	GJ 258	07:04:26.94	+68:17:20.5	M3.0 V	8.170		
J07047+249	Ross 874	07:04:49.44	+24:59:50.6	M1.5 V	8.273		
J07051-101	1R070511.2-100801	07:05:12.10	-10:07:51.6	M5.0 V	10.196		•
J07052+084	G 108-52	07:05:12.39	+08:25:45.7	M2.0 V	8.829		
J07076+486	GJ 3426	07:07:37.70	+48:41:08.6	M4.3 V	9.106		
J07078+672	GJ 3425	07:07:49.68	+67:12:03.7	M1.5 V	7.872		
J07081-228	LP 840-16	07:08:06.53	-22:48:51.0	M2.0 V	8.094		
J07086+307	GJ 3429	07:08:39.72	+30:42:51.6	M0.5 V	8.329		
J07095+698	GJ 3427	07:09:31.85	+69:50:53.1	M3.0 V	8.862		
J07100+385	QYAur	07:10:01.23	+38:31:31.0	M4.5 V	6.731	Binary (SB2)	
J07102+376	GJ 3430	07:10:13.32	+37:40:05.9	M4.0 V	10.297	Binary	
J07105-087	1R071032.6-084232	07:10:31.37	-08:42:46.7	M3.5 V	9.054		
J07111+434	LP 206-11	07:11:11.97	+43:29:49.0	M5.5 V	9.979	Binary	
J07119+773	TYC 4530-1414-1	07:11:57.13	+77:21:57.4	M1.5 V	7.723	Binary (SB1)	
J07121+522	GJ 3432	07:12:11.14	+52:16:20.4	M1.0 V	8.118		
J07129+357	1R071259.5+354655	07:12:59.62	+35:47:03.1	M2.5 V	8.834		
J07140+507	G 193-39	07:14:04.29	+50:43:28.9	M0.5 V	8.443	Binary	
J07163+271	GJ 268.3	07:16:19.73	+27:08:29.9	M2.5 V	7.013	Binary	
J07163+331	GJ 1096	07:16:17.89	+33:09:03.4	M5.0 V	9.763		
J07172-050	PM J07172-0501	07:17:17.54	-05:01:09.8	M3.5 V	8.873		
J07174+195	GJ 3437	07:17:29.57	+19:34:12.4	M3.2 V	9.017		
J07181+392	Ross 987	07:18:07.89	+39:16:27.4	M0.0 V	7.209	Binary	
J07182+137	PM J07182+1342	07:18:12.86	+13:42:16.2	M3.5 V	9.361		
J07195+328	GJ 270	07:19:31.79	+32:49:42.8	M0.0 V	7.184		
J07199+840	TYC 4618-116-1	07:19:57.65	+84:04:36.8	M2.5 V	8.305		
J07200-087	Scholz's star	07:20:03.21	-08:46:51.9	M9.5+T5	10.628	Binary	
J07212+005	TYC 178-2187-1	07:31:12.97	+00:33:13.8	M0.5 V	8.305		
J07227+306	GJ 3439	07:22:41.50	+30:40:02.3	M4.0 V	9.506		
J07232+460	GJ 272	07:23:14.71	+46:05:10.9	M0.5 V	7.343		
J07274+052	Luyten's Star	07:27:25.11	+05:12:33.8	M3.5 V	5.714	Binary	
J07274+220	Ross 878	07:27:28.31	+22:02:35.6	M1.5 V	7.818		
J07282-187	GJ 3442	07:28:13.09	-18:47:25.2	M4.5 V	9.049		•
J07287-032	GJ 1097	07:28:45.91	-03:18:05.9	M3.0 V	7.544		
J07295+359	1R072931.4+355607	07:29:31.04	+35:55:58.5	M1.5 V	8.644	Triple	
J07307+481	GJ 275.2 A	07:30:42.46	+48:11:38.2	M4.0 V	9.141	Triple	•
J07310+460	1R073101.9+460030	07:31:01.27	+46:00:24.8	M4.0 V	9.948	Quadruple*	
J07319+362S	LynA	07:31:57.38	+36:13:06.2	M2.5 V	6.771	Triple	
J07319+362N	BLLyn	07:31:56.97	+36:13:43.2	M3.5 V	7.571	Triple	
J07319+392	GJ 3445	07:31:56.74	+39:13:34.0	M2.48 V	9.164		•
J07320+173E	GJ 3447	07:32:02.63	+17:19:07.0	M0.0 V	8.169	Triple	
J07320+173W	GJ 3448	07:32:01.87	+17:19:09.4	M3.2 V	9.739	Triple	
J07320+686	GJ 9235	07:32:01.51	+68:37:13.6	M1.5 V	7.745		
J07325+248	G 88-37	07:32:30.71	+24:53:42.4	M3.0 V	8.987		
J07342+009	GJ 1099	07:34:17.57	+00:58:59.7	M2.5 V	8.261		
J07344+629	GJ 9236	07:34:26.27	+62:56:27.6	M0.5 V	7.340		
J07346+223	GJ 3453	07:34:39.31	+22:20:13.9	M1.0 V	8.362		
J07346+318	Castor C	07:34:37.19	+31:52:08.6	M0.5 V	6.073	Sextuple (EB/DESB2)	
J07349+147	TYC 777-141-1	07:34:56.25	+14:45:52.5	M3.0 V	7.287	Binary	
J07353+548	GJ 3452	07:35:21.67	+54:50:59.2	M2.5 V	7.772		
J07354+482	LP 162-39	07:35:26.96	+48:14:33.0	M1.0 V	8.620		
J07359+785	LP 17-66	07:35:57.31	+78:32:49.7	M3.0 V	9.214		•
J07361-031	GJ 282 C	07:36:07.15	-03:06:43.4	M1.0 V	6.791	Quadruple (SB1)	
J07364+070	GJ 3454	07:36:25.37	+07:04:38.2	M4.5 V	8.180	Binary	

Table B.1: Carmencita, the CARMENES input catalogue (continued).

Karmn	Name	α (2016.0)	δ (2016.0)	Spectral type	J [mag]	Multiplicity[a]	DR1[b]
J07365-006	PM J07365-0039	07:36:30.27	-00:39:37.3	M3.5 V	9.422		•
J07366+440	G 111-20	07:36:39.13	+44:04:43.5	M3.5 V	9.961	Binary	
J07383+344	TYC 2461-826-1	07:38:19.92	+34:27:00.6	M0.0 V	8.485		
J07384+240	1R073829.3+240014	07:38:29.32	+24:00:07.1	M3.5 V	8.928		
J07386-212	GJ 3459	07:38:41.48	-21:13:36.1	dM3.0	7.848		
J07393+021	Ross 880	07:39:22.88	+02:10:57.3	M0.0 V	6.769		
J07395+334	GJ 3457	07:39:35.62	+33:27:42.6	M2.0 V	8.420	Binary	•
J07403-174	GJ 283 B	07:40:20.66	-17:24:54.5	M6.5 V	10.155	Binary	•
J07418+050	GJ 3461	07:41:52.56	+05:02:23.1	M3.0 V	8.910	Triple (SB2)	
J07421+500	LP 162-55	07:42:10.07	+50:04:28.5	M2.5 V	8.455		•
J07431+181	GJ 3462	07:43:11.67	+18:10:34.8	M1.5 V	8.117		
J07446+035	YZCMi	07:44:39.80	+03:33:01.7	M4.0 V	6.581		
J07467+574	G 193-65	07:46:41.97	+57:26:49.5	M4.5 V	9.699		
J07470+760	LP 17-75	07:47:06.48	+76:03:13.1	M4.0 V	9.976		•
J07472+503	1R074714.1+502032	07:47:13.84	+50:20:39.8	M4.0 V	8.855		
J07482+203	Wolf 1421	07:48:18.04	+20:21:49.4	M1.5 V	8.120		
J07493+849	GJ 3456	07:49:17.72	+84:58:32.5	M3.0 V	8.988		•
J07497-033	PM J07497-0320	07:49:41.97	-03:20:34.9	M3.5 V	8.891		
J07518+055	GJ 3463	07:51:51.86	+05:32:50.6	M5.0 V	9.966		
J07519-000	GJ 1103 A	07:51:54.95	-00:00:24.4	M4.5 V	8.496		
J07523+162	LP 423-31	07:52:24.13	+16:12:09.4	M6.0 V	10.879		
J07545+085	1R075434.3+083213	07:54:33.90	+08:32:25.5	M2.5 V	8.538	Binary (SB1)	
J07525+063	GJ 3465	07:52:33.63	+06:18:22.0	M3.0 V	9.608		
J07545-096	PM J07545-0941	07:54:32.60	-09:41:47.9	M3.5 V	9.697	Binary	
J07558+833	GJ 1101	07:55:51.23	+83:22:55.4	M4.5: V	8.744		
J07581+072	GJ 3467	07:58:08.74	+07:17:00.9	M5.0 V	9.272		
J07582+413	GJ 1105	07:58:13.01	+41:18:02.3	M3.5 V	7.734		•
J07583+496	LP 163-47	07:58:23.26	+49:39:41.3	M4.0 V	8.706		
J07585+155N	GJ 3468	07:58:30.88	+15:30:12.6	M4.5 V	9.970	Triple	•
J07585+155S	GJ 3469 A	07:58:30.37	+15:29:58.8	M4.5 V	10.429	Triple	
J07590+153	GJ 3470	07:59:05.63	+15:23:28.3	M2.0 V	8.794		
J07591+173	1R075908.2+171957	07:59:07.07	+17:19:46.8	M4.0 V	9.468		
J08005+258	TYC 1930-667-1	08:00:34.87	+25:53:32.6	M2.0 V	8.204		
J08017+237	TYC 1926-794-1	08:01:43.44	+23:42:25.3	M1.5 V	7.670		
J08023+033	GJ 3473	08:02:22.45	+03:20:13.6	M4.0 V	9.627	Binary	
J08025-130	LP 724-16	08:02:33.09	-13:05:33.4	M2.5 V	9.421		
J08031+203	PM J08031+2022	08:03:10.06	+20:22:14.3	M3.5 V	9.242	Binary	•
J08033+528	G 194-7	08:03:20.18	+52:50:27.3	M1.5 V	8.058	Binary	
J08066+558	GJ 3477	08:06:36.75	+55:53:37.1	M2.0 V	8.050	Binary	
J08068+367	GJ 3479	08:06:48.21	+36:45:32.5	M3.0 V	8.976		
J08069+422	G 111-56	08:06:54.99	+42:17:28.7	M4.0 V	9.724		
J08082+211	GJ 3482	08:08:12.85	+21:06:12.6	M3.0 V	6.860	Triple	
J08083+585	GJ 3480	08:08:17.82	+58:31:08.4	M3.0 V	8.804		
J08089+328	FPCncB	08:08:55.38	+32:49:01.4	M3.0 V	7.999	Quadruple (SB2)	
J08095+219	GJ 3484	08:09:30.59	+21:54:16.2	M2.0 V	8.332		
J08103+095	PM J08103+0935	08:10:20.65	+09:35:15.4	M2.5 V	8.382		
J08105-138	HD 68146B	08:10:34.02	-13:48:50.1	M2.5 V	8.276	Binary	
J08108+039	GJ 3485	08:10:53.75	+03:58:28.2	M4.0 V	9.238		
J08117+531	G 194-14	08:11:47.07	+53:11:48.4	M2.5 V	9.293		
J08119+087	Ross 619	08:11:58.72	+08:45:01.4	M4.5 V	8.424		
J08126-215	GJ 300	08:12:40.90	-21:33:18.1	M3.5 V	7.601		
J08158+346	LP 311-8	08:15:53.78	+31:36:35.8	M1.0 V	8.935		•
J08161+013	GJ 2066	08:16:07.58	+01:18:10.2	M2.0 V	6.625		•
J08175+209	LP 367-67	08:17:31.31	+20:59:48.7	M2.5 V	8.989		
J08178+311	GJ 3491	08:17:51.20	+31:07:49.4	M1.0 V	7.943		•
J08202+055	PM J08202+0532	08:20:13.29	+05:32:08.2	M2.0 V	8.526		
J08258+690	GJ 3497	08:25:50.76	+69:01:40.7	M7.0 V	10.078		
J08282+201	GJ 1110	08:28:12.37	+20:08:11.4	M4.0 V	9.397		
J08283+350	GJ 308	08:28:20.83	+35:00:53.6	M0.0 V	7.633	Binary	

Table B.1: Carmencita, the CARMENES input catalogue (continued).

Karmn	Name	α (2016.0)	δ (2016.0)	Spectral type	J [mag]	Multiplicity[a]	DR1[b]
J08283+553	PM J08283+5522	08:28:18.75	+55:22:40.6	M2.5 V	9.235		
J08286+660	1R082839.4+660229	08:28:41.33	+66:02:25.4	M4.0 V	9.197	Binary	
J08293+039	PM J08293+0355E	08:29:21.81	+03:55:08.2	M2.5 V	7.932		
J08298+267	DXCnc	08:29:48.02	+26:46:23.8	M6.5 V	8.235		
J08313-060	GJ 3501	08:31:21.14	-06:02:02.8	M2.0 V	7.998	Triple	•
J08314-060	GJ 3502	08:31:26.75	-06:02:13.6	M3.0 V	8.716	Triple	•
J08313-104	GJ 3503	08:31:22.81	-10:29:58.9	M4.0 V	10.070		
J08315+730	LP 35-219	08:31:32.36	+73:03:50.1	M4.0 V	8.780		
J08316+193S	CUCnc	08:31:37.32	+19:23:37.5	M3.5 V	7.509	Quintuple (EB)	
J08316+193N	CCncA	08:31:37.17	+19:23:47.6	M4.0 V	8.625	Quintuple	•
J08317+057	1R083147.3+054504	08:31:47.89	+05:45:17.0	M1.0 V	8.915		
J08321+844	GJ 3496	08:32:13.99	+84:24:34.8	M3.5 V	9.441		
J08325+451	Wolf 312	08:32:35.78	+45:10:16.3	M2.5 V	8.880		
J08334+185	GJ 3505	08:33:25.06	+18:31:34.9	M4.5 V	10.263		
J08344-011	GJ 2070	08:34:26.13	-01:08:46.3	M3.0 V	8.810		
J08353+141	LSPM J0835+1408	08:35:19.75	+14:08:31.9	M4.5 V	9.163	Triple (ST3)	
J08358+680	GJ 3506	08:35:46.65	+68:04:00.1	M3.0 V	7.861		
J08364+264	LP 311-37	08:36:26.45	+26:28:18.9	M2.0 V	8.964	Binary	
J08364+672	GJ 310	08:36:22.51	+67:17:42.9	M0.5 V	6.425	Binary	•
J08371+151	GJ 3508	08:37:07.82	+15:07:31.2	M3.0 V	8.122		
J08375+035	LSPM J0837+0333	08:37:30.28	+03:33:43.1	M4.0 V	9.853		
J08387+516	StKM 1-711	08:38:42.06	+51:41:31.9	M1.5 V	8.695		
J08398+089	GJ 3510	08:39:47.80	+08:56:21.0	M2.0 V	9.470	Binary	
J08402+314	LSPM J0840+3127	08:40:16.24	+31:27:08.7	M3.5 V	8.122		
J08404+184	AZCnc	08:40:28.77	+18:24:01.5	M6.0 V	11.053		
J08409-234	GJ 317	08:40:58.67	-23:27:09.7	M3.5 V	7.934		•
J08410+676	GJ 3509	08:41:01.83	+67:39:33.1	M4.0 V	10.290		
J08413+594	GJ 3512	08:41:19.58	+59:29:30.0	dM5.5	9.615		•
J08427+095	GJ 319 A	08:42:44.77	+09:33:14.0	M0.0 V	6.687	Quadruple (SB1)	
J08428+095	GJ 319 C	08:42:52.47	+09:33:01.3	M2.5 V	8.122	Quadruple	•
J08443-104	GJ 3513	08:44:22.71	-10:24:20.1	M3.5 V	9.799		
J08447+182	G 9-19	08:44:45.08	+18:12:59.2	M3.5 V	8.942		
J08449-066	PM J08449-0637	08:44:55.59	-06:37:28.2	M3.5 V	9.325	Binary	
J08517+181	Ross 622	08:51:42.78	+18:07:29.1	M1.5 V	8.281		
J08526+283	GJ 324 B	08:52:40.28	+28:18:54.9	M4.5 V	8.560	Binary	
J08531-202	PM J08531-2017	08:53:10.96	-20:17:19.3	M3.0 V	9.323		
J08536-034	GJ 3517	08:53:35.61	-03:29:35.4	M9.0 V	11.212		•
J08537+149	StKM 1-730	08:53:43.67	+14:58:09.7	M0.0 V	8.165		
J08540-131	GJ 326 A	08:54:05.69	-13:07:39.9	M2.5 V	8.048	Binary	•
J08551+015	Ross 623	08:55:07.67	+01:32:30.7	M0.0 V	7.191		
J08555+664	PM J08555+6628	08:55:31.46	+66:28:06.6	M3.0 V	8.824		
J08563+126	G 41-8	08:56:19.49	+12:39:45.8	M6.0 V	9.585	Binary	
J08570+116	GJ 330	08:57:04.65	+11:38:43.9	M1.0 V	7.311	Binary	
J08572+194	LP 426-35	08:57:15.55	+19:24:15.2	M3.5 V	9.447		
J08582+197	GJ 1116 A	08:58:14.09	+19:45:45.3	M5.5 V	7.791	Binary	
J08588+210	G 41-13	08:58:52.53	+21:04:29.1	M2.0 V	10.058		
J08595+537	G 194-47	08:59:35.41	+53:43:47.5	M3.5 V	9.014	Binary	
J08589+084	GJ 3522	08:58:56.73	+08:28:20.8	M3.5 V	6.507	Binary	
J08599+729	GJ 3520	08:59:59.70	+72:57:35.8	M5.0 V	9.731		
J09003+218	LP 368-128	09:00:22.95	+21:49:55.4	M6.5 V	9.436		
J09005+465	GJ 1119	09:00:31.74	+46:35:02.7	M4.5 V	8.604		
J09008+052W	Ross 686	09:00:48.25	+05:14:38.1	M3.0 V	8.605	Binary	•
J09008+052E	Ross 687	09:00:50.05	+05:14:26.3	M3.0 V	8.845	Binary	•
J09011+019	Ross 625	09:01:10.07	+01:56:33.7	M3.0 V	7.932	Triple	
J09023+084	GJ 3528	09:02:20.55	+08:28:03.3	M3.0 V	8.145		
J09023+177	PM J09023+1746	09:02:22.91	+17:46:31.8	M4.0 V	9.645		
J09028+680	GJ 3526	09:02:53.41	+68:03:52.1	M4.0 V	8.453		
J09029+716	LSPM J0902+7138	09:02:55.82	+71:38:11.0	M1.5 V	9.731		
J09033+056	LP 546-37	09:03:20.91	+05:40:08.5	M7.0 V	10.766		•

Table B.1: Carmencita, the CARMENES input catalogue (continued).

Karmn	Name	α (2016.0)	δ (2016.0)	Spectral type	J [mag]	Multiplicity[a]	DR1[b]
J09037+520	G 194-52	09:03:43.39	+52:02:49.1	M3.5 V	8.964		•
J09038+129	LP 486-43	09:03:53.41	+12:59:24.8	M2.0 V	8.919		•
J09040-159	1R090406.8-155512	09:04:05.44	-15:55:19.0	M2.5 V	9.156	Binary*	
J09050+028	GJ 3530	09:05:04.11	+02:50:03.9	M1.5 V	8.177	Binary	
J09057+186	LP 426-56	09:05:43.02	+18:36:27.6	M2.5 V	8.957		
J09062+128	GJ 3531	09:06:13.79	+12:51:30.1	M3.5 V	9.243		
J09070-221	GJ 3533	09:07:02.40	-22:08:56.6	M4.5 V	9.533		
J09087+665	GJ 3532	09:08:46.58	+66:35:36.4	M2.5 V	9.168		
J09091+227	2M09090798+2247413	09:09:07.88	+22:47:40.1	M4.5 V	10.474		
J09093+401	GJ 1121	09:09:23.06	+40:05:55.5	M4.0 V	10.135		
J09095+328	GJ 336	09:09:30.18	+32:48:59.1	M0.5 V	7.035	Binary	
J09096+067	GJ 3537	09:09:39.07	+06:42:11.8	M3.0 V	9.294		
J09099+004	G 46-24	09:09:59.43	+00:23:39.5	M1.0 V	8.892		
J09115+126	LP 487-10	09:11:32.14	+12:37:18.3	M2.5 V	9.408		
J09115+466	GJ 336.1	09:11:30.27	+46:37:00.7	M0.5 V	7.900		
J09120+279	GJ 3540	09:12:02.44	+27:54:16.2	M3.0 V	8.430	Binary (SB2)	
J09133+688	G 234-57A	09:13:23.43	+68:52:27.1	M2.5 V	7.775	Binary	
J09140+196	LP 427-16	09:14:03.02	+19:40:03.2	M3.0 V	8.424	Binary (SB1)	
J09143+526	HD 79210	09:14:20.05	+52:41:02.7	M0.0 V	4.889	Triple (SB1)	•
J09144+526	HD 79211	09:14:21.91	+52:41:00.3	M0.0 V	4.779	Triple	•
J09156-105	G 161-7	09:15:35.96	-10:35:50.2	M5.0 V	8.605	Binary	•
J09160+293	G 47-31	09:16:05.04	+29:19:36.3	M2.0 V	8.915		•
J09161+018	RX J0916.1+0153	09:16:10.24	+01:53:07.2	M4.0 V	8.770		
J09163-186	GJ 3543	09:16:20.29	-18:37:30.6	M1.5 V	7.351		
J09165+841	GJ 3536	09:16:24.75	+84:11:06.4	M1.5 V	8.618		•
J09168+248	2M09165078+2448559	09:16:50.70	+24:48:54.0	M4.5 V	10.466		•
J09177+462	RX J0917.7+4612	09:17:44.52	+46:12:24.4	M2.5 V	8.126	Binary	
J09177+584	GJ 3542	09:17:46.04	+58:25:02.7	M5.0 V	10.261		
J09187+267	GJ 3548	09:18:45.99	+26:45:05.4	M1.5 V	8.296	Binary	
J09193+385S	GJ 1122	09:19:18.62	+38:31:15.9	M5.0 V	9.924	Binary	
J09193+385N	G 115-69	09:19:18.71	+38:31:23.3	M5.0 V	10.048	Binary	
J09193+620	GJ 3547	09:19:22.21	+62:03:10.7	M1.0 V	8.168	Binary (EB/SB2)	
J09200+308	TYC 2493-1386-1	09:20:00.38	+30:52:39.1	M1.5 V	8.309	Triple	
J09201+037	1R092010.8+034731	09:20:10.74	+03:47:27.0	M3.5 V	9.310		
J09209+033	GJ 3553	09:20:58.28	+03:21:48.3	M4.0 V	9.363		
J09213+731	GJ 3550	09:21:16.03	+73:06:33.1	M5.0 V	10.365		
J09218+435	GJ 3554	09:21:48.61	+43:30:26.5	M4.5 V	9.431	Binary	
J09218-023	RAVE J092148.1-021943	09:21:48.32	-02:19:43.2	M2.5 V	8.441		
J09228+467	G 115-72	09:22:51.31	+46:46:58.8	M1.0 V	8.533	Binary	
J09231+223	BD+22 2086B	09:23:06.01	+22:18:25.6	M0.0 V	8.497	Binary	
J09238+001	GJ 3555	09:23:52.36	+00:08:13.8	M1.0 V	8.506		
J09248+306	LSPM J0924+3041	09:24:50.68	+30:41:34.2	M3.5 V	9.490		
J09256+634	G 235-25	09:25:39.51	+63:29:14.9	M4.5 V	9.818	Binary	
J09275+506	GJ 3556	09:27:30.19	+50:39:10.1	M2.5 V	8.481		
J09286-121	LP 727-31	09:28:41.63	-12:10:02.0	M2.5 V	8.837		
J09288-073	Ross 439	09:28:53.16	-07:22:27.2	M2.5 V	8.446	Binary	
J09289-073	GJ 347 B	09:28:55.53	-07:22:23.3	M4.5 V	10.370	Binary	
J09291+259	LP 370-26	09:29:09.83	+25:58:05.0	M5.0 V	10.906		
J09300+396	GJ 3558	09:30:01.84	+39:37:21.1	M2.5 V	8.467		
J09302+265	LSPM J0930+2630	09:30:14.24	+26:30:22.7	M3.0 V	8.866		
J09307+003	GJ 1125	09:30:43.98	+00:19:12.8	M3.5 V	7.697		
J09308+024	1R093051.2+022741	09:30:50.81	+02:27:21.5	M4.0 V	9.415		
J09313-134	Ross 440	09:31:20.26	-13:29:18.9	M3.0 V	6.361	Binary	•
J09315+202	Ross 84	09:31:33.05	+20:16:43.6	M2.0 V	8.783		
J09319+363	GJ 353	09:31:56.06	+36:19:04.4	M0.0 V	7.121		
J09328+269	HD 82443B	09:32:48.07	+26:59:39.9	M5.5 V	10.356	Binary	
J09352+612	GJ 3560	09:35:13.45	+61:14:37.6	M2.5 V	8.463		
J09360-061	GJ 3561	09:36:04.10	-06:07:01.2	M3.5 V	9.854		
J09360-216	GJ 357	09:36:01.80	-21:39:54.7	M2.5 V	7.337		

Table B.1: Carmencita, the CARMENES input catalogue (continued).

Karmn	Name	α (2016.0)	δ (2016.0)	Spectral type	J [mag]	Multiplicity[a]	DR1[b]
J09362+375	GJ 9303	09:36:04.14	+37:33:08.9	M0.0 V	8.085	Triple (SB2)	
J09370+405	GJ 3562	09:37:03.29	+40:34:37.7	M3.8 V	9.766		•
J09394+146	LP 428-20	09:39:29.77	+14:38:48.5	M3.5 V	9.393		
J09394+317	G 117-34	09:39:24.04	+31:45:13.7	M1.5 V	8.486	Binary	
J09410+220	Ross 92	09:41:02.58	+22:01:20.5	M4.5 V	9.627		
J09411+132	Ross 85	09:41:09.64	+13:12:32.1	M1.5 V	6.971		
J09423+559	GJ 363	09:42:21.84	+55:58:53.1	M3.0 V	8.374		
J09425+700	GJ 360	09:42:32.74	+70:01:57.6	M2.5 V	6.917	Binary	•
J09428+700	GJ 362	09:42:49.63	+70:02:17.6	M3.5 V	7.326	Binary	•
J09425-192	GJ 3563	09:42:35.14	-19:14:08.6	M2.5 V	8.298		
J09430+237	LP 370-35	09:43:01.12	+23:49:18.3	M1.0 V	8.994	Triple	•
J09439+269	Ross 93	09:43:54.92	+26:58:06.8	M3.5 V	8.035		•
J09447-182	GJ 1129	09:44:45.55	-18:12:51.7	M3.5 V	8.122		
J09449-123	G 161-71	09:44:53.83	-12:20:53.7	M5.0 V	8.496		•
J09461-044	GJ 3566	09:46:08.66	-04:25:40.6	M4.0 V	9.688	Binary	•
J09468+760	Ross 434	09:46:48.87	+76:02:22.1	M1.5 V	7.437		•
J09473+263	Ross 94	09:47:22.15	+26:18:06.9	M0.0 V	8.141		
J09475+129	GJ 3568	09:47:34.71	+12:56:42.8	M4.0 V	9.267		•
J09506-138	LP 728-70	09:50:40.70	-13:48:40.2	M4.0 V	8.579	Binary (SB2)	
J09488+156	G 43-2	09:48:50.18	+15:38:48.5	M3.0 V	9.303		
J09511-123	GJ 369	09:51:10.88	-12:20:10.8	dM0.5	6.988		
J09526-156	LP 728-71	09:52:41.65	-15:36:15.9	M3.5 V	9.320		
J09527+554	G 195-43	09:52:45.26	+55:28:16.2	M1.5 V	8.989	Binary	•
J09531-036	GJ 372	09:53:11.67	-03:41:31.8	M2.0 V	6.998	Binary (SB2)	
J09535+507	LP 126-73	09:53:32.64	+50:45:04.2	M1.5 V	8.733		
J09539+209	GJ 3571	09:53:54.78	+20:56:53.1	M4.0 V	9.208		
J09557+353	Wolf 330	09:55:43.55	+35:21:36.8	M3.5 V	8.850		
J09561+627	GJ 373	09:56:07.96	+62:47:09.1	M0.5 V	6.030	Binary (SB?)	
J09564+226	GJ 3573	09:56:26.42	+22:38:56.9	M4.0 V	9.621		
J09579+118	GJ 3576	09:57:57.54	+11:48:26.3	M4.0 V	10.092	Binary*	•
J09587+555	G 196-1	09:58:46.62	+55:32:59.0	M1.0 V	8.899		
J09589+059	LP 549-6	09:58:56.31	+05:57:58.8	M4.5 V	9.937		
J09593+438W	GJ 3577	09:59:18.65	+43:50:21.9	M3.5 V	9.682	Binary	
J09593+438E	GJ 3578	09:59:20.78	+43:50:22.1	M5.0 V	9.917	Binary	
J09597+472	GJ 3579	09:59:46.11	+47:12:06.9	M4.0 V	9.756		
J09597+721	PM J09597+7211	09:59:45.30	+72:12:01.3	M3.5 V	9.059		
J10004+272	GJ 375.2	10:00:26.69	+27:16:03.5	M0.5 V	8.382	Triple*	
J10007+323	Wolf 335	10:00:43.01	+32:18:23.1	M1.0 V	8.780		
J10020+697	LP 37-57	10:02:05.67	+69:45:25.6	M4.0 V	9.768		
J10023+480	GJ 378	10:02:20.74	+48:04:56.1	M1.0 V	6.949		
J10027+149	GJ 3582	10:02:42.62	+14:59:09.2	M4.61	9.649		
J10028+484	G 195-55	10:02:48.79	+48:27:28.7	M5.5 V	9.963	Binary	•
J10035+059	GJ 3583	10:03:32.76	+05:57:45.4	M3.5 V	9.290		
J10040+187	GJ 9312	10:04:05.80	+18:47:41.5	M0.5 V	8.365	Binary	
J10043+503	G 196-3	10:04:21.23	+50:23:10.1	M2.5 V	8.081	Binary	
J10067+417	GJ 3585	10:06:43.45	+41:42:46.1	M1.0 V	8.209		
J10068-127	PM J10068-1246	10:06:51.98	-12:46:54.3	M4.5 V	9.749		
J10069+126	LP 489-35	10:06:57.49	+12:40:51.6	M1.5 V	8.776		
J10079+692	GJ 1131	10:07:56.60	+69:14:46.1	M4.0 V	10.096		
J10087+027	LP 549-23	10:08:44.52	+02:43:49.6	M3.0 V	8.590		
J10087+355	Wolf 346	10:08:42.37	+35:32:51.3	M1.5 V	9.167		
J10088+692	TYC 4384-1735-1	10:08:52.40	+69:16:35.8	M0.5 V	8.711		
J10094+512	GJ 3586	10:09:29.22	+51:17:06.4	M4.65	9.299		
J10094+544	PM J10094+5424	10:09:26.88	+54:24:22.5	M2.0 V	8.644		•
J10120-026	GJ 381	10:12:05.23	-02:41:14.8	M2.5 V	7.021	Binary	
J10117+353	Wolf 351	10:11:44.11	+35:18:40.1	M4.0 V	10.112		
J10122-037	ANSex	10:12:17.50	-03:44:48.3	M1.5 V	5.888		
J10125+570	LP 92-48	10:12:34.10	+57:03:40.5	M3.5 V	7.759		
J10130+233	G 54-18	10:13:00.45	+23:20:45.9	M3.5 V	9.194	Binary	•

Table B.1: Carmencita, the CARMENES input catalogue (continued).

Karmn	Name	α (2016.0)	δ (2016.0)	Spectral type	J [mag]	Multiplicity[a]	DR1[b]
J10143+210	DKLeo	10:14:19.03	+21:04:26.8	M0.5 V	7.074	Binary	•
J10133+467	LP 167-17	10:13:20.56	+46:47:24.5	M5.5 V	10.873		
J10148+213	G 54-19	10:14:52.91	+21:23:42.5	M4.5 V	9.725		
J10151+314	GJ 3590	10:15:06.87	+31:25:07.0	M4.0 V	9.326	Binary	
J10155-164	PM J10155-1628E	10:15:34.86	-16:28:20.4	M4.0 V	9.363		
J10158+174	LSPM J1015+1729	10:15:54.26	+17:29:27.2	M3.5 V	8.696		
J10167-119	GJ 386	10:16:45.49	-11:57:52.1	dM3.0	7.323		
J10182-204	LP 790-2	10:18:13.39	-20:28:39.3	M4.5 V	8.999	Triple (SB2)	
J10185-117	LP 729-54	10:18:34.77	-11:43:04.2	M4.0 V	9.007	Binary	•
J10196+198	ADLeo	10:19:35.72	+19:52:11.3	M3.0 V	5.449		•
J10200+289	G 118-51	10:20:00.23	+28:57:09.5	M3.0 V	9.159		•
J10206+492	GJ 3595	10:20:37.15	+49:17:43.2	M3.0 V	9.396		•
J10238+438	LP 212-62	10:23:52.13	+43:53:33.2	M5.0 V	10.039		
J10240+366	PM J10240+3639	10:24:05.04	+36:39:30.2	M3.5 V	9.429		
J10243+119	GJ 3598	10:24:20.16	+11:57:23.5	M2.5 V	8.847	Binary	
J10251-102	GJ 390	10:25:10.09	-10:13:41.3	M1.0 V	6.895		
J10255+263	GJ 3599	10:25:29.93	+26:23:09.8	M3.0 V	9.030		
J10260+504W	GJ 3600	10:26:01.99	+50:27:00.0	M4.0 V	9.268	Binary	•
J10260+504E	GJ 3601	10:26:02.64	+50:27:13.0	M4.0 V	9.404	Binary	
J10273+799	PM J10273+7959	10:27:22.67	+79:59:50.0	M2.0 V	8.669		
J10278+028	G 44-19	10:27:49.12	+02:51:35.5	M3.5 V	9.438		
J10284+482	GJ 3602	10:28:28.86	+48:14:17.7	M3.5 V	9.055	Binary*	
J10286+322	GJ 3604	10:28:40.73	+32:14:21.7	M2.5 V	9.043	Binary	
J10289+008	Ross 446	10:28:54.91	+00:50:15.9	dM2	6.176		
J10303+328	GJ 3607	10:30:23.19	+32:50:07.3	M3.0 V	8.867		
J10315+570	GJ 397.1 B	10:31:30.64	+57:05:20.4	M5.0 V	9.738	Triple	•
J10320+033	PM J10320+0318	10:32:02.31	+03:18:54.9	M2.0 V	8.365		
J10345+463	GJ 3610	10:34:29.53	+46:18:07.2	M3.0 V	9.195	Binary	
J10350-094	LP 670-17	10:35:01.36	-09:24:41.5	dM3.0	8.276		
J10354+694	GJ 3612	10:35:21.96	+69:26:48.5	M4.0 V	7.898	Binary (SB2)	
J10359+288	RX J1035.9+2853	10:35:57.12	+28:53:30.3	M3.0 V	9.245		•
J10360+051	RYSex	10:36:00.52	+05:07:14.8	M4.0 V	8.463		•
J10364+415	G 146-48	10:36:27.19	+41:30:02.8	M2.5 V	8.647	Binary	
J10367+153	PM J10367+1521A	10:36:44.96	+15:21:38.6	M3.5 V	8.748	Triple	•
J10368+509	LP 127-502	10:36:48.58	+50:55:00.7	M4.5 V	9.866	Binary (SB2?)	
J10379+127	LP 490-42 A	10:37:55.03	+12:46:37.6	M3.0 V	8.730	Binary	
J10384+485	GJ 3613	10:38:29.47	+48:31:43.4	M3.0 V	9.495		
J10385+354	LP 262-400	10:38:32.66	+35:29:53.7	M2.5 V	8.676		
J10389+250	StKM 1-873	10:38:56.64	+25:05:39.0	M2.0 V	8.982		
J10396-069	GJ 399	10:39:39.79	-06:55:27.2	dM2.5	7.664		
J10403+015	TYC 254-88-1	10:40:21.42	+01:34:36.6	M1.0 V	8.787		
J10416+376	GJ 1134	10:41:35.91	+37:36:33.4	M4.0 V	8.493		•
J10430-092	PM J10430-0912	10:43:00.72	-09:12:35.0	M5.5 V	9.667	Binary	
J10443+124	LP 490-63	10:44:18.52	+12:25:11.5	M3.5 V	9.422		•
J10448+324	GJ 3616 A	10:44:52.40	+32:24:41.3	M3.0 V	9.494	Triple	
J10453+385	GJ 400 A	10:45:21.43	+38:30:44.8	M0.5 V	6.354	Binary	
J10456-191	GJ 401	10:45:36.98	-19:07:01.3	M0.5 V	8.069	Binary	
J10460+096	GJ 3619	10:46:03.81	+09:41:47.1	M3.5 V	9.441		
J10472+404	LP 213-67	10:47:12.19	+40:26:43.2	M6.5 V	11.384	Triple	
J10474+025	Ross 895	10:47:24.47	+02:35:32.7	M2.0 V	8.878	Binary	
J10482-113	GJ 3622	10:48:13.24	-11:20:34.1	M6.5 V	8.857		
J10485+191	GJ 3623	10:48:32.84	+19:09:00.3	M3.0 V	9.491		
J10497+355	GJ 1138	10:49:44.71	+35:32:34.3	M5.0 V	8.537	Binary	•
J10504+331	GJ 3626	10:50:26.08	+33:05:54.0	M3.5 V	8.899	Binary (SB1)	
J10506+517	GJ 3628	10:50:37.91	+51:45:01.6	M4.1 V	9.828	Binary	
J10508+068	EELeo	10:50:51.11	+06:48:16.2	M4.0 V	7.319	Binary	•
J10513+361	GJ 3629	10:51:20.33	+36:07:24.5	M3.0 V	9.422	Binary	
J10520+005	GJ 3630	10:52:02.83	+00:32:38.5	M4.0 V	9.426	Triple (ST3/SQ4)	•
J10520+139	GJ 403	10:52:03.01	+13:59:54.5	M4.0 V	8.607		

Table B.1: Carmencita, the CARMENES input catalogue (continued).

Karmn	Name	α (2016.0)	δ (2016.0)	Spectral type	J [mag]	Multiplicity[a]	DR1[b]
J10522+059	GJ 3631	10:52:13.50	+05:55:08.9	M5.5 V	9.834		
J10546-073	LP 671-8	10:54:41.77	-07:18:39.4	M4.0 V	8.877	Binary	
J10555-093	GJ 3632	10:55:34.19	-09:21:18.7	M3.5 V	9.419		
J10563+042	PM J10563+0415	10:56:22.32	+04:15:44.6	M2.5 V	9.179		
J10564+070	CNLeo	10:56:24.77	+07:00:09.8	M6.0 V	7.085		
J10576+695	Ross 447	10:57:36.16	+69:35:48.8	M0.0 V	7.514		
J10584-107	LP 731-76	10:58:27.78	-10:46:31.8	M5.0 V	9.512		•
J11000+228	Ross 104	11:00:03.76	+22:49:54.1	M2.5 V	6.314		
J11003+728	G 254-11A	11:00:23.29	+72:52:17.6	M2.0 V	8.934	Binary	•
J11008+120	GJ 3636	11:00:50.58	+12:04:08.7	M5.5 V	10.676		•
J11013+030	GJ 3637	11:01:20.81	+03:00:10.8	M5.0 V	9.708		
J11014+568	StKM 1-902	11:01:26.72	+56:52:04.0	M1.0 V	8.994		
J11023+165E	GJ 1141 A	11:02:19.29	+16:30:27.1	M1.0 V	8.270	Binary	
J11023+165W	GJ 1141 B	11:02:18.02	+16:30:30.8	M1.0 V	8.353	Binary	
J11026+219	DSLeo	11:02:38.51	+21:58:00.9	M1.0 V	6.522		
J11030+037	Wolf 360	11:03:04.39	+03:44:19.2	M2.5 V	9.307		
J11031+152	LP 431-50	11:03:08.01	+15:17:50.3	M3.5 V	8.890		•
J11031+366	GJ 3639	11:03:09.74	+36:39:09.1	M3.5 V	9.464		
J11033+359	HD 95735	11:03:19.43	+35:56:55.2	M1.5 V	4.203		
J11036+136	LP 491-51	11:03:21.05	+13:37:58.2	M4.0 V	8.759	Binary (SB1)	
J11042+400	GJ 3640	11:04:15.64	+40:00:15.1	M0.0 V	8.025		•
J11044+304	LSPM J1104+3027	11:04:28.35	+30:27:30.9	M3.0 V	10.929		
J11054+435	GJ 412 A	11:05:22.09	+43:31:51.4	M1.0 V	5.538	Binary	
J11055+435	WXUMa	11:05:24.50	+43:31:33.3	M5.5 V	8.742	Binary	•
J11055+450	GJ 3641	11:05:33.91	+45:00:27.9	M0.0 V	8.107	Binary	•
J11057+102	GJ 3643	11:05:43.80	+10:13:58.1	M3.0 V	8.643		•
J11075+437	PM J11075+4345	11:07:31.88	+43:45:56.3	M3.0 V	9.941		
J11081-052	GJ 1142 A	11:08:06.48	-05:13:54.2	M3.0 V	8.797	Binary	
J11108+479	GJ 3646	11:10:51.05	+47:56:53.7	M4.0 V	10.082		
J11110+304E	HD 97101	11:11:05.90	+30:26:42.5	K7 V	5.764	Binary	
J11110+304W	HD 97101B	11:11:03.29	+30:26:38.0	M2.0 V	6.592	Binary	
J11113+434	GJ 9351 A	11:11:18.88	+43:24:55.8	M2.5 V	7.333	Binary	
J11118+335	GJ 3647	11:11:51.52	+33:32:13.1	M3.5 V	8.297	Binary	•
J11126+189	GJ 3649	11:12:38.95	+18:56:05.5	dM1.5	7.445		
J11131+002	Wolf 370	11:13:09.63	+00:14:16.7	M0.0 V	7.471	Binary	
J11151+734	HD 97584B	11:15:09.56	+73:28:38.0	M2.5 V	7.880	Binary	•
J11152+194	GJ 3652	11:15:12.62	+19:27:04.3	M3.5 V	8.919		
J11152-181	GJ 421 C	11:15:15.67	-18:07:47.8	M3.0 V	9.643	Triple	
J11154+410	G 122-8	11:15:26.72	+41:05:12.5	M3.5 V	8.974		
J11159+553	GJ 3653	11:15:53.69	+55:19:49.2	M0.5 V	8.090		
J11195+466	LP 169-22	11:19:31.09	+46:41:33.4	M5.5 V	10.087		
J11200+658	GJ 424	11:19:57.14	+65:50:50.3	M0.0 V	6.306	Binary	
J11201-104	LP 733-99	11:20:05.89	-10:29:46.4	M2.0 V	7.814		
J11214-204	HD 98712B	11:21:26.84	-20:27:11.5	M2.5 V	6.638	Binary	
J11216+061	GJ 1146	11:21:37.67	+06:08:00.7	M3.5 V	9.766		•
J11231+258	GJ 3657	11:23:06.77	+25:53:31.7	M5.0 V	10.294		
J11233+448	GJ 3658	11:23:20.14	+44:48:36.5	M2.0 V	9.146		
J11237+085	Wolf 386	11:23:43.49	+08:33:51.6	M0.5 V	7.994		
J11238+106	LSPM J1123+1037	11:23:50.12	+10:37:07.0	M0.5 V	7.787	Quadruple	
J11239-183	Ross 1002	11:23:56.61	-18:21:49.5	M3.0 V	9.172		
J11247+675	Ross 448	11:24:46.53	+67:33:08.5	M1.0 V	8.659		
J11249+024	StKM 1-941	11:24:58.52	+02:28:26.8	M1.0 V	8.660		
J11240+381	1R112405.0+380809	11:24:04.53	+38:08:10.7	M4.5 V	9.928	Binary	
J11254+782	GJ 3660	11:25:26.06	+78:15:52.9	d/sdM4	8.733	Binary	
J11266+379	PM J11266+3756	11:26:37.40	+37:56:22.8	M2.0 V	8.572	Binary	
J11276+039	GJ 3664	11:27:38.47	+03:58:36.1	M0.0 V	7.848		
J11289+101	Wolf 398	11:28:55.45	+10:10:48.2	M4.0 V	8.478		
J11302+076	K2-18	11:30:14.43	+07:35:16.1	dM2.5	9.763		
J11306-080	LP 672-42	11:30:41.44	-08:05:38.9	M3.5 V	8.033		•

Table B.1: Carmencita, the CARMENES input catalogue (continued).

Karmn	Name	α (2016.0)	δ (2016.0)	Spectral type	J [mag]	Multiplicity[a]	DR1[b]
J11307+549	StKM 1-950	11:30:43.80	+54:57:29.1	M1.0 V	8.846	Binary*	•
J11311-149	GJ 3668	11:31:08.84	-14:57:43.2	M5.0 V	9.359		•
J11315+022	LP 552-68	11:31:32.21	+02:13:34.8	M2.5 V	8.999		
J11317+226	Ross 903	11:31:42.72	+22:40:02.2	M0.5 V	7.171		
J11351-056	GJ 3672	11:35:07.66	-05:39:38.2	M4.5 V	10.269		
J11355+389	GJ 3673	11:35:30.94	+38:55:33.4	M3.5 V	9.034	Binary	
J11376+587	Ross 112	11:37:38.30	+58:42:38.2	M2.5 V	8.978		
J11404+770	LP 19-403	11:40:27.09	+77:04:19.0	M2.0 V	8.379		
J11417+427	Ross 1003	11:41:43.80	+42:45:05.7	M4.0 V	7.608		
J11420+147	Ross 115	11:42:01.43	+14:46:39.9	M3.0 V	8.859		
J11421+267	Ross 905	11:42:12.16	+26:42:10.6	M2.5 V	6.900		•
J11423+230	LP 375-23	11:42:18.14	+23:01:37.3	M0.5 V	8.649	Binary	
J11433+253	GJ 3682	11:43:23.27	+25:18:13.2	M4.0 V	9.507		•
J11451+183	LP 433-47	11:45:11.57	+18:20:53.8	M4.0 V	9.162		•
J11467-140	GJ 443	11:46:43.69	-14:01:04.4	M3.0 V	7.965		
J11470+700	GJ 3684 A	11:47:04.37	+70:01:57.7	M4.0 V	9.309	Binary	
J11474+667	1R114728.8+664405	11:47:28.27	+66:44:02.6	M5.0 V	9.684		•
J11476+002	GJ 3685	11:47:40.41	+00:15:18.5	M4.0 V	8.991	Binary	
J11476+786	GJ 445	11:47:45.46	+78:41:35.9	M4.0 V	6.724		•
J11477+008	FIVir	11:47:45.05	+00:47:56.8	dM4	6.505		•
J11483-112	GJ 3688	11:48:18.61	-11:17:15.0	M3.0 V	9.028		•
J11485+076	G 10-52	11:48:35.63	+07:41:37.8	M3.5 V	9.476		•
J11496+220	BPM 87650	11:49:40.33	+22:03:52.5	M0.0 V	8.403		
J11509+483	GJ 1151	11:50:55.24	+48:22:23.2	M4.5 V	8.488		
J11511+352	GJ 450	11:51:06.98	+35:16:23.3	M1.5 V	6.419		
J11519+075	RX J1151.9+0731	11:51:56.69	+07:31:25.2	M2.5 V	8.812	Binary	•
J11529+244	GJ 3691	11:52:57.55	+24:28:46.9	M4.1 V	9.937		•
J11532-073	GJ 452	11:53:15.91	-07:22:35.8	M2.5 V	8.303		
J11533+430	TYC 3016-577-1	11:53:23.24	+43:02:56.3	M1.0 V	8.417		
J11538+069	GJ 3693	11:53:53.01	+06:59:41.9	M8.0 V	11.256		
J11541+098	Ross 119	11:54:07.98	+09:48:10.0	M4.0 V	8.699		
J11549-021	PM J11549-0206	11:54:56.83	-02:06:08.4	M3.0 V	9.547		
J11551+009	Ross 129	11:55:06.42	+00:58:26.1	M1.5 V	8.170		
J11557-189	GJ 3694	11:55:44.87	-18:54:36.6	M3.5 V	9.967		
J11557-227	LP 851-346	11:55:42.42	-22:25:01.8	M7.5 V	10.930		
J11575+118	Ross 122	11:57:32.06	+11:49:43.7	M2.0 V	8.429		
J11582+425	GJ 3696	11:58:17.81	+42:34:23.0	M4.0 V	9.594		
J11521+039	StM 162	11:52:09.87	+03:57:21.4	M4.0 V	8.382	Binary	
J11589+426	GJ 3697	11:58:58.99	+42:39:40.8	M2.0 V	8.638	Binary	
J11585+595	G 197-38	11:58:33.53	+59:33:22.2	M0.0 V	8.296	Binary	
J12006-138	GJ 3698	12:00:36.36	-13:49:36.6	M3.5 V	8.852	Binary	
J12016-122	GJ 3700	12:01:40.72	-12:13:57.6	M3.0 V	8.685	Binary	
J12054+695	Ross 689	12:05:28.29	+69:32:21.7	M4.0 V	8.740		
J12057+784	LSPM J1205+7825	12:05:45.99	+78:25:51.6	M2.5 V	8.575		
J12023+285	GJ 455	12:02:17.12	+28:35:13.4	sdM3.5	9.132	Binary (SB2)	
J12088+303	1R120847.7+302120	12:08:49.63	+30:21:00.5	M2.5 V	8.988		•
J12093+210	StM 165	12:09:21.70	+21:03:05.8	M2.5 V	9.472		
J12100-150	GJ 3707	12:10:05.54	-15:04:28.4	dM3.5	7.768		
J12063-132	1R120622.6-131453	12:06:22.22	-13:14:57.2	M3.5 V	8.702	Binary	
J12109+410	GJ 9393	12:10:56.90	+41:03:31.7	M0.0 V	7.851		
J12104-131	LP 734-34	12:10:28.65	-13:10:29.5	M4.5 V	9.292	Binary (SB2)	•
J12111-199	GJ 3708	12:11:11.52	-19:57:41.0	dM3.0	7.895	Binary	
J12112-199	GJ 3709	12:11:16.71	-19:58:24.7	M2.5 V	8.596	Binary	
J12121+488	GJ 3713	12:12:11.68	+48:48:58.3	M2.5 V	9.258	Binary	•
J12122+714	LP 39-66	12:12:13.89	+71:25:26.2	M3.0 V	8.815		
J12123+544S	HD 238090	12:12:21.29	+54:29:10.2	M0.0 V	6.875	Binary	
J12123+544N	GJ 458 B	12:12:21.58	+54:29:24.6	M3.0 V	9.171	Binary	
J12124+121	PM J12124+1211	12:12:25.99	+12:11:38.2	M2.0 V	9.391		
J12124+396	GJ 3714	12:12:29.65	+39:40:25.2	M1.0 V	8.121	Binary	•

Table B.1: Carmencita, the CARMENES input catalogue (continued).

Karmn	Name	α (2016.0)	δ (2016.0)	Spectral type	J [mag]	Multiplicity[a]	DR1[b]
J12133+166	IVCom	12:13:19.91	+16:41:32.3	M1.5 V	8.867		
J12144+245	GJ 3717	12:14:26.04	+24:35:20.5	M2.0 V	8.754		
J12151+487	GJ 458.2	12:15:08.46	+48:43:56.4	M0.5 V	7.610		
J12154+391	GJ 3718	12:15:27.93	+39:11:15.4	M1.5 V	8.607		
J12156+526	StKM 2-809	12:15:39.55	+52:39:08.7	M4.0 V	8.588		
J12142+006	GJ 1154	12:14:15.53	+00:37:21.8	M4.5 V	8.456		
J12162+508	RX J1216.2+5053	12:16:14.90	+50:53:36.7	M4.0 V		Binary	
J12168+029	GJ 1155 A	12:16:51.16	+02:58:09.0	M3.0 V	9.234	Binary	•
J12168+248	PM J12168+2451E	12:16:52.62	+24:51:06.0	M1.5 V	8.993		
J12189+111	GLVir	12:18:58.02	+11:07:37.0	M4.5 V	8.525		
J12169+311	GJ 3719	12:16:58.27	+31:09:22.6	M3.0 V	9.909	Binary (SB2)	
J12191+318	LP 320-626	12:19:05.55	+31:50:43.5	M3.5 V	8.289	Triple (SB2)	
J12194+283	Wolf 408	12:19:23.31	+28:22:57.8	M0.5 V	7.666		•
J12198+527	StKM 1-1007	12:19:47.76	+52:46:43.1	M0.0 V	8.281		
J12199+364	G 123-36	12:29:55.22	+36:26:40.0	M1.0 V	8.784		
J12204+005	GJ 461	12:20:25.59	+00:35:00.4	M0.0 V	6.861	Binary	
J12214+306W	G 148-48	12:21:26.79	+30:38:31.4	M5.0 V	9.987	Binary	
J12214+306E	LP 320-416	12:21:26.49	+30:38:33.6	M4.5 V	10.057	Binary	
J12217+682	LP 39-245	12:21:46.41	+68:16:07.3	M3.0 V	8.828		
J12223+251	Wolf 409	12:22:20.46	+25:10:08.6	M0.5 V	8.409		
J12225+123	BD+28 2110	12:22:33.90	+27:36:16.5	M0.0 V	8.055		
J12230+640	Ross 690	12:22:58.52	+64:01:56.9	M3.0 V	7.937		
J12235+279	Wolf 411	12:23:34.55	+27:54:49.6	M0.0 V	8.480		
J12228-040	G 13-33	12:22:50.33	-04:04:47.5	M4.5 V	9.662	Binary	
J12238+125	HD 107888	12:23:53.60	+12:34:46.2	M0.0 V	7.483		•
J12248-182	Ross 695	12:24:53.73	-18:15:09.2	dM2.0	7.734		
J12235+671	GJ 3722	12:23:33.85	+67:11:16.4	M2.5 V	7.598	Binary	
J12251+604	LP 95-135	12:25:05.64	+60:25:06.0	M1.0 V	9.872	Binary	
J12269+270	CXCom	12:26:57.47	+27:00:49.7	M4.5 V	10.197	Triple	•
J12274+374	G 148-61	12:27:29.12	+37:26:35.1	M1.5 V	8.873		
J12277-032	G 13-39A	12:27:44.38	-03:15:01.3	M3.5 V	8.763	Binary	
J12288-106N	Ross 948A	12:28:52.85	-10:39:48.6	M2.0 V	7.682	Binary	
J12288-106S	Ross 948B	12:28:52.65	-10:39:50.8	M2.0 V	7.652	Binary	
J12289+084	Wolf 414	12:28:56.90	+08:25:27.3	M3.5 V	7.844	Binary	
J12290+417	GJ 3729	12:29:02.65	+41:43:45.9	M3.5 V	8.786	Binary (SB2(3?))	
J12292+535	GJ 1159 A	12:29:12.22	+53:32:47.0	M4.0 V	9.983	Binary	
J12294+229	GJ 3730	12:29:26.92	+22:59:46.4	M4.0 V	9.823		
J12299-054W	GJ 3731	12:29:53.57	-05:27:29.2	M3.5 V	8.818	Triple (SB2)	
J12299-054E	GJ 3732	12:29:54.05	-05:27:25.2	M4.0 V	9.792	Triple	
J12312+086	Wolf 417	12:31:15.12	+08:48:29.8	M0.5 V	6.782		
J12323+315	GJ 3733	12:32:19.79	+31:36:03.2	M3.0 V	9.374		
J12324+203	GJ 3734	12:32:26.37	+20:23:28.0	M2.5 V	9.092		•
J12327+682	LP 39-249	12:32:44.66	+68:15:42.1	M0.0 V	8.353		
J12332+090	Wolf 424 A	12:33:15.48	+09:01:19.5	M5.0 V	6.995	Binary	
J12349+322	PM J12349+3214	12:34:54.03	+32:14:29.2	M3.5 V	9.459		
J12350+098	Wolf 427	12:35:00.22	+09:49:37.5	M2.5 V	7.995		
J12363-043	GJ 3736	12:36:22.35	-04:22:41.7	M3.0 V	9.579		
J12368-019	PM J12368-0159	12:36:51.96	-01:59:02.0	M3.5 V	9.440		•
J12373-208	LP 795-38	12:37:21.52	-20:52:42.4	dM4.0	8.972		
J12387-043	GJ 1162	12:38:46.47	-04:19:20.2	M4.3 V	9.329		
J12388+116	Wolf 433	12:38:51.18	+11:41:42.1	M3.5 V	7.581		
J12390+470	G 123-049A	12:39:05.24	+47:02:21.4	M2.5 V		Binary	•
J12397+255	GJ 3739	12:39:43.32	+25:30:43.3	M4.0 V	10.242		
J12416+482	GJ 3741	12:41:38.24	+48:14:22.3	M1.0 V	8.376		•
J12417+567	RX J1241.7+5645	12:41:47.59	+56:45:13.7	M3.5 V	9.483		
J12428+418	G 123-55	12:42:49.10	+41:53:47.8	M4.0 V	8.118		
J12436+251	GJ 1163	12:43:35.62	+25:06:21.1	M3.5 V	8.972		
J12440-111	LP 735-29	12:44:00.22	-11:10:32.8	M4.5 V	9.516		
J12470+466	Ross 991	12:46:59.81	+46:37:28.6	M2.5 V	8.104		•

Table B.1: Carmencita, the CARMENES input catalogue (continued).

Karmn	Name	α (2016.0)	δ (2016.0)	Spectral type	J [mag]	Multiplicity[a]	DR1[b]
J12471-035	GJ 3747	12:47:09.24	-03:34:18.0	M3.0 V	8.767		
J12479+097	Wolf 437	12:47:55.53	+09:44:57.7	M3.5 V	7.195		
J12364+352	G 123-45	12:36:28.17	+35:11:59.0	M4.5 V	9.113	Binary (SB1)	
J12485+495	RX J1248.5+4933	12:48:34.67	+49:33:53.8	M3.5 V	8.684		
J12481+472	GJ 3749	12:48:10.07	+47:13:23.2	M3.5 V	9.607	Binary	•
J12495+094	Wolf 439	12:49:33.74	+09:28:31.6	M3.5 V	9.091		
J12505+269	GJ 3755	12:50:34.35	+26:55:20.3	M3.8 V	9.947		
J12508-213	APMPM J1251-2121	12:50:53.16	-21:21:18.9	M7.5 V	11.160		
J12490+661	DPDra	12:49:01.61	+66:06:35.2	M3.0 V	6.880	Triple (ST3)	
J12513+221	GJ 1166A	12:51:23.71	+22:06:15.7	M3.0 V	9.132	Triple	
J12576+352E	BFCVn	12:57:39.89	+35:13:27.9	M0.0 V	7.401	Quadruple	
J12576+352W	GJ 490 B	12:57:38.94	+35:13:16.9	M4.5 V	8.872	Quadruple	
J12594+077	GJ 3757	12:59:23.31	+07:43:54.8	M5.0 V	10.740		
J13000-056	Ross 972	13:00:03.58	-05:37:47.1	M3.0 V	8.655		
J13005+056	FNVir	13:00:32.51	+05:41:11.6	M4.5 V	8.553		
J12583+405	LP 41-165	12:58:21.97	+40:33:20.7	M1.5 V	8.699	Binary	
J13007+123	Wolf 462	13:00:45.87	+12:22:32.1	M0.0 V	6.437	Triple	
J13019+335	G 164-38	13:01:55.96	+33:35:23.0	M1.0 V	8.969		•
J13027+415	G 123-84	13:02:46.65	+41:31:06.6	M3.5 V	9.033		
J13047+559	GJ 497 A	13:04:46.29	+55:54:10.6	M0.5 V	7.853	Binary	
J13054+371	GJ 3760 A	13:05:29.44	+37:08:07.6	M2.5 V	8.216	Binary	
J13068+308	GJ 3762	13:06:50.53	+30:50:46.4	M6.0 V	10.226		
J13084+169	GJ 9428	13:08:24.64	+16:58:18.5	M1.0 V	8.492		
J13088+163	GJ 3763	13:08:49.96	+16:22:00.9	M2.5 V	9.264		
J13089+490	GJ 3765	13:08:55.46	+49:04:50.3	M0.5 V	7.897		
J13102+477	G 177-25	13:10:11.62	+47:45:08.8	M5.0 V	9.584		
J13113+285	GJ 3766	13:11:21.13	+28:32:34.4	M5.0 V	10.841		
J13118+253	GJ 3767	13:11:51.24	+25:20:48.1	M5.0 V	10.736		
J13119+658	PM J13119+6550	13:11:59.17	+65:50:01.3	M3.0 V	9.706		•
J13130+201	GJ 1168	13:13:04.08	+20:11:29.0	M3.5 V	8.867		
J13140+038	GJ 3772	13:14:05.05	+03:53:59.0	M3.8 V	9.490		
J13095+289	GJ 1167 A	13:09:34.56	+28:59:03.1	M4.8V	9.476		•
J13142+792	G 255-29A	13:14:14.06	+79:14:45.9	M1.0 V	8.603	Binary	
J13165+278	GJ 1169	13:16:31.95	+27:52:33.5	M4.0 V	9.267		
J13167-123	LP 737-14	13:16:45.10	-12:20:21.2	M3.5 V	9.489		
J13143+133	LP 497-33	13:14:20.08	+13:19:57.9	M6.0 V	9.754	Binary	
J13168+170	HD 115404B	13:16:52.28	+17:00:55.7	M0.5 V	6.532	Binary	
J13168+231	GJ 3774	13:16:53.38	+23:10:05.5	M1.5 V	8.424		
J13179+362	GJ 1170	13:17:58.30	+36:17:51.5	M1.0 V	8.112		
J13180+022	GJ 3775	13:18:01.42	+02:14:00.4	M3.5 V	8.787	Binary	
J13182+733	PM J13182+7322	13:18:13.82	+73:22:05.6	M3.5 V	9.541	Binary*	
J13195+351W	GJ 507 A	13:19:34.10	+35:06:24.2	M0.5 V	6.383	Quadruple	
J13195+351E	GJ 507 B	13:19:35.18	+35:06:12.4	M3.0 V	8.287	Quadruple (SB1)	
J13197+477	HD 115953	13:19:45.90	+47:46:40.5	M2.0 V	5.338	Triple	
J13196+333	Ross 1007	13:19:39.74	+33:20:45.2	M1.5 V	7.266		
J13209+342	Ross 1008	13:20:58.67	+34:16:39.4	M1.0 V	7.398		•
J13215+035	LSPM J1321+0332	13:21:30.15	+03:33:02.1	M1.0 V	8.877		
J13215+037	GJ 3778	13:21:34.69	+03:45:54.5	M2.0 V	8.531		•
J13229+244	Ross 1020	13:22:56.03	+24:27:49.8	M4.0 V	8.728		
J13235+292	HD 116495A	13:23:32.21	+29:14:18.9	M0.0 V	6.259	Binary	
J13239+694	LP 40-109	13:23:56.16	+69:27:03.5	M0.0 V	8.426		•
J13247-050	G 14-52	13:24:46.56	-05:04:24.8	M4.0 V	9.465		
J13251-114	PM J13251-1126	13:25:11.61	-11:26:33.7	M3.0 V	9.156		
J13254+377	BD+38 2445	13:25:28.07	+37:43:10.9	M0.0 V	8.274	Binary	
J13255+688	2M13253177+6850106	13:25:31.76	+68:50:09.8	M0.0 V	10.039		
J13260+275	PM J13260+2735A	13:26:02.70	+27:35:03.7	M3.0 V	9.249	Triple*	
J13282+300	BD+30 2400	13:28:17.53	+30:02:43.0	M0.0 V	8.378	Triple	•
J13283-023W	Ross 486A	13:28:21.24	-02:21:45.0	dM3.0	7.515	Binary	
J13283-023E	Ross 486B	13:28:21.68	-02:21:39.6	M4.0 V	9.240	Binary	

Table B.1: Carmencita, the CARMENES input catalogue (continued).

Karmn	Name	α (2016.0)	δ (2016.0)	Spectral type	J [mag]	Multiplicity[a]	DR1[b]
J13293+114	GJ 513	13:29:21.67	+11:26:07.6	M3.0 V	8.368		
J13294-143	1R132923.9-142206	13:29:24.21	-14:22:13.0	M3.5 V	9.061		•
J13299+102	Ross 490	13:30:01.01	+10:22:20.6	M1.0 V	5.902		•
J13300-087	Ross 476	13:30:01.59	-08:42:33.0	M4.0 V	9.599	Binary	
J13305+191	GJ 1171	13:30:30.49	+19:09:13.5	M5.0 V	10.065		•
J13318+233	GJ 3790	13:31:50.26	+23:23:21.1	M2.5 V	8.608		
J13317+292	DGCVn	13:31:46.33	+29:16:34.3	M4.0 V	7.561	Binary	
J13319+311	GJ 9448 B	13:31:58.08	+31:08:05.3	M0.0 V	7.564	Binary	
J13326+309	LP 323-169	13:32:38.85	+30:59:05.3	M4.5 V	9.620	Binary	
J13327+168	VWCom	13:32:44.93	+16:48:35.8	M2.5 V	7.643	Binary	
J13335+704	PM J13335+7029	13:33:33.27	+70:29:41.6	M3.5 V	9.227		
J13343+046	Wolf 1487	13:34:21.67	+04:40:00.7	M0.0 V	7.213		
J13348+201	GJ 3793	13:34:49.40	+20:11:35.7	M3.5 V	9.671		
J13348+745	GJ 9453 B	13:34:49.83	+74:30:12.6	M3.5 V	9.574	Binary	
J13358+146	G 150-17	13:35:50.73	+14:41:07.4	M2.5 V	8.638		
J13369+229	Ross 1021	13:36:55.35	+22:57:58.2	M2.5 V	8.979		
J13378+481	GJ 520 A	13:37:50.84	+48:08:14.8	M0.0 V	6.943	Triple	
J13376+481	GJ 520 C	13:37:40.09	+48:07:52.0	M4.0 V	10.122	Triple	
J13386+258	Ross 1022	13:38:36.37	+25:49:50.7	M3.0 V	8.751		
J13386-115	1R133841.3-113137	13:38:41.05	-11:32:09.1	M4.5 V	9.714		
J13388-022	Ross 488	13:38:53.11	-02:15:48.5	M2.0 V	8.595		
J13401+437	Ross 1026	13:40:07.19	+43:46:42.8	M3.5 V	8.544		
J13413-091	PM J13413-0907	13:41:21.33	-09:07:16.4	M2.5 V	9.444		
J13414+489	StM 186	13:41:27.84	+48:54:43.4	M3.5 V	9.002	Binary	
J13394+461	GJ 521	13:39:24.04	+46:11:17.6	M1.5 V	7.054	Binary	
J13415+148	GJ 3799	13:41:31.58	+14:49:27.6	M1.5 V	8.855		
J13417+582	StM 187	13:41:46.48	+58:15:18.9	M3.5 V	8.733	Binary	
J13427+332	Ross 1015	13:42:43.13	+33:17:12.9	M3.5 V	7.787		
J13430+090	GJ 3802	13:43:00.91	+09:04:21.8	M3.0 V	9.093		
J13434+111	TYC 896-760-1	13:43:25.03	+11:06:42.1	M0.5 V	8.428		
J13421-160	GJ 3800	13:42:09.28	-16:00:24.1	M4e	8.971	Binary	•
J13444+516	Ross 492	13:44:27.00	+51:41:08.6	M2.5 V	8.989	Binary	
J13445+249	LP 379-98 A	13:44:33.38	+24:57:03.6	M1.0 V	8.699	Binary	
J13450+176	Wolf 497	13:45:05.59	+17:46:38.2	M0.0 V	6.997		
J13455+609	MCC 699	13:45:31.28	+60:58:58.3	M0.5 V	8.150		
J13457+148	HD 119850	13:45:45.74	+14:53:06.2	M1.5 V	5.181		•
J13458-179	GJ 3804	13:45:50.37	-17:58:14.5	dM3.5	7.745		
J13477+214	BD+22 2632A	13:47:42.49	+21:27:36.3	M0.0 V	8.215	Binary	•
J13481-137	LP 738-14	13:48:06.52	-13:44:39.8	M4.5 V	10.413	Binary	•
J13482+236	GJ 1179 A	13:48:11.69	+23:36:50.7	M5.0 V	10.082	Binary	
J13485+563	Ross 493	13:48:34.32	+56:20:09.6	M1.5 V	8.612		
J13488+041	Wolf 1494	13:48:48.61	+04:05:59.4	M4.5 V	9.755		
J13490+026	Wolf 1495 A	13:49:01.16	+02:47:23.6	M1.5 V	7.839	Binary	
J13507-216	GJ 3810	13:50:43.96	-21:41:33.0	M3.0 V	8.871	Binary	
J13503-216	LP 798-41	13:50:23.73	-21:37:25.9	M3.5 V	9.458	Binary	
J13508+367	Ross 1019	13:50:51.18	+36:44:18.5	M4.0 V	9.299		
J13518+127	RX J1351.8+1247	13:51:53.02	+12:47:07.0	M2.0 V	8.788		
J13526+144	Wolf 515	13:52:36.26	+14:25:15.7	M2.0 V	8.013	Binary	
J13528+656	GJ 533.1	13:52:48.61	+65:37:17.7	M1.5 V	8.523	Binary	
J13528+668	GJ 3815	13:52:49.25	+66:48:57.2	M5.0 V	10.539		
J13536+776	LP 21-224	13:53:39.91	+77:37:07.9	M4.0 V	8.635		
J13529+536	LP 97-259	13:52:55.76	+56:36:17.0	M1.0 V	8.648		
J13534+129	Ross 835	13:53:27.37	+12:56:22.9	M0.0 V	6.945	Binary	
J13537+521	PM J13537+5210A	13:53:45.89	+52:10:27.3	M3.5 V	9.128	Binary	
J13537+788	GJ 534.2	13:53:45.76	+78:51:08.7	M0.0 V	7.639		•
J13582+125	Ross 837	13:58:13.56	+12:34:55.4	M3.5 V	8.269		
J13582-120	LP 739-2	13:58:15.80	-12:02:58.4	M4.5 V	9.728		
J13583-132	LP 739-3	13:58:19.96	-13:16:26.0	M4.0 V	9.488		
J13587-000	GJ 3818	13:58:43.20	-00:04:54.3	M4.0 V	9.963		•

Table B.1: Carmencita, the CARMENES input catalogue (continued).

Karmn	Name	α (2016.0)	δ (2016.0)	Spectral type	J [mag]	Multiplicity[a]	DR1[b]
J13591-198	GJ 3820	13:59:09.78	-19:50:06.6	M4.5 V	8.334		
J14010-026	HD 122303	14:01:02.31	-02:39:07.9	M1.0 V	6.516		
J14019+154	GJ 536.1 A	14:01:58.86	+15:29:40.7	M0.0 V	7.728	Binary	•
J14019+432	PM J14019+4316A	14:01:58.67	+43:16:41.1	M2.5 V	9.281	Binary	•
J14023+136	GJ 3822	14:02:19.73	+13:41:20.4	M0.5 V	7.563		
J14024-210	GJ 3821	14:02:29.43	-21:00:42.9	M3.5 V	9.163		
J14025+463S	GJ 537 A	14:02:34.03	+46:20:23.0	M0.5 V	6.269	Binary	
J14025+463N	GJ 537 B	14:02:34.19	+46:20:26.4	M0.5 V	6.264	Binary	
J14039+242	LSPM J1403+2440	14:03:54.74	+24:40:44.2	M2.5 V	8.935		
J14041+207	StKM 1-1119	14:04:09.06	+20:44:30.9	M1.0 V	8.590	Triple	
J14062+693	NLTT 36313	14:06:14.66	+69:18:38.8	M3.0 V	8.731		
J14082+805	GJ 540	14:08:14.37	+80:35:41.5	M1.0 V	7.179		
J14083+758	GJ 3826	14:08:20.91	+75:51:13.2	M1.5 V	8.349		
J14121-005	GJ 3828 A	14:12:10.22	-00:35:00.3	M2.5 V	9.352	Triple	•
J14130-120	GQVir	14:13:04.19	-12:01:32.9	M4.5 V	9.040	Binary (SB2)	
J14142-153	GJ 3832	14:14:16.87	-15:21:15.9	M3.5 V	9.687	Quadruple	
J14144+234	GJ 3834	14:14:26.33	+23:27:26.4	M3.5 V	9.516		
J14152+450	Ross 992	14:15:15.96	+45:00:49.7	M3.0 V	8.014		
J14153+153	LP 439-350	14:15:20.63	+15:23:01.5	M2.0 V	8.654		
J14155+046	GJ 1182	14:15:31.75	+04:39:19.1	M5.69	9.433	Binary (SB2)	•
J14157+594	LP 97-674 A	14:15:42.13	+59:27:29.1	M2.2 V	8.850	Binary	
J14159+362	G 165-58	14:15:56.39	+36:16:42.2	M3.5 V	8.940		•
J14161+233	LP 81-30	14:16:11.25	+23:23:26.5	M1.0 V	8.713		
J14170+105	GJ 3838	14:17:04.56	+10:35:34.3	M1.5 V	8.185		
J14170+317	GJ 3839	14:17:02.14	+31:42:44.7	M4.5 V	8.443	Binary (SB2/ST3)	
J14171+088	PM J14171+0851	14:17:07.18	+08:51:37.1	M4.5 V	9.109	Binary (SB2)	
J14174+454	GJ 541.2	14:17:24.45	+45:26:39.8	M0.0 V	7.389	Binary	
J14173+454	RX J1417.3+4525	14:17:22.17	+45:25:45.7	dM5.0	9.467	Binary	
J14175+025	RX J1417.5+0233	14:17:30.18	+02:33:42.5	M3.0 V	9.274		•
J14177+214	LP 381-94	14:17:47.76	+21:25:58.8	M1.0 V	8.534		
J14179-005	GJ 3840	14:17:58.75	-00:31:33.8	M2.5 V	9.040		
J14189+386	LP 220-78	14:18:58.09	+38:38:22.5	M1.0 V	8.500		
J14191-073	Wolf 534	14:19:09.81	-07:18:24.0	M3.0 V	9.665		
J14194+029	LP 560-1	14:19:29.37	+02:54:34.1	M5.0 V	9.954		
J14200+390	IZBoo	14:20:04.66	+39:03:02.5	M3.0 V	8.572		
J14201-096	Ross 848	14:20:06.71	-09:37:26.8	M4.0 V	8.740		
J14212-011	GJ 3843	14:21:15.31	-01:07:29.8	M4.0 V	8.948		
J14215-079	PM J14215-0755	14:21:33.96	-07:55:18.0	M4.0 V	9.456		
J14219+376	LP 270-68	14:21:55.61	+37:39:45.5	M1.5 V	8.982		
J14227+164	LP 440-13	14:22:43.19	+16:24:47.2	M5.0 V	10.303		
J14231-222	GJ 3845	14:23:07.49	-22:17:16.7	M4.5 V	10.402		
J14249+088	GJ 3846	14:24:56.58	+08:53:18.0	M3.0 V	8.420		
J14210+275	GJ 3844	14:21:03.13	+27:35:34.5	M2.5 V	8.928	Binary	
J14251+518	HD 126660B	14:25:11.17	+51:49:46.6	M2.5 V	7.883	Binary	
J14255-118	LP 740-10	14:25:33.79	-11:48:51.5	M4.0 V	9.353		
J14257+236W	GJ 548 A	14:25:44.40	+23:36:43.6	M0.0 V	6.769	Binary	•
J14257+236E	GJ 548 B	14:25:47.58	+23:36:55.8	M0.5 V	6.889	Binary	
J14259+142	V358Boo	14:25:55.87	+14:12:09.6	M0.0 V	8.147		•
J14269+241	LSPM J1426+2408	14:26:58.63	+24:08:56.9	M1.0 V	8.908		•
J14279-003S	GJ 1183 A	14:27:55.69	-00:22:30.5	M4.65	9.305	Binary	
J14279-003N	GJ 1183 B	14:27:56.01	-00:22:18.3	M4.70	9.345	Binary	
J14280+139	LP 500-35	14:28:03.75	+13:56:05.4	M7.0 V	11.014		
J14283+053	LP 560-27	14:28:21.12	+05:19:00.3	M3.0 V	8.724	Binary	
J14282+053	LP 560-26	14:28:17.18	+05:18:44.8	M3.5 V	8.932	Binary	
J14294+155	Ross 130	14:29:28.53	+15:32:18.3	M2.0 V	7.229		
J14299+295	GJ 3853	14:29:59.26	+29:33:54.9	M4.0 V	10.072		
J14306+597	GJ 3855	14:30:36.08	+59:43:27.4	M6.5 V	10.790		•
J14307-086	HD 127339	14:30:46.35	-08:38:50.6	M0.5 V	6.616		
J14310-122	Wolf 1478	14:31:00.72	-12:17:52.3	dM3.5	7.803		

Table B.1: Carmencita, the CARMENES input catalogue (continued).

Karmn	Name	α (2016.0)	δ (2016.0)	Spectral type	J [mag]	Multiplicity[a]	DR1[b]
J14312+754	LSPM J1431+7526	14:31:12.59	+75:26:41.7	M4.0 V	9.792		•
J14320+738	G 255-55	14:32:01.99	+73:49:23.3	M2.0 V	8.139		•
J14321+081	LP 560-35	14:32:07.99	+08:11:31.4	M6.0 V	10.108		
J14321+160	GJ 3856	14:32:11.00	+16:00:48.2	M5.0 V	9.288		
J14322+496	GJ 3858	14:32:13.58	+49:39:04.2	M3.5 V	9.277		•
J14331+610	G 224-13A	14:33:06.93	+61:00:43.9	M2.5 V	8.171	Binary	
J14342-125	HNLib	14:34:16.42	-12:31:00.9	M3.5 V	6.838		
J14366+143	StKM 1-1170	14:36:38.98	+14:21:52.6	M1.0 V	8.676		
J14368+583	GJ 3861	14:36:54.24	+58:20:43.6	M3.0 V	8.079	Binary (SB2)	•
J14371+756	LSPM J1437+7536N	14:37:09.94	+75:36:54.7	M2.0 V	8.650	Binary	
J14376+677	G 239-22	14:37:39.32	+67:45:34.9	M1.5 V	8.917	Binary	
J14388+422	GPM 219.718548+42.229288	14:38:51.66	+42:13:43.9	M1.5 V	8.793		
J14415+064	LP 560-66	14:41:32.72	+06:27:41.2	M1.5 V	8.843		
J14423+660	GJ 9492	14:42:20.79	+66:03:20.2	M2.0 V	7.306	Binary	
J14438+667	NLTT 38291	14:43:50.67	+66:44:34.6	M1.0 V	8.935		
J14472+570	RX J1447.2+5701	14:47:13.67	+57:01:54.4	M4.0 V	9.914		
J14485+101	LP 501-17	14:48:32.79	+10:06:55.7	M3.5 V	9.475		
J14501+323	LP 326-34	14:50:11.14	+32:18:13.8	M3.5 V	9.144		
J14511+311	LP 326-38	14:51:09.97	+31:06:37.4	M4.0 V	8.408		
J14524+123	GJ 3871	14:52:28.47	+12:23:29.2	M2.5 V	7.967		
J14525+001	Wolf 555	14:52:32.27	+00:10:02.8	M2.5 V	8.999		
J14469+170	Ross 994	14:46:59.22	+17:05:07.5	M1.5 V	8.600	Binary	
J14538+235	Ross 52A	14:53:50.59	+23:33:22.5	M3.5 V	7.438	Binary	•
J14544+161	CEBoo	14:54:29.55	+16:06:01.9	M1.0: V	6.633	Triple	
J14544+355	Ross 1041	14:54:28.10	+35:32:43.5	M3.5 V	8.243		
J14548+099	Ross 1028b	14:54:53.15	+09:56:30.1	M2.0 V	8.217		
J14549+411	GJ 3875	14:54:54.61	+41:08:50.5	M4.5 V	10.249	Binary (SB)	•
J14557+072	G 66-42	14:55:47.82	+07:17:47.7	M0.5 V	8.412		
J14564+168	G 136-35	14:56:28.16	+16:48:29.1	M1.5 V	8.960	Binary (SB)	
J14574-214	HD 131976	14:57:27.70	-21:25:07.9	M1.0 V	4.550	Quadruple (SB2)	
J14575+313	Ross 53A	14:57:31.43	+31:23:25.9	M2.0 V	8.444	Binary	
J14578+566	GJ 1187	14:57:54.28	+56:39:14.1	M5.5 V	10.207		
J15009+454	GJ 572	15:00:55.91	+45:25:39.8	M0.5 V	6.198	Binary	
J15011+354	Ross 1042	15:01:11.98	+35:27:10.5	M2.0 V	8.670		
J15013+055	GJ 3885	15:01:20.20	+05:32:48.5	M3.0 V	8.326		
J15018+550	GJ 3891	15:05:48.60	+55:04:45.8	M3.5 V	9.239		
J15030+704	LP 41-431	15:03:01.68	+70:26:14.0	M3.0 V	8.871		
J15043+294	GJ 575.1	15:04:22.56	+29:28:39.9	M2.5 V	9.220		•
J15043+603	Ross 1051	15:04:17.09	+60:23:07.4	M1.0 V	7.701		
J15049-211	GJ 3888	15:04:57.53	-21:07:03.9	M4.5 V	10.174		
J15060+453	PM J15060+4521	15:06:03.02	+45:21:52.8	M1.5 V	8.999		
J15073+249	GJ 579	15:07:22.59	+24:56:15.8	M0.0 V	7.296		
J15011+071	Ross 1030a	15:01:10.20	+07:09:46.5	M3.5 V	8.682	Binary	
J15079+762	LSPM J1507+7613	15:07:56.64	+76:14:01.8	M4.5 V	9.235	Triple	
J15081+623	LSPM J1508+6221	15:08:11.53	+62:21:56.4	M4.0 V	9.296	Binary	
J15095+031	Ross 1047	15:09:34.95	+03:10:08.3	M3.0 V	7.720		
J15100+193	GJ 3893	15:10:04.82	+19:21:20.2	M4.3 V	9.056		
J15118-102	GJ 3894	15:11:49.55	-10:14:22.1	M4.5 V	9.651		•
J15119+179	GJ 3895	15:11:55.49	+17:57:07.4	M4.0 V	9.556		
J15147+645	LP 67-339	15:14:45.76	+64:33:50.3	M3.5 V	9.785	Binary	
J15151+333	LP 272-63	15:15:06.93	+33:17:57.0	M2.0 V	9.207		
J15156+638	PM J15156+6349	15:15:37.69	+63:49:50.8	M1.5 V	8.992		
J15166+391	LP 222-65	15:16:40.44	+39:10:47.4	M7.0 V	10.796		
J15126+457	GJ 3898	15:12:37.60	+45:43:52.3	M4.0 V	8.977	Binary	
J15188+292	StKM 1-1229	15:18:49.75	+29:15:06.4	M1.0 V	8.624	Triple*	
J15193+678	GJ 3902	15:19:17.35	+67:51:24.0	M3.0 V	9.568		
J15194-077	HOLib	15:19:25.51	-07:43:21.7	M3.0 V	6.706		
J15197+046	PM J15197+0439	15:19:45.88	+04:39:36.0	M4.0 V	9.546		
J15210+309	PM J15210+3057	15:21:00.56	+30:57:00.9	M2.5 V	8.963		

Table B.1: Carmencita, the CARMENES input catalogue (continued).

Karmn	Name	α (2016.0)	δ (2016.0)	Spectral type	J [mag]	Multiplicity[a]	DR1[b]
J15214+042	TYC 344-504-1	15:21:25.39	+04:14:49.9	M1.5 V	8.553		•
J15218+209	OTSer	15:21:53.03	+20:58:42.0	M1.0 V	6.610		
J15219+185	LP 442-37	15:21:56.83	+18:35:47.9	M1.5 V	8.714		
J15238+174	Ross 508	15:23:50.70	+17:27:37.3	M4.92	9.105		
J15191-127	GJ 3900	15:19:10.93	-12:45:09.3	M4.0 V	8.507	Binary (SB2)	•
J15238+561	StKM 1-1240	15:23:54.01	+56:09:31.5	M1.0 V	8.794	Triple (SB2)	
J15238+584	G 224-65	15:23:51.06	+58:28:11.2	M4.0 V	9.905		
J15273+415	TYC 3055-1525-1	15:27:19.05	+41:30:09.9	M1.5 V	8.363	Binary	
J15276+408	G 179-29	15:27:38.85	+40:52:02.2	M1.0 V	8.480		
J15280+257	GJ 587.1	15:28:01.43	+25:47:22.9	M0.0 V	8.143		
J15290+467	RX J1529.0+4646	15:29:02.77	+46:46:23.5	M4.5 V	9.942	Binary	
J15305+094	LP 502-56	15:30:30.13	+09:26:04.4	M5.5 V	9.569		
J15297+428	GJ 3907	15:29:44.63	+42:52:38.9	M4.68	9.587	Binary	
J15336+462	GJ 3911	15:33:39.33	+46:15:06.1	M3.6 V	9.417		
J15319+288	GJ 3910	15:31:53.50	+28:51:10.2	M4.0 V	9.673	Binary (SB1)	•
J15339+379	GJ 588.1	15:33:54.82	+37:54:48.4	M0.5 V	8.226	Binary	
J15340+513	LP 135-414	15:34:03.52	+51:22:06.8	M4.5 V	9.370		
J15345+142	Ross 512	15:34:29.76	+14:16:15.5	M4.0 V	9.642		
J15349-143	2MUCD 11346	15:34:55.92	-14:18:54.5	M8.6V	11.380		
J15353+177S	Ross 513	15:35:19.17	+17:42:44.3	M2.5 V	8.694	Binary	
J15353+177N	Ross 513B	15:35:18.98	+17:43:01.7	M4.5 V	10.282	Binary	
J15357+221	GJ 3913	15:35:45.31	+22:09:01.6	M3.5 V	8.681		
J15368+375	BKCrB	15:36:49.97	+37:34:48.0	M0.0 V	8.397	Binary	
J15369-141	Ross 802	15:36:58.13	-14:08:11.8	dM4.0	8.432		
J15386+371	G 179-42	15:38:36.68	+37:07:28.0	M3.5 V	9.979		
J15400+434N	GJ 1194 A	15:40:05.37	+43:29:34.1	M3.0 V	8.312	Binary	•
J15400+434S	GJ 1194 B	15:40:05.54	+43:29:30.0	M4.0 V	8.893	Binary	
J15412+759	UU UMi	15:41:20.12	+75:59:22.5	M3.5 V	8.260	Binary (SB2)	
J15416+184	StKM 1-1264	15:41:37.17	+18:28:09.2	M1.5 V	8.955	Triple	
J15421-194	GJ 595	15:42:04.27	-19:28:34.9	M3.0 V	7.920	Binary (SB1)	•
J15474-108	GJ 3916	15:47:24.21	-10:53:53.2	M2.5 V	7.582	Triple (ST3)	
J15476+226	1R154741.3+224108	15:47:40.51	+22:41:16.0	M4.5 V	9.543		
J15474+451	LP 177-102	15:47:27.03	+45:07:54.5	M4.0 V	9.082	Binary (EB/SB2)	•
J15480+043	RX J1548.0+0421	15:48:02.78	+04:21:38.4	M2.5 V	9.058	Binary*	
J15488+305	PM J15488+3030	15:48:48.60	+30:30:38.7	M3.0 V	8.958		
J15493+250	G 168-13	15:49:20.38	+25:03:48.5	M2.0 V	8.884		
J15496+510	GJ 3920	15:49:35.62	+51:03:02.0	M2.0 V	8.573		
J15499+796	LP 23-35	15:49:53.83	+79:39:53.6	M5.0 V	9.721		
J15501+009	Wolf 587	15:50:11.41	+00:57:32.0	M3.0 V	8.677		
J15512+306	TYC 2572-633-1	15:51:14.63	+30:40:42.2	M1.5 V	8.974		
J15513+295	GJ 3923	15:51:21.51	+29:30:59.2	M3.5 V	8.961		•
J15496+348	GJ 3919	15:49:37.37	+34:49:07.8	M4.0 V	8.728	Binary	
J15531+347N	Ross 806	15:53:06.69	+34:45:05.9	M3.0 V	8.001	Triple	
J15531+347S	GJ 3926	15:53:06.97	+34:44:39.5	M3.0 V	8.994	Triple	
J15538+641	NLTT 41533	15:53:48.31	+64:09:36.2	M0.5 V	8.441		
J15555+352	GJ 3928	15:55:31.51	+35:12:05.2	M4.0 V	8.928	Binary	
J15557+686	RX J1555.7+6840	15:55:47.10	+68:40:16.0	M2.5 V	8.593		
J15569+376	RX J1556.9+3738	15:56:58.12	+37:38:14.3	M2.5 V	9.417		
J15578+090	LSPM J1557+0901	15:57:48.42	+09:01:07.6	M4.0 V	9.282		
J15581+494	V1022Her	15:58:10.41	+49:27:05.5	M1.0 V	8.732		
J15583+354	GJ 3929	15:58:18.61	+35:24:29.4	M3.5 V	8.694		
J15587+346	StM 258	15:58:45.75	+34:48:53.8	M3.5 V	8.809		
J15597+440	RX J1559.7+4403	15:59:47.20	+44:03:59.6	M2.0 V	8.509	Binary	•
J15598-082	GJ 606	15:59:53.60	-08:15:12.0	M1.0 V	7.185		
J16008+403	GJ 3933	16:00:50.40	+40:19:38.7	M3.0 V	9.216		
J16017+301	GJ 607	16:01:43.15	+30:10:52.9	M3.0 V	8.666		•
J16018+304	GJ 3935	16:01:52.43	+30:27:37.0	M2.5 V	9.530	Binary	
J16017+304	GJ 3936	16:01:44.35	+30:27:42.9	M4.5 V	10.427	Binary	
J16028+205	GJ 609	16:02:49.85	+20:35:01.2	M4.0 V	8.132		

Table B.1: Carmencita, the CARMENES input catalogue (continued).

Karmn	Name	α (2016.0)	δ (2016.0)	Spectral type	J [mag]	Multiplicity[a]	DR1[b]
J16033+175	PM J16033+1735	16:03:20.60	+17:35:55.0	M2.0 V	8.821		
J16043-062	GJ 3937	16:04:19.91	-06:16:59.9	M4.5 V	10.452		•
J16046+263	BPM 91242	16:04:36.85	+26:20:44.6	M0.5 V	8.251		
J16048+391	HD 144579B	16:04:50.08	+39:09:36.6	M4.0 V	9.903	Binary	
J16054+769	GJ 3941	16:05:26.51	+76:54:58.5	M3.0 V	8.632		
J16062+290	LP 329-30	16:06:13.41	+29:02:01.6	M2.0 V	8.473		
J16066+083	GJ 611.3	16:06:40.66	+08:23:19.6	M1.0 V	8.422	Triple	
J16074+059	GJ 3939	16:07:27.90	+05:57:56.0	M3.8 V	9.525		
J16082-104	GJ 1198	16:08:14.56	-10:26:35.1	M4.5 V	10.257		
J16090+529	GJ 3942	16:09:03.50	+52:56:39.0	M0.5 V	7.185		
J16092+093	LP 504-59	16:09:15.90	+09:21:11.0	M3.0 V	7.969		
J16102-193	K2-33	16:10:14.73	-19:19:09.8	dM3.0	11.095		
J16120+033	TYC 371-1053-1	16:12:04.68	+03:18:19.8	M2.0 V	8.127	Binary	•
J16126-188	LP 804-27	16:12:41.82	-18:52:35.2	M3.0 V	7.555		•
J16139+337	sig CrB C	16:13:55.90	+33:46:22.7	M2.5 V	8.598	Quintuple	
J16144-028	LP 624-54	16:14:25.19	-02:50:54.9	M5.0 V	11.303		
J16145+191	GJ 1200	16:14:30.36	+19:06:16.7	M3.5 V	8.990		
J16147+048	GJ 3946	16:14:43.36	+04:52:09.7	M3.5 V	9.476		
J16155+244	GJ 3947	16:15:32.10	+24:27:50.9	M1.5 V	8.645		
J16167+672S	HD 147379	16:16:41.37	+67:14:21.2	M0.0 V	5.779	Binary	
J16167+672N	EWDra	16:16:43.98	+67:15:23.9	M3.0 V	6.908	Binary	
J16180+062	1R161804.9+061702	16:18:05.01	+06:17:12.0	M3.0 V	8.950		•
J16170+552	CRDra	16:17:05.52	+55:16:01.9	M1.0 V	6.600	Binary	•
J16204-042	GJ 618.1 A	16:20:24.34	-04:16:02.6	M0.0 V	7.950	Binary	
J16220+228	V1169Her	16:22:01.12	+22:50:22.8	M1.5 V	8.904		
J16247+229	LSPM J1624+2254	16:24:43.71	+22:54:19.3	M1.0 V	8.016		
J16254+543	GJ 625	16:25:25.41	+54:18:12.0	M1.5 V	6.608		
J16241+483	GJ 623	16:24:11.16	+48:21:03.1	M3.0 V	6.638	Binary	
J16255+323	LP 330-13	16:25:32.91	+32:18:34.1	M2.0 V	8.868		
J16259+834	TYC 4647-2406-1	16:25:59.21	+83:24:23.2	M1.5 V	8.642		•
J16255+260	GJ 3953	16:25:32.12	+26:01:38.0	M3.0 V	14.776	Binary	
J16268-173	GJ 3954	16:26:47.75	-17:23:40.5	M5e	9.548	Binary	
J16280+155	GJ 3955	16:28:02.04	+15:33:52.1	M3.6 V	9.375	Binary	
J16303-126	V2306Oph	16:30:17.96	-12:40:04.3	M3.0 V	5.950		
J16313+408	GJ 3959	16:31:18.59	+40:51:56.6	M6.0 V	9.461		
J16315+175	GJ 1202	16:31:34.69	+17:33:35.9	M4.0 V	8.926		
J16327+126	GJ 1203	16:32:44.36	+12:36:43.8	M3.0 V	8.429		•
J16328+098	GJ 3960	16:32:53.09	+09:50:28.5	M3.5 V	8.988		•
J16342+543	LP 137-37	16:34:13.28	+54:23:48.5	M1.0 V	8.720		
J16302-146	GJ 2121	16:30:12.52	-14:39:53.0	M2.5 V	8.416	Binary	•
J16343+571	CMDra	16:34:18.14	+57:10:03.3	M4.5 V	8.501	Triple (EB/SB2)	
J16360+088	GJ 1204	16:36:05.09	+08:48:46.7	M4.0 V	9.419		
J16395+505	G 202-68	16:39:30.81	+50:33:57.0	M1.0 V	8.628		•
J16401+007	GJ 3967	16:40:06.17	+00:42:16.3	M5.0 V	9.116		
J16403+676	GJ 3971	16:40:19.87	+67:36:10.6	M7.0 V	9.854		
J16408+363	Ross 812	16:40:48.72	+36:19:02.9	M2.0 V	8.069		
J16420+192	PM J16420+1916	16:42:00.72	+19:16:11.6	M2.5 V	8.692		
J16462+164	GJ 3972	16:46:13.35	+16:28:33.2	M3.0 V	7.951		
J16465+345	LP 276-22	16:46:31.03	+34:34:49.0	M6.0 V	10.533		
J16354+350	V1200Her	16:35:27.61	+35:00:55.3	M4.0 V	8.615	Binary	
J16487-157	GJ 3973	16:48:45.95	-15:44:23.7	M1.5 Vk:	7.656		•
J16508-048	GJ 3975	16:50:52.99	-04:50:38.8	M3.5 V	9.465		
J16509+224	GJ 3976	16:50:57.98	+22:27:12.1	M5.0 V	9.136		
J16528+630	GSC 04194-01561	16:52:49.82	+63:04:41.2	M4.5 V	9.592		
J16529+400	GJ 3979	16:52:54.92	+40:05:04.6	M3.0 V	9.389		
J16542+119	Ross 644	16:54:11.44	+11:54:57.9	M0.0 V	7.886		
J16487+106	LSPM J1648+1038	16:48:46.40	+10:38:51.1	M2.5 V	7.820	Binary	
J16554-083S	V1054Oph	16:55:27.89	-08:20:25.2	M3.0 V	5.270	Quintuple (ST3)	
J16554-083N	Wolf 629	16:55:24.34	-08:19:35.7	M3.5 V	7.555	Quintuple	

Table B.1: Carmencita, the CARMENES input catalogue (continued).

Karmn	Name	α (2016.0)	δ (2016.0)	Spectral type	J [mag]	Multiplicity[a]	DR1[b]
J16555-083	GJ 644 C	16:55:34.38	-08:23:54.7	M7.0 V	9.776	Quintuple	•
J16570-043	GJ 1207	16:57:06.25	-04:21:02.3	dM4	7.971		
J16573+124	GJ 3980	16:57:23.12	+13:28:06.6	M4.0 V	10.036		•
J16573+271	PM J16573+2708	16:57:22.27	+27:08:31.2	M2.0 V	9.356	Binary	•
J16574+777	GJ 3986	16:57:29.79	+77:43:06.3	M3.0 V	8.982		
J16577+132	GJ 647	16:57:46.15	+13:17:31.1	M0.0 V	7.872	Binary	
J16578+473	HD 153557B	16:57:53.40	+47:22:06.7	M1.5 V	6.874	Triple	
J16581+257	Ross 860	16:58:08.71	+25:44:30.8	M1.0 V	6.448		
J16584+139	GJ 3981 A	16:58:24.81	+13:58:10.9	M4.0 V	8.801	Binary	
J16587+688	LP 43-338	16:58:42.17	+68:53:55.8	M1.5 V	8.749		•
J16591+209	V1234Her	16:59:09.58	+20:58:18.3	M3.5 V	8.338	Binary	
J17003+253	GJ 3983	17:00:20.18	+25:21:05.1	M3.2 V	9.404		
J17006+063	G 139-4	17:00:38.65	+06:18:42.0	M1.0 V	8.586		
J17010+082	GJ 3984	17:01:01.85	+08:12:23.5	M3.8 V	9.437		
J17027-060	GJ 3987	17:02:49.45	-06:04:07.6	M0	7.802		
J17033+514	GJ 3988	17:03:24.10	+51:24:32.6	M5.0 V	8.768		
J17038+321	LP 331-57 A	17:03:53.09	+32:11:47.6	M2.0 V	7.886	Triple (SB2?)	
J17043+169	GJ 1209	17:04:22.49	+16:55:37.5	M3.0 V	8.571		•
J17052-050	HD 154363B	17:05:12.80	-05:05:57.4	M1.5 V	6.780	Binary	
J17058+260	LP 387-37	17:05:52.55	+26:05:27.4	M1.5 V	8.887	Binary	
J17071+215	Ross 863	17:07:06.96	+21:33:14.1	M3.0 V	7.875		•
J17082+516	G 203-44	17:08:12.71	+51:38:10.6	M1.0 V	8.794		
J17076+073	GJ 1210	17:07:40.31	+07:22:00.6	M5.0 V	9.284	Binary	•
J17098+119	GJ 3990	17:09:52.36	+11:55:32.8	M4.0 V	9.611		
J17095+436	GJ 3991	17:09:32.03	+43:40:48.4	M3.5 V	7.380	Binary (SB1)	
J17104+279	StM 336	17:10:25.49	+27:58:38.6	M2.5 V	8.987	Binary	
J17121+456	HD 155876	17:12:08.21	+45:39:32.6	M3.0 V	5.552	Binary	
J17115+384	Wolf 654	17:11:35.04	+38:26:33.2	M4.0 V	7.630		
J17118-018	GJ 660	17:11:51.82	-01:51:10.5	M3.0 V	7.462	Binary	•
J17146+269	GJ 3994	17:14:39.87	+26:55:44.4	M2.0 V	8.861		
J17153+049	GJ 1214	17:15:19.56	+04:57:38.1	M4.5 V	9.750		
J17136-084	V2367Oph	17:13:40.00	-08:25:21.4	M3.5 V	8.120	Binary (SB2)	
J17158+190	GJ 3997	17:15:49.95	+19:00:00.3	M0.5 V	7.212	Binary	
J17160+110	GJ 3998	17:16:00.49	+11:03:22.1	M1.0 V	7.634		
J17166+080	GJ 2128	17:16:40.68	+08:03:29.1	M2.5 V	7.933		
J17177+116	GJ 1215	17:17:43.71	+11:40:05.3	M5.0 V	9.817	Binary	
J17177-118	GJ 3999	17:17:45.28	-11:48:59.0	M3.0 V	8.818	Binary	•
J17183+181	GJ 4002	17:18:22.44	+18:08:52.4	M3.0 V	9.050	Binary	
J17183-017	GJ 4001	17:18:21.82	-01:46:55.4	M0.0 V	7.554	Binary	
J17199+265	V647Her	17:19:53.95	+26:30:08.7	M3.5 V	7.273	Binary	
J17198+265	V639Her	17:19:52.70	+26:30:08.3	M4.5 V	8.229	Binary	
J17198+417	GJ 671	17:19:53.12	+41:42:36.4	M2.5 V	7.712		
J17207+492	GJ 1216	17:20:47.19	+49:15:01.4	M4.0 V	10.124		•
J17219+214	GJ 4003	17:21:54.44	+21:25:51.3	M4.0 V	9.344		
J17225+055	PM J17225+0531	17:22:33.80	+05:31:15.1	M2.5 V	8.966		
J17242-043	GJ 4005	17:24:16.69	-04:21:54.1	M2.5 V	8.515		
J17276+144	GJ 1219	17:27:38.65	+14:28:56.4	M4.0 V	9.693		
J17285+374	Wolf 750	17:28:30.41	+37:27:04.1	M3.5 V	9.387		
J17303+055	Wolf 751	17:30:22.76	+05:32:50.7	M1.0 V	6.240		
J17312+820	GJ 1220	17:31:14.95	+82:05:27.8	M4.0 V	9.572		
J17316+047	Wolf 755	17:31:37.97	+01:47:48.0	M1.5 V	8.586		•
J17321+504	GJ 4011	17:32:07.82	+50:24:41.7	M2.5 V	9.008		
J17328+543	G 226-64	17:32:53.06	+54:20:19.6	M2.0 V	8.935		
J17338+169	V1274Her	17:33:53.03	+16:55:11.0	M6.0 V	8.895		
J17340+446	RX J1734.0+4447B	17:34:05.47	+44:47:08.4	M3.5 V		Binary	
J17355+616	GJ 685	17:35:35.07	+61:40:45.4	M0.5 V	6.884	Triple	•
J17364+683	GJ 687	17:36:24.97	+68:20:00.6	M3.0 V	5.335		
J17376+220	GJ 4015	17:37:36.52	+22:05:45.2	M4.1 V	9.764		•
J17378+185	GJ 686	17:37:54.39	+18:35:45.9	M1.5 V	6.360		•

Table B.1: Carmencita, the CARMENES input catalogue (continued).

Karmn	Name	α (2016.0)	δ (2016.0)	Spectral type	J [mag]	Multiplicity[a]	DR1[b]
J17386+612	GJ 4021	17:38:40.87	+61:14:00.0	M4.0 V	10.245		
J17388+080	GJ 4016	17:38:51.16	+08:01:31.7	M2.5 V	8.702		•
J17395+277S	GJ 4018	17:39:30.73	+27:45:40.8	M0.5 V	8.097	Triple	
J17395+277N	GJ 4019	17:39:32.26	+27:46:33.5	M3.0 V	8.828	Triple	
J17419+407	G 204-25	17:41:57.04	+40:44:44.3	M1.5 V	8.917		
J17421-088	Wolf 1471	17:42:09.85	-08:49:07.8	M3.0 V	9.812		
J17423+574	2M17422264+5726521	17:42:22.63	+57:26:52.0	M0.0 V	10.484		
J17425-166	GJ 690.1	17:42:32.15	-16:38:35.9	M2.5 V	9.441		
J17430+057	GJ 4024	17:43:01.06	+05:47:20.5	M1.0 V	7.441	Binary	
J17431+854	G 259-20	17:43:07.85	+85:26:25.5	M2.0 V	8.736	Binary	
J17432-185	Ross 133	17:43:17.37	-18:31:27.7	M1.5 V	8.872		
J17439+433	GJ 694	17:43:55.98	+43:22:33.3	M2.5 V	6.812		
J17460+246	GJ 4026	17:46:04.22	+24:39:13.1	M4.0 V	8.814		
J17455+468	GJ 694.2	17:45:33.50	+46:51:19.8	M0.0 V	7.636	Binary	
J17464+277	GJ 695 C	17:46:24.65	+27:42:49.8	M3.5 V	5.772	Quadruple	
J17469+228	StKM 1-1528	17:46:55.96	+22:48:01.6	M1.0 V	8.674		
J17481+159	PM J17481+1558	17:48:11.19	+15:58:48.4	M3.0 V	9.610		
J17502+237	GJ 4030	17:50:14.74	+23:45:58.1	M3.3 V	9.320		
J17515+147	GJ 4031	17:51:30.58	+14:45:32.4	M3.0 V	9.653		
J17521+647	G 227-20	17:52:11.83	+64:46:02.9	M0.5 V	8.249		
J17464-087	Wolf 1473	17:46:29.28	-08:42:43.4	M3.5 V	8.198	Binary (SB2)	
J17530+169	GJ 4032 A	17:53:00.32	+16:54:59.5	M3.0 V	8.699	Binary	
J17542+073	GJ 1222	17:54:16.48	+07:22:40.2	M4.0 V	8.772		
J17547+128	LSPM J1754+1251	17:54:43.24	+12:51:18.6	M2.0 V	8.738		
J17570+157	GJ 4038	17:57:03.33	+15:46:39.3	M3.0 V	8.329	Binary	•
J17572+707	LP 44-162	17:57:15.43	+70:42:06.4	M7.5 V	11.452		
J17578+046	Barnard's Star	17:57:47.64	+04:44:21.9	M3.5 V	5.244		
J17578+465	GJ 4040	17:57:50.94	+46:35:28.4	M2.5 V	7.847	Binary	
J17589+807	LP 24-152	17:58:55.00	+80:42:53.9	M3.5 V	8.994		•
J18010+508	Wolf 1403	18:01:05.86	+50:49:38.9	M1.5 V	8.927		•
J18012+355	G 182-34	18:01:16.14	+35:35:41.4	M3.5 V	9.695		
J18022+642	LP 71-82	18:02:17.09	+64:15:38.1	M5.0 V	8.541		
J18027+375	GJ 1223	18:02:46.49	+37:30:44.7	dM5.0	9.720		
J18031+179	Wolf 792	18:03:06.02	+17:54:20.0	M1.0 V	8.664		•
J18037+247	Ross 820	18:03:47.68	+25:45:16.7	M0.0 V	8.021		•
J18042+359	GJ 4041	18:04:17.70	+35:57:21.5	M0.5 V	7.728	Binary	
J18051-030	HD 165222	18:05:08.19	-03:01:58.1	M0.0 V	6.161		
J18063+728	NLTT 46021	18:06:18.11	+72:49:20.1	M0.0 V	8.488		
J18074+184	Wolf 806	18:07:27.99	+18:27:54.1	M1.0 V	8.646		•
J18075-159	GJ 1224	18:07:32.15	-15:57:52.6	M4.0 V	8.639		
J18096+318	LP 334-11	18:09:40.77	+31:52:16.0	M1.0 V	8.232		
J18103+512	Wolf 1412	18:10:23.37	+51:15:55.0	M2.0 V	8.996		•
J18109+220	StKM 1-1582	18:10:56.18	+22:01:31.2	M0.0 V	8.437		
J18116+061	LP 569-163	18:11:36.49	+06:06:27.9	M3.0 V	9.266	Binary	
J18131+260	V1334Her	18:13:06.83	+26:01:51.3	M4.0 V	8.899		
J18134+054	LP 569-15	18:13:28.12	+05:26:54.8	M1.5 V	8.432	Binary	
J18135+055	LP 569-16	18:13:33.09	+05:32:08.4	M4.0 V	9.702	Binary	•
J18157+189	HD 348274	18:15:43.54	+18:56:12.7	M0.0 V	7.757		
J18160+139	GJ 708.2	18:16:02.36	+13:54:40.2	M0.0 V	7.343		
J18163+015	GJ 708.3	18:16:17.74	+01:31:17.1	M3.0 V	8.738		
J18165+048	G 140-51	18:16:31.37	+04:52:52.3	M5.0 V	9.798		
J18165+455	GJ 709	18:16:31.07	+45:33:33.7	M0.5 V	7.264		
J18174+483	V401Dra	18:17:25.05	+48:22:03.1	dM2.0	7.770		•
J18180+387E	GJ 4048	18:18:03.73	+38:46:16.2	M3.0 V	8.040	Binary	
J18180+387W	GJ 4049	18:18:02.88	+38:46:17.4	M4.0 V		Binary	•
J18189+661	GJ 4053	18:18:58.38	+66:11:26.2	M4.5 V	8.740		•
J18193-057	GJ 4051	18:19:21.68	-05:46:33.5	M2.0 V	9.233		
J18195+420	PM J18195+4201	18:19:34.48	+42:01:37.4	M1.5 V	8.788		•
J18209-010	GJ 1226 A	18:20:56.62	-01:03:14.2	M3.5 V	8.754	Binary	

Table B.1: Carmencita, the CARMENES input catalogue (continued).

Karmn	Name	α (2016.0)	δ (2016.0)	Spectral type	J [mag]	Multiplicity[a]	DR1[b]
J18221+063	Ross 136	18:22:05.40	+06:20:39.4	M4.0 V	8.671		
J18224+620	GJ 1227	18:22:24.92	+62:02:42.0	M4.0 V	8.640		
J18227+379	G 205-19	18:22:43.47	+37:57:41.1	M1.0 V	8.542		
J18234+281	Ross 708A	18:23:28.24	+28:10:01.0	M3.5 V	8.306	Binary	•
J18240+016	GJ 4056	18:24:05.35	+01:41:12.3	M2.5 V	8.297		•
J18248+282	Ross 710	18:24:52.32	+28:17:22.3	M1.5 V	8.821	Binary	
J18250+246	HD 336196	18:25:04.75	+24:37:57.3	M0.0 V	7.899		
J18255+383	GJ 4058	18:25:31.82	+38:21:00.8	M0.0 V	8.285		
J18264+113	GJ 4059	18:26:24.58	+11:20:52.9	M3.5 V	8.918	Binary	
J18292+638	TYC 4222-2195-1	18:29:13.36	+63:51:10.9	M1.5 V	8.721		
J18296+338	2M18294012+3350130	18:29:40.02	+33:50:13.3	M3.0 V	9.841		
J18312+068	LP 570-92	18:31:16.21	+06:50:08.2	M1.0 V	7.579		
J18319+406	GJ 4062	18:31:58.24	+40:41:17.6	M3.5 V	8.065		
J18346+401	GJ 4063	18:34:36.73	+40:07:23.1	M4.0 V	7.184		
J18352+243	G 184-13A	18:35:13.42	+24:18:39.2	M2.5 V	8.590	Binary	
J18352+414	GJ 4064	18:35:18.38	+41:29:14.5	M2.0 V	8.446		•
J18353+457	GJ 720 A	18:35:19.08	+45:44:44.4	M0.5 V	6.881	Binary	•
J18354+457	GJ 720 B	18:35:27.99	+45:45:46.7	M2.5 V	8.886	Binary	
J18356+329	LSPM J1835+3259	18:35:37.79	+32:59:41.2	M8.5 V	10.270		
J18358+800	GJ 4068	18:35:52.58	+80:05:42.9	M4.0 V	8.989		•
J18362+567	G 227-39	18:36:12.72	+56:44:37.8	M0.0 V	8.354		
J18363+136	Ross 149	18:36:19.43	+13:36:30.8	M4.0 V	8.186		•
J18387+047	LP 570-22	18:38:47.63	+04:46:01.7	M0.5 V	8.320	Binary	
J18394+690	RX J1839.4+6903	18:39:25.71	+69:03:06.8	M2.0 V	8.533		
J18395+298	LP 335-12	18:39:33.18	+29:52:12.9	M6.5 V	11.011		•
J18395+301	LP 335-13	18:39:32.00	+30:09:52.1	M0.0 V	8.065		
J18399+334	GJ 4067	18:39:59.94	+33:24:58.9	M3.5 V	9.131		
J18400+726	LP 44-334	18:40:02.20	+72:40:57.2	M6.5 V	10.974	Binary	
J18387-144	GJ 2138	18:38:44.87	-14:29:35.1	M2.5 V	7.661	Binary	
J18402-104	Wolf 1466	18:40:17.68	-10:28:04.1	M1.0 V	8.262		
J18405+595	G 227-43	18:40:35.77	+59:30:53.6	M2.0 V	8.777		
J18409+315	BD+31 3330B	18:40:55.33	+31:31:37.3	M1.0 V	8.210	Triple	
J18409-133	Ross 720	18:40:57.20	-13:22:57.3	dM1.0	7.397		
J18411+247S	GJ 1230 A	18:41:10.35	+24:47:15.8	M4.5 V	7.528	Triple (SB2)	
J18411+247N	GJ 1230 B	18:41:10.39	+24:47:20.5	M4.5 V	8.860	Triple	•
J18416+397	GJ 4069	18:41:37.04	+39:42:09.3	M4.0 V	9.216		
J18419+318	Ross 145	18:41:58.66	+31:49:49.9	M3.0 V	7.523		
J18427+139	V816Her	18:42:44.94	+13:54:22.4	M5.0 V	8.361		
J18427+596N	HD 173739	18:42:43.94	+59:38:18.1	M3.0 V	5.189	Binary	
J18427+596S	HD 173740	18:42:43.94	+59:38:06.5	M3.5 V	5.721	Binary	•
J18432+253	TYC 2112-920-1	18:43:14.51	+25:22:43.1	M1.0 V	8.771		
J18433+406	V492Lyr	18:43:21.96	+40:40:30.8	M7.5 V	11.313	Binary	•
J18451+063	1R184510.6+062016	18:45:10.23	+06:20:14.7	M1.0 V	7.656		•
J18453+188	G 184-24	18:45:22.79	+18:51:54.3	M4.0 V	9.273		
J18480-145	GJ 4077	18:48:01.01	-14:34:55.0	dM2.5	8.375		
J18482+076	G 141-36	18:48:17.94	+07:41:25.2	M5.0 V	8.853		
J18487+615	LSPM J1848+6135	18:48:47.07	+61:35:06.3	M2.0 V	8.967		
J18498-238	V1216Sgr	18:49:50.11	-23:50:13.6	M3.5 V	6.222		•
J18499+186	G 184-31	18:49:54.34	+18:40:24.2	M4.5 V	9.380		•
J18500+030	Ross 142	18:50:00.63	+03:05:10.7	M0.5 V	7.724		
J18507+479	GJ 4083	18:50:45.66	+47:58:17.3	M3.5 V	8.686		•
J18515+027	BD+02 3698	18:51:35.59	+02:46:19.2	M0.5 V	8.432		
J18516+244	GJ 4084	18:51:40.44	+24:27:31.7	M3.0 V	8.925		
J18518+165	HD 229793	18:51:50.93	+16:34:52.1	M0.0 V	7.162		
J18519+130	1R185200.0+130005	18:51:59.66	+13:00:01.1	M2.0 V	8.345		
J18534+028	G 141-46	18:53:25.68	+02:50:49.4	M2.5 V	8.834		
J18548+008	BD+00 4050	18:54:53.14	+00:51:44.8	M0.0 V	7.789		
J18548+109	HD 230017B	18:54:53.86	+10:58:45.1	M3.5 V	7.139	Triple*	
J18554+084	GJ 735	18:55:27.51	+08:24:07.9	M3.0 V	6.311	Binary (SB2)	

Table B.1: Carmencita, the CARMENES input catalogue (continued).

Karmn	Name	α (2016.0)	δ (2016.0)	Spectral type	J [mag]	Multiplicity[a]	DR1[b]
J18563+544	GJ 4091 B	18:56:18.29	+54:29:45.5	M2.0 V		Quadruple (SB2)	
J18564+463	GJ 4089	18:56:26.40	+46:22:58.5	M4.1 V	9.598		
J18571+075	GJ 4088	18:57:10.40	+07:34:14.7	M2.0 V	8.331		
J18576+535	G 229-20A	18:57:38.42	+53:31:14.4	M3.5 V	8.906	Triple	
J18580+059	HD 176029	18:57:59.93	+05:54:09.7	M1.0 V	6.239		
J18596+079	GJ 4092	18:59:39.00	+07:59:11.2	M0.5 V	7.971		
J19025+704	GJ 4093	19:02:30.83	+70:25:53.6	M2.5 V	8.958		
J19025+754	LSPM J1902+7525	19:02:32.79	+75:25:06.6	M1.5 V	9.797		•
J19032+034	G 141-57	19:03:13.40	+03:24:01.4	M3.0 V	8.665		
J19032+639	GJ 4094	19:03:17.46	+63:59:35.9	M3.5 V	7.785	Triple	
J19032-135	GJ 741	19:03:16.10	-13:34:12.9	M4.0 V	10.375		
J19041+211	1R190405.9+211030	19:04:06.24	+21:10:32.7	M2.0 V	8.750	Binary*	
J19044+590	LSPM J1907+5905	19:07:24.98	+59:05:11.9	M3.0 V	8.457	Binary	
J19045+240	TYC 2122-1204-1	19:04:31.24	+24:01:54.8	M2.0 V	8.789		
J19072+208	HD 349726	19:07:12.66	+20:52:31.9	M2.0 V	7.278	Binary	
J19070+208	Ross 730	19:07:05.02	+20:53:11.4	M2.0 V	7.295	Binary	
J19082+265	GJ 1231	19:08:15.55	+26:34:57.6	M5.0 V	10.361		
J19084+322	GJ 4098	19:08:29.67	+32:16:48.0	M3.0 V	7.905		•
J19077+325	GJ 747	19:07:44.54	+32:32:59.3	M3.0 V	7.242	Binary	•
J19093+382	GJ 4099	19:09:19.01	+39:12:00.7	M2.0 V	7.967	Triple	
J19095+391	LSPM J1909+3910	19:09:31.54	+39:10:48.4	M2.0 V	8.841	Triple	
J19093-147	Ross 727	19:09:20.08	-14:45:02.4	M2.5 V	8.425		•
J19098+176	GJ 1232	19:09:50.16	+17:39:59.6	M4.0 V	8.819		
J19106+015	GJ 4100	19:10:38.38	+01:32:07.3	M1.5 V	8.929	Binary	
J19116+050	TYC 471-1564-1	19:11:47.89	+05:00:37.4	M1.0 V	8.413		
J19124+355	GJ 4105	19:12:29.70	+35:33:50.2	M2.0 V	8.399		•
J19122+028	Wolf 1062	19:12:16.50	+02:53:02.6	M3.5 V	7.087	Binary	
J19146+193N	Ross 733	19:14:38.46	+19:19:10.7	M4.5 V	7.579	Binary	
J19146+193S	Ross 734	19:14:38.51	+19:18:29.9	M4.0 V	9.101	Binary	
J19169+051N	V1428Aql	19:16:54.64	+05:09:46.7	M2.5 V	5.583	Binary	
J19169+051S	V1298Aql	19:16:56.97	+05:08:39.7	M8.0 V	9.908	Binary	
J19185+580	LSPM J1918+5803	19:18:30.48	+58:03:16.6	M1.0 V	8.979	Binary*	
J19205-076	GJ 754.1 B	19:20:33.38	-07:39:46.6	M2.5 V	8.221	Binary	•
J19206+731S	2M19204172+7311434	19:20:41.75	+73:11:42.4	M4.0 V	10.604	Binary*	•
J19206+731N	2M19204172+7311467	19:20:41.76	+73:11:45.5	M4.5 V	10.795	Binary*	
J19216+208	GJ 1235	19:21:37.62	+20:51:40.0	M4.0 V	8.796		
J19218+286	V2078Cyg	19:21:52.48	+28:40:02.3	M1.5 V	8.352		
J19220+070	GJ 1236	19:22:01.28	+07:02:23.2	M4.0 V	8.524		•
J19228+307	GSC 02654-01527	19:22:48.64	+30:45:13.5	M0.0 V	7.859		
J19234+666	NLTT 47788	19:23:24.51	+66:39:54.2	M1.0 V	8.864		•
J19215+425	1R192132.1+423041	19:21:32.18	+42:30:54.8	M2.0 V	8.624	Binary	
J19242+797	TYC 4592-101-1	19:24:15.66	+79:43:37.3	M1.0 V	8.665	Binary	
J19237+797	PM J19237+7944	19:23:46.46	+79:44:37.6	M1.5 V	8.806	Binary	
J19242+755	GJ 1238	19:24:17.89	+75:33:21.3	M6.0 V	9.908		
J19251+283	Ross 164	19:25:08.74	+28:21:19.8	M3.5 V	8.442		
J19255+096	LSPM J1925+0938	19:25:31.00	+09:38:19.4	M8/9V	11.214		
J19260+244	G 185-23	19:26:01.84	+24:26:18.7	M4.5 V	9.625		
J19268+167	GJ 4110	19:26:49.42	+16:42:58.3	M3.5 V	9.000		•
J19284+289	TYC 2137-1575-1	19:28:25.51	+28:54:09.6	M0.0 V	8.016		•
J19289+066	PM J19289+0638	19:28:55.70	+06:38:24.5	M1.5 V	8.977		
J19312+361	G 125-15	19:31:12.38	+36:07:28.2	M4.5 V	9.609	Triple (SB2)	
J19326+005	GJ 761.2	19:32:38.15	+00:34:39.5	M0.0 V	7.635		
J19336+395	Ross 1063	19:33:39.75	+39:31:29.9	M1.5 V	8.120		
J19346+045	HD 184489	19:34:40.40	+04:35:02.0	M0.0 V	6.714		
J19349+532	Wolf 1108	19:34:55.56	+53:15:31.3	M2.5 V	8.554		
J19351+084S	GJ 4114	19:35:06.24	+08:27:37.9	M0.5 V	7.329	Triple	
J19351+084N	GJ 4115	19:35:06.33	+08:27:43.4	M2.5 V	8.864	Triple	•
J19358+413	Ross 1064	19:35:51.00	+41:19:06.7	M0.0 V	7.563		
J19395+718	GJ 4120	19:39:32.22	+71:52:12.1	M0.5 V	8.023		

Table B.1: Carmencita, the CARMENES input catalogue (continued).

Karmn	Name	α (2016.0)	δ (2016.0)	Spectral type	J [mag]	Multiplicity[a]	DR1[b]
J19419+031	GJ 1242	19:41:53.93	+03:09:08.3	M2.0 V	9.304		
J19354+377	RX J1935.4+3746	19:35:29.02	+37:46:06.7	M3.5 V	7.562	Binary (SB1)	
J19422-207	2M19421282-2045477	19:42:12.81	-20:45:50.4	M5.1 V	9.598		
J19420-210	LP 869-19	19:42:00.74	-21:04:09.4	M3.5 V	8.692	Binary (SB2)	
J19457+271	Ross 165A	19:45:45.41	+27:07:11.7	M4.0 V	7.998	Binary	
J19457+323	GJ 4122	19:45:50.25	+32:23:16.8	M1.5 V	7.572		
J19463+320	HD 331161A	19:46:24.51	+32:00:55.2	M0.5 V	6.883	Binary	•
J19464+320	HD 331161B	19:46:24.83	+32:00:51.1	M2.5 V	7.323	Binary	
J19468-019	PM J19468-0157	19:46:50.63	-01:57:40.1	M3.0 V	8.512		
J19470+352	LSPM J1947+3516	19:47:03.30	+35:16:55.5	M2.0 V	8.839		
J19486+359	G 125-34	19:48:40.88	+35:55:12.6	M3.5 V	8.909		
J19500+325	GJ 4124	19:50:03.10	+32:35:05.5	M3.0 V	8.647	Binary	
J19502+317	GJ 4125	19:50:16.11	+31:47:05.7	M2.1 V	9.178	Binary	
J19510+104	GJ 9671 B	19:51:00.97	+10:24:38.0	M4.0 V	8.888	Binary	
J19511+464	GJ 1243	19:51:09.60	+46:29:04.5	M4.0 V	8.586		
J19512+622	G 260-35	19:51:11.69	+62:17:15.7	M2.0 V	8.348		
J19535+341	GJ 4127	19:53:32.73	+34:08:32.2	M1.5 V	8.329		
J19539+444W	V1581Cyg	19:53:55.14	+44:24:44.4	M5.5 V	7.791	Triple	•
J19539+444E	GJ 1245 B	19:53:55.66	+44:24:46.5	M5.5 V	8.275	Triple	
J19540+325	GJ 4128	19:54:02.88	+32:33:55.8	M2.5 V	8.946		
J19546+202	TYC 1624-397-1	19:54:37.52	+20:13:05.5	M0.0 V	8.068		
J19558+512	Wolf 1122	19:55:53.62	+51:16:27.7	M1.5 V	8.658		
J19565+591	GJ 9677 A	19:56:33.06	+59:09:40.3	M0.0 V	7.423	Binary	
J19564+591	GJ 9677 B	19:56:23.96	+59:09:19.7	M3.5 V	9.653	Binary	
J19573-125	GJ 773 B	19:57:23.71	-12:33:58.5	M5.0 V	10.212	Binary	
J19582+020	GJ 4129	19:58:15.38	+02:02:02.5	M2.5 V	8.371		
J19582+650	G 260-38	19:58:16.31	+65:02:25.0	M3.5 V	8.740		
J20011+002	LP 634-16	20:01:06.21	+00:16:12.0	M2.0 V	8.106		
J20005+593	1R200031.8+592127	20:00:31.98	+59:21:29.9	M4.1 V	9.636	Binary	
J20034+298	GJ 777 B	20:03:27.42	+29:51:51.1	M4.5 V	9.554	Binary	
J20037+644	1R200348.4+642542	20:03:47.80	+64:25:45.3	M0.0 V	8.267		
J20038+059	GJ 1248	20:03:50.47	+05:59:31.4	M2.5 V	8.632		
J20039-081	GJ 4132	20:03:58.37	-08:07:51.4	M4.0 V	9.184		
J20050+544	V1513Cyg	20:05:00.07	+54:25:48.8	sdM1	8.830	Triple (SB1)	
J20057+529	Wolf 1131	20:05:44.59	+52:58:21.1	M4.0 V	9.095		
J20079-015	GJ 4136	20:07:57.91	-01:32:31.5	M3.0 V	9.586		
J20082+333	GJ 1250	20:08:18.35	+33:18:19.0	M4.77	9.961		
J20093-012	PM J20093-0113	20:09:18.20	-01:13:44.3	M5.0 V	9.403		
J20105+065	LP 574-21	20:10:34.49	+06:32:10.7	M4.0 V	8.021	Triple (SB2)	
J20112+161	GJ 783.2 B	20:11:12.80	+16:11:14.4	M4.0 V	9.627	Binary	
J20112+379	LSPM J2011+3757	20:11:12.85	+37:57:48.1	M1.5 V	8.593		•
J20129+342	LP 283-5	20:12:54.72	+34:16:54.5	M1.0 V	8.213	Binary	
J20132+029	[R78b] 440	20:13:12.94	+02:56:02.3	M1.0 V	8.739	Binary	
J20138+133	Ross 754	20:13:52.27	+13:23:20.0	M1.0 V	8.309		
J20139+066	GJ 784.2 A	20:13:58.71	+06:41:06.8	M3.3 V	9.090	Binary	
J20151+635	LP 106-240	20:15:10.64	+63:31:16.4	M0.0 V	8.384		
J20165+351	G 210-11	20:16:32.04	+35:10:37.6	M2.0 V	8.905		
J20187+158	GJ 4143	20:18:44.75	+15:50:45.3	M2.5 V	8.174		
J20195+080	GJ 4144	20:19:34.60	+08:00:27.1	M3.0 V	9.190	Binary*	
J20198+229	LP 395-8 A	20:19:49.36	+22:56:38.1	M3.0 V	8.166	Quadruple* (SB2)	
J20220+216	TYC 1643-120-1	20:22:01.62	+21:47:19.7	M2.0 V	8.741	Binary*	
J20223+322	PM J20223+3217	20:22:18.82	+32:17:15.1	M3.5 V	8.810		
J20229+106	G 143-48	20:22:55.79	+10:40:44.5	M3.0 V	9.953		
J20232+671	LP 73-196	20:23:18.57	+67:10:12.9	M5.0 V	10.075	Binary	•
J20260+585	Wolf 1069	20:26:05.84	+58:34:31.4	dM5.0	9.029		
J20287-114	LP 755-19	20:28:43.80	-11:28:32.4	M1.5 V	8.394		
J20269+275	GJ 4146	20:26:56.29	+27:31:03.1	M2.0 V	8.762	Binary	
J20298+096	HUDel	20:29:49.04	+09:41:22.2	M4.5 V	8.228	Binary	
J20305+654	GJ 793	20:30:33.18	+65:27:02.9	M2.5 V	6.735		

Table B.1: Carmencita, the CARMENES input catalogue (continued).

Karmn	Name	α (2016.0)	δ (2016.0)	Spectral type	J [mag]	Multiplicity[a]	DR1[b]
J20301+798	1R203011.0+795040	20:30:07.75	+79:50:47.4	M3.0 V	8.480	Binary (SB2)	•
J20336+617	GJ 1254	20:33:41.53	+61:45:28.2	M4.0 V	8.287		
J20314+385	Ross 188	20:31:25.91	+38:33:55.8	M5.0 V	9.193	Binary	
J20337+233	GJ 4148	20:33:43.10	+23:22:15.4	M3.0 V	9.110	Binary	
J20339+643	GJ 4150	20:33:58.81	+64:19:08.1	M3.5 V	9.228		
J20347+033	GJ 4149	20:34:43.33	+03:20:43.6	M2.5 V	8.446		•
J20349+592	Wolf 1074	20:34:54.81	+59:17:26.0	M4.0 V	9.318		
J20367+388	GJ 4152	20:36:46.27	+38:50:30.3	M3.5 V	9.270		•
J20373+219	Wolf 1351	20:37:20.77	+21:56:47.8	M0.5 V	8.157	Binary	
J20403+616	TYC 4246-488-1	20:40:18.59	+61:41:28.4	M1.0 V	8.154		
J20405+154	GJ 1256	20:40:35.33	+15:30:09.3	M4.5 V	8.641		
J20407+199	GJ 797 B	20:40:44.65	+19:54:08.2	M2.5 V	8.160	Triple	
J20409-101	GJ 4155	20:40:56.32	-10:06:43.1	M1.5 V	8.535	Binary (SB)	
J20418-324	ATMicA	20:41:51.44	-32:26:13.3	M4.5 V	5.807	SKG	
J20451-313	AUMic	20:45:09.88	-31:20:33.0	M0.5 V	5.436	SKG	
J20429-189	Ross 751	20:42:57.83	-18:55:19.8	M1.5 V	7.557		•
J20433+047	LP 575-35	20:43:24.35	+04:45:52.9	M5.0 V	10.083		
J20435+240	Wolf 1360	20:43:34.69	+24:07:40.2	M2.5 V	8.241		
J20436+642	G 262-26	20:43:42.13	+64:16:52.5	M0.0 V	8.399		
J20436-001	GJ 4159	20:43:41.71	-00:10:37.5	M1.0 V	8.484		
J20433+553	Wolf 1084	20:43:20.89	+55:21:20.5	M5.0 V	9.563	Binary	
J20443+197	HD 352860	20:44:21.98	+19:44:49.8	M0.0 V	7.359	Binary	
J20445+089S	GJ 4160	20:44:30.94	+08:54:12.6	M1.5 V	8.136	Triple	
J20445+089N	GJ 4161	20:44:30.67	+08:54:27.1	M0.5 V	8.607	Triple (SB2)	
J20450+444	GJ 806	20:45:04.75	+44:30:01.0	M1.5 V	7.329		
J20496-003	Wolf 882	20:49:39.86	-00:21:06.7	M3.5 V	9.099		
J20488+197	GJ 4163	20:48:52.27	+19:43:01.6	M3.3 V	9.236	Binary	
J20525-169	LP 816-60	20:52:32.67	-16:58:28.4	M4.0 V	7.090		
J20519+691	GJ 4170	20:52:00.55	+69:10:07.6	M1.0 V	8.452	Binary	•
J20533+621	HD 199305	20:53:19.79	+62:09:03.4	M1.0 V	5.429		•
J20535+106	GJ 4169	20:53:32.53	+10:36:55.0	M5.0 V	9.348		
J20549+675	LP 74-35	20:54:54.90	+67:35:09.8	M2.0 V	8.749		
J20532-023	LP 636-19	20:53:14.87	-02:21:21.7	M3.0 V	9.329	Binary	
J20556-140N	GJ 810 A	20:55:39.31	-14:02:15.6	M4.0 V	8.117	Triple (SB2)	•
J20556-140S	GJ 810 B	20:55:38.68	-14:04:02.4	M5.0 V	9.717	Triple	
J20567-104	Wolf 896	20:56:46.56	-10:27:12.7	dM2.5	7.766		•
J20568-048	FRAqr	20:56:49.39	-04:50:52.6	M4.0 V	7.816	Triple (SB2)	
J20574+223	Wolf 1373	20:57:26.24	+22:21:42.4	M3.0 V	8.410		
J20586+342	GJ 4173	20:58:42.31	+34:16:24.7	M0.5 V	8.073		•
J21001+495	G 212-14	21:00:09.24	+49:35:20.8	M2.0 V	8.546		•
J21000+400	V1396Cyg	21:00:06.23	+40:04:08.6	M2.0 VM0.5V	6.668	Binary	•
J21012+332	GJ 4176	21:01:16.51	+33:14:30.7	M4.0 V	8.439	Quadruple	
J21013+332	GJ 4177	21:01:21.03	+33:14:25.9	M4.0 V	8.936	Quadruple	
J21019-063	Wolf 906	21:01:58.39	-06:19:14.5	M2.5 V	7.563		
J21027+349	G 211-9	21:02:46.40	+34:54:31.2	M4.5 V	9.846		
J21044+455	TYC 3588-5589-1	21:04:28.94	+45:35:42.3	M2.0 V	8.993		
J21048-169	Ross 769	21:04:52.36	-16:58:04.6	M1.5 V	8.285		
J21014+207	GJ 4175	21:01:24.40	+20:43:31.6	M3.5 V	9.941	Binary	
J21055+061	PM J21055+0609N	21:05:32.09	+06:09:16.2	M3.0 V	8.694	Binary*	
J21057+502	PM J21057+5015E	21:05:45.54	+50:15:44.1	M3.5 V	9.543	Binary*	•
J21059+044	GJ 4180	21:05:56.52	+04:25:38.0	M2.5 V	8.574		
J21074+468	PM J21074+4651	21:07:28.14	+46:51:55.4	M2.0 V	9.488		
J21076-130	1R210736.5-130500	21:07:36.86	-13:04:59.6	M3.0 V	8.734		
J21087-044S	GJ 9721	21:08:45.41	-04:25:36.7	M1.0 V	7.146	Triple	
J21087-044N	GJ 9721B	21:08:44.75	-04:25:18.3	M3.0 V	9.481	Triple	
J21092-133	Wolf 918	21:09:18.21	-13:18:40.9	M1.0 V	7.688		
J21100-193	1R211004.9-192005	21:10:05.46	-19:19:59.1	M2.0 V	8.112	Binary	
J21123+359	LP 285-9	21:12:22.66	+35:55:24.7	M1.5 V	8.490		
J21127-073	PM J21127-0719	21:12:45.71	-07:19:56.5	M3.5 V	9.902		

Table B.1: Carmencita, the CARMENES input catalogue (continued).

Karmn	Name	α (2016.0)	δ (2016.0)	Spectral type	J [mag]	Multiplicity[a]	DR1[b]
J21109+294	Ross 824	21:10:54.47	+29:25:18.6	M1.5 V	7.799	Binary	
J21137+087	LSPM J2113+0846N	21:13:44.77	+08:46:09.1	M2.0 V	8.384	Triple	
J21138+180	Ross 772	21:13:53.01	+18:05:58.8	M3.0 V	8.970		
J21145+508	LSPM J2114+5052	21:14:32.61	+50:52:31.6	M2.5 V	8.456		
J21147+380	GJ 822.1 C	21:14:47.09	+38:01:21.0	M2.5 V	8.337	Quadruple	
J21152+257	GJ 4184	21:15:12.76	+25:47:41.2	M3.0 V	8.403		
J21160+298E	Ross 776	21:16:06.06	+29:51:51.5	M3.3 V	8.448	Triple	
J21160+298W	Ross 826	21:16:04.10	+29:51:46.7	M3.3 V	9.295	Triple	
J21164+025	LSPM J2116+0234	21:16:27.55	+02:34:50.8	M3.0 V	8.219		
J21173+208N	Ross 773A	21:17:23.09	+20:53:59.2	M3.0 V	8.683	Binary	
J21173+208S	Ross 773B	21:17:23.00	+20:54:03.4	M4.0 V	8.911	Binary	•
J21173+640	G 262-38	21:17:22.75	+64:02:39.1	M5.0 V	10.043		
J21176-089N	GJ 4187	21:17:36.07	-08:54:11.7	M2.5 V	8.467	Triple	
J21176-089S	GJ 4188	21:17:39.55	-08:54:49.6	M3.0 V	9.517	Triple	•
J21185+302	1R211833.8+301434	21:18:33.83	+30:14:34.3	M1.5 V	8.643		
J21221+229	TYC 2187-512-1	21:22:06.41	+22:55:55.0	M1.0 V	7.400		
J21243+085	GJ 4192	21:24:19.08	+08:30:03.6	M3.5 V	9.667		
J21245+400	LSPM J2124+4003	21:24:33.07	+40:04:06.7	M5.5 V	10.339		
J21267+037	GJ 828.1	21:26:42.41	+03:44:12.9	M0.0 V	7.794		
J21272-068	Wolf 920	21:27:16.89	-06:50:45.8	M0.5 V	8.046		
J21275+340	V2160Cyg	21:27:32.60	+34:01:25.7	M1.5 V	8.031		•
J21277+072	Ross 778	21:27:46.19	+07:17:45.9	M1.0 V	8.373		
J21280+179	LP 457-38	21:28:05.57	+17:54:02.7	M1.5 V	8.907		
J21283-223	GJ 4197	21:28:18.04	-22:18:36.5	M2.5 V	8.501		
J21296+176	Ross 775	21:29:37.94	+17:38:41.9	M3.0 V	6.249	Binary (EB?/SB2)	
J21313-097	BBCap	21:31:19.92	-09:47:27.5	M4.5 V	7.316	Binary	
J21323+245	GJ 4201 A	21:32:22.33	+24:33:41.9	M4.0 V	8.476	Binary	
J21338+017S	GJ 4203	21:33:49.11	+01:46:44.9	M4.0 V	9.646	Binary	
J21338+017N	GJ 4204	21:33:49.13	+01:46:50.0	M4.0 V	9.977	Binary	
J21338-068	Wolf 923	21:33:49.04	-06:51:18.4	M4.0 V	9.562		
J21348+515	Wolf 926	21:34:51.13	+51:32:18.6	M2.5 V	8.038		
J21366+394	V2168Cyg	21:36:38.29	+39:27:18.0	M0.0 V	7.111	Binary	
J21369+561	Ross 215	21:36:58.82	+56:07:07.2	M1.5 V	8.695		
J21374-059	PM J21374-0555	21:37:29.02	-05:55:05.7	M3.0 V	8.779	Binary	
J21378+530	Ross 199	21:37:50.77	+53:04:49.9	M0.0 V	7.753		
J21376+016	1R213740.3+013711	21:37:40.28	+01:37:12.7	M4.5 V	8.802	Binary	•
J21380+277	GJ 835	21:38:00.96	+27:43:24.4	M0.0 V	6.809	Triple	
J21402+370	LP 286-1	21:40:12.27	+37:03:24.1	M0.5 V	8.460		
J21399+276	GJ 4210	21:39:54.70	+27:36:39.8	M2.0 V	8.211	Binary	
J21421-121	Ross 206	21:42:07.58	-12:09:59.3	M3.0 V	8.922		
J21419+276	GJ 4212	21:41:58.03	+27:41:14.2	M4.0 V	9.825	Binary	
J21441+170S	GJ 4214	21:44:09.31	+17:03:35.0	M4.0 V	9.313	Binary	
J21441+170N	GJ 4215	21:44:08.25	+17:04:37.3	M5.2 V	10.078	Binary	
J21442+066	GJ 4213	21:44:12.64	+06:38:26.6	M3.0 V	8.271	Binary (SB1)	
J21449+442	G 215-12	21:44:53.78	+44:16:58.4	M1.5 V	8.100	Binary	
J21450+198	G 126-32B	21:45:04.90	+19:53:31.7	M1.5 V		Triple*	
J21450-057	Wolf 937	21:45:00.59	-05:47:20.3	M3.0 V	9.034		
J21454-059	Wolf 939	21:45:24.74	-05:54:11.5	M3.5 V	9.604		
J21463+382	LSPM J2146+3813	21:46:22.29	+38:13:03.1	M5.0 V	7.949		
J21466+668	G 264-12	21:46:41.30	+66:48:14.0	M4.0 V	8.837		
J21466-001	Wolf 940	21:46:41.24	-00:10:31.9	dM4.0	8.364	Binary	
J21469+466	Wolf 944	21:46:56.68	+46:38:06.1	M4.0 V	9.089		
J21472-047	PM J21472-0444	21:47:17.73	-04:44:40.6	M4.5 V	9.416		
J21474+627	TYC 4266-736-1	21:47:24.39	+62:45:13.7	M0.0 V	8.771	Binary	•
J21478+502	Wolf 945	21:47:53.64	+50:14:54.6	M4.0 V	9.311		•
J21479+058	Ross 779	21:47:57.57	+05:49:16.4	M2.0 V	8.626		•
J21481+014	GJ 4221	21:48:10.46	+01:26:42.0	M3.0 V	9.824		
J21482+279	GJ 4225	21:48:15.02	+27:55:31.0	M2.0 V	8.508		
J21512+128	GJ 4227	21:51:18.24	+12:50:33.2	M4.0 V	9.349		•

Table B.1: Carmencita, the CARMENES input catalogue (continued).

Karmn	Name	α (2016.0)	δ (2016.0)	Spectral type	J [mag]	Multiplicity[a]	DR1[b]
J21518+136	GJ 4228	21:51:48.53	+13:36:13.8	M4.0 V	9.311	Binary	
J21516+592	TYC 3980-1081-1	21:51:38.15	+59:17:40.0	M4.0 V	6.529	Binary	
J21521+274	GJ 4232	21:52:12.12	+27:24:48.2	M5.0 V	9.984		
J21539+417	GJ 839	21:53:59.55	+41:46:38.7	M0.0 V	7.572		
J21566+197	Ross 263	21:56:37.83	+19:46:06.8	M3.0 V	8.928		
J21569-019	GJ 4239	21:56:56.61	-01:53:59.5	M5.0 V	9.880		
J21574+081	Wolf 953	21:57:26.64	+08:08:15.5	M1.5 V	7.723		
J21584+755	GJ 842.2	21:58:25.51	+75:35:21.0	M0.5 V	7.601		
J21585+612	LSPM J2158+6117	21:58:36.41	+61:17:07.8	M6.0 V	11.292		
J21593+418	GJ 4246	21:59:22.08	+41:51:25.4	M3.0 V	8.982		
J22012+283	V374Peg	22:01:13.58	+28:18:25.6	M3.5 V	7.635		
J21521+056	GJ 4231	21:52:10.52	+05:37:33.5	M2.4 V	8.248	Binary	
J22012+323	Wolf 1154 A	22:01:14.13	+32:23:13.9	M1.5 V	8.829	Triple	
J22018+164	Ross 265	22:01:49.49	+16:28:05.2	M2.5 V	7.009	Triple*	
J22020-194	GJ 843	22:02:01.85	-19:28:58.0	dM3.5	8.046		
J22021+014	HD 209290	22:02:09.79	+01:23:56.4	M0.5 V	6.196		•
J22033+674	GJ 4251	22:03:22.74	+67:29:55.1	M4.5 V	9.410		
J22051+051	Wolf 983	22:05:07.30	+05:08:14.2	M4.0 V	9.518		
J22035+036	1R220330.8+034001	22:03:33.39	+03:40:21.4	M4.0 V	9.742	Binary	•
J22057+656	GJ 4258	22:05:44.55	+65:38:58.9	M1.5 V	8.422	Binary	•
J22058-119	Wolf 1548	22:05:51.00	-11:54:53.7	M0.0 V	7.221	Binary	
J22060+393	GJ 4256	22:06:00.76	+39:17:55.6	M3.0 V	8.912		
J22067+034	Wolf 990	22:06:46.87	+03:24:58.7	M4.0 V	9.409		
J22088+117	PM J22088+1144	22:08:50.44	+11:44:12.4	M4.5 V	9.901		•
J22095+118	LP 519-38	22:09:31.86	+11:52:51.6	M3.0 V	9.901		
J22096-046	Wolf 1329	22:09:41.56	-04:38:27.0	M3.5 V	6.510		
J22097+410	GJ 4260	22:09:43.64	+41:02:09.5	M3.0 V	8.755		
J22102+587	UCAC4 744-073158	22:10:15.18	+58:42:21.9	M2.0 V	9.860		
J22107+079	Wolf 1003 A	22:10:44.98	+07:54:32.9	M0.5 V	7.936	Binary	
J22112+410	G 214-14	22:11:16.65	+41:00:58.6	M0.0 V	8.228		
J22112-025	GJ 4262	22:11:13.95	-02:32:38.2	M2.0 V	8.688		•
J22114+409	1R221124.3+410000	22:11:24.04	+40:59:59.8	M5.5 V	9.725		
J22115+184	Ross 271	22:11:30.46	+18:25:37.2	M2.0 V	6.725		
J22117-207	WT 2221	22:11:42.27	-20:44:19.3	M3.5 V	9.676	Binary	
J22125+085	Wolf 1014	22:12:36.06	+08:33:00.9	M3.0 V	8.277		
J22129+550	LF 4 +54 152	22:12:56.63	+55:04:50.8	M0.0 V	8.125	Binary*	
J22134-147	Wolf 1556	22:13:28.46	-14:44:58.8	M3.5 V	9.449		•
J22135+259	GJ 4264	22:13:35.90	+25:58:08.1	M4e	9.511		•
J22137-176	GJ 1265	22:13:43.82	-17:41:13.6	dM4.5	8.955		
J22138+052	Wolf 1019	22:13:53.53	+05:16:34.9	M1.5 V	8.541	Binary	•
J22154+662	GJ 4267	22:15:26.16	+66:13:31.1	M3.0 V	8.749		
J22142+255	1R221419.3+253411	22:14:17.88	+25:34:05.6	M4.3 V	10.177	Binary	
J22160+546	GJ 4269	22:16:02.99	+54:40:00.5	M4.0 V	9.718	Binary	
J22163+709	GJ 1266	22:16:23.03	+70:56:39.2	M2.0 V	8.746		•
J22173-088N	FGAqr	22:17:18.47	-08:48:16.9	M4.0 V	9.024	Triple	
J22173-088S	Wolf 1561 B	22:17:18.16	-08:48:23.4	M5.0 V	9.459	Triple	
J22176+565	PM J22176+5633	22:17:37.21	+56:33:11.1	M1.5 V	8.992		
J22202+067	Wolf 1034	22:20:13.57	+06:43:36.5	M2.5 V	9.500		
J22228+280	GJ 4275	22:22:51.34	+28:01:46.4	M3.8 V	9.758		
J22231-176	GJ 4274	22:23:07.34	-17:36:37.8	M4.5 V	8.242		
J22234+324	Wolf 1225 A	22:23:29.44	+32:27:29.9	M3.0 V	6.898	Binary	
J22249+520	GJ 1268	22:24:56.33	+52:00:25.6	M5.1 V	10.155		
J22250+356	Wolf 1231	22:25:01.66	+35:40:05.3	M2.0 V	8.537		
J22252+594	GJ 4276	22:25:17.32	+59:24:44.9	M3.5 V	8.745		
J22262+030	Wolf 1201	22:26:15.24	+03:00:11.3	M4.0 V	9.623	Binary	
J22264+583	PM J22264+5823	22:26:24.73	+58:23:03.9	M3.0 V	9.461		•
J22270+068	GJ 4279	22:27:03.00	+06:49:32.1	M4.0 V	9.020		
J22279+576	HD 239960A	22:27:58.11	+57:41:38.5	M3.0 V	5.575	Binary	
J22287+189	GJ 9784	22:28:46.13	+18:55:52.1	M1.0 V	7.819		

Table B.1: Carmencita, the CARMENES input catalogue (continued).

Karmn	Name	α (2016.0)	δ (2016.0)	Spectral type	J [mag]	Multiplicity[a]	DR1[b]
J22289-134	GJ 4281	22:28:53.99	-13:25:36.2	M6.5 V	10.768		•
J22290+016	LP 640-74	22:29:05.91	+01:39:45.0	M0.5 V	7.616		
J22298+414	GJ 1270	22:29:50.68	+41:28:55.8	M4.0 V	8.849		
J22300+488	PM J22300+4851A	22:30:04.10	+48:51:33.8	M4.5 V	9.524	Binary	
J22330+093	GJ 863	22:33:02.81	+09:22:43.0	M1.0 V	7.208		
J22333-096	GJ 4282 A	22:33:22.77	-09:36:53.6	M2.6 V	8.534	Binary	
J22347+040	GJ 4283	22:34:46.11	+04:02:39.7	M3.0 V	8.964		
J22348-010	GJ 4284	22:34:54.85	-01:04:54.5	M4.5 V	10.388		
J22353+746	G 242-3	22:35:20.75	+74:41:20.1	M0.0 V	8.425		•
J22373+299	LP 344-27	22:37:23.33	+29:59:05.6	M1.5 V	8.959		
J22361-008	HD 214100	22:36:09.75	-00:50:39.8	M1.0 V	7.038	Binary	•
J22374+395	GJ 4287	22:37:29.83	+39:22:45.9	M0.0 V	6.639	Triple	
J22387+252	G 127-42	22:38:44.65	+25:13:30.5	M3.5 V	9.769		
J22385-152	EZAqr	22:38:36.17	-15:17:22.7	M5.5 V	6.553	Triple (ST3)	
J22387-206S	FKAqr	22:38:46.09	-20:37:17.4	M1.5 V	5.669	Quadruple (SB2)	
J22387-206N	FLAqr	22:38:45.77	-20:36:52.9	M3.5 V	7.344	Quadruple (SB1)	
J22406+445	GJ 4290	22:40:42.53	+44:35:47.0	M3.5 V	9.216		
J22415+188	GJ 9793	22:41:35.30	+18:49:28.9	M0.0 V	7.883		
J22415+260	1R224134.7+260210	22:41:35.76	+26:02:13.8	M3.5 V	9.044		
J22426+176	GJ 1271	22:42:39.99	+17:40:17.6	M2.5 V	8.062		
J22433+221	GJ 4292	22:43:23.65	+22:08:18.1	M5.0 V	10.143		
J22437+192	RX J2243.7+1916	22:43:43.73	+19:16:52.4	M3.0 V	9.242		
J22441+405	TYC 3218-905-1	22:44:06.16	+40:29:58.1	M1.0 V	8.199	Binary	
J22440+405	TYC 3218-907-1	22:44:04.51	+40:29:58.5	M1.0 V	8.167	Binary	
J22457+016	LP 641-4	22:45:46.48	+01:41:22.0	M1.0 V	8.915	Binary	
J22464-066	GJ 4294	22:46:27.09	-06:39:35.0	M5.0 V	10.790		
J22468+443	ELac	22:46:48.68	+44:19:55.0	M4.0 V	6.106		
J22476+184	LP 461-11	22:47:39.35	+18:26:40.4	M2.5 V	9.102		
J22479+318	GJ 4297	22:47:54.67	+31:52:18.4	M3.0 V	9.087		
J22489+183	PM J22489+1819	22:48:54.56	+18:19:56.9	M4.5 V	9.957		
J22503-070	HD 216133	22:50:19.31	-07:05:22.7	M0.5 V	6.932		
J22506+348	GJ 1274	22:50:38.79	+34:51:26.8	M2+ V	8.280		
J22507+286	GJ 4300	22:50:45.77	+28:36:07.7	M2.5 V	8.810		•
J22509+499	1R225056.4+495906	22:50:55.28	+49:59:13.2	M4.0 V	9.804		
J22518+317	GTPeg	22:51:54.19	+31:45:14.4	M3.5 V	7.697		
J22524+099	GJ 9801 B	22:52:30.31	+09:54:04.9	M3.0 V	9.657	Triple	
J22526+750	LP 48-305	22:52:40.21	+75:04:16.7	M4.5 V	9.089		•
J22543+609	Ross 226	22:54:19.95	+60:59:41.5	M3.0 V	8.836		
J22547-054	GJ 4302	22:54:47.14	-05:28:21.1	M4.0 V	9.650		
J22532-142	ILAqr	22:53:17.79	-14:16:00.1	M4.0 V	5.934		
J22559+057	GJ 4304	22:55:57.20	+05:45:14.0	M1.0 V	8.130	Binary	•
J22559+178	GJ 4306	22:55:59.87	+17:48:38.0	M1.0 V	7.319		
J22565+165	HD 216899	22:56:33.65	+16:33:07.8	M1.5 V	5.360		
J22576+373	G 189-53A	22:57:40.20	+37:19:17.8	M3.0 V	8.975	Binary	•
J23028+436	1R230251.9+433814	23:02:52.29	+43:38:15.5	M4.0 V	9.316		
J23036+097	PM J23036+0942	23:03:37.56	+09:42:59.0	M3.5 V	9.992		
J23045+667	GJ 1278	23:04:31.03	+66:45:50.5	M0.5 V	7.094		
J23051+519	PM J23051+5159	23:05:06.47	+51:59:11.6	M3.5 V	9.680		•
J23060+639	GJ 9809	23:06:05.27	+63:55:33.4	M0.3 V	7.815		•
J23051+452	LSPM J2305+4517	23:05:09.00	+45:17:32.9	M3.5 V	9.297	Binary*	
J23063+126	LP 521-79	23:06:24.19	+12:36:25.6	M0.5 V	8.375	Quadruple (SB2/3?)	
J23064-050	2MUCD 12171	23:06:30.37	-05:02:36.7	M7.5 V	11.354		
J23065+717	GJ 4311	23:06:39.95	+71:43:32.5	M2.0 V	8.336		
J23075+686	GJ 4312	23:07:33.27	+68:40:06.1	M3.0 V	8.624		
J23081+033	GJ 889.1	23:08:07.49	+03:19:48.5	M0.0 V	7.865		
J23083-154	HKAqr	23:08:19.67	-15:24:36.1	M0.0 V	7.979		
J23088+065	StKM 1-2100	23:08:52.60	+06:33:39.9	M0.0 V	8.047		
J23089+551	G 233-42	23:09:58.62	+55:06:48.1	M5.0 V	10.541	Binary	•
J23096-019	GJ 4314	23:09:39.64	-01:58:29.9	M3.5 V	8.671	Triple (SB2)	

Table B.1: Carmencita, the CARMENES input catalogue (continued).

Karmn	Name	α (2016.0)	δ (2016.0)	Spectral type	J [mag]	Multiplicity[a]	DR1[b]
J23107-192	GJ 1281	23:10:42.22	-19:13:57.9	M2.5 V	8.976		
J23113+085	G 28-46	23:11:23.45	+08:30:56.4	M3.0 V	8.466	Binary*	
J23121-141	GJ 4316	23:12:11.11	-14:06:23.2	M3.0 V	9.064		
J23166+196	GJ 893.4	23:16:39.52	+19:37:14.2	M2.0 V	8.134	Binary	
J23142-196N	GJ 2154 A	23:14:17.13	-19:38:38.5	M0.5 Vk	7.471	Binary	
J23142-196S	GJ 2154 B	23:14:16.97	-19:38:45.4	M4.0 V	9.411	Binary	
J23174+196	GJ 4326	23:17:28.54	+19:36:45.1	M2.0 V	8.020	Binary	
J23161+067	GJ 4319	22:34:26.25	-00:28:12.9	M3.0 V	10.369		•
J23174+382	GJ 4327	23:17:24.09	+38:12:34.8	M3.0 V	7.761	Binary (SB2)	
J23175+063	GJ 4329	23:17:34.73	+06:23:24.5	M3.0 V	8.776	Binary*	
J23182+462	Ross 244	23:18:18.44	+46:17:23.6	M0.5 V	7.890		
J23182+795	LP 12-69	23:18:19.85	+79:34:45.8	M3.0 V	9.712		
J23193+154	StKM 1-2115	23:19:21.03	+15:24:13.5	M1.0 V	8.887		
J23194+790	HD 220140B	23:19:25.64	+79:00:04.8	M3.5 V	8.036	SKG	
J23228+787	LP 12-90	23:22:54.97	+78:47:39.6	M5.0 V	10.418	SKG	
J23215+568	LSPM J2321+5651	23:21:32.23	+56:51:19.7	M1.0 V	8.903		
J23216+172	GJ 4333	23:21:36.85	+17:17:03.3	M3.5 V	7.391		
J23220+569	G 217-6	23:22:01.52	+56:59:21.4	M3.0 V	9.473		
J23229+372	PM J23229+3717	23:22:58.46	+37:17:13.3	M2.0 V	8.797		
J23234+155	LP 522-65	23:23:24.72	+15:34:09.2	M2.0 V	8.255		
J23245+578	Ross 302	23:24:30.39	+57:51:11.0	M1.5 V	6.795		
J23249+506	PM J23549+5036	23:54:56.57	+50:36:15.0	M3.0 V	8.798		•
J23252+009	Wolf 1038	23:25:16.81	+00:57:44.1	M1.0 V	8.964		
J23256+531	GJ 4334	23:25:42.10	+53:08:11.1	M5.0 V	9.878		
J23262+088	GJ 2155	23:26:12.93	+08:53:41.2	M0.0 V	7.763		
J23261+170	PM J23261+1700	23:26:12.00	+17:00:06.9	M4.0 V	9.356	Binary	
J23265+121	GJ 4336	23:26:33.26	+12:09:37.9	M2.5 V	8.962		•
J23262+278	V595Peg	23:26:17.02	+27:52:02.8	M3.0 V	8.455	Binary	
J23293+414N	GJ 4337	23:29:24.06	+41:28:06.0	M3.0 V	7.925	Triple	
J23293+414S	GJ 4338	23:29:23.18	+41:27:51.4	M4.2 V	8.017	Triple	
J23317-027	AFPsc	23:31:45.03	-02:44:40.7	M4.5 V	9.507	Binary	
J23301-026	2M23301129-0237227	23:30:11.41	-02:37:23.9	M6.0 V	10.648	Binary	
J23308+157	LP 462-51	23:30:53.52	+15:47:38.8	M1.0 V	8.413	Binary	
J23318+199E	EQPegA	23:31:52.83	+19:56:13.2	M3.5 V	6.162	Quadruple (SB2)	
J23318+199W	EQPegB	23:31:53.20	+19:56:14.3	M4.0 V	7.101	Quadruple (SB1)	
J23323+540	G 217-12	23:32:20.61	+54:01:48.5	M2.0 V	8.920		
J23302-203	GJ 1284	23:30:13.80	-20:23:30.7	M2.0 V	7.200	Quintuple (SB2)	
J23327-167	GJ 897	23:32:46.98	-16:45:12.3	M3.0 V	6.712	Quintuple	
J23340+001	Wolf 1039	23:34:02.28	+00:10:30.9	M2.5 V	7.664		
J23350+252	Ross 298	23:35:03.91	+25:15:00.7	M3.0 V	9.138		
J23351-023	GJ 1286	23:35:11.30	-02:23:34.1	M5.0 V	9.148		
J23354+300	GJ 4342	23:35:24.05	+30:03:40.6	M3.5 V	9.399		
J23357+419	GJ 4346	23:35:45.48	+41:58:06.3	M1.0 V	8.108		
J23364+554	Ross 303	23:36:26.53	+55:29:42.1	M1.5 V	8.448		
J23376-128	LP 763-3	23:37:38.56	-12:50:33.3	M5.5 V	11.462		•
J23381-162	GJ 4352	23:38:07.84	-16:14:11.4	M2.0 V	7.813		
J23386+391	GJ 4354	23:38:41.41	+39:09:17.9	M3.3 V	9.580		
J23350+016	GJ 900	23:35:00.64	+01:36:19.9	M0.0 V	6.881	Binary	•
J23389+210	GJ 4356	23:38:56.00	+21:01:24.5	M4.3 V	9.941	Binary	
J23401+606	GJ 4358 A	23:40:07.91	+60:41:14.4	M1.0 V	8.136	Binary	
J23414+200	TYC 1727-1708-1	23:41:28.99	+20:02:31.0	M0.5 V	8.487	Binary	
J23419+441	HHAnd	23:41:55.20	+44:10:13.4	M5.0 V	6.884		
J23423+349	PM J23423+3458	23:42:22.21	+34:58:25.5	M4.0 V	9.315		•
J23428+308	GJ 1288	23:42:52.33	+30:49:16.9	M5.0 V	9.637		
J23431+365	GJ 1289	23:43:07.56	+36:32:10.7	M4.5 V	8.110		
J23438+325	GJ 905.2 A	23:43:52.84	+32:35:37.8	M1.5 V	7.863	Triple	
J23438+610	G 217-18	23:43:51.95	+61:02:07.5	M3.0 V	9.392		
J23443+216	GJ 1290	23:44:21.41	+21:36:06.4	M3.4 V	9.070		•
J23439+647	Ross 676	23:44:00.86	+64:44:30.4	M0.3 V	8.149	Binary (SB2)	

Table B.1: Carmencita, the CARMENES input catalogue (continued).

Karmn	Name	α (2016.0)	δ (2016.0)	Spectral type	J [mag]	Multiplicity[a]	DR1[b]
J23455-161	GJ 4360 A	23:45:30.82	-16:10:28.8	M5.0 V	9.206	Binary	
J23462+284	PM J23462+2826	23:46:14.17	+28:26:05.0	M3.5 V	8.957		•
J23480+490	Ross 249	23:48:04.16	+49:00:58.4	M3.0 V	8.765		
J23489+098	[R78b] 377	23:48:58.98	+09:51:53.3	M1.0 V	8.891	Binary	
J23492+024	BRPsc	23:49:13.58	+02:23:48.9	dM1	5.827		
J23492+100	GJ 4363	23:49:15.05	+10:05:32.7	M3.0 V	9.459		
J23496+083	GJ 4364	23:49:37.78	+08:21:29.1	M1.0 V	8.276		
J23505-095	GJ 4367	23:50:32.33	-09:33:39.5	dM4.0	8.943		
J23506+099	GJ 4368	23:50:36.86	+09:56:57.5	M3.0 V	7.672	Binary	
J23509+384	GJ 4369	23:50:53.91	+38:29:30.1	M3.8 V	9.800		
J23517+069	GJ 4370	23:51:44.72	+06:58:11.8	M3.0 V	8.841	Binary	•
J23523-146	GJ 4371	23:52:23.92	-14:41:28.2	M4.5 V	10.436		
J23535+121	PM J23535+1206S	23:53:35.69	+12:06:14.8	M2.5 V	8.670	Binary	
J23541+516	GJ 4373	23:54:10.95	+51:41:11.0	M3.5 V	9.574		•
J23544+081	GJ 4374	23:54:26.50	+08:09:42.6	M3.0 V	9.243		
J23548+385	RX J2354.8+3831	23:54:51.28	+38:31:34.8	M4.0 V	8.937		
J23554-039	GJ 4376	23:55:26.51	-03:58:59.8	M3.5 V	9.866		
J23560+150	LP 523-78	23:56:00.14	+15:01:37.9	M2.5 V	9.382		
J23556-061	GJ 912	23:55:39.27	-06:08:39.4	M2.5Vk	7.600	Binary (SB1)	
J23569+230	G 129-45	23:56:54.75	+23:05:04.2	M1.5 V	8.483	Binary	
J23573-129E	GJ 4378	23:57:20.81	-12:58:48.6	M4.0 V	8.636	Quadruple	
J23573-129W	GJ 4379	23:57:19.59	-12:58:40.3	M3.0 V	9.128	Quadruple (SB2)	•
J23577+197	GJ 4380	23:57:45.32	+19:46:03.4	M3.7 V	9.035		
J23577+233	GJ 1292	23:57:45.32	+23:18:00.1	M3.5 V	7.800		•
J23578+386	GJ 4381	23:57:49.68	+38:37:44.4	M3.0 V	8.691	Binary	
J23582-174	LP 764-40 A	23:58:13.95	-17:24:34.6	M2.0 V	8.311	Binary	
J23585+076	Wolf 1051	23:58:32.74	+07:39:25.0	M3.0 V	7.907	Triple (ST3)	
J23587+467	GJ 913	23:58:44.50	+46:43:44.9	M0.0 V	6.659	Binary	
J23590+208	G 129-51	23:59:00.74	+20:51:37.2	M2.5 V	9.072	Binary*	
J23598+477	GJ 4385	23:59:50.89	+47:45:41.3	M5.0 V	10.866		

[a] An asterisk (∗) means that further multiplicity is possible, generally hinted by *Gaia*.

[b] The star is part of the first data release (DR1) of CARMENES, which includes all the spectra collected in four years of GTO operations (Ribas et al., 2023).

Appendix C

Long tables of Chapter 3

Table C.1: Star candidates belonging to multiple systems not tabulated by the Washington Double Star Catalog (WDS).

Identifier	Name[a]	Spectral type	α (J2015.5)	δ (J2015.5)	π [mas]	$\mu_\alpha \cos\delta$ [mas a^{-1}]	μ_δ [mas a^{-1}]	$\mu_{\rm total}$ [mas a^{-1}]	G [mag]	θ [deg]	ρ [arcsec]
J00026+383	2M J00024011+3821453	M4.0 V	00:02:40.00	+38:21:44.1	24.54 ± 0.24	-70.31 ± 0.27	-22.34 ± 0.19	73.77 ± 0.27	13.1900 ± 0.0012	34.0	1.419
			00:02:40.06	+38:21:45.4	24.16 ± 0.38	-57.16 ± 0.54	-35.59 ± 0.20	67.33 ± 0.47	13.3648 ± 0.0014		
I01007+2356	PM J01007+2356	K7 V	01:00:46.85	+23:56:54.4	24.75 ± 0.04	129.88 ± 0.06	8.41 ± 0.06	130.15 ± 0.06	10.7186 ± 0.0007	4.7	1.480
			01:00:46.85	+23:56:55.9	…	…	…	…	14.6491 ± 0.0089		
J01074-025	RAVE J010727.5-023326	K5 V	01:07:27.46	−02:33:27.4	6.77 ± 0.05	-54.38 ± 0.09	-62.33 ± 0.05	82.72 ± 0.07	12.1930 ± 0.0003	165.2	1.363
			01:07:27.48	−02:33:28.8	6.42 ± 0.08	-54.13 ± 0.17	-61.36 ± 0.07	81.82 ± 0.12	14.5322 ± 0.0020		
J02026+105	RX J0202.4+1034	M4.5 V	02:02:28.15	+10:34:51.9	70.43 ± 0.53	-54.60 ± 1.07	-96.95 ± 0.77	111.27 ± 0.85	11.8652 ± 0.0012	25.3	0.904
			02:02:28.18	+10:34:52.7	68.79 ± 1.20	-101.45 ± 2.02	-58.95 ± 1.43	117.33 ± 1.89	12.3296 ± 0.0064		
J02287+156	BPM 85139	M2.0 V	02:28:47.14	+15:38:53.6	28.53 ± 0.11	170.91 ± 0.18	-9.17 ± 0.17	171.15 ± 0.18	11.5139 ± 0.0037	147.7	0.814
			02:28:47.17	+15:38:52.9	…	…	…	…	13.0258 ± 0.0055		
J02289+226	BPM 85140	M2.0 V	02:28:58.41	+22:36:24.5	17.16 ± 0.04	148.78 ± 0.08	-48.74 ± 0.07	156.56 ± 0.08	11.3170 ± 0.0006	147.4	3.022
			02:28:58.52	+22:36:21.9	17.19 ± 0.53	134.47 ± 1.13	-36.20 ± 0.99	139.26 ± 1.12	12.0611 ± 0.0003		
J03207+397	LP 198-637	M1.5 V	03:20:45.41	+39:42:59.4	31.60 ± 0.51	126.71 ± 1.33	-129.25 ± 0.86	181.00 ± 1.12	10.9868 ± 0.0020	278.1	0.783
			03:20:45.35	+39:42:59.7	…	…	…	…	11.2553 ± 0.0065		
I03276+0956	GJ 3226	K7 V	03:27:38.21	+09:56:05.3	22.80 ± 0.09	77.33 ± 0.15	-24.81 ± 0.14	81.22 ± 0.15	10.5483 ± 0.0014	296.8	1.541
			03:27:38.12	+09:56:06.0	23.82 ± 0.12	57.31 ± 0.19	-13.65 ± 0.21	58.91 ± 0.19	10.5825 ± 0.0008		
J03284+352	LSPM J0328+3515	M2.0 V	03:28:29.35	+35:15:18.7	20.90 ± 0.09	99.21 ± 0.15	-121.12 ± 0.08	156.56 ± 0.11	12.1366 ± 0.0007	204.2	1.230
			03:28:29.31	+35:15:17.5	21.14 ± 0.09	95.48 ± 0.15	-108.47 ± 0.08	144.51 ± 0.12	12.1711 ± 0.0010		
J03544-091	StKM 1-430	M1.0 V	03:54:25.52	−09:09:29.2	47.39 ± 0.04	-95.44 ± 0.06	110.84 ± 0.05	146.27 ± 0.06	10.5351 ± 0.0006	153.2	3.177
			03:54:25.62	−09:09:32.1	47.40 ± 0.06	-96.46 ± 0.09	98.93 ± 0.08	138.17 ± 0.09	11.8800 ± 0.0012		
J05530+047	G 106-007	M1.5 V	05:53:04.74	+04:43:02.7	24.70 ± 0.10	258.57 ± 0.28	-295.56 ± 0.20	392.71 ± 0.24	11.3303 ± 0.0011	278.1	1.517
			05:53:04.64	+04:43:02.9	…	…	…	…	15.8285 ± 0.0108		
I07245+1836	PM J07245+1836	K7 V	07:24:32.30	+18:36:31.3	19.99 ± 0.05	53.55 ± 0.09	-36.35 ± 0.08	64.72 ± 0.09	10.8267 ± 0.0005	326.9	1.836
			07:24:32.23	+18:36:32.9	…	…	…	…	12.6023 ± 0.0024		
J07418+050[b]	G 050-001	M2.5 V+	07:41:52.56	+05:02:23.1	36.09 ± 0.07	-248.35 ± 0.13	-87.34 ± 0.10	263.26 ± 0.12	11.6216 ± 0.0009	136.1	1.006
			07:41:52.61	+05:02:22.4	…	…	…	…	16.1257 ± 0.0263		
J07545-096	2M J07543272-0941478	M3.5 V	07:54:32.61	−09:41:47.9	27.81 ± 0.10	-91.49 ± 0.16	-13.16 ± 0.11	92.43 ± 0.16	12.6737 ± 0.0014	129.9	1.233
			07:54:32.67	−09:41:48.7	…	…	…	…	13.9321 ± 0.0029		
I08192+5752	PM J08192+5752	K7 V	08:19:14.01	+57:52:26.8	19.67 ± 0.04	39.66 ± 0.06	-79.76 ± 0.06	89.08 ± 0.06	10.7381 ± 0.0005	93.3	1.475
			08:19:14.19	+57:52:26.6	19.71 ± 0.14	40.66 ± 0.23	-72.23 ± 0.46	82.89 ± 0.42	14.1599 ± 0.0067		
J09050+028	LP 546-48	M1.5 V	09:05:04.12	+02:50:03.8	42.58 ± 0.25	-312.21 ± 0.39	29.17 ± 0.42	313.57 ± 0.39	10.9288 ± 0.0021	253.0	1.214
			09:05:04.04	+02:50:03.5	…	…	…	…	12.1972 ± 0.0021		
J09527+554	G 195-043	M1.5 V	09:52:45.24	+55:28:16.3	28.51 ± 0.36	298.92 ± 0.59	-201.23 ± 0.64	360.34 ± 0.61	11.3624 ± 0.0008	331.1	2.716
			09:52:45.14	+55:28:18.9	27.15 ± 0.12	285.07 ± 0.23	-190.75 ± 0.15	343.00 ± 0.21	16.4864 ± 0.0034		
I10526+0029	PM J10526+0029	K7 V	10:52:39.52	+00:29:01.5	25.18 ± 0.08	-91.32 ± 0.10	-31.13 ± 0.08	96.48 ± 0.09	10.1687 ± 0.0016	251.0	1.594

Table C.1: Star candidates belonging to multiple systems not tabulated by the Washington Double Star Catalog (continued).

Identifier	Name[a]	Spectral type	α (J2015.5)	δ (J2015.5)	π [mas]	$\mu_\alpha \cos\delta$ [mas a^{-1}]	μ_δ [mas a^{-1}]	$\mu_{\rm total}$ [mas a^{-1}]	G [mag]	θ [deg]	ρ [arcsec]
			10:52:39.42	+00:29:01.0	…	…	…	…	12.7067 ± 0.0042		
I11585+4626[c]	PM J11585+4626	K7 V	11:58:33.82	+46:26:28.9	16.20 ± 0.06	-129.71 ± 0.07	1.77 ± 0.06	129.72 ± 0.07	10.9651 ± 0.0011	333.9	1.540
			11:58:33.77	+46:26:30.4	14.50 ± 0.14	-141.05 ± 0.31	1.26 ± 0.17	141.05 ± 0.31	11.5845 ± 0.0015		
J12191+318[b]	LP 320-626	M4.0 V+	12:19:05.57	+31:50:43.6	…	…	…	…	11.1940 ± 0.0006	225.2	1.764
			12:19:05.48	+31:50:42.2	35.13 ± 0.09	-295.73 ± 0.10	5.02 ± 0.11	295.77 ± 0.10	13.9526 ± 0.0023		
J12390+470	G 123-049	M2.0 V	12:39:05.24	+47:02:21.4	…	…	…	…	11.1336 ± 0.0044	110.4	0.463
			12:39:05.28	+47:02:21.2	43.50 ± 0.05	384.45 ± 0.07	-118.41 ± 0.08	402.27 ± 0.07	11.2091 ± 0.0009		
J12513+221	GJ 1166A	M3.0 V	12:51:23.72	+22:06:15.7	30.32 ± 0.51	-177.34 ± 0.98	50.54 ± 0.79	184.40 ± 0.96	12.1313 ± 0.0019	91.8	1.263
			12:51:23.81	+22:06:15.6	…	…	…	…	13.3117 ± 0.0038		
J13282+300	BD+30 2400	M0.0 V	13:28:17.54	+30:02:43.1	25.33 ± 0.08	-186.41 ± 0.25	-183.87 ± 0.13	261.84 ± 0.20	10.5043 ± 0.0006	320.1	1.243
			13:28:17.48	+30:02:44.1	…	…	…	…	14.1569 ± 0.0103		
J13445+249	LP 379-098	M1.0 V	13:44:33.39	+24:57:03.7	22.31 ± 0.33	-245.17 ± 0.54	-96.38 ± 0.39	263.43 ± 0.52	11.5057 ± 0.0021	355.8	0.879
			13:44:33.39	+24:57:04.6	…	…	…	…	11.8891 ± 0.0098		
J13490+026	Wolf 1495	M1.5 V	13:49:01.18	+02:47:23.3	…	…	…	…	10.7706 ± 0.0210	315.7	0.680
			13:49:01.15	+02:47:23.8	55.78 ± 0.75	149.68 ± 1.64	-333.14 ± 1.56	365.22 ± 1.57	10.8252 ± 0.0075		
I15380+3224[c]	PM J15380+3224	K7 V	15:38:04.49	+32:24:31.9	16.48 ± 0.23	-63.14 ± 0.31	-78.46 ± 0.38	100.71 ± 0.36	11.2639 ± 0.0021	143.8	1.061
			15:38:04.53	+32:24:31.0	15.10 ± 0.25	-74.75 ± 0.39	-83.43 ± 0.48	112.02 ± 0.44	11.3307 ± 0.0019		
J16573+271	2M J16572235+2708304	M2.0 V	16:57:22.27	+27:08:31.1	27.12 ± 0.12	-34.09 ± 0.21	44.34 ± 0.26	55.93 ± 0.24	12.3752 ± 0.0011	117.6	1.048
			16:57:22.34	+27:08:30.6	…	…	…	…	13.2959 ± 0.0025		
I17068+3212	PM J17068+3212	K7 V	17:06:48.88	+32:11:59.3	31.93 ± 0.02	53.18 ± 0.03	-74.71 ± 0.04	91.70 ± 0.04	10.7788 ± 0.0003	31.4	3.279
			17:06:49.00	+32:12:02.2	31.93 ± 0.03	46.05 ± 0.09	-82.76 ± 0.06	94.71 ± 0.07	12.6244 ± 0.0004		
J18116+061	NLTT 46076	M3.0 V	18:11:36.49	+06:06:27.8	…	…	…	…	11.9662 ± 0.0074	139.6	0.625
			18:11:36.51	+06:06:27.3	…	…	…	…	13.5146 ± 0.0077		
J18400+726	LP 044-334	M6.5 V	18:40:02.20	+72:40:57.1	51.04 ± 0.52	-43.74 ± 0.83	184.49 ± 1.09	189.60 ± 1.08	15.3854 ± 0.0114	110.3	0.821
			18:40:02.32	+72:40:56.5	…	…	…	…	15.7040 ± 0.0035		
I18447+6241	PM J18447+6241	K7 V	18:44:47.49	+62:41:08.3	22.52 ± 0.03	-33.82 ± 0.06	56.65 ± 0.05	65.98 ± 0.05	10.7927 ± 0.0006	277.5	1.342
			18:44:47.30	+62:41:08.7	…	…	…	…	14.7260 ± 0.0167		
I21088+1247	BD+12 4554	K7 V	21:08:51.84	+12:47:36.9	23.81 ± 0.04	85.71 ± 0.06	-67.99 ± 0.05	109.40 ± 0.06	10.4390 ± 0.0005	2.5	1.833
			21:08:51.85	+12:47:38.7	…	…	…	…	14.4780 ± 0.0077		
I21415+4925	PM J21415+4925	K7 V	21:41:31.36	+49:25:38.1	29.93 ± 0.02	33.99 ± 0.04	-85.44 ± 0.04	91.95 ± 0.04	9.9125 ± 0.0003	308.8	1.609
			21:41:31.26	+49:25:39.3	30.10 ± 0.10	50.32 ± 0.60	-88.08 ± 0.83	101.44 ± 0.78	13.2790 ± 0.0044		
J22012+323	TYC 2723-908-1	M1.5 V	22:01:14.12	+32:23:13.9	32.55 ± 0.08	118.50 ± 0.09	62.63 ± 0.15	134.03 ± 0.11	11.4391 ± 0.0012	239.8	1.295
			22:01:14.04	+32:23:13.1	32.10 ± 0.20	107.88 ± 0.27	53.40 ± 0.31	120.37 ± 0.28	12.8902 ± 0.0022		
I22142+1712	PM J22142+1712	K7 V	22:14:12.84	+17:12:24.4	17.18 ± 0.05	-10.52 ± 0.08	-84.77 ± 0.07	85.42 ± 0.07	10.7551 ± 0.0006	268.2	1.510
			22:14:12.73	+17:12:24.4	…	…	…	…	15.4819 ± 0.0194		
I22569+0031	PM J22569+0031	K7 V	22:56:54.65	+00:31:23.6	…	…	…	…	10.9107 ± 0.0145	22.4	0.907

Table C.1: Star candidates belonging to multiple systems not tabulated by the Washington Double Star Catalog (continued).

Identifier	Name[a]	Spectral type	α (J2015.5)	δ (J2015.5)	π [mas]	$\mu_\alpha \cos\delta$ [mas a^{-1}]	μ_δ [mas a^{-1}]	$\mu_{\rm total}$ [mas a^{-1}]	G [mag]	θ [deg]	ρ [arcsec]
			22:56:54.67	+00:31:24.4	17.57 ± 0.68	13.04 ± 1.16	-82.42 ± 0.87	83.44 ± 0.88	11.0021 ± 0.0058		
I22596+2154	PM J22596+2154	K7 V	22:59:41.42	+21:54:05.8	26.30 ± 0.05	127.97 ± 0.09	-59.09 ± 0.06	140.96 ± 0.09	10.1878 ± 0.0006	37.3	2.093
			22:59:41.51	+21:54:07.6	…	…	…	…	13.3417 ± 0.0037		
J23051+452	LSPM J2305+4517	M3.5 V	23:05:08.99	+45:17:32.9	21.94 ± 0.17	184.58 ± 0.26	67.37 ± 0.27	196.49 ± 0.26	12.3370 ± 0.0021	80.7	0.785
			23:05:09.06	+45:17:33.1	…	…	…	…	14.3079 ± 0.0029		
J23489+098	[R78b] 377	M1.0 V	23:48:58.97	+09:51:53.4	21.08 ± 0.05	147.68 ± 0.09	-52.74 ± 0.05	156.82 ± 0.08	11.3848 ± 0.0009	20.1	1.945
			23:48:59.02	+09:51:55.2	20.76 ± 0.08	141.19 ± 0.18	-43.69 ± 0.06	147.80 ± 0.17	13.9181 ± 0.0013		
J23590+208	G 129-051	M2.5 V	23:59:00.73	+20:51:37.3	14.96 ± 0.79	228.92 ± 1.25	-104.85 ± 0.57	251.79 ± 1.16	12.0177 ± 0.0072	170.7	0.521
			23:59:00.73	+20:51:36.7	…	…	…	…	12.3273 ± 0.0186		

[a] Primaries "A" are always brighter than secondaries "B" in the G band.
[b] Previously identified as spectroscopic binaries in Reipurth & Mikkola (2012a) and Jeffers et al. (2018).
[c] Common proper motion pairs with $\Delta\pi > 5$ % labelled in Fig. 3.8

Table C.2: Average colours for K5 V to L6 sources. The number in parentheses indicates the number of useful data points.

Spectral type	$FUV - NUV$ [mag]	$NUV - u$ [mag]	$u - B_T$ [mag]	$B_T - B$ [mag]	$B - g$ [mag]	$g - G_{BP}$ [mag]	$G_{BP} - V_T$ [mag]	$V_T - V$ [mag]	$V - G$ [mag]	$G - r$ [mag]
K5 V	3.59 ± 0.95 (2)	5.37 (1)	…	0.24 ± 0.40 (6)	0.63 ± 0.23 (11)	0.32 ± 0.11 (11)	0.04 ± 0.08 (8)	0.26 ± 0.07 (4)	0.45 ± 0.04 (9)	−0.03 ± 0.21 (13)
K7 V	3.26 ± 0.65 (7)	4.23 ± 0.75 (36)	2.66 ± 0.83 (59)	0.49 ± 0.43 (98)	0.62 ± 0.16 (107)	0.48 ± 0.13 (101)	0.02 ± 0.12 (94)	0.21 ± 0.16 (96)	0.61 ± 0.10 (100)	−0.06 ± 0.12 (103)
M0.0 V	2.83 ± 0.61 (22)	4.05 ± 0.83 (37)	2.87 ± 0.73 (54)	0.46 ± 0.36 (108)	0.65 ± 0.14 (113)	0.51 ± 0.12 (117)	0.08 ± 0.09 (113)	0.15 ± 0.11 (109)	0.71 ± 0.09 (115)	−0.17 ± 0.14 (120)
M0.5 V	2.40 ± 0.42 (14)	4.01 ± 0.96 (22)	2.85 ± 0.82 (36)	0.43 ± 0.36 (70)	0.66 ± 0.13 (72)	0.53 ± 0.11 (72)	0.07 ± 0.14 (69)	0.17 ± 0.16 (68)	0.77 ± 0.10 (72)	−0.18 ± 0.11 (71)
M1.0 V	2.29 ± 0.44 (11)	4.72 ± 0.82 (43)	2.48 ± 0.70 (42)	0.35 ± 0.40 (86)	0.72 ± 0.14 (135)	0.51 ± 0.10 (140)	0.09 ± 0.16 (87)	0.15 ± 0.16 (87)	0.82 ± 0.09 (135)	−0.23 ± 0.10 (140)
M1.5 V	2.24 ± 0.49 (13)	4.95 ± 0.98 (43)	2.53 ± 0.66 (32)	0.28 ± 0.47 (63)	0.72 ± 0.13 (115)	0.51 ± 0.15 (121)	0.12 ± 0.17 (65)	0.10 ± 0.20 (65)	0.89 ± 0.11 (115)	−0.30 ± 0.13 (121)
M2.0 V	1.90 ± 0.66 (12)	5.30 ± 0.78 (36)	2.08 ± 0.69 (29)	0.36 ± 0.59 (54)	0.76 ± 0.05 (118)	0.49 ± 0.11 (124)	0.15 ± 0.24 (55)	0.11 ± 0.26 (53)	0.95 ± 0.10 (117)	−0.37 ± 0.10 (124)
M2.5 V	1.66 ± 0.65 (9)	5.37 ± 1.07 (37)	2.35 ± 0.85 (21)	0.35 ± 0.55 (30)	0.79 ± 0.07 (138)	0.48 ± 0.09 (145)	0.12 ± 0.18 (31)	0.16 ± 0.18 (29)	1.04 ± 0.09 (137)	−0.47 ± 0.11 (146)
M3.0 V	1.33 ± 0.45 (12)	5.17 ± 0.93 (38)	1.82 ± 0.37 (8)	0.42 ± 0.37 (20)	0.80 ± 0.11 (157)	0.47 ± 0.09 (173)	0.09 ± 0.12 (20)	0.17 ± 0.11 (20)	1.13 ± 0.09 (156)	−0.55 ± 0.11 (173)
M3.5 V	1.31 ± 0.36 (23)	4.72 ± 1.13 (46)	2.18 ± 0.80 (7)	0.20 ± 0.59 (14)	0.85 ± 0.07 (217)	0.46 ± 0.09 (237)	0.13 ± 0.19 (12)	0.14 ± 0.19 (13)	1.24 ± 0.09 (215)	−0.66 ± 0.10 (237)
M4.0 V	1.49 ± 0.56 (29)	3.91 ± 1.36 (36)	2.43 ± 0.63 (2)	0.05 ± 0.50 (5)	0.90 ± 0.07 (167)	0.46 ± 0.08 (203)	0.23 ± 0.24 (6)	0.04 ± 0.24 (6)	1.38 ± 0.09 (165)	−0.77 ± 0.09 (203)
M4.5 V	1.04 ± 0.65 (15)	2.96 ± 0.90 (18)	…	…	0.97 ± 0.08 (95)	0.47 ± 0.10 (116)	…	…	1.54 ± 0.10 (96)	−0.92 ± 0.10 (116)
M5.0 V	1.12 ± 0.42 (8)	2.75 ± 0.77 (12)	…	…	0.98 ± 0.19 (35)	0.46 ± 0.16 (60)	…	…	1.71 ± 0.16 (38)	−1.10 ± 0.16 (60)
M5.5 V	1.52 ± 0.34 (2)	2.80 ± 0.58 (7)	…	…	1.13 ± 0.21 (14)	0.49 ± 0.13 (26)	…	…	2.04 ± 0.12 (14)	−1.37 ± 0.10 (26)
M6.0 V	0.84 ± 0.15 (2)	0.89 ± 1.78 (5)	…	…	1.24 ± 0.04 (2)	0.48 ± 0.20 (14)	…	…	2.01 (1)	−1.73 ± 0.24 (14)
M6.5 V	…	…	…	…	1.07 ± 0.20 (2)	0.49 ± 0.15 (7)	…	…	2.72 ± 0.21 (2)	−2.00 ± 0.17 (7)
M7.0 V	…	2.90 (1)	…	…	1.30 (1)	0.46 ± 0.19 (5)	…	…	2.80 (1)	−2.08 ± 0.28 (5)
M7.5 V	…	…	…	…	…	0.42 ± 0.16 (3)	…	…	…	−2.06 ± 0.12 (3)
M8.0 V	…	…	…	…	…	0.56 ± 0.15 (4)	…	…	…	−2.23 ± 0.08 (6)
M8.5 V	…	…	…	…	…	0.52 ± 0.01 (2)	…	…	…	−2.16 ± 0.13 (3)
M9.0 V	…	…	…	…	…	0.72 (1)	…	…	…	−2.01 ± 0.07 (2)
M9.5 V	…	…	…	…	…	…	…	…	…	−1.96 (1)
L0.0	…	…	…	…	…	…	…	…	…	−1.98 ± 0.16 (10)
L0.5	…	…	…	…	…	…	…	…	…	−1.92 ± 0.18 (5)
L1.0	…	…	…	…	…	…	…	…	…	−1.98 ± 0.12 (14)
L1.5	…	…	…	…	…	…	…	…	…	−1.99 ± 0.08 (4)
L2.0	…	…	…	…	…	…	…	…	…	−1.88 ± 0.08 (11)
L2.5	…	…	…	…	…	…	…	…	…	−1.90 ± 0.04 (4)
L3.0	…	…	…	…	…	…	…	…	…	−1.88 ± 0.12 (3)
L3.5	…	…	…	…	…	…	…	…	…	−2.02 ± 0.15 (2)
L4.0	…	…	…	…	…	…	…	…	…	−1.86 ± 0.10 (3)
L4.5	…	…	…	…	…	…	…	…	…	…
L5.0	…	…	…	…	…	…	…	…	…	−2.01 (1)
L5.5	…	…	…	…	…	…	…	…	…	−2.04 (1)
L6.0	…	…	…	…	…	…	…	…	…	−2.09 (1)

Table C.2: Average colours for K5 V to L6 sources. The number in parentheses indicates the number of useful data points (continued).

Spectral type	$r-i$ [mag]	$i-G_{RP}$ [mag]	$G_{RP}-J$ [mag]	$J-H$ [mag]	$H-Ks$ [mag]	$Ks-W1$ [mag]	$W1-W2$ [mag]	$W2-W3$ [mag]	$W3-W4$ [mag]
K5 V	0.41 ± 0.07 (13)	0.40 ± 0.20 (12)	0.95 ± 0.06 (13)	0.57 ± 0.03 (14)	0.14 ± 0.03 (14)	0.08 ± 0.06 (14)	0.04 ± 0.19 (15)	–0.02 ± 0.20 (15)	0.01 ± 0.13 (10)
K7 V	0.60 ± 0.12 (106)	0.34 ± 0.12 (99)	1.12 ± 0.05 (104)	0.63 ± 0.03 (112)	0.17 ± 0.03 (112)	0.11 ± 0.04 (109)	–0.03 ± 0.06 (109)	0.05 ± 0.06 (112)	0.06 ± 0.11 (112)
M0.0 V	0.74 ± 0.14 (119)	0.36 ± 0.11 (117)	1.22 ± 0.05 (118)	0.63 ± 0.04 (120)	0.19 ± 0.03 (119)	0.12 ± 0.05 (116)	0.02 ± 0.09 (117)	0.02 ± 0.08 (119)	0.10 ± 0.09 (118)
M0.5 V	0.80 ± 0.13 (70)	0.36 ± 0.08 (71)	1.28 ± 0.05 (72)	0.63 ± 0.03 (72)	0.21 ± 0.03 (71)	0.12 ± 0.05 (70)	0.05 ± 0.09 (70)	0.03 ± 0.07 (71)	0.11 ± 0.09 (73)
M1.0 V	0.87 ± 0.11 (140)	0.36 ± 0.09 (139)	1.32 ± 0.04 (139)	0.62 ± 0.04 (140)	0.21 ± 0.03 (138)	0.14 ± 0.04 (138)	0.05 ± 0.09 (138)	0.06 ± 0.06 (138)	0.09 ± 0.11 (141)
M1.5 V	0.96 ± 0.14 (124)	0.37 ± 0.11 (121)	1.37 ± 0.05 (119)	0.63 ± 0.04 (121)	0.21 ± 0.03 (121)	0.14 ± 0.04 (122)	0.06 ± 0.08 (121)	0.06 ± 0.06 (123)	0.09 ± 0.11 (125)
M2.0 V	1.05 ± 0.12 (125)	0.38 ± 0.11 (126)	1.44 ± 0.05 (127)	0.61 ± 0.05 (128)	0.23 ± 0.03 (128)	0.15 ± 0.04 (126)	0.09 ± 0.07 (126)	0.07 ± 0.05 (126)	0.10 ± 0.12 (122)
M2.5 V	1.17 ± 0.11 (147)	0.40 ± 0.10 (144)	1.51 ± 0.05 (147)	0.59 ± 0.04 (150)	0.24 ± 0.03 (147)	0.16 ± 0.05 (147)	0.11 ± 0.05 (149)	0.08 ± 0.04 (149)	0.12 ± 0.13 (144)
M3.0 V	1.29 ± 0.11 (173)	0.41 ± 0.10 (172)	1.58 ± 0.05 (172)	0.59 ± 0.04 (172)	0.25 ± 0.03 (171)	0.16 ± 0.04 (173)	0.13 ± 0.05 (172)	0.09 ± 0.05 (172)	0.13 ± 0.14 (162)
M3.5 V	1.40 ± 0.13 (240)	0.44 ± 0.12 (235)	1.66 ± 0.05 (237)	0.58 ± 0.05 (242)	0.26 ± 0.03 (241)	0.17 ± 0.04 (241)	0.15 ± 0.05 (239)	0.10 ± 0.05 (239)	0.15 ± 0.15 (226)
M4.0 V	1.53 ± 0.15 (205)	0.47 ± 0.13 (201)	1.76 ± 0.06 (202)	0.58 ± 0.04 (206)	0.27 ± 0.03 (206)	0.18 ± 0.04 (201)	0.17 ± 0.04 (200)	0.12 ± 0.04 (199)	0.19 ± 0.17 (169)
M4.5 V	1.71 ± 0.13 (116)	0.49 ± 0.09 (116)	1.87 ± 0.06 (116)	0.56 ± 0.04 (116)	0.29 ± 0.03 (116)	0.20 ± 0.04 (114)	0.19 ± 0.03 (114)	0.15 ± 0.04 (115)	0.23 ± 0.21 (88)
M5.0 V	1.85 ± 0.21 (59)	0.59 ± 0.14 (59)	2.02 ± 0.12 (61)	0.58 ± 0.03 (62)	0.31 ± 0.03 (62)	0.21 ± 0.03 (62)	0.20 ± 0.03 (61)	0.16 ± 0.04 (60)	0.28 ± 0.28 (43)
M5.5 V	2.12 ± 0.15 (26)	0.64 ± 0.13 (26)	2.14 ± 0.08 (27)	0.57 ± 0.04 (27)	0.33 ± 0.02 (26)	0.23 ± 0.03 (26)	0.21 ± 0.05 (27)	0.17 ± 0.05 (27)	0.23 ± 0.16 (21)
M6.0 V	2.32 ± 0.25 (13)	0.83 ± 0.12 (12)	2.33 ± 0.16 (12)	0.60 ± 0.08 (15)	0.37 ± 0.03 (15)	0.23 ± 0.02 (15)	0.21 ± 0.04 (15)	0.21 ± 0.07 (15)	0.33 ± 0.22 (5)
M6.5 V	2.68 ± 0.14 (7)	0.82 ± 0.10 (7)	2.49 ± 0.07 (7)	0.61 ± 0.03 (7)	0.37 ± 0.02 (7)	0.24 ± 0.04 (7)	0.20 ± 0.03 (7)	0.23 ± 0.03 (7)	0.10 ± 0.15 (4)
M7.0 V	2.62 ± 0.26 (5)	0.99 ± 0.15 (5)	2.52 ± 0.17 (5)	0.58 ± 0.06 (5)	0.38 ± 0.04 (5)	0.26 ± 0.09 (5)	0.21 ± 0.03 (5)	0.23 ± 0.08 (5)	0.21 ± 0.07 (3)
M7.5 V	2.66 ± 0.09 (3)	0.91 ± 0.05 (3)	2.52 ± 0.09 (3)	0.64 ± 0.01 (3)	0.37 ± 0.03 (3)	0.25 ± 0.05 (3)	0.21 ± 0.01 (3)	0.27 ± 0.06 (3)	…
M8.0 V	2.77 ± 0.10 (6)	1.03 ± 0.10 (6)	2.75 ± 0.12 (9)	0.66 ± 0.03 (9)	0.41 ± 0.03 (9)	0.25 ± 0.04 (9)	0.24 ± 0.05 (9)	0.28 ± 0.04 (8)	…
M8.5 V	2.70 ± 0.05 (2)	1.12 ± 0.02 (2)	2.93 ± 0.05 (4)	0.64 ± 0.05 (4)	0.46 ± 0.01 (4)	0.33 ± 0.04 (4)	0.28 ± 0.05 (4)	0.35 ± 0.08 (4)	0.32 ± 0.05 (3)
M9.0 V	2.43 ± 0.09 (2)	1.17 ± 0.02 (3)	3.06 ± 0.08 (5)	0.67 ± 0.06 (5)	0.46 ± 0.04 (5)	0.35 ± 0.03 (5)	0.29 ± 0.03 (5)	0.49 ± 0.08 (5)	0.30 (1)
M9.5 V	2.39 (1)	1.18 (1)	3.12 ± 0.11 (2)	0.84 ± 0.07 (2)	0.57 ± 0.03 (2)	0.34 ± 0.02 (2)	0.28 ± 0.02 (2)	0.45 ± 0.08 (2)	…
L0.0	2.43 ± 0.16 (10)	1.16 ± 0.03 (9)	3.07 ± 0.05 (11)	0.75 ± 0.05 (12)	0.50 ± 0.05 (12)	0.33 ± 0.04 (12)	0.27 ± 0.04 (12)	0.49 ± 0.15 (12)	…
L0.5	2.38 ± 0.19 (5)	1.17 ± 0.02 (4)	3.15 ± 0.06 (6)	0.73 ± 0.06 (7)	0.53 ± 0.06 (7)	0.33 ± 0.02 (7)	0.26 ± 0.02 (7)	0.45 ± 0.07 (7)	…
L1.0	2.41 ± 0.10 (14)	1.20 ± 0.04 (14)	3.18 ± 0.10 (15)	0.82 ± 0.05 (15)	0.51 ± 0.06 (15)	0.36 ± 0.05 (15)	0.24 ± 0.04 (15)	0.46 ± 0.10 (14)	…
L1.5	2.39 ± 0.03 (5)	1.23 ± 0.06 (4)	3.23 ± 0.06 (7)	0.80 ± 0.08 (8)	0.52 ± 0.04 (8)	0.40 ± 0.09 (8)	0.27 ± 0.03 (8)	0.55 ± 0.11 (6)	…
L2.0	2.34 ± 0.08 (12)	1.16 ± 0.03 (11)	3.24 ± 0.10 (12)	0.85 ± 0.09 (14)	0.53 ± 0.07 (14)	0.40 ± 0.06 (14)	0.27 ± 0.02 (14)	0.54 ± 0.15 (14)	…
L2.5	2.31 ± 0.05 (5)	1.20 ± 0.04 (4)	3.31 ± 0.07 (5)	0.91 ± 0.04 (6)	0.54 ± 0.08 (6)	0.45 ± 0.06 (6)	0.26 ± 0.03 (6)	0.56 ± 0.32 (6)	…
L3.0	2.34 ± 0.11 (5)	1.25 ± 0.01 (2)	3.48 ± 0.09 (3)	1.00 ± 0.08 (6)	0.64 ± 0.07 (6)	0.58 ± 0.09 (6)	0.33 ± 0.07 (6)	0.43 ± 0.17 (6)	…
L3.5	2.40 ± 0.11 (2)	1.35 ± 0.04 (2)	3.37 ± 0.03 (2)	0.93 ± 0.05 (2)	0.58 ± 0.05 (2)	0.58 ± 0.06 (2)	0.30 ± 0.01 (2)	0.53 ± 0.13 (2)	…
L4.0	2.22 ± 0.13 (4)	1.31 ± 0.07 (3)	3.50 ± 0.15 (4)	0.90 ± 0.09 (5)	0.57 ± 0.07 (5)	0.53 ± 0.09 (5)	0.27 ± 0.02 (5)	0.32 ± 0.14 (5)	…
L4.5	2.06 (1)	…	…	1.13 (1)	0.69 (1)	0.82 (1)	0.37 (1)	0.66 (1)	…
L5.0	2.15 ± 0.21 (5)	1.53 (1)	3.75 (1)	1.01 ± 0.16 (5)	0.59 ± 0.14 (5)	0.70 ± 0.09 (5)	0.38 ± 0.11 (6)	0.52 ± 0.33 (6)	…
L5.5	2.13 (1)	…	…	0.88 (1)	0.56 (1)	0.67 (1)	0.28 (1)	0.62 (1)	…
L6.0	2.07 (1)	1.71 (1)	3.49 (1)	0.69 (1)	0.34 (1)	0.75 (1)	0.34 (1)	0.76 (1)	…

Table C.3: Basic properties of M-dwarf hosted exoplanets.

Name	Planet	a [au]	P_{orb} [days]	$\mathcal{M}_p$[a] [$\mathcal{M}_\oplus$]	$\mathcal{R}_p$[a] [$\mathcal{R}_\oplus$]	References[b]	S_{eff} [$S_\odot$]	$T_{eq,p}$ [K]	Potentially HZ
GX And	b	$0.072^{+0.003}_{-0.004}$	$11.4407^{+0.0017}_{-0.0016}$	$> 3.03^{+0.46}_{-0.44}$	(> 1.53)	Pin18	4.89 ± 0.10	413.9 ± 8.7	
K2-149	b	$0.083^{+0.027}_{-0.027}$	$11.332^{+0.0013}_{-0.0013}$	(3.85)	$1.64^{+0.20}_{-0.18}$	Hir18	9.82 ± 0.25	493 ± 13	
CD-44 170	b	$0.101^{+0.009}_{-0.013}$	$15.8190^{+0.0049}_{-0.0026}$	$> 13^{+4.1}_{-6.6}$	(> 3.63)	Tuo14	4.51 ± 0.35	406 ± 32	
LHS 1140	b	$0.0875^{+0.0041}_{-0.0041}$	$24.73712^{+0.00025}_{-0.00025}$	$6.65^{+1.82}_{-1.82}$	$1.43^{+0.10}_{-0.10}$	Dit17	0.5780 ± 0.0072	242.7 ± 3.0	Yes
	c	$0.02675^{+0.00070}_{-0.00070}$	$3.777931^{+0.000006}_{-0.000006}$	$1.81^{+0.39}_{-0.39}$	$1.282^{+0.024}_{-0.024}$	Men19	6.184 ± 0.077	438.9 ± 5.4	
2MASS J01021226-6145216	b	$0.03946^{+0.00095}_{-0.00168}$	$3.7955213^{+0.0000011}_{-0.0000011}$	(1750)	$12.106^{+0.179}_{-0.179}$	Bak18	16.18 ± 1.14	558 ± 39	
BD+61 195	b	$0.0905^{+0.0011}_{-0.0011}$	$13.8508^{+0.0053}_{-0.0051}$	$> 5.63^{+0.67}_{-0.68}$	(> 2.25)	Per19	5.52 ± 0.12	426.7 ± 9.0	
YZ Cet	b	$0.01557^{+0.00052}_{-0.00052}$	$1.96876^{+0.00021}_{-0.00021}$	$> 0.75^{+0.13}_{-0.13}$	(> 0.93)	Ast17b	9.08 ± 0.14	483.1 ± 7.6	
	c	$0.0209^{+0.0007}_{-0.0007}$	$3.06008^{+0.00022}_{-0.00022}$	$> 0.98^{+0.14}_{-0.14}$	(> 1.00)	Ast17b	5.037 ± 0.079	417.0 ± 6.5	
	d	$0.02764^{+0.00093}_{-0.00093}$	$4.65627^{+0.00042}_{-0.00042}$	$> 1.14^{+0.17}_{-0.17}$	(> 1.05)	Ast17b	2.880 ± 0.045	362.6 ± 5.7	
K2-150	b	$0.0727^{+0.0027}_{-0.0027}$	$10.59357^{+0.00084}_{-0.00084}$	(5.26)	$2.00^{+0.27}_{-0.21}$	Hir18	4.24 ± 0.10	399.5 ± 9.8	
K2-151	b	$0.0365^{+0.0014}_{-0.0014}$	$3.835592^{+0.000023}_{-0.000023}$	(2.44)	$1.35^{+0.16}_{-0.14}$	Hir18	24.48 ± 0.34	619.1 ± 8.7	
BD-17 400	b	$0.0197^{+0.0005}_{-0.0005}$	$1.22003^{+0.00006}_{-0.00004}$	$> 1.78^{+0.34}_{-0.33}$	(> 1.20)	Ast17a	215.2 ± 3.4	1066 ± 17	
	c	$0.057^{+0.001}_{-0.001}$	$5.974^{+0.001}_{-0.001}$	$> 4.18^{+0.61}_{-0.59}$	(> 1.88)	Ast17a	25.70 ± 0.41	626.7 ± 9.9	
	d	$0.698^{+0.018}_{-0.019}$	$257.8^{+3.6}_{-3.5}$	$> 10.5^{+2.3}_{-2.1}$	(> 3.21)	Ast17a	0.1714 ± 0.0027	179.1 ± 2.8	
GJ 96	b	$0.291^{+0.005}_{-0.005}$	$73.94^{+0.33}_{-0.38}$	$> 19.66^{+2.20}_{-2.30}$	(> 4.74)	Hob18	0.754 ± 0.011	259.4 ± 3.8	Yes
CD-23 1056	b	$0.25^{+0.01}_{-0.01}$	$53.435^{+0.042}_{-0.042}$	$> 114^{+22}_{-22}$	(> 13.1)	Sta17	1.45 ± 0.12	306 ± 25	Yes
LP 413-32 B	b	$0.164^{+0.03}_{-0.03}$	$31.393463^{+0.000067}_{-0.000069}$	(4.01)	$1.70^{+0.36}_{-0.36}$	Fei19	1.354 ± 0.066	300 ± 15	Yes
BD-21 784	b	$0.053^{+0.004}_{-0.007}$	$5.2354^{+0.0027}_{-0.0065}$	$> 10.2^{+7.2}_{-4.1}$	(> 3.10)	Tuo14	48.8 ± 2.9	736 ± 43	
LPM 178	b	$0.06070^{+0.00001}_{-0.00001}$	$8.63300^{+0.00155}_{-0.00155}$	$> 10.60^{+0.06}_{-0.06}$	(> 3.29)	Bon13b	5.89 ± 0.10	433.6 ± 7.5	
	c	$0.1254^{+0.0001}_{-0.0001}$	$25.6450^{+0.0235}_{-0.0235}$	$> 6.8^{+0.9}_{-0.9}$	(> 2.52)	Bon13b	1.380 ± 0.024	301.6 ± 5.2	Yes
	d	$1.0304^{+0.0086}_{-0.0086}$	$660.89^{+7.56}_{-7.56}$	$> 29.4^{+2.9}_{-2.9}$	(> 5.91)	Bon13b	0.02044 ± 0.00035	105.2 ± 1.8	
Melotte 25 VA 50	b	$0.0299^{+0.0005}_{-0.0005}$	$3.484552^{+0.000031}_{-0.000037}$	(11.6)	$3.43^{+0.95}_{-0.31}$	Man16a	8.68 ± 0.15	477.7 ± 8.1	
HG 8-15	b	$0.0562^{+0.0013}_{-0.0014}$	$6.342^{+0.002}_{-0.002}$	$4.7^{+0.5}_{-0.3}$	$1.8^{+0.2}_{-0.1}$	Die18	31.61 ± 0.49	660 ± 10	
	c	$0.0946^{+0.0031}_{-0.0030}$	$13.850^{+0.006}_{-0.006}$	$6.5^{+1.5}_{-0.5}$	$2.6^{+0.7}_{-0.2}$	Die18	11.16 ± 0.17	509 ± 7.8	
	d	$0.1937^{+0.0064}_{-0.0059}$	$40.718^{+0.005}_{-0.005}$	$4.9^{+1.7}_{-0.6}$	$1.9^{+0.7}_{-0.2}$	Die18	22.661 ± 0.041	355.5 ± 5.5	
LP 834-042	b	$0.14339^{+0.00003}_{-0.00003}$	$30.5987^{+0.0083}_{-0.0084}$	$> 23.54^{+0.88}_{-0.89}$	(> 5.14)	Ast17a	1.341 ± 0.019	299.5 ± 4.2	Yes
	c	$0.36175^{+0.00048}_{-0.00047}$	$122.6196^{+0.2429}_{-0.2371}$	$> 21.09^{+1.24}_{-1.26}$	(> 4.88)	Ast17a	0.2108 ± 0.0030	188.6 ± 2.7	

Table C.3: Basic properties of M-dwarf hosted exoplanets (continued).

Name	Planet	a [au]	$P_{\rm orb}$ [days]	$\mathcal{M}_{\rm p}$[a] [$\mathcal{M}_\oplus$]	$\mathcal{R}_{\rm p}$[a] [$\mathcal{R}_\oplus$]	References[b]	$S_{\rm eff}$ [$S_\odot$]	$T_{\rm eq,p}$ [K]	Potentially HZ
	d	$0.19394^{+0.00017}_{-0.00018}$	$48.1345^{+0.0628}_{-0.0661}$	$> 7.60^{+1.05}_{-1.05}$	(> 2.63)	Ast17a	0.733 ± 0.010	257.5 ± 3.7	Yes
	e	$0.08208^{+0.00003}_{-0.00004}$	$13.2543^{+0.0078}_{-0.0104}$	$> 3.28^{+0.64}_{-0.64}$	(> 1.62)	Ast17a	4.094 ± 0.058	395.9 ± 5.6	
LEHPM 3808	b	$0.0306^{+0.0033}_{-0.0057}$	$3.360080^{+0.000065}_{-0.000070}$	(1.98)	$1.247^{+0.089}_{-0.083}$	Gun19	17.89 ± 1.44	572 ± 46	
	c	$0.0472^{+0.0030}_{-0.0033}$	$5.660172^{+0.000035}_{-0.000035}$	(6.88)	$2.42^{+0.13}_{-0.13}$	Gun19	7.52 ± 0.14	460.9 ± 8.3	
	d	$0.0733^{+0.0042}_{-0.0042}$	$11.38014^{+0.00011}_{-0.00010}$	(5.48)	$2.13^{+0.12}_{-0.12}$	Gun19	3.119 ± 0.052	369.9 ± 6.2	
LP 358-499	b	$0.033^{+0.002}_{-0.002}$	$3.0712^{+0.0001}_{-0.0001}$	(2.29)	$1.31^{+0.08}_{-0.08}$	Wel17	32.26 ± 0.39	663.3 ± 8.0	
	c	$0.045^{+0.003}_{-0.003}$	$4.8682^{+0.0001}_{-0.0003}$	(3.07)	$1.48^{+0.09}_{-0.09}$	Wel17	17.35 ± 0.21	568.0 ± 6.8	
	d	$0.077^{+0.005}_{-0.005}$	$11.0234^{+0.0008}_{-0.0003}$	(5.15)	$2.02^{+0.13}_{-0.13}$	Wel17	5.925 ± 0.071	434.2 ± 5.2	
HD 285968	b	$0.066^{+0.001}_{-0.001}$	$8.776^{+0.001}_{-0.002}$	$> 9.06^{+1.54}_{-0.70}$	(> 2.87)	Tri18	8.37 ± 0.17	473.5 ± 9.5	
Wolf 1539	b	$2.41^{+0.04}_{-0.04}$	2288^{+59}_{-59}	$> 260.61^{+22.25}_{-22.25}$	(> 13.9)	How10	0.002714 ± 0.000052	63.5 ± 1.2	
LPM 198	b	$0.103^{+0.006}_{-0.014}$	$17.380^{+0.018}_{-0.020}$	$> 8.3^{+3.5}_{-5.3}$	(> 2.81)	Tuo14	2.29 ± 0.18	342.3 ± 27.1	Yes
	c	$0.1290^{+0.0070}_{-0.0017}$	$24.329^{+0.052}_{-0.066}$	$> 6.4^{+3.7}_{-4.1}$	(> 2.43)	Tuo14	1.459 ± 0.064	306 ± 13	
LP 656-38	b	$0.03282^{+0.00054}_{-0.00056}$	$5.3636^{+0.0007}_{-0.0007}$	$> 2.02^{+0.26}_{-0.25}$	(> 1.23)	Ast17a	3.392 ± 0.049	377.7 ± 5.5	
	c	$0.1264^{+0.0021}_{-0.0022}$	$40.54^{+0.21}_{-0.19}$	$> 2.31^{+0.50}_{-0.49}$	(> 1.32)	Ast17a	0.2287 ± 0.0033	192.5 ± 2.8	
Kapteyn's	b	$0.168^{+0.006}_{-0.008}$	$48.616^{+0.036}_{-0.036}$	$> 4.8^{+0.9}_{-1.0}$	(> 1.98)	Ang14	0.454 ± 0.014	228.4 ± 6.9	Yes
	c	$0.311^{+0.038}_{-0.014}$	$121.54^{+0.25}_{-0.25}$	$> 7.0^{+1.2}_{-1.0}$	(> 2.54)	Ang14	0.132 ± 0.012	167.9 ± 13.8	
LP 892-26	b	0.089	$14.207^{+0.007}_{-0.007}$	$> 6.60^{+0.01}_{-0.01}$	(> 2.43)	Ast15	4.1	395	
NGTS-1	b	$0.0326^{+0.0047}_{-0.0045}$	$2.647298^{+0.000020}_{-0.000020}$	$258.1^{+20.9}_{-23.8}$	$14.91^{+6.84}_{-3.70}$	Bay18	63.9 ± 1.4	786.8 ± 16.9	
HATS-6	b	$0.03623^{+0.00042}_{-0.00057}$	$3.3252725^{+0.0000021}_{-0.0000021}$	$101.4^{+22.2}_{-22.2}$	$11.19^{+0.21}_{-0.21}$	Har15	53.5 ± 1.2	752.7 ± 16.8	
BD-06 1339	b	$0.0428^{+0.0007}_{-0.0007}$	$3.8728^{+0.0004}_{-0.0004}$	$> 8.5^{+1.3}_{-1.3}$	(> 2.81)	LoC13	56.7 ± 1.3	763.9 ± 17.8	
	c	$0.457^{+0.007}_{-0.007}$	$125.95^{+0.44}_{-0.44}$	$> 53^{+8}_{-8}$	(> 8.42)	LoC13	0.498 ± 0.012	233.8 ± 5.4	Yes
HD 42581	b	$0.97^{+0.12}_{-0.09}$	471^{+22}_{-12}	$> 32^{+17}_{-16}$	(> 6.21)	Tuo14	0.0576 ± 0.0035	136.3 ± 8.3	
PM J06168+2435	b	$0.0962^{+0.0054}_{-0.0061}$	$14.5665^{+0.0016}_{-0.0020}$	(7.64)	$2.67^{+0.46}_{-0.42}$	Sch16	4.79 ± 0.10	411.8 ± 8.9	
Luyten's star	b	$0.091101^{+0.000019}_{-0.000017}$	$18.6498^{+0.0059}_{-0.0052}$	$> 2.89^{+0.27}_{-0.26}$	(> 1.45)	Ast17a	1.193 ± 0.042	291 ± 10	Yes
	c	$0.036467^{+0.000002}_{-0.000002}$	$4.7234^{+0.0004}_{-0.0004}$	$> 1.18^{+0.16}_{-0.16}$	(> 1.06)	Ast17a	7.44 ± 0.26	460 ± 16	
LP 424-4	b	$0.0348^{+0.0014}_{-0.0014}$	$3.33714^{+0.00017}_{-0.00017}$	$14.0^{+1.7}_{-1.7}$	$4.2^{+0.6}_{-0.6}$	Bon12	33.07 ± 0.41	667.4 ± 8.2	
NGC 2632 JS 183	b	$0.0653^{+0.0039}_{-0.0045}$	$10.13389^{+0.00068}_{-0.00077}$	$0.361^{+0.069}_{-0.069}$	$3.47^{+0.78}_{-0.53}$	Obe16	5.13 ± 0.27	419 ± 22	
K2-146	b	$0.0266^{+0.0010}_{-0.0010}$	$2.644646^{+0.000043}_{-0.000043}$	(5.48)	$2.2^{+0.23}_{-0.23}$	Hir18	17.47 ± 0.38	569 ± 13	

Table C.3: Basic properties of M-dwarf hosted exoplanets (continued).

Name	Planet	a [au]	$P_{\rm orb}$ [days]	$\mathcal{M}_{\rm p}$[a] [$\mathcal{M}_\oplus$]	$\mathcal{R}_{\rm p}$[a] [$\mathcal{R}_\oplus$]	References[b]	$S_{\rm eff}$ [$S_\odot$]	$T_{\rm eq,p}$ [K]	Potentially HZ
LP 844-8	b	$1.15^{+0.05}_{-0.05}$	692^{+2}_{-2}	$> 572.07^{+15.89}_{-15.89}$	(> 13.3)	Ang12	0.01695 ± 0.00029	100.4 ± 8.9	
	c	5.5	7100^{+8000}_{-1500}	509	(> 13.5)	Ang12	0.00074	45	
NGC 2632 JS 597	b	$0.05023^{+0.00042}_{-0.00043}$	$5.840002^{+0.000676}_{-0.000602}$	(5.83)	$2.231^{+0.151}_{-0.145}$	Liv19	12.57 ± 0.38	524 ± 16	
	c	$0.11283^{+0.00095}_{-0.00097}$	$19.660302^{+0.003496}_{-0.003337}$	(7.64)	$2.668^{+0.201}_{-0.194}$	Liv19	2.490 ± 0.075	350 ± 11	
BD+02 2098	b	$4.5^{+0.2}_{-0.2}$	4100^{+300}_{-300}	$> 2.30^{+0.13}_{-0.13}$	(> 1.32)	Rob13	0.004911 ± 0.000060	73.68 ± 0.90	
K2-117	b	$0.019^{+0.001}_{-0.001}$	$1.291505^{+0.000040}_{-0.000040}$	(4.84)	$1.96^{+0.12}_{-0.12}$	Dre17	123.1 ± 2.6	927 ± 20	
	c	$0.051^{+0.002}_{-0.002}$	$5.444820^{+0.000397}_{-0.000417}$	(5.26)	$2.03^{+0.13}_{-0.13}$	Dre17	17.09 ± 0.36	565 ± 12	
BD+48 1829	b	$0.039435^{+0.00023}_{-0.00023}$	$3.822^{+0.001}_{-0.001}$	$> 13.02^{+2.03}_{-2.01}$	(> 3.62)	Hob19	37.08 ± 0.67	687 ± 13	
LTT 3758	b	$0.0153^{+0.0005}_{-0.0005}$	$1.628931^{+0.000027}_{-0.000027}$	$1.66^{+0.23}_{-0.23}$	$1.43^{+0.16}_{-0.16}$	Sou17, Bon18b	19.88 ± 0.25	587.7 ± 7.3	
	c	$0.0476^{+0.0017}_{-0.0017}$	$8.929^{+0.010}_{-0.010}$	$> 2.64^{+0.44}_{-0.44}$	(> 1.40)	Bon18b	2.054 ± 0.026	333.2 ± 4.2	
K2-239	b	$0.0441^{+0.0008}_{-0.0008}$	$5.240^{+0.001}_{-0.001}$	$1.4^{+0.4}_{-0.4}$	$1.1^{+0.1}_{-0.1}$	Die18	3.697 ± 0.048	385.9 ± 5.0	
	c	$0.0576^{+0.0009}_{-0.0009}$	$7.775^{+0.001}_{-0.001}$	$0.9^{+0.3}_{-0.3}$	$1.1^{+0.1}_{-0.1}$	Die18	2.167 ± 0.026	337.7 ± 4.4	
	d	$0.0685^{+0.0012}_{-0.0012}$	$10.115^{+0.001}_{-0.001}$	$1.3^{+0.4}_{-0.4}$	$1.1^{+0.1}_{-0.1}$	Die18	1.532 ± 0.048	309.7 ± 4.0	
LP 905-36	b	$0.0287^{+0.0010}_{-0.0011}$	$2.64561^{+0.00066}_{-0.00066}$	$7.0^{+0.9}_{-0.8}$[c]	(> 2.54)	Bon11	35.02 ± 0.56	677.0 ± 10.7	
Lalande 21185	b	0.0695	$9.8693^{+0.0016}_{-0.0016}$	3.8	(> 1.75)	But17	3.84 ± 0.27	390 ± 27	
Innes' star	b	$0.119^{+0.014}_{-0.009}$	$26.161^{+0.082}_{-0.098}$	$> 9.9^{+5.6}_{-4.0}$	(> 3.13)	Tuo14	1.264 ± 0.056	295 ± 13	Yes
K2-22	b	0.009	$0.381078^{+0.000003}_{-0.000003}$	(20.2)	$4.75^{+0.35}_{-0.36}$	Dre17	1000	1565	
PM J11293-0127	b	$0.0769^{+0.0039}_{-0.0039}$	$10.05449^{+0.00026}_{-0.00026}$	$8.4^{+2.1}_{-2.1}$	$2.18^{+0.3}_{-0.3}$	Alm15, Sin16	10.20 ± 0.20	497.4 ± 9.9	
	c	$0.1399^{+0.0070}_{-0.0070}$	$24.64354^{+0.00117}_{-0.00117}$	$2.1^{+2.1}_{-1.3}$	$1.85^{+0.27}_{-0.27}$	Alm15, Sin16	3.083 ± 0.062	368.8 ± 7.4	
	d	$0.2076^{+0.0104}_{-0.0104}$	$44.55983^{+0.00590}_{-0.00590}$	$11.1^{+3.5}_{-3.5}$	$1.51^{+0.23}_{-0.23}$	Alm15, Sin16	1.400 ± 0.028	302.8 ± 6.0	Yes
PM J11302+0735	b	$0.1429^{+0.0060}_{-0.0065}$	$32.939614^{+0.000101}_{-0.000084}$	$8.43^{+1.44}_{-1.35}$	$2.38^{+0.22}_{-0.22}$	Clo17, Sar18	1.293 ± 0.021	296.8 ± 4.8	Yes
	c	$0.060^{+0.003}_{-0.003}$	$8.962^{+0.008}_{-0.008}$	$> 7.51^{+1.33}_{-1.33}$	(> 2.66)	Clo17	7.33 ± 0.12	458.0 ± 7.3	
CD-31 9113	b	$0.060^{+0.004}_{-0.008}$	$7.3697^{+0.0034}_{-0.0036}$	$> 5.3^{+2.0}_{-1.9}$	(> 2.19)	Tuo14	9.43 ± 0.65	487.7 ± 33.4	
	c	3.6	3693^{+253}_{-253}	44.6	(> 7.73)	Del13	0.0026	63	
Ross 1003	b	$0.166^{+0.001}_{-0.001}$	$41.380^{+0.002}_{-0.001}$	$> 96.70^{+1.41}_{-1.02}$	(> 11.9)	Tri18	0.5440 ± 0.0061	239.0 ± 2.7	Yes
	c	$0.912^{+0.005}_{-0.002}$	$532.58^{+4.14}_{-2.52}$	$> 68.06^{+4.91}_{-2.19}$	(> 9.40)	Tri18	0.01802 ± 0.00021	102.0 ± 1.2	
Ross 905	b	$0.028^{+0.001}_{-0.001}$	$2.644^{+0.001}_{-0.001}$	$> 21.36^{+0.20}_{-0.21}$	$4.170^{+0.168}_{-0.168}$	Mac14, Tri18	30.48 ± 0.45	653.9 ± 9.7	
LP 613-39	b	$0.0910^{+0.0130}_{-0.0160}$	$18.4498^{+0.0015}_{-0.0015}$	(5.83)	$2.25^{+0.53}_{-0.96}$	Sch16	1.470 ± 0.054	306.4 ± 11.3	Yes

Table C.3: Basic properties of M-dwarf hosted exoplanets (continued).

Name	Planet	a [au]	$P_{\rm orb}$ [days]	$\mathcal{M}_{\rm p}$[a] [$\mathcal{M}_\oplus$]	$\mathcal{R}_{\rm p}$[a] [$\mathcal{R}_\oplus$]	References[b]	$S_{\rm eff}$ [$S_\odot$]	$T_{\rm eq,p}$ [K]	Potentially HZ
FI Vir	b	$0.0496^{+0.0017}_{-0.0017}$	$9.8658^{+0.0070}_{-0.0070}$	$> 1.4^{+0.21}_{-0.21}$	(> 1.11)	Bon18b	1.556 ± 0.023	310.8 ± 4.5	
K2-152	b	$0.1735^{+0.0054}_{-0.0054}$	$32.6527^{+0.0035}_{-0.0035}$	(8.30)	$2.81^{+0.34}_{-0.30}$	Hir18	2.944 ± 0.054	364.6 ± 6.6	
K2-153	b	$0.0601^{+0.0021}_{-0.0021}$	$7.51554^{+0.00098}_{-0.00098}$	(4.89)	$2.00^{+0.26}_{-0.22}$	Hir18	14.82 ± 0.33	546 ± 12	
K2-137	b	$0.0058^{+0.0006}_{-0.0006}$	$0.179715^{+0.000006}_{-0.000006}$	(0.65)	$0.89^{+0.09}_{-0.09}$	Smi18	841 ± 18	1499 ± 33	
K2-154	b	$0.0408^{+0.0012}_{-0.0012}$	$3.67635^{+0.00017}_{-0.00017}$	(6.08)	$2.23^{+0.37}_{-0.24}$	Hir18	59.04 ± 0.96	772 ± 13	
	c	$0.0683^{+0.0021}_{-0.0021}$	$7.95478^{+0.00063}_{-0.00063}$	(5.48)	$2.10^{+0.25}_{-0.23}$	Hir18	21.07 ± 0.34	596.3 ± 9.7	
Ross 1020	b	$0.026^{+0.001}_{-0.001}$	$3.023^{+0.001}_{-0.001}$	$> 7.0^{+0.5}_{-0.5}$	(> 2.54)	Luq18	12.16 ± 0.16	519.7 ± 6.6	
HD 122303	b	$0.067^{+0.001}_{-0.001}$	$8.708^{+0.002}_{-0.001}$	$> 6.51^{+0.69}_{-0.40}$	(> 2.42)	Tri18	9.66 ± 0.16	490.6 ± 8.2	
Proxima Cen	b	$0.0485^{+0.0041}_{-0.0041}$	$11.186^{+0.001}_{-0.001}$	$> 1.27^{+0.19}_{-0.17}$	(> 1.07)	Ang16	0.653 ± 0.017	250.2 ± 6.4	Yes
K2-240	b	$0.0513^{+0.0009}_{-0.0009}$	$6.034^{+0.001}_{-0.001}$	$5.0^{+0.5}_{-0.2}$	$2.0^{+0.2}_{-0.1}$	Die18	23.88 ± 0.58	615 ± 15	
	c	$0.1159^{+0.0020}_{-0.0020}$	$20.523^{+0.001}_{-0.001}$	$4.6^{+0.7}_{-0.3}$	$1.8^{+0.3}_{-0.1}$	Die18	4.68 ± 0.11	409 ± 10	
HO Lib	b	$0.041^{+0.001}_{-0.001}$	$5.368^{+0.001}_{-0.001}$	$> 15.20^{+0.22}_{-0.27}$	(> 4.03)	Tri18	7.14 ± 0.10	455.0 ± 6.4	
	c	$0.074^{+0.001}_{-0.001}$	$12.919^{+0.003}_{-0.002}$	$> 5.652^{+0.386}_{-0.239}$	(> 2.20)	Tri18	2.192 ± 0.031	338.6 ± 4.7	
	d	$0.029^{+0.001}_{-0.001}$	$3.153^{+0.001}_{-0.006}$	$> 1.657^{+0.240}_{-0.161}$	(> 1.18)	Tri18	14.27 ± 0.20	541.0 ± 7.6	
K2-286	b	$0.1768^{+0.0175}_{-0.0205}$	$27.359^{+0.005}_{-0.005}$	(5.26)	$2.1^{+0.2}_{-0.2}$	Die19	2.891 ± 0.063	362.9 ± 7.9	
MCC 759	b	$0.0608^{+0.0068}_{-0.0068}$	$6.905^{+0.040}_{-0.040}$	$> 7.14^{+0.59}_{-0.59}$	(> 2.67)	Per17	17.5 ± 0.2	569.1 ± 6.4	
USco J161014.7-191909	b	$0.0409^{+0.0021}_{-0.0023}$	$5.424865^{+0.000035}_{-0.000031}$	< 11.76	$5.04^{+0.34}_{-0.37}$	Dav16, Man16b	60.9 ± 1.9	778 ± 25	
LP 804-27	b	0.36	$111.7^{+0.7}_{-0.7}$	> 667.415	(> 13.2)	App10	0.23	193	
HD 147379	b	$0.3193^{+0.0002}_{-0.0002}$	$86.54^{+0.07}_{-0.06}$	$> 24.7^{+1.8}_{-2.4}$	(> 5.28)	Rei18	0.959 ± 0.023	275.4 ± 6.5	Yes
MCC 767	b	$0.078361^{+0.000044}_{-0.000046}$	$14.628^{+0.012}_{-0.013}$	$> 2.82^{+0.51}_{-0.51}$	(> 1.45)	Sua17	2.412 ± 0.033	346.8 ± 4.8	
V2306 Oph	b	$0.0375^{+0.0012}_{-0.0013}$	$4.8869^{+0.0005}_{-0.0005}$	$> 1.91^{+0.26}_{-0.25}$	(> 1.23)	Ast17a	7.70 ± 0.12	463.6 ± 7.1	
	c	$0.0890^{+0.0029}_{-0.0031}$	$17.8719^{+0.0059}_{-0.0059}$	$> 3.41^{+0.43}_{-0.41}$	(> 1.66)	Ast17a	1.366 ± 0.021	300.9 ± 4.6	Yes
	d	$0.470^{+0.015}_{-0.017}$	$217.21^{+0.55}_{-0.52}$	$> 7.70^{+1.12}_{-1.06}$	(> 2.66)	Ast17a	0.04899 ± 0.00077	130.9 ± 2.1	
BD+25 3173	b	$1.135^{+0.035}_{-0.035}$	$598.3^{+4.2}_{-4.2}$	$> 104.244^{+10.170}_{-10.170}$	(> 12.5)	Jon10	0.03372 ± 0.00036	119.3 ± 1.3	
LHS 3275	b	$0.01411^{+0.00032}_{-0.00032}$	$1.58040456^{+0.00000016}_{-0.00000016}$	$6.55^{+0.98}_{-0.98}$	$2.85^{+0.20}_{-0.20}$	Cha09, Har13	19.51 ± 0.25	584.9 ± 7.6	
BD+11 3149	b	$0.029^{+0.001}_{-0.001}$	$2.64977^{+0.00081}_{-0.00077}$	$> 2.47^{+0.27}_{-0.27}$	(> 1.36)	Aff16	55.6 ± 1.5	760 ± 20	
	c	$0.089^{+0.003}_{-0.003}$	$13.740^{+0.016}_{-0.016}$	$> 6.26^{+0.79}_{-0.76}$	(> 2.36)	Aff16	5.90 ± 0.16	434 ± 11	
HD 156384C	b	$0.0505^{+0.0053}_{-0.0044}$	$7.2004^{+0.0017}_{-0.0017}$	$> 5.6^{+1.4}_{-1.3}$	(> 2.23)	Ang13	5.86 ± 0.14	433 ± 10	

Table C.3: Basic properties of M-dwarf hosted exoplanets (continued).

Name	Planet	a [au]	$P_{\rm orb}$ [days]	$\mathcal{M}_{\rm p}$[a] [$\mathcal{M}_\oplus$]	$\mathcal{R}_{\rm p}$[a] [$\mathcal{R}_\oplus$]	References[b]	$S_{\rm eff}$ [$S_\odot$]	$T_{\rm eq,p}$ [K]	Potentially HZ
	c	$0.125^{+0.012}_{-0.013}$	$28.14^{+0.03}_{-0.03}$	$> 3.8^{+1.5}_{-1.2}$	(> 1.78)	Ang13	0.956 ± 0.016	275.2 ± 4.7	Yes
	d	$0.276^{+0.024}_{-0.030}$	$91.61^{+0.81}_{-0.89}$	$> 5.1^{+1.8}_{-1.7}$	(> 2.08)	Ang13	0.1962 ± 0.0052	185.2 ± 4.9	
	e	$0.213^{+0.020}_{-0.020}$	$62.24^{+0.55}_{-0.55}$	$> 2.7^{+1.6}_{-1.4}$	(> 1.47)	Ang13	0.3294 ± 0.0050	210.9 ± 3.2	Yes
	f	$0.156^{+0.014}_{-0.017}$	$39.026^{+0.194}_{-0.211}$	$> 2.7^{+1.4}_{-1.2}$	(> 1.42)	Ang13	0.614 ± 0.015	246.4 ± 6.0	Yes
	g	$0.549^{+0.052}_{-0.058}$	$256.2^{+13.8}_{-7.9}$	$> 4.6^{+2.6}_{-2.3}$	(> 1.98)	Ang13	0.04958 ± 0.00092	131.3 ± 2.4	
CD-46 11540	b	0.039	$4.6938^{+0.0070}_{-0.0070}$	> 11.09	(> 3.32)	Bon07	11	507	
CD-51 10924	b	$1.8049^{+0.0302}_{-0.0302}$	$1051.1^{+0.5}_{-0.5}$	$> 1497.9^{+2.9}_{-2.9}$	(> 12.8)	Sah16	0.02763 ± 0.00050	113.5 ± 2.0	
	c	$6.6675^{+0.4684}_{-0.4684}$	$7462.9^{+105.4}_{-101.4}$	$> 2190^{+32}_{-32}$	(> 12.6)	Sah16	0.002024 ± 0.000037	59.0 ± 1.1	
	d	$0.0410^{+0.0007}_{-0.0007}$	$3.6005^{+0.0002}_{-0.0002}$	$> 4.4^{+0.3}_{-0.3}$	(> 1.94)	Sah16	53.50 ± 0.96	753 ± 14	
	e	$0.1882^{+0.0032}_{-0.0032}$	$35.39^{+0.03}_{-0.04}$	$> 8.1^{+0.7}_{-0.7}$	(> 2.71)	Sah16	2.541 ± 0.046	351.4 ± 6.3	
BD+68 946	b	$0.71^{+0.01}_{-0.01}$	$38.140^{+0.015}_{-0.015}$	$> 19^{+3}_{-3}$	(> 4.57)	Sta17	0.0439 ± 0.0010	127.4 ± 2.8	
CD-44 11909	b	$0.08^{+0.014}_{-0.004}$	$17.478^{+0.062}_{-0.040}$	$> 4.4^{+3.7}_{-2.4}$	(> 1.92)	Tuo14	1.268 ± 0.159	295 ± 37	Yes
	c	$0.176^{+0.030}_{-0.009}$	$57.32^{+0.45}_{-0.48}$	$> 8.7^{+5.8}_{-4.6}$	(> 2.81)	Tuo14	0.262 ± 0.031	199 ± 24	Yes
BD+18 3421	b	$0.091^{+0.004}_{-0.004}$	$15.53209^{+0.00166}_{-0.00167}$	$> 7.1^{+0.9}_{-0.9}$	(> 2.58)	Aff19	3.34 ± 0.22	376 ± 25	
Barnard's star	b	$0.404^{+0.018}_{-0.018}$	$232.80^{+0.38}_{-0.41}$	$> 3.23^{+0.44}_{-0.44}$	(> 1.58)	Rib18	0.02180 ± 0.00044	106.9 ± 2.2	
Kepler-83	b	0.0785	$9.770469^{+0.000022}_{-0.000022}$	(7.03)	$2.53^{+0.16}_{-0.16}$	Row14	15	547	
	c	0.0514	$5.169796^{+0.000016}_{-0.000016}$	(4.74)	$1.94^{+0.13}_{-0.13}$	Row14	35	676	
	d	0.1270	$20.090227^{+0.000102}_{-0.000102}$	(6.08)	$2.30^{+0.35}_{-0.35}$	Row14	5.7	430	
Kepler-446	b	$0.0159^{+0.0007}_{-0.0007}$	$1.5654090^{+0.0000033}_{-0.0000033}$	$4.5^{+0.5}_{-0.5}$	$1.50^{+0.25}_{-0.25}$	Mui15	19.61 ± 0.39	586 ± 12	
	c	$0.0248^{+0.0011}_{-0.0011}$	$3.0361790^{+0.0000055}_{-0.0000055}$	3^{+1}_{-1}	$1.11^{+0.18}_{-0.18}$	Mui15	8.11 ± 0.16	469.6 ± 9.3	
	d	$0.0352^{+0.0016}_{-0.0016}$	$5.148921^{+0.000022}_{-0.000022}$	4^{+1}_{-1}	$1.35^{+0.22}_{-0.22}$	Mui15	4.008 ± 0.079	393.8 ± 7.8	
Kepler-303	b	0.0265	$1.937055^{+0.000004}_{-0.000004}$	(0.66)	$0.89^{+0.05}_{-0.05}$	Row14	125	930	
	c	0.0628	$7.061149^{+0.000019}_{-0.000019}$	(1.55)	$1.14^{+0.09}_{-0.09}$	Row14	22	604	
Kepler-617	b	0.0233	$1.682696148^{+0.000001112}_{-0.000001112}$	(2.32)	$1.32^{+0.07}_{-0.07}$	Mor16	94	867	
Kepler-236	b	0.0698	$8.295611^{+0.000032}_{-0.000032}$	(3.40)	$1.57^{+0.12}_{-0.12}$	Row14	15	552	
	c	0.1416	$23.968127^{+0.000174}_{-0.000174}$	(4.94)	$2.00^{+0.17}_{-0.17}$	Row14	3.8	388	
Kepler-235	b	0.035	$3.340222^{+0.000005}_{-0.000005}$	(5.83)	$2.23^{+0.10}_{-0.10}$	Row14	71	810	
	c	0.037	$7.824904^{+0.000055}_{-0.000055}$	(2.02)	$1.28^{+0.08}_{-0.08}$	Row14	64	788	

Table C.3: Basic properties of M-dwarf hosted exoplanets (continued).

Name	Planet	a [au]	$P_{\rm orb}$ [days]	$\mathcal{M}_{\rm p}$[a] [$\mathcal{M}_\oplus$]	$\mathcal{R}_{\rm p}$[a] [$\mathcal{R}_\oplus$]	References[b]	$S_{\rm eff}$ [$S_\odot$]	$T_{\rm eq,p}$ [K]	Potentially HZ
	d	0.122	$20.060548^{+0.000099}_{-0.000099}$	(5.26)	$2.05^{+0.10}_{-0.10}$	Row14	5.9	434	
	e	0.213	$46.183669^{+0.000425}_{-0.000425}$	(5.95)	$2.22^{+0.29}_{-0.29}$	Row14	1.9	328	
Kepler-52	b	…	$7.877407^{+0.000020}_{-0.000020}$	(6.08)	$2.34^{+0.22}_{-0.22}$	Row14	22	604	
	c	…	$16.384888^{+0.000080}_{-0.000080}$	(4.01)	$1.71^{+0.08}_{-0.08}$	Row14	8.4	474	
	d	…	$36.445171^{+0.000253}_{-0.000253}$	(4.74)	$1.95^{+0.21}_{-0.21}$	Row14	2.9	363	
Kepler-155	b	0.056	$5.931194^{+0.000008}_{-0.000008}$	(5.26)	$2.09^{+0.21}_{-0.21}$	Row14	55	758	
	c	0.242	$52.661793^{+0.000236}_{-0.000236}$	(5.83)	$2.24^{+0.15}_{-0.15}$	Row14	2.9	365	
V1428 Aql	b	$0.3357^{+0.0099}_{-0.0100}$	$105.90^{+0.09}_{-0.10}$	$> 12.2^{+1.0}_{-1.4}$	(> 3.40)	Kam18	0.2891 ± 0.0035	204.1 ± 2.5	Yes
Kepler-138	b	$0.0746^{+0.0021}_{-0.0021}$	$10.3126^{+0.0004}_{-0.0006}$	$0.066^{+0.059}_{-0.037}$	$0.522^{+0.032}_{-0.032}$	Jhu15	10.34 ± 0.14	499.1 ± 6.5	
	c	$0.0905^{+0.0026}_{-0.0026}$	$13.7813^{+0.0001}_{-0.0001}$	$1.970^{+1.912}_{-1.120}$	$1.197^{+0.070}_{-0.070}$	Jhu15	7.026 ± 0.092	453.1 ± 5.9	
	d	$0.1277^{+0.0036}_{-0.0036}$	$23.0881^{+0.0009}_{-0.0008}$	$0.640^{+0.674}_{-0.387}$	$2.1^{+2.2}_{-1.2}$	Jhu15	3.531 ± 0.046	381.5 ± 5.0	
LSPM J1928+4437	b	0.0116	$1.2137672^{+0.0000046}_{-0.0000046}$	(0.39)	$0.78^{+0.22}_{-0.22}$	Mui12b	22	600	
	c	0.006	$0.45328509^{+0.00000097}_{-0.00000097}$	(0.33)	$0.73^{+0.20}_{-0.20}$	Mui12b	81	834	
	d	0.0154	$1.865169^{+0.000014}_{-0.000014}$	(0.13)	$0.57^{+0.18}_{-0.18}$	Mui12b	12	521	
Kepler-49	b	0.0642	$7.203871^{+0.000008}_{-0.000008}$	(6.21)	$2.35^{+0.09}_{-0.09}$	Row14	23	609	
	c	0.0847	$10.912732^{+0.000021}_{-0.000021}$	(5.10)	$2.06^{+0.09}_{-0.09}$	Row14	13	530	
	d	0.0323	$2.576549^{+0.000003}_{-0.000003}$	(3.55)	$1.60^{+0.07}_{-0.07}$	Row14	90	858	
	e	0.1208	$18.596108^{+0.000079}_{-0.000079}$	(3.33)	$1.56^{+0.08}_{-0.08}$	Row14	6.5	444	
LSPM J1930+4149	b	$0.0514^{+0.0028}_{-0.0028}$	$8.689090^{+0.000024}_{-0.000024}$	(1.28)	$1.08^{+0.15}_{-0.15}$	Age17	1.982 ± 0.039	330.2 ± 6.6	
Kepler-45	b	0.03	$2.455239^{+0.000004}_{-0.000004}$	$160.497^{+28.604}_{-28.604}$	$10.76^{+1.23}_{-1.23}$	Jon12	90	856	
Kepler-231	b	0.0788	$10.065275^{+0.000027}_{-0.000027}$	(4.10)	$1.73^{+0.12}_{-0.12}$	Row14	13	530	
	c	0.1215	$19.271566^{+0.000099}_{-0.000099}$	(4.74)	$1.93^{+0.19}_{-0.19}$	Row14	5.5	427	
Kepler-54	b	0.0655	$8.010260^{+0.000030}_{-0.000030}$	(5.15)	$2.07^{+0.12}_{-0.12}$	Row14	11	509	
	c	0.0862	$12.072389^{+0.000100}_{-0.000100}$	(4.23)	$1.75^{+0.12}_{-0.12}$	Row14	6.5	444	
	d	0.1246	$20.995694^{+0.000143}_{-0.000143}$	(3.26)	$1.53^{+0.08}_{-0.08}$	Row14	3.1	369	
Kepler-252	b	0.0631	$6.668391^{+0.000031}_{-0.000031}$	(1.90)	$1.23^{+0.12}_{-0.12}$	Row14	36	680	
	c	0.0873	$10.848463^{+0.000015}_{-0.000015}$	(5.37)	$2.15^{+0.13}_{-0.13}$	Row14	19	578	
Kepler-32	b	0.05	$5.90124^{+0.00010}_{-0.00010}$	(5.89)	$2.2^{+0.2}_{-0.2}$	Fab12	26	629	

Table C.3: Basic properties of M-dwarf hosted exoplanets (continued).

Name	Planet	a [au]	$P_{\rm orb}$ [days]	$\mathcal{M}_{\rm p}$[a] [$\mathcal{M}_\oplus$]	$\mathcal{R}_{\rm p}$[a] [$\mathcal{R}_\oplus$]	References[b]	$S_{\rm eff}$ [$S_\odot$]	$T_{\rm eq,p}$ [K]	Potentially HZ
	c	0.09	$8.7522^{+0.0003}_{-0.0003}$	(4.94)	$2.0^{+0.2}_{-0.2}$	Fab12	8.0	469	
	d	0.13	$22.7802^{+0.0005}_{-0.0005}$	(7.96)	$2.7^{+0.2}_{-0.2}$	Fab12	3.9	390	
	e	0.033	$2.8960^{+0.0003}_{-0.0003}$	(4.36)	$1.85^{+0.01}_{-0.01}$	Fab12	60	7734	
	f	0.013	$0.74296^{+0.00007}_{-0.00007}$	(0.47)	$0.82^{+0.07}_{-0.07}$	Fab12	385	1233	
Kepler-125	b	0.0427	$4.164389^{+0.000003}_{-0.000003}$	(6.34)	$2.37^{+0.10}_{-0.10}$	Row14	31	655	
	c	0.0531	$5.774464^{+0.000047}_{-0.000047}$	(0.32)	$0.74^{+0.05}_{-0.05}$	Row14	20	587	
Kepler-186	b	$0.0343^{+0.0046}_{-0.0046}$	$3.8867907^{+0.0000062}_{-0.0000063}$	(1.21)	$1.07^{+0.12}_{-0.12}$	Qui14	48.6 ± 1.2	735 ± 19	
	c	$0.0451^{+0.0070}_{-0.0070}$	$7.267302^{+0.000012}_{-0.000011}$	(2.02)	$1.25^{+0.14}_{-0.14}$	Qui14	28.09 ± 0.71	641 ± 16	
	d	$0.0781^{+0.0100}_{-0.0100}$	$13.342996^{+0.000025}_{-0.000024}$	(2.65)	$1.40^{+0.16}_{-0.16}$	Qui14	9.37 ± 0.24	487 ± 12	
	e	$0.110^{+0.015}_{-0.015}$	$22.407704^{+0.000074}_{-0.000072}$	(2.05)	$1.27^{+0.15}_{-0.14}$	Qui14	4.72 ± 0.12	410 ± 10	
	f	$0.432^{+0.171}_{-0.053}$	$129.9441^{+0.0013}_{-0.0012}$	(1.65)	$1.17^{+0.08}_{-0.08}$	Tor15	0.306 ± 0.084	207 ± 57	Yes
Kepler-445	b	$0.0229^{+0.0010}_{-0.0010}$	$2.984151^{+0.000011}_{-0.000011}$	(3.55)	$1.58^{+0.23}_{-0.23}$	Mui15	14.79 ± 0.40	546 ± 15	
	c	$0.0318^{+0.0013}_{-0.0013}$	$4.871229^{+0.000011}_{-0.000011}$	(6.74)	$2.51^{+0.36}_{-0.36}$	Mui15	7.70 ± 0.21	464 ± 13	
	d	$0.0448^{+0.0019}_{-0.0019}$	$8.15275^{+0.00040}_{-0.00040}$	(1.86)	$1.25^{+0.19}_{-0.19}$	Mui15	3.87 ± 0.11	390 ± 11	
Kepler-267	b	0.0370	$3.353728^{+0.000007}_{-0.000007}$	(5.04)	$1.98^{+0.09}_{-0.09}$	Row14	43	712	
	c	0.0597	$6.877450^{+0.000016}_{-0.000016}$	(5.59)	$2.13^{+0.11}_{-0.11}$	Row14	16	560	
	d	0.1539	$28.464515^{+0.000180}_{-0.000180}$	(5.71)	$2.27^{+0.12}_{-0.12}$	Row14	2.5	349	
HD 204961	b	$3.56^{+0.28}_{-0.28}$	3657^{+104}_{-104}	$> 216^{+29}_{-28}$	(> 13.8)	Wit14	0.002304 ± 0.000088	61.0 ± 2.3	
	c	$0.163^{+0.006}_{-0.006}$	$35.68^{+0.03}_{-0.03}$	$> 5.40^{+0.95}_{-0.95}$	(> 2.16)	Wit14	1.099 ± 0.042	285 ± 11	Yes
BD-05 5715	b	$2.35^{+0.22}_{-0.22}$	1882^{+250}_{-250}	$> 318^{+99}_{-99}$	(> 13.5)	Sta17	0.005115 ± 0.000077	74.4 ± 1.1	
	c	6.5640	8775	> 245.7	(> 13.9)	Mon14	0.00066	45	
LP 819-052	b	$0.026^{+0.001}_{-0.001}$	$3.651^{+0.001}_{-0.001}$	$> 6.4^{+0.5}_{-0.5}$	(> 2.36)	Luq18	5.378 ± 0.068	423.8 ± 5.4	
LP 700-6	b	$0.0214^{+0.0013}_{-0.0013}$	$2.260455^{+0.000041}_{-0.000041}$	(6.08)	$2.32^{+0.24}_{-0.24}$	Hir16	25.50 ± 0.50	625 ± 12	
K2-21	b	$0.076^{+0.002}_{-0.003}$	$9.325038^{+0.000379}_{-0.000403}$	(4.45)	$1.84^{+0.10}_{-0.10}$	Dre17	16.93 ± 0.32	565 ± 11	
	c	$0.107^{+0.003}_{-0.004}$	$15.50192^{+0.00092}_{-0.00093}$	(7.18)	$2.49^{+0.17}_{-0.19}$	Dre17	8.54 ± 0.14	475.8 ± 8.0	
LHS 3844	b	$0.00623^{+0.00015}_{-0.00015}$	$0.46292792^{+0.0000016}_{-0.0000016}$	(2.25)	$1.32^{+0.02}_{-0.02}$	Van18	69.82 ± 0.74	804.5 ± 8.6	
IL Aqr	b	$0.214^{+0.001}_{-0.001}$	$61.082^{+0.006}_{-0.010}$	$> 760.9^{+1.0}_{-1.0}$	(> 13.1)	Tri18	0.2823 ± 0.0066	202.9 ± 4.8	Yes
	c	$0.134^{+0.001}_{-0.001}$	$30.126^{+0.011}_{-0.003}$	$> 241.5^{+0.7}_{-0.6}$	(> 13.7)	Tri18	0.720 ± 0.017	256.4 ± 6.0	Yes

Table C.3: Basic properties of M-dwarf hosted exoplanets (continued).

Name	Planet	a [au]	P_{orb} [days]	$\mathcal{M}_p$[a] [$\mathcal{M}_\oplus$]	$\mathcal{R}_p$[a] [$\mathcal{R}_\oplus$]	References[b]	S_{eff} [$S_\odot$]	$T_{eq,p}$ [K]	Potentially HZ
	d	$0.021^{+0.001}_{-0.001}$	$1.938^{+0.001}_{-0.001}$	$> 6.910^{+0.220}_{-0.270}$	(> 2.54)	Tri18	29.31 ± 0.68	648 ± 15	
	e	$0.345^{+0.001}_{-0.001}$	$124.4^{+0.3}_{-0.7}$	$> 15.43^{+1.29}_{-1.27}$	(> 3.92)	Tri18	0.1086 ± 0.0025	159.8 ± 3.7	
2MUCD 12171	b	$0.01111^{+0.00034}_{-0.00034}$	$1.51087081^{+0.00000060}_{-0.00000060}$	$0.85^{+0.72}_{-0.72}$	$1.086^{+0.035}_{-0.035}$	Gil17	4.357 ± 0.046	402.1 ± 4.3	
	c	$0.01521^{+0.00047}_{-0.00047}$	$2.4218233^{+0.0000017}_{-0.0000017}$	$1.38^{+0.61}_{-0.61}$	$1.056^{+0.035}_{-0.035}$	Gil17	2.325 ± 0.025	343.7 ± 3.7	
	d	$0.02144^{+0.00066}_{-0.00063}$	$4.049610^{+0.000063}_{-0.000063}$	$0.41^{+0.27}_{-0.27}$	$0.772^{+0.030}_{-0.030}$	Gil17	1.170 ± 0.013	289.5 ± 3.1	Yes
	e	$0.02817^{+0.00083}_{-0.00087}$	$6.099615^{+0.000011}_{-0.000011}$	$0.62^{+0.58}_{-0.58}$	$0.918^{+0.039}_{-0.039}$	Gil17	0.6777 ± 0.0073	252.5 ± 2.7	Yes
	f	$0.0371^{+0.0011}_{-0.0011}$	$9.206690^{+0.000015}_{-0.000015}$	$0.68^{+0.18}_{-0.18}$	$1.045^{+0.038}_{-0.038}$	Gil17	0.3907 ± 0.0042	220.0 ± 2.3	Yes
	g	$0.0451^{+0.0014}_{-0.0014}$	$12.35294^{+0.00012}_{-0.00012}$	$1.34^{+0.88}_{-0.88}$	$1.127^{+0.041}_{-0.041}$	Gil17	0.2644 ± 0.0028	199.6 ± 2.1	Yes
	h	$0.063^{+0.027}_{-0.013}$	$18.767^{+0.004}_{-0.003}$	(0.39)	$0.752^{+0.032}_{-0.031}$	Gil17, Lug17	0.136 ± 0.030	169 ± 38	

[a] The planetary masses and radii shown in parentheses correspond to our adopted mass-radius relation.

[b] Aff16: Affer et al. (2016); Aff19: Affer et al. (2019); Age17: Angelo et al. (2017); Alm15: Almenara et al. (2015); Ang12: Anglada-Escudé et al. (2012); Ang13: Anglada-Escudé et al. (2013); Ang14: Anglada-Escudé et al. (2014); Ang16: Anglada-Escudé et al. (2016); App10: Apps et al. (2010); Ast15: Astudillo-Defru et al. (2015); Ast17a: Astudillo-Defru et al. (2017a); Ast17b: Astudillo-Defru et al. (2017b); Bak18: Bakos et al. (2018); Bay18: Bayliss et al. (2018); Bid14: Biddle et al. (2014); Bon07: Bonfils et al. (2007); Bon11: Bonfils et al. (2011); Bon13b: Bonfils et al. (2013b); Bon17: Bonfils et al. (2018c); Bon18a: Bonfils et al. (2018b); Bon18b: Bonfils et al. (2018a); But17: Butler et al. (2017); Cha09: Charbonneau et al. (2009); Clo17: Cloutier et al. (2017); Dav16: David et al. (2016); Del13: Delfosse et al. (2013); Die18a: (Díez Alonso et al., 2018b); Die18b: (Díez Alonso et al., 2018a); Die19: (Díez Alonso et al., 2019); Dit17: Dittmann et al. (2017); Dre17: Dressing et al. (2017); Fab12: Fabrycky et al. (2012); Fei19: Feinstein et al. (2019); Gil17: Gillon et al. (2017); Gil17: Gillon et al. (2017); Gun19: Günther et al. (2019); Har13: Harpsøe et al. (2013); Har15: Hartman et al. (2015); Hir16: Hirano et al. (2016); Hir18: Hirano et al. (2018); Hob18: Hobson et al. (2018); Hob19: Hobson et al. (2019); How10: Howard et al. (2010); Jhu15: Jontof-Hutter et al. (2015); Jon10: Johnson et al. (2010b); Jon12: Johnson et al. (2012); Kam18: Kaminski et al. (2018); Liv19: Livingston et al. (2019); LoC13: Lo Curto et al. (2013); Lug17: Luger et al. (2017); Luq18: Luque et al. (2018); Mac14: Maciejewski et al. (2014); Man16a: Mann et al. (2016a); Man16b: Mann et al. (2016b); Men19: Ment et al. (2019); Mon14: Montet et al. (2014); Mor16: Morton et al. (2016); Mui12: Muirhead et al. (2012); Mui15: Muirhead et al. (2015); Obe16: Obermeier et al. (2016); Per17: Perger et al. (2017); Per19: Perger et al. (2019); Pin18: Pinamonti et al. (2018); Qui14: Quirrenbach et al. (2014); Rei18: Reiners et al. (2018a); Rob13: Astropy Collaboration et al. (2013); Row14: Rowe et al. (2014); Sah16: Sahlmann et al. (2016); San15: Sanchís-Ojeda et al. (2015); Sar18: Sarkis et al. (2018); Sch16: Schlieder et al. (2016); Sin16: Sinukoff et al. (2016); Sou17: Southworth et al. (2017); Smi18: Smith (2018); Sta17: Stassun et al. (2017); Sua17: Suárez Mascareño et al. (2017c); Tor15: Torres et al. (2015); Tri18: Trifonov et al. (2018); Tuo14: Tuomi et al. (2014); Van18: Vanderspek et al. (2019); Wel17: Wells et al. (2018); Wit14: Wittenmyer et al. (2014).

[c] Bonfils et al. (2011) gave true mass for LP 905-36 b calculated with a Markov chain analysis, $\mathcal{M}_p = 8.4^{+4.0}_{-1.5}\,\mathcal{M}_\oplus$, but we adopt the minimum mass, $\mathcal{M}_2 \sin i$, for consistency.

Appendix D

Long tables of Chapter 4

Table D.1: Description of the online table used in Chapter 4.

Parameter	Units	Column(s)	Description
			Identification
ID_star, ID_system	…	1, 2	Star and system identifiers[a]
Name	…	3	Discovery name or most common name[b]
Karmn	…	4	Carmencita star identifier (JHHMMm+DDd)[d]
GJ	…	5	Gliese-Jahreiss catalogue number[d]
RA_J2016, DE_J2016	hms, dms	6, 7	Right ascension and declination in the epoch J2016.0
SpT, SpTnum, SpT_ref	…	8–10	Spectral type, its numerical format, and the reference[e]
N_planet	…	11	Number of confirmed planets[f]
			Multiplicity
Type, Class	…	12, 13	Type of system and multiplicity class[g]
Component, System	…	14, 15	Component designation and resolution of the components in the multiple system[h]
SB, SB_ref	…	16, 17	Type of spectroscopic system and reference[h]
Remarks	…	18	Annotations and remarks
WDS_…	…	19–28	Washington double star catalogue data[i]
theta_deg	deg	29	Positional angle[j]
rho_arcsec	arcsec	30	Projected separation
s_au	au	31	Physical separation
muratio, deltaPA, deltad	…	32–34	μratio, ΔPA, Δd criteria for physical parity
crit_…	Boolean	35–41	Criteria for unresolved companions[k]
Candidate	Boolean	42	Candidate to unresolved companion[l]
			Stellar parameters
Teff_K, eTeff_K, Teff_K_ref	K	43–45	Effective temperature
logg, elogg	dex	46, 47	Surface gravity
L_Lsol, eL_Lsol, L_ref	$\mathcal{L}_\odot$	48–50	Luminosity and uncertainty
R1_Rsol, eR1_Rsol	$\mathcal{R}_\odot$	51, 52	Radius and uncertainty
M1_Msol, eM1_Msol, RM1_ref	$\mathcal{M}_\odot$	53–55	Mass and uncertainty
M2_Msol, eM2_Msol, RM2_ref	$\mathcal{M}_\odot$	56–58	Mass and uncertainty for the unresolved companion
Mt_Msol, eMt_Msol	$\mathcal{M}_\odot$	59, 60	Total mass of the system
q	…	61	Mass ratio
Ug_J, eUg_J	J	62, 63	Binding energy
Porb_d, ePorb_d, Porb_d_ref	d	64–66	Orbital period
			Astrometry and photometry
_id	…	67–70	Catalog identifiers
ra, ra_error	deg	71, 72	Barycentric right ascension and uncertainty in the epoch J2016.0
dec, dec_error	deg	73, 74	Barycentric declination and uncertainty in the epoch J2016.0
parallax, parallax_error	mas	75–77	Parallax and uncertainty
d_pc, ed_pc, d_ref	pc	78, 79	Distance, uncertainty, and reference
pm, pm_error, pm_ref	mas a^{-1}	80–82	Total proper motion and reference
pmra, pmra_error	mas a^{-1}	83, 84	Proper motion in right ascension, uncertainty, and reference
pmdec, pmdec_error	mas a^{-1}	85, 86	Proper motion in declination, uncertainty, and reference
rv, rv_error, rv_ref	km s^{-1}	87–89	Radial velocity, uncertainty, and reference
ruwe	…	90	Renormalised unite weight error from *Gaia* DR3
l, b	deg	91, 92	Galactic longitude and latitude in the epoch J2016.0
RA_J2000, DE_J2000	deg	93, 94	Right ascension and declination in the epoch J2016.0
NN_mag, eNN_mag	mag	95–116	Photometric magnitudes and quality flags in up to 10 passbands[m]
			Statistical indicators (Gaia DR3)
[Statistics DR3]	…	117–130	Statistical indicators in *Gaia* DR3[n]

a) `ID_star` is a unique identifier that sorts the table by right ascension but priorising that components of the same system (equal `ID_system`) are together and sorted by decreasing brightness.

b) Name of the star, obeying the following priority (n designates a natural number): Proper name, variable in constellation (V* Vn Con; but not suspected variables, SV*), Henry Draper (HD n, with $n \leq 225300$), Gliese-Jahreiss (GJ n, only if $n < 3000$), Bonner Durchmusterung (BD±n n), Luyten (LP n-n), Giclas (G n-n, only if unique Giclas designation), Luyten (LHS n), other designations in chronological order (Haro, StKM/StM, 1RXS/RXS, HIP, LSPM, PM, NLTT, GSC, TYC, MCC, R78b, I81, 2MUCD), catalog identifier (*Gaia* DR3, 2MASS, UCAC4).

c) "HHMMm+DDd" are the truncated equatorial coordinates. For stars in a close binary system, a position of the star in the system is added as "N", "S", "E" or "W".

d) Gliese-Jahreiss designation (GJ n) is given regardless of the denomination in the `Name` column, and regardless of the n number.

e) `SpTnum` = 10.0 for O0.0 V, 20.0 for B0.0 V, 30.0 for A0.0 V, 40.0 for F0.0 V, 50.0 for G0.0 V, 60.0 for K0.0 V, 70.0 for M0.0 V, 70.5 for M0.5 V, 80.0 for L0.0. Reference 'This work' refers to a photometric estimation of the spectral type based on the absolute magnitudes of Cifuentes et al. (2020).

f) Information extracted from the NASA Exoplanet Archive.

g) For the cases were it exists evidence of an unresolved component, we include an asterisk (∗) at the end of the type (i.e. 'Single*' and 'Multiple*') and the class (e.g. 'Single*' or 'Binary*').

h) SB1: Single-lined double; SB2: Double-lined double; ST2: Double-lined triple; ST3: Triple-lined triple; SQ: Triple- or quadruple-lined quadruple.

i) `id`: WDS identifier; `disc`: Discoverer code plus number, if assigned; `comp`: Component designations; `obs1`, `obs2`: First and last observation years; `pa2`: Positional angle in the more recent measurement; `sep2`: Separation in the more recent measurement; `mag1`, `mag2`: Magnitudes of the two components. More details can be found in the WDS website: `http://www.astro.gsu.edu/wds/`.

j) Measured eastward from the north in the epoch 2016.0.

k) Criteria for physical parity as described in Eqn. 4.5 (`crit_parity`) and in Table 4.2 (1–6: `crit_ruwe`, `crit_ipd`, `crit_rv`, `crit_rv_error`, `crit_non_single`, `crit_DR3_non_single`). Orbital: Orbital model for an astrometric binary; OrbitalTargetedSearch: Orbital model for a priori known systems, with a subset containing suffix 'Validated'; SB1: Single-lined spectroscopic binary; SB2: Double-lined spectroscopic binary; SB2C: Double-lined spectroscopic binary with circular orbit; AstroSpectroSB1: Combined astrometric + single lined spectroscopic orbital model.

l) It refers to unknown unresolved binaries. That is, if an unresolved companion already exists (e.g. an spectroscopic binary), the value is 'false'.

m) `BP`, `G`, `RP`: G_{B_P}, G, and G_{R_P} from *Gaia* DR3; `J`, `H`, `Ks`: J, H, and K_s from 2MASS; `W1`, `W2`, `W3`, `W4`: $W1$, $W2$, $W3$, and $W4$ from AllWISE. The photometric uncertainties in the *Gaia* passbands have been calculated by us $\Delta\lambda = |-2.5/\ln 10 \times \Delta F_\lambda / F_\lambda|$, where F_λ and ΔF_λ re the flux and its error in the λ passband, using the errors in the corresponding fluxes, and the zero points as provided by VizieR.

n) Statistics from DR3 related to the criteria for unresolved binarity: `astrometric_excess_noise`, `astrometric_excess_noise_sig`, `phot_bp_rp_excess_factor`, `phot_bp_n_blended_transits`, `phot_rp_n_blended_transits`, `phot_variable_flag`, `rv_chisq_pvalue`, `rv_amplitude_robust`, `rv_nb_transits`, `renormalised_gof`, `astrometric_n_obs_al`, `astrometric_n_good_obs_al`, `ipd_gof_harmonic_amplitude`, `duplicated_source` (see Sect. 4.3.2).

Table D.2: Complete sample with the description of multiple systems.

WDS id	WDS disc	Name	Karmn	Spectral type	α (2016.0)	δ (2016.0)	System	Component	ρ [arcsec]	θ [deg]	ϖ [mas]	$\mu_{\rm total}$ [mas a^{-1}]	$\mathcal{L}$ [$10^{-4}\,\mathcal{L}_\odot$]	$\mathcal{M}$ [$\mathcal{M}_\odot$]
00012+1357	LSC 2	BD+13 5195A	J00012+139N	M0.5 V	00:01:13.21	+13:58:32.7	(AB)+C	AB	0.247	170.0	27.34	150.86	…	…
00012+1357	WNO 12	BD+13 5195B	J00012+139S	M0.0 V	00:01:12.89	+13:58:22.0	…	C	11.657	203.8	27.71	152.02	1019.35 ± 5.62	0.692 ± 0.026
…	…	PM J00026+3821A	J00026+383	M4.0 V	00:02:40.00	+38:21:44.1	AB	A	…	…	24.62	74.86	…	0.357 ± 0.033
…	…	PM J00026+3821B	…	M3.5 V	00:02:40.05	+38:21:45.3	…	B*	1.415	28.1	25.39	71.14	…	0.330 ± 0.034
…	…	StKM 1-2199	J00033+046	M1.5 V	00:03:18.97	+04:41:11.6	…	…	…	…	34.88	88.03	394.76 ± 2.03	0.511 ± 0.029
…	…	HD 38A	…	K6 V	00:05:42.38	+45:48:40.9	Aab+B+C	Aab	…	…	26.59	903.28	…	…
00057+4549	STT 547	HD 38B	J00056+458	M0.0 V	00:05:42.30	+45:48:35.0	…	B	6.034	188.4	86.80	859.02	…	0.640 ± 0.027
00057+4549	STT 547	GJ 2	J00051+457	M1.0 V	00:05:12.22	+45:47:09.2	…	C	328.479	253.8	86.82	883.80	435.76 ± 2.26	0.492 ± 0.012
…	…	GJ 1002	J00067-075	M5.5 V	00:06:42.32	-07:32:47.3	…	…	…	…	86.93	2059.86	14.07 ± 0.07	0.107 ± 0.009
…	…	G 217-32A	J00077+603	M4.0 V	00:07:43.28	+60:22:54.0	AB	A	…	…	206.35	321.59	…	0.235 ± 0.037
00077+6022	JNN 247	G 217-32B	…	M5.0 V	00:07:43.40	+60:22:53.8	…	B	0.848	100.4	65.00	368.61	…	0.193 ± 0.039
…	…	PM J00078+6736	J00078+676	M2.0 V	00:07:50.65	+67:36:23.9	…	…	…	…	65.21	106.84	436.13 ± 4.29	0.492 ± 0.030
…	…	GJ 3007	J00079+080	M4.0 V	00:07:58.74	+08:00:12.8	…	…	…	…	39.65	544.03	193.29 ± 1.70	0.399 ± 0.016
…	…	1R000806.3+475659	J00081+479	M4.0 V	00:08:06.23	+47:57:02.4	Aab	Aab(2)	…	…	32.26	124.13	…	…
…	…	GJ 3008	J00084+174	M0.0 V	00:08:27.18	+17:25:26.4	…	…	…	…	36.80	113.87	598.00 ± 2.32	0.587 ± 0.028
00089+2050	BEU 1	GJ 3010	J00088+208	M5.0 V	00:08:53.86	+20:50:21.4	(AB)	AB	0.152	74.2	53.62	264.70	…	0.300 ± 0.035
…	…	G 31-29	J00110+052	M1.0 V	00:11:04.89	+05:12:33.4	…	…	…	…	45.99	265.51	874.37 ± 12.45	0.645 ± 0.027
…	…	LSPM J0011+5908	J00115+591	M6.0 V	00:11:29.94	+59:08:21.2	…	…	…	…	55.26	1477.10	11.29 ± 0.05	0.116 ± 0.009
…	…	LP 348-40	J00118+229	M3.5 V	00:11:53.17	+22:59:01.2	…	…	…	…	26.97	243.70	164.18 ± 1.10	0.390 ± 0.016
…	…	G 130-53	J00119+330	M3.5 V	00:11:55.73	+33:03:10.7	…	…	…	…	107.39	683.41	153.33 ± 0.89	0.376 ± 0.016
…	…	1R001213.6+302906	J00122+304	M4.5 V	00:12:13.49	+30:28:43.8	…	…	…	…	48.83	61.99	584.88 ± 34.92	0.489 ± 0.031
…	…	TYC 4298-613-1	J00131+703	M1.0 V	00:13:11.68	+70:23:54.9	…	…	…	…	47.75	145.71	849.73 ± 3.70	0.650 ± 0.027
00133+6919	KUI 1	GJ 11 A	J00132+693	M3.5 V	00:13:18.00	+69:19:32.4	AB	A	0.849	276.7	13.37	784.08	…	0.322 ± 0.034
…	…	GJ 11 B	…	M3.0 V	00:13:18.21	+69:19:32.3	…	B	1.100	98.7	31.53	774.33	…	…
…	…	UPM J0013+2733	J00133+275	M4.5 V	00:13:19.55	+27:33:29.1	…	…	…	…	48.73	116.63	152.59 ± 0.82	0.428 ± 0.018
…	…	GJ 3014	J00136+806	M1.5 V	00:13:40.36	+80:39:59.8	AB	A	…	…	…	311.44	461.06 ± 2.94	0.522 ± 0.029
00137+8038	LDS1503	GJ 3015	J00137+806	M5.0 V	00:13:44.59	+80:39:52.3	…	B	12.757	126.2	24.19	316.44	20.27 ± 0.15	0.164 ± 0.011
00155-1608	HEI299	GJ 1005	J00154-161	M4.0 V	00:15:28.77	-16:08:11.7	(AB)	AB	0.417	236.6	51.98	951.27	…	0.212 ± 0.039
…	…	LP 49-338	J00156+722	M2.0 V	00:15:37.59	+72:17:03.5	…	…	…	…	51.98	358.92	293.55 ± 1.59	0.468 ± 0.018
…	…	GJ 12	J00158+135	M4.0 V	00:15:49.92	+13:33:27.6	…	…	…	…	200.53	700.38	74.68 ± 0.32	0.255 ± 0.012
00160-1637	BWL 2	1R001557.5-163659	J00159-166	M4.1 V	00:15:57.94	-16:36:57.5	(AB)	AB	0.051	140.9	39.03	117.74	…	0.322 ± 0.034
…	…	EZPsc	J00162+198W	M4.0 V	00:16:15.44	+19:51:25.3	Aab+B	Aab(2)	…	…	30.35	1044.65	…	0.491 ± 0.003
00164+1950	LDS 863	GJ 1006 B	J00162+198E	M4.0 V	00:16:16.96	+19:51:38.5	…	B	25.141	58.5	82.19	1030.67	88.32 ± 0.59	0.274 ± 0.011
…	…	GJ 1007	J00169+051	M4.0 V	00:16:56.20	+05:07:16.4	…	…	…	…	56.10	630.38	78.38 ± 0.53	0.280 ± 0.013
…	…	GJ 3022	J00169+200	M3.5 V	00:16:57.03	+20:03:55.7	AB+C	A	…	…	65.11	239.54	…	0.319 ± 0.034
00169+2004	CRC 43	G 131-47B	…	M3.5 V	00:16:57.10	+20:03:55.4	…	B	1.077	106.5	65.05	233.36	…	0.313 ± 0.034
…	…	LP 404-54	…	M5.0 V	00:15:13.81	+19:47:40.5	…	C*	1751.981	236.2	56.16	233.80	33.49 ± 0.20	0.188 ± 0.011
…	…	Ross 680	J00173+291	M2.0 V	00:17:21.17	+29:11:05.7	…	…	…	…	29.31	812.80	458.04 ± 2.43	0.522 ± 0.029
…	…	GJ 3025	J00176-086	M0.0 V	00:17:41.23	-08:40:55.8	…	…	…	…	29.14	304.40	1011.74 ± 9.86	0.680 ± 0.026
…	…	LP 404-81	J00179+209	M1.0 V	00:17:58.87	+20:57:18.6	A+B	A	…	…	28.87	445.15	681.37 ± 2.55	0.612 ± 0.027

Table D.2: Complete sample with the description of multiple systems (continued).

WDS id	WDS disc	Name	Karmn	Spectral type	α (2016.0)	δ (2016.0)	System	Component	ρ [arcsec]	θ [deg]	ϖ [mas]	$\mu_{\rm total}$ [mas a^{-1}]	$\mathcal{L}$ [$10^{-4}\,\mathcal{L}_\odot$]	$\mathcal{M}$ [$\mathcal{M}_\odot$]
00180+2057	LDS 864	LP 404-80	…	M3.0 V	00:17:58.33	+20:57:13.0	…	B	9.426	233.7	43.77	443.59	432.11 ± 2.19	0.510 ± 0.019
…	…	GJ 16	J00182+102	M1.5 V	00:18:16.59	+10:12:09.6	…	…	…	…	31.20	29.63	411.22 ± 3.15	0.511 ± 0.029
…	…	HD 1326	J00183+440	M1.0 V	00:18:27.17	+44:01:29.2	A+B	A	…	…	36.10	2920.70	239.65 ± 2.18	0.395 ± 0.012
00184+4401	GRB 34	HD 1326B	J00184+440	M3.5 V	00:18:30.07	+44:01:43.5	…	B	34.349	65.5	36.06	2882.50	34.75 ± 0.14	0.164 ± 0.010
…	…	GJ 3027	J00188+278	M4.0 V	00:18:54.07	+27:48:48.1	…	…	…	…	59.63	410.00	75.64 ± 0.35	0.275 ± 0.013
…	…	GJ 1008	J00190-099	M0.0 V	00:19:05.52	-09:57:58.3	…	…	…	…	280.71	303.67	839.44 ± 3.66	0.672 ± 0.026
…	…	GJ 2003	J00201-170	M1+ Vk:	00:20:08.54	-17:03:41.2	…	…	…	…	280.69	142.53	334.46 ± 1.68	0.446 ± 0.017
…	…	GJ 3028	J00204+330	M5.5 V	00:20:30.78	+33:04:52.6	…	…	…	…	53.06	1379.44	14.53 ± 0.07	0.147 ± 0.010
…	…	[I81] M 134	J00207+596	M2.5 V	00:20:47.70	+59:36:15.6	…	…	…	…	49.48	117.69	329.12 ± 1.80	0.497 ± 0.019
…	…	StKM 1-25	J00209+176	M0.0 V	00:20:57.24	+17:38:14.7	…	…	…	…	43.79	91.16	687.19 ± 3.27	0.618 ± 0.027
…	…	G 217-43	J00210+557	M2.0 V	00:21:05.02	+55:43:55.6	…	…	…	…	81.57	443.46	691.48 ± 3.33	0.615 ± 0.027
…	…	G 171-51	J00218+382	M3.0 V	00:21:54.79	+38:16:24.2	…	…	…	…	35.12	700.25	232.41 ± 1.94	0.468 ± 0.019
…	…	GJ 3030	J00219+492	M2.5 V	00:21:58.20	+49:12:37.3	AB	A	…	…	33.45	211.68	…	0.430 ± 0.031
00220+4913	SKF1600	LP 149-56 B	…	M5.0 V	00:21:58.00	+49:12:38.4	…	B	2.276	301.0	22.71	211.19	…	0.197 ± 0.039
…	…	GJ 1011	J00234+243	M4.0 V	00:23:27.73	+24:18:26.5	…	…	…	…	40.34	254.16	47.37 ± 0.19	0.212 ± 0.011
…	…	GJ 1010 A	J00234+771	M2.5 V	00:23:24.80	+77:11:22.2	A+B	A	…	…	33.87	838.64	376.84 ± 1.92	0.503 ± 0.019
00243+7711	LDS1506	GJ 1010 B	J00235+771	M4.5 V	00:23:27.78	+77:11:27.5	…	B	11.253	61.7	33.75	838.76	55.38 ± 0.28	0.232 ± 0.012
…	…	LSPM J0024+2626	J00240+264	M4.0 V	00:24:03.96	+26:26:28.9	…	…	…	…	60.20	151.89	165.78 ± 3.31	0.418 ± 0.018
…	…	G 130-67	J00244+360	M1.0 V	00:24:26.30	+36:03:54.0	…	…	…	…	52.27	292.46	593.32 ± 3.03	0.580 ± 0.028
…	…	GJ 3033	J00245+300	M5.0 V	00:24:35.60	+30:02:29.7	…	…	…	…	52.29	585.98	62.23 ± 0.32	0.265 ± 0.013
…	…	GJ 3034	J00253+228	M4.71	00:25:20.33	+22:53:03.7	…	…	…	…	26.04	519.80	46.24 ± 0.20	0.209 ± 0.011
…	…	GJ 21	J00268+701	M1.0 V	00:26:52.27	+70:08:30.4	…	…	…	…	27.74	200.45	479.69 ± 2.44	0.542 ± 0.029
…	…	GJ 3035	J00271+496	M4.0 V	00:27:07.39	+49:41:49.3	…	…	…	…	51.32	430.86	88.43 ± 0.39	0.299 ± 0.014
00279+2220	FRV 1	LP 349-25	J00279+223	M8.0 Ve	00:27:56.46	+22:19:29.7	(AB)	AB	0.117	17.3	61.90	434.79	…	0.106 ± 0.047
…	…	GJ 1012	J00286-066	dM4.0	00:28:39.11	-06:40:02.0	…	…	…	…	61.87	865.14	152.11 ± 1.09	0.347 ± 0.012
00289+5023	DAE 1	GJ 3036	J00288+503	M3.7 V	00:28:54.66	+50:22:35.3	(AB)	AB	0.320	85.0	44.81	467.17	…	0.238 ± 0.037
…	…	GJ 1013	J00315-058	M3.7 V	00:31:35.79	-05:52:30.0	…	…	…	…	70.78	1112.30	88.57 ± 0.45	0.280 ± 0.013
…	…	G 217-56	J00322+544	M4.5 V	00:32:15.34	+54:28:55.3	…	…	…	…	74.71	487.74	96.07 ± 0.39	0.313 ± 0.014
00321+6715	MCY 1	V547Cas	J00324+672N	M2.0 V	00:32:34.33	+67:14:03.6	(AB)+C	AB	0.310	276.0	74.21	1782.54	…	0.421 ± 0.031
00321+6715	VYS 2	GJ 22 B	J00324+672S	M3.0 V	00:32:34.28	+67:13:59.8	…	C	3.790	184.0	71.02	1721.48	…	0.264 ± 0.036
…	…	GJ 3039	J00325+074	M4.0 V	00:32:34.91	+07:29:25.7	AB	A	…	…	49.95	121.86	…	0.506 ± 0.029
00326+0729	MCT 1	GJ 3039	…	M3.0 V	00:32:34.89	+07:29:26.4	…	B	0.720	333.6	101.09	123.57	…	0.378 ± 0.032
00329-0434	JNN 12	GR* 50	J00328-045	M4.5 V	00:32:53.21	-04:34:09.4	(AB)	AB	0.978	194.4	100.40	154.70	…	0.260 ± 0.036
…	…	G 132-4	J00333+368	M3.0 V	00:33:21.17	+36:50:28.6	…	…	…	…	28.43	513.00	249.90 ± 1.09	0.486 ± 0.019
…	…	V493AndA	J00341+253	M0.0 V	00:34:08.48	+25:23:48.5	AB+C	A	…	…	28.23	127.91	…	0.680 ± 0.026
00341+2524	SKF 220	V493AndB	…	K7 V	00:34:08.59	+25:23:48.2	…	B	1.536	102.3	52.85	129.46	…	0.679 ± 0.026
…	…	UCAC4 578-001365	…	M4.0 V	00:34:20.04	+25:28:12.9	…	C*	307.226	30.6	43.03	127.04	71.47 ± 1.95	0.266 ± 0.013
…	…	GJ 3040	J00346+711	M3.5 V	00:34:39.40	+71:11:36.6	…	…	…	…	20.10	626.48	86.52 ± 0.41	0.276 ± 0.013
00357+0233	LAW 7	LP 585-55	J00357+025	M5.0 V	00:35:43.30	+02:33:10.9	(AB)	AB	0.446	104.3	19.72	239.17	…	0.185 ± 0.040
00358+5241	RAO 682	G 172-11	J00358+526	M2.5 V	00:35:54.70	+52:41:09.3	A+(BC)	A	…	…	19.67	798.14	…	0.419 ± 0.031

Table D.2: Complete sample with the description of multiple systems (continued).

WDS id	WDS disc	Name	Karmn	Spectral type	α (2016.0)	δ (2016.0)	System	Component	ρ [arcsec]	θ [deg]	ϖ [mas]	$\mu_{\rm total}$ [mas a^{-1}]	$\mathcal{L}$ [$10^{-4}\,\mathcal{L}_\odot$]	$\mathcal{M}$ [$\mathcal{M}_\odot$]
00358+5241	GIC 11	G 217-59	…	M3.0 V	00:35:55.04	+52:41:33.7	…	BC	24.573	55.7	51.80	795.48	…	0.215 ± 0.038
…	…	GJ 1014	J00359+104	M5.0 V	00:35:56.70	+10:28:29.4	…	…	…	…	36.15	1151.32	21.52 ± 0.11	0.157 ± 0.010
…	…	GJ 3042	J00361+455	M2.0 V	00:36:08.05	+45:30:55.3	…	…	…	…	41.17	285.12	390.74 ± 175.97	0.439 ± 0.067
…	…	G 172-14	J00374+515	M0.5 V	00:37:25.07	+51:33:06.8	…	…	…	…	41.18	506.35	732.28 ± 3.39	0.618 ± 0.027
…	…	PM J00380+1656	J00380+169	M3.0 V	00:38:03.75	+16:56:01.3	…	…	…	…	69.47	142.34	117.75 ± 0.52	0.326 ± 0.014
…	…	GJ 3044	J00382+523	M0.0 V	00:38:15.16	+52:19:53.3	…	…	…	…	43.90	156.40	752.94 ± 2.82	0.639 ± 0.027
…	…	GJ 3045	J00385+514	M3.0 V	00:38:33.48	+51:27:58.4	…	…	…	…	30.73	231.31	134.33 ± 0.68	0.328 ± 0.014
…	…	Wolf 1056	J00389+306	M2.5 V	00:39:00.98	+30:36:58.8	…	…	…	…	47.59	1558.15	251.40 ± 1.11	0.418 ± 0.011
00395+1454	GIC 12	LP 465-061	J00395+149S	M4.0 V	00:39:33.91	+14:54:19.6	A+(BC)	A	…	…	43.44	333.74	…	0.310 ± 0.034
00395+1454	JNN 249	LP 465-62	J00395+149N	M4.5 V	00:39:34.16	+14:54:35.4	…	BC	16.188	12.5	55.83	328.89	…	0.308 ± 0.034
…	…	Wolf 10	J00395+605	M2.42 V	00:39:33.51	+60:33:10.9	…	…	…	…	78.90	332.44	421.38 ± 2.44	0.495 ± 0.029
…	…	2M00402129+6112490	J00403+612	M2.0 V	00:40:21.40	+61:12:48.2	…	…	…	…	34.82	73.93	374.04 ± 1.95	0.470 ± 0.012
…	…	GJ 3047	J00409+313	M3.3 V	00:40:56.19	+31:22:51.2	…	…	…	…	34.26	334.19	112.15 ± 0.64	0.340 ± 0.015
…	…	GJ 1015 A	J00413+558	M4.2 V	00:41:21.44	+55:50:03.2	A+B	A	…	…	27.12	332.50	…	0.280 ± 0.035
00415+5550	GIC 13	GJ 1015 B	…	DBQ5	00:41:22.64	+55:50:07.2	…	B	10.854	68.4	19.33	324.16	…	0.500 ± 0.100
…	…	PM J00427+4349	J00427+438	M2.5 V	00:42:47.79	+43:49:24.0	…	…	…	…	44.39	55.19	259.09 ± 1.16	0.466 ± 0.018
…	…	FFAnd	J00428+355	M1.0 V	00:42:48.59	+35:32:56.9	Aab	Aab(2)	…	…	46.82	273.37	…	…
…	…	GJ 1019	J00435+284	M4.0 V	00:43:35.44	+28:26:24.4	…	…	…	…	43.73	1071.52	43.22 ± 0.18	0.202 ± 0.011
…	…	GJ 3052	J00443+091	M4.5 V	00:44:21.54	+09:07:34.5	…	…	…	…	43.66	813.09	132.31 ± 1.10	0.371 ± 0.016
…	…	GJ 3051	J00443+126	M3.5 V	00:44:19.64	+12:36:59.8	…	…	…	…	47.61	337.85	158.32 ± 0.82	0.382 ± 0.016
…	…	GJ 3053	J00449-152	M4.5 V	00:44:59.68	-15:16:27.1	…	…	…	…	46.13	676.15	44.18 ± 0.23	0.219 ± 0.012
00459+3347	LAW 8	G 132-25	J00459+337	M4.5 V	00:45:57.01	+33:47:11.3	(AB)	AB	0.262	127.6	47.93	263.15	…	0.196 ± 0.039
…	…	PM J00463+3522	J00463+353	M1.5 Ve	00:46:21.76	+35:22:10.6	…	…	…	…	40.01	121.34	346.23 ± 1.67	0.463 ± 0.030
…	…	G 172-22	J00464+506	M4.0 V	00:46:30.66	+50:38:35.3	…	…	…	…	50.65	470.57	149.72 ± 0.70	0.396 ± 0.017
…	…	PM J00468+1603	J00468+160	M2.0 V	00:46:53.16	+16:03:01.8	…	…	…	…	66.83	128.89	277.92 ± 1.34	0.454 ± 0.018
…	…	LSPM J0048+7518	J00484+753	M3.0 V	00:48:30.66	+75:18:47.2	…	…	…	…	49.93	226.34	263.78 ± 1.21	0.470 ± 0.018
…	…	GJ 3057	J00487+270	M2.5 V	00:48:45.34	+27:01:04.4	…	…	…	…	34.50	328.24	228.43 ± 1.31	0.410 ± 0.016
…	…	GJ 3058	J00489+445	M3.0 V	00:48:58.46	+44:35:06.9	AB	A	…	…	30.95	182.00	…	0.391 ± 0.032
00490+4435	MCT 2	GJ 3058	…	M3.0 V	00:48:58.37	+44:35:06.6	…	B	1.006	256.7	49.71	181.78	…	0.367 ± 0.033
…	…	PM J00490+6544	J00490+657	M2.5 V	00:49:05.09	+65:44:36.8	…	…	…	…	30.72	132.46	312.69 ± 2.16	0.483 ± 0.018
…	…	RX J0050.2+0837	J00502+086	M4.5 V	00:50:17.59	+08:37:33.6	Aab	Aab(2)	…	…	49.80	75.62	…	…
00505+2450	LDS3203	FTPscA	J00505+248	M3.0 V	00:50:33.49	+24:48:59.7	AB	A	1.020	322.0	45.13	205.83	…	0.335 ± 0.034
…	…	FTPscB	…	…	00:50:33.45	+24:49:00.4	…	B	0.887	320.8	29.56	202.83	…	…
…	…	BPM 84579	J00511+225	M1.5 V	00:51:10.71	+22:34:43.8	…	…	…	…	29.76	120.57	548.80 ± 5.39	0.550 ± 0.028
…	…	Wolf 33	J00514+583	M0.0 V	00:51:33.02	+58:18:13.8	…	…	…	…	30.44	1618.53	455.66 ± 1.43	0.496 ± 0.018
…	…	HD 4967	…	K5 V	00:51:34.73	-22:54:40.7	A+B	A	…	…	16.31	672.69	…	0.722 ± 0.025
00516-2255	LDS1082	HD 4967B	J00515-229	M5.5 V	00:51:35.91	-22:54:35.4	…	B	17.073	72.1	66.73	680.57	13.34 ± 0.08	0.129 ± 0.010
…	…	G 69-27	J00520+205	M1.0 V	00:52:00.27	+20:34:56.6	…	…	…	…	…	211.39	659.59 ± 2.59	0.601 ± 0.027
…	…	LSPM J0053+1903	J00532+190	M2.5 V	00:53:12.84	+19:03:25.0	…	…	…	…	37.57	161.71	234.53 ± 1.34	0.442 ± 0.017
…	…	G 172-28	J00538+459	M0.0 V	00:53:53.72	+45:56:41.6	…	…	…	…	52.67	313.34	699.65 ± 3.60	0.622 ± 0.027

Table D.2: Complete sample with the description of multiple systems (continued).

WDS id	WDS disc	Name	Karmn	Spectral type	α (2016.0)	δ (2016.0)	System	Component	ρ [arcsec]	θ [deg]	ϖ [mas]	$\mu_{\rm total}$ [mas a^{-1}]	$\mathcal{L}$ [$10^{-4}\,\mathcal{L}_\odot$]	$\mathcal{M}$ [$\mathcal{M}_\odot$]
…	…	Ross 317	J00540+691	M2.0 V	00:54:00.72	+69:10:56.9	…	…	…	…	65.09	273.99	214.65 ± 4.47	0.396 ± 0.016
…	…	G 69-32	J00548+275	M4.5 V	00:54:48.49	+27:31:03.9	…	…	…	…	65.07	341.78	74.02 ± 0.34	0.291 ± 0.014
…	…	GJ 1024	J00566+174	M3.8 V	00:56:39.14	+17:27:30.3	…	…	…	…	31.82	743.02	91.08 ± 0.54	0.284 ± 0.013
…	…	G 172-30	J00570+450	M3.0 V	00:57:03.64	+45:05:08.7	…	…	…	…	44.66	629.52	149.81 ± 0.84	0.330 ± 0.011
…	…	BD+05 127	J00577+058	M0.0 V	00:57:44.49	+05:51:20.6	…	…	…	…	34.56	55.54	576.84 ± 3.35	0.592 ± 0.028
…	…	1R005802.4+391912	J00580+393	M4.5 V	00:58:01.01	+39:19:11.5	…	…	…	…	34.27	109.93	43.49 ± 0.24	0.217 ± 0.012
…	…	GJ 3068	J01008+669	M3.5 V	01:00:48.83	+66:56:53.8	…	…	…	…	36.46	242.48	135.21 ± 0.71	0.351 ± 0.015
…	…	GJ 1025	J01009-044	M4.0 V	01:00:57.71	-04:26:49.5	…	…	…	…	54.85	1323.95	50.94 ± 0.35	0.221 ± 0.012
…	…	Wolf 44	J01013+613	M2.0 V	01:01:20.86	+61:21:43.7	…	…	…	…	76.11	888.89	202.20 ± 0.84	0.370 ± 0.011
…	…	GJ 3069	J01019+541	M5.0 V	01:01:58.94	+54:10:55.8	…	…	…	…	56.15	325.64	19.52 ± 0.08	0.141 ± 0.008
…	…	GJ 3072	J01023-104	M0.0 V	01:02:21.16	-10:25:28.7	…	…	…	…	68.39	178.83	…	0.677 ± 0.026
…	…	Ross 318	J01025+716	M3.0 V	01:02:38.16	+71:40:41.2	…	…	…	…	44.32	1787.93	307.28 ± 1.99	0.472 ± 0.013
…	…	Wolf 46	J01026+623	M1.5 V	01:02:40.55	+62:20:43.6	A+B	A	…	…	80.79	736.67	487.34 ± 3.21	0.536 ± 0.029
01026+6221	WNO 51	V388Cas	J01033+623	M5.0 V	01:03:21.51	+62:21:57.2	…	B	294.459	75.5	94.97	735.44	46.11 ± 0.24	0.231 ± 0.012
…	…	GJ 1026 A	J01032+200	M2.0 V	01:03:14.92	+20:05:53.1	AB	A	…	…	90.01	674.09	…	0.413 ± 0.031
01032+2006	LDS 873	GJ 1026 B	…	M3.5 V	01:03:15.07	+20:05:54.5	…	B	2.482	56.6	47.38	676.83	…	0.304 ± 0.034
01032+3141	RAO 183	GJ 3073	J01032+316	M3.2 V	01:03:14.23	+31:40:59.7	(AB)	AB	0.202	147.7	121.46	209.40	…	0.405 ± 0.069
01032+7113	JNN 250	LP 29-70	J01032+712	M4.0 V	01:03:16.13	+71:13:11.8	(AB)	AB	0.147	34.2	101.42	510.53	…	0.333 ± 0.034
01037+4051	BWL 5	G 132-50	J01036+408	M0.0 Ve	01:03:40.31	+40:51:26.6	(AB)+C+D	AB	0.264	308.9	101.37	195.87	…	0.685 ± 0.026
01037+4051	LDS3225	G 132-51A	J01037+408	M2.6 V	01:03:42.24	+40:51:13.5	…	C	25.562	120.9	62.77	204.43	215.28 ± 1.82	0.450 ± 0.018
01037+4051	LDS3225	LP 194-20	…	M3.8 V	01:03:42.46	+40:51:13.1	…	D	27.859	118.9	62.77	208.49	…	0.294 ± 0.035
…	…	StKM 1-112	J01041+108	M1.0 V	01:04:11.07	+10:51:35.4	…	…	…	…	24.90	71.97	538.49 ± 3.95	0.565 ± 0.028
…	…	GJ 1028	J01048-181	dM5.0	01:04:55.25	-18:07:20.8	…	…	…	…	36.32	1381.30	22.21 ± 0.16	0.137 ± 0.009
…	…	GJ 1029	J01056+284	M5.5 V	01:05:39.97	+28:29:30.6	Aab	Aab(2)	…	…	…	1926.77	…	0.034 ± 0.002
…	…	GJ 1030	J01066+152	M2.0 V	01:06:41.39	+15:16:18.1	…	…	…	…	32.81	273.61	475.81 ± 3.06	0.525 ± 0.029
…	…	LSPM J0106+1913	J01066+192	M3.0 V	01:06:36.93	+19:13:29.6	…	…	…	…	32.53	226.73	160.77 ± 0.79	0.341 ± 0.011
…	…	LP 12-502	J01069+804	M4.5 V	01:06:56.00	+80:27:34.0	…	…	…	…	32.31	208.20	110.16 ± 0.61	0.360 ± 0.016
…	…	G 2-21	J01078+128	M1.5 V	01:07:52.53	+12:52:51.4	…	…	…	…	28.68	276.82	394.17 ± 1.71	0.502 ± 0.029
…	…	LP 707-16	J01102-118	M3.0 V	01:10:17.75	-11:51:19.3	…	…	…	…	102.28	248.87	180.86 ± 1.42	0.410 ± 0.017
01114+1526	BEU 2	GJ 3076	J01114+154	M5.93	01:11:25.63	+15:26:19.9	(AB)	AB	0.441	284.6	79.93	231.87	…	0.226 ± 0.043
…	…	LP 467-15	J01116+120	M2.0 V	01:11:36.66	+12:05:02.3	…	…	…	…	44.98	292.92	180.76 ± 0.78	0.362 ± 0.015
01119+0455	RAO 683	GJ 3077	J01119+049N	M3.5 V	01:11:56.01	+04:54:56.6	(AB)+C	AB	0.440	357.7	40.45	665.19	…	0.293 ± 0.035
01119+0455	GIC 20	GJ 3078	J01119+049S	M4.0 V	01:11:58.39	+04:54:04.0	…	C	63.506	146.0	46.93	648.10	46.79 ± 0.22	0.211 ± 0.011
…	…	YZCet	J01125-169	M4.0 Ve	01:12:31.98	-16:59:46.2	…	…	…	…	35.23	1363.33	22.88 ± 0.12	0.137 ± 0.009
…	…	Wolf 58	J01133+589	M1.5 Ve	01:13:20.12	+58:55:20.3	AB	A	…	…	54.35	210.93	…	0.539 ± 0.029
…	…	G3- 414108140954108672	…	M5.0 V	01:13:19.97	+58:55:18.6	…	B*	2.082	213.9	58.00	200.51	…	0.179 ± 0.040
…	…	GJ 1033	J01134-229	M4.0 V	01:13:24.20	-22:54:07.3	…	…	…	…	48.79	153.27	76.88 ± 0.41	0.277 ± 0.013
…	…	PM J01141+7904	J01141+790	M3.0 V	01:14:06.69	+79:04:01.9	…	…	…	…	64.67	89.71	333.30 ± 4.19	0.440 ± 0.031
…	…	LP 351-6	J01147+253	M1.5 V	01:14:49.86	+25:18:57.6	…	…	…	…	64.57	422.33	502.15 ± 2.64	0.535 ± 0.029
01158+4702	LAW 9	1R011549.5+470159	J01158+470	M4.5 V	01:15:50.51	+47:02:02.1	(AB)+(CD)	AB	0.267	267.4	269.06	186.53	…	…

Table D.2: Complete sample with the description of multiple systems (continued).

WDS id	WDS disc	Name	Karmn	Spectral type	α (2016.0)	δ (2016.0)	System	Component	ρ [arcsec]	θ [deg]	ϖ [mas]	$\mu_{\rm total}$ [mas a^{-1}]	$\mathcal{L}$ [$10^{-4}\,\mathcal{L}_\odot$]	$\mathcal{M}$ [$\mathcal{M}_\odot$]
01158+4702	FMR 42	LP 151-21	…	M5.0 V	01:15:49.20	+47:02:25.7	…	CD	27.195	330.4	36.03	198.56	…	0.190 ± 0.039
…	…	Wolf 59	J01161+601	M0.5 V	01:16:10.94	+60:09:09.6	…	…	…	…	35.97	428.48	515.71 ± 2.23	0.563 ± 0.028
…	…	GJ 3084	J01178+054	M0.5 V	01:17:53.34	+05:28:16.0	…	…	…	…	44.17	640.24	384.29 ± 2.26	0.479 ± 0.018
…	…	Ross 324	J01178+286	M0.5 V	01:17:50.21	+28:40:09.6	…	…	…	…	23.93	431.54	207.05 ± 0.91	0.366 ± 0.015
…	…	GJ 56.1	J01182-128	M2.0 V	01:18:16.20	-12:54:10.2	…	…	…	…	30.47	697.94	397.62 ± 2.32	0.500 ± 0.029
…	…	GJ 1035	J01198+841	M5.0 V	01:19:41.88	+84:09:40.4	…	…	…	…	…	1090.97	32.12 ± 0.16	0.183 ± 0.011
…	…	Ross 788	J01214+243	M0.0 V	01:21:29.78	+24:19:50.2	…	…	…	…	21.43	340.62	859.10 ± 3.73	0.661 ± 0.026
01222+2209	CRC 44	LP 351-34	J01221+221	M4.0 V	01:22:10.58	+22:09:00.6	(AB)	AB	0.248	359.9	39.08	287.16	…	0.207 ± 0.041
…	…	GJ 3093	J01227+005	M5.0 V	01:22:44.77	+00:31:55.7	AB	A	…	…	55.25	559.58	…	0.220 ± 0.038
01227+0032	LDS3270	GJ 3094	…	M5.0 V	01:22:44.83	+00:31:56.5	…	B	1.173	43.2	59.85	580.70	…	0.167 ± 0.041
…	…	Wolf 66 A	J01256+097	M4.0 V	01:25:36.89	+09:45:18.5	AB	A	…	…	42.10	455.85	…	0.270 ± 0.036
01256+0945	JOD 1	Wolf 66 B	…	…	01:25:36.86	+09:45:18.0	…	B	0.598	213.6	69.21	…	…	…
…	…	Wolf 1523	J01317+209	M2.0 V	01:32:44.80	+20:59:13.5	…	…	…	…	36.89	441.64	303.38 ± 1.72	0.448 ± 0.017
…	…	GJ 3098	J01324-219	M1.5 Vk:	01:32:25.53	-21:54:32.7	…	…	…	…	87.60	1065.06	369.99 ± 1.62	0.498 ± 0.018
…	…	LP 768-113	J01339-176	dM4.0	01:33:58.05	-17:38:26.8	…	…	…	…	65.52	190.97	89.10 ± 0.46	0.267 ± 0.011
…	…	1R013514.2-071254	J01352-072	M4.0 V	01:35:14.03	-07:12:52.2	…	…	…	…	55.78	108.44	…	…
…	…	EXCet	…	K0/1 V	01:37:35.65	-06:45:39.1	A+B	A	…	…	69.20	197.86	4565.07 ± 17.60	0.880 ± 0.132
01376-0645	CAB 3	LP 648-20	J01369-067	M3.5 V	01:36:55.36	-06:47:39.6	…	B	612.075	258.6	54.56	200.55	101.79 ± 0.61	0.322 ± 0.014
…	…	TYC 4031-2527-1	J01373+610	M1.5 V	01:37:21.44	+61:05:27.6	…	…	…	…	…	66.75	1011.45 ± 12.79	0.660 ± 0.026
…	…	Ross 10	J01383+572	M2.5 V	01:38:21.23	+57:13:51.4	…	…	…	…	38.68	398.10	130.70 ± 0.59	0.324 ± 0.014
…	…	GJ 3103	J01384+006	M2.5 V	01:38:30.49	+00:39:08.4	…	…	…	…	53.67	543.94	359.01 ± 1.63	0.486 ± 0.030
…	…	BLCet	J01390-179	M5.0 V	01:39:05.17	-17:56:53.9	AB	A	…	…	68.02	3428.81	…	0.129 ± 0.044
01388-1758	LDS 838	UCet	…	M6.0 V	01:39:05.20	-17:56:51.7	…	B	2.259	10.5	26.82	3231.91	…	0.118 ± 0.045
01395+0503	JOD 2	GJ 3104	J01395+050	M3.0 V	01:39:31.32	+05:03:20.3	(AB)	AB	0.271	209.0	41.56	187.30	…	0.491 ± 0.030
…	…	GJ 3105	J01402+317	M4.21	01:40:17.16	+31:47:30.4	…	…	…	…	41.70	465.64	135.34 ± 2.27	0.375 ± 0.016
01431+2101	JNN 251	RX J0143.1+2101	J01431+210	M4.0 V	01:43:11.75	+21:01:10.4	(AB)	AB	0.355	325.8	23.02	96.35	…	0.409 ± 0.031
…	…	GJ 3108	J01432+278	M1.0 V	01:43:16.64	+27:50:31.1	…	…	…	…	75.89	551.81	842.50 ± 4.11	0.648 ± 0.027
…	…	GJ 70	J01433+043	M2.0 V	01:43:19.73	+04:19:05.7	…	…	…	…	48.22	873.90	225.82 ± 1.22	0.396 ± 0.011
…	…	PM J01437-0602	J01437-060	M3.5 V	01:43:45.20	-06:02:40.6	(Aab)	Aab(2)	…	…	32.54	58.38	…	…
…	…	Wolf 1530	J01449+163	M4.0 V	01:44:57.63	+16:20:32.5	…	…	…	…	367.71	849.89	52.94 ± 0.24	0.226 ± 0.012
01466-0839	JOD 3	GJ 3113	J01466-086	M4.0 V	01:46:37.29	-08:39:00.5	(AB)	AB	0.182	5.3	373.84	451.35	…	0.387 ± 0.033
…	…	G 173-18	J01453+465	M2.0 V	01:45:18.81	+46:32:11.3	Aab	Aab(2)	…	…	47.42	444.34	…	…
…	…	Wolf 87	J01480+212	M2.5 V	01:48:04.37	+21:12:20.8	…	…	…	…	23.40	409.52	206.73 ± 1.43	0.413 ± 0.017
…	…	GJ 3119	J01510-061	M4.5 Ve	01:51:04.69	-06:07:09.3	…	…	…	…	41.55	607.06	25.29 ± 0.12	0.172 ± 0.011
…	…	Wolf 90	J01514+213	M4.0 V	01:51:24.17	+21:23:33.9	…	…	…	…	26.04	347.55	61.73 ± 0.33	0.246 ± 0.012
…	…	GJ 3117	J01518+644	M2.5 V	01:51:51.72	+64:26:02.8	AB	A	…	…	45.42	306.37	336.69 ± 162.31	0.467 ± 0.119
01519+6426	GIC 27	GJ 3118	…	DA5.6	01:51:51.69	+64:25:49.3	…	B	13.503	180.7	88.31	301.94	…	0.500 ± 0.100
…	…	Ross 555	J01518-108	M2.0 V	01:51:49.30	-10:48:21.1	…	…	…	…	46.70	783.75	200.70 ± 0.86	0.383 ± 0.015
…	…	BD-21 332	J01531-210	M2.0 Ve	01:53:11.67	-21:05:42.2	Aab	Aab(2)	…	…	47.49	281.99	…	…
…	…	PM J01538-1459A	J01538-149	M3.0 V	01:53:50.97	-14:59:51.5	AB	A	…	…	61.67	114.18	…	0.516 ± 0.029

Table D.2: Complete sample with the description of multiple systems (continued).

WDS id	WDS disc	Name	Karmn	Spectral type	α (2016.0)	δ (2016.0)	System	Component	ρ [arcsec]	θ [deg]	ϖ [mas]	$\mu_{\rm total}$ [mas a^{-1}]	$\mathcal{L}$ [$10^{-4}\,\mathcal{L}_\odot$]	$\mathcal{M}$ [$\mathcal{M}_\odot$]
01538-1500	BRG 7	PM J01538-1459B	…	M1.5 V	01:53:50.79	-14:59:50.5	…	B	2.854	291.4	39.10	115.33	…	0.512 ± 0.029
…	…	1RO15426.6+574136	J01544+576	M3.5 Ve	01:54:28.04	+57:41:27.7	A+B	A	…	…	39.42	199.20	255.20 ± 1.76	0.492 ± 0.019
01545+5741	NSN 1	LSPM J0154+5741N	…	M4.5 V	01:54:28.05	+57:41:36.4	…	B	8.669	0.4	53.73	207.78	44.47 ± 0.31	0.205 ± 0.011
…	…	LSPM J0155+3758	J01550+379	M5.0 V	01:55:02.64	+37:57:54.6	…	…	…	…	94.71	532.97	35.81 ± 0.17	0.195 ± 0.011
…	…	G 73-5	J01556+028	M1.5 V	01:55:36.98	+02:52:53.8	…	…	…	…	59.11	413.23	637.34 ± 10.28	0.587 ± 0.028
01568+3033	KO 4	LP 296-57	J01567+305	M4.5 V	01:56:45.99	+30:33:28.6	A+B	A	299.135	190.5	57.82	211.06	97.48 ± 0.90	0.337 ± 0.015
…	…	LP 296-56	…	M5.0 V	01:56:41.74	+30:28:34.6	…	B	299.134	190.6	57.80	208.62	32.82 ± 0.25	0.186 ± 0.011
…	…	GJ 1041 A	J01592+035E	M1.0 V	01:59:12.66	+03:31:09.6	A+Bab	A	…	…	58.24	264.35	…	0.555 ± 0.028
01592+0330	LDS3331	GJ 1041 B	J01592+035W	M3.0 V	01:59:12.89	+03:31:12.1	…	Bab(2)	4.176	54.2	60.77	269.39	…	…
…	…	V596Cas	J01593+585	M4.0 V	01:59:24.17	+58:31:13.0	…	…	…	…	31.21	374.04	171.26 ± 1.35	0.425 ± 0.018
…	…	GJ 3123	J02000+437	M3.0 V	02:00:03.00	+43:45:23.9	…	…	…	…	29.64	299.03	371.03 ± 2.34	0.474 ± 0.030
…	…	GJ 3124	J02001+366	M3.8 V	02:00:07.50	+36:39:43.8	…	…	…	…	29.56	266.52	112.27 ± 0.62	0.318 ± 0.014
…	…	TZAri	J02002+130	M3.5: V	02:00:14.16	+13:02:38.7	…	…	…	…	44.86	2083.39	26.40 ± 0.13	0.148 ± 0.009
…	…	GJ 3127	J02007-103	M3.5 V	02:00:46.86	-10:21:26.6	…	…	…	…	44.87	521.54	131.85 ± 0.76	0.370 ± 0.016
…	…	GJ 3126	J02015+637	M2.5 V	02:01:34.72	+63:46:10.5	…	…	…	…	49.33	275.12	260.90 ± 1.79	0.419 ± 0.012
…	…	GJ 3125	J02019+735	M4.5 Ve	02:01:55.13	+73:32:30.2	AB	A	…	…	26.74	…	…	…
02019+7332	JNN 252	G3- 558611490992292480	…	M5.5 V	02:01:55.18	+73:32:30.4	…	B	0.307	45.3	31.85	281.78	…	0.152 ± 0.042
…	…	Wolf 109	…	K5 V	02:02:02.81	+03:56:20.0	A+BC	A	…	…	26.64	466.14	1184.99 ± 6.10	0.700 ± 0.105
02021+0355	OSV 1	Wolf 109 B	J02020+039	M2.0 V	02:02:03.11	+03:56:37.4	…	B	17.961	14.4	41.87	465.77	299.82 ± 8.81	0.406 ± 0.032
…	…	G3- 2517912315149114240	…	…	02:02:03.16	+03:56:36.9	…	C	17.739	16.8	41.90	…	…	…
…	…	GJ 3128	J02022+103	M5.5 V	02:02:15.51	+10:20:09.4	…	…	…	…	76.29	729.74	11.76 ± 0.06	0.119 ± 0.009
…	…	PM J02024+1034B	J02026+105	M4.5 V	02:02:28.15	+10:34:51.9	A+B	A	…	…	28.13	109.34	…	0.266 ± 0.036
02025+1035	WSS 1	PM J02024+1034A	…	M5.5 V	02:02:28.18	+10:34:52.7	…	B	0.911	23.3	38.11	117.33	…	0.226 ± 0.038
…	…	GJ 3129	J02027+135	M5.0 V	02:02:44.86	+13:34:31.9	Aab	Aab(2)	…	…	24.61	473.30	…	…
…	…	RX J0202.8+0446	J02028+047	M3.5 Ve	02:02:52.00	+04:47:00.4	…	…	…	…	223.73	150.90	158.65 ± 1.39	0.383 ± 0.016
…	…	GJ 3131	J02033-212	M2.5 V	02:03:20.52	-21:13:50.2	AabB	Aab(2)	…	…	58.02	471.89	…	…
…	…	GJ 3131 B	…	…	02:03:20.25	-21:13:51.5	…	B*	4.008	251.9	34.35	450.04	…	0.1475 ± 0.058
…	…	GJ 3132	J02044-018	M4.5 V	02:04:26.87	-01:53:06.0	…	…	…	…	84.06	822.41	68.42 ± 0.33	0.260 ± 0.013
02051-1737	BEU 3	GJ 84	J02050-176	M2.5 V	02:05:06.31	-17:36:55.5	AabB	AabB(1)	0.244	100.7	66.76	1286.46	…	…
…	…	Wolf 116	J02055+056	M1.0 V	02:05:30.35	+05:41:43.0	…	…	…	…	…	301.59	661.35 ± 4.74	0.597 ± 0.027
…	…	V374And	J02069+451	M0.0 V	02:06:57.61	+45:10:56.9	Aab	Aab(2)	…	…	48.92	537.61	…	0.680
…	…	G 173-37	J02070+496	M3.5 Ve	02:07:04.24	+49:38:36.6	…	…	…	…	84.39	487.87	135.17 ± 0.59	0.318 ± 0.010
…	…	GJ 3134	J02071+642	M4.5 V	02:07:10.89	+64:17:08.7	…	…	…	…	27.83	278.20	57.47 ± 0.28	0.236 ± 0.012
…	…	G 242-81	J02082+802	M0.0 V	02:08:18.76	+80:13:11.1	…	…	…	…	28.92	556.27	711.03 ± 4.97	0.630 ± 0.027
…	…	GJ 3136	J02088+494	M4.0 Ve	02:08:54.01	+49:26:51.8	…	…	…	…	…	375.08	176.80 ± 0.74	0.415 ± 0.032
…	…	GJ 3139	J02096-143	M2.5 V	02:09:36.70	-14:21:38.2	…	…	…	…	108.26	623.31	330.39 ± 2.15	0.461 ± 0.030
…	…	G 35-32	J02116+185	M3.0 V	02:11:41.19	+18:33:42.3	…	…	…	…	69.64	334.94	204.62 ± 1.09	0.411 ± 0.017
…	…	Wolf 124	J02123+035	M1.5 V	02:12:19.10	+03:34:02.6	…	…	…	…	68.79	2557.19	322.05 ± 1.30	0.470 ± 0.012
02133+3649	JNN 18	1RO21320.6+364837	J02133+368	M4.5 V	02:13:20.68	+36:48:51.6	(AB)	AB	0.213	82.4	26.04	92.11	…	0.213 ± 0.038
…	…	GJ 3142	J02129+000	M4.0 V	02:12:55.22	+00:00:17.3	…	…	…	…	48.08	556.17	76.74 ± 0.40	0.277 ± 0.013

Table D.2: Complete sample with the description of multiple systems (continued).

WDS id	WDS disc	Name	Karmn	Spectral type	α (2016.0)	δ (2016.0)	System	Component	ρ [arcsec]	θ [deg]	ϖ [mas]	$\mu_{\rm total}$ [mas a^{-1}]	$\mathcal{L}$ [$10^{-4}\,\mathcal{L}_\odot$]	$\mathcal{M}$ [$\mathcal{M}_\odot$]
…	…	LP 649-72	J02142-039	M5.5 V	02:14:13.11	-03:57:46.1	…	…	…	…	46.67	532.92	12.80 ± 0.07	0.136 ± 0.010
…	…	GJ 1045	J02149+174	M4.0 V	02:15:00.20	+17:25:00.8	…	…	…	…	46.75	584.12	68.69 ± 0.31	0.261 ± 0.013
…	…	Wolf 127	J02153+074	M1.5 V	02:15:22.39	+07:29:32.5	…	…	…	…	54.45	577.56	360.68 ± 2.55	0.491 ± 0.018
…	…	GJ 3143	J02155+339	M4.2 V	02:15:34.63	+33:57:35.0	…	…	…	…	107.30	414.45	249.16 ± 1.31	0.396 ± 0.032
…	…	GJ 3145	J02158-126	M3.5 V	02:15:49.43	-12:40:24.2	…	…	…	…	25.80	543.01	257.57 ± 2.08	0.494 ± 0.020
…	…	GJ 3146	J02164+135	M5.0 Ve	02:16:30.40	+13:35:05.9	…	…	…	…	51.47	664.72	11.55 ± 0.06	0.128 ± 0.010
…	…	GJ 3147	J02171+354	M7.0 V	02:17:10.74	+35:26:28.4	…	…	…	…	69.83	607.26	13.54 ± 0.06	0.141 ± 0.010
…	…	G 35-39	J02185+207	M2.5 V	02:18:35.93	+20:47:44.8	…	…	…	…	52.27	292.61	179.77 ± 1.28	0.361 ± 0.015
…	…	RX J0218.6+1219	J02186+123	M2.5 V	02:18:36.75	+12:18:56.0	…	…	…	…	32.62	185.61	411.18 ± 2.31	0.498 ± 0.029
…	…	GJ 3150	J02190+238	M3.6 V	02:19:02.67	+23:52:53.7	…	…	…	…	58.51	307.13	86.91 ± 0.40	0.296 ± 0.014
…	…	Ross 19	J02190+353	M3.5 V	02:19:03.89	+35:21:11.8	…	…	…	…	50.51	795.17	151.70 ± 0.86	0.374 ± 0.016
02206+3748	LDS3370	GJ 3151	J02204+377	M2.5 V	02:20:25.74	+37:47:29.6	(AB)	AB	2.000	89.0	49.07	349.30	…	0.414 ± 0.031
…	…	GJ 3153	J02207+029	M6.0 V	02:20:46.42	+02:58:32.9	…	…	…	…	95.16	330.57	42.92 ± 0.21	0.216 ± 0.012
…	…	GJ 1047 A	J02210+368	M3.0 V	02:21:05.05	+36:52:55.2	AB+C	A	…	…	70.02	927.46	…	0.278 ± 0.035
02212+3653	WNO 7	GJ 1047 B	…	M4.5 V	02:21:05.01	+36:52:56.4	…	B	1.237	340.4	65.49	925.86	…	0.259 ± 0.036
02212+3653	GIC 31	GJ 1047 C	…	M3.5 V	02:21:02.88	+36:52:38.6	…	C	30.910	237.5	80.05	921.31	60.94 ± 0.26	0.228 ± 0.012
…	…	GJ 96	J02222+478	M0.5 V	02:22:14.99	+47:52:48.8	…	…	…	…	45.42	220.07	657.93 ± 3.86	0.601 ± 0.027
…	…	StKM 1-261	J02230+181	M0.5 V	02:23:06.15	+18:10:31.6	…	…	…	…	38.80	218.67	…	…
…	…	LP 353-51	J02234+227	M0.5 V	02:23:26.76	+22:44:05.0	…	…	…	…	32.11	149.70	650.86 ± 2.39	0.599 ± 0.027
…	…	GJ 3156	J02247+259	M0.5 V	02:24:46.00	+25:58:31.5	…	…	…	…	36.57	197.30	533.43 ± 2.34	0.558 ± 0.028
…	…	StKM 1-265	J02254+246	M2.0 V	02:25:28.00	+24:40:36.9	…	…	…	…	109.95	89.94	576.99 ± 3.71	0.557 ± 0.028
…	…	GJ 3157	J02256+375	M5e	02:25:38.83	+37:32:32.8	…	…	…	…	96.74	293.78	151.70 ± 0.79	0.399 ± 0.017
02273+5433	LAW10	1R022716.4+543258	J02272+545	M4.5 V	02:27:17.31	+54:32:46.1	(AB)	AB	0.677	185.8	49.95	151.50	…	0.210 ± 0.038
…	…	PM J02274+0310	J02274+031	M4.0 V	02:27:27.43	+03:10:54.7	…	…	…	…	33.43	122.39	80.21 ± 0.76	0.283 ± 0.013
02278+0426	A 2329	HD 15285	J02277+044	M1.0 V	02:27:46.05	+04:25:58.8	AB	AB	0.630	109.3	44.22	255.09	…	…
…	…	GJ 3159	J02282+014	M3.0 V	02:28:17.41	+01:26:29.0	…	…	…	…	57.33	310.15	147.38 ± 1.06	0.345 ± 0.015
…	…	TYC 1221-1171-1	J02283+219	M0.5 V	02:28:22.17	+21:59:45.3	…	…	…	…	40.87	56.52	1211.57 ± 45.27	0.699 ± 0.026
02290-1959	RST2280	HD 15468	…	K4.5 Vk	02:29:02.40	-19:58:40.8	(AB)+C	AB	0.182	145.3	53.35	646.40	…	0.699 ± 0.105
02290-1959	UC 744	GJ 100 C	J02285-200	M2.5 V	02:28:32.62	-20:02:22.5	…	C	474.569	242.1	43.84	649.19	126.10 ± 0.65	0.318 ± 0.014
…	…	LSPM J0228+1538	J02287+156	M2.0 V	02:28:47.15	+15:38:53.6	AB	A	…	…	43.82	171.10	…	0.520 ± 0.029
02288+1539	RAO 536	StKM 2-212B	…	…	02:28:47.18	+15:38:52.9	…	B	0.804	146.7	43.86	…	…	…
…	…	GJ 3160	J02289+120	M2.5 V	02:28:54.68	+12:05:22.3	Aab	Aab(2)	…	…	48.98	81.71	…	…
…	…	StKM 2-213A	J02289+226	M2.0 V	02:28:58.41	+22:36:24.5	A+B	A	…	…	83.66	156.39	…	0.721 ± 0.025
02290+2236	CFN 2	StKM 2-213B	…	M0.5 V	02:28:58.52	+22:36:21.9	…	B	3.012	149.6	…	140.86	…	0.609 ± 0.028
…	…	LP 410-33	J02292+195	M2.5 Ve	02:29:14.32	+19:32:31.9	…	…	…	…	36.90	270.77	612.28 ± 3.80	0.558 ± 0.028
…	…	GJ 3137	J02293+884	M3.5 V	02:29:14.09	+88:24:20.3	…	…	…	…	35.77	437.01	159.16 ± 0.65	0.360 ± 0.015
…	…	Ross 21	J02314+573	M3.5 V	02:31:29.87	+57:22:43.3	…	…	…	…	28.20	1115.77	119.49 ± 0.92	0.329 ± 0.014
…	…	LP 530-26	J02330+078	M2.0 V	02:33:04.78	+07:49:41.0	…	…	…	…	34.63	231.24	522.43 ± 5.62	0.541 ± 0.029
…	…	GJ 102	J02336+249	M3.5 Ve	02:33:37.23	+24:55:26.9	…	…	…	…	36.56	677.52	55.55 ± 0.23	0.215 ± 0.009
…	…	GJ 3165	J02337+150	M3.0 V	02:33:47.96	+15:00:17.8	…	…	…	…	42.04	438.16	91.68 ± 0.43	0.285 ± 0.013

Table D.2: Complete sample with the description of multiple systems (continued).

WDS id	WDS disc	Name	Karmn	Spectral type	α (2016.0)	δ (2016.0)	System	Component	ρ [arcsec]	θ [deg]	ϖ [mas]	$\mu_{\rm total}$ [mas a^{-1}]	$\mathcal{L}$ [$10^{-4}\,\mathcal{L}_\odot$]	$\mathcal{M}$ [$\mathcal{M}_\odot$]
…	…	GJ 3164	J02340+417	M3.0 V	02:34:00.46	+41:46:50.4	…	…	…	…	58.33	297.00	98.83 ± 0.42	0.297 ± 0.013
…	…	G 174-4	J02345+566	M2.0 V	02:34:34.87	+56:36:42.1	…	…	…	…	44.81	240.69	583.07 ± 5.10	0.554 ± 0.028
…	…	GJ 3166	J02353+235	M4.0 V	02:35:22.50	+23:34:29.5	…	…	…	…	23.62	111.79	202.38 ± 5.05	0.435 ± 0.018
…	…	GJ 104	J02358+202	M2.0 V	02:35:53.59	+20:13:09.3	…	…	…	…	51.61	286.55	397.25 ± 1.73	0.487 ± 0.012
02361+0653	GKI 1	HD 16160	…	K3 V	02:36:06.81	+06:53:36.0	(AB)+C	AB	1.730	289.5	50.97	2312.10	2771.37 ± 81.28	0.780 ± 0.117
02361+0653	PLQ 32	BXCet	J02362+068	M4.0 V	02:36:17.20	+06:52:41.1	…	C	164.247	318.4	28.44	2312.99	81.17 ± 0.42	0.261 ± 0.012
…	…	GJ 3168	J02364+554	M3.0 V	02:36:26.63	+55:28:30.2	…	…	…	…	…	358.33	228.52 ± 2.77	0.464 ± 0.019
…	…	G 36-26	J02367+226	M5.0 V	02:36:44.08	+22:40:20.2	…	…	…	…	38.66	376.42	25.09 ± 0.10	0.172 ± 0.011
…	…	GJ 3169	J02367+320	M3.5 V	02:36:47.30	+32:04:18.9	AB	A	…	…	17.21	336.16	…	0.285 ± 0.035
02369+3204	LDS3404	GJ 3170	…	M3.0 V	02:36:47.44	+32:04:20.0	…	B	2.064	58.2	16.81	338.06	…	0.257 ± 0.036
…	…	GJ 3174	J02392+074	M3.7 V	02:39:17.85	+07:28:14.9	…	…	…	…	25.11	499.67	60.61 ± 0.30	0.243 ± 0.012
…	…	G 75-35	J02412-045	M4.5 V	02:41:15.51	-04:32:18.8	…	…	…	…	46.01	357.49	44.25 ± 0.36	0.219 ± 0.012
…	…	StKM 1-291	J02419+435	M1.0 V	02:41:58.94	+43:34:19.0	…	…	…	…	50.01	49.84	737.12 ± 30.43	0.620 ± 0.028
…	…	LP 410-81	J02424+182	M1.5 V	02:42:25.80	+18:14:44.0	…	…	…	…	32.61	241.21	705.27 ± 5.64	0.607 ± 0.027
…	…	Wolf 1132	J02438-088	M1.5 V	02:43:53.88	-08:49:57.8	…	…	…	…	100.15	973.37	241.51 ± 1.45	0.398 ± 0.016
…	…	HD 16895	…	F8 V	02:44:12.53	+49:13:41.0	A+B	A	…	…	45.42	346.40	…	1.203 ± 0.180
02442+4914	STF 296	GJ 107 B	J02441+492	M1.5 V	02:44:10.79	+49:13:53.0	…	B	20.932	305.1	45.24	322.95	…	0.509 ± 0.029
…	…	VXAri	J02442+255	dM3	02:44:16.53	+25:31:18.3	…	…	…	…	27.86	937.72	170.73 ± 0.88	0.349 ± 0.011
02444+1057	JNN 300	MCC 401	J02443+109W	M1.0 V	02:44:21.45	+10:57:40.2	(AB)+C	AB	0.249	322.6	32.85	86.18	…	…
02444+1057	SKF 20	2M02442272+1057349	J02443+109E	M5.0 Ve	02:44:22.81	+10:57:34.2	…	C	20.917	106.7	71.22	93.99	217.08 ± 1.41	0.346 ± 0.033
02457+4456	LDS5393	GJ 3178	J02456+449	M0.5 V	02:45:40.30	+44:56:53.5	A+B	A	17.980	66.2	138.34	428.98	707.84 ± 2.71	0.613 ± 0.027
…	…	GJ 3179	…	M5.0 V	02:45:41.85	+44:57:00.8	…	B	17.984	66.2	138.44	440.90	20.99 ± 0.47	0.155 ± 0.010
…	…	GJ 3180	J02462-049	M6.0 V	02:46:16.73	-04:59:50.7	…	…	…	…	34.18	2529.50	14.45 ± 0.08	0.125 ± 0.009
…	…	GJ 3181	J02465+164	M6.0 V	02:46:33.79	+16:25:01.1	…	…	…	…	68.34	1007.59	9.43 ± 0.05	0.104 ± 0.009
…	…	2M02483695+6211228	J02486+621	M5.5 V	02:48:37.25	+62:11:21.3	…	…	…	…	51.38	153.80	18.05 ± 0.19	0.142 ± 0.010
…	…	PM J02489-1432W	J02489-145W	M2.0 V	02:48:59.45	-14:32:14.2	A+B	A	…	…	51.27	170.54	342.53 ± 2.92	0.463 ± 0.013
02490-1432	KPP2871	PM J02489-1432E	J02489-145E	M2.5 V	02:49:00.02	-14:32:15.5	…	B	8.354	99.0	50.05	180.26	273.58 ± 1.47	0.432 ± 0.013
…	…	G 246-12	J02502+628	M2.5 V	02:50:16.95	+62:51:16.4	…	…	…	…	81.20	303.05	207.62 ± 0.98	0.414 ± 0.017
…	…	GJ 3184	J02518+062	M3.0 V	02:51:51.15	+06:13:39.6	…	…	…	…	33.49	484.90	155.46 ± 1.01	0.355 ± 0.015
02518+2929	CRC 45	GJ 3183	J02518+294	M4.0 V	02:51:49.63	+29:29:10.4	(AB)	AB	0.890	243.6	25.40	168.63	…	0.251 ± 0.036
…	…	RBS 365	J02519+224	dM4.0	02:51:54.22	+22:27:28.2	…	…	…	…	46.89	155.52	268.93 ± 1.71	0.404 ± 0.032
…	…	GJ 3186	J02524+269	M2.0 V	02:52:25.03	+26:58:26.2	…	…	…	…	89.68	231.37	600.88 ± 2.55	0.576 ± 0.028
…	…	Teegarden's Star	J02530+168	M7.0 V	02:53:04.71	+16:51:51.7	…	…	…	…	89.37	5122.57	8.55 ± 0.05	0.104 ± 0.047
…	…	LP 411-18	J02534+174	M3.5 V	02:53:26.14	+17:24:28.4	…	…	…	…	130.20	252.85	180.66 ± 3.73	0.410 ± 0.017
…	…	HD 18143A	…	…	02:55:39.38	+26:52:20.5	A+B+C	A	…	…	20.78	327.70	…	1.079 ± 0.021
02556+2652	STF 326	HD 18143B	…	K7.5 V	02:55:39.14	+26:52:16.9	…	B	4.781	221.3	21.35	327.98	…	0.719 ± 0.025
02556+2652	LDS 883	HD 18143C	J02555+268	M4.0 V	02:55:36.11	+26:52:17.6	…	C	43.787	266.3	41.71	328.06	106.92 ± 0.47	0.331 ± 0.015
…	…	LP 591-156	J02560-006	M5.0 V	02:56:04.17	-00:36:32.0	…	…	…	…	45.45	266.17	22.52 ± 0.11	0.161 ± 0.010
02562+2359	JNN 253	LSPM J0256+2359	J02562+239	M5.0 V	02:56:14.06	+23:59:07.4	(AB)	AB	0.107	98.4	59.84	183.53	…	0.255 ± 0.036
…	…	Ross 364	J02565+554W	M1.0 V	02:56:35.79	+55:26:06.8	A+B	A	…	…	71.60	858.30	720.47 ± 3.03	0.615 ± 0.027

Table D.2: Complete sample with the description of multiple systems (continued).

WDS id	WDS disc	Name	Karmn	Spectral type	α (2016.0)	δ (2016.0)	System	Component	ρ [arcsec]	θ [deg]	ϖ [mas]	$\mu_{\rm total}$ [mas a^{-1}]	$\mathcal{L}$ [$10^{-4}\,\mathcal{L}_\odot$]	$\mathcal{M}$ [$\mathcal{M}_\odot$]
02565+5526	LDS5401	Ross 365	J02565+554E	M2.5 V	02:56:36.49	+55:26:22.3	…	B	16.600	21.0	24.10	844.15	…	0.483 ± 0.030
…	…	LP 14-53	J02573+765	M4.0 V	02:57:21.43	+76:33:04.9	…	…	…	…	26.57	798.30	72.79 ± 0.33	0.238 ± 0.012
…	…	Ross 791	J02575+107	M4.0 V	02:57:32.96	+10:47:17.9	…	…	…	…	26.54	1803.80	84.20 ± 0.48	0.272 ± 0.013
…	…	GJ 3189	J02581-128	sdM3.0	02:58:10.53	-12:52:57.4	…	…	…	…	36.96	605.17	51.63 ± 0.28	0.195 ± 0.011
…	…	Ross 331	J02591+366	M3.7 V	02:59:11.44	+36:36:35.7	AB	A	…	…	40.82	644.87	…	0.366 ± 0.033
02592+3637	CRC 46	Ross 331B	…	M6.0 V	02:59:11.45	+36:36:37.6	…	B	1.889	3.9	43.62	648.91	…	0.131 ± 0.043
…	…	GJ 3191	J02592+317	M3.3 V	02:59:16.77	+31:46:27.8	…	…	…	…	37.01	190.13	192.89 ± 1.02	0.424 ± 0.017
02598+3856	LAW 11	G 134-63	J02597+389	M4.5 V	02:59:46.67	+38:55:34.6	(AB)	AB	0.876	17.3	42.79	250.28	…	0.218 ± 0.038
…	…	GJ 3193	J03018-165S	M3.0 V	03:01:50.98	-16:35:40.3	A+B	A	…	…	260.99	456.80	…	0.285 ± 0.035
03019-1633	RST2292	GJ 3192	J03018-165N	M2.5 V	03:01:50.63	-16:35:35.2	…	B	7.211	315.0	50.49	450.46	…	0.261 ± 0.037
…	…	GJ 9108	J03026-181	M2.5 V	03:02:38.51	-18:09:56.1	…	…	…	…	44.43	435.93	292.37 ± 1.87	0.467 ± 0.018
…	…	StM 20	J03033-080	M3.0 V	03:03:21.47	-08:05:16.0	…	…	…	…	44.51	125.55	576.61 ± 44.39	0.533 ± 0.031
…	…	GJ 3197	J03037-128	M3.5 V	03:03:48.10	-12:51:21.0	A+B	A	…	…	44.52	259.64	152.70 ± 1.05	0.375 ± 0.016
03037-1251	LDS3450	GJ 3196	J03036-128	M3.5 V	03:03:40.99	-12:50:33.7	…	B	114.293	294.5	61.87	255.81	133.60 ± 0.94	0.349 ± 0.015
…	…	GJ 3198	J03040-203	M4.0 V	03:04:05.05	-20:22:50.7	…	…	…	…	40.08	688.31	147.75 ± 0.97	0.368 ± 0.016
…	…	HD 18757	…	G1.5 V	03:04:11.26	+61:42:09.9	A+B	A	…	…	49.32	1000.79	10444.81 ± 35.05	1.030 ± 0.155
03042+6142	LDS9142	GJ 3195	J03047+617	M3.0 V	03:04:45.06	+61:43:57.7	…	B	263.299	65.8	49.31	1000.09	229.77 ± 1.05	0.437 ± 0.017
03076-0358	HDS396	GJ 3202	J03075-039	M0.0 V	03:07:33.51	-03:58:23.2	(AB)	AB	0.082	162.4	54.90	470.78	…	…
…	…	LP 355-27	J03077+249	M4.5 V	03:07:47.13	+24:57:53.3	…	…	…	…	61.06	261.83	76.21 ± 0.36	0.295 ± 0.014
…	…	GJ 1055	J03090+100	M5.0 V	03:09:00.48	+10:01:16.3	…	…	…	…	86.96	652.48	22.79 ± 0.12	0.151 ± 0.010
03095+4544	HDS 404	GJ 125	J03095+457	M2.0 V	03:09:30.17	+45:43:52.7	(AB)	AB	0.510	20.2	43.16	581.18	…	0.622 ± 0.027
…	…	EKCet	J03102+059	M2.5 V	03:10:15.34	+05:54:22.5	…	…	…	…	43.25	576.45	228.27 ± 1.29	0.410 ± 0.016
…	…	GJ 3204	J03104+584	M2.0 V	03:10:26.72	+58:26:05.5	…	…	…	…	33.98	222.41	365.27 ± 1.81	0.494 ± 0.018
…	…	GJ 1053	J03109+737	M6.0 V	03:11:05.27	+73:46:02.5	…	…	…	…	32.94	2118.60	21.91 ± 0.13	0.147 ± 0.010
…	…	LP 652-62	J03110-046	M3.0 V	03:11:04.90	-04:36:41.1	…	…	…	…	145.69	304.49	230.58 ± 1.35	0.438 ± 0.017
…	…	1R031114.2+010655	J03112+011	M5.5 V	03:11:15.60	+01:06:30.6	…	…	…	…	139.70	115.06	19.17 ± 0.10	0.159 ± 0.010
…	…	Wolf 132	J03118+196	M0.5 V	03:11:48.26	+19:40:11.3	…	…	…	…	52.64	314.74	672.18 ± 5.42	0.585 ± 0.028
03119+6131	HDS 407	GJ 3206	J03119+615	M0.0 V	03:11:56.89	+61:31:14.6	(AB)	AB	0.522	185.7	23.95	86.96	…	…
…	…	CDCet	J03133+047	M4.5 V	03:13:24.78	+04:46:30.7	…	…	…	…	42.72	1744.02	29.75 ± 0.17	0.162 ± 0.009
…	…	LP 53-55	J03136+653	M1.5 V	03:13:37.88	+65:21:19.5	…	…	…	…	42.85	193.07	256.11 ± 1.40	0.410 ± 0.016
…	…	GJ 3208	J03142+286	M6.0 V	03:14:12.85	+28:40:27.6	…	…	…	…	58.62	812.01	11.51 ± 0.06	0.128 ± 0.010
…	…	Ross 369A	J03145+594	M2.5 V	03:14:33.17	+59:26:13.8	AB	A	…	…	42.46	250.95	…	0.444 ± 0.031
…	…	Ross 369B	…	M3.0 V	03:14:33.10	+59:26:13.2	…	B*	0.775	221.0	42.53	237.34	…	0.368 ± 0.033
…	…	RX J0314.7+1127	J03147+114	M2.0 V	03:14:47.26	+11:27:26.7	…	…	…	…	18.29	75.42	…	0.587 ± 0.028
…	…	Ross 346	J03147+485	M1.5 V	03:14:45.11	+48:31:05.5	…	…	…	…	38.82	367.80	500.54 ± 3.43	0.536 ± 0.029
…	…	Ross 370A	J03162+581S	M2.0 V	03:16:14.73	+58:09:57.3	A+B	A	…	…	79.45	550.45	304.01 ± 2.52	0.449 ± 0.017
03162+5810	MLB 115	Ross 370B	J03162+581N	M2.0 V	03:16:14.75	+58:10:02.4	…	B	5.041	2.0	58.12	523.34	264.69 ± 2.33	0.417 ± 0.016
…	…	PM J03167+3855	J03167+389	M3.5 V	03:16:46.02	+38:55:27.7	…	…	…	…	55.24	63.83	209.88 ± 6.93	0.444 ± 0.019
03172+4522	PRV 2	GJ 3213	J03172+453	M3.0 V	03:17:11.82	+45:22:20.9	(AB)	AB	0.042	206.6	44.43	270.09	…	0.391 ± 0.032
…	…	GJ 3215	J03177+252	M2.5 V	03:17:46.17	+25:15:00.6	…	…	…	…	82.66	865.99	297.53 ± 1.85	0.444 ± 0.017

Table D.2: Complete sample with the description of multiple systems (continued).

WDS id	WDS disc	Name	Karmn	Spectral type	α (2016.0)	δ (2016.0)	System	Component	ρ [arcsec]	θ [deg]	ϖ [mas]	$\mu_{\rm total}$ [mas a^{-1}]	$\mathcal{L}$ [$10^{-4}\,\mathcal{L}_\odot$]	$\mathcal{M}$ [$\mathcal{M}_\odot$]
…	…	HD 275122	J03181+382	M1.5 V	03:18:08.09	+38:14:58.3	…	…	…	…	33.81	725.86	623.67 ± 3.01	0.579 ± 0.028
…	…	Wolf 140	J03181+426	M3.5 V	03:18:07.31	+42:40:06.8	…	…	…	…	59.55	252.44	156.30 ± 0.82	0.380 ± 0.016
…	…	StKM 1-354	J03185+103	M1.5 V	03:18:35.36	+10:18:43.2	…	…	…	…	37.51	167.76	484.76 ± 2.26	0.540 ± 0.029
…	…	GJ 3216	J03186+326	M1.0 V	03:18:38.59	+32:39:55.3	…	…	…	…	27.48	231.71	549.17 ± 2.70	0.567 ± 0.028
…	…	Ross 371	J03187+606	M3.5 V	03:18:43.66	+60:36:21.1	…	…	…	…	116.27	597.29	348.03 ± 6.16	0.459 ± 0.030
03194+6156	JNN 254	G 246-33	J03194+619	M4.0 V	03:19:29.28	+61:56:01.5	(AB)	AB	0.386	239.8	44.35	292.21	…	0.278 ± 0.039
…	…	LP 198-637 A	J03207+397	M1.5 V	03:20:45.42	+39:42:59.3	AB	A	…	…	67.07	177.60	…	0.558 ± 0.028
03208+3943	RAO 187	LP 198-637 B	…	M1.5 V	03:20:45.35	+39:42:59.6	…	B	0.795	293.2	36.82	180.92	…	0.522 ± 0.029
…	…	GJ 133	J03213+799	M2.0 V	03:21:24.29	+79:58:06.8	…	…	…	…	36.50	501.04	244.96 ± 1.26	0.401 ± 0.011
…	…	GJ 3218	J03217-066	M2.0 V	03:21:47.27	-06:40:25.0	…	…	…	…	17.63	326.95	333.84 ± 2.06	0.455 ± 0.012
…	…	GJ 1058	J03220+029	M4.5 V	03:22:04.46	+02:56:22.7	…	…	…	…	39.91	823.48	27.82 ± 0.13	0.157 ± 0.010
…	…	GJ 3219	J03224+271	M0.0 V	03:22:28.40	+27:09:20.8	…	…	…	…	73.62	230.09	876.64 ± 4.42	0.665 ± 0.026
…	…	GJ 1059	J03230+420	M5.0 V	03:23:02.16	+42:00:15.8	…	…	…	…	73.58	741.20	20.55 ± 0.10	0.142 ± 0.010
…	…	GJ 3221	J03233+116	M3.5 Ve	03:23:22.15	+11:41:11.0	…	…	…	…	37.35	291.26	188.84 ± 0.91	0.394 ± 0.016
…	…	1R032338.7+054117	J03236+056	M4.5 V	03:23:39.25	+05:41:14.1	…	…	…	…	53.11	108.50	210.30 ± 1.42	0.507 ± 0.021
…	…	GJ 140 A	J03241+237	M1.5 V	03:24:06.73	+23:47:04.2	AB+C	A	…	…	46.06	246.23	…	0.583 ± 0.028
03242+2347	WOR 4	GJ 140 B	…	M3.0 V	03:24:06.67	+23:47:06.6	…	B	2.593	339.7	62.64	231.12	…	0.467 ± 0.030
03242+2347	LDS 884	GJ 140 C	J03242+237	M2.5 V	03:24:13.10	+23:46:17.3	…	C	99.222	118.2	41.57	233.16	316.38 ± 1.52	0.486 ± 0.018
…	…	PM J03247+4447A	J03247+447	M1.5 V	03:24:42.31	+44:47:41.4	AB	A	…	…	28.36	105.26	…	0.552 ± 0.028
03247+4448	KPP3523	PM J03247+4447B	…	M3.5 V	03:24:42.23	+44:47:39.7	…	B	1.912	206.5	38.98	89.93	…	0.340 ± 0.033
03257+0551	JNN 255	GJ 3224	J03257+058	M4.5 V	03:25:42.04	+05:51:48.2	(AB)	AB	0.225	162.3	26.07	246.27	…	0.204 ± 0.038
03263+1709	JNN 256	PM J03263+1709	J03263+171	M4.0 V	03:26:23.74	+17:09:30.1	(AB)	AB	0.945	222.9	35.80	108.79	…	0.319 ± 0.034
…	…	GJ 3225	J03267+192	M4.5 V	03:26:44.97	+19:14:37.7	…	…	…	…	31.70	160.56	38.96 ± 0.19	0.204 ± 0.011
…	…	CKAri	J03272+273	M1.0 Ve	03:27:14.22	+27:23:07.8	…	…	…	…	31.54	116.46	543.83 ± 3.68	0.567 ± 0.028
…	…	ATO J051.8788+22.2102	J03275+222	M4.5 V	03:27:30.94	+22:12:36.9	…	…	…	…	71.66	104.42	191.98 ± 1.10	0.452 ± 0.018
…	…	LSPM J0328+3515A	J03284+352	M2.0 V	03:28:29.35	+35:15:18.6	AB	A	…	…	57.99	156.47	…	0.524 ± 0.029
03284+3515	KPP4352	LSPM J0328+3515B	…	M1.5 V	03:28:29.32	+35:15:17.4	…	B	1.225	200.3	61.36	144.49	…	0.520 ± 0.029
…	…	GJ 3228	J03286-156	M3.5 Ve	03:28:39.18	-15:37:16.4	A+B	A	…	…	31.47	189.19	85.08 ± 3.44	0.293 ± 0.015
03286-1537	LDS3498	GJ 3229	…	M3.5 V	03:28:39.36	-15:37:32.6	…	B	16.424	170.6	67.88	204.04	70.48 ± 0.31	0.264 ± 0.013
…	…	1R033021.4+344044	J03303+346	M4.0 V	03:30:23.37	+34:40:31.7	A+BC	A	…	…	58.47	56.66	…	…
…	…	G3- 221088045766546816	…	M1/2 V	03:30:16.90	+34:39:50.2	…	B*	89.956	242.5	26.64	53.59	…	0.411 ± 0.031
…	…	G3- 221088050062935680	…	M3.0 V	03:30:16.80	+34:39:49.2	…	C*	91.483	242.3	48.27	52.34	…	0.359 ± 0.033
…	…	GJ 3227	J03288+264	M4.0 V	03:28:49.84	+26:29:10.2	…	…	…	…	48.26	262.15	65.65 ± 0.37	0.254 ± 0.012
…	…	LSPM J0330+5413	J03308+542	M5.0 V	03:30:48.61	+54:13:55.1	…	…	…	…	48.34	152.03	11.58 ± 0.05	0.118 ± 0.009
03309+7041	JNN 257	LP 31-368	J03309+706	M3.5 V	03:30:56.01	+70:41:06.4	(AB)	AB	0.354	315.2	30.28	607.40	…	0.296 ± 0.035
…	…	GJ 143.3	J03317+143	M2.5 V	03:31:47.18	+14:19:07.0	…	…	…	…	30.42	675.27	204.13 ± 1.16	0.386 ± 0.016
03326+2844	JNN 24	RX J0332.6+2843	J03325+287	M4.5 V	03:32:35.85	+28:43:54.1	(ABC)	ABC	0.098	282.4	39.77	100.09	…	…
…	…	V577Per	…	K2 V	03:33:13.60	+46:15:23.7	A+B	A	…	…	27.45	188.42	1014.02 ± 28.06	0.820 ± 0.012
03332+4615	ES 560	HD 21845B	J03332+462	M0.0 V	03:33:14.16	+46:15:16.2	…	B	9.502	142.3	55.31	185.83	…	0.688 ± 0.026
…	…	Ross 563	J03340+585	M0.5 V	03:34:01.11	+58:35:52.3	…	…	…	…	32.96	348.57	1173.61 ± 7.05	0.686 ± 0.026

Table D.2: Complete sample with the description of multiple systems (continued).

WDS id	WDS disc	Name	Karmn	Spectral type	α (2016.0)	δ (2016.0)	System	Component	ρ [arcsec]	θ [deg]	ϖ [mas]	$\mu_{\rm total}$ [mas a^{-1}]	$\mathcal{L}$ [$10^{-4}\,\mathcal{L}_\odot$]	$\mathcal{M}$ [$\mathcal{M}_\odot$]
…	…	GJ 3235	J03346-048	M3.8 V	03:34:40.07	-04:50:38.5	Aabc	Aabc(3)	…	…	59.55	520.01	…	…
…	…	1R033609.2+311853	J03361+313	M4.5 V	03:36:08.85	+31:18:37.4	…	…	…	…	25.90	175.56	52.98 ± 0.26	0.242 ± 0.012
…	…	GJ 3237	J03366+034	M5.0 V	03:36:40.97	+03:29:17.6	…	…	…	…	21.22	171.39	186.43 ± 1.30	0.476 ± 0.020
…	…	GJ 3236	J03372+691	M3.8 V	03:37:14.55	+69:10:47.9	Aab	Aab(EB)	…	…	27.51	196.46	…	0.657 ± 0.023
…	…	GJ 3239	J03375+178N	M2.5 V	03:37:33.54	+17:51:14.1	Aab+Bab	Aab(2)	…	…	42.04	172.97	…	…
03376+1751	LDS3512	GJ 3240	J03375+178S	M3.5 V	03:37:34.09	+17:51:00.0	…	Bab(EB?)	16.150	150.6	112.39	172.61	…	…
…	…	KPTau	J03394+249	M3.5 Ve	03:39:29.85	+24:58:05.7	…	…	…	…	21.15	228.67	110.09 ± 0.73	0.315 ± 0.014
…	…	Wolf 204	J03396+254E	M3.0 V	03:39:36.47	+25:28:11.6	A+B	A	…	…	43.80	626.22	290.22 ± 2.81	0.494 ± 0.019
03396+2530	LDS9158	Wolf 205	J03396+254W	M3.5 V	03:39:40.77	+25:28:39.1	…	B	64.329	64.7	41.87	622.15	231.86 ± 1.81	0.439 ± 0.017
…	…	HD 278874	…	K2 V	03:39:48.92	+33:28:24.3	Aab+B	Aab(2)	…	…	29.00	36.21	…	…
03398+3328	ES 327	HD 278874B	J03397+334	M3.0 V	03:39:47.79	+33:28:30.7	…	B	15.472	294.3	…	38.83	568.68 ± 3.97	0.521 ± 0.029
…	…	TYC 3720-426-1	J03416+552	M0.0 Ve	03:41:37.46	+55:13:05.0	…	…	…	…	11.38	151.56	976.90 ± 4.67	0.673 ± 0.026
…	…	LSPM J0343+4554A	J03430+459	M4.0 V	03:43:01.79	+45:54:17.4	AB	A	…	…	11.73	199.94	…	0.235 ± 0.037
03430+4554	JNN 259	LSPM J0343+4554B	…	M4.5 V	03:43:01.72	+45:54:17.9	…	B	0.886	305.6	65.13	213.60	…	0.231 ± 0.037
…	…	GJ 3247	J03433-095	M4.5 V	03:43:22.53	-09:33:46.1	…	…	…	…	95.22	519.04	63.40 ± 0.91	0.267 ± 0.013
…	…	GJ 150.1 A	J03438+166	M0.0 V	03:43:52.74	+16:40:14.2	A+B	A	…	…	43.83	353.41	754.91 ± 2.48	0.633 ± 0.027
03439+1640	GIC 44	GJ 150.1 B	J03437+166	M1.0 V	03:43:45.42	+16:39:57.2	…	B	106.541	260.8	49.53	347.26	453.19 ± 1.98	0.530 ± 0.029
…	…	HD 278968	J03445+349	M0.0 V	03:44:31.21	+34:58:20.8	…	…	…	…	…	254.27	784.51 ± 2.74	0.649 ± 0.027
…	…	G 221-21	J03454+729	M1.5 V	03:45:28.68	+72:59:25.2	(AB)+C	A	…	…	27.48	487.29	…	0.549 ± 0.028
03454+7259	LDS1581	LP 31-210	…	…	…	…	…	B	8.100	179.8	27.48	…	…	…
03454+7259	WIS 99	LP 31-200	…	M3.5 Ve	03:43:44.04	+72:53:42.2	…	C	574.149	233.5	25.61	488.28	51.72 ± 0.25	0.223 ± 0.012
…	…	PM J03455+7018	J03455+703	M1.0 V	03:45:32.34	+70:18:00.4	…	…	…	…	37.82	137.73	395.25 ± 2.11	0.512 ± 0.029
…	…	G 6-33	J03459+147	M1.5 V	03:45:54.96	+14:42:47.2	…	…	…	…	73.21	283.12	662.74 ± 3.05	0.597 ± 0.027
…	…	HD 23453	J03463+262	M1.0 V	03:46:20.60	+26:12:52.7	…	…	…	…	37.35	433.72	739.35 ± 3.48	0.626 ± 0.027
…	…	TYC 4521-1342-1	J03467+821	M1.0 V	03:46:42.67	+82:07:50.1	…	…	…	…	27.05	109.54	742.46 ± 4.37	0.623 ± 0.027
…	…	GJ 3249	J03467-112	M2.5 V	03:46:46.04	-11:17:40.5	…	…	…	…	25.83	582.16	185.89 ± 3.10	0.391 ± 0.016
…	…	GJ 3250	J03473+086	M5.0 V	03:47:21.40	+08:41:36.7	…	…	…	…	25.78	803.41	24.90 ± 0.19	0.159 ± 0.010
…	…	G 80-21	J03473-019	M3.0 V	03:47:23.53	-01:58:24.3	…	…	…	…	62.65	328.20	317.72 ± 2.22	0.502 ± 0.039
…	…	Ross 588	J03479+027	M0.5 V	03:47:57.68	+02:47:09.3	…	…	…	…	38.83	579.87	342.39 ± 2.13	0.451 ± 0.017
03480+6840	KUI 13	HD 23189	…	K2 V	03:48:01.40	+68:40:26.4	A+(BC)	A	…	…	38.91	279.83	1046.22 ± 5.04	0.820 ± 0.123
03480+6840	KUI 13	GJ 153 C	J03480+686	M2 V	03:48:02.08	+68:40:42.9	…	BC	17.206	13.2	25.43	288.83	…	0.467 ± 0.030
…	…	GJ 3248	J03486+735	M1.0 V	03:48:39.73	+73:32:30.9	…	…	…	…	25.57	482.03	256.76 ± 1.16	0.411 ± 0.016
…	…	GJ 3251	J03505+634	M1.5 V	03:50:33.69	+63:27:14.9	…	…	…	…	27.92	230.99	1332.76 ± 6.09	0.708 ± 0.026
…	…	GJ 1065	J03507-060	M3.0 V	03:50:43.81	-06:06:03.6	…	…	…	…	41.91	1441.79	51.45 ± 0.39	0.222 ± 0.012
…	…	PM J03510+1413	J03510+142	M4.5 V	03:51:00.87	+14:13:38.7	A+B	A	…	…	41.95	102.59	374.12 ± 2.75	0.434 ± 0.031
03510+1414	JLM 1	UPM J0350+1414	…	M3.5 V	03:50:59.58	+14:14:00.5	…	B	28.818	319.2	49.65	94.89	159.59 ± 1.63	0.469 ± 0.020
…	…	GJ 3252	J03510-008	M8.0 V	03:51:00.04	-00:52:52.4	…	…	…	…	58.04	470.09	8.22 ± 0.05	0.125 ± 0.010
…	…	HD 275867	…	K2 V	03:52:00.35	+39:47:43.7	A+B	A	…	…	58.03	62.07	2050.28 ± 9.78	0.820 ± 0.123
03520+3947	GRV 197	TYC 2868-639-1	J03519+397	M0.0 V	03:51:58.19	+39:46:55.8	…	B	53.919	207.5	38.92	64.40	859.01 ± 5.45	0.662 ± 0.026
…	…	Wolf 227	J03526+170	M5.0 V	03:52:42.24	+17:00:53.8	(Aab)	Aab(2)	…	…	26.76	777.27	…	…

Table D.2: Complete sample with the description of multiple systems (continued).

WDS id	WDS disc	Name	Karmn	Spectral type	α (2016.0)	δ (2016.0)	System	Component	ρ [arcsec]	θ [deg]	ϖ [mas]	$\mu_{\rm total}$ [mas a^{-1}]	$\mathcal{L}$ [$10^{-4}\,\mathcal{L}_\odot$]	$\mathcal{M}$ [$\mathcal{M}_\odot$]
…	…	Ross 567	J03531+625	M3.0 V	03:53:10.51	+62:34:03.8	…	…	…	…	39.09	270.93	167.54 ± 0.76	0.347 ± 0.011
…	…	2M03542008-1437388	J03543-146	M6.5 V	03:54:20.02	-14:37:37.2	…	…	…	…	…	111.80	10.98 ± 0.31	0.136 ± 0.010
…	…	GJ 3256	J03544-091	M1.0 V	03:54:25.52	-09:09:29.2	AB	A	…	…	39.15	146.38	…	0.506 ± 0.029
…	…	GJ 3256 B	…	M3.0 V	03:54:25.61	-09:09:32.0	…	B*	3.182	153.6	33.28	138.31	…	0.344 ± 0.033
…	…	LP 413-108	J03548+163	M4.0 V	03:54:53.37	+16:18:55.9	…	…	…	…	27.71	133.30	276.38 ± 2.68	0.405 ± 0.032
…	…	1R035632.5+315746	J03565+319	M3.5 V	03:56:33.26	+31:57:23.8	…	…	…	…	69.51	139.28	376.01 ± 2.18	0.455 ± 0.030
…	…	Ross 23	J03567+039	M1.5 V	03:56:47.95	+53:33:30.5	…	…	…	…	24.18	501.26	642.36 ± 2.93	0.585 ± 0.028
…	…	HD 24916	…	K4 V	03:57:28.50	-01:09:36.4	A+Bab	A	…	…	44.67	234.33	…	0.721 ± 0.108
03575-0110	BU 543	HD 24916B	J03574-011	M2.5 V	03:57:28.68	-01:09:25.7	…	Bab	10.968	14.1	46.64	251.75	…	…
…	…	Ross 24	J03586+520	M1.0 V	03:58:36.92	+52:01:21.7	…	…	…	…	80.06	429.52	352.25 ± 2.53	0.485 ± 0.018
…	…	G 7-14	J03588+125	M4.0 V	03:58:49.38	+12:30:18.3	…	…	…	…	59.43	403.12	119.85 ± 0.67	0.352 ± 0.015
…	…	Wolf 1322	J03598+260	M3.0 V	03:59:54.53	+26:05:19.5	…	…	…	…	56.99	774.40	251.17 ± 4.91	0.488 ± 0.020
…	…	Ross 25	J04011+513	M3.8 V	04:01:08.18	+51:23:06.4	A+B	A	…	…	55.83	883.46	125.09 ± 0.63	0.337 ± 0.015
…	…	LSPM J0401+5131	…	DC8	04:01:02.14	+51:31:17.2	…	B*	494.032	353.4	55.98	883.24	…	0.500 ± 0.100
…	…	GJ 3261	J04056+057	M4e	04:05:38.94	+05:44:40.4	AB+C	A	…	…	62.67	47.98	…	0.630 ± 0.027
04056+0545	MCT 3	G3- 3296932486866670720	…	…	04:05:38.89	+05:44:40.1	…	B	0.817	251.9	25.34	…	…	…
…	…	ATO J061.4727+05.5235	…	M3.0 V	04:05:53.46	+05:31:24.6	…	C*	824.788	164.8	100.73	49.85	227.47 ± 1.68	0.494 ± 0.020
…	…	LP 31-301	J04059+712E	M4.0 V	04:05:58.09	+71:16:34.7	A+BC	A	…	…	24.98	415.87	69.28 ± 0.38	0.262 ± 0.013
04058+7117	LDS1589	LP 31-302 A	J04059+712W	M5.0 V	04:05:57.21	+71:16:32.4	…	B	4.828	240.7	24.87	408.76	…	0.148 ± 0.042
04058+7117	LEP 123	LP 31-302 B	…	M6.0 V	04:05:57.02	+71:16:31.9	…	C	5.832	241.4	68.12	413.74	…	0.130 ± 0.044
…	…	PM J04061-0534	J04061-055	M3.5 V	04:06:06.90	-05:34:46.9	…	…	…	…	30.98	147.05	63.82 ± 0.27	0.250 ± 0.012
…	…	LP 474-123	J04077+142	M0.0 V	04:07:44.14	+14:13:22.1	A+B	A	…	…	31.02	233.82	1038.15 ± 5.12	0.694 ± 0.026
04077+1413	LDS5187	LP 474-124	J04079+142	M2.5 V	04:07:54.99	+14:12:58.2	…	B	159.493	98.6	103.50	234.83	292.69 ± 1.49	0.496 ± 0.019
…	…	LP 32-16	J04081+743	M3.5 V	04:08:13.87	+74:22:51.6	…	…	…	…	81.20	899.05	73.58 ± 0.32	0.253 ± 0.012
…	…	LP 31-433	J04083+691	M4.5 V	04:08:24.60	+69:10:57.9	…	…	…	…	56.21	279.79	58.43 ± 0.85	0.256 ± 0.013
…	…	HD 281621	J04086+336	M0.5 V	04:08:38.07	+33:38:15.3	(AB)	AB	…	…	47.41	541.74	…	0.543 ± 0.029
04094+0546	LAW 12	LP 534-29	J04093+057	M4.5 V	04:09:22.50	+05:46:25.2	(AB)	AB	0.247	130.0	47.54	254.91	…	0.153 ± 0.042
…	…	LP 714-37	J04108-128	M5.5 V	04:10:47.88	-12:51:48.4	AB	A	…	…	22.74	421.99	…	0.136 ± 0.043
04108-1252	PHB 1	LP 714-37 B	…	M6.5 V	04:10:47.98	-12:51:49.4	…	B	1.722	123.7	20.83	418.94	…	0.104 ± 0.047
…	…	Ross 27	J04112+495	M3.5 V	04:11:13.29	+49:31:45.0	…	…	…	…	44.40	480.41	108.19 ± 0.51	0.312 ± 0.014
…	…	GJ 3266	J04122+647	M4.0 V	04:12:18.25	+64:43:48.7	…	…	…	…	65.43	657.85	43.32 ± 0.19	0.202 ± 0.011
…	…	LP 414-117	J04123+162	M4.0 V	04:12:21.90	+16:15:02.9	Aab+B	Aab(2)	…	…	52.78	156.84	…	0.652 ± 0.052
…	…	LSPM J0409+1622	…	M5.5 V	04:09:57.30	+16:22:41.3	…	B*	2131.567	282.5	65.49	161.15	…	0.151 ± 0.042
04130+5237	PRV1	Ross 28	J04129+526	M4.0 V	04:12:58.22	+52:36:28.9	(AB)	AB	0.057	294.1	35.49	893.94	…	0.247 ± 0.037
…	…	Ross 29A	J04131+505	M4.0 V	04:13:09.43	+50:31:38.0	AB	A	…	…	37.57	440.74	…	0.256 ± 0.036
04132+5032	CHR 15	Ross 29B	…	M4.5 V	04:13:09.56	+50:31:39.1	…	B	1.643	51.1	43.65	432.33	…	0.213 ± 0.038
…	…	LSPM J0413+4737E	J04137+476	M2.5 V	04:13:47.70	+47:37:42.5	…	…	…	…	39.82	161.35	604.36 ± 6.30	0.553 ± 0.028
…	…	GJ 3262	J04139+829	M0.0 V	04:13:56.69	+82:55:03.0	…	…	…	…	39.84	264.59	1547.11 ± 19.88	0.759 ± 0.025
…	…	G 39-3	J04148+277	M3.5 Ve	04:14:53.80	+27:45:26.0	…	…	…	…	16.09	260.87	225.24 ± 1.16	0.461 ± 0.018
…	…	HD 26965	…	K0 V	04:15:13.91	-07:40:05.1	A+B+C	A	…	…	…	4089.84	…	0.845 ± 0.127

Table D.2: Complete sample with the description of multiple systems (continued).

WDS id	WDS disc	Name	Karmn	Spectral type	α (2016.0)	δ (2016.0)	System	Component	ρ [arcsec]	θ [deg]	ϖ [mas]	$\mu_{\rm total}$ [mas a^{-1}]	$\mathcal{L}$ [10^{-4} $\mathcal{L}_\odot$]	$\mathcal{M}$ [$\mathcal{M}_\odot$]
04153-0739	STF 518	HD 26976	…	DA2.9	04:15:19.39	-07:40:22.6	…	B	83.337	102.2	15.88	4018.59	…	0.500 ± 0.100
04153-0739	STF 518	DYEri	J04153-076	M4.5 V	04:15:19.12	-07:40:15.3	…	C	78.097	97.5	54.57	4083.72	69.46 ± 0.39	0.266 ± 0.014
…	…	GJ 2033 A	J04166-125	M1.0 V	04:16:41.59	-12:33:19.3	AB	A	…	…	54.63	251.29	…	0.534 ± 0.029
04167-1233	HDS 544	GJ 2033 B	…	M2.5 V	04:16:41.80	-12:33:19.8	…	B	2.990	99.3	54.59	200.50	…	0.424 ± 0.031
…	…	LP 714-47	J04167-120	M0.0 V	04:16:45.65	-12:05:05.6	…	…	…	…	70.87	203.40	735.47 ± 3.97	0.619 ± 0.027
…	…	GJ 3270	J04173+088	M5.0 V	04:17:18.68	+08:49:16.0	…	…	…	…	32.13	400.23	68.11 ± 0.37	0.278 ± 0.013
…	…	LSPM J0417+4103A	J04177+410	M3.5 V	04:17:44.44	+41:03:10.1	AB	A	…	…	32.40	219.80	…	0.404 ± 0.032
04177+4103	NSN 546	LSPM J0417+4103B	…	M4.5 V	04:17:44.24	+41:03:09.2	…	B	2.427	249.6	62.82	231.80	…	0.224 ± 0.038
…	…	HIP 20122	J04188+013	M2.0 V	04:18:51.45	+01:23:35.0	…	…	…	…	43.00	59.65	725.30 ± 11.14	0.593 ± 0.028
…	…	UPM J0419+0944	J04191+097	M3.0 V	04:19:08.15	+09:44:50.2	…	…	…	…	71.82	138.27	90.91 ± 0.47	0.284 ± 0.013
…	…	LP 654-39	J04191-074	M3.5 V	04:19:06.41	-07:27:43.6	…	…	…	…	47.80	182.82	155.23 ± 0.90	0.404 ± 0.017
…	…	LSPM J0419+4233	J04198+425	M8/9V	04:19:52.90	+42:33:07.4	…	…	…	…	44.84	1535.49	4.74 ± 0.03	0.109 ± 0.010
…	…	Ross 592	J04199+364	M1.5 V	04:19:59.96	+36:29:04.1	…	…	…	…	42.63	497.03	449.81 ± 2.23	0.525 ± 0.029
…	…	PM J04205+8131	J04205+815	M3.0 V	04:20:34.24	+81:31:54.4	…	…	…	…	46.34	140.83	396.54 ± 1.96	0.490 ± 0.030
…	…	XEST 16-045	J04206+272	M4.5 V	04:20:39.20	+27:17:31.4	…	…	…	…	82.90	28.01	1483.86 ± 14.82	…
04207+1514	JNN261	LP 415-363	J04207+152	M4.0 V	04:20:48.16	+15:14:08.2	(AB)	AB	0.220	91.2	28.24	181.83	…	0.338 ± 0.034
…	…	GJ 3274	J04218+213	M3.5 V	04:21:50.22	+21:19:39.2	…	…	…	…	28.77	257.43	148.13 ± 0.87	0.369 ± 0.016
…	…	GJ 3271	J04219+751	M3.0 V	04:21:59.86	+75:08:20.5	…	…	…	…	75.61	728.35	220.08 ± 0.93	0.402 ± 0.016
…	…	GJ 3275	J04221+192	M3.0 V	04:22:08.13	+19:15:21.4	…	…	…	…	50.45	106.52	405.81 ± 2.66	0.487 ± 0.030
…	…	TYC 78-257-1	…	…	04:21:04.26	+03:16:07.9	A+B	A	…	…	50.64	139.56	2519.01 ± 12.78	0.7418 ± 0.022
…	…	RX J0422.4+0337	J04224+036	M3.5 V	04:22:25.19	+03:37:08.5	…	B*	1748.607	43.9	25.97	143.01	208.87 ± 1.22	0.443 ± 0.018
…	…	LP 31-339	J04224+740	M1.5 V	04:22:28.52	+74:01:21.5	…	…	…	…	27.07	327.30	432.58 ± 1.90	0.521 ± 0.029
…	…	LSPM J0422+1031	J04225+105	M3.5 V	04:22:32.25	+10:31:19.3	…	…	…	…	44.12	247.15	255.46 ± 1.48	0.423 ± 0.012
…	…	GJ 1070	J04225+390	M5.0 V	04:22:34.31	+39:00:34.0	…	…	…	…	199.61	844.50	34.15 ± 0.18	0.190 ± 0.011
…	…	LP 415-30	J04227+205	M4.0 V	04:22:42.99	+20:34:11.9	…	…	…	…	199.69	115.40	183.41 ± 2.78	0.441 ± 0.018
…	…	G 8-31	J04229+259	M4.5 V	04:22:59.30	+25:59:10.4	…	…	…	…	199.45	246.98	58.33 ± 0.26	0.238 ± 0.012
…	…	TYC 3337-1716-1	J04234+495	M2.5 V	04:23:26.84	+49:34:15.6	…	…	…	…	45.93	214.40	330.65 ± 2.20	0.498 ± 0.019
…	…	1R042323.2+805511	J04234+809	M4.0 V	04:23:29.60	+80:55:08.8	…	…	…	…	45.62	121.25	422.78 ± 17.95	0.471 ± 0.030
…	…	LP 535-73	J04238+092	M3.0 V	04:23:50.83	+09:12:19.4	…	…	…	…	19.11	114.41	673.23 ± 4.05	0.556 ± 0.028
…	…	INTau	J04238+149	M3.5 V	04:23:50.50	+14:55:17.0	…	…	…	…	68.56	117.51	411.84 ± 8.32	0.471 ± 0.030
…	…	1R042441.9-064725	J04247-067	M4.0 V	04:24:42.78	-06:47:31.2	Aabc	Aabc(3)	…	…	39.46	147.33	…	…
…	…	GJ 3280	J04248+324	M2.5 V	04:24:49.49	+32:26:56.0	…	…	…	…	32.80	259.61	257.74 ± 1.12	0.437 ± 0.017
…	…	PM J04251+5131	J04251+515	M2.0 V	04:25:09.86	+51:31:56.2	…	…	…	…	32.78	122.30	541.62 ± 27.70	0.536 ± 0.030
…	…	GJ 3282	J04252+080S	M2.5 V	04:25:15.25	+08:02:55.8	Aab+B	Aab(2)	…	…	52.84	140.04	…	…
04252+0803	LDS3584	GJ 3283	J04252+080N	M4.0 V	04:25:17.09	+08:04:03.9	…	B	73.393	21.9	24.78	146.66	…	0.300 ± 0.035
04244+1705	OCC 615	HD 27848	…	…	04:24:22.38	+17:04:43.8	AB+C+DE+F	AB	…	…	40.25	103.39	…	…
…	…	V991Tau	…	K4 V	04:25:00.35	+16:59:05.2	…	C	641.168	121.9	29.97	94.41	…	0.771 ± 0.116
04252+1716	AST 4	V805Tau	J04252+172	M3.5 V	04:25:13.67	+17:16:05.1	…	DE	1002.145	47.1	97.45	110.65	…	0.575 ± 0.028
…	…	LP 415-881	…	M7.0 V	04:26:19.16	+17:03:01.7	…	F	1677.610	93.4	42.21	105.70	…	0.144 ± 0.042
…	…	TYC 1273-9-1	J04274+203	M1.5 V	04:27:24.97	+20:22:44.5	…	…	…	…	25.00	84.54	292.41 ± 1.29	0.440 ± 0.017

Table D.2: Complete sample with the description of multiple systems (continued).

WDS id	WDS disc	Name	Karmn	Spectral type	α (2016.0)	δ (2016.0)	System	Component	ρ [arcsec]	θ [deg]	ϖ [mas]	$\mu_{\rm total}$ [mas a^{-1}]	$\mathcal{L}$ [$10^{-4}\,\mathcal{L}_\odot$]	$\mathcal{M}$ [$\mathcal{M}_\odot$]
04277+5935	BWL16	GJ 3287	J04276+595	M3.8 V	04:27:41.56	+59:35:13.5	(AB)	AB	4.239	184.1	7.52	225.85	…	0.255 ± 0.036
…	…	GJ 3291	J04278+117	M4.2 V	04:27:53.89	+11:46:46.8	…	…	…	…	36.85	593.07	141.19 ± 0.72	0.360 ± 0.015
…	…	V1102Tau	J04284+176	M2.0 V	04:28:28.89	+17:41:44.9	AB	A	…	…	48.41	118.08	…	0.645 ± 0.027
04285+1742	GUE 5	HG 7-232B	…	M3.0 V	04:28:29.01	+17:41:45.3	…	B	1.663	74.7	51.41	108.17	…	0.381 ± 0.032
…	…	HD 28343	J04290+219	M0.5 V	04:29:00.05	+21:55:24.5	…	…	…	…	27.92	187.05	1182.29 ± 6.36	0.727 ± 0.025
…	…	GJ 3292	J04293+142	M3.8 V	04:29:18.76	+14:14:02.0	…	…	…	…	26.97	300.06	146.35 ± 1.28	0.391 ± 0.017
04295+2617	SMN 11	FW Tau	J04294+262	M5.5 V	04:29:29.71	+26:16:52.8	(ABC)	ABC	0.105	317.0	27.85	17.58	…	…
…	…	PM J04302+7049	J04302+708	M1.5 V	04:30:11.72	+70:49:14.3	…	…	…	…	32.99	118.86	327.29 ± 1.78	0.467 ± 0.018
…	…	V546Per	J04304+398	M5.0 V	04:30:25.67	+39:50:50.4	…	…	…	…	48.00	628.65	35.57 ± 0.14	0.194 ± 0.011
…	…	LP 655-23	J04308-088	M4.0 V	04:30:52.04	-08:49:22.0	A+B	A	…	…	49.97	161.83	145.83 ± 1.06	0.391 ± 0.017
04309-0849	KO 2	Koenigstuhl 2B	…	M8.0 V	04:30:51.58	-08:49:03.5	…	B	19.809	339.8	22.20	157.34	7.72 ± 0.15	0.146 ± 0.010
…	…	PM J04310+3647A	J04310+367	M3.0 V	04:30:59.95	+36:47:54.7	AB	A	…	…	57.14	63.11	…	0.401 ± 0.032
…	…	PM J04310+3647B	…	M3.0 V	04:30:59.91	+36:47:54.0	…	B	0.793	215.4	46.52	60.11	…	0.366 ± 0.033
…	…	GJ 169.1 A	J04311+589	M4.0 V	04:31:14.21	+58:58:04.7	A+B	A	…	…	23.99	2424.35	95.39 ± 0.62	0.276 ± 0.011
04312+5858	STI2051	GJ 169.1 B	…	DC5	04:31:15.33	+58:58:10.1	…	B	10.263	58.2	22.36	2361.13	…	0.500 ± 0.100
…	…	PM J04312+4217	J04312+422	M2.5 Ve	04:31:14.99	+42:17:08.9	…	…	…	…	25.66	122.32	344.48 ± 2.07	0.509 ± 0.019
04314+2411	LEI 14	V927Tau	J04313+241	M4.5: V+	04:31:23.83	+24:10:52.6	(AB)	AB	0.260	292.0	28.24	19.77	…	…
…	…	LP 475-1095	J04326+098	M1.5 Ve	04:32:37.96	+09:51:06.5	…	…	…	…	41.13	124.68	1291.73 ± 34.82	0.686 ± 0.026
…	…	LP 595-23	J04329+001E	M0.5 V	04:32:56.07	+00:06:14.7	A+B+C	A	…	…	29.04	184.91	499.69 ± 2.41	0.548 ± 0.028
04329+0007	LDS 121	G 82-28	J04329+001S	M4.0 Ve	04:32:55.38	+00:06:28.3	…	B	17.079	322.7	29.68	190.36	114.99 ± 0.64	0.322 ± 0.014
04329+0007	LDS 121	LP 595-21	J04329+001N	M4.0 V	04:32:55.32	+00:06:33.2	…	C	21.662	328.7	28.88	202.02	73.62 ± 0.75	0.271 ± 0.013
…	…	V697TauA	J04333+239	M3.0 V	04:33:23.91	+23:59:26.0	AB	A	…	…	19.96	111.52	…	0.484 ± 0.030
…	…	V697TauB	…	M1.5 V	04:33:23.87	+23:59:26.5	…	B	0.767	309.5	18.36	107.60	…	…
…	…	GJ 3296	J04335+207	M5.0 V	04:33:34.48	+20:44:40.7	…	…	…	…	19.31	557.27	29.93 ± 0.12	0.176 ± 0.011
…	…	PM J04343+4302	J04343+430	M2.65 V	04:34:22.55	+43:02:13.3	…	…	…	…	21.20	94.90	297.59 ± 1.43	0.464 ± 0.013
…	…	LP 595-11	J04347-004	M4.0 V	04:34:45.24	-00:26:50.2	…	…	…	…	40.74	244.65	93.57 ± 0.78	0.308 ± 0.014
04350+0840	RAO 549	StKM 1-495	J04350+086	M1.0 Ve	04:35:02.65	+08:39:30.5	(AB)	AB	0.320	97.0	43.84	90.95	…	…
…	…	LP 775-31	J04352-161	M8.0 Ve	04:35:16.33	-16:06:52.2	Aab	Aab(2)	…	…	52.83	353.47	…	…
…	…	GJ 3302	J04366+112	M4.0 V	04:36:39.94	+11:13:22.8	…	…	…	…	35.79	635.73	84.09 ± 0.40	0.291 ± 0.013
…	…	LP 84-34	J04369+593	M2.0 V	04:36:58.75	+59:21:57.7	…	…	…	…	20.92	190.55	310.86 ± 1.24	0.482 ± 0.018
…	…	1RO43657.1-161258	J04369-162	M3.5 V	04:36:57.49	-16:13:07.0	…	…	…	…	21.90	87.52	500.96 ± 4.03	0.498 ± 0.029
…	…	LP 415-1644	J04373+193	M4.0 V	04:37:22.00	+19:21:16.9	…	…	…	…	89.05	97.37	…	…
…	…	HD 232979	J04376+528	M0.0 V	04:37:41.47	+52:53:29.4	…	…	…	…	41.54	564.14	757.04 ± 4.92	0.643 ± 0.027
04376-0228	WAL 32	HD 29391	…	F0 V	04:37:36.18	-02:28:25.8	A+(BC)	A	66.700	162.5	…	77.72	…	1.750 ± 0.050
04376-0228	KAS 1	GJ 3305	J04376-024	M1.1 V	04:37:37.51	-02:29:29.7	…	BC	66.962	162.6	38.87	72.38	…	0.706 ± 0.026
…	…	GJ 173	J04376-110	M1.5 V	04:37:41.62	-11:02:23.1	…	…	…	…	91.84	299.84	329.57 ± 1.45	0.451 ± 0.012
…	…	GJ 3304 A	J04382+282	M4.0 V	04:38:13.13	+28:12:58.4	AB	A	…	…	33.16	404.45	…	0.267 ± 0.036
04382+2813	BEU 6	GJ 3304 B	…	M4.5 V	04:38:13.05	+28:12:59.0	…	B	1.202	304.5	31.95	394.70	…	0.228 ± 0.037
…	…	LP 715-39	J04386-115	M3.5 V	04:38:36.86	-11:30:18.6	…	…	…	…	24.53	361.03	207.07 ± 1.39	0.414 ± 0.017
…	…	G 8-48A	J04388+217	M3.5 V	04:38:53.72	+21:47:51.7	AB+C	A	…	…	25.50	285.83	…	0.414 ± 0.031

Table D.2: Complete sample with the description of multiple systems (continued).

WDS id	WDS disc	Name	Karmn	Spectral type	α (2016.0)	δ (2016.0)	System	Component	ρ [arcsec]	θ [deg]	ϖ [mas]	$\mu_{\rm total}$ [mas a^{-1}]	$\mathcal{L}$ [$10^{-4}\,\mathcal{L}_\odot$]	$\mathcal{M}$ [$\mathcal{M}_\odot$]
04390+2149	JNN 262	LP 358-478	…	M5.5 Ve	04:38:53.79	+21:47:51.0	…	B	1.238	124.6	181.24	284.57	…	0.380 ± 0.032
04390+2149	LDS1183	G 8-48B	…	M5.0 V	04:38:54.69	+21:47:45.0	…	C	15.002	116.3	181.27	274.20	28.16 ± 0.40	0.198 ± 0.012
…	…	V583Aur	…	K5 V	04:39:25.47	+33:32:43.9	A+(BC)	A	…	…	44.83	52.35	3249.50 ± 20.07	…
04393+3331	JNN 263	PM J04393+3331	J04393+335	M4.0 V	04:39:23.22	+33:31:48.7	…	BC	61.936	207.1	…	50.28	…	…
…	…	LP 415-302	J04395+162	M5.5 Ve	04:39:31.54	+16:15:30.2	…	…	…	…	23.25	799.07	16.60 ± 0.07	0.135 ± 0.010
…	…	PM J04398+2509	J04398+251	M3.5 V	04:39:48.86	+25:09:25.4	…	…	…	…	38.08	105.73	88.18 ± 0.43	0.279 ± 0.013
…	…	LP 655-48	J04403-055	M6.0 V	04:40:23.63	-05:30:06.1	…	…	…	…	38.17	358.15	6.32 ± 0.03	0.107 ± 0.009
…	…	GJ 9163 A	J04404-091	M0.0 V	04:40:29.13	-09:11:48.5	AB	A	…	…	38.12	179.28	…	0.545 ± 0.028
04406-0912	WOR 17	GJ 9163 B	…	M1.0 V	04:40:29.15	-09:11:46.8	…	B	1.715	9.6	22.94	124.61	…	0.535 ± 0.029
…	…	TOI-2457	J04406-128	M0.0 V	04:40:40.16	-12:53:26.6	…	…	…	…	19.49	24.78	870.01 ± 5.24	0.679 ± 0.026
…	…	GJ 3307	J04407+022	M2.0 V	04:40:42.67	+02:13:52.7	…	…	…	…	73.51	177.22	590.81 ± 5.52	0.564 ± 0.028
…	…	G 39-30A	J04413+327	M4.0 V	04:41:24.22	+32:42:19.9	AB	A	…	…	26.59	310.42	…	0.409 ± 0.031
04413+3242	JNN 264	G 39-30B	…	M4.0 V	04:41:24.22	+32:42:21.4	…	B	1.473	359.3	52.82	301.62	…	0.298 ± 0.035
…	…	TYC 694-1183-1	J04414+132	M0.5 V	04:41:29.78	+13:13:16.0	Aab	Aab	…	…	46.64	100.97	…	…
…	…	LP 84-59	J04422+577	M0.0 V	04:42:15.86	+57:42:18.2	…	…	…	…	16.85	576.53	790.91 ± 8.46	0.641 ± 0.027
…	…	LP 415-1896	J04423+207	M2.0 V	04:42:23.76	+20:46:34.9	…	…	…	…	94.31	299.49	477.00 ± 2.52	0.534 ± 0.029
…	…	LP 415-345	J04425+204	M3.0 V	04:42:30.40	+20:27:10.8	Aab+B+C	Aab(2)	…	…	27.10	97.45	…	…
…	…	LP 415-3051	…	M3.0 V	04:42:58.58	+20:36:16.8	…	B*	674.349	35.9	39.11	91.26	160.48 ± 1.04	0.385 ± 0.016
…	…	G2-3411054848866601472	…	M6.0 V	04:43:55.36	+20:08:40.5	…	C*	1631.351	132.8	35.68	93.82	12.77 ± 0.21	0.148 ± 0.010
…	…	PM J04429+0935	J04429+095	M1.0 V	04:42:55.14	+09:35:53.7	A+B	A	…	…	25.37	82.04	568.80 ± 3.59	0.574 ± 0.028
…	…	G3- 3293060625388613248	…	M6.5 V	04:42:53.91	+09:35:50.3	…	B*	18.386	259.1	…	77.51	9.72 ± 0.11	0.126 ± 0.010
…	…	HD 285968	J04429+189	M2.5 V	04:42:56.52	+18:57:11.5	…	…	…	…	100.92	1295.36	358.08 ± 2.37	0.468 ± 0.012
…	…	PM J04429+2128	J04429+214	M3.5 V	04:42:55.90	+21:28:24.8	…	…	…	…	33.44	123.58	181.62 ± 1.59	0.363 ± 0.011
…	…	Haro 6-36	J04433+296	M5.5 V	04:43:20.23	+29:40:05.7	…	…	…	…	36.01	22.58	2282.44 ± 48.94	…
…	…	HD 283779	J04444+278	M1.5 V	04:44:26.17	+27:51:37.2	…	…	…	…	89.19	437.44	293.26 ± 1.16	0.441 ± 0.017
…	…	PM J04458-1426	J04458-144	M4.0 V	04:45:52.69	-14:26:23.6	…	…	…	…	75.67	142.89	218.23 ± 1.50	0.453 ± 0.018
…	…	PM J04468-1116A	J04468-112	M3.0 V	04:46:51.63	-11:16:48.6	AB	A	…	…	76.31	153.74	…	0.372 ± 0.032
04469-1117	JNN 28	PM J04468-1116B	…	M6.0 V	04:46:51.53	-11:16:48.2	…	B	1.518	285.0	48.75	147.07	…	0.289 ± 0.035
…	…	GJ 3313	J04471+021	M0.0 V	04:47:11.55	+02:09:39.6	…	…	…	…	22.45	193.33	538.44 ± 3.03	0.569 ± 0.028
…	…	RX J0447.2+2038	J04472+206	M5.0 V	04:47:12.35	+20:38:09.2	…	…	…	…	21.89	132.32	123.97 ± 0.75	0.428 ± 0.032
…	…	LP 416-43	J04480+170	M0.5 V	04:48:00.98	+17:03:21.1	Aab+B	Aab	…	…	33.65	82.10	…	0.13180 …0.004
…	…	UCAC4 536-010184	…	M4.5 V	04:49:36.67	+17:01:58.6	…	B*	1374.841	93.4	21.57	87.10	75.26 ± 0.47	0.293 ± 0.014
…	…	1R044847.6+100302	J04488+100	M3.0 Ve	04:48:47.32	+10:03:01.4	Aab	Aab(2)	…	…	94.37	101.41	…	…
04494+4828	JNN265	G 81-34	J04494+484	M4.0 V	04:49:29.77	+48:28:42.9	(AB)	AB	0.740	250.0	11.13	264.56	…	0.304 ± 0.035
…	…	EM* LkCa 18A	J04499+236	M1.0 V	04:49:56.34	+23:41:00.1	AB	A	…	…	7.43	173.62	…	0.647 ± 0.027
04499+2341	KPP3177	EM* LkCa 18B	…	M1.5 V	04:49:56.51	+23:41:00.1	…	B	2.380	90.0	83.99	162.99	…	0.509 ± 0.029
…	…	LP 32-204	J04499+711	M3.5 V	04:49:56.29	+71:09:46.5	…	…	…	…	47.26	183.39	132.65 ± 0.70	0.348 ± 0.015
…	…	GJ 3315	J04502+459	M1.0 V	04:50:15.59	+45:58:46.2	…	…	…	…	102.59	305.58	397.19 ± 1.23	0.512 ± 0.029
…	…	BPM 85800	J04504+199	M1.5 V	04:50:25.49	+19:59:09.1	…	…	…	…	49.43	145.65	471.15 ± 2.40	0.533 ± 0.029
…	…	GJ 1072	J04508+221	M5.0 V	04:50:51.65	+22:07:14.7	…	…	…	…	49.11	759.23	21.98 ± 0.10	0.159 ± 0.010

Table D.2: Complete sample with the description of multiple systems (continued).

WDS id	WDS disc	Name	Karmn	Spectral type	α (2016.0)	δ (2016.0)	System	Component	ρ [arcsec]	θ [deg]	ϖ [mas]	$\mu_{\rm total}$ [mas a^{-1}]	$\mathcal{L}$ [$10^{-4}\,\mathcal{L}_\odot$]	$\mathcal{M}$ [$\mathcal{M}_\odot$]
…	…	GJ 3316	J04508+261	M2.5 V	04:50:51.21	+26:07:22.3	…	…	…	…	16.29	623.45	172.89 ± 0.97	0.376 ± 0.016
…	…	Wolf 1539	J04520+064	M3.5 V	04:52:05.90	+06:28:30.7	…	…	…	…	42.69	342.44	158.33 ± 1.02	0.350 ± 0.012
…	…	LP 776-25	J04524-168	M3.3 V	04:52:24.55	-16:49:25.3	…	…	…	…	24.93	243.44	295.75 ± 1.51	0.499 ± 0.019
…	…	GJ 1073	J04525+407	M5.0 V	04:52:36.26	+40:42:06.6	…	…	…	…	24.96	1606.93	58.14 ± 0.25	0.238 ± 0.012
…	…	LP 84-48	J04536+623	M3.5 V	04:53:40.79	+62:18:59.9	…	…	…	…	22.66	361.91	96.58 ± 0.35	0.293 ± 0.013
…	…	LSPM J0453+1549	J04538+158	M2.5 V	04:53:50.10	+15:49:12.6	…	…	…	…	29.47	176.11	166.00 ± 0.73	0.368 ± 0.015
…	…	GJ 180	J04538-177	M2.0 V	04:53:50.44	-17:46:34.6	…	…	…	…	35.55	763.06	236.80 ± 1.12	0.398 ± 0.011
…	…	1R045430.9+650451	J04544+650	M4.0 V	04:54:29.98	+65:04:39.5	…	…	…	…	20.48	118.11	73.45 ± 0.30	0.270 ± 0.013
04559+0440	EGN 4	HD 31412	…	F9.5 V	04:55:56.03	+04:40:10.5	(AB)+C	AB	0.443	17.7	19.43	233.46	…	1.114 ± 0.167
04559+0440	LDS9181	HD 31412B	J04559+046	M2.0 V	04:55:54.60	+04:40:13.5	…	C	21.657	277.9	19.48	234.00	791.43 ± 5.69	0.600 ± 0.027
…	…	LP 202-2	J04560+432	M4.0 V	04:56:04.12	+43:13:53.0	…	…	…	…	28.74	420.36	66.13 ± 0.38	0.255 ± 0.012
…	…	GJ 1074	J04587+509	M1.0 V	04:58:46.84	+50:56:32.4	…	…	…	…	28.68	604.82	513.22 ± 2.02	0.558 ± 0.028
…	…	GJ 181	J04588+498	M0.0 V	04:58:50.76	+49:50:55.6	…	…	…	…	105.43	159.39	796.11 ± 3.90	0.642 ± 0.027
…	…	GJ 182	J04595+017	M0.0 Ve	04:59:34.88	+01:46:59.2	…	…	…	…	71.90	102.65	1422.03 ± 6.60	0.739 ± 0.025
…	…	Ross 794	J05012+248	M2.0 V	05:01:15.79	+24:52:18.2	…	…	…	…	6.02	456.24	456.28 ± 2.43	0.519 ± 0.029
…	…	LSPM J0501+2237	J05013+226	M4.5 V	05:01:17.95	+22:36:55.3	…	…	…	…	60.82	356.57	23.39 ± 0.10	0.165 ± 0.010
…	…	GJ 3321	J05018+037	M1.5 V	05:01:50.71	+03:45:53.1	…	…	…	…	39.10	186.47	337.11 ± 1.66	0.474 ± 0.018
…	…	1R050156.7+010845	J05019+011	M4.0 V	05:01:56.70	+01:08:41.4	…	…	…	…	52.77	97.03	340.51 ± 2.04	0.432 ± 0.031
…	…	GJ 3322 A	J05019+099	M4.0 V	05:01:58.83	+09:58:57.1	AabB	Aab(2)	…	…	31.90	125.62	…	0.022
05020+0959	HDS 654	GJ 3322 B	…	M2.5 V	05:01:58.89	+09:58:55.9	…	B	1.398	146.7	52.85	128.14	…	0.426 ± 0.031
…	…	GJ 3323	J05019-069	M4.0 Ve	05:01:56.83	-06:56:54.9	…	…	…	…	38.24	767.60	36.40 ± 0.24	0.173 ± 0.009
…	…	HD 32450A	J05024-212	M2.0 V	05:02:28.28	-21:15:28.4	AB	A	…	…	42.99	316.71	…	0.611 ± 0.027
05025-2115	DON 91	HD 32450B	…	M3.0 V	05:02:28.26	-21:15:27.5	…	B	0.888	345.8	20.16	260.93	…	0.372 ± 0.032
…	…	HD 285190	J05032+213	M1.5 V+	05:03:16.21	+21:23:54.0	Aab+(BC)	Aab(2)	…	…	43.63	169.67	…	…
05033+2125	LAW 13	LP 359-186	…	M5.0 V	05:03:05.77	+21:22:33.8	…	BC	166.404	241.2	19.84	177.43	…	0.251 ± 0.045
…	…	GJ 3325	J05033-173	M3.0 V	05:03:19.83	-17:22:31.8	…	…	…	…	57.90	499.86	92.97 ± 0.49	0.259 ± 0.010
…	…	GJ 184	J05034+531	M0.5 V	05:03:26.22	+53:07:17.9	A+B	A	…	…	44.27	2014.91	515.22 ± 2.40	0.563 ± 0.028
05034+5308	WDK 1	BD+52 911B	…	…	05:03:25.60	+53:07:18.7	…	B	5.600	278.5	24.62	2030.03	…	0.100 ± 0.050
…	…	GJ 3326	J05042+110	M5.0 V	05:04:14.69	+11:03:27.0	…	…	…	…	24.57	204.64	30.94 ± 0.14	0.180 ± 0.011
…	…	UPM J0505+4414	J05050+442	M5.0 V	05:05:06.06	+44:14:03.3	…	…	…	…	38.34	99.41	27.86 ± 0.15	0.169 ± 0.010
…	…	GJ 3327	J05051-120	M3.0 V	05:05:11.55	-12:00:30.9	…	…	…	…	39.39	260.57	154.14 ± 0.96	0.354 ± 0.015
…	…	GJ 3328	J05060+043	M1.0 V	05:06:04.44	+04:20:16.1	…	…	…	…	33.18	413.12	393.82 ± 2.32	0.511 ± 0.029
…	…	RX J0506.2+0439	J05062+046	M4.0 V	05:06:12.96	+04:39:25.7	…	…	…	…	79.04	94.79	280.33 ± 1.85	0.398 ± 0.032
…	…	GJ 3331	J05068-215E	M1.5 V	05:06:49.97	-21:35:09.4	A+BC	A	…	…	43.28	49.64	931.51 ± 8.79	0.627 ± 0.027
05069-2135	DON 93	GJ 3332	J05068-215W	M3.5 V	05:06:49.48	-21:35:04.3	…	B	8.489	306.7	80.56	65.51	…	0.516 ± 0.029
05069-2135	DON 93	BD-21 1074C	…	M2.5 V	05:06:49.55	-21:35:04.7	…	C	7.560	308.5	63.13	69.22	…	0.424 ± 0.031
…	…	RX J0507.2+3731A	J05072+375	M5.0 V	05:07:14.33	+37:30:42.1	AB	A	…	…	74.07	102.11	…	0.187 ± 0.041
…	…	RX J0507.2+3731B	…	M5.0 V	05:07:14.37	+37:30:42.1	…	B*	0.476	93.2	54.28	96.09	…	0.166 ± 0.041
…	…	TYC 1853-1649-1	J05076+275	M0.5 V	05:07:36.74	+27:30:03.8	…	…	…	…	38.54	107.00	…	…
05078+1759	CRC 48	Wolf 230	J05078+179	M3.0 V	05:07:49.34	+17:58:53.5	Aabc	Aabc(2)	0.063	84.4	48.89	263.54	…	…

Table D.2: Complete sample with the description of multiple systems (continued).

WDS id	WDS disc	Name	Karmn	Spectral type	α (2016.0)	δ (2016.0)	System	Component	ρ [arcsec]	θ [deg]	ϖ [mas]	$\mu_{\rm total}$ [mas a^{-1}]	$\mathcal{L}$ [$10^{-4}\,\mathcal{L}_\odot$]	$\mathcal{M}$ [$\mathcal{M}_\odot$]
05083+7538	JNN 266	LP 15-315	J05083+756	M4.5 V	05:08:19.36	+75:38:13.3	(AB)	AB	0.095	352.3	83.69	237.23	…	0.201 ± 0.039
05085-2102	YMG 9	2M05082729-2101444	J05084-210	M5.0 V	05:08:27.34	-21:01:44.6	(AB)	AB	0.029	272.6	51.00	36.58	…	0.414 ± 0.031
05086-1810	WSI 72	GJ 190	J05085-181	M3.5 V	05:08:35.61	-18:10:41.8	(AB)	AB	0.041	224.5	27.86	1487.47	…	0.465 ± 0.030
…	…	Ross 388	J05091+154	M3.5 V	05:09:10.11	+15:27:22.8	…	…	…	…	27.85	649.24	395.01 ± 2.83	0.488 ± 0.030
…	…	G 97-23	J05103+095	M2.0 V	05:10:18.12	+09:30:01.8	…	…	…	…	62.46	353.27	578.29 ± 4.23	0.556 ± 0.028
…	…	LSPM J0510+2714	J05103+272	M7.0 V	05:10:19.83	+27:13:51.8	…	…	…	…	47.50	665.89	6.92 ± 0.04	0.113 ± 0.010
…	…	GJ 3336 A	J05103+488	M2.5 V	05:10:22.30	+48:50:26.3	AB	A	…	…	60.19	428.14	…	0.464 ± 0.030
05104+4850	HEI 321	GJ 3336 B	…	M2.0 V	05:10:22.48	+48:50:25.5	…	B	2.009	112.5	40.99	426.80	…	0.457 ± 0.030
…	…	G 86-28	J05106+297	M3.0 V	05:10:39.22	+29:46:48.9	…	…	…	…	44.25	253.57	83.14 ± 0.42	0.270 ± 0.013
…	…	GJ 3337	J05109+186	M4.0 V	05:10:57.16	+18:37:24.1	…	…	…	…	69.89	690.53	68.29 ± 0.32	0.260 ± 0.013
…	…	StKM 1-549	J05111+158	M1.0 Ve	05:11:09.78	+15:48:57.0	…	…	…	…	53.08	63.81	1171.33 ± 52.24	0.690 ± 0.027
…	…	LP 477-36	J05114+101	M1.0 V	05:11:29.68	+10:07:12.2	…	…	…	…	39.54	221.80	936.70 ± 10.56	0.650 ± 0.027
…	…	GJ 192	J05127+196	M2.0 V	05:12:42.54	+19:40:00.2	…	…	…	…	42.04	368.87	269.16 ± 1.49	0.421 ± 0.011
…	…	GJ 3340	J05151-073	M1.0 V	05:15:08.33	-07:20:55.4	…	…	…	…	42.10	508.34	343.64 ± 1.78	0.479 ± 0.018
…	…	UPM J0515+2336	J05152+236	M5.0 V	05:15:17.58	+23:36:25.2	…	…	…	…	186.05	65.40	150.58 ± 4.90	0.349 ± 0.016
…	…	LSPM J0515+5911	J05155+591	M7.5 V	05:15:31.19	+59:11:01.3	…	…	…	…	119.57	1012.71	9.43 ± 0.11	0.136 ± 0.010
05173+3208	RAO 201	G 86-37	J05173+321	M3.5 V	05:17:20.09	+32:07:29.7	(AB)	AB	0.170	214.5	118.82	308.44	…	0.441 ± 0.031
…	…	Capella	…	G3 III:	…	…	Aab+BC	Aab(2)	…	…	46.83	433.47	…	4.909 ± 0.022
05167+4600	FRH 1	Capella H	J05173+458	M1.0 V	05:17:24.00	+45:50:16.1	…	B	722.840	141.8	48.52	437.93	…	0.537 ± 0.029
05167+4600	ST 3	Capella L	…	M4.0 V	05:17:24.04	+45:50:12.6	…	C	3.457	173.5	43.50	420.38	…	0.272 ± 0.036
…	…	TYC 4351-466-1	J05173+721	M1.0 V	05:17:21.23	+72:10:49.8	…	…	…	…	108.27	117.79	416.93 ± 1.59	0.500 ± 0.018
…	…	PM J05187+4629	J05187+464	M4.5 V	05:18:44.62	+46:29:57.9	…	…	…	…	72.17	115.11	321.34 ± 4.10	0.412 ± 0.031
…	…	1R051929.3+645435	J05195+649	M3.5 V	05:19:31.21	+64:54:36.2	…	…	…	…	72.24	151.99	251.64 ± 2.88	0.399 ± 0.032
…	…	GJ 3342	J05206+587N	M3.5 V	05:20:41.70	+58:47:25.2	A+B	A	…	…	98.23	524.57	224.15 ± 2.80	0.459 ± 0.019
05207+5848	GIC 46	GJ 3343	J05206+587S	M3.5 V	05:20:41.05	+58:47:12.0	…	B	14.107	200.9	74.14	519.48	101.44 ± 0.59	0.322 ± 0.014
…	…	GJ 3345	J05211+557	M3.5 V	05:21:10.47	+55:45:46.5	…	…	…	…	48.19	309.78	222.36 ± 1.46	0.429 ± 0.017
…	…	PM J05223+3031	J05223+305	M3.0 V	05:22:20.65	+30:31:08.3	…	…	…	…	44.04	113.73	210.68 ± 0.94	0.445 ± 0.018
…	…	TYC 4532-731-1	J05226+795	M0.5 V	05:22:39.87	+79:34:30.3	…	…	…	…	36.19	100.16	555.01 ± 2.35	0.575 ± 0.028
…	…	PM J05228+2016	J05228+202	M2.5 Ve	05:22:50.18	+20:16:36.5	AB	A	…	…	50.43	46.07	…	0.487 ± 0.030
…	…	G3- 3402193923314210944	…	…	05:22:50.43	+20:16:36.6	…	B	3.548	87.2	50.52	…	…	…
…	…	PM J05243-1601A	J05243-160	M4.5 V	05:24:19.14	-16:01:15.8	AB	A	…	…	50.58	39.99	…	0.371 ± 0.033
05243-1601	BRG 21	PM J05243-1601B	…	M3.5 V	05:24:19.17	-16:01:15.6	…	B	0.444	66.9	43.80	34.25	…	0.339 ± 0.033
…	…	LP 717-36	J05256-091	M3.5 V	05:25:41.70	-09:09:15.8	AB	A	…	…	44.02	205.70	…	0.353 ± 0.033
05257-0909	DAE 2	G3- 3014628959425010688	…	M3.5 V	05:25:41.73	-09:09:15.3	…	B	0.723	41.9	…	183.57	…	0.310 ± 0.034
…	…	Ross 41	J05280+096	M3.5 V	05:27:59.94	+09:38:26.0	…	…	…	…	86.10	780.65	67.93 ± 0.31	0.221 ± 0.009
…	…	GJ 1080	J05282+029	M3.5 V	05:28:14.24	+02:57:56.6	Aab+B	Aab	…	…	33.42	1157.54	…	…
05282+0258	SKF 270	GJ 1080 B	…	M6.0 V	05:28:14.27	+02:57:51.9	…	B	4.698	175.2	66.20	1168.06	…	0.122 ± 0.044
…	…	HD 35956	…	G0 V	05:28:51.74	+12:32:59.6	Aab+B+CD	Aab(1)	…	…	56.12	231.78	…	…
05289+1233	TOK 94	HD 35956B	…	M1.0 V	05:28:52.11	+12:33:01.4	…	B	5.830	71.4	20.70	237.81	…	0.564 ± 0.028
05289+1233	LDS6186	GJ 3348A	J05289+125	M4.0 V	05:28:56.61	+12:31:50.4	…	C	99.391	134.1	108.33	230.59	…	0.263 ± 0.060

Table D.2: Complete sample with the description of multiple systems (continued).

WDS id	WDS disc	Name	Karmn	Spectral type	α (2016.0)	δ (2016.0)	System	Component	ρ [arcsec]	θ [deg]	ϖ [mas]	$\mu_{\rm total}$ [mas a^{-1}]	$\mathcal{L}$ [$10^{-4}\,\mathcal{L}_\odot$]	$\mathcal{M}$ [$\mathcal{M}_\odot$]
05289+1233	RAO 552	GJ 3348B	…	…	05:28:56.61	+12:31:50.2	…	D	99.461	134.2	33.57	…	…	…
…	…	GJ 2043	J05294+155E	M0.0: V	05:29:26.92	+15:34:36.2	A+B	A	…	…	27.45	152.85	456.65 ± 3.51	0.543 ± 0.029
05296+1534	LDS6187	GJ 2043 B	J05294+155W	M4.0 V	05:29:26.02	+15:34:43.4	…	B	14.862	298.9	97.32	138.81	32.76 ± 0.13	0.173 ± 0.010
…	…	Ross 406	J05298+320	M2.5 V	05:29:52.40	+32:04:40.4	…	…	…	…	42.84	709.93	245.33 ± 0.93	0.426 ± 0.017
…	…	Wolf 1450	J05298-034	M3.0 V	05:29:51.70	-03:26:37.6	…	…	…	…	42.82	559.50	215.44 ± 1.01	0.422 ± 0.017
…	…	LSPM J0530+1514	J05306+152	M3.0 V	05:30:37.09	+15:14:26.3	…	…	…	…	80.34	182.76	147.29 ± 0.80	0.345 ± 0.015
…	…	HD 36395	J05314-036	M1.5 V	05:31:28.21	-03:41:11.5	…	…	…	…	47.04	2226.53	657.08 ± 16.58	0.590 ± 0.028
05321-0305	JNN 39	V1311Ori	J05320-030	M2.0 V+	05:32:04.51	-03:05:30.0	(AB)+C+D+E	AB	0.171	293.0	19.12	41.38	…	0.700 ± 0.027
05321-0305	JNN 39	PM J05319-0303W	…	M5.0 V	05:31:57.88	-03:03:37.6	…	C	150.006	318.5	22.63	54.71	337.69 ± 5.08	0.394 ± 0.032
05321-0305	JNN 39	2M05315816-0303397	…	M3.5 V	05:31:58.17	-03:03:40.7	…	D	144.834	319.0	82.31	54.64	175.72 ± 1.03	0.461 ± 0.019
05321-0305	JNN 39	ESO-HA 737	…	M5.0 V	05:32:05.97	-03:01:16.8	…	E	254.187	4.9	46.25	51.30	110.16 ± 0.67	0.360 ± 0.016
…	…	Ross 42	J05322+098	M3.5 V	05:32:14.46	+09:49:11.5	Aab	Aab(2)	…	…	75.57	281.96	…	0.400
…	…	G 98-7	J05328+338	M3.5 V	05:32:51.57	+33:49:39.8	…	…	…	…	24.47	493.99	53.78 ± 0.23	0.213 ± 0.011
05333+4449	AST 3	GJ 1081	J05333+448	M3.5 V	05:33:19.20	+44:48:52.9	(AB)	AB	0.323	46.7	63.36	381.20	…	0.363 ± 0.033
…	…	V371Ori	J05337+019	M3.0 Ve	05:33:44.55	+01:56:41.0	Aab	Aab(1)	…	…	39.91	278.07	…	…
…	…	RX J0534.0-0221	J05339-023	M3.0 V	05:33:59.83	-02:21:33.3	…	…	…	…	30.56	59.18	660.15 ± 4.91	0.552 ± 0.028
…	…	PM J05334+4809	…	M0.0 V	05:33:28.97	+48:09:26.2	A+BC+D	A	…	…	76.20	66.93	653.27 ± 2.87	0.610 ± 0.027
…	…	PM J05341+4732A	J05341+475	M2.5 V	05:34:10.56	+47:32:02.8	…	B*	2282.136	169.4	74.95	69.01	…	0.492 ± 0.030
…	…	PM J05341+4732B	…	M3.0 V	05:34:10.62	+47:32:05.2	…	C*	2279.958	169.3	75.18	61.85	…	0.367 ± 0.033
…	…	UPM J0533+4809	…	M3.5 V	05:33:16.22	+48:09:23.3	…	D*	127.551	268.7	36.27	65.01	119.19 ± 2.21	0.351 ± 0.016
…	…	GJ 3352	J05341+512	M1.0 V	05:34:08.57	+51:12:52.8	…	…	…	…	20.90	227.66	623.11 ± 2.49	0.592 ± 0.028
…	…	Ross 45	J05342+103N	M3.0 V	05:34:15.05	+10:19:08.0	A+Bab	A	…	…	37.69	387.58	258.09 ± 1.69	0.465 ± 0.018
05342+1019	LDS6189	Ross 45B	J05342+103S	M4.5 V	05:34:15.00	+10:19:03.0	…	Bab	5.028	188.0	50.35	379.22	…	…
…	…	Ross 46	J05348+138	M3.0 V	05:34:51.99	+13:52:40.4	…	…	…	…	35.20	413.93	156.71 ± 0.61	0.343 ± 0.011
…	…	Wolf 1457	J05360-076	dM4.0	05:36:00.20	-07:38:51.0	…	…	…	…	38.86	479.46	126.63 ± 0.76	0.314 ± 0.011
…	…	V2689Ori	J05365+113	M0.0 V	05:36:30.99	+11:19:39.4	A+B	A	…	…	37.12	56.42	821.94 ± 4.56	0.654 ± 0.027
05365+1120	TOK255	PM J05366+1117	J05366+112	M4.0 Ve	05:36:38.46	+11:17:47.8	…	B	156.630	135.4	34.81	60.93	90.40 ± 0.73	0.273 ± 0.010
…	…	LSPM J0539+4038	J05394+406	M8.0 Ve	05:39:25.71	+40:38:29.5	…	…	…	…	39.76	1055.41	5.89 ± 0.03	0.113 ± 0.010
…	…	LP 33-191	J05394+747	M3.5 V	05:39:25.44	+74:46:02.6	…	…	…	…	34.70	147.59	120.02 ± 0.57	0.330 ± 0.014
…	…	V1402Ori	J05402+126	M1.5 Ve	05:40:16.07	+12:38:56.4	Aab	Aab(2)	…	…	57.08	261.39	…	…
…	…	V538Aur	…	K1 V	05:41:20.34	+53:28:43.4	A+B	A	…	…	…	523.48	4863.31 ± 137.03	0.860 ± 0.129
05413+5329	ENG 22	HD 233153	J05415+534	M1.0 V	05:41:30.74	+53:29:15.0	…	B	98.035	71.2	32.06	515.97	573.08 ± 2.66	0.568 ± 0.028
05404+2448	WNO45	V780Tau	J05404+248	M5.5 V	05:40:25.82	+24:48:02.0	(AB)	AB	0.658	92.2	32.27	390.93	…	0.132 ± 0.043
…	…	GJ 9188	J05419+153	M0.0 V	05:41:58.95	+15:20:13.3	…	…	…	…	46.20	90.07	702.52 ± 2.67	0.621 ± 0.027
…	…	V1352Ori	J05421+124	M4.0 V	05:42:11.45	+12:28:56.5	…	…	…	…	45.57	2540.13	63.27 ± 0.27	0.229 ± 0.010
…	…	GJ 2045	J05422-054	M5.0 V	05:42:12.53	-05:27:40.3	…	…	…	…	97.89	969.56	18.33 ± 0.08	0.143 ± 0.010
…	…	1R054232.1+152459	J05425+154	M3.5 V	05:42:31.70	+15:25:00.2	…	…	…	…	47.51	106.30	…	…
…	…	PM J05455-1158	J05455-119	M4.5 V	05:45:32.04	-11:58:02.3	…	…	…	…	47.22	86.59	92.76 ± 0.46	0.307 ± 0.014
…	…	PM J05456+7255	J05456+729	M3.0 V	05:45:39.09	+72:55:14.6	…	…	…	…	33.79	139.63	218.16 ± 1.03	0.425 ± 0.017
…	…	PM J05458+7254	J05458+729	M2.5 V	05:45:50.02	+72:54:09.0	…	…	…	…	35.40	139.41	224.62 ± 1.09	0.432 ± 0.017

Table D.2: Complete sample with the description of multiple systems (continued).

WDS id	WDS disc	Name	Karmn	Spectral type	α (2016.0)	δ (2016.0)	System	Component	ρ [arcsec]	θ [deg]	ϖ [mas]	$\mu_{\rm total}$ [mas a^{-1}]	$\mathcal{L}$ [$10^{-4}\,\mathcal{L}_\odot$]	$\mathcal{M}$ [$\mathcal{M}_\odot$]
05466+4407	CRC 49	Wolf 237	J05466+441	M4.0 V	05:46:37.60	+44:07:14.0	AabB	AabB(2)	3.712	222.7	27.67	670.09	…	…
…	…	TYC 4106-420-1	J05468+665	M0.5 V	05:46:48.92	+66:30:13.1	…	…	…	…	39.50	121.53	635.41 ± 5.89	0.574 ± 0.028
…	…	GJ 3366	J05471-052	M4.5 V	05:47:09.69	-05:12:20.3	…	…	…	…	…	768.26	40.79 ± 0.17	0.195 ± 0.011
…	…	GJ 3367	J05472-000	M0	05:47:17.89	-00:00:49.9	…	…	…	…	58.20	102.95	707.09 ± 3.86	0.618 ± 0.027
…	…	GJ 3368	J05484+077	M4.0 V	05:48:24.15	+07:45:34.3	…	…	…	…	58.23	282.11	86.78 ± 0.40	0.296 ± 0.014
…	…	PM J05511+1216	J05511+122	M4.0 V	05:51:10.51	+12:16:09.4	…	…	…	…	46.64	89.83	190.38 ± 3.85	0.372 ± 0.016
…	…	G 106-7	J05530+047	M1.5 V	05:53:04.75	+04:43:02.6	AB	A	…	…	57.76	391.42	…	0.595 ± 0.028
…	…	G 106-7B	…	M5.5 V	05:53:04.65	+04:43:02.8	…	B*	1.520	278.2	50.83	387.78	…	0.139 ± 0.043
05530+2508	RAO 206	LSPM J0553+2507	J05530+251	M3.0 V	05:53:01.92	+25:07:40.9	(AB)	AB	0.259	2.7	175.31	191.68	…	0.367 ± 0.033
…	…	Ross 59	J05532+242	M1.5 V	05:53:14.24	+24:15:22.1	Aab	Aab(2)	…	…	39.31	625.08	…	0.076 ± 0.002
…	…	RX J0554.7+1055	J05547+109	M3.0 V	05:54:45.58	+10:55:55.9	…	…	…	…	27.22	156.47	269.87 ± 1.84	0.476 ± 0.019
…	…	PM J05558+4036	J05558+406	M1.0 V	05:55:48.31	+40:36:48.0	AB	A	…	…	26.30	122.73	…	0.544 ± 0.028
…	…	G3- 3458612029599345664	…	M3.0 V	05:55:48.41	+40:36:47.7	…	B*	1.200	103.0	25.91	138.62	…	0.368 ± 0.033
…	…	1R055641.0-101837	J05566-103	M3.5 V	05:56:40.63	-10:18:35.8	…	…	…	…	25.96	130.74	85.20 ± 0.41	0.293 ± 0.014
…	…	PM J05587+2557	J05587+259	M1.0 V	05:58:47.68	+25:57:40.1	…	…	…	…	77.14	98.96	485.71 ± 2.23	0.550 ± 0.028
05588+2121	JNN268	G 104-9	J05588+213	M5.0 V	05:58:53.53	+21:20:54.5	(AB)	AB	0.455	99.8	68.41	487.62	…	0.164 ± 0.041
…	…	EGCam	J05596+585	M0.5 V	05:59:37.77	+58:35:30.8	A+B	A	…	…	65.44	254.17	440.26 ± 1.82	0.527 ± 0.029
05599+5834	GIC 61	GJ 3372	J05599+585	M4.2 V	05:59:55.68	+58:34:11.2	…	B	161.111	119.6	63.36	252.69	60.62 ± 0.23	0.243 ± 0.012
…	…	GJ 3379	J06000+027	M3.5 Ve	06:00:03.83	+02:42:22.9	…	…	…	…	29.12	311.77	63.55 ± 0.29	0.234 ± 0.009
…	…	GJ 3373	J06008+681	M3.5 V	06:00:50.71	+68:09:05.3	A+B	A	…	…	30.27	1175.81	152.66 ± 0.71	0.375 ± 0.016
06007+6809	LDS1201	GJ 3374	J06007+681	M4.0 V	06:00:47.81	+68:08:11.6	…	B	56.075	196.8	30.05	1174.60	117.60 ± 0.59	0.326 ± 0.014
…	…	GJ 3378	J06011+595	M4.0 V	06:01:10.82	+59:35:35.0	…	…	…	…	30.04	934.54	83.30 ± 0.41	0.249 ± 0.010
…	…	LSPM J0601+1305	J06017+130	M2.5 Ve	06:01:45.54	+13:05:00.7	…	…	…	…	30.23	145.98	224.93 ± 1.01	0.432 ± 0.017
…	…	GJ 3382	J06023-203	M3.5 V	06:02:22.56	-20:19:35.3	…	…	…	…	40.50	556.62	67.38 ± 0.39	0.241 ± 0.012
…	…	GJ 3380	J06024+498	M5.0 V	06:02:29.31	+49:51:42.6	…	…	…	…	45.19	852.65	21.41 ± 0.11	0.134 ± 0.009
…	…	LP 57-46	J06024+663	M4.5 V	06:02:26.51	+66:20:32.3	…	…	…	…	45.13	582.95	55.95 ± 0.23	0.250 ± 0.013
…	…	PM J06025+3707	J06025+371	M1.0 V	06:02:35.46	+37:07:36.2	…	…	…	…	83.97	138.30	578.82 ± 3.73	0.547 ± 0.028
…	…	Wolf 261	J06034+478	M4.2 V	06:03:29.48	+47:48:06.0	…	…	…	…	66.44	562.68	125.47 ± 0.59	0.361 ± 0.016
…	…	1R060335.0+153132	J06035+155	M0.0 V	06:03:34.74	+15:31:30.4	…	…	…	…	87.53	68.32	1903.04 ± 77.82	0.815 ± 0.025
…	…	1R060334.8+165128	J06035+168	M4.0 V	06:03:34.49	+16:51:45.4	…	…	…	…	87.35	93.78	124.65 ± 28.81	0.359 ± 0.047
…	…	Ross 60	J06039+261	M3.0 V	06:03:54.54	+26:08:46.0	…	…	…	…	87.97	640.80	85.01 ± 0.42	0.274 ± 0.013
…	…	LP 86-173	J06054+608	M4.5 V	06:05:30.04	+60:49:09.8	…	…	…	…	47.26	840.47	80.39 ± 0.41	0.249 ± 0.012
…	…	PM J06066+4633A	J06066+465	M3.0 V	06:06:37.78	+46:33:47.0	AB	A	…	…	29.07	67.55	…	0.398 ± 0.032
06066+4634	KPP3658	PM J06066+4633B	…	M3.5 V	06:06:37.77	+46:33:45.2	…	B	1.790	182.3	81.50	84.00	…	0.331 ± 0.034
…	…	Ross 70	J06071+335	M2.0 V	06:07:11.91	+33:32:30.9	…	…	…	…	81.46	421.94	371.91 ± 2.20	0.490 ± 0.030
…	…	1R060732.5+471154	J06075+472	M4.5 V	06:07:31.91	+47:12:23.3	…	…	…	…	97.60	192.04	136.35 ± 0.74	0.377 ± 0.016
…	…	HD 291290	J06097+001	M0.0 V	06:09:46.30	+00:09:30.8	…	…	…	…	44.56	192.85	1002.68 ± 6.20	0.693 ± 0.026
…	…	PM J06102+2234	J06102+225	M4.0 V	06:10:17.81	+22:34:17.2	A+BC	A	…	…	172.68	158.78	121.97 ± 0.61	0.355 ± 0.015
…	…	LP 362-121	J06103+225	M5.0 V	06:10:22.52	+22:34:18.1	…	B	65.155	89.2	77.08	166.63	…	0.175 ± 0.041
06104+2234	LAW 14	G3- 3425067888342287616	…	…	06:10:22.50	+22:34:17.9	…	C	64.941	89.4	…	…	…	…

Table D.2: Complete sample with the description of multiple systems (continued).

WDS id	WDS disc	Name	Karmn	Spectral type	α (2016.0)	δ (2016.0)	System	Component	ρ [arcsec]	θ [deg]	ϖ [mas]	$\mu_{\rm total}$ [mas a^{-1}]	$\mathcal{L}$ [$10^{-4}\,\mathcal{L}_\odot$]	$\mathcal{M}$ [$\mathcal{M}_\odot$]
…	…	LSPM J0610+7212	J06103+722	M2.5 V	06:10:18.09	+72:11:58.0	…	…	…	…	46.40	160.32	290.05 ± 1.13	0.494 ± 0.019
…	…	GJ 226	J06103+821	M2.0 V	06:10:20.24	+82:06:02.9	…	…	…	…	35.10	1337.19	239.14 ± 1.04	0.406 ± 0.011
…	…	TYC 135-239-1	J06105+024	M0.0 V	06:10:31.41	+02:25:30.3	…	…	…	…	35.10	62.81	1178.64 ± 64.36	0.712 ± 0.027
06106-2152	NAJ 1	HD 42581	J06105-218	M0.5 V	06:10:34.46	-21:52:04.2	(AB)	AB	4.891	179.7	43.25	731.87	545.28 ± 13.88	0.563 ± 0.028
…	…	Wolf 1058	J06107+259	M1.5 V	06:10:46.51	+25:55:53.3	…	…	…	…	32.56	594.86	569.45 ± 7.01	0.561 ± 0.028
06109+1020	KAM1	Ross 79	J06109+103	M2.5 V	06:10:54.88	+10:18:50.6	(AB)	AB	1.157	355.9	56.93	934.18	…	0.454 ± 0.032
…	…	GJ 3388	J06140+516	M3.5 V	06:14:01.72	+51:40:06.5	…	…	…	…	38.56	386.61	86.95 ± 0.37	0.277 ± 0.013
…	…	G 106-35	J06145+025	M3.0 V	06:14:34.76	+02:30:19.7	…	…	…	…	44.68	493.68	193.70 ± 1.51	0.425 ± 0.017
06173+0506	CAT 1	HD 43587	…	G0 V	06:17:15.90	+05:06:02.6	(AB)+(CD)	AB(1)	0.840	70.9	214.04	269.29	…	1.300 ± 0.000
06173+0506	PRV 3	GJ 231.1 B	J06171+051	M3.5 V	06:17:10.42	+05:07:05.3	…	CD	103.189	307.4	33.04	261.65	…	0.300 ± 0.035
…	…	LP 779-34	J06151-164	M4.0 V	06:15:11.90	-16:26:21.4	…	…	…	…	24.71	379.97	46.90 ± 0.23	0.211 ± 0.011
…	…	TYC 4525-194-1	J06171+751	M2.0 Ve	06:18:07.08	+75:06:04.3	Aabc	Aabc(3?)	…	…	52.11	77.87	…	…
…	…	LSPM J0617+8353	J06171+838	M3.5 V	06:17:04.81	+83:53:32.5	…	…	…	…	24.82	188.78	157.08 ± 1.90	0.336 ± 0.014
…	…	G 103-29	J06185+250	M4.0 V	06:18:34.83	+25:03:00.6	…	…	…	…	58.06	324.78	172.94 ± 0.82	0.401 ± 0.017
…	…	Ross 417	J06193-066	M3.0 V	06:19:20.74	-06:39:32.1	…	…	…	…	47.73	625.97	92.86 ± 0.54	0.287 ± 0.013
…	…	TYC 743-1836-1	J06194+139	M0.5 V	06:19:29.61	+13:57:02.3	…	…	…	…	40.54	115.03	768.13 ± 2.94	0.636 ± 0.027
…	…	GJ 3391	J06212+442	M2.0 Ve	06:21:13.26	+44:14:26.7	AB	A	…	…	27.78	294.38	…	0.571 ± 0.028
06212+4415	CRC 50	G3- 962141157559432064	…	M5.0 V	06:21:13.21	+44:14:25.5	…	B	1.334	203.2	27.97	288.78	…	0.173 ± 0.040
…	…	LP 420-5	J06216+163	M1.0 V	06:21:36.85	+16:18:33.8	A+B	A	…	…	62.84	281.57	355.02 ± 2.85	0.487 ± 0.018
06215+1618	LDS894	LP 420-6	J06217+163	M2.5 V	06:21:44.17	+16:19:19.9	…	B	115.018	66.4	32.63	283.64	203.11 ± 1.08	0.385 ± 0.016
…	…	GJ 2049	J06218-227	M1 Vk	06:21:53.08	-22:43:19.7	…	…	…	…	60.71	687.88	893.70 ± 4.81	0.651 ± 0.027
…	…	TYC 2425-1286-1	J06223+334	M1.0 V	06:22:20.65	+33:26:54.6	…	…	…	…	74.14	113.71	1721.47 ± 26.29	0.761 ± 0.025
…	…	LP 720-10	J06236-096	M3.5 V	06:23:38.41	-09:38:51.5	AB	A	…	…	74.21	62.21	…	0.299 ± 0.035
06236-0938	JNN 270	LP 720-10 B	…	M8.0 V	06:23:38.29	-09:38:51.4	…	B	1.836	273.0	192.01	63.64	…	0.100 ± 0.050
…	…	TYC 141-24-1	J06237+020	M1.5 V	06:23:46.49	+05:02:40.1	…	…	…	…	50.41	78.91	624.56 ± 3.30	0.581 ± 0.028
06239+4540	RAO 210	LP 160-22	J06238+456	M5.0 V	06:23:51.20	+45:40:00.0	(AB)	AB	0.602	273.4	50.39	282.93	…	0.167 ± 0.041
…	…	Ross 64	J06246+234	M4.0 V	06:24:41.93	+23:25:50.8	…	…	…	…	129.30	749.61	34.45 ± 0.23	0.171 ± 0.009
…	…	GJ 3393	J06258+561	M4.0 V	06:25:53.21	+56:10:16.9	…	…	…	…	53.27	516.23	45.39 ± 0.20	0.207 ± 0.011
…	…	1R062614.2+234942	J06262+238	M1.5 Ve	06:26:14.52	+23:49:36.4	…	…	…	…	66.52	136.66	431.13 ± 3.02	0.522 ± 0.029
…	…	Ross 603A	J06277+093	M2.0 V	06:27:43.80	+09:23:51.3	AB	A	…	…	104.96	245.06	…	0.456 ± 0.030
06277+0924	CRC 51	Ross 603B	…	M3.5 V	06:27:43.74	+09:23:50.5	…	B	1.170	221.8	52.89	264.74	…	0.327 ± 0.034
…	…	V577Mon	J06293-028	M4.5 V	06:29:24.18	-02:49:01.9	AB	A	…	…	32.62	1098.83	…	0.230 ± 0.037
06293-0248	B2601	Ross 614 B	…	M4.5 V	06:29:24.19	-02:49:01.7	…	B	0.313	48.6	38.05	1098.83	…	0.228 ± 0.037
…	…	G 108-4	J06298-027	M4.0 V	06:29:50.47	-02:47:49.0	Aab	Aab(2)	…	…	44.36	264.66	…	…
…	…	PM J06306+4539	J06306+456	M1.0 V	06:30:37.39	+45:39:23.0	…	…	…	…	21.63	131.61	363.81 ± 1.42	0.466 ± 0.017
…	…	PM J06307+3947	J06307+397	M2.0 V	06:30:47.39	+39:47:38.5	…	…	…	…	43.10	129.54	170.51 ± 0.61	0.351 ± 0.015
…	…	GJ 3395	J06310+500	M0.8 V	06:31:00.97	+50:02:45.5	…	…	…	…	44.93	201.46	471.63 ± 1.90	0.537 ± 0.029
…	…	GJ 3396	J06318+414	M5.84	06:31:50.73	+41:29:42.2	…	…	…	…	61.43	208.66	131.98 ± 0.58	0.357 ± 0.070
…	…	TYC 2928-1568-1	J06322+378	M1.5 V	06:32:14.91	+37:48:10.6	…	…	…	…	30.33	160.15	888.61 ± 25.23	0.636 ± 0.027
…	…	PM J06323-0943	J06323-097	M4.5 V	06:32:20.28	-09:43:29.9	…	…	…	…	30.32	56.94	103.08 ± 2.55	0.325 ± 0.015

Table D.2: Complete sample with the description of multiple systems (continued).

WDS id	WDS disc	Name	Karmn	Spectral type	α (2016.0)	δ (2016.0)	System	Component	ρ [arcsec]	θ [deg]	ϖ [mas]	$\mu_{\rm total}$ [mas a^{-1}]	$\mathcal{L}$ [$10^{-4}\,\mathcal{L}_\odot$]	$\mathcal{M}$ [$\mathcal{M}_\odot$]
…	…	LP 57-192	J06325+641	M4.0 V	06:32:31.27	+64:06:12.2	…	…	…	…	32.58	560.21	165.63 ± 0.81	0.418 ± 0.017
…	…	G 103-41	J06345+315	M3.5 V	06:34:33.48	+31:30:05.1	…	…	…	…	35.44	192.39	175.03 ± 0.69	0.403 ± 0.017
06354-0403	JNN271	1R063531.2-040314	J06354-040	M5.5 V	06:35:29.75	-04:03:17.2	(AB)	AB	0.043	165.0	31.96	121.86	…	0.186 ± 0.039
…	…	GJ 3398	J06361+116	M5.0 V	06:36:06.16	+11:36:49.5	…	…	…	…	34.90	876.52	52.60 ± 0.23	0.225 ± 0.012
…	…	LP 420-4	J06361+201	M2.5 V	06:36:12.05	+20:08:10.3	…	…	…	…	43.90	236.63	164.69 ± 0.67	0.366 ± 0.015
…	…	HD 260655	J06371+175	M0.0 V	06:37:09.94	+17:33:58.7	…	…	…	…	…	835.76	364.95 ± 1.58	0.440 ± 0.011
…	…	LP 780-32	J06396-210	dM4.0	06:39:37.20	-21:01:32.4	AB	A	…	…	31.67	225.54	136.81 ± 4.35	0.326 ± 0.013
…	…	G3- 2926756741750933120	…	M4.0 V	06:39:37.22	-21:01:31.9	…	B*	0.556	35.1	105.69	146.66	…	0.266 ± 0.036
06401+2835	CRC 52	GJ 3399	J06400+285	M2.5 V	06:40:05.54	+28:35:10.5	(AB)	AB	0.269	91.3	25.93	245.94	…	0.476 ± 0.030
…	…	LP 780-23	J06401-164	M2.5 V	06:40:08.72	-16:27:21.5	AB	A	…	…	173.57	319.03	…	…
…	…	LP 780-23 B	…	…	06:40:08.72	-16:27:21.7	…	B*	0.199	187.9	37.23	…	…	…
…	…	Wolf 289	J06414+157	M4.0 V	06:41:28.23	+15:45:42.6	…	…	…	…	91.65	318.30	186.02 ± 0.83	0.416 ± 0.017
…	…	GJ 3404	J06421+035	M3.0 V	06:42:11.24	+03:34:48.5	A+B	A	…	…	67.60	261.94	182.11 ± 0.93	0.369 ± 0.012
06423+0334	GIC 65	GJ 3405	J06422+035	M4.0 V	06:42:13.39	+03:35:26.8	…	B	50.055	40.0	37.87	257.50	71.60 ± 0.37	0.267 ± 0.013
…	…	G 110-14	J06435+166	M4.5 V	06:43:34.53	+16:41:35.5	…	…	…	…	51.62	208.68	93.06 ± 2.89	0.329 ± 0.016
…	…	GJ 3406A	J06438+511	M2.5 V	06:43:49.95	+51:08:06.0	AB	A	…	…	52.14	874.58	…	0.359 ± 0.033
06438+5108	LDS6200	GJ 3406B	…	M4.5 V	06:43:49.77	+51:08:05.8	…	B	1.700	265.8	77.54	916.52	…	0.259 ± 0.036
06448+7153	BAG 22	GJ 2050	J06447+718	M0.5 V	06:44:45.25	+71:53:06.7	(AB)	AB	0.630	64.1	31.69	558.83	…	0.560 ± 0.028
…	…	HD 263175	…	K3 V	06:46:04.47	+32:33:22.0	A+B	A	…	…	47.29	467.06	2218.02 ± 7.94	0.780 ± 0.117
06461+3233	LDS6201	HD 263175B	J06461+325	M1.0 V	06:46:06.88	+32:33:16.6	…	B	30.855	100.1	28.96	472.87	278.81 ± 1.20	0.429 ± 0.016
…	…	1R064645.7+155739	J06467+159	M1.0 Ve	06:46:45.62	+15:57:41.8	…	…	…	…	59.48	102.50	541.77 ± 2.45	0.565 ± 0.028
…	…	G 108-27	J06474+054	M4.0 V	06:47:27.57	+05:24:23.3	…	…	…	…	39.95	308.45	175.68 ± 0.87	0.404 ± 0.017
…	…	LP 121-58	J06486+532	M1.5 V	06:48:38.72	+53:17:24.3	…	…	…	…	26.93	357.19	641.38 ± 3.40	0.584 ± 0.028
…	…	1R064855.9+210754	J06489+211	M2.5 V	06:48:55.18	+21:08:02.8	…	…	…	…	27.11	72.41	330.27 ± 1.71	0.461 ± 0.030
…	…	GJ 1092	J06490+371	M4.0 V	06:49:05.73	+37:06:25.0	…	…	…	…	43.05	1603.32	43.79 ± 0.16	0.203 ± 0.011
…	…	LP 661-2	J06509-091	M3.5 V	06:50:59.37	-09:10:59.3	…	…	…	…	43.06	584.19	151.38 ± 1.27	0.373 ± 0.016
06523-0510	WSI 125	HD 50281	…	K3.5 V	06:52:17.47	-05:10:25.4	(AB)+C	AB	0.175	149.6	37.07	543.70	…	0.745 ± 0.112
06523-0510	WNO 17	HD 50281B	J06523-051	M2.0 V+	06:52:17.42	-05:11:24.3	…	C	58.833	180.6	17.17	576.48	…	0.445 ± 0.031
…	…	GJ 3413	J06524+182	M3.5 V	06:52:24.45	+18:17:06.9	…	…	…	…	40.77	175.88	169.69 ± 1.04	0.397 ± 0.016
06541+6052	HEI 334	GJ 3412	J06540+608	M3.0 V	06:54:05.43	+60:52:02.4	(AB)	AB(1)	0.351	253.1	40.35	1093.13	…	…
…	…	HD 265866	J06548+332	M3.0 V	06:54:48.03	+33:15:59.1	…	…	…	…	41.83	828.58	163.26 ± 0.94	0.342 ± 0.012
…	…	TYC 756-1685-1	J06564+121	M1.0 V	06:56:25.84	+12:07:31.4	…	…	…	…	40.34	98.10	1366.51 ± 39.35	0.715 ± 0.026
06565+4004	KUI27	GJ 3415	…	K4.5 V	06:56:28.28	+40:04:20.6	A+B	A	37.808	6.8	48.95	452.03	1944.33 ± 7.69	0.730 ± 0.110
…	…	GJ 3416	J06564+400	M1.0 V	06:56:28.64	+40:04:58.3	…	B	37.895	6.2	117.73	446.75	642.93 ± 2.58	0.593 ± 0.028
…	…	LP 34-110	J06564+759	M1.0 V	06:53:24.30	+72:55:09.3	…	…	…	…	50.45	346.36	1170.26 ± 17.73	0.693 ± 0.026
…	…	G 107-36	J06565+440	M4.5 V	06:56:31.24	+44:01:45.0	…	…	…	…	36.34	708.19	101.14 ± 0.51	0.321 ± 0.014
…	…	1R065728.1+740529	J06574+740	M4.0 Ve	06:57:25.77	+74:05:26.1	…	…	…	…	43.22	96.24	…	…
…	…	GJ 3417 A	J06579+623	M6.0 V	06:57:57.83	+62:19:11.0	AB	A	…	…	43.45	614.04	…	0.207 ± 0.038
06579+6220	HEN 2	GJ 3417 B	…	M5.0 V	06:57:57.66	+62:19:10.5	…	B	1.284	246.9	242.97	573.10	…	0.129 ± 0.044
…	…	G 192-59	J06582+511	M2.0 V	06:58:12.70	+51:08:32.4	…	…	…	…	242.97	364.19	441.91 ± 1.94	0.517 ± 0.029

Table D.2: Complete sample with the description of multiple systems (continued).

WDS id	WDS disc	Name	Karmn	Spectral type	α (2016.0)	δ (2016.0)	System	Component	ρ [arcsec]	θ [deg]	ϖ [mas]	$\mu_{\rm total}$ [mas a^{-1}]	$\mathcal{L}$ [$10^{-4}\,\mathcal{L}_\odot$]	$\mathcal{M}$ [$\mathcal{M}_\odot$]
…	…	GJ 1093	J06594+193	M5.0 Ve	06:59:29.84	+19:20:41.5	…	…	…	…	24.17	1275.43	16.35 ± 0.09	0.120 ± 0.009
…	…	G 88-2	J06594+195	M3.0 V	06:59:28.65	+19:30:30.4	…	…	…	…	35.23	269.52	158.26 ± 0.73	0.382 ± 0.016
…	…	PM J06596+0545	J06596+057	M2.5 Ve	06:59:41.55	+05:45:38.9	…	…	…	…	39.37	70.32	344.17 ± 2.14	0.508 ± 0.019
…	…	1R070005.1-190115	J07001-190	M5.0 V	07:00:07.00	-19:01:25.1	Aab	Aab(2)	…	…	46.17	170.88	…	…
…	…	PM J07009-0221	J07009-023	M3.0 V	07:00:59.74	-02:21:32.2	…	…	…	…	48.58	68.30	226.16 ± 1.15	0.433 ± 0.017
…	…	PM J07012+0052	J07012+008	M2.5 V	07:01:15.54	+00:52:40.4	…	…	…	…	35.91	104.42	476.53 ± 10.10	0.522 ± 0.029
…	…	GJ 3423	J07033+346	M4.0 Ve	07:03:23.09	+34:41:53.6	…	…	…	…	30.18	151.83	74.58 ± 0.28	0.253 ± 0.010
…	…	LP 16-379	J07034+767	M3.5 V	07:03:29.98	+76:46:21.9	…	…	…	…	38.99	233.75	122.79 ± 0.57	0.334 ± 0.015
07039+5242	BEU 8	GJ 3421	J07039+527	M5.0 V	07:03:56.92	+52:41:51.8	(AB)	AB	0.165	335.5	31.64	1143.04	…	0.202 ± 0.039
07043-1031	BEU 9	Ross 54	J07042-105	M3.5 V	07:04:17.55	-10:30:44.6	(AB)	AB(2)	0.108	289.7	40.67	826.29	…	…
…	…	GJ 258	J07044+682	M3.0 V	07:04:26.94	+68:17:20.5	…	…	…	…	52.35	349.83	217.05 ± 1.10	0.392 ± 0.011
…	…	Ross 874	J07047+249	M1.5 V	07:04:49.44	+24:59:50.6	…	…	…	…	79.16	326.17	430.16 ± 1.58	0.518 ± 0.029
…	…	1R070511.2-100801	J07051-101	M5.0 V	07:05:12.10	-10:07:51.6	…	…	…	…	56.64	146.49	31.70 ± 0.14	0.182 ± 0.011
…	…	G 108-52	J07052+084	M2.0 V	07:05:12.39	+08:25:45.7	…	…	…	…	39.56	425.52	172.20 ± 0.98	0.353 ± 0.015
…	…	GJ 3426	J07076+486	M4.3 V	07:07:37.70	+48:41:08.6	…	…	…	…	100.02	305.76	36.29 ± 0.12	0.183 ± 0.011
…	…	GJ 3425	J07078+672	M1.5 V	07:07:49.68	+67:12:03.7	…	…	…	…	63.74	280.71	403.42 ± 3.41	0.509 ± 0.029
…	…	LP 840-16	J07081-228	M2.0 V	07:08:06.53	-22:48:51.0	…	…	…	…	65.31	471.01	259.09 ± 1.15	0.413 ± 0.016
…	…	GJ 3429	J07086+307	M0.5 V	07:08:39.72	+30:42:51.6	…	…	…	…	43.89	197.24	549.10 ± 3.55	0.569 ± 0.028
…	…	GJ 3427	J07095+698	M3.0 V	07:09:31.85	+69:50:53.1	…	…	…	…	…	324.11	238.73 ± 1.05	0.446 ± 0.018
…	…	QYAur	J07100+385	M4.5 V	07:10:01.23	+38:31:31.0	Aab	Aab(2)	…	…	38.76	1041.98	…	0.399 ± 0.001
…	…	GJ 3430	J07102+376	M4.0 V	07:10:13.32	+37:40:05.9	A+B	A	…	…	…	350.22	53.23 ± 1.28	0.226 ± 0.012
07103+3739	GIC 69	GJ 3431	…	DQ8	07:10:14.04	+37:40:15.0	…	B	12.472	43.1	33.46	357.87	…	0.500 ± 0.100
…	…	1R071032.6-084232	J07105-087	M3.5 V	07:10:31.37	-08:42:46.7	…	…	…	…	65.98	129.38	131.45 ± 0.72	0.346 ± 0.015
…	…	LP 206-11	J07111+434	M5.5 V	07:11:11.97	+43:29:49.0	AB	A	…	…	66.06	675.37	…	0.120 ± 0.045
07112+4330	MTG1	LP 206-11 B	…	…	07:11:12.02	+43:29:49.3	…	B	0.634	65.5	41.99	…	…	…
…	…	TYC 4530-1414-1	J07119+773	M1.5 V	07:11:57.13	+77:21:57.4	Aab	Aab(1)	…	…	40.33	88.25	…	…
…	…	GJ 3432	J07121+522	M1.0 V	07:12:11.14	+52:16:20.4	…	…	…	…	53.03	295.08	594.22 ± 2.57	0.574 ± 0.028
…	…	1R071259.5+354655	J07129+357	M2.5 Ve	07:12:59.62	+35:47:03.1	…	…	…	…	52.90	66.50	243.95 ± 1.05	0.451 ± 0.018
…	…	G 193-39	J07140+507	M0.5 V	07:14:04.29	+50:43:28.9	AB	A	…	…	46.49	299.13	…	0.566 ± 0.028
07141+5044	KPP3199	G 193-39B	…	M5.0 V	07:14:04.09	+50:43:28.4	…	B	1.892	256.2	38.83	301.87	…	0.189 ± 0.039
07163+2709	BEU 10	GJ 268.3	J07163+271	M2.5 V	07:16:19.73	+27:08:29.9	(AB)	AB(2)	0.060	154.5	66.91	201.19	…	0.727 ± 0.012
…	…	GJ 1096	J07163+331	M5.0 V	07:16:17.89	+33:09:03.4	…	…	…	…	38.87	448.75	39.39 ± 0.20	0.206 ± 0.011
…	…	PM J07172-0501	J07172-050	M3.5 V	07:17:17.54	-05:01:09.8	…	…	…	…	44.69	574.06	49.73 ± 0.35	0.218 ± 0.011
…	…	GJ 3437	J07174+195	M3.2 V	07:17:29.57	+19:34:12.4	…	…	…	…	36.59	417.61	162.91 ± 0.70	0.364 ± 0.015
07181+3916	RAO 216	Ross 987	J07181+392	M0.0 V	07:18:07.89	+39:16:27.4	(AB)	AB	0.107	67.3	25.87	244.37	…	0.524 ± 0.029
…	…	PM J07182+1342	J07182+137	M3.5 V	07:18:12.86	+13:42:16.2	…	…	…	…	28.59	44.09	165.89 ± 0.75	0.392 ± 0.016
…	…	GJ 270	J07195+328	M0.0 V	07:19:31.79	+32:49:42.8	…	…	…	…	69.20	536.19	745.86 ± 3.85	0.630 ± 0.027
…	…	TYC 4618-116-1	J07199+840	M2.5 V	07:19:57.65	+84:04:36.8	…	…	…	…	41.00	89.65	112.02 ± 0.62	0.298 ± 0.013
07200-0847	BUG 17	Scholz's star	J07200-087	M9.5+T5	07:20:03.21	-08:46:51.9	(AB)	AB	0.381	63.5	114.35	125.25	…	0.116 ± 0.055
…	…	TYC 178-2187-1	J07212+005	M0.5 V	07:31:12.97	+00:33:13.8	…	…	…	…	114.29	100.59	658.56 ± 4.71	0.607 ± 0.027

Table D.2: Complete sample with the description of multiple systems (continued).

WDS id	WDS disc	Name	Karmn	Spectral type	α (2016.0)	δ (2016.0)	System	Component	ρ [arcsec]	θ [deg]	ϖ [mas]	$\mu_{\rm total}$ [mas a^{-1}]	$\mathcal{L}$ [$10^{-4}\,\mathcal{L}_\odot$]	$\mathcal{M}$ [$\mathcal{M}_\odot$]
…	…	GJ 3439	J07227+306	M4.0 V	07:22:41.50	+30:40:02.3	…	…	…	…	44.35	719.15	156.09 ± 0.87	0.379 ± 0.016
…	…	GJ 272	J07232+460	M0.5 V	07:23:14.71	+46:05:10.9	…	…	…	…	91.61	266.76	542.28 ± 2.73	0.558 ± 0.028
07274+0514	WDK 2	Luyten's Star	J07274+052	M3.5 V	07:27:25.11	+05:12:33.8	(AB)	AB	0.170	327.0	179.06	3735.42	108.89 ± 1.00	0.297 ± 0.012
…	…	Ross 878	J07274+220	M1.5 V	07:27:28.31	+22:02:35.6	…	…	…	…	27.43	298.23	477.33 ± 2.02	0.527 ± 0.029
…	…	GJ 3442	J07282-187	M4.5 V	07:28:13.09	-18:47:25.2	…	…	…	…	39.87	616.89	57.38 ± 1.07	0.236 ± 0.012
…	…	GJ 1097	J07287-032	M3.0 V	07:28:45.91	-03:18:05.9	…	…	…	…	39.93	902.58	187.98 ± 1.04	0.367 ± 0.011
07295+3556	JNN 57	1R072931.4+355607	J07295+359	M1.5 V	07:29:31.04	+35:55:58.5	(AB)+C	AB	0.074	25.9	19.55	122.54	…	0.654 ± 0.027
07295+3556	UC 1586	2M07293670+3554531	…	M3.0 V	07:29:36.67	+35:54:51.3	…	C	95.884	134.5	37.92	108.79	…	0.385 ± 0.032
…	…	GJ 275.2 A	J07307+481	M4.0 V	07:30:42.46	+48:11:38.2	A+BC	A	0.054		…	1287.99	…	0.207 ± 0.038
07307+4813	GIC 75	GJ 275.2 B	…	DA	07:30:46.99	+48:10:05.7	…	B	103.053	153.9	87.03	1281.73	…	0.500 ± 0.100
07307+4813	WNO 49	G 107-70B	…	DA	07:30:46.96	+48:10:06.3	…	C	102.385	153.9	87.24	…	…	0.500 ± 0.100
…	…	1R073138.4+455718	…	M3.0 V	07:31:38.47	+45:57:15.8	Aab+B+C	Aab	…	…	197.96	93.78	…	…
…	…	1R073101.9+460030	J07310+460	M4.0 V	07:31:01.27	+46:00:24.8	…	B*	431.391	296.0	30.20	101.75	438.36 ± 4.02	0.470 ± 0.030
…	…	G3- 975312928903090560	…	M4.5 V	07:31:09.03	+45:56:55.6	…	C*	307.796	266.3	128.99	100.74	65.93 ± 0.49	0.273 ± 0.013
…	…	LynA	J07319+362S	M2.5 V	07:31:57.38	+36:13:06.2	A+BC	A	…	…	49.45	351.29	388.95 ± 2.56	0.468 ± 0.030
07319+3613	LDS6206	BLLyn	J07319+362N	M3.5 V	07:31:56.97	+36:13:43.2	…	B	37.364	352.4	34.38	370.92	187.91 ± 0.75	0.397 ± 0.010
07319+3613	BEU 11	LynB	…	M5.0 V	07:31:57.36	+36:13:04.6	…	C	1.560	190.0	33.53	347.61	…	0.205 ± 0.038
…	…	GJ 3445	J07319+392	M2.48 V	07:31:56.74	+39:13:34.0	…	…	…	…	35.44	293.58	471.99 ± 13.25	0.496 ± 0.030
…	…	GJ 3447	J07320+173E	M0.0 V	07:32:02.63	+17:19:07.0	(AB)+C	A	…	…	31.25	285.23	…	0.620 ± 0.027
07320+1720	HDS1065	G 88-36B	…	…	…	…	…	B	5.090	115.8	75.35	285.75	…	…
07320+1720	WOR 27	GJ 3448	J07320+173W	M3.2 V	07:32:01.87	+17:19:09.4	…	C	11.127	282.5	59.31	281.89	159.27 ± 0.87	0.360 ± 0.015
…	…	GJ 9235	J07320+686	M1.5 V	07:32:01.51	+68:37:13.6	…	…	…	…	110.83	210.11	732.07 ± 3.32	0.608 ± 0.027
…	…	G 88-37	J07325+248	M3.0 V	07:32:30.71	+24:53:42.4	…	…	…	…	63.55	231.15	280.93 ± 1.15	0.486 ± 0.019
…	…	GJ 1099	J07342+009	M2.5 V	07:34:17.57	+00:58:59.7	…	…	…	…	61.14	599.58	180.91 ± 0.86	0.385 ± 0.016
…	…	GJ 9236	J07344+629	M0.5 V	07:34:26.27	+62:56:27.6	…	…	…	…	42.20	507.61	257.85 ± 0.95	0.388 ± 0.015
…	…	GJ 3453	J07346+223	M1.0 V	07:34:39.31	+22:20:13.9	…	…	…	…	58.49	199.08	496.87 ± 2.77	0.546 ± 0.028
07346+3153	STF1110	Castor	…	A1 V	07:34:35.95	+31:53:18.6	(AabBab)+Cab	AabBab(2+2)	5.380	52.6	33.48	240.28	…	4.933 ± 0.023
07346+3153	STF1110	Castor C	J07346+318	M0.5 V	07:34:37.19	+31:52:08.6	…	Cab(DEB)	71.756	167.2	293.60	223.55	…	1.19840 ± 0.007
…	…	TYC 777-141-1	J07349+147	M3.0 Ve	07:34:56.25	+14:45:52.5	AB	A	…	…	51.60	108.94	…	0.446 ± 0.031
07349+1446	CRC 53	G3- 3165346543026736512	…	…	07:34:56.18	+14:45:52.9	…	B	1.018	291.7	94.22	109.05	…	…
…	…	GJ 3452	J07353+548	M2.5 V	07:35:21.67	+54:50:59.2	…	…	…	…	52.72	114.33	196.34 ± 0.93	0.364 ± 0.011
…	…	LP 162-39	J07354+482	M1.0 V	07:35:26.96	+48:14:33.0	…	…	…	…	59.87	222.98	532.91 ± 2.85	0.558 ± 0.028
…	…	LP 17-66	J07359+785	M3.0 V	07:35:57.31	+78:32:49.7	…	…	…	…	38.14	238.75	194.03 ± 0.74	0.426 ± 0.017
…	…	V869Mon	…	K3 V	07:39:59.40	-03:35:55.5	A+B+Cab	A	…	…	42.33	286.81	…	0.787 ± 0.118
07400-0336	BGH 3	HD 61606B	…	K7 V	07:40:02.97	-03:36:17.8	…	B	57.903	112.7	165.21	294.21	1009.21 ± 4.63	0.640 ± 0.096
…	…	GJ 282 C	J07361-031	M1.0 V	07:36:07.15	-03:06:43.4	…	Cab(1)	3894.176	296.7	59.06	302.35	…	0.742 ± 0.058
07364+0705	HEN3	GJ 3454	J07364+070	M4.5 V	07:36:25.37	+07:04:38.2	(AB)	AB	0.722	279.0	44.60	383.93	…	0.176 ± 0.040
…	…	PM J07365-0039	J07365-006	M3.5 V	07:36:30.27	-00:39:37.3	…	…	…	…	41.03	107.56	190.81 ± 2.05	0.422 ± 0.017
…	…	G 111-20	J07366+440	M3.5 V	07:36:39.13	+44:04:43.5	A+B	A	…	…	51.72	348.25	…	0.432 ± 0.031
07367+4405	NSN 578	G 111-20B	…	M6.5 V	07:36:38.87	+44:04:46.5	…	B	4.122	317.5	76.40	349.53	…	0.105 ± 0.047

Table D.2: Complete sample with the description of multiple systems (continued).

WDS id	WDS disc	Name	Karmn	Spectral type	α (2016.0)	δ (2016.0)	System	Component	ρ [arcsec]	θ [deg]	ϖ [mas]	$\mu_{\rm total}$ [mas a^{-1}]	$\mathcal{L}$ [10^{-4} $\mathcal{L}_\odot$]	$\mathcal{M}$ [$\mathcal{M}_\odot$]
…	…	TYC 2461-826-1	J07383+344	M0.0 V	07:38:19.92	+34:27:00.6	…	…	…	…	…	121.21	991.07 ± 17.24	0.689 ± 0.026
…	…	1R073829.3+240014	J07384+240	M3.5 V	07:38:29.32	+24:00:07.1	…	…	…	…	44.68	180.35	142.06 ± 0.66	0.361 ± 0.015
…	…	GJ 3459	J07386-212	dM3.0	07:38:41.48	-21:13:36.1	…	…	…	…	39.62	659.14	113.53 ± 0.55	0.284 ± 0.010
…	…	Ross 880	J07393+021	M0.0 V	07:39:22.88	+02:10:57.3	…	…	…	…	42.32	286.45	775.50 ± 4.16	0.638 ± 0.027
…	…	GJ 3457	J07395+334	M2.0 V	07:39:35.62	+33:27:42.6	A+B	A	…	…	35.15	236.68	818.81 ± 17.83	0.610 ± 0.027
07397+3328	LDS3755	GJ 3458	…	M6.0 V	07:39:36.51	+33:27:49.5	…	B	13.099	58.2	35.26	237.05	11.91 ± 0.17	0.155 ± 0.011
…	…	GJ 283 A	…	DZQA6	07:40:22.06	-17:24:57.8	A+B	A	…	…	83.88	1261.34	…	0.500 ± 0.100
07402-1724	LUY5693	GJ 283 B	J07403-174	M6.5 Ve	07:40:20.66	-17:24:54.5	…	B	20.338	99.5	65.48	1270.98	8.29 ± 0.04	0.107 ± 0.047
…	…	GJ 3461	J07418+050	M3.0 V	07:41:52.56	+05:02:23.1	AabB	Aab(EB)	…	…	32.35	263.05	…	…
07419+0502	CFN 5	G 50-1B	…	…	07:41:52.61	+05:02:22.4	…	B	1.014	130.9	89.82	…	…	…
…	…	LP 162-55	J07421+500	M2.5 V	07:42:10.07	+50:04:28.5	…	…	…	…	47.73	195.83	257.35 ± 5.89	0.464 ± 0.019
…	…	GJ 3462	J07431+181	M1.5 V	07:43:11.67	+18:10:34.8	…	…	…	…	71.32	472.06	938.46 ± 6.50	0.649 ± 0.027
…	…	YZCMi	J07446+035	M4.0 Ve	07:44:39.80	+03:33:01.7	…	…	…	…	40.18	565.33	111.34 ± 0.82	0.415 ± 0.031
…	…	G 193-65	J07467+574	M4.5 V	07:46:41.97	+57:26:49.5	…	…	…	…	54.87	234.80	96.31 ± 0.54	0.335 ± 0.015
…	…	LP 17-75	J07470+760	M4.0 V	07:47:06.48	+76:03:13.1	…	…	…	…	80.02	414.88	96.09 ± 0.41	0.313 ± 0.014
…	…	1R074714.1+502032	J07472+503	M4.0 Ve	07:47:13.84	+50:20:39.8	…	…	…	…	147.00	81.37	78.57 ± 0.36	0.271 ± 0.014
…	…	Wolf 1421	J07482+203	M1.5 V	07:48:18.04	+20:21:49.4	…	…	…	…	35.23	1756.92	187.13 ± 0.76	0.347 ± 0.014
…	…	GJ 3456	J07493+849	M3.0 V	07:49:17.72	+84:58:32.5	…	…	…	…	38.99	383.89	212.85 ± 1.06	0.420 ± 0.017
…	…	PM J07497-0320	J07497-033	M3.5 V	07:49:41.97	-03:20:34.9	…	…	…	…	58.90	171.22	117.19 ± 1.15	0.348 ± 0.015
…	…	GJ 3463	J07518+055	M5.0 V	07:51:51.86	+05:32:50.6	…	…	…	…	264.13	603.72	30.09 ± 0.13	0.177 ± 0.011
…	…	GJ 1103 A	J07519-000	M4.5 V	07:51:54.95	-00:00:24.4	…	…	…	…	49.34	801.43	46.94 ± 0.32	0.211 ± 0.011
…	…	LP 423-31	J07523+162	M6.0 V	07:52:24.13	+16:12:09.4	…	…	…	…	73.97	395.30	19.48 ± 0.12	0.174 ± 0.011
…	…	1R075434.3+083213	J07545+085	M2.5 V	07:54:33.90	+08:32:25.5	Aab	Aab(1)	…	…	145.62	213.07	…	…
…	…	GJ 3465	J07525+063	M3.0 V	07:52:33.63	+06:18:22.0	…	…	…	…	85.22	214.56	215.86 ± 1.17	0.450 ± 0.018
…	…	PM J07545-0941	J07545-096	M3.5 V	07:54:32.60	-09:41:47.9	AB	A	…	…	23.42	90.90	…	0.392 ± 0.032
07545-0942	CFN 6	PM J07545-0941B	…	…	07:54:32.66	-09:41:48.7	…	B	1.227	130.6	23.57	…	…	…
…	…	GJ 1101	J07558+833	M4.5: V	07:55:51.23	+83:22:55.4	…	…	…	…	88.72	666.30	74.17 ± 0.31	0.262 ± 0.013
…	…	GJ 3467	J07581+072	M5.0 V	07:58:08.74	+07:17:00.9	…	…	…	…	83.48	327.27	47.63 ± 0.31	0.213 ± 0.011
…	…	GJ 1105	J07582+413	M3.5 V	07:58:13.01	+41:18:02.3	…	…	…	…	…	721.00	87.32 ± 0.48	0.255 ± 0.010
…	…	LP 163-47	J07583+496	M4.0 V	07:58:23.26	+49:39:41.3	…	…	…	…	17.88	811.01	110.22 ± 0.59	0.336 ± 0.015
…	…	GJ 3468	J07585+155N	M4.5 V	07:58:30.88	+15:30:12.6	A+(BC)	A	…	…	18.14	139.95	139.97 ± 0.81	0.382 ± 0.016
07586+1530	LDS3768	GJ 3469 A	J07585+155S	M4.5 V	07:58:30.37	+15:29:58.8	…	B	15.708	208.1	18.39	143.68	…	0.225 ± 0.038
07586+1530	SKF2835	GJ 3469 B	…	M5.0 V	07:58:30.34	+15:29:57.8	…	C	16.815	207.9	83.38	136.71	…	0.190 ± 0.039
…	…	GJ 3470	J07590+153	M2.0 V	07:59:05.63	+15:23:28.3	…	…	…	…	83.40	194.26	391.79 ± 2.01	0.493 ± 0.030
…	…	1R075908.2+171957	J07591+173	M4.0 V	07:59:07.07	+17:19:46.8	…	…	…	…	83.52	97.01	…	…
…	…	TYC 1930-667-1	J08005+258	M2.0 V	08:00:34.87	+25:53:32.6	…	…	…	…	25.87	122.18	987.25 ± 8.40	0.650 ± 0.027
…	…	TYC 1926-794-1	J08017+237	M1.5 V	08:01:43.44	+23:42:25.3	…	…	…	…	37.05	186.08	640.27 ± 23.97	0.576 ± 0.028
…	…	GJ 3473	J08023+033	M4.0 V	08:02:22.45	+03:20:13.6	A+B	A	…	…	…	554.68	149.78 ± 0.72	0.343 ± 0.011
08024+0320	LDS5160	GJ 3474	…	M6.0 V	08:02:20.22	+03:19:37.4	…	B	49.260	222.8	34.13	551.81	11.52 ± 0.09	0.128 ± 0.010
…	…	LP 724-16	J08025-130	M2.5 V	08:02:33.09	-13:05:33.4	…	…	…	…	42.76	291.96	291.77 ± 11.59	0.466 ± 0.020

Table D.2: Complete sample with the description of multiple systems (continued).

WDS id	WDS disc	Name	Karmn	Spectral type	α (2016.0)	δ (2016.0)	System	Component	ρ [arcsec]	θ [deg]	ϖ [mas]	$\mu_{\rm total}$ [mas a^{-1}]	$\mathcal{L}$ [$10^{-4}\,\mathcal{L}_\odot$]	$\mathcal{M}$ [$\mathcal{M}_\odot$]
08032+2022	JNN 60	PM J08031+2022	J08031+203	M3.5 V	08:03:10.06	+20:22:14.3	(AB)	AB	0.206	17.8	36.89	110.90	…	0.455 ± 0.032
08033+5251	HDS1149	G 194-7	J08033+528	M1.5 V	08:03:20.18	+52:50:27.3	(AB)	AB	0.287	218.2	64.00	767.31	…	0.629 ± 0.045
08066+5554	CRC 54	GJ 3477	J08066+558	M2.0 V	08:06:36.75	+55:53:37.1	(AB)	AB	0.174	236.5	84.70	154.63	…	0.550 ± 0.029
…	…	GJ 3479	J08068+367	M3.0 V	08:06:48.21	+36:45:32.5	…	…	…	…	38.70	417.51	114.76 ± 0.55	0.322 ± 0.014
…	…	G 111-56	J08069+422	M4.0 V	08:06:54.99	+42:17:28.7	…	…	…	…	64.12	353.75	70.46 ± 0.32	0.264 ± 0.013
08082+2106	COU 91	GJ 3482	J08082+211	M3.0 V	08:08:12.85	+21:06:12.6	A+BC	A	…	…	66.31	463.21	999.07 ± 6.46	0.705 ± 0.026
08082+2106	CRC 55	GJ 3481	…	K7 Ve	08:08:13.29	+21:06:03.9	…	BC(2)	10.655	144.6	66.43	453.31	…	…
…	…	GJ 3480	J08083+585	M3.0 V	08:08:17.82	+58:31:08.4	…	…	…	…	61.37	185.60	105.26 ± 0.39	0.307 ± 0.014
08090+3249	BDT 2	FPCnc	…	K6 V	08:08:56.33	+32:49:08.3	(AB)+Cab	AB	0.207	69.6	61.80	203.10	…	…
08090+3249	DYR 1	FPCncB	J08089+328	M3.0 V	08:08:55.38	+32:49:01.4	…	Cab(2)	13.927	240.0	28.63	214.09	…	…
…	…	GJ 3484	J08095+219	M2.0 V	08:09:30.59	+21:54:16.2	…	…	…	…	78.16	326.02	306.03 ± 1.21	0.478 ± 0.018
…	…	PM J08103+0935	J08103+095	M2.5 V	08:10:20.65	+09:35:15.4	…	…	…	…	33.75	86.55	426.80 ± 2.74	0.505 ± 0.029
…	…	HD 68146	…	F6.5 V	08:10:39.55	-13:47:56.2	A+BC	A	…	…	38.67	257.61	…	1.232 ± 0.185
08107-1348	LDS204	HD 68146B	J08105-138	M2.5 V	08:10:34.02	-13:48:50.1	…	B	96.934	236.2	71.03	259.91	…	0.463 ± 0.030
08107-1348	JOD 4	G3- 5725122965265271680	…	M4.0 V	08:10:33.96	-13:48:49.9	…	C	97.537	236.6	70.99	245.49	…	0.274 ± 0.036
…	…	GJ 3485	J08108+039	M4.0 V	08:10:53.75	+03:58:28.2	…	…	…	…	70.27	358.58	142.46 ± 0.72	0.361 ± 0.015
…	…	G 194-14	J08117+531	M2.5 V	08:11:47.07	+53:11:48.4	…	…	…	…	116.60	334.28	359.61 ± 2.32	0.471 ± 0.030
…	…	Ross 619	J08119+087	M4.5 V	08:11:58.72	+08:45:01.4	…	…	…	…	36.37	5205.34	27.95 ± 0.17	0.153 ± 0.009
…	…	GJ 300	J08126-215	M3.5 V	08:12:40.90	-21:33:18.1	…	…	…	…	22.93	694.12	82.76 ± 0.41	0.260 ± 0.012
…	…	LP 311-8	J08158+346	M1.0 V	08:15:53.78	+31:36:35.8	…	…	…	…	23.17	214.62	1138.48 ± 17.87	0.693 ± 0.026
…	…	GJ 2066	J08161+013	M2.0 V	08:16:07.58	+01:18:10.2	…	…	…	…	26.56	381.04	278.67 ± 1.55	0.436 ± 0.012
…	…	LP 367-67	J08175+209	M2.5 V	08:17:31.31	+20:59:48.7	…	…	…	…	51.56	427.91	371.26 ± 2.93	0.484 ± 0.030
…	…	GJ 3491	J08178+311	M1.0 V	08:17:51.20	+31:07:49.4	…	…	…	…	95.66	229.91	493.50 ± 1.95	0.543 ± 0.029
…	…	PM J08202+0532	J08202+055	M2.0 V	08:20:13.29	+05:32:08.2	…	…	…	…	66.34	75.55	312.10 ± 1.84	0.455 ± 0.017
…	…	GJ 3497	J08258+690	M7.0 V	08:25:50.76	+69:01:40.7	…	…	…	…	28.47	1451.45	16.85 ± 0.22	0.148 ± 0.010
…	…	GJ 1110	J08282+201	M4.0 V	08:28:12.37	+20:08:11.4	…	…	…	…	27.73	685.79	139.95 ± 0.58	0.336 ± 0.014
…	…	GJ 308	J08283+350	M0.0 V	08:28:20.83	+35:00:53.6	AB	A	…	…	109.34	1086.44	…	0.473 ± 0.046
08286+3502	WOR19	G3- 903444927988618752	…	…	08:28:20.82	+35:00:54.0	…	B	0.487	340.4	109.25	…	…	…
…	…	PM J08283+5522	J08283+553	M2.5 V	08:28:18.75	+55:22:40.6	…	…	…	…	36.11	106.35	233.73 ± 0.96	0.441 ± 0.017
08286+6602	JNN 273	1R082839.4+660229	J08286+660	M4.0 V	08:28:41.33	+66:02:25.4	(AB)	AB	0.294	146.4	…	101.92	…	0.274 ± 0.038
…	…	PM J08293+0355E	J08293+039	M2.5 V	08:29:21.81	+03:55:08.2	…	…	…	…	48.58	116.89	357.26 ± 2.01	0.475 ± 0.012
…	…	DXCnc	J08298+267	M6.5 V	08:29:48.02	+26:46:23.8	…	…	…	…	31.28	1270.86	7.67 ± 0.03	0.103 ± 0.048
08313-0601	BAG 49	GJ 3501	J08313-060	M2.0 V	08:31:21.14	-06:02:02.8	(AB)+C	AB	0.121	76.8	166.98	436.18	…	0.587 ± 0.028
08313-0601	LDS 221	GJ 3502	J08314-060	M3.0 V	08:31:26.75	-06:02:13.6	…	C	84.405	97.3	43.26	441.13	307.15 ± 1.57	0.479 ± 0.018
…	…	GJ 3503	J08313-104	M4.0 V	08:31:22.81	-10:29:58.9	…	…	…	…	39.36	676.43	36.19 ± 0.16	0.196 ± 0.011
…	…	LP 35-219	J08315+730	M4.0 V	08:31:32.36	+73:03:50.1	…	…	…	…	70.88	669.51	93.09 ± 0.46	0.276 ± 0.012
08317+1924	BEU 12	CUCnc	J08316+193S	M3.5 V	08:31:37.32	+19:23:37.5	(AabB)+CD	AabB(EB)	0.345	222.9	32.94	258.23	…	0.834 ± 0.001
08317+1924	LDS 905	CCncA	J08316+193N	M4.0 V	08:31:37.17	+19:23:47.6	…	C	10.363	348.5	68.03	266.18	…	0.259 ± 0.036
08317+1924	DEL 1	CCncB	…	M5.0 V	08:31:37.16	+19:23:46.7	…	D	9.435	346.9	41.80	242.46	…	0.208 ± 0.038
…	…	1R083147.3+054504	J08317+057	M1.0 Ve	08:31:47.89	+05:45:17.0	…	…	…	…	57.83	93.30	1049.84 ± 16.60	0.674 ± 0.026

Table D.2: Complete sample with the description of multiple systems (continued).

WDS id	WDS disc	Name	Karmn	Spectral type	α (2016.0)	δ (2016.0)	System	Component	ρ [arcsec]	θ [deg]	ϖ [mas]	$\mu_{\rm total}$ [mas a^{-1}]	$\mathcal{L}$ [$10^{-4}\,\mathcal{L}_\odot$]	$\mathcal{M}$ [$\mathcal{M}_\odot$]
…	…	GJ 3496	J08321+844	M3.5 V	08:32:13.99	+84:24:34.8	…	…	…	…	67.62	432.48	89.12 ± 0.41	0.281 ± 0.013
…	…	Wolf 312	J08325+451	M2.5 V	08:32:35.78	+45:10:16.3	…	…	…	…	107.85	155.67	252.21 ± 1.47	0.432 ± 0.017
…	…	GJ 3505	J08334+185	M4.5 V	08:33:25.06	+18:31:34.9	…	…	…	…	52.96	648.79	46.99 ± 0.30	0.211 ± 0.011
…	…	GJ 2070	J08344-011	M3.0 V	08:34:26.13	-01:08:46.3	…	…	…	…	…	479.24	79.46 ± 0.40	0.264 ± 0.013
…	…	LSPM J0835+1408	J08353+141	M4.5 V	08:35:19.75	+14:08:31.9	Aabc	Aabc(3)	…	…	30.09	171.72	…	…
…	…	GJ 3506	J08358+680	M3.0 V	08:35:46.65	+68:04:00.1	…	…	…	…	31.43	1008.72	179.89 ± 0.71	0.362 ± 0.011
…	…	LP 311-37	J08364+264	M2.0 V	08:36:26.45	+26:28:18.9	AB	A	…	…	27.09	199.63	…	0.473 ± 0.030
08364+2628	KPP3209	LP 311-37 B	…	M6.5 V	08:36:26.29	+26:28:17.9	…	B	2.445	246.7	…	202.70	…	0.107 ± 0.047
08364+6718	YR 13	GJ 310	J08364+672	M0.5 V	08:36:22.51	+67:17:42.9	(AB)	AB	0.259	239.8	76.39	1072.67	…	0.661 ± 0.026
…	…	GJ 3508	J08371+151	M3.0 V	08:37:07.82	+15:07:31.2	…	…	…	…	76.28	903.19	265.52 ± 1.65	0.472 ± 0.018
…	…	LSPM J0837+0333	J08375+035	M4.0 V	08:37:30.28	+03:33:43.1	…	…	…	…	112.99	186.28	56.64 ± 0.27	0.234 ± 0.012
…	…	StKM 1-711	J08387+516	M1.5 V	08:38:42.06	+51:41:31.9	…	…	…	…	62.47	141.61	573.78 ± 2.66	0.567 ± 0.028
…	…	GJ 3510	J08398+089	M2.0 V	08:39:47.80	+08:56:21.0	A+B	A	…	…	32.08	284.72	173.99 ± 1.05	0.355 ± 0.015
08398+0856	LDS3806	GJ 3511	…	M4.5 V	08:39:48.25	+08:56:21.1	…	B	6.645	88.7	32.03	282.64	47.42 ± 0.25	0.212 ± 0.011
…	…	LSPM J0840+3127	J08402+314	M3.5 V	08:40:16.24	+31:27:08.7	…	…	…	…	32.16	238.18	98.82 ± 0.54	0.274 ± 0.010
…	…	AZCnc	J08404+184	M6.0 V	08:40:28.77	+18:24:01.5	…	…	…	…	34.02	925.95	8.55 ± 0.05	0.117 ± 0.010
…	…	GJ 317	J08409-234	M3.5 V	08:40:58.67	-23:27:09.7	…	…	…	…	…	928.02	223.23 ± 2.04	0.406 ± 0.014
…	…	GJ 3509	J08410+676	M4.0 V	08:41:01.83	+67:39:33.1	…	…	…	…	28.12	761.15	68.04 ± 0.29	0.259 ± 0.013
…	…	GJ 3512	J08413+594	dM5.5	08:41:19.58	+59:29:30.0	…	…	…	…	46.09	1305.77	16.88 ± 0.08	0.122 ± 0.009
…	…	GJ 319 A	J08427+095	M0.0 V	08:42:44.77	+09:33:14.0	AB+C	A	…	…	36.61	670.38	…	0.610
08427+0935	ST 8	GJ 319 B	…	M4.0 V	08:42:44.84	+09:33:15.1	…	B	1.512	40.5	36.45	610.58	…	0.270 ± 0.036
08427+0935	LUY6218	GJ 319 C	J08428+095	M2.5 V	08:42:52.47	+09:33:01.3	…	C	114.573	96.3	29.45	653.39	208.03 ± 1.09	0.415 ± 0.017
…	…	GJ 3513	J08443-104	M3.5 V	08:44:22.71	-10:24:20.1	…	…	…	…	27.25	603.95	150.76 ± 0.80	0.372 ± 0.016
…	…	G 9-19	J08447+182	M3.5 V	08:44:45.08	+18:12:59.2	…	…	…	…	31.87	510.61	372.62 ± 2.28	0.456 ± 0.030
08449-0637	JNN 63	PM J08449-0637	J08449-066	M3.5 V	08:44:55.59	-06:37:28.2	(AB)	AB	0.274	23.2	40.34	137.75	…	…
…	…	Ross 622	J08517+181	M1.5 V	08:51:42.78	+18:07:29.1	…	…	…	…	56.59	901.53	216.97 ± 0.98	0.376 ± 0.015
…	…	55 Cnc	…	K0 IV-V	08:52:35.22	+28:19:47.2	A+B	A	…	…	50.35	538.90	6005.81 ± 100.88	…
08526+2820	LDS6219	GJ 324 B	J08526+283	M4.5 V	08:52:40.28	+28:18:54.9	…	B	84.826	128.1	56.01	539.75	79.01 ± 0.53	0.259 ± 0.011
…	…	PM J08531-2017	J08531-202	M3.0 V	08:53:10.96	-20:17:19.3	…	…	…	…	56.23	123.21	152.91 ± 0.91	0.352 ± 0.015
…	…	GJ 3517	J08536-034	M9.0 Ve	08:53:35.61	-03:29:35.4	…	…	…	…	64.43	553.84	2.87 ± 0.02	0.079 ± 0.012
…	…	StKM 1-730	J08537+149	M0.0 V	08:53:43.67	+14:58:09.7	…	…	…	…	41.73	83.64	804.48 ± 10.57	0.618 ± 0.027
…	…	GJ 326 A	J08540-131	M2.5 V	08:54:05.69	-13:07:39.9	AB	A	…	…	40.82	668.71	…	0.318 ± 0.034
08539-1308	ST 9	GJ 326 B	…	M3.5 V	08:54:05.63	-13:07:39.8	…	B	0.919	275.8	47.74	631.53	…	0.305 ± 0.034
…	…	Ross 623	J08551+015	M0.0 V	08:55:07.67	+01:32:30.7	…	…	…	…	39.61	1046.84	970.55 ± 4.09	0.682 ± 0.026
…	…	PM J08555+6628	J08555+664	M3.0 V	08:55:31.46	+66:28:06.6	…	…	…	…	44.34	94.03	264.23 ± 1.69	0.470 ± 0.018
08563+1239	JNN 274	G 41-8	J08563+126	M6.0 V	08:56:19.49	+12:39:45.8	(AB)	AB	1.824	210.3	44.52	251.17	…	0.171 ± 0.040
08571+1139	HDS1296	GJ 330	J08570+116	M1.0 V	08:57:04.65	+11:38:43.9	(AB)	AB	0.703	237.3	44.15	311.03	…	0.509 ± 0.029
…	…	LP 426-35	J08572+194	M3.5 V	08:57:15.55	+19:24:15.2	…	…	…	…	45.38	196.36	276.39 ± 67.04	0.376 ± 0.043
…	…	GJ 1116 A	J08582+197	M5.5 V	08:58:14.09	+19:45:45.3	AB	A	…	…	28.06	937.77	…	0.111 ± 0.046
08582+1945	LDS3836	GJ 1116 B	…	M7.0 V	08:58:14.21	+19:45:46.7	…	B	2.175	50.9	147.72	773.57	…	0.127 ± 0.044

Table D.2: Complete sample with the description of multiple systems (continued).

WDS id	WDS disc	Name	Karmn	Spectral type	α (2016.0)	δ (2016.0)	System	Component	ρ [arcsec]	θ [deg]	ϖ [mas]	$\mu_{\rm total}$ [mas a^{-1}]	$\mathcal{L}$ [$10^{-4}\,\mathcal{L}_\odot$]	$\mathcal{M}$ [$\mathcal{M}_\odot$]
…	…	G 41-13	J08588+210	M2.0 V	08:58:52.53	+21:04:29.1	…	…	…	…	123.20	363.62	…	0.322 ± 0.034
08596+5344	CRC 56	G 194-47	J08595+537	M3.5 V	08:59:35.41	+53:43:47.5	(AB)	AB	0.485	220.7	19.69	324.42	…	0.290 ± 0.035
…	…	GJ 3522	J08589+084	M3.5 V	08:58:56.73	+08:28:20.8	AB	A(2)	…	…	21.98	492.32	…	0.235 ± 0.001
08589+0829	DEL 2	G3- 585250248258396416	…	…	08:58:56.76	+08:28:20.9	…	B	0.447	81.7	111.87	…	…	…
…	…	GJ 3520	J08599+729	M5.0 V	08:59:59.70	+72:57:35.8	…	…	…	…	32.01	962.14	35.71 ± 0.13	0.195 ± 0.011
…	…	LP 368-128	J09003+218	M6.5 V	09:00:22.95	+21:49:55.4	…	…	…	…	46.06	784.81	7.76 ± 0.04	0.103 ± 0.048
…	…	GJ 1119	J09005+465	M4.5 Ve	09:00:31.74	+46:35:02.7	…	…	…	…	44.51	705.49	49.39 ± 0.21	0.204 ± 0.009
…	…	Ross 686	J09008+052W	M3.0 V	09:00:48.25	+05:14:38.1	A+B	A	…	…	81.37	333.91	262.86 ± 1.62	0.469 ± 0.018
09008+0516	OSV 2	Ross 687	J09008+052E	M3.0 V	09:00:50.05	+05:14:26.3	…	B	29.459	113.7	42.56	328.91	207.33 ± 1.75	0.414 ± 0.017
09012+0157	CRC 57	Ross 625	J09011+019	M3.0 V	09:01:10.07	+01:56:33.7	(AB)+C	AB(2)	0.182	148.8	44.00	387.95	…	…
09012+0157	CRC 57	Ross 625B	…	M6.0 V	09:01:10.16	+01:56:31.0	…	C	3.051	155.6	50.82	404.21	…	0.111 ± 0.046
…	…	GJ 3528	J09023+084	M3.0 V	09:02:20.55	+08:28:03.3	…	…	…	…	…	651.46	352.55 ± 2.17	0.473 ± 0.030
…	…	PM J09023+1746	J09023+177	M4.0 V	09:02:22.91	+17:46:31.8	…	…	…	…	35.56	141.53	84.46 ± 0.35	0.292 ± 0.014
…	…	GJ 3526	J09028+680	M4.0 V	09:02:53.41	+68:03:52.1	…	…	…	…	50.50	391.40	86.12 ± 0.39	0.271 ± 0.012
…	…	LSPM J0902+7138	J09029+716	M1.5 V	09:02:55.82	+71:38:11.0	…	…	…	…	54.28	174.76	357.82 ± 1.44	0.473 ± 0.030
…	…	LP 546-37	J09033+056	M7.0 V	09:03:20.91	+05:40:08.5	…	…	…	…	279.25	377.92	…	…
…	…	G 194-52	J09037+520	M3.5 V	09:03:43.39	+52:02:49.1	…	…	…	…	39.62	335.51	129.83 ± 0.66	0.344 ± 0.015
…	…	LP 486-43	J09038+129	M2.0 V	09:03:53.41	+12:59:24.8	…	…	…	…	39.79	214.36	761.64 ± 7.64	0.599 ± 0.027
…	…	V405Hya	…	K2 V	09:04:20.57	-15:54:51.8	A+B	A	…	…	58.91	112.03	2581.76 ± 12.41	0.820 ± 0.123
…	…	1R090406.8-155512	J09040-159	M2.5 V	09:04:05.44	-15:55:19.0	…	B*	220.022	82.9	68.21	113.77	245.78 ± 1.55	0.453 ± 0.018
…	…	GJ 3530	J09050+028	M1.5 V	09:05:04.11	+02:50:03.9	AB	A	…	…	60.06	314.11	…	0.487 ± 0.030
09051+0250	RAO 232	GJ 3530	…	M3.5 V	09:05:04.03	+02:50:03.5	…	B	1.220	253.9	60.25	336.22	…	0.335 ± 0.034
…	…	LP 426-56	J09057+186	M2.5 V	09:05:43.02	+18:36:27.6	…	…	…	…	60.69	397.28	603.56 ± 11.58	0.554 ± 0.028
…	…	GJ 3531	J09062+128	M3.5 V	09:06:13.79	+12:51:30.1	…	…	…	…	20.63	407.05	244.99 ± 6.18	0.481 ± 0.020
…	…	GJ 3533	J09070-221	M4.5 V	09:07:02.40	-22:08:56.6	…	…	…	…	51.92	508.98	51.19 ± 0.27	0.238 ± 0.012
…	…	GJ 3532	J09087+665	M2.5 V	09:08:46.58	+66:35:36.4	…	…	…	…	40.66	264.00	129.40 ± 3.29	0.322 ± 0.015
…	…	2M09090798+2247413	J09091+227	M4.5 V	09:09:07.88	+22:47:40.1	…	…	…	…	47.87	109.41	53.93 ± 0.78	0.245 ± 0.013
…	…	GJ 1121	J09093+401	M4.0 V	09:09:23.06	+40:05:55.5	…	…	…	…	74.41	807.61	54.83 ± 0.61	0.230 ± 0.012
…	…	GJ 336	J09095+328	M0.5 V	09:09:30.18	+32:48:59.1	AB	A	…	…	38.85	715.71	…	0.656 ± 0.027
09095+3250	COU 1561	BD+33 1814B	…	M0.0 V	09:09:30.17	+32:48:59.5	…	B	0.483	353.0	76.94	…	…	…
…	…	GJ 3537	J09096+067	M3.0 V	09:09:39.07	+06:42:11.8	…	…	…	…	34.35	91.36	146.99 ± 0.88	0.367 ± 0.016
…	…	G 46-24	J09099+004	M1.0 V	09:09:59.43	+00:23:39.5	…	…	…	…	34.48	506.47	280.68 ± 1.35	0.430 ± 0.017
…	…	LP 487-10	J09115+126	M2.5 V	09:11:32.14	+12:37:18.3	…	…	…	…	70.62	378.85	721.32 ± 12.48	0.578 ± 0.028
…	…	GJ 336.1	J09115+466	M0.5 V	09:11:30.27	+46:37:00.7	…	…	…	…	56.11	352.70	643.41 ± 2.45	0.597 ± 0.027
…	…	GJ 3540	J09120+279	M3.0 V	09:12:02.44	+27:54:16.2	Aab	Aab(2)	…	…	159.66	489.68	…	…
…	…	G 234-57A	J09133+688	M2.5 V	09:13:23.43	+68:52:27.1	AB	A	…	…	52.93	288.04	672.86 ± 12.64	0.494 ± 0.030
09134+6853	RAO 568	G 234-57B	…	M2.0 V	09:13:23.34	+68:52:26.7	…	B	0.596	231.8	30.52	275.37	…	0.463 ± 0.030
…	…	LP 427-16	J09140+196	M3.0 V	09:14:03.02	+19:40:03.2	Aab	Aab(1)	…	…	42.97	217.28	…	…
…	…	HD 79210	J09143+526	M0.0 V	09:14:20.05	+52:41:02.7	Aab+B	Aab(1)	…	…	42.71	1647.20	…	…
09144+5241	STF1321	HD 79211	J09144+526	M0.0 V	09:14:21.91	+52:41:00.3	…	B	17.075	97.9	38.06	1705.85	772.68 ± 20.80	0.632 ± 0.027

Table D.2: Complete sample with the description of multiple systems (continued).

WDS id	WDS disc	Name	Karmn	Spectral type	α (2016.0)	δ (2016.0)	System	Component	ρ [arcsec]	θ [deg]	ϖ [mas]	$\mu_{\rm total}$ [mas a^{-1}]	$\mathcal{L}$ [$10^{-4}\,\mathcal{L}_\odot$]	$\mathcal{M}$ [$\mathcal{M}_\odot$]
09156-1036	MTG 2	G 161-7	J09156-105	M5.0 V	09:15:35.96	-10:35:50.2	(AB)	AB	0.146	62.1	38.00	440.48	…	0.159 ± 0.042
…	…	G 47-31	J09160+293	M2.0 V	09:16:05.04	+29:19:36.3	…	…	…	…	89.07	544.57	452.92 ± 2.55	0.522 ± 0.029
…	…	RX J0916.1+0153	J09161+018	M4.0 Ve	09:16:10.24	+01:53:07.2	…	…	…	…	73.86	115.19	106.69 ± 0.72	0.323 ± 0.016
…	…	GJ 3543	J09163-186	M1.5 V	09:16:20.29	-18:37:30.6	…	…	…	…	65.88	347.01	327.45 ± 1.87	0.441 ± 0.011
…	…	GJ 3536	J09165+841	M1.5 V	09:16:24.75	+84:11:06.4	…	…	…	…	38.94	658.85	338.59 ± 163.73	0.449 ± 0.116
…	…	2M09165078+2448559	J09168+248	M4.5 V	09:16:50.70	+24:48:54.0	…	…	…	…	105.29	141.95	102.87 ± 0.56	0.347 ± 0.015
09177+4612	JNN 68	RX J0917.7+4612	J09177+462	M2.5 V	09:17:44.52	+46:12:24.4	(AB)	AB	0.190	348.0	64.68	131.04	…	0.591 ± 0.028
…	…	GJ 3542	J09177+584	M5.0 V	09:17:46.04	+58:25:02.7	…	…	…	…	64.64	1171.23	25.97 ± 0.11	0.162 ± 0.010
09188+2647	LDS6226	GJ 3548	J09187+267	M1.5 V	09:18:45.99	+26:45:05.4	A+B	A	76.454	302.6	64.71	404.42	455.75 ± 2.34	0.518 ± 0.029
…	…	GJ 3549	…	M5.0 Ve	09:18:41.19	+26:45:46.6	…	B	76.454	302.7	33.65	402.96	24.30 ± 0.15	0.169 ± 0.010
…	…	GJ 1122	J09193+385S	M5.0 V	09:19:18.62	+38:31:15.9	A+B	A	…	…	31.81	234.55	52.79 ± 0.23	0.242 ± 0.012
09193+3831	GIC 84	G 115-69	J09193+385N	M5.0 V	09:19:18.71	+38:31:23.3	…	B	7.500	7.5	…	238.98	…	0.215 ± 0.038
09194+6203	RAO 569	GJ 3547	J09193+620	M1.0 Ve	09:19:22.21	+62:03:10.7	(AB)	AB	0.790	189.0	33.00	481.74	…	…
09200+3053	RAO 570	TYC 2493-1386-1	J09200+308	M1.5 Ve	09:20:00.38	+30:52:39.1	(AB)+C	AB	0.430	71.3	59.84	81.54	…	…
09200+3053	CRB 80	2M09195883+3052156	…	M5.0 V	09:19:58.74	+30:52:15.0	…	C	32.038	221.2	79.45	82.62	27.70 ± 0.52	0.196 ± 0.012
…	…	1R092010.8+034731	J09201+037	M3.5 V	09:20:10.74	+03:47:27.0	…	…	…	…	79.66	139.64	167.55 ± 5.65	0.394 ± 0.018
…	…	GJ 3553	J09209+033	M4.0 V	09:20:58.28	+03:21:48.3	…	…	…	…	42.19	1179.28	82.45 ± 0.49	0.269 ± 0.013
…	…	GJ 3550	J09213+731	M5.0 V	09:21:16.03	+73:06:33.1	…	…	…	…	115.49	974.40	21.48 ± 0.08	0.146 ± 0.010
09218+4330	LAW 17	GJ 3554	J09218+435	M4.5 V	09:21:48.61	+43:30:26.5	(AB)	AB	0.710	124.0	33.06	323.07	…	0.297 ± 0.035
…	…	RAVE J092148.1-021943	J09218-023	M2.5 V	09:21:48.32	-02:19:43.2	…	…	…	…	64.94	177.10	90.07 ± 0.54	0.265 ± 0.012
…	…	G 115-72	J09228+467	M1.0 V	09:22:51.31	+46:46:58.8	A+B	A	…	…	65.67	238.54	730.83 ± 3.53	0.607 ± 0.027
09229+4647	KPP3219	G 115-72B	…	…	09:22:51.44	+46:47:02.0	…	B	3.412	22.7	48.74	226.53	…	0.262 ± 0.036
…	…	BD+22 2086A	…	K5 V	09:23:06.19	+22:18:17.6	A+B	A	…	…	40.70	218.39	2015.37 ± 8.48	0.700 ± 0.105
09231+2218	HDS1348	BD+22 2086B	J09231+223	M0.0 V	09:23:06.01	+22:18:25.6	…	B	8.301	343.4	85.80	223.16	…	0.641 ± 0.027
…	…	GJ 3555	J09238+001	M1.0 V	09:23:52.36	+00:08:13.8	…	…	…	…	61.32	305.88	493.22 ± 2.98	0.546 ± 0.028
…	…	LSPM J0924+3041	J09248+306	M3.5 V	09:24:50.68	+30:41:34.2	…	…	…	…	28.50	198.06	225.22 ± 1.24	0.460 ± 0.018
09256+6329	JNN 275	G 235-25	J09256+634	M4.5 V	09:25:39.51	+63:29:14.9	(AB)	AB	0.126	92.7	196.26	420.18	…	0.288 ± 0.035
…	…	GJ 3556	J09275+506	M2.5 V	09:27:30.19	+50:39:10.1	…	…	…	…	194.14	265.31	621.40 ± 3.79	0.563 ± 0.028
…	…	LP 727-31	J09286-121	M2.5 V	09:28:41.63	-12:10:02.0	…	…	…	…	35.93	391.43	499.92 ± 3.92	0.534 ± 0.029
…	…	Ross 439	J09288-073	M2.5 V	09:28:53.16	-07:22:27.2	A+B	A	…	…	55.73	732.01	192.22 ± 0.83	0.398 ± 0.016
09288-0722	GIC 87	GJ 347 B	J09289-073	M4.5 V	09:28:55.53	-07:22:23.3	…	B	35.610	83.6	147.66	731.82	30.18 ± 0.13	0.177 ± 0.011
…	…	LP 370-26	J09291+259	M5.0 V	09:29:09.83	+25:58:05.0	…	…	…	…	…	1082.47	17.21 ± 0.09	0.149 ± 0.010
…	…	GJ 3558	J09300+396	M2.5 V	09:30:01.84	+39:37:21.1	…	…	…	…	69.46	205.27	255.60 ± 1.03	0.462 ± 0.018
…	…	LSPM J0930+2630	J09302+265	M3.0 V	09:30:14.24	+26:30:22.7	…	…	…	…	157.27	206.22	237.43 ± 1.19	0.473 ± 0.019
…	…	GJ 1125	J09307+003	M3.5 V	09:30:43.98	+00:19:12.8	…	…	…	…	99.16	790.95	115.62 ± 0.55	0.292 ± 0.010
…	…	1R093051.2+022741	J09308+024	M4.0 V	09:30:50.81	+02:27:21.5	…	…	…	…	45.14	88.96	114.20 ± 1.96	0.343 ± 0.015
09313-1329	KUI 41	Ross 440	J09313-134	M3.0 V	09:31:20.26	-13:29:18.9	AB	A	0.379	102.5	45.15	700.39	…	0.391 ± 0.033
…	…	G3- 5690031948585514368	…	…	09:31:20.22	-13:29:18.9	…	B	0.502	265.9	42.63	…	…	…
…	…	Ross 84	J09315+202	M2.0 V	09:31:33.05	+20:16:43.6	…	…	…	…	41.75	807.29	228.23 ± 2.14	0.410 ± 0.016
…	…	GJ 353	J09319+363	M0.0 V	09:31:56.06	+36:19:04.4	…	…	…	…	48.96	564.65	423.82 ± 2.63	0.505 ± 0.018

Table D.2: Complete sample with the description of multiple systems (continued).

WDS id	WDS disc	Name	Karmn	Spectral type	α (2016.0)	δ (2016.0)	System	Component	ρ [arcsec]	θ [deg]	ϖ [mas]	$\mu_{\rm total}$ [mas a^{-1}]	$\mathcal{L}$ [10^{-4} $\mathcal{L}_\odot$]	$\mathcal{M}$ [$\mathcal{M}_\odot$]
09327+2659	LDS3903	DXLeo	…	G9 V(k)	09:32:43.58	+26:59:14.8	A+B	A	65.558	64.4	47.60	287.22	4708.24 ± 16.38	0.900 ± 0.135
…	…	HD 82443B	J09328+269	M5.5 V	09:32:48.07	+26:59:39.9	…	B	65.013	67.3	81.36	284.17	29.79 ± 0.19	0.189 ± 0.011
…	…	GJ 3560	J09352+612	M2.5 V	09:35:13.45	+61:14:37.6	…	…	…	…	23.19	123.91	254.60 ± 1.09	0.434 ± 0.017
…	…	GJ 3561	J09360-061	M3.5 V	09:36:04.10	-06:07:01.2	…	…	…	…	…	747.42	92.25 ± 0.44	0.306 ± 0.014
…	…	GJ 357	J09360-216	M2.5 V	09:36:01.80	-21:39:54.7	…	…	…	…	53.66	1000.01	161.20 ± 0.84	0.341 ± 0.011
…	…	HD 82939	…	G5 V	09:36:15.78	+37:31:44.1	A+Bab	A	…	…	23.47	134.64	2187.00 ± 15.44	0.980 ± 0.147
09361+3733	SKF 254	GJ 9303	J09362+375	M0.0 V	09:36:04.14	+37:33:08.9	…	Bab(2)	162.314	301.5	159.91	134.34	…	…
…	…	GJ 3562	J09370+405	M3.8 V	09:37:03.29	+40:34:37.7	…	…	…	…	36.51	189.48	78.38 ± 0.37	0.280 ± 0.013
…	…	LP 428-20	J09394+146	M3.5 V	09:39:29.77	+14:38:48.5	…	…	…	…	36.63	180.10	96.32 ± 0.50	0.293 ± 0.013
…	…	G 117-34	J09394+317	M1.5 V	09:39:24.04	+31:45:13.7	AB	A	…	…	42.09	284.64	…	0.459 ± 0.030
09394+3145	NSN 596	G 117-34B	…	M7.5 V	09:39:23.89	+31:45:14.1	…	B	2.004	282.9	42.22	312.79	…	0.100 ± 0.049
…	…	Ross 92	J09410+220	M4.5 V	09:41:02.58	+22:01:20.5	…	…	…	…	25.74	671.41	28.92 ± 0.12	0.173 ± 0.010
…	…	Ross 85	J09411+132	M1.5 V	09:41:09.64	+13:12:32.1	…	…	…	…	34.17	675.39	339.21 ± 2.01	0.449 ± 0.012
…	…	GJ 363	J09423+559	M3.0 V	09:42:21.84	+55:58:53.1	…	…	…	…	65.22	873.10	168.44 ± 0.72	0.362 ± 0.012
…	…	GJ 360	J09425+700	M2.5 Ve	09:42:32.74	+70:01:57.6	A+B	A	…	…	49.31	724.44	348.80 ± 1.48	0.498 ± 0.013
09427+7004	OSV 3	GJ 362	J09428+700	M3.5 Ve	09:42:49.63	+70:02:17.6	…	B	88.780	76.9	39.69	721.57	240.39 ± 0.84	0.420 ± 0.013
…	…	GJ 3563	J09425-192	M2.5 V	09:42:35.14	-19:14:08.6	…	…	…	…	47.85	522.62	208.21 ± 0.89	0.415 ± 0.017
…	…	LP 370-35	J09430+237	M1.0 V	09:43:01.12	+23:49:18.3	A+B+C	A	…	…	46.81	269.52	541.75 ± 223.84	0.560 ± 0.028
09430+2349	GOM 35	LSPM J0943+2349S	…	M6.0 V	09:43:00.94	+23:49:13.2	…	B	5.731	206.0	…	267.91	…	0.108 ± 0.047
09430+2349	LDS3917	LP 370-34	…	M7.0 V	09:42:56.96	+23:51:16.1	…	C	130.856	334.1	43.48	267.86	7.49 ± 0.10	0.108 ± 0.009
…	…	Ross 93	J09439+269	M3.5 V	09:43:54.92	+26:58:06.8	…	…	…	…	39.41	586.64	179.35 ± 0.87	0.362 ± 0.011
…	…	GJ 1129	J09447-182	M3.5 Ve	09:44:45.55	-18:12:51.7	…	…	…	…	19.09	1609.66	93.86 ± 0.54	0.268 ± 0.010
…	…	G 161-71	J09449-123	M5.0 V	09:44:53.83	-12:20:53.7	…	…	…	…	42.23	333.75	89.06 ± 0.45	0.387 ± 0.030
…	…	GJ 3566	J09461-044	M4.0 V	09:46:08.66	-04:25:40.6	AB	A	…	…	34.31	578.71	…	0.229 ± 0.037
09461-0425	JNN 276	G 161-74B	…	M5.0 V	09:46:08.66	-04:25:39.4	…	B	1.191	358.9	42.36	576.97	…	0.170 ± 0.040
…	…	Ross 434	J09468+760	M1.5 V	09:46:48.87	+76:02:22.1	…	…	…	…	41.11	1004.25	423.76 ± 1.80	0.522 ± 0.029
…	…	Ross 94	J09473+263	M0.0 V	09:47:22.15	+26:18:06.9	…	…	…	…	43.51	411.82	1107.65 ± 4.51	0.711 ± 0.026
…	…	GJ 3568	J09475+129	M4.0 V	09:47:34.71	+12:56:42.8	…	…	…	…	157.89	243.06	123.28 ± 0.61	0.334 ± 0.015
…	…	LP 728-70	J09506-138	M4.0 V	09:50:40.70	-13:48:40.2	Aab	Aab(2)	…	…	31.90	187.98	…	…
…	…	G 43-2	J09488+156	M3.0 V	09:48:50.18	+15:38:48.5	…	…	…	…	157.88	229.71	82.28 ± 0.39	0.269 ± 0.013
…	…	GJ 369	J09511-123	dM0.5	09:51:10.88	-12:20:10.8	…	…	…	…	134.90	1847.30	461.67 ± 2.25	0.508 ± 0.012
…	…	LP 728-71	J09526-156	M3.5 V	09:52:41.65	-15:36:15.9	…	…	…	…	30.57	179.24	81.39 ± 0.41	0.267 ± 0.013
…	…	G 195-43	J09527+554	M1.5 V	09:52:45.26	+55:28:16.2	AB	A	…	…	63.89	354.45	…	0.562 ± 0.029
09527+5528	RAO 238	G 195-43B	…	M6.0 V	09:52:45.16	+55:28:18.8	…	B	2.716	342.5	74.39	342.98	…	0.117 ± 0.045
…	…	GJ 372	J09531-036	M2.0 V	09:53:11.67	-03:41:31.8	Aab	Aab(2)	…	…	…	68.74	473.34	…	1.043 ± 0.057
…	…	LP 126-73	J09535+507	M1.5 V	09:53:32.64	+50:45:04.2	…	…	…	…	…	38.50	524.29	322.93 ± 1.82	0.463 ± 0.018
…	…	GJ 3571	J09539+209	M4.0 Ve	09:53:54.78	+20:56:53.1	…	…	…	…	…	28.49	523.78	25.69 ± 0.11	0.161 ± 0.010
…	…	Wolf 330	J09557+353	M3.5 Ve	09:55:43.55	+35:21:36.8	…	…	…	…	…	29.90	314.77	151.82 ± 0.81	0.374 ± 0.016
…	…	GJ 373	J09561+627	M0.5 V	09:56:07.96	+62:47:09.1	Aab	Aab(?)	…	…	…	37.25	657.83	…	…
…	…	GJ 3573	J09564+226	M4.0 V	09:56:26.42	+22:38:56.9	…	…	…	…	…	64.24	532.49	64.35 ± 0.31	0.251 ± 0.012

Table D.2: Complete sample with the description of multiple systems (continued).

WDS id	WDS disc	Name	Karmn	Spectral type	α (2016.0)	δ (2016.0)	System	Component	ρ [arcsec]	θ [deg]	ϖ [mas]	$\mu_{\rm total}$ [mas a^{-1}]	$\mathcal{L}$ [$10^{-4}\,\mathcal{L}_\odot$]	$\mathcal{M}$ [$\mathcal{M}_\odot$]
…	…	GJ 3576	J09579+118	M4.0 V	09:57:57.54	+11:48:26.3	A+B	A	…	…	40.29	451.50	80.70 ± 0.53	0.305 ± 0.014
…	…	LP 489-1	…	M5.0 V	09:56:45.21	+11:34:23.6	…	B*	1356.049	231.6	40.17	456.96	28.92 ± 0.15	0.173 ± 0.010
…	…	G 196-1	J09587+555	M1.0 V	09:58:46.62	+55:32:59.0	…	…	…	…	51.74	242.72	610.72 ± 8.15	0.575 ± 0.028
…	…	LP 549-6	J09589+059	M4.5 V	09:58:56.31	+05:57:58.8	…	…	…	…	51.73	193.34	32.71 ± 0.15	0.185 ± 0.011
…	…	GJ 3577	J09593+438W	M3.5 V	09:59:18.65	+43:50:21.9	A+B	A	…	…	26.36	242.55	138.56 ± 0.66	0.380 ± 0.016
09593+4350	GIC 91	GJ 3578	J09593+438E	M5.0 V	09:59:20.78	+43:50:22.1	…	B	23.063	89.4	…	242.07	111.28 ± 0.56	0.338 ± 0.015
…	…	GJ 3579	J09597+472	M4.0 V	09:59:46.11	+47:12:06.9	…	…	…	…	27.21	284.91	86.60 ± 0.41	0.296 ± 0.014
…	…	PM J09597+7211	J09597+721	M3.5 V	09:59:45.30	+72:12:01.3	…	…	…	…	40.36	97.75	114.77 ± 0.56	0.322 ± 0.014
…	…	GJ 375.2	J10004+272	M0.5 V	10:00:26.69	+27:16:03.5	AC+B	A	…	…	56.73	118.42	…	0.679 ± 0.026
10004+2716	TOK 273	2M10003572+2717054	…	M6.5 V	10:00:35.70	+27:17:07.5	…	B	136.040	61.9	66.44	118.34	9.54 ± 0.11	0.125 ± 0.010
…	…	G3- 740041664172917376	…	M7.5 V	10:00:26.56	+27:16:05.7	…	C*	2.882	320.9	34.03	117.20	…	0.101 ± 0.049
…	…	Wolf 335	J10007+323	M1.0 V	10:00:43.01	+32:18:23.1	…	…	…	…	83.68	1208.02	377.44 ± 1.78	0.475 ± 0.018
…	…	LP 37-57	J10020+697	M4.0 V	10:02:05.67	+69:45:25.6	…	…	…	…	29.43	232.04	44.28 ± 0.16	0.219 ± 0.012
…	…	GJ 378	J10023+480	M1.0 V	10:02:20.74	+48:04:56.1	…	…	…	…	29.42	1604.96	592.56 ± 2.53	0.579 ± 0.028
…	…	GJ 3582	J10027+149	M4.61	10:02:42.62	+14:59:09.2	…	…	…	…	29.41	283.17	59.04 ± 0.50	0.240 ± 0.012
10028+4828	CRC 58	G 195-55	J10028+484	M5.5 V	10:02:48.79	+48:27:28.7	(AB)	AB	0.200	306.0	29.44	425.96	…	0.169 ± 0.041
…	…	GJ 3583	J10035+059	M3.5 V	10:03:32.76	+05:57:45.4	…	…	…	…	37.04	587.97	155.79 ± 0.95	0.379 ± 0.016
10041+1848	TOK 889	GJ 9312	J10040+187	M0.5 V	10:04:05.80	+18:47:41.5	(AB)	AB	0.033	113.1	31.49	275.15	…	…
…	…	G 196-3	J10043+503	M2.5 V	10:04:21.23	+50:23:10.1	A+B	A	…	…	38.63	246.66	441.92 ± 1.80	0.506 ± 0.029
10044+5023	REB 1	G 196-3B	…	L3beta	10:04:20.41	+50:22:56.1	…	B	16.070	209.1	32.09	246.29	1.11 ± 0.03	…
…	…	GJ 3585	J10067+417	M1.0 V	10:06:43.45	+41:42:46.1	…	…	…	…	30.29	479.34	415.23 ± 2.01	0.499 ± 0.018
…	…	PM J10068-1246	J10068-127	M4.5 V	10:06:51.98	-12:46:54.3	…	…	…	…	57.18	81.30	76.34 ± 16.29	0.296 ± 0.037
…	…	LP 489-35	J10069+126	M1.5 V	10:06:57.49	+12:40:51.6	…	…	…	…	57.18	324.45	311.51 ± 1.90	0.455 ± 0.017
…	…	GJ 1131	J10079+692	M4.0 V	10:07:56.60	+69:14:46.1	…	…	…	…	56.59	909.36	38.08 ± 0.15	0.188 ± 0.011
…	…	LP 549-23	J10087+027	M3.0 V	10:08:44.52	+02:43:49.6	…	…	…	…	48.74	456.50	317.65 ± 1.64	0.452 ± 0.030
…	…	Wolf 346	J10087+355	M1.5 V	10:08:42.37	+35:32:51.3	…	…	…	…	41.31	234.01	114.71 ± 0.49	0.302 ± 0.013
…	…	TYC 4384-1735-1	J10088+692	M0.5 V	10:08:52.40	+69:16:35.8	…	…	…	…	100.90	197.42	864.16 ± 3.58	0.661 ± 0.026
…	…	GJ 3586	J10094+512	M4.65	10:09:29.22	+51:17:06.4	…	…	…	…	45.28	937.45	47.12 ± 0.21	0.212 ± 0.011
…	…	PM J10094+5424	J10094+544	M2.0 V	10:09:26.88	+54:24:22.5	…	…	…	…	99.88	149.51	401.27 ± 1.94	0.501 ± 0.029
10121-0241	DEL 3	GJ 381	J10120-026	M2.5 V	10:12:05.23	-02:41:14.8	(AB)	AB(2)	0.072	270.1	62.87	798.92	…	…
…	…	Wolf 351	J10117+353	M4.0 V	10:11:44.11	+35:18:40.1	…	…	…	…	…	281.48	56.73 ± 0.23	0.235 ± 0.012
…	…	ANSex	J10122-037	M1.5 V	10:12:17.50	-03:44:48.3	…	…	…	…	45.05	287.61	418.61 ± 2.83	0.496 ± 0.013
…	…	LP 92-48	J10125+570	M3.5 V	10:12:34.10	+57:03:40.5	…	…	…	…	73.70	634.64	116.41 ± 0.56	0.290 ± 0.010
10130+2321	RAO 241	G 54-18	J10130+233	M3.5 V	10:13:00.45	+23:20:45.9	(AB)	AB	0.614	16.0	55.33	301.16	…	0.366 ± 0.033
10143+2104	BWL 25	DKLeo	J10143+210	M0.5 V	10:14:19.03	+21:04:26.8	(AB)	AB(1)	0.095	320.2	77.48	225.49	…	…
…	…	LP 167-17	J10133+467	M5.5 Ve	10:13:20.56	+46:47:24.5	…	…	…	…	55.29	266.25	25.25 ± 0.14	0.186 ± 0.011
…	…	G 54-19	J10148+213	M4.5 V	10:14:52.91	+21:23:42.5	…	…	…	…	50.39	288.59	57.68 ± 0.93	0.254 ± 0.013
…	…	GJ 3590	J10151+314	M4.0 V	10:15:06.87	+31:25:07.0	AB	A	…	…	42.50	219.97	…	0.344 ± 0.033
10151+3125	CRC 59	G 118-43B	…	M3.5 V	10:15:06.76	+31:25:08.1	…	B	1.829	306.4	105.98	217.31	…	0.306 ± 0.034
…	…	PM J10155-1628E	J10155-164	M4.0 V	10:15:34.86	-16:28:20.4	…	…	…	…	25.74	479.16	228.94 ± 1.36	0.464 ± 0.019

Table D.2: Complete sample with the description of multiple systems (continued).

WDS id	WDS disc	Name	Karmn	Spectral type	α (2016.0)	δ (2016.0)	System	Component	ρ [arcsec]	θ [deg]	ϖ [mas]	$\mu_{\rm total}$ [mas a^{-1}]	$\mathcal{L}$ [$10^{-4}\,\mathcal{L}_\odot$]	$\mathcal{M}$ [$\mathcal{M}_\odot$]
…	…	LSPM J1015+1729	J10158+174	M3.5 V	10:15:54.26	+17:29:27.2	…	…	…	…	25.84	290.75	93.03 ± 0.54	0.287 ± 0.013
…	…	GJ 386	J10167-119	dM3.0	10:16:45.49	-11:57:52.1	…	…	…	…	47.00	734.48	320.63 ± 1.83	0.475 ± 0.013
…	…	LP 790-2	J10182-204	M4.5 V	10:18:13.39	-20:28:39.3	Aab+B	Aab(2)	…	…	…	412.59	…	0.427 ± 0.001
10183-2029	LDS3975	LP 790-1	…	M4.5 V	10:18:11.66	-20:28:19.3	…	B	31.519	309.3	51.49	407.26	46.68 ± 0.25	0.226 ± 0.012
…	…	LP 729-54	J10185-117	M4.0 V	10:18:34.77	-11:43:04.2	A+B	A	…	…	46.97	421.93	172.24 ± 1.46	0.367 ± 0.012
10185-1143	LDS3977	LP 729-55	…	M3.5 Ve	10:18:35.83	-11:43:06.2	…	B	15.788	97.1	47.03	422.28	22.77 ± 0.13	0.162 ± 0.010
…	…	ADLeo	J10196+198	M3.0 V	10:19:35.72	+19:52:11.3	…	…	…	…	81.02	500.51	238.49 ± 1.73	0.431 ± 0.011
…	…	G 118-51	J10200+289	M3.0 V	10:20:00.23	+28:57:09.5	…	…	…	…	86.62	511.22	107.58 ± 0.39	0.291 ± 0.013
…	…	GJ 3595	J10206+492	M3.0 V	10:20:37.15	+49:17:43.2	…	…	…	…	60.51	392.53	151.44 ± 0.63	0.350 ± 0.015
…	…	LP 212-62	J10238+438	M5.0 V	10:23:52.13	+43:53:33.2	…	…	…	…	84.33	178.72	40.45 ± 0.21	0.224 ± 0.012
…	…	PM J10240+3639	J10240+366	M3.5 V	10:24:05.04	+36:39:30.2	…	…	…	…	84.30	148.05	193.59 ± 2.42	0.425 ± 0.017
10243+1157	RAO 245	GJ 3598	J10243+119	M2.5 V	10:24:20.16	+11:57:23.5	(AB)	AB	0.110	325.0	58.63	177.93	…	0.376 ± 0.032
…	…	GJ 390	J10251-102	M1.0 V	10:25:10.09	-10:13:41.3	…	…	…	…	27.55	703.74	461.94 ± 2.35	0.530 ± 0.029
…	…	GJ 3599	J10255+263	M3.0 V	10:25:29.93	+26:23:09.8	…	…	…	…	27.65	591.17	161.58 ± 0.82	0.386 ± 0.016
…	…	GJ 3600	J10260+504W	M4.0 V	10:26:01.99	+50:27:00.0	A+B	A	…	…	27.86	654.77	97.45 ± 0.45	0.295 ± 0.013
10261+5029	LDS1241	GJ 3601	J10260+504E	M4.0 V	10:26:02.64	+50:27:13.0	…	B	14.379	25.7	69.59	659.62	84.52 ± 0.35	0.292 ± 0.014
…	…	PM J10273+7959	J10273+799	M2.0 V	10:27:22.67	+79:59:50.0	…	…	…	…	90.99	128.32	424.24 ± 7.40	0.512 ± 0.029
…	…	G 44-19	J10278+028	M3.5 V	10:27:49.12	+02:51:35.5	…	…	…	…	76.05	502.39	193.30 ± 3.42	0.425 ± 0.018
…	…	GJ 3602	J10284+482	M3.5 V	10:28:28.86	+48:14:17.7	AB	A	…	…	50.45	615.83	…	0.270 ± 0.038
…	…	G 146-35B	…	…	10:28:28.87	+48:14:17.8	…	B*	0.196	48.9	50.33	…	…	…
…	…	GJ 3604	J10286+322	M2.5 V	10:28:40.73	+32:14:21.7	AB	A	…	…	63.33	499.85	…	0.307 ± 0.034
10287+3214	KPP3229	G 118-61B	…	M4.0 V	10:28:40.84	+32:14:23.1	…	B	1.989	45.4	29.44	514.32	…	0.282 ± 0.035
…	…	Ross 446	J10289+008	dM2	10:28:54.91	+00:50:15.9	…	…	…	…	47.11	948.29	257.06 ± 1.71	0.414 ± 0.012
…	…	GJ 3607	J10303+328	M3.0 V	10:30:23.19	+32:50:07.3	…	…	…	…	51.14	553.01	303.87 ± 2.05	0.506 ± 0.019
10318+5706	LDS2314	GJ 397.1	…	K5 V	10:31:43.09	+57:06:59.9	A+(BC)	A	141.959	225.6	58.18	185.37	872.48 ± 3.36	0.700 ± 0.105
10318+5706	RAO 252	GJ 397.1 B	J10315+570	M5.0 V	10:31:30.64	+57:05:20.4	…	BC	142.037	225.6	76.16	161.31	…	…
…	…	PM J10320+0318	J10320+033	M2.0 V	10:32:02.31	+03:18:54.9	…	…	…	…	56.82	40.58	860.94 ± 9.67	0.620 ± 0.027
…	…	GJ 3610	J10345+463	M3.0 V	10:34:29.53	+46:18:07.2	A+B	A	…	…	26.96	424.70	174.98 ± 1.20	0.403 ± 0.017
10345+4618	LDS3999	GJ 3611	…	M4.5 V	10:34:25.22	+46:18:20.8	…	B	46.701	286.9	27.12	429.93	24.23 ± 0.13	0.168 ± 0.010
…	…	LP 670-17	J10350-094	dM3.0	10:35:01.36	-09:24:41.5	…	…	…	…	63.61	293.87	192.01 ± 1.23	0.371 ± 0.011
…	…	GJ 3612	J10354+694	M4.0 V	10:35:21.96	+69:26:48.5	Aab	Aab(2)	…	…	…	1773.72	…	0.389 ± 0.003
…	…	RX J1035.9+2853	J10359+288	M3.0 V	10:35:57.12	+28:53:30.3	…	…	…	…	39.60	141.60	243.89 ± 7.08	0.480 ± 0.020
…	…	RYSex	J10360+051	M4.0 V	10:36:00.52	+05:07:14.8	…	…	…	…	104.76	666.43	135.43 ± 0.75	0.359 ± 0.011
…	…	G 146-48	J10364+415	M2.5 V	10:36:27.19	+41:30:02.8	AB	A	…	…	52.12	336.63	…	0.494 ± 0.030
10364+4130	RAO 253	G 146-48B	…	M5.5 V	10:36:27.02	+41:30:01.8	…	B	2.122	241.3	95.05	345.11	…	0.155 ± 0.041
10367+1522	DAE 3	PM J10367+1521A	J10367+153	M3.5 V	10:36:44.96	+15:21:38.6	A+BC	A	0.730	228.6	54.62	135.56	…	0.295 ± 0.035
10367+1522	DAE 3	PM J10367+1521B	…	M4.5 V	10:36:44.92	+15:21:37.9	…	BC	0.858	218.7	39.57	118.34	…	…
…	…	LP 127-502	J10368+509	M4.5 V	10:36:48.58	+50:55:00.7	Aab	Aab(2?)	…	…	55.92	319.05	…	…
…	…	LP 490-42 A	J10379+127	M3.0 V	10:37:55.03	+12:46:37.6	AB	A	…	…	40.84	223.11	…	0.363 ± 0.033
10379+1247	CRC 60	LP 490-42 B	…	M3.0 V	10:37:55.05	+12:46:36.8	…	B	0.826	155.9	26.86	249.10	…	0.376 ± 0.032

Table D.2: Complete sample with the description of multiple systems (continued).

WDS id	WDS disc	Name	Karmn	Spectral type	α (2016.0)	δ (2016.0)	System	Component	ρ [arcsec]	θ [deg]	ϖ [mas]	$\mu_{\rm total}$ [mas a^{-1}]	$\mathcal{L}$ [$10^{-4}\,\mathcal{L}_\odot$]	$\mathcal{M}$ [$\mathcal{M}_\odot$]
…	…	GJ 3613	J10384+485	M3.0 V	10:38:29.47	+48:31:43.4	…	…	…	…	66.49	215.04	225.94 ± 1.13	0.461 ± 0.018
…	…	LP 262-400	J10385+354	M2.5 V	10:38:32.66	+35:29:53.7	…	…	…	…	36.75	515.87	219.75 ± 1.05	0.427 ± 0.017
…	…	StKM 1-873	J10389+250	M2.0 V	10:38:56.64	+25:05:39.0	…	…	…	…	36.72	191.10	296.60 ± 1.12	0.443 ± 0.017
…	…	GJ 399	J10396-069	dM2.5	10:39:39.79	-06:55:27.2	…	…	…	…	44.64	725.55	313.94 ± 2.17	0.459 ± 0.012
…	…	TYC 254-88-1	J10403+015	M1.0 V	10:40:21.42	+01:34:36.6	…	…	…	…	54.49	70.12	622.21 ± 4.13	0.590 ± 0.028
…	…	GJ 1134	J10416+376	M4.0 V	10:41:35.91	+37:36:33.4	…	…	…	…	27.77	1500.56	54.72 ± 0.31	0.215 ± 0.009
10430-0913	WSI 112	PM J10430-0912	J10430-092	M5.5 V	10:43:00.72	-09:12:35.0	(AB)	AB	0.575	136.2	27.72	2009.04	…	0.153 ± 0.042
…	…	LP 490-63	J10443+124	M3.5 V	10:44:18.52	+12:25:11.5	…	…	…	…	26.56	274.62	207.59 ± 1.00	0.441 ± 0.018
…	…	GJ 3616 A	J10448+324	M3.0 V	10:44:52.40	+32:24:41.3	AB+C	A	…	…	36.36	214.33	…	0.336 ± 0.034
10449+3224	CRC 61	GJ 3616 B	…	M4.0 V	10:44:52.43	+32:24:40.1	…	B	1.296	160.3	62.28	226.22	…	0.287 ± 0.035
10449+3224	LDS1258	GJ 3617	…	M5.0 V	10:44:54.79	+32:24:23.4	…	C	35.225	120.7	66.84	211.36	…	0.184 ± 0.040
…	…	GJ 400 A	J10453+385	M0.5 V	10:45:21.43	+38:30:44.8	AB	A	…	…	56.01	155.18	…	0.642 ± 0.027
10454+3831	HO 532	G3- 776067093937332992	…	M2.5 V	10:45:21.39	+38:30:44.4	…	B	0.684	232.7	60.10	159.02	…	0.393 ± 0.032
…	…	GJ 401	J10456-191	M0.5 V	10:45:36.98	-19:07:01.3	AB	A	…	…	42.55	1963.77	…	0.506 ± 0.029
10457-1907	LDS4013	GJ 401 B	…	DQ	10:45:36.93	-19:06:54.7	…	B	6.655	354.5	22.90	1962.56	…	0.500 ± 0.100
…	…	GJ 3619	J10460+096	M3.5 V	10:46:03.81	+09:41:47.1	…	…	…	…	45.85	287.36	148.75 ± 0.86	0.370 ± 0.016
10472+4027	CLO 5	LP 213-67	J10472+404	M6.5 Ve	10:47:12.19	+40:26:43.2	(AB)+C	AB	0.101	345.6	46.20	300.14	…	0.135 ± 0.043
10472+4027	LDS4016	LP 213-68	…	M8.0 V	10:47:13.36	+40:26:48.7	…	C	14.382	67.5	44.88	303.57	8.00 ± 0.17	0.149 ± 0.010
10474+0236	HDS1542	Ross 895	J10474+025	M2.0 V	10:47:24.47	+02:35:32.7	(AB)	AB	0.528	258.3	46.80	181.27	…	0.423 ± 0.032
…	…	GJ 3622	J10482-113	M6.5 V	10:48:13.24	-11:20:34.1	…	…	…	…	40.15	1635.97	7.46 ± 0.04	0.102 ± 0.048
…	…	GJ 3623	J10485+191	M3.0 V	10:48:32.84	+19:09:00.3	…	…	…	…	58.25	256.84	122.49 ± 0.53	0.333 ± 0.014
10498+3533	BEU 14	GJ 1138	J10497+355	M5.0 V	10:49:44.71	+35:32:34.3	(AB)	AB	0.281	54.2	41.44	1261.32	…	0.219 ± 0.038
…	…	GJ 3626	J10504+331	M3.5 V	10:50:26.08	+33:05:54.0	Aab	Aab(1)	…	…	23.15	638.33	…	0.436 ± 0.017
…	…	LZUMa	…	G5 V	10:50:39.98	+51:47:58.8	A+B	A	…	…	53.90	196.65	3514.87 ± 816.83	0.980 ± 0.147
10507+5148	LDS3019	GJ 3628	J10506+517	M4.1 V	10:50:37.91	+51:45:01.6	…	B	178.251	186.2	25.24	191.40	111.80 ± 0.55	0.339 ± 0.015
10509+0648	RAO256	EELeo	J10508+068	M4.0 V	10:50:51.11	+06:48:16.2	(AB)	AB	0.098	214.2	76.01	1184.61	79.95 ± 0.56	0.246 ± 0.011
10513+3607	BWL26	GJ 3629	J10513+361	M3.0 V	10:51:20.33	+36:07:24.5	(AB)	AB	0.206	119.6	37.15	198.40	…	0.414 ± 0.031
…	…	GJ 3630	J10520+005	M4.0 V	10:52:02.83	+00:32:38.5	Aabc	Aabc(3/4)	…	…	19.48	407.59	…	…
…	…	GJ 403	J10520+139	M4.0 V	10:52:03.01	+13:59:54.5	…	…	…	…	86.65	1142.17	88.32 ± 0.39	0.279 ± 0.013
…	…	GJ 3631	J10522+059	M5.5 V	10:52:13.50	+05:55:08.9	…	…	…	…	47.40	698.13	30.73 ± 0.15	0.179 ± 0.011
…	…	LP 671-8	J10546-073	M4.0 V	10:54:41.77	-07:18:39.4	AB	A	…	…	129.75	410.62	…	0.303 ± 0.035
10547-0719	CRC 62	G3- 3763681220170173952	…	…	10:54:41.83	-07:18:39.1	…	B	0.844	66.0	99.56	…	…	…
…	…	GJ 3632	J10555-093	M3.5 V	10:55:34.19	-09:21:18.7	…	…	…	…	35.08	522.15	87.27 ± 0.41	0.278 ± 0.013
…	…	PM J10563+0415	J10563+042	M2.5 V	10:56:22.32	+04:15:44.6	…	…	…	…	42.74	113.88	245.51 ± 1.66	0.453 ± 0.018
…	…	CNLeo	J10564+070	M6.0 V	10:56:24.77	+07:00:09.8	…	…	…	…	47.29	4715.33	10.10 ± 0.09	0.108 ± 0.047
…	…	Ross 447	J10576+695	M0.0 V	10:57:36.16	+69:35:48.8	…	…	…	…	55.19	632.69	934.57 ± 3.20	0.680 ± 0.026
…	…	LP 731-76	J10584-107	M5.0 V	10:58:27.78	-10:46:31.8	…	…	…	…	30.03	210.47	42.28 ± 0.21	0.197 ± 0.009
…	…	Ross 104	J11000+228	M2.5 V	11:00:03.76	+22:49:54.1	…	…	…	…	29.95	511.84	195.79 ± 93.22	0.370 ± 0.095
…	…	G 254-11A	J11003+728	M2.0 V	11:00:23.29	+72:52:17.6	AB	A	…	…	33.38	423.20	…	0.486 ± 0.030
11004+7252	NSN 608	G 254-11B	…	M4.0 V	11:00:23.11	+72:52:18.3	…	B	1.061	309.1	71.54	414.68	…	0.280 ± 0.035

Table D.2: Complete sample with the description of multiple systems (continued).

WDS id	WDS disc	Name	Karmn	Spectral type	α (2016.0)	δ (2016.0)	System	Component	ρ [arcsec]	θ [deg]	ϖ [mas]	$\mu_{\rm total}$ [mas a^{-1}]	$\mathcal{L}$ [$10^{-4}\,\mathcal{L}_\odot$]	$\mathcal{M}$ [$\mathcal{M}_\odot$]
…	…	GJ 3636	J11008+120	M5.5 V	11:00:50.58	+12:04:08.7	…	…	…	…	74.24	187.54	31.99 ± 0.27	0.197 ± 0.011
…	…	GJ 3637	J11013+030	M5.0 V	11:01:20.81	+03:00:10.8	…	…	…	…	39.49	1146.90	39.25 ± 0.22	0.191 ± 0.011
…	…	StKM 1-902	J11014+568	M1.0 V	11:01:26.72	+56:52:04.0	…	…	…	…	39.36	194.90	755.37 ± 3.68	0.629 ± 0.027
…	…	GJ 1141 A	J11023+165E	M1.0 V	11:02:19.29	+16:30:27.1	A+B	A	…	…	45.40	164.09	513.84 ± 3.05	0.550 ± 0.028
11024+1631	LDS 917	GJ 1141 B	J11023+165W	M1.0 V	11:02:18.02	+16:30:30.8	…	B	18.685	281.4	45.23	168.37	481.57 ± 2.83	0.536 ± 0.029
…	…	DSLeo	J11026+219	M1.0 Ve	11:02:38.51	+21:58:00.9	…	…	…	…	201.41	151.83	563.47 ± 2.47	0.575 ± 0.028
…	…	Wolf 360	J11030+037	M2.5 V	11:03:04.39	+03:44:19.2	…	…	…	…	53.58	244.83	…	…
…	…	LP 431-50	J11031+152	M3.5 Ve	11:03:08.01	+15:17:50.3	…	…	…	…	41.63	427.34	…	…
…	…	GJ 3639	J11031+366	M3.5 V	11:03:09.74	+36:39:09.1	…	…	…	…	54.97	190.86	119.20 ± 0.51	0.351 ± 0.015
…	…	HD 95735	J11033+359	M1.5 V	11:03:19.43	+35:56:55.2	…	…	…	…	34.55	4811.68	230.42 ± 6.91	0.398 ± 0.014
…	…	LP 491-51	J11036+136	M4.0 V	11:03:21.05	+13:37:58.2	Aab	Aab(1)	…	…	49.20	207.70	…	…
…	…	GJ 3640	J11042+400	M0.0 V	11:04:15.64	+40:00:15.1	…	…	…	…	51.79	225.85	976.99 ± 4.46	0.678 ± 0.026
…	…	LSPM J1104+3027	J11044+304	M3.0 V	11:04:28.35	+30:27:30.9	…	…	…	…	78.17	168.16	182.11 ± 0.94	0.356 ± 0.023
…	…	GJ 412 A	J11054+435	M1.0 V	11:05:22.09	+43:31:51.4	A+B	A	…	…	46.74	4505.31	230.89 ± 1.87	0.382 ± 0.011
11055+4332	VBS 18	WXUMa	J11055+435	M5.5 V	11:05:24.50	+43:31:33.3	…	B	31.854	124.7	53.45	4444.91	9.57 ± 0.05	0.115 ± 0.045
…	…	GJ 3641	J11055+450	M0.0 V	11:05:33.91	+45:00:27.9	AB	A	…	…	53.43	254.23	…	0.632 ± 0.027
11056+4501	NSN 609	G 176-8B	…	M6.0 V	11:05:33.92	+45:00:30.5	…	B	2.560	2.5	35.90	269.33	…	0.120 ± 0.045
…	…	GJ 3643	J11057+102	M3.0 V	11:05:43.80	+10:13:58.1	…	…	…	…	35.70	930.73	168.50 ± 1.07	0.371 ± 0.015
…	…	PM J11075+4345	J11075+437	M3.0 V	11:07:31.88	+43:45:56.3	…	…	…	…	48.60	117.73	101.43 ± 0.44	0.301 ± 0.014
…	…	GJ 1142 A	J11081-052	M3.0 V	11:08:06.48	-05:13:54.2	A+B	A	…	…	…	443.17	277.25 ± 1.62	0.482 ± 0.019
11080-0509	LDS 852	GJ 1142 B	…	DA3	11:07:59.89	-05:09:33.1	…	B	278.996	339.3	44.61	446.11	…	0.500 ± 0.100
…	…	GJ 3646	J11108+479	M4.0 V	11:10:51.05	+47:56:53.7	…	…	…	…	42.63	598.83	76.50 ± 0.39	0.276 ± 0.013
…	…	HD 97101	J11110+304E	K7 V	11:11:05.90	+30:26:42.5	A+B	A	…	…	142.10	623.58	1236.01 ± 8.02	0.640 ± 0.096
11111+3027	STT 231	HD 97101B	J11110+304W	M2.0 V	11:11:03.29	+30:26:38.0	…	B	34.153	262.4	36.49	639.04	511.07 ± 1.72	0.539 ± 0.029
…	…	GJ 9351 A	J11113+434	M2.5 V	11:11:18.88	+43:24:55.8	AB	A	…	…	57.01	782.79	…	0.432 ± 0.031
11114+4325	KUI 55	GJ 9351 B	…	M2.5 V	11:11:18.56	+43:24:55.3	…	B	3.568	262.5	…	764.96	…	0.440 ± 0.031
…	…	GJ 3647	J11118+335	M3.5 V	11:11:51.52	+33:32:13.1	AB	A	…	…	28.96	211.07	…	0.320 ± 0.034
…	…	LSPM J1111+3332E	…	…	…	…	…	B	…	…	41.27	197.47	…	…
…	…	GJ 3649	J11126+189	dM1.5	11:12:38.95	+18:56:05.5	…	…	…	…	41.20	21.84	456.48 ± 2.23	0.510 ± 0.012
11132+0014	YSC 208	Wolf 370	J11131+002	M0.0 V	11:13:09.63	+00:14:16.7	(AB)	AB	0.292	339.0	61.22	456.20	…	0.670 ± 0.032
11152+7329	STF1516	HD 97584	…	K4 V	11:15:10.39	+73:28:32.5	A+B	A	67.600	102.9	78.57	418.80	2152.23 ± 5.97	0.730 ± 0.110
…	…	HD 97584B	J11151+734	M2.5 V	11:15:09.56	+73:28:38.0	…	B	6.481	327.1	34.41	396.51	209.63 ± 0.93	0.416 ± 0.017
…	…	GJ 3652	J11152+194	M3.5 V	11:15:12.62	+19:27:04.3	…	…	…	…	65.47	512.69	134.04 ± 0.78	0.350 ± 0.015
…	…	GJ 421 A	…	K7 V	11:15:20.90	-18:08:49.2	A+B+C	A	…	…	35.30	748.09	…	0.695 ± 0.104
11154-1807	LDS 342	GJ 421 B	…	K5 V	11:15:19.61	-18:08:52.0	…	B	18.567	261.4	34.94	752.44	1010.88 ± 4.59	0.700 ± 0.105
11154-1807	LDS 342	GJ 421 C	J11152-181	M3.0 V	11:15:15.67	-18:07:47.8	…	C	96.651	309.5	49.98	753.07	108.79 ± 0.51	0.313 ± 0.014
…	…	G 122-8	J11154+410	M3.5 V	11:15:26.72	+41:05:12.5	…	…	…	…	…	247.04	204.74 ± 1.36	0.411 ± 0.017
…	…	GJ 3653	J11159+553	M0.5 V	11:15:53.69	+55:19:49.2	…	…	…	…	40.73	200.30	733.95 ± 3.11	0.605 ± 0.027
…	…	LP 169-22	J11195+466	M5.5 V	11:19:31.09	+46:41:33.4	…	…	…	…	38.25	682.13	12.86 ± 0.07	0.126 ± 0.010
11200+6551	TAM 1	GJ 424	J11200+658	M0.0 V	11:19:57.14	+65:50:50.3	(AB)	AB	0.132	334.0	38.34	2952.33	…	0.531 ± 0.029

Table D.2: Complete sample with the description of multiple systems (continued).

WDS id	WDS disc	Name	Karmn	Spectral type	α (2016.0)	δ (2016.0)	System	Component	ρ [arcsec]	θ [deg]	ϖ [mas]	$\mu_{\rm total}$ [mas a^{-1}]	$\mathcal{L}$ [$10^{-4}\,\mathcal{L}_\odot$]	$\mathcal{M}$ [$\mathcal{M}_\odot$]
…	…	LP 733-99	J11201-104	M2.0 V	11:20:05.89	-10:29:46.4	…	…	…	…	32.20	198.88	414.88 ± 2.99	0.506 ± 0.029
…	…	HD 98712A	…	K7 V	11:21:26.87	-20:27:15.3	AB	A	…	…	47.74	191.29	…	0.650 ± 0.097
11214-2027	STN 22	HD 98712B	J11214-204	M2.5 V	11:21:26.84	-20:27:11.5	…	B	3.811	354.4	36.46	255.49	…	0.421 ± 0.031
…	…	GJ 1146	J11216+061	M3.5 V	11:21:37.67	+06:08:00.7	…	…	…	…	64.20	1758.39	72.59 ± 0.34	0.235 ± 0.012
…	…	GJ 3657	J11231+258	M5.0 V	11:23:06.77	+25:53:31.7	…	…	…	…	28.93	1061.30	25.81 ± 0.14	0.162 ± 0.010
…	…	GJ 3658	J11233+448	M2.0 V	11:23:20.14	+44:48:36.5	…	…	…	…	99.46	351.11	366.15 ± 2.60	0.478 ± 0.030
…	…	Wolf 386	J11237+085	M0.5 V	11:23:43.49	+08:33:51.6	…	…	…	…	82.00	1021.78	420.33 ± 1.98	0.521 ± 0.029
…	…	GJ 426.1 A	…	F1 IV	11:23:55.62	+10:31:44.9	(AabB)+C	Aab	…	…	36.94	169.81	…	…
11239+1032	STF1536	GJ 426.1 B	…	F5 V	11:23:55.75	+10:31:44.7	…	B	2.050	95.1	34.04	185.02	…	1.330 ± 0.200
11239+1032	STF1536	LSPM J1123+1037	J11238+106	M0.5 V	11:23:50.12	+10:37:07.0	…	C	332.098	345.9	32.04	173.50	767.99 ± 13.39	0.634 ± 0.027
…	…	Ross 1002	J11239-183	M3.0 V	11:23:56.61	-18:21:49.5	…	…	…	…	27.91	612.81	102.04 ± 0.60	0.302 ± 0.014
…	…	Ross 448	J11247+675	M1.0 V	11:24:46.53	+67:33:08.5	…	…	…	…	28.05	393.02	362.59 ± 1.63	0.493 ± 0.018
…	…	StKM 1-941	J11249+024	M1.0 V	11:24:58.52	+02:28:26.8	…	…	…	…	72.12	275.17	322.14 ± 1.49	0.437 ± 0.016
…	…	1R112405.0+380809	J11240+381	M4.5 V	11:24:04.53	+38:08:10.7	A+B	A	…	…	72.99	121.95	49.52 ± 0.23	0.233 ± 0.012
11241+3808	RED23	2MUCD 10984	…	M8.5 V	11:24:05.06	+38:08:05.3	…	B	8.250	130.6	53.17	126.02	…	0.111 ± 0.054
…	…	GJ 3660	J11254+782	d/sdM4	11:25:26.06	+78:15:52.9	A+B	A	…	…	53.19	672.13	253.30 ± 1.11	0.433 ± 0.017
11254+7817	LDS 920	GJ 3661	…	M3.0 V	11:25:13.53	+78:16:55.0	…	B	72.909	328.4	39.82	671.49	181.53 ± 0.76	0.363 ± 0.015
…	…	PM J11266+3756	J11266+379	M2.0 V	11:26:37.40	+37:56:22.8	AB	A	…	…	40.43	150.84	…	0.554 ± 0.028
11266+3756	KPP3238	PM J11266+3756B	…	M1.5 V	11:26:37.31	+37:56:22.5	…	B	1.145	254.9	39.47	150.58	…	0.498 ± 0.029
…	…	GJ 3664	J11276+039	M0.0 V	11:27:38.47	+03:58:36.1	…	…	…	…	32.57	98.48	1045.91 ± 5.46	0.689 ± 0.026
…	…	Wolf 398	J11289+101	M4.0 V	11:28:55.45	+10:10:48.2	…	…	…	…	219.33	935.04	91.65 ± 0.57	0.266 ± 0.011
…	…	K2-18	J11302+076	dM2.5	11:30:14.43	+07:35:16.1	…	…	…	…	43.22	155.46	272.31 ± 1.61	0.433 ± 0.013
…	…	LP 672-42	J11306-080	M3.5 V	11:30:41.44	-08:05:38.9	…	…	…	…	102.75	437.49	160.57 ± 0.70	0.343 ± 0.011
…	…	StKM 1-950	J11307+549	M1.0 V	11:30:43.80	+54:57:29.1	A+B	A	…	…	44.27	111.40	835.36 ± 5.44	0.641 ± 0.027
…	…	G3- 844502037681090688	…	M6.0 V	11:30:42.66	+54:56:57.0	…	B*	33.615	197.0	37.39	112.07	13.69 ± 0.13	0.131 ± 0.010
…	…	GJ 3668	J11311-149	M5.0 V	11:31:08.84	-14:57:43.2	…	…	…	…	37.89	1433.08	31.60 ± 0.22	0.182 ± 0.011
…	…	LP 552-68	J11315+022	M2.5 V	11:31:32.21	+02:13:34.8	…	…	…	…	143.54	792.86	313.43 ± 1.51	0.484 ± 0.018
…	…	Ross 903	J11317+226	M0.5 V	11:31:42.72	+22:40:02.2	…	…	…	…	29.96	585.58	567.56 ± 3.30	0.568 ± 0.028
…	…	GJ 3672	J11351-056	M4.5 V	11:35:07.66	-05:39:38.2	…	…	…	…	25.46	994.67	35.58 ± 0.19	0.194 ± 0.011
11355-3856	CRC 63	GJ 3673	J11355+389	M3.5 V	11:35:30.94	+38:55:33.4	AB	A	0.339	65.6	75.49	754.70	…	0.386 ± 0.033
…	…	G 122-34B	…	M3.0 V	11:35:30.95	+38:55:33.4	…	B	0.196	87.8	71.80	754.70	…	0.346 ± 0.034
…	…	Ross 112	J11376+587	M2.5 V	11:37:38.30	+58:42:38.2	…	…	…	…	48.81	414.06	611.04 ± 5.80	0.553 ± 0.028
…	…	LP 19-403	J11404+770	M2.0 V	11:40:27.09	+77:04:19.0	…	…	…	…	…	542.43	558.91 ± 2.64	0.552 ± 0.028
…	…	Ross 1003	J11417+427	M4.0 V	11:41:43.80	+42:45:05.7	…	…	…	…	52.12	582.49	149.18 ± 0.65	0.350 ± 0.014
…	…	Ross 115	J11420+147	M3.0 V	11:42:01.43	+14:46:39.9	…	…	…	…	36.63	353.99	258.47 ± 1.31	0.465 ± 0.018
…	…	Ross 905	J11421+267	M2.5 V	11:42:12.16	+26:42:10.6	…	…	…	…	415.18	1209.56	241.90 ± 1.20	0.414 ± 0.012
…	…	LP 375-23	J11423+230	M0.5 V	11:42:18.14	+23:01:37.3	A+B	A	…	…	42.67	209.12	562.02 ± 2.63	0.582 ± 0.028
11423+2302	LDS 926	LP 375-24	…	M4.0 V	11:42:20.98	+23:03:14.8	…	B	105.050	22.0	68.96	209.27	96.86 ± 0.44	0.294 ± 0.013
…	…	GJ 3682	J11433+253	M4.0 V	11:43:23.27	+25:18:13.2	…	…	…	…	148.20	229.78	265.46 ± 4.18	0.444 ± 0.018
…	…	LP 433-47	J11451+183	M4.0 V	11:45:11.57	+18:20:53.8	…	…	…	…	31.51	411.30	227.61 ± 1.26	0.463 ± 0.018

Table D.2: Complete sample with the description of multiple systems (continued).

WDS id	WDS disc	Name	Karmn	Spectral type	α (2016.0)	δ (2016.0)	System	Component	ρ [arcsec]	θ [deg]	ϖ [mas]	$\mu_{\rm total}$ [mas a^{-1}]	$\mathcal{L}$ [$10^{-4}\,\mathcal{L}_\odot$]	$\mathcal{M}$ [$\mathcal{M}_\odot$]
…	…	GJ 443	J11467-140	M3.0 V	11:46:43.69	-14:01:04.4	…	…	…	…	31.61	1059.90	379.08 ± 2.64	0.472 ± 0.030
…	…	GJ 3684 A	J11470+700	M4.0 V	11:47:04.37	+70:01:57.7	AB	A	…	…	46.68	347.22	…	0.324 ± 0.034
11471+7002	NSN 621	GJ 3684 B	…	M3.5 V	11:47:04.25	+70:01:58.4	…	B	0.873	318.6	67.26	334.67	…	0.307 ± 0.034
…	…	1R114728.8+664405	J11474+667	M5.0 V	11:47:28.27	+66:44:02.6	…	…	…	…	24.22	110.02	80.25 ± 0.79	0.289 ± 0.010
…	…	GJ 3685	J11476+002	M4.0 V	11:47:40.41	+00:15:18.5	A+B	A	…	…	38.99	330.04	123.65 ± 0.94	0.339 ± 0.011
11477+0016	LDS5207	GJ 3686	…	M5e	11:47:41.77	+00:15:04.4	…	B	24.744	124.5	38.99	322.04	…	0.126 ± 0.044
…	…	GJ 445	J11476+786	M4.0 V	11:47:45.46	+78:41:35.9	…	…	…	…	83.76	889.55	79.81 ± 0.51	0.254 ± 0.012
…	…	FIVir	J11477+008	dM4	11:47:45.05	+00:47:56.8	…	…	…	…	…	1365.51	38.56 ± 0.26	0.173 ± 0.010
…	…	GJ 3688	J11483-112	M3.0 V	11:48:18.61	-11:17:15.0	…	…	…	…	…	733.60	281.29 ± 2.31	0.425 ± 0.031
…	…	G 10-52	J11485+076	M3.5 V	11:48:35.63	+07:41:37.8	…	…	…	…	43.80	221.18	98.96 ± 0.47	0.318 ± 0.014
…	…	BPM 87650	J11496+220	M0.0 V	11:49:40.33	+22:03:52.5	…	…	…	…	392.75	132.52	1871.25 ± 15.15	0.808 ± 0.024
…	…	GJ 1151	J11509+483	M4.5 V	11:50:55.24	+48:22:23.2	…	…	…	…	65.84	1820.46	34.51 ± 0.18	0.168 ± 0.009
…	…	GJ 450	J11511+352	M1.5 V	11:51:06.98	+35:16:23.3	…	…	…	…	32.82	372.60	323.22 ± 1.66	0.440 ± 0.012
11519+0731	BWL 66	RX J1151.9+0731	J11519+075	M2.5 Ve	11:51:56.69	+07:31:25.2	(AB)	AB(2)	0.514	107.1	71.23	150.54	…	…
…	…	GJ 3691	J11529+244	M4.1 V	11:52:57.55	+24:28:46.9	…	…	…	…	18.05	325.98	40.47 ± 0.16	0.209 ± 0.011
…	…	GJ 452	J11532-073	M2.5 V	11:53:15.91	-07:22:35.8	…	…	…	…	203.89	534.44	284.29 ± 1.82	0.460 ± 0.018
…	…	TYC 3016-577-1	J11533+430	M1.0 V	11:53:23.24	+43:02:56.3	…	…	…	…	203.83	177.20	548.56 ± 1.98	0.567 ± 0.028
…	…	GJ 3693	J11538+069	M8.0 V	11:53:53.01	+06:59:41.9	…	…	…	…	34.61	947.89	8.66 ± 0.06	0.129 ± 0.010
…	…	Ross 119	J11541+098	M4.0 Ve	11:54:07.98	+09:48:10.0	…	…	…	…	34.62	806.20	62.41 ± 0.39	0.231 ± 0.012
…	…	PM J11549-0206	J11549-021	M3.0 V	11:54:56.83	-02:06:08.4	…	…	…	…	55.99	107.77	140.39 ± 0.69	0.359 ± 0.015
…	…	Ross 129	J11551+009	M1.5 V	11:55:06.42	+00:58:26.1	…	…	…	…	38.84	741.06	547.58 ± 3.89	0.554 ± 0.028
…	…	GJ 3694	J11557-189	M3.5 V	11:55:44.87	-18:54:36.6	…	…	…	…	40.18	609.07	81.34 ± 0.39	0.286 ± 0.013
…	…	LP 851-346	J11557-227	M7.5 V	11:55:42.42	-22:25:01.8	…	…	…	…	40.29	418.69	6.49 ± 0.04	0.119 ± 0.010
…	…	Ross 122	J11575+118	M2.0 V	11:57:32.06	+11:49:43.7	…	…	…	…	41.46	723.41	426.28 ± 2.00	0.511 ± 0.029
…	…	GJ 3696	J11582+425	M4.0 V	11:58:17.81	+42:34:23.0	…	…	…	…	84.18	398.77	94.75 ± 0.45	0.310 ± 0.014
11522+0357	CRC 64	StM 162	J11521+039	M4.0 V	11:52:09.87	+03:57:21.4	(AB)	AB	0.337	26.0	84.16	158.65	…	0.296 ± 0.035
11590+4240	PKO 32	GJ 3697	J11589+426	M2.0 V	11:58:58.99	+42:39:40.8	(AB)	AB	0.303	232.8	59.60	335.59	…	…
11588+5934	WOR 21	G 197-38	J11585+595	M0.0 V	11:58:33.53	+59:33:22.2	(AB)	AB	0.903	286.5	59.68	712.92	…	…
…	…	GJ 3698	J12006-138	M3.5 V	12:00:36.36	-13:49:36.6	A+B	A	…	…	74.88	477.06	277.14 ± 2.30	0.419 ± 0.031
12007-1348	LDS4166	GJ 3699	…	M4.5 V	12:00:35.98	-13:49:40.6	…	B	6.791	233.9	…	468.87	…	0.194 ± 0.039
…	…	GJ 3700	J12016-122	M3.0 V	12:01:40.72	-12:13:57.6	A+B	A	…	…	59.92	237.56	305.10 ± 2.25	0.507 ± 0.020
12017-1214	CRC 65	L 829-10 B	…	M7.0 V	12:01:40.90	-12:13:52.0	…	B	6.122	24.4	39.42	245.96	…	0.101 ± 0.049
…	…	Ross 689	J12054+695	M4.0 V	12:05:28.29	+69:32:21.7	…	…	…	…	69.14	460.17	103.39 ± 0.50	0.297 ± 0.012
…	…	LSPM J1205+7825	J12057+784	M2.5 V	12:05:45.99	+78:25:51.6	…	…	…	…	69.13	204.94	255.48 ± 1.24	0.435 ± 0.017
…	…	GJ 455	J12023+285	sdM3.5	12:02:17.12	+28:35:13.4	Aab	Aab(2)	…	…	60.95	788.79	…	…
…	…	1R120847.7+302120	J12088+303	M2.5 V	12:08:49.63	+30:21:00.5	…	…	…	…	53.89	93.75	313.28 ± 1.38	0.484 ± 0.018
…	…	StM 165	J12093+210	M2.5 V	12:09:21.70	+21:03:05.8	…	…	…	…	43.66	161.21	329.22 ± 6.30	0.452 ± 0.031
…	…	GJ 3707	J12100-150	dM3.5	12:10:05.54	-15:04:28.4	…	…	…	…	43.62	715.19	163.68 ± 1.08	0.362 ± 0.013
12064-1315	JNN77	1R120622.6-131453	J12063-132	M3.5 V	12:06:22.22	-13:14:57.2	(AB)	AB	0.425	54.1	43.58	102.51	…	0.466 ± 0.031
…	…	GJ 9393	J12109+410	M0.0 V	12:10:56.90	+41:03:31.7	…	…	…	…	43.23	229.44	600.49 ± 2.24	0.602 ± 0.027

Table D.2: Complete sample with the description of multiple systems (continued).

WDS id	WDS disc	Name	Karmn	Spectral type	α (2016.0)	δ (2016.0)	System	Component	ρ [arcsec]	θ [deg]	ϖ [mas]	$\mu_{\rm total}$ [mas a^{-1}]	$\mathcal{L}$ [$10^{-4}\,\mathcal{L}_\odot$]	$\mathcal{M}$ [$\mathcal{M}_\odot$]
…	…	LP 734-34	J12104-131	M4.5 V	12:10:28.65	-13:10:29.5	Aab	Aab(2)	…	…	139.34	422.76	…	0.013
…	…	GJ 3708	J12111-199	dM3.0	12:11:11.52	-19:57:41.0	A+B	A	…	…	35.49	281.54	166.78 ± 0.86	0.343 ± 0.010
12113-1958	LDS 390	GJ 3709	J12112-199	M2.5 V	12:11:16.71	-19:58:24.7	…	B	85.283	120.8	95.52	278.50	85.89 ± 0.43	0.275 ± 0.013
…	…	GJ 3713	J12121+488	M2.5 V	12:12:11.68	+48:48:58.3	AB	A	…	…	110.23	371.62	…	0.392 ± 0.032
12122+4849	SKF1634	G 122-74B	…	M4.5 V	12:12:11.74	+48:48:55.5	…	B	2.848	167.9	52.82	382.48	…	0.221 ± 0.038
…	…	LP 39-66	J12122+714	M3.0 V	12:12:13.89	+71:25:26.2	…	…	…	…	72.86	409.18	240.42 ± 1.06	0.477 ± 0.019
…	…	HD 238090	J12123+544S	M0.0 V	12:12:21.29	+54:29:10.2	A+B	A	…	…	76.19	250.12	695.72 ± 2.31	0.620 ± 0.027
12123+5429	VYS 5	GJ 458 B	J12123+544N	M3.0 V	12:12:21.58	+54:29:24.6	…	B	14.655	10.1	50.13	255.62	67.73 ± 0.28	0.259 ± 0.013
…	…	PM J12124+1211	J12124+121	M2.0 V	12:12:25.99	+12:11:38.2	…	…	…	…	61.65	73.33	350.00 ± 2.08	0.481 ± 0.030
12125+3940	HDS1727	GJ 3714	J12124+396	M1.0 V	12:12:29.65	+39:40:25.2	(AB)	AB	0.483	333.9	30.46	224.65	…	0.560 ± 0.028
…	…	IVCom	J12133+166	M1.5 V	12:13:19.91	+16:41:32.3	…	…	…	…	49.58	679.56	427.50 ± 2.41	0.507 ± 0.018
…	…	GJ 3717	J12144+245	M2.0 V	12:14:26.04	+24:35:20.5	…	…	…	…	42.35	371.53	359.35 ± 1.92	0.486 ± 0.030
…	…	GJ 458.2	J12151+487	M0.5 V	12:15:08.46	+48:43:56.4	…	…	…	…	41.50	231.72	792.43 ± 6.12	0.637 ± 0.027
…	…	GJ 3718	J12154+391	M1.5 V	12:15:27.93	+39:11:15.4	…	…	…	…	41.67	337.93	418.22 ± 2.52	0.514 ± 0.029
…	…	StKM 2-809	J12156+526	M4.0 Ve	12:15:39.55	+52:39:08.7	…	…	…	…	55.58	105.25	328.98 ± 4.21	0.477 ± 0.012
…	…	GJ 1154	J12142+006	M4.5 Ve	12:14:15.53	+00:37:21.8	…	…	…	…	39.16	992.84	34.61 ± 0.25	0.206 ± 0.011
…	…	G3- 1547529669400723968	…	M2/3 V	12:16:14.94	+50:53:38.4	AB	A	…	…	42.67	86.59	…	0.362 ± 0.033
12163+5054	CRC 66	RX J1216.2+5053	J12162+508	M4.0 V	12:16:14.90	+50:53:36.7	…	B	1.785	192.0	54.19	86.61	…	0.308 ± 0.034
…	…	GJ 1155 A	J12168+029	M3.0 V	12:16:51.16	+02:58:09.0	AB	A	…	…	54.31	700.55	…	0.348 ± 0.033
12169+0258	LDS 935	GJ 1155 B	…	DA	12:16:51.17	+02:58:06.9	…	B	2.126	177.9	44.32	711.07	…	0.500 ± 0.100
…	…	PM J12168+2451E	J12168+248	M1.5 V	12:16:52.62	+24:51:06.0	…	…	…	…	44.27	51.85	298.84 ± 1.41	0.445 ± 0.017
…	…	GLVir	J12189+111	M4.5 Ve	12:18:58.02	+11:07:37.0	…	…	…	…	25.30	1285.97	22.07 ± 0.12	0.152 ± 0.009
…	…	GJ 3719	J12169+311	M3.0 V	12:16:58.27	+31:09:22.6	Aab	Aab(2)	…	…	32.83	133.17	…	…
…	…	LP 320-626	J12191+318	M3.5 V	12:19:05.55	+31:50:43.5	AabB	Aab(2)	…	…	35.26	321.46	…	…
12191+3151	RAO 274	LP 320-626	…	M3.5 V	12:19:05.47	+31:50:42.2	…	B	1.739	220.6	25.34	295.65	…	…
…	…	Wolf 408	J12194+283	M0.5 V	12:19:23.31	+28:22:57.8	…	…	…	…	34.81	652.53	814.53 ± 4.58	0.640 ± 0.027
…	…	StKM 1-1007	J12198+527	M0.0 V	12:19:47.76	+52:46:43.1	…	…	…	…	78.29	209.58	684.47 ± 3.22	0.617 ± 0.027
…	…	G 123-36	J12199+364	M1.0 V	12:29:55.22	+36:26:40.0	…	…	…	…	26.25	204.34	438.43 ± 4.56	0.527 ± 0.029
…	…	GJ 461	J12204+005	M0.0 V	12:20:25.59	+00:35:00.4	AB	A	…	…	74.20	60.60	…	0.609 ± 0.027
12204+0035	RST5366	G3- 3699797155055781760	…	M2.5 V	12:20:25.60	+00:35:01.3	…	B	0.882	14.6	24.78	129.05	…	0.418 ± 0.031
…	…	G 148-48	J12214+306W	M5.0 V	12:21:26.79	+30:38:31.4	A+B	A	…	…	24.73	339.77	18.53 ± 0.21	0.144 ± 0.010
12215+3038	GIC 106	LP 320-416	J12214+306E	M4.5 V	12:21:26.49	+30:38:33.6	…	B	4.497	298.9	86.90	317.63	…	0.141 ± 0.042
…	…	LP 39-245	J12217+682	M3.0 V	12:21:46.41	+68:16:07.3	…	…	…	…	35.62	429.42	168.82 ± 0.84	0.371 ± 0.015
…	…	Wolf 409	J12223+251	M0.5 V	12:22:20.46	+25:10:08.6	…	…	…	…	63.21	723.19	559.65 ± 2.91	0.584 ± 0.028
…	…	BD+28 2110	J12225+123	M0.0 V	12:22:33.90	+27:36:16.5	…	…	…	…	54.83	148.54	894.83 ± 4.86	0.667 ± 0.026
…	…	Ross 690	J12230+640	M3.0 V	12:22:58.52	+64:01:56.9	…	…	…	…	31.04	769.71	335.88 ± 1.52	0.484 ± 0.014
…	…	Wolf 411	J12235+279	M0.0 V	12:23:34.55	+27:54:49.6	…	…	…	…	31.04	183.00	608.70 ± 2.78	0.599 ± 0.027
12228-0405	BWL 29	G 13-33	J12228-040	M4.5 V	12:22:50.33	-04:04:47.5	(AB)	AB	0.107	144.8	25.19	263.33	…	0.184 ± 0.044
…	…	HD 107888	J12238+125	M0.0 V	12:23:53.60	+12:34:46.2	…	…	…	…	35.78	173.35	775.49 ± 3.08	0.637 ± 0.027
…	…	Ross 695	J12248-182	dM2.0	12:24:53.73	-18:15:09.2	…	…	…	…	90.69	2555.76	96.99 ± 0.37	0.270 ± 0.010

Table D.2: Complete sample with the description of multiple systems (continued).

WDS id	WDS disc	Name	Karmn	Spectral type	α (2016.0)	δ (2016.0)	System	Component	ρ [arcsec]	θ [deg]	ϖ [mas]	$\mu_{\rm total}$ [mas a^{-1}]	$\mathcal{L}$ [$10^{-4}\,\mathcal{L}_\odot$]	$\mathcal{M}$ [$\mathcal{M}_\odot$]
12236+6711	HDS1745	GJ 3722	J12235+671	M2.5 V	12:23:33.85	+67:11:16.4	(AB)	AB	0.621	33.3	40.70	268.66	…	0.350 ± 0.033
12251+6025	GIC 108	LP 95-135	J12251+604	M1.0 V	12:25:05.64	+60:25:06.0	A+B	A	19.987	65.4	102.30	198.04	516.78 ± 2.59	0.552 ± 0.028
…	…	LP 95-136	…	M1.5 V	12:25:08.10	+60:25:14.3	…	B	19.987	65.5	32.37	200.57	433.44 ± 2.23	0.520 ± 0.029
…	…	HD 108421A	…	K2 V	12:27:13.83	+27:01:24.9	AB+C	A	…	…	32.40	265.14	…	0.770 ± 0.116
12272+2701	STF1643	HD 108421B	…	K4 V	12:27:13.84	+27:01:27.6	…	B	2.756	4.1	27.75	256.19	…	0.729 ± 0.109
12272+2701	LEP 54	CXCom	J12269+270	M4.5 V	12:26:57.47	+27:00:49.7	…	C	221.398	260.9	36.36	265.95	77.61 ± 1.50	0.298 ± 0.014
…	…	G 148-61	J12274+374	M1.5 V	12:27:29.12	+37:26:35.1	…	…	…	…	51.58	249.10	307.45 ± 1.17	0.452 ± 0.017
…	…	G 13-39A	J12277-032	M3.5 V	12:27:44.38	-03:15:01.3	AB	A	…	…	32.86	295.11	…	0.396 ± 0.032
12277-0315	CRC 67	G 13-39B	…	M4.5 V	12:27:44.41	-03:14:59.9	…	B	1.469	14.9	32.65	319.40	…	0.221 ± 0.038
…	…	Ross 948A	J12288-106N	M2.0 V	12:28:52.85	-10:39:48.6	A+B	A	…	…	47.50	279.65	…	0.469 ± 0.030
12288-1040	RST3792	Ross 948B	J12288-106S	M2.0 V	12:28:52.65	-10:39:50.8	…	B	3.771	233.3	53.14	280.43	…	0.461 ± 0.030
12290+0826	WSI 113	Wolf 414	J12289+084	M3.5 V	12:28:56.90	+08:25:27.3	(AB)	AB	0.072	69.8	53.02	683.10	…	0.356 ± 0.033
12290+4144	BWL 31	GJ 3729	J12290+417	M3.5 V	12:29:02.65	+41:43:45.9	(AB)	AabB(2/3?)	0.050	255.5	50.42	286.43	…	…
…	…	GJ 1159 A	J12292+535	M4.0 V	12:29:12.22	+53:32:47.0	A+B	A	…	…	190.33	1228.81	89.20 ± 0.40	0.300 ± 0.014
12294+5333	LDS3046	GJ 1159 B	…	M6.0 V	12:29:11.96	+53:33:08.3	…	B	21.394	353.7	296.31	1230.60	9.73 ± 0.06	0.116 ± 0.009
…	…	GJ 3730	J12294+229	M4.0 V	12:29:26.92	+22:59:46.4	…	…	…	…	34.94	173.83	82.96 ± 0.48	0.289 ± 0.013
…	…	GJ 3731	J12299-054W	M3.5 V	12:29:53.57	-05:27:29.2	Aab+B	Aab(2)	…	…	34.64	646.28	…	…
12298-0527	B2737	GJ 3732	J12299-054E	M4.0 V	12:29:54.05	-05:27:25.2	…	B	8.153	60.5	48.29	633.07	…	0.257 ± 0.036
…	…	Wolf 417	J12312+086	M0.5 V	12:31:15.12	+08:48:29.8	…	…	…	…	20.21	823.04	627.57 ± 3.32	0.599 ± 0.027
…	…	GJ 3733	J12323+315	M3.0 V	12:32:19.79	+31:36:03.2	…	…	…	…	124.34	473.16	276.47 ± 5.11	0.482 ± 0.019
…	…	GJ 3734	J12324+203	M2.5 V	12:32:26.37	+20:23:28.0	…	…	…	…	114.09	49.52	179.03 ± 1.13	0.408 ± 0.017
…	…	LP 39-249	J12327+682	M0.0 V	12:32:44.66	+68:15:42.1	…	…	…	…	19.71	215.82	878.12 ± 3.28	0.664 ± 0.026
…	…	Wolf 424 A	J12332+090	M5.0 V	12:33:15.48	+09:01:19.5	AB	A	…	…	59.63	1808.82	…	0.140 ± 0.043
12335+0901	REU1	Wolf 424 B	…	M5.5 V	12:33:15.52	+09:01:18.6	…	B	1.149	145.3	51.25	1722.48	…	0.143 ± 0.042
…	…	PM J12349+3214	J12349+322	M3.5 V	12:34:54.03	+32:14:29.2	…	…	…	…	35.47	79.89	254.04 ± 1.51	0.491 ± 0.019
…	…	Wolf 427	J12350+098	M2.5 V	12:35:00.22	+09:49:37.5	…	…	…	…	67.14	551.02	331.44 ± 1.51	0.482 ± 0.012
…	…	GJ 3736	J12363-043	M3.0 V	12:36:22.35	-04:22:41.7	…	…	…	…	86.78	502.65	174.92 ± 0.99	0.378 ± 0.016
…	…	PM J12368-0159	J12368-019	M3.5 V	12:36:51.96	-01:59:02.0	…	…	…	…	40.60	176.91	194.26 ± 1.17	0.426 ± 0.017
…	…	LP 795-38	J12373-208	dM4.0	12:37:21.52	-20:52:42.4	…	…	…	…	39.19	429.67	202.80 ± 1.02	0.401 ± 0.014
…	…	GJ 1162	J12387-043	M4.3 V	12:38:46.47	-04:19:20.2	…	…	…	…	42.12	773.98	91.94 ± 0.47	0.305 ± 0.014
…	…	Wolf 433	J12388+116	M3.5 V	12:38:51.18	+11:41:42.1	…	…	…	…	91.27	1182.67	276.45 ± 1.60	0.446 ± 0.013
…	…	G 123-049A	J12390+470	M2.5 Ve	12:39:05.24	+47:02:21.4	(AB)	A	…	…	39.53	…	…	…
12391+4702	CFN 9	G 123-049B	…	M2.0 V	12:39:05.30	+47:02:21.2	…	B	0.661	115.1	45.90	402.46	…	0.444 ± 0.031
…	…	GJ 3739	J12397+255	M4.0 V	12:39:43.32	+25:30:43.3	…	…	…	…	62.55	240.19	59.91 ± 0.29	0.242 ± 0.012
…	…	GJ 3741	J12416+482	M1.0 V	12:41:38.24	+48:14:22.3	…	…	…	…	…	267.98	396.01 ± 2.39	0.507 ± 0.029
…	…	RX J1241.7+5645	J12417+567	M3.5 V	12:41:47.59	+56:45:13.7	…	…	…	…	23.21	116.23	136.82 ± 0.67	0.354 ± 0.015
…	…	G 123-55	J12428+418	M4.0 Ve	12:42:49.10	+41:53:47.8	…	…	…	…	39.11	550.33	163.84 ± 0.79	0.382 ± 0.012
…	…	GJ 1163	J12436+251	M3.5 Ve	12:43:35.62	+25:06:21.1	…	…	…	…	39.29	370.26	184.47 ± 2.43	0.414 ± 0.017
…	…	LP 735-29	J12440-111	M4.5 V	12:44:00.22	-11:10:32.8	…	…	…	…	40.36	502.79	41.38 ± 0.19	0.211 ± 0.011
…	…	Ross 991	J12470+466	M2.5 V	12:46:59.81	+46:37:28.6	…	…	…	…	40.19	817.84	351.80 ± 1.70	0.469 ± 0.030

Table D.2: Complete sample with the description of multiple systems (continued).

WDS id	WDS disc	Name	Karmn	Spectral type	α (2016.0)	δ (2016.0)	System	Component	ρ [arcsec]	θ [deg]	ϖ [mas]	$\mu_{\rm total}$ [mas a^{-1}]	$\mathcal{L}$ [10^{-4} $\mathcal{L}_\odot$]	$\mathcal{M}$ [$\mathcal{M}_\odot$]
…	…	GJ 3747	J12471-035	M3.0 V	12:47:09.24	-03:34:18.0	…	…	…	…	64.80	508.13	200.56 ± 1.28	0.407 ± 0.016
…	…	Wolf 437	J12479+097	M3.5 V	12:47:55.53	+09:44:57.7	…	…	…	…	47.22	1108.26	122.75 ± 0.79	0.311 ± 0.013
…	…	G 123-45	J12364+352	M4.5 V	12:36:28.17	+35:11:59.0	Aab	Aab(1)	…	…	24.83	375.94	…	…
…	…	RX J1248.5+4933	J12485+495	M3.5 Ve	12:48:34.67	+49:33:53.8	…	…	…	…	57.12	109.89	377.59 ± 11.59	0.469 ± 0.030
12482+4714	LHS2637	GJ 3749	J12481+472	M3.5 V	12:48:10.07	+47:13:23.2	(AB)	AB	0.830	169.0	35.35	593.19	…	0.336 ± 0.033
…	…	Wolf 439	J12495+094	M3.5 V	12:49:33.74	+09:28:31.6	…	…	…	…	26.86	426.63	159.06 ± 1.01	0.383 ± 0.016
…	…	GJ 3755	J12505+269	M3.8 V	12:50:34.35	+26:55:20.3	…	…	…	…	81.57	261.34	…	…
…	…	APMPM J1251-2121	J12508-213	M7.5 Ve	12:50:53.16	-21:21:18.9	…	…	…	…	32.85	558.72	13.35 ± 0.14	0.182 ± 0.012
12490+6607	DEL 4	DPDra	J12490+661	M3.0 V	12:49:01.61	+66:06:35.2	(AabB)	AabB(3)	0.269	221.4	29.98	447.63	…	0.463 ± 0.001
…	…	GJ 1166A	J12513+221	M3.0 V	12:51:23.71	+22:06:15.7	A+BC	A	…	…	45.28	182.91	342.08 ± 8.14	0.507 ± 0.020
12515+2207	LDS 940	LP 377-78 B	…	M3.5 V	12:51:28.60	+22:07:06.3	…	B	84.764	53.3	45.47	180.19	…	0.336 ± 0.033
12515+2207	RAO 284	GJ 1166 B	…	M3.5 V	12:51:23.80	+22:06:15.7	…	C	1.268	91.6	78.48	180.35	…	0.304 ± 0.034
12576+3514	BWL 35	BFCVn	J12576+352E	M0.0 V	12:57:39.89	+35:13:27.9	(AB)+(CD)	AB	0.082	156.6	78.46	297.85	…	0.562 ± 0.028
12576+3514	BWL 35	GJ 490 B	J12576+352W	M4.5 Ve	12:57:38.94	+35:13:16.9	…	CD	16.046	226.7	37.64	317.47	…	0.336 ± 0.033
…	…	GJ 3757	J12594+077	M5.0 V	12:59:23.31	+07:43:54.8	…	…	…	…	37.59	677.91	21.86 ± 0.11	0.159 ± 0.010
…	…	Ross 972	J13000-056	M3.0 V	13:00:03.58	-05:37:47.1	…	…	…	…	42.01	346.78	185.01 ± 1.56	0.415 ± 0.017
…	…	FNVir	J13005+056	M4.5 Ve	13:00:32.51	+05:41:11.6	…	…	…	…	65.58	967.81	36.32 ± 0.28	0.188 ± 0.010
12584+4033	HDS1819	LP 41-165	J12583+405	M1.5 V	12:58:21.97	+40:33:20.7	(AB)	AB	0.187	195.2	65.60	268.38	…	0.613 ± 0.029
13008+1223	BEU 16	Wolf 462	J13007+123	M0.0 V	13:00:45.87	+12:22:32.1	(ABC)	AB	0.525	60.0	28.08	629.61	…	0.551 ± 0.028
13008+1223	GDM 1	Ross 458C	…	T8.5p	…	…	…	C	12.060	220.2	34.85	639.45	…	…
…	…	G 164-38	J13019+335	M1.0 V	13:01:55.96	+33:35:23.0	…	…	…	…	33.35	449.63	384.64 ± 1.94	0.480 ± 0.018
…	…	G 123-84	J13027+415	M3.5 V	13:02:46.65	+41:31:06.6	…	…	…	…	36.68	577.05	245.25 ± 1.15	0.482 ± 0.019
…	…	GJ 497 A	J13047+559	M0.5 V	13:04:46.29	+55:54:10.6	AB	A	…	…	43.80	167.46	…	0.687 ± 0.026
13048+5555	WOR 23	GJ 497 B	…	M1.0 V	13:04:46.36	+55:54:08.7	…	B	2.019	161.7	37.11	169.95	…	0.544 ± 0.028
…	…	GJ 3760 A	J13054+371	M2.5 V	13:05:29.44	+37:08:07.6	AB	A	…	…	39.85	391.69	…	0.464 ± 0.030
13055+3708	HDS1830	GJ 3760 B	…	M2.0 V	13:05:29.46	+37:08:07.2	…	B	0.477	141.9	123.64	345.22	…	0.463 ± 0.030
…	…	GJ 3762	J13068+308	M6.0 V	13:06:50.53	+30:50:46.4	…	…	…	…	26.29	508.51	20.81 ± 0.08	0.154 ± 0.010
…	…	GJ 9428	J13084+169	M1.0 V	13:08:24.64	+16:58:18.5	…	…	…	…	26.23	124.83	439.07 ± 18.86	0.520 ± 0.029
…	…	GJ 3763	J13088+163	M2.5 V	13:08:49.96	+16:22:00.9	…	…	…	…	42.82	558.87	227.02 ± 9.60	0.434 ± 0.020
…	…	GJ 3765	J13089+490	M0.5 V	13:08:55.46	+49:04:50.3	…	…	…	…	42.77	114.23	361.58 ± 1.29	0.464 ± 0.017
…	…	G 177-25	J13102+477	M5.0 V	13:10:11.62	+47:45:08.8	…	…	…	…	36.74	885.73	30.24 ± 0.11	0.162 ± 0.009
…	…	GJ 3766	J13113+285	M5.0 V	13:11:21.13	+28:32:34.4	…	…	…	…	154.70	603.28	21.63 ± 0.09	0.158 ± 0.010
…	…	GJ 3767	J13118+253	M5.0 V	13:11:51.24	+25:20:48.1	…	…	…	…	25.98	493.64	41.10 ± 0.22	0.211 ± 0.011
…	…	PM J13119+6550	J13119+658	M3.0 V	13:11:59.17	+65:50:01.3	…	…	…	…	…	152.67	279.05 ± 1.26	0.408 ± 0.011
…	…	GJ 1168	J13130+201	M3.5 V	13:13:04.08	+20:11:29.0	…	…	…	…	35.20	627.69	198.19 ± 1.02	0.430 ± 0.017
…	…	GJ 3772	J13140+038	M3.8 V	13:14:05.05	+03:53:59.0	…	…	…	…	41.90	736.12	88.67 ± 0.46	0.280 ± 0.013
…	…	GJ 1167 A	J13095+289	M4.8V	13:09:34.56	+28:59:03.1	…	…	…	…	34.78	395.26	35.72 ± 0.19	0.195 ± 0.011
…	…	G 255-29A	J13142+792	M1.0 V	13:14:14.06	+79:14:45.9	AB	A	…	…	33.89	297.31	…	0.631 ± 0.027
13143+7915	KPP3265	G 255-29B	…	M2.0 V	13:14:13.78	+79:14:47.1	…	B	1.383	325.5	57.13	295.36	…	0.478 ± 0.030
…	…	GJ 1169	J13165+278	M4.0 V	13:16:31.95	+27:52:33.5	…	…	…	…	56.81	777.15	67.09 ± 0.30	0.240 ± 0.012

Table D.2: Complete sample with the description of multiple systems (continued).

WDS id	WDS disc	Name	Karmn	Spectral type	α (2016.0)	δ (2016.0)	System	Component	ρ [arcsec]	θ [deg]	ϖ [mas]	$\mu_{\rm total}$ [mas a^{-1}]	$\mathcal{L}$ [$10^{-4}\,\mathcal{L}_\odot$]	$\mathcal{M}$ [$\mathcal{M}_\odot$]
…	…	LP 737-14	J13167-123	M3.5 V	13:16:45.10	-12:20:21.2	…	…	…	…	83.50	289.65	111.96 ± 3.17	0.339 ± 0.016
13143+1320	LAW 2	LP 497-33	J13143+133	M6.0 V	13:14:20.08	+13:19:57.9	(AB)	AB(2)	0.172	96.4	37.42	306.81	…	…
…	…	HD 115404	…	K2 V	13:16:51.76	+17:00:57.6	A+B	A	…	…	83.46	689.14	2979.43 ± 25.18	0.820 ± 0.123
13169+1701	BU 800	HD 115404B	J13168+170	M0.5 V	13:16:52.28	+17:00:55.7	…	B	7.671	104.6	51.13	701.23	…	0.541 ± 0.029
…	…	GJ 3774	J13168+231	M1.5 V	13:16:53.38	+23:10:05.5	…	…	…	…	35.92	283.60	536.26 ± 2.91	0.552 ± 0.028
…	…	GJ 1170	J13179+362	M1.0 V	13:17:58.30	+36:17:51.5	…	…	…	…	33.68	345.03	501.91 ± 1.74	0.553 ± 0.028
13180+0214	CRC 68	GJ 3775	J13180+022	M3.5 V	13:18:01.42	+02:14:00.4	AB	A	0.701	243.0	54.45	290.74	…	0.218 ± 0.038
…	…	G3- 3688439268658769408	…	M4.5 V	13:18:01.41	+02:14:00.2	…	B	0.342	225.1	33.87	290.74	…	0.211 ± 0.038
…	…	PM J13182+7322	J13182+733	M3.5 V	13:18:13.82	+73:22:05.6	A+B	A	…	…	58.90	129.46	137.10 ± 0.64	0.354 ± 0.015
…	…	PM J13182+7322B	…	M7.0 V	13:18:13.11	+73:22:12.4	…	B*	7.387	335.7	46.55	122.66	…	0.100 ± 0.049
13196+3507	BAG 11	GJ 507 A	J13195+351W	M0.5 V	13:19:34.10	+35:06:24.2	(AB)+Cab	AB(2)	0.073	182.7	76.10	870.64	…	0.684 ± 0.022
13196+3507	HJ 529	GJ 507 B	J13195+351E	M3.0 V	13:19:35.18	+35:06:12.4	…	Cab(1)	17.793	131.6	41.62	883.65	…	…
13198+4747	CHR 193	HD 115953	J13197+477	M2.0 V	13:19:45.90	+47:46:40.5	AB+C	AB(2)	0.088	97.2	47.32	227.71	…	…
13198+4747	HU 644	HD 115953B	…	M2.0 V	13:19:45.97	+47:46:40.6	…	C	0.666	85.5	112.67	227.71	…	0.473 ± 0.030
…	…	Ross 1007	J13196+333	M1.5 V	13:19:39.74	+33:20:45.2	…	…	…	…	75.62	330.74	545.68 ± 2.66	0.553 ± 0.028
…	…	Ross 1008	J13209+342	M1.0 V	13:20:58.67	+34:16:39.4	…	…	…	…	18.87	567.80	483.53 ± 214.18	0.541 ± 0.029
…	…	LSPM J1321+0332	J13215+035	M1.0 V	13:21:30.15	+03:33:02.1	…	…	…	…	18.86	192.61	365.15 ± 2.88	0.467 ± 0.017
…	…	GJ 3778	J13215+037	M2.0 V	13:21:34.69	+03:45:54.5	…	…	…	…	36.50	519.37	320.53 ± 1.96	0.490 ± 0.019
…	…	Ross 1020	J13229+244	M4.0 V	13:22:56.03	+24:27:49.8	…	…	…	…	36.51	1061.67	86.85 ± 0.58	0.272 ± 0.012
…	…	HD 116495A	J13235+292	M0.0 V	13:23:32.21	+29:14:18.9	AB	A	…	…	37.64	531.64	…	0.710 ± 0.026
13235+2914	HO 260	HD 116495B	…	K6 V	13:23:32.33	+29:14:19.0	…	B	1.659	88.4	38.51	515.54	…	0.654 ± 0.027
…	…	LP 40-109	J13239+694	M0.0 V	13:23:56.16	+69:27:03.5	…	…	…	…	40.46	180.01	744.36 ± 2.65	0.638 ± 0.027
…	…	G 14-52	J13247-050	M4.0 V	13:24:46.56	-05:04:24.8	…	…	…	…	40.38	309.86	128.77 ± 2.63	0.302 ± 0.014
…	…	PM J13251-1126	J13251-114	M3.0 V	13:25:11.61	-11:26:33.7	…	…	…	…	51.44	238.84	498.98 ± 3.50	0.492 ± 0.018
…	…	BD+38 2445	J13254+377	M0.0 V	13:25:28.07	+37:43:10.9	AB	A	…	…	51.51	205.97	…	0.661 ± 0.026
13260+3743	SKF 942	BD+38 2445B	…	M4.5 V	13:25:28.31	+37:43:10.4	…	B	2.847	99.7	72.27	213.36	…	0.258 ± 0.037
…	…	2M13253177+6850106	J13255+688	M0.0 V	13:25:31.76	+68:50:09.8	…	…	…	…	42.54	46.15	823.44 ± 3.59	0.644 ± 0.027
…	…	PM J13255+2738	…	M1.0 V	13:25:35.66	+27:38:08.9	A+BC	A	…	…	39.91	71.21	570.45 ± 2.86	0.579 ± 0.028
…	…	PM J13260+2735A	J13260+275	M3.0 V	13:26:02.70	+27:35:03.7	…	B*	404.411	117.2	39.95	72.89	…	0.481 ± 0.030
13260+2735	KPP3896	PM J13260+2735B	…	M2.5 V	13:26:02.63	+27:35:02.5	…	C	404.111	117.4	44.08	63.57	…	0.391 ± 0.032
…	…	BD+30 2400	J13282+300	M0.0 V	13:28:17.53	+30:02:43.0	AB+C	A	…	…	46.99	260.99	…	0.724 ± 0.025
13283+3003	CFN 11	BD+30 2400B	…	…	13:28:17.48	+30:02:44.1	…	B	1.247	324.0	47.09	…	…	…
13284+3005	LDS1390	LP 323-115	…	M7.0 V	13:28:20.69	+30:03:15.8	…	C	52.481	51.3	72.89	259.70	10.25 ± 0.14	0.142 ± 0.010
…	…	Ross 486A	J13283-023W	dM3.0	13:28:21.24	-02:21:45.0	A+B	A	…	…	30.71	517.21	259.47 ± 1.78	0.424 ± 0.013
13283-0222	B 2753	Ross 486B	J13283-023E	M4.0 V	13:28:21.68	-02:21:39.6	…	B	8.472	50.2	43.82	503.74	48.50 ± 0.84	0.231 ± 0.012
…	…	GJ 513	J13293+114	M3.0 V	13:29:21.67	+11:26:07.6	…	…	…	…	30.10	1235.48	248.46 ± 1.65	0.440 ± 0.013
…	…	1R132923.9-142206	J13294-143	M3.5 V	13:29:24.21	-14:22:13.0	…	…	…	…	231.12	116.41	198.11 ± 1.45	0.430 ± 0.017
…	…	Ross 490	J13299+102	M1.0 V	13:30:01.01	+10:22:20.6	…	…	…	…	223.48	1556.96	424.22 ± 2.99	0.487 ± 0.012
…	…	Wolf 485	…	DA3.5	13:30:12.44	-08:34:37.0	A+B	A	…	…	30.23	1207.51	…	0.500 ± 0.100
13303-0834	LDS 448	Ross 476	J13300-087	M4.0 V	13:30:01.59	-08:42:33.0	…	B	502.447	198.7	54.97	1210.61	49.55 ± 0.26	0.234 ± 0.012

Table D.2: Complete sample with the description of multiple systems (continued).

WDS id	WDS disc	Name	Karmn	Spectral type	α (2016.0)	δ (2016.0)	System	Component	ρ [arcsec]	θ [deg]	ϖ [mas]	$\mu_{\rm total}$ [mas a^{-1}]	$\mathcal{L}$ [$10^{-4}\,\mathcal{L}_\odot$]	$\mathcal{M}$ [$\mathcal{M}_\odot$]
…	…	GJ 1171	J13305+191	M5.0 V	13:30:30.49	+19:09:13.5	…	…	…	…	35.54	1378.97	28.83 ± 0.15	0.172 ± 0.010
…	…	GJ 3790	J13318+233	M2.5 V	13:31:50.26	+23:23:21.1	…	…	…	…	35.35	284.20	201.30 ± 1.26	0.407 ± 0.016
13318+2917	BEU 17	DGCVn	J13317+292	M4.0 V	13:31:46.33	+29:16:34.3	(AB)	AB(2)	0.190	85.4	47.96	285.30	…	…
13320+3108	WOR 24	GJ 9448 B	J13319+311	M0.0 V	13:31:58.08	+31:08:05.3	AB	A	0.134	125.5	41.82	132.92	…	0.668 ± 0.039
…	…	G3- 1468339715235126784	…	…	13:31:58.10	+31:08:05.6	…	B	0.384	42.1	53.52	…	…	…
13327+3100	BWL36	LP 323-169	J13326+309	M4.5 V	13:32:38.85	+30:59:05.3	(AB)	AB	0.137	213.8	70.11	208.43	…	0.274 ± 0.036
…	…	VWCom	J13327+168	M2.5 V	13:32:44.93	+16:48:35.8	AB	A	…	…	…	354.79	…	0.401 ± 0.032
13328+1649	VYS 6	GJ 516 B	…	M4.0 Ve	13:32:45.08	+16:48:37.4	…	B	2.713	54.0	43.52	376.03	…	0.361 ± 0.033
…	…	PM J13335+7029	J13335+704	M3.5 V	13:33:33.27	+70:29:41.6	…	…	…	…	43.32	132.93	123.10 ± 0.45	0.334 ± 0.015
…	…	Wolf 1487	J13343+046	M0.0 V	13:34:21.67	+04:40:00.7	…	…	…	…	42.28	197.24	953.40 ± 7.14	0.683 ± 0.026
…	…	GJ 3793	J13348+201	M3.5 V	13:34:49.40	+20:11:35.7	…	…	…	…	41.85	191.37	625.12 ± 25.37	0.531 ± 0.029
13349+7430	LDS1775	GJ 9453	…	K5 V	13:34:51.91	+74:30:01.1	A+B	A	14.800	323.3	69.84	439.09	2438.88 ± 15.15	0.700 ± 0.105
…	…	GJ 9453 B	J13348+745	M3.5 V	13:34:49.83	+74:30:12.6	…	B	14.192	324.0	44.55	437.06	331.23 ± 1.72	0.444 ± 0.031
…	…	G 150-17	J13358+146	M2.5 V	13:35:50.73	+14:41:07.4	…	…	…	…	70.57	275.10	324.75 ± 1.75	0.453 ± 0.030
…	…	Ross 1021	J13369+229	M2.5 V	13:36:55.35	+22:57:58.2	…	…	…	…	49.51	198.31	206.46 ± 1.04	0.413 ± 0.017
…	…	GJ 520 A	J13378+481	M0.0 V	13:37:50.84	+48:08:14.8	AB+C	A	…	…	48.03	277.90	…	0.663 ± 0.026
13379+4808	ES 608	GJ 520 B	…	M1.5 V	13:37:50.77	+48:08:16.3	…	B	1.621	335.4	123.78	244.96	…	0.541 ± 0.029
13379+4808	LDS5784	GJ 520 C	J13376+481	M4.0 V	13:37:40.09	+48:07:52.0	…	C	109.969	258.0	84.22	257.67	54.87 ± 0.21	0.230 ± 0.012
…	…	Ross 1022	J13386+258	M3.0 V	13:38:36.37	+25:49:50.7	…	…	…	…	37.22	583.81	242.76 ± 1.86	0.450 ± 0.018
…	…	1R133841.3-113137	J13386-115	M4.5 V	13:38:41.05	-11:32:09.1	…	…	…	…	29.57	172.73	69.46 ± 0.39	0.262 ± 0.013
…	…	Ross 488	J13388-022	M2.0 V	13:38:53.11	-02:15:48.5	…	…	…	…	45.81	311.57	187.75 ± 1.05	0.369 ± 0.015
…	…	Ross 1026	J13401+437	M3.5 V	13:40:07.19	+43:46:42.8	…	…	…	…	…	1125.83	159.71 ± 1.13	0.384 ± 0.016
…	…	PM J13413-0907	J13413-091	M2.5 V	13:41:21.33	-09:07:16.4	…	…	…	…	56.79	103.29	149.97 ± 0.83	0.348 ± 0.015
13415+4855	RAO 298	StM 186	J13414+489	M3.5 V	13:41:27.84	+48:54:43.4	(AB)	AB	0.355	351.9	97.91	193.13	…	…
13394+4611	JOD 6	GJ 521	J13394+461	M1.5 V+	13:39:24.04	+46:11:17.6	(AB)	AB	0.447	15.8	29.94	391.46	…	0.525 ± 0.029
…	…	GJ 3799	J13415+148	M1.5 V	13:41:31.58	+14:49:27.6	…	…	…	…	28.89	258.55	512.12 ± 10.23	0.549 ± 0.028
…	…	StM 187	J13417+582	M3.5 Ve	13:41:46.48	+58:15:18.9	AB	A	…	…	29.06	101.05	…	0.358 ± 0.033
13418+5815	JNN 94	G3- 1658968054798747008	…	M4.0 V	13:41:46.39	+58:15:18.6	…	B	0.762	252.9	56.11	81.41	…	0.269 ± 0.036
…	…	Ross 1015	J13427+332	M3.5 V	13:42:43.13	+33:17:12.9	…	…	…	…	49.55	721.13	91.12 ± 0.42	0.261 ± 0.010
…	…	GJ 3802	J13430+090	M3.0 V	13:43:00.91	+09:04:21.8	…	…	…	…	55.08	352.29	159.05 ± 3.65	0.383 ± 0.017
…	…	TYC 896-760-1	J13434+111	M0.5 V	13:43:25.03	+11:06:42.1	…	…	…	…	52.62	147.97	795.57 ± 5.07	0.633 ± 0.027
13422-1600	WSI 114	GJ 3800	J13421-160	M4e	13:42:09.28	-16:00:24.1	(AB)	AB	0.737	17.7	117.03	497.80	…	0.289 ± 0.035
13446+5142	KUI64	Ross 492	J13444+516	M2.5 V	13:44:27.00	+51:41:08.6	(AB)	AB	1.050	51.1	24.59	760.00	…	0.343 ± 0.048
…	…	LP 379-98 A	J13445+249	M1.0 V	13:44:33.38	+24:57:03.6	AB	A	…	…	86.90	262.46	…	0.599 ± 0.027
13446+2457	RAO 301	LP 379-98 B	…	M1.0 V	13:44:33.38	+24:57:04.5	…	B	0.887	356.4	85.54	256.64	…	0.537 ± 0.029
…	…	Wolf 497	J13450+176	M0.0 V	13:45:05.59	+17:46:38.2	…	…	…	…	32.66	1887.91	451.52 ± 1.60	0.486 ± 0.012
…	…	MCC 699	J13455+609	M0.5 V	13:45:31.28	+60:58:58.3	…	…	…	…	37.86	60.61	1002.74 ± 4.52	0.682 ± 0.026
…	…	HD 119850	J13457+148	M1.5 V	13:45:45.74	+14:53:06.2	…	…	…	…	28.88	2296.01	378.79 ± 7.77	0.498 ± 0.014
…	…	GJ 3804	J13458-179	dM3.5	13:45:50.37	-17:58:14.5	…	…	…	…	29.10	632.04	140.59 ± 0.88	0.328 ± 0.011
…	…	BD+22 2632A	J13477+214	M0.0 V	13:47:42.49	+21:27:36.3	AB	A	…	…	36.49	119.73	…	0.619 ± 0.027

Table D.2: Complete sample with the description of multiple systems (continued).

WDS id	WDS disc	Name	Karmn	Spectral type	α (2016.0)	δ (2016.0)	System	Component	ρ [arcsec]	θ [deg]	ϖ [mas]	$\mu_{\rm total}$ [mas a^{-1}]	$\mathcal{L}$ [$10^{-4}\,\mathcal{L}_\odot$]	$\mathcal{M}$ [$\mathcal{M}_\odot$]
13477+2128	HDS1939	BD+22 2632B	…	M3.5 V	13:47:42.54	+21:27:35.2	…	B	1.303	150.8	36.07	119.20	…	0.342 ± 0.033
…	…	LP 738-14	J13481-137	M4.5 V	13:48:06.52	-13:44:39.8	AB	A	…	…	70.90	858.15	…	0.183 ± 0.040
13481-1345	DEA1	LP 738-14 B	…	T5.5	…	…	…	B	67.340	291.5	38.24	857.92	…	…
…	…	GJ 1179 A	J13482+236	M5.0 V	13:48:11.69	+23:36:50.7	A+B	A	…	…	35.92	1487.63	16.78 ± 0.09	0.136 ± 0.010
13484+2337	LDS4410	GJ 1179 B	…	DC9	13:48:01.28	+23:34:48.4	…	B	188.131	229.5	56.13	1490.91	…	0.500 ± 0.100
…	…	Ross 493	J13485+563	M1.5 V	13:48:34.32	+56:20:09.6	…	…	…	…	82.04	366.09	586.60 ± 2.63	0.570 ± 0.028
…	…	Wolf 1494	J13488+041	M4.5 V	13:48:48.61	+04:05:59.4	…	…	…	…	53.55	180.33	44.88 ± 0.22	0.221 ± 0.012
…	…	Wolf 1495 A	J13490+026	M1.5 V	13:49:01.16	+02:47:23.6	AB	A	…	…	40.69	365.48	…	0.420 ± 0.031
13490+0247	RAO 302	Wolf 1495 B	…	…	13:49:01.19	+02:47:23.2	…	B	0.679	133.1	27.74	365.22	…	…
…	…	GJ 3810	J13507-216	M3.0 V	13:50:43.96	-21:41:33.0	A+B	A	…	…	45.42	379.05	181.12 ± 1.23	0.385 ± 0.016
13507-2140	LDS 461	LP 798-41	J13503-216	M3.5 V	13:50:23.73	-21:37:25.9	…	B	375.007	311.2	51.29	378.00	106.82 ± 0.64	0.331 ± 0.015
…	…	Ross 1019	J13508+367	M4.0 V	13:50:51.18	+36:44:18.5	…	…	…	…	77.90	447.25	76.46 ± 0.33	0.276 ± 0.013
…	…	RX J1351.8+1247	J13518+127	M2.0 Ve	13:51:53.02	+12:47:07.0	…	…	…	…	24.41	91.68	337.77 ± 1.60	0.475 ± 0.018
…	…	Wolf 515	J13526+144	M2.0 V	13:52:36.26	+14:25:15.7	A+B	A	…	…	24.34	284.44	…	0.517 ± 0.029
13526+1425	JOD 7	Wolf 515 B	…	M3.5 V	13:52:36.26	+14:25:16.9	…	B	1.204	359.8	64.80	294.25	…	0.304 ± 0.034
…	…	GJ 533.1	J13528+656	M1.5 V	13:52:48.61	+65:37:17.7	(AB)	AB	…	…	44.80	562.38	…	0.514 ± 0.029
…	…	GJ 3815	J13528+668	M5.0 V	13:52:49.25	+66:48:57.2	…	…	…	…	61.00	723.77	21.07 ± 0.08	0.155 ± 0.010
…	…	LP 21-224	J13536+776	M4.0 Ve	13:53:39.91	+77:37:07.9	…	…	…	…	91.02	224.76	86.22 ± 0.31	0.295 ± 0.019
…	…	LP 97-259	J13529+536	M1.0 V	13:52:55.76	+56:36:17.0	…	…	…	…	90.95	211.10	472.19 ± 1.89	0.544 ± 0.028
13535+1257	BEU18	Ross 835	J13534+129	M0.0 V	13:53:27.37	+12:56:22.9	(AB)	AB	0.278	9.0	35.96	628.21	…	…
…	…	PM J13537+5210A	J13537+521	M3.5 V	13:53:45.89	+52:10:27.3	AB	A	…	…	42.23	134.34	…	0.441 ± 0.031
13538+5210	JNN 96	PM J13537+5210B	…	M2.5 V	13:53:45.88	+52:10:28.3	…	B	1.027	351.7	74.45	130.52	…	0.439 ± 0.031
…	…	GJ 534.2	J13537+788	M0.0 V	13:53:45.76	+78:51:08.7	…	…	…	…	74.45	277.86	750.31 ± 2.89	0.628 ± 0.027
…	…	Ross 837	J13582+125	M3.5 Ve	13:58:13.56	+12:34:55.4	…	…	…	…	39.53	792.17	63.69 ± 0.37	0.213 ± 0.009
…	…	LP 739-2	J13582-120	M4.5 V	13:58:15.80	-12:02:58.4	…	…	…	…	39.28	340.49	49.75 ± 0.24	0.234 ± 0.012
…	…	LP 739-3	J13583-132	M4.0 V	13:58:19.96	-13:16:26.0	…	…	…	…	72.97	348.28	53.73 ± 0.26	0.228 ± 0.012
…	…	GJ 3818	J13587-000	M4.0 V	13:58:43.20	-00:04:54.3	…	…	…	…	73.92	543.64	103.66 ± 0.53	0.305 ± 0.014
…	…	GJ 3820	J13591-198	M4.5 V	13:59:09.78	-19:50:06.6	…	…	…	…	109.98	590.77	75.29 ± 0.62	0.263 ± 0.010
…	…	HD 122303	J14010-026	M1.0 V	14:01:02.31	-02:39:07.9	…	…	…	…	109.98	1019.56	433.61 ± 2.26	0.505 ± 0.012
…	…	GJ 536.1 A	J14019+154	M0.0 V	14:01:58.86	+15:29:40.7	AB	A	…	…	59.31	105.24	…	0.593 ± 0.028
14019+1530	ALD 112	GJ 536.1 B	…	M0.5 V	14:01:58.89	+15:29:39.1	…	B	1.621	162.3	60.03	118.04	…	0.588 ± 0.028
…	…	PM J14019+4316A	J14019+432	M2.5 V	14:01:58.67	+43:16:41.1	AB	A	…	…	36.00	82.70	…	0.389 ± 0.032
14020+4317	KPP3910	PM J14019+4316B	…	M3.0 V	14:01:58.69	+43:16:43.1	…	B	1.960	7.1	43.49	83.90	…	0.382 ± 0.032
…	…	GJ 3822	J14023+136	M0.5 V	14:02:19.73	+13:41:20.4	…	…	…	…	72.73	171.99	648.18 ± 2.71	0.594 ± 0.028
…	…	GJ 3821	J14024-210	M3.5 V	14:02:29.43	-21:00:42.9	…	…	…	…	55.21	618.88	126.58 ± 0.86	0.339 ± 0.015
…	…	GJ 537 A	J14025+463S	M0.5 V	14:02:34.03	+46:20:23.0	A+B	A	…	…	55.19	576.57	…	0.524 ± 0.029
14024+4620	SWI 1	GJ 537 B	J14025+463N	M0.5 V	14:02:34.19	+46:20:26.4	…	B	3.742	25.3	31.83	583.81	…	0.506 ± 0.029
…	…	LSPM J1403+2440	J14039+242	M2.5 V	14:03:54.74	+24:40:44.2	…	…	…	…	40.56	161.57	286.52 ± 1.25	0.462 ± 0.018
…	…	BD+21 2602	…	K4 V	14:04:09.85	+20:45:32.5	A+BC	A	…	…	27.87	127.65	1762.73 ± 6.48	0.730 ± 0.110
14042+2046	J 1128	StKM 1-1119	J14041+207	M1.0 Ve	14:04:09.06	+20:44:30.9	…	B	62.660	190.2	29.63	132.08	…	…

Table D.2: Complete sample with the description of multiple systems (continued).

WDS id	WDS disc	Name	Karmn	Spectral type	α (2016.0)	δ (2016.0)	System	Component	ρ [arcsec]	θ [deg]	ϖ [mas]	$\mu_{\rm total}$ [mas a^{-1}]	$\mathcal{L}$ [$10^{-4}\,\mathcal{L}_\odot$]	$\mathcal{M}$ [$\mathcal{M}_\odot$]
14042+2046	J 1128	G3- 1247168140942467200	…	…	14:04:09.06	+20:44:31.2	…	C	62.307	190.3	31.03	…	…	…
…	…	NLTT 36313	J14062+693	M3.0 V	14:06:14.66	+69:18:38.8	…	…	…	…	14.16	199.13	310.28 ± 1.42	0.452 ± 0.030
…	…	GJ 540	J14082+805	M1.0 V	14:08:14.37	+80:35:41.5	…	…	…	…	22.00	583.70	646.17 ± 2.90	0.586 ± 0.028
…	…	GJ 3826	J14083+758	M1.5 V	14:08:20.91	+75:51:13.2	…	…	…	…	21.87	546.27	385.66 ± 5.43	0.509 ± 0.019
14121-0035	WSI 129	GJ 3828 A	J14121-005	M2.5 V	14:12:10.22	-00:35:00.3	(AB)+C	AB	0.529	170.5	22.03	750.90	…	0.361 ± 0.033
14121-0035	LDS4442	GJ 3828 B	…	M6.5 V	14:12:11.36	-00:35:12.6	…	C	21.040	125.9	24.70	752.91	4.85 ± 0.06	0.100 ± 0.050
…	…	GQVir	J14130-120	M4.5 V	14:13:04.19	-12:01:32.9	Aab	Aab(2)	…	…	25.40	725.08	…	…
14144-1521	CVN 25	HD 124498A	…	K7 V	14:14:21.24	-15:21:24.8	AB+C	A	0.306	208.4	…	209.20	…	0.733 ± 0.026
14144-1521	RST3869	HD 124498B	…	M2.0 V	14:14:21.34	-15:21:24.4	…	B	1.553	78.4	24.10	229.25	…	0.471 ± 0.030
14144-1521	LDS 483	GJ 3832	J14142-153	M3.5 V	14:14:16.87	-15:21:15.9	…	C	63.743	278.0	75.88	231.00	150.21 ± 0.89	0.397 ± 0.017
…	…	GJ 3834	J14144+234	M3.5 V	14:14:26.33	+23:27:26.4	…	…	…	…	75.60	492.02	162.69 ± 0.78	0.388 ± 0.016
…	…	Ross 992	J14152+450	M3.0 V	14:15:15.96	+45:00:49.7	…	…	…	…	52.32	710.71	253.74 ± 0.91	0.429 ± 0.011
…	…	LP 439-350	J14153+153	M2.0 V	14:15:20.63	+15:23:01.5	…	…	…	…	41.45	186.82	291.05 ± 1.87	0.466 ± 0.018
…	…	GJ 1182	J14155+046	M5.69	14:15:31.75	+04:39:19.1	Aab	Aab(2)	…	…	25.37	1070.70	…	0.258 ± 0.002
…	…	LP 97-674 A	J14157+594	M2.2 V	14:15:42.13	+59:27:29.1	A+B	A	…	…	131.10	184.40	360.20 ± 1.68	0.491 ± 0.018
14157+5928	LDS2707	LP 97-674 B	…	M3.0 V	14:15:41.61	+59:27:25.9	…	B	5.061	231.1	62.15	189.23	…	0.413 ± 0.031
…	…	G 165-58	J14159+362	M3.5 V	14:15:56.39	+36:16:42.2	…	…	…	…	62.28	303.35	71.03 ± 0.26	0.248 ± 0.012
…	…	LP 81-30	J14161+233	M1.0 V	14:16:11.25	+23:23:26.5	…	…	…	…	66.83	203.00	387.93 ± 1.77	0.509 ± 0.029
…	…	GJ 3838	J14170+105	M1.5 V	14:17:04.56	+10:35:34.3	…	…	…	…	51.65	301.67	359.45 ± 2.81	0.487 ± 0.030
14170+3143	DEL 5	GJ 3839	J14170+317	M4.5 Ve	14:17:02.14	+31:42:44.7	(AB)	AB(2/3)	0.247	157.5	25.35	606.11	…	…
…	…	PM J14171+0851	J14171+088	M4.5 V	14:17:07.18	+08:51:37.1	Aab	Aab(2)	…	…	39.77	139.55	…	…
…	…	GJ 541.2	J14174+454	M0.0 V	14:17:24.45	+45:26:39.8	A+B	A	…	…	54.69	47.49	711.76 ± 2.58	0.625 ± 0.027
14174+4527	VVO 12	RX J1417.3+4525	J14173+454	dM5.0	14:17:22.17	+45:25:45.7	…	B	59.202	203.9	31.24	47.89	76.76 ± 0.58	0.273 ± 0.010
…	…	RX J1417.5+0233	J14175+025	M3.0 V	14:17:30.18	+02:33:42.5	…	…	…	…	…	70.45	271.08 ± 2.02	0.477 ± 0.019
…	…	LP 381-94	J14177+214	M1.0 V	14:17:47.76	+21:25:58.8	…	…	…	…	44.58	185.25	1112.43 ± 14.00	0.686 ± 0.026
…	…	GJ 3840	J14179-005	M2.5 V	14:17:58.75	-00:31:33.8	…	…	…	…	60.10	391.98	161.51 ± 0.97	0.363 ± 0.015
…	…	LP 220-78	J14189+386	M1.0 V	14:18:58.09	+38:38:22.5	…	…	…	…	59.99	737.76	651.44 ± 3.70	0.598 ± 0.027
…	…	Wolf 534	J14191-073	M3.0 V	14:19:09.81	-07:18:24.0	…	…	…	…	48.98	1351.08	62.01 ± 0.27	0.215 ± 0.011
…	…	LP 560-1	J14194+029	M5.0 V	14:19:29.37	+02:54:34.1	…	…	…	…	48.97	246.22	60.87 ± 0.31	0.261 ± 0.013
…	…	IZBoo	J14200+390	M3.0 Ve	14:20:04.66	+39:03:02.5	…	…	…	…	17.49	71.53	685.27 ± 3.52	0.565 ± 0.028
…	…	Ross 848	J14201-096	M4.0 V	14:20:06.71	-09:37:26.8	…	…	…	…	25.39	1036.46	85.27 ± 0.63	0.274 ± 0.013
…	…	GJ 3843	J14212-011	M4.0 V	14:21:15.31	-01:07:29.8	…	…	…	…	25.49	648.81	67.32 ± 0.37	0.258 ± 0.013
…	…	PM J14215-0755	J14215-079	M4.0 V	14:21:33.96	-07:55:18.0	…	…	…	…	39.74	130.49	128.13 ± 1.02	0.341 ± 0.015
…	…	LP 270-68	J14219+376	M1.5 V	14:21:55.61	+37:39:45.5	…	…	…	…	42.55	469.43	374.34 ± 1.55	0.501 ± 0.019
…	…	LP 440-13	J14227+164	M5.0 V	14:22:43.19	+16:24:47.2	…	…	…	…	47.21	195.81	113.14 ± 0.65	0.341 ± 0.015
…	…	GJ 3845	J14231-222	M4.5 V	14:23:07.49	-22:17:16.7	…	…	…	…	47.21	545.98	55.75 ± 0.29	0.232 ± 0.012
…	…	GJ 3846	J14249+088	M3.0 V	14:24:56.58	+08:53:18.0	…	…	…	…	47.19	570.88	108.73 ± 0.69	0.293 ± 0.013
14211+2736	CRC 69	GJ 3844	J14210+275	M2.5 V	14:21:03.13	+27:35:34.5	(AB)	AB	0.677	85.1	43.83	301.67	…	0.468 ± 0.030
14252+5151	STT 580	HD 126660	…	F7 V	14:25:11.39	+51:50:56.3	A+B	A	70.160	182.5	51.10	464.15	…	1.210 ± 0.182
…	…	HD 126660B	J14251+518	M2.5 V	14:25:11.17	+51:49:46.6	…	B	69.674	181.7	55.39	469.65	222.34 ± 0.94	0.392 ± 0.011

Table D.2: Complete sample with the description of multiple systems (continued).

WDS id	WDS disc	Name	Karmn	Spectral type	α (2016.0)	δ (2016.0)	System	Component	ρ [arcsec]	θ [deg]	ϖ [mas]	$\mu_{\rm total}$ [mas a^{-1}]	$\mathcal{L}$ [$10^{-4}\,\mathcal{L}_\odot$]	$\mathcal{M}$ [$\mathcal{M}_\odot$]
…	…	LP 740-10	J14255-118	M4.0 V	14:25:33.79	-11:48:51.5	…	…	…	…	57.92	296.82	272.54 ± 2.93	0.509 ± 0.020
14257+2338	BU 1442	GJ 548 A	J14257+236W	M0.0 V	14:25:44.40	+23:36:43.6	A+B	A	45.200	74.4	40.07	1369.12	847.75 ± 4.67	0.648 ± 0.027
…	…	GJ 548 B	J14257+236E	M0.5 V	14:25:47.58	+23:36:55.8	…	B	45.350	74.4	…	1371.68	733.70 ± 4.01	0.618 ± 0.027
…	…	V358Boo	J14259+142	M0.0 Ve	14:25:55.87	+14:12:09.6	…	…	…	…	74.80	66.90	…	0.622 ± 0.093
…	…	LSPM J1426+2408	J14269+241	M1.0 V	14:26:58.63	+24:08:56.9	…	…	…	…	30.17	160.22	526.05 ± 3.24	0.555 ± 0.028
…	…	GJ 1183 A	J14279-003S	M4.65	14:27:55.69	-00:22:30.5	A+B	A	…	…	46.25	363.55	80.53 ± 0.49	0.284 ± 0.013
14279-0032	GIC 120	GJ 1183 B	J14279-003N	M4.70	14:27:56.01	-00:22:18.3	…	B	13.073	21.8	45.89	366.95	76.86 ± 0.49	0.297 ± 0.014
…	…	LP 500-35	J14280+139	M7.0 V	14:28:03.75	+13:56:05.4	…	…	…	…	108.79	615.68	8.32 ± 0.04	0.115 ± 0.010
…	…	LP 560-27	J14283+053	M3.0 V	14:28:21.12	+05:19:00.3	A+B	A	…	…	46.01	377.91	177.07 ± 1.08	0.381 ± 0.016
14284+0520	LDS 961	LP 560-26	J14282+053	M3.5 V	14:28:17.18	+05:18:44.8	…	B	60.904	255.2	30.66	378.25	136.89 ± 1.44	0.378 ± 0.016
…	…	Ross 130	J14294+155	M2.0 V	14:29:28.53	+15:32:18.3	…	…	…	…	49.46	1673.55	397.97 ± 1.96	0.500 ± 0.012
…	…	GJ 3853	J14299+295	M4.0 V	14:29:59.26	+29:33:54.9	…	…	…	…	41.10	522.71	85.23 ± 0.34	0.293 ± 0.014
…	…	GJ 3855	J14306+597	M6.5 V	14:30:36.08	+59:43:27.4	…	…	…	…	22.11	823.39	5.77 ± 0.03	0.101 ± 0.009
…	…	HD 127339	J14307-086	M0.5 V	14:30:46.35	-08:38:50.6	…	…	…	…	22.01	1293.18	965.25 ± 4.78	0.682 ± 0.026
…	…	Wolf 1478	J14310-122	dM3.5	14:31:00.72	-12:17:52.3	…	…	…	…	77.44	570.53	124.83 ± 0.83	0.306 ± 0.011
…	…	LSPM J1431+7526	J14312+754	M4.0 V	14:31:12.59	+75:26:41.7	…	…	…	…	30.93	201.28	34.49 ± 0.12	0.178 ± 0.010
…	…	G 255-55	J14320+738	M2.0 V	14:32:01.99	+73:49:23.3	…	…	…	…	184.00	219.96	472.73 ± 1.98	0.525 ± 0.029
…	…	LP 560-35	J14321+081	M6.0 V	14:32:07.99	+08:11:31.4	…	…	…	…	89.33	477.20	18.32 ± 0.09	0.127 ± 0.011
…	…	GJ 3856	J14321+160	M5.0 V	14:32:11.00	+16:00:48.2	…	…	…	…	33.42	191.86	66.54 ± 0.28	0.256 ± 0.013
…	…	GJ 3858	J14322+496	M3.5 V	14:32:13.58	+49:39:04.2	…	…	…	…	33.34	592.90	91.46 ± 0.58	0.285 ± 0.013
…	…	G 224-13A	J14331+610	M2.5 V	14:33:06.93	+61:00:43.9	AB	A	…	…	55.03	207.18	…	0.413 ± 0.031
14331+6101	CRC 70	G 224-13B	…	M3.0 V	14:33:06.80	+61:00:43.6	…	B	0.971	251.5	59.50	206.02	…	0.376 ± 0.032
…	…	HNLib	J14342-125	M3.5 V	14:34:16.42	-12:31:00.9	…	…	…	…	84.22	691.25	100.75 ± 0.69	0.291 ± 0.013
…	…	StKM 1-1170	J14366+143	M1.0 V	14:36:38.98	+14:21:52.6	…	…	…	…	84.31	60.77	1283.35 ± 7.68	0.709 ± 0.026
…	…	GJ 3861	J14368+583	M3.0 Ve	14:36:54.24	+58:20:43.6	Aab	Aab(2)	…	…	39.36	937.75	…	…
…	…	LSPM J1437+7536N	J14371+756	M2.0 V	14:37:09.94	+75:36:54.7	A+B	A	…	…	31.32	219.27	167.49 ± 0.55	0.347 ± 0.014
14372+7537	LDS1803	LSPM J1437+7536S	…	M4.0 V	14:37:13.27	+75:36:41.5	…	B	18.130	136.7	61.48	214.13	112.68 ± 0.42	0.299 ± 0.013
…	…	G 239-22	J14376+677	M1.5 V	14:37:39.32	+67:45:34.9	(AB)	AB	…	…	54.93	281.05	…	0.567 ± 0.028
…	…	GPM 219.718548+42.229288	J14388+422	M1.5 V	14:38:51.66	+42:13:43.9	…	…	…	…	…	134.84	547.06 ± 5.10	0.506 ± 0.029
…	…	LP 560-66	J14415+064	M1.5 V	14:41:32.72	+06:27:41.2	…	…	…	…	47.43	439.95	498.76 ± 2.83	0.546 ± 0.028
…	…	GJ 9492	J14423+660	M2.0 V	14:42:20.79	+66:03:20.2	A+B	A	…	…	47.41	301.51	…	0.412 ± 0.031
14424+6603	GKI 4	GJ 9492 B	…	L0	14:42:21.17	+66:03:20.1	…	B	2.290	93.6	59.18	337.31	…	0.104 ± 0.052
…	…	NLTT 38291	J14438+667	M1.0 V	14:43:50.67	+66:44:34.6	…	…	…	…	37.51	251.26	652.89 ± 2.54	0.595 ± 0.028
…	…	RX J1447.2+5701	J14472+570	M4.0 V	14:47:13.67	+57:01:54.4	…	…	…	…	40.66	87.07	…	…
…	…	LP 501-17	J14485+101	M3.5 V	14:48:32.79	+10:06:55.7	…	…	…	…	40.49	361.92	286.77 ± 1.97	0.491 ± 0.019
…	…	LP 326-34	J14501+323	M3.5 V	14:50:11.14	+32:18:13.8	…	…	…	…	36.18	193.39	314.21 ± 1.46	0.444 ± 0.031
…	…	LP 326-38	J14511+311	M4.0 Ve	14:51:09.97	+31:06:37.4	…	…	…	…	61.47	389.31	103.92 ± 51.81	0.305 ± 0.083
…	…	GJ 3871	J14524+123	M2.5 V	14:52:28.47	+12:23:29.2	…	…	…	…	75.48	235.83	420.46 ± 1.77	0.502 ± 0.013
…	…	Wolf 555	J14525+001	M2.5 V	14:52:32.27	+00:10:02.8	…	…	…	…	34.76	352.08	446.84 ± 7.13	0.506 ± 0.029
14470+1705	RAO 320	Ross 994	J14469+170	M1.5 V	14:46:59.22	+17:05:07.5	(AB)	AB	1.096	185.4	45.62	548.58	…	0.563 ± 0.028

Table D.2: Complete sample with the description of multiple systems (continued).

WDS id	WDS disc	Name	Karmn	Spectral type	α (2016.0)	δ (2016.0)	System	Component	ρ [arcsec]	θ [deg]	ϖ [mas]	$\mu_{\rm total}$ [mas a^{-1}]	$\mathcal{L}$ [$10^{-4}\,\mathcal{L}_\odot$]	$\mathcal{M}$ [$\mathcal{M}_\odot$]
…	…	Ross 52A	J14538+235	M3.5 V	14:53:50.59	+23:33:22.5	AB	A	…	…	21.17	697.94	…	0.327 ± 0.034
14540+2335	REU 2	Ross 52B	…	M4.5 V	14:53:50.66	+23:33:22.5	…	B	0.880	89.2	20.92	761.38	…	0.238 ± 0.037
14545+1606	FRT 1	CEBoo	J14544+161	M1.0: V	14:54:29.55	+16:06:01.9	ABab	A	4.917	40.5	44.08	303.00	…	0.477 ± 0.030
14545+1606	MEL 2	GJ 569 B	…	M8.5 V	14:54:29.77	+16:06:05.6	…	Bab	4.908	40.8	53.91	367.41	…	0.125 ± 0.016
…	…	Ross 1041	J14544+355	M3.5 V	14:54:28.10	+35:32:43.5	…	…	…	…	106.84	854.39	155.28 ± 0.80	0.348 ± 0.012
…	…	Ross 1028b	J14548+099	M2.0 V	14:54:53.15	+09:56:30.1	…	…	…	…	57.79	508.62	519.13 ± 3.76	0.563 ± 0.028
…	…	GJ 3875	J14549+411	M4.5 V	14:54:54.61	+41:08:50.5	Aab	Aab	…	…	53.23	272.51	…	…
…	…	G 66-42	J14557+072	M0.5 V	14:55:47.82	+07:17:47.7	…	…	…	…	64.01	300.42	1152.71 ± 10.90	0.706 ± 0.026
…	…	G 136-35	J14564+168	M1.5 V	14:56:28.16	+16:48:29.1	Aab	Aab	…	…	68.93	324.13	…	…
…	…	KXLib	…	K4 V	14:57:29.18	-21:25:23.3	A+BabC	A	…	…	37.35	2008.68	…	0.746 ± 0.112
14575-2125	HN 28	HD 131976	J14574-214	M1.0 V	14:57:27.70	-21:25:07.9	…	Bab(2)	25.762	306.6	31.39	1933.94	…	…
14575-2125	BUG 4	GJ 570 D	…	T8	14:57:14.96	-21:21:47.8	…	C	234.000	317.0	92.47	1972.88	…	…
…	…	Ross 53A	J14575+313	M2.0 V	14:57:31.43	+31:23:25.9	AB	A	…	…	95.96	1354.84	…	0.632 ± 0.027
14575+3124	HDS2112	Ross 53B	…	M0.5 V	14:57:31.41	+31:23:26.6	…	B	0.783	338.6	34.07	1354.46	…	0.610 ± 0.027
…	…	GJ 1187	J14578+566	M5.5 V	14:57:54.28	+56:39:14.1	…	…	…	…	34.14	705.09	14.76 ± 0.08	0.126 ± 0.009
…	…	GJ 572	J15009+454	M0.5 V	15:00:55.91	+45:25:39.8	AB	A	…	…	28.86	398.22	…	0.620 ± 0.027
15009+4526	HDS2118	BD+45 2247B	…	M4.5 V	15:00:55.96	+45:25:37.9	…	B	2.004	165.3	28.88	409.02	…	0.243 ± 0.037
…	…	Ross 1042	J15011+354	M2.0 V	15:01:11.98	+35:27:10.5	…	…	…	…	49.12	312.63	304.92 ± 1.38	0.477 ± 0.018
…	…	GJ 3885	J15013+055	M3.0 V	15:01:20.20	+05:32:48.5	…	…	…	…	49.84	450.43	154.16 ± 0.75	0.332 ± 0.011
…	…	GJ 3891	J15018+550	M3.5 V	15:05:48.60	+55:04:45.8	…	…	…	…	89.60	481.59	128.37 ± 1.32	0.365 ± 0.016
…	…	LP 41-431	J15030+704	M3.0 V	15:03:01.68	+70:26:14.0	…	…	…	…	89.53	444.88	259.62 ± 1.09	0.466 ± 0.018
…	…	GJ 575.1	J15043+294	M2.5 V	15:04:22.56	+29:28:39.9	…	…	…	…	37.92	294.68	275.62 ± 1.35	0.452 ± 0.017
…	…	Ross 1051	J15043+603	M1.0 V	15:04:17.09	+60:23:07.4	…	…	…	…	24.81	681.03	380.79 ± 1.60	0.505 ± 0.019
…	…	GJ 3888	J15049-211	M4.5 V	15:04:57.53	-21:07:03.9	…	…	…	…	…	686.05	71.29 ± 0.34	0.266 ± 0.013
…	…	PM J15060+4521	J15060+453	M1.5 V	15:06:03.02	+45:21:52.8	…	…	…	…	…	117.83	749.45 ± 3.01	0.609 ± 0.027
…	…	GJ 579	J15073+249	M0.0 V	15:07:22.59	+24:56:15.8	…	…	…	…	38.93	979.55	762.02 ± 3.02	0.641 ± 0.027
15012+0710	RAO 326	Ross 1030a	J15011+071	M3.5 V	15:01:10.20	+07:09:46.5	(AB)	AB	0.104	201.7	58.15	503.18	…	0.488 ± 0.030
15079+7612	MET 10	HD 135363	…	G5 V	15:07:55.68	+76:12:05.4	(AB)+C	AB	0.363	133.1	43.02	208.70	…	0.797 ± 0.119
15079+7612	LEP 72	LSPM J1507+7613	J15079+762	M4.5 V	15:07:56.64	+76:14:01.8	…	C	116.445	1.7	37.03	207.10	244.03 ± 1.19	0.371 ± 0.032
…	…	LSPM J1508+6221	J15081+623	M4.0 V	15:08:11.53	+62:21:56.4	AB	A	…	…	37.28	233.61	…	0.313 ± 0.034
15082+6222	CRC 71	G3- 1619631553142673664	…	M3.5 V	15:08:11.66	+62:21:56.7	…	B	0.900	69.6	31.91	233.02	…	0.312 ± 0.034
…	…	Ross 1047	J15095+031	M3.0 V	15:09:34.95	+03:10:08.3	…	…	…	…	34.50	770.81	257.95 ± 1.25	0.425 ± 0.011
…	…	GJ 3893	J15100+193	M4.3 V	15:10:04.82	+19:21:20.2	…	…	…	…	31.86	452.25	97.41 ± 0.47	0.315 ± 0.014
…	…	GJ 3894	J15118-102	M4.5 V	15:11:49.55	-10:14:22.1	…	…	…	…	34.85	999.70	42.58 ± 0.20	0.215 ± 0.012
…	…	GJ 3895	J15119+179	M4.0 V	15:11:55.49	+17:57:07.4	…	…	…	…	37.24	699.72	126.47 ± 0.60	0.339 ± 0.015
15148+6434	RAO 332	LP 67-339	J15147+645	M3.5 V	15:14:45.76	+64:33:50.3	(AB)	AB	0.359	298.2	58.95	568.23	…	0.202 ± 0.039
…	…	LP 272-63	J15151+333	M2.0 V	15:15:06.93	+33:17:57.0	…	…	…	…	42.69	362.69	177.81 ± 0.72	0.359 ± 0.015
…	…	PM J15156+6349	J15156+638	M1.5 V	15:15:37.69	+63:49:50.8	…	…	…	…	72.00	126.66	399.71 ± 2.40	0.514 ± 0.029
…	…	LP 222-65	J15166+391	M7.0 V	15:16:40.44	+39:10:47.4	…	…	…	…	35.19	212.01	18.42 ± 0.09	0.183 ± 0.011
15126+4544	MCT 8	GJ 3898	J15126+457	M4.0 Ve	15:12:37.60	+45:43:52.3	(AB)	AB	0.509	220.0	35.23	513.64	…	0.284 ± 0.035

Table D.2: Complete sample with the description of multiple systems (continued).

WDS id	WDS disc	Name	Karmn	Spectral type	α (2016.0)	δ (2016.0)	System	Component	ρ [arcsec]	θ [deg]	ϖ [mas]	$\mu_{\rm total}$ [mas a^{-1}]	$\mathcal{L}$ [10^{-4} $\mathcal{L}_\odot$]	$\mathcal{M}$ [$\mathcal{M}_\odot$]
…	…	StKM 1-1229	J15188+292	M1.0 V	15:18:49.75	+29:15:06.4	AB+C	A	…	…	73.46	98.17	…	0.608 ± 0.029
…	…	G3- 1275127175448008448	…	M0.0 V	15:18:49.78	+29:15:06.7	…	B*	0.588	50.9	36.57	78.58	…	0.625 ± 0.028
15189+2915	LDS5168	UCAC4 597-051773	…	M3.5 V	15:18:48.67	+29:14:05.7	…	C	62.256	193.1	49.53	86.82	116.01 ± 0.67	0.346 ± 0.015
…	…	GJ 3902	J15193+678	M3.0 V	15:19:17.35	+67:51:24.0	…	…	…	…	60.00	614.29	140.60 ± 0.55	0.359 ± 0.015
…	…	HOLib	J15194-077	M3.0 V	15:19:25.51	-07:43:21.7	…	…	…	…	54.30	1225.14	123.26 ± 0.65	0.295 ± 0.010
…	…	PM J15197+0439	J15197+046	M4.0 V	15:19:45.88	+04:39:36.0	…	…	…	…	51.46	102.52	59.26 ± 0.27	0.240 ± 0.012
…	…	PM J15210+3057	J15210+309	M2.5 V	15:21:00.56	+30:57:00.9	…	…	…	…	52.66	99.25	235.14 ± 1.50	0.416 ± 0.016
…	…	TYC 344-504-1	J15214+042	M1.5 V	15:21:25.39	+04:14:49.9	…	…	…	…	33.21	95.70	430.88 ± 2.33	0.512 ± 0.029
…	…	OTSer	J15218+209	M1.0 V	15:21:53.03	+20:58:42.0	…	…	…	…	23.90	151.81	454.40 ± 2.11	0.518 ± 0.029
…	…	LP 442-37	J15219+185	M1.5 V	15:21:56.83	+18:35:47.9	…	…	…	…	46.78	213.40	561.41 ± 2.42	0.564 ± 0.028
…	…	Ross 508	J15238+174	M4.92	15:23:50.70	+17:27:37.3	…	…	…	…	31.56	1318.87	38.05 ± 0.19	0.202 ± 0.011
15192-1245	CRC 72	GJ 3900	J15191-127	M4.0 V	15:19:10.93	-12:45:09.3	(AB)	AabB(2)	0.135	8.2	31.35	761.62	…	…
…	…	StKM 1-1240	J15238+561	M1.0 Ve	15:23:54.01	+56:09:31.5	Aab+B	Aab(2)	…	…	316.48	88.93	…	…
15239+5610	VVO 14	PM J15237+5609	…	M0.0 V	15:23:46.47	+56:09:06.0	…	B	67.990	248.1	57.04	87.64	851.63 ± 3.28	0.665 ± 0.026
…	…	G 224-65	J15238+584	M4.0 V	15:23:51.06	+58:28:11.2	…	…	…	…	47.80	348.95	78.80 ± 0.31	0.281 ± 0.013
15270+4128	SKF1924	TYC 3055-1525-1	J15273+415	M1.5 V	15:27:19.05	+41:30:09.9	A+B	A	34.317	1.0	27.78	120.44	…	…
…	…	PM J15273+4130N	…	M6.5 V	15:27:19.11	+41:30:44.2	…	B	34.282	1.1	72.32	122.65	13.08 ± 0.12	0.150 ± 0.010
…	…	G 179-29	J15276+408	M1.0 V	15:27:38.85	+40:52:02.2	…	…	…	…	74.78	304.94	630.36 ± 2.43	0.594 ± 0.028
…	…	GJ 587.1	J15280+257	M0.0 V	15:28:01.43	+25:47:22.9	…	…	…	…	42.11	112.49	564.66 ± 3.12	0.576 ± 0.028
15290+4646	JNN 103	RX J1529.0+4646	J15290+467	M4.5 V	15:29:02.77	+46:46:23.5	(AB)	AB	0.222	202.0	32.99	123.10	…	0.230 ± 0.037
…	…	RX J1532.6+4653	…	M1.0 V	15:32:37.17	+46:53:04.6	…	…	…	…	30.21	123.80	507.59 ± 1.94	0.548 ± 0.028
…	…	LP 502-56	J15305+094	M5.5 V	15:30:30.13	+09:26:04.4	…	…	…	…	41.00	256.53	13.99 ± 0.07	0.115 ± 0.008
15297+4252	JNN 278	GJ 3907	J15297+428	M4.68	15:29:44.63	+42:52:38.9	(AB)	AB	0.560	3.7	76.78	760.24	…	0.228 ± 0.037
…	…	GJ 3911	J15336+462	M3.6 V	15:33:39.33	+46:15:06.1	…	…	…	…	30.78	199.81	132.74 ± 0.56	0.348 ± 0.015
…	…	GJ 3910	J15319+288	M4.0 V	15:31:53.50	+28:51:10.2	Aab	Aab(1)	…	…	22.10	544.00	…	…
…	…	GJ 588.1	J15339+379	M0.5 V	15:33:54.82	+37:54:48.4	AB	A	…	…	69.07	81.90	…	0.583 ± 0.028
15339+3755	BEU 20	G3- 1375767330164975616	…	M2.5 V	15:33:54.89	+37:54:48.3	…	B	0.834	99.3	68.81	82.68	…	0.422 ± 0.031
…	…	LP 135-414	J15340+513	M4.5 V	15:34:03.52	+51:22:06.8	…	…	…	…	31.29	335.59	65.77 ± 0.25	0.273 ± 0.013
…	…	Ross 512	J15345+142	M4.0 V	15:34:29.76	+14:16:15.5	…	…	…	…	61.24	685.85	99.46 ± 0.49	0.318 ± 0.014
…	…	2MUCD 11346	J15349-143	M8.6V	15:34:55.92	-14:18:54.5	…	…	…	…	61.20	976.35	3.78 ± 0.03	0.104 ± 0.052
…	…	Ross 513	J15353+177S	M2.5 V	15:35:19.17	+17:42:44.3	A+B	A	…	…	6.33	1222.21	106.84 ± 0.45	0.290 ± 0.013
15354+1743	LDS 977	Ross 513B	J15353+177N	M4.5 V	15:35:18.98	+17:43:01.7	…	B	17.637	351.2	29.31	1221.56	23.02 ± 0.09	0.152 ± 0.010
…	…	GJ 3913	J15357+221	M3.5 V	15:35:45.31	+22:09:01.6	…	…	…	…	57.01	719.72	158.07 ± 1.07	0.382 ± 0.016
…	…	BKCrB	J15368+375	M0.0 V	15:36:49.97	+37:34:48.0	AB	A	…	…	57.03	291.14	…	0.6220 ± 0.093
15368+3735	LDS4572	LP 273-44	…	…	…	…	…	B	15.278	89.3	75.59	287.84	…	…
…	…	Ross 802	J15369-141	dM4.0	15:36:58.13	-14:08:11.8	…	…	…	…	52.73	773.31	113.90 ± 0.63	0.295 ± 0.011
…	…	G 179-42	J15386+371	M3.5 V	15:38:36.68	+37:07:28.0	…	…	…	…	52.66	367.18	140.78 ± 0.67	0.359 ± 0.015
…	…	GJ 1194 A	J15400+434N	M3.0 V	15:40:05.37	+43:29:34.1	A+B	A	…	…	70.32	1229.91	105.50 ± 0.51	0.288 ± 0.013
15400+4330	VBS 25	GJ 1194 B	J15400+434S	M4.0 V	15:40:05.54	+43:29:30.0	…	B	4.487	155.3	38.25	1208.54	…	0.189 ± 0.039
…	…	UU UMi	J15412+759	M3.5 V	15:41:20.12	+75:59:22.5	Aab	Aab(2)	…	…	35.83	1077.66	…	0.502 ± 0.071

Table D.2: Complete sample with the description of multiple systems (continued).

WDS id	WDS disc	Name	Karmn	Spectral type	α (2016.0)	δ (2016.0)	System	Component	ρ [arcsec]	θ [deg]	ϖ [mas]	$\mu_{\rm total}$ [mas a^{-1}]	$\mathcal{L}$ [$10^{-4}\,\mathcal{L}_\odot$]	$\mathcal{M}$ [$\mathcal{M}_\odot$]
…	…	HD 140232	…	A8 Vam	15:41:54.65	+18:27:51.4	AB+C	A	…	…	100.31	82.17	…	1.810 ± 0.272
15419+1828	DRS 17	G3- 1197801408884577408	…	M3.5 V	15:41:54.81	+18:27:51.5	…	B	2.359	87.6	63.36	82.28	…	0.319 ± 0.034
15419+1828	TOK 302	StKM 1-1264	J15416+184	M1.5 Ve	15:41:37.17	+18:28:09.2	…	C	249.250	274.1	91.90	91.89	1106.36 ± 19.33	0.668 ± 0.026
…	…	GJ 595	J15421-194	M3.0 V	15:42:04.27	-19:28:34.9	Aab	Aab(1)	…	…	…	2261.94	…	…
…	…	GJ 3916	J15474-108	M2.5 V	15:47:24.21	-10:53:53.2	Aabc	Aabc(3)	…	…	59.09	482.66	…	0.672 ± 0.048
…	…	1R154741.3+224108	J15476+226	M4.5 V	15:47:40.51	+22:41:16.0	…	…	…	…	69.04	186.83	164.85 ± 2.27	0.446 ± 0.019
…	…	LP 177-102	J15474+451	M4.0 V	15:47:27.03	+45:07:54.5	Aab	Aab(EB)	…	…	50.47	318.39	…	0.516 ± 0.012
…	…	RX J1548.0+0421	J15480+043	M2.5 V	15:48:02.78	+04:21:38.4	A+B	A	…	…	42.51	58.85	299.27 ± 1.99	0.502 ± 0.019
…	…	UCAC4 472-052890	…	M4.0 V	15:47:54.89	+04:18:02.9	…	B*	245.615	208.7	78.56	58.38	94.76 ± 0.46	0.310 ± 0.014
…	…	PM J15488+3030	J15488+305	M3.0 V	15:48:48.60	+30:30:38.7	…	…	…	…	63.38	103.80	277.11 ± 1.48	0.482 ± 0.019
…	…	G 168-13	J15493+250	M2.0 V	15:49:20.38	+25:03:48.5	…	…	…	…	54.79	390.77	256.11 ± 1.34	0.435 ± 0.017
…	…	GJ 3920	J15496+510	M2.0 V	15:49:35.62	+51:03:02.0	…	…	…	…	46.87	480.73	254.48 ± 1.48	0.434 ± 0.017
…	…	LP 23-35	J15499+796	M5.0 V	15:49:53.83	+79:39:53.6	…	…	…	…	46.78	252.39	73.49 ± 0.69	0.291 ± 0.010
…	…	Wolf 587	J15501+009	M3.0 V	15:50:11.41	+00:57:32.0	…	…	…	…	159.92	189.62	144.99 ± 0.83	0.342 ± 0.015
…	…	TYC 2572-633-1	J15512+306	M1.5 Ve	15:51:14.63	+30:40:42.2	…	…	…	…	20.54	181.48	905.27 ± 30.30	0.640 ± 0.027
…	…	GJ 3923	J15513+295	M3.5 V	15:51:21.51	+29:30:59.2	…	…	…	…	54.18	498.11	127.33 ± 0.73	0.340 ± 0.015
15496+3449	BWL 41	GJ 3919	J15496+348	M4.0 Ve	15:49:37.37	+34:49:07.8	(AB)	AB	0.208	98.6	56.08	966.80	…	0.293 ± 0.035
15531+3445	RAO 340	Ross 806	J15531+347N	M3.0 V	15:53:06.69	+34:45:05.9	(AB)+C	AB	0.433	304.9	56.11	559.77	…	0.481 ± 0.030
15531+3445	LDS6309	GJ 3926	J15531+347S	M3.0 V	15:53:06.97	+34:44:39.5	…	C	26.607	172.6	25.37	570.00	176.19 ± 0.83	0.405 ± 0.017
…	…	NLTT 41533	J15538+641	M0.5 V	15:53:48.31	+64:09:36.2	…	…	…	…	26.80	228.67	764.47 ± 3.93	0.636 ± 0.027
…	…	GJ 3928	J15555+352	M4.0 V	15:55:31.51	+35:12:05.2	AB	A	…	…	30.98	279.97	…	0.366 ± 0.033
15555+3512	MCT 9	G 180-11B	…	M5.0 V	15:55:31.39	+35:12:04.7	…	B	1.630	252.4	91.48	266.99	…	0.184 ± 0.040
…	…	RX J1555.7+6840	J15557+686	M2.5 Ve	15:55:47.10	+68:40:16.0	…	…	…	…	91.36	140.05	367.74 ± 1.63	0.484 ± 0.030
…	…	RX J1556.9+3738	J15569+376	M2.5 V	15:56:58.12	+37:38:14.3	…	…	…	…	26.17	94.77	476.95 ± 10.61	0.506 ± 0.029
…	…	LSPM J1557+0901	J15578+090	M4.0 V	15:57:48.42	+09:01:07.6	…	…	…	…	…	212.20	98.54 ± 0.47	0.317 ± 0.014
…	…	V1022Her	J15581+494	M1.0 Ve	15:58:10.41	+49:27:05.5	…	…	…	…	29.19	189.79	694.71 ± 4.37	0.590 ± 0.028
…	…	GJ 3929	J15583+354	M3.5 V	15:58:18.61	+35:24:29.4	…	…	…	…	31.81	348.81	118.00 ± 0.45	0.292 ± 0.011
…	…	StM 258	J15587+346	M3.5 V	15:58:45.75	+34:48:53.8	…	…	…	…	76.64	90.55	315.58 ± 8.53	0.436 ± 0.031
…	…	RX J1559.7+4403	J15597+440	M2.0 Ve	15:59:47.20	+44:03:59.6	A+B	A	…	…	48.38	69.95	1092.28 ± 19.82	0.665 ± 0.026
15598+4404	JNN 106	PM J15597+4403B	…	M8.0 V	15:59:46.70	+44:04:01.0	…	B	5.622	284.3	29.05	68.31	…	0.106 ± 0.047
…	…	GJ 606	J15598-082	M1.0 V	15:59:53.60	-08:15:12.0	…	…	…	…	31.07	204.06	381.38 ± 2.40	0.476 ± 0.012
…	…	GJ 3933	J16008+403	M3.0 V	16:00:50.40	+40:19:38.7	…	…	…	…	87.50	410.82	134.10 ± 0.54	0.350 ± 0.015
…	…	GJ 607	J16017+301	M3.0 V	16:01:43.15	+30:10:52.9	…	…	…	…	86.28	358.19	186.29 ± 0.78	0.391 ± 0.016
…	…	GJ 3935	J16018+304	M2.5 V	16:01:52.43	+30:27:37.0	A+B	A	…	…	100.52	190.95	178.80 ± 0.75	0.383 ± 0.016
16019+3027	LDS4626	GJ 3936	J16017+304	M4.5 V	16:01:44.35	+30:27:42.9	…	B	104.711	273.3	93.81	188.24	63.82 ± 0.73	0.219 ± 0.011
…	…	GJ 609	J16028+205	M4.0 V	16:02:49.85	+20:35:01.2	…	…	…	…	66.99	1571.06	72.64 ± 0.30	0.241 ± 0.010
…	…	PM J16033+1735	J16033+175	M2.0 V	16:03:20.60	+17:35:55.0	…	…	…	…	40.33	55.81	878.93 ± 12.93	0.622 ± 0.027
…	…	GJ 3937	J16043-062	M4.5 V	16:04:19.91	-06:16:59.9	…	…	…	…	20.89	869.82	26.06 ± 0.25	0.175 ± 0.011
…	…	BPM 91242	J16046+263	M0.5 V	16:04:36.85	+26:20:44.6	…	…	…	…	25.39	129.04	637.04 ± 2.38	0.602 ± 0.027
…	…	HD 144579	…	G8 V	16:04:56.01	+39:09:24.3	A+B	A	…	…	22.54	573.29	4140.87 ± 12.13	0.940 ± 0.141

Table D.2: Complete sample with the description of multiple systems (continued).

WDS id	WDS disc	Name	Karmn	Spectral type	α (2016.0)	δ (2016.0)	System	Component	ρ [arcsec]	θ [deg]	ϖ [mas]	$\mu_{\rm total}$ [mas a^{-1}]	$\mathcal{L}$ [$10^{-4}\,\mathcal{L}_\odot$]	$\mathcal{M}$ [$\mathcal{M}_\odot$]
16048+3910	WNO 47	HD 144579B	J16048+391	M4.0 V	16:04:50.08	+39:09:36.6	…	B	69.998	280.1	169.88	564.44	30.52 ± 0.11	0.166 ± 0.010
…	…	GJ 3941	J16054+769	M3.0 V	16:05:26.51	+76:54:58.5	…	…	…	…	168.77	353.09	276.28 ± 1.48	0.482 ± 0.019
…	…	LP 329-30	J16062+290	M2.0 V	16:06:13.41	+29:02:01.6	…	…	…	…	169.30	405.78	869.00 ± 5.18	0.619 ± 0.027
16067+0823	JOD 9	GJ 611.3	J16066+083	M1.0 V	16:06:40.66	+08:23:19.6	(AB)+C	AB	0.599	291.0	23.58	513.49	…	0.610 ± 0.027
16067+0823	JOY 6	G3- 4451575895400385536	…	…	16:06:40.51	+08:23:20.4	…	C	2.407	290.4	23.81	…	…	…
…	…	GJ 3939	J16074+059	M3.8 V	16:07:27.90	+05:57:56.0	…	…	…	…	87.20	366.88	158.64 ± 1.06	0.383 ± 0.016
…	…	GJ 1198	J16082-104	M4.5 V	16:08:14.56	-10:26:35.1	…	…	…	…	85.41	1353.47	50.15 ± 0.23	0.219 ± 0.012
…	…	GJ 3942	J16090+529	M0.5 V	16:09:03.50	+52:56:39.0	…	…	…	…	85.43	213.40	649.64 ± 2.37	0.599 ± 0.027
…	…	LP 504-59	J16092+093	M3.0 Ve	16:09:15.90	+09:21:11.0	…	…	…	…	42.22	405.12	177.74 ± 0.98	0.355 ± 0.011
…	…	K2-33	J16102-193	dM3.0	16:10:14.73	-19:19:09.8	…	…	…	…	66.54	25.81	1054.64 ± 10.66	…
…	…	TYC 371-1053-1	J16120+033	M2.0 V	16:12:04.68	+03:18:19.8	A+B	A	…	…	48.75	66.33	774.53 ± 11.50	0.602 ± 0.027
16121+0318	SKF2840	1R161204.8+031850	…	M3.5 V	16:12:05.06	+03:18:52.4	…	B	33.100	10.0	40.30	73.41	107.25 ± 2.13	0.273 ± 0.013
…	…	LP 804-27	J16126-188	M3.0 V	16:12:41.82	-18:52:35.2	…	…	…	…	33.38	217.11	…	0.440 ± 0.031
…	…	sig CrB A	…	F6 V	16:14:40.51	+33:51:29.6	Aab+B+(CD)	Aab(2)	…	…	77.48	282.06	…	0.231 ± 0.001
16147+3352	STF2032	sig CrB B	…	G1 V	16:14:40.01	+33:51:25.8	…	B	7.231	238.5	58.54	301.27	9935.25 ± 17.97	1.030 ± 0.155
16147+3352	YSC 152	sig CrB C	J16139+337	M2.5 V	16:13:55.90	+33:46:22.7	…	CD	635.058	241.1	40.65	300.69	…	0.432 ± 0.031
…	…	LP 624-54	J16144-028	M5.0 V	16:14:25.19	-02:50:54.9	…	…	…	…	23.44	367.49	7.51 ± 0.05	0.108 ± 0.009
…	…	GJ 1200	J16145+191	M3.5 V	16:14:30.36	+19:06:16.7	…	…	…	…	52.54	2035.67	103.97 ± 0.48	0.305 ± 0.014
…	…	GJ 3946	J16147+048	M3.5 V	16:14:43.36	+04:52:09.7	…	…	…	…	31.93	416.37	166.18 ± 0.86	0.392 ± 0.016
…	…	GJ 3947	J16155+244	M1.5 V	16:15:32.10	+24:27:50.9	…	…	…	…	33.71	256.12	361.06 ± 1.56	0.491 ± 0.018
…	…	HD 147379	J16167+672S	M0.0 V	16:16:41.37	+67:14:21.2	A+B	A	…	…	33.71	504.96	962.91 ± 5.28	0.680 ± 0.026
16167+6714	ENG 57	EWDra	J16167+672N	M3.0 V	16:16:43.98	+67:15:23.9	…	B	64.529	13.6	35.64	491.15	294.12 ± 1.14	0.449 ± 0.014
…	…	1R161804.9+061702	J16180+062	M3.0 Ve	16:18:05.01	+06:17:12.0	…	…	…	…	34.17	92.76	320.46 ± 4.55	0.450 ± 0.031
16171+5516	BLA 3	CRDra	J16170+552	M1.0 V	16:17:05.52	+55:16:01.9	(AB)	AB(2)	0.097	8.5	119.58	439.85	…	…
…	…	GJ 618.1 A	J16204-042	M0.0 V	16:20:24.34	-04:16:02.6	A+B	A	…	…	68.45	416.69	1014.40 ± 5.86	0.691 ± 0.026
16204-0416	WIL 3	GJ 618.1 B	…	L2.4V	16:20:25.72	-04:16:32.0	…	B	35.907	144.8	57.57	415.28	1.08 ± 0.06	0.075 ± 0.011
…	…	V1169Her	J16220+228	M1.5 Ve	16:22:01.12	+22:50:22.8	…	…	…	…	65.50	85.58	1157.76 ± 16.87	0.677 ± 0.026
…	…	LSPM J1624+2254	J16247+229	M1.0 V	16:24:43.71	+22:54:19.3	…	…	…	…	41.09	180.71	587.98 ± 13.14	0.572 ± 0.028
…	…	GJ 625	J16254+543	M1.5 V	16:25:25.41	+54:18:12.0	…	…	…	…	57.20	465.07	144.88 ± 0.69	0.303 ± 0.010
16240+4822	HEN 1	GJ 623	J16241+483	M3.0 V	16:24:11.16	+48:21:03.1	(AB)	AB(1)	0.327	55.9	18.09	1254.76	…	…
…	…	LP 330-13	J16255+323	M2.0 V	16:25:32.91	+32:18:34.1	…	…	…	…	42.42	184.66	254.78 ± 1.44	0.434 ± 0.017
…	…	TYC 4647-2406-1	J16259+834	M1.5 V	16:25:59.21	+83:24:23.2	…	…	…	…	32.04	106.46	463.34 ± 1.81	0.533 ± 0.029
16255+2602	RAO 347	GJ 3953	J16255+260	M3.0 V	16:25:32.12	+26:01:38.0	(AB)	AB	0.285	54.8	56.68	190.85	…	…
16268-1724	WSI 131	GJ 3954	J16268-173	M5e	16:26:47.75	-17:23:40.5	(AB)	AB	0.691	172.7	52.59	524.83	…	0.185 ± 0.039
16280+1533	JNN279	GJ 3955	J16280+155	M3.6 V	16:28:02.04	+15:33:52.1	(AB)	AB(2)	0.558	35.1	…	307.67	…	…
…	…	V2306Oph	J16303-126	M3.0 V	16:30:17.96	-12:40:04.3	…	…	…	…	20.17	1187.66	109.31 ± 0.79	0.289 ± 0.011
…	…	GJ 3959	J16313+408	M6.0 V	16:31:18.59	+40:51:56.6	…	…	…	…	20.93	338.19	26.95 ± 0.12	0.158 ± 0.010
…	…	GJ 1202	J16315+175	M4.0 V	16:31:34.69	+17:33:35.9	…	…	…	…	19.84	873.35	107.96 ± 0.43	0.292 ± 0.013
…	…	GJ 1203	J16327+126	M3.0 V	16:32:44.36	+12:36:43.8	…	…	…	…	39.33	776.89	210.00 ± 1.02	0.395 ± 0.011
…	…	GJ 3960	J16328+098	M3.5 V	16:32:53.09	+09:50:28.5	…	…	…	…	158.72	276.61	86.50 ± 0.48	0.276 ± 0.013

Table D.2: Complete sample with the description of multiple systems (continued).

WDS id	WDS disc	Name	Karmn	Spectral type	α (2016.0)	δ (2016.0)	System	Component	ρ [arcsec]	θ [deg]	ϖ [mas]	$\mu_{\rm total}$ [mas a^{-1}]	$\mathcal{L}$ [$10^{-4}\,\mathcal{L}_\odot$]	$\mathcal{M}$ [$\mathcal{M}_\odot$]
…	…	LP 137-37	J16342+543	M1.0 V	16:34:13.28	+54:23:48.5	…	…	…	…	59.73	591.36	480.63 ± 1.91	0.541 ± 0.029
16302-1440	WSI 132	GJ 2121	J16302-146	M2.5 V	16:30:12.52	-14:39:53.0	(AB)	AB	0.105	100.5	41.52	571.32	…	0.435 ± 0.031
…	…	CMDra	J16343+571	M4.5 V	16:34:18.14	+57:10:03.3	Aab+B	Aab(EB)	…	…	50.62	1623.35	…	0.445 ± 0.001
16345+5709	LDS1436	GJ 630.1 B	…	DQ8	16:34:19.37	+57:10:28.1	…	B	26.726	21.9	36.80	1634.85	…	0.500 ± 0.100
…	…	GJ 1204	J16360+088	M4.0 V	16:36:05.09	+08:48:46.7	…	…	…	…	87.33	542.06	57.04 ± 0.34	0.235 ± 0.012
…	…	G 202-68	J16395+505	M1.0 V	16:39:30.81	+50:33:57.0	…	…	…	…	30.80	514.38	239.84 ± 0.81	0.396 ± 0.016
…	…	GJ 3967	J16401+007	M5.0 V	16:40:06.17	+00:42:16.3	…	…	…	…	89.13	236.37	39.62 ± 0.24	0.206 ± 0.011
…	…	GJ 3971	J16403+676	M7.0 V	16:40:19.87	+67:36:10.6	…	…	…	…	46.44	456.21	27.66 ± 0.29	0.196 ± 0.011
…	…	Ross 812	J16408+363	M2.0 V	16:40:48.72	+36:19:02.9	…	…	…	…	19.70	212.79	421.80 ± 2.12	0.508 ± 0.029
…	…	PM J16420+1916	J16420+192	M2.5 V	16:42:00.72	+19:16:11.6	…	…	…	…	19.73	77.66	481.17 ± 3.60	0.519 ± 0.029
…	…	GJ 3972	J16462+164	M3.0 V	16:46:13.35	+16:28:33.2	…	…	…	…	43.35	590.54	248.23 ± 1.07	0.413 ± 0.012
…	…	LP 276-22	J16465+345	M6.0 V	16:46:31.03	+34:34:49.0	…	…	…	…	…	542.48	10.78 ± 0.04	0.134 ± 0.010
16355+3501	BWL 44	V1200Her	J16354+350	M4.0 Ve	16:35:27.61	+35:00:55.3	(AB)	AB	0.092	25.6	30.84	200.15	…	0.330 ± 0.034
…	…	GJ 3973	J16487-157	M1.5 Vk:	16:48:45.95	-15:44:23.7	…	…	…	…	32.67	220.40	510.00 ± 2.33	0.545 ± 0.028
…	…	GJ 3975	J16508-048	M3.5 V	16:50:52.99	-04:50:38.8	…	…	…	…	40.69	786.19	80.11 ± 0.58	0.265 ± 0.013
…	…	GJ 3976	J16509+224	M5.0 V	16:50:57.98	+22:27:12.1	…	…	…	…	45.62	401.79	30.59 ± 0.12	0.178 ± 0.011
…	…	GSC 04194-01561	J16528+630	M4.5 V	16:52:49.82	+63:04:41.2	…	…	…	…	38.11	212.34	45.22 ± 0.22	0.222 ± 0.012
…	…	GJ 3979	J16529+400	M3.0 V	16:52:54.92	+40:05:04.6	…	…	…	…	116.04	233.33	278.28 ± 7.40	0.412 ± 0.032
…	…	Ross 644	J16542+119	M0.0 V	16:54:11.44	+11:54:57.9	…	…	…	…	53.07	628.96	474.85 ± 2.52	0.507 ± 0.018
16488+1039	CRC 73	LSPM J1648+1038	J16487+106	M2.5 V	16:48:46.40	+10:38:51.1	(AB)	AB(2)	0.102	176.3	53.76	177.27	…	…
16555-0820	KUI 75	V1054Oph	J16554-083S	M3.0 V	16:55:27.89	-08:20:25.2	(AB)+C+D	AB(2)	0.225	106.9	55.42	1202.11	…	0.640 ± 0.021
16555-0820	LDS 573	Wolf 629	J16554-083N	M3.5 V	16:55:24.34	-08:19:35.7	…	C	72.292	313.2	43.18	1214.87	57.29 ± 0.40	0.207 ± 0.010
16555-0820	WNO 55	GJ 644 C	J16555-083	M7.0 V	16:55:34.38	-08:23:54.7	…	D	230.576	155.3	37.64	1191.21	5.64 ± 0.03	0.101 ± 0.049
…	…	GJ 1207	J16570-043	dM4	16:57:06.25	-04:21:02.3	…	…	…	…	32.88	611.15	67.66 ± 0.60	0.257 ± 0.009
…	…	GJ 3980	J16573+124	M4.0 V	16:57:23.12	+13:28:06.6	…	…	…	…	32.95	225.63	94.15 ± 1.39	0.309 ± 0.014
…	…	PM J16573+2708	J16573+271	M2.0 V	16:57:22.27	+27:08:31.2	AB	A	…	…	60.84	55.64	…	0.425 ± 0.031
16574+2709	CFN 13	PM J16573+2708B	…	…	16:57:22.34	+27:08:30.6	…	B	1.044	121.2	44.12	…	…	…
…	…	GJ 3986	J16574+777	M3.0 V	16:57:29.79	+77:43:06.3	…	…	…	…	91.42	254.66	208.29 ± 0.87	0.415 ± 0.017
16578+1317	HDS2399	GJ 647	J16577+132	M0.0 V	16:57:46.15	+13:17:31.1	(AB)	AB	0.102	193.4	66.88	104.81	…	0.728 ± 0.026
…	…	V1090Her	…	K3 V	16:57:52.95	+47:22:04.4	A+B+C	A	…	…	66.93	308.70	…	0.775 ± 0.116
16579+4722	A 1874	HD 153557B	J16578+473	M1.5 V	16:57:53.40	+47:22:06.7	…	B	5.091	63.0	54.34	301.44	…	0.475 ± 0.030
16579+4722	STFA 32	V1089Her	…	K3 V	16:57:42.01	+47:21:47.9	…	C	112.378	261.6	18.99	296.94	…	0.764 ± 0.115
…	…	Ross 860	J16581+257	M1.0 V	16:58:08.71	+25:44:30.8	…	…	…	…	…	521.01	450.03 ± 2.13	0.497 ± 0.012
16584+1358	YSC61	GJ 3981 A	J16584+139	M4.0 V	16:58:24.81	+13:58:10.9	AB	A	0.549	236.4	71.47	399.08	…	0.263 ± 0.037
…	…	GJ 3981 B	…	…	16:58:24.79	+13:58:10.8	…	B	0.298	263.8	32.26	…	…	…
…	…	LP 43-338	J16587+688	M1.5 V	16:58:42.17	+68:53:55.8	…	…	…	…	79.85	565.45	372.78 ± 1.86	0.500 ± 0.019
…	…	V1234Her	J16591+209	M3.5 Ve	16:59:09.58	+20:58:18.3	AB	A	…	…	79.84	120.04	…	0.370 ± 0.033
16592+2058	JNN 111	PM J16591+2058B	…	M4.0 V	16:59:09.62	+20:58:17.9	…	B	0.653	129.7	73.26	139.45	…	0.268 ± 0.036
…	…	GJ 3983	J17003+253	M3.2 V	17:00:20.18	+25:21:05.1	…	…	…	…	18.72	182.98	124.65 ± 0.46	0.316 ± 0.014
…	…	G 139-4	J17006+063	M1.0 V	17:00:38.65	+06:18:42.0	…	…	…	…	18.64	315.70	549.03 ± 2.84	0.568 ± 0.028

Table D.2: Complete sample with the description of multiple systems (continued).

WDS id	WDS disc	Name	Karmn	Spectral type	α (2016.0)	δ (2016.0)	System	Component	ρ [arcsec]	θ [deg]	ϖ [mas]	$\mu_{\rm total}$ [mas a^{-1}]	$\mathcal{L}$ [$10^{-4}\,\mathcal{L}_\odot$]	$\mathcal{M}$ [$\mathcal{M}_\odot$]
…	…	GJ 3984	J17010+082	M3.8 V	17:01:01.85	+08:12:23.5	…	…	…	…	19.37	306.52	95.24 ± 0.55	0.291 ± 0.013
…	…	GJ 3987	J17027-060	M0	17:02:49.45	-06:04:07.6	…	…	…	…	103.18	151.44	488.47 ± 2.60	0.554 ± 0.028
…	…	GJ 3988	J17033+514	M5.0 V	17:03:24.10	+51:24:32.6	…	…	…	…	62.52	622.70	39.68 ± 0.19	0.183 ± 0.009
…	…	LP 331-57 A	J17038+321	M2.0 V	17:03:53.09	+32:11:47.6	AabB	Aab(2?)	…	…	27.85	216.04	…	…
17039+3212	DAE 6	LP 331-57 B	…	M4.0 V	17:03:53.14	+32:11:46.4	…	B	1.393	151.3	35.23	185.92	…	0.232 ± 0.037
…	…	GJ 1209	J17043+169	M3.0 V	17:04:22.49	+16:55:37.5	…	…	…	…	45.07	1140.03	147.01 ± 0.75	0.345 ± 0.015
…	…	HD 154363	…	K4/5 V	17:05:02.41	-05:04:17.7	A+B	A	…	…	34.44	1461.66	1307.20 ± 6.44	0.730 ± 0.110
17050-0504	LDS 585	HD 154363B	J17052-050	M1.5 V	17:05:12.80	-05:05:57.4	…	B	184.423	122.7	34.58	1457.06	337.16 ± 1.58	0.478 ± 0.012
…	…	LP 387-37	J17058+260	M1.5 V	17:05:52.55	+26:05:27.4	AB	A	…	…	37.61	291.03	…	0.553 ± 0.028
17059+2606	LDS4721	LP 387-36	…	DC7	17:05:52.54	+26:05:46.7	…	B	19.244	359.6	41.32	285.38	…	0.500 ± 0.100
…	…	Ross 863	J17071+215	M3.0 V	17:07:06.96	+21:33:14.1	…	…	…	…	47.42	464.00	204.83 ± 0.82	0.379 ± 0.012
…	…	G 203-44	J17082+516	M1.0 V	17:08:12.71	+51:38:10.6	…	…	…	…	48.16	376.70	743.43 ± 2.72	0.617 ± 0.027
17077+0722	YSC62	GJ 1210	J17076+073	M5.0 V	17:07:40.31	+07:22:00.6	(AB)	AB	0.122	283.5	59.12	618.93	…	0.163 ± 0.041
…	…	GJ 3990	J17098+119	M4.0 V	17:09:52.36	+11:55:32.8	…	…	…	…	21.14	371.52	68.88 ± 1.09	0.261 ± 0.013
…	…	GJ 3991	J17095+436	M3.5 V	17:09:32.03	+43:40:48.4	Aab	Aab(1)	…	…	18.00	430.81	…	…
…	…	StM 336	J17104+279	M2.5 V	17:10:25.49	+27:58:38.6	A+B	A	…	…	54.11	91.91	215.47 ± 0.94	0.397 ± 0.016
17104+2759	SKF 366	CTI 170958.5+275905	…	M5.5 V	17:10:28.32	+27:58:08.4	…	B	48.112	128.8	59.14	91.23	12.16 ± 0.07	0.122 ± 0.009
…	…	HD 155876	J17121+456	M3.0 V	17:12:08.21	+45:39:32.6	AB	A	…	…	43.71	1661.81	…	0.376 ± 0.033
17121+4540	KUI 79	G3- 1364668825433435776	…	…	17:12:08.21	+45:39:33.7	…	B	1.133	357.1	43.63	…	…	…
…	…	Wolf 654	J17115+384	M4.0 V	17:11:35.04	+38:26:33.2	…	…	…	…	30.81	217.81	184.71 ± 0.77	0.372 ± 0.013
…	…	GJ 660	J17118-018	M3.0 V	17:11:51.82	-01:51:10.5	AB	A	…	…	36.01	639.91	…	0.282 ± 0.043
17119-0151	LPM629	G3- 4367834134894197888	…	…	17:11:51.82	-01:51:10.3	…	B	0.216	357.7	36.22	…	…	…
…	…	GJ 3994	J17146+269	M2.0 V	17:14:39.87	+26:55:44.4	…	…	…	…	39.04	336.83	384.19 ± 6.98	0.490 ± 0.030
…	…	GJ 1214	J17153+049	M4.5 V	17:15:19.56	+04:57:38.1	…	…	…	…	22.55	948.00	37.50 ± 0.22	0.200 ± 0.011
17121+4540	KUI 79	V2367Oph	J17136-084	M3.5 V	17:13:40.00	-08:25:21.4	Aab	Aab(2)	0.662	289.4	49.49	600.61	…	…
…	…	GJ 3997	J17158+190	M0.5 V	17:15:49.95	+19:00:00.3	AB	A	…	…	52.28	151.20	…	0.499 ± 0.029
17158+1900	JOD 11	BD+19 3268B	…	M4.5 V	17:15:49.84	+19:00:00.3	…	B	1.471	271.0	26.36	89.24	…	0.244 ± 0.037
…	…	GJ 3998	J17160+110	M1.0 V	17:16:00.49	+11:03:22.1	…	…	…	…	63.17	373.65	469.14 ± 2.22	0.537 ± 0.029
…	…	GJ 2128	J17166+080	M2.5 V	17:16:40.68	+08:03:29.1	…	…	…	…	36.36	286.72	237.65 ± 1.04	0.402 ± 0.011
…	…	GJ 1215	J17177+116	M5.0 V	17:17:43.71	+11:40:05.3	(AB)	AB	…	…	23.76	566.80	…	0.154 ± 0.041
…	…	GJ 3999	J17177-118	M3.0 V	17:17:45.28	-11:48:59.0	A+B	A	…	…	23.55	292.10	312.91 ± 1.80	0.484 ± 0.018
17178-1149	LDS 593	GJ 4000	…	M3.0 V	17:17:44.51	-11:48:31.1	…	B	30.072	337.8	75.29	292.36	269.55 ± 1.51	0.506 ± 0.020
17183+1809	BWL45	GJ 4002	J17183+181	M3.0 V	17:18:22.44	+18:08:52.4	(AB)	AB	0.452	324.5	47.33	244.52	…	0.329 ± 0.034
17184-0147	BAG51	GJ 4001	J17183-017	M0.0 V	17:18:21.82	-01:46:55.4	(AB)	AB	0.521	291.3	51.77	160.45	…	0.615 ± 0.027
…	…	V647Her	J17199+265	M3.5 V	17:19:53.95	+26:30:08.7	A+B	A	…	…	35.28	411.40	199.89 ± 1.03	0.432 ± 0.018
17199+2629	OSV 5	V639Her	J17198+265	M4.5 V	17:19:52.70	+26:30:08.3	…	B	16.860	268.9	35.52	420.84	77.24 ± 0.40	0.298 ± 0.014
…	…	GJ 671	J17198+417	M2.5 V	17:19:53.12	+41:42:36.4	…	…	…	…	99.79	877.18	180.28 ± 0.77	0.353 ± 0.011
…	…	GJ 1216	J17207+492	M4.0 V	17:20:47.19	+49:15:01.4	…	…	…	…	22.74	1296.78	39.02 ± 0.17	0.190 ± 0.011
…	…	GJ 4003	J17219+214	M4.0 V	17:21:54.44	+21:25:51.3	…	…	…	…	57.00	293.77	61.49 ± 0.30	0.245 ± 0.012
…	…	PM J17225+0531	J17225+055	M2.5 V	17:22:33.80	+05:31:15.1	…	…	…	…	36.19	99.21	234.22 ± 1.56	0.441 ± 0.017

Table D.2: Complete sample with the description of multiple systems (continued).

WDS id	WDS disc	Name	Karmn	Spectral type	α (2016.0)	δ (2016.0)	System	Component	ρ [arcsec]	θ [deg]	ϖ [mas]	$\mu_{\rm total}$ [mas a^{-1}]	$\mathcal{L}$ [$10^{-4}\,\mathcal{L}_\odot$]	$\mathcal{M}$ [$\mathcal{M}_\odot$]
…	…	GJ 4005	J17242-043	M2.5 V	17:24:16.69	-04:21:54.1	…	…	…	…	69.64	264.75	253.01 ± 1.52	0.460 ± 0.018
…	…	GJ 1219	J17276+144	M4.0 V	17:27:38.65	+14:28:56.4	…	…	…	…	69.64	1169.53	64.43 ± 0.25	0.235 ± 0.012
…	…	Wolf 750	J17285+374	M3.5 V	17:28:30.41	+37:27:04.1	…	…	…	…	43.60	188.78	107.24 ± 0.44	0.310 ± 0.014
…	…	Wolf 751	J17303+055	M1.0 V	17:30:22.76	+05:32:50.7	…	…	…	…	26.86	251.09	521.06 ± 2.99	0.563 ± 0.028
…	…	GJ 1220	J17312+820	M4.0 V	17:31:14.95	+82:05:27.8	…	…	…	…	28.44	564.93	33.06 ± 0.12	0.186 ± 0.011
…	…	Wolf 755	J17316+047	M1.5 V	17:31:37.97	+01:47:48.0	…	…	…	…	…	208.41	342.86 ± 1.78	0.478 ± 0.018
…	…	GJ 4011	J17321+504	M2.5 V	17:32:07.82	+50:24:41.7	…	…	…	…	37.95	526.57	273.67 ± 2.17	0.479 ± 0.019
…	…	G 226-64	J17328+543	M2.0 V	17:32:53.06	+54:20:19.6	…	…	…	…	46.30	506.37	215.09 ± 0.82	0.374 ± 0.015
…	…	V1274Her	J17338+169	M6.0 V	17:33:53.03	+16:55:11.0	…	…	…	…	59.00	187.78	94.16 ± 1.97	0.317 ± 0.066
…	…	RX J1734.0+4447A	…	M2.0 V	17:34:05.43	+44:47:08.9	AB	A	…	…	73.72	115.42	…	0.381 ± 0.032
17341+4447	CRC 74	RX J1734.0+4447B	J17340+446	M3.5 V	17:34:05.47	+44:47:08.4	…	B	0.633	146.4	7.19	94.46	…	0.328 ± 0.034
17350+6153	BU 962	HD 160269A	…	G0 IV/V	17:35:00.16	+61:52:20.8	(AB)+C	AB(1)	0.625	300.5	80.21	522.56	…	…
17350+6153	LDS2736	GJ 685	J17355+616	M0.5 V	17:35:35.07	+61:40:45.4	…	C	738.164	160.3	33.65	577.33	589.33 ± 2.28	0.579 ± 0.028
…	…	GJ 687	J17364+683	M3.0 V	17:36:24.97	+68:20:00.6	…	…	…	…	33.85	1309.76	224.17 ± 1.78	0.434 ± 0.024
…	…	GJ 4015	J17376+220	M4.1 V	17:37:36.52	+22:05:45.2	…	…	…	…	68.61	310.38	71.87 ± 0.29	0.267 ± 0.013
…	…	GJ 686	J17378+185	M1.5 V	17:37:54.39	+18:35:45.9	…	…	…	…	44.06	1351.97	298.36 ± 1.47	0.429 ± 0.012
17387+6114	HOM 1	HD 160934B	J17386+612	M4.0 V	17:38:39.61	+61:14:16.8	(AB)+C	AB	0.020	18.4	44.13	42.26	…	…
17387+6114	VVO 17	GJ 4021	…	M4.0 V	17:38:40.87	+61:14:00.0	…	C	19.052	151.4	44.27	49.61	109.72 ± 0.47	0.336 ± 0.015
…	…	GJ 4016	J17388+080	M2.5 V	17:38:51.16	+08:01:31.7	…	…	…	…	68.95	236.37	210.10 ± 1.22	0.392 ± 0.016
17397+2746	LDS 999	GJ 4018	J17395+277S	M0.5 V	17:39:30.73	+27:45:40.8	A+(BC)	A	56.439	21.0	58.88	201.22	739.04 ± 3.54	0.621 ± 0.027
17397+2746	JOD 12	GJ 4019	J17395+277N	M3.0 V	17:39:32.26	+27:46:33.5	…	BC	56.440	21.0	37.54	202.31	…	0.450 ± 0.031
…	…	G 204-25	J17419+407	M1.5 V	17:41:57.04	+40:44:44.3	…	…	…	…	39.23	271.77	633.73 ± 2.22	0.583 ± 0.028
…	…	Wolf 1471	J17421-088	M3.0 V	17:42:09.85	-08:49:07.8	…	…	…	…	92.88	964.49	80.31 ± 0.33	0.249 ± 0.012
…	…	2M17422264+5726521	J17423+574	M0.0 V	17:42:22.63	+57:26:52.0	…	…	…	…	92.90	14.84	710.85 ± 4.08	0.619 ± 0.027
…	…	GJ 690.1	J17425-166	M2.5 V	17:42:32.15	-16:38:35.9	…	…	…	…	34.87	699.66	103.69 ± 0.44	0.286 ± 0.013
17430+0547	HDS2506	GJ 4024	J17430+057	M1.0 V	17:43:01.06	+05:47:20.5	(AB)	AB	0.255	99.2	51.77	257.98	…	…
…	…	G 259-20	J17431+854	M2.0 V	17:43:07.85	+85:26:25.5	A+B	A	…	…	49.63	291.24	260.89 ± 5.02	0.414 ± 0.017
17432+8526	LUH 12	2M17430860+8526594	…	L5	17:43:07.13	+85:26:55.2	…	B	29.739	358.3	34.08	291.00	0.85 ± 0.02	…
…	…	Ross 133	J17432-185	M1.5 V	17:43:17.37	-18:31:27.7	…	…	…	…	33.87	574.92	386.59 ± 9.76	0.509 ± 0.020
…	…	GJ 694	J17439+433	M2.5 V	17:43:55.98	+43:22:33.3	…	…	…	…	19.17	603.29	251.60 ± 1.26	0.458 ± 0.018
…	…	GJ 4026	J17460+246	M4.0 V	17:46:04.22	+24:39:13.1	…	…	…	…	41.45	629.21	97.04 ± 0.46	0.294 ± 0.013
17456+4651	JOD 13	GJ 694.2	J17455+468	M0.0 V	17:45:33.50	+46:51:19.8	(AB)	AB	0.670	77.0	154.35	36.97	…	0.593 ± 0.028
17465+2743	TRN 2	HD 161797	…	G5 IV	17:46:27.17	+27:43:02.2	(AB)+C+D	AB	1.780	254.8	127.48	833.79	…	…
17465+2743	STF2220	GJ 695 B	…	M2.5 V	17:46:24.69	+27:42:49.5	…	C	35.364	248.9	41.56	899.45	…	0.422 ± 0.031
17465+2743	AC 7	GJ 695 C	J17464+277	M3.5 V	17:46:24.65	+27:42:49.8	…	D	35.759	249.7	34.60	719.40	…	0.375 ± 0.032
…	…	StKM 1-1528	J17469+228	M1.0 V	17:46:55.96	+22:48:01.6	…	…	…	…	27.90	93.31	570.74 ± 2.15	0.575 ± 0.028
…	…	PM J17481+1558	J17481+159	M3.0 V	17:48:11.19	+15:58:48.4	…	…	…	…	55.66	119.73	163.47 ± 0.69	0.365 ± 0.015
…	…	GJ 4030	J17502+237	M3.3 V	17:50:14.74	+23:45:58.1	…	…	…	…	27.90	563.73	124.77 ± 0.67	0.337 ± 0.015
…	…	GJ 4031	J17515+147	M3.0 V	17:51:30.58	+14:45:32.4	…	…	…	…	232.14	215.46	195.83 ± 0.99	0.428 ± 0.017
…	…	G 227-20	J17521+647	M0.5 V	17:52:11.83	+64:46:02.9	…	…	…	…	88.82	347.39	730.57 ± 2.63	0.623 ± 0.027

Table D.2: Complete sample with the description of multiple systems (continued).

WDS id	WDS disc	Name	Karmn	Spectral type	α (2016.0)	δ (2016.0)	System	Component	ρ [arcsec]	θ [deg]	ϖ [mas]	$\mu_{\rm total}$ [mas a^{-1}]	$\mathcal{L}$ [$10^{-4}\,\mathcal{L}_\odot$]	$\mathcal{M}$ [$\mathcal{M}_\odot$]
…	…	Wolf 1473	J17464-087	M3.5 V	17:46:29.28	-08:42:43.4	Aab	Aab(2)	…	…	34.47	430.41	…	0.396 ± 0.002
…	…	GJ 4032 A	J17530+169	M3.0 V	17:53:00.32	+16:54:59.5	AB	A	…	…	59.46	331.97	…	0.319 ± 0.034
17530+1655	CRC 27	GJ 4032 B	…	M4.0 V	17:53:00.38	+16:54:59.2	…	B	0.852	112.4	54.02	313.37	…	0.279 ± 0.035
…	…	GJ 1222	J17542+073	M4.0 V	17:54:16.48	+07:22:40.2	…	…	…	…	64.90	664.62	103.80 ± 0.75	0.303 ± 0.011
…	…	LSPM J1754+1251	J17547+128	M2.0 V	17:54:43.24	+12:51:18.6	…	…	…	…	33.21	153.20	214.77 ± 1.25	0.374 ± 0.015
…	…	GJ 4038	J17570+157	M3.0 V	17:57:03.33	+15:46:39.3	AB	A	…	…	44.16	302.88	…	0.349 ± 0.033
17571+1547	MCT 10	G 183-13B	…	M3.0 V	17:57:03.41	+15:46:39.1	…	B	1.221	101.5	67.29	291.04	…	0.356 ± 0.033
…	…	LP 44-162	J17572+707	M7.5 V	17:57:15.43	+70:42:06.4	…	…	…	…	67.35	326.76	11.99 ± 0.14	0.171 ± 0.011
…	…	Barnard's Star	J17578+046	M3.5 V	17:57:47.64	+04:44:21.9	…	…	…	…	66.16	10393.35	35.91 ± 0.28	0.175 ± 0.009
…	…	GJ 4040	J17578+465	M2.5 V	17:57:50.94	+46:35:28.4	AB	A	…	…	48.37	578.34	206.46 ± 0.86	0.387 ± 0.012
17578+4635	BDK9	G 204-39B	…	T7	…	…	…	B	197.004	130.6	88.69	594.57	…	…
…	…	LP 24-152	J17589+807	M3.5 V	17:58:55.00	+80:42:53.9	…	…	…	…	69.82	668.97	372.51 ± 24.02	0.459 ± 0.031
…	…	Wolf 1403	J18010+508	M1.5 V	18:01:05.86	+50:49:38.9	…	…	…	…	46.57	211.58	608.52 ± 2.55	0.584 ± 0.028
…	…	G 182-34	J18012+355	M3.5 Ve	18:01:16.14	+35:35:41.4	…	…	…	…	32.24	572.26	168.87 ± 0.65	0.396 ± 0.016
…	…	LP 71-82	J18022+642	M5.0 V	18:02:17.09	+64:15:38.1	…	…	…	…	63.37	431.12	32.26 ± 0.14	0.169 ± 0.010
…	…	GJ 1223	J18027+375	dM5.0	18:02:46.49	+37:30:44.7	…	…	…	…	84.01	1154.51	24.22 ± 0.10	0.144 ± 0.009
…	…	Wolf 792	J18031+179	M1.0 V	18:03:06.02	+17:54:20.0	…	…	…	…	57.99	352.27	408.48 ± 8.02	0.495 ± 0.019
…	…	Ross 820	J18037+247	M0.0 V	18:03:47.68	+25:45:16.7	…	…	…	…	52.65	234.74	822.30 ± 4.61	0.648 ± 0.027
18043+3557	JOD 14	GJ 4041	J18042+359	M0.5 V	18:04:17.70	+35:57:21.5	(AB)	AB	0.297	339.0	55.10	276.68	…	0.587 ± 0.028
…	…	HD 165222	J18051-030	M0.0 V	18:05:08.19	-03:01:58.1	…	…	…	…	95.52	659.78	330.03 ± 1.99	0.441 ± 0.011
…	…	NLTT 46021	J18063+728	M0.0 V	18:06:18.11	+72:49:20.1	…	…	…	…	65.75	236.68	733.44 ± 2.58	0.630 ± 0.027
…	…	Wolf 806	J18074+184	M1.0 V	18:07:27.99	+18:27:54.1	…	…	…	…	29.68	238.82	592.35 ± 2.53	0.573 ± 0.028
…	…	GJ 1224	J18075-159	M4.0 Ve	18:07:32.15	-15:57:52.6	…	…	…	…	49.80	709.11	28.55 ± 0.17	0.157 ± 0.009
…	…	LP 334-11	J18096+318	M1.0 V	18:09:40.77	+31:52:16.0	…	…	…	…	…	201.53	391.05 ± 1.30	0.484 ± 0.018
…	…	Wolf 1412	J18103+512	M2.0 V	18:10:23.37	+51:15:55.0	…	…	…	…	161.41	162.19	205.63 ± 1.05	0.365 ± 0.015
…	…	StKM 1-1582	J18109+220	M0.0 V	18:10:56.18	+22:01:31.2	…	…	…	…	153.88	41.29	1491.76 ± 7.71	0.754 ± 0.025
…	…	LP 569-163	J18116+061	M3.0 V	18:11:36.49	+06:06:27.9	(AB)	A	…	…	153.97	118.07	…	…
18116+0606	CFN 14	LP 569-163 B	…	…	18:11:36.51	+06:06:27.3	…	B	0.629	144.2	114.92	…	…	…
…	…	V1334Her	J18131+260	M4.0 V	18:13:06.83	+26:01:51.3	…	…	…	…	37.84	224.18	117.10 ± 0.61	0.332 ± 0.017
…	…	LP 569-15	J18134+054	M1.5 V	18:13:28.12	+05:26:54.8	A+B	A	…	…	27.27	238.09	632.76 ± 3.58	0.586 ± 0.028
18136+0527	LDS1007	LP 569-16	J18135+055	M4.0 V	18:13:33.09	+05:32:08.4	…	B	322.188	13.3	…	238.14	167.43 ± 0.89	0.394 ± 0.016
…	…	HD 348274	J18157+189	M0.0 V	18:15:43.54	+18:56:12.7	…	…	…	…	43.23	429.87	690.14 ± 7.95	0.605 ± 0.027
…	…	GJ 708.2	J18160+139	M0.0 V	18:16:02.36	+13:54:40.2	…	…	…	…	29.78	510.75	662.36 ± 3.16	0.613 ± 0.027
…	…	GJ 708.3	J18163+015	M3.0 V	18:16:17.74	+01:31:17.1	…	…	…	…	55.75	757.81	117.98 ± 0.81	0.306 ± 0.014
…	…	G 140-51	J18165+048	M5.0 V	18:16:31.37	+04:52:52.3	…	…	…	…	55.77	435.77	36.49 ± 0.18	0.178 ± 0.009
…	…	GJ 709	J18165+455	M0.5 V	18:16:31.07	+45:33:33.7	…	…	…	…	55.72	337.61	620.48 ± 2.60	0.592 ± 0.028
…	…	V401Dra	J18174+483	dM2.0	18:17:25.05	+48:22:03.1	…	…	…	…	96.23	66.55	447.04 ± 2.36	0.510 ± 0.029
…	…	GJ 4048	J18180+387E	M3.0 V	18:18:03.73	+38:46:16.2	AB	A	…	…	56.20	1089.90	114.55 ± 0.41	0.284 ± 0.010
18180+3846	GIC 151	GJ 4049	J18180+387W	M4.0 V	18:18:02.88	+38:46:17.4	…	B	9.971	277.4	…	1116.56	…	0.204 ± 0.038
…	…	GJ 4053	J18189+661	M4.5 Ve	18:18:58.38	+66:11:26.2	…	…	…	…	37.16	620.58	24.68 ± 0.14	0.150 ± 0.010

Table D.2: Complete sample with the description of multiple systems (continued).

WDS id	WDS disc	Name	Karmn	Spectral type	α (2016.0)	δ (2016.0)	System	Component	ρ [arcsec]	θ [deg]	ϖ [mas]	$\mu_{\rm total}$ [mas a^{-1}]	$\mathcal{L}$ [$10^{-4}\,\mathcal{L}_\odot$]	$\mathcal{M}$ [$\mathcal{M}_\odot$]
…	…	GJ 4051	J18193-057	M2.0 V	18:19:21.68	-05:46:33.5	…	…	…	…	50.77	544.91	252.78 ± 1.19	0.432 ± 0.017
…	…	PM J18195+4201	J18195+420	M1.5 V	18:19:34.48	+42:01:37.4	…	…	…	…	50.95	59.88	554.43 ± 2.06	0.557 ± 0.028
…	…	GJ 1226 A	J18209-010	M3.5 V	18:20:56.62	-01:03:14.2	AB	A	…	…	44.84	1094.63	…	0.285 ± 0.035
18210-0101	WOR 35	GJ 1226 B	…	M4.0 V	18:20:56.63	-01:03:12.8	…	B	1.435	6.1	33.31	1107.99	…	0.270 ± 0.036
…	…	Ross 136	J18221+063	M4.0 V	18:22:05.40	+06:20:39.4	…	…	…	…	51.06	1195.56	109.60 ± 0.63	0.295 ± 0.011
…	…	GJ 1227	J18224+620	M4.0 V	18:22:24.92	+62:02:42.0	…	…	…	…	50.55	1561.71	32.78 ± 0.17	0.161 ± 0.010
…	…	G 205-19	J18227+379	M1.0 V	18:22:43.47	+37:57:41.1	…	…	…	…	100.93	401.06	793.86 ± 13.72	0.619 ± 0.027
…	…	Ross 708A	J18234+281	M3.5 V	18:23:28.24	+28:10:01.0	AB	A	…	…	54.27	199.56	…	0.320 ± 0.034
18235+2810	JOD 15	Ross 708B	…	M5.5 V	18:23:28.25	+28:09:59.7	…	B	1.264	175.3	54.57	216.99	…	0.158 ± 0.041
…	…	GJ 4056	J18240+016	M2.5 V	18:24:05.35	+01:41:12.3	…	…	…	…	60.73	281.95	221.36 ± 1.04	0.403 ± 0.016
18249+2817	RAO 391	Ross 710	J18248+282	M1.5 V	18:24:52.32	+28:17:22.3	(AB)	AB	0.143	313.3	95.57	189.54	…	0.573 ± 0.028
…	…	HD 336196	J18250+246	M0.0 V	18:25:04.75	+24:37:57.3	…	…	…	…	95.56	450.44	660.88 ± 4.68	0.603 ± 0.027
…	…	GJ 4058	J18255+383	M0.0 V	18:25:31.82	+38:21:00.8	…	…	…	…	28.75	749.11	450.70 ± 1.48	0.543 ± 0.029
…	…	GJ 4059	J18264+113	M3.5 V	18:26:24.58	+11:20:52.9	A+B	A	…	…	28.84	276.07	…	0.423 ± 0.031
18264+1121	NI 38	LSPM J1826+1120S	…	DA	18:26:24.42	+11:20:45.1	…	B	8.196	196.8	70.97	281.07	…	0.500 ± 0.100
…	…	TYC 4222-2195-1	J18292+638	M1.5 V	18:29:13.36	+63:51:10.9	…	…	…	…	26.18	217.06	467.23 ± 14.51	0.536 ± 0.029
…	…	2M18294012+3350130	J18296+338	M3.0 V	18:29:40.02	+33:50:13.3	…	…	…	…	82.00	75.41	254.45 ± 0.99	0.491 ± 0.019
…	…	LP 570-92	J18312+068	M1.0 V	18:31:16.21	+06:50:08.2	…	…	…	…	54.33	182.49	430.36 ± 2.13	0.509 ± 0.019
…	…	GJ 4062	J18319+406	M3.5 V	18:31:58.24	+40:41:17.6	…	…	…	…	131.60	423.15	160.86 ± 0.61	0.342 ± 0.011
…	…	GJ 4063	J18346+401	M4.0 V	18:34:36.73	+40:07:23.1	…	…	…	…	42.77	214.33	218.01 ± 0.93	0.413 ± 0.016
…	…	G 184-13A	J18352+243	M2.5 V	18:35:13.42	+24:18:39.2	AB	A	…	…	42.77	294.62	…	0.415 ± 0.031
18352+2419	KPP3331	G 184-13B	…	M3.5 V	18:35:13.44	+24:18:41.7	…	B	2.466	4.5	167.29	302.61	…	0.331 ± 0.034
…	…	GJ 4064	J18352+414	M2.0 V	18:35:18.38	+41:29:14.5	…	…	…	…	…	376.89	219.65 ± 0.91	0.378 ± 0.015
…	…	GJ 720 A	J18353+457	M0.5 V	18:35:19.08	+45:44:44.4	A+B	A	…	…	83.07	580.29	700.35 ± 2.75	0.617 ± 0.027
18355+4546	LDS6329	GJ 720 B	J18354+457	M2.5 V	18:35:27.99	+45:45:46.7	…	B	112.139	56.2	98.19	582.11	93.70 ± 0.52	0.288 ± 0.013
…	…	LSPM J1835+3259	J18356+329	M8.5 V	18:35:37.79	+32:59:41.2	…	…	…	…	…	758.63	2.93 ± 0.01	0.114 ± 0.054
…	…	GJ 4068	J18358+800	M4.0 Ve	18:35:52.58	+80:05:42.9	…	…	…	…	33.70	244.24	97.33 ± 0.37	0.315 ± 0.014
…	…	G 227-39	J18362+567	M0.0 V	18:36:12.72	+56:44:37.8	…	…	…	…	68.30	403.55	1038.72 ± 5.01	0.698 ± 0.026
…	…	Ross 149	J18363+136	M4.0 V	18:36:19.43	+13:36:30.8	…	…	…	…	48.48	331.47	104.77 ± 0.49	0.300 ± 0.011
18388+0446	RAO 395	LP 570-22	J18387+047	M0.5 V	18:38:47.63	+04:46:01.7	(AB)	AB	0.427	153.3	73.06	187.09	…	0.523 ± 0.031
…	…	RX J1839.4+6903	J18394+690	M2.0 Ve	18:39:25.71	+69:03:06.8	…	…	…	…	73.38	200.86	684.85 ± 4.04	0.581 ± 0.028
…	…	LP 335-12	J18395+298	M6.5 Ve	18:39:33.18	+29:52:12.9	…	…	…	…	55.02	238.81	6.98 ± 0.04	0.113 ± 0.010
…	…	LP 335-13	J18395+301	M0.0 V	18:39:32.00	+30:09:52.1	…	…	…	…	66.13	192.79	667.98 ± 2.19	0.619 ± 0.027
…	…	GJ 4067	J18399+334	M3.5 V	18:39:59.94	+33:24:58.9	…	…	…	…	80.84	289.65	157.05 ± 0.66	0.381 ± 0.016
…	…	LP 44-334	J18400+726	M6.5 V	18:40:02.20	+72:40:57.2	AB	A	…	…	36.77	187.35	…	0.107 ± 0.047
18400+7241	CFN 15	LP 44-334 B	…	…	18:40:02.32	+72:40:56.6	…	B	0.832	140.8	36.93	…	…	…
18387-1429	HDS2641	GJ 2138	J18387-144	M2.5 V	18:38:44.87	-14:29:35.1	(AB)	AB	0.107	358.0	47.05	579.86	…	0.418 ± 0.031
…	…	Wolf 1466	J18402-104	M1.0 V	18:40:17.68	-10:28:04.1	…	…	…	…	45.03	574.97	247.66 ± 0.97	0.403 ± 0.016
…	…	G 227-43	J18405+595	M2.0 V	18:40:35.77	+59:30:53.6	…	…	…	…	92.99	309.24	375.34 ± 1.68	0.492 ± 0.030
…	…	BD+31 3330	…	K2.5 V	18:40:54.99	+31:31:45.7	A+BC	A	…	…	92.96	841.17	2351.22 ± 7.15	0.820 ± 0.123

Table D.2: Complete sample with the description of multiple systems (continued).

WDS id	WDS disc	Name	Karmn	Spectral type	α (2016.0)	δ (2016.0)	System	Component	ρ [arcsec]	θ [deg]	ϖ [mas]	$\mu_{\rm total}$ [mas a^{-1}]	$\mathcal{L}$ [$10^{-4}\,\mathcal{L}_\odot$]	$\mathcal{M}$ [$\mathcal{M}_\odot$]
18409+3132	HJ1337	BD+31 3330B	J18409+315	M1.0 V	18:40:55.33	+31:31:37.3	…	B	9.446	152.2	81.74	…	…	…
…	…	BD+31 3330C	…	…	18:40:55.31	+31:31:37.5	…	C	9.210	153.1	55.69	…	…	…
…	…	Ross 720	J18409-133	dM1.0	18:40:57.20	-13:22:57.3	…	…	…	…	62.91	677.86	506.17 ± 3.41	0.547 ± 0.028
…	…	GJ 1230 A	J18411+247S	M4.5 V	18:41:10.35	+24:47:15.8	Aab+B	Aab(2)	…	…	…	512.79	…	0.463 ± 0.001
18411+2447	LDS6330	GJ 1230 B	J18411+247N	M4.5 Ve	18:41:10.39	+24:47:20.5	…	B	4.725	5.6	40.89	501.94	…	0.145 ± 0.042
…	…	GJ 4069	J18416+397	M4.0 V	18:41:37.04	+39:42:09.3	…	…	…	…	48.52	315.35	44.23 ± 0.20	0.204 ± 0.011
…	…	Ross 145	J18419+318	M3.0 V	18:41:58.66	+31:49:49.9	…	…	…	…	54.10	300.44	165.64 ± 0.63	0.341 ± 0.011
…	…	V816Her	J18427+139	M5.0 V	18:42:44.94	+13:54:22.4	…	…	…	…	49.25	355.60	74.44 ± 0.38	0.272 ± 0.013
18428+5938	STF2398	HD 173739	J18427+596N	M3.0 V	18:42:43.94	+59:38:18.1	AB	A	11.400	180.8	98.84	2221.02	152.45 ± 2.35	0.336 ± 0.012
…	…	HD 173740	J18427+596S	M3.5 V	18:42:43.94	+59:38:06.5	…	B	11.565	179.9	77.74	2330.18	90.22 ± 0.31	0.266 ± 0.012
…	…	TYC 2112-920-1	J18432+253	M1.0 V	18:43:14.51	+25:22:43.1	…	…	…	…	40.44	215.40	528.52 ± 2.47	0.562 ± 0.028
…	…	V492Lyr	J18433+406	M7.5 Ve	18:43:21.96	+40:40:30.8	(AB)	AB	…	…	36.26	603.49	…	0.101 ± 0.048
…	…	1R184510.6+062016	J18451+063	M1.0 Ve	18:45:10.23	+06:20:14.7	…	…	…	…	43.87	86.44	493.76 ± 2.21	0.545 ± 0.028
…	…	G 184-24	J18453+188	M4.0 V	18:45:22.79	+18:51:54.3	…	…	…	…	60.91	297.39	55.06 ± 0.34	0.231 ± 0.012
…	…	GJ 4077	J18480-145	dM2.5	18:48:01.01	-14:34:55.0	…	…	…	…	35.56	334.96	188.75 ± 0.87	0.361 ± 0.012
…	…	G 141-36	J18482+076	M5.0 V	18:48:17.94	+07:41:25.2	…	…	…	…	37.64	450.85	21.83 ± 0.11	0.139 ± 0.009
…	…	LSPM J1848+6135	J18487+615	M2.0 V	18:48:47.07	+61:35:06.3	…	…	…	…	69.28	174.31	223.68 ± 0.94	0.405 ± 0.016
…	…	V1216Sgr	J18498-238	M3.5 Ve	18:49:50.11	-23:50:13.6	…	…	…	…	69.89	668.14	40.79 ± 0.27	0.177 ± 0.009
…	…	G 184-31	J18499+186	M4.5 V	18:49:54.34	+18:40:24.2	…	…	…	…	219.79	299.35	34.36 ± 0.16	0.190 ± 0.011
…	…	Ross 142	J18500+030	M0.5 V	18:50:00.63	+03:05:10.7	…	…	…	…	48.70	448.36	614.37 ± 3.10	0.590 ± 0.028
…	…	GJ 4083	J18507+479	M3.5 V	18:50:45.66	+47:58:17.3	…	…	…	…	122.55	281.90	187.07 ± 0.74	0.392 ± 0.016
…	…	BD+02 3698	J18515+027	M0.5 V	18:51:35.59	+02:46:19.2	…	…	…	…	31.44	326.23	933.18 ± 6.23	0.669 ± 0.026
…	…	GJ 4084	J18516+244	M3.0 V	18:51:40.44	+24:27:31.7	…	…	…	…	30.95	357.42	128.17 ± 0.76	0.320 ± 0.014
…	…	HD 229793	J18518+165	M0.0 V	18:51:50.93	+16:34:52.1	…	…	…	…	49.47	532.16	536.53 ± 2.37	0.568 ± 0.028
…	…	1R185200.0+130005	J18519+130	M2.0 Ve	18:51:59.66	+13:00:01.1	…	…	…	…	35.98	157.31	622.29 ± 10.42	0.566 ± 0.028
…	…	G 141-46	J18534+028	M2.5 V	18:53:25.68	+02:50:49.4	…	…	…	…	35.95	299.46	168.64 ± 2.71	0.349 ± 0.015
…	…	BD+00 4050	J18548+008	M0.0 V	18:54:53.14	+00:51:44.8	…	…	…	…	26.55	145.01	822.44 ± 3.73	0.649 ± 0.027
…	…	HD 230017A	…	M0.0 V	18:54:53.67	+10:58:42.4	A+B+C	A	…	…	46.82	133.27	1266.03 ± 10.71	0.730 ± 0.025
18550+1058	VYS 8	HD 230017B	J18548+109	M3.5 V	18:54:53.86	+10:58:45.1	…	B	3.792	45.1	12.31	89.29	…	0.364 ± 0.033
…	…	PM J18542+1058	…	M4.0 V	18:54:17.14	+10:58:11.0	…	C*	538.890	266.7	49.23	114.61	89.09 ± 0.57	0.300 ± 0.014
…	…	GJ 735	J18554+084	M3.0 V	18:55:27.51	+08:24:07.9	Aab	Aab(2)	…	…	…	114.60	…	…
…	…	MCC 806A	…	…	18:56:16.00	+54:31:42.3	AB+C	A	…	…	47.83	…	…	…
18563+5432	HDS2682	MCC 806B	…	…	18:56:15.98	+54:31:42.4	…	B	0.232	296.8	45.26	…	…	…
18563+5432	GIC154	GJ 4091 B	J18563+544	M2.0 V	18:56:18.29	+54:29:45.5	…	C(2)	118.495	170.3	64.73	349.10	…	…
…	…	GJ 4089	J18564+463	M4.1 V	18:56:26.40	+46:22:58.5	…	…	…	…	45.14	309.79	75.77 ± 0.30	0.275 ± 0.013
…	…	GJ 4088	J18571+075	M2.0 V	18:57:10.40	+07:34:14.7	…	…	…	…	34.13	191.40	485.85 ± 2.64	0.548 ± 0.028
…	…	G 229-20A	J18576+535	M3.5 V	18:57:38.42	+53:31:14.4	AB+C	A	…	…	104.91	261.44	…	0.368 ± 0.033
18576+5331	LDS4802	LP 141-13	…	M3.0 V	18:57:38.34	+53:31:12.2	…	B	2.290	197.0	66.60	245.56	…	0.359 ± 0.033
18576+5331	LDS4802	LP 141-14	…	DC	18:57:39.78	+53:30:32.5	…	C	43.653	163.9	46.53	246.40	…	0.500 ± 0.100
…	…	HD 176029	J18580+059	M1.0 V	18:57:59.93	+05:54:09.7	…	…	…	…	119.92	1236.30	666.70 ± 2.97	0.604 ± 0.027

Table D.2: Complete sample with the description of multiple systems (continued).

WDS id	WDS disc	Name	Karmn	Spectral type	α (2016.0)	δ (2016.0)	System	Component	ρ [arcsec]	θ [deg]	ϖ [mas]	$\mu_{\rm total}$ [mas a^{-1}]	$\mathcal{L}$ [$10^{-4}\,\mathcal{L}_\odot$]	$\mathcal{M}$ [$\mathcal{M}_\odot$]
…	…	GJ 4092	J18596+079	M0.5 V	18:59:39.00	+07:59:11.2	…	…	…	…	119.89	408.58	884.16 ± 6.31	0.660 ± 0.026
…	…	GJ 4093	J19025+704	M2.5 V	19:02:30.83	+70:25:53.6	…	…	…	…	120.40	215.31	225.54 ± 1.33	0.433 ± 0.017
…	…	LSPM J1902+7525	J19025+754	M1.5 V	19:02:32.79	+75:25:06.6	…	…	…	…	31.33	204.59	345.93 ± 1.24	0.454 ± 0.017
…	…	G 141-57	J19032+034	M3.0 V	19:03:13.40	+03:24:01.4	…	…	…	…	36.01	205.36	241.87 ± 1.17	0.449 ± 0.018
19033+6400	JOD 16	GJ 4094	J19032+639	M3.5 V	19:03:17.46	+63:59:35.9	(AB)+C	AB	0.236	141.0	46.83	63.09	…	…
19033+6400	JOD 16	StKM 1-1676B	…	M2.0 V	19:03:17.96	+63:59:37.4	…	C	3.578	65.1	31.63	144.33	…	0.455 ± 0.030
…	…	GJ 741	J19032-135	M4.0 V	19:03:16.10	-13:34:12.9	…	…	…	…	33.64	695.97	33.87 ± 0.15	0.189 ± 0.011
…	…	1R190405.9+211030	J19041+211	M2.0 Ve	19:04:06.24	+21:10:32.7	(AB)	A	…	…	76.54	131.32	…	0.544 ± 0.029
…	…	PM J19041+2110 B	…	…	19:04:06.24	+21:10:33.2	…	B*	0.526	353.4	48.23	…	…	…
…	…	LSPM J1907+5905	J19044+590	M3.0 V	19:07:24.98	+59:05:11.9	AB	A	…	…	47.49	175.37	…	0.434 ± 0.031
19074+5905	KPP3335	LSPM J1907+5905B	…	M6.0 V	19:07:24.72	+59:05:14.7	…	B	3.394	323.7	62.16	166.16	…	0.132 ± 0.043
…	…	TYC 2122-1204-1	J19045+240	M2.0 V	19:04:31.24	+24:01:54.8	…	…	…	…	48.35	147.85	365.16 ± 1.70	0.484 ± 0.030
…	…	HD 349726	J19072+208	M2.0 V	19:07:12.66	+20:52:31.9	A+B	A	…	…	47.15	584.53	145.15 ± 0.83	0.311 ± 0.010
19072+2053	LDS1017	Ross 730	J19070+208	M2.0 V	19:07:05.02	+20:53:11.4	…	B	114.053	290.2	47.03	592.12	141.07 ± 0.94	0.309 ± 0.010
…	…	GJ 1231	J19082+265	M5.0 V	19:08:15.55	+26:34:57.6	…	…	…	…	52.25	537.21	34.33 ± 0.18	0.190 ± 0.011
…	…	GJ 4098	J19084+322	M3.0 V	19:08:29.67	+32:16:48.0	…	…	…	…	546.98	300.16	153.99 ± 0.62	0.332 ± 0.011
19074+3230	KUI 90	GJ 747	J19077+325	M3.0 V	19:07:44.54	+32:32:59.3	(AB)	AB	0.135	248.4	71.50	1678.52	…	0.288 ± 0.035
19093+3912	JOD 17	GJ 4099	J19093+382	M2.0 V	19:09:19.01	+39:12:00.7	(AB)+C	AB	0.299	162.5	73.75	210.22	…	0.605 ± 0.027
19093+3912	FMR 144	LSPM J1909+3910	J19095+391	M2.0 V	19:09:31.54	+39:10:48.4	…	C	162.605	116.4	31.23	213.14	334.29 ± 1.43	0.501 ± 0.019
…	…	Ross 727	J19093-147	M2.5 V	19:09:20.08	-14:45:02.4	…	…	…	…	27.05	501.02	282.20 ± 1.78	0.458 ± 0.018
…	…	GJ 1232	J19098+176	M4.0 V	19:09:50.16	+17:39:59.6	…	…	…	…	33.26	768.23	44.00 ± 0.22	0.193 ± 0.010
…	…	GJ 4100	J19106+015	M1.5 V	19:10:38.38	+01:32:07.3	A+B	A	…	…	128.31	255.58	513.69 ± 2.64	0.546 ± 0.028
19106+0132	GWP 2820	GJ 4100 B	…	M4.5 Ve	19:10:37.90	+01:32:18.7	…	B	13.516	327.8	81.74	255.11	…	0.135 ± 0.043
…	…	TYC 471-1564-1	J19116+050	M1.0 V	19:11:47.89	+05:00:37.4	…	…	…	…	37.63	126.80	548.80 ± 2.56	0.572 ± 0.028
…	…	GJ 4105	J19124+355	M2.0 V	19:12:29.70	+35:33:50.2	…	…	…	…	35.97	265.65	209.22 ± 0.96	0.391 ± 0.016
19121+0254	AST1	Wolf 1062	J19122+028	M3.5 V	19:12:16.50	+02:53:02.6	(AB)	AB	0.192	333.0	46.25	1846.10	…	0.371 ± 0.033
…	…	Ross 733	J19146+193N	M4.5 V	19:14:38.46	+19:19:10.7	A+B	A	…	…	129.22	752.72	424.44 ± 2.28	0.482 ± 0.030
19147+1918	LDS1020	Ross 734	J19146+193S	M4.0 V	19:14:38.51	+19:18:29.9	…	B	40.772	179.1	30.64	755.49	104.67 ± 0.42	0.327 ± 0.015
…	…	V1428Aql	J19169+051N	M2.5 V	19:16:54.64	+05:09:46.7	A+B	A	…	…	30.89	1453.23	329.58 ± 2.93	0.475 ± 0.013
19169+0510	LDS6334	V1298Aql	J19169+051S	M8.0 V	19:16:56.97	+05:08:39.7	…	B	75.500	152.5	125.45	1491.52	4.29 ± 0.03	0.103 ± 0.052
…	…	LSPM J1918+5803	J19185+580	M1.0 V	19:18:30.48	+58:03:16.6	AB	A	…	…	45.88	178.63	…	0.583 ± 0.028
…	…	G3- 2143230844400445696	…	M8.0 V	19:18:30.33	+58:03:18.1	…	B*	1.925	323.8	43.49	190.05	…	0.100 ± 0.050
…	…	GJ 754.1 B	J19205-076	M2.5 V	19:20:33.38	-07:39:46.6	A+B	A	…	…	22.07	191.46	…	0.286 ± 0.035
19206-0740	LDS 678	GJ 754.1 A	…	DBQA5	19:20:34.86	-07:40:02.7	…	B	27.168	126.2	…	173.04	…	0.500 ± 0.100
…	…	2M19204172+7311434	J19206+731S	M4.0 V	19:20:41.75	+73:11:42.4	A+B	A	…	…	…	74.49	72.37 ± 0.71	0.228 ± 0.014
…	…	2M19204172+7311467	J19206+731N	M4.5 V	19:20:41.76	+73:11:45.5	…	B*	3.182	0.0	56.04	82.50	…	0.240 ± 0.037
…	…	GJ 1235	J19216+208	M4.0 Ve	19:21:37.62	+20:51:40.0	…	…	…	…	34.09	1738.79	44.99 ± 0.25	0.195 ± 0.010
…	…	V2078Cyg	J19218+286	M1.5 V	19:21:52.48	+28:40:02.3	…	…	…	…	34.04	901.75	403.94 ± 1.51	0.514 ± 0.029
…	…	GJ 1236	J19220+070	M4.0 V	19:22:01.28	+07:02:23.2	…	…	…	…	43.12	863.35	64.33 ± 0.27	0.235 ± 0.012
…	…	GSC 02654-01527	J19228+307	M0.0 V	19:22:48.64	+30:45:13.5	…	…	…	…	54.73	115.48	1107.82 ± 12.63	0.704 ± 0.026

Table D.2: Complete sample with the description of multiple systems (continued).

WDS id	WDS disc	Name	Karmn	Spectral type	α (2016.0)	δ (2016.0)	System	Component	ρ [arcsec]	θ [deg]	ϖ [mas]	$\mu_{\rm total}$ [mas a^{-1}]	$\mathcal{L}$ [$10^{-4}\,\mathcal{L}_\odot$]	$\mathcal{M}$ [$\mathcal{M}_\odot$]
…	…	NLTT 47788	J19234+666	M1.0 V	19:23:24.51	+66:39:54.2	…	…	…	…	62.91	209.84	506.72 ± 2.18	0.549 ± 0.028
19215+4231	JNN 122	1R192132.1+423041	J19215+425	M2.0 Ve	19:21:32.18	+42:30:54.8	(AB)	AB	0.126	154.4	68.25	151.93	…	0.541 ± 0.029
…	…	TYC 4592-101-1	J19242+797	M1.0 V	19:24:15.66	+79:43:37.3	A+B	A	…	…	57.34	88.20	741.53 ± 3.46	0.620 ± 0.027
19239+7944	LDS1906	PM J19237+7944	J19237+797	M1.5 V	19:23:46.46	+79:44:37.6	…	B	98.614	307.7	50.40	87.77	624.07 ± 2.96	0.588 ± 0.028
…	…	GJ 1238	J19242+755	M6.0 V	19:24:17.89	+75:33:21.3	…	…	…	…	88.01	698.05	16.06 ± 0.07	0.119 ± 0.008
…	…	Ross 164	J19251+283	M3.5 V	19:25:08.74	+28:21:19.8	…	…	…	…	87.98	431.01	166.62 ± 86.70	0.352 ± 0.099
…	…	LSPM J1925+0938	J19255+096	M8/9V	19:25:31.00	+09:38:19.4	…	…	…	…	130.85	255.76	11.63 ± 0.13	0.102 ± 0.048
…	…	G 185-23	J19260+244	M4.5 V	19:26:01.84	+24:26:18.7	…	…	…	…	35.57	206.57	65.28 ± 0.27	0.272 ± 0.013
…	…	GJ 4110	J19268+167	M3.5 Ve	19:26:49.42	+16:42:58.3	…	…	…	…	29.76	210.36	162.10 ± 0.99	0.387 ± 0.016
…	…	TYC 2137-1575-1	J19284+289	M0.0 V	19:28:25.51	+28:54:09.6	…	…	…	…	56.26	41.87	691.21 ± 2.53	0.624 ± 0.027
…	…	PM J19289+0638	J19289+066	M1.5 V	19:28:55.70	+06:38:24.5	…	…	…	…	56.22	101.34	448.06 ± 2.52	0.526 ± 0.029
…	…	G 125-15	J19312+361	M4.5 V	19:31:12.38	+36:07:28.2	Aab+B	Aab(2)	…	…	61.26	167.85	…	…
19312+3607	GIC 158	G 125-14	…	M4.5 V	19:31:11.56	+36:08:12.8	…	B	45.782	347.4	67.54	167.38	91.67 ± 0.42	0.305 ± 0.014
…	…	GJ 761.2	J19326+005	M0.0 V	19:32:38.15	+00:34:39.5	…	…	…	…	119.75	219.55	740.37 ± 3.82	0.636 ± 0.027
…	…	Ross 1063	J19336+395	M1.5 V	19:33:39.75	+39:31:29.9	…	…	…	…	28.21	477.69	259.33 ± 1.40	0.438 ± 0.017
…	…	HD 184489	J19346+045	M0.0 V	19:34:40.40	+04:35:02.0	…	…	…	…	67.55	609.74	763.97 ± 3.40	0.652 ± 0.027
…	…	Wolf 1108	J19349+532	M2.5 V	19:34:55.56	+53:15:31.3	…	…	…	…	67.35	567.87	132.32 ± 63.09	0.326 ± 0.085
19352+0825	BAG 27	GJ 4114	J19351+084S	M0.5 V	19:35:06.24	+08:27:37.9	(AB)+C	AB	0.311	26.6	57.60	84.67	…	0.644 ± 0.050
19352+0825	VYS9	GJ 4115	J19351+084N	M2.5 V	19:35:06.33	+08:27:43.4	…	C	5.635	14.5	28.10	65.00	257.20 ± 3.79	0.436 ± 0.017
…	…	Ross 1064	J19358+413	M0.0 V	19:35:51.00	+41:19:06.7	…	…	…	…	43.73	316.28	1284.29 ± 16.38	0.712 ± 0.026
…	…	GJ 4120	J19395+718	M0.5 V	19:39:32.22	+71:52:12.1	…	…	…	…	42.38	482.57	480.45 ± 3.07	0.510 ± 0.018
…	…	GJ 1242	J19419+031	M2.0 V	19:41:53.93	+03:09:08.3	…	…	…	…	37.06	549.63	145.37 ± 1.11	0.322 ± 0.014
…	…	RX J1935.4+3746	J19354+377	M3.5 V	19:35:29.02	+37:46:06.7	Aab	Aab(1)	…	…	55.40	162.48	…	…
…	…	2M19421282-2045477	J19422-207	M5.1 V	19:42:12.81	-20:45:50.4	…	…	…	…	37.06	154.60	48.52 ± 0.23	0.209 ± 0.012
…	…	LP 869-19	J19420-210	M3.5 V	19:42:00.74	-21:04:09.4	Aab	Aab(2)	…	…	21.14	262.23	…	…
…	…	Ross 165A	J19457+271	M4.0 V	19:45:45.41	+27:07:11.7	AB	A	…	…	32.93	1225.43	…	0.245 ± 0.037
19458+2710	KUI 95	Ross 165B	…	M4.0 V	19:45:45.55	+27:07:12.8	…	B	2.270	60.4	25.34	1220.47	…	0.206 ± 0.038
…	…	GJ 4122	J19457+323	M1.5 V	19:45:50.25	+32:23:16.8	…	…	…	…	59.74	441.14	277.71 ± 1.07	0.428 ± 0.016
…	…	HD 331161A	J19463+320	M0.5 V	19:46:24.51	+32:00:55.2	A+B	A	…	…	73.71	607.80	531.00 ± 2.21	0.552 ± 0.028
19464+3201	KAM 3	HD 331161B	J19464+320	M2.5 V	19:46:24.83	+32:00:51.1	…	B	5.707	135.1	91.80	638.05	…	0.443 ± 0.031
…	…	PM J19468-0157	J19468-019	M3.0 V	19:46:50.63	-01:57:40.1	…	…	…	…	39.68	119.23	325.04 ± 7.43	0.493 ± 0.020
…	…	LSPM J1947+3516	J19470+352	M2.0 V	19:47:03.30	+35:16:55.5	…	…	…	…	39.59	164.93	503.14 ± 2.32	0.534 ± 0.029
…	…	G 125-34	J19486+359	M3.5 V	19:48:40.88	+35:55:12.6	…	…	…	…	53.78	293.20	69.53 ± 0.30	0.262 ± 0.013
19500+3235	JOD 18	GJ 4124	J19500+325	M3.0 V	19:50:03.10	+32:35:05.5	(AB)	AB	0.222	345.1	64.24	242.56	…	…
19503+3147	RAO 418	GJ 4125	J19502+317	M2.1 V	19:50:16.11	+31:47:05.7	(AB)	AB	0.640	39.6	64.21	364.83	…	0.400 ± 0.032
…	…	HD 187691	…	F8 V	19:51:01.91	+10:24:54.4	A+B	A	…	…	175.79	277.69	27700.41 ± 534.64	1.180 ± 0.177
19510+1025	J 124	GJ 9671 B	J19510+104	M4.0 V	19:51:00.97	+10:24:38.0	…	B	21.477	220.2	61.00	288.38	147.95 ± 1.04	0.369 ± 0.016
…	…	GJ 1243	J19511+464	M4.0 Ve	19:51:09.60	+46:29:04.5	…	…	…	…	28.03	322.76	71.83 ± 0.28	0.271 ± 0.012
…	…	G 260-35	J19512+622	M2.0 V	19:51:11.69	+62:17:15.7	…	…	…	…	83.14	290.26	634.34 ± 2.32	0.577 ± 0.028
…	…	GJ 4127	J19535+341	M1.5 V	19:53:32.73	+34:08:32.2	…	…	…	…	40.23	228.28	538.09 ± 1.97	0.552 ± 0.028

Table D.2: Complete sample with the description of multiple systems (continued).

WDS id	WDS disc	Name	Karmn	Spectral type	α (2016.0)	δ (2016.0)	System	Component	ρ [arcsec]	θ [deg]	ϖ [mas]	$\mu_{\rm total}$ [mas a^{-1}]	$\mathcal{L}$ [$10^{-4}\,\mathcal{L}_\odot$]	$\mathcal{M}$ [$\mathcal{M}_\odot$]
19539+4425	MCY3	V1581Cyg	J19539+444W	M5.5 V	19:53:55.14	+44:24:44.4	(AB)+C	AB	0.410	183.3	29.53	619.31	…	0.135 ± 0.043
19539+4425	GIC159	GJ 1245 B	J19539+444E	M5.5 V	19:53:55.66	+44:24:46.5	…	C	5.945	69.6	82.36	593.94	12.99 ± 0.10	0.127 ± 0.010
…	…	GJ 4128	J19540+325	M2.5 V	19:54:02.88	+32:33:55.8	…	…	…	…	39.24	236.14	858.84 ± 5.52	0.613 ± 0.027
…	…	TYC 1624-397-1	J19546+202	M0.0 V	19:54:37.52	+20:13:05.5	…	…	…	…	45.42	73.50	780.28 ± 3.60	0.646 ± 0.027
…	…	Wolf 1122	J19558+512	M1.5 V	19:55:53.62	+51:16:27.7	…	…	…	…	52.78	585.88	358.27 ± 1.67	0.489 ± 0.018
…	…	GJ 9677 A	J19565+591	M0.0 V	19:56:33.06	+59:09:40.3	A+B	A	…	…	…	431.05	1393.72 ± 13.18	0.747 ± 0.025
19566+5910	GIC 161	GJ 9677 B	J19564+591	M3.5 V	19:56:23.96	+59:09:19.7	…	B	72.939	253.7	74.79	444.25	144.84 ± 0.53	0.342 ± 0.015
…	…	HD 188807	…	K7 V	19:57:19.54	-12:34:13.0	A+B	A	…	…	56.26	523.41	1086.17 ± 4.34	0.640 ± 0.096
19573-1234	LDS4824	GJ 773 B	J19573-125	M5.0 V	19:57:23.71	-12:33:58.5	…	B	62.695	76.6	35.81	525.78	34.56 ± 0.19	0.206 ± 0.011
…	…	GJ 4129	J19582+020	M2.5 V	19:58:15.38	+02:02:02.5	…	…	…	…	41.75	887.32	164.81 ± 0.70	0.366 ± 0.015
…	…	G 260-38	J19582+650	M3.5 V	19:58:16.31	+65:02:25.0	…	…	…	…	…	394.41	157.85 ± 0.69	0.382 ± 0.016
…	…	LP 634-16	J20011+002	M2.0 V	20:01:06.21	+00:16:12.0	…	…	…	…	…	224.69	358.05 ± 2.11	0.485 ± 0.030
…	…	1R200031.8+592127	J20005+593	M4.1 V	20:00:31.98	+59:21:29.9	AB	A	…	…	58.84	132.56	…	0.309 ± 0.034
20006+5922	JNN124	G3-2237179062111268096	…	…	20:00:32.02	+59:21:29.7	…	B	0.374	121.4	100.69	…	…	…
…	…	HD 190360	…	G7 IV-V	20:03:38.25	+29:53:40.1	A+B	A	…	…	100.56	861.92	11241.75 ± 182.61	…
20036+2954	LDS6339	GJ 777 B	J20034+298	M4.5 V	20:03:27.42	+29:51:51.1	…	B	178.054	232.3	80.10	860.49	49.73 ± 0.20	0.234 ± 0.012
…	…	1R200348.4+642542	J20037+644	M0.0 V	20:03:47.80	+64:25:45.3	…	…	…	…	92.61	98.74	1190.73 ± 12.94	0.722 ± 0.025
…	…	GJ 1248	J20038+059	M2.5 V	20:03:50.47	+05:59:31.4	…	…	…	…	91.46	940.69	96.37 ± 0.46	0.258 ± 0.012
…	…	GJ 4132	J20039-081	M4.0 V	20:03:58.37	-08:07:51.4	…	…	…	…	283.84	558.85	109.86 ± 0.84	0.336 ± 0.015
…	…	V1513Cyg	J20050+544	sdM1	20:05:00.07	+54:25:48.8	(AabB)	Aab(1)	…	…	64.93	1470.28	…	…
20050+5426	MGN1	Wolf 1130 B	…	T8p	…	…	…	B	188.540	115.0	283.84	…	…	…
…	…	Wolf 1131	J20057+529	M4.0 V	20:05:44.59	+52:58:21.1	…	…	…	…	31.24	277.53	145.54 ± 0.76	0.365 ± 0.015
…	…	GJ 4136	J20079-015	M3.0 V	20:07:57.91	-01:32:31.5	…	…	…	…	69.63	405.55	95.66 ± 0.43	0.292 ± 0.013
…	…	GJ 1250	J20082+333	M4.77	20:08:18.35	+33:18:19.0	…	…	…	…	52.99	506.19	55.31 ± 13.13	0.216 ± 0.031
…	…	PM J20093-0113	J20093-012	M5.0 V	20:09:18.20	-01:13:44.3	…	…	…	…	71.05	376.60	27.03 ± 0.14	0.144 ± 0.012
…	…	LP 574-21	J20105+065	M4.0 V	20:10:34.49	+06:32:10.7	Aab+B	Aab(2)	…	…	20.81	208.13	…	…
20106+0632	LUH 15	2M20103539+0634367	…	M8.5 V	20:10:35.44	+06:34:33.5	…	B	143.531	5.6	58.60	213.72	3.00 ± 0.03	0.114 ± 0.054
…	…	HD 191785	…	K0 V	20:11:05.61	+16:11:23.2	A+B	A	…	…	131.28	575.39	4626.61 ± 18.13	0.880 ± 0.132
20111+1611	GIC 163	GJ 783.2 B	J20112+161	M4.0 V	20:11:12.80	+16:11:14.4	…	B	103.843	94.8	41.89	577.77	78.99 ± 0.32	0.281 ± 0.013
…	…	LSPM J2011+3757	J20112+379	M1.5 V	20:11:12.85	+37:57:48.1	…	…	…	…	336.03	187.54	672.18 ± 3.43	0.591 ± 0.028
…	…	LP 283-5	J20129+342	M1.0 V	20:12:54.72	+34:16:54.5	A+B	A	…	…	83.79	405.26	930.29 ± 3.50	0.683 ± 0.026
20130+3416	LDS1035	LP 283-4	…	M1.0 V	20:12:54.41	+34:16:37.6	…	B	17.283	192.8	47.08	412.00	793.89 ± 3.97	0.633 ± 0.027
…	…	StKM 1-1767a	…	K5 V	20:13:11.14	+02:56:20.5	A+B	A	…	…	50.91	108.28	1551.77 ± 7.12	0.700 ± 0.105
20132+0256	CRI 26	[R78b] 440	J20132+029	M1.0 V	20:13:12.94	+02:56:02.3	…	B	32.497	123.9	27.68	110.73	707.14 ± 4.16	0.613 ± 0.027
…	…	Ross 754	J20138+133	M1.0 V	20:13:52.27	+13:23:20.0	…	…	…	…	55.15	422.35	750.02 ± 3.23	0.623 ± 0.027
…	…	GJ 784.2 A	J20139+066	M3.3 V	20:13:58.71	+06:41:06.8	A+B	A	…	…	65.76	634.75	172.59 ± 1.07	0.400 ± 0.017
20139+0641	GIC 164	V1412Aql	…	DC7	20:13:55.41	+06:42:35.5	…	B	101.455	330.9	33.49	635.70	…	0.500 ± 0.100
…	…	LP 106-240	J20151+635	M0.0 V	20:15:10.64	+63:31:16.4	…	…	…	…	50.24	377.93	949.14 ± 377.17	0.683 ± 0.026
…	…	G 210-11	J20165+351	M2.0 V	20:16:32.04	+35:10:37.6	…	…	…	…	40.12	333.21	281.11 ± 1.13	0.457 ± 0.018
…	…	GJ 4143	J20187+158	M2.5 V	20:18:44.75	+15:50:45.3	…	…	…	…	53.42	184.10	247.21 ± 0.94	0.427 ± 0.017

Table D.2: Complete sample with the description of multiple systems (continued).

WDS id	WDS disc	Name	Karmn	Spectral type	α (2016.0)	δ (2016.0)	System	Component	ρ [arcsec]	θ [deg]	ϖ [mas]	$\mu_{\rm total}$ [mas a^{-1}]	$\mathcal{L}$ [$10^{-4}\,\mathcal{L}_\odot$]	$\mathcal{M}$ [$\mathcal{M}_\odot$]
…	…	GJ 4144	J20195+080	M3.0 V	20:19:34.60	+08:00:27.1	AB	A	…	…	53.64	210.99	…	0.427 ± 0.031
…	…	G3- 4250232535851803136	…	M3.0 V	20:19:34.55	+08:00:26.9	…	B*	0.777	258.3	53.84	200.82	…	0.387 ± 0.032
…	…	LP 395-8 A	J20198+229	M3.0 V	20:19:49.36	+22:56:38.1	AabB+C	Aab(2)	…	…	22.22	135.40	…	0.124 ± 0.001
20198+2257	KPP4191	LP 395-8 B	…	M3.5 V	20:19:49.35	+22:56:40.0	…	B	1.918	355.5	89.91	137.73	…	0.318 ± 0.034
…	…	G3- 1829571684884360832	…	…	20:19:48.73	+22:56:44.8	…	C*	11.019	307.4	…	142.76	…	0.1504 ± 0.059
…	…	TYC 1643-120-1	J20220+216	M2.0 V	20:22:01.62	+21:47:19.7	A+B	A	…	…	…	131.82	355.01 ± 2.22	0.477 ± 0.030
…	…	PM J20220+2147B	…	M4/5 V	20:22:01.98	+21:47:21.8	…	B*	5.445	67.5	23.49	133.78	…	0.158 ± 0.041
…	…	PM J20223+3217	J20223+322	M3.5 V	20:22:18.82	+32:17:15.1	…	…	…	…	51.18	148.03	160.50 ± 0.89	0.385 ± 0.016
…	…	G 143-48	J20229+106	M3.0 V	20:22:55.79	+10:40:44.5	…	…	…	…	39.00	548.17	151.33 ± 0.77	0.373 ± 0.016
…	…	LP 73-196	J20232+671	M5.0 V	20:23:18.57	+67:10:12.9	AB	A	…	…	40.35	278.28	…	0.178 ± 0.040
20233+6710	LAW 19	LP 73-196 B	…	M5.5 V	20:23:18.43	+67:10:12.1	…	B	1.145	225.6	40.36	291.47	…	0.156 ± 0.041
…	…	Wolf 1069	J20260+585	dM5.0	20:26:05.84	+58:34:31.4	…	…	…	…	40.39	602.40	29.24 ± 0.27	0.159 ± 0.010
…	…	LP 755-19	J20287-114	M1.5 Ve	20:28:43.80	-11:28:32.4	…	…	…	…	90.02	186.32	213.38 ± 1.20	0.448 ± 0.018
20269+2731	RAO 432	GJ 4146	J20269+275	M2.0 V	20:26:56.29	+27:31:03.1	(AB)	AB	0.203	335.5	35.33	281.66	…	0.511 ± 0.030
20298+0941	AST 2	HUDel	J20298+096	M4.5 V	20:29:49.04	+09:41:22.2	(AB)	AB(1)	0.161	93.8	60.67	676.97	…	0.412 ± 0.007
…	…	GJ 793	J20305+654	M2.5 V	20:30:33.18	+65:27:02.9	…	…	…	…	41.51	526.09	195.56 ± 1.25	0.374 ± 0.011
20287-1129	BWL55	1R203011.0+795040	J20301+798	M3.0 Ve	20:30:07.75	+79:50:47.4	Aab	Aab(2)	5.611	34.0	169.22	108.40	…	…
…	…	GJ 1254	J20336+617	M4.0 V	20:33:41.53	+61:45:28.2	…	…	…	…	23.86	1058.07	175.89 ± 1.38	0.378 ± 0.013
20314+3833	JNN 284	Ross 188	J20314+385	M5.0 V	20:31:25.91	+38:33:55.8	(AB)	AB	0.118	252.4	46.05	748.29	…	0.256 ± 0.036
…	…	GJ 4148	J20337+233	M3.0 V	20:33:43.10	+23:22:15.4	AB	A	…	…	…	304.69	…	0.447 ± 0.031
20337+2322	JNN 285	G 186-29B	…	M4.0 V	20:33:43.11	+23:22:14.5	…	B	0.909	172.5	27.50	322.24	…	0.301 ± 0.035
…	…	GJ 4150	J20339+643	M3.5 V	20:33:58.81	+64:19:08.1	…	…	…	…	53.84	441.98	237.64 ± 1.65	0.445 ± 0.018
…	…	GJ 4149	J20347+033	M2.5 V	20:34:43.33	+03:20:43.6	…	…	…	…	27.74	558.88	287.35 ± 1.47	0.462 ± 0.018
…	…	Wolf 1074	J20349+592	M4.0 V	20:34:54.81	+59:17:26.0	…	…	…	…	…	244.58	125.22 ± 0.51	0.337 ± 0.015
…	…	GJ 4152	J20367+388	M3.5 V	20:36:46.27	+38:50:30.3	…	…	…	…	44.56	227.57	73.84 ± 0.28	0.253 ± 0.012
…	…	Wolf 1351	J20373+219	M0.5 V	20:37:20.77	+21:56:47.8	A+B	A	…	…	44.52	279.80	922.02 ± 64.01	0.630 ± 0.029
20373+2157	MCT 11	GJ 4153 B	…	M4.5 V	20:37:23.97	+21:56:21.4	…	B	51.773	120.7	36.01	301.36	66.67 ± 0.33	0.256 ± 0.013
…	…	TYC 4246-488-1	J20403+616	M1.0 V	20:40:18.59	+61:41:28.4	…	…	…	…	113.22	117.58	537.60 ± 3.27	0.558 ± 0.028
…	…	GJ 1256	J20405+154	M4.5 V	20:40:35.33	+15:30:09.3	…	…	…	…	113.25	1477.37	42.26 ± 0.19	0.191 ± 0.010
20408+1956	LDS1045	HD 197076	…	G5 V	20:40:45.28	+19:56:12.9	A+(BC)	A	…	…	52.47	334.03	…	1.001 ± 0.150
20408+1956	RAO 23	GJ 797 B	J20407+199	M2.5 V	20:40:44.65	+19:54:08.2	…	BC	125.058	184.1	80.18	339.09	…	…
…	…	GJ 4155	J20409-101	M1.5 V	20:40:56.32	-10:06:43.1	Aab	Aab	…	…	43.47	155.85	…	…
…	…	ATMicA	J20418-324	M4.5 V	20:41:51.44	-32:26:13.3	AB+C	A	…	…	120.20	484.79	…	0.420 ± 0.031
20452-3120	LDS 720	ATMicB	…	M4.5 Ve	20:41:51.54	-32:26:15.1	…	B	2.102	145.0	36.05	423.10	…	0.414 ± 0.031
20452-3120	LDS 720	AUMic	J20451-313	M0.5 V	20:45:09.88	-31:20:33.0	…	C	4681.175	32.9	36.15	457.00	990.15 ± 7.63	0.654 ± 0.027
…	…	Ross 751	J20429-189	M1.5 V	20:42:57.83	-18:55:19.8	…	…	…	…	48.39	1048.64	556.52 ± 2.76	0.564 ± 0.028
…	…	LP 575-35	J20433+047	M5.0 V	20:43:24.35	+04:45:52.9	…	…	…	…	97.24	469.44	…	0.159 ± 0.041
…	…	Wolf 1360	J20435+240	M2.5 Ve	20:43:34.69	+24:07:40.2	…	…	…	…	29.02	150.57	348.02 ± 1.56	0.475 ± 0.030
…	…	G 262-26	J20436+642	M0.0 V	20:43:42.13	+64:16:52.5	…	…	…	…	29.06	326.18	334.83 ± 1.32	0.446 ± 0.017
…	…	GJ 4159	J20436-001	M1.0 V	20:43:41.71	-00:10:37.5	…	…	…	…	36.20	440.43	464.18 ± 2.22	0.548 ± 0.028

Table D.2: Complete sample with the description of multiple systems (continued).

WDS id	WDS disc	Name	Karmn	Spectral type	α (2016.0)	δ (2016.0)	System	Component	ρ [arcsec]	θ [deg]	ϖ [mas]	$\mu_{\rm total}$ [mas a^{-1}]	$\mathcal{L}$ [$10^{-4}\,\mathcal{L}_\odot$]	$\mathcal{M}$ [$\mathcal{M}_\odot$]
20433+5521	LLO1	Wolf 1084	J20433+553	M5.0 V	20:43:20.89	+55:21:20.5	(AB)	AB(2)	0.086	20.2	31.29	1919.02	…	0.268
20444+1945	CAR 2	HD 352860	J20443+197	M0.0 V	20:44:21.98	+19:44:49.8	(AB)	AB	0.226	81.8	34.23	555.61	…	…
…	…	GJ 4160	J20445+089S	M1.5 V	20:44:30.94	+08:54:12.6	A+Bab	A	…	…	55.78	223.80	…	0.565 ± 0.028
20446+0854	LDS1046	GJ 4161	J20445+089N	M0.5 V	20:44:30.67	+08:54:27.1	…	Bab(2)	15.094	344.5	38.88	230.26	…	…
…	…	GJ 806	J20450+444	M1.5 V	20:45:04.75	+44:30:01.0	…	…	…	…	106.28	511.70	259.29 ± 0.98	0.413 ± 0.011
…	…	Wolf 882	J20496-003	M3.5 V	20:49:39.86	-00:21:06.7	…	…	…	…	55.19	366.38	206.12 ± 0.95	0.439 ± 0.018
20488+1943	JNN 286	GJ 4163	J20488+197	M3.3 V	20:48:52.27	+19:43:01.6	(AB)	AB	0.233	178.6	55.22	257.20	…	0.377 ± 0.035
…	…	LP 816-60	J20525-169	M4.0 V	20:52:32.67	-16:58:28.4	…	…	…	…	169.06	311.33	62.69 ± 0.40	0.219 ± 0.010
20520+6910	JOD 19	GJ 4170	J20519+691	M1.0 V	20:52:00.55	+69:10:07.6	(AB)	AB	0.470	171.6	168.95	231.52	…	0.474 ± 0.030
…	…	HD 199305	J20533+621	M1.0 V	20:53:19.79	+62:09:03.4	…	…	…	…	26.27	773.10	525.60 ± 4.57	0.562 ± 0.028
…	…	GJ 4169	J20535+106	M5.0 V	20:53:32.53	+10:36:55.0	…	…	…	…	26.31	665.25	40.84 ± 0.19	0.210 ± 0.011
…	…	LP 74-35	J20549+675	M2.0 V	20:54:54.90	+67:35:09.8	…	…	…	…	95.18	198.43	414.46 ± 1.80	0.509 ± 0.029
20532-0221	JNN126	LP 636-19	J20532-023	M3.0 V	20:53:14.87	-02:21:21.7	(AB)	AB	0.138	327.3	95.18	195.08	…	0.445 ± 0.031
…	…	GJ 810 A	J20556-140N	M4.0 V	20:55:39.31	-14:02:15.6	Aab+B	Aab(2)	…	…	58.80	1493.30	…	0.121 ± 0.009
20555-1400	LDS6418	GJ 810 B	J20556-140S	M5.0 V	20:55:38.68	-14:04:02.4	…	B	107.268	184.9	32.78	1497.19	26.26 ± 0.13	0.153 ± 0.009
…	…	Wolf 896	J20567-104	dM2.5	20:56:46.56	-10:27:12.7	…	…	…	…	32.79	1125.07	312.25 ± 1.75	0.466 ± 0.013
…	…	FRAqr	J20568-048	M4.0 V	20:56:49.39	-04:50:52.6	Aab+B	Aab(2)	…	…	50.15	826.32	…	…
20568-0449	LDS6420	Ross 193B	…	DC10	20:56:48.62	-04:50:43.1	…	B	15.006	309.4	94.40	807.72	…	0.500 ± 0.100
…	…	Wolf 1373	J20574+223	M3.0 V	20:57:26.24	+22:21:42.4	…	…	…	…	42.42	798.71	133.63 ± 0.87	0.308 ± 0.013
…	…	GJ 4173	J20586+342	M0.5 V	20:58:42.31	+34:16:24.7	…	…	…	…	94.19	324.95	639.77 ± 2.64	0.597 ± 0.027
…	…	G 212-14	J21001+495	M2.0 V	21:00:09.24	+49:35:20.8	…	…	…	…	32.70	296.48	532.43 ± 2.22	0.541 ± 0.029
21000+4004	KUI 103	V1396Cyg	J21000+400	M2.0 V	21:00:06.23	+40:04:08.6	(AB)	AB(2)	0.885	58.2	50.81	652.26	…	…
21013+3315	CRC 75	GJ 4176	J21012+332	M4.0 V	21:01:16.51	+33:14:30.7	(AB)+(CD)	AB	0.232	6.3	30.67	364.63	…	0.406 ± 0.032
21011+3315	JNN 288	GJ 4177	J21013+332	M4.0 V	21:01:21.03	+33:14:25.9	…	CD	56.912	94.8	31.47	333.46	…	0.341 ± 0.034
…	…	Wolf 906	J21019-063	M2.5 V	21:01:58.39	-06:19:14.5	…	…	…	…	27.88	498.67	296.13 ± 1.30	0.451 ± 0.012
…	…	G 211-9	J21027+349	M4.5 V	21:02:46.40	+34:54:31.2	…	…	…	…	27.87	362.28	174.68 ± 0.82	0.460 ± 0.019
…	…	TYC 3588-5589-1	J21044+455	M2.0 V	21:04:28.94	+45:35:42.3	…	…	…	…	94.07	173.29	587.57 ± 2.34	0.557 ± 0.028
…	…	Ross 769	J21048-169	M1.5 V	21:04:52.36	-16:58:04.6	…	…	…	…	59.62	2236.05	261.50 ± 1.50	0.415 ± 0.016
21014+2043	JNN 289	GJ 4175	J21014+207	M3.5 V	21:01:24.40	+20:43:31.6	(AB)	AB	0.377	25.4	58.91	557.25	…	0.248 ± 0.037
…	…	PM J21055+0609N	J21055+061	M3.0 V	21:05:32.09	+06:09:16.2	A+B	A	…	…	53.83	52.64	248.97 ± 1.36	0.485 ± 0.019
…	…	PM J21055+0609S	…	M5.5 V	21:05:32.17	+06:09:11.2	…	B*	5.094	166.0	47.71	61.85	…	0.139 ± 0.043
…	…	PM J21057+5015E	J21057+502	M3.5 V	21:05:45.54	+50:15:44.1	A+B	A	…	…	38.59	100.51	271.86 ± 1.50	0.508 ± 0.020
…	…	PM J21057+5015W	…	M3.5 V	21:05:42.60	+50:15:58.1	…	B*	31.465	296.4	30.52	97.27	180.42 ± 0.92	0.437 ± 0.018
…	…	GJ 4180	J21059+044	M2.5 V	21:05:56.52	+04:25:38.0	…	…	…	…	24.95	215.22	408.63 ± 2.12	0.492 ± 0.030
…	…	PM J21074+4651	J21074+468	M2.0 V	21:07:28.14	+46:51:55.4	…	…	…	…	24.97	100.93	438.11 ± 1.84	0.503 ± 0.029
…	…	1R210736.5-130500	J21076-130	M3.0 Ve	21:07:36.86	-13:04:59.6	…	…	…	…	45.14	106.44	203.86 ± 1.17	0.437 ± 0.018
21088-0426	HDS3013	GJ 9721	J21087-044S	M1.0 V	21:08:45.41	-04:25:36.7	(AB)+C	AB	0.192	340.0	57.57	85.47	…	…
21088-0426	VVO 18	GJ 9721B	J21087-044N	M3.0 V	21:08:44.75	-04:25:18.3	…	C	20.894	331.9	69.26	53.58	186.56 ± 0.95	0.417 ± 0.017
…	…	Wolf 918	J21092-133	M1.0 V	21:09:18.21	-13:18:40.9	…	…	…	…	65.74	2119.70	190.69 ± 0.97	0.351 ± 0.014
…	…	1R211004.9-192005	J21100-193	M2.0 V	21:10:05.46	-19:19:59.1	A+B	A	…	…	36.42	128.41	896.94 ± 5.59	0.600 ± 0.027

Table D.2: Complete sample with the description of multiple systems (continued).

WDS id	WDS disc	Name	Karmn	Spectral type	α (2016.0)	δ (2016.0)	System	Component	ρ [arcsec]	θ [deg]	ϖ [mas]	$\mu_{\rm total}$ [mas a^{-1}]	$\mathcal{L}$ [$10^{-4}\,\mathcal{L}_\odot$]	$\mathcal{M}$ [$\mathcal{M}_\odot$]
21100-1920	LDS 734	UCAC4 354-189365	…	M5.0 V	21:10:04.71	-19:20:32.0	…	B	34.542	197.8	38.69	129.86	620.35 ± 29.47	0.497 ± 0.030
…	…	LP 285-9	J21123+359	M1.5 V	21:12:22.66	+35:55:24.7	…	…	…	…	34.89	201.98	534.67 ± 3.26	0.554 ± 0.028
…	…	PM J21127-0719	J21127-073	M3.5 V	21:12:45.71	-07:19:56.5	…	…	…	…	47.53	111.19	185.68 ± 0.99	0.416 ± 0.017
21109+2925	BAG29	Ross 824	J21109+294	M1.5 V	21:10:54.47	+29:25:18.6	(AB)	AB	0.188	174.4	43.34	371.86	…	0.658 ± 0.039
21137+0846	RAO 449	LSPM J2113+0846N	J21137+087	M2.0 V	21:13:44.77	+08:46:09.1	(AB)+C	AB	0.377	322.0	69.12	178.26	…	0.482 ± 0.030
21137+0846	UC 4412	LSPM J2113+0846S	…	M1.5 V	21:13:44.56	+08:46:01.1	…	C	8.563	200.9	63.10	166.83	375.14 ± 2.70	0.493 ± 0.030
…	…	Ross 772	J21138+180	M3.0 V	21:13:53.01	+18:05:58.8	…	…	…	…	53.58	449.37	347.31 ± 1.71	0.464 ± 0.030
…	…	LSPM J2114+5052	J21145+508	M2.5 V	21:14:32.61	+50:52:31.6	…	…	…	…	93.88	211.51	467.76 ± 1.99	0.512 ± 0.029
21148+3803	AGC 13	GJ 9728 B	…	…	21:14:47.68	+38:02:50.6	(AB)+(CD)	AB	1.050	189.7	93.87	472.40	…	2.6300 ± 0.120
21148+3803	JOD 20	GJ 822.1 C	J21147+380	M2.5 V	21:14:47.09	+38:01:21.0	…	CD	89.862	184.4	72.70	453.21	…	0.437 ± 0.031
…	…	GJ 4184	J21152+257	M3.0 V	21:15:12.76	+25:47:41.2	…	…	…	…	71.72	300.40	471.35 ± 2.78	0.503 ± 0.029
21161+2951	BWL 56	Ross 776	J21160+298E	M3.3 V	21:16:06.06	+29:51:51.5	(AB)+C	AB	0.058	163.1	71.68	203.76	…	0.380 ± 0.032
21161+2951	LDS1053	Ross 826	J21160+298W	M3.3 V	21:16:04.10	+29:51:46.7	…	C	26.031	259.3	42.59	214.61	109.38 ± 0.46	0.335 ± 0.015
…	…	LSPM J2116+0234	J21164+025	M3.0 V	21:16:27.55	+02:34:50.8	…	…	…	…	30.23	250.53	241.76 ± 1.46	0.410 ± 0.012
…	…	Ross 773A	J21173+208N	M3.0 V	21:17:23.09	+20:53:59.2	A+B	A	…	…	74.39	420.04	414.91 ± 2.68	0.479 ± 0.030
21174+2053	KUI 106	Ross 773B	J21173+208S	M4.0 V	21:17:23.00	+20:54:03.4	…	B	4.337	341.2	…	422.14	…	0.369 ± 0.033
…	…	G 262-38	J21173+640	M5.0 V	21:17:22.75	+64:02:39.1	…	…	…	…	33.73	342.80	114.87 ± 2.12	0.322 ± 0.015
21176-0854	JOD 21	GJ 4187	J21176-089N	M2.5 V	21:17:36.07	-08:54:11.7	(AB)+C	AB	0.479	188.8	51.31	84.74	…	0.461 ± 0.031
21176-0854	VVO 19	GJ 4188	J21176-089S	M3.0 V	21:17:39.55	-08:54:49.6	…	C	63.991	126.4	51.37	78.19	204.92 ± 1.71	0.411 ± 0.017
…	…	1R211833.8+301434	J21185+302	M1.5 Ve	21:18:33.83	+30:14:34.3	…	…	…	…	83.49	63.45	790.66 ± 3.57	0.628 ± 0.027
…	…	TYC 2187-512-1	J21221+229	M1.0 V	21:22:06.41	+22:55:55.0	…	…	…	…	34.10	160.33	416.86 ± 2.32	0.483 ± 0.012
…	…	GJ 4192	J21243+085	M3.5 V	21:24:19.08	+08:30:03.6	…	…	…	…	37.15	240.54	279.24 ± 42.07	0.374 ± 0.037
…	…	LSPM J2124+4003	J21245+400	M5.5 V	21:24:33.07	+40:04:06.7	…	…	…	…	213.13	697.68	19.12 ± 0.10	0.159 ± 0.010
…	…	GJ 828.1	J21267+037	M0.0 V	21:26:42.41	+03:44:12.9	…	…	…	…	214.57	66.87	1033.35 ± 4.90	0.699 ± 0.026
…	…	Wolf 920	J21272-068	M0.5 V	21:27:16.89	-06:50:45.8	…	…	…	…	21.74	400.29	286.41 ± 1.74	0.411 ± 0.016
…	…	V2160Cyg	J21275+340	M1.5 V	21:27:32.60	+34:01:25.7	…	…	…	…	36.38	333.36	680.43 ± 4.48	0.603 ± 0.027
…	…	Ross 778	J21277+072	M1.0 V	21:27:46.19	+07:17:45.9	…	…	…	…	39.37	684.31	480.70 ± 3.03	0.541 ± 0.029
…	…	LP 457-38	J21280+179	M1.5 V	21:28:05.57	+17:54:02.7	…	…	…	…	36.81	174.63	644.14 ± 3.08	0.586 ± 0.028
…	…	GJ 4197	J21283-223	M2.5 V	21:28:18.04	-22:18:36.5	…	…	…	…	36.74	333.87	262.88 ± 1.49	0.469 ± 0.018
21313-0947	BLA 9	Ross 775	J21313-097	M4.5 V	21:31:19.92	-09:47:27.5	(AB)	AB	0.156	122.8	66.21	1248.01	…	0.228 ± 0.001
…	…	BBCap	J21296+176	M3.0 V	21:29:37.94	+17:38:41.9	Aab	Aab(EB?)	…	…	112.99	1075.79	…	…
…	…	GJ 4201 A	J21323+245	M4.0 V	21:32:22.33	+24:33:41.9	AB	A	…	…	55.82	229.20	…	0.324 ± 0.034
21324+2434	MCT 12	GJ 4201 B	…	M4.0 V	21:32:22.23	+24:33:41.1	…	B	1.548	240.8	56.17	216.79	…	0.300 ± 0.035
…	…	GJ 4203	J21338+017S	M4.0 V	21:33:49.11	+01:46:44.9	A+B	A	…	…	64.15	727.05	55.98 ± 0.44	0.233 ± 0.012
21338+0147	BLZ 1	GJ 4204	J21338+017N	M4.0 V	21:33:49.13	+01:46:50.0	…	B	5.173	3.2	53.81	723.26	…	0.207 ± 0.038
…	…	Wolf 923	J21338-068	M4.0 V	21:33:49.04	-06:51:18.4	…	…	…	…	50.26	518.43	58.05 ± 0.41	0.238 ± 0.012
…	…	Wolf 926	J21348+515	M2.5 V	21:34:51.13	+51:32:18.6	…	…	…	…	29.05	555.58	274.19 ± 1.45	0.445 ± 0.012
…	…	V2168Cyg	J21366+394	M0.0 V	21:36:38.29	+39:27:18.0	AB	A	…	…	…	263.42	…	0.630 ± 0.027
21366+3928	VYS 10	GJ 834 B	…	M2.5 V	21:36:38.20	+39:27:17.8	…	B	1.003	260.8	62.49	245.73	…	0.435 ± 0.031
…	…	Ross 215	J21369+561	M1.5 V	21:36:58.82	+56:07:07.2	…	…	…	…	62.53	153.57	679.51 ± 3.30	0.600 ± 0.027

Table D.2: Complete sample with the description of multiple systems (continued).

WDS id	WDS disc	Name	Karmn	Spectral type	α (2016.0)	δ (2016.0)	System	Component	ρ [arcsec]	θ [deg]	ϖ [mas]	$\mu_{\rm total}$ [mas a^{-1}]	$\mathcal{L}$ [$10^{-4}\,\mathcal{L}_\odot$]	$\mathcal{M}$ [$\mathcal{M}_\odot$]
21375-0555	JNN 133	PM J21374-0555	J21374-059	M3.0 V	21:37:29.02	-05:55:05.7	AB	A	0.219	172.0	26.58	169.19	…	…
…	…	G3- 2670835278558316160	…	…	21:37:29.01	-05:55:05.5	…	B	0.261	316.3	75.25	…	…	…
…	…	Ross 199	J21378+530	M0.0 V	21:37:50.77	+53:04:49.9	…	…	…	…	51.82	317.05	1297.77 ± 13.35	0.728 ± 0.025
21376+0137	JNN291	1R213740.3+013711	J21376+016	M4.5 V	21:37:40.28	+01:37:12.7	(AB)	AB	0.420	345.0	60.30	99.36	…	0.445 ± 0.031
21379+2743	HDS3080	GJ 835	J21380+277	M0.0 V	21:38:00.96	+27:43:24.4	(AB)C	AB	0.167	109.0	…	485.01	…	0.558 ± 0.028
21379+2743	SKF 245	BD+27 4120B	…	M5.0 V	21:38:01.04	+27:43:27.6	…	C	3.336	16.3	46.97	487.70	…	0.195 ± 0.039
…	…	LP 286-1	J21402+370	M0.5 V	21:40:12.27	+37:03:24.1	…	…	…	…	47.24	490.75	536.90 ± 1.81	0.569 ± 0.028
21399+2737	HDS3083	GJ 4210	J21399+276	M2.0 V	21:39:54.70	+27:36:39.8	(AB)	AB	0.085	298.4	46.20	353.56	…	0.508 ± 0.029
…	…	Ross 206	J21421-121	M3.0 V	21:42:07.58	-12:09:59.3	…	…	…	…	92.65	692.97	412.28 ± 3.03	0.483 ± 0.030
21420+2741	RAO 465	GJ 4212	J21419+276	M4.0 V	21:41:58.03	+27:41:14.2	(AB)	AB	2.562	302.9	62.14	296.96	…	0.296 ± 0.035
…	…	GJ 4214	J21441+170S	M4.0 V	21:44:09.31	+17:03:35.0	A+B	A	…	…	61.85	252.08	75.44 ± 0.31	0.274 ± 0.013
21440+1705	LDS6358	GJ 4215	J21441+170N	M5.2 V	21:44:08.25	+17:04:37.3	…	B	64.149	346.4	48.93	245.38	35.79 ± 0.15	0.195 ± 0.011
…	…	GJ 4213	J21442+066	M3.0 Ve	21:44:12.64	+06:38:26.6	Aab	Aab(1)	…	…	40.10	364.35	…	…
21448+4425	COU 2234	G 215-12	J21449+442	M1.5 V	21:44:53.78	+44:16:58.4	(AB)	AB	0.107	84.3	48.93	670.31	…	0.534 ± 0.029
…	…	G 126-32A	…	M1.0 V	21:45:04.94	+19:53:31.8	ABC	A	…	…	29.31	219.44	…	0.527 ± 0.029
21451+1954	RAO 466	G 126-32B	J21450+198	M1.5 V	21:45:04.90	+19:53:31.7	…	B	0.564	253.2	31.05	240.74	…	0.484 ± 0.030
…	…	G 126-32C	…	…	21:45:05.04	+19:53:36.9	…	C*	5.317	16.4	31.93	232.18	…	0.143 ± 0.058
…	…	Wolf 937	J21450-057	M3.0 V	21:45:00.59	-05:47:20.3	…	…	…	…	27.36	467.42	101.66 ± 0.51	0.302 ± 0.014
…	…	Wolf 939	J21454-059	M3.5 V	21:45:24.74	-05:54:11.5	…	…	…	…	27.36	371.17	128.06 ± 0.66	0.341 ± 0.015
…	…	LSPM J2146+3813	J21463+382	M5.0 V	21:46:22.29	+38:13:03.1	…	…	…	…	32.59	201.01	45.87 ± 0.20	0.202 ± 0.009
…	…	G 264-12	J21466+668	M4.0 V	21:46:41.30	+66:48:14.0	…	…	…	…	43.57	443.63	103.78 ± 0.45	0.284 ± 0.011
…	…	Wolf 940	J21466-001	dM4.0	21:46:41.24	-00:10:31.9	(AB)	A	…	…	43.57	920.67	95.47 ± 0.54	0.272 ± 0.010
21467-0010	BNG 2	Wolf 940 B	…	T8+/Y?	…	…	…	B	31.640	250.5	28.71	919.00	…	…
…	…	Wolf 944	J21469+466	M4.0 V	21:46:56.68	+46:38:06.1	…	…	…	…	38.92	278.80	93.00 ± 0.64	0.307 ± 0.014
…	…	PM J21472-0444	J21472-047	M4.5 V	21:47:17.73	-04:44:40.6	…	…	…	…	57.18	257.05	30.29 ± 0.15	0.177 ± 0.011
…	…	TYC 4266-736-1	J21474+627	M0.0 V	21:47:24.39	+62:45:13.7	A+B	A	…	…	26.83	173.75	870.84 ± 6.24	0.667 ± 0.026
21474+6245	WIS 354	LSPM J2147+6246	…	M6.0 V	21:47:25.40	+62:46:22.4	…	B	69.038	5.8	26.58	175.12	11.90 ± 0.13	0.131 ± 0.010
…	…	Wolf 945	J21478+502	M4.0 V	21:47:53.64	+50:14:54.6	…	…	…	…	33.90	813.93	113.31 ± 0.95	0.320 ± 0.014
…	…	Ross 779	J21479+058	M2.0 V	21:47:57.57	+05:49:16.4	…	…	…	…	33.90	458.26	567.25 ± 2.45	0.566 ± 0.028
…	…	GJ 4221	J21481+014	M3.0 V	21:48:10.46	+01:26:42.0	…	…	…	…	33.94	226.43	184.76 ± 0.99	0.415 ± 0.017
…	…	GJ 4225	J21482+279	M2.0 V	21:48:15.02	+27:55:31.0	…	…	…	…	37.09	721.44	170.31 ± 0.68	0.351 ± 0.015
…	…	GJ 4227	J21512+128	M4.0 V	21:51:18.24	+12:50:33.2	…	…	…	…	37.15	686.04	142.00 ± 0.63	0.361 ± 0.015
21518+1336	CRC 40	GJ 4228	J21518+136	M4.0 V	21:51:48.53	+13:36:13.8	(AB)	AB	10.909	121.6	51.13	211.25	…	0.240 ± 0.037
…	…	TYC 3980-1081-1	J21516+592	M4.0 V	21:51:38.15	+59:17:40.0	A+B	A	…	…	31.99	79.89	231.04 ± 4.09	0.467 ± 0.019
21516+5918	KPP4552	UCAC4 747-070768	…	DAH	21:51:39.93	+59:17:34.5	…	B	14.642	111.9	45.53	88.85	…	0.500 ± 0.100
…	…	GJ 4232	J21521+274	M5.0 V	21:52:12.12	+27:24:48.2	…	…	…	…	45.24	806.23	89.39 ± 0.42	0.281 ± 0.013
…	…	GJ 839	J21539+417	M0.0 V	21:53:59.55	+41:46:38.7	…	…	…	…	104.44	527.45	1031.11 ± 4.48	0.695 ± 0.026
…	…	Ross 263	J21566+197	M3.0 V	21:56:37.83	+19:46:06.8	…	…	…	…	54.55	488.18	188.98 ± 1.49	0.394 ± 0.016
…	…	GJ 4239	J21569-019	M5.0 V	21:56:56.61	-01:53:59.5	…	…	…	…	32.49	1419.70	27.60 ± 0.13	0.168 ± 0.010
…	…	Wolf 953	J21574+081	M1.5 V	21:57:26.64	+08:08:15.5	…	…	…	…	133.81	386.95	565.14 ± 3.17	0.560 ± 0.028

Table D.2: Complete sample with the description of multiple systems (continued).

WDS id	WDS disc	Name	Karmn	Spectral type	α (2016.0)	δ (2016.0)	System	Component	ρ [arcsec]	θ [deg]	ϖ [mas]	$\mu_{\rm total}$ [mas a^{-1}]	$\mathcal{L}$ [$10^{-4}\,\mathcal{L}_\odot$]	$\mathcal{M}$ [$\mathcal{M}_\odot$]
…	…	GJ 842.2	J21584+755	M0.5 V	21:58:25.51	+75:35:21.0	…	…	…	…	123.65	232.45	747.29 ± 3.89	0.623 ± 0.027
…	…	LSPM J2158+6117	J21585+612	M6.0 V	21:58:36.41	+61:17:07.8	…	…	…	…	29.46	815.50	12.65 ± 0.07	0.115 ± 0.009
…	…	GJ 4246	J21593+418	M3.0 V	21:59:22.08	+41:51:25.4	…	…	…	…	62.59	423.27	159.25 ± 0.59	0.360 ± 0.015
…	…	V374Peg	J22012+283	M3.5 Ve	22:01:13.58	+28:18:25.6	…	…	…	…	64.94	375.25	99.29 ± 0.53	0.319 ± 0.011
21522+0538	JOD 23	GJ 4231	J21521+056	M2.4 V	21:52:10.52	+05:37:33.5	(AB)	AB	0.132	263.6	28.73	191.80	…	0.508 ± 0.058
…	…	Wolf 1154 A	J22012+323	M1.5 V	22:01:14.13	+32:23:13.9	A(BC)	A	…	…	29.02	133.62	…	0.493 ± 0.030
22012+3223	GRV1283	Wolf 1154 B	…	M3.5 V	22:01:14.04	+32:23:13.2	…	B	1.302	235.5	35.60	119.08	…	0.323 ± 0.034
…	…	2M22011701+3222062	…	T2.5	…	…	…	C	…	…	47.42	125.77	…	…
22018+1628	YSC 165	Ross 265	J22018+164	M2.5 V	22:01:49.49	+16:28:05.2	(AB)+C	AB	0.355	36.3	45.79	421.76	…	0.505 ± 0.031
…	…	Ross 268	…	M3.5 V	22:06:23.02	+17:22:22.1	…	C*	5100.550	50.2	61.13	371.56	116.63 ± 0.52	0.347 ± 0.015
…	…	GJ 843	J22020-194	dM3.5	22:02:01.85	-19:28:58.0	…	…	…	…	30.17	933.09	145.39 ± 1.16	0.327 ± 0.011
…	…	HD 209290	J22021+014	M0.5 V	22:02:09.79	+01:23:56.4	…	…	…	…	23.62	531.35	638.60 ± 5.17	0.596 ± 0.028
…	…	GJ 4251	J22033+674	M4.5 V	22:03:22.74	+67:29:55.1	…	…	…	…	41.26	608.37	102.62 ± 0.49	0.303 ± 0.014
…	…	Wolf 983	J22051+051	M4.0 V	22:05:07.30	+05:08:14.2	…	…	…	…	104.92	479.50	161.43 ± 0.75	0.386 ± 0.016
22035+0340	JNN293	1R220330.8+034001	J22035+036	M4.0 V	22:03:33.39	+03:40:21.4	(AB)	AB	0.412	351.9	47.75	126.77	…	0.248 ± 0.037
…	…	GJ 4258	J22057+656	M1.5 V	22:05:44.55	+65:38:58.9	A+B	A	…	…	…	380.08	373.21 ± 2.57	0.470 ± 0.012
22058+6539	NI 44	G 264-18B	…	M4.5 V	22:05:45.29	+65:38:53.9	…	B	6.782	137.7	…	377.33	57.83 ± 0.37	0.237 ± 0.012
…	…	Wolf 1548	J22058-119	M0.0 V	22:05:51.00	-11:54:53.7	A+B	A	…	…	100.79	319.26	1476.70 ± 47.95	0.747 ± 0.026
22059-1155	WNO 57	LP 759-25	…	M6.0 Ve	22:05:35.44	-11:04:31.8	…	B	3030.622	355.7	101.97	322.49	10.00 ± 0.06	0.118 ± 0.009
…	…	GJ 4256	J22060+393	M3.0 V	22:06:00.76	+39:17:55.6	…	…	…	…	102.94	464.23	164.44 ± 1.22	0.366 ± 0.015
…	…	Wolf 990	J22067+034	M4.0 V	22:06:46.87	+03:24:58.7	…	…	…	…	52.43	569.30	78.81 ± 0.53	0.281 ± 0.013
…	…	PM J22088+1144	J22088+117	M4.5 V	22:08:50.44	+11:44:12.4	…	…	…	…	66.45	103.82	203.54 ± 1.19	0.498 ± 0.020
…	…	LP 519-38	J22095+118	M3.0 V	22:09:31.86	+11:52:51.6	…	…	…	…	46.85	208.15	258.81 ± 1.54	0.465 ± 0.018
…	…	Wolf 1329	J22096-046	M3.5 V	22:09:41.56	-04:38:27.0	…	…	…	…	46.58	1132.80	283.03 ± 1.83	0.448 ± 0.014
…	…	GJ 4260	J22097+410	M3.0 V	22:09:43.64	+41:02:09.5	…	…	…	…	38.21	485.43	249.93 ± 1.37	0.457 ± 0.018
…	…	UCAC4 744-073158	J22102+587	M2.0 V	22:10:15.18	+58:42:21.9	…	…	…	…	60.96	29.80	307.54 ± 1.61	0.479 ± 0.018
…	…	Wolf 1003 A	J22107+079	M0.5 V	22:10:44.98	+07:54:32.9	AB	A	…	…	50.80	255.11	…	0.596 ± 0.028
22107+0755	WOR 10	Wolf 1003 B	…	M1.0 V	22:10:44.98	+07:54:33.8	…	B	0.894	5.4	40.46	241.13	…	0.568 ± 0.028
…	…	G 214-14	J22112+410	M0.0 V	22:11:16.65	+41:00:58.6	…	…	…	…	40.35	313.80	486.65 ± 2.11	0.563 ± 0.028
…	…	GJ 4262	J22112-025	M2.0 V	22:11:13.95	-02:32:38.2	…	…	…	…	82.89	433.31	262.26 ± 2.07	0.441 ± 0.017
…	…	1R221124.3+410000	J22114+409	M5.5 V	22:11:24.04	+40:59:59.8	…	…	…	…	40.38	113.38	26.43 ± 0.10	0.160 ± 0.009
…	…	Ross 271	J22115+184	M2.0 V	22:11:30.46	+18:25:37.2	…	…	…	…	29.80	375.38	435.24 ± 3.02	0.506 ± 0.029
…	…	WT 2221	J22117-207	M3.5 V	22:11:42.27	-20:44:19.3	A+B	A	…	…	177.93	160.10	340.88 ± 2.19	0.443 ± 0.031
22117-2044	FMR 18	WT 2220	…	M3.0 V	22:11:41.51	-20:44:12.0	…	B	12.876	304.6	45.59	159.43	55.47 ± 0.38	0.232 ± 0.012
…	…	Wolf 1014	J22125+085	M3.0 V	22:12:36.06	+08:33:00.9	…	…	…	…	142.05	679.53	186.37 ± 0.78	0.362 ± 0.011
…	…	LF 4 +54 152	J22129+550	M0.0 V	22:12:56.63	+55:04:50.8	AB	A	…	…	77.94	109.13	…	0.6220 ± 0.093
…	…	G3- 2005884249925303168	…	M6.5 V	22:13:00.46	+55:05:48.3	…	B*	66.265	29.8	35.01	108.97	…	0.109 ± 0.046
…	…	Wolf 1556	J22134-147	M3.5 V	22:13:28.46	-14:44:58.8	…	…	…	…	29.20	408.23	244.01 ± 1.94	0.480 ± 0.019
…	…	GJ 4264	J22135+259	M4e	22:13:35.90	+25:58:08.1	…	…	…	…	84.86	227.21	96.90 ± 0.41	0.314 ± 0.014
…	…	GJ 1265	J22137-176	dM4.5	22:13:43.82	-17:41:13.6	…	…	…	…	80.20	909.89	36.06 ± 0.24	0.175 ± 0.010

Table D.2: Complete sample with the description of multiple systems (continued).

WDS id	WDS disc	Name	Karmn	Spectral type	α (2016.0)	δ (2016.0)	System	Component	ρ [arcsec]	θ [deg]	ϖ [mas]	$\mu_{\rm total}$ [mas a^{-1}]	$\mathcal{L}$ [$10^{-4}\,\mathcal{L}_\odot$]	$\mathcal{M}$ [$\mathcal{M}_\odot$]
22139+0517	JOD 24	Wolf 1019	J22138+052	M1.5 V	22:13:53.53	+05:16:34.9	(AB)	AB	3.053	317.9	61.98	189.46	…	0.507 ± 0.029
…	…	GJ 4267	J22154+662	M3.0 V	22:15:26.16	+66:13:31.1	…	…	…	…	61.82	208.93	142.86 ± 0.78	0.362 ± 0.015
22143+2534	BWL57	1R221419.3+253411	J22142+255	M4.3 V	22:14:17.88	+25:34:05.6	(AB)	AB	0.141	304.0	61.76	166.68	…	0.352 ± 0.033
…	…	V447Lac	…	K1 V	22:15:54.53	+54:40:23.5	A+B	A	…	…	69.30	223.87	4489.55 ± 18.72	0.860 ± 0.129
22159+5440	GIC 177	GJ 4269	J22160+546	M4.0 V	22:16:02.99	+54:40:00.5	…	B	76.900	107.4	39.68	221.35	…	0.272 ± 0.036
…	…	GJ 1266	J22163+709	M2.0 V	22:16:23.03	+70:56:39.2	…	…	…	…	33.02	863.79	253.12 ± 1.30	0.408 ± 0.016
22173-0847	LDS 782	FGAqr	J22173-088N	M4.0 V	22:17:18.47	-08:48:16.9	A+(BC)	A	7.900	215.6	66.55	544.62	40.71 ± 0.47	0.195 ± 0.011
22173-0847	BEU 22	Wolf 1561 B	J22173-088S	M5.0 V	22:17:18.16	-08:48:23.4	…	BC	7.900	215.6	49.78	555.64	…	0.158 ± 0.041
…	…	PM J22176+5633	J22176+565	M1.5 V	22:17:37.21	+56:33:11.1	…	…	…	…	47.97	122.47	1199.15 ± 82.71	0.681 ± 0.028
…	…	Wolf 1034	J22202+067	M2.5 V	22:20:13.57	+06:43:36.5	…	…	…	…	69.02	399.86	76.51 ± 0.43	0.242 ± 0.012
22212+3745	NSN 753	LSPM J2221+3744A	…	M1.5 V	22:21:13.22	+37:44:50.8	AB	A	2.053	248.8	28.86	159.43	…	0.509 ± 0.029
22212+3745	NSN 753	LSPM J2221+3744B	…	M2.0 V	22:21:13.06	+37:44:50.2	…	B	1.980	250.3	25.95	165.62	…	0.466 ± 0.030
…	…	GJ 4275	J22228+280	M3.8 V	22:22:51.34	+28:01:46.4	…	…	…	…	54.62	402.72	135.75 ± 0.64	0.376 ± 0.016
…	…	GJ 4274	J22231-176	M4.5 Ve	22:23:07.34	-17:36:37.8	…	…	…	…	44.10	781.91	35.04 ± 0.24	0.176 ± 0.009
…	…	Wolf 1225 A	J22234+324	M3.0 V	22:23:29.44	+32:27:29.9	AB	A	…	…	44.37	350.39	…	0.437 ± 0.031
22234+3228	WOR 11	Wolf 1225 B	…	M3.4 V	22:23:29.34	+32:27:29.5	…	B	1.252	254.0	44.37	306.69	…	0.434 ± 0.031
…	…	GJ 1268	J22249+520	M5.1 V	22:24:56.33	+52:00:25.6	…	…	…	…	27.71	490.89	28.40 ± 0.13	0.171 ± 0.010
…	…	Wolf 1231	J22250+356	M2.0 V	22:25:01.66	+35:40:05.3	…	…	…	…	27.65	163.04	211.93 ± 1.09	0.394 ± 0.016
…	…	GJ 4276	J22252+594	M3.5 V	22:25:17.32	+59:24:44.9	…	…	…	…	37.08	333.29	205.64 ± 1.27	0.400 ± 0.014
…	…	Wolf 1201	J22262+030	M4.0 V	22:26:15.24	+03:00:11.3	A+B	A	…	…	23.81	668.79	115.11 ± 0.82	0.344 ± 0.015
22263+0301	LDS4967	GJ 4277 B	…	M6.0 V	22:26:14.97	+03:00:00.4	…	B	11.565	200.5	48.14	675.07	21.66 ± 0.13	0.158 ± 0.010
…	…	PM J22264+5823	J22264+583	M3.0 V	22:26:24.73	+58:23:03.9	…	…	…	…	34.85	147.29	161.33 ± 0.78	0.386 ± 0.016
…	…	GJ 4279	J22270+068	M4.0 V	22:27:03.00	+06:49:32.1	…	…	…	…	35.26	186.47	65.35 ± 0.35	0.254 ± 0.012
22280+5742	KR60	HD 239960A	J22279+576	M3.0 V	22:27:58.11	+57:41:38.5	AB	A	2.052	206.5	84.44	758.87	…	0.306 ± 0.034
…	…	DOCep	…	M4.0 V	22:27:57.93	+57:41:38.8	…	B	1.420	280.0	30.90	1159.08	…	0.199 ± 0.039
…	…	GJ 9784	J22287+189	M1.0 V	22:28:46.13	+18:55:52.1	…	…	…	…	29.77	210.47	619.64 ± 2.66	0.597 ± 0.027
…	…	GJ 4281	J22289-134	M6.5 V	22:28:53.99	-13:25:36.2	…	…	…	…	34.07	1095.16	6.89 ± 0.04	0.104 ± 0.047
…	…	LP 640-74	J22290+016	M0.5 V	22:29:05.91	+01:39:45.0	…	…	…	…	29.27	200.07	754.74 ± 4.65	0.630 ± 0.027
…	…	GJ 1270	J22298+414	M4.0 V	22:29:50.68	+41:28:55.8	…	…	…	…	31.00	1274.43	75.93 ± 0.32	0.252 ± 0.010
…	…	PM J22300+4851A	J22300+488	M4.5 V	22:30:04.10	+48:51:33.8	AB	A	…	…	38.41	96.16	…	0.350 ± 0.033
22300+4851	JNN 294	PM J22300+4851B	…	M4.5 V	22:30:03.87	+48:51:33.1	…	B	2.344	252.4	36.46	106.07	…	0.238 ± 0.037
…	…	GJ 863	J22330+093	M1.0 V	22:33:02.81	+09:22:43.0	…	…	…	…	33.19	556.38	360.49 ± 1.97	0.458 ± 0.012
…	…	GJ 4282 A	J22333-096	M2.6 V	22:33:22.77	-09:36:53.6	AB	A	…	…	36.41	158.89	…	0.380 ± 0.032
22334-0937	MCT 13	GJ 4282 B	…	M2.5 V	22:33:22.87	-09:36:53.7	…	B	1.399	95.5	49.58	139.59	…	0.382 ± 0.032
…	…	GJ 4283	J22347+040	M3.0 V	22:34:46.11	+04:02:39.7	…	…	…	…	49.10	160.66	109.81 ± 0.55	0.295 ± 0.013
…	…	GJ 4284	J22348-010	M4.5 V	22:34:54.85	-01:04:54.5	…	…	…	…	37.39	1118.60	48.94 ± 0.23	0.216 ± 0.011
…	…	G 242-3	J22353+746	M0.0 V	22:35:20.75	+74:41:20.1	…	…	…	…	50.76	262.63	1095.50 ± 22.56	0.696 ± 0.026
…	…	LP 344-27	J22373+299	M1.5 V	22:37:23.33	+29:59:05.6	…	…	…	…	49.91	299.20	513.19 ± 2.74	0.544 ± 0.028
22360-0050	JOD 25	HD 214100	J22361-008	M1.0 V	22:36:09.75	-00:50:39.8	(AB)	AB	0.631	291.7	56.69	632.79	…	0.610 ± 0.027
22375+3923	HDS3211	GJ 4287	J22374+395	M0.0 V	22:37:29.83	+39:22:45.9	(AB)+C	AB	0.261	11.0	36.56	365.03	…	…

Table D.2: Complete sample with the description of multiple systems (continued).

WDS id	WDS disc	Name	Karmn	Spectral type	α (2016.0)	δ (2016.0)	System	Component	ρ [arcsec]	θ [deg]	ϖ [mas]	$\mu_{\rm total}$ [mas a^{-1}]	$\mathcal{L}$ [$10^{-4}\,\mathcal{L}_\odot$]	$\mathcal{M}$ [$\mathcal{M}_\odot$]
22375+3923	KIR 5	G 216-7B	…	M9.5	22:37:32.51	+39:22:33.7	…	C	33.332	111.5	32.79	351.15	2.42 ± 0.02	0.078 ± 0.012
…	…	G 127-42	J22387+252	M3.5 V	22:38:44.65	+25:13:30.5	…	…	…	…	32.75	284.85	161.19 ± 0.76	0.386 ± 0.016
22385-1519	BLA 10	EZAqr	J22385-152	M5.5 V	22:38:36.17	-15:17:22.7	(AabB)	AabB(3)	0.095	245.8	58.41	3259.86	…	0.333 ± 0.005
22388-2037	HJ 3126	FKAqr	J22387-206S	M1.5 V	22:38:46.09	-20:37:17.4	Aab+Bab	Aab(2)	24.887	349.6	42.66	456.11	…	0.489 ± 0.008
…	…	FLAqr	J22387-206N	M3.5 V	22:38:45.77	-20:36:52.9	…	Bab(1)	24.883	349.6	30.22	429.84	…	0.296 ± 0.007
…	…	GJ 4290	J22406+445	M3.5 V	22:40:42.53	+44:35:47.0	…	…	…	…	31.97	478.30	407.24 ± 12.61	0.471 ± 0.030
…	…	GJ 9793	J22415+188	M0.0 V	22:41:35.30	+18:49:28.9	…	…	…	…	37.15	268.53	1143.69 ± 20.68	0.702 ± 0.026
…	…	1R224134.7+260210	J22415+260	M3.5 V	22:41:35.76	+26:02:13.8	…	…	…	…	33.51	63.05	324.20 ± 2.00	0.447 ± 0.031
…	…	GJ 1271	J22426+176	M2.5 V	22:42:39.99	+17:40:17.6	…	…	…	…	26.76	1218.10	345.97 ± 2.37	0.465 ± 0.030
…	…	GJ 4292	J22433+221	M5.0 V	22:43:23.65	+22:08:18.1	…	…	…	…	64.58	390.11	45.02 ± 0.18	0.221 ± 0.012
…	…	RX J2243.7+1916	J22437+192	M3.0 V	22:43:43.73	+19:16:52.4	…	…	…	…	25.90	106.47	409.73 ± 13.14	0.481 ± 0.030
…	…	TYC 3218-905-1	J22441+405	M1.0 V	22:44:06.16	+40:29:58.1	A+B	A	…	…	68.92	147.00	398.71 ± 1.45	0.489 ± 0.018
22441+4029	LDS1064	TYC 3218-907-1	J22440+405	M1.0 V	22:44:04.51	+40:29:58.5	…	B	18.823	271.0	36.07	133.27	399.40 ± 1.66	0.489 ± 0.018
…	…	LP 641-4	J22457+016	M1.0 V	22:45:46.48	+01:41:22.0	AB	A	…	…	59.63	210.48	…	0.520 ± 0.029
22458+0141	NSN 760	LP 641-4 B	…	M6.5 V	22:45:46.51	+01:41:19.5	…	B	2.533	170.7	38.29	194.61	…	0.105 ± 0.047
…	…	GJ 4294	J22464-066	M5.0 V	22:46:27.09	-06:39:35.0	…	…	…	…	38.48	879.92	24.67 ± 0.13	0.170 ± 0.011
…	…	ELac	J22468+443	M4.0 Ve	22:46:48.68	+44:19:55.0	…	…	…	…	26.50	842.23	125.77 ± 0.85	0.337 ± 0.012
…	…	LP 461-11	J22476+184	M2.5 V	22:47:39.35	+18:26:40.4	…	…	…	…	47.32	433.03	241.62 ± 9.93	0.478 ± 0.022
…	…	GJ 4297	J22479+318	M3.0 V	22:47:54.67	+31:52:18.4	…	…	…	…	134.08	495.59	118.15 ± 0.48	0.307 ± 0.014
…	…	PM J22489+1819	J22489+183	M4.5 V	22:48:54.56	+18:19:56.9	…	…	…	…	147.50	130.21	49.91 ± 0.22	0.219 ± 0.011
…	…	HD 216133	J22503-070	M0.5 V	22:50:19.31	-07:05:22.7	…	…	…	…	48.59	148.74	591.79 ± 2.75	0.590 ± 0.028
…	…	GJ 1274	J22506+348	M2+ V	22:50:38.79	+34:51:26.8	…	…	…	…	48.73	896.32	274.95 ± 1.20	0.452 ± 0.017
…	…	GJ 4300	J22507+286	M2.5 V	22:50:45.77	+28:36:07.7	…	…	…	…	59.20	199.23	239.43 ± 1.20	0.447 ± 0.018
…	…	1R225056.4+495906	J22509+499	M4.0 V	22:50:55.28	+49:59:13.2	…	…	…	…	59.24	123.60	135.56 ± 0.59	0.402 ± 0.017
…	…	GTPeg	J22518+317	M3.5 Ve	22:51:54.19	+31:45:14.4	…	…	…	…	59.75	526.02	262.27 ± 1.26	0.419 ± 0.031
22524+0950	LDS6388	HD 216385	…	F6 V	22:52:24.64	+09:50:09.1	A+(BC)	A	249.637	19.6	56.72	523.35	52617.38 ± 1081.20	1.250 ± 0.188
22524+0950	RAO30	GJ 9801 B	J22524+099	M3.0 V	22:52:30.31	+09:54:04.9	…	BC	250.246	19.6	48.11	530.18	…	0.345 ± 0.034
…	…	LP 48-305	J22526+750	M4.5 V	22:52:40.21	+75:04:16.7	…	…	…	…	47.91	180.65	68.82 ± 0.39	0.279 ± 0.013
…	…	Ross 226	J22543+609	M3.0 V	22:54:19.95	+60:59:41.5	…	…	…	…	28.24	717.82	134.41 ± 0.61	0.350 ± 0.015
…	…	GJ 4302	J22547-054	M4.0 V	22:54:47.14	-05:28:21.1	…	…	…	…	…	696.98	117.96 ± 5.89	0.349 ± 0.018
…	…	ILAqr	J22532-142	M4.0 V	22:53:17.79	-14:16:00.1	Aab	Aab(2)	…	…	36.72	1170.88	…	0.318 ± 0.034
…	…	GJ 4304	J22559+057	M1.0 V	22:55:57.20	+05:45:14.0	A+B	A	…	…	…	446.04	586.61 ± 3.24	0.572 ± 0.028
22560+0546	LDS5021	GJ 4305	…	DA8.1	22:55:56.09	+05:45:18.4	…	B	17.168	284.6	32.13	439.47	…	0.500 ± 0.100
…	…	GJ 4306	J22559+178	M1.0 V	22:55:59.87	+17:48:38.0	…	…	…	…	27.85	112.80	554.72 ± 2.39	0.563 ± 0.028
…	…	HD 216899	J22565+165	M1.5 V	22:56:33.65	+16:33:07.8	…	…	…	…	76.26	1073.03	525.73 ± 5.17	0.548 ± 0.028
…	…	G 189-53A	J22576+373	M3.0 V	22:57:40.20	+37:19:17.8	AB	A	…	…	79.23	658.43	…	0.373 ± 0.032
22577+3719	KPP3388	G 189-53B	…	M5.0 V	22:57:40.10	+37:19:15.6	…	B	2.522	210.7	36.03	668.95	…	0.203 ± 0.039
…	…	1R230251.9+433814	J23028+436	M4.0 V	23:02:52.29	+43:38:15.5	…	…	…	…	42.80	137.69	42.02 ± 0.15	0.199 ± 0.011
…	…	PM J23036+0942	J23036+097	M3.5 V	23:03:37.56	+09:42:59.0	…	…	…	…	31.22	107.10	277.95 ± 1.46	0.483 ± 0.019
…	…	GJ 1278	J23045+667	M0.5 V	23:04:31.03	+66:45:50.5	…	…	…	…	40.41	315.35	1030.77 ± 5.18	0.692 ± 0.026

Table D.2: Complete sample with the description of multiple systems (continued).

WDS id	WDS disc	Name	Karmn	Spectral type	α (2016.0)	δ (2016.0)	System	Component	ρ [arcsec]	θ [deg]	ϖ [mas]	$\mu_{\rm total}$ [mas a^{-1}]	$\mathcal{L}$ [$10^{-4}\,\mathcal{L}_\odot$]	$\mathcal{M}$ [$\mathcal{M}_\odot$]
…	…	PM J23051+5159	J23051+519	M3.5 V	23:05:06.47	+51:59:11.6	…	…	…	…	58.58	121.96	318.43 ± 1.50	0.442 ± 0.031
…	…	GJ 9809	J23060+639	M0.3 V	23:06:05.27	+63:55:33.4	…	…	…	…	58.61	183.38	681.87 ± 3.61	0.603 ± 0.027
…	…	LSPM J2305+4517	J23051+452	M3.5 V	23:05:09.00	+45:17:32.9	AB	A	…	…	48.62	198.80	…	0.485 ± 0.030
…	…	G2-1935209944573613568	…	…	23:05:09.06	+45:17:33.1	…	B*	0.688	78.0	43.64	…	…	…
23064+1235	HDS3291	LP 521-79	J23063+126	M0.5 V	23:06:24.19	+12:36:25.6	(AB)+C	AB(2/3?)	0.467	336.3	50.41	320.69	…	…
23064+1235	GIC 188	G 67-47	…	M3 IV(e)	23:06:25.69	+12:36:55.9	…	C	37.439	36.0	27.66	322.41	130.34 ± 1.14	…
…	…	2MUCD 12171	J23064-050	M7.5 Ve	23:06:30.37	-05:02:36.7	…	…	…	…	26.82	1046.82	5.35 ± 0.03	0.106 ± 0.009
…	…	GJ 4311	J23065+717	M2.0 V	23:06:39.95	+71:43:32.5	…	…	…	…	26.25	1329.33	228.60 ± 1.36	0.410 ± 0.016
…	…	GJ 4312	J23075+686	M3.0 V	23:07:33.27	+68:40:06.1	…	…	…	…	59.84	1143.30	120.11 ± 0.62	0.309 ± 0.014
…	…	GJ 889.1	J23081+033	M0.0 V	23:08:07.49	+03:19:48.5	…	…	…	…	40.13	557.18	316.45 ± 1.35	0.433 ± 0.016
…	…	HKAqr	J23083-154	M0.0 Ve	23:08:19.67	-15:24:36.1	…	…	…	…	141.89	108.68	673.80 ± 3.36	0.608 ± 0.027
…	…	StKM 1-2100	J23088+065	M0.0 V	23:08:52.60	+06:33:39.9	…	…	…	…	62.55	103.94	1130.74 ± 31.91	0.702 ± 0.026
…	…	G 233-42	J23089+551	M5.0 V	23:09:58.62	+55:06:48.1	A+B	A	…	…	80.74	411.27	21.25 ± 0.08	0.156 ± 0.010
23100+5507	NSN 11	LSPM J2309+5506E	…	DA	23:09:59.29	+55:06:50.2	…	B	6.150	69.6	79.80	410.18	…	0.500 ± 0.100
…	…	GJ 4314	J23096-019	M3.5 V	23:09:39.64	-01:58:29.9	AabB	Aab(2)	…	…	36.83	458.40	…	…
23097-0158	CRC 76	G 28-44B	…	M4.0 V	23:09:39.68	-01:58:28.3	…	B	1.697	22.5	58.35	483.31	…	0.286 ± 0.035
…	…	GJ 1281	J23107-192	M2.5 V	23:10:42.22	-19:13:57.9	…	…	…	…	86.87	1435.04	174.71 ± 1.18	0.355 ± 0.015
…	…	G 28-46	J23113+085	M3.0 V	23:11:23.45	+08:30:56.4	AB	A	…	…	24.92	458.92	239.41 ± 33.33	0.426 ± 0.035
…	…	G 28-46B	…	…	23:11:23.47	+08:30:56.4	…	B*	0.248	77.7	24.83	…	…	…
…	…	GJ 4316	J23121-141	M3.0 V	23:12:11.11	-14:06:23.2	…	…	…	…	48.52	720.48	113.47 ± 0.53	0.320 ± 0.014
23167+1937	HDS3316	GJ 893.4	J23166+196	M2.0 V	23:16:39.52	+19:37:14.2	(AB)	AB	0.129	7.8	32.01	252.63	…	0.622 ± 0.038
…	…	GJ 2154 A	J23142-196N	M0.5 Vk	23:14:17.13	-19:38:38.5	A+B	A	…	…	30.06	444.84	748.87 ± 4.05	0.622 ± 0.027
23142-1938	LDS5060	GJ 2154 B	J23142-196S	M4.0 V	23:14:16.97	-19:38:45.4	…	B	7.223	198.2	59.41	451.31	105.55 ± 0.84	0.288 ± 0.013
23175+1937	BEU23	GJ 4326	J23174+196	M2.0 V	23:17:28.54	+19:36:45.1	(AB)	AB	0.145	220.2	42.18	375.65	…	0.400 ± 0.032
…	…	GJ 4319	J23161+067	M3.0 V	22:34:26.25	-00:28:12.9	…	…	…	…	55.50	297.50	171.64 ± 0.91	0.399 ± 0.016
…	…	GJ 4327	J23174+382	M3.0 V	23:17:24.09	+38:12:34.8	Aab	Aab(2)	…	…	39.11	475.88	…	…
…	…	GJ 4329	J23175+063	M3.0 V	23:17:34.73	+06:23:24.5	A+B	A	…	…	123.06	302.15	197.08 ± 0.91	0.403 ± 0.016
…	…	GJ 4319	…	M3.5 V	23:16:08.65	+06:44:32.2	…	B*	1803.432	314.7	118.16	304.89	124.16 ± 0.78	0.336 ± 0.015
…	…	Ross 244	J23182+462	M0.5 V	23:18:18.44	+46:17:23.6	…	…	…	…	40.31	355.18	660.25 ± 2.52	0.602 ± 0.027
…	…	LP 12-69	J23182+795	M3.0 V	23:18:19.85	+79:34:45.8	…	…	…	…	39.31	511.17	226.14 ± 1.14	0.461 ± 0.018
…	…	StKM 1-2115	J23193+154	M1.0 V	23:19:21.03	+15:24:13.5	…	…	…	…	45.12	149.64	638.12 ± 3.17	0.591 ± 0.028
…	…	V368Cep	…	G9 V	23:19:27.78	+79:00:13.8	A+B+C	A	…	…	74.22	215.92	3480.02 ± 11.81	0.900 ± 0.135
23194+7900	LDS2035	HD 220140B	J23194+790	M3.5 V	23:19:25.64	+79:00:04.8	…	B	10.905	214.1	47.72	218.08	305.75 ± 1.31	0.428 ± 0.031
23194+7900	MKR 1	LP 12-90	J23228+787	M5.0 V	23:22:54.97	+78:47:39.6	…	C	962.738	141.1	45.66	217.44	30.51 ± 0.17	0.207 ± 0.012
…	…	LSPM J2321+5651	J23215+568	M1.0 V	23:21:32.23	+56:51:19.7	…	…	…	…	53.66	190.84	597.83 ± 2.98	0.579 ± 0.028
…	…	GJ 4333	J23216+172	M3.5 V	23:21:36.85	+17:17:03.3	…	…	…	…	48.61	1483.04	172.03 ± 0.95	0.375 ± 0.015
…	…	G 217-6	J23220+569	M3.0 V	23:22:01.52	+56:59:21.4	…	…	…	…	109.85	398.39	237.37 ± 0.99	0.445 ± 0.018
…	…	PM J23229+3717	J23229+372	M2.0 V	23:22:58.46	+37:17:13.3	…	…	…	…	32.79	89.99	244.44 ± 1.39	0.425 ± 0.017
…	…	LP 522-65	J23234+155	M2.0 V	23:23:24.72	+15:34:09.2	…	…	…	…	32.34	467.44	358.36 ± 1.41	0.490 ± 0.018
…	…	Ross 302	J23245+578	M1.5 V	23:24:30.39	+57:51:11.0	…	…	…	…	32.42	288.73	547.80 ± 3.12	0.559 ± 0.028

Table D.2: Complete sample with the description of multiple systems (continued).

WDS id	WDS disc	Name	Karmn	Spectral type	α (2016.0)	δ (2016.0)	System	Component	ρ [arcsec]	θ [deg]	ϖ [mas]	$\mu_{\rm total}$ [mas a^{-1}]	$\mathcal{L}$ [$10^{-4}\,\mathcal{L}_\odot$]	$\mathcal{M}$ [$\mathcal{M}_\odot$]
…	…	PM J23549+5036	J23249+506	M3.0 V	23:54:56.57	+50:36:15.0	…	…	…	…	31.40	54.62	135.28 ± 0.69	0.351 ± 0.015
…	…	Wolf 1038	J23252+009	M1.0 V	23:25:16.81	+00:57:44.1	…	…	…	…	61.79	657.67	556.23 ± 3.39	0.570 ± 0.028
…	…	GJ 4334	J23256+531	M5.0 V	23:25:42.10	+53:08:11.1	…	…	…	…	56.76	1065.05	93.76 ± 0.53	0.330 ± 0.015
…	…	GJ 2155	J23262+088	M0.0 V	23:26:12.93	+08:53:41.2	…	…	…	…	77.44	561.15	708.98 ± 3.60	0.624 ± 0.027
23262+1700	JNN138	PM J23261+1700	J23261+170	M4.0 V	23:26:12.00	+17:00:06.9	(AB)	AB	0.273	1.7	94.56	133.35	…	0.280 ± 0.035
…	…	GJ 4336	J23265+121	M2.5 V	23:26:33.26	+12:09:37.9	…	…	…	…	48.64	744.79	234.80 ± 0.97	0.442 ± 0.017
23263+2752	JNN139	V595Peg	J23262+278	M3.0 V	23:26:17.02	+27:52:02.8	(AB)	AB	0.109	328.7	37.24	60.29	…	0.484 ± 0.030
23294+4128	GIC 193	GJ 4337	J23293+414N	M3.0 V	23:29:24.06	+41:28:06.0	A+(BC)	A	17.701	214.1	45.91	411.68	218.46 ± 0.86	0.453 ± 0.018
23294+4128	BWL 59	GJ 4338	J23293+414S	M4.2 V	23:29:23.18	+41:27:51.4	…	BC	17.707	214.0	42.61	405.83	…	0.353 ± 0.033
…	…	AFPsc	J23317-027	M4.5 V	23:31:45.03	-02:44:40.7	A+B	A	…	…	42.60	118.45	253.93 ± 1.55	0.365 ± 0.033
23317-0245	CAB24	2M23301129-0237227	J23301-026	M6.0 V	23:30:11.41	-02:37:23.9	…	B	1469.115	287.3	38.62	122.01	147.11 ± 1.53	0.420 ± 0.018
23309+1547	LDS5096	LP 462-51	J23308+157	M1.0 V	23:30:53.52	+15:47:38.8	(AB)	AB	2.000	320.0	51.07	198.04	…	0.500 ± 0.029
…	…	EQPegA	J23318+199E	M3.5 Ve	23:31:52.83	+19:56:13.2	Aab+Bab	Aab(2)	…	…	26.84	581.09	…	…
23317+1956	WIR 1	EQPegB	J23318+199W	M4.0 Ve	23:31:53.20	+19:56:14.3	…	Bab(1)	5.376	77.6	60.92	552.72	…	…
…	…	G 217-12	J23323+540	M2.0 V	23:32:20.61	+54:01:48.5	…	…	…	…	49.05	217.31	430.72 ± 2.03	0.513 ± 0.029
…	…	HD 221503	…	K6 V	23:32:49.78	-16:50:47.8	A+Bab+CD	A	…	…	56.59	405.45	1267.48 ± 6.60	0.690 ± 0.104
22577-2937	SHY10	GJ 1284	J23302-203	M2.0 Ve	23:30:13.80	-20:23:30.7	…	Bab(2)	12953.999	189.8	26.79	375.23	…	0.133 ± 0.004
23328-1651	LDS 816	GJ 897	J23327-167	M3.0 Ve	23:32:46.98	-16:45:12.3	…	C	337.883	353.2	26.75	681.85	…	…
23328-1645	VOU 28	G3- 2395220664463236992	…	…	23:32:46.98	-16:45:11.7	…	D	0.724	356.4	25.07	…	…	…
…	…	Wolf 1039	J23340+001	M2.5 V	23:34:02.28	+00:10:30.9	…	…	…	…	113.44	1365.84	262.17 ± 1.30	0.433 ± 0.012
…	…	Ross 298	J23350+252	M3.0 V	23:35:03.91	+25:15:00.7	…	…	…	…	43.33	208.10	87.68 ± 0.34	0.261 ± 0.012
…	…	GJ 1286	J23351-023	M5.0 Ve	23:35:11.30	-02:23:34.1	…	…	…	…	23.54	1148.37	14.75 ± 0.08	0.113 ± 0.009
…	…	GJ 4342	J23354+300	M3.5 V	23:35:24.05	+30:03:40.6	…	…	…	…	31.00	328.99	244.14 ± 5.49	0.480 ± 0.020
…	…	GJ 4346	J23357+419	M1.0 V	23:35:45.48	+41:58:06.3	…	…	…	…	31.30	718.17	742.92 ± 4.99	0.615 ± 0.027
…	…	Ross 303	J23364+554	M1.5 V	23:36:26.53	+55:29:42.1	…	…	…	…	42.20	499.31	546.70 ± 2.27	0.558 ± 0.028
…	…	LP 763-3	J23376-128	M5.5 Ve	23:37:38.56	-12:50:33.3	…	…	…	…	44.58	361.40	23.37 ± 0.53	0.193 ± 0.012
…	…	GJ 4352	J23381-162	M2.0 V	23:38:07.84	-16:14:11.4	…	…	…	…	78.88	291.26	198.05 ± 1.11	0.364 ± 0.011
…	…	GJ 4354	J23386+391	M3.3 V	23:38:41.41	+39:09:17.9	…	…	…	…	85.41	567.55	93.24 ± 0.43	0.288 ± 0.013
23350+0136	MEL9	GJ 900	J23350+016	M0.0 V	23:35:00.64	+01:36:19.9	(AB)	AB	1.294	357.0	24.15	341.22	…	…
…	…	GJ 4356	J23389+210	M4.3 V	23:38:56.00	+21:01:24.5	A+B	A	…	…	24.17	328.86	217.21 ± 1.41	0.482 ± 0.019
23389+2101	LDS5108	GJ 4357	…	DA	23:38:56.63	+21:01:21.1	…	B	9.495	110.7	62.88	325.25	…	0.500 ± 0.100
…	…	GJ 4358 A	J23401+606	M1.0 V	23:40:07.91	+60:41:14.4	AB	A	…	…	18.39	299.68	…	0.476 ± 0.030
23401+6041	SKF 283	GJ 4358 B	…	M3.0 V	23:40:08.17	+60:41:12.9	…	B	2.408	127.7	18.55	302.70	…	0.356 ± 0.033
…	…	TYC 1727-1708-1	J23414+200	M0.5 V	23:41:28.99	+20:02:31.0	A+B	A	…	…	31.94	225.26	…	0.592 ± 0.028
23415+2002	UC 5005	LSPM J2341+2002S	…	M2.0 V	23:41:28.97	+20:02:27.0	…	B	4.024	184.1	48.27	222.83	…	0.430 ± 0.031
…	…	HHAnd	J23419+441	M5.0 V	23:41:55.20	+44:10:13.4	…	…	…	…	97.68	1595.62	22.62 ± 0.17	0.141 ± 0.009
…	…	PM J23423+3458	J23423+349	M4.0 V	23:42:22.21	+34:58:25.5	…	…	…	…	38.61	150.76	204.09 ± 2.57	0.466 ± 0.019
…	…	GJ 1288	J23428+308	M5.0 V	23:42:52.33	+30:49:16.9	…	…	…	…	55.83	450.80	31.32 ± 0.16	0.181 ± 0.011
…	…	GJ 1289	J23431+365	M4.5 Ve	23:43:07.56	+36:32:10.7	…	…	…	…	24.25	953.91	55.99 ± 0.35	0.217 ± 0.010
23439+3232	JOD 26	GJ 905.2 A	J23438+325	M1.5 V	23:43:52.84	+32:35:37.8	(AB)+C	AB(2)	0.109	308.0	39.28	223.77	…	…

Table D.2: Complete sample with the description of multiple systems (continued).

WDS id	WDS disc	Name	Karmn	Spectral type	α (2016.0)	δ (2016.0)	System	Component	ρ [arcsec]	θ [deg]	ϖ [mas]	$\mu_{\rm total}$ [mas a^{-1}]	$\mathcal{L}$ [$10^{-4}\,\mathcal{L}_\odot$]	$\mathcal{M}$ [$\mathcal{M}_\odot$]
23439+3232	LDS1070	GJ 905.2 B	…	DA3.8	23:43:50.45	+32:32:45.8	…	C	174.652	190.0	45.59	224.05	…	0.500 ± 0.100
…	…	G 217-18	J23438+610	M3.0 V	23:43:51.95	+61:02:07.5	…	…	…	…	45.63	787.75	79.75 ± 0.31	0.264 ± 0.013
…	…	GJ 1290	J23443+216	M3.4 V	23:44:21.41	+21:36:06.4	…	…	…	…	43.79	462.48	133.34 ± 0.63	0.349 ± 0.015
…	…	Ross 676	J23439+647	M0.3 V	23:44:00.86	+64:44:30.4	Aab	Aab(2)	…	…	24.96	553.71	…	…
…	…	GJ 4360 A	J23455-161	M5.0 V	23:45:30.82	-16:10:28.8	AB	A	…	…	90.49	370.59	…	…
23455-1610	MTG5	GJ 4360 B	…	…	23:45:30.81	-16:10:29.1	…	B	0.323	194.5	89.73	…	…	…
…	…	PM J23462+2826	J23462+284	M3.5 V	23:46:14.17	+28:26:05.0	…	…	…	…	18.32	103.73	88.61 ± 0.35	0.280 ± 0.013
…	…	Ross 249	J23480+490	M3.0 V	23:48:04.16	+49:00:58.4	…	…	…	…	55.39	630.08	135.21 ± 0.71	0.291 ± 0.013
…	…	[R78b] 377	J23489+098	M1.0 V	23:48:58.98	+09:51:53.3	ABC	A	…	…	25.68	156.75	…	0.636 ± 0.027
23490+0952	KPP4328	[R78b] 377B	…	M3.5 V	23:48:59.02	+09:51:55.2	…	B	1.949	19.7	25.65	148.46	…	0.317 ± 0.034
…	…	BRPsc	J23492+024	dM1	23:49:13.58	+02:23:48.9	…	…	…	…	138.23	1387.11	266.00 ± 1.61	0.425 ± 0.012
…	…	GJ 4363	J23492+100	M3.0 V	23:49:15.05	+10:05:32.7	…	…	…	…	65.65	381.33	234.93 ± 1.69	0.471 ± 0.019
…	…	GJ 4364	J23496+083	M1.0 V	23:49:37.78	+08:21:29.1	…	…	…	…	65.38	144.91	518.39 ± 3.41	0.559 ± 0.028
…	…	GJ 4367	J23505-095	dM4.0	23:50:32.33	-09:33:39.5	…	…	…	…	63.77	764.31	107.06 ± 0.95	0.295 ± 0.011
…	…	GJ 4368	J23506+099	M3.0 V	23:50:36.86	+09:56:57.5	AB	A	…	…	52.05	700.59	…	0.482 ± 0.030
23506+0957	BEU 24	GJ 4368 B	…	M4.0 V	23:50:36.94	+09:56:57.3	…	B	1.170	101.0	46.94	649.02	…	0.282 ± 0.035
…	…	GJ 4369	J23509+384	M3.8 V	23:50:53.91	+38:29:30.1	…	…	…	…	42.64	219.87	88.24 ± 0.52	0.299 ± 0.014
…	…	GJ 4370	J23517+069	M3.0 V	23:51:44.72	+06:58:11.8	AB	A	…	…	42.61	292.30	…	0.358 ± 0.033
23517+0658	CRC 77	G 30-26B	…	M3.0 V	23:51:44.86	+06:58:11.3	…	B	2.181	103.0	38.72	299.55	…	0.355 ± 0.033
…	…	GJ 4371	J23523-146	M4.5 V	23:52:23.92	-14:41:28.2	…	…	…	…	72.68	476.88	54.20 ± 1.55	0.245 ± 0.013
…	…	StKM 2-1787	…	K4 V	23:53:35.58	+12:06:20.4	A+B	A	…	…	249.39	120.69	1065.90 ± 4.89	0.730 ± 0.110
23536+1207	VYS 11	PM J23535+1206S	J23535+121	M2.5 Ve	23:53:35.69	+12:06:14.8	…	B	5.785	165.1	249.97	119.44	…	0.573 ± 0.028
…	…	GJ 4373	J23541+516	M3.5 V	23:54:10.95	+51:41:11.0	…	…	…	…	44.91	270.79	138.78 ± 0.60	0.356 ± 0.015
…	…	GJ 4374	J23544+081	M3.0 V	23:54:26.50	+08:09:42.6	…	…	…	…	91.84	291.13	461.83 ± 23.78	0.504 ± 0.030
…	…	RX J2354.8+3831	J23548+385	M4.0 V	23:54:51.28	+38:31:34.8	…	…	…	…	45.03	157.68	103.47 ± 0.55	0.312 ± 0.010
…	…	GJ 4376	J23554-039	M3.5 V	23:55:26.51	-03:58:59.8	…	…	…	…	71.11	522.42	…	0.410 ± 0.031
…	…	LP 523-78	J23560+150	M2.5 V	23:56:00.14	+15:01:37.9	…	…	…	…	29.85	206.28	234.43 ± 1.10	0.442 ± 0.017
…	…	GJ 912	J23556-061	M2.5Vk	23:55:39.27	-06:08:39.4	Aab	Aab(1)	…	…	60.89	611.70	…	0.580 ± 0.020
…	…	G 129-45	J23569+230	M1.5 V	23:56:54.75	+23:05:04.2	A+B	A	…	…	29.87	273.13	901.25 ± 4.07	0.679 ± 0.026
23570+2305	GIC 196	G 129-46	…	M1.73 V	23:56:55.00	+23:04:58.7	…	B	6.488	148.8	77.03	271.30	451.20 ± 2.52	0.531 ± 0.029
23573-1259	BWL 67	GJ 4378	J23573-129E	M4.0 V	23:57:20.81	-12:58:48.6	(AB)+Cab	AB	0.755	342.6	38.34	211.92	…	0.352 ± 0.033
23573-1259	LDS 830	GJ 4379	J23573-129W	M3.0 V	23:57:19.59	-12:58:40.3	…	Cab(2)	19.719	294.8	59.39	209.62	…	…
…	…	GJ 4380	J23577+197	M3.7 V	23:57:45.32	+19:46:03.4	…	…	…	…	38.26	503.23	147.64 ± 0.78	0.368 ± 0.016
…	…	GJ 1292	J23577+233	M3.5 V	23:57:45.32	+23:18:00.1	…	…	…	…	59.50	1444.53	286.19 ± 10.55	0.490 ± 0.021
23578+3838	MCT 14	GJ 4381	J23578+386	M3.0 V	23:57:49.68	+38:37:44.4	(AB)	AB	0.476	210.3	45.09	218.86	…	0.419 ± 0.031
…	…	LP 764-40 A	J23582-174	M2.0 Ve	23:58:13.95	-17:24:34.6	AB	A	…	…	25.46	220.68	…	0.482 ± 0.030
23582-1725	DAE 8	LP 764-40 B	…	M2.0 Ve	23:58:13.94	-17:24:32.5	…	B	2.080	357.0	28.11	226.62	…	0.483 ± 0.030
…	…	Wolf 1051	J23585+076	M3.0 V	23:58:32.74	+07:39:25.0	Aabc	Aabc(3)	…	…	19.28	325.95	…	0.789 ± 0.018
23587+4644	BAG 34	GJ 913	J23587+467	M0.0 V	23:58:44.50	+46:43:44.9	Aab	AB(2?)	0.068	82.6	27.88	652.95	…	…
…	…	G 129-51	J23590+208	M2.5 V	23:59:00.74	+20:51:37.2	AB	A	…	…	60.38	300.02	…	0.537 ± 0.029

Table D.2: Complete sample with the description of multiple systems (continued).

WDS id	WDS disc	Name	Karmn	Spectral type	α (2016.0)	δ (2016.0)	System	Component	ρ [arcsec]	θ [deg]	ϖ [mas]	$\mu_{\rm total}$ [mas a^{-1}]	$\mathcal{L}$ [$10^{-4}\,\mathcal{L}_\odot$]	$\mathcal{M}$ [$\mathcal{M}_\odot$]
…	…	G 129-51B	…	M2.0 V	23:59:00.75	+20:51:36.7	…	B*	0.563	165.6	46.89	301.61	…	0.455 ± 0.030
…	…	GJ 4385	J23598+477	M5.0 V	23:59:50.89	+47:45:41.3	…	…	…	…	47.64	894.90	21.06 ± 0.09	0.155 ± 0.010

Table D.3: Components of multiple system that do not comply with one or more of the criteria for physical parity.

Name[a]	Component[b]	α (J2016.0)	δ (J2016.0)	μratio	ΔPA	Δd	ρ[c] [arcsec]	Cause[d]
PM J00026+3821 B	B*	00:02:40.05	+38:21:45.3	0.214	12.254	0.031	1.415	1
G 217-32 B	B	00:07:43.40	+60:22:53.8	0.196	9.161	0.0032	0.848	1
LP 296-56	B	01:56:41.74	+30:28:34.6	0.012	0.027	0.163	299.1	3
PM J02024+1034 A	B	02:02:28.18	+10:34:52.7	0.545	32.513	0.012	0.911	1
LP 198-637 B	B	03:20:45.35	+39:42:59.6	0.152	8.738	0.0051	0.795	1
PM J03247+4447 B	B	03:24:42.23	+44:47:39.7	0.191	4.590	0.0048	1.912	1
Gaia EDR3 3296932486866670720	B	04:05:38.89	+05:44:40.1	0.331	1.614	…	0.817	1, 2
GJ 2033 B	B	04:16:41.80	-12:33:19.8	0.334	11.137	0.0069	2.990	1
HG 7-232 B	B	04:28:29.01	+17:41:45.3	0.227	11.403	0.047	1.663	1
V697 Tau B	B	04:33:23.87	+23:59:26.5	0.200	11.095	0.150	0.767	1
GJ 3305 (J04376-024)	BC	04:37:37.51	-02:29:29.7	0.274	14.659	0.077	0.098	1
PM J04393+3331 (J04393+335)	BC	04:39:23.22	+33:31:48.7	0.147	7.913	0.333	0.126	1
GJ 9163 B	B	04:40:29.15	-09:11:46.8	0.441	1.954	0.0064	1.715	1
GJ 3322 B	B	05:01:58.89	+09:58:55.9	0.152	8.744	0.0015	1.398	1
HD 32450 B	B	05:02:28.26	-21:15:27.5	0.247	6.461	0.0063	0.888	1
LP 359-186	BC	05:03:05.77	+21:22:33.8	0.046	0.799	0.104	0.302	1, 2
GJ 3332 (J05068-215W)	B	05:06:49.48	-21:35:04.3	0.881	58.265	0.0018	8.489	1
BD-21 1074 C	C	05:06:49.55	-21:35:04.7	0.309	8.384	0.0029	1.1	1
GJ 3343 (J05206+587S)	B	05:20:41.05	+58:47:12.0	0.021	1.037	0.104	14	3
PM J05243-1601 B	B	05:24:19.17	-16:01:15.6	0.964	52.141	0.0066	0.4	1
GJ 3348A (J05289+125)	C	05:28:56.61	+12:31:50.4	0.023	1.307	0.169	99.39	2
PM J05319-0303W	C	05:31:57.88	-03:03:37.6	0.254	4.659	0.034	150.0	5
2MASS J05315816-0303397	D	05:31:58.17	-03:03:40.7	0.257	5.562	0.048	144.8	5
ESO-HA 737	E	05:32:05.97	-03:01:16.8	0.209	5.090	0.046	254.2	5
PM J06066+4633 B	B	06:06:37.77	+46:33:45.2	0.198	2.085	0.00038	1.790	1

Table D.3: Components of multiple system that do not comply with one or more of the criteria for physical parity (continued).

Name[a]	Component[b]	α (J2016.0)	δ (J2016.0)	μratio	ΔPA	Δd	ρ[c] [arcsec]	Cause[d]
LP 362-121 (J06103+225)	B	06:10:22.52	+22:34:18.1	0.057	1.898	0.258	65.16	2
Ross 603 B	B	06:27:43.74	+09:23:50.5	0.167	8.901	0.0052	1.170	1
Gaia EDR3 2926756741750933120	B*	06:39:37.22	-21:01:31.9	0.590	11.207	0.025	0.556	1
2MASS J07293670+3554531	C	07:29:36.67	+35:54:51.3	0.171	6.262	0.0063	95.88	3
Castor C (J07346+318)	Cab	07:34:37.19	+31:52:08.6	0.220	11.459	0.034	TBD	1
FP Cnc B (J08089+328)	Cab	08:08:55.38	+32:49:01.4	0.189	10.740	0.022	< 0.92 au	1
GJ 1116 B	B	08:58:14.21	+19:45:46.7	0.236	5.329	0.011	2.175	1
LP 489-1	B*	09:56:45.21	+11:34:23.6	0.326	18.840	0.032	1356.0	TBD
GJ 397.1 B (J10315+570)	BC	10:31:30.64	+57:05:20.4	0.166	3.931	…	0.284	1, 2
PM J10367+1521 B	BC	10:36:44.92	+15:21:37.9	0.174	5.147	…	0.132	1, 2
GJ 3616 B	B	10:44:52.43	+32:24:40.1	0.067	2.466	0.129	1.296	1
GJ 3617	C	10:44:54.79	+32:24:23.4	0.079	4.417	0.125	35.23	TBD
GJ 3628 (J10506+517)	B	10:50:37.91	+51:45:01.6	0.219	12.290	0.013	178.3	3
HD 98712 B (J11214-204)	B	11:21:26.84	-20:27:11.5	0.266	5.851	0.046	3.811	1
GJ 426.1 B	B	11:23:55.75	+10:31:44.7	0.213	11.741	0.020	2.050	1
Gaia EDR3 3699797155055781760	B	12:20:25.60	+00:35:01.3	0.641	30.528	0.0055	0.882	1
GJ 490 B (J12576+352W)	CD	12:57:38.94	+35:13:16.9	0.106	5.090	0.117	0.171	1
PM J13260+2735 B	C	13:26:02.63	+27:35:02.5	0.201	8.729	0.0015	1.485	1
GJ 520 B	B	13:37:50.77	+48:08:16.3	0.166	5.256	0.000046	1.621	1
Gaia EDR3 1658968054798747008	B	13:41:46.39	+58:15:18.6	0.360	13.784	0.0078	0.762	1
GJ 536.1 B	B	14:01:58.89	+15:29:39.1	0.167	7.680	0.0020	1.621	1
PM J14019+4316 B	B	14:01:58.69	+43:16:43.1	0.151	8.700	0.00081	1.960	1
HD 124498 B	B	14:14:21.34	-15:21:24.4	0.175	9.130	0.077	1.553	1
G 224-13 B	B	14:33:06.80	+61:00:43.6	0.190	10.854	0.0018	0.971	1
GJ 9492 B	B	14:42:21.17	+66:03:20.1	0.221	11.795	0.0013	2.290	1

Table D.3: Components of multiple system that do not comply with one or more of the criteria for physical parity (continued).

Name[a]	Component[b]	α (J2016.0)	δ (J2016.0)	μratio	ΔPA	Δd	ρ[c] [arcsec]	Cause[d]
GJ 569 B	Bab	14:54:29.77	+16:06:05.6	0.215	7.832	0.067	0.097	1
Gaia EDR3 1275127175448008448	B*	15:18:49.78	+29:15:06.7	0.302	8.736	0.037	0.588	1
Gaia EDR3 1375767330164975616	B	15:33:54.89	+37:54:48.3	0.234	13.506	0.0022	0.834	1
LP 331-57 B	B	17:03:53.14	+32:11:46.4	0.175	3.536	0.0055	1.393	1
BD+19 3268 B	B	17:15:49.84	+19:00:00.3	0.699	3.435	0.0044	1.471	1
RX J1734.0+4447 B (J17340+446)	B	17:34:05.47	+44:47:08.4	0.403	17.500	0.058	0.633	1
GJ 4021	C	17:38:40.87	+61:14:00.0	0.232	11.069	0.016	19.05	1
GJ 695 C (J17464+277)	E	17:46:24.65	+27:42:49.8	0.160	0.847	0.0039	0.575	1
HD 230017 B (J18548+109)	B	18:54:53.86	+10:58:45.1	0.512	6.480	0.0041	3.792	1
PM J18542+1058	C*	18:54:17.14	+10:58:11.0	0.170	2.601	0.0078	538.9	1
StKM 1-1676 B	C	19:03:17.96	+63:59:37.4	0.824	54.189	…	3.578	1
GJ 4115 (J19351+084N)	C	19:35:06.33	+08:27:43.4	0.462	17.584	0.062	5.635	1
GJ 1245 B (J19539+444E)	C	19:53:55.66	+44:24:46.5	0.174	9.449	0.0068	5.945	1
LP 395-8 B	B	20:19:49.35	+22:56:40.0	0.184	10.601	0.000044	1.918	1
GJ 4153 B	B	20:37:23.97	+21:56:21.4	0.072	0.221	0.217	51.77	2
AT Mic B	B	20:41:51.54	-32:26:15.1	0.298	13.947	0.012	2.102	1
PM J21055+0609S	B*	21:05:32.17	+06:09:11.2	0.175	5.680	0.000069	5.094	1
GJ 9721 B (J21087-044N)	C	21:08:44.75	-04:25:18.3	0.652	12.094	0.012	20.89	1
GJ 4188 (J21176-089S)	C	21:17:39.55	-08:54:49.6	0.166	7.927	0.098	63.99	1
GJ 4201 B	B	21:32:22.23	+24:33:41.1	0.181	9.559	0.0029	1.548	1
GJ 834 B	B	21:36:38.20	+39:27:17.8	0.181	9.172	0.0041	1.003	1
UCAC4 747-070768	B	21:51:39.93	+59:17:34.5	0.384	20.069	0.041	14.64	1
Ross 268	C*	22:06:23.02	+17:22:22.1	0.210	8.636	0.081	5100.6	1
LP 759-25	B	22:05:35.44	-11:04:31.8	0.053	3.002	0.323	3030.6	3
Wolf 1225 B	B	22:23:29.34	+32:27:29.5	0.271	12.352	0.0040	1.252	1

Table D.3: Components of multiple system that do not comply with one or more of the criteria for physical parity (continued).

Name[a]	Component[b]	α (J2016.0)	δ (J2016.0)	μratio	ΔPA	Δd	ρ[c] [arcsec]	Cause[d]
DO Cep	B	22:27:57.93	+57:41:38.8	0.438	19.178	0.0023	1.420	1
GJ 4282 B	B	22:33:22.87	-09:36:53.7	0.172	5.466	0.0022	1.399	1
2M J23301129-0237227 (J23301-026)	B	23:30:11.41	-02:37:23.9	0.069	3.658	0.232	1469.1	4
EQ Peg B (J23318+199W)	Bab	23:31:53.20	+19:56:14.3	0.152	8.006	0.0015	5.376	1
GJ 897 (J23327-167)	C	23:32:46.98	-16:45:12.3	0.938	66.572	…[e]	337.9	2
LSPM J2350+1013	C*	23:50:24.02	+10:13:47.9	0.152	7.831	0.051	1818.3	TBD

[a] Karmn identification in parentheses, when available.
[b] Component within the system it belongs to. An asterisk (*) denotes new components found.
[c] Projected separation of the closest component.
[d] Causes: 1: Presence of a very close companion ($\lesssim$ 220 au), also applicable to the primary; 2: Parallactic distances and proper motions from a source different than *Gaia* DR3, with larger uncertainties, or missing values; 3: Component A is candidate to binary; 4: Candidate to binary system; 5: Young stellar object candidate. These systems undergo a process of dynamical stabilisation; TBD: To be determined.
[e] Parallax from Hipparcos (van Leeuwen, 2007) removed because of very large relative error.

Table D.4: Star candidates belonging to multiple systems not tabulated by WDS.

Name	Karmn	Spectral type	Component[a]	Class[b]	α (J2016.0)	δ (J2016.0)	π [mas]	$\mu_{\rm total}$ [mas a^{-1}]	G [mag]	θ [deg]	ρ [arcsec]	Notes[c]
PM J00026+3821A	J00026+383	M4.0 V	A	Binary*	00:02:40.00	+38:21:44.1	24.622 ± 0.210	74.86 ± 0.21	13.193			
PM J00026+3821B		…	B*		00:02:40.05	+38:21:45.3	25.392 ± 0.368	71.14 ± 0.46	13.388	28.1	1.415	•
GJ 3022	J00169+200	M3.5 V	A	Triple*	00:16:57.03	+20:03:55.7	29.310 ± 0.097	239.54 ± 0.21	13.183			
G 131-47B		M3.5 V	B		00:16:57.10	+20:03:55.4	29.139 ± 0.071	233.36 ± 0.32	13.261	106.5	1.077	
LP 404-54		M5.0 V	C*		00:15:13.81	+19:47:40.5	28.873 ± 0.034	233.80 ± 0.05	14.874	236.2	1752.0	
V493 And A	J00341+253	M0.0 V	A	Triple*	00:34:08.48	+25:23:48.5	20.101 ± 0.039	127.91 ± 0.05	11.226			•
V493 And B		K7 V	B		00:34:08.59	+25:23:48.2	19.720 ± 0.037	129.46 ± 0.06	11.276	102.3	1.536	
UCAC4 578-001365		M4.0 V	C*		00:34:20.04	+25:28:12.9	19.672 ± 0.234	127.04 ± 0.35	15.058	30.6	307.2	
Wolf 58	J01133+589	M1.5 Ve	A	Binary*	01:13:20.12	+58:55:20.3	36.025 ± 0.017	210.93 ± 0.02	10.894			•
Gaia EDR3 414108140954108672		M5.0 V	B*		01:13:19.97	+58:55:18.6	35.974 ± 0.088	200.51 ± 0.11	14.516	213.9	2.082	
GJ 3131	J02033-212	M2.5 V	Aab	Triple*	02:03:20.52	-21:13:50.2	46.672 ± 0.041	471.89 ± 0.05	10.169			
GJ 3131 B		…	B*		02:03:20.25	-21:13:51.5	46.747 ± 0.307	450.04 ± 0.47	18.661	251.9	4.008	
Ross 369A	J03145+594	M2.5 V	A	Binary*	03:14:33.17	+59:26:13.8	36.823 ± 0.126	250.95 ± 0.18	11.571			
Ross 369B		M3.0 V	B*		03:14:33.10	+59:26:13.2	36.496 ± 0.167	237.34 ± 0.24	12.236	221.0	0.775	
1RXS J033021.4+344044	J03303+346	M4.0 V	A	Triple*	03:30:23.37	+34:40:31.7	…	56.66 ± 2.14	13.371			•
Gaia EDR3 221088045766546816		M1.5 V	B*		03:30:16.90	+34:39:50.2	11.375 ± 0.057	53.59 ± 0.08	14.389	242.5	89.96	
Gaia EDR3 221088050062935680		M3.0 V	C*		03:30:16.80	+34:39:49.2	11.725 ± 0.234	52.34 ± 0.36	14.788	242.3	91.48	
GJ 3256	J03544-091	M1.0 V	A	Binary*	03:54:25.52	-09:09:29.2	47.406 ± 0.023	146.38 ± 0.03	10.540			
GJ 3256 B		M3.0 V	B*		03:54:25.61	-09:09:32.0	47.545 ± 0.035	138.31 ± 0.04	11.889	153.6	3.182	•
Ross 25	J04011+513	M4.0 V	A	Binary*	04:01:08.18	+51:23:06.4	39.816 ± 0.021	883.46 ± 0.03	12.435			
LSPM J0401+5131		DC8	B*		04:01:02.14	+51:31:17.2	39.836 ± 0.077	883.24 ± 0.12	17.113	353.4	494.0	
GJ 3261	J04056+057	M4.0 Ve	A	Triple*	04:05:38.94	+05:44:40.4	16.094 ± 0.103	47.98 ± 0.15	12.028			
Gaia EDR3 3296932486866670720		…	B		04:05:38.89	+05:44:40.1	…	…	12.814	251.9	0.817	
ATO J061.4727+05.5235		M3.0 V	C*		04:05:53.46	+05:31:24.6	15.876 ± 0.026	49.85 ± 0.03	14.012	164.8	824.8	
LP 414-117	J04123+162	M4.0 V	Aab	Triple*	04:12:21.90	+16:15:02.9	28.240 ± 0.091	156.84 ± 0.15	12.669			•
LSPM J0409+1622		M5.5 V	B*		04:09:57.30	+16:22:41.3	28.769 ± 0.051	161.15 ± 0.08	15.525	282.5	2131.6	
TYC 78-257-1		…	A	Binary*	04:21:04.26	+03:16:07.9	26.974 ± 0.022	139.56 ± 0.03	9.154			
RX J0422.4+0337	J04224+036	M3.5 V	B*		04:22:25.19	+03:37:08.5	27.846 ± 0.026	143.01 ± 0.04	12.774	43.9	1748.6	
LP 415-345	J04425+204	M3.0 V	Aab	Quadruple*	04:42:30.40	+20:27:10.8	20.476 ± 0.022	97.45 ± 0.03	12.146			•

Table D.4: Star candidates belonging to multiple systems not tabulated by WDS (continued).

Name	Karmn	Spectral type	Component[a]	Class[b]	α (J2016.0)	δ (J2016.0)	π [mas]	$\mu_{\rm total}$ [mas a^{-1}]	G [mag]	θ [deg]	ρ [arcsec]	Notes[c]
LP 415-3051		M3.0 V	B		04:42:58.58	+20:36:16.8	19.426 ± 0.020	91.26 ± 0.03	13.767	35.9	674.3	
Gaia DR2 3411054848866601472		M6.0 V	C*		04:43:55.36	+20:08:40.5	19.484 ± 0.118	93.82 ± 0.18	17.282	132.8	1631.4	
PM J04429+0935	J04429+095	M1.0 V	A	Binary*	04:42:55.14	+09:35:53.7	28.741 ± 0.024	82.04 ± 0.03	11.142			
Gaia EDR3 3293060625388613248		M6.5 V	B		04:42:53.91	+09:35:50.3	28.684 ± 0.086	77.51 ± 0.12	16.753	259.1	18.39	
LP 416-43	J04480+170	M0.5 V	Aab	Triple*	04:48:00.98	+17:03:21.1	20.164 ± 0.088	82.10 ± 0.14	10.526			
UCAC4 536-010184		M4.5 V	B*		04:49:36.67	+17:01:58.6	19.838 ± 0.027	87.10 ± 0.04	14.761	93.4	1374.8	
RX J0507.2+3731A	J05072+375	M5.0 V	A	Binary*	05:07:14.33	+37:30:42.1	43.800 ± 4.000	102.11 ± 4.90	13.950			•
RX J0507.2+3731B		M5.0 V	B*		05:07:14.37	+37:30:42.1	44.022 ± 0.461	96.09 ± 0.82	14.300	93.2	0.476	
PM J05334+4809		M0.0 V	A	Quadruple*	05:33:28.97	+48:09:26.2	30.270 ± 0.018	66.93 ± 0.02	10.788			
PM J05341+4732A	J05341+475	M2.5 V	B		05:34:10.56	+47:32:02.8	30.050 ± 0.027	69.01 ± 0.03	11.635	169.4	2282.1	
PM J05341+4732B		M3.0 V	C		05:34:10.62	+47:32:05.2	30.039 ± 0.023	61.85 ± 0.03	12.671	169.3	2280.0	
UPM J0533+4809		M3.5 V	D		05:33:16.22	+48:09:23.3	30.229 ± 0.235	65.01 ± 0.31	13.236	268.7	127.6	
G 106-7	J05530+047	M1.5 V	A	Binary*	05:53:04.75	+04:43:02.6	24.715 ± 0.056	391.42 ± 0.10	11.325			
G 106-7B		M5.5 V	B*		05:53:04.65	+04:43:02.8	24.818 ± 0.208	387.78 ± 0.40	16.120	278.2	1.520	•
PM J05558+4036	J05558+406	M1.0 V	A	Binary*	05:55:48.31	+40:36:48.0	27.777 ± 0.043	122.73 ± 0.05	11.423			
Gaia EDR3 3458612029599345664		M3.0 V	B*		05:55:48.41	+40:36:47.7	27.966 ± 0.110	138.62 ± 0.12	12.814	103.0	1.200	
LP 780-32	J06396-210	dM4.0 V	A	Binary*	06:39:37.20	-21:01:32.4	63.738 ± 0.886	225.54 ± 0.94	12.267			•
Gaia EDR3 2926756741750933120		M4.0 V	B*		06:39:37.22	-21:01:31.9	65.308 ± 0.325	146.66 ± 0.34	12.022	35.1	0.556	
LP 780-23	J06401-164	M2.5 V	A	Binary*	06:40:08.72	-16:27:21.5	…	319.03 ± 11.31	12.315			•
LP 780-23 B		…	B*		06:40:08.72	-16:27:21.7	…	…	12.438	187.9	0.199	
1RXS J073138.4+455718		M3.0 V	Aab	Quadruple*	07:31:38.47	+45:57:15.8	17.880 ± 0.416	93.78 ± 0.48	12.766			
1RXS J073101.9+460030	J07310+460	M4.0 V	B		07:31:01.27	+46:00:24.8	18.141 ± 0.052	101.75 ± 0.06	12.896	296.0	431.4	
Gaia EDR3 975312928903090560		M4.5 V	C*		07:31:09.03	+45:56:55.6	18.388 ± 0.034	100.74 ± 0.04	15.219	266.3	307.8	
GJ 3461	J07418+050	M3.0 V	Aab	Binary*	07:41:52.56	+05:02:23.1	36.109 ± 0.030	263.05 ± 0.04	11.624			
G 50-1B		…	B*		07:41:52.61	+05:02:22.4	…	…	16.860	130.9	1.014	
1RXS J090406.8-155512	J09040-159	M2.5 V	A	Binary*	09:04:05.44	-15:55:19.0	36.628 ± 0.021	113.77 ± 0.03	11.754			
V405 Hya		K2.0 V	B*		09:04:20.57	-15:54:51.8	36.512 ± 0.022	112.03 ± 0.03	8.464	82.9	220.0	
GJ 3576	J09579+118	M4.0 V	A	Binary*	09:57:57.54	+11:48:26.3	39.565 ± 0.048	451.50 ± 0.06	13.184			
LP 489-1		M5.0 V	B*		09:56:45.21	+11:34:23.6	40.843 ± 0.032	456.96 ± 0.04	14.267	231.6	1356.0	

Table D.4: Star candidates belonging to multiple systems not tabulated by WDS (continued).

Name	Karmn	Spectral type	Component[a]	Class[b]	α (J2016.0)	δ (J2016.0)	π [mas]	$\mu_{\rm total}$ [mas a^{-1}]	G [mag]	θ [deg]	ρ [arcsec]	Notes[c]
GJ 375.2	J10004+272	M0.5 V	A	Triple*	10:00:26.69	+27:16:03.5	27.767 ± 0.016	118.42 ± 0.02	10.528			
2MASS J10003572+2717054		M6.5 V	B		10:00:35.70	+27:17:07.5	27.723 ± 0.103	118.34 ± 0.13	16.928	61.9	136.0	
Gaia EDR3 740041664172917376		M7.5 V	C*		10:00:26.56	+27:16:05.7	26.561 ± 0.349	117.20 ± 0.34	17.609	320.9	2.882	
GJ 3602	J10284+482	M3.5 V	A	Binary*	10:28:28.86	+48:14:17.7	48.600 ± 3.300	615.83 ± 11.31	12.616			•
G 146-35B		…	B*		10:28:28.87	+48:14:17.8	…	…	12.633	48.9	0.196	
StKM 1-950	J11307+549	M1.0 V	A	Binary*	11:30:43.80	+54:57:29.1	24.778 ± 0.018	111.40 ± 0.02	11.019			
Gaia EDR3 844502037681090688		M6.0 V	B*		11:30:42.66	+54:56:57.0	24.731 ± 0.056	112.07 ± 0.07	16.672	197.0	33.61	
PM J13182+7322	J13182+733	M3.5 V	A	Binary*	13:18:13.82	+73:22:05.6	39.534 ± 0.021	129.46 ± 0.04	12.396			
PM J13182+7322B		M7.0 V	B*		13:18:13.11	+73:22:12.4	39.276 ± 0.098	122.66 ± 0.16	16.888	335.7	7.387	
PM J13255+2738		M1.0 V	A	Triple*	13:25:35.66	+27:38:08.9	21.996 ± 0.019	71.21 ± 0.03	11.689			
PM J13260+2735A	J13260+275	M3.0 V	B*		13:26:02.70	+27:35:03.7	21.868 ± 0.070	72.89 ± 0.11	12.410	117.2	404.4	
PM J13260+2735B		M2.5 V	C		13:26:02.63	+27:35:02.5	22.030 ± 0.057	63.57 ± 0.09	13.131	117.4	404.1	
BD+30 2400	J13282+300	M0.0 V	A	Triple*	13:28:17.53	+30:02:43.0	24.698 ± 0.058	260.99 ± 0.07	10.509			
BD+30 2400B		…	B		13:28:17.48	+30:02:44.1	…	…	14.577	324.0	1.247	
LP 323-115		M7.0 V	C*		13:28:20.69	+30:03:15.8	24.101 ± 0.117	259.70 ± 0.14	17.314	51.3	52.48	
StKM 1-1229	J15188+292	M1.0 V	A	Triple*	15:18:49.75	+29:15:06.4	20.173 ± 0.523	98.17 ± 0.53	11.682			
Gaia EDR3 1275127175448008448		M0.0 V	B*		15:18:49.78	+29:15:06.7	20.926 ± 0.337	78.58 ± 0.30	11.489	50.9	0.588	
UCAC4 597-051773		M3.5 V	C		15:18:48.67	+29:14:05.7	19.839 ± 0.018	86.82 ± 0.02	14.157	193.1	62.26	
RX J1548.0+0421	J15480+043	M2.5 V	A	Binary*	15:48:02.78	+04:21:38.4	34.436 ± 0.027	58.85 ± 0.04	11.718			
UCAC4 472-052890		M4.0 V	B*		15:47:54.89	+04:18:02.9	34.579 ± 0.023	58.38 ± 0.03	13.186	208.7	245.6	
HD 230017A		M0.0 V	A	Triple*	18:54:53.67	+10:58:42.4	53.423 ± 0.108	133.27 ± 0.16	8.799			
HD 230017B	J18548+109	M3.5 V	B		18:54:53.86	+10:58:45.1	53.644 ± 0.043	89.29 ± 0.06	11.441	45.1	3.792	
PM J18542+1058		M4.0 V	C*		18:54:17.14	+10:58:11.0	53.838 ± 0.024	114.61 ± 0.03	12.362	266.7	538.9	
1RXS J190405.9+211030	J19041+211	M2.0 Ve	A	Binary*	19:04:06.24	+21:10:32.7	27.742 ± 0.079	131.32 ± 0.10	11.429			
PM J19041+2110 B		…	B*		19:04:06.24	+21:10:33.2	…	…	21.153	353.4	0.526	
LSPM J1918+5803	J19185+580	M1.0 V	A	Binary*	19:18:30.48	+58:03:16.6	26.266 ± 0.012	178.63 ± 0.02	11.271			
Gaia EDR3 2143230844400445696		M8.0 V	B*		19:18:30.33	+58:03:18.1	26.310 ± 0.231	190.05 ± 0.40	17.978	323.8	1.925	
2MASS J19204172+7311434	J19206+731S	M4.0 V	A	Binary*	19:20:41.75	+73:11:42.4	32.782 ± 0.014	74.49 ± 0.02	13.598			
2MASS J19204172+7311467	J19206+731N	M4.5 V	B*		19:20:41.76	+73:11:45.5	32.791 ± 0.014	82.50 ± 0.02	13.830	0.0	3.182	•

Table D.4: Star candidates belonging to multiple systems not tabulated by WDS (continued).

Name	Karmn	Spectral type	Component[a]	Class[b]	α (J2016.0)	δ (J2016.0)	π [mas]	$\mu_{\rm total}$ [mas a^{-1}]	G [mag]	θ [deg]	ρ [arcsec]	Notes[c]
GJ 4144	J20195+080	M3.0 V	A	Binary*	20:19:34.60	+08:00:27.1	26.833 ± 0.129	210.99 ± 0.19	12.393			
Gaia EDR3 4250232535851803136		M3.0 V	B*		20:19:34.55	+08:00:26.9	26.582 ± 0.128	200.82 ± 0.18	12.760	258.3	0.777	
LP 395-8 A	J20198+229	M3.0 V	Aab	Quadruple*	20:19:49.36	+22:56:38.1	33.897 ± 0.026	135.40 ± 0.03	11.023			
LP 395-8 B		M3.5 V	B		20:19:49.35	+22:56:40.0	33.896 ± 0.053	137.73 ± 0.06	12.875	355.5	1.918	
Gaia EDR3 1829571684884360832		…	C*		20:19:48.73	+22:56:44.8	33.938 ± 0.342	142.76 ± 0.36	19.419	307.4	11.02	•
TYC 1643-120-1	J20220+216	M2.0 V	A	Binary*	20:22:01.62	+21:47:19.7	37.091 ± 0.028	131.82 ± 0.03	11.290			
PM J20220+2147B		M4/5 V	B*		20:22:01.98	+21:47:21.8	37.147 ± 0.042	133.78 ± 0.04	14.815	67.5	5.445	
PM J21055+0609N	J21055+061	M3.0 V	A	Binary*	21:05:32.09	+06:09:16.2	44.368 ± 0.033	52.64 ± 0.04	11.459			
PM J21055+0609S		M5.5 V	B*		21:05:32.17	+06:09:11.2	44.365 ± 0.033	61.85 ± 0.04	14.855	166.0	5.094	
PM J21057+5015E	J21057+502	M3.5 V	A	Binary*	21:05:45.54	+50:15:44.1	27.714 ± 0.015	100.51 ± 0.02	12.453			
PM J21057+5015W		M3.5 V	B*		21:05:42.60	+50:15:58.1	27.653 ± 0.016	97.27 ± 0.03	12.983	296.4	31.47	
G 126-32A		M1.0 V	A	Triple*	21:45:04.94	+19:53:31.8	27.661 ± 0.127	219.44 ± 0.14	11.554			
G 126-32B	J21450+198	M1.5 V	B		21:45:04.90	+19:53:31.7	26.818 ± 0.296	240.74 ± 0.41	11.946	253.2	0.564	
G 126-32C		…	C*		21:45:05.04	+19:53:36.9	26.252 ± 0.803	232.18 ± 1.02	19.824	16.4	5.317	
a Ross 265	J22018+164	M2.5 V	AB	Triple*	22:01:49.49	+16:28:05.2	61.790 ± 2.230	421.76 ± 3.03	9.971			•
Ross 268		M3.5 V	C*		22:06:23.02	+17:22:22.1	56.763 ± 0.032	371.56 ± 0.04	11.830	50.2	5100.6	
LF 4 +54 152	J22129+550	M0.0 V	A	Binary*	22:12:56.63	+55:04:50.8	18.385 ± 0.153	109.13 ± 0.25	10.222			
Gaia EDR3 2005884249925303168		M6.5 V	B*		22:13:00.46	+55:05:48.3	18.550 ± 0.079	108.97 ± 0.12	17.702	29.8	66.26	•
LSPM J2305+4517	J23051+452	M3.5 V	A	Binary*	23:05:09.00	+45:17:32.9	22.102 ± 0.157	198.80 ± 0.18	12.356			
Gaia DR2 1935209944573613568		…	B*		23:05:09.06	+45:17:33.1	…	…	14.308	78.0	0.688	•
G 28-46	J23113+085	M3.0 V	A	Binary*	23:11:23.45	+08:30:56.4	49.800 ± 3.300	458.92 ± 11.31	11.857			•
G 28-46B		…	B*		23:11:23.47	+08:30:56.4	…	…	11.863	77.7	0.248	•
GJ 4329	J23175+063	M3.0 V	A	Binary*	23:17:34.73	+06:23:24.5	48.918 ± 0.027	302.15 ± 0.04	11.429			
GJ 4319		M3.5 V	B*		23:16:08.65	+06:44:32.2	48.976 ± 0.026	304.89 ± 0.04	11.994	314.7	1803.4	
G 129-51	J23590+208	M2.5 V	A	Binary*	23:59:00.74	+20:51:37.2	19.284 ± 0.448	300.02 ± 0.54	12.265			
G 129-51B		M2.0 V	B*		23:59:00.75	+20:51:36.7	19.478 ± 0.146	301.61 ± 0.18	12.862	165.6	0.563	•

[a] An asterisk (*) denotes the new component found in each system.

[b] An asterisk (*) denotes the upgraded multiplicity order as the new found component is included.

[c] PM J00026+3821B: Component included in Table A.1 of Cifuentes et al. (2020), but not in WDS. V493 And A: Candidate to binary (criteria 1 and 2 in Table 4.2), thus a quadruple system. Wolf 58: The star has confirmed planet(s). 1RXS J033021.4+344044: Proper motions does not come from *Gaia*. GJ 3256 B: Component included in Table A.1 of Cifuentes et al. (2020), but not in WDS. LP 414-117: Hyades? LP 415-345: Hyades? RX J0507.2+3731A: Parallax and proper motions do not come from *Gaia*. G 106-7B: Component included in Table A.1 of Cifuentes et al. (2020), but not in WDS. LP 780-32: The star has confirmed planet(s). LP 780-23: Proper motions does not come from *Gaia*. GJ 3602: Parallax and proper motions do not come from *Gaia*. 2MASS J19204172+7311467: The star has confirmed planet(s). Gaia EDR3 1829571684884360832: Blended background object in the epoch of *Gaia*. Ross 265: Parallax and proper motions do not come from *Gaia*. *Gaia* EDR3 2005884249925303168: White dwarf candidate (Jiménez-Esteban et al., 2018). *Gaia* DR2 1935209944573613568: Component included in Table A.1 of Cifuentes et al. (2020), but not in WDS. G 28-46: Parallax and proper motions do not come from *Gaia*. G 28-46B: Sabotta et al. (2021) finds a 2225-day periodicity. G 129-51B: Component included in Table A.1 of Cifuentes et al. (2020), but not in WDS.

Table D.5: Spectroscopic binaries in Carmencita.

Name	Karmn	Type[a]	P_{orb} [d]	a [au]	Reference[b]
HD 38A		SB	…	…	Str93
1R000806.3+475659	J00081+479	SB2	4.4	0.04	Shk10 / Fou18
EZPsc	J00162+198W	SB2	3.95652 ± 0.00008	0.038623	Bar18
FFAnd	J00428+355	SB2	…	…	Bop77 / Giz02
RX J0050.2+0837	J00502+086	SB2	…	…	Jeff18
GJ 1029	J01056+284	SB2	95.76 ± 0.18	0.1331	Bar18 / Win20a
PM J01437-0602	J01437-060	SB2	…	…	Fou18
G 173-18	J01453+465	SB2	157.9	0.56	Giz02 / Shk10
BD-21 332	J01531-210	SB2	2.9	0.04	Shk10
GJ 1041 B	J01592+035W	SB2	356.4	0.93	Shk10
GJ 3129	J02027+135	SB2	27.8	0.13	Jen09 / Shk10
GJ 3131	J02033-212	SB2	…	…	Jeff18
V374And	J02069+451	SB2	897.0 ± 2.3	…	Spe19
GJ 3160	J02289+120	SB2	…	…	Jeff18
GJ 3235	J03346-048	ST3	…	…	Jeff18
GJ 3236	J03372+691	EB/SB2	0.7712600 ± 0.0000023	0.0143	Irw09 / Shk10
GJ 3239	J03375+178N	SB2	33.2	0.18	Shk10 / Fou18
GJ 3240	J03375+178S	EB?/SB2	0.4	0.01	Shk10
HD 278874		SB2	…	…	Mon18
Wolf 227	J03526+170	SB2	…	…	Bon13 / Jeff18
HD 24916B	J03574-011	SB	…	…	Zak79
LP 414-117	J04123+162	SB2	128.114	64.56	Ben08
1R042441.9-064725	J04247-067	ST3	1.9	0.02	Shk10
GJ 3282	J04252+080S	SB2	…	…	Jeff18
LP 775-31	J04352-161	SB2	…	…	Rei09
TYC 694-1183-1	J04414+132	SB	…	…	Mer09
LP 415-345	J04425+204	SB2	…	…	Sta97
LP 416-43	J04480+170	SB	8.49474 ± 0.00007	6.2	Gri85
1R044847.6+100302	J04488+100	SB2	…	…	Jeff18
GJ 3322 A	J05019+099	SB2	…	…	Del98 / Del99b
HD 285190	J05032+213	SB2	…	…	Jeff18 / Fou18
Wolf 230	J05078+179	ST2	15.04547 ± 0.00041	0.082527	Jeff18 / Win20
Capella		SB2	104.02173 ± 0.00022	0.7357	She85 / Tor09
GJ 1080	J05282+029	SB	…	…	Jen09
HD 35956		SB1	…	…	Kat13
Ross 42	J05322+098	SB2	61.1	0.23	Mar87 / Shk10 / Rei12
V371Ori	J05337+019	SB1	…	…	Rei12 / Bar21
Ross 45B	J05342+103S	SB	…	…	Rei12
V1402Ori	J05402+126	SB2	138.9	0.52	Shk10
Wolf 237	J05466+441	SB2	…	…	Jeff18
Ross 59	J05532+242	SB2	721 ± 2	0.6656	Bar18
TYC 4525-194-1	J06171+751	ST3?	…	…	Fou18
G 108-4	J06298-027	SB2	46.9	0.16	Shk10
1R070005.1-190115	J07001-190	SB2	6.56025 ± 0.00030	0.002797	Bar21
QYAur	J07100+385	SB2	10.42673 ± 0.00010	0.0687	TP86 / Win20a
TYC 4530-1414-1	J07119+773	SB1	…	…	Jeff18
1R073138.4+455718		SB2?	…	…	Fou18
Castor		SB2+SB2	167570 ± 840	104.9	Vin40 / Tor22
Castor C	J07346+318	EB/DESB2	0.8142822	0.01809	Joy26 / Giz02
GJ 282 C	J07361-031	SB1	6591 ± 177	6.224	Bar21
GJ 3461	J07418+050	SB2	…	…	Jeff18
1R075434.3+083213	J07545+085	SB1	…	…	Jeff18
FPCncB	J08089+328	SB2	395.5	0.92	Shk10

Table D.5: Spectroscopic binaries in Carmencita (continued).

Name	Karmn	Type[a]	P_{orb} [d]	a [au]	Reference[b]
CUCnc	J08316+193S	EB	2.771468 ± 0.000004	0.036240	Del99a / Del99b / Tor10
LSPM J0835+1408	J08353+141	ST3	…	…	Ski18
GJ 319 A	J08427+095	SB1	20.9491 ± 0.0019	0.021	Duq88
GJ 3540	J09120+279	SB2	…	…	Jeff18
LP 427-16	J09140+196	SB1	…	…	Bar21
HD 79210	J09143+526	SB1	…	…	Jeff18
GJ 3547	J09193+620	EB/SB2	20.2	0.16	Shk10 / Skr21
GJ 9303	J09362+375	SB2	…	…	Mal14a
LP 728-70	J09506-138	SB2	…	…	Jeff18
GJ 372	J09531-036	SB2	47.709 ± 0.053	39.06	Har96 / Jeff18 / Bar18
GJ 373	J09561+627	SB?	…	…	Rei12
LP 790-2	J10182-204	SB2	5.922845 ± 0.000061	0.048242	Bar18
GJ 3612	J10354+694	SB2	119.41 ± 0.04	0.3464	Bar18
LP 127-502	J10368+509	SB2?	…	…	Fou18
GJ 3626	J10504+331	SB1	2996 ± 31	0.2355	Bar21
GJ 3630	J10520+005	ST3/SQ4	28.1	0.11	Shk10
LP 491-51	J11036+136	SB1	…	…	Jeff18
GJ 426.1 A		SB	…	…	Abt76
GJ 455	J12023+285	SB2	…	…	Giz02
LP 734-34	J12104-131	SB2	33.6551 ± 0.0046	0.0479	Win20a
GJ 3719	J12169+311	SB2	…	…	Fou18
LP 320-626	J12191+318	SB2	…	…	Jeff18
GJ 3729	J12290+417	SB2/3?	…	…	Shk12 / Bow15 / Fou18
GJ 3731	J12299-054W	SB2	…	…	Jeff18
G 123-45	J12364+352	SB1	34.7557 ± 0.0041	0.0219	Win20a
DPDra	J12490+661	ST3	54.075 ± 0.006	…	Del99b
GJ 507 B	J13195+351E	SB1	…	…	Jeff18
GQVir	J14130-120	SB2	…	…	Jeff18
GJ 1182	J14155+046	SB2	154.20 ± 0.10	0.35835	Bar18
GJ 3839	J14170+317	SB2/ST3	…	…	Del99b / Rei12 / Fou18
PM J14171+0851	J14171+088	SB2	…	…	Jeff18
GJ 3861	J14368+583	SB2	…	…	Giz02 / Jeff18
GJ 3875	J14549+411	SB	…	…	Ski18
G 136-35	J14564+168	SB	…	…	Ski18
HD 131976	J14574-214	SB2	…	…	Mar87
GJ 3900	J15191-127	SB2	…	…	Bon13
StKM 1-1240	J15238+561	SB2	…	…	Fou18
GJ 3910	J15319+288	SB1	…	…	Jen09
UU UMi	J15412+759	SB2	5240 ± 410	4.7	Bar18 / Bar21
GJ 595	J15421-194	SB1	…	…	Nid02
GJ 3916	J15474-108	ST3	3028 ± 23	3.59	Bar21
LP 177-102	J15474+451	EB/SB2	3.5500184	0.036535	Moc02 / Har11 / Bir12
sig CrB A		SB2	1.13979142 ± 0.00000008	0.013106	Str03 / Rag09
CMDra	J16343+571	EB/SB2	1.268	0.017502	Mor09 / Tor10 / Scha19
V1054Oph	J16554-083S	ST3	2.965522 ± 0.000014	0.05	Joy47 / Pet84 / Del98
LP 331-57 A	J17038+321	SB2?	…	…	Shk09/Fou18
GJ 3991	J17095+436	SB1	…	…	Rei97a / Del99b
V2367Oph	J17136-084	SB2	…	…	Rei12 / Jeff18
Wolf 1473	J17464-087	SB2	83.926 ± 0.032	0.27559	Mal14a / Win20a
GJ 1230 A	J18411+247S	SB2	5.06880 ± 0.00005	…	GR96 / Del99b
GJ 735	J18554+084	SB2	…	…	Mar87 / Giz02 / Kar04
GJ 4091 B	J18563+544	SB2	…	…	Fou18
G 125-15	J19312+361	SB2	0.7	0.01	Shk10

Table D.5: Spectroscopic binaries in Carmencita (continued).

Name	Karmn	Type[a]	P_{orb} [d]	a [au]	Reference[b]
RX J1935.4+3746	J19354+377	SB1	…	…	Shk09/Jeff18
LP 869-19	J19420-210	SB2	…	…	Mal14a
V1513Cyg	J20050+544	SB1	…	…	Joy47 / Mac08
LP 574-21	J20105+065	SB2	40.1	0.19	Shk10
LP 395-8 A	J20198+229	SB2	1.1293392 ± 0.0000067	0.01057	Bar18
1R203011.0+795040	J20301+798	SB2	…	…	Jeff18
GJ 4155	J20409-101	SB	…	…	Rei12
GJ 4161	J20445+089N	SB2	…	…	Jeff18
GJ 810 A	J20556-140N	SB2	812 ± 51	0.841	Bar18
FRAqr	J20568-048	SB2	…	…	Jeff18
Ross 775	J21296+176	EB?/SB2	53.221 ± 0.004	…	Mar87 / Del99b
GJ 4213	J21442+066	SB1	…	…	Jeff18
EZAqr	J22385-152	ST3	3.78652 ± 0.00001	1189	Del99c
FKAqr	J22387-206S	SB2	4.08322 ± 0.00004	0.039372	Her65 / Del99b
FLAqr	J22387-206N	SB1	1.795 ± 0.017	0.00353	Davi14
LP 521-79	J23063+126	SB2/3?	58.9	0.31	Shk10
GJ 4314	J23096-019	SB2	…	…	Jeff18
GJ 4327	J23174+382	SB2	…	…	Jeff18
EQPegA	J23318+199E	SB2	…	…	Del99b
EQPegB	J23318+199W	SB1	…	…	Del99b
GJ 1284	J23302-203	SB2	11.838033 ± 0.000076	6.48275	Giz02 / Jeff18 / Car21
Ross 676	J23439+647	SB2	3.0	0.04	Shk10
GJ 912	J23556-061	SB1	5188 ± 58	0.505	Bar21
GJ 4379	J23573-129W	SB2	…	…	Giz02 / Jeff18
Wolf 1051	J23585+076	ST3	4634 ± 17	0.4436	Bar21

[a] A spectroscopic binary (SB) that displays one or two lines in the spectrum is a single- or double-lined spectroscopic binary, respectively, and abbreviated as SB1 or SB2. A spectroscopic triple (ST) showing two or three lines is a double- or triple-lined spectroscopic triple, and abbreviated as ST2 or ST3. Spectroscopic quadruples (SQ) are much more rare, and typically are three- or four-lined systems, denominated SQ3 and SQ4, respectively.

[b] And07: Andrade (2007); Bar18: Baroch et al. (2018); Bar21: Baroch et al. (2021); Ben00: Benedict et al. (2000); Bon13: Bonfils et al. (2013a); Bop74: Bopp (1974); Bow15: Bowler et al. (2015); BS08: Bender & Simon (2008); Cat06: Catala et al. (2006); Che16: Chelli et al. (2016); Cor14: Cortes-Contreras et al. (2014); Cor17: Cortés-Contreras et al. (2017a); Cur06: CURTIS (1906); Dav14: Davenport et al. (2014); Del98: Delfosse et al. (1998b); Del99a: Delfosse et al. (1999b); Del99b: Delfosse et al. (1999a); Ell15: Elliott et al. (2015); Fou18: Fouqué et al. (2018); Giz00a: Gizis et al. (2000a); Giz00b: Gizis et al. (2000c); Giz02: Gizis et al. (2002); Gli91: Gliese & Jahreiß (1991); GR96: Gizis & Reid (1996); Har11: Hartman et al. (2011); HC81: Harrington et al. (1981a); HM65: Herbig & Moorhead (1965); Ire08: Ireland et al. (2008); Irw09: Irwin et al. (2009); Jan12 : Janson et al. (2012) ; Jan14a: Janson et al. (2014c); Jan14b: Janson et al. (2014a); Jef18: Jeffers et al. (2018); Jen09: Jenkins et al. (2009); Jod13: Jódar et al. (2013); Joy26: Joy & Sanford (1926); Joy47: Joy (1947); Kar04: Karataş et al. (2004); Kat13: Katoh et al. (2013); Kon10 : Konopacky et al. (2010) ; Lan01: Lane et al. (2001); Law06: Law et al. (2006); Lin12: Lindegren et al. (2012); Malo14a: Malo et al. (2014b); Malo14b: Malo et al. (2014c); Mar00: Martín et al. (2000); Mar87: Marcy et al. (1987); Maz01: Mazeh et al. (2001); Mer09: Mermilliod et al. (2009); Mon18: Montes et al. (2018); Mor09: Morales et al. (2009); Nid02: Nidever et al. (2002); Pet84: Pettersen et al. (1984); Pou04: Pourbaix et al. (2004); Rag09: Raghavan et al. (2009); Rei09: Reiners & Basri (2009); Rei12: Reipurth & Mikkola (2012a); Rei97a: Reid & Gizis (1997); Sam07: Samus' et al. (2017); Scha19: Schanche et al. (2019); Schl12b: Schlieder et al. (2012b); Schw19: Schweitzer et al. (2019); Sha17: Shan et al. (2017); Sha21: Shara et al. (2021); Shk10: Shkolnik et al. (2010); Shk12: Shkolnik et al. (2012); Ski18: Skinner et al. (2018); Spe19: Sperauskas et al. (2019); Sta97: Stauffer et al. (1997); Ste14: Stebbins (1914); Str77: Strand (1977); Str93: Strassmeier et al. (1993); Tok10: Tokovinin et al. (2010); Tok97: Tokovinin (1997); Tor15: Torres et al. (2015); TP86: Tomkin & Pettersen (1986); Vin40: Vinter Hansen et al. (1940); Zak79: Zakhozhaj (1979).

Table D.6: Multiple systems containing M dwarfs and FGK primaries.

Name	Karmn	Spectral type	Component	Class	α	δ	π [mas]	$\mu_{\rm total}$ [mas a^{-1}]	G [mag]	θ [deg]	ρ [arcsec]	Notes[a]
HD 4967		K5 V	A		00:51:34.73	−22:54:40.7	65.090 ± 0.025	672.69 ± 0.05	8.416			
HD 4967B	J00515-229	M5.5 V	B		00:51:35.91	−22:54:35.4	65.073 ± 0.050	680.57 ± 0.09	14.366	72.1	17.1	
EXCet		K0/1 V	A		01:37:35.65	−06:45:39.1	41.564 ± 0.024	197.86 ± 0.03	7.466			
LP 648-20	J01369-067	M3.5 V	B		01:36:55.36	−06:47:39.6	41.699 ± 0.045	200.55 ± 0.05	12.709	258.6	612.075	
Wolf 109		K5 V	A		02:02:02.81	+03:56:20.0	27.827 ± 0.021	466.14 ± 0.03	10.081			
Wolf 109 B	J02020+039	M2.0 V	B		02:02:03.11	+03:56:37.4	28.922 ± 0.353	465.77 ± 0.48	12.412	14.4	18.0	
G3-2517912315149114240		…	C		02:02:03.16	+03:56:36.9	…	…	12.832	16.8	17.739	
HD 15468		K4.5 Vk	AB		02:29:02.40	−19:58:40.8	51.606 ± 0.136	646.40 ± 0.17	8.394	145.3	0.182	
GJ 100 C	J02285-200	M2.5 V	C		02:28:32.62	−20:02:22.5	50.972 ± 0.032	649.19 ± 0.04	11.784	242.1	474.569	
HD 16160		K3 V	AB		02:36:06.81	+06:53:36.0	138.340 ± 0.318	2312.10 ± 0.50	5.498	289.5	1.730	
BXCet	J02362+068	M4.0 V	C		02:36:17.20	+06:52:41.1	138.437 ± 0.042	2312.99 ± 0.06	10.333	289.5	164.180	
HD 16895		F8 V	A		02:44:12.53	+49:13:41.0	89.685 ± 0.164	346.40 ± 0.24	3.983			•
GJ 107 B	J02441+492	M1.5 V	B		02:44:10.79	+49:13:53.0	89.374 ± 0.032	322.95 ± 0.04	9.140	305.1	20.932	
HD 18757		G1.5 V	A		03:04:11.26	+61:42:09.9	42.459 ± 0.020	1000.79 ± 0.02	6.484			
GJ 3195	J03047+617	M3.0 V	B		03:04:45.06	+61:43:57.7	42.534 ± 0.026	1000.09 ± 0.03	11.493	65.8	263.299	
V577Per		K2 V	A		03:33:13.60	+46:15:23.7	27.482 ± 0.031	188.42 ± 0.04	8.016			
HD 21845B	J03332+462	M0.0 V	B		03:33:14.16	+46:15:16.2	27.481 ± 0.016	185.83 ± 0.02	10.497	142.3	9.502	•
HD 278874		K2 V	Aab		03:39:48.92	+33:28:24.3	25.434 ± 0.032	36.21 ± 0.04	8.707			
HD 278874B	J03397+334	M3.0 V	B		03:39:47.79	+33:28:30.7	25.571 ± 0.041	38.83 ± 0.06	11.771	294.3	15.47	
HD 23189		K2 V	A		03:48:01.40	+68:40:26.4	55.825 ± 0.013	279.83 ± 0.02	8.772			
GJ 153 C	J03480+686	M2 V	BC		03:48:02.08	+68:40:42.9	55.984 ± 0.105	288.83 ± 0.21	10.478	26.3/13.2	0.763/17.206	
HD 275867		K2 V	A		03:52:00.35	+39:47:43.7	30.985 ± 0.016	62.07 ± 0.02	9.136			
TYC 2868-639-1	J03519+397	M0.0 V	B		03:51:58.19	+39:46:55.8	31.021 ± 0.020	64.40 ± 0.03	10.393	207.5	53.919	
HD 24916		K4 V	A		03:57:28.50	−01:09:36.4	65.426 ± 0.023	234.33 ± 0.03	7.673			
HD 24916B	J03574-011	M2.5 V	Bab		03:57:28.68	−01:09:25.7	65.492 ± 0.044	251.75 ± 0.06	10.438	14.1	11.0	
HD 26965		K0 V	A		04:15:13.91	−07:40:05.1	199.608 ± 0.121	4089.84 ± 0.16	4.180			
HD 26976		DA2.9	B		04:15:19.39	−07:40:22.6	199.691 ± 0.051	4018.59 ± 0.06	9.542	102.2	83.337	
HD 27848		…	AB		04:24:22.38	+17:04:43.8	19.959 ± 0.026	103.39 ± 0.04	6.856			•
V991Tau		K4 V	C		04:25:00.35	+16:59:05.2	18.356 ± 0.019	94.41 ± 0.03	9.970	121.9	641.2	

Table D.6: Multiple systems containing M dwarfs and FGK primaries (continued).

Name	Karmn	Spectral type	Component	Class	α	δ	π [mas]	$\mu_{\rm total}$ [mas a^{-1}]	G [mag]	θ [deg]	ρ [arcsec]	Notes[a]
V805Tau	J04252+172	M3.5 V	DE		04:25:13.67	+17:16:05.1	19.313 ± 0.193	110.65 ± 0.26	11.998	47.1	1002.145	
LP 415-881		M7.0 V	F		04:26:19.16	+17:03:01.7	21.204 ± 0.061	105.70 ± 0.09	16.338	93.4	1677.610	
HD 29391		F0 V	A		04:37:36.18	−02:28:25.8	33.439 ± 0.078	77.72 ± 0.13	5.141	162.5	66.7	
GJ 3305	J04376-024	M1.1 V	BC		04:37:37.51	−02:29:29.7	36.009 ± 0.476	72.38 ± 0.63	9.801	208.2/162.6	0.098/66.963	
V583Aur		K5 V	A		04:39:25.47	+33:32:43.9	11.128 ± 0.018	52.35 ± 0.03	11.002			•
PM J04393+3331	J04393+335	M4.0 V	BC		04:39:23.22	+33:31:48.7	7.425 ± 0.848	50.28 ± 1.83	13.052	50.6/207.1	0.126/61.936	
HD 31412		F9.5 V	AB		04:55:56.03	+04:40:10.5	27.865 ± 0.027	233.46 ± 0.04	6.891	17.7	0.443	
HD 31412B	J04559+046	M2.0 V	C		04:55:54.60	+04:40:13.5	27.851 ± 0.026	234.00 ± 0.03	11.031	277.9	21.657	
HD 35956		G0 V	Aab		05:28:51.74	+12:32:59.6	33.788 ± 0.294	231.78 ± 0.42	6.597			
HD 35956B		M1.0 V	B		05:28:52.11	+12:33:01.4	35.405 ± 0.020	237.81 ± 0.03	10.760	71.4	5.8	
GJ 3348A	J05289+125	M4.0 V	C		05:28:56.61	+12:31:50.4	39.500 ± 10.200	230.59 ± 11.31	13.146	134.1	99.391	
GJ 3348B		…	D		05:28:56.61	+12:31:50.2	…	…	13.222	134.2	99.461	
V538Aur		K1 V	A		05:41:20.34	+53:28:43.4	81.499 ± 0.025	523.48 ± 0.03	5.991			
HD 233153	J05415+534	M1.0 V	B		05:41:30.74	+53:29:15.0	81.464 ± 0.023	515.97 ± 0.03	8.919	71.2	98.035	
HD 43587		G0 V	AB		06:17:15.90	+05:06:02.6	51.616 ± 0.124	269.29 ± 0.20	5.565	70.9	0.840	
GJ 231.1 B	J06171+051	M3.5 V	CD		06:17:10.42	+05:07:05.3	52.139 ± 0.083	261.65 ± 0.11	12.136	156.90/307.4	0.545/103.19	
HD 263175		K3 V	A		06:46:04.47	+32:33:22.0	38.828 ± 0.022	467.06 ± 0.03	8.501			
HD 263175B	J06461+325	M1.0 V	B		06:46:06.88	+32:33:16.6	38.873 ± 0.017	472.87 ± 0.02	11.288	100.1	30.855	
HD 50281		K3.5 V	AB		06:52:17.47	−05:10:25.4	114.355 ± 0.042	543.70 ± 0.04	6.231	149.6	0.175	
HD 50281B	J06523-051	M2.0 V+	C		06:52:17.42	−05:11:24.3	114.291 ± 0.022	576.48 ± 0.03	9.098	180.6	58.833	
GJ 3415		K4.5 V	A		06:56:28.28	+40:04:20.6	39.870 ± 0.023	452.03 ± 0.03	8.687	6.8	37.808	
GJ 3416	J06564+400	M1.0 V	B		06:56:28.64	+40:04:58.3	39.925 ± 0.021	446.75 ± 0.03	10.299	6.2	37.9	
V869Mon		K3 V	A		07:39:59.40	−03:35:55.5	71.032 ± 0.024	286.81 ± 0.03	6.890			
HD 61606B		K7 V	B		07:40:02.97	−03:36:17.8	70.992 ± 0.025	294.21 ± 0.03	8.335	112.7	57.9	
GJ 282 C	J07361-031	M1.0 V	Cab		07:36:07.15	−03:06:43.4	70.275 ± 0.131	302.35 ± 0.17	9.142	296.7	3894.176	
HD 68146		F6.5 V	A		08:10:39.55	−13:47:56.2	44.340 ± 0.053	257.61 ± 0.06	5.399			
HD 68146B	J08105-138	M2.5 V	B		08:10:34.02	−13:48:50.1	44.520 ± 0.049	259.91 ± 0.06	11.008	236.2	96.934	
G3-5725122965265271680		M4.0 V	C		08:10:33.96	−13:48:49.9	44.150 ± 0.203	245.49 ± 0.32	12.781	236.6	97.537	
V405Hya		K2 V	A		09:04:20.57	−15:54:51.8	36.512 ± 0.022	112.03 ± 0.03	8.464			
1R090406.8-155512	J09040-159	M2.5 V	B*		09:04:05.44	−15:55:19.0	36.628 ± 0.021	113.77 ± 0.03	11.754	82.9	220.022	•

Table D.6: Multiple systems containing M dwarfs and FGK primaries (continued).

Name	Karmn	Spectral type	Component	Class	α	δ	π [mas]	$\mu_{\rm total}$ [mas a^{-1}]	G [mag]	θ [deg]	ρ [arcsec]	Notes[a]
BD+22 2086A		K5 V	A		09:23:06.19	+22:18:17.6	29.405 ± 0.020	218.39 ± 0.02	9.274			
BD+22 2086B	J09231+223	M0.0 V	B		09:23:06.01	+22:18:25.6	29.444 ± 0.022	223.16 ± 0.02	10.641	343.4	8.301	
DXLeo		G9 V(k)	A		09:32:43.58	+26:59:14.8	55.329 ± 0.021	287.22 ± 0.02	6.813	64.4	65.558	
HD 82443B	J09328+269	M5.5 V	B		09:32:48.07	+26:59:39.9	55.292 ± 0.071	284.17 ± 0.09	13.826	67.3	65.013	
HD 82939		G5 V	A		09:36:15.78	+37:31:44.1	25.740 ± 0.023	134.64 ± 0.02	10.292			
GJ 9303	J09362+375	M0.0 V	Bab		09:36:04.14	+37:33:08.9	25.836 ± 0.023	134.34 ± 0.02	8.069	301.5	162.314	
GJ 397.1		K5 V	A		10:31:43.09	+57:06:59.9	57.010 ± 0.014	185.37 ± 0.02	9.003	225.6	141.959	
GJ 397.1 B	J10315+570	M5.0 V	BC		10:31:30.64	+57:05:20.4	…	161.31 ± 11.31	13.519	154.5/225.6	0.284/142.037	
LZUMa		G5 V	A		10:50:39.98	+51:47:58.8	37.386 ± 0.070	196.65 ± 0.17	8.047			•
GJ 3628	J10506+517	M4.1 V	B		10:50:37.91	+51:45:01.6	37.889 ± 0.028	191.40 ± 0.03	12.763	186.2	178.3	
HD 97584		K4 V	A		11:15:10.39	+73:28:32.5	69.136 ± 0.015	418.80 ± 0.02	7.312	102.9	67.600	
HD 97584B	J11151+734	M2.5 V	B		11:15:09.56	+73:28:38.0	69.134 ± 0.018	396.51 ± 0.03	10.609	327.1	6.481	
GJ 426.1 A		F1 IV	Aab		11:23:55.62	+10:31:44.9	42.355 ± 0.398	169.81 ± 0.99	3.907			
GJ 426.1 B		F5 V	B		11:23:55.75	+10:31:44.7	41.496 ± 0.351	185.02 ± 0.97	6.842	95.1	2.050	
HD 108421A		K2 V	A		12:27:13.83	+27:01:24.9	36.504 ± 0.027	265.14 ± 0.03	8.485			
HD 108421B		K4 V	B		12:27:13.84	+27:01:27.6	36.511 ± 0.031	256.19 ± 0.04	8.857	4.1	2.8	
HD 115404		K2 V	A		13:16:51.76	+17:00:57.6	91.018 ± 0.024	689.14 ± 0.04	6.298			
HD 115404B	J13168+170	M0.5 V	B		13:16:52.28	+17:00:55.7	90.948 ± 0.023	701.23 ± 0.04	8.870	104.6	7.671	
GJ 9453		K5 V	A		13:34:51.91	+74:30:01.1	25.386 ± 0.026	439.09 ± 0.05	9.384	323.3	14.8	
GJ 9453 B	J13348+745	M3.5 V	B		13:34:49.83	+74:30:12.6	25.492 ± 0.015	437.06 ± 0.03	12.363	324.0	14.192	
BD+21 2602		K4 V	A		14:04:09.85	+20:45:32.5	24.815 ± 0.015	127.65 ± 0.02	9.793			
StKM 1-1119	J14041+207	M1.0 Ve	B		14:04:09.06	+20:44:30.9	…	132.08 ± 3.76	11.499	190.2	62.7	
G3-1247168140942467200		…	C		14:04:09.06	+20:44:31.2	…	…	11.660	190.3	62.307	
HD 126660		F7 V	A		14:25:11.39	+51:50:56.3	69.069 ± 0.158	464.15 ± 0.23	3.917	182.5	70.160	•
HD 126660B	J14251+518	M2.5 V	B		14:25:11.17	+51:49:46.6	68.812 ± 0.032	469.65 ± 0.05	10.498	181.7	69.674	
KXLib		K4 V	A		14:57:29.18	–21:25:23.3	169.884 ± 0.065	2008.68 ± 0.09	5.364			
HD 131976	J14574-214	M1.0 V	Bab		14:57:27.70	–21:25:07.9	168.770 ± 21.540	1933.94 ± 26.20	7.249	306.6	25.762	•
GJ 570 D		T8	C		15:07:55.68	+76:12:05.4	169.300 ± 1.700	1972.88 ± 5.62		317.0	234.000	•
HD 135363		G5 V	AB		15:07:55.68	+76:12:05.4	33.711 ± 0.052	208.70 ± 0.10	8.429	133.1	0.36	

Table D.6: Multiple systems containing M dwarfs and FGK primaries (continued).

Name	Karmn	Spectral type	Component	Class	α	δ	π [mas]	$\mu_{\rm total}$ [mas a^{-1}]	G [mag]	θ [deg]	ρ [arcsec]	Notes[a]
LSPM J1507+7613	J15079+762	M4.5 V	C		15:07:56.64	+76:14:01.8	33.714 ± 0.027	207.10 ± 0.06	12.379	1.7	116.445	
HD 144579		G8 V	A		16:04:56.01	+39:09:24.3	69.641 ± 0.014	573.29 ± 0.02	6.461			
HD 144579B	J16048+391	M4.0 V	B		16:04:50.08	+39:09:36.6	69.637 ± 0.019	564.44 ± 0.03	12.855	280.1	69.998	
HD 146361A		F6 V	Aab		16:14:40.51	+33:51:29.6	44.057 ± 0.046	282.06 ± 0.07	5.431			
HD 146362		G1 V	B		16:14:40.01	+33:51:25.8	44.134 ± 0.018	301.27 ± 0.03	6.438	238.5	7.231	
TZCrB	J16139+337	M2.5 V	CD		16:13:55.90	+33:46:22.7	44.267 ± 0.159	300.69 ± 0.24	11.269	28.7/241.1	0.507/635.058	
V1090Her		K3 V	A		16:57:52.95	+47:22:04.4	55.751 ± 0.016	308.70 ± 0.03	7.521			
HD 153557B	J16578+473	M1.5 V	B		16:57:53.40	+47:22:06.7	55.771 ± 0.017	301.44 ± 0.03	10.419	63.0	5.091	
V1089Her		K3 V	C		16:57:42.01	+47:21:47.9	55.718 ± 0.016	296.94 ± 0.03	7.622	261.6	112.378	
HD 154363		K4/5 V	A		17:05:02.41	−05:04:17.7	95.567 ± 0.024	1461.66 ± 0.03	7.265			
HD 154363B	J17052-050	M1.5 V	B		17:05:12.80	−05:05:57.4	95.560 ± 0.021	1457.06 ± 0.03	9.178	122.7	184.42	
HD 160269A		G0 IV/V	AB		17:35:00.16	+61:52:20.8	69.283 ± 0.200	522.56 ± 0.33	5.069	300.5	0.625	
GJ 685	J17355+616	M0.5 V	C		17:35:35.07	+61:40:45.4	69.892 ± 0.015	577.33 ± 0.02	9.175	160.3	738.164	
BD+31 3330		K2.5 V	A		18:40:54.99	+31:31:45.7	41.745 ± 0.016	841.17 ± 0.02	8.260			
BD+31 3330B	J18409+315	M1.0 V	B		18:40:55.33	+31:31:37.3	…	…	11.037	152.2	9.45	
BD+31 3330C		…	C		18:40:55.31	+31:31:37.5	…	…	11.139	153.1	9.210	
HD 187691		F8 V	A		19:51:01.91	+10:24:54.4	51.313 ± 0.090	277.69 ± 0.11	4.976			
GJ 9671 B	J19510+104	M4.0 V	B		19:51:00.97	+10:24:38.0	51.373 ± 0.040	288.38 ± 0.05	11.765	220.2	21.5	
HD 191785		K0 V	A		20:11:05.61	+16:11:23.2	48.926 ± 0.023	575.39 ± 0.03	7.113			
GJ 783.2 B	J20112+161	M4.0 V	B		20:11:12.80	+16:11:14.4	48.928 ± 0.032	577.77 ± 0.04	12.614	94.8	103.843	
StKM 1-1767a		K5 V	A		20:13:11.14	+02:56:20.5	27.359 ± 0.018	108.28 ± 0.02	9.821			
[R78b] 440	J20132+029	M1.0 V	B		20:13:12.94	+02:56:02.3	27.359 ± 0.023	110.73 ± 0.03	10.984	123.9	32.5	
HD 197076		G5 V	A		20:40:45.28	+19:56:12.9	47.746 ± 0.020	334.03 ± 0.02	6.285			
GJ 797 B	J20407+199	M2.5 V	BC		20:40:44.65	+19:54:08.2	…	339.09 ± 1.98	11.394	268.9/184.1	0.268/125.0584	
V447Lac		K1 V	A		22:15:54.53	+54:40:23.5	45.591 ± 0.017	223.87 ± 0.02	7.283			
GJ 4269	J22160+546	M4.0 V	B		22:16:02.99	+54:40:00.5	45.625 ± 0.020	221.35 ± 0.03	12.732	107.4	76.900	
HD 216385		F6 V	A		22:52:24.64	+09:50:09.1	36.558 ± 0.108	523.35 ± 0.20	5.022	19.6	249.637	
GJ 9801 B	J22524+099	M3.0 V	BC		22:52:30.31	+09:54:04.9	37.250 ± 0.760	530.18 ± 11.31	12.411	19.6	250.246	•
V368Cep		G9 V	A		23:19:27.78	+79:00:13.8	52.784 ± 0.014	215.92 ± 0.02	7.293			

Table D.6: Multiple systems containing M dwarfs and FGK primaries (continued).

Name	Karmn	Spectral type	Component	Class	α	δ	π [mas]	$\mu_{\rm total}$ [mas a^{-1}]	G [mag]	θ [deg]	ρ [arcsec]	Notes[a]
HD 220140B	J23194+790	M3.5 V	B		23:19:25.64	+79:00:04.8	52.840 ± 0.021	218.08 ± 0.04	10.915	214.1	10.905	
LP 12-90	J23228+787	M5.0 V	C		23:22:54.97	+78:47:39.6	52.834 ± 0.030	217.44 ± 0.05	14.020	141.1	962.738	
StKM 2-1787		K4 V	A		23:53:35.58	+12:06:20.4	26.840 ± 0.020	120.69 ± 0.03	10.426			
PM J23535+1206S	J23535+121	M2.5 V	B		23:53:35.69	+12:06:14.8	26.792 ± 0.035	119.44 ± 0.04	11.297	165.1	5.785	

[a] HD 16895: Candidate to unresolved binary; HD 21845B: Candidate to unresolved binary; HD 27848: Hyades moving group (Röser et al., 2011; Kopytova et al., 2016; Lodieu et al., 2019; Freund et al., 2020); V583 Aur: Candidate to unresolved binary; GJ 3348A: Proper motions from Zacharias et al. (2012); 1RXS J090406.8-155512: Desidera et al. (2021) recognises the pair but it is not tabulated in WDS; GJ 397.1 B: Proper motions from Zacharias et al. (2012); LZ UMa: Candidate to unresolved binary; StKM 1-1119: Proper motions from Zacharias et al. (2012); HD 126660: Candidate to unresolved binary; HD 131976: Parallax and proper motions from van Leeuwen (2007); GJ 570 D: Parallax and proper motions from Faherty et al. (2012); Weinberger et al. (2016); GJ 9801 B: Parallax and proper motions from Dawson & De Robertis (2005); Zacharias et al. (2012).

Table D.7: Multiple systems containing M dwarfs and white dwarfs.

Name	Karmn	Spectral type	Component	Class	α	δ	π [mas]	μ_{total} [mas a^{-1}]	G [mag]	θ [deg]	ρ [arcsec]	Notes[a]
GJ 1015 A	J00413+558	M4.2 V	A	A+B	00:41:21.44	+55:50:03.2	43.735 ± 0.022	332.50 ± 0.02	12.732			
GJ 1015 B		DBQ5	B		00:41:22.64	+55:50:07.2	43.659 ± 0.022	324.16 ± 0.03	13.998	68.4	10.854	
GJ 3117	J01518+644	M2.5 V	A	AB	01:51:51.72	+64:26:02.8	57.825 ± 0.016	306.37 ± 0.02	10.409			
GJ 3118		DA5.6	B		01:51:51.69	+64:25:49.3	57.799 ± 0.016	301.94 ± 0.02	13.947	180.7	13.503	
Ross 25	J04011+513	M3.8 V	A	A+B	04:01:08.18	+51:23:06.4	39.816 ± 0.021	883.46 ± 0.03	12.435			
LSPM J0401+5131		DC8	B*		04:01:02.14	+51:31:17.2	39.836 ± 0.077	883.24 ± 0.12	17.113	353.4	494.0	
HD 26965		K0 V	A	A+B+C	04:15:13.91	−07:40:05.1	199.608 ± 0.121	4089.84 ± 0.16	4.180			
HD 26976		DA2.9	B		04:15:19.39	−07:40:22.6	199.691 ± 0.051	4018.59 ± 0.06	9.542	102.2	83.337	
DYEri	J04153-076	M4.5 V	C		04:15:19.12	−07:40:15.3	199.452 ± 0.069	4083.72 ± 0.08	9.775 97.5	78.097		
GJ 169.1 A	J04311+589	M4.0 V	A	A+B	04:31:14.21	+58:58:04.7	181.244 ± 0.050	2424.35 ± 0.07	9.703			
GJ 169.1 B		DC5	B		04:31:15.33	+58:58:10.1	181.273 ± 0.020	2361.13 ± 0.03	12.336	58.2	10.263	
GJ 3430	J07102+376	M4.0 V	A	A+B	07:10:13.32	+37:40:05.9	44.601 ± 0.437	350.22 ± 0.61	13.232			
GJ 3431		DQ8	B		07:10:14.04	+37:40:15.0	41.029 ± 0.036	357.87 ± 0.05	15.512	43.1	12.5	
GJ 275.2 A	J07307+481	M4.0 V	AB	(AB)+CD	07:30:42.46	+48:11:38.2	88.723 ± 0.030	1287.99 ± 0.03	12.116			•
GJ 275.2 B		DA	C		07:30:46.99	+48:10:05.7	83.484	1281.73 ± 3.61	15.065	153.9	103.053	•
G 107-70B		DA	D		07:30:46.96	+48:10:06.3			15.252	318.1/153.9	0.667/102.38	
GJ 283 A		DZQA6	A	A+B	07:40:22.06	−17:24:57.8	109.344 ± 0.018	1261.34 ± 0.02	12.970			
GJ 283 B	J07403-174	M6.5 Ve	B		07:40:20.66	−17:24:54.5	109.254 ± 0.039	1270.98 ± 0.05	13.957	99.5	20.338	
GJ 401	J10456-191	M0.5 V	A	AB	10:45:36.98	−19:07:01.3	53.172 ± 0.022	1963.77 ± 0.03	10.291			
GJ 401 B		DQ	B		10:45:36.93	−19:06:54.7	53.190 ± 0.034	1962.56 ± 0.06	15.441	354.5	6.655	
GJ 1142 A	J11081-052	M3.0 V	A	A+B	11:08:06.48	−05:13:54.2	40.180 ± 0.026	443.17 ± 0.03	11.472			
GJ 1142 B		DA3	B		11:07:59.89	−05:09:33.1	40.293 ± 0.032	446.11 ± 0.04	13.091	339.3	278.996	
GJ 1155 A	J12168+029	M3.0 V	A	AB	12:16:51.16	+02:58:09.0	42.820 ± 0.035	700.55 ± 0.05	12.080			
GJ 1155 B		DA	B		12:16:51.17	+02:58:06.9	42.773 ± 0.043	711.07 ± 0.06	15.330	177.9	2.126	
Wolf 485		DA3.5	A	A+B	13:30:12.44	−08:34:37.0	62.148 ± 0.044	1207.51 ± 0.06	12.355			
Ross 476	J13300-087	M4.0 V	B		13:30:01.59	−08:42:33.0	62.281 ± 0.042	1210.61 ± 0.06	12.706	198.7	502.447	
GJ 1179 A	J13482+236	M5.0 V	A	A+B	13:48:11.69	+23:36:50.7	84.225 ± 0.027	1487.63 ± 0.04	13.442			
GJ 1179 B		DC9	B		13:48:01.28	+23:34:48.4	84.311 ± 0.029	1490.91 ± 0.04	15.338	229.5	188.131	
CMDra	J16343+571	M4.5 V	Aab	Aab+B	16:34:18.14	+57:10:03.3	67.288 ± 0.034	1623.35 ± 0.06	11.491			•

Table D.7: Multiple systems containing M dwarfs and white dwarfs (continued).

Name	Karmn	Spectral type	Component	Class	α	δ	π [mas]	$\mu_{\rm total}$ [mas a^{-1}]	G [mag]	θ [deg]	ρ [arcsec]	Notes[a]
GJ 630.1 B		DQ8	B		16:34:19.37	+57:10:28.1	67.354 ± 0.021	1634.85 ± 0.04	14.849	21.9	26.726	
LP 387-37	J17058+260	M1.5 V	A	AB	17:05:52.55	+26:05:27.4	28.746 ± 0.019	291.03 ± 0.03	11.284			
LP 387-36		DC7	B		17:05:52.54	+26:05:46.7	28.841 ± 0.054	285.38 ± 0.07	17.034	359.6	19.24	
GJ 4059	J18264+113	M3.5 V	A	A+B	18:26:24.58	+11:20:52.9	37.056 ± 0.024	276.07 ± 0.03	11.728			
LSPM J1826+1120S		DA	B		18:26:24.42	+11:20:45.1	37.055 ± 0.066	281.07 ± 0.09	16.962	196.8	8.196	•
G 229-20A	J18576+535	M3.5 V	A	AB+C	18:57:38.42	+53:31:14.4	40.348 ± 0.015	261.44 ± 0.03	12.019			
LP 141-13		M3.0 V	B		18:57:38.34	+53:31:12.2	40.365 ± 0.015	245.56 ± 0.03	12.103	197.0	2.290	
LP 141-14		DC	C		18:57:39.78	+53:30:32.5	40.393 ± 0.051	246.40 ± 0.10	16.942	163.9	43.653	
GJ 754.1 B	J19205-076	M2.5 V	B	A+B	19:20:33.38	−07:39:46.6	95.178 ± 0.031	191.46 ± 0.04	10.972			
GJ 754.1 A		DBQA5	A		19:20:34.86	−07:40:02.7	95.176 ± 0.029	173.04 ± 0.04	12.253	126.2	27.168	
GJ 784.2 A	J20139+066	M3.3 V	A	A+B	20:13:58.71	+06:41:06.8	43.570 ± 0.022	634.75 ± 0.03	11.951			
V1412Aql		DC7	B		20:13:55.41	+06:42:35.5	43.574 ± 0.038	635.70 ± 0.05	15.664	330.9	101.5	
FRAqr	J20568-048	M4.0 V	Aab	Aab+B	20:56:49.39	−04:50:52.6	61.824 ± 0.074	826.32 ± 0.09	10.660			
Ross 193B		DC10	B		20:56:48.62	−04:50:43.1	61.760 ± 0.052	807.72 ± 0.07	16.347	309.4	15.006	
TYC 3980-1081-1	J21516+592	M4.0 V	A	A+B	21:51:38.15	+59:17:40.0	123.057 ± 0.594	79.89 ± 1.67	9.409			
UCAC4 747-070768		DAH	B		21:51:39.93	+59:17:34.5	118.155 ± 0.016	88.85 ± 0.03	14.373	111.9	14.642	
LF 4 +54 152	J22129+550	M0.0 V	A	AB	22:12:56.63	+55:04:50.8	18.385 ± 0.153	109.13 ± 0.25	10.222			
G3-2005884249925303168		M6.5 V	B*		22:13:00.46	+55:05:48.3	18.550 ± 0.079	108.97 ± 0.12	17.702	29.8	66.265	•
GJ 4304	J22559+057	M1.0 V	A	A+B	22:55:57.20	+05:45:14.0	40.347 ± 0.024	446.04 ± 0.03	10.415			
GJ 4305		DA8.1	B		22:55:56.09	+05:45:18.4	40.325 ± 0.072	439.47 ± 0.07	16.041	284.6	17.2	
G 233-42	J23089+551	M5.0 V	A	A+B	23:09:58.62	+55:06:48.1	60.921 ± 0.027	411.27 ± 0.04	13.986			
LSPM J2309+5506E		DA	B		23:09:59.29	+55:06:50.2	60.895 ± 0.030	410.18 ± 0.04	15.604	69.6	6.150	
GJ 4356	J23389+210	M4.3 V	A	A+B	23:38:56.00	+21:01:24.5	25.402 ± 0.028	328.86 ± 0.04	12.907			
GJ 4357		DA	B		23:38:56.63	+21:01:21.1	25.367 ± 0.100	325.25 ± 0.13	17.683	110.7	9.5	
GJ 905.2 A	J23438+325	M1.5 V	AB	(AB)+C	23:43:52.84	+32:35:37.8		223.77 ± 13.69	10.611	308.00	0.109	
GJ 905.2 B		DA3.8	C		23:43:50.45	+32:32:45.8	53.762 ± 0.027	224.05 ± 0.04	12.967	190.0	174.652	

[a] GJ 275.2 A: Quadruple system, with (AB) separated ∼ 0.054 arcsec (Harrington et al., 1981b); GJ 275.2 B: Parallax from Khrutskaya et al. (2010), proper motions from Monet et al. (2003); LSPM J1826+1120S: Candidate to unresolved double white dwarf based on position in HR diagram; GJ 754.1 B: White dwarf candidate from position in HR diagram (see also Jiménez-Esteban et al., 2018).

Table D.8: Stars with detected planets in our sample.

Karmn	Name	System class	Component	Number of planets[a]	Discovery reference[b]	Flag[c]
J00067-075	GJ 1002	Single	-	2	Sua23	1
J00183+440	HD 1326	Binary	A	2	How14, Pin18	13
J00449-152	GJ 3053	Single	-	2	Dit17, Men19	…
J01023-104	GJ 3072	Single	-	1	Fen20	…
J01026+623	Wolf 46	Binary	A	1	Per19	1
J01066+192	LSPM J0106+1913	Single	-	2	Cha22	2
J01125-169	YZ Cet	Single	-	3	Ast17b	3
J02002+130	TZ Ari	Single	-	1	Qui22	1
J02222+478	GJ 96	Single	-	1	Hob18	…
J02489-145W	PM J02489-1432W	Binary	A	1	Kos21	2
J02530+168	Teegarden's Star	Single	-	2	Zec19	1
	HD 18143A	Triple	A	2	Fen22	…
J02573+765	LP 14-53	Single	-	1	Sot21	2
J03018-165S	GJ 3193	Binary	A	2	Win19b, Win22	…
J03133+047	CD Cet	Single	-	1	Bau20	1
	HD 26965	Triple	A	1	Dia18	…
J04167-120	LP 714-47	Single	-	1	Dre20	2
J04343+430	PM J04343+4302	Single	-	1	Blu21	2
	HD 29391	Triple	A	1	Mac15	…
J04429+189	HD 285968	Single	-	1	For09	13
J04520+064	Wolf 1539	Single	-	1	How10	…
J04538-177	GJ 180	Single	-	3	Tuo14	…
J05019-069	GJ 3323	Single	-	2	Ast17a	…
J06105-218	HD 42581	Binary	AB	2	Tuo14, Fen20	…
J06371+175	HD 260655	Single	-	2	Luq22	2
J06548+332	HD 265866	Single	-	1	Sto20	1
J07274+052	Luyten's Star	Binary	AB	2[d]	Ast17a	…
J07590+153	GJ 3470	Single	-	1	Bon12	…
J08023+033	GJ 3473	Binary	A	2	Kem20	2
J08409-234	GJ 317	Single	-	2	Joh07	…
J08413+594	GJ 3512	Single	-	2	Mor19	1
	55 Cnc	Binary	A	5	But97, Mar02, Mc04, Fis08	…
J08551+015	Ross 623	Single	-	1	Rob13	…
J08588+210	G 41-13	Single	-	1	Stef20	…
J09144+526	HD 79211	Triple	B	1	Gon20	1
J09286-121	LP 727-31	Single	-	1	Ree22	…
J09360-216	GJ 357	Single	-	3	Luq19	12
J09561+627	GJ 373	Binary	Aab (SB?, Rei12)	1	Fen20	…
J10023+480	GJ 378	Single	-	1	Hob19	…
J10088+692	TYC 4384-1735-1	Single	-	1	Blu20	2
J10185-117	LP 729-54	Binary	A	2	Now20	2
J10289+008	Ross 446	Single	-	1	Ama21	1
J10564+070	CN Leo	Single	-	0[e]	Tuo19	…
J11033+359	HD 95735	Single	-	2	Dia19, Ros21	3
J11110+304E	HD 97101	Binary	A	2	Ded21	…
J11302+076	K2-18	Single	-	2	Mon15, Clo17	2
J11417+427	Ross 1003	Single	-	2	Hag10, Tri18	13
J11421+267	Ross 905	Single	-	1	But04	3
J11477+008	FI Vir	Single	-	1	Bon18	…
J11509+483	GJ 1151	Single	-	1[f]	Bla23	1
J12123+544S	HD 238090	Binary	A	1	Sto20	1
J12388+116	Wolf 433	Single	-	1	Fen20	…

Table D.8: Planets with detected planets in our sample (continued).

Karmn	Name	System class	Component	Number of planets[a]	Discovery reference[b]	Flag[c]
J12479+097	Wolf 437	Single	-	1	Tri21	1
J13007+123	Wolf 462	Triple	AB	1[g]	Bur10	…
J13119+658	PM J13119+6550	Single	-	2	Dem20	…
	HD 115404	Binary	A	2	Fen22	…
J13229+244	Ross 1020	Single	-	1	Luq18	1
J13255+688	2M J13253177+6850106	Single	-	2	Gon22	1
J13299+102	Ross 490	Single	-	1	Dam22	1
J14010-026	HD 122303	Single	-	1	Sua17a	3
J15194-077	HO Lib	Single	-	3	Bon05, May09, Udr07	3
J15238+174	Ross 508	Single	-	1	Har22	…
J15583+354	GJ 3929	Single	-	2	Kem22, Bea22	1
J16090+529	GJ 3942	Single	-	1	Per17	…
J16102-193	K2-33	Single	-	1	Dav16	…
J16126-188	LP 804-27	Single	-	1	App10	…
J16167+672S	HD 147379	Binary	A	1	Rei18a	1
J16254+543	GJ 625	Single	-	1	SM17b	…
J16303-126	V2306 Oph	Single	-	3	Wri16	…
	V1090 Her	Triple	A	3	Fen22	…
J16581+257	Ross 860	Single	-	1	Joh10	…
J17153+049	GJ 1214	Single	-	1	Cha09	…
J17160+110	GJ 3998	Single	-	2	Aff16	…
J17355+616	GJ 685	Triple	C	1	Pin19	…
J17364+683	GJ 687	Single	-	2	Lur14	…
J17378+185	GJ 686	Single	-	1	Aff19	3
J17578+046	Barnard's Star	Single	-	0[h]	Rib18 (Lub21)	…
J18353+457	GJ 720 A	Binary	A	1	Gon21	…
	LP 141-14	Triple	C	1	Van20	…
J18580+059	HD 176029	Single	-	1	Tol21	1
J19169+051N	V1428 Aql	Binary	A	1	Kam18	1
J19206+731S	2M J19204172+7311434	Binary*	A	1	Cad22	…
	HD 190360	Binary	A	2	Nae03, Vog05	…
J20138+133	Ross 754	Single	-	1	Mal21	…
J20451-313	AU Mic	SKG	C	2	Pla20, Mar21	2
J21164+025	LSPM J2116+0234	Single	-	1	Lal19	1
J21221+229	TYC 2187-512-1	Single	-	1	Qui22	1
J21466+668	G 264-12	Single	-	2	Ama21	1
J21474+627	TYC 4266-736-1	Binary	A	1	Esp22	2
J22096-046	Wolf 1329	Single	-	2	But06, Mon14	…
J22102+587	UCAC4 744-073158	Single	-	1	Fuk22	…
J22137-176	GJ 1265	Single	-	1	Luq18	1
J22252+594	GJ 4276	Single	-	1[i]	Nag19	1
J22532-142	IL Aqr	Single	-	4[j]	Mar98/Del98, Mar01, Riv05, Riv10	3
J23064-050	2MUCD 12171	Single	-	7[k]	Gil16, Gil17	…
J23318+199E	EQ Peg A	Quadruple	Aab (SB2, Del99b)	1	Cur22	…

[a] In the majority of cases these planets are classified as 'Confirmed' (to the date of publication of this work) by the NASA Exoplanet Archive. A few notable stars have been included, despite of the controversial nature of the detections (e.g. Barnard's Star or CN Leo).

[b] References: Aff16: Affer et al. (2016); Aff19: Affer et al. (2019); Ama21: Amado et al. (2021); App10: Apps et al. (2010); Ast17a: Astudillo-Defru et al. (2017b); Ast17b: Astudillo-Defru et al. (2017a); Bau20: Bauer et al. (2020); Bea22: Beard et al. (2022); Bla23: Blanco-Pozo et al. (2023); Blu21: Bluhm et al. (2021); Bon05: Bonfils

et al. (2005a); Bon12: Bonfils et al. (2012); Bon18: Bonfils et al. (2018b); Burg10: Burgasser et al. (2010); But97: Butler et al. (1997); But04: Butler et al. (2004); But06: Butler et al. (2006); Cad22: Cadieux et al. (2022); Cha09: Charbonneau et al. (2009); Cha22: Chaturvedi et al. (2022); Clou17: Cloutier et al. (2017); Cur22: Curiel et al. (2022); Dam22: Damasso et al. (2022); Davi16: David et al. (2016); Ded21: Dedrick et al. (2021); Dem20: Demory et al. (2020); Dia18: Díaz et al. (2018); Dia19: Díaz et al. (2019); Dit17: Dittmann et al. (2017); Dre20: Dreizler et al. (2020); Esp22: Espinoza et al. (2022); Fen20: Feng et al. (2020); Fen22: Feng et al. (2022); Fis08: Fischer et al. (2008); For09: Forveille et al. (2009); Fuk22: Fukui et al. (2022); Gon20: González-Álvarez et al. (2020); Gon21: González-Álvarez et al. (2021); Gon22: González-Álvarez et al. (2022); Gil16: Gillon et al. (2016); Gil17: Gillon et al. (2017); Hag10: Haghighipour et al. (2010); Har22: Harakawa et al. (2022); Hob18: Hobson et al. (2018); Hob19: Hobson et al. (2019); How10: Howard et al. (2010); How14: Howell et al. (2014); Joh07: Johnson et al. (2007); Joh10: Johnson et al. (2010c); Kam18: Kaminski et al. (2018); Kem20: Kemmer et al. (2020); Kem22: Kemmer et al. (2022); Kos21: Kossakowski et al. (2021); Lal19: Lalitha et al. (2019); Lub21: Lubin et al. (2021); Luq18: Luque et al. (2018); Luq19: Luque et al. (2019b); Luq22: Luque et al. (2022b); Mac15: Macintosh et al. (2015); Mal21: Maldonado et al. (2021); Mar01: Marcy et al. (2001); Mar02: Marcy et al. (2002); Mar98: Marcy et al. (1998); Mar21: Martioli et al. (2021); May09: Mayor et al. (2009); Mc04: McArthur et al. (2004); Men19: Ment et al. (2019); Mon14: Montet et al. (2014); Mon15: Montet et al. (2015); Mor19: Morales et al. (2019); Nae03: Naef et al. (2003); Nag19: Nagel et al. (2019); Now20: Nowak et al. (2020); Per17: Perger et al. (2017); Per19: Perger et al. (2019); Pin18: Pinamonti et al. (2018); Pin19: Pinamonti et al. (2019); Pla20: Plavchan et al. (2020); Qui22: Quirrenbach et al. (2022); Ree22: Reefe et al. (2022); Rei12: Reiners et al. (2012); Rei18a: Reiners et al. (2018a); Rib18: Ribas et al. (2018); Riv05: Rivera et al. (2005); Riv10: Rivera et al. (2010); Rob13: Astropy Collaboration et al. (2013); Ros21: Rosenthal et al. (2021); Sua17b: Suárez Mascareño et al. (2017b); Sot21: Soto et al. (2021); Ste20: Stefansson et al. (2020); Sto20: Stock et al. (2020); Sua17a: Suárez Mascareño et al. (2017a); Sua23: Suárez Mascareño et al. (2023); Tol21: Toledo-Padrón et al. (2021); Tri18: Trifonov et al. (2018); Tri21: Trifonov et al. (2021); Tuo14: Tuomi et al. (2014); Tuo19: Tuomi et al. (2019); Udr07: Udry & Santos (2007); Van20: Vanderburg et al. (2020); Vog05: Vogt et al. (2005); Win19b: Winters et al. (2019b); Win22: Winters et al. (2022); Wri16: Wright et al. (2016); Zec19: Zechmeister et al. (2019).

[c] 1: Planet discovered by CARMENES; 2: Transiting planet confirmed with CARMENES follow-up observations; 3: Reanalysis with CARMENES data.

[d] Planets d and e are unconfirmed.

[e] Planets b and c are unconfirmed/controversial.

[f] Planet b (Mahadevan et al., 2021) is a false positive planet.

[g] Planet detected in Ross 458B.

[h] Unconfirmed/controversial planet.

[i] Planet c is unconfirmed.

[j] Delfosse et al. (1998a) and Marcy et al. (1998) simultaneously detected this Jovian-mass planet (published in *Astronomy & Astrophysics* and *Astrophysical Journal Letters*, respectively).

[k] Planet i is unconfirmed.

Table D.9: Eclipsing binaries in our sample.

Karmn	Name	P [d]	$\mathcal{M}_1$ [$\mathcal{M}_\odot$]	$\mathcal{M}_2$ [$\mathcal{M}_\odot$]	$\mathcal{R}_1$ [$\mathcal{R}_\odot$]	$\mathcal{R}_2$ [$\mathcal{R}_\odot$]	a [au]	Reference[a]
J03372+691	GJ 3236	0.7712600 ± 0.0000023	0.376 ± 0.017	0.281 ± 0.015	0.3828 ± 0.0072	0.2992 ± 0.0075	0.01430	Irw09, Shk10
J03375+178S	GJ 3240	< 0.4	…	…	…	…	0.01	Shk10
J07346+318	Castor C	0.8142822 ± 0.0000010	0.5992 ± 0.0047	0.5992 ± 0.0047	0.6191 ± 0.0057	0.6191 ± 0.0057	0.01819	Joy26, Giz02, Tor22
J08316+193S	CU Cnc	2.771468 ± 0.000004	0.4349 ± 0.0012	0.39922 ± 0.00089	0.4323 ± 0.0055	0.3916 ± 0.0094	0.03624	Del99a, Del99b, Tor10
J09193+620	GJ 3547	20.2	…	…	…	…	0.16	Shk10, Skr21
J15474+451	LP 177-102	3.5500184 0.0000018	0.2576 ± 0.0085	0.2585 ± 0.0080	0.2895 ± 0.0068	0.2895 ± 0.0068	0.03654	Moc02, Har11, Bir12
J16343+571	CM Dra	1.268	0.23102 ± 0.00089	0.21409 ± 0.00083	0.2534 ± 0.0019	0.2398 ± 0.0018	0.01750	Mor09, Tor10, Scha19
J21296+176	Ross 775	53.221 ± 0.004	0.114 ± 0.001	0.114 ± 0.001	…	…	…	Mar87, Del99b

[a] Bir12 : Birkby et al. (2012); Del99a : Delfosse et al. (1999a); Del99b : Delfosse et al. (1999b); Giz02 : Gizis et al. (2002); Har11 : Hartman et al. (2011); Irw09 : Irwin et al. (2009); Jef18 : Jeffers et al. (2018); Joy26 : Joy & Sanford (1926); Mar87 : Marcy et al. (1987); Moc02 : Mochnacki et al. (2002); Mor09 : Morales et al. (2009); Scha19 : Schanche et al. (2019); Shk10 : Shkolnik et al. (2010); Shk10 : Shkolnik et al. (2010); Skr21 : Skrzypinski (2021); Tor10 : Torres et al. (2010); Tor22 : Torres et al. (2022).

D.10 Descriptive charts of multiple systems

WDS 00212-4246 (KO 1)

A: LEHPM 494, Königstuhl 1A
B: 2MASS J00210589-4244433, Königstuhl 1B

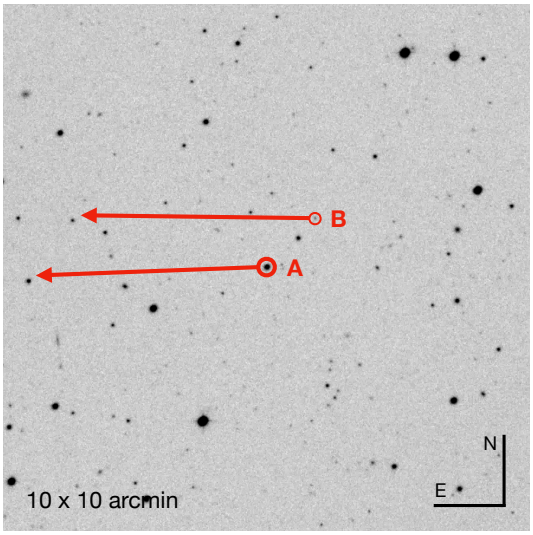

	A-B	
WDS	KO 1	
ρ	77.77	arcsec
θ	316.9	deg
μ ratio	0.050	
ΔPA	2.8	deg
$\Delta d/d$	0.016	
d	26.79	pc
s	2083	au
$P_{\rm orb}$	288	10^3 a
$-U_g^*$	7.33	10^{33} J

Component	A	B	
SpT	m5.5 V	L0.6: V	
α	00:21:11.11	00:21:06.29	
δ	−42:45:40.4	−42:44:43.5	
π	37.332 ± 0.038	37.93 ± 0.40	mas
$\mu_\alpha \cos\delta$	255.184 ± 0.031	257.82 ± 0.37	mas a^{-1}
μ_δ	−12.475 ± 0.039	−0.03 ± 0.39	mas a^{-1}
γ	…	+2 ± 1[a]	km s^{-1}
G	15.3454 ± 0.0028	18.4345 ± 0.0062	mag
J	12.001 ± 0.022	13.521 ± 0.025	mag
$\mathcal{L}$	15.47 ± 0.17	2.95 ± 0.11	$10^{-4}\mathcal{L}_\odot$
$T_{\rm eff}$	2900 ± 50	2200 ± 25	K
$\mathcal{M}$	0.109	0.0793	$\mathcal{M}_\odot$
ruwe	1.074	2.540	
Qflag 2MASS	AAA	AAA	
Qflag AllWISE	AAAU	AAAU	

[a] Mohanty & Basri (2003)

WDS 00212-426 is a known physical pair of ultra-cool dwarfs (mid-M and early-L). The updated physical separation of 2083 au is wider than previously reported. This is the least massive pair in our sample, with a total mass of 0.19$\mathcal{M}_\odot$. With a separation of 1.3 arcmin, it was dubbed as 'the widest ultracool binary' by Caballero (2007). The authors also noted that confirming the binarity of the B component would help to support the hypothesis that wide triples are more prevalent than wide binaries. *Gaia* DR3 ruwe value indicates, in fact, a probable multiplicity of the B component.

WDS 01568+3033 (KO 4)

A: NLTT 6496, Königstuhl 4A, Karmn J01567+305
B: NLTT 6491, Königstuhl 4B

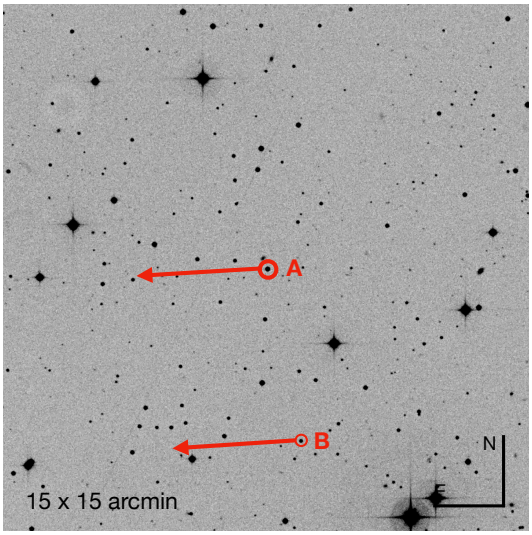

	A-B	
WDS	KO 4	
ρ	299.1	arcsec
θ	190.6	deg
μ ratio	0.012	
ΔPA	0.027	deg
$\Delta d/d$	0.19	
d	31.40	pc
s	9392	au
$P_{\rm orb}$	1699	10^3 a
$-U_g^*$	8.27	10^{33} J

Component	A	B	
SpT	M4.5 V	m5 V	
α	01:56:45.99	01:56:41.74	
δ	+30:33:28.6	+30:28:34.6	
π	31.850 ± 0.076	26.645 ± 0.044	mas
$\mu_\alpha \cos\delta$	210.625 ± 0.092	208.183 ± 0.042	mas a^{-1}
μ_δ	−13.523 ± 0.090	−13.464 ± 0.044	mas a^{-1}
γ	…	…	km s^{-1}
G	13.5151 ± 0.0029	15.1596 ± 0.0028	mag
J	10.323 ± 0.023	11.917 ± 0.023	mag
$\mathcal{L}$	98.6 ± 1.4	31.72 ± 0.46	$10^{-4}\mathcal{L}_\odot$
$T_{\rm eff}$	3100 ± 50	3100 ± 50	K
$\mathcal{M}$	0.287	0.153	$\mathcal{M}_\odot$
ruwe	4.582	1.109	
Qflag 2MASS	AAA	AAA	
Qflag AllWISE	AAAB	AAAU	

WDS 01568+3033 (Königstuhl 4A and 4B) is a wide multiple system of two intermediate M dwarfs, and one of the least bound systems found (Caballero et al., 2012). *Gaia* DR3 enlarges the distance given by the authors by more than 60%. While the pair complies with the proper motion criteria for physical parity, it exists a notable dissimilarity in distances, accompanied by an indication of poor astrometric quality. This high ruwe value of the primary is probably due to unresolved binarity, which affects the *Gaia* parallax determination.

WDS 04309-0849 (KO 2)

A: LP 655-23, Königstuhl 2A, Karmn J04308-088

B: DENIS J043051.5-084900, Königstuhl 2B

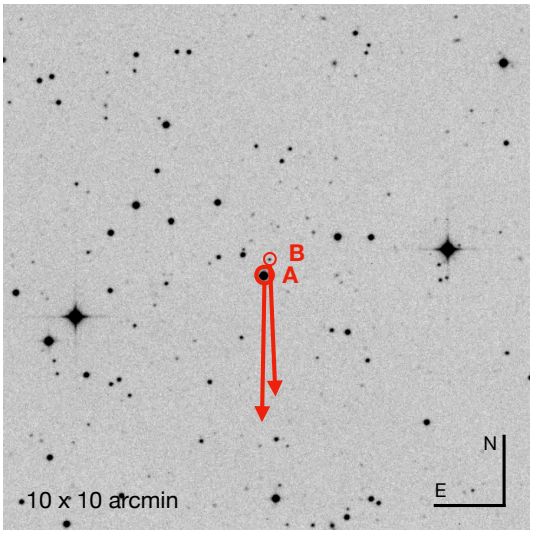

	A-B	
WDS	KO 2	
ρ	19.81	arcsec
θ	339.8	deg
μ ratio	0.053	
ΔPA	2.6	deg
$\Delta d/d$	0.038	
d	30.15	pc
s	597	au
$P_{\rm orb}$	25.1	10^3 a
$-U_g^*$	93.8	10^{33} J

Component	A	B	
SpT	M4.0 V	M8 V	
α	04:30:52.04	04:30:51.58	
δ	−08:49:22.0	−08:49:03.5	
π	33.165 ± 0.061	31.95 ± 0.24	mas
$\mu_\alpha \cos\delta$	3.286 ± 0.069	−3.97 ± 0.23	mas a^{-1}
μ_δ	−161.794 ± 0.053	−157.29 ± 0.19	mas a^{-1}
γ	+1.7 ± 3.5[a]	…	km s^{-1}
G	12.8742 ± 0.0028	17.4264 ± 0.0040	mag
J	9.853 ± 0.024	12.897 ± 0.022	mag
$\mathcal{L}$	142.2 ± 1.9	7.10 ± 0.19	$10^{-4}\mathcal{L}_\odot$
$T_{\rm eff}$	3200 ± 50	2300 ± 25	K
$\mathcal{M}$	0.339	0.0936	$\mathcal{M}_\odot$
ruwe	3.370	1.687	
Qflag 2MASS	AAA	AAA	
Qflag AllWISE	AAAC	AAAU	

[a] Terrien et al. (2015)

WDS 04309-0849 is a known physical pair of spectroscopically characterised ultra-cool dwarfs (mid- and late-M). The separation of almost 20 arcsec reported in *Gaia* DR3 increases the projected separation calculated by Caballero et al. 2007. Their ruwe values suggest a possible binarity, at least for the brightest component.

WDS 06104+2234 (LAW 14 + *New*)

A: 2MASS J06101775+2234199, Karmn J06102+225
BaBb: LP 362-121, Karmn J06103+225

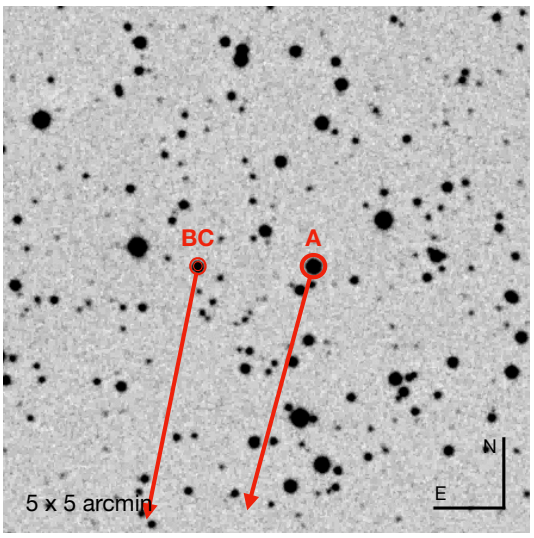

	A-BaBb	
WDS	…	
ρ	65.16	arcsec
θ	89.2	deg
μ ratio	0.060	
ΔPA	1.90	deg
$\Delta d/d$	0.20	
d	28.65	pc
s	1867	au
$P_{\rm orb}$	143.3	10^3 a
$-U_g^*$	66.4	10^{33} J

Component	**A**	**BaBb**	
SpT	M4.0 V	M6 V + m7 V[a]	
α	06:10:17.81	06:10:22.52	
δ	+22:34:17.2	+22:34:18.1	
π	34.900 ± 0.028	43.9 ± 3.7[b]	mas
$\mu_\alpha \cos\delta$	42.256 ± 0.033	39[c]	mas a^{-1}
μ_δ	−153.057 ± 0.025	−162[c]	mas a^{-1}
γ	−10.390 ± 9.806	+9 ± 4[d]	km s^{-1}
G	12.9716 ± 0.0029	14.1549 ± 0.0040	mag
J	9.876 ± 0.021	10.644 ± 0.022	mag
L	121.5 ± 1.5	…	$10^{-4}\mathcal{L}_\odot$
$T_{\rm eff}$	3100 ± 50	…	K
$\mathcal{M}$	0.289	0.12 + 0.10	$\mathcal{M}_\odot$
ruwe	1.402	…	
Qflag 2MASS	AAA	AAA	
Qflag AllWISE	AAAC	AAAC	

[a] From upper limits given by Law et al. (2008).
[b] Dittmann et al. (2014).
[c] Lépine & Shara (2005).
[d] Newton et al. (2014).

Karmn J06102+225 and LP 362-121 are two nearby mid-M dwarfs, the latter resolved to be a close binary (LAW 14; Law et al. 2008), and the former having a visual (non-physical) companion in the background (Janson et al. 2014). We redefine this system as triple. Next *Gaia* releases might determine more accurately the parameters for the BaBb components, for which we compiled data from several sources from the literature.

New

A: BD+37 1541

B: Gaia DR2 943408949754423680

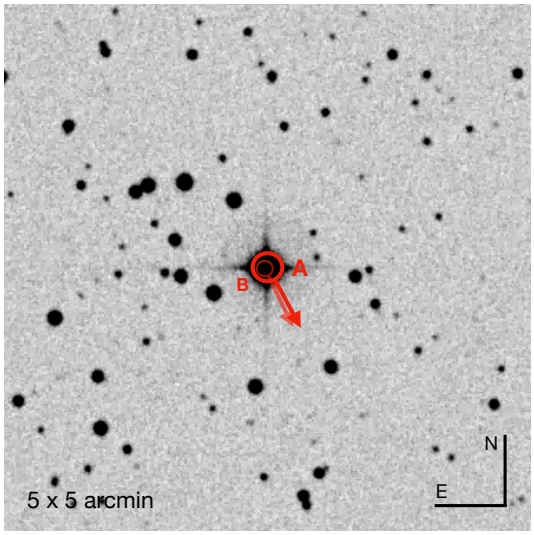

	A-B	
WDS	…	
ρ	3.88	arcsec
θ	201.5	deg
μ ratio	0.016	
ΔPA	0.70	deg
$\Delta d/d$	0.0072	
d	218.8	pc
s	849	au
$P_{\rm orb}$	19.5	10^3 a
$-U_g^*$	1306	10^{33} J

Component	A	B	
SpT	f0: V	m2.5 V	
α	06:35:38.65	06:35:38.53	
δ	+37:51:13.6	+37:51:10.0	
π	4.569 ± 0.019	4.60 ± 0.11	mas
$\mu_\alpha \cos\delta$	−11.831 ± 0.018	−11.69 ± 0.13	mas a^{-1}
μ_δ	−19.999 ± 0.015	−20.33 ± 0.11	mas a^{-1}
γ	+0.7 ± 1.6	…	km s^{-1}
G	9.1409 ± 0.0028	16.439 ± 0.019	mag
J	8.342 ± 0.023	…	mag
$\mathcal{L}$	79030 ± 1750	…	$10^{-4}\mathcal{L}_\odot$
$T_{\rm eff}$	6400 ± 50	…	K
$\mathcal{M}$	1.61	0.391	$\mathcal{M}_\odot$
ruwe	0.905	1.099	
Qflag 2MASS	AAA	…	
Qflag AllWISE	AAAB	…	

BD+37 1541 is an early-F star (estimated by us) in which vicinity *Gaia* DR3 resolves a physical companion candidate at 3.9 arcsec that is seven magnitudes fainter in the G passband, but shares similar proper motions and parallactic distances. The brightness of the very close primary strongly limits the characterisation of the early-M-dwarf secondary.

WDS 06511+1844 (FMR 83)

A: LSPM J0651+1843

B: LSPM J0651+1845

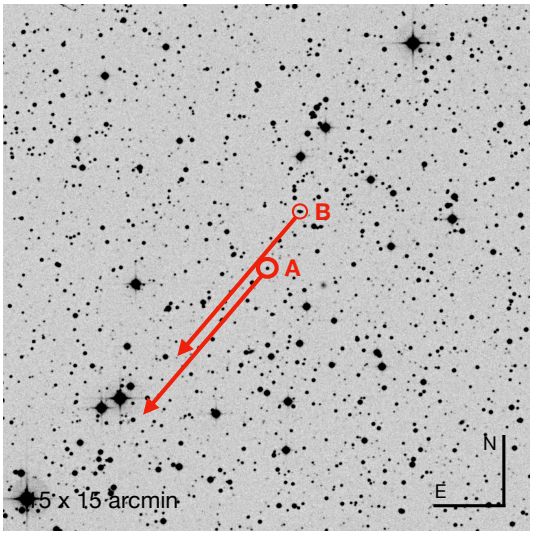

	A-B	
WDS	FMR 83	
ρ	111.7	arcsec
θ	330.6	deg
μ ratio	0.0020	
ΔPA	0.016	deg
$\Delta d/d$	0.0028	
d	63.85	pc
s	7133	au
$P_{\rm orb}$	1461	10^3 a
$-U_g^*$	7.11	10^{33} J

Component	A	B	
SpT	m4.5 V	m4.5 V	
α	06:51:00.84	06:51:04.70	
δ	+18:45:16.1	+18:43:38.7	
π	15.662 ± 0.050	15.617 ± 0.052	mas
$\mu_\alpha \cos\delta$	199.532 ± 0.048	199.078 ± 0.055	mas a^{-1}
μ_δ	−244.131 ± 0.040	−243.713 ± 0.043	mas a^{-1}
γ	…	…	km s^{-1}
G	15.9303 ± 0.0029	15.9455 ± 0.0029	mag
J	12.981 ± 0.021	12.983 ± 0.023	mag
$\mathcal{L}$	37.94 ± 0.92	37.65 ± 0.95	$10^{-4}\mathcal{L}_\odot$
$T_{\rm eff}$	3100 ± 50	3100 ± 50	K
$\mathcal{M}$	0.170	0.169	$\mathcal{M}_\odot$
ruwe	1.057	1.068	
Qflag 2MASS	AAA	AAA	
Qflag AllWISE	AABU	AABU	

LSPM J0651+1843 and LSPM J0651+1845 are the components of a known binary system of mid-M dwarfs. Spectral types of both stars photometrically estimated by us. Rica and Caballero (2012) characterised this pair and described it as an 'ultrafragile' system. In this work we refine their parameters with the *Gaia* DR3 solution, and also redefine the nomenclature of their components based on their bolometric luminosity (and G band magnitude).

New

AaAb: 1RXS J073138.4+455718
B: 2MASS J07310905+4556573, Karmn J07310+460
C: PYC J07311+4556

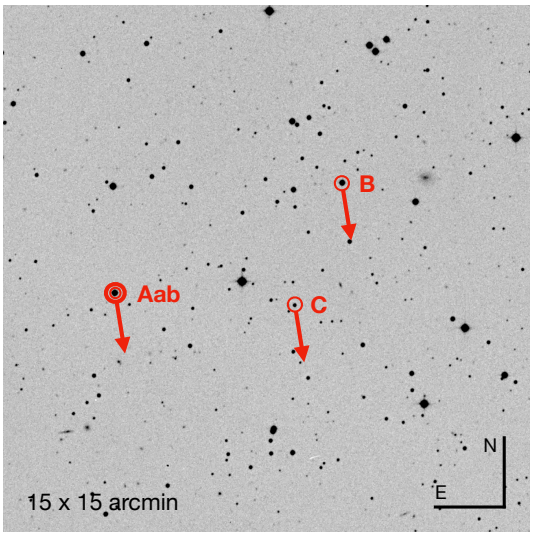

	AaAb-B	AaAb-C	
WDS	…	…	
ρ	431.4	307.8	arcsec
θ	296.0	266.3	deg
μ ratio	0.086	0.079	
ΔPA	0.76	1.5	deg
$\Delta d/d$	0.014	0.028	
d	55.93		pc
s	24127	17215	au
$P_{\rm orb}$	4217	2542	10^3 a
$-U_g^*$	17.5	11.2	10^{33} J

Component	AaAb	B	C	
SpT	M3 + m4.5 V[a]	M4.0 V	m4.5 V	
α	07:31:38.47	07:31:01.27	07:31:09.03	
δ	+45:57:15.8	+46:00:24.8	+45:56:55.6	
π	17.88 ± 0.42	18.141 ± 0.052	18.388 ± 0.034	mas
$\mu_\alpha \cos\delta$	−13.69 ± 0.39	−13.516 ± 0.059	−12.167 ± 0.034	mas a^{-1}
μ_δ	−92.77 ± 0.28	−100.846 ± 0.034	−99.999 ± 0.024	mas a^{-1}
γ	…	…	…	km s^{-1}
G	12.7665 ± 0.0083	12.8963 ± 0.0029	15.2193 ± 0.0030	mag
J	9.776 ± 0.021	9.948 ± 0.023	11.898 ± 0.022	mag
$\mathcal{L}$	…	445.8 ± 7.1	65.1 ± 1.1	$10^{-4}\mathcal{L}_\odot$
$T_{\rm eff}$	…	3200 ± 50	3100 ± 50	K
$\mathcal{M}$	0.789	0.504	0.231	$\mathcal{M}_\odot$
ruwe	20.805	2.230	1.105	
Qflag 2MASS	AAA	AAA	AAA	
Qflag AllWISE	AAAB	AAAB	AAAU	

[a] From the difference in magnitudes reported in JNN 58.

Since the primary of this trio of early-to-mid M dwarfs is a 0.2-arcsec close binary (JNN 58; Janson et al., 2014b), this is a quadruple system. Components B and C are separated about 431 and 308 arcsec from the primary, respectively. Remarkably, the C component is PYC J07311+4556, a young candidate member in the β Pictoris moving group as reported by Schlieder et al. (2012a). For this reason, for the B component we report bolometric luminosity and effective temperature values not in agreement with the expected figures for the main sequence. Additionally, its large ruwe value might be indicative of a non-resolved companion, in which case the system would turn out to be quintuple.

WDS 07400-0336 (BGH 3 + *New*)

A: HD 61606 A

B: HD 61606 B

C: BD-02 2198, Karmn J07361-031

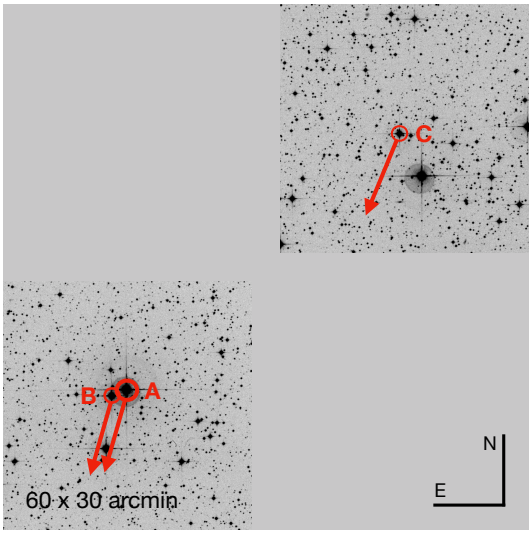

	A-B	A-C	
WDS	BGH 3	…	
ρ	57.9	3894	arcsec
θ	112.7	296.7	deg
μ ratio	0.033	0.054	
ΔPA	1.18	0.049	deg
$\Delta d/d$	0.00056	0.011	
d	14.08		pc
s	815	54823	au
$P_{\rm orb}$	26.6	10907	10^3 a
$-U_g^*$	1026	24.4	10^{33} J

Component	A	B	C	
SpT	K3 V	K7 V	M1.0 V	
α	07:39:59.40	07:40:02.97	07:36:07.15	
δ	−03:35:55.5	−03:36:17.8	−03:06:43.4	
π	71.032 ± 0.024	70.992 ± 0.025	70.27 ± 0.13	mas
$\mu_\alpha \cos\delta$	70.078 ± 0.024	66.008 ± 0.024	74.129 ± 0.144	mas a^{-1}
μ_δ	−278.117 ± 0.019	−286.706 ± 0.020	−293.118 ± 0.095	mas a^{-1}
γ	−18.35 ± 0.18	−19.01 ± 0.19	−17.19 ± 0.37	km s^{-1}
G	6.8898 ± 0.0028	8.3347 ± 0.0028	9.1424 ± 0.0029	mag
J	5.493 ± 0.027	6.377 ± 0.024	6.791 ± 0.034	mag
$\mathcal{L}$	…	…	608.8 ± 9.4	$10^{-4}\mathcal{L}_\odot$
$T_{\rm eff}$	…	…	3700 ± 50	K
$\mathcal{M}$	0.766	0.619	0.547	$\mathcal{M}_\odot$
ruwe	1.065	1.022	6.531	
Qflag 2MASS	EAA	AAA	AAA	
Qflag AllWISE	BBAA	BAAA	AAAA	

WDS 07400-0336 is a known pair of K dwarfs with a projected physical separation of 815 au. Poveda et al. (2009) found that the wide early-M dwarf BD-02 2198 is an co-eval, co-moving and equi-distant companion of this pair. Ishikawa et al. (2020) concluded that this object was not a member of the system, based on the study of scape velocities and chemical abundances (from Montes et al. 2018). However, the large value of the ruwe indicator of C points towards unresolved binarity, in which case the system would be quadruple (i.e. a binary of binaries). This is the closest system of our sample (14.1 pc), but also the most separated one (55 000 au).

New

A: 1RXS J074948.5-031712
B: 2MASS J07495087-0317194
C: 2MASS J07494215-0320338, Karmn J07497-033

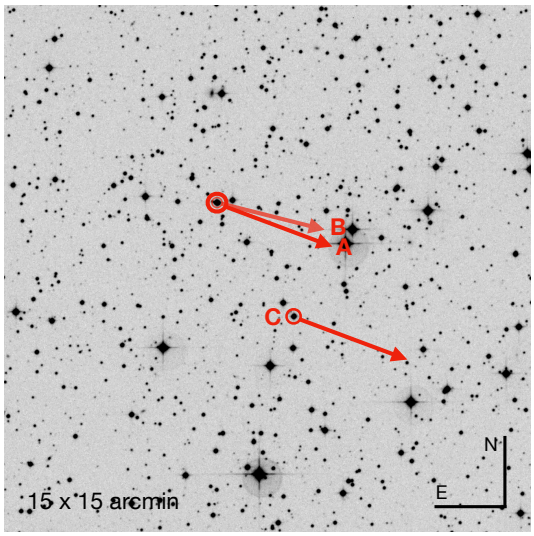

	A-B	A-C	
WDS	…	…	
ρ	1.936	234.9	arcsec
θ	266.3	214.0	deg
μ ratio	0.24	0.084	
ΔPA	5.48	1.56	deg
$\Delta d/d$	0.00043	0.015	
d	17.04		pc
s	32.82	4002	au
$P_{\rm orb}$	0.333	327	10^3 a
$-U_g^*$	4832	81.4	10^{33} J

Component	A	B	C	
SpT	M3.5 V	m4: V	M3.5 V	
α	07:49:50.75	07:49:50.62	07:49:41.97	
δ	−03:17:20.3	−03:17:20.4	−03:20:34.9	
π	58.683 ± 0.047	58.658 ± 0.045	57.83 ± 0.15	mas
$\mu_\alpha \cos\delta$	−174.257 ± 0.044	−139.058 ± 0.046	−161.90 ± 0.14	mas a^{-1}
μ_δ	−65.329 ± 0.033	−37.451 ± 0.040	−55.71 ± 0.11	mas a^{-1}
γ	…	…	−24.2 ± 5.1[a]	km s^{-1}
G	11.5510 ± 0.0028	11.9199 ± 0.0028	11.8027 ± 0.0028	mag
J	8.039 ± 0.030	…	8.891 ± 0.027	mag
$\mathcal{L}$	…	…	113.8 ± 1.7	$10^{-4}\mathcal{L}_\odot$
$T_{\rm eff}$	…	…	3200 ± 50	K
$\mathcal{M}$	0.3195	0.2814	0.3074	$\mathcal{M}_\odot$
ruwe	1.575	1.744	5.936	
Qflag 2MASS	AAA	…	AAA	
Qflag AllWISE	AAAA	…	AAAA	

[a] Terrien et al. (2015)

At less than 2 arcsec of the M3.5-dwarf 1RXS J074948.5-031712, *Gaia* DR3 resolves a source of similar apparent brightness that is equidistant and co-moving. Although its μ ratio exceeds the limit set by our criteria for physical parity, we expect this deviation due to the closeness of the pair (less than 2 arcsec). Separated 235 arcsec from this pair is Karmn J07498-033, which astrometry is indicative of physical connection with the primary. Additionally, the large value of its ruwe indicator suggests an additional binarity for this star, meaning that the entire system would be quadruple.

WDS 08371+3908 (KO 6)

A: LP 209-28, Königstuhl 6A

B: LP 209-27, Königstuhl 6B

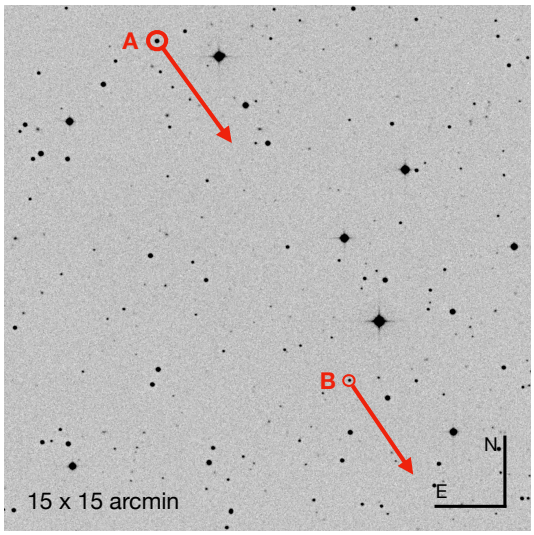

	A-B	
WDS	KO 6	
ρ	666.7	arcsec
θ	208.5	deg
μ ratio	0.034	
ΔPA	0.37	deg
$\Delta d/d$	0.43	
d	104.7	pc
s	69837	au
$P_{\rm orb}$	31557	10^3 a
$-U_g^*$	2.26	10^{33} J

Component	A	B	
SpT	m3: V	m4: V	
α	08:37:04.54	08:36:37.28	
δ	+39:07:56.9	+38:58:10.7	
π	9.546 ± 0.027	6.688± 0.069	mas
$\mu_\alpha \cos\delta$	−119.169 ± 0.027	−116.409 ± 0.065	mas a^{-1}
μ_δ	−186.435 ± 0.023	−179.564 ± 0.052	mas a^{-1}
γ	…	…	km s^{-1}
G	15.0067 ± 0.0028	16.8107 ± 0.0029	mag
J	12.816 ± 0.022	14.009 ± 0.026	mag
$\mathcal{L}$	144.8 ± 2.1	81.8 ± 3.2	$10^{-4}\mathcal{L}_\odot$
$T_{\rm eff}$	3700 ± 50	3200 ± 50	K
$\mathcal{M}$	0.342	0.261	$\mathcal{M}_\odot$
ruwe	1.042	0.964	
Qflag 2MASS	AAA	AAA	
Qflag AllWISE	AABU	AAUU	

LP 209-28 and LP 209-27 (KO6 AB) is a pair proposed as a binary system by Caballero et al. (2012). *Gaia* DR3 introduces a notable dissimilarity in distance between components, accompanied by a good single-star model fitting (i.e. ruwe < 1.4). This means that we do not expect additional multiplicity in either component, and the difference in parallactic determination would not be the cause of close, unresolved companions. We find that the separation of ρ during 10 epochs of observation spanning 62 years increases by 0.248 arcsec (4 milliarcsecond per year). Therefore, we propose this system as a visual pair.

New

A: HD 77825

B: 1RXS J090406.8-155512, Karmn J09040-159

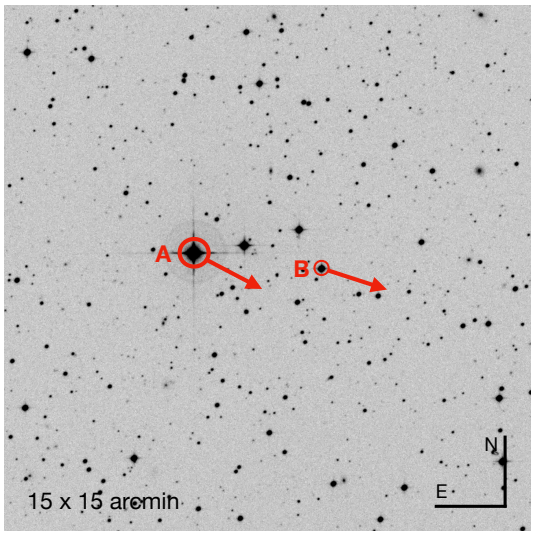

	A-B	
WDS	…	
ρ	220.0	arcsec
θ	262.9	deg
μ ratio	0.020	
ΔPA	0.71	deg
$\Delta d/d$	0.0032	
d	27.39	pc
s	6026	au
$P_{\rm orb}$	538	10^3 a
$-U_g^*$	93.4	10^{33} J

Component	A	B	
SpT	K2 V	M2.5 V	
α	09:04:20.57	09:04:05.44	
δ	−15:54:51.8	−15:55:19.0	
π	36.512 ± 0.022	36.628 ± 0.022	mas
$\mu_\alpha \cos\delta$	−107.828 ± 0.083	−109.034 ± 0.072	mas a^{-1}
μ_δ	−30.936 ± 0.079	−32.638 ± 0.076	mas a^{-1}
γ	+4.39 ± 0.24	+4.44 ± 0.33	km s^{-1}
G	8.4640 ± 0.0028	11.7538 ± 0.0029	mag
J	7.005 ± 0.024	9.156 ± 0.026	mag
$\mathcal{L}$	2601 ± 28	250.1 ± 3.1	$10^{-4}\mathcal{L}_\odot$
$T_{\rm eff}$	4800 ± 50	3400 ± 50	K
$\mathcal{M}$	0.756	0.422	$\mathcal{M}_\odot$
ruwe	1.002	1.114	
Qflag 2MASS	AAA	AAA	
Qflag AllWISE	AAAA	AAAB	

HD 77825 and 1RXS J090406.8-155512 (Karmn J09040-159) form a physical pair of spectroscopically-derived K2 V and M2.5 V stars located at less than 30 pc. All astrometric measurements from *Gaia* DR3 support the binarity, including their radial velocities from *Gaia* DR2.

New

A: 2MASS J13181352+7322073, Karmn J13182+733

B: Gaia DR2 1688578285187648128

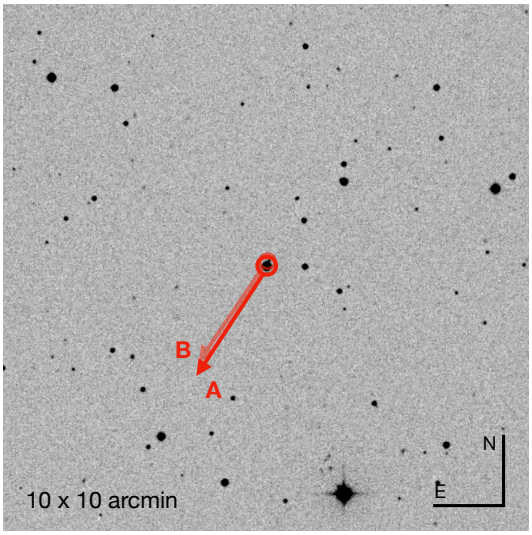

	A-B	
WDS	…	
ρ	7.39	arcsec
θ	155.7	deg
μ ratio	0.065	
ΔPA	1.01	deg
$\Delta d/d$	0.007	
d	25.29	pc
s	187	au
$P_{\rm orb}$	4.38	10^3 a
$-U_g^*$	297	10^{33} J

Component	A	B	
SpT	M3.5 V	m7 V	
α	13:18:13.82	13:18:13.11	
δ	+73:22:05.6	+73:22:12.4	
π	39.534 ± 0.021	39.276 ± 0.098	mas
$\mu_\alpha \cos\delta$	72.055 ± 0.027	70.05 ± 0.11	mas a^{-1}
μ_δ	−107.549 ± 0.027	−100.69 ± 0.12	mas a^{-1}
γ	…	…	km s^{-1}
G	12.3962 ± 0.0028	16.9130 ± 0.0030	mag
J	9.541 ± 0.022	12.660 ± 0.025	mag
$\mathcal{L}$	143.2 ± 1.3	6.20 ± 0.17	$10^{-4}\mathcal{L}_\odot$
$T_{\rm eff}$	3300 ± 50	2500 ± 50	K
$\mathcal{M}$	0.340	0.092	$\mathcal{M}_\odot$
ruwe	1.422	0.814	
Qflag 2MASS	AAA	ABA	
Qflag AllWISE	AAAB	…	

Karmn J13182+733 is an M3.5 V star with a resolved companion at 7.4 arcsec (187 au) to the south. The astrometry of this companion indicates a physical relation to the primary, and its photometry and empirically derived parameters are compatible with a mid- to late-M dwarf.

New

A: HD 130666

B: 2MASS J14474531+4934020

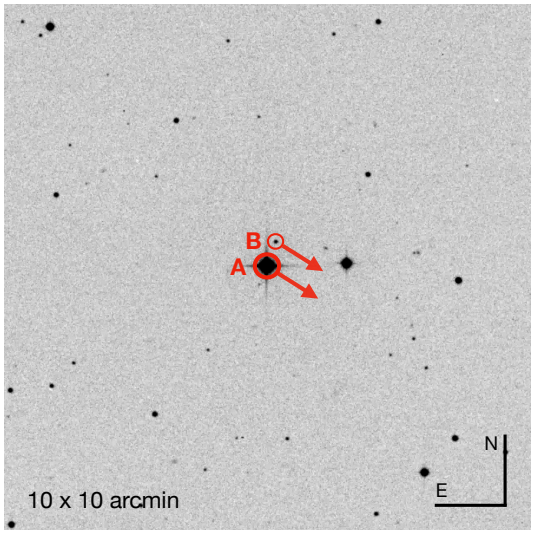

	A-B	
WDS	…	
ρ	29.54	arcsec
θ	336.6	deg
μ ratio	0.051	
ΔPA	21.5	deg
$\Delta d/d$	0.0066	
d	104.0	pc
s	3072	au
$P_{\rm orb}$	146	10^3 a
$-U_g^*$	130	10^{33} J

Component	A	B	
SpT	G5	m4.5 V	
α	14:47:46.40	14:47:45.19	
δ	+49:33:34.1	+49:34:01.2	
π	9.614 ± 0.033	9.551 ± 0.069	mas
$\mu_\alpha \cos\delta$	−63.589 ± 0.032	−62.076 ± 0.068	mas a^{-1}
μ_δ	−51.374 ± 0.038	−47.446 ± 0.081	mas a^{-1}
γ	−50.165 ± 0.179	…	km s^{-1}
G	8.4416 ± 0.0028	17.2739 ± 0.0030	mag
J	7.031 ± 0.030	14.032 ± 0.028	mag
$\mathcal{L}$	38260 ± 9487	36.85 ± 1.14	$10^{-4}\mathcal{L}_\odot$
$T_{\rm eff}$	4900 ± 50	3000 ± 50	K
$\mathcal{M}$	1.36	0.167	$\mathcal{M}_\odot$
ruwe	2.094	1.123	
Qflag 2MASS	AAF	AAA	
Qflag AllWISE	AAAA	AABU	

HD 130666 is a bright Sun-like star with mid-M dwarf physical companion separated by 29.5 arsec. The components are well-characterised, both astrometric and photometrically, in *Gaia* DR3. The ruwe indicator in the primary is higher than expected for a single-star model fit.

New

A: TYC 2565-684-1

B: 2MASS J15080798+3310222

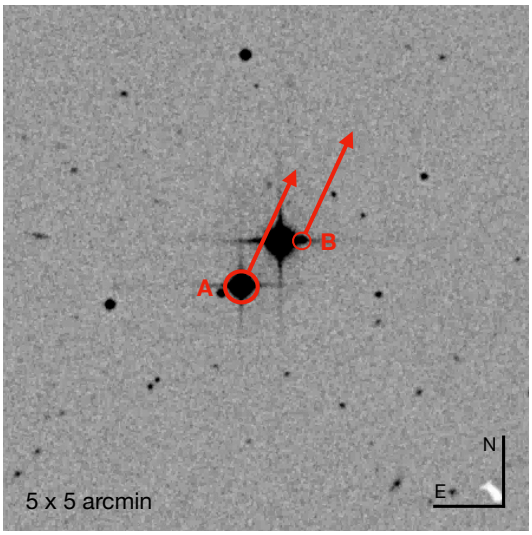

	A-B	
WDS	…	
ρ	43.64	arcsec
θ	306.2	deg
μ ratio	0.0041	
ΔPA	0.23	deg
$\Delta d/d$	0.0054	
d	198.1	pc
s	8644	au
$P_{\rm orb}$	787	10^3 a
$-U_g^*$	79.1	10^{33} J

Component	A	B	
SpT	g1 V	m3 V	
α	15:08:10.72	15:08:07.92	
δ	+33:09:57.8	+33:10:23.6	
π	5.048 ± 0.019	5.021 ± 0.061	mas
$\mu_\alpha \cos\delta$	−39.926 ± 0.015	−40.224 ± 0.050	mas a^{-1}
μ_δ	77.094 ± 0.018	76.905 ± 0.063	mas a^{-1}
γ	−19.2 ± 3.4	…	km s^{-1}
G	10.9314 ± 0.0028	16.9843 ± 0.0028	mag
J	9.895 ± 0.020	14.081 ± 0.037	mag
$\mathcal{L}$	11814 ± 152	128.2 ± 5.3	$10^{-4}\mathcal{L}_\odot$
$T_{\rm eff}$	5700 ± 50	3200 ± 50	K
$\mathcal{M}$	1.04	0.324	$\mathcal{M}_\odot$
ruwe	1.499	1.043	
Qflag 2MASS	AAA	AAA	
Qflag AllWISE	AAAC	…	

TYC 2565-684-1 is a bright dwarf, estimated to be of early-G type, with a fainter companion that we classify photometrically as m3 V. The pair complies with the conditions for physical parity. It is located 13 arcsec westward from the bright background star BD+33 2544 ($G \sim 9.8$ mag).

WDS 15092+3304 (HJ 566 + *New*)

A: HD 134494

B: BD+33 2548 B

C: Gaia DR2 1288848427727490048

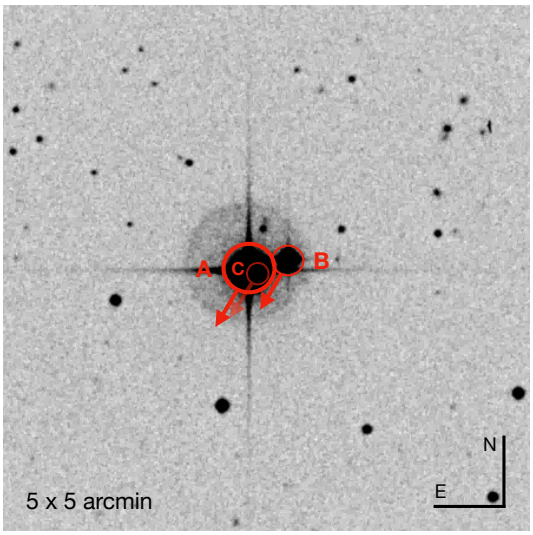

	A-B	A-C	
WDS	HJ 566	…	
ρ	23.4	5.85	arcsec
θ	285.0	180.3	deg
μ ratio	0.0089	0.0066	
ΔPA	0.46	0.21	deg
$\Delta d/d$	0.0063	0.12	
d	276.1		pc
s	6456	1615	au
$P_{\rm orb}$	314	42.1	10^3 a
$-U_g^*$	837	907	10^{33} J

Component	A	B	C	
SpT	K0 IV	f9 V	m3 V	
α	15:09:09.91	15:09:08.11	15:09:09.91	
δ	+33:03:37.4	+33:03:43.4	+33:03:31.5	
π	3.622 ± 0.021	3.645 ± 0.019	4.12 ± 0.10	mas
$\mu_\alpha \cos\delta$	13.284 ± 0.015	13.423 ± 0.015	11.27 ± 0.11	mas a^{-1}
μ_δ	−23.059 ± 0.020	−22.866 ± 0.019	−24.23 ± 0.11	mas a^{-1}
γ	+0.15 ± 0.13	+0.02 ± 0.61	…	km s^{-1}
G	8.0455 ± 0.0028	11.2661 ± 0.0028	17.0507 ± 0.0055	mag
J	6.511 ± 0.021	10.359 ± 0.021	…	mag
$\mathcal{L}$	391600 ± 10700	16294 ± 307	…	$10^{-4}\mathcal{L}_\odot$
$T_{\rm eff}$	4800 ± 50	6100 ± 50	…	K
$\mathcal{M}$	2.55	1.12	0.349	$\mathcal{M}_\odot$
ruwe	1.011	1.172	1.343	
Qflag 2MASS	AAA	AAA	…	
Qflag AllWISE	BAAA	AAAB	…	

HD 134494 (K0, Cannon et al. 1993) has a known physical companion, BD+33 2548B, which we estimate to be a late-F dwarf or early-G. We propose a second candidate to physical companion resolved by *Gaia* at 5.9 arcsec from the primary and 9 mag fainter in G, which we estimate it to be an m3 V star. Based on the bolometric luminosity and the absolute brightnesses in G and J, we propose a new classification of the primary as subgiant.

WDS 16329+0315 (DSG 7 + LEP 79 + DAM 649)

Aabc: HD 149162

B: G 17-23, Karmn J16330+031

C: LSPM J1633+0311S

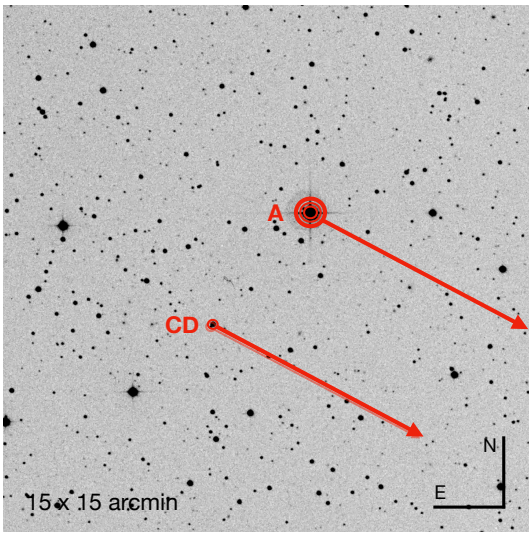

	AaAbAc-BC	
WDS	LEP 79	
ρ	252.0	arcsec
θ	138.4	deg
μ ratio	0.013	
ΔPA	0.67	deg
$\Delta d/d$	0.0015	
d	45.25	pc
s	11406	au
$P_{\rm orb}$	959	10^3 a
$-U_g^*$	121.0	10^{33} J

Component	AaAbAc	B	C	
SpT	K0 Ve + k5 V + m5 V	M3.0 V	D:	
α	16:32:51.24	16:33:02.42	16:33:02.71	
δ	+03:14:42.8	+03:11:34.4	+03:11:29.7	
π	22.09 ± 0.52	22.130 ± 0.016	22.01 ± 0.11	mas
$\mu_\alpha \cos\delta$	−373.83 ± 0.51	−369.147 ± 0.017	−369.41 ± 0.13	mas a^{-1}
μ_δ	−183.10 ± 0.48	−186.158 ± 0.014	−189.69 ± 0.11	mas a^{-1}
γ	−64.1 ± 7.3	…	…	km s^{-1}
G	8.5855 ± 0.0028	13.3872 ± 0.0028	17.7936 ± 0.0030	mag
J	7.159 ± 0.024	10.625 ± 0.026	16.31 ± 0.28	mag
$\mathcal{L}$	…	167.0 ± 2.0	…	$10^{-4}\mathcal{L}_\odot$
$T_{\rm eff}$	…	3300 ± 50	…	K
$\mathcal{M}$	0.87 + 0.68 + 0.19	0.363	0.0985	$\mathcal{M}_\odot$
ruwe	28.569	1.145	0.997	
Qflag 2MASS	AAA	AAA	DDU	
Qflag AllWISE	AAAA	AAAC	…	

From the triple system HD 149162 (AaAbAc, DSG 7), the component Aa is spectroscopically classified as an early-K dwarf. We estimate photometrically the spectral types of Ab and Ac. At 252 arcsec from A, the M3 V G 17-23 (Karmn J16330+031) was reported to be a physical companion of the triple system (LEP 79). For this M dwarf, a close companion named LSPM J1633+0311S was additionally found at 6.4 arcsec (DAM 649), and classified as a white dwarf by Montes et al. (2018). Three of the five components are resolved by *Gaia* DR3 and 2MASS. González-Peinado et al. (2018) described this system in detail with the astrometry from *Gaia* DR1. We revisit this quintuple system with the latest astrometry from *Gaia* DR3.

WDS 19312+3607 (GIC 158)

Aab: G 125-15

B: G 125-14, Karmn J19312+361AB

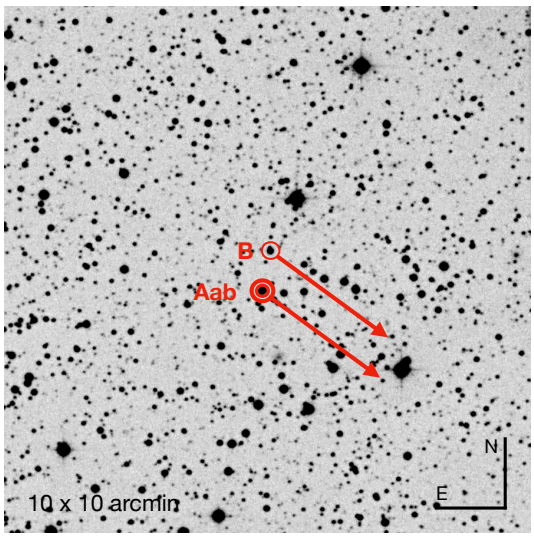

	Aab-B	
WDS	GIC 158	
ρ	45.78	arcsec
θ	347.4	deg
μ ratio	0.0085	
ΔPA	0.461	deg
$\Delta d/d$	0.00072	
d	40.08	pc
s	1835	au
$P_{\rm orb}$	101.9	10^3 a
$-U_g^*$	160.4	10^{33} J

Component	**Aab**	**B**	
SpT	M4.5 V + M5[a]	M4.5 V	
α	19:31:12.38	19:31:11.56	
δ	+36:07:28.2	+36:08:12.8	
π	24.948 ± 0.022	24.966 ± 0.015	mas
$\mu_\alpha \cos\delta$	−129.778 ± 0.022	−130.266 ± 0.015	mas a^{-1}
μ_δ	−106.444 ± 0.026	−105.102 ± 0.018	mas a^{-1}
γ	−22.31 ± 1.24[a]	…	km s^{-1}
G	12.6849 ± 0.0029	13.9120 ± 0.0028	mag
J	9.609 ± 0.022	10.924 ± 0.022	mag
$\mathcal{L}$	…	93.92 ± 0.94	$10^{-4}\mathcal{L}_\odot$
$T_{\rm eff}$	…	3200 ± 50	K
$\mathcal{M}$	0.40 + 0.19	0.280	$\mathcal{M}_\odot$
ruwe	1.358	1.203	
Qflag 2MASS	AAA	AAA	
Qflag AllWISE	AAAB	AAAU	

[a] Shkolnik et al. (2010)

G 125-15 is an active (Reid et al. 2004) mid-M-dwarf and double-lined spectroscopic binary (Shkolnik et al. 2010), with a known physical companion at 45.8 arcsec. The trio was investigated in detail by Caballero et al. (2010). In particular, they studied the age of the system and ruled out previous determinations of youth. Their photometrically estimated distance, as well as other previous determinations, are substantially different from the latest trigonometric value from *Gaia* DR3, which in turn enlarges the physical separation up to 1835 au.

WDS 20198+2257 (KPP 4191 + *New*)

Aab: LP 395-8 A, Karmn J20198+229

B: LP 395-8 B

C: Gaia DR2 1829571684884360832

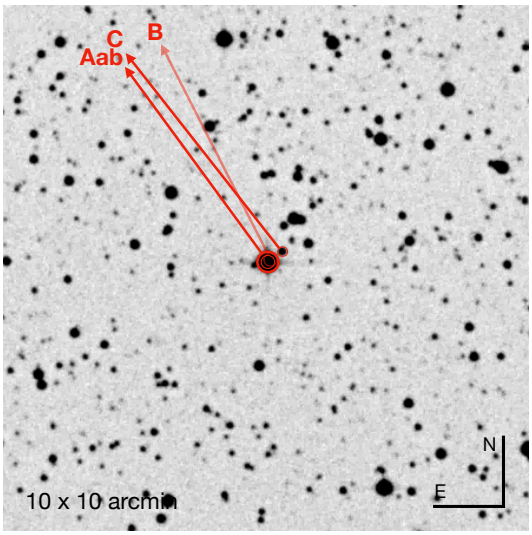

	Aab-B	Aab-C	
WDS	KPP 4191	…	
ρ	1.92	11.02	arcsec
θ	355.5	307.4	deg
μ ratio	0.19	0.054	
ΔPA	10.6	0.0093	deg
$\Delta d/d$	0.000044	0.0012	
d	29.50		pc
s	56.6	325	au
$P_{\rm orb}$	0.432	5.95	10^3 a
$-U_g^*$	9231	5954	10^{33} J

Component	Aab	B	C	
SpT	M3.0 V + m0 V[a]	m3.5 V	m9: V	
α	20:19:49.36	20:19:49.35	20:19:48.72	
δ	+22:56:38.1	+22:56:40.0	+22:56:44.8	
π	33.897 ± 0.026	33.896 ± 0.053	33.94 ± 0.34	mas
$\mu_\alpha \cos\delta$	83.565 ± 0.019	63.613 ± 0.041	88.09 ± 0.25	mas a^{-1}
μ_δ	106.536 ± 0.019	122.155 ± 0.039	112.33 ± 0.26	mas a^{-1}
γ	…	…	…	km s^{-1}
G	11.0225 ± 0.0029	12.8748 ± 0.0028	19.4441 ± 0.0039	mag
J	8.166 ± 0.021	…	13.82 ± 0.11	mag
$\mathcal{L}$	…	…	…	$10^{-4}\mathcal{L}_\odot$
$T_{\rm eff}$	…	…	…	K
$\mathcal{M}$	0.348 + 0.621[a]	0.305	0.077	$\mathcal{M}_\odot$
ruwe	1.484	1.639	1.046	
Qflag 2MASS	AAA	…	BBA	
Qflag AllWISE	AAAA	…	…	

[a] Baroch et al. (2018)

LP 395-8 AB is a known binary system of M dwarfs located at less than 30 pc, which small projected separation (1.9 arcsec) affects the quality of the astrometric data. The primary (LP 395-8 A) was identified to be a spectroscopic binary by Baroch et al. (2018). To this known triple system, we add a fourth candidate to physical companion and estimated to be a very late-M dwarf from its intrinsic brightness in G and J.

WDS 22259-7501 (TOK 434 + DUN 238 + KO 5)

A: HD 212168, Königstuhl 5A
BaBb: CPD-75 1748B, Königstuhl 5B
C: DENIS J222644.3-750342, Königstuhl 5C

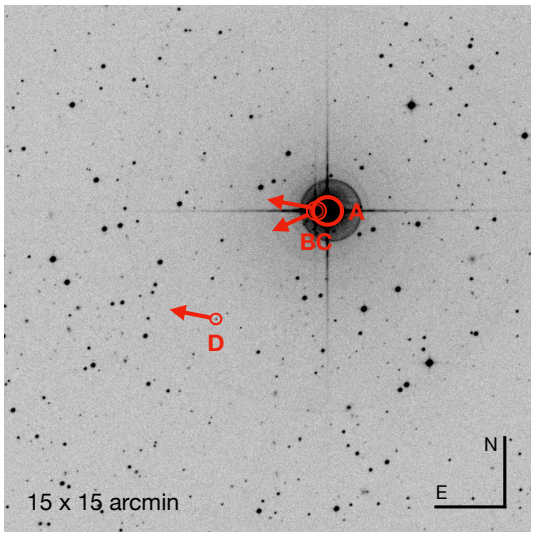

	A-BaBb	A-C	
WDS	DUN 238	KO 5	
ρ	20.89	264.8	arcsec
θ	79.3	128.9	deg
μ ratio	0.49	0.029	
ΔPA	19.08	1.268	deg
$\Delta d/d$	0.0007	0.002	
d	23.41		pc
s	489.2	6199	au
$P_{\rm orb}$	10.25	462.3	10^3 a
$-U_g^*$	2895	29.7	10^{33} J

Component	A	BaBb	C	
SpT	G0 V	k3 V+	M8	
α	22:25:51.39	22:25:56.69	22:26:44.66	
δ	−75:00:56.3	−75:00:52.4	−75:03:42.3	
π	42.722 ± 0.020	42.69 ± 0.25	42.637 ± 0.078	mas
$\mu_\alpha \cos\delta$	57.385 ± 0.021	33.33 ± 0.29	58.739 ± 0.084	mas a^{-1}
μ_δ	12.835 ± 0.023	−3.78 ± 0.30	11.779± 0.092	mas a^{-1}
γ	+14.51 ± 0.14	+17.86 ± 0.59	+17 ± 2[a]	km s^{-1}
G	5.9771 ± 0.0028	8.3805 ± 0.0028	16.7983 ± 0.0031	mag
J	5.262 ± 0.276	6.559 ± 0.029	12.353 ± 0.023	mag
$\mathcal{L}$	15900 ± 290	…	7.06 ± 0.11	$10^{-4}\mathcal{L}_\odot$
$T_{\rm eff}$	5900 ± 50	…	2400 ± 50	K
$\mathcal{M}$	1.11	0.720	0.0935	$\mathcal{M}_\odot$
ruwe	1.017	16.764	1.189	
Qflag 2MASS	DEE	AAA	AAA	
Qflag AllWISE	BBAA	BAAA	AAAU	

[a] Burgasser et al. (2015)

The G0 dwarf HD 212168 and the close binary CPD −75° 1748B (TOK 434), separated 21 arcsec, form a triple system, which is additionally orbited by the M8.5 V star DENIS J222644.3-750342, separated 265 arcsec. Caballero et al. (2012) confirmed the physical binding. The Sun-lile primary and the low-mass companion share common parallax, proper motion and radial velocity. *Gaia* DR3 astrometric data for the K-dwarf secondary is, however, affected by its close binarity (ρ = 0.3 arcsec).

WDS 23059+0614 (SLW 1299 + SLW 1300)

A: SLW J2305+0613 A

B: SLW J2305+0613 B

C: SLW J2305+0613 C

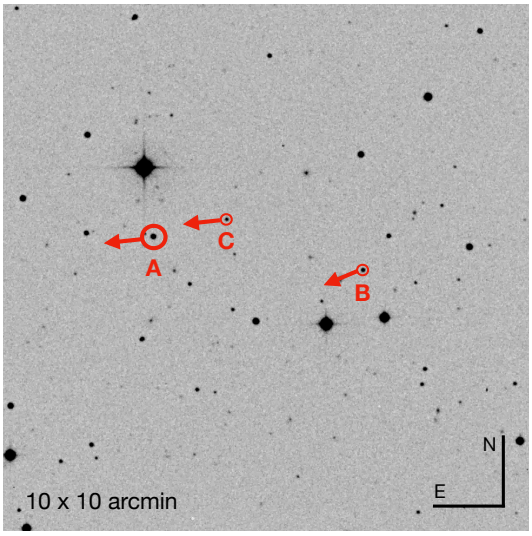

	A-B	A-C	
WDS	SLW 1299	SLW 1230	
ρ	242.4	86.00	arcsec
θ	260.9	283.1	deg
μ ratio	0.11	0.029	
ΔPA	6.14	1.47	deg
$\Delta d/d$	0.40	0.022	
d	216.9		pc
s	52578	186579	au
$P_{\rm orb}$	16642	3518	10^3 a
$-U_g^*$	6.82	15.5	10^{33} J

Component	A	B	C	
SpT	M1.7	M3.2	M3.7	
α	23:05:51.69	23:05:35.65	23:05:46.08	
δ	+06:13:34.6	+06:12:56.1	+06:13:54.1	
π	4.609 ± 0.041	7.743 ± 0.084	4.71 ± 0.10	mas
$\mu_\alpha \cos\delta$	43.584 ± 0.044	42.158 ± 0.092	42.78 ± 0.12	mas a^{-1}
μ_δ	−5.291 ± 0.084	−9.784 ± 0.064	−6.308 ± 0.084	mas a^{-1}
γ	…	…	…	km s^{-1}
G	16.5216 ± 0.0062	18.146 ± 0.036	18.896 ± 0.029	mag
J	12.913 ± 0.025	13.826 ± 0.026	14.397 ± 0.034	mag
$\mathcal{L}$	517 ± 22	196 ± 18	118 ± 11	$10^{-4}\mathcal{L}_\odot$
$T_{\rm eff}$	3500 ± 50	3300 ± 50	3200 ± 50	K
$\mathcal{M}$	0.525	0.386	0.312	$\mathcal{M}_\odot$
ruwe	1.081	1.086	0.937	
Qflag 2MASS	AAA	AAA	AAA	
Qflag AllWISE	AABU	AAUU	AAUU	

The pairs SLW J2305+0613 AB and BC are two known binary systems (SDSS SLoWPoKES Catalog; Dhital et al. 2010) of early-M dwarfs. We analyse the pairs A-B and A-C to test the candidacy for a triple system. We find that the parallactic distance of B differs by 40% to that of the primary, and also present a moderately large difference in proper motion. Given that the quality indicator ruwe does not indicate unreliable astrometry, we propose the B component to be a foreground star. Therefore, the pair A-B is visual, and the trio A-B-C does not qualify as a triple system.

WDS 23315-0405 (KO 3 + CLO 4 + GZA 1)

A: HD 221356, Königstuhl 3A
BC: 2MASSW J2331016-040618, Königstuhl 3BC
D: 2MASS J23313095-0405234

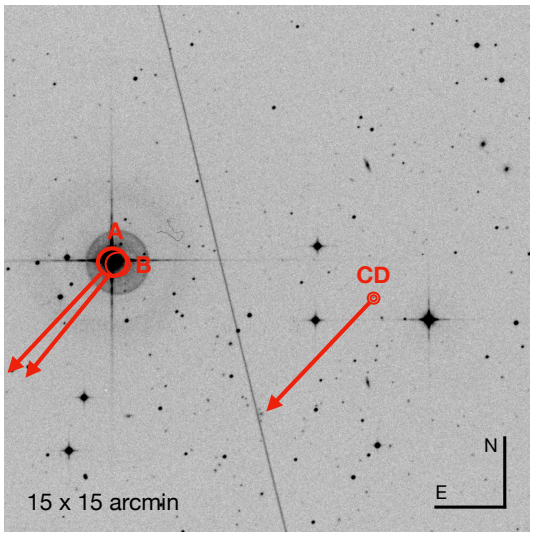

	A-BC	A-D	
WDS	KO 3	GZA 1	
ρ	451.7	12.46	arcsec
θ	261.7	221.6	deg
μ ratio	0.012	0.033	
ΔPA	0.080	1.75	deg
$\Delta d/d$	0.005	0.004	
d	25.832		pc
s	11670	322	au
$P_{\rm orb}$	1205	5560	10^3 a
$-U_g^*$	26.6	468.4	10^{33} J

Component	A	BC	D	
SpT	F7 V	M8.0 V + L3.0 V	L1	
α	23:31:31.69	23:31:01.82	23:31:31.14	
δ	−04:05:17.7	−04:06:22.5	−04:05:27.0	
π	38.711 ± 0.024	38.51 ± 0.16	38.54 ± 0.36	mas
$\mu_\alpha \cos\delta$	178.130 ± 0.028	176.34 ± 0.17	169.94 ± 0.41	mas a^{-1}
μ_δ	−191.845 ± 0.017	−189.38 ± 0.13	−194.59 ± 0.30	mas a^{-1}
γ	−12.47 ± 0.18	…	…	km s^{-1}
G	6.3626 ± 0.0028	17.2032 ± 0.0037	18.527 ± 0.013	mag
J	5.488 ± 0.019	12.938 ± 0.024	12.198	mag
$\mathcal{L}$	13740 ± 150	…	…	$10^{-4}\mathcal{L}_\odot$
$T_{\rm eff}$	6000 ± 50	…	…	K
$\mathcal{M}$	1.09	0.161	0.0792	$\mathcal{M}_\odot$
ruwe	0.857	1.215	1.198	
Qflag 2MASS	AAA	AAA	UUB	
Qflag AllWISE	BAAA	AABU	…	

The triple system consisting of the F7 V HD 221356 and the 0.573 arcsec double (CLO 4; Gizis et al. 2003) 2MASSW J2331016-040618 (M8.0 V and L3.0 V), was confirmed to be a physically bound system by Caballero (2007). Gauza et al. (2012) reported a fourth component (L1 ± 1) separated by 12.5 arcsec from the primary.

WDS 23536+1207 (VYS 11)

A: StKM 2-1787

B: TYC 1174-955-2, Karmn J23535+121

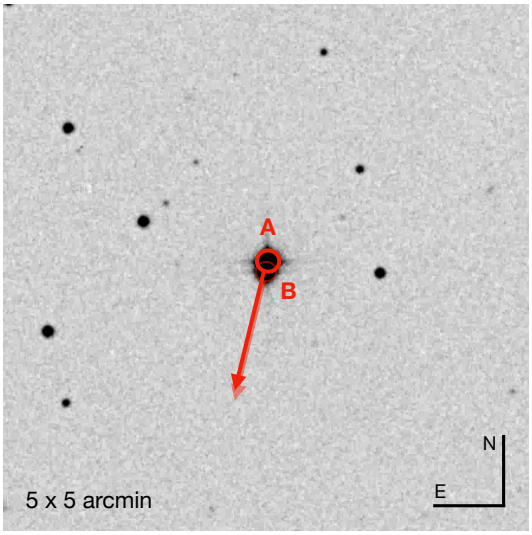

	A-B	
WDS	VYS 11	
ρ	5.78	arcsec
θ	165.1	deg
μ ratio	0.039	
ΔPA	2.190	deg
$\Delta d/d$	0.0018	
d	37.26	pc
s	215.5	au
$P_{\rm orb}$	3.987	10^3 a
$-U_g^*$	2774	10^{33} J

Component	A	B	
SpT	K4 V	M2.5 V	
α	23:53:35.58	23:53:35.69	
δ	+12:06:20.4	+12:06:14.8	
π	26.839 ± 0.019	26.792 ± 0.035	mas
$\mu_\alpha \cos\delta$	40.265 ± 0.023	44.122 ± 0.039	mas a^{-1}
μ_δ	−113.773 ± 0.014	−110.989 ± 0.022	mas a^{-1}
γ	−21.69 ± 0.49	…	km s^{-1}
G	10.4261 ± 0.0028	11.2967± 0.0028	mag
J	8.403 ± 0.019	8.670 ± 0.029	mag
$\mathcal{L}$	1103.5 ± 9.2	702.7 ± 8.8	$10^{-4}\mathcal{L}_\odot$
$T_{\rm eff}$	4000 ± 50	3500 ± 50	K
$\mathcal{M}$	0.629	0.538	$\mathcal{M}_\odot$
ruwe	1.183	1.520	
Qflag 2MASS	AAA	AAA	
Qflag AllWISE	AAAA	…	

Using the latest astrometric data from *Gaia* DR3, we revisit the known binary system of StKM 2-1787 and TYC 1174-955-2, which comprises a mid-K dwarf and an early-M dwarf. We measure an orbital period of approximately 4000 years at a separation of 216 au. We confirm the binarity that Montes et al. (2018) left on hold, as new *Gaia* astrometry could come to settle the issue.

Appendix E

Code

In this Appendix the most relevant pieces of code used in this work can be found. Their purposes are mainly to access databases and to automate repetitive tasks. They aim for syntax simplicity and a good effort has been made to consciously abide with the style guides[1]. The full suite of code produced during this thesis can be found in the GitHub: https://github.com/ccifuentesr/.

[1] For instance, the Python's PEP 8 (https://peps.python.org/pep-0008/).

E.1 `Aladin` search

The following is a working example for a 10-arcmin automatic cone search around the source defined as $1, loading a 15×15 arcmin^2 first generation DSS image, the WDS catalog, and the main astro-photometric catalogues used in this work. Use the `Tool > Macro controller` option to input this macro:

```
reset
get DSS.ESO(POSS2UKSTU_IR, 15, 15) $1 10'
pause 3  # giving time for image to load and stay on the background
get Simbad $1 10'  # Simbad
get VizieR(B/wds/wds) $1 10'  # WDS
get VizieR(II/335/galex_ais) $1 10'  # Galex DR5
get VizieR(I/259/tyc2) $1 10'  # Tycho-2
get VizieR(I/355/gaiadr3) $1 10'  # Gaia DR3
get VizieR(I/350/gaiaedr3) $1 10'  # Gaia EDR3
get VizieR(I/345/gaia2) $1 10'  # Gaia DR2
get VizieR(V/139/sdss9) $1 10'  # SDSS9
get VizieR(I/322A/out) $1 10'  # UCAC4
get VizieR(II/336/apass9) $1 10'  # APASS9
get VizieR(II/349/ps1) $1 10'  # Pan-STARRS1
get VizieR(I/327/cmc15) $1 10'  # CMC15
get VizieR(II/246/out) $1 10'  # 2MASS
get VizieR(II/328/allwise) $1 10'  # AllWISE
get VizieR(II/311/wise) $1 10'  # WISE
get VizieR(II/365/catwise ) $1 10'  # CatWISE
```

`get hips(CDS/P/SDSS9/color)`, SDSS and `get hips(CDS/P/DSS2/color)`, second generation DSS, are other surveys available for loading image adquisition. In the cases in which a close binarity is suspected, the use of several images from different epochs makes it possible to actually eyesight the change of position of the stars in the sky. Similarly, the syntax `get VizieR( ... )` accepts any catalog identifier from the VizieR database (`https://vizier.cds.unistra.fr/viz-bin/VizieR`).

`TOPCAT` and `Aladin` are able to exchange data, from 'Interop' menu, 'Send table to...' option. The table is then loaded as a layer in `Aladin`, with the possibility of scrolling through the objects.

E.2 *Gaia* ADQL

The vast amount of information stored in the *Gaia* Archive (https://gea.esac.esa.int/archive/) can be retrieved using Astronomical Data Query Language (ADQL), a semantic derivative (or dialtect) of Structured Query Language (SQL). These are working examples of code snippets used in this work to obtain tailored *Gaia* data. In this work they have also been implemented programmatically within other codes using `Python`'s `astroquery.gaia` package. Fields in <angle brackets> refer to user's input.

```
> Retrieval of all of the Gaia columns for a given <gaia_id>.

SELECT *
FROM gaiadr3.gaia_source
WHERE source_id = <gaia_id>

> Search by coordinates <ra>, <dec> of any source within a <radius> in degrees,
limiting to a difference in <parallax> of less than 10%.

SELECT * , distance(POINT('ICRS', <ra>, <dec>),
POINT('ICRS', gaia.ra, gaia.dec)) AS dist
FROM gaiadr3.gaia_source AS gaia
WHERE 1=CONTAINS(POINT('ICRS', <ra>, <dec>),
CIRCLE('ICRS', gaia.ra, gaia.dec, <radius>))
AND abs(1-(gaia.parallax/ <parallax>)) < 0.10)

> Example of double cross match with AllWISE

SELECT mytab.*, gaia.*
FROM user_ccifuentes. <user_table> AS mytab
LEFT OUTER JOIN gaiadr3.allwise_best_neighbour AS xmatch
ON mytab.<gaia_id> = xmatch.source_id
LEFT OUTER JOIN gaiadr2.allwise_original_valid AS wise
ON xmatch.original_ext_source_id = wise.allwise_oid
```

E.3 Software

Table E.1: Software widely used in this work.

Software	Author(s)	Webpage
Aladin[a]	Bonnarel et al. (2000)	https://aladin.u-strasbg.fr
IRAF[b]	NOAO	http://iraf.noao.edu (404)
PARSEC	Bressan et al. (2012)	http://stev.oapd.inaf.it/cgi-bin/cmd
SteParKin[c]	Montes et al. (2001)	https://github.com/dmontesg/SteParKin
TOPCAT[d]	Taylor (2005)	http://www.star.bris.ac.uk/~mbt/topcat/

[a] Developed by the CDS.

[b] IRAF was written by the National Optical Astronomy Observatories (NOAO), but http://iraf.noao.edu does no longer exist. The latest NOAO release had a large number of problems, due to its complicated package structure, a buggy installation procedure, major bugs in the code itself (with increasing difficulty to adapt to 64-bit architectures), and (most important) major issues in the licensing and security bugs. With this, development and maintenance of IRAF is discontinued since 2013. The IRAF community distribution (https://iraf-community.github.io) notes that "[users] should be aware that IRAF is 35 years old legacy code and institutional support for IRAF and its usage is going away quickly". The same source also recommends to search for alternative solutions (e.g. in Astropy) and *not to* start new projects using IRAF. See Space Telescope Science Institute (STScI) newsletter (Vol. 2018, issue 35) "Removing the Institute's Dependence on IRAF (You can do it too!)" on the imperious necessity for de-IRAFing the community.

[c] SteParKin is based on D. Montes' and H. Tabernero's original code, originally written in FORTRAN and later in IDL, and adapted to Python by A. J. Domínguez-Fernández.

Table E.2: Python libraries most often used in this work.

Software	Author(s)
AstroPy	Astropy Collaboration et al. (2022)
emcee	Foreman-Mackey et al. (2013)
IPython	Perez & Granger (2007)
Matplotlib	Hunter (2007)
NumPy	Harris et al. (2020)
Pandas	Wes McKinney (2010)
SciPy	Virtanen et al. (2020)

List of Figures

List of Tables

GOBIERNO
DE ESPAÑA

MINISTERIO
DE CIENCIA, INNOVACIÓN
Y UNIVERSIDADES